

Joachim Kurzke · Ian Halliwell

Propulsion and Power

An Exploration of Gas Turbine
Performance Modeling



Springer

Propulsion and Power

Joachim Kurzke · Ian Halliwell

Propulsion and Power

An Exploration of Gas Turbine
Performance Modeling



Springer

Joachim Kurzke
Dachau
Germany

Ian Halliwell
Heath, Ohio
USA

ISBN 978-3-319-75977-7 ISBN 978-3-319-75979-1 (eBook)
<https://doi.org/10.1007/978-3-319-75979-1>

Library of Congress Control Number: 2018932197

© Springer International Publishing AG, part of Springer Nature 2018

This work is subject to copyright. All rights are reserved by the Publisher, whether the whole or part of the material is concerned, specifically the rights of translation, reprinting, reuse of illustrations, recitation, broadcasting, reproduction on microfilms or in any other physical way, and transmission or information storage and retrieval, electronic adaptation, computer software, or by similar or dissimilar methodology now known or hereafter developed.

The use of general descriptive names, registered names, trademarks, service marks, etc. in this publication does not imply, even in the absence of a specific statement, that such names are exempt from the relevant protective laws and regulations and therefore free for general use.

The publisher, the authors and the editors are safe to assume that the advice and information in this book are believed to be true and accurate at the date of publication. Neither the publisher nor the authors or the editors give a warranty, express or implied, with respect to the material contained herein or for any errors or omissions that may have been made. The publisher remains neutral with regard to jurisdictional claims in published maps and institutional affiliations.

Printed on acid-free paper

This Springer imprint is published by the registered company Springer International Publishing AG part of Springer Nature

The registered company address is: Gewerbestrasse 11, 6330 Cham, Switzerland

Preface

In the preliminary design of a gas turbine engine, a great deal of information is brought together from many sources. One problem that many young engineers have is in remembering what they have learned in order to apply it. If we were to ask you to name your first-grade teacher, most of you would be able to. Why? It's because over the course of our lives, we each build a personal matrix in which all the events, experiences, and encounters—even the most detailed—are stored and linked, simply but solidly. So, when we are asked about something personal, we can immediately go to our matrix, trace through the connections, and pull out the relevant information.

As young engineers, we have no equivalent technical matrix and often only a vague idea of how to relate one piece of technology to another. This is due mainly to the fact that technical subjects must be taught as separate classes, because there is simply so much! The extent of any overlap is often not obvious, and connections are not made in the first encounters, usually because of a lack of understanding at the time.

But understanding can only be based on experience or familiarity, to which there is no shortcut! Typically, one becomes comfortable with a technical topic from the presentation of the same material by different people with different points of view, by reading a variety of textbooks, by attending more advanced courses, or from informal—but frequent—discussions with a more senior colleague who is interested in telling the story.

In college, we were not comfortable with any of this stuff, but gradually, over the course of many years, more and more pieces of the puzzle fell into place, a broader picture emerged and began to make sense. It wasn't so difficult after all but whenever that occurred, our reaction was invariably “Why didn't somebody tell me that?” Our approach addresses many such questions, based on numerous examples encountered in our own careers. For some readers, certain topics may be too simple, but for others, they are keystones that are neglected all too frequently. Their inclusion allows critical technical steps to be taken and accelerates gas turbine understanding. One important example is an appreciation of velocity diagrams, their interpretation, and the ability to use them to advantage.

This book is written for anyone interested in preliminary design of gas turbine engines, their operation, and their performance. But it is much more than that. For practicing engineers, we offer some new and unique approaches to performance analysis, interpretation of test data, and rapid answers to *what-if* questions. For students and teachers, we supply some fresh ways of looking at engine technology to make the learning and teaching experience more enjoyable and encourage further exploration. We present industrial systems modeling and performance prediction, but we connect them solidly to a knowledge of thermodynamics and turbomachinery supplied typically by university courses in propulsion and power generation. The book is intended for teachers as a source of information for lecture materials and exercises for their students. It is illustrated extensively with examples and data from real engine cycles, all of which can be reproduced with GasTurb™ or other equivalent software.

The book discusses the practical application of thermodynamic, aerodynamic, and mechanical principles. We describe the theoretical background of the simulation elements and the relevant correlations through which they are applied, however we refrain from detailed derivations. We try to explain things simply. We want the readers to understand the subject themselves, rather than be impressed by our knowledge, so we are not worried about being accused of writing popular science.

While working in industry under pressure, who remembers all the complex mathematical derivations? Most of the time, you don't need them, except perhaps to develop a new product or design tool—and such activities should not be based on extrapolation of an existing idea but on confident extensions of engineering fundamentals. Therefore, you should know the basic physical laws and how to apply them. We want to teach you to make best use of existing software. We want to prevent you from doing too much trial and error. We want you to avoid some of the errors we made! Having said that, errors cannot be avoided sometimes, but their effects can be minimized, and much can be learned by always checking results for plausibility.

It is hoped that this book complements the many other useful texts available on gas turbine design and performance. It passes on the views of two engineers with many years of experience in industry. Imagine you are talking to us and exchanging ideas. The book is a conversation and it is hoped that is reflected in its style and in its title.

Joachim Kurzke
Dachau, Germany

Ian Halliwell
Heath, Ohio, USA

Contents

Part A Simulation Tasks

1	New Engine Design	3
1.1	Nomenclature	3
1.2	Generation of Shaft Power	5
1.2.1	Ideal Thermodynamic Cycles	5
1.2.2	The Efficiency of Shaft Power Generation	11
1.2.3	Combined Cycle	19
1.3	Aircraft Propulsion	22
1.3.1	Turbojet	22
1.3.2	More Definitions of Efficiency	26
1.3.3	Turbofan	34
1.4	Fundamental Design Decisions	42
1.4.1	Turbofan: Mixed Flow or Separate Flow?	43
1.4.2	Dry or Reheated Turbofan?	48
1.4.3	Convergent or Convergent-Divergent Nozzle?	53
1.4.4	Single or Two Stage High Pressure Turbine?	56
1.5	Conceptual Turbofan Design	66
1.5.1	Flow Annulus	66
1.5.2	Direct Drive or with a Gearbox?	70
1.5.3	Conventional Turbofans with Bypass Ratios Between 6 and 14	72
1.5.4	Turbofan with Gearbox	81
1.5.5	Comparison	82
1.5.6	The Fundamental Differences	88
1.6	Mission Analysis	90
1.6.1	General Requirements	90
1.6.2	Single Point Design	91
1.6.3	Multi-point Design	93

1.6.4	High Speed Propulsion	100
1.7	References	114
2	Engine Families	115
2.1	Baseline Engine	116
2.2	Derivative Engine	118
2.2.1	Fan and Booster	118
2.2.2	Core Compressor	120
2.2.3	Combustor	121
2.2.4	High Pressure Turbine	121
2.2.5	Low Pressure Turbine	122
2.3	Optimizing the Growth Engine	122
2.3.1	Design Variables	122
2.3.2	Design Constraints	123
2.3.3	Figure of Merit	124
2.3.4	Ranges for the Design Variables	124
2.3.5	Starting Point	125
2.3.6	Graphical User Interface	125
2.4	Exploring the Design Space	128
2.5	References	130
3	Modeling an Engine	131
3.1	Sources of Data	132
3.1.1	Magazines and Marketing Brochures	132
3.1.2	Official Engine Data	132
3.1.3	Calculated Engine Cycle Data	133
3.1.4	Measurements Made by the Gas Turbine User	133
3.1.5	Measurements in an Engine Maintenance Shop	134
3.2	Data Correction	135
3.2.1	Correction to Standard Day Atmosphere	136
3.2.2	Data Enrichment	139
3.3	Cycle Reference Point	141
3.3.1	Trial and Error Method	141
3.3.2	Multi Point Analysis	142
3.3.3	Optimized Data Match	142
3.3.4	Unable to Create a Reasonable Model?	143
3.4	Off-Design	143
3.4.1	Compressor Maps	144
3.4.2	Turbine Maps	145
3.4.3	More Simulation Details	146
3.5	References	146

4 Engine Model Examples	147
4.1 J57-19W	147
4.1.1 Cycle Reference Point	148
4.1.2 Off-Design Simulation	153
4.2 CFM56-3	166
4.2.1 Check of the Data	167
4.2.2 Cycle Reference Point	179
4.2.3 Off-Design	183
4.2.4 Preliminary Model Calibration.	189
4.2.5 Refined Model	197
4.2.6 Some Final Remarks.	199
4.3 F107-WR-400	201
4.3.1 Cycle Reference Point Max Continuous ISA SLS.	201
4.3.2 Off-Design Model.	207
4.4 References	212
5 Model-Based Performance Analysis	213
5.1 The Analysis by Synthesis Methodology	214
5.1.1 The Model	215
5.1.2 Data Preprocessing	215
5.1.3 Definition of the AnSyn Factors	216
5.1.4 A Simple Analysis Example	220
5.1.5 How to Deal with Missing and Additional Measurements	222
5.1.6 AnSyn and Optimization.	223
5.1.7 Application of the AnSyn Factors	224
5.2 AnSyn During Engine Development	226
5.2.1 Sensor Checking	227
5.2.2 Test Analysis	229
5.2.3 Model Improvement Potential	229
5.3 AnSyn in Engine Maintenance Shops	232
5.3.1 Baseline Model for Diagnostics	233
5.3.2 Engine Diagnostics	233
5.4 AnSyn for Engine Performance Monitoring	235
5.4.1 Baseline Model for Monitoring	235
5.4.2 Trend Monitoring	236
5.5 Interpretation of the AnSyn Factors	237
5.5.1 Component Degradation	238
5.5.2 Model Faults	240
5.5.3 Sensor Faults	240
5.5.4 Measurement Errors	243
5.6 Concluding Remarks	246
5.7 References	247

6	Inlet Flow Distortion	249
6.1	Types of Inlet Flow Distortion	250
6.1.1	Pressure Distortion	250
6.1.2	Temperature Distortion	253
6.2	Parallel Compressor Theory	253
6.2.1	Theory and Experiment	257
6.2.2	Compressor Coupling	261
6.3	Impact of Distortion on Thermodynamics	263
6.4	Changes Due to Control System Actions	265
6.4.1	Unintended Reactions	266
6.4.2	Intended Actions	266
6.5	Reprise	266
6.6	References	267
7	Transient Performance Simulation	269
7.1	Transient Basics	270
7.1.1	Overcoming Rotor Inertia	270
7.1.2	Transient Control Strategies	271
7.2	Engine Geometry	273
7.2.1	Steady State Geometry	273
7.2.2	A Turbofan Example	274
7.3	An Enhanced Approach	277
7.3.1	Tip Clearance	277
7.3.2	Heat Transfer	278
7.3.3	Burner	281
7.3.4	Other Transient Phenomena	281
7.4	Transient Behavior of a Turbofan	282
7.4.1	Accelerating the Cold Engine	282
7.4.2	Decelerating the Hot Engine and Re-slam	286
7.5	Concluding Remarks	290
7.6	References	291

Part B Preliminary Design

1	Engines	295
1.1	The Role of Preliminary Design in Systems Studies	295
1.2	Approach and Implementation	299
1.2.1	Building an Engine Model	299
1.2.2	Component Models	299
1.2.3	Design Constraints	301
1.2.4	Trade Studies Revisited	302
1.2.5	Component Hierarchy	304

1.2.6	The Cycle Design Point	305
1.2.7	Individual Component Design Points	306
1.3	Engine Development—The Role of Performance	309
2	Compressors	313
2.1	Function, Environment, and Basic Efficiency	313
2.1.1	Introduction	313
2.1.2	Limitations of Isentropic Efficiency	317
2.1.3	Polytropic Efficiency	318
2.1.4	Additional Operational Functions	320
2.2	Velocity Diagrams	321
2.2.1	Introduction	321
2.2.2	Sign Convention for Angles and Circumferential Velocities	324
2.2.3	Construction	326
2.2.4	Use of Velocity Diagrams	326
2.2.5	Stage Characteristics	329
2.3	Preliminary Compressor Design	333
2.3.1	Flow in a Blade Passage	334
2.3.2	Mean Line Analysis	335
2.3.3	Three-Dimensional Flow and Radial Equilibrium	335
2.3.4	Diffusion, Turning and Blockage	336
2.3.5	Mean Line Loss Models	342
2.3.6	The Structure of the Mean Line Design Code CSPAN	344
2.3.7	Structure of the Mean Line Analysis in GasTurb	346
2.4	Compressor Design Envelopes	347
2.4.1	Introduction	347
2.4.2	Specification of Design Space	348
2.4.3	Primary Design Variables	350
2.4.4	A Core Compressor with 11 Stages—An Example	351
2.4.5	A Core Driven Fan—A More Complex Example	355
2.5	References	356
3	Turbines	357
3.1	Function, Environment and Basic Efficiency	357
3.1.1	Limitations of Isentropic Efficiency	362
3.1.2	Polytropic Efficiency	364
3.2	Velocity Diagrams	367
3.2.1	Introduction	367
3.2.2	Sign Convention for Angles and Circumferential Velocities	370
3.2.3	Construction	371
3.2.4	Use of Velocity Diagrams	371

3.2.5	Stage Characteristics	374
3.3	Preliminary Turbine Design	380
3.3.1	HP Turbine	380
3.3.2	LP Turbine	381
3.3.3	Mean Line Analysis	382
3.3.4	Development of a Mean Line Code	385
3.3.5	Structure of a Mean Line Code	386
3.3.6	Mean Line Loss Models	388
3.3.7	Loss Components	391
3.3.8	Effects of Cooling Air	393
3.4	Turbine Design Envelopes	394
3.4.1	Introduction	394
3.4.2	Specification	395
3.4.3	Primary Design Variables	396
3.4.4	Solution and Interpretation	397
3.5	Vaneless Counter-Rotation	401
3.6	References	408
4	Mechanical Design	411
4.1	Introduction	411
4.2	Flow Path	413
4.2.1	Compressors	413
4.2.2	Low-Bypass-Ratio Fan or LP Compressor	413
4.2.3	High-Bypass-Ratio Fan	414
4.2.4	Splitters	416
4.2.5	Booster	416
4.2.6	HP Compressor	416
4.2.7	Combustor	418
4.2.8	HP Turbine	418
4.2.9	LP Turbine	420
4.2.10	Afterburners	421
4.2.11	Nozzles	421
4.3	Frames and Ducts	422
4.3.1	Front Frame	422
4.3.2	Main Frame	423
4.3.3	Turbine Center Frame	423
4.3.4	Rear Frame	424
4.4	Shafts	424
4.5	Disk	425
4.5.1	Disk Design Methodology	426
4.5.2	Rim Load	427
4.5.3	Disk Temperature	429
4.5.4	Disk Stress	430

4.5.5	Material Properties	431
4.5.6	Design Margins	432
4.5.7	Stress Distribution	433
4.6	Engine Weight	433
4.7	References	436

Part C Off-Design

1	Component Performance	439
1.1	Inlet	439
1.1.1	Aircraft Engines	439
1.1.2	Power Generation	448
1.2	Off-Design Behavior of Compressors	451
1.2.1	About Compressor Maps	452
1.2.2	Compressor Map Coordinates	461
1.2.3	Compressors with Variable Guide Vanes	468
1.2.4	Fan Maps	473
1.2.5	Secondary Effects	483
1.2.6	Scaling Compressor Maps	487
1.2.7	The Map Preparation Program Smooth C	496
1.2.8	A Simple Map Scaling Procedure	498
1.2.9	Advanced Map Scaling	499
1.2.10	Map Scaling During Off-Design	501
1.3	Turbine Performance	503
1.3.1	Operational Behavior	503
1.3.2	The Map Preparation Program Smooth T	512
1.3.3	Turbine Map Format	515
1.3.4	Tip Clearance	518
1.3.5	Variable Geometry Turbines	520
1.3.6	Vaneless Counter-Rotating Turbines	520
1.4	Combustor	522
1.4.1	Efficiency	522
1.4.2	Pressure Loss	525
1.4.3	Temperature Distribution at the Combustor Exit	528
1.5	Mixer	529
1.5.1	How Mixing Increases Thrust	530
1.5.2	Mixer Geometry	531
1.5.3	Fully Mixed Thrust	532
1.5.4	Unmixed Thrust	533
1.5.5	Mixer Efficiency and Mixer Velocity Coefficient	533
1.5.6	Thrust Gain Potential	534
1.5.7	Practical Mixers	536

1.5.8	Mixer Design Example	537
1.5.9	Mixer Off-Design	539
1.6	Afterburner	541
1.6.1	The Need for a Precise Afterburner Simulation	542
1.6.2	Geometry and Nomenclature	543
1.6.3	Afterburner Operation	544
1.6.4	Reheat Efficiency	546
1.6.5	EJ 200 Example	550
1.7	Nozzles	558
1.7.1	Convergent Nozzles	559
1.7.2	Convergent-Divergent Nozzles	563
1.8	References	573
2	Understanding Off-Design Behavior	577
2.1	Turbojet	578
2.1.1	Off-Design Behavior of the Components	578
2.1.2	Component Synergy	582
2.1.3	Booster Operating Line	593
2.2	Turbofan	594
2.2.1	Fan Operating Line	595
2.2.2	Turbofan Booster Operating Line	597
2.2.3	Low Pressure Turbine	605
2.3	Multi-spool Turboshaft	607
2.4	Single Spool Turboshaft	608
2.5	References	610

Part D Basics

1	Gas Properties and Standard Atmosphere	613
1.1	The Half Ideal Gas	613
1.1.1	Enthalpy	614
1.1.2	Entropy Function	615
1.2	Numerical Values	615
1.2.1	Specific Heat, Enthalpy and Entropy Function	615
1.2.2	Temperature Rise Due to Combustion	616
1.2.3	Fuel	616
1.3	Standard Atmosphere	617
1.4	Reference	618
2	Spreadsheet Calculations	619
2.1	Frequently Needed Equations	619
2.1.1	Some Simple Correlations	619
2.1.2	Compressor	620
2.1.3	Turbine	622

2.1.4	Isentropic and Polytropic Efficiency	625
2.1.5	Combustor	625
2.1.6	Nozzle	626
2.2	Cycle Calculation for a Turbojet Engine	627
2.2.1	Requirement	627
2.2.2	Solution	627
2.2.3	Summary	637
3	Non-dimensional Performance	639
3.1	Non-dimensional Compressor Performance	639
3.2	Non-dimensional Engine Performance	644
3.2.1	Practical Correction to Standard Day Conditions	647
3.2.2	How to Determine the Exponents	648
3.2.3	Aircraft Engines with Afterburners	649
3.2.4	Gas Turbines with Heat Exchanger	650
3.3	References	650
4	Reynolds Number Corrections	651
4.1	Reynolds Number Index	651
4.2	Turbomachinery Loss Correlations with Reynolds Number	653
4.2.1	Compressor	654
4.2.2	Turbine	655
4.2.3	Some Additional Remarks	656
4.3	Applying the Pipe Flow Analogy in Performance Programs	657
4.4	Variations of the Pipe Flow Analogy	658
4.5	Mass Flow Correction	659
4.6	References	660
5	Efficiency of a Cooled Turbine	661
5.1	Single Stage Turbine	663
5.1.1	Simulation Principle	663
5.1.2	About NGV Cooling Air	666
5.1.3	Exchange Rates	667
5.2	Two-Stage Turbine	668
5.3	Equivalent Single Stage Turbine	670
5.3.1	The Virtual RIT Method	673
5.3.2	The Virtual T4 Method	674
5.3.3	Sensitivity Analysis	674
5.3.4	Application	677
5.4	Thermodynamic Efficiency	677
5.4.1	Comparison of Turbine Efficiency Estimates	679
5.4.2	Efficiency Definition Affects the Results of Cycle Studies	681

5.5	Efficiency Losses Due to Cooling	682
5.5.1	Some Numbers	682
5.5.2	A Real-World Example	683
5.6	References	685
6	Secondary Air System	687
6.1	SAS in the Performance Model	687
6.2	SAS Calculation	690
6.2.1	Interstage Bleed	691
6.3	Turbine Cooling Air	692
6.3.1	Multi-stage Turbines	694
6.4	References	696
7	Mathematics	697
7.1	The Off-Design Simulation Task	697
7.2	Basic Algorithms	700
7.2.1	Newton	700
7.2.2	Regula Falsi	701
7.2.3	Newton-Raphson	702
7.3	Application to Performance Calculations	704
7.4	More About the Analytical Technique	704
7.4.1	Hierarchy of Iterations	706
7.4.2	Steady State Performance	707
7.4.3	Limiters	708
7.4.4	Dynamic Engine Simulation	709
7.5	About Convergence Problems	711
7.5.1	A Solution Exists, but the Program Does not Find It	711
7.5.2	No Solution Exists	713
7.6	References	714
8	Optimization	715
8.1	Parametric Studies	715
8.2	Numerical Optimization	716
8.2.1	A Gradient Strategy	717
8.2.2	Adaptive Random Search Strategy	718
8.2.3	Constraints	720
8.2.4	Application	720
8.3	References	722
9	Monte Carlo Simulations	723
9.1	Statistical Background	723
9.1.1	Normal Distribution and Standard Deviation	723
9.1.2	Probability Distribution and Confidence Level	726

9.2	Measurement Uncertainty	727
9.2.1	Systematic Errors	727
9.2.2	A Conventional Test Analysis Procedure	727
9.2.3	Core Flow Analysis	728
9.3	Engine Design Uncertainty	730
9.4	Engine Manufacturing Tolerance	735
9.4.1	Random Variations	736
9.4.2	Correlations	736
9.4.3	Control System Tolerance	736
9.4.4	A Turboshaft Example	737
9.5	References	738
Appendix	739
Index	745

About the Authors

Professors teaching at a University have written most of the technical textbooks, with students as their main audience. This book, however, was written by two engineers who have spent most of their working lives in the gas turbine industry. They know from experience in industry what the challenges are—not the derivation of complex equations from basic principles, but the application of knowledge that is well understood.

Joachim Kurzke spent his engineering life dealing with gas turbine performance, first at the Technical University of Munich, Institute for Flight Propulsion. There he learnt a lot from Prof. H. G. Münzberg who had acquired his gas turbine expertise during the times of pencil and slide ruler. As a young engineer, Kurzke confronted his professor with printouts from a computer—for good reason he never accepted the argument: *These numbers must be right because the computer cannot be wrong*. The outcome of every numerical examination needed an explanation, based on the laws of physics.

In 1976, after finishing his doctoral thesis, Kurzke joined the performance department of the company which is now MTU Aero Engines and stayed there for 28 years. He worked on a multitude of different engine projects, designed the engine performance program MOPS for MTU, and applied it to the everyday problems in the performance department.

MOPS is due to the modular design very flexible and can be adapted easily to new requirements, however, its use requires significant training in gas turbine performance. This observation resulted in the development of the performance program GasTurb™, which Kurzke developed in parallel to his job at MTU. This software concentrates on the user interface, without neglecting any detail which is required for professional gas turbine performance work. After more than 20 years in the public domain, GasTurb™ is well known and acknowledged all over the world.

Kurzke has published numerous papers dealing with gas turbine performance, and was a member of several RTO (former AGARD) working groups, as well as the SAE E33 committee “Thrust in Flight”. He is still a member of the ASME/IGTI Aircraft Engine and Education Committees.

Ian Halliwell obtained his B.Sc. in Aeronautical Engineering and M.Sc. in Aerodynamics from Imperial College, London, followed by a Ph.D. in Experimental Gas Dynamics from the University of Southampton. His professional career began in 1975 at Rolls-Royce, Derby in Turbine Aerodynamics Research. He then crossed the Atlantic to work for Pratt and Whitney Canada in Mississauga and subsequently GE in Cincinnati, where he moved into the preliminary design of complete engine systems and spent several years on the High Speed Civil Transport program. During that period, he also began teaching in GE after-hours education.

While continuing to model complete engine systems, his teaching activities increased after moving to the small business world, as a contractor to the NASA Glenn Research Center and becoming more involved with AIAA and ASME/IGTI. Dr. Halliwell is an Associate Fellow of the AIAA, Past-Chair of the AIAA Air Breathing Propulsion Technical Committee and Past-Chair of the AIAA Gas Turbine Engines Technical Committee. He was given an AIAA Sustained Service Award in 2012. He is currently active as a Member of the AIAA Gas Turbine Engines and Inlets, Nozzles and Propulsion Systems Integration Technical Committees and the ASME/IGTI Aircraft Engines and Education Committees. His connection to students and university faculty was enhanced during the 14 years he organized the AIAA International Engine Design Competition for undergraduate teams. He first met Joachim Kurzke in 2001 and the seeds were sown for this book a few years later.

In addition to teaching from an industrial base, his current special interests include the development of new design tools for gas turbine engines and the investigation of new engine architectures. Full vaneless counter-rotating and exoskeletal systems—both axial and radial—occupy some of his time.

Acknowledgements

The authors are indebted to our friend, Robert Hill, for his vital role in the production of this book. Bob stepped in at a late stage of the project and reviewed the whole manuscript. He undertook an immense task and used his engineering knowledge, intellect, and humor to improve the content, the structure and the accuracy of the material. His support throughout a long series of international Skype calls meant a lot.

Robert Hill (Editor) graduated in Mathematics with a B.A. from Queens' College, Cambridge University and Ph.D. from the University of Manchester Institute of Science and Technology (UMIST). He then worked as an engineer for nearly 40 years in the aircraft engine industry, starting in the Technical Design department at Rolls-Royce in Derby in 1978. This was followed by 10 years in the Performance Department at MTU in Munich, where he first met Joachim Kurzke. During this time he worked on a large range of engines, from small to large, in collaborative projects with Pratt & Whitney (in Hartford and Canada) as well as with General Electric. The last 26 years were spent at Rolls-Royce Deutschland before retirement in 2017. For most of the last 20 years, he was in Future Programmes and studied the conceptual cycle design of advanced engines for the corporate and regional aircraft market. This regularly involved jointly evolving the performance of engines with the requirements coming from the aircraft manufacturers.

Introduction

This book shows how gas turbine engine systems can be modeled accurately using simple tools and limited data. It describes and discusses an industrial approach to engine simulation but, in a unique manner, it connects the models and results to fundamental engineering principles that form the basis of any academic course or text on propulsion or power generation. While gas turbines are used for aircraft propulsion and ground-based power generation and common elements of both applications are discussed, our treatise is focused primarily on propulsion.

Part A discusses the design of new engines. Some typical broad examples of solutions to overall system modeling requirements are described, where contemporary questions are asked and answered. Some of the thought processes involved are addressed, as well as the interpretation and calibration of various data sources used to set performance for the models. Three detailed examples of real engines are presented, where specific characteristics and difficulties are outlined, and the shift from design point to off-design operation is introduced. The analysis of model based performance is evaluated through its application to engine development and its significance in engine maintenance shops. The important effects of inlet flow distortion are introduced and quantified. Finally, high-fidelity transient engine behavior is engaged in a simple fashion, and the effects of heat transfer are coupled with cold acceleration and hot deceleration of an engine. A reader may explore this part of the book to find problems similar to his or her own, where suggestions as to how they may be tackled will also be found.

Modeling at this level occurs in preliminary engine design and the stage is set in Part B. Here, the preliminary design environment is defined, system modeling is outlined, and the types and roles of design constraints are illustrated. The critical function of performance in engine development is also characterized. For components, we focus on the aerodynamic design of axial compressors and turbines. We illustrate how a full appreciation of velocity diagrams captures the quality of a compressor or turbine stage, including trends caused by changing the flow field or

blading geometry. This leads on to a description of mean line models and an initial breakdown of losses in compressors and turbines. The effects of bleed air in compressors and cooling air in turbines are considered. One easy way to capture numerous design parameters in one location and ensure that nothing is neglected is to construct *design envelopes*, so their generation is presented in a general discussion about axial compressors and turbines. In any new engine program, two questions are always asked, usually prematurely; “What does it look like” and “What does it weigh?” As the answers are very important to many people, we devote the last section of Part B to the creation of engine geometry models.

The appeal of any new engine concept to a customer depends not on its performance at its selected design point but on its behavior over a complete flight mission or, in fact, over its entire life. The ability to predict the off-design performance of the components, especially in the complete engine assembly, is therefore essential. Part C refers the reader to off-design models for the most important gas turbine components. Here, the principles of scaling and validating compressor and turbine maps are discussed in more detail than in other sources. New and original information on afterburner and convergent-divergent nozzle models is also presented. Another comprehensive section offers an understanding of overall off-design behavior of an engine and explains how the components relate to each other and are integrated to make a complete gas turbine system. A simple turbojet and a turbofan are used as illustrations and are supplemented by short discussions of single- and multi-spool turboshaft machines.

Part D completes the connection between our modeling techniques and conventional gas turbine course materials. It covers gas properties and the standard atmosphere and moves on to basic equations and correlations that can be used in manual calculations or to set up spreadsheets. (It is recommended that students refrain from using gas turbine performance software until they have hand-calculated their way through a simple turbojet and a turbofan cycle and are proficient in accounting for efficiencies and work balance!) Various approaches are cited that depend on the starting point. A turbojet cycle calculation is provided as an example. Non-dimensional performance is explained in an unusual way, without referring to higher mathematics. Reynolds number corrections to component performance are indispensable and are discussed in a very clear manner. Further highlights are the sections on modeling cooled turbines and the secondary air system. Part D concludes with an outline of useful mathematical tools, convergence issues, and optimization.

All the figures with numerical results contain truly calculated results—they are not cartoons. Many of the figures can be reproduced exactly by the reader using GasTurb™. However, the results from another commercial gas turbine performance code will be very close to those in this book. If there are significant differences between the GasTurb™ output and other results, then—in the absence of an error—you are likely to have used different input data or boundary conditions.

Part A

Simulation Tasks

Chapter 1

New Engine Design



The first step of any gas turbine design is the selection of the thermodynamic cycle. The cycle consists of a sequence of thermodynamic processes that involve transfer of heat and work. The ideal cycle for the simplest gas turbine consists of an isentropic compression, heat addition at constant pressure and an isentropic expansion. In Europe, this cycle is named after James Prescott Joule, a brewer living in England from 1818 to 1889 who recognized the equivalence of heat and work. In the US, this cycle is named after the mechanical engineer George Brayton living in Boston from 1830 to 1892 who invented a machine with constant pressure combustion.

1.1 Nomenclature

When it comes to nomenclature, conflict between author and reader is almost inevitable because the simulation of an overall system deals with various disciplines whose practitioners are all accustomed to their own standards.

Gas turbine performance is the dominating topic in this book, therefore we employ the most popular terms and abbreviations from this engineering discipline. Our preferred system of units is the SI system—with few exceptions.

The thermodynamic station nomenclature described in the SAE Aerospace Standard AS755 is generally accepted in the aircraft engine industry. Station numbers are used as indices to the parameter names.

Most of the parameter names are familiar. Remarkable peculiarities are the use of W for mass flow rate (instead of \dot{m}), T for total temperature, and P for total pressure, both without subscript “ t ”.

To calculate the performance of any gas turbine, it is sufficient to know P and T at each station. But what are these total quantities and how are they connected with the true pressures and temperatures?

Imagine a gas flowing with a certain velocity through a duct. Measuring devices moving with the gas would measure the static pressure P_s and the static temperature T_s of the gas. If there is no heat or work transfer to or from the flow, then—according to the first law of thermodynamics—the sum of static enthalpy $h(T_s)$ and kinetic energy is constant:

$$h(T) = h(T_s) + \frac{V^2}{2} \quad (1.1-1)$$

The relationship between enthalpy and temperature depends on specific heat C_p only. For a gas with constant specific heat we can state

$$C_p T = C_p T_s + \frac{V^2}{2} \quad (1.1-2)$$

So, in a duct with arbitrary cross section, the *total temperature* T remains constant. Friction along the duct wall, boundary layer behavior, turbulence, local flow separation etc.—none of these changes total temperature as long as there is no heat transfer through the duct walls.

For incompressible flow, *total pressure* P is defined as the sum of static pressure P_s and dynamic head, the product of density ρ and kinetic energy:

$$P = P_s + \rho \frac{V^2}{2} \quad (1.1-3)$$

Pressure losses in a duct reduce the total pressure. We can describe a total pressure loss as a fraction of the dynamic head at the duct inlet.

In compressible flow, the density of the gas ρ is a function of static pressure, static temperature, and the gas constant R :

$$\rho = \frac{P_s}{R T_s} \quad (1.1-4)$$

The Mach number $M = V/V_{sonic}$ is the most important descriptor of compressible flow. Sonic velocity in an ideal gas is given by

$$V_{sonic} = \sqrt{\gamma R T_s} \quad (1.1-5)$$

Introducing Mach number and the isentropic exponent $\gamma = C_p/(C_p - R)$ into Eq. (1.1-2) leads to the following relationship between total and static temperatures:

$$\frac{T}{T_s} = 1 + \frac{\gamma - 1}{2} M^2 \quad (1.1-6)$$

Total pressure is the static pressure a compressible gas retains when brought to rest isentropically from a velocity that corresponds to a Mach number M:

$$\frac{P}{P_s} = \left(1 + \frac{\gamma - 1}{2} M^2\right)^{\frac{\gamma}{\gamma-1}} \quad (1.1-7)$$

We quantify duct loss in compressible flow by total pressure loss ΔP expressed as a fraction of the total pressure at the duct inlet.

Total temperatures and total pressures dominate in gas turbine performance calculations. They are the currencies in which we work, and they avoid the need to account for static and dynamic quantities separately. In this text T and P (without an index t like in many other books) stand for total quantities. To refer to static pressure or temperature we use the subscript s.

A comprehensive nomenclature list is found in the appendix.

1.2 Generation of Shaft Power

1.2.1 Ideal Thermodynamic Cycles

Any book about gas turbine performance should have a section on thermodynamic cycles. Here, we limit ourselves to gas turbine cycles which have either been put into practice or are subjects of recent research work. An ideal cycle is composed of compression and expansion processes that operate with 100% efficiency and other connecting processes with zero total pressure losses. In the current context, we also assume for convenience that the kinetic energy at the gas exhaust exit is negligible.

We begin our discussion with an ideal (i.e. lossless) cycle turboshaft engine. We first introduce the fundamental system and then discuss various options to increase the power output per unit mass flow. Figure 1.2-1 shows a gas turbine composed of the components compressor, combustion chamber, high pressure turbine (HPT) and power turbine (PT). The HPT drives the compressor; the PT provides useful power for driving a generator, for example.

Figure 1.2-2 shows the temperature-entropy diagram of the ideal Joule (Brayton) cycle. Maybe you expect that the temperature differences $2 \rightarrow 3$ and $4 \rightarrow 45$ are the same because the power delivered by the HPT PW_{HPT} must be equal to the power needed by the compressor PW_C . Obviously, that is not the case because a rigorous power balance involves not only the temperature differences but also the significant changes in specific heat:

$$PW_C = W_2 C_{P,C} (T_3 - T_2) = W_4 C_{P,HPT} (T_4 - T_{45}) = PW_{HPT} \quad (1.2-1)$$

In this equation, W stands for mass flow rate. Specific heat of air and combustion products increases with both temperature and fuel/air ratio. At the compressor inlet C_P is 1004.5 J/(kg*K), but in the hot part of the engine it is more than

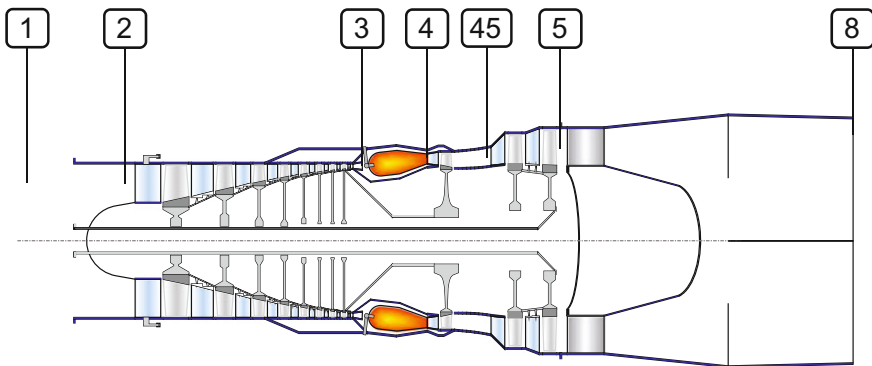


Fig. 1.2-1 Turboshaft station nomenclature

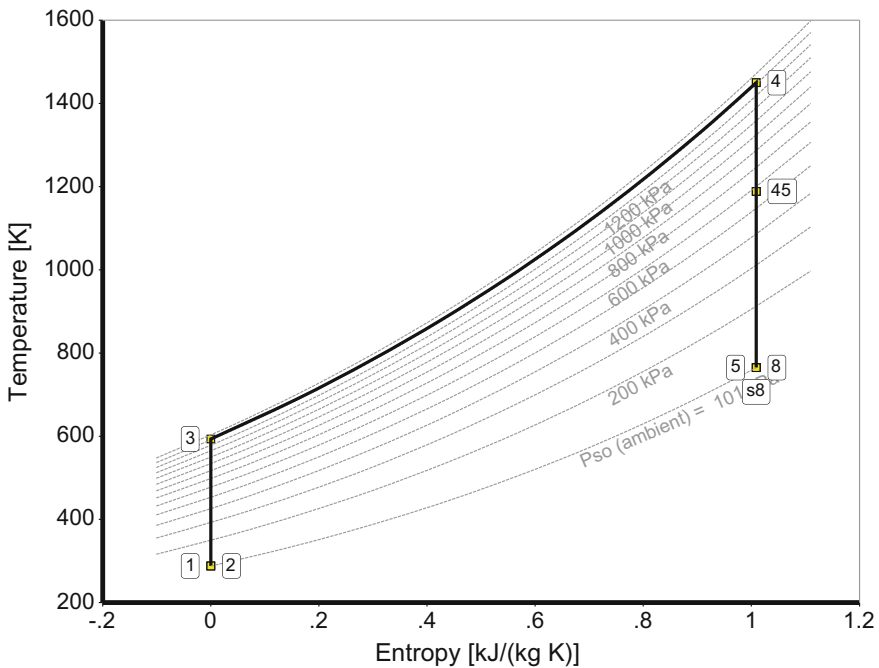


Fig. 1.2-2 Temperature-Entropy diagram of the ideal Joule (Brayton) cycle

1200 J/(kg*K). The variability of C_P is best considered by working with differences in total enthalpy.

$$PW_C = W_2(H_3 - H_2) = W_4(H_4 - H_{45}) = PW_{HPT} \quad (1.2-3)$$

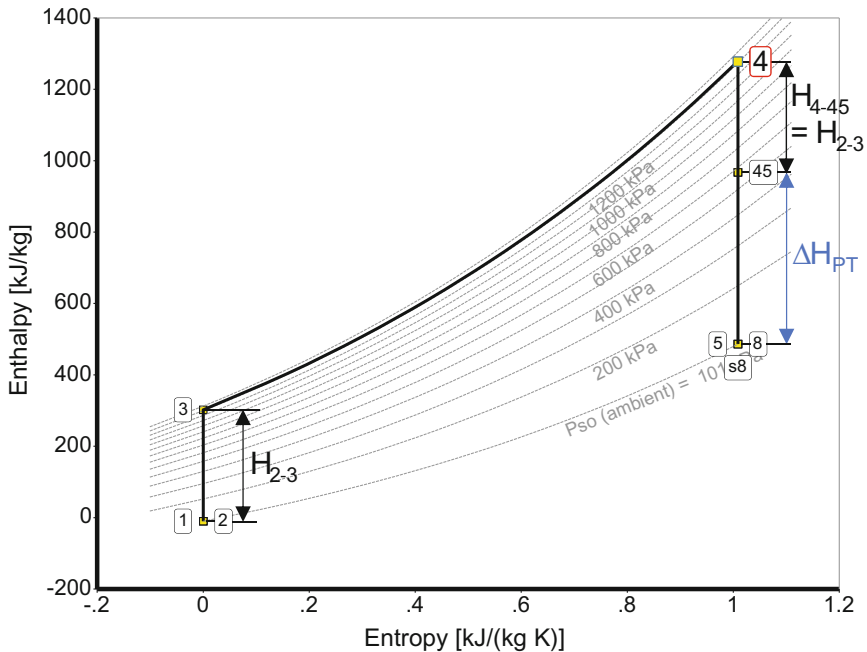


Fig. 1.2-3 Enthalpy-Entropy diagram of the ideal Joule (Brayton) cycle

The mass flow rates W_2 and W_4 are equal if we use a fuel with infinite heating value for the heat addition. The power balance between compressor and turbine becomes simply

$$H_{2-3} = H_{4-45} \quad (1.2-3)$$

We can see and measure the specific power (i.e. power per unit mass flow) of the various components directly when we use enthalpy-entropy instead of temperature-entropy in Fig. 1.2-3.

1.2.1.1 Methods to Increase the Power Output

Increasing the power output per unit mass flow is of interest, especially for aircraft engines, because engine size and weight are proportional to mass flow rate W_2 . Figure 1.2-4 shows the influence of burner exit temperature T_4 on the enthalpy difference ΔH_{PT} over the power turbine. It is obvious that increasing T_4 raises the enthalpy difference available for power generation because the power turbine inlet pressure P_{45} and temperature T_{45} increase. We get more specific work (work ΔH_{PT} per unit mass flow) when we increase T_4 .

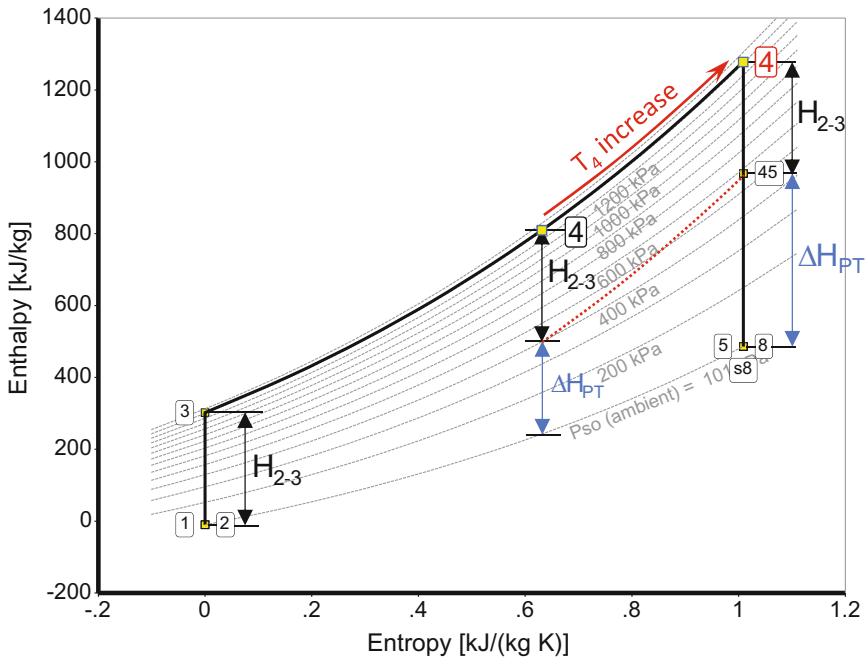


Fig. 1.2-4 Influence of T_4 on shaft power output

We can generalize our conclusion from Fig. 1.2-4 and apply it to any Joule cycle derivative: raising burner exit temperature always yields more work per unit mass flow because the constant pressure lines in the enthalpy-entropy diagram diverge from left to right.

There are more ways than raising T_4 to increase the power output of a gas turbine. For example, we can reduce the power needed for the gas compression by splitting this process into two equal parts and cooling the compressed air from T_{24} at constant pressure back to T_2 (see Fig. 1.2-5). Now the sum of the two compressor work processes $H_{2-24} + H_{25-3}$ is less than the work needed for a one-step compression process from station 2 to 3_{Joule} . The power output per unit mass flow increases by ΔH_C . A real-world application of this cycle is the LMS-100 gas turbine from GE.

Another way to increase the power turbine output is sequential combustion where the HPT exhaust gas is reheated in a second combustion chamber back to the inlet temperature of the gas generator turbine (Fig. 1.2-6). The enthalpy downstream of the HPT H_{42} follows from the power balance with the compressor, thus we know the temperature at the inlet to the second combustor T_{42} . Due to the higher power turbine inlet temperature T_{45} we get more work per unit mass flow (ΔH_{PT}) than from the ideal Joule process. A real-world application of sequential combustion is the GT24/26 gas turbine from GE (previously Alstom).

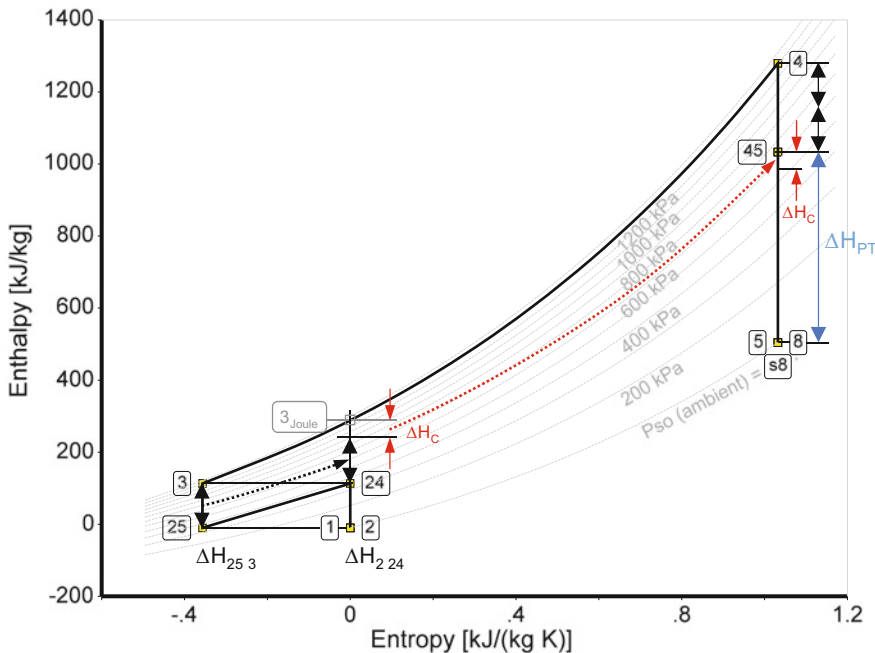


Fig. 1.2-5 Compressor intercooling increases power output

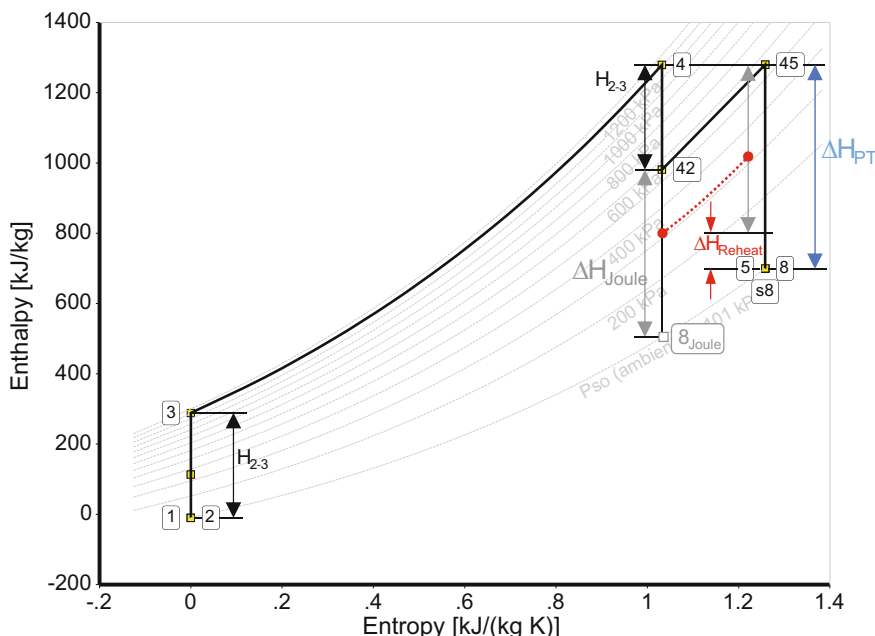


Fig. 1.2-6 Reheating the gas generator exhaust gas (sequential combustion) increases power output

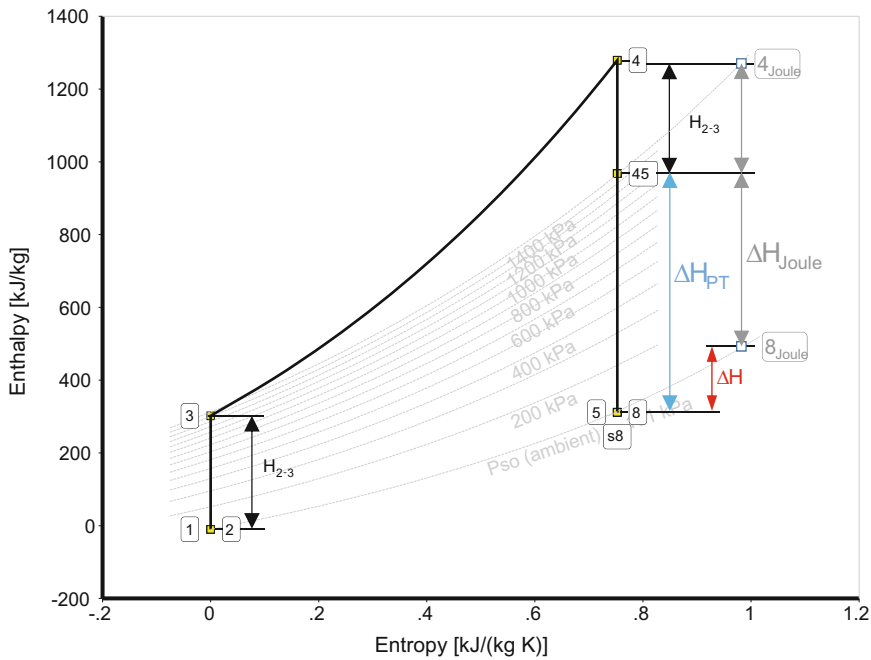


Fig. 1.2-7 Constant volume combustion increases power output

Now we have considered power increase by modifications of the compression and the expansion processes. What about the heat addition part of the cycle?

We can replace the constant pressure combustion by constant volume combustion. This is the *Humphrey* cycle. Pulse detonation engines and wave rotor combustors attempt to make constant volume combustion a reality.

Figure 1.2-7 shows that the power output potential is significantly higher than that of the ideal Joule cycle. Research is in progress, but constant volume combustion is nowhere near a practical application, so we will not consider this cycle further.

The effectiveness of inter-cooling and sequential combustion to increase the specific power of the ideal Joule cycle depends on pressure ratio (see Fig. 1.2-8). It should be noted that the curves can be shifted upwards or downwards by increasing or decreasing the combustor exit temperature T_4 .

1.2.1.2 Methods for Reducing Fuel Consumption

Fuel burn is especially important today because of the effects of CO₂ and other emissions on the environment. This, along with noise generation, is now tightly regulated and monitored throughout the world and the relevant international rules

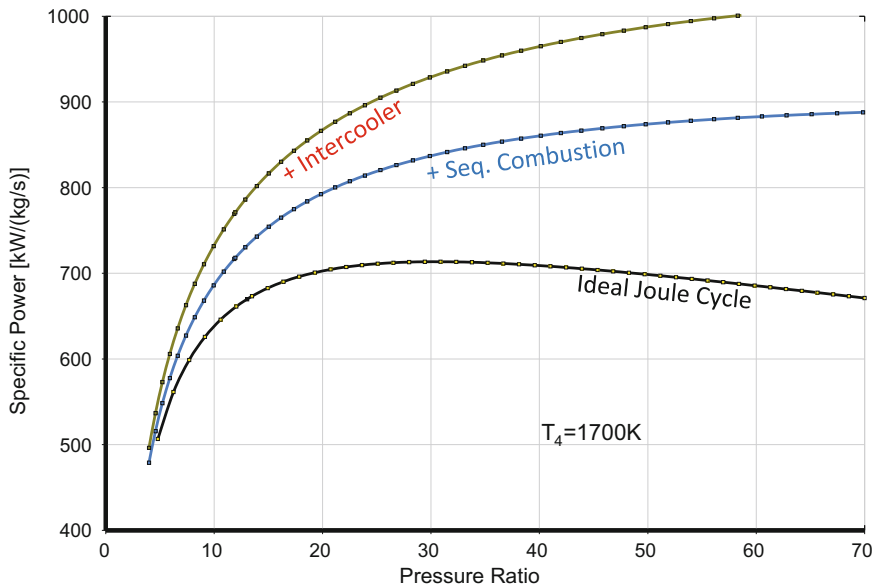


Fig. 1.2-8 Power output per unit mass flow

that govern emissions are part of the externally-imposed design criteria for any new engine. The amount of fuel burned in the combustion chamber depends on the total temperature difference $T_4 - T_3$. Compressor intercooling yields more shaft power, but needs more fuel since $T_4 - T_3$ is bigger than in the Joule cycle. Similarly, the higher shaft power output of a machine with sequential combustion must also be paid for with more fuel. Whether the extra power is worth the additional fuel depends on pressure ratio P_3/P_2 and T_4 .

However, we can definitely reduce the amount of fuel needed by introducing a heat exchanger which transfers part of the exhaust energy to the entrance of the combustion chamber (Fig. 1.2-9). Note that this energy transfer is only feasible if T_6 is greater than T_3 and that is not the case if the pressure ratio P_3/P_2 is high.

1.2.2 *The Efficiency of Shaft Power Generation*

1.2.2.1 **Ideal Cycles**

Cycle efficiency is generally defined as the ratio of power output to power input. The following simple formula for the thermal efficiency of the ideal Joule cycle is found in many basic textbooks:

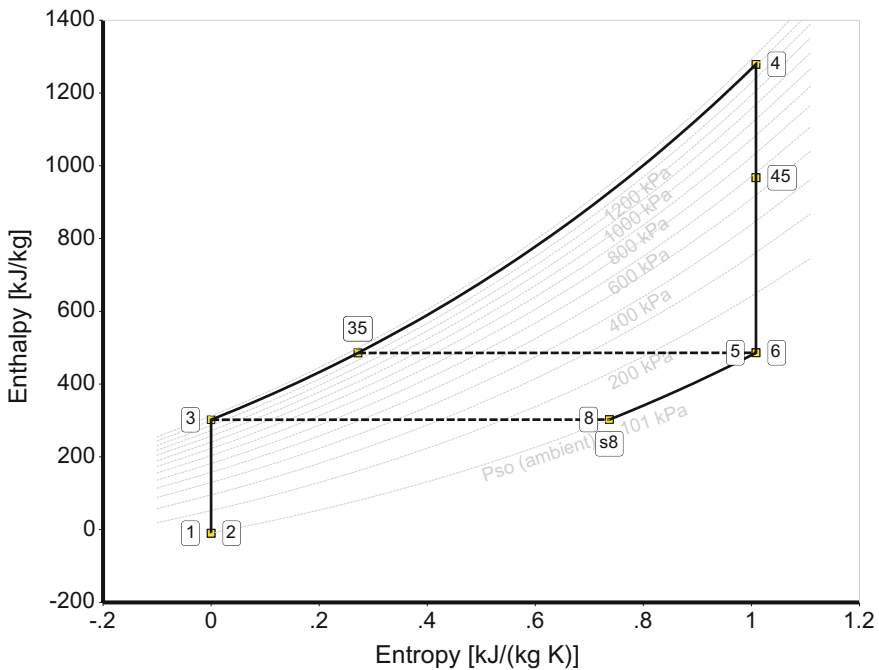


Fig. 1.2-9 Ideal Joule cycle with heat exchanger

$$\eta_{therm} = 1 - \left(\frac{P_2}{P_3} \right)^{\frac{\gamma-1}{\gamma}} \quad (1.2-4)$$

The magnitude of the isentropic exponent γ influences the efficiency, see Fig. 1.2-10. If $\gamma = 1.4$ this yields the highest value—but this is an over simplistic view because γ varies significantly with temperature and gas composition within a gas turbine ($\gamma = 1.4$ at the engine inlet, $\gamma \approx 1.3$ at the combustor exit). Figure 1.2-10 shows that the difference in ideal cycle efficiency due to the variability of γ can be more than 5%.

Note that the efficiency of the ideal Joule cycle decreases slightly when burner exit temperature goes up. The efficiency difference between that of the Joule cycle and the most efficient thermodynamic cycle—the *Carnot* cycle—gets larger with T_4 .

Increasing combustion temperature may not seem to be the right way to go when aiming for high efficiency power generation. However, such a conclusion is premature: remember that we are talking only about ideal cycles here. It will be found later, that higher T_4 yields better thermal efficiency in real-world engine cycles where component efficiencies are of course less than 100%.

According to Eq. (1.2-4), the efficiency of the ideal Joule process is independent of burner exit temperature T_4 . In the following we keep burner exit temperature constant at 1700 K and focus on the effect of overall pressure ratio on cycle

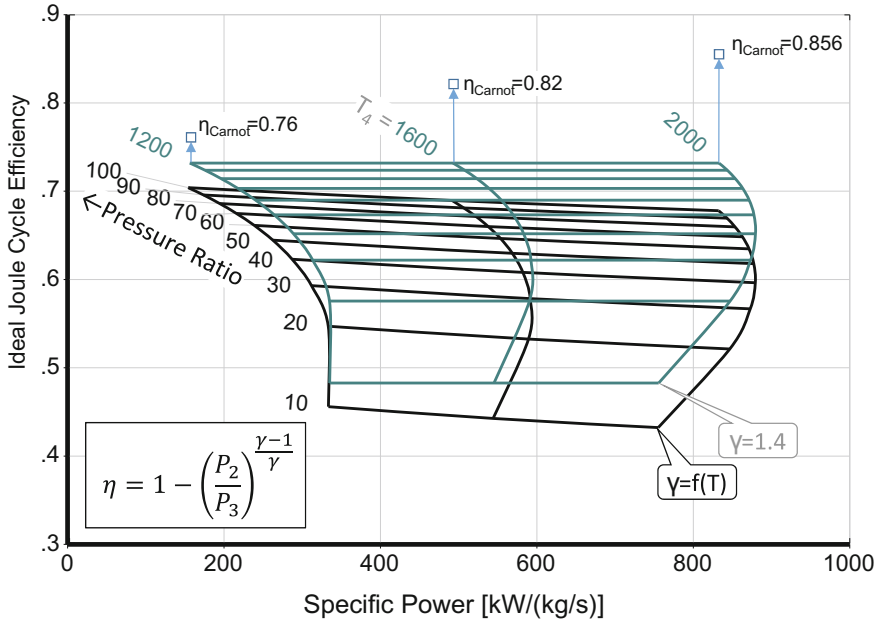


Fig. 1.2-10 Ideal Joule and Carnot cycle efficiency ($T_2 = 288.15$ K)

efficiency. All the following calculations employ realistic values of the gas properties. Cycle thermal efficiency is defined as the ratio of useful power PW_{SD} to the power provided by the fuel Q_{Fuel}

$$\eta_{therm,Q} = \frac{PW_{SD}}{Q_{Fuel}} \quad (1.2-5)$$

By considering an energy balance across the combustion chamber, we determine the power added to the system by burning fuel:

$$Q_{Fuel} = W_4H_4 - W_3H_3 \quad (1.2-6)$$

The efficiency of the ideal Joule cycle rises continuously with pressure ratio, see Fig. 1.2-11 which is valid for $T_4 = 1700$ K. We can improve the efficiency of that cycle by adding a heat exchanger, as already mentioned above. However, this is only beneficial at pressure ratios lower than about 31, where turbine exit temperature is higher than compressor exit temperature.

Redistribution of the compression between two machines, combined with cooling the air back to ambient temperature with an intercooler after the first compressor, decreases thermal efficiency. This is because the amount of additional energy needed in the combustion chamber due to the higher temperature difference

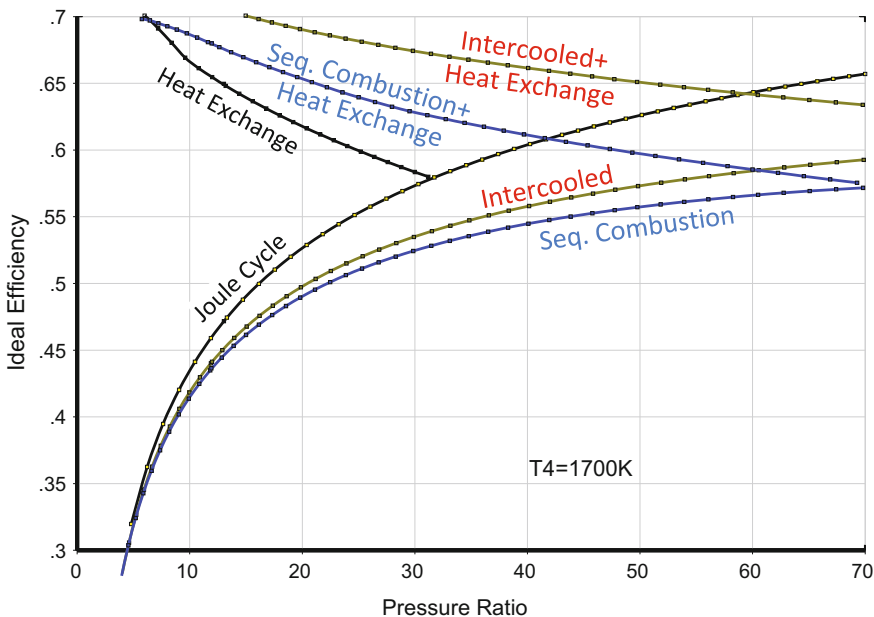


Fig. 1.2-11 Efficiency of ideal cycles for shaft power generation

is greater than the gain in output shaft power. The advantage of intercooling is reflected not in improved thermal efficiency but in increased power output per unit mass flow (remember Fig. 1.2-8).

However, intercooling does increase the temperature difference between turbine exit and compressor exit ($T_6 - T_3$). Therefore, adding a heat exchanger to an intercooled machine is very effective and increases thermal efficiency significantly over a wide range of pressure ratios.

Introducing sequential combustion reduces thermal efficiency because the pressure is lower in the second combustion chamber than in the first. Why is heat addition worse at low pressure than at high pressure?

Let us explain this with the temperature-entropy diagram for an ideal gas. Constant pressure lines in this diagram have a shallow gradient where pressure is low and are steep where pressure is high. We now consider a given temperature increase from T_A to T_B . Adding heat at constant pressure yields a certain entropy increase if pressure is high and a larger entropy increase if pressure is low. The integral of $T \times ds$ —which is the area below a constant pressure line—represents the amount of heat required for the temperature change. So, for a given temperature change from T_A to T_B we need more heat for a low pressure process than for a high pressure process. Using more heat for the same temperature change is obviously a lot less efficient.

Adding a heat exchanger to a machine with sequential combustion improves thermal efficiency, but not as much as in case of the intercooled machine.

1.2.2.2 Real Cycles

Let us bring more realism to our cycle studies. Table 1.2-1 summarizes and quantifies the loss assumptions for the next cycle studies. Note that the polytropic efficiency of cooled turbines depends on T_4 . Higher T_4 requires more cooling air—turbine efficiency gets worse. Figure 1.2-12 shows the thermal efficiency of real Joule cycles as functions of compressor pressure ratio and burner exit temperature.

Figure 1.2-13 shows efficiencies of real cycles with $T_4 = 1700$ K, calculated with the loss assumptions in Table 1.2-1. The efficiency of all real cycles comes out worse than its lossless counterparts, as may be seen by comparing Fig. 1.2-11 with Fig. 1.2-13.

The cycle with sequential combustion is the least efficient. The main reason for that is the low pressure in the second combustion chamber. This pressure is low because the HP turbine efficiency is less than unity and the work to be done by the HPT exceeds that in the ideal cycle due to the losses in the compressor.

The exit temperature of the compressors with intercooling in the real cycle is higher than that in the ideal cycle. The temperature difference $T_4 - T_3$ is not increased as much by intercooling so the efficiency of a real intercooled cycle is closer to that of the Joule cycle.

A further comment on sequential combustion is that the thermal efficiency of this sort of gas turbine engine is not attractive. What is the advantage of such an engine? We have seen from Fig. 1.2-8 that sequential combustion increases the specific power significantly; the exhaust gas temperature is much higher than that of the Joule cycle (Fig. 1.2-14). If we add a heat recovery steam generator to the power generation station then we can convert part of the gas turbine exhaust energy to

Table 1.2-1 Efficiencies and other loss assumptions

Compressors	$\eta_{\text{pol}} = 0.9$
Cooled turbines	$\eta_{\text{pol}} = 1.0625 - 0.000125 * T_4$
Uncooled turbines	$\eta_{\text{pol}} = 0.9$
Exhaust pressure ratio (for low kinetic energy)	$P_8/P_{\text{amb}} = 1.03$
Combustor total pressure ratio	$P_4/P_3 = 0.95$
Combustor efficiency	$\eta_{3-4} = 1$
2nd Combustor total pressure ratio	$P_{45}/P_{43} = 0.95$
Intercooler pressure ratio	$P_{25}/P_{24} = 0.95$
Intercooler exit temperature	$T_{25} = T_2 = 288.15$ K
Heat exchanger effectiveness	$\eta_{\text{eff}} = 0.8$
Heat exchanger (cold side)	$P_{35}/P_3 = 0.975$
Heat exchanger (hot side)	$P_8/P_6 = 0.95$
Gas generator mechanical efficiency (Accessory drive)	$\eta_{\text{mech}} = 0.99$
Power turbine mechanical efficiency (Generator losses)	$\eta_{\text{mech}} = 0.98$

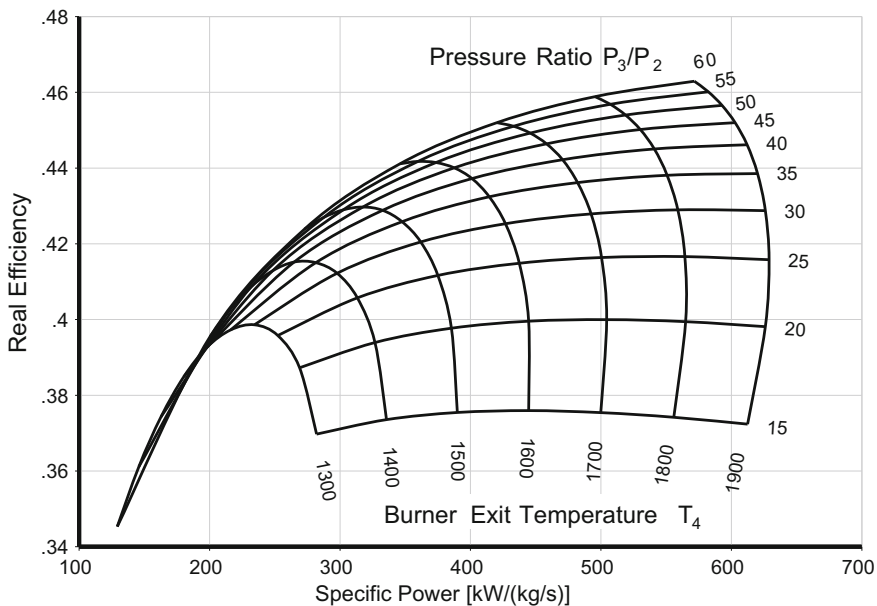


Fig. 1.2-12 Thermal efficiency of the Joule (Brayton) cycle. Losses as in Table 1.2-1

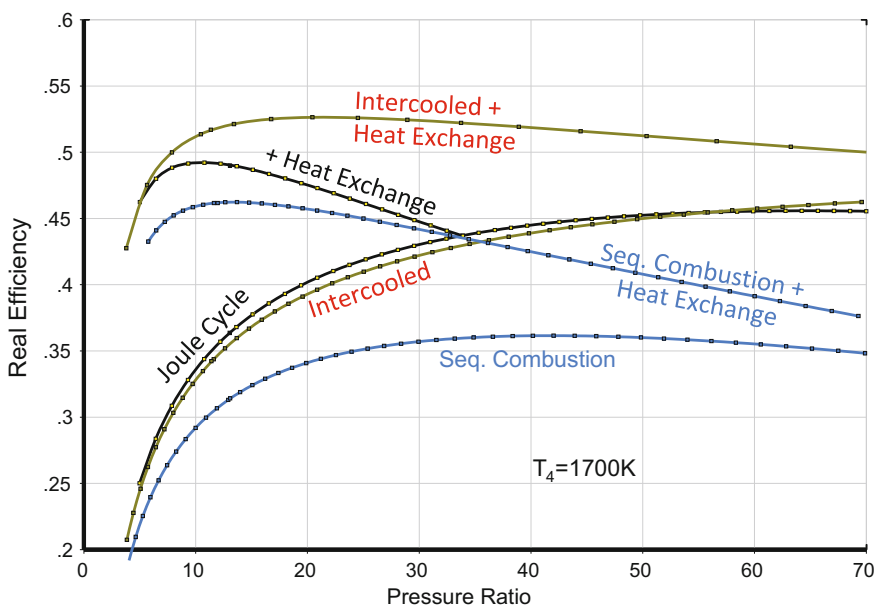


Fig. 1.2-13 Thermal efficiency of real cycles with $T_4 = 1700$ K

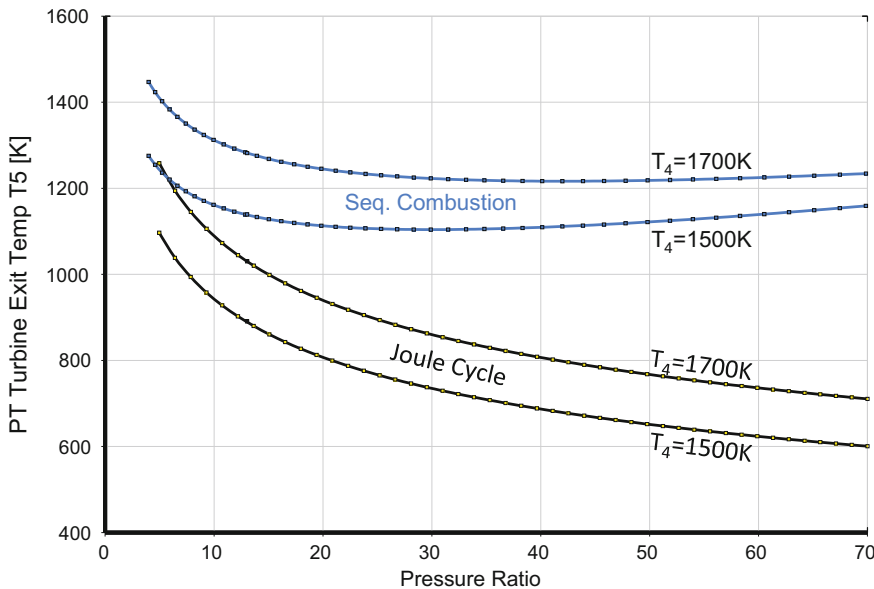


Fig. 1.2-14 Typical exhaust gas temperatures for real cycles

useful power. The thermal efficiency of the combined cycle is much higher than that of the gas turbine alone and can exceed 60%. The machine with sequential combustion in a combined cycle application takes advantage of a much higher exhaust gas temperature than the simple Joule configuration.

1.2.2.3 Back to the Definition of Efficiency

Up to now we have defined thermal efficiency in the thermodynamic way as the ratio of shaft power delivered to heat energy supplied. The source of the heat was immaterial. It could have come from the sun in a solar thermal power station in the desert, for example. Normally, however, we must burn fuel to add heat to a cycle. Then the cost of the heat depends on the amount of fuel burned W_F . A revised definition of thermal efficiency takes that into account:

$$\eta_{therm} = \frac{PW_{SD}}{W_F FHV} \quad (1.2-7)$$

FHV is the lower fuel heating value at 25 °C.

The maximum amount of heat available from burning either liquid or gaseous fuel depends on the chemical compositions of the fuel and the incoming gas—which might be dry or humid air, for example. Ideal combustion occurs when the fuel is mixed completely with the gas and there is sufficient time for all relevant

chemical reactions, in other words—chemical equilibrium is achieved. The fuel/air ratio at which the highest temperature is reached is the stoichiometric value. Injecting more fuel (a rich burn situation) or less fuel (a lean burn situation) leads to a burner exit temperature less than maximum. The derivative $\partial T_4 / \partial W_F$ is zero at stoichiometric fuel/air ratio.

It is important to realize that stoichiometric combustion yields the highest possible T_4 , but not the highest thermal efficiency. Using a little less fuel than that needed for stoichiometric burning changes neither T_4 nor the shaft power delivered (PW_{SD}) but it does reduce $W_F \times FHV$. Consequently, thermal efficiency with $\text{far} = \text{far}_{\text{stoich}} - \epsilon$ is definitely higher than with stoichiometric combustion. It makes no sense to consider stoichiometric combustion as the ultimate target for the development of gas turbines.

We obtain the best fuel flow-based thermal efficiency when the fuel/air ratio is 60...70% of the stoichiometric fuel/air ratio. This rule of thumb holds for liquid and gaseous hydrocarbon fuels including hydrogen.

The energy-based definition of thermal efficiency—Eq. (1.2-5)—does not consider where the added heat comes from. The difference between the energy-based and fuel flow-based efficiency definitions increases with fuel/air ratio, as shown in Fig. 1.2-15. Note that the peak value of the fuel-based thermal efficiency is lower and occurs at smaller fuel/air ratio.

In the remainder of the book, we shall refer to fuel-based thermal efficiency only.

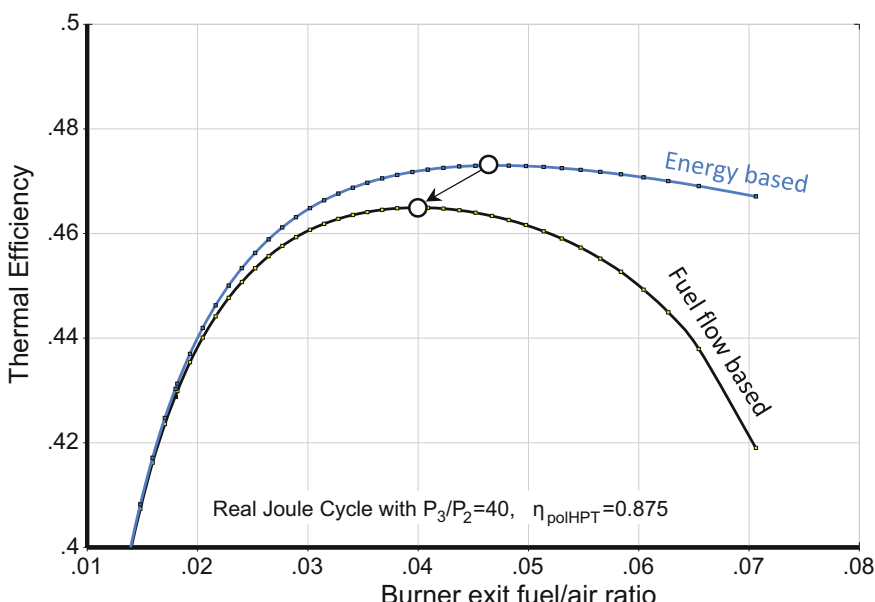


Fig. 1.2-15 Energy and fuel flow based thermal efficiency (generic hydrocarbon fuel)

1.2.3 *Combined Cycle*

The exhaust of a gas turbine contains a large amount of energy which can be used to generate steam in a *Heat Recovery Steam Generator* (HRSG). This steam can be used in industrial processes for heating or driving one or more turbines. Some of the steam can also be injected into the burner of the gas turbine for NOx reduction and power enhancement. Moreover, steam can be used for cooling blades and vanes of the gas turbine.

If the steam is used in a power generation plant for driving an additional generator through a steam turbine, then the total electrical power output increases as well as the overall efficiency of the plant. Such a combination of a gas turbine with waste heat recovery and a steam turbine is called a *Combined Cycle*. If the steam is not used for driving a turbine but for process applications in the chemical industry, for example, then we talk about *Cogeneration*.

Let us consider a simple combined cycle. The numbers are taken from Appendix C-16 in [1]. The gas turbine has a thermal efficiency of 0.33 and delivers 12.2 MW electric power as well as 57.2 kg/s of exhaust gas with a temperature of 704 K. The reference does not contain more details of the gas turbine cycle, but it is easy to re-engineer the main data at least approximately. We can estimate compressor pressure ratio and burner exit temperature to be 14.6 and 1233 K respectively. The upper left portion of Fig. 1.2-16 shows the Joule cycle of the gas turbine in the temperature-entropy diagram for air and combustion gases. This high temperature cycle is commonly called a topping cycle.

The *Rankine Cycle* in the lower right part of the same figure—the bottoming cycle—is drawn in a temperature-entropy diagram for steam. The scale of the temperature axis is valid for both cycles, but the scales of the entropy axes are different. Therefore, there are no numbers on the x-axis of Fig. 1.2-16.

The bottoming cycle consists of the heat recovery steam generator, the steam turbine and the condenser.

1.2.3.1 The Heat Recovery Steam Generator (HRSG)

Heat recovery steam generators can be very complex devices, especially if a large amount of heat is to be recovered from the gas turbine exhaust. The simplest HRSG delivers steam at one pressure only. More heat can be extracted if two or even three steam pressure levels are employed.

A single pressure Heat Recovery Steam Generator HRSG (Fig. 1.2-17) is assembled on the water side of an economizer for heating the feed water, an evaporator in which the water evaporates and a superheater for heating the steam to the desired temperature.

The temperature of the gas turbine exhaust may be increased in a burner before it approaches the superheater. The HRSG should be designed for the unfired mode, i.e. with the duct burner not operating.

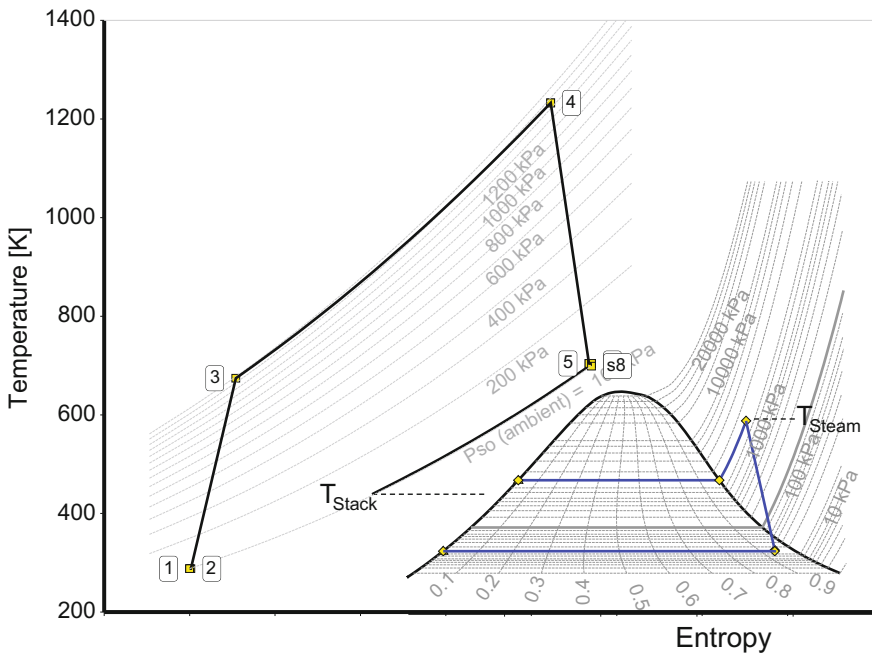


Fig. 1.2-16 Joule and Rankine cycles in the temperature-entropy diagram

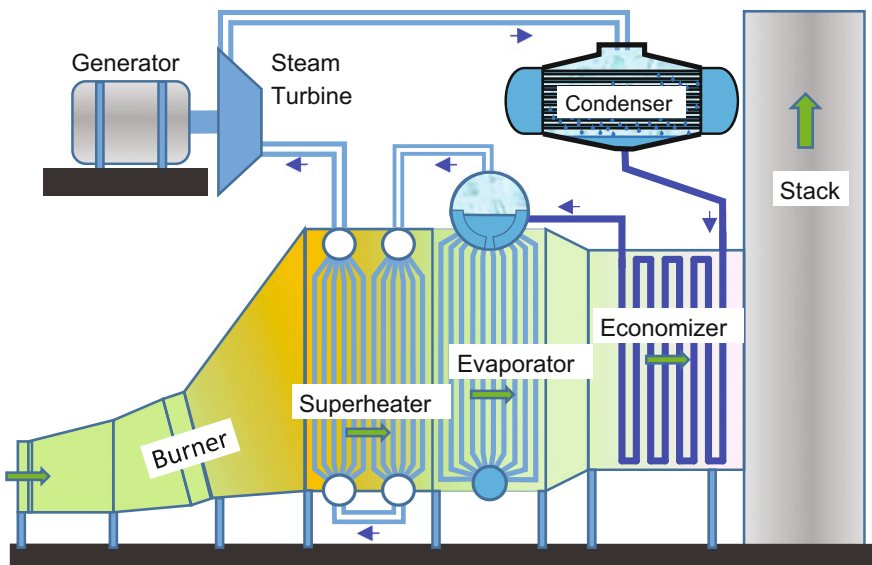


Fig. 1.2-17 Single pressure heat recovery steam generator for a combined cycle

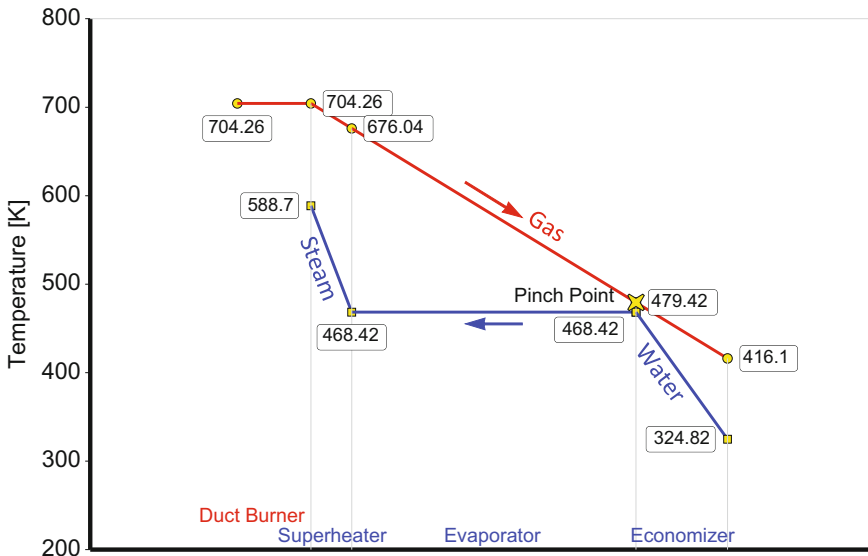


Fig. 1.2-18 Pinch point diagram—numerical example from Appendix C-16 in Ref. 1

Steam temperature and pressure are input values; the amount of steam generated is a result. Selecting the steam pressure defines the temperature in the evaporator.

The theoretical maximum gas-side temperature difference available for heat transfer is the difference between the duct burner exit temperature and the evaporation temperature. In real applications, there must be a temperature difference between the gas and the water temperature at the water side inlet to the evaporator. This point in the HRSG temperature plot (Fig. 1.2-18) is called the pinch point. $\text{Pinch } \Delta T = T_{\text{Pinch Point}} - T_{\text{Evap}}$ of practical devices is at least 5–15 °C. The smaller the pinch ΔT is, the more surface it takes to exchange the heat.

The gas leaving the evaporator enters the economizer. If the temperature differential between the gas and the water in the economizer is the same as in the evaporator, boiling tends to occur at the economizer exit. Boiling in the economizer should be avoided, especially at off-design operating conditions, because the steam could block the flow. The problem would be water hammer and tube-to-tube differential expansion. Therefore, the outlet water temperature of the economizer must be kept several degrees below the saturation value. The water temperature difference of 5–10 °C between the economizer exit and the evaporator is the *Approach ΔT*.

1.2.3.2 Steam Turbine

Most steam turbines used for power generation are condensing turbines which exhaust directly to condensers. There the saturation pressure is well below atmospheric and is a function of the cooling medium temperature.

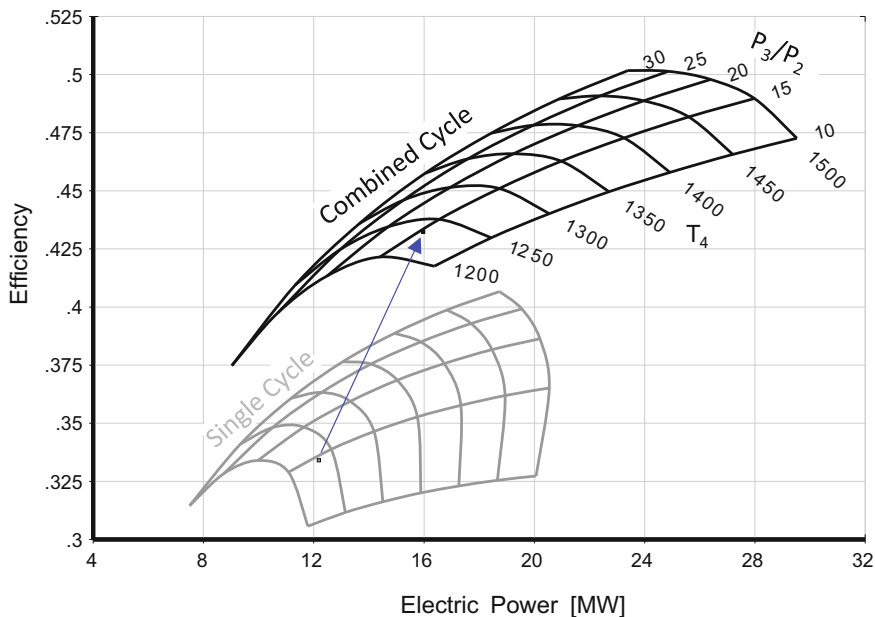


Fig. 1.2-19 Single cycle gas turbine and combined cycle performance

1.2.3.3 Combined Cycle Output

The gas turbine of our numerical example delivers 12.2 MW electric power with a thermal efficiency of 0.33. From the steam turbine of the bottoming cycle we acquire another 3.8 MW. The blue arrow in Fig. 1.2-19 indicates the resulting efficiency increase to 0.43 from the additional power.

Figure 1.2-19 also shows the efficiency and electric power potential for increasing the pressure ratio and burner exit temperature of the gas turbine cycle—the topping cycle. Further improvements are feasible when going to two or three steam pressure levels in the bottoming cycle. Combined cycle efficiencies of more than 0.6 have been demonstrated in large modern electric power stations.

1.3 Aircraft Propulsion

1.3.1 Turbojet

Figure 1.3-1 shows a turbojet engine composed of the components compressor, combustion chamber, high pressure turbine HPT and a convergent-divergent nozzle. The turbine provides the power for driving the compressor, the remaining energy in the exhaust is converted into jet velocity.

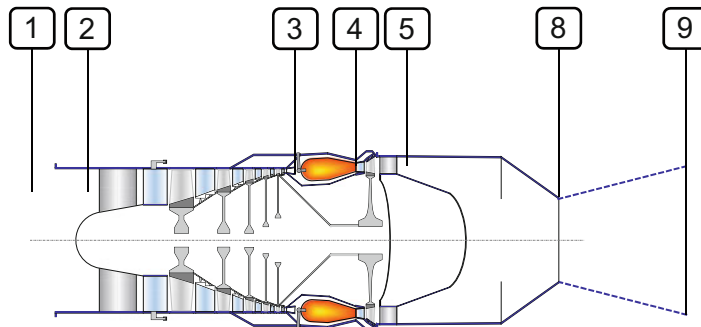


Fig. 1.3-1 Turbojet station nomenclature

We can consider the turbojet as a turboshaft in which a nozzle replaces the power turbine. The machine creates kinetic energy instead of shaft power. Thus, the thermal efficiency of a stationary turbojet is:

$$\eta_{therm} = \frac{W_9 \frac{V_9^2}{2}}{W_F FHV} \quad (1.3-1)$$

1.3.1.1 Ideal Turbojet Cycle

The compressor and the turbine of an ideal turbojet work with 100% efficiency. There are no pressure losses in the combustion chamber. Achieving the ideal jet velocity V_{9id} requires a lossless convergent-divergent nozzle which expands the jet to ambient pressure. The area ratio A_9/A_8 of the ideally matched nozzle depends on the pressure ratio P_8/P_{amb} .

Figure 1.3-2 shows the enthalpy-entropy diagram of the ideal turbojet cycle for two values of burner exit temperature T_4 . The kinetic energy of the jet increases with T_4 due to the diverging constant pressure lines in the enthalpy-entropy diagram. Thrust per unit mass flow is proportional to the ideal jet velocity as long as the turbojet is not moving.

1.3.1.2 A Method to Increase Turbojet Thrust

The permissible material temperatures or more precisely the centrifugal stresses in the turbine rotors set a limit for how much we can increase thrust by increasing T_4 . Downstream of the turbine, however, there are no rotating parts. Therefore, we can reheat the turbine exhaust gases in an afterburner to much higher temperatures than

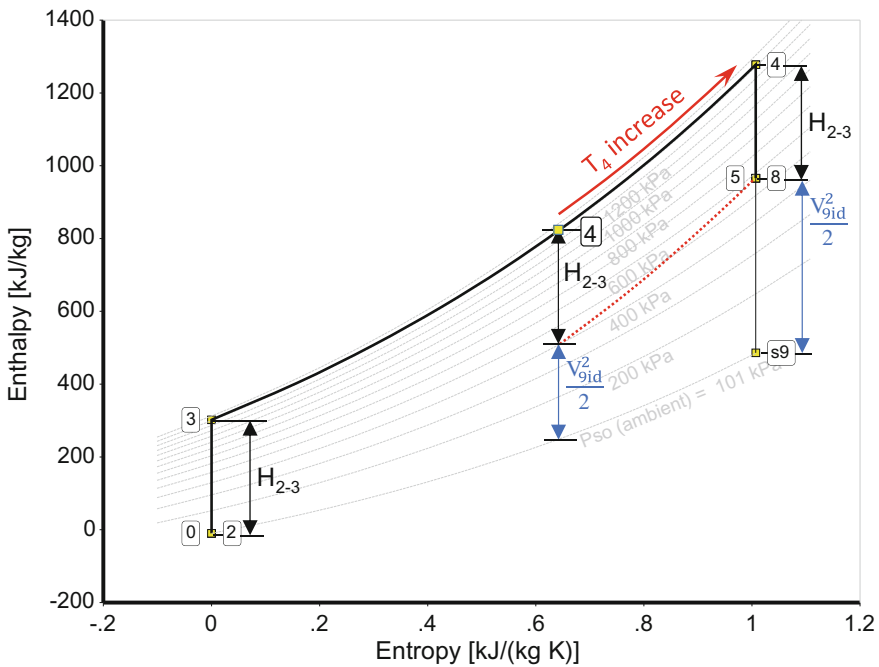


Fig. 1.3-2 Ideal cycle of the turbojet

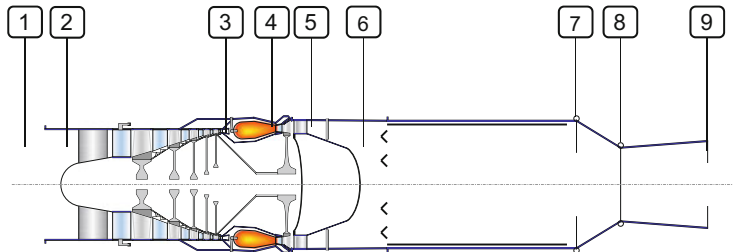


Fig. 1.3-3 Turbojet with afterburner

in the combustion chamber between compressor and turbine (Fig. 1.3-4). When we burn all the oxygen remaining after the first combustion process then we get the highest possible exhaust gas temperature $T_{8\text{stoich}}$. In practice, we cannot achieve this temperature because the afterburner hardware and the nozzle need cooling. Nevertheless, we can reheat the turbine exhaust gases to a very large extent, which increases jet velocity and consequently thrust.

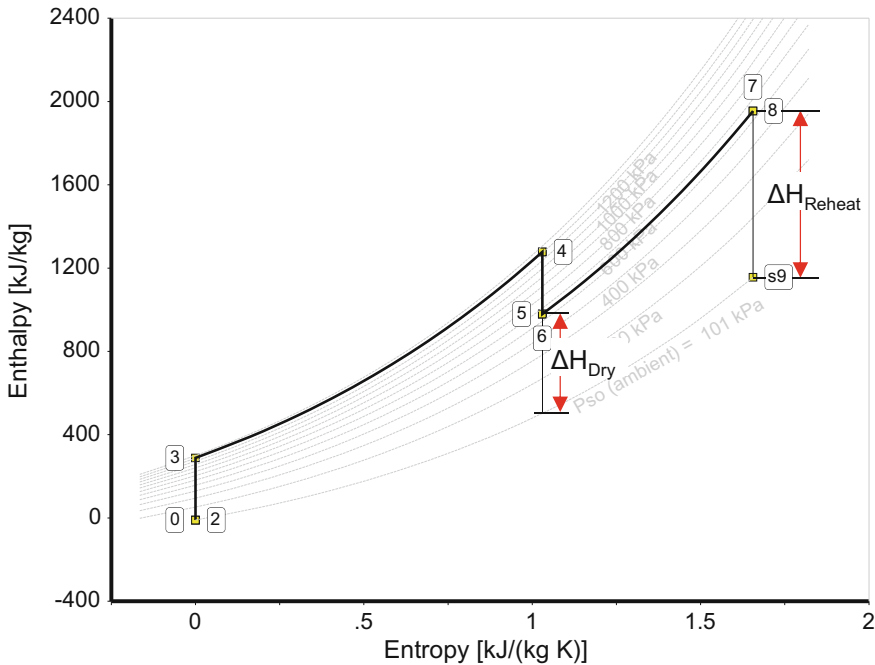


Fig. 1.3-4 Enthalpy-entropy diagram of an ideal reheated turbojet

1.3.1.3 Effect of Flight Velocity

We can compare the thermal efficiency of a turbojet directly with that of the ideal turboshaft if the turbojet is not moving, i.e. at static conditions. The kinetic energy of the jet is equivalent to the specific power of the turboshaft.

If our turbojet propels an aircraft which flies with the velocity V_0 then we must take account of the kinetic energy of the incoming air. The thermal efficiency of the turbojet is the increase in the kinetic energy relative to the energy provided:

$$\eta_{therm} = \frac{W_9 \frac{V_0^2}{2} - W_2 \frac{V_0^2}{2}}{W_F FHV} \quad (1.3-2)$$

Increasing flight velocity (flight Mach number) of an ideal turbojet which has fixed values for T_4/T_2 and compressor pressure ratio P_3/P_2 increases thermal efficiency, see Fig. 1.3-5.

This is because the thermodynamic cycle pressure ratio P_3/P_{amb} increases due to the compression of the air upstream of the engine—the ram effect. If we reduced the compressor pressure ratio of the turbojet at higher flight velocities in such a way that P_3/P_{amb} remains constant then we would get constant thermal efficiency, as indicated by the dashed lines in Fig. 1.3-5.

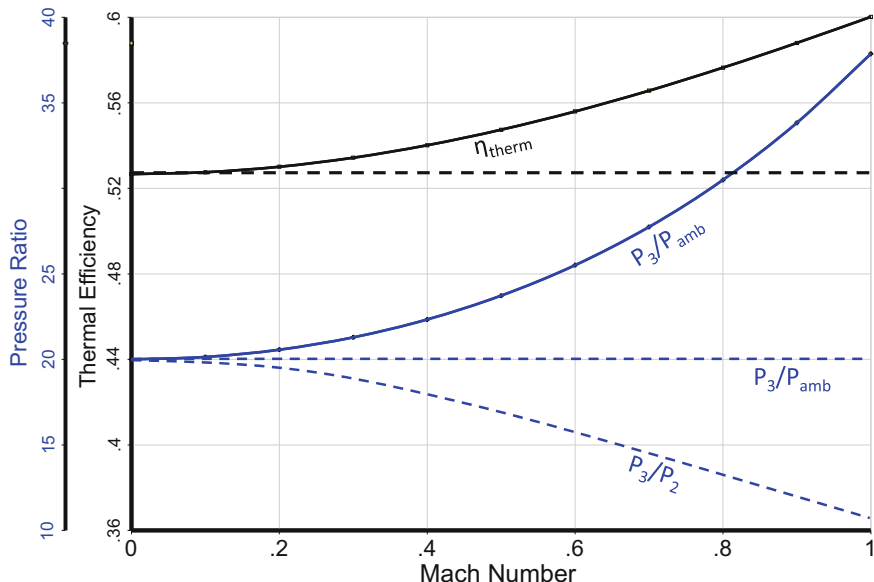


Fig. 1.3-5 Thermal efficiency of an ideal turbojet ($T_4 = 1700 \text{ K}$, $T_2 = 288.15 \text{ K}$)

1.3.2 More Definitions of Efficiency

Thermal efficiency is the efficiency of the thermodynamic cycle. It describes the conversion of the heat added to the cycle (here described by the product of fuel flow and lower heating value of the fuel) to kinetic energy.

We can split thermal efficiency of *turbofans* into core efficiency and transmission efficiency. *Core efficiency* is the ratio of energy available after all the power requirements of the core stream compression processes are satisfied—that means at the core exit—and the energy available from the fuel:

$$\eta_{core} = \frac{W_{core}(\Delta H_{is} - V_0^2/2)}{W_F FHV} \quad (1.3-3)$$

The enthalpy difference ΔH_{is} is evaluated assuming an isentropic expansion from the gas state at the core exit to ambient pressure at the engine exit.

Transmission efficiency describes the quality of the energy transfer from the core stream to the bypass stream. It is defined as ratio of the energy at the nozzle exit(s) to the energy at the core exit. Transmission efficiency is dominated by the efficiencies of the fan and the low pressure turbine, and these are equally important.

The task of an aircraft engine is to produce thrust. The ratio of useful propulsive energy—the product of thrust and flight velocity—to the kinetic energy added by

the engine is the *propulsive efficiency*: The kinetic energy of the jet relative to the environment is the loss in the process which converts the kinetic energy to thrust.

$$\eta_{Prop} = \frac{F_N V_0}{W_9 \frac{V_9^2 - V_0^2}{2}} \quad (1.3-4)$$

If the nozzle flow is expanded fully to ambient pressure and the inlet mass flow W_0 is equal to the nozzle mass flow W_9 then net thrust F_N equals $W(V_9 - V_0)$ and the formula simplifies to

$$\eta_{Prop} = \frac{2V_0}{V_0 + V_9} \quad (1.3-5)$$

Unfortunately thrust $F_N = W(V_9 - V_0)$ approaches zero when propulsive efficiency gets close to 1 which requires that $V_9 \approx V_0$.

The product of thermal efficiency and propulsive efficiency is the *overall efficiency*, the ratio of useful work done in overcoming the drag of the airplane to the energy provided by the fuel:

$$\eta_{overall} = \frac{W_9 \frac{V_9^2}{2} - W_2 \frac{V_0^2}{2}}{W_F FHV} \frac{F_N V_0}{W_9 \frac{V_9^2 - V_0^2}{2}} \quad (1.3-6)$$

Assuming $W_9 = W_2$ yields

$$\eta_{overall} = \frac{F_N V_0}{W_F FHV} \quad (1.3-7)$$

Overall efficiency is rarely used because it is zero if the aircraft is not moving. However, we can easily convert the equation into something useful by introducing specific fuel consumption $SFC = W_F/F_N$:

$$\eta_{overall} = \frac{V_0}{SFC FHV} \quad (1.3-8)$$

$$SFC = \frac{V_0}{\eta_{overall} FHV} = \frac{V_0}{\eta_{therm} \eta_{prop} FHV} \quad (1.3-9)$$

This equation does not yield $SFC = 0$ for $V_0 = 0$ because η_{prop} is also zero for $V_0 = 0$. Nevertheless, SFC is inseparably linked with the flight velocity.

Figure 1.3-6 is a graphical representation of Eq. (1.3-9) for a typical cruise condition of modern airliners, 35000 ft/Mach 0.8, i.e. flight velocity $V_0 = 237$ m/s and $FHV = 43.1$ MJ/kg. Note that this carpet is not a result of thermodynamic cycle calculations. It only shows how thermal and propulsive efficiency are connected to SFC.

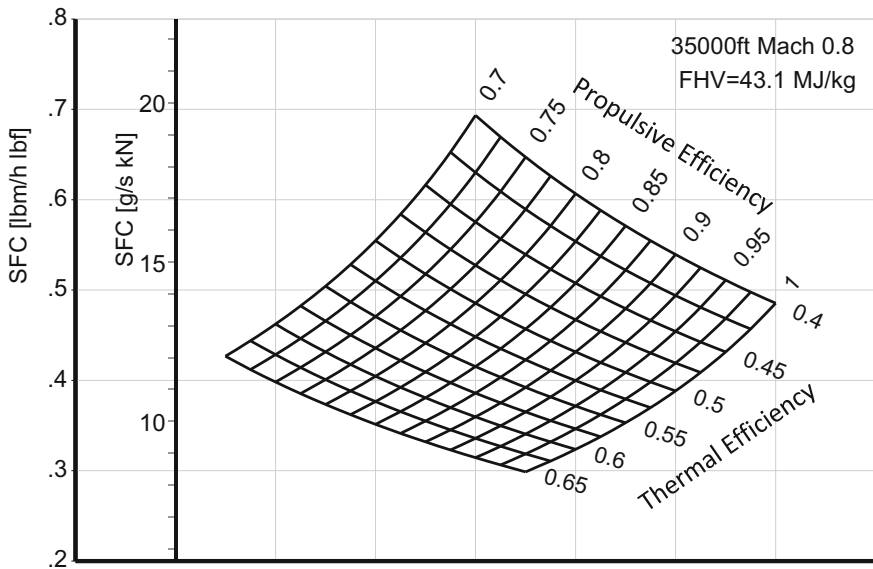


Fig. 1.3-6 Correlation of thermal and propulsive efficiency with SFC

1.3.2.1 Real Turbojet Cycle

Now let us consider a realistic turbojet engine. The various losses are listed in Table 1.3-1. Cooling air and other parasitic flows are considered indirectly: turbine efficiency is a function of burner exit temperature in this study.

Note that for the ideal turbojet cycle we have assumed a convergent-divergent nozzle which expands the jet exactly to ambient pressure. In the following, we calculate the performance for an engine with a convergent nozzle in which the static exit pressure P_{s8} is higher than ambient pressure. Gross thrust of the convergent nozzle is

$$F_G = W_8 V_8 C_{FG} + A_8 (P_{s8} - P_{amb}) \quad (1.3-10)$$

Table 1.3-1 Loss assumptions for the dry turbojet

Compressor	$\eta_{pol} = 0.9$
Turbine	$\eta_{pol} = 1.0625 - 0.000125 * T_4$
Combustor total pressure ratio	$P_4/P_3 = 0.95$
Combustion efficiency	$\eta_{3-4} = 0.999$
Exhaust pressure loss	$P_6/P_5 = 0.98$
Gas generator mechanical efficiency (Accessory drive)	$\eta_{mech} = 0.99$
Convergent nozzle thrust coefficient	$C_{FG} = 0.995$

In the efficiency evaluations, we use V_{9eq} as the equivalent jet velocity, where

$$V_{9eq} = F_G/W_8 \quad (1.3-11)$$

In Fig. 1.3-7 we see the various efficiencies for two burner exit temperatures as functions of flight velocity V_0 . Note that each calculated cycle represents a different engine design—the numbers do not describe how a specific turbojet behaves when the aircraft accelerates from flight velocity zero to 330 m/s.

Overall efficiency increases with flight velocity mainly because propulsive efficiency improves. Thermal efficiency gets only a little bit better within the flight velocity range considered. Note that higher overall efficiency does not result in lower SFC—the flight velocity effect in Eq. (1.3-9) dominates.

In this example thermal efficiency is not affected much by the burner exit temperature. The slightly higher η_{therm} value for $T_4 = 1500$ K is a result of the implied turbine efficiency benefit: for lower turbine entry temperature, we need less cooling air, and this is taken into account by a higher turbine efficiency value. Propulsive efficiency gets better when the engines are designed for lower T_4 because the jet velocity V_{9eq} is then lower.

What we do not see in this figure is the size of the engines. For the same thrust, the hotter turbojets need about 14% less mass flow—these engines will be lighter by a similar amount.

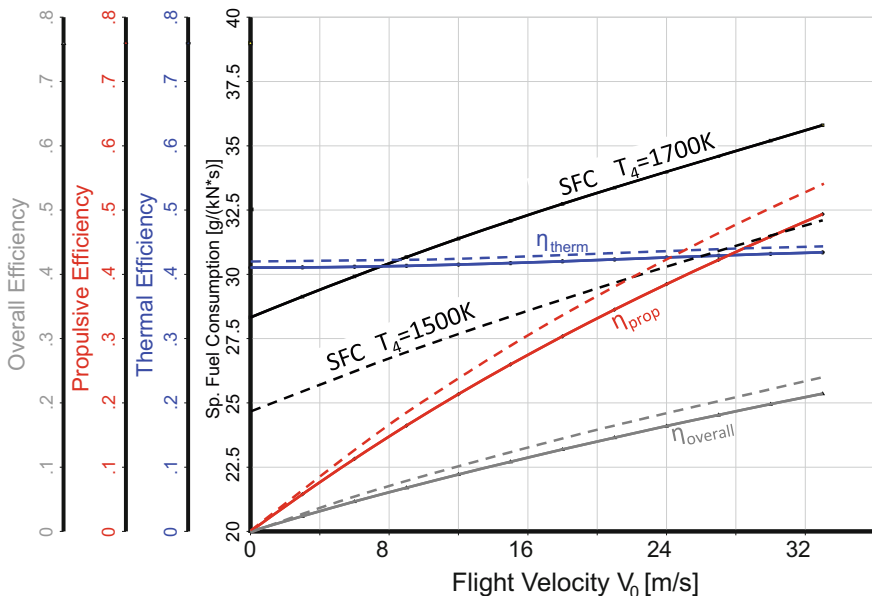


Fig. 1.3-7 Efficiencies of dry turbojets with $T_4 = 1700$ K and $T_4 = 1500$ K

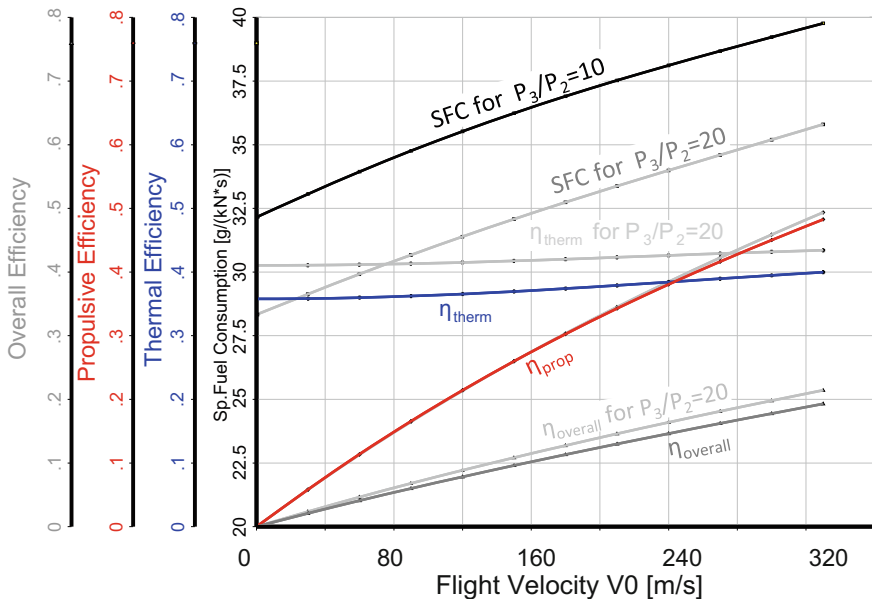


Fig. 1.3-8 Efficiencies of a turbojet for compressor pressure ratios $P_3/P_2 = 10$ and $P_3/P_2 = 20$. Burner exit temperature $T_4 = 1700$ K, ISA sea level

Figure 1.3-8 shows the effect of a reduction in compressor pressure ratio from 20 to 10 for constant burner exit temperature $T_4 = 1700$ K. Thermal efficiency decreases because $P_3/P_2 = 10$ is much too low for such a high value of T_4 , and this is reflected in Fig. 1.3-9. Propulsive efficiency at constant flight velocity is virtually independent of the change in pressure ratio since the specific thrust F_N/W_2 does not change. Note that the equivalent jet velocity V_{9eq} is directly connected with specific thrust:

$$V_{9eq} = \frac{W_2}{W_9} \left(\frac{F_N}{W_2} + V_0 \right) \quad (1.3-12)$$

Thus, overall efficiency decreases and SFC increases as a consequence of falling thermal efficiency.

1.3.2.2 Efficiency of the Turbojet with Reheat (Afterburner)

We can increase the thrust of our turbojet significantly by adding an afterburner, also called a (thrust-) augmenter or a reheat system. The latter term describes best what happens with respect to the thermodynamic cycle. It is common to call the engine a “wet” engine when the afterburner is lit—in contrast to the “dry” engine operation when the afterburner is switched off (Table 1.3-2).

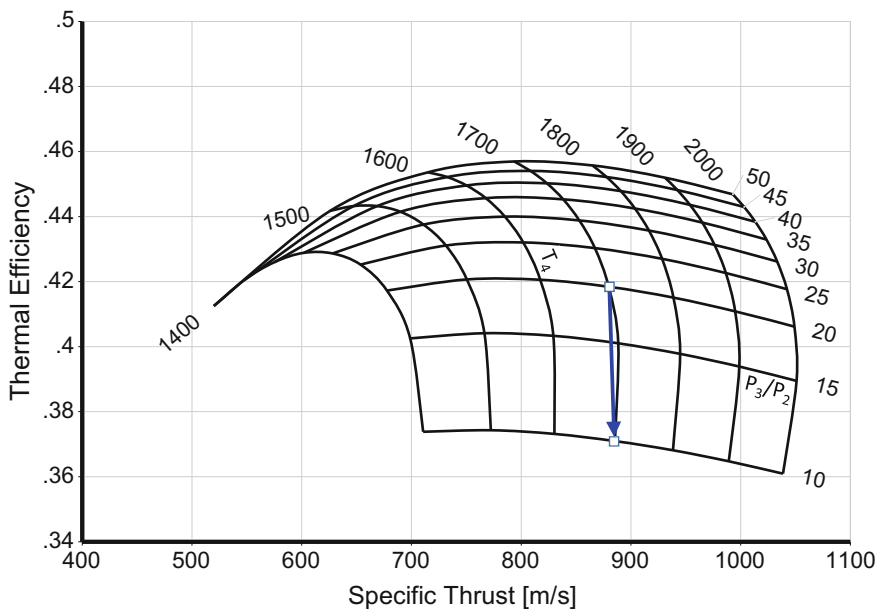


Fig. 1.3-9 Thermal efficiency of the turbojet for $V_0 = 160 \text{ m/s}$ (polytropic turbine efficiency = 0.85)

Table 1.3-2 Loss assumptions for the reheated turbojet

Compressor	$\eta_{\text{pol}} = 0.9$
Turbine	$\eta_{\text{pol}} = 1.0625 - 0.000125 * T_4$
Combustor total pressure ratio	$P_4/P_3 = 0.95$
Combustion efficiency	$\eta_{3-4} = 0.999$
Reheat flame-holder total pressure ratio	$P_6/P_5 = 0.98$
Reheat entry Mach number	$M_6 = 0.25$
Reheat combustion efficiency	$\eta_{6-7} = 0.95$
Reheat exit temperature	$T_7 = 2100 \text{ K}$
Gas generator mechanical efficiency (Accessory drive)	$\eta_{\text{mech}} = 0.99$
Convergent nozzle thrust coefficient	$C_{FG} = 0.995$

The six curves in Fig. 1.3-10 begin with the SFC and specific thrust values of the unreheated turbojet. As we move upwards and to the right along the pressure ratio curves, the reheat exit temperature increases until the maximum reheat exit temperature of $T_7 = 2100 \text{ K}$ is reached. Thus, each of the lines represents the relevant operating range from minimum to maximum reheat.

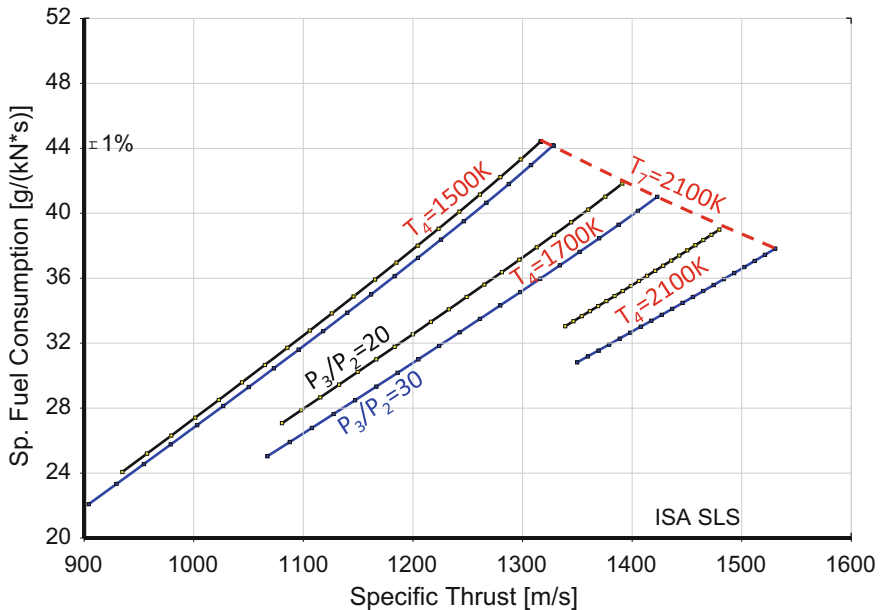


Fig. 1.3-10 Turbojet with reheat SFC increase from “dry” to full reheat ($T_7 = 2100\text{ K}$)

Low T_4 and high P_3/P_2 lead to moderate reheat inlet temperatures T_6 . The thrust boost potential (the thrust difference between min reheat and max reheat) depends on T_6 .

The higher thrust is not free: we need much more fuel per unit thrust compared to the bare engine. Why does SFC increase so much? It is true that the combustion efficiency in an afterburner is much worse than in the main combustion chamber, however, that is not the main reason for the very high fuel consumption. Let us have a look at the temperature-entropy diagram of an ideal lossless turbojet with reheat, operating at sea level static conditions (Fig. 1.3-11). In this diagram, the area below the T - s curve represents the heat transferred.

We look at the dry engine first. The area A-3-4-B-A represents the heat added in the main combustor. The useful work (the kinetic energy of the jet) we would get when the afterburner is unlit is proportional to the area 0-3-4-D-0. The relation of these two areas in the T - s diagram is the heat-based thermal efficiency as defined in Eq. 1.2-5.

We can make a similar comparison of areas in the T - s diagram for the reheat system. The heat added is proportional to the area B-6-8-C-B, the gain in kinetic jet energy is equivalent to the area D-6-8-s9-D. The ratio of these two areas is the thermal efficiency of the reheat system.

Without any calculation, it is obvious that the thermal efficiency of the reheat system is much worse than the thermal efficiency of the dry engine. The reason is that P_6 is much lower than P_3 .

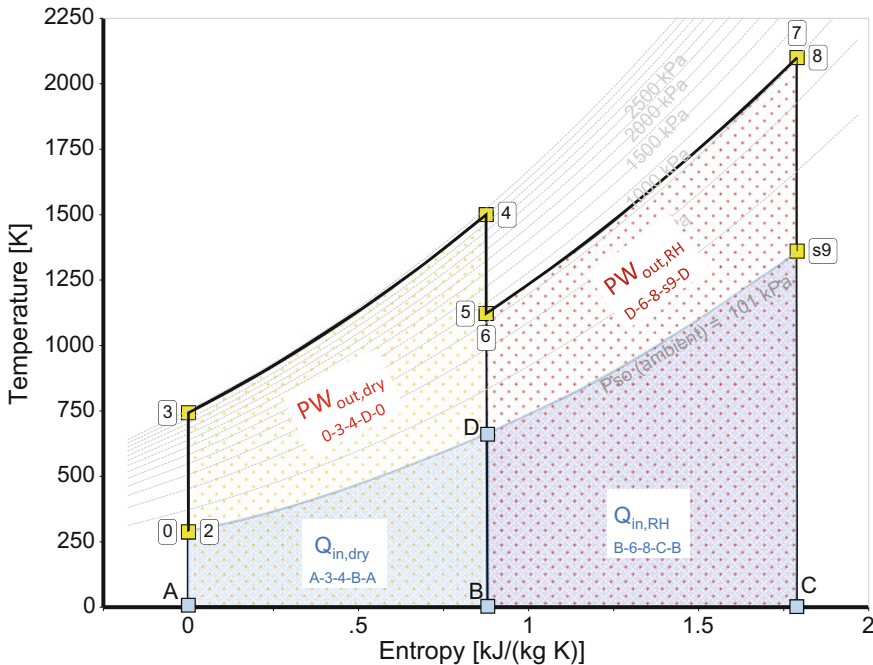


Fig. 1.3-11 Temperature-Entropy diagram of an ideal reheated turbojet

Next, we look at the sea level static performance of reheated turbojets with pressure ratios between 10 and 60. Burner exit temperature $T_4 = 1500$ K is the same for all engines. Our figures of merit are—instead of heat based thermal efficiencies—three definitions of specific fuel consumption:

$$\begin{aligned} \text{SFC}_{\text{dry}} &= W_{\text{FB}}/F_{\text{dry}} \\ \text{SFC}_{\text{RHsystem}} &= W_{\text{FRH}}/(F_{\text{RH}} - F_{\text{dry}}) \\ \text{SFC}_{\text{overall}} &= (W_{\text{FB}} + W_{\text{FRH}})/F_{\text{RH}} \end{aligned}$$

Figure 1.3-12 shows values of the three types of SFC and the pressure ratio P_6/P_{amb} against the overall compressor pressure ratio P_3/P_2 . There is a maximum in P_6/P_{amb} at an overall pressure ratio of 30. Both the lowest reheat system SFC and the lowest overall SFC occur at almost the same value of P_3/P_2 .

This parametric study confirms our previous statement: when it comes to both thermal efficiency and specific fuel consumption, it is a bad idea to add heat at pressures lower than that of the main burner inlet P_3 .

So what can we do if reheat SFC is unacceptably high even when compressor pressure ratio is optimal? If afterburner efficiency is poor, then we can improve it possibly by making the jet pipe longer. This provides more residence time for the chemical reactions. When afterburner efficiency is acceptable, and the compressor

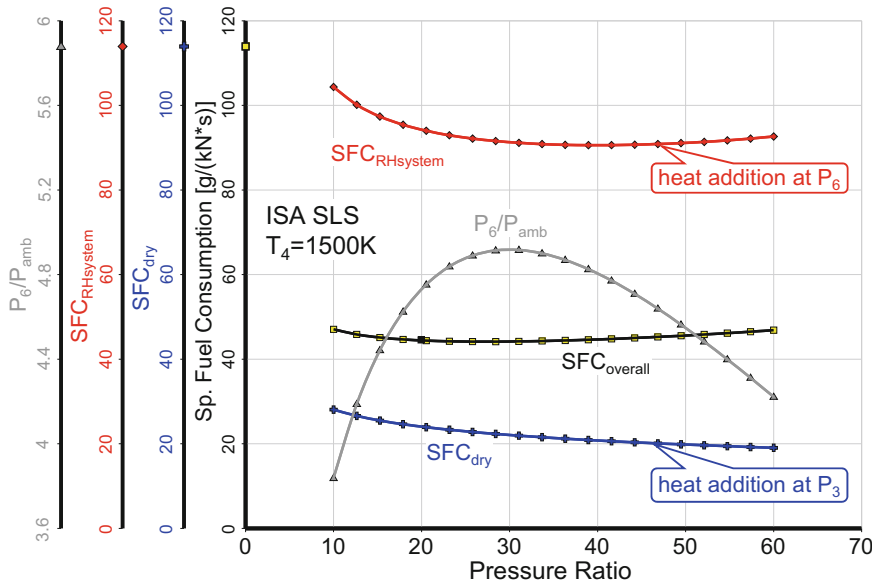


Fig. 1.3-12 SFC of reheated turbojets (ISA Sea Level Static, $T_7 = 2100\text{ K}$)

pressure ratio is near its optimum, then the only remaining options are to reduce T_7 (Fig. 1.3-10) or to increase main burner exit temperature T_4 (Fig. 1.3-13). Note that along each line of constant T_4 , the lowest SFC occurs where P_6/P_{amb} is highest.

1.3.3 Turbofan

The jet velocity of turbojets is generally very high and that results in poor propulsive efficiency for subsonic flight. How can we correct that defect? The solution is simple: we extract energy from the hot gas stream with a low pressure turbine (LPT) located between the high pressure turbine (HPT) and the nozzle. The jet velocity becomes smaller due to the additional power extraction and the propulsive efficiency of the primary exhaust stream increases.

The LPT provides a certain amount of shaft power which we can use to drive either a compressor with low mass flow and high pressure ratio or one with high mass flow and low pressure ratio. In the latter case, the excess compressed air is expanded in a second outer nozzle and delivers additional thrust.

We can adjust both the primary and the secondary nozzle exit velocities as we like. If we extract a lot of energy from the primary gas stream, we get a low primary jet velocity. If we use this energy to supply a second jet with a similar jet velocity, then we get a very significant increase in propulsive efficiency compared with that of our original turbojet.

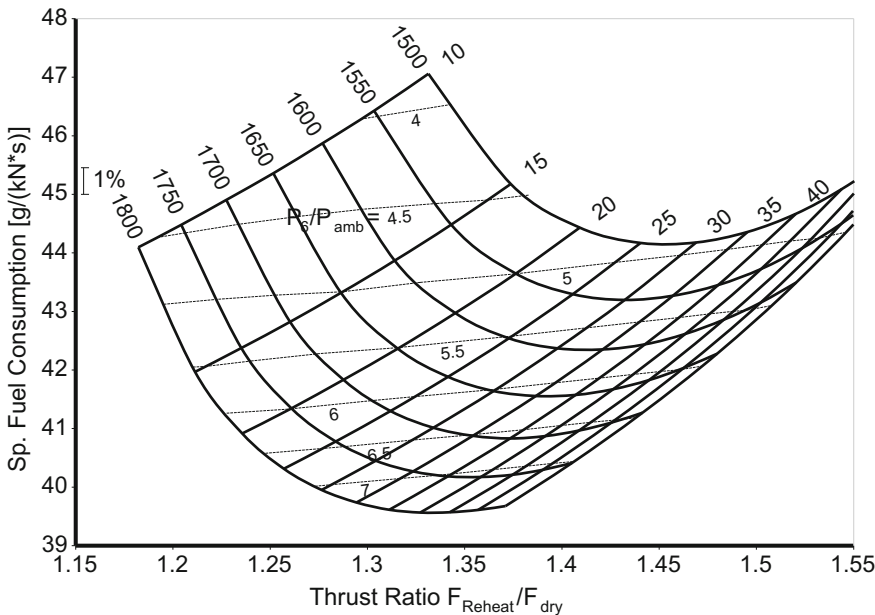


Fig. 1.3-13 Turbojet SFC and thrust boost ratio for $T_7 = 2100$ K

Figure 1.3-14 shows the configuration of an engine with enhanced propulsive efficiency. In the middle, we have the original turbojet, followed by the low pressure turbine and the primary nozzle. The additional compressor—usually called the fan—is in front of the “turbojet”. Nobody calls this part of the turbofan a “turbojet”. It is called the core of the engine or the *gas generator*.

In the following we will do some parametric studies, for which we use the loss assumptions in Table 1.3-3. These losses are representative of high bypass engines as used currently in commercial aviation. Losses due to turbine cooling are accounted for by a reduction in HP turbine efficiency as a function of burner exit temperature T_4 . For example, the relationship in Table 1.3-3 yields $\eta_{pol} = 0.875$ for $T_4 = 1500$ K and 0.85 for 1700 K.

The total pressure losses in the bypass duct (the ratio P_{16}/P_{13}) are mainly due to wall friction. When the bypass ratio is high, then the ratio of wall area to flow cross section area is low. This justifies a slight increase in P_{16}/P_{13} with bypass ratio as described by the corresponding equation in Table 1.3-3.

With all these assumptions, when we look at a turbofan with bypass ratio 6 and $T_4 = 1600$ K for cruise conditions (35000 ft altitude, flight Mach number 0.8) we obtain $SFC = 16.0$ g/(kN*s) or 0.566 lbm/(lbf*h), which is typical for engines in service since 1995.

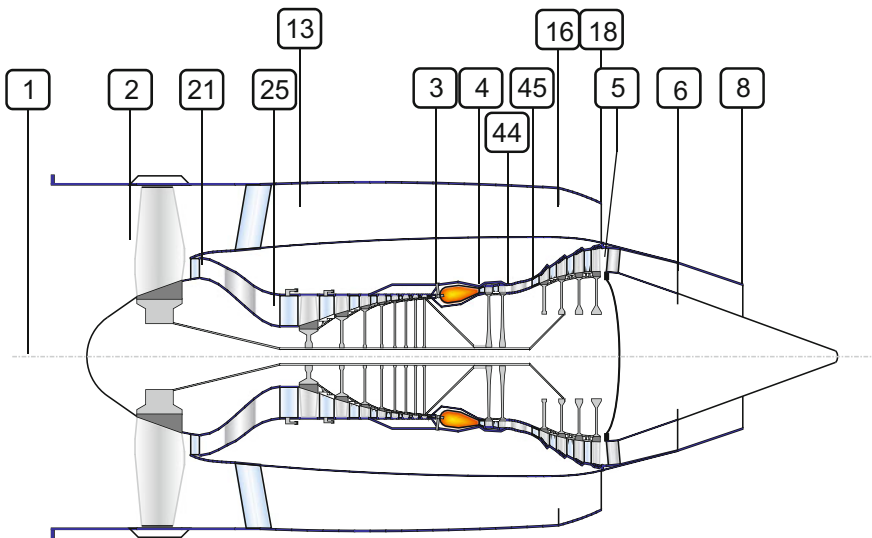


Fig. 1.3-14 Turbofan nomenclature

Table 1.3-3 Loss assumptions for the turbofan at cruise conditions $35000 \text{ ft/M} = 0.8$

Fan	$\eta_{\text{pol}} = 0.91$
Compressor interduct	$P_{25}/P_{21} = 0.98$
Compressor	$\eta_{\text{pol}} = 0.9$
Combustor total pressure loss	$P_4/P_3 = 0.95$
HP turbine	$\eta_{\text{pol}} = 1.0625 - 0.000125 * T_4$
Turbine interduct	$P_{45}/P_{44} = 0.98$
LP turbine	$\eta_{\text{pol}} = 0.91$
Turbine exit duct	$P_6/P_5 = 0.98$
Bypass duct pressure loss	$\frac{P_{16}}{P_{13}} = 1 - \frac{0.05}{(BPR + 1)^{0.4}}$
Gas generator mechanical efficiency (represents accessory drive)	$\eta_{\text{mech}} = 0.98$
High pressure air leakage to bypass	0.5% of W_{25}
High pressure air leakage to LPT exit	1% of W_{25}
High pressure air to overboard	1% of W_{25}

1.3.1.1 Jet Velocity Ratio

Parametric studies of turbojet engines are easy to handle because there are only two main design variables: the compressor pressure ratio P_3/P_2 and the burner exit temperature T_4 . With the turbofan we have two more variables: the bypass ratio (i.e. the mass flow ratio W_{13}/W_{21}) and the fan pressure ratio or that of the bypass stream P_{13}/P_2 . Fortunately, we can eliminate one of the additional variables by introducing

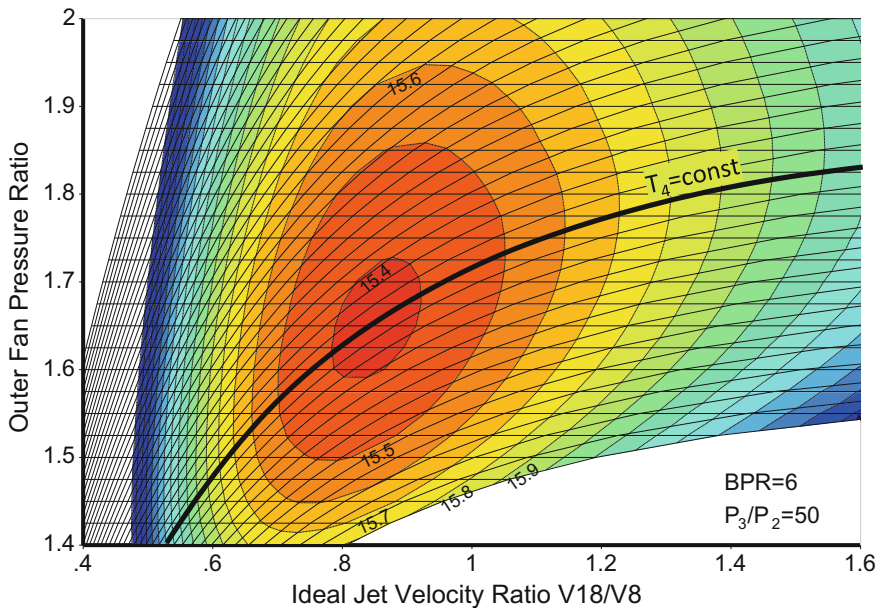


Fig. 1.3-15 Contour lines for constant SFC (cruise conditions $35000 \text{ ft/M} = 0.8$)

the condition that the inner and outer jet velocities shall be optimally matched. Theory says that to achieve the best specific fuel consumption, the ideal jet velocity ratio $V_{18\text{id}}/V_{8\text{id}}$ should be equal to the product of fan and LPT efficiency. In this context, *ideal* means that both jets are expanded fully to ambient pressure.

As a rule of thumb, we can use $V_{18\text{id}}/V_{8\text{id}} = 0.8$ for generic cycle calculations since modern fans and low pressure turbines have efficiencies around 0.9. Figure 1.3-15 shows in an example that SFC is essentially minimal for all fan pressure ratios in the region of $V_{18\text{id}}/V_{8\text{id}} = 0.8$. The SFC increases very little when we deviate from the numerical optimum. Choosing a slightly lower value for the jet velocity ratio (for constant burner exit temperature T_4) simplifies the aerodynamic design of the fan and LPT.

1.3.1.2 Parametric Studies

After this lengthy preamble, let us discuss a study in which bypass ratio and burner exit temperature are the variables. In each cycle calculation the overall pressure ratio P_3/P_2 is constant at 50 and the fan pressure ratio is adjusted in such a way that $V_{18\text{id}}/V_{8\text{id}} = 0.8$ is maintained.

First, let us see what happens to propulsive efficiency when we go from the turbojet (bypass ratio 0) to turbofans with a bypass ratio of 15. Higher bypass ratio means higher propulsive efficiency—that's the popular opinion. However, as

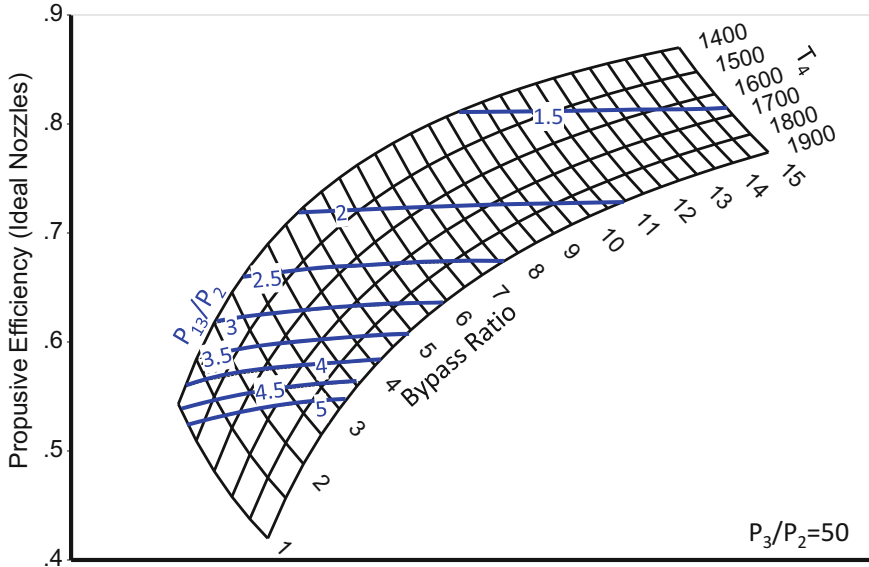


Fig. 1.3-16 Propulsive efficiency with ideal convergent-divergent nozzles (35000 ft/0.8 ISA)

Fig. 1.3-16 shows, this is only true for constant T_4 . Note that, for example, we can get 0.72 as propulsive efficiency with bypass ratios between 4.5 and 11 along the line for $P_{13}/P_2 = 2$.

It is no wonder that contours of constant fan pressure ratio are essentially those of constant propulsive efficiency, since the bypass nozzle pressure ratio P_{18}/P_{amb} —which determines bypass jet velocity V_{18} —is directly connected to P_{13}/P_2 .

By the way: what is propulsive efficiency of a bypass engine with two nozzles? We can calculate it using the previously mentioned definition—Eq. (1.3-4)—using an equivalent exhaust jet velocity $V_{9\text{eq}}$ which we define as

$$V_{9\text{eq}} = \frac{F_{G8} + F_{G18}}{W_8 + W_{18}} \quad (1.3-13)$$

In the following we focus on engines with single-stage fans. The pressure ratio of such fans is lower than two, propulsive efficiency higher than ≈ 0.725 (Fig. 1.3-16).

The expression for specific fuel consumption is composed of flight velocity, fuel heating value and the product of thermal and propulsive efficiencies, (Eq. 1.3-9). It is a good idea to look at the two efficiency terms separately. Let us fix propulsive efficiency and calculate specific fuel consumption for various values of thermal efficiency. The main driving parameters for thermal efficiency are compressor pressure ratio P_3/P_2 and burner exit temperature T_4 . We adjust bypass ratio in such a way that we get the desired propulsive efficiency. However, to generate the carpet plot in Fig. 1.3-17, it is convenient to set propulsive efficiency and solve for bypass ratio. In this context, bypass ratio is no longer an input variable, it is a result.

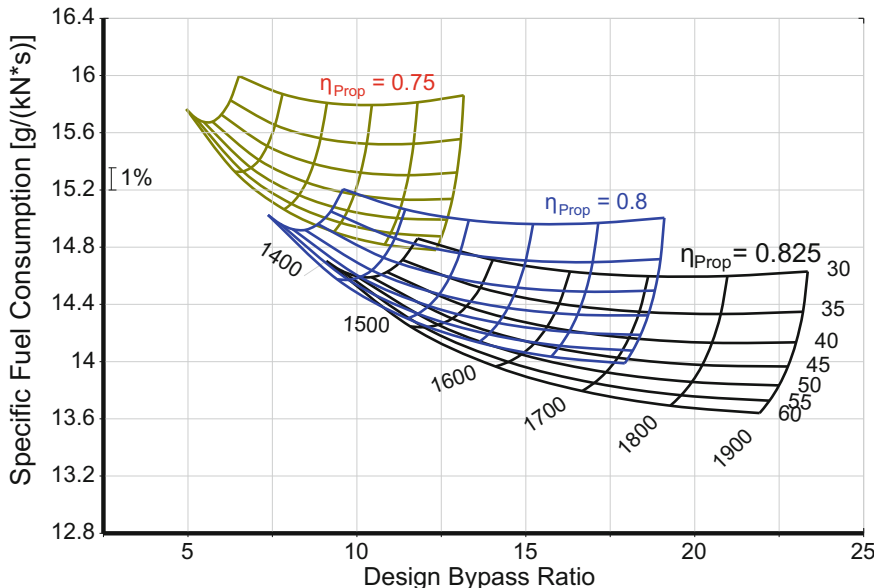


Fig. 1.3-17 Specific fuel consumption of turbofans at 35000 ft/0.8 ISA

Figure 1.3-17 shows specific fuel consumption for propulsive efficiencies of 0.75, 0.8 and 0.825. Increasing T_4 above 1700 K produces only a small gain in SFC. The same is true for overall pressure ratios above 60. The three carpets show indirectly how thermal efficiency changes, since each of the three carpets is valid for constant propulsive efficiency. Note that the range of bypass ratios gets bigger with increasing propulsive efficiency.

So what about specific thrust? The answer is very simple: it is directly connected with propulsive efficiency and flight velocity and rearranging Eq. (1.3-5) yields

$$\frac{F_N}{W} \approx 2V_0 \frac{(1 - \eta_{prop})}{\eta_{prop}} \quad (1.3-14)$$

At a given thrust, the engine inlet diameter of a turbofan with 80% propulsive efficiency is 282% (i.e. nearly three times!) of that of a turbojet (Fig. 1.3-18).

Propulsive efficiency is essentially fixed when fan diameter and thrust are given. In such a case, the only way to improve specific fuel consumption is to increase thermal efficiency. This can be done by raising compressor pressure ratio P_3/P_2 and/or burner exit temperature T_4 .

Of course, reducing the losses in the gas generator and the fan will also improve thermal efficiency. Figure 1.3-19 shows thermal efficiency calculated with the loss assumptions in Table 1.3-3 but with improved rotating components. The losses, i.e. the “1 minus efficiency” terms, are 10% lower in the fan, the compressor and the

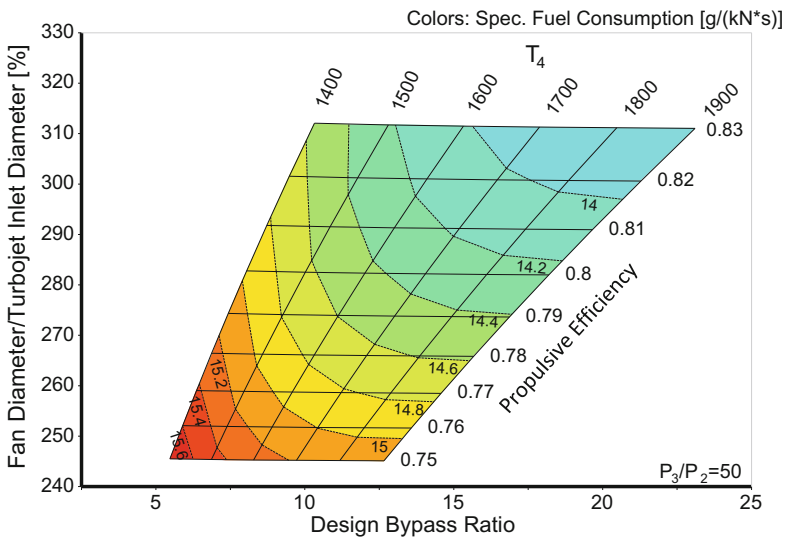


Fig. 1.3-18 Engine inlet diameter of turbofans compared to turbojets of the same thrust

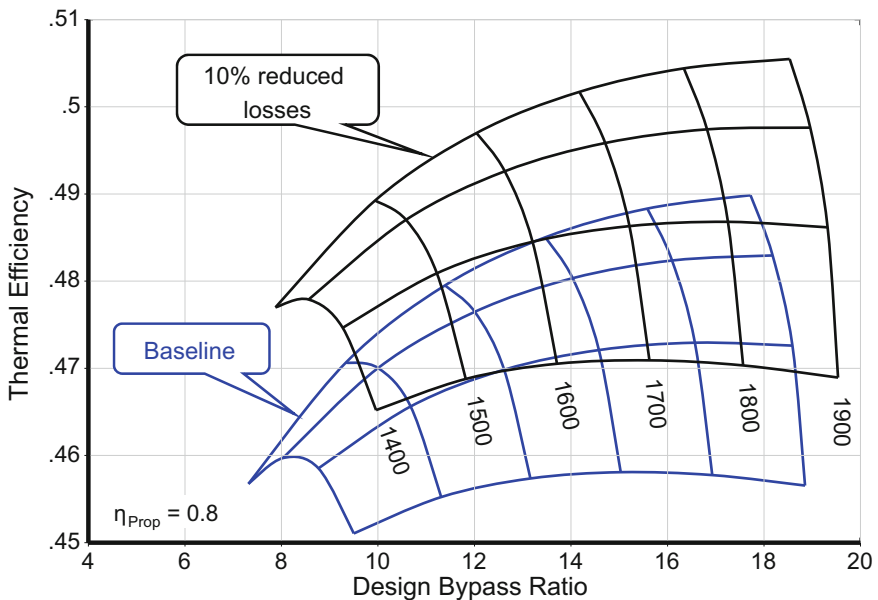


Fig. 1.3-19 Thermal efficiency of turbofans at cruise (35000 ft/0.8 ISA)

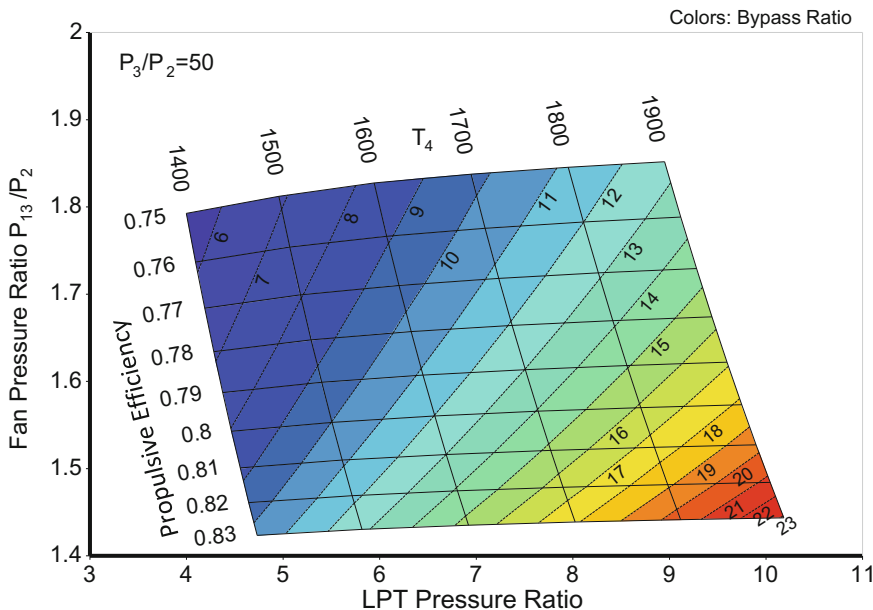


Fig. 1.3-20 Fan and low pressure turbine pressure ratio, OPR = 50

turbines. Such an improvement of the turbomachinery would be hard to achieve, but thermal efficiency would increase by only two points.

Finally let us have a quick look at the low pressure system (Fig. 1.3-20). Fan pressure ratio P_{13}/P_2 correlates well with propulsive efficiency as already mentioned. Low pressure turbine pressure ratio increases with burner exit temperature T_4 . This is no surprise if you recall Fig. 1.2-4!

1.3.1.3 Some Final Remarks

The loss assumptions for the turbofan (Table 1.3-3) and those for the power-generating gas turbine (Table 1.2-1) are very similar. However, thermal efficiencies of the aircraft engine are about 3 points higher (compare Fig. 1.2-12 with Fig. 1.3-19). What is the reason for that?

Again, it can be explained simply: the inlet temperature T_2 of an aircraft engine at cruise is 41 K lower than that of a ground-based engine at standard day conditions ($T_2 = 288.15$ K). The temperature ratio T_4/T_2 of the aircraft engine is higher and that gives it an advantage. The higher thermal efficiencies of an aircraft engine at cruise compared to that of land-based gas turbines is not a measure of superior technology, it is due to basic thermodynamics.

The first high bypass ratio turbofans (JT9D, CF6-6, RB211) were certificated in the early 70s of the 20th century. SFC at cruise conditions was between 0.62 and

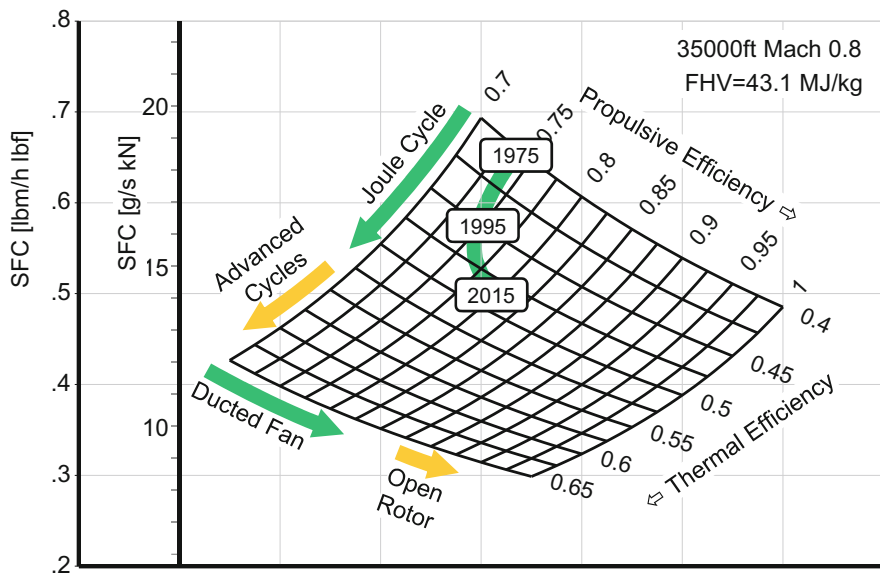


Fig. 1.3-21 Turbofan SFC trend over time

0.66 lbm/(h lbf). Within the following 20 years, until 1995, bypass ratio did not change much (it remained around 5) but significant progress in thermal efficiency reduced SFCs to 0.58. A further 20 years of development again improved thermal efficiency—but less than during the previous 20 years. By 2015, cruise SFC went down to 0.5 lbm/(h lbf)—5% improvement in propulsive efficiency (bypass ratio increased from 5 to 12) contributed much to that success.

In the future we will see further increases in both thermal and propulsive efficiency. Significant SFC reductions, however, require major changes in engine architecture. Open rotor engines aim at propulsive efficiencies above 90%, advanced thermodynamic cycles strive for higher thermal efficiencies. Whether gas turbines will ever achieve cruise SFCs lower than 0.4 lbm/(h lbf) is still an unanswered question (Fig. 1.3-21).

1.4 Fundamental Design Decisions

The engine of a fighter aircraft looks very different to that of a passenger aircraft. The reason for that is: The mission defines the thermodynamic cycle. Engines for supersonic aircraft must have a small frontal area, otherwise the aircraft drag would be excessive. Commercial airliners need engines with low fuel consumption. That

leads to turbofan engines with high bypass ratio which have inherently low thrust per frontal area.

While the mission defines the basic type of engine, it does not determine all the design details. The selection and the general arrangement of the components is a complex interdisciplinary optimization task. In the following we discuss some of the fundamental design decisions to be made in the early phase of any project.

1.4.1 Turbofan: Mixed Flow or Separate Flow?

Turbofan engines for subsonic transport aircraft come in two variants: with mixer (single nozzle) and without (two nozzles), see Fig. 1.4-1.

There are many arguments (cost, weight, noise, reverse thrust...) for and against both versions. Here we look primarily at the differences in the thermodynamic cycles.

1.4.1.1 Separate Flow Turbofan

The gas generator of the turbofan produces a certain amount of gas power. How do we distribute this power optimally between kinetic energy of the core stream and shaft power for driving the fan? We have discussed this problem already: Theoretically, the best ideal jet velocity ratio is

$$\left(\frac{V_{18}}{V_8} \right)_{id} = \eta_{2-18} \eta_{45-8} \quad (1.4-1)$$

In this equation η_{2-18} stands for the efficiency of the secondary stream, whose losses occur in the fan and the bypass duct. Similarly, η_{45-8} reflects the losses of the low pressure turbine and its downstream duct. The two ideal velocities are those of lossless nozzles which expand the flow to ambient pressure. This requires a convergent-divergent nozzle if the total-static pressure ratio is bigger than the critical pressure value.



Fig. 1.4-1 Turbofans with one or two nozzles

In practice, we need not care about the subtle differences between η_{2-18} and fan efficiency, η_{45-8} and low pressure turbine efficiency because deviating from the numerical optimum does not affect specific fuel consumption very much. Choosing $(V_{18}/V_8)_{id} = 0.8$ at cruise conditions is a good rule of thumb for matching the two jet velocities of any high bypass ratio turbofan optimally.

1.4.1.2 Mixed Flow Turbofan

In a mixed flow turbofan simulation, we obviously cannot apply the jet velocity ratio rule—there is only one nozzle. A different condition exists here for an optimal match of the core and the bypass streams: The mixer only works satisfactorily if the total pressure ratio P_{16}/P_6 is close to 1.0. Small deviations from 1.0 are acceptable, but in general this ratio should be in the range $0.9 \dots P_{16}/P_6 \dots 1.05$ at cruise conditions.

1.4.1.3 Comparison at Constant Propulsive Efficiency

Propulsive efficiency is rarely used in cycle studies as an input variable. This is because propulsive efficiency is generally not among the input quantities of cycle codes—it is a result, an output. However, when we look at a real-world engine design problem, the required propulsive efficiency is often implicit in the aircraft requirements.

Imagine an engine design task for a new commercial airliner. The airframe designer requests a certain thrust at top of climb (35000 ft, $M = 0.8$ ISA), which he has derived from the aircraft drag and lift characteristics. Additionally, he specifies the nacelle dimensions, either because the engine must fit into an already existing nacelle or because the undercarriage of the aircraft does not allow for a bigger nacelle, for example.

The size of the nacelle sets an upper limit for the fan diameter and hence the corrected flow of the engine, which happens to be at the top of climb. We can design our engine exactly for this corrected flow or—if we want some margin for later thrust growth—we design it for somewhat less corrected flow. In either case we know the maximum corrected flow in advance.

Now remember the basics: corrected flow per area depends only on local Mach number, total pressure, and total temperature. Pressure and temperature, we know from the flight condition. What about a local Mach number? The nacelle specialists certainly know the Mach number for the maximum corrected flow the intake can accept at its throat. With this Mach number, we can calculate the maximum true air mass flow at the top of climb from the known data.

Alternatively, we could consider the flow conditions at the fan face—there the local Mach number cannot exceed 0.7. With this Mach number, the known corrected flow, and the fan hub/tip radius ratio (a mechanical design constraint), we can calculate the fan diameter. Hopefully the fan fits into the given nacelle—otherwise something is wrong in the specification.

Now we know flight velocity V_0 , net thrust F_N and engine mass flow W_2 for top of climb. We can calculate propulsive efficiency from Eq. (1.4-2) which is the inversion of Eq. (1.3-14):

$$\eta_{prop} \approx \frac{2V_0}{\frac{F_N}{W_2} + 2V_0} \quad (1.4-2)$$

At the end of the day we are interested in an engine with low specific fuel consumption. The formula for SFC is composed of thermal efficiency, propulsive efficiency, and the constant values of flight velocity V_0 and fuel heating value FHV. If we do parametric studies for a given propulsive efficiency, then any change in SFC is a consequence of better or worse thermal efficiency. Since the engine maker can only influence the thermal efficiency of his machine it is more than adequate to do parametric studies with constant propulsive efficiency. And that's what we are going to do now.

In our study, all separate flow turbofans have the optimum jet velocity ratio, all mixed flow turbofans have equal total pressures at the bypass and core exits. The component loss assumptions for both engine configurations are those listed in Table 1.3-3. Figure 1.4-2 shows thermal efficiency for both separate flow and mixed flow turbofans. Note that losses due to mixing the two streams are not considered. Thus, the difference between the black and the blue carpets represents the ideal case; in reality the thermal efficiency advantage of the mixed flow engine will be smaller.

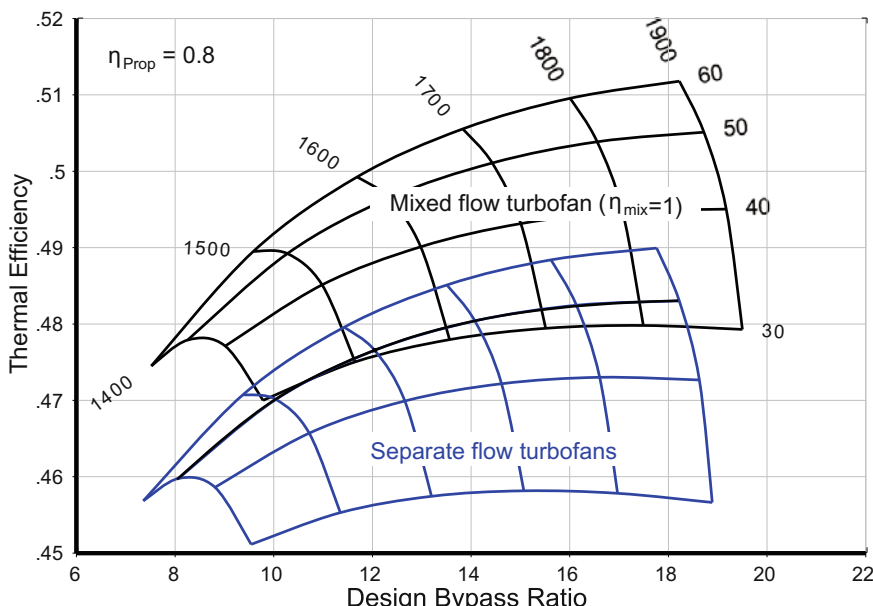


Fig. 1.4-2 Thermal efficiency with optimized fan pressure ratio

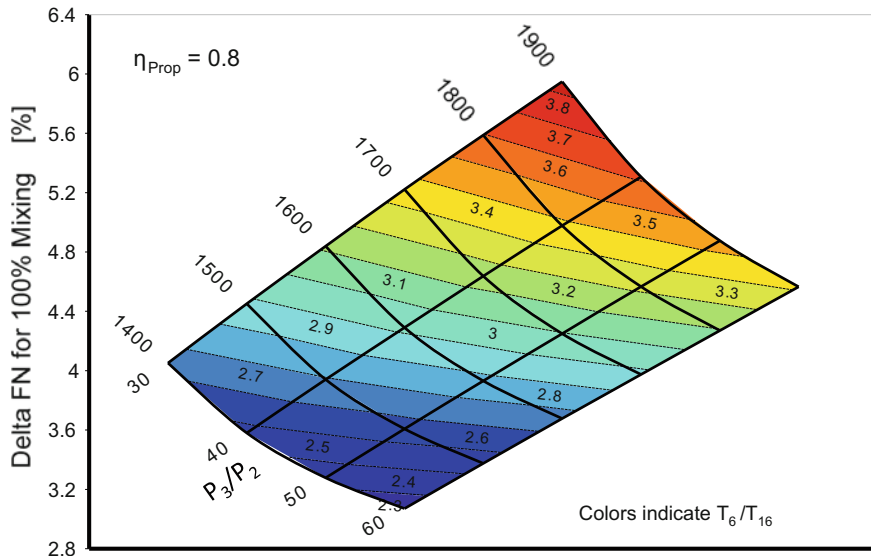


Fig. 1.4-3 Net thrust gain due to mixing core and bypass flow ($\eta_{\text{mix}} = 1$)

What exactly is *Delta FN for 100% Mixing* shown in Fig. 1.4-3? It is calculated as the difference between the gross thrust of the fully mixed stream ($\eta_{\text{mix}} = 1$) and the gross thrust of two separate streams which see the same core and bypass exit conditions, as a percentage of the net thrust. The percentage number looks big because net thrust is much lower than gross thrust.

The contour lines for the hot-to-cold stream temperature ratio T_6/T_{16} in Fig. 1.4-3 show that the thrust gain comes mainly from the temperature difference between the two streams. The bigger the temperature ratio, the higher the gain in thrust.

The performance differences between the two engine architectures are not big, but the components on the low pressure spool are quite different. The optimized fan pressure ratio of the separate flow turbofan is noticeably higher than that of the optimized mixed flow turbofans, see Fig. 1.4-4. Consequently, the pressure ratio of the mixed flow turbofan LPT is much lower (Fig. 1.4-5). There is the opportunity to compensate for the added weight of the mixer with a reduced number of LP turbine stages and a lower low pressure spool speed.

Note that in Fig. 1.4-4 the fan pressure ratio for both engine architectures is essentially independent of design bypass ratio. This is a consequence of keeping propulsive efficiency constant in our parametric study.

Up to now we have discussed the performance of ideal mixers, which produce a uniform temperature distribution without any friction loss. The thrust gain of real mixers depends on their shape, the mixing chamber length and diameter. Lobed annular mixers can achieve 75% of the theoretical thrust gain, plain annular mixers 30% when bypass ratio is in the range of four to six. With higher bypass ratios, it

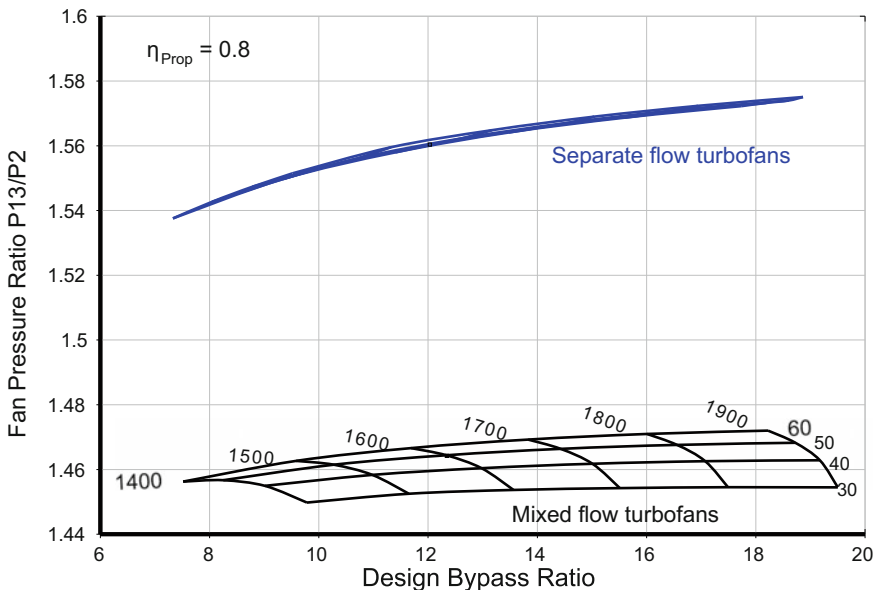


Fig. 1.4-4 Optimum fan pressure ratio for propulsive efficiency $\eta_{\text{prop}} = 0.8$ (35000 ft/0.8 ISA)

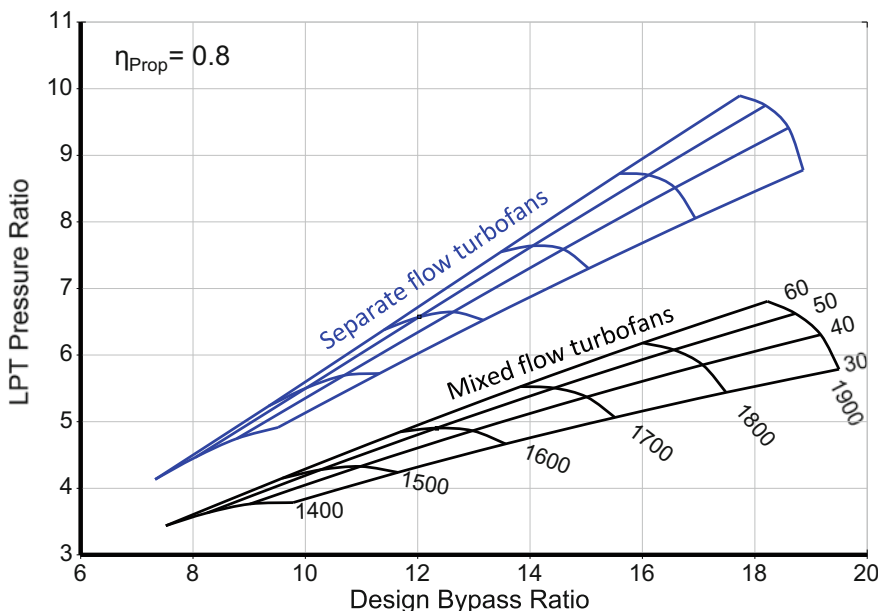


Fig. 1.4-5 Pressure ratio of the low pressure turbine

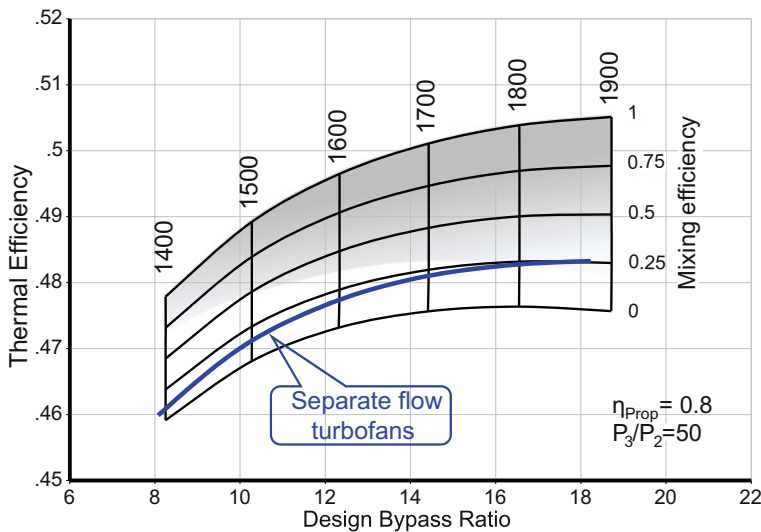


Fig. 1.4-6 Effect of mixing efficiency for engines with $P_3/P_2 = 50$ (35000 ft/0.8 ISA)

becomes increasingly difficult to achieve a uniform temperature distribution at the end of the mixing chamber, so mixing efficiency drops. The gray area in Fig. 1.4-6 marks the region of unrealistic mixer performance aims.

Mixed flow turbofans offer better thermal efficiency and SFC only for modest bypass ratios. The ultra-high bypass ratio engines of the future will have two nozzles.

1.4.2 Dry or Reheated Turbofan?

The predominant aim for a fighter aircraft is almost always to achieve high aircraft thrust/weight ratio, in the interests of speed, agility and weapons carrying capability. This means engine thrust/weight ratio needs to be high. Even more importantly, engine specific thrust (and also thrust per frontal area) must be high because this results in reduced aircraft fuselage cross section. Any growth in engine diameter has a considerable effect on airframe size and weight. For supersonic vehicles, the size penalty of medium to high bypass ratio engines (which inherently have low specific thrust) overwhelms any SFC benefit.

Despite the importance of frontal area, we cannot ignore fuel consumption. For engines with afterburners, specific fuel consumption can get quite high. Using fuel to heat low-pressure air is a highly inefficient process, whose only attractions are that it is basically simple, and it provides the engine with a greatly increased thrust capability without increasing diameter.

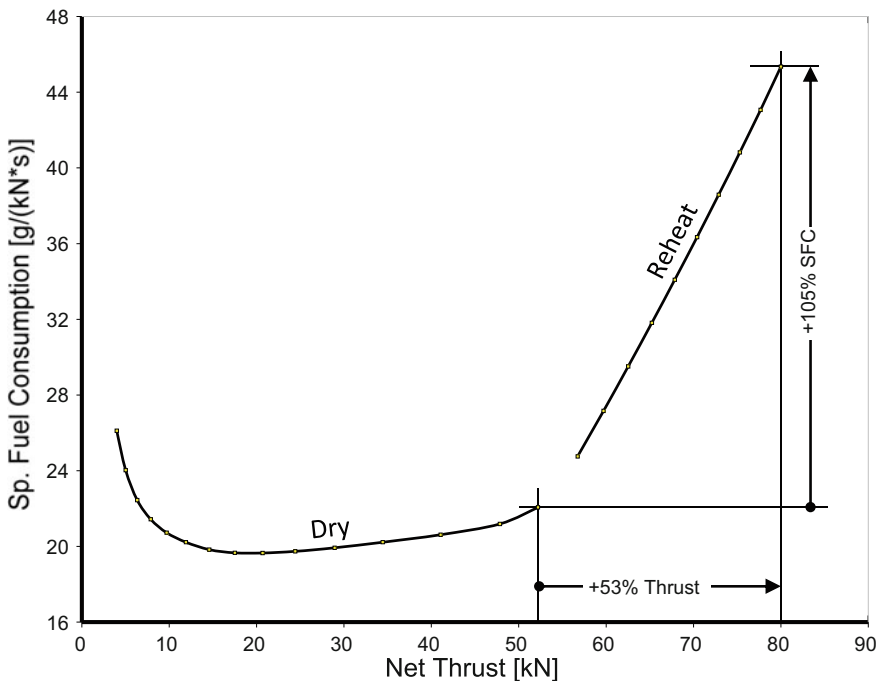


Fig. 1.4-7 Thrust and SFC for a turbofan (BPR = 0.5, ISA SLS)

Because of the high fuel consumption, afterburning is seldom used for more than a few minutes to provide short bursts of power for take off, high climb rates, acceleration, and high angle of attack combat maneuvering.

The next figure shows the SFC for both dry and reheated operation of a mixed flow turbofan with bypass ratio 0.5 which illustrates the vast difference between dry and reheated fuel consumption. Note also that thrust increases by 53% which is achieved without increasing the frontal area of the engine. However, the weight and complexity penalty must not be underestimated (Figs. 1.4-7, 1.4-8).

1.4.2.1 Reheated Turbofans for Supersonic Flight

In the following cycle study, we examine turbofan engines which all deliver the same thrust at supersonic flight at $M = 2$ and 11 km altitude. Combustor and reheat exit temperature are constant, as well as all component efficiencies. All engines have convergent-divergent nozzles with an area ratio of $A_9/A_8 = 1.5$. The fan pressure ratio is adjusted in such a way that the ratio of bypass exit to core exit pressures P_{16}/P_6 is equal to 1.0. The Mach number at the fan inlet is 0.5; the total mass flow W_2 is adjusted in each case in such a way that the required thrust is achieved.

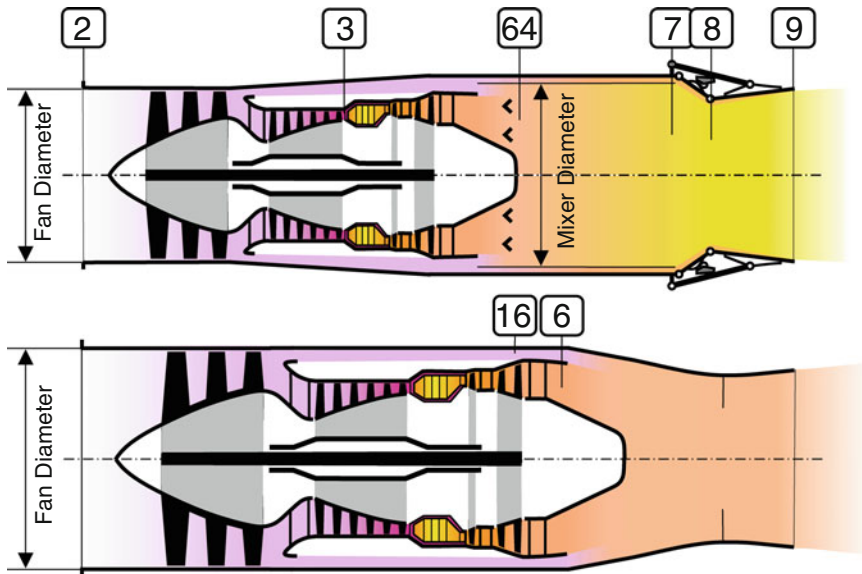


Fig. 1.4-8 Dry and reheated turbofans for supersonic flight

The Mach number M_{64} , after mixing core and bypass flow and before (in the calculation) the reheat combustion begins, not only determines the total pressure losses but also limits the temperature increase in the afterburner.

Rayleigh flow (adding heat in a frictionless pipe of cross sectional area) causes the so-called fundamental pressure loss. Figure 1.4-9 shows not only this pressure loss but also the limit for the reheat exit temperature T_7 for the assumption $T_{64} = 1000$ K. In this example, it is impossible to get more than 1800 K reheat exit temperature when the reheat inlet Mach number is 0.4.

If we select an inlet Mach number of 0.22 for our parametric study, we get the result shown in Fig. 1.4-10. The fundamental pressure losses vary because the reheat inlet temperature T_{64} depends on overall pressure ratio P_3/P_2 and bypass ratio. High bypass ratios have inherently low reheat inlet temperature T_{64} . More fuel is needed for reheating the gas to the given afterburner exit temperature of $T_7 = 1950$ K.

The lowest bypass ratio is the best both from an SFC and an engine size point of view. Pressure ratios of around 12 are best to achieve low reheat fuel consumption, but higher pressure ratios help to minimize the engine size and would also improve the SFC during dry operation.

All the cycles in Fig. 1.4-10 are feasible, but in the red region the reheat pressure losses exceed 4%. Cycles with low bypass ratio have less pressure losses. To avoid the high pressure loss, it is necessary to increase the jet pipe diameter for high bypass ratio engines which means M_{64} must be lower than 0.22. In contrast, the

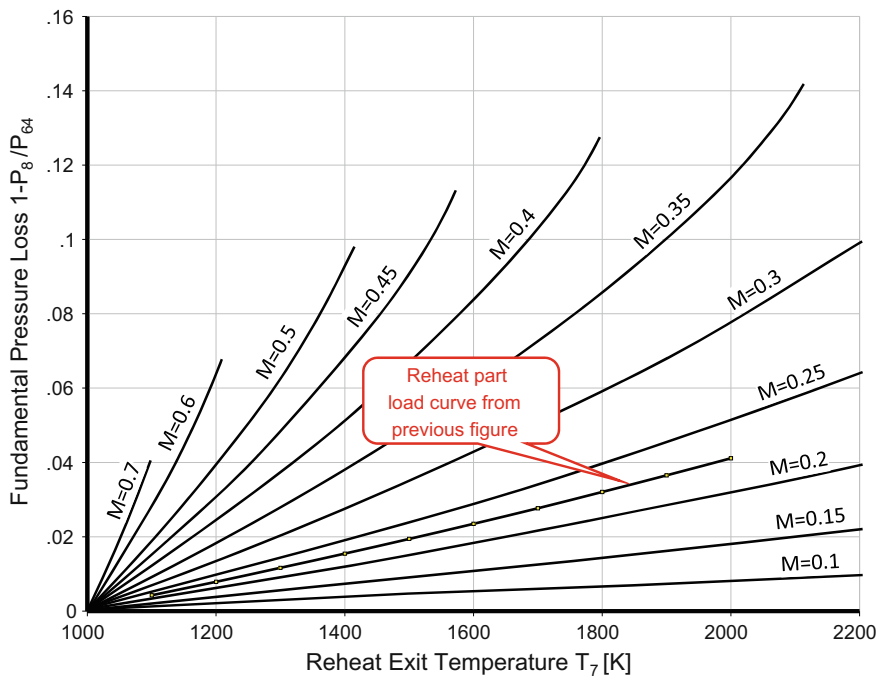


Fig. 1.4-9 Total pressure loss due to heat addition

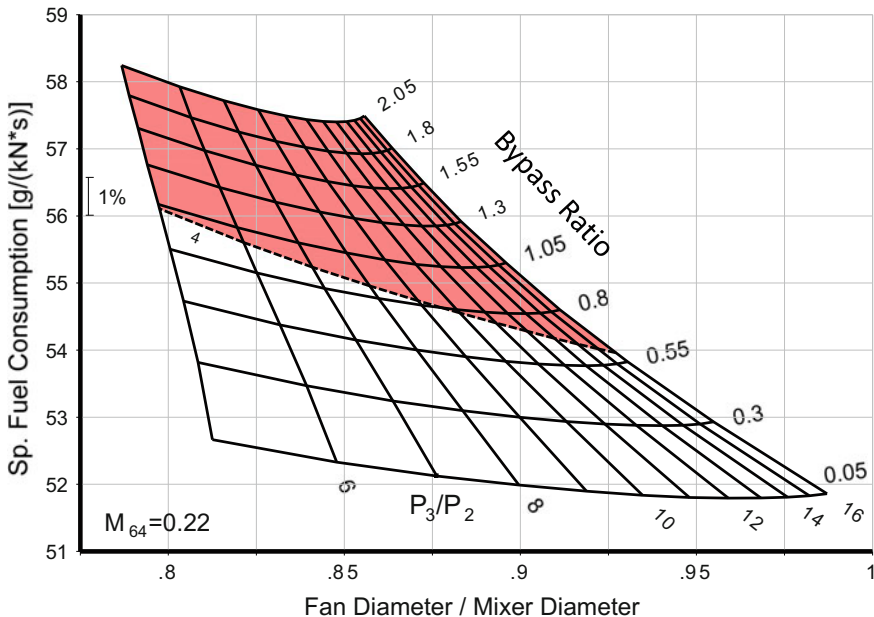


Fig. 1.4-10 Mixer Mach No $M_{64} = 0.22$, $A_9/A_8 = 1.5$

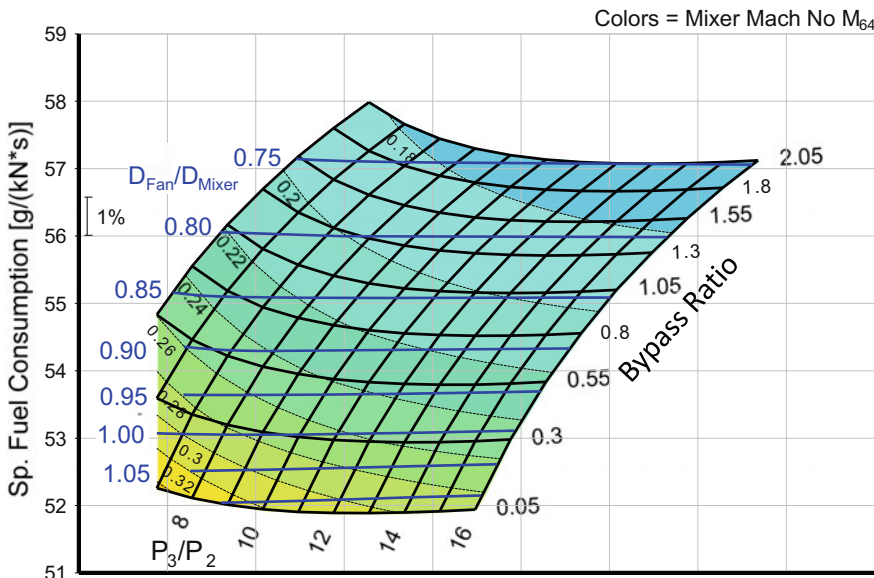


Fig. 1.4-11 Result for 4% heat addition pressure loss

engines with low bypass ratio can afford a higher reheat inlet Mach number without suffering excessive pressure loss.

Let us modify the boundary condition of our parametric study now: we adjust the reheat inlet Mach number in such a way that all engines have the same fundamental pressure loss of 4%. The color contours in Fig. 1.4-11 indicate the required reheat inlet Mach numbers. The blue lines are lines of constant diameter ratio $D_{\text{Fan}}/D_{\text{Mixer}}$.

The fan diameter of an engine with afterburner is generally smaller than the diameter of the afterburner, except at the very low bypass ratio of the second parametric study.

1.4.2.2 Dry Turbofans for Supersonic Flight

For supersonic cruise without an afterburner we make the same assumptions for the cycle as before. The exception is the mixer Mach number M_{64} . There is no need to keep it low and therefore we set this property at 0.5.

In a comparison with Figs. 1.4-10, 1.4-12 shows that the fan diameter of dry turbofans is much bigger than the diameter in the mixer area—the fan face dimensions set the engine diameter. Taking the fan inlet area as a measure of engine size leads to the conclusion that a dry engine is about 50% bigger in mass flow than a reheated engine with the same thrust.

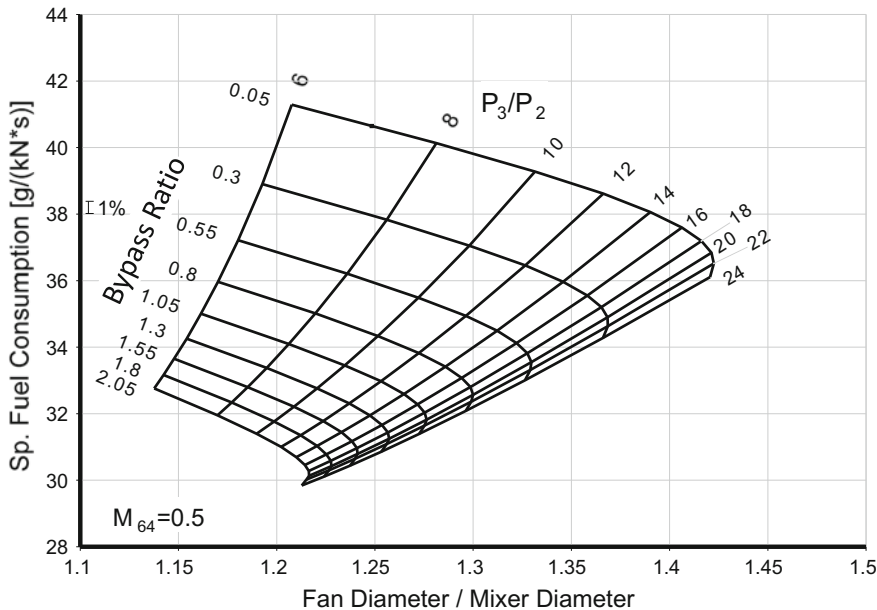


Fig. 1.4-12 Dry turbofan SFC and diameter ratio for constant thrust at supersonic flight (36089 ft Mach 2)

Thrust/weight ratio of the dry engine will be significantly lower than that of the reheated engines. Thrust per frontal area is low which results in increased aircraft fuselage cross section, airframe size and weight. For supersonic vehicles, the size penalty of medium to high bypass ratio overwhelms any SFC benefit.

1.4.3 Convergent or Convergent-Divergent Nozzle?

Most engines have simple conical nozzles of fixed geometry; the throat area is constant. Variable area nozzles are required for engine cycles where large variations in throat area are necessary, usually because of afterburning. Convergent nozzles are of a simpler design, they are shorter than convergent-divergent nozzles and weigh less. Why use the longer, heavier, and more complex nozzle?

A convergent-divergent nozzle produces more thrust than the convergent variant when the pressure ratio of total to static pressure P/P_s is big enough and the area ratio A_0/A_8 is adequate, see Fig. 1.4-13. It obviously does not make sense to use a convergent-divergent nozzle with a high bypass ratio turbofan because the nozzle pressure ratio is not much bigger than 2 even during Max Climb at altitude.

The nozzle pressure ratios of low bypass ratio engines, as they are used with fighter aircraft, are much bigger: around 4 at sea level Take Off.

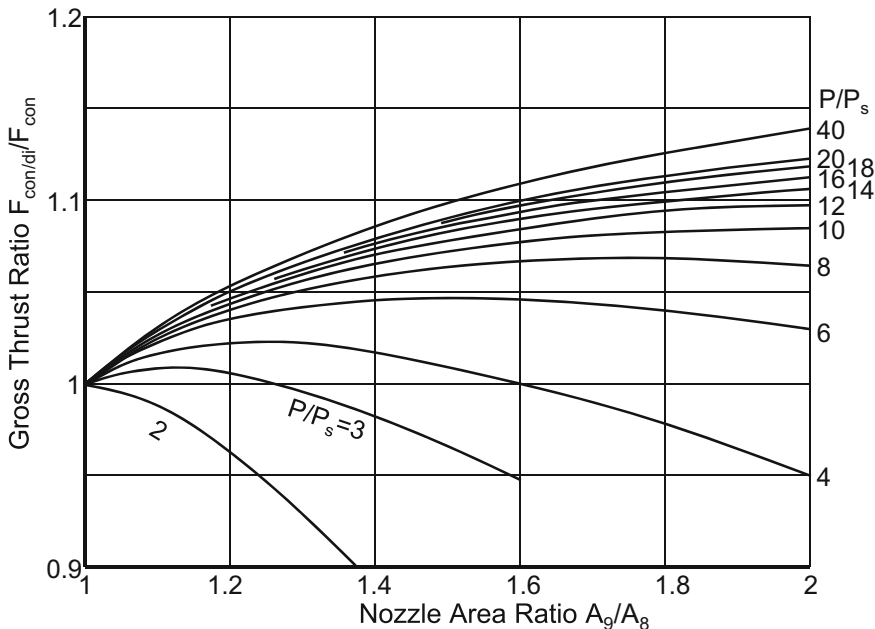


Fig. 1.4-13 Thrust ratio of the convergent-divergent to the convergent nozzle

A convergent-divergent nozzle delivers more thrust, but the thrust advantage at Take Off is too small to justify the additional weight. Things change significantly in the flight envelope. Nozzle pressure ratio increases with Mach number up to more than 15 in our example of a low bypass ratio turbofan, see Fig. 1.4-14.

Let us go back to Fig. 1.4-13 for a few moments: why do the constant pressure ratio lines reach a maximum gross thrust ratio at a certain area ratio A_9/A_8 ? Let us have a look at the flow in the divergent part of the nozzle. There, the Mach number increases to supersonic values; the static pressure drops below the pressure in the throat. The bigger the nozzle exit area A_9 , the lower the static pressure P_{s9} . Whether P_{s9} is greater, equal, or less than ambient pressure depends on the combination of nozzle pressure ratio P/P_{s9} and the area ratio A_9/A_8 . We get the highest amount of thrust if the expansion leads to $P_{s9} = P_{\text{amb}}$ —this is the ideal case.

The lower the nozzle pressure ratio, the lower the optimal area ratio. Therefore, economic part load operation of an engine demands A_9/A_8 be as low as practical, in the range from 1.03 to 1.06. During non-afterburning (dry) operation the throat area A_8 is comparatively small.

Higher area ratios only make sense if the pressure ratio is above 5, which is the case during high speed flight. Supersonic flight with high Mach numbers is only feasible with an afterburner switched on. Then, the throat area A_8 is much bigger than during dry operation. If we design the nozzle mechanically in such a way that

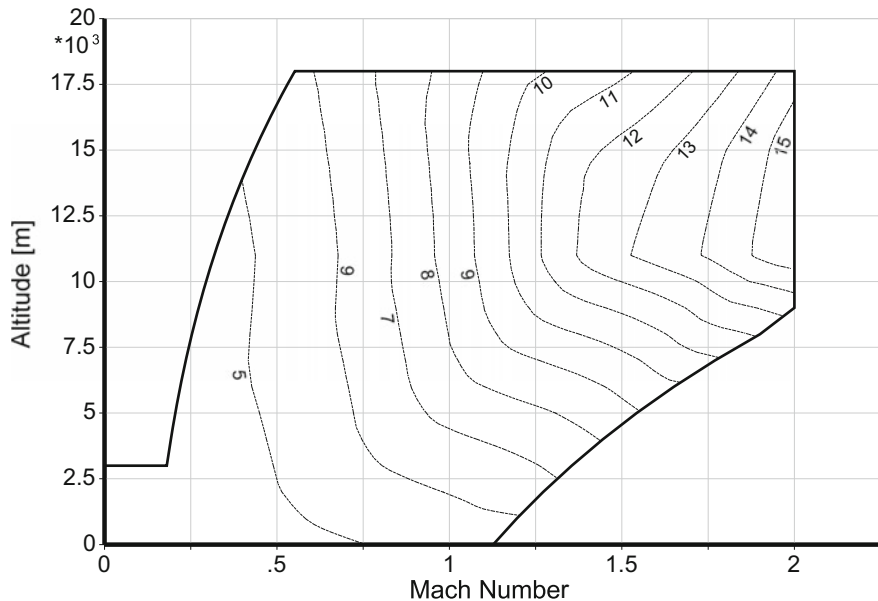


Fig. 1.4-14 Nozzle pressure ratio of a low bypass ratio turbofan with afterburner

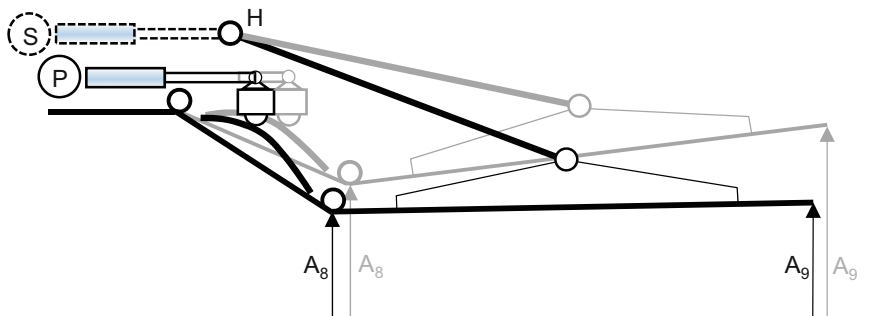


Fig. 1.4-15 Kinematics of a convergent-divergent nozzle

the area ratio A_9/A_8 increases with throat area, we can fulfill the requirements for dry part load and maximum afterburner operation simultaneously.

In Fig. 1.4-15, the primary actuator P controls the throat area A_8 . The nozzle exit area A_9 varies as function of A_8 in such a way that A_9/A_8 increases with A_8 if the hinge H is attached to the engine casing.

However, the direct connection between throat and exit area is not the best solution for all flight cases. Think of “super cruise”—flying supersonically without igniting the afterburner. The Max Dry nozzle throat area is small, but the pressure ratio is very high, between 10 and 12 (Fig. 1.4-14). The divergent part of the nozzle

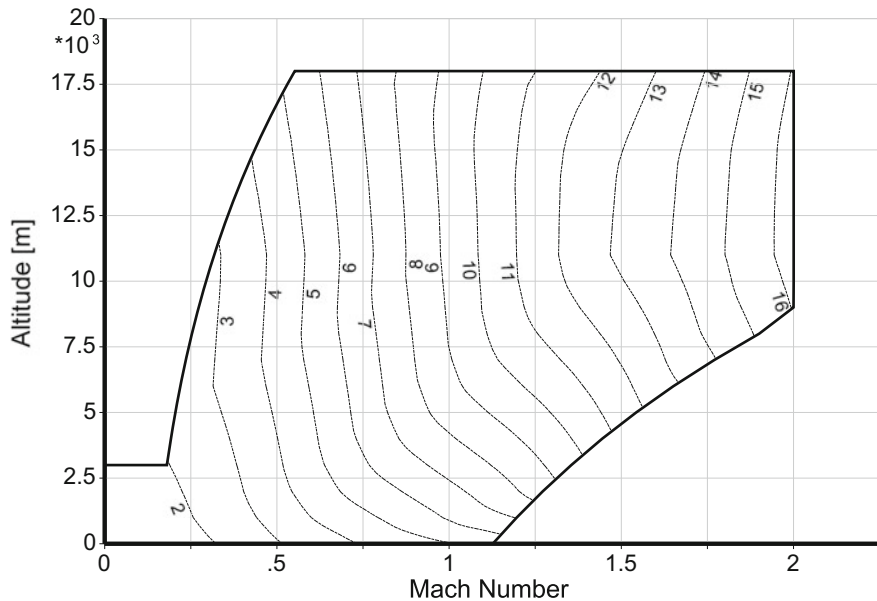


Fig. 1.4-16 Percent net thrust gain with a convergent-divergent nozzle of area ratio $A_9/A_8 = 1.6$

enhances thrust only marginally under these conditions because A_9/A_8 is so near unity if we are able to control the throat area only.

With two actuators, we can control A_9 independently from A_8 . This not only allows us to fly faster without afterburner, it also improves the reheat part load specific fuel consumption while flying supersonically.

Figure 1.4-16 compares augmented turbofan engines with convergent and convergent-divergent nozzle with an area ratio A_9/A_8 of 1.6. The dotted lines mark constant net thrust deltas in %. You might be surprised that the numbers are significantly bigger than those in Fig. 1.4-13. The reason is that Fig. 1.4-13 compares gross thrust while Fig. 1.4-16 compares net thrust.

The decision between the simple convergent nozzle and the more complex convergent-divergent nozzle with one or two actuators depends on the mission of the aircraft. Installed engine performance should be considered because the outer nozzle geometry affects the boat-tail drag of the aircraft significantly and the weight of the variable nozzle systems is considerable.

1.4.4 Single or Two Stage High Pressure Turbine?

In the 1000 kW class there are two modern gas turbines for helicopter propulsion: the MTR390 (Fig. 1.4-17) and the T800 (Fig. 1.4-18). One of the main differences

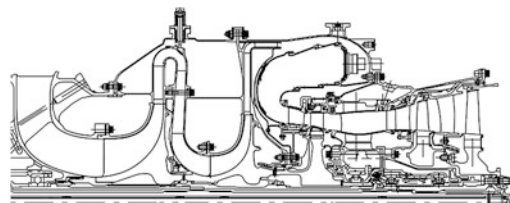


Fig. 1.4-17 MTR 390 cross section (adapted from Ref. [2])

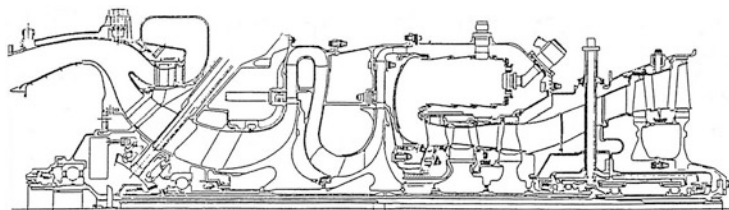


Fig. 1.4-18 T800-802 cross section (adapted from Ref. [3])

between those two engines is that the MTR390 has a single stage gas generator turbine while the T800 has two high pressure turbine stages.

In the following we show that from a conceptual cycle design point of view, both engines are optimum solutions for the number of gas generator turbine stages they have. We begin the design studies with a generic reference cycle which is neither that of the MTR390 nor that of the T800, but close to both:

Take off power	960 kW
Spec. fuel consumption	289 g/kWh
Mass flow	3.5 kg/s
Pressure ratio	13

Selecting an optimum cycle is not a trivial task. First, we should define what “optimum” is. This depends very much on the application, but usually involves cost. The cost of engine operation is due mainly to fuel and maintenance. Procurement cost is another issue. Of course, even the minimum cost engine must fulfill the power requirements without exceeding given weight and volume limits.

An optimal engine has low fuel consumption, low weight, and small volume. It is composed of as few parts as possible with long service life in mind. The selection of materials and manufacturing technology depends very much on the intended production price.

1.4.4.1 Simple Cycle Study

The thermodynamic cycle of this type of engine is simple: it is the Joule process. The parameters to be optimized are mainly the pressure ratio of the compressor and the turbine inlet temperature. Figure 1.4-19 shows results from a parametric variation at constant isentropic component efficiencies ($\eta_C = 0.8$, $\eta_{HPT} = 0.85$, $\eta_{LPT} = 0.89$).

The figure is valid for 5% turbine cooling air, independent of burner exit temperature—this is obviously unrealistic. Figure 1.4-20 shows the influence of cooling air on the results for constant compressor pressure ratio $P_3/P_2 = 13$. Two turbine efficiency definitions are employed—they differ in the bookkeeping of the working potential of the various cooling air streams. Which efficiency definition we use has significant impact on the results: keeping the thermodynamic efficiency constant leads to less sensitivity of SFC to cooling air compared to the cases with constant stage-by-stage efficiency.

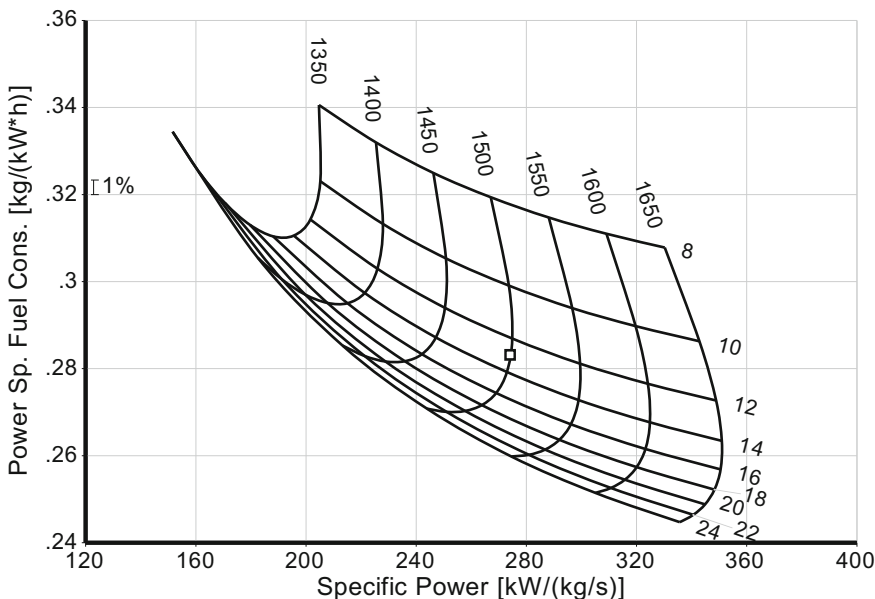


Fig. 1.4-19 Simple parametric study

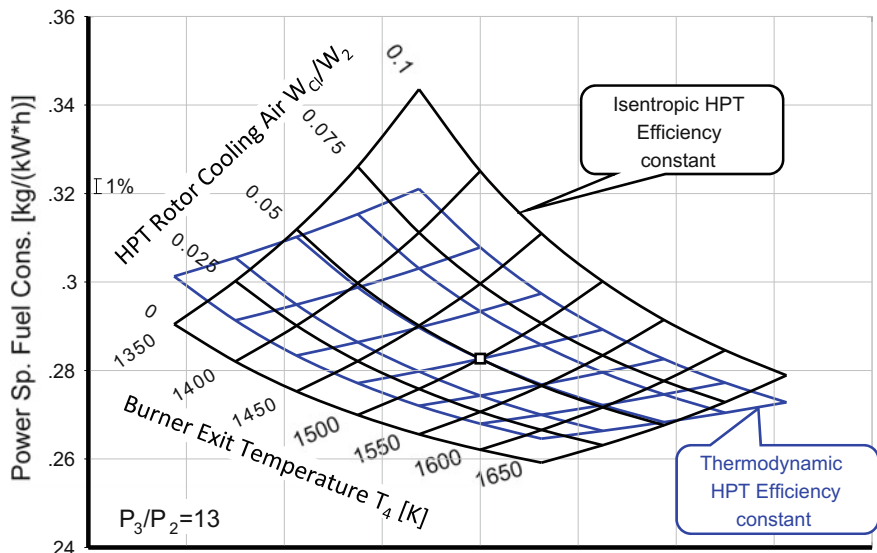


Fig. 1.4-20 Influence of cooling air with two turbine efficiency definitions

The amount of cooling air required for a given burner exit temperature depends on the cooling technology applied, on the material used and on the number of turbine stages. But we will discuss this further in the next subsection.

From Fig. 1.4-19 we can see that for high specific power (which results in an engine of low weight and volume) we need high burner exit temperatures T_4 . Moreover, high temperature leads to low specific fuel consumption.

Let us assume now that the maximum tolerable burner exit temperature is 1500 K for manufacturing cost or durability reasons. Keeping this constraint in mind, we read from Fig. 1.4-19 that the pressure ratio for minimum SFC is approximately 23.

The engines in this class operate with a burner exit temperature in the range of 1450–1550 K, but with much lower pressure ratio than 23. Is it possible that they are not designed to the optimum cycle? In fact, they are optimum engines. The present cycle parameter study is too simplistic to find the real optimum.

1.4.4.2 Realistic Optimization

Constant *isentropic* component efficiencies have been assumed for calculating the numbers in Fig. 1.4-19. This is standard practice, but not fully correct. Rerunning the parametric study with constant *polytropic* efficiencies leads to an optimum pressure ratio that is only slightly lower than 23. Switching to polytropic efficiencies is not the key to getting the right answer; it is necessary to go into more depth.

Another topic to be considered is the number of turbine stages which is either one or two. There is no such thing as a 1½ stage turbine. It is necessary to run the parametric study twice, once for a single-stage turbine and a second time for a two-stage turbine.

1.4.4.3 Engines with Single Stage Turbines

The efficiency of a turbine depends very much on the aerodynamic loading and on some geometrical parameters. We now do a turbine velocity diagram analysis. The resulting efficiency is adjusted with the help of a calibration factor in such a way that, for the reference cycle ($P_3/P_2 = 13$, $T_4 = 1500$ K), we get the value 0.85 for HPT efficiency. This reference point is marked with a little square in all the figures.

Mass flow is the same for all engines, as are the compressor entry dimensions. The gas generator spool speed follows from common assumptions for Mach number and blade tip speed at the compressor face.

Turbine mean diameter and radius ratio are also fixed. Thus, for each cycle we get the same turbine exit area A_{44} and blade root stress level, expressed as $A_{44}N^2$. The absolute shaft power PW_{SD} changes with specific power—a result of the thermodynamic cycle calculation.

Figure 1.4-21 differs significantly from Fig. 1.4-19. The pressure ratio for the lowest specific fuel consumption along the contour for burner exit temperature

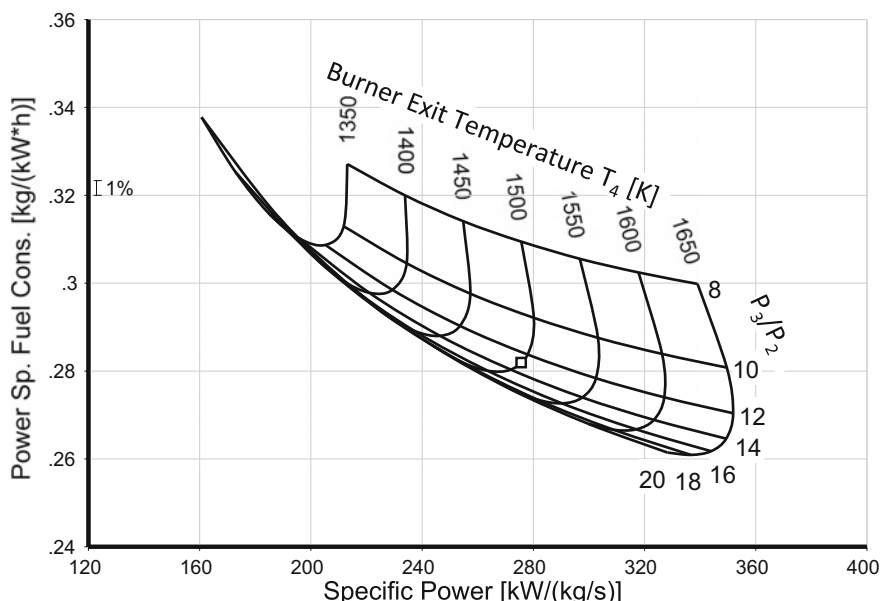


Fig. 1.4-21 Single stage HPT with η_{HPT} from velocity diagram analysis

1500 K is now only 15. This value is much nearer to the MTR390 compressor pressure ratio of 13 and very different to the value which was previously found to be optimum (it was 23).

The next figure (Fig. 1.4-22) shows some features of the single-stage turbine. High Mach numbers and swirl generate big losses in the duct downstream of the HP turbine and possibly also in the low-pressure turbine. Turbine exit Mach numbers above 0.5 and absolute swirl angles above 30° (relative to the axis) should be avoided.

Next let us have a look at another important result which is only available if a turbine velocity triangle analysis is part of the parametric study: we can calculate a value for the mean rotor blade metal temperature. The only thing we need to know in addition to the velocity triangles is the blade cooling effectiveness, which is defined as

$$\eta_{cl} = \frac{T_{41rel} - T_{metal}}{T_{41rel} - T_3} \quad (1.4-3)$$

Let us assume that we can achieve a rotor blade cooling effectiveness of 0.555 with 5% of the compressor mass flow as cooling air. Then we get the blade metal temperatures shown on the x-axis of Fig. 1.4-23.

Note that for constant burner exit temperature this metal temperature is not constant. This results on one side from the increase in cooling air temperature with

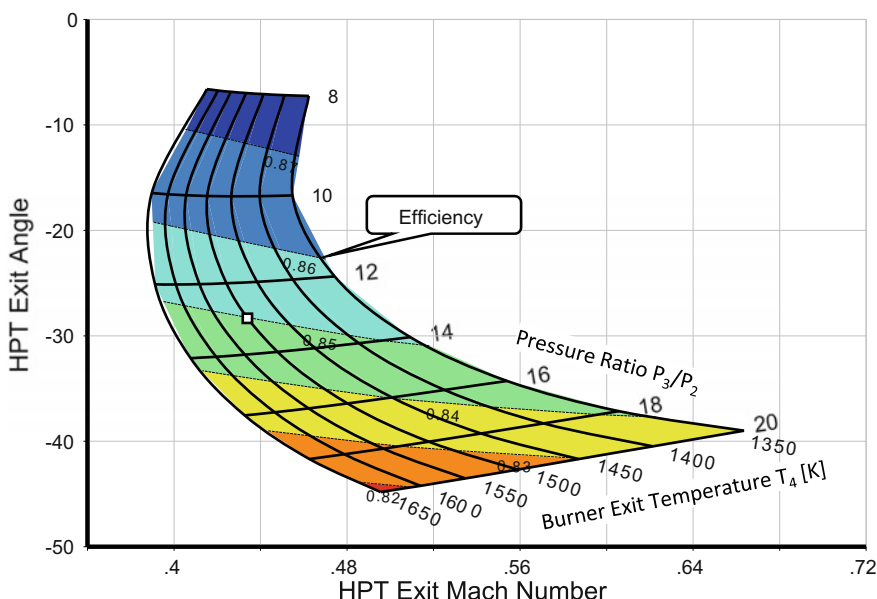


Fig. 1.4-22 HPT exit flow conditions

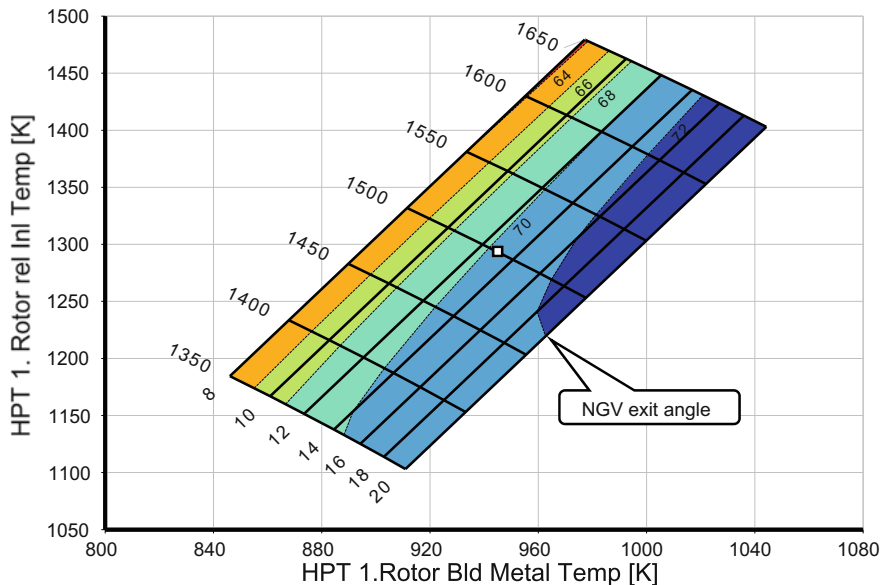


Fig. 1.4-23 Rotor blade metal temperature for $W_{c1}/W_2 = 0.05$

compressor pressure ratio. On the other side, the difference between the absolute rotor inlet temperature T_{41} and the rotor inlet temperature in the relative system $T_{41\text{rel}}$ increases with the aerodynamic turbine loading $\Delta H/U^2$. Compressor pressure ratio is directly connected with the specific work ΔH of the turbine and circumferential speed U is invariant in our case. Therefore, the total temperature in the relative system of the rotor $T_{41\text{rel}}$ decreases with increasing pressure ratio at constant T_{41} .

1.4.4.4 Design with Prescribed Rotor Blade Metal Temperature

The price of a turbine blade depends very much on the material used. Single crystal blades allow high metal temperatures; however, they are very expensive. For any material, there is a blade metal temperature limit which depends on the stress level and on the blade life requirement.

As mentioned above, in this study the blade stress level expressed as AN^2 is constant. Therefore, it is not necessary to consider the relation between blade life, stress level and temperature in this special case.

All the previous parametric studies were done with 5% cooling air. To achieve a constant metal temperature across a range of cycles, we need to vary the amount of cooling air since the hot gas temperature and the cooling air temperature are also changing.

Cooling effectiveness depends on the intended cooling technology and the amount of cooling air. The following empirical correlation describes approximately how much cooling air is required for multi-pass convection cooling:

$$\frac{W_{cl}}{W_2} = 0.04 \frac{\eta_{cl}}{1 - \eta_{cl}} \quad (1.4-4)$$

Keeping rotor blade metal temperature constant requires the cooling effectiveness shown in Fig. 1.4-24. The amount of cooling air increases with compressor pressure ratio because the temperature of the cooling air increases.

In Fig. 1.4-25 the pressure ratio for minimum specific fuel consumption and burner exit temperature of 1500 K is again 15. An important observation from this figure is that, in spite of the significant increase in the cooling air flow, the specific fuel consumption continues to fall when the burner exit temperature increases. But we cannot easily deduce the best burner exit temperature for minimum specific fuel consumption from this parametric study. We must consider other arguments.

One approach is that there might be a limit to the low-pressure turbine inlet temperature. For cost reasons, an uncooled design is preferred. In Fig. 1.4-25, if we look at the dashed line which marks the PT inlet temperature of 1150 K, we observe that an optimum engine in terms of fuel consumption, would be a machine with pressure ratio 14 and burner exit temperature 1575 K.

In our example, however, T_4 is limited at 1500 K. Choosing a pressure ratio slightly smaller than 15 makes it easier to achieve the compressor efficiency goal

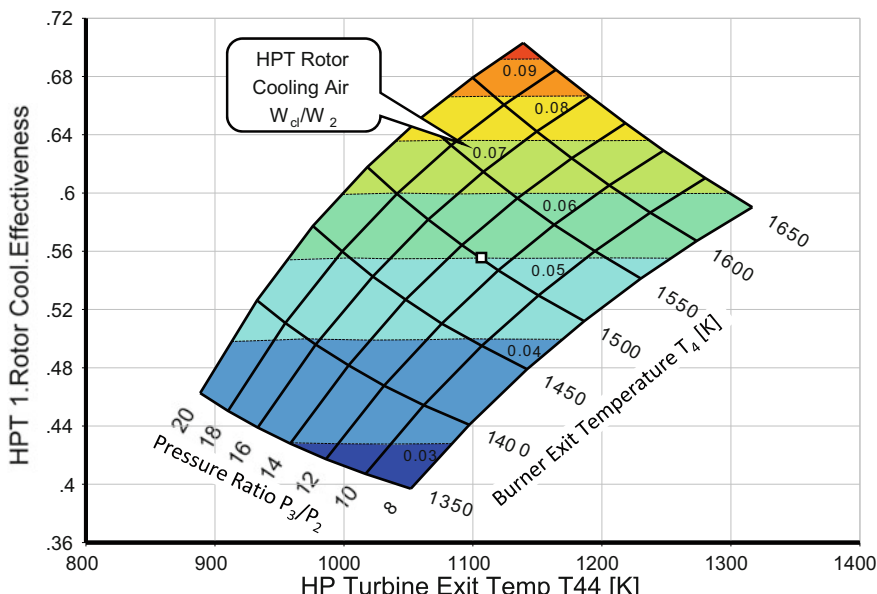


Fig. 1.4-24 Cooling effectiveness required for constant rotor blade metal temperature

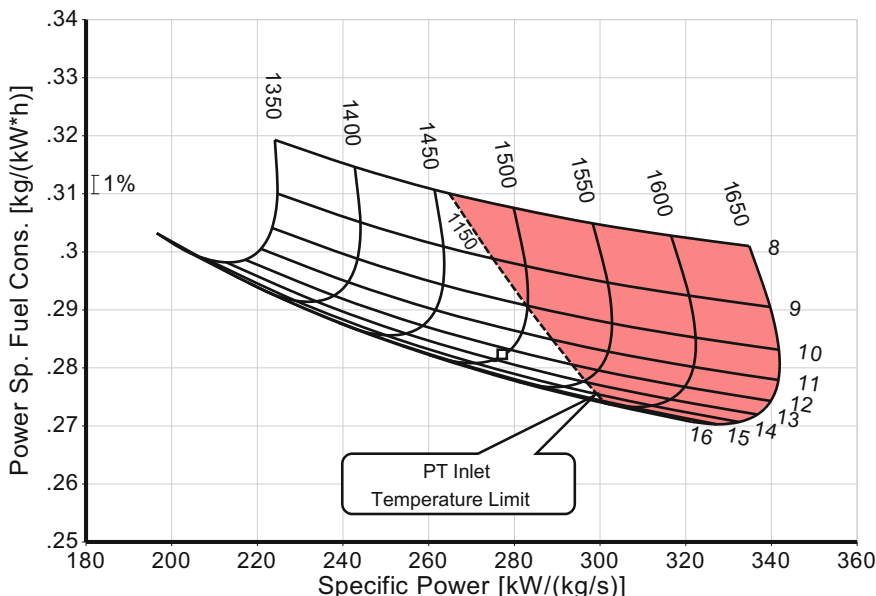


Fig. 1.4-25 Parametric study with single-stage HP turbines and constant blade metal temperature

without too much increase in SFC. Additionally, we get a bit more specific power and have some room for future engine power growth. It really makes sense to choose a pressure ratio of 13 for an engine like the MTR390 which has a single stage high pressure turbine.

1.4.4.5 Engines with Two-Stage Turbines

Selecting the number of turbine stages is another non-trivial task. The advantages of the single-stage design are that it has fewer cooling air requirements, that the engine is lighter and also has a smaller volume. The costs of manufacturing and maintenance are lower. On the other hand, the two-stage design gives a better efficiency, a lower HP turbine exit Mach number and less swirl in the flow downstream of the turbine.

The two-stage turbine needs more cooling, but not simply because there is one more stage. The main reason is that the inlet temperature in the rotating coordinate system of the first rotor is significantly higher. We take that into account with a combination of higher permissible blade metal temperature, improved cooling technology and an increased amount of cooling air. Note that is common practice to assume that the cooling air of the first rotor does work in the second stage.

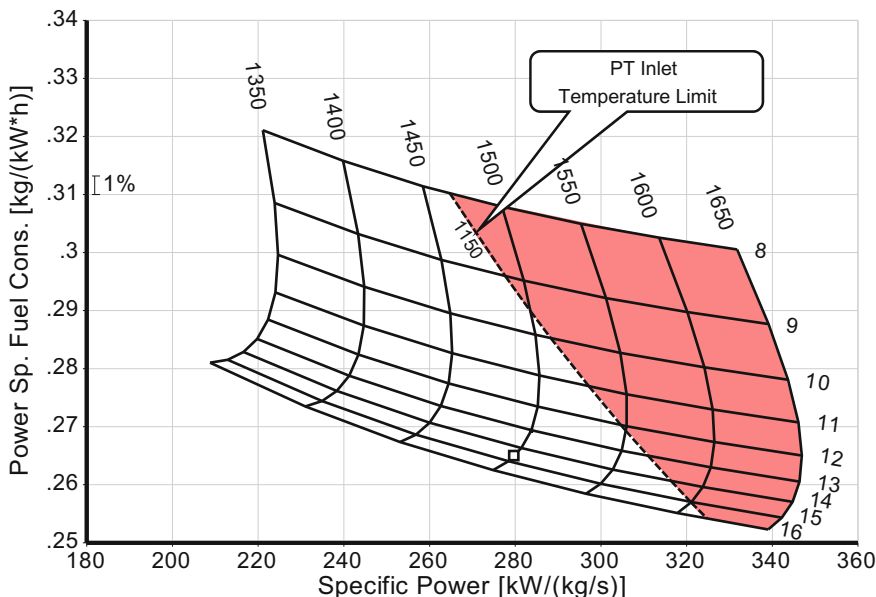


Fig. 1.4-26 Parametric study with two stage HP turbine with constant blade metal temperature of the first rotor

If we look at the specific fuel consumption and the specific power in Fig. 1.4-26 and compare it with the preceding figure, we see that an optimum design for a turboshaft with a two-stage gas generator turbine benefits from choosing a pressure ratio higher than 13. The advantage in terms of fuel consumption is significant.

1.4.4.6 Conclusion

A simple, conventional cycle study obviously does not yield a realistic result. We find answers for compressor pressure ratio and burner exit temperature that are in line with reality only if we consider the constraints imposed by the components.

The example shown was only one of many alternatives. The computer makes it easy to repeat the exercise for examples with different levels of component efficiencies. We can also consider the details of the power turbine design. As demonstrated by the figures, there are many parameters to be checked while selecting an optimum cycle. But always remember: the computer does not think—that is left to the user.

1.5 Conceptual Turbofan Design

1.5.1 Flow Annulus

A cycle design point calculation yields the mass flows, total temperatures, and total pressures. However, the size of the engine is not directly visible from these numbers, except for the exhaust area. That is the reason why performance calculation programs are sometimes called 0-D programs. This characterization creates the impression that these programs are primitive and vastly inferior to any 3-D CFD program. However, 0-D performance programs can—when the component maps have been calibrated with measured data—predict thrust and fuel consumption very accurately as well as temperatures, pressures, and spool speeds for any operating condition, all without knowing the engine geometry in detail.

As mentioned above, thermodynamic cycle calculations deal only with total pressures and temperatures. Static pressures and temperatures are not relevant, apart from the ambient pressure downstream of the exhaust. When we want to know more about the flow annulus, then we need to make assumptions about the Mach numbers in all thermodynamic stations.

1.5.1.1 Local Mach Numbers

Station 2 defines the engine inlet diameter which should not be bigger than necessary—therefore high Mach numbers are preferred. Just the opposite is true at the entry to the combustion chamber (Station 3) where high velocity would endanger burner stability. The local Mach number is moderate because the sonic velocity is high (due to the relatively high T_3) and the absolute velocity is low.

The temperature at the inlet to the core compressor is higher than at the fan face, so is the local sonic velocity. Therefore, the Mach number at this location is lower than at station 2. Mach numbers at the exit of the turbines are moderate, again due to the high local sonic velocity.

1.5.1.2 Hub/Tip Radius Ratio

Mach number, mass flow, total temperature and pressure determine the flow area. If we also estimate the hub/tip radius ratio r_h/r_t , then we can calculate the hub and tip radii at each of the thermodynamic stations around the turbomachines. Figure 1.5-1 shows typical values for turbofans together with local Mach numbers.

Low hub/tip radius ratios are desirable at the engine inlet to minimize overall engine diameter and hence nacelle drag, weight and increased ground clearance. The lower limit is often set by the ability to accommodate the roots of the fan blades.

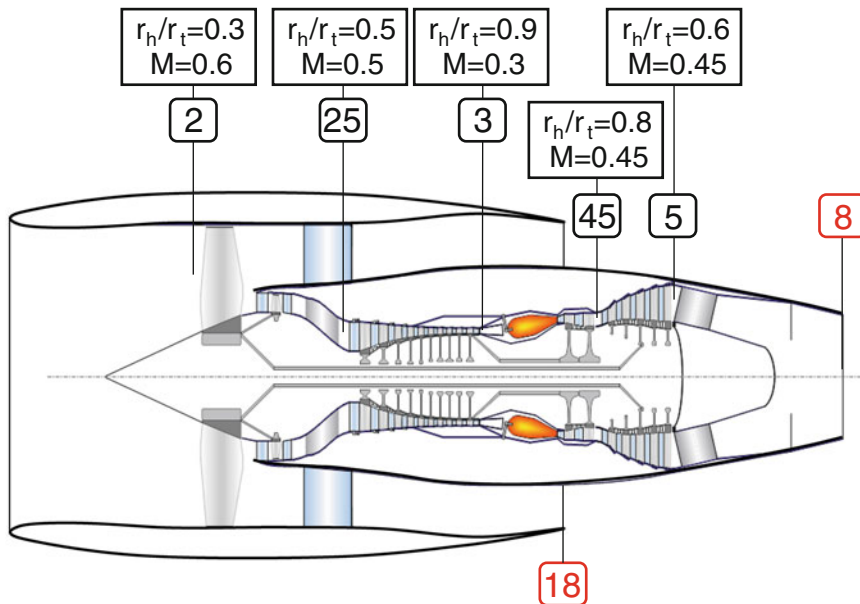


Fig. 1.5-1 Typical hub/tip radius ratios and Mach numbers for a turbofan

1.5.1.3 Relationships Between Components

High circumferential speed is advantageous for stage pressure ratio. However, non-dimensional speed reduces along a multi-stage compressor as temperature rises. Therefore, the speed tends to be too high at the front and too low at the rear. To compensate for this, the exit radius is raised by selecting a high hub/tip radius. This can be assisted by using a constant tip radius, which in turn leads to short blade height $r_t - r_h$ and tip clearance may become a problem: If the blade height gets too small, then the relative tip clearance (expressed in percentage of the blade height) becomes unacceptable due to losses in efficiency and stall margin.

The HP compressor exit radius does not limit the HP turbine radius. At the turbine inlet, we need a much bigger annulus area since the density of the gas is considerably lower than at the compressor exit. Thus, we can make the turbine diameter bigger than the compressor exit diameter without getting blades which are too short. The benefit for the turbine is higher circumferential speed which reduces the aerodynamic loading. The mean turbine diameter is typically 10% bigger than the compressor exit diameter.

The fan dictates the rotational speed of the low pressure turbine (LPT). For acceptable aerodynamic loading and for minimizing the stage count, we need the highest feasible circumferential speed. Therefore, in high bypass ratio engines the LPT entry diameter is up to 60% bigger than the HPT exit diameter.

The space available in the nacelle limits the exit diameter of the LP turbine. It usually cannot be more than 20% bigger than the outer diameter of the core entry. Another way to set the LPT exit diameter is to choose a hub/tip radius ratio of 0.6.

1.5.1.4 Spool Speed

Selecting spool speed is a complex compromise between aerodynamic and stress requirements. Compressor stage count depends on circumferential speed since stage loading $\Delta H/U^2$ must remain within limits. The length of the engine depends on the number of stages and the magnitude of the radius differences between the turbomachines.

Estimating the rotational spool speeds based on the conditions at the fan and the HP compressor entry is a suitable starting point. Given corrected flow $W\sqrt{T/P}$, absolute Mach number, hub/tip radius ratio and blade tip circumferential speed yield revolutions per minute. The blade tip relative Mach number is a byproduct of this calculation.

1.5.1.5 Core Size

Local Mach numbers, hub/tip radius ratios and AN² at turbine exit (as a measure of blade root stress) have always been used in conceptual design studies of gas turbines. In the recent years a new term has become popular in this context: the so-called *core size*. It is defined as

$$cs = \frac{W_{25}\sqrt{\Theta_3}}{\delta_3} \quad (1.5-1)$$

In this formula W_{25} is the core compressor inlet mass flow, Θ_3 is the corrected compressor exit temperature $T_3/288.15$ K and δ_3 is the corrected compressor exit pressure $P_3/101.325$ Pa.

From this definition, we can immediately see that only properties of the high pressure compressor are considered. It is obvious that this definition of core size cannot describe burner volume effects or whether there are one or two HP turbine stages.

If *core size* does not stand for the size of the core in total, the question arises if it can be used to describe at least the size of the core compressor. To check that, we expand the above formula as follows:

$$cs = k \frac{W_{25}\sqrt{T_3}}{P_3} = k \frac{W_{25}A_3}{W_3 R} \frac{W_3 R \sqrt{T_3}}{A_3 P_3} = k \frac{W_{25}A_3}{W_3 R} f(M_3) \quad (1.5-2)$$

The mass flow ratio W_{25}/W_3 reflects an interstage bleed offtake. If air is bled off, then the compressor size upstream of the bleed offtake location increases and this is reflected in an increase of c_s .

For further examination of c_s we assume that for a given application of the compressor, W_{25}/W_3 is constant. In any case, the Mach number M_3 will be selected such that it is as high as possible within the limits of stable burner operation because high velocities are favorable for the design of the last compressor stage. Therefore, we can consider the Mach number M_3 also as constant.

Thus, the term *core size* as defined here is proportional to the compressor exit area since both W_{25}/W_3 and M_3 are constant (except for minor variations) within any conceptual design study. Since also the hub/tip radius ratio at the compressor exit is within narrow limits we can say:

Core size is proportional to the blade height of the last compressor stage.

The difficulties of manufacturing small high quality blades and maintaining tight tip clearance during operation amplify with decreasing blade height. Introducing an efficiency penalty and eventually an increased surge margin requirement for compressors with small *core size* can be adequate in a sophisticated conceptual engine design study. However, there is no hard limit for minimum blade height which could justify restricting the design space to engines with a certain minimum core size.

The uncritical use of core size as engine quality criterion can be misleading if the term is understood as a measure of the geometrical size, of the volume or of the weight of the gas generator. Consider the following two cases:

- (1) The geometry of a gas generator changes despite constant *core size* if
 - A two-stage turbine replaces a single stage high pressure turbine.
 - In a cycle study with constant overall pressure ratio, the booster pressure ratio is decreased and the HPC pressure ratio is increased in such a way that more HPC stages are needed.
 - The gas generator spool speed is increased and the HPC stage count decreases as a consequence.
 - Inlet mass flow (and thus inlet area) is increased and simultaneously the pressure ratio (and the required number of stages) is decreased in such a way that core size is constant.
- (2) The geometry of a gas generator does not change, but *core size* varies during off-design operation if
 - Bleed air is taken from the burner.
 - Power is taken from the gas generator spool.
 - The efficiencies of compressor and turbine decrease due to deterioration.
 - HPT flow capacity is modified by re-staggering the nozzle guide vanes.
 - LPT flow capacity is modified.
 - The engine is operated transiently.

As a summary: the term *core size* is only useful as a correlating parameter for size effects on compressor efficiency and eventually for correlating surge margin requirements. If the geometry of a compressor is given, then it makes no sense to use *core size* as a criterion for anything.

1.5.2 Direct Drive or with a Gearbox?

Cruise specific fuel consumption of turbofan engines depends on core efficiency, transmission efficiency and propulsive efficiency. Core efficiency depends on the core component efficiencies, the overall pressure ratio and the burner exit temperature.

The aerodynamic quality of the turbomachines has already reached a very high level—there is little room for further improvements. Increasing burner exit temperature did contribute to better core cycle efficiency in the past but increasing it further yields less and less improvement in thermodynamic efficiency because present day T_4 values are already near to the theoretical optimum. Increasing the cycle pressure ratio above 50 will also lead only to small improvements in core efficiency.

So, we can significantly decrease turbofan specific fuel consumption only if we increase propulsive efficiency and using higher bypass ratios (i.e. lower specific thrust) is the key to success.

Let us examine the theoretical SFC reduction potential with a simple cycle study. All cycle input data are constant, except bypass ratio and fan pressure ratio. If we were to do the study as a systematic variation of these two parameters, many of their combinations would not make sense. Therefore, for each bypass ratio, we adjust fan pressure ratio in such a way that the ratio of fan jet velocity V_{18} to core jet velocity V_8 is constant. Convince yourself with a parametric study that a jet velocity ratio of $V_{18}/V_8 = \eta_{\text{Fan}} \times \eta_{\text{LPT}} \approx 0.8$ yields the lowest SFC for any bypass ratio.

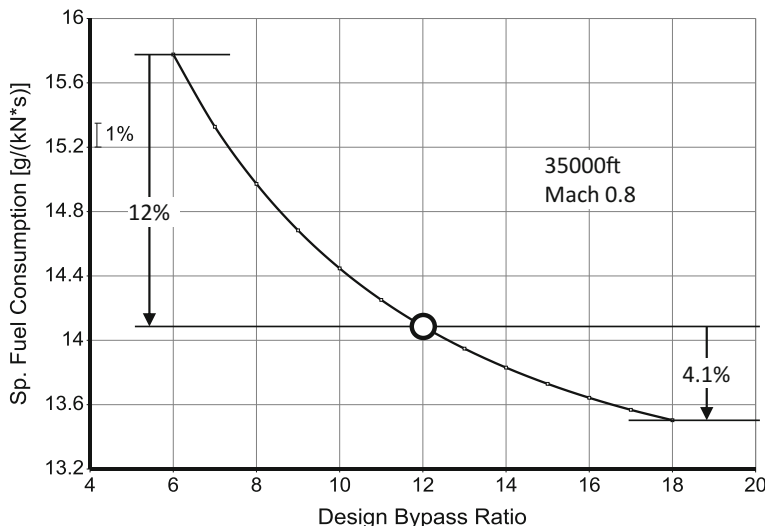
Table 1.5-1 summarizes the most important constant input data for this simple cycle study; only some minor details of the secondary air system (which are difficult to describe) are missing. Note that the table contains neither a thrust value nor one for mass flow—the size of the engine has no effect on the thermodynamic cycle. Figure 1.5-2 shows the result: Going from a bypass ratio of 6 to 12 yields 12% lower SFC, increasing the bypass ratio by another 6 to 18 leads to a further 4.1% SFC reduction.

The question is: What do the engines look like that achieve this SFC level? In the following we will show how the flow path changes with bypass ratio. All the engines have the same core, the same overall pressure ratio and the same burner exit temperature T_4 . In other words: we consider an engine family with a common core. The thermodynamic data of this core are listed in Table 1.5-1, and for fixing its size we set the standard day corrected flow of the compressor $W_{25} \sqrt{\Theta_{25}/\delta_{25}}$ to 25 kg/s.

Any change in bypass ratio requires a new fan, a redesigned booster and a new low pressure turbine. For conventional direct drive two spool turbofans we examine

Table 1.5-1 Main assumptions for the simple cycle study

Flight condition	Altitude 35000 ft	Mach 0.8
Fan outer efficiency	Polytropic	0.91
Fan inner efficiency	Polytropic	0.91
Booster efficiency	Polytropic	0.91
HPC efficiency	Polytropic	0.91
Burner efficiency		0.9995
HPT efficiency	Polytropic	0.89
NGV cooling air	% of W_{25}	8
1st Rotor cooling air	% of W_{25}	5
LPT efficiency	Polytropic	0.91
Compressor interduct pressure loss	%	2
Burner pressure loss	%	5
Turbine interduct pressure loss	%	2
Turbine exit duct pressure loss	%	1
Bypass pressure loss	%	1
Accessory parasitic power	% of PW_{HPT}	1
T_4	K	1700
Fan inner and booster pressure ratio P_{24}/P_2		2.551
HPC pressure ratio	-	18
Overall pressure ratio P_3/P_2	-	45
Jet velocity ratio V_{18}/V_8	-	0.8

**Fig. 1.5-2** Specific fuel consumption result from a simple thermodynamic cycle study

bypass ratios between 6 and 14 and for turbofans with gearbox we consider bypass ratios between 10 and 18. We compare the fundamental differences between conventional turbofans and those with a gearbox for the bypass ratio of 12—the middle of the bypass ratio range.

The cycle design point is *Max Climb* rating at the flight condition Mach 0.8/35000 ft, which is typical for commercial airliners.

Different rules apply for optimizing turbofans of conventional designs and those with a gearbox. Various criteria need to be considered for optimizing the respective engines and their components. We begin with conventional direct drive turbofans.

1.5.3 Conventional Turbofans with Bypass Ratios Between 6 and 14

The corrected flow at the entry of the gas generator $W_{25}\sqrt{\Theta_{25}/\delta_{25}}$ is 25 kg/s. The true air flow is almost the same ($W_{25} \approx 20.9$ kg/s) for all members of the engine family because the pressure ratio P_{25}/P_2 is constant and the temperature ratio T_{25}/T_2 changes only slightly due to minor changes in booster efficiency. The total airflow of the bypass ratio 6 engine, for example, is $W_2 = 146.4$ kg/s and it delivers 29.8 kN net thrust.

Now let us go to the details of engine design; we want to see how the various engines look. The simple thermodynamic cycle calculation yields only total pressures and total temperatures—if we want to know the geometry of the engine then we also need to know the static conditions. We get these by setting appropriate local Mach numbers at the thermodynamic stations indicated in Fig. 1.5-3. We can select all these local Mach numbers freely except for stations 8 and 18. The thermodynamic cycle directly determines them.

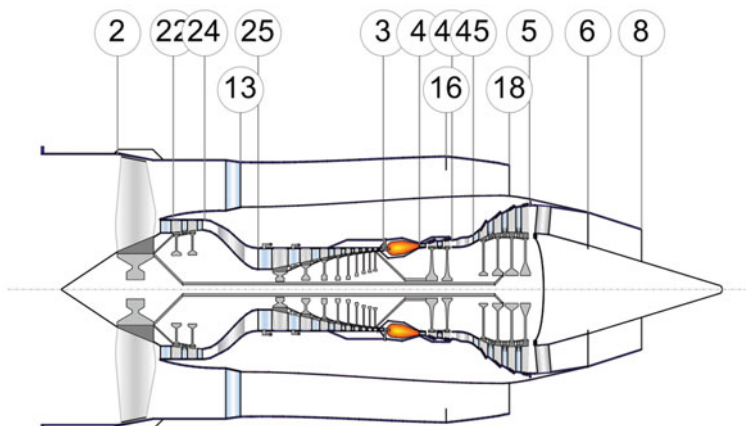


Fig. 1.5-3 Conventional turbofan, bypass ratio 6

Table 1.5-2 Mach numbers at selected thermodynamic stations of Fig. 1.5-3

Station	Mach number
22	0.5
24	0.5
45	0.4
5	A result of the LPT design
6	Same as in station 5
13	0.45
16	0.478

Mach number, mass flow, total temperature and total pressure determine the required flow areas. The Mach number at the fan face (station 2) together with the hub/tip radius ratio determines the fan tip diameter. We choose $M_2 = 0.6$ for *Max Climb*—this leaves some room for higher mass flow within the same nacelle. The selected hub/tip radius ratio of 0.28 is at the lower limit because some room must remain for the blade attachment.

All the Mach numbers and hub/tip radius ratios from station 25 to station 44 remain unchanged because we are considering an engine family with a given core. Reasonable Mach numbers are chosen for the other stations, as in Table 1.5-2.

The lengths of the compressors and turbines depend on the stage count and the blade aspect ratios. Low aspect ratios are favorable for compressor stability; high aspect ratios make both compressor and turbine shorter. There is no strict rule saying how large the blade aspect ratios must be. Our numbers are typical of modern turbofans.

As mentioned before, the gas generator of our turbofan engine family is the same for all bypass ratios, for both direct drive and geared configurations. So, we can now limit our exploration of engine geometry to the fan, the booster and the low pressure turbine.

1.5.3.1 Fan and Booster

The core stream pressure increases in the hub region of the fan and in the booster from P_2 to P_{24} . The specified values of P_{24}/P_2 (2.551) and pressure loss in the compressor interduct (2%) lead to $P_{25}/P_2 = 2.5$. Combining this with the HPC pressure ratio of 18, gives us the overall pressure ratio $P_3/P_2 = 45$. Combustor exit temperature (T_4), LPT inlet temperature (T_{45}) and LPT inlet pressure (P_{45}) are all the same in our engines.

We make use of the energy available at the LPT inlet for three processes. First, we extract the power we need for compressing the core stream in the fan and the booster. Second, we generate the shaft power necessary for compressing the bypass stream to P_{18} . Third we generate thrust in the core nozzle.

The power we extract in the first process is always the same. In the other two processes, we have a choice; we generate thrust in either the core or the bypass

nozzle. High shaft power extraction from the core flow delivers much thrust in the bypass nozzle and little thrust in the core nozzle, low power extraction does the opposite. Theoretically, the best thrust distribution between core and bypass thrust happens when the jet velocity ratio V_{18}/V_8 is equal to the product of fan and LPT efficiency.

We can use a constant value of $V_{18}/V_8 = 0.8$ for all bypass ratios since the sum of core and bypass thrust is only a weak function of the jet velocity ratio near to the optimum. Assuming constant V_{18}/V_8 makes the fan pressure ratio a function of bypass ratio. Increasing bypass ratio leads to decreasing fan pressure ratio, decreasing bypass jet velocity and decreasing core jet velocity—propulsive efficiency gets better.

The lower the fan pressure ratio, the lower the required circumferential fan speed U becomes. In a first parametric study we adjust the fan tip speed in such a way that the average pitch line loading $\Delta H/U^2$ is 0.4. This choice leads to a relatively high rotational speed, which is beneficial for both the booster and LP turbine efficiencies and hence contributes to low specific fuel consumption. We can achieve 91% polytropic efficiency with the selected aerodynamic loading [4]. The disadvantage of our choice is the noise which accompanies the high fan tip speed.

Both the fan tip and hub diameters increase with bypass ratio because their radius ratio is constant. The increase in core inlet radius with bypass ratio benefits the aerodynamic loading of the booster stages. However, the effect of decreasing the fan tip speed dominates so much that the booster stage pitch line loading would increase significantly if the number of stages were not increased.

If we kept the aerodynamic loading of the booster stages exactly constant, then we would need more booster stages than is practical. The bypass ratio 6 engine has two booster stages in our example. Additional stages in higher bypass ratio engines prevent an excessive increase in the aerodynamic stage loading. The limited increase of the loading results in only a modest drop in booster efficiency (according to a correlation in [4]) as shown in Fig. 1.5-4. This reduction affects specific fuel consumption only very slightly: a 1% booster efficiency drop increases SFC by only 0.12%.

In our study we assume that the fan root pressure ratio is lower than that in the bypass stream because the circumferential speed in the hub region is much lower:

$$\frac{P_{22}}{P_2} = 1 + 0.8 \left(\frac{P_{13}}{P_2} - 1 \right) \quad (1.5-3)$$

The booster pressure ratio P_{24}/P_{22} must increase slightly with bypass ratio because P_{22}/P_2 decreases with fan pressure ratio P_{13}/P_2 .

1.5.3.2 Bypass

The pressure loss in the bypass duct has a significant effect on the specific fuel consumption. 1% reduction in P_{16}/P_{13} increases SFC by 0.6% if BPR = 6 and the

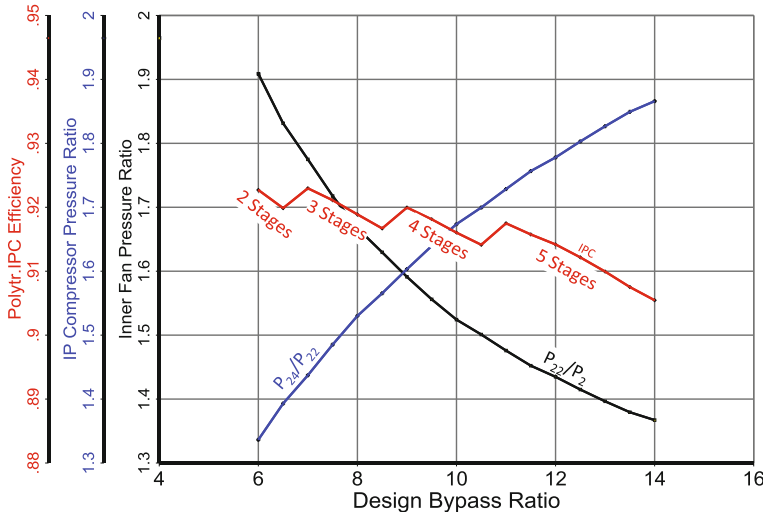


Fig. 1.5-4 Booster pressure ratio and efficiency

penalty increases to 1.4% if the bypass ratio is 12. The use of a constant pressure ratio P_{16}/P_{13} is inadequate in an ambitious cycle study. Therefore, we make the bypass pressure loss a function of the ratio of the bypass length to the hydraulic diameter of the duct. The pressure loss in an engine with bypass ratio 6 is assumed to be 1.8%. This value decreases to 0.9% in a bypass ratio 12 engine.

1.5.3.3 Low Pressure Turbine

We determine the efficiency of the low pressure turbine with the help of a simple velocity diagram analysis. The velocity triangles are assumed to be symmetrical and the loading $\Delta H/U^2$ —which is the same for all stages—is optimally matched to the flow factor V_{ax}/U as indicated by the dotted line in the Smith Chart (Fig. 1.5-5).

If we employed only four LPT stages in all engines, then as BPR increases we would get excessive aerodynamic stage loading and consequently poor LPT efficiency because the rotational speed of the low pressure spool decreases from 7603 rpm (BPR = 6) to 4110 rpm (BPR = 12). Increasing the LPT diameter helps a little but we still must increase the number of LPT stages with bypass ratio to achieve an acceptable LPT efficiency. Figure 1.5-6 shows how the efficiency varies with bypass ratio and the number of LPT stages. The blue line indicates a reasonable assumption for the number of stages versus bypass ratio.

We could always get better efficiency with an additional turbine stage. However, that would mean more weight, length and manufacturing cost. Our stage count selection is a compromise between performance and other requirements. Figure 1.5-7 shows that the SFC of our engines is nearly as good as our simple thermodynamic cycle has predicted (i.e. the black line with the circle).

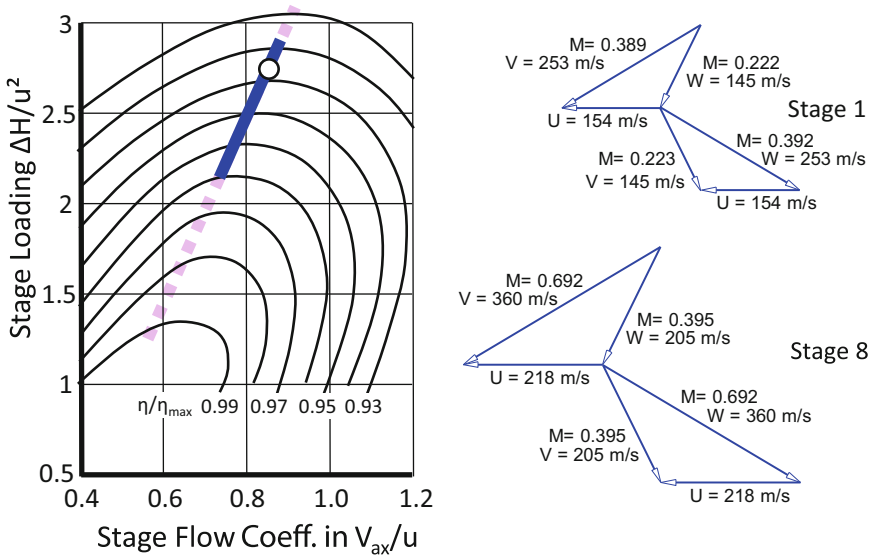


Fig. 1.5-5 The 8 stage LPT design point of the bypass ratio 12 turbofan in the Smith Chart

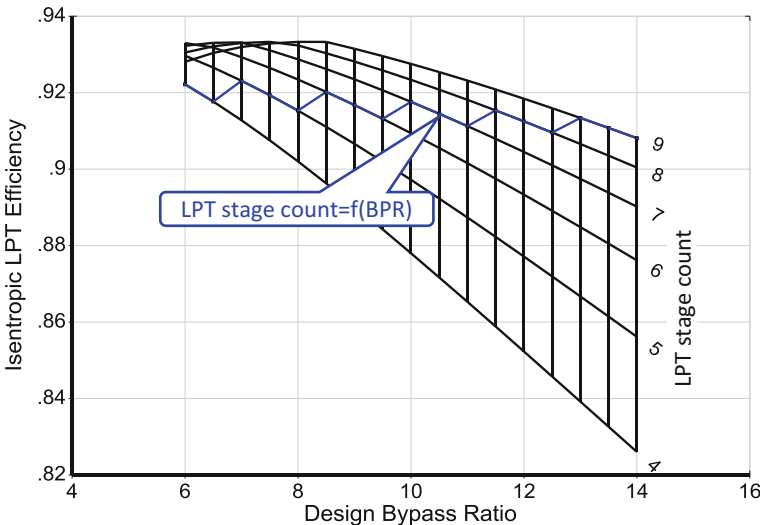


Fig. 1.5-6 LPT efficiency result from the velocity diagram analysis

The next two figures show some details of the LPT design. Our model describes a sort of “rubber engine” which changes its shape with design bypass ratio. Both the inner radius of the LPT at the turbine inlet and exit grow with bypass ratio. The slope of the hub at the turbine inlet increases also because this gives a shorter transition duct from the HPT to the LPT.

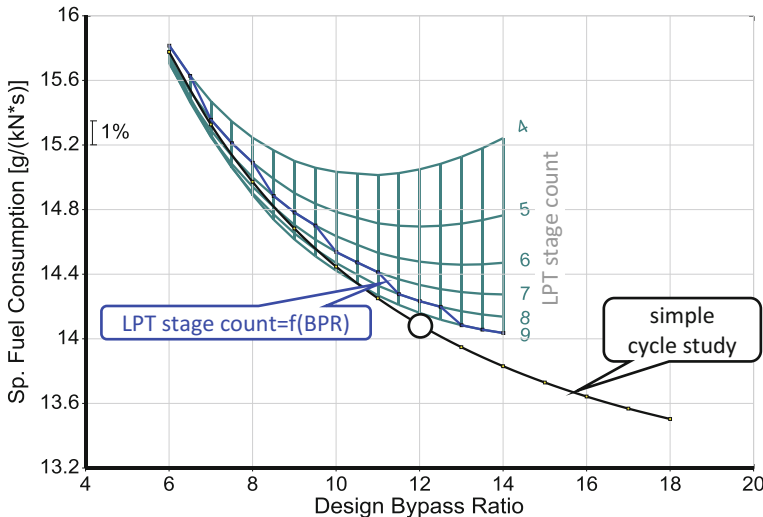


Fig. 1.5-7 Effect of LPT stage count on SFC

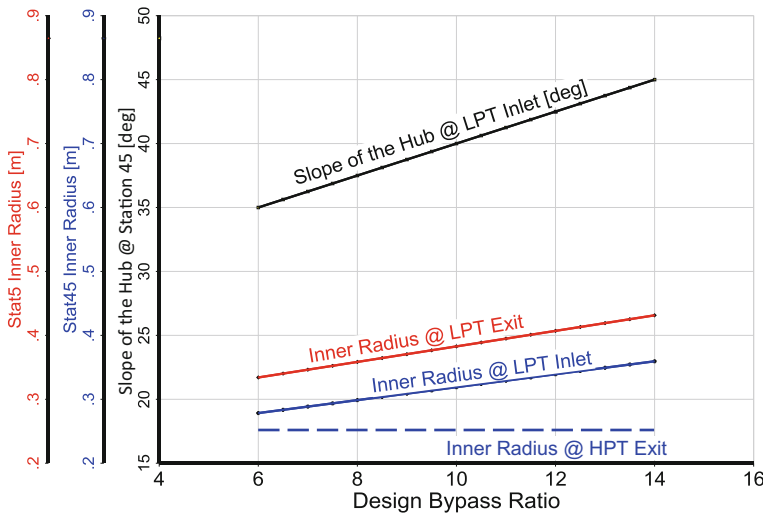


Fig. 1.5-8 Boundary conditions for the LPT

We do the velocity diagram analysis with the geometric boundary conditions of Fig. 1.5-8. Among many other details we get from the velocity diagram analysis are the hub/tip radius ratio as well as the Mach number at the LP turbine exit (Fig. 1.5-9). These two quantities influence the shape and dimensions of the exhaust system.

With all these assumptions, we get a reasonable idea of the behavior of our “rubber engine” model.

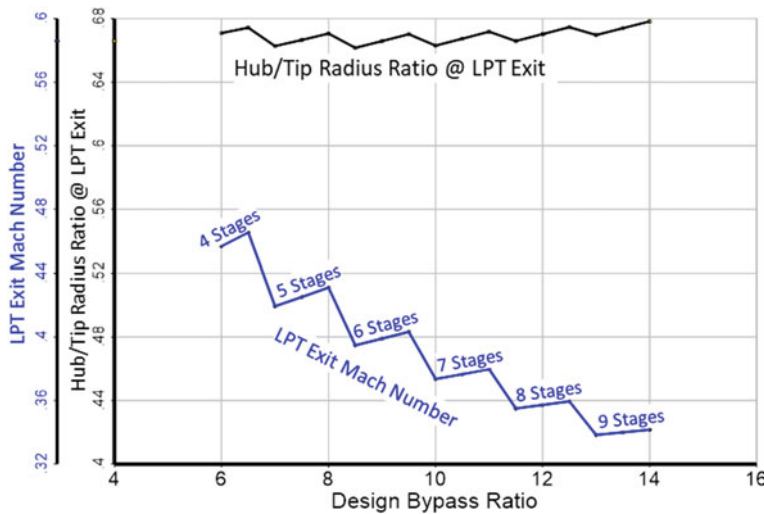


Fig. 1.5-9 Calculated hub/tip radius ratio and Mach number at the LPT exit

1.5.3.4 Effect of Spool Speed

In the next investigation we compare turbofans with and without a gearbox in a parametric study where fan tip speed is the major driver. It varies between 400 and 650 m/s and results in relative tip Mach numbers at Max Climb from 1.53 (BPR = 14) to 2.18 (BPR = 6).

Polytropic fan efficiency drops as soon as we deviate from the optimal aerodynamic loading of $\Delta H/U^2 = 0.4$, and this is seen in Fig. 1.5-10. Figure 1.5-11 shows that the best isentropic efficiency we can achieve increases slightly with bypass ratio because fan pressure ratio falls. Isentropic LPT efficiency is also affected by low circumferential speed in a different manner. That is illustrated in Fig. 1.5-12, where the range of efficiency difference over fan tip speed tends to be maintained as bypass ratio increases.

Figure 1.5-13 shows how SFC changes with fan tip speed. Low fan tip speed is certainly desirable for noise reasons; however, it increases specific fuel consumption, especially for the low bypass ratio engines.

SFC optimized engines with bypass ratios 6 and 12 have quite different cross sections. Note that in Fig. 1.5-14, not only is the annulus different but so are the disk shapes in the booster and the LPT. The stresses in each of the disks have been calculated—their shape is optimized for weight. The disk bore diameter can be much bigger in the high bypass ratio engine because of the low rotational speed. Therefore, the weight penalty for an 8 stage LPT, for example, is not as large as might be expected.

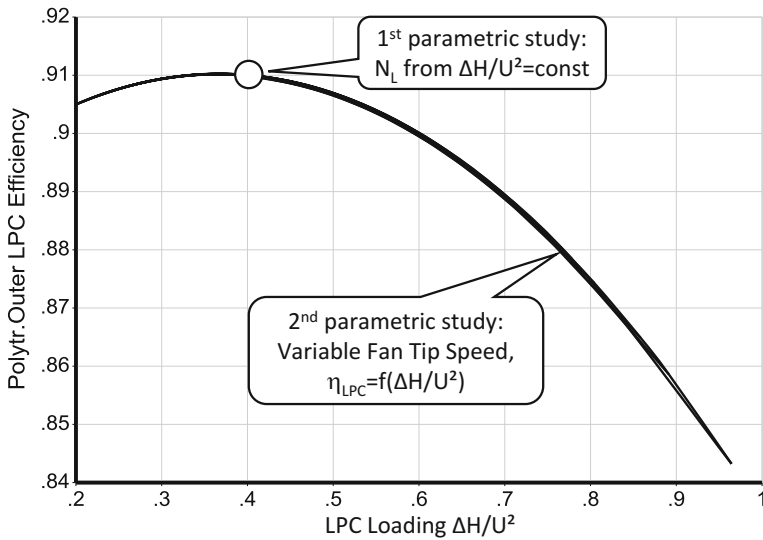


Fig. 1.5-10 Polytropic fan efficiency as function of the average pitch line loading $\Delta H/U^2$ [4]

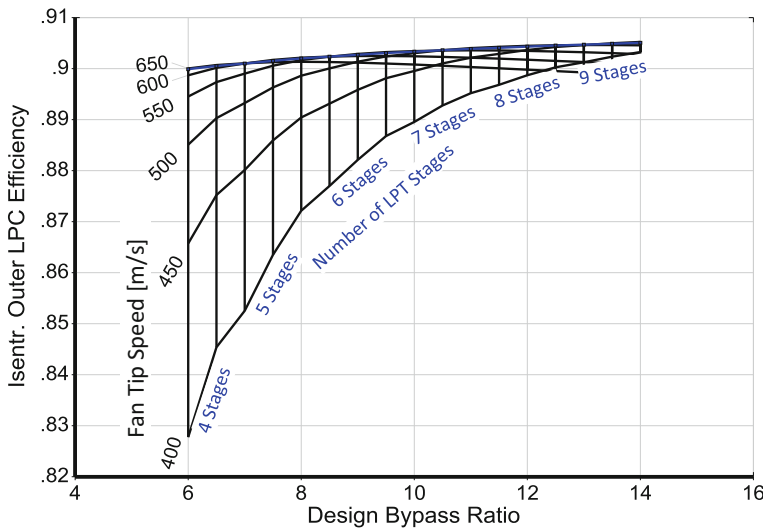


Fig. 1.5-11 Calculated isentropic fan efficiency

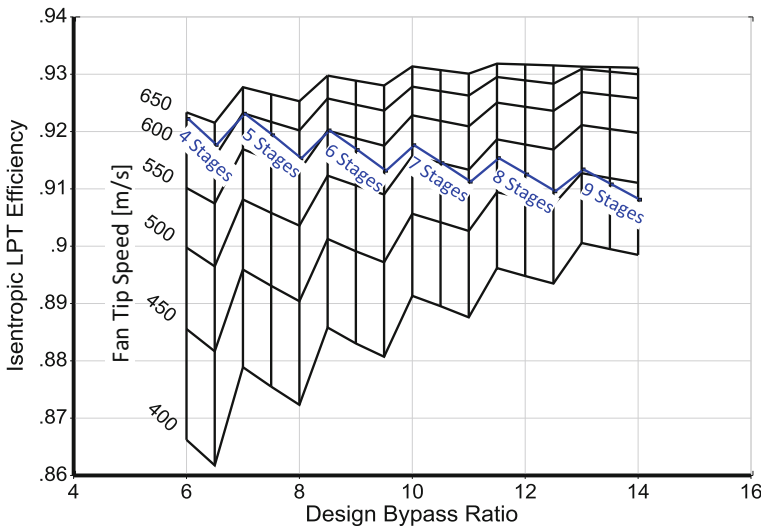


Fig. 1.5-12 Isentropic LPT efficiency

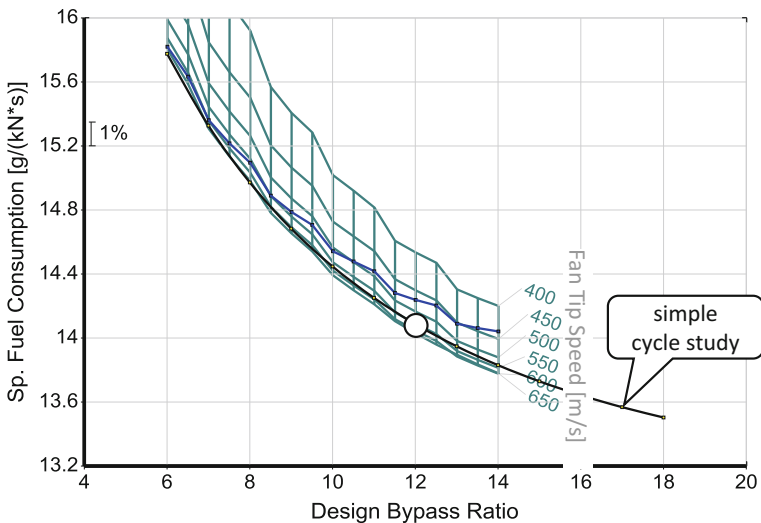


Fig. 1.5-13 Effect of fan tip speed on SFC

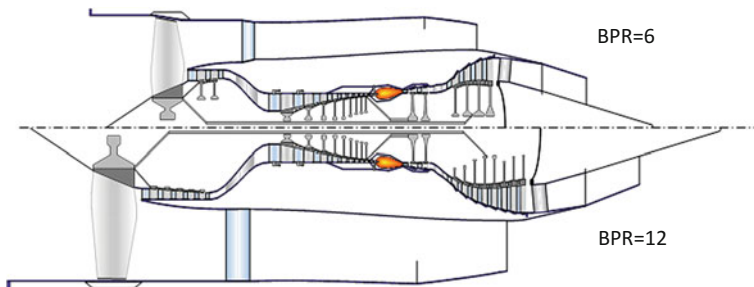


Fig. 1.5-14 Comparison of conventional turbofan models with $BPR = 6$ and 12

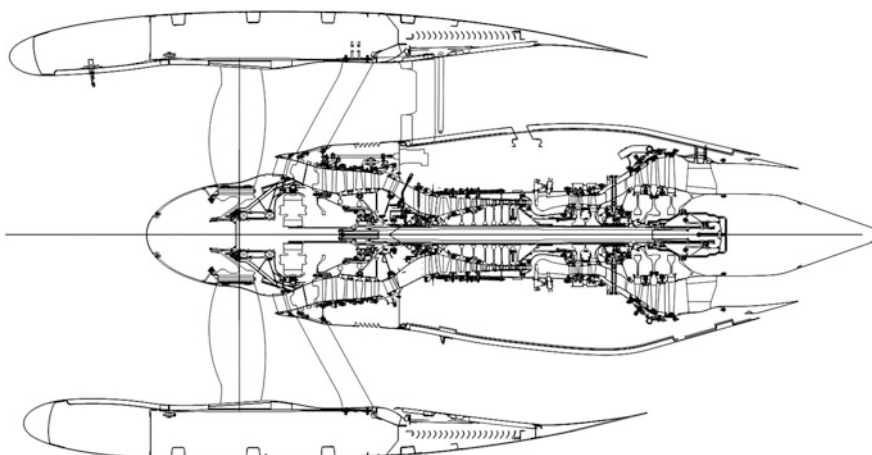


Fig. 1.5-15 PW1000G PurePower® Geared Turbofan™ Reproduced with permission from United Technologies Corporation, Pratt and Whitney

1.5.4 Turbofan with Gearbox

Conventional turbofans would need to have excessive numbers of low pressure turbine stages when the bypass ratio exceeds 12. Introducing a gearbox makes the rotational speed of the fan independent of that of the booster and the low pressure turbine. We need fewer booster and LPT stages and at the same time maintain the low aerodynamic loading levels required for good efficiency.

The bearing arrangement in a turbofan with gearbox differs from that of a direct drive turbofan, in which the front bearing structure is inside the compressor interduct. Mounting the gearbox and the fan spool requires an additional structure between fan and booster. Figure 1.5-15 shows as an example of a turbofan with gearbox the cross section of the PW1000G PurePower® Geared Turbofan™.

The layout of our study engine with bypass ratio 12 in Fig. 1.5-16, is very like that of the PW1000G. In the following analysis, we examine such turbofans with three booster and three LPT stages over a range of bypass ratio from 12 to 18. The flow path

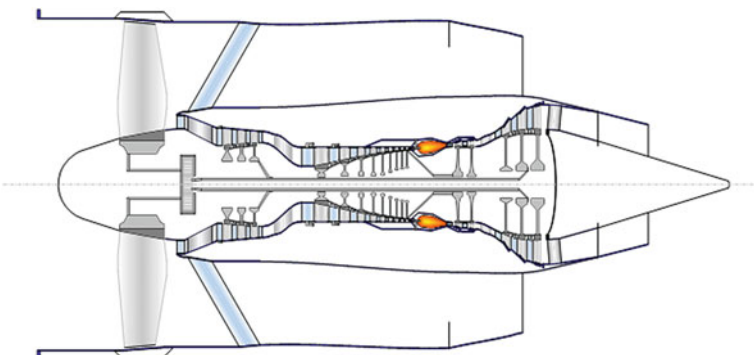


Fig. 1.5-16 Cross section of a turbofan with gearbox (bypass ratio 12)

of the core stream does not change very much. The important characteristic which changes with bypass ratio is not visible in the engine cross section: it is the gear ratio.

For the conventional turbofan we established the LP spool speed from the average fan pitch line loading of 0.4. The numbers of booster and LPT stages were increased with bypass ratio to keep the respective stage loadings within reasonable limits. This approach not only gave us the optimum fan efficiency but also the highest possible booster and LP turbine efficiencies.

Fan and LPT spool speeds for turbofans with gearbox are consequences of optimizing the gear ratio. Fan efficiency changes with average pitch line loading, as shown in Fig. 1.5-10, and LP turbine efficiency is a result of the velocity triangle analysis.

Figure 1.5-17 shows AN^2 (a measure of blade root stress) at the exit of the LPT for gear ratios between 2 and 3. The coloured contour bands represent specific fuel consumption of engines with bypass ratio 12. All the loss assumptions for the cycle calculation described above are the same as those used for the direct drive turbofan. We assume that the gearbox losses are 0.8% of the transferred shaft power.

The point with gear ratio 2.5 and $AN^2 = 40$ is a compromise between blade root stress, SFC and fan tip speed. Selecting a point with lower gear ratio and higher fan tip speed would yield only a slightly better SFC, but the noise generated by the fan would be significantly higher.

Repeating the parametric study for bypass ratio 18 yields the data in Fig. 1.5-18. It is reasonable to choose the gear ratio 3 as a practical design point because we get a lower fan tip speed and less blade root stress in the last LPT stage. In the following parametric study, we make the gear ratio a linear function of the design bypass ratio.

1.5.5 Comparison

Now we compare engines with and without gearbox more directly. Figure 1.5-19 compares sections of the most efficient direct drive turbofan and the optimized turbofan with gearbox each with a bypass ratio of 12 with gearbox. For thrust (see Fig. 1.5-20) and SFC (compare the numbers in Fig. 1.5-13 with those in

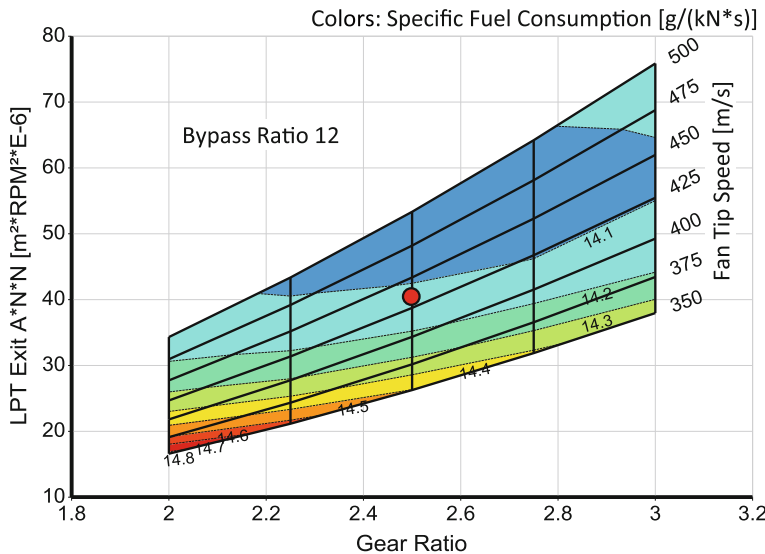


Fig. 1.5-17 Optimizing the gear ratio for the bypass ratio 12 engine

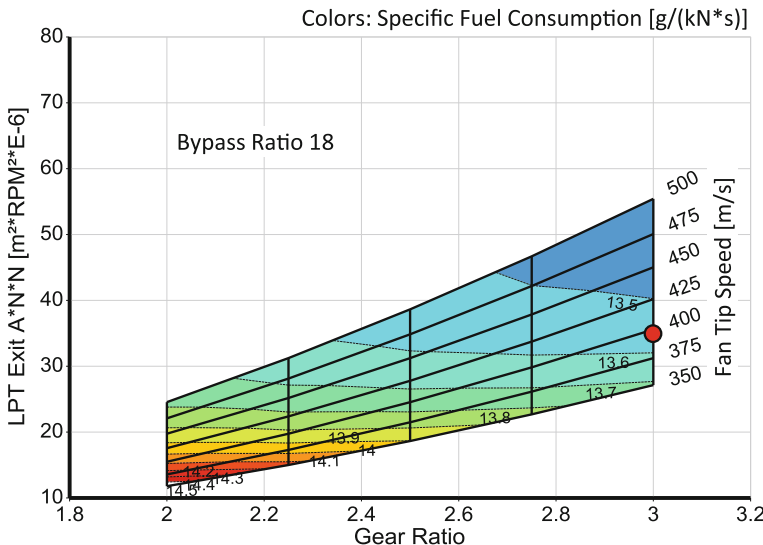


Fig. 1.5-18 Optimizing the gear ratio for the bypass ratio 18 engine

Fig. 1.5-17), the engines are essentially equal, however, there are many other significant differences worthy of discussion.

In the following figures, practical bypass ratio 12 engine designs are indicated by blue solid circles. The white open circles mark the design points of a conventional bypass ratio 6 turbofan and a bypass ratio 18 turbofan with gearbox.

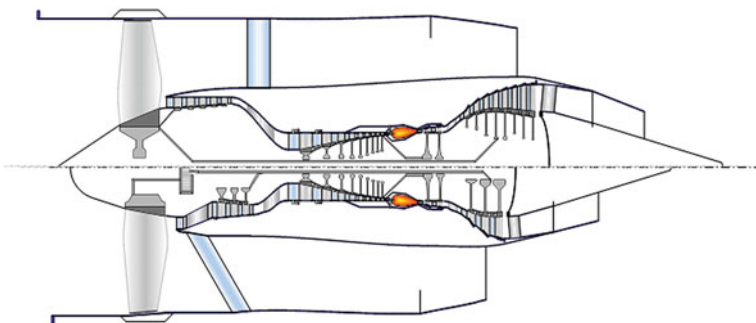


Fig. 1.5-19 Turbofans with and without gearbox, common core, bypass ratio 12

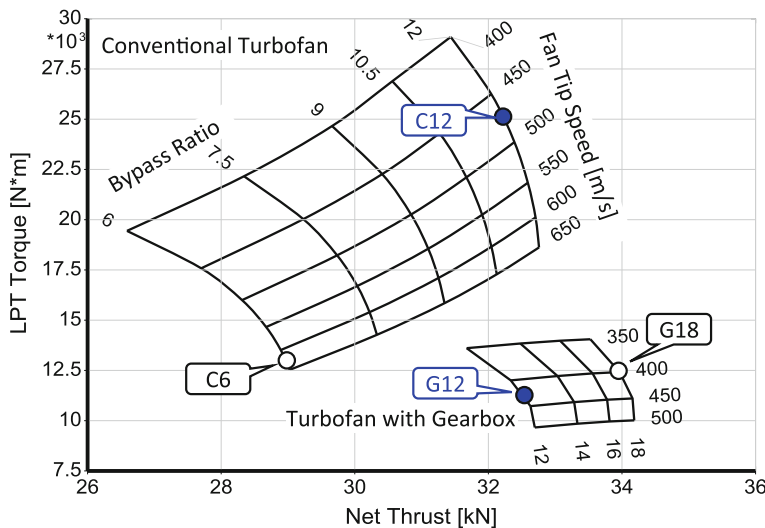


Fig. 1.5-20 Low pressure turbine torque

1.5.5.1 Mechanics

From the engine cross sections, we can immediately see that the booster and LPT disks of the turbofan with gearbox have a much smaller bore radius and a bigger bore width than those of its conventional counterpart. On the other hand, fewer stages are sufficient to achieve the same SFC. The fan will be lighter because of the lower rotational speed, but the weight penalty of the gearbox and the additional oil cooler must also be considered. In summary, it is difficult to know which of the two engines will be lighter.

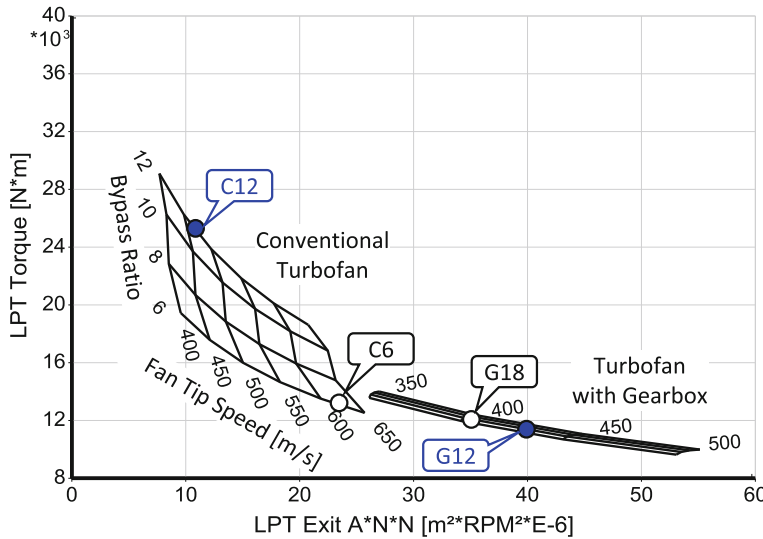


Fig. 1.5-21 LPT torque and AN^2 at the LPT exit

The power to be transferred to the fan and the booster is the same for the two BPR 12 engines. However, remember that the torque in the LPT shaft is inversely proportional to the spool speed. The upper limit for the bypass ratio of a conventional turbofan may be restricted by the disk bore diameter of the core components and the resulting maximum permissible LPT shaft torque.

The low LPT shaft torque advantage of the turbofan with gearbox is accompanied by a very significant increase in the blade root stress in the last LPT stage, expressed as AN^2 in Fig. 1.5-21. The actual blade root stress can be reduced by using noticeably tapered hollow blades made from a material with low density. It is a challenge to design tapered turbine blades for highly efficient work extraction as the pitch to chord ratio at the blade root will be quite different to that at the blade tip. Conventional LP turbines do not pose such a stress problem and their aerodynamic design can be optimized without exceptional mechanical constraints.

1.5.5.2 Aerodynamics

The differences in the aerodynamics of the booster and the LPT originate from the dissimilar spool speeds. As we see from Fig. 1.5-22, the booster stages of a direct drive turbofan produce only a very modest pressure ratio because the circumferential speed is so low.

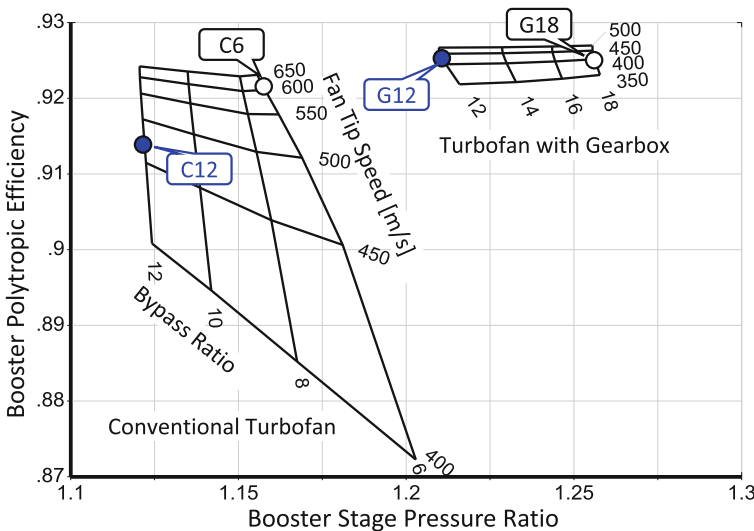


Fig. 1.5-22 Stage pressure ratio and efficiency of the booster

With a gearbox, however, we can achieve quite high stage pressure ratios and therefore the booster stage count of such a turbofan can be lower than in a direct drive turbofan. Similarly, the modest aerodynamic loading of the LPT allows a lower stage count for this component.

Figure 1.5-23 shows the blade tip speed of the fan—which can be regarded as a crude measure of fan noise—and the LPT efficiency. The two BPR 12 engines have similar fan tip speeds and will therefore not differ noticeably in fan noise.

The efficiency of the three stage LPT of the turbofan with gearbox is better than that of its conventional eight stage LPT counterpart due to the lower aerodynamic loading, see Fig. 1.5-24. Note that in this preliminary engine design study we did not apply any efficiency decrement for the mechanically challenging blade design of the high speed LPT.

Figure 1.5-25 shows the specific fuel consumption over the full range of bypass ratios for the uninstalled engine at Max Climb rating. No minimum exists as SFC gets continuously better when bypass ratio increases. However, if we consider the engine together with the nacelle, then we reach a minimum for the corresponding *installed SFC* because nacelle drag increases with bypass ratio. This minimum is somewhere in the region between bypass ratios 13 and 16. The precise number depends on the aircraft design and its mission.

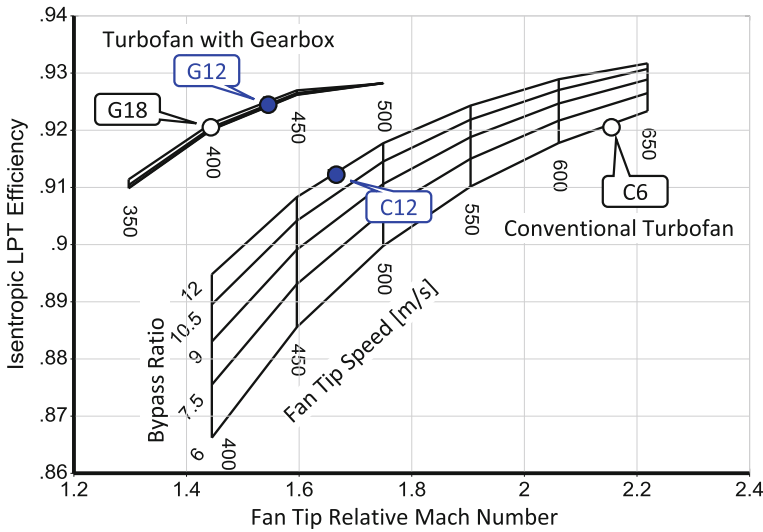


Fig. 1.5-23 LPC (Fan) tip speed and LPT efficiency

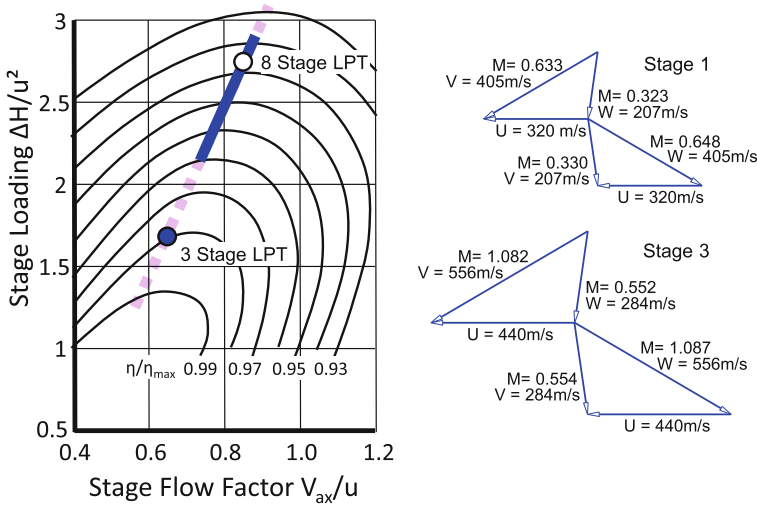


Fig. 1.5-24 The 3 stage LPT design point of the bypass ratio 12 turbofan with gearbox

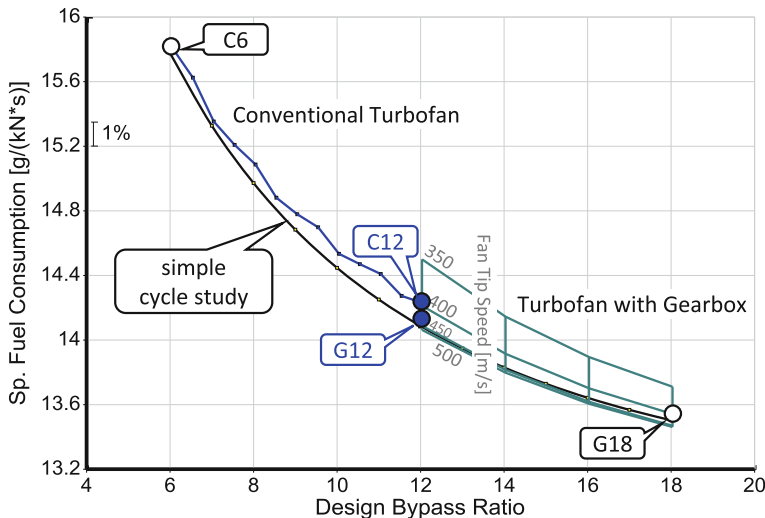


Fig. 1.5-25 Specific fuel consumption

1.5.6 The Fundamental Differences

Four selected engine design points are marked in the preceding figures. Let's compare their cross sections in Figs. 1.5-3, 1.5-14, 1.5-19 and 1.5-26 to see the main differences in the flow paths. Table 1.5-3 lists the design parameters that are most relevant for the comparison of turbofans with and without a gearbox.

The fundamental differences between the two engine configurations are highlighted with bold letters in the columns 2 and 3. Note that we see no significant SFC advantage for the turbofan with gearbox if we compare it with a conventional turbofan at a bypass ratio of 12.

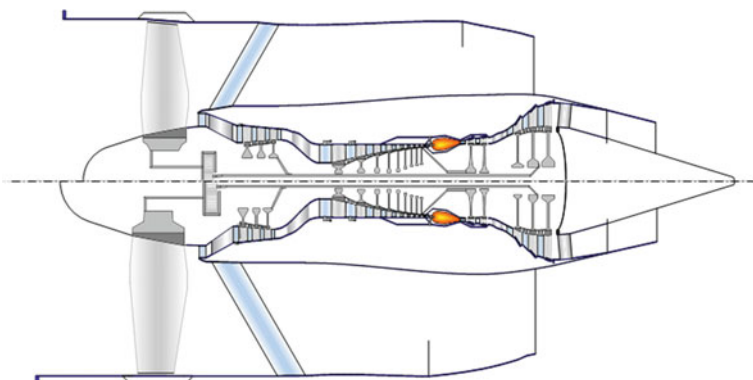


Fig. 1.5-26 Turbofans with gearbox, bypass ratio 12 and 18

Table 1.5-3 Important design parameters

Engine configuration	C6	C12	G12	G18
Bypass ratio	6	12	12	18
Gear ratio	n/a	n/a	2.5	3
Fan tip diameter [m]	1.60	2.19	2.19	2.64
Fan pressure ratio	2.136	1.543	1.548	1.358
Fan tip relative mach number	2.18	1.66	1.54	1.44
Booster pressure ratio	1.34	1.78	1.77	1.98
Booster stage count	2	5	3	3
LPT pressure ratio	7.23	8.96	8.96	9.75
LPT torque [kN*m]	12.8	25.2	11.2	12.5
LPT AN ² [m ² RPM ² *10 ⁻⁶]	24.8	10.8	40	35
LPT stage loading ΔH/U ²	2.10	2.71	1.69	2.08
LPT isentropic efficiency	0.922	0.913	0.925	0.920
LPT stage count	4	8	3	3
SFC@Max Climb, 35000 ft Mach 0.8	15.8	14.2	14.1	13.6

Noise is of course not relevant during flight at altitude. Nevertheless, we can use fan tip relative Mach number at Max Climb as an indicator of take off noise. Due to our spool speed selection, the direct drive turbofan emits more noise than the variant with gearbox.

The fan is not the only source of noise, because the low pressure turbine also contributes to the total acoustic emission. Noise originating in the high speed LPT of the turbofan with gearbox is generated at a very high frequency, much higher than the noise from the LPT of a direct drive turbofan. This is an advantage because high frequency noise attenuates quickly with increasing distance.

Table 1.5-4 shows mass data and parts count for the low pressure components. These data have been calculated with rather crude assumptions which are certainly debatable. Nevertheless, the blade and vane counts of the direct drive turbofan will be much bigger in any case than those of the turbofan with gearbox.

The booster of the engine variant with gearbox has about the same mass as the booster of an engine with direct drive—despite the lower stage count and the

Table 1.5-4 Component mass and parts count

Engine configuration	C6	C12	G12	G18
Bypass ratio	6	12	12	18
Gear ratio	n/a	n/a	2.5	3
Fan mass [kg]	333	826	736	1370
No of rotor blades	30	30	30	30
No of bypass exit vanes	19	19	25	25
No of core exit vanes	74	111	52	69
Booster mass [kg]	45.4	128	100	109
No of blades and vanes	568	2072	890	1106
LPT mass [kg]	252	500	244	221
No of blades and vanes	1207	3599	733	736

smaller diameter. This is because the disks are much heavier since they rotate so fast. The three stage LPT of the turbofan with gearbox is lighter than the eight-stage turbine of the engine with direct drive, but it is heavier than the stage count ratio of 3/8 would lead us to expect. This is again due to the high rotational speed, which results in heavy disks.

If we consider the weight of the gearbox and the indispensable oil cooler, it's hard to conclude which of the engines is lighter overall. To make a reliable weight statement would require more detailed design studies.

1.6 Mission Analysis

Market requirements drive any new gas turbine design project. These requirements originate from the application of the engine: the aircraft must be able to fly its missions economically. Mission performance is what a customer pays for. The mission determines the engine cycle, while engine size is usually based on an individual maneuver.

1.6.1 General Requirements

It is self-evident that the overall efficiency should be as high as possible under any given set of circumstances. However, quite severe compromises in thermal and propulsive efficiency are often necessary. In pursuit of reduced fuel burn, a low value of SFC is frequently selected as the arbiter of success, but if low SFC can only be achieved by high engine weight, then it is possible that more fuel could be used. In such a situation, we must take a broad view of mission analysis and "fly the mission" in an analytical sense to estimate how much fuel is needed. In addition to fuel costs, an overarching restriction has been placed on us in relatively recent years by international mandates on emissions. These are separate from the internal design limits that all engine companies espouse and—like noise restrictions—are unavoidable in the interests of our environment.

Figure 1.6-1 shows performance and other design considerations for three different applications of a turbojet. Fuel consumption is not the top priority for a business jet engine, where low acquisition costs and long life are more important. Simple designs with limited overall pressure ratio and burner exit temperature are the consequence. A lift engine needs to have high power per weight and volume; here SFC is less important. Low fuel consumption is important if the aircraft mission contains long cruise phases. The fuel weight reduction easily compensates the relatively high weight of the engine.

As said before, an engine is competitive almost always, if thermal and propulsive efficiencies are high. That means specific fuel consumption $SFC = W_F/F_N$ must be low. Weight is also important; it is measured by the ratios thrust/weight, thrust/volume, and thrust/mass flow (= specific thrust). Thrust per frontal area is an important criterion for supersonic aircraft propulsion.

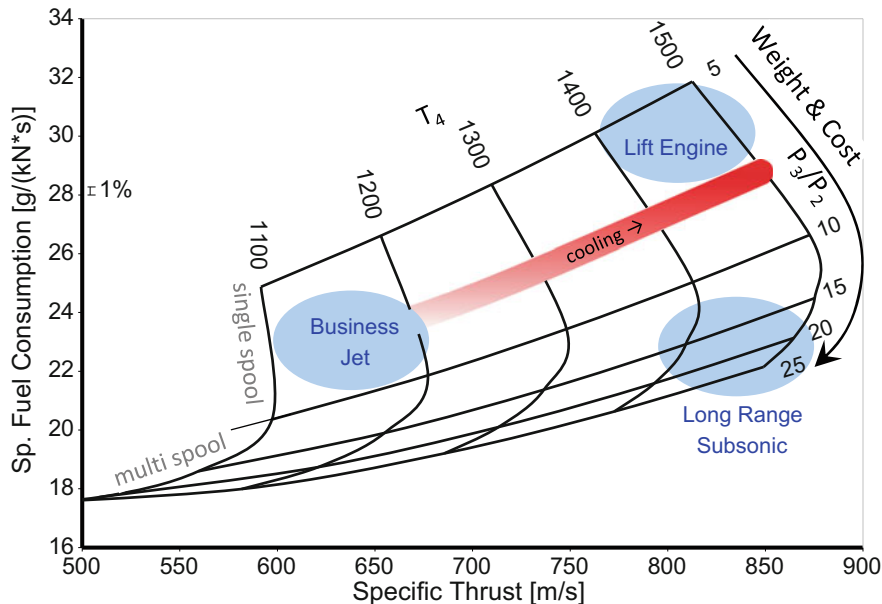


Fig. 1.6-1 Performance and design considerations for a turbojet

Environmental legislation requires both low noise (which favors high bypass ratio due to the lower jet velocity) and low emissions which is easier to achieve if burner pressure is low. The engine must operate without surge or flame-out during transients, and it must be tolerant to inlet flow distortion, rain, and hail ingestion. In other words: operability must be guaranteed. Additionally, manufacturing cost should be low, the engine should be reliable and easy to maintain, and all parts should be accessible without difficulty.

To achieve all that, a new engine must approach the limits of technology in aerodynamics, thermodynamics, structural design, and materials. Risks are high because the interactions of all the disciplines involved preclude an infallible prediction of how the system will behave. Thus, in pursuit of that, a thorough analysis of the system is needed.

1.6.2 Single Point Design

Performance is most important for some applications like power generation in which the gas turbine often operates at full power in a narrow range of ambient conditions for very long periods between shut-downs. We can select the cycle for such an application such that performance is best at the nominal operating condition. However, virtually all gas turbines need to run at a range of ambient pressures,

temperatures, and spool speeds. Note that industrial gas turbines for power generation operate at a constant physical speed after start-up, but the corrected speed—which really determines the operating point—is affected by ambient temperature and that can vary significantly from day to night and from winter to summer. Part-load operation is also essential, so we must consider the off-design behavior even in the very early design phase. Moreover, we should consider other applications than those the engine was designed for and should also consider potential derivatives, mostly power-enhanced versions of the baseline engine.

Figure 1.6-2 shows the result from a typical parametric cycle design point study. Overall pressure ratio P_3/P_2 and burner exit temperature T_4 are the main variables; the compressor inlet mass flow (i.e. engine size) is constant in this exercise.

From cost considerations, it is desirable to make use of an uncooled power turbine. Let us assume that this limits its inlet temperature T_{45} to 1300 K. For the same cost reason, we intend to use a single stage high pressure turbine HPT, and this restricts its pressure ratio to about four. The “forbidden” regions in the carpet are highlighted in color. For the best cycle in terms of specific fuel consumption we get a pressure ratio of about 20 and a burner exit temperature T_4 of 1710 K.

It is quite common to use figures with boundaries that limit the design space but keep in mind that such boundaries usually are not so hard! In our example, the permissible temperature for the low pressure turbine inlet temperature T_{45} depends on the material. The HPT pressure ratio will affect the achievable efficiency, but there is no such thing like a hard stop at $P_4/P_{45} = 4$.

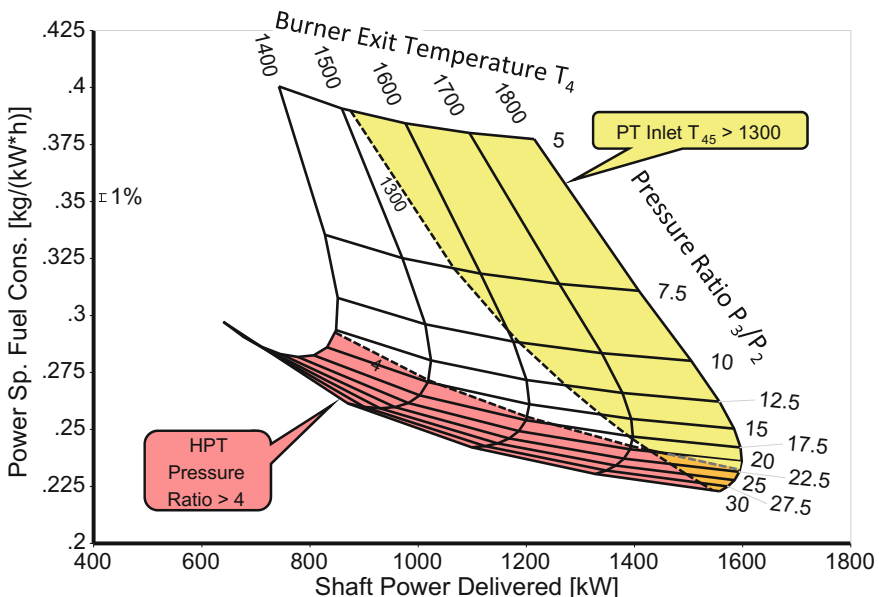


Fig. 1.6-2 Two-spool turboshaft cycle parametric study

During the last years the term *core size* has become popular as a quality criterion to be considered during preliminary design. Unless a customer is adamant about using existing hardware, there is no firm limit at all for the *core size* and therefore a line of constant core size can never be a strict technical boundary for the engine design space.

1.6.3 *Multi-point Design*

The term *Multi-point Design* can be misleading. You might think that the results from several cycle design calculations—each of which fulfills the requirements of a different operating condition—are somehow combined into a single cycle which fulfills all the requirements simultaneously. This, however, is impossible to do. There can be only one cycle design point because this determines the flow areas at the various thermodynamic stations implicitly.

Looking at the printout of a cycle design calculation makes this obvious because it contains the nozzle throat and exit areas as well as calculated values of corrected flow $W\sqrt{T}/P$ at all the other thermodynamic stations. Now remember that corrected flow per area $W\sqrt{T}/(P \times A)$ depends primarily on the local Mach number. If you make reasonable assumptions for the cycle design point Mach numbers at the thermodynamic stations, then you get all the local flow areas from the $W\sqrt{T}/P$ values.

The Mach numbers at the thermodynamic stations (except stations 8 and 9) are all subsonic. In a theoretical *Multi-point Design* study, you could adjust the local Mach numbers in such a way that you get the same flow area for each of these thermodynamic stations from several cycle design calculations. However, one problem would remain. Even if you could get the same areas with reasonable Mach numbers at all thermodynamic stations, the turbine throat areas would still be different for each cycle design point. This is because the Mach number in the throat of the inlet guide vane of any turbine is always sonic or very close. Thus $W\sqrt{T}/(P \times A)$ is the same for all turbines and we can calculate the turbine throat area unambiguously from $W\sqrt{T}/P$.

In general, each cycle design calculation yields different flow area values, not only for the nozzle throat but also for the areas at all the other thermodynamic stations. Combining the results from two or more cycle design calculations into one cycle would be only feasible if the nozzle(s) and the turbine(s) had variable geometry. If we want to design an engine with fixed nozzle area and no variable guide vanes in the turbines, then there can be only one cycle design point.

A *Multi-point Design* exercise, as we understand it, begins with a single cycle design point calculation which defines the geometry of the engine. Then we do off-design calculations (i.e. calculations with given geometry) for all the other operating conditions which need to be considered. It is here that the phrase “compromise to optimize” comes into effect! The successful design must meet the

most-demanding maneuver but in so-doing it may turn out to be “over-designed” for other operating conditions.

1.6.3.1 Commercial Aircraft

The mission of a commercial subsonic aircraft for passenger transport consists of the sequence *roll to runway—take off—climb—cruise—descent—land—roll to gate*. The engine ratings during these phases are *Ground Idle—Take Off—Climb—Cruise—Flight Idle—Reverse—Ground Idle*.

Two of these operating conditions are most relevant for the design of a turbofan: *Hot Day Take Off* at sea level and Max Climb at cruise altitude. The highest burner exit temperatures and spool speeds occur during Take Off when ambient temperature is 15 °C above ISA temperature (our definition of a hot day). The air is much colder at the end of the climb and what is then more important for the gas turbine is that the total temperature T_2 at the engine face is much lower than it was at Take Off. Since the absolute spool speeds at Max Climb are still relatively high, the corrected spool speeds $N_L/\sqrt{T_2}$ and $N_H/\sqrt{T_{25}}$ are much higher than at Take Off.

Figure 1.6-3 shows typical variations of some relevant parameters at Max Climb, cruise and Hot Day Take Off as the relative corrected LP spool speed changes. The cycle design point is Max Climb at 11 km altitude, Mach 0.8. The most important off-design points are cruise and the mechanical design point Hot Day Take Off at sea level, Mach 0.2, ISA + 15 K. Note that the fan efficiency at cruise is significantly higher than at Max Climb, which is usually the fan design point. This efficiency difference is the main reason the specific fuel consumption reaches its minimum during cruise.

From a cycle design point of view, the other segments of the mission are not demanding. However, they are important for the design of the combustion chamber, customer bleed air system, oil system and for the operability of the engine.

Typically, the cycle selection for a commercial airliner leads to a two-point design:

1. The cycle design point is Max Climb at cruise altitude. This cycle determines the size of the annulus areas at all thermodynamic stations.
2. The mechanical and cooling system design point is Hot Day Take Off where maximum temperatures and spool speeds are encountered. This is an off-design operating point from an aero-thermodynamic point of view.

So, we set the cycle design Mach numbers at Max Climb at all thermodynamic stations as high as the design constraints allow for compressors, ducts and turbines. The Mach number at the fan face determines the fan inlet diameter (together with the corrected flow and an assumption for the hub/tip radius ratio). Bear in mind that the fan efficiency in the cycle design point calculation must be kept lower than the efficiency we expect under cruise conditions.

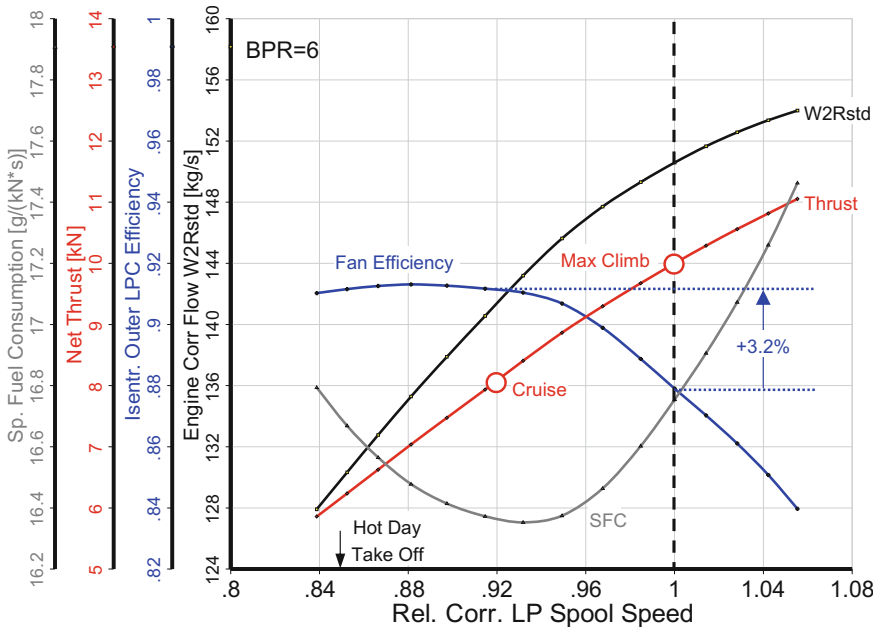


Fig. 1.6-3 Typical relations between Max Climb, Cruise and Hot Day Take Off

We can present the most important parameters in carpet plots, just as in the case of a single-point design. The carpet lines in Fig. 1.6-4 denote the cycle design point data of a bypass ratio 6 turbofan which delivers 10 kN of Max Climb thrust at 11 km altitude, Mach 0.8, ISA. The colors represent an off-design number: the relative high pressure spool speed needed for 32 kN Hot Day Take Off thrust at sea level, Mach 0.2, ISA + 15 K. Of course, we could have shown any of the Hot Day Take Off cycle properties as contour lines in the cycle design carpet but regardless of this, by identifying the corresponding relative LP spool speeds, we can evaluate and compare data from the two most important operating conditions in a single picture.

1.6.3.2 Fighter Aircraft

The engine selection for a fighter aircraft is a more complex iterative process which seeks the lightest aircraft/engine combination considering a mix of several missions. Many military missions are much more demanding than those of a commercial airliner. However, there are purely subsonic military missions with long cruise legs (ferry flights) and those with extended loiter phases.

In great contrast to commercial flights, are missions like “Minimum Time Intercept” which require high acceleration and climb rates to quickly reach supersonic velocity at high altitude. The aircraft must not only be able to fly these

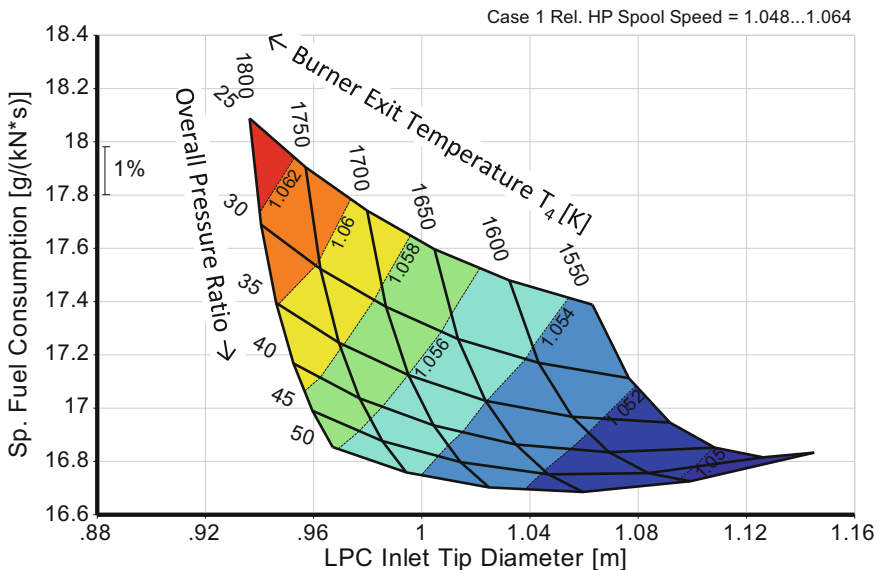


Fig. 1.6-4 Max Climb and Take Off results in a single picture

missions economically, it also must have enough thrust to accomplish specific maneuvers which, for example, require minimum sustained turn rates or a certain specific excess power.

Let us consider a low bypass ratio turbofan engine in the context of the flight envelope. The limiting parameter for the maximum achievable thrust depends on the prevailing altitude and Mach number combination. At such a condition, we must not surpass certain limiting values for the spool speeds N_L and N_H , the corrected fan speed $N_L/\sqrt{T_2}$, compressor exit temperature T_3 , the pressure P_3 in the combustion chamber and the temperature T_{45} at the low pressure turbine inlet.

- Excessive spool speed would be a problem for the compressor and turbine disks.
- Fan flutter sets the maximum permissible value for $N_L/\sqrt{T_2}$.
- Compressor exit temperature T_3 is the temperature of the last compressor disk—the disk material determines how much T_3 is tolerable. Moreover, T_3 is the temperature of the turbine cooling air, which in turn affects the AN² limit for the HP turbine.
- The combustion chamber is a pressure vessel which can withstand only a certain P_3 value.
- The low pressure turbine inlet temperature T_{45} is the substitute for burner exit temperature T_4 which is impossible to measure.

Figure 1.6-5 shows which of the limiters determines the maximal achievable thrust. In the upper left region of the flight envelope this happens to be the corrected fan speed $N_L/\sqrt{T_2}$. Maximum permissible T_3 and T_{45} are the active limits in the

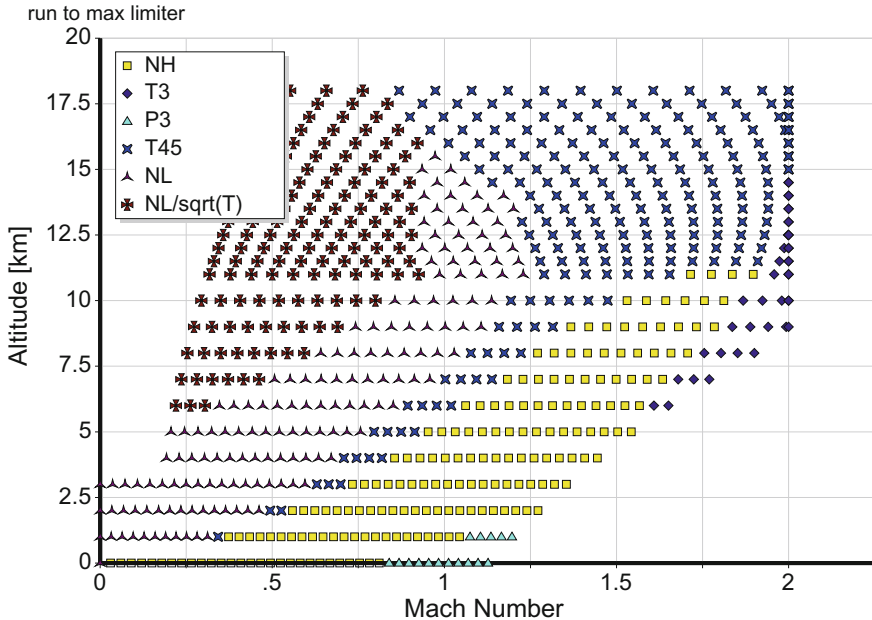


Fig. 1.6-5 Limiters in the flight envelope

upper right region, where the aircraft flies supersonically. The P_3 limiter comes into play during low-level high-speed flight. Spool speeds and T_{45} are the active limiters in the center of the flight envelope.

In Fig. 1.6-6 we have identified some typical parts of fighter aircraft missions in the flight envelope. The dashed lines mark the corrected fan speed for maximum thrust and all the limiters from Fig. 1.6-5 are active. The line of $\text{Rel } N_L/\sqrt{T_2} = 1$ divides the flight envelope into two roughly equal parts. Selecting sea level static conditions (the origin of the plot) as the cycle design point is a good compromise.

Of course, it is not sufficient to consider only the cycle design point—we must also scrutinize the operation at the corners of the flight envelope. Special attention should be given to the upper left corner, where we encounter the lowest Reynolds numbers and the biggest impact of any power offtake on the cycle.

Figure 1.6-7 shows how the *Reynolds Number Index* varies within the flight envelope. This index relates the prevailing Reynolds number to that at sea-level static conditions. RNI is very low in the upper left corner of the flight envelope because the Reynolds numbers encountered there are only about 10% of those at sea level static. Decreasing Reynolds numbers weaken the cycle because component efficiencies deteriorate, and the flow capacities of compressors and turbines are reduced. The operating line in the core compressor map moves upwards and since the surge line moves downwards, the reduction in surge margin is magnified quite markedly.

Any mechanical power offtake (electrical or hydraulic power for aircraft purposes) shifts the core compressor operating line towards the surge line. This shift is

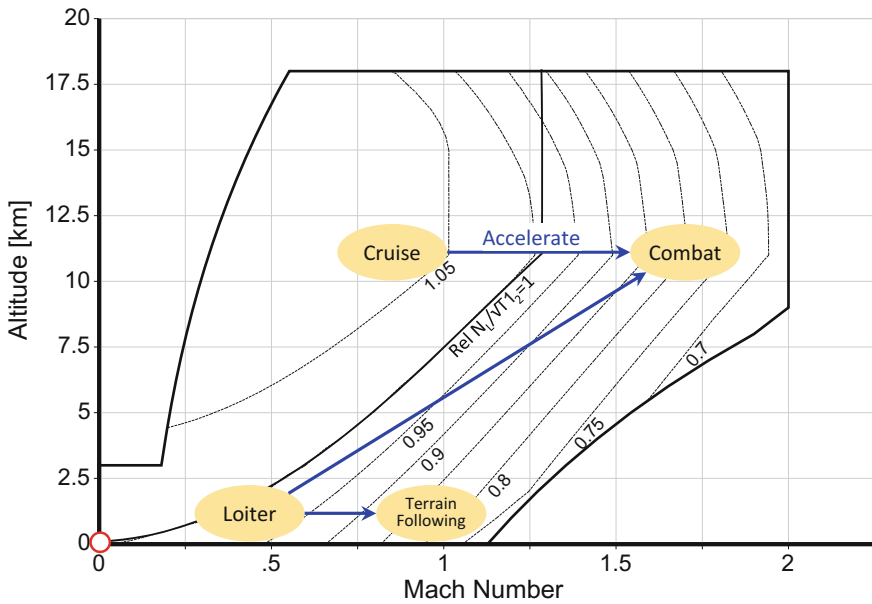


Fig. 1.6-6 Flight envelope of a fighter aircraft with lines of constant relative $N_L / \sqrt{T_2}$

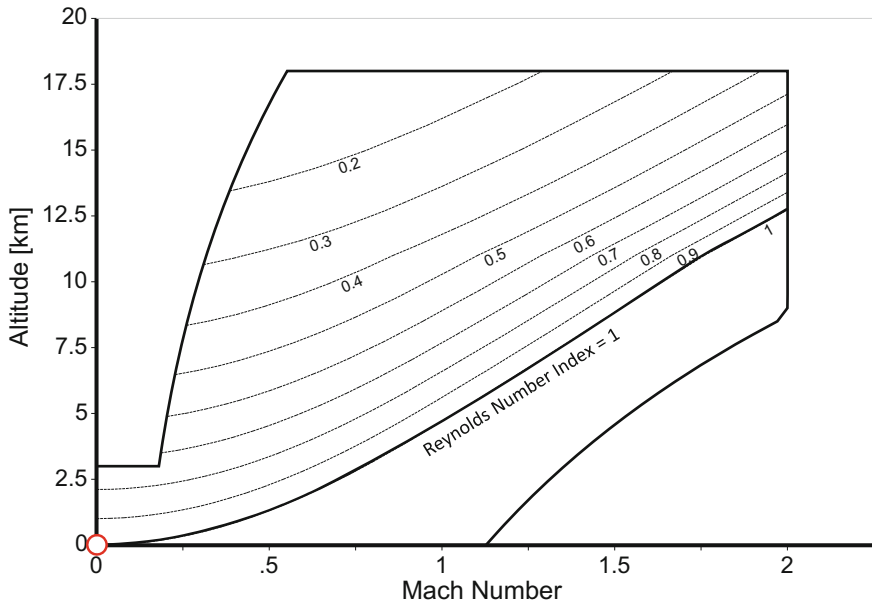


Fig. 1.6-7 Reynolds number index $RNI = Re/Re_{SLS}$

small at sea level because the power offtake is only a small fraction of the high pressure turbine power. However, the same power offtake is a much bigger fraction of turbine power when inlet total pressure P_2 is low. Have a look at Fig. 1.6-8: 1 kW power offtake at sea level is equivalent to 12 kW power offtake at 18 km Mach 0.55. The resulting shift of the core compressor operating line is significant.

The erosion of core compressor surge margin at altitude is not only due to Reynolds number and power offtake effects. Even moderate inlet flow distortion and engine deterioration can lead to surge if the surge margin at the cycle design point is not sufficient.

The upper left-hand region of the flight envelope is an aero-thermodynamic problem area in general. The most critical conditions from a stress and cooling point of view happen to be at the lower right corner of the flight envelope, corresponding to maximum Mach number at a modest altitude—where dynamic pressure effects are highest.

The engine cannot be defined without checking the aircraft performance. The mission segments that use most fuel should be targeted for any compromises in the design of both engine and aircraft. It is unlikely that any single maneuver, due to the small amount of fuel used when compared to a mission phase, will have much influence on the cycle. However, individual maneuvers determine the engine size.

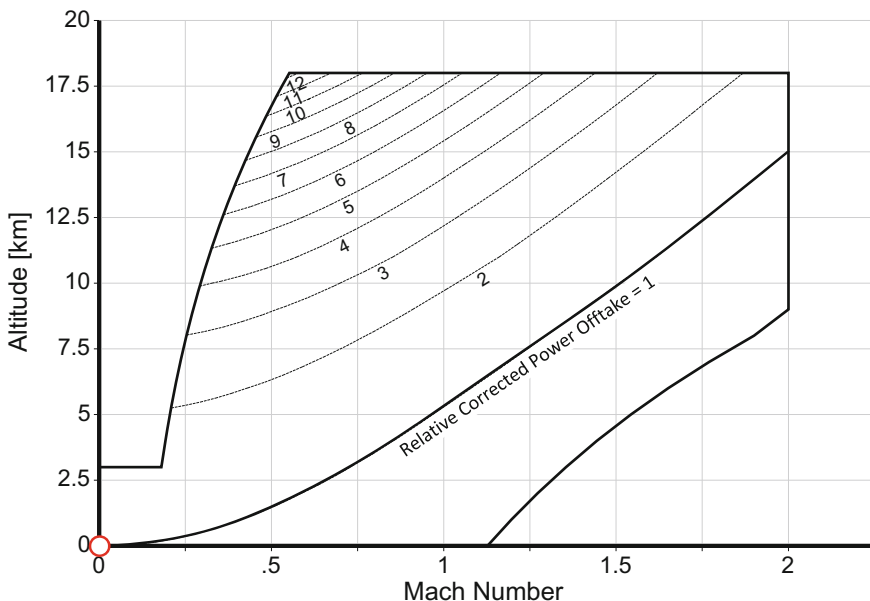


Fig. 1.6-8 Relative corrected power offtake

1.6.4 High Speed Propulsion

What are the limits of the gas turbine; how fast can we fly with a turbofan or a turbojet? We will show that the highest achievable speed is somewhere between the flight Mach numbers 3 and 4. If we want to fly faster, we need a ramjet, perhaps in combination with a gas turbine which operates only during take off, acceleration and the return segments of the mission. First, we look at the thermodynamic cycles of turbojets and turbofans and calculate the so-called *point performance* for altitude/Mach number combinations on a line in the middle of the flight envelope, where we are likely to fly most often.

The left and right boundaries of this flight envelope are lines of constant equivalent air speed EAS. The lower EAS boundary represents an aerodynamic limit (the maximum lift coefficient), the upper EAS boundary is a structural limit of the air vehicle, where the pressure difference across the engine casings are greatest. The EAS boundary values in Fig. 1.6-9 are typical for modern fighter aircraft which achieve a maximum speed of around Mach 2. Aircraft designed for Mach 3+—like the famous Blackbird SR-71—have more narrow flight envelopes, typically 310 to 420 knots EAS for the lower and upper EAS limits respectively.

Lines of constant stagnation temperature T_2 are also features of the flight envelope in Fig. 1.6-9. In the top right corner, this temperature is close to the material temperature limit of modern compressor disks. There would be only a small temperature margin left for compressing air—if that made sense at all.

1.6.4.1 Point Performance

Point performance is the result of a thermodynamic cycle design calculation for some combination of altitude and Mach number. The *cycle design* calculation mode yields a different engine geometry for each different pass through the mathematical model.

Let us consider points on a flight path in the middle of the SR-71 flight envelope with an EAS of 375 knots. Specific fuel consumption and specific thrust (thrust per unit of airflow, expressed as $N/(kg/s) = m/s$) are two most important characteristics. For a given thrust: does the engine with the highest specific thrust have the smallest dimensions?

1.6.4.2 Turbojet

We begin our studies with the simplest gas turbine, the straight turbojet without afterburner. Figure 1.6-10 shows the thermodynamic stations.

We use the following assumptions in our cycle studies, beginning with the aircraft intake.

- (i) The total pressure recovery is a function of Mach number (defined in MIL-E-5007):

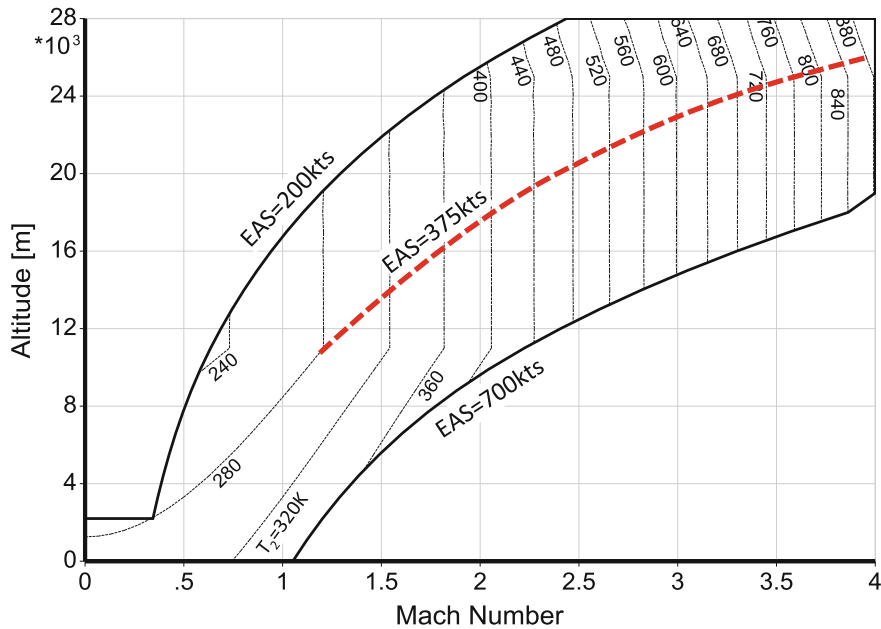


Fig. 1.6-9 Flight envelope with lines of constant T_2

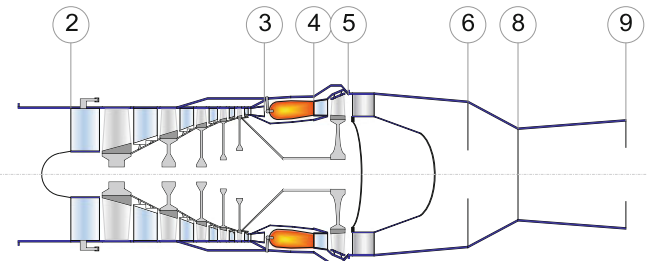


Fig. 1.6-10 Turbojet nomenclature

$$\frac{P_2}{P_1} = 1 - 0.075 * (M - 1)^{1.35} \quad (1.6-1)$$

- (ii) The polytropic efficiencies of compressors and turbines are 0.9 and burner pressure ratio P_4/P_3 is 0.97.
- (iii) The amount of turbine cooling air depends on burner exit temperature as follows. If T_4 is 1500 K then 2% of the compressor air flow is needed for cooling the turbine inlet guide vanes and 1% is needed for cooling the other turbine parts. The amounts of cooling air increase linearly with temperature and reach 10 and 6% respectively for T_4 of 2000 K.

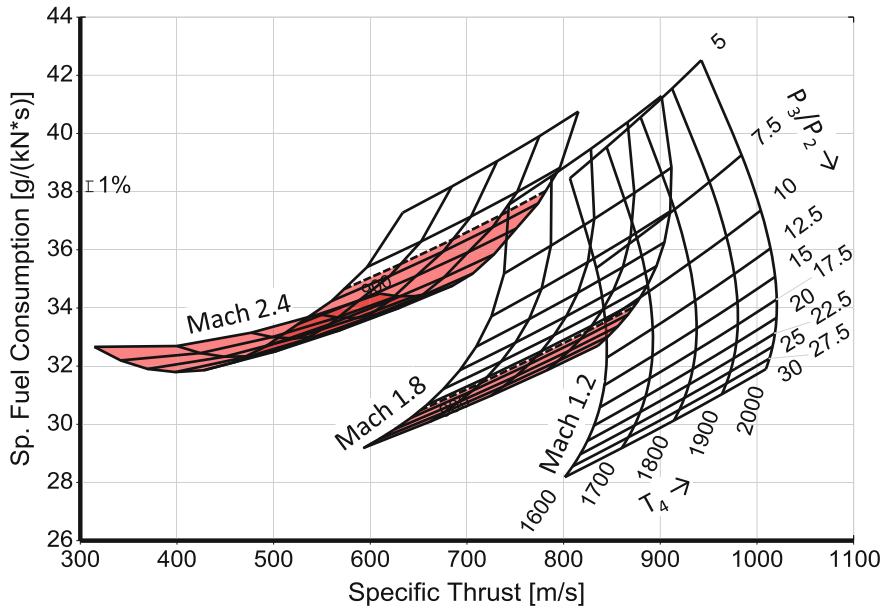


Fig. 1.6-11 Dry turbojet point performance

- (iv) Turbine exit duct pressure ratio P_6/P_5 is 0.98.
- (v) The convergent-divergent nozzle has an ideally-matched area ratio A_9/A_8 which means that the exit area is such that the static pressure P_{s9} matches the ambient pressure P_{amb} .

Figure 1.6-11 contains specific thrust and specific fuel consumption SFC for a series of three altitude/Mach number combinations on the 375 knots flight path. The highest burner exit temperature always yields the highest specific thrust. For the two lower Mach numbers of 1.2 and 1.8, a compressor pressure ratio of more than 30 results in the lowest specific fuel consumption. At a flight Mach number of 2.4 we see minimum SFCs at pressure ratios of around 21.

However, this thermodynamically-optimal pressure ratio is not feasible because the compressor exit temperature T_3 would then exceed 900 K. This limit emerges from the maximum tolerable disk material temperature. Cooling the turbine disk requires air with sufficient pressure and the only source of this is compressor delivery, unless an additional special cooling device is introduced. So, the pressure ratio is restricted to around 21 at Mach 1.8 and to maybe as low as 9 at Mach 2.4. In Fig. 1.6-11 the colored areas in the two respective carpets indicate forbidden regions.

We do the next cycle study with burner exit temperature $T_4 = 1900$ K and adjust the pressure ratio for each point on the flight path in such a way that the compressor

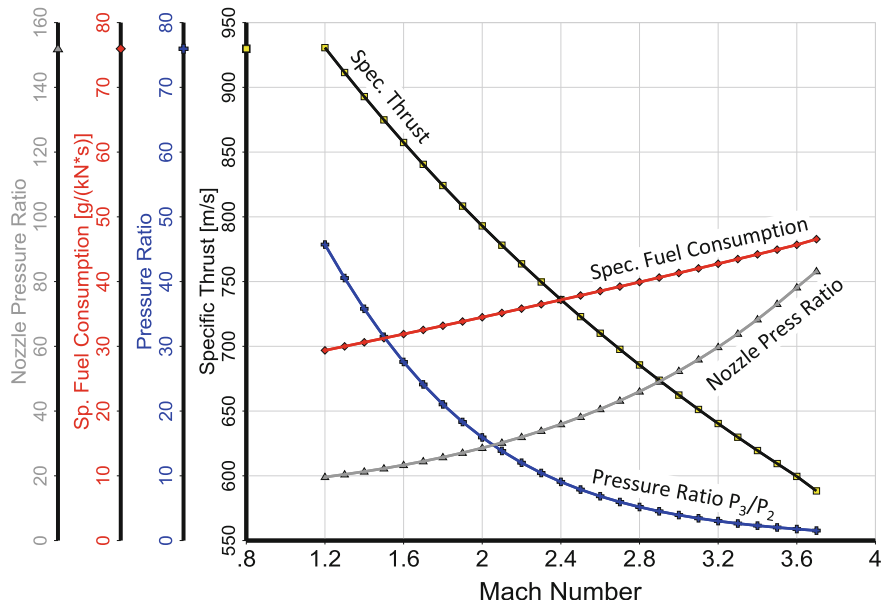


Fig. 1.6-12 Dry turbojet with $T_3 = 900$ K, $T_4 = 1900$ K

delivery temperature is $T_3 = 900$ K. The cycle study covers the full Mach number range along the 375 knot flight path. Figure 1.6-12 shows how four important cycle parameters (nozzle pressure ratio, SFC, overall pressure ratio and specific thrust) vary along the flight path as Mach number is increased. The highest achievable Mach number is slightly below 4.

Specific thrust decreases from 931 to 588 m/s (-37%). This loss in specific thrust is accompanied by an increase of specific fuel consumption of +58%, from 29.4 to 46.6 g/(kN × s). Above Mach 3 the pressure ratio decreases from 4 to a value little more than unity at Mach 3.7.

Note that the nozzle pressure ratio increases up to nearly 100 at the right-hand end of the Mach number range despite the decreasing compressor pressure ratio. The nozzle inlet pressure P_8 is driven almost exclusively by the compression in the engine intake. Thus, the quality of the propulsion system is dominated at very high flight speed by the intake and nozzle performance. Compressor and turbine efficiencies are no longer important in a turbojet for very high Mach number applications. The temperature-entropy diagram for Mach number 3.7 turbojet makes that obvious (Fig. 1.6-13). The turbomachinery is now useless weight!

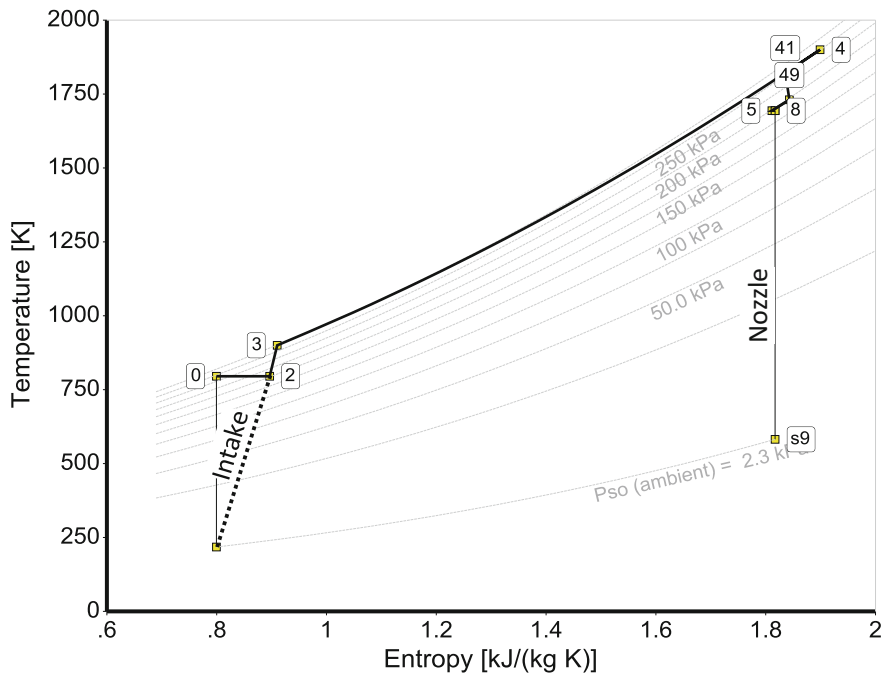


Fig. 1.6-13 Temperature—entropy diagram, dry turbojet, 25360 m/Mach 3.7

1.6.4.3 Turbojet with Reheat (Afterburner)

We can increase thrust of the straight turbojet by adding a reheat system (an afterburner), which makes use of the remaining oxygen in the flow and increases the gas temperature from T_5 (the turbine exit temperature) to the reheat exit temperature T_7 of 2000 K. Notice that the absence of rotating parts raises the allowable temperature limit considerably. This is a lower-cost alternative to scaling up the existing engine that requires additional fuel and makes the “dry” turbojet a “wet” turbojet (Fig. 1.6-14).

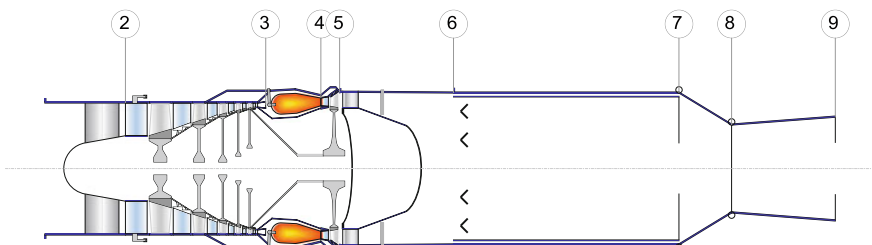


Fig. 1.6-14 Reheated turbojet nomenclature

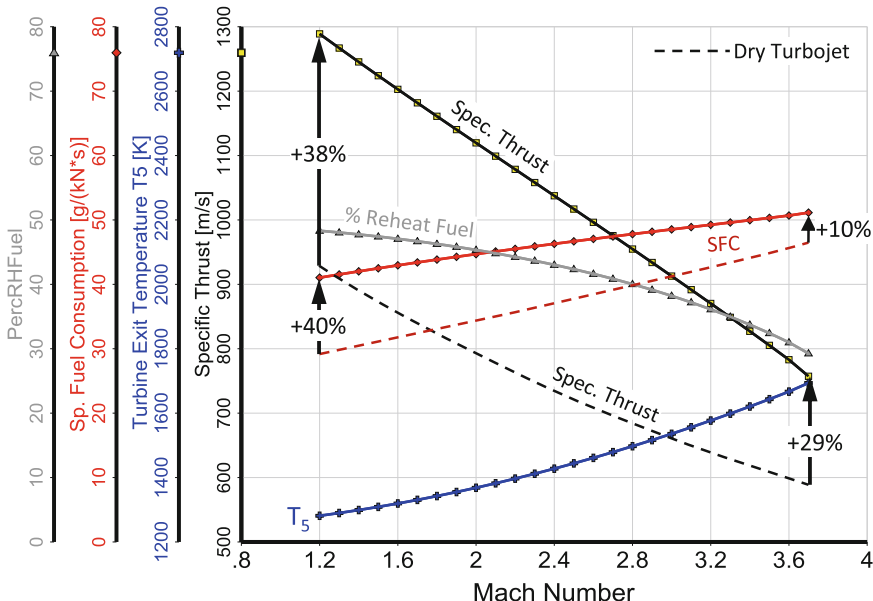


Fig. 1.6-15 Reheated turbojet with $T_3 = 900$ K

The afterburner efficiency is significantly lower than in that of the primary combustion chamber due to the higher gas velocity in the reheat pipe; we use 0.9 for reheat efficiency in our cycle calculations, compared with 0.995 for the main burner. Cooling the afterburner casing and nozzle requires about 10% of the engine total mass flow. The cooling air is made to mix with the hot gases upstream of the nozzle throat.

Figure 1.6-15 compares specific thrust and specific fuel consumption of the dry turbojet with the wet (the reheated) version. The afterburner increases specific thrust significantly (+38%) at the low Mach number end, accompanied by a 40% increase in specific fuel consumption. At the high Mach number end of the flight path the thrust boost is reduced to +29%, the increase of specific fuel consumption (+10%) is moderate.

Reheat SFC is worse than dry engine SFC but not only because of the poor reheat efficiency. When the flight Mach number is low, much heat is added at the turbine exit pressure P_5 which is significantly lower than the pressure in the main burner P_3 . Thermodynamically, this is not desirable because the entropy rise for a given temperature difference increases with decreasing pressure. At the high Mach number end of the flight path the pressures P_3 and P_5 are of similar magnitude. The higher specific fuel consumption is mainly a result of the low reheat efficiency.

1.6.4.4 Turbofan with Reheat

Turbofans offer lower specific fuel consumption than turbojets when reheat is switched off. With reheat, the contrary is true and afterburner SFC of the turbofan is worse than that of the turbojet. Figure 1.6-16 shows cycle design data on the 375 knots flight path of our current example for bypass ratio 1 turbofans with maximum permissible pressure ratio, i.e. with $T_3 = 900$ K. There is a comparatively small loss in specific thrust relative to the “wet” turbojet at Mach = 1.2 which essentially disappears at the high Mach numbers. Specific fuel consumption of the augmented turbofan is higher than that of the turbojet because so much more heat must be added to the relatively inefficient afterburner. Note that the reheat inlet temperature of the turbofan is much lower and so the amount of fuel burnt in the afterburner is much more than in the turbojet. Another reason for the SFC difference is that the pressure in the turbofan afterburner is lower than in that of the turbojet. The topmost line (marked with triangles) in Fig. 1.6-16 highlights the importance of the turbofan afterburner for high speed propulsion: 65–75% of the total fuel is burned there. In the turbojet afterburner, more than 50% of the total fuel is burnt in the main combustor, see Fig. 1.6-15.

A low bypass ratio turbofan can be an attractive option, especially at the high Mach number end of the flight path, because it offers SFC and noise advantages if operated dry at low flight Mach numbers, take off and landing. The penalty of higher SFC in the augmented mode compared to the “wet” turbojet is moderate.

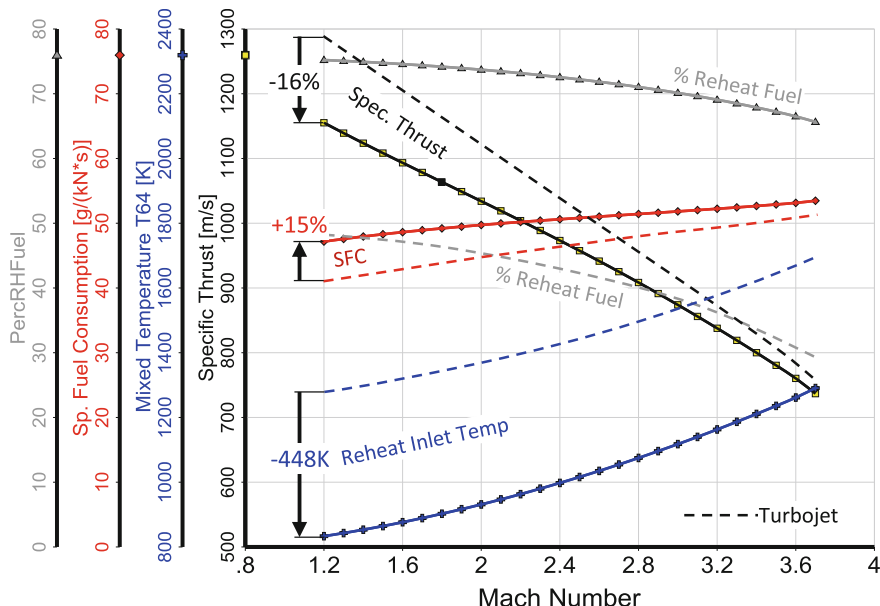


Fig. 1.6-16 Reheated turbofan (bypass ratio 1), $T_3 = 900$ K

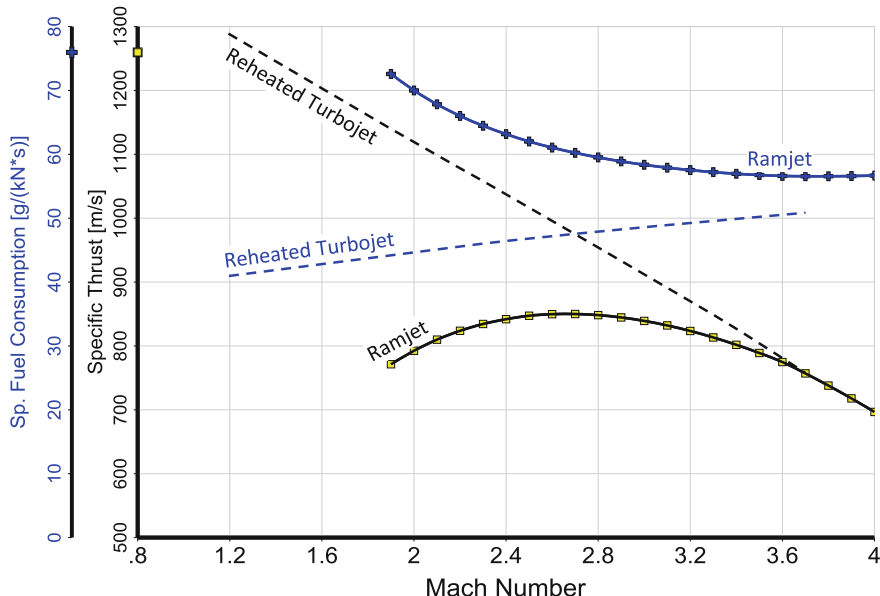


Fig. 1.6-17 Ramjet performance

1.6.4.5 Ramjet

We can consider the ramjet as a degenerated, reheated turbojet—one with a compressor pressure ratio of unity. Figure 1.6-17 compares the ramjet cycle with that of the reheated turbojet described above. At the top Mach number of the reheated turbojet (Mach 3.7) the specific thrust for both engine configurations is the same. The higher specific fuel consumption of the ramjet at Mach 3.7 is caused mainly by burner efficiency differences which we have assumed for this exercise. In the turbojet, the main part of the heat addition occurs in the core combustor which has nearly 100% burner efficiency. Combustion in the ramjet is equivalent to that of an afterburner, so its efficiency is only about 90%. This difference between the burning efficiencies of the two engine configurations is somewhat academic. Within the accuracy limits of our cycle study, the point performances of reheated turbojet and ramjet cycles are essentially the same at around Mach 3.6.

1.6.4.6 Acceleration to High Mach Numbers

The previous examinations compared many different engine cycles. All of them were designed for altitude/Mach number combinations on the 375 knots EAS flight path. Now we select one of these engines—a turbojet with reheat—and investigate its off-design behavior. The flight condition for the cycle design point is Mach 3 at

an altitude of 22700 m. The efficiency and loss assumptions are the same as before, with a compressor pressure ratio corresponding to the maximum T_3 limit of 900 K.

The engine must be able to operate not only at the flight condition of the cycle design point but also demonstrate acceptable performance throughout the 375 knots flight path. The engine inlet temperature changes drastically: At Mach 1.2/11000 m where the acceleration to Mach 3 begins, the total temperature at the engine face T_2 is only 279 K but at the end of the acceleration T_2 exceeds 600 K, a change with dramatic consequences!

We intend to run the engine with the maximum permissible rotational spool speed N all along the flight path. This creates a problem because, when Mach number is lower than 3, T_2 is lower than 600 K. But now the aerodynamic spool speed $N/\sqrt{T_2}$ is bigger, and in fact is higher than the cycle design point value. At the beginning of the acceleration the aerodynamic spool speed is given by multiplying the design value by the ratio of the square roots of the temperatures, i.e. $\sqrt{(601.4/279)} = 1.47$ of the cycle design point value if the true spool speed N is kept constant. For the compressor, that means that the aerodynamic speed margin at the cycle design point must be 47% if unrestricted operation along the flight path is to be achieved.

What happens if we design the compressor for the mass flow, pressure ratio and efficiency of the cycle design point? If we do that, then all the operating points during the acceleration to Mach 3 will be on the design point speed line in the compressor map. The corrected spool speed will come down only if we accelerate further to Mach 3.1 or 3.2, as shown in Fig. 1.6-18.

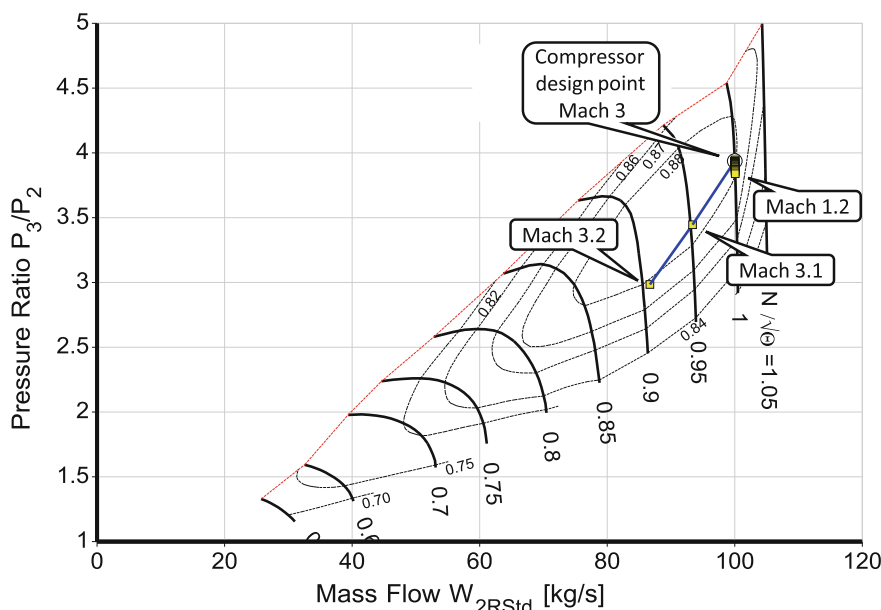


Fig. 1.6-18 Compressor A design pressure ratio 3.94

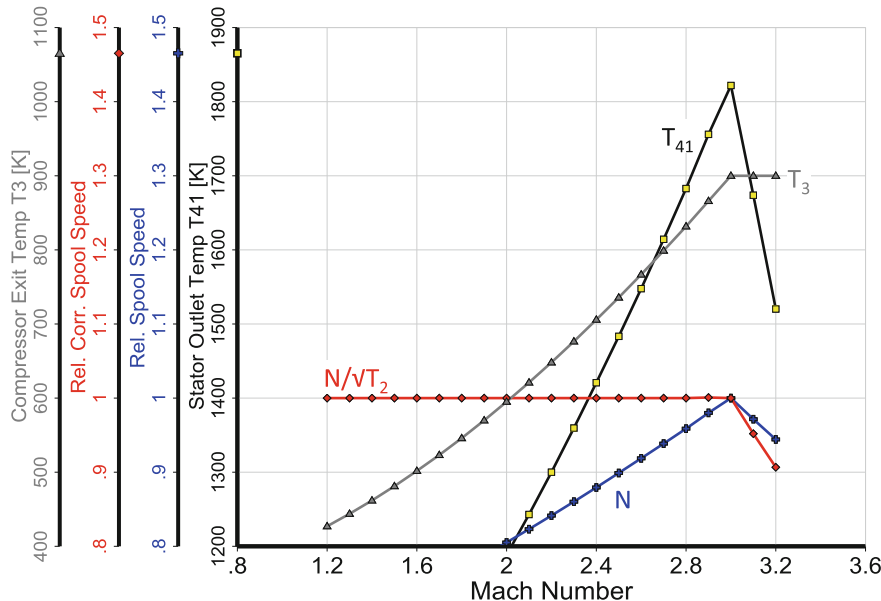


Fig. 1.6-19 Engine control parameters for compressor A

Figure 1.6-19 shows how the spool speed N , the corrected speed $N/\sqrt{T_2}$, the compressor exit temperature T_3 and the turbine rotor inlet temperature T_{41} vary over the flight envelope. The engine uses the maximum permissible turbine inlet temperature only at Mach 3, the cycle design point. The maximum permissible T_3 of 900 K prevents the use of the design point turbine temperature and spool speed when the Mach number is any greater than 3. When the Mach number is less than 3, keeping $N/\sqrt{T_2}$ constant forces both the spool speed N and the turbine inlet temperature to drop.

Numerous questions still arise. At the beginning of the acceleration (Mach 1.2), how comfortable are we with the spool speed and the turbine inlet temperature? Does the engine deliver sufficient thrust to the aircraft? What can we do if we need more thrust?

We can design the compressor for a much higher pressure ratio and higher corrected flow than that of the current cycle design point. Let us examine two alternate compressors B and C, one with a design pressure ratio of 7 and another with a pressure ratio of 10.

Figure 1.6-20 shows the operating line of compressor B and Fig. 1.6-21 that of the alternate compressor design C. Note that there is a significant size difference between the three compressors A, B and C. At the cycle design point the Standard Day corrected mass flow is 100 kg/s. Compressor B, which is designed for the pressure ratio 7, delivers $W_{2Rstd} = 150$ kg/s at the compressor design speed which is 25% higher than that of the cycle design point, see Fig. 1.6-20. Compressor C is even bigger (200 kg/s) and, at its higher pressure ratio, is designed for 143% of the corrected speed of the cycle design point.

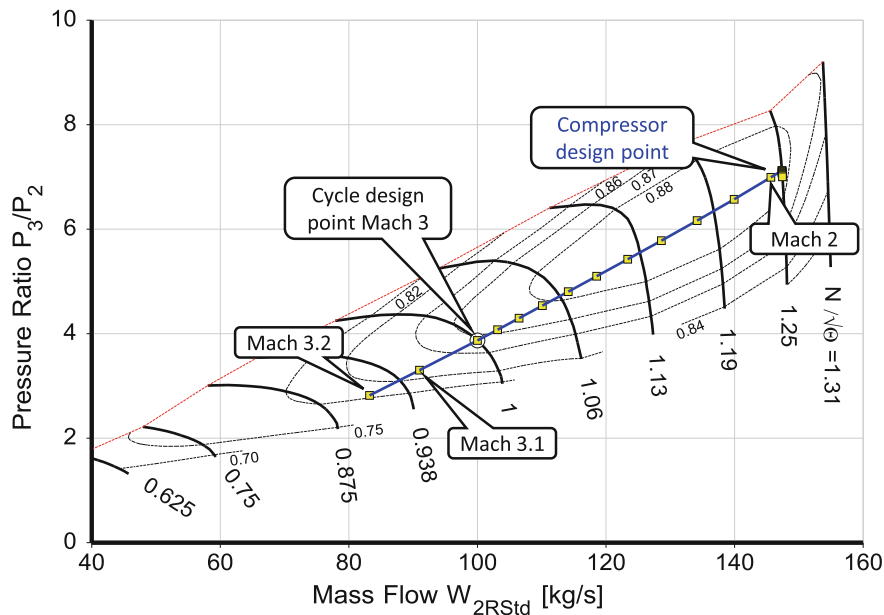


Fig. 1.6-20 Compressor B design pressure ratio 7

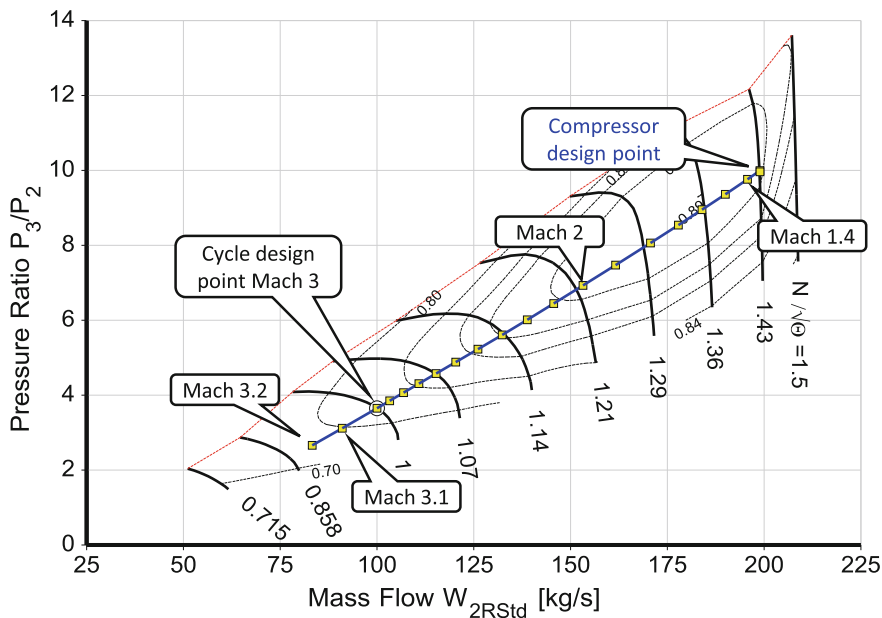


Fig. 1.6-21 Compressor C design pressure ratio 10

At the original cycle design point, all three compressors have the same corrected flow of $W_{2Rstd} = 100 \text{ kg/s}$ and almost the same pressure ratio. So why are the pressure ratios at the new cycle design conditions not identical? The variations are caused by the compressor efficiency differences at the cycle design point in the maps for compressors B and C. Compressor A has a cycle design point efficiency of 0.8811, see Table 1.6-1, while compressor B operates at Mach 3 with an efficiency slightly below 0.87 (Fig. 1.6-20) and the efficiency of compressor C is much less, at only 0.81. Pressure ratio decreases with efficiency because the compressor inlet and exit temperatures ($T_2 = 601.4 \text{ K}$, $T_3 = 900 \text{ K}$) are the same in all engines.

Figure 1.6-22 shows how the controlled variables behave along the flight path. Turbine rotor inlet temperature T_{41} is limited to 1822 K which corresponds to the design burner exit temperature $T_4 = 1900 \text{ K}$. Maximum permissible relative spool speed N is 1.0 and the compressor exit temperature T_3 must not exceed 900 K. The big difference between the two compressor variants B and C is in the corrected spool speed margins, which are 1.25 (compressor B) and 1.43 (compressor C) respectively.

At the high-speed end, above Mach 3, the T_3 value remains constant, but the other controlled parameters are reduced in all three alternative engine designs. The engine with compressor B (design mass flow $W_{2Rstd} = 150 \text{ kg/s}$, design pressure ratio 7) operates at the T_{41} limit between the Mach numbers 2 and 3 and at the $N/\sqrt{T_2}$ limit at lower Mach numbers. The bigger turbojet, with the compressor C ($W_{2Rstd} = 200 \text{ kg/s}$, design pressure ratio 10), operates at the $N/\sqrt{T_2}$ limit only when Mach number is less than 1.3. The relative spool speed limit of 1.0 is active only in the Mach number range from 1.3 to 1.7.

Table 1.6-1 Turbojet cycle design point, altitude 22700 m, Mach 3

Station	W kg/s	T K	P kPa	WRstd kg/s	Reheat on	
amb		216.65	3.571		FN	= 66.62 kN
1	72.979	601.44	132.084		TSFC	= 48.53 g/(kN*s)
2	72.979	601.44	106.832	100.000	FN/W2	= 912.88 m/s
3	72.979	900.00	420.672	31.066	Prop Eff	= 0.6792
31	63.200	900.00	420.672		eta core	= 0.6495
4	65.197	1900.00	408.052	41.571		
41	71.327	1821.81	408.052	44.535	WF	= 1.99774 kg/s
49	71.327	1565.58	190.849	91.899	WFRH	= 1.23562 kg/s
5	74.976	1535.83	190.849	91.899	WF total	= 3.23336 kg/s
6	74.976	1535.83	187.032		A8	= 0.4900 m ²
61	67.479	1535.83	187.032			
7	68.714	2000.00	185.648		XM8	= 1.00000
8	76.212	1956.35	185.648	108.382	P8/Pamb	= 51.9885
Bleed	0.000	900.00	420.672		WB1d/W2	= 0.00000
<hr/>						
P2/P1 = 0.8088 P4/P3 = 0.9700 P6/P5 = 0.9800						
Efficiencies: isentr polytr RN1 P/P						
Compressor	0.8811	0.9000	0.439	3.938	WC1N/W2	= 0.08400
Burner	0.9999			0.970	WC1R/W2	= 0.05000
Turbine	0.9074	0.9000	0.467	2.138	Loading	= 100.00 %
Reheat	0.9000			0.993	e45 th	= 0.88689
<hr/>						
Spool mech Eff	0.9999	Nom Spd	8055 rpm		XM61	= 0.18000
Con-Di Nozzle:					XM7	= 0.21434
A9*(Ps9-Pamb)	4.62E-6				far7	= 0.04619
					PWX	= 0.00 kw
<hr/>						
A9/A8						
CFGid						

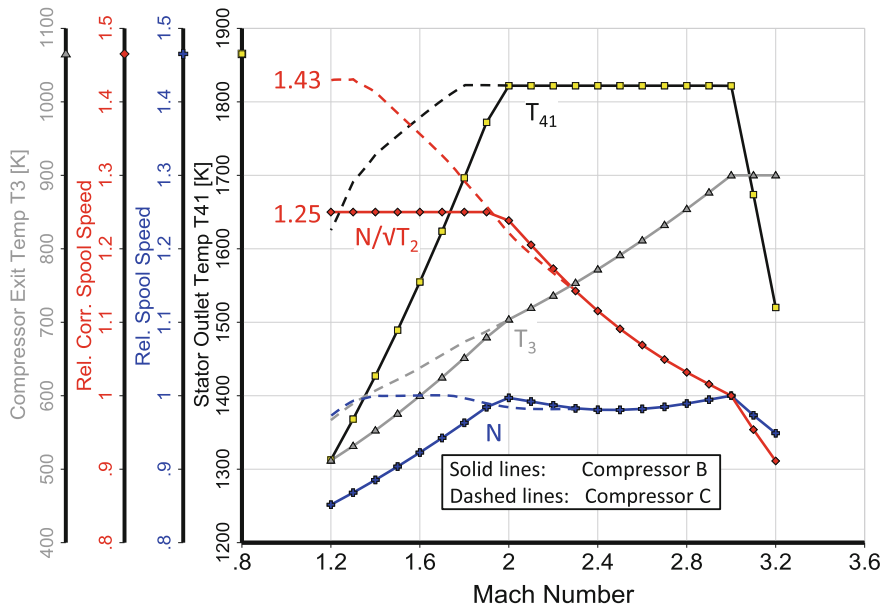


Fig. 1.6-22 Engine control parameters for compressors B and C

We could improve this rather simple control system by making use of variable geometry features that are usually required for such an engine in practice. We could influence the relationship between mass flow and spool speed with variable guide vanes in the compressor. This could improve the performance of the compressor C turbojet between Mach 1.3 and Mach 1.7, for example. Another fine trim in the engine control system could be a sophisticated schedule for the nozzle throat area.

Thrust and SFC of our three turbojets are very different during the acceleration from Mach 1.2 to Mach 3 (Figs. 1.6-23 and 1.6-24). All engines deliver the same thrust and SFC at the end of the acceleration (Mach 3). The engine with compressor C, designed for pressure ratio 10, delivers the best performance. However, this is the heaviest engine because it needs more compressor stages and is designed for twice as much corrected flow than variant A. Not surprisingly, it will also be the most expensive!

Whether compressor A or B (or a similar one) is the best choice depends on the aircraft mission. Thrust, fuel consumption and weight of the propulsion system, including the aircraft intake, will determine the optimum compressor design mass flow and pressure ratio. For the Blackbird SR-71, a compressor with pressure ratio 7.5 was the best choice.

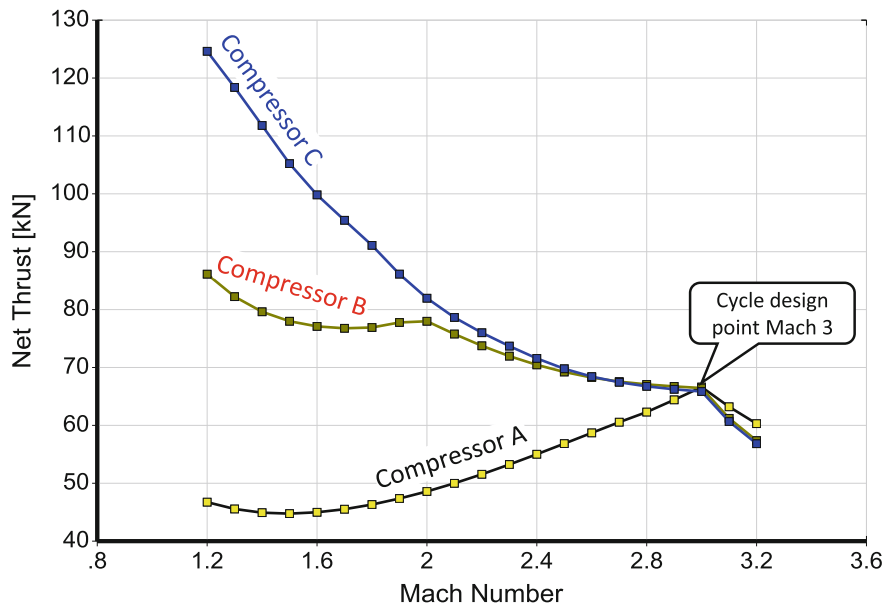


Fig. 1.6-23 Thrust for three compressor variants

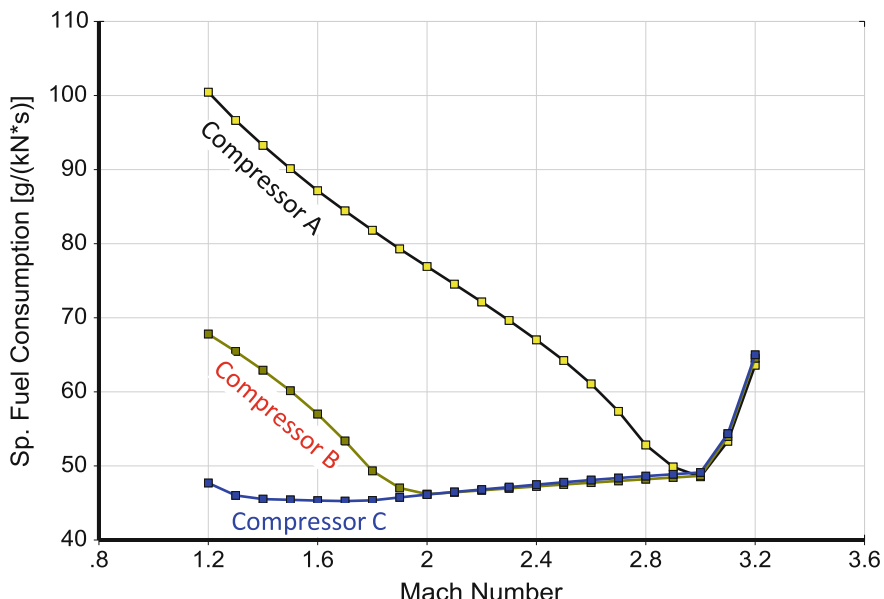


Fig. 1.6-24 SFC for three compressor variants

1.7 References

1. Giampaolo, T.: Gas Turbine Handbook Principles and Practice, 5th edn. The Fairmont Press, Inc, USA (2014)
2. Abdullahi, H., Kurpjuhn, B., Reiser, M., Spirkl, A.: Sand Ingestion Tests on the MTR390 Turboshaft Engine Reference EP03, 24th European Rotorcraft Forum. Marseille, France (1998)
3. Cosner, A., Rutledge, G.: Successful Performance Development Program for the T800-LHT-800 Turboshaft Engine SAE Technical Paper 891048, (1989)
4. Walsh, P.P., Fletcher, P.: Gas Turbine Performance, 2nd edn, Blackwell Science Ltd (2004)

Chapter 2

Engine Families



We have already seen that gas turbine engines may be categorized in terms of their architecture, namely simple turbojet, low bypass ratio turbofan, etc. However, within almost any manufacturing company, different engine families are also encountered. What is an engine family? Usually this is defined by a series of units all based on a common core or gas generator. A great deal of thought and planning from marketing and engineering departments precedes the initial or baseline engine design because this will influence the overall sales to a high degree. The siblings of an engine family are called derivatives and they come about by designing alternative IP and LP systems around the common core, which is retained as far as possible. The derivative engines will generate higher or lower levels of thrust than the baseline but the baseline must be configured with precisely that objective in mind. This usually means compromising the baseline somewhat to allow for either growth or reduction, which may risk reduced sales of the original version in the hope of the greater sales of the derivatives. There are some special, but very simple rules, involving aerodynamic similarity, that allow a new IP/LP system to operate with a fixed gas generator.

Famous turbofan engine families are the Pratt and Whitney PW4000 (thrust range 52,000–98,000 lbf), the Rolls-Royce Trent (from 53,000 to 115,000 lbf), the CFM56 family (24,000–34,000 lbf) and the GE Aviation CF6 (40,000–70,000 lbf). The CF6 core is also the ancestor of the LM2500 family which provides shaft power (16–35 MW) for ships, electricity generators and pipeline compressors. Rolls-Royce offers the MT30, a 36 MW derivative of the Boeing 777 engine, the Trent 800, for ship propulsion and power generation, as do other companies.

In an ideal world, the gas generator of an engine family would consist of identical parts. In reality, the cores of the engines are similar, but not identical. While the maximum permissible spool speed is very much limited by a common value of tolerable disk stress, the aerodynamics and the tolerable burner exit temperature differ. The flow capacity of compressors and turbines can vary within the same annulus due to re-staggered or re-designed blades and vanes. New materials and more sophisticated cooling schemes can increase the temperature capability of the turbine.

Adapting an existing engine to a new application creates a new member or derivative of the engine family. This is a very common design task and much more frequent than the design of a completely new engine, which may happen only once in a decade or so. The main motivation for derivative engines is economic, with the focus of keeping development costs and technical risk as low as possible. This leads to many constraints and boundary conditions imposed on the given gas generator and makes the cycle selection for a derivative engine a challenge.

Traditionally the advanced projects engineer explores the design space of a new engine with extensive parametric studies. He presents the results as x-y plots which might include contour lines for important quantities. Showing the boundaries of the design space in a single figure is easy if there are only two design parameters. However, if there are more than two design parameters, then more than one figure is required to fully describe the design space. Searching for the best engine cycle becomes time consuming and difficult if the number of design variables exceeds three or four.

Instead of screening a wide range for the design variables with systematic parameter variations it is also possible to do an automatic search for the optimum engine design with the help of numerical optimization routines. This is the approach we describe in the following two sections, where we will optimize the 25% thrust growth derivative of a turbofan engine.

2.1 Baseline Engine

As an illustrative example, we shall start from an existing small engine as used for business jets. These types of engine have rather low overall pressure ratios and moderate burner exit temperatures compared to the big turbofan engines used in commercial airliners. Fuel costs are less important than engine acquisition cost because business jets fly only a few hundreds of hours per year, but SFC is still important as an enabler for range.

The aerodynamic design point of the baseline engine is Max Climb rating at an altitude of 11,000 m, Mach 0.8 on an ISA day. Table 2.1-1 lists the cycle parameters for this operating condition and Fig. 2.1-1 shows the relevant station numbers.

The mechanical design point of the engine is the Hot Day Take Off case at sea level, Mach 0.2, ISA + 15. This operating point is an off-design case from a cycle calculation point of view. Therefore, we require component maps to complete our engine performance model. If neither measured nor calculated maps are available, then scaled versions of maps from similar turbomachines may be used. We scale the *GasTurb Standard maps* in such a way that reading them at the operating conditions of the aerodynamic design point yields exactly the data in Table 2.1-1.

We differentiate here between the aerodynamic design point and the mechanical design point. The aerodynamic design point is defined by the operating conditions where performance or fuel-burn is optimized. In contrast, the mechanical design

Table 2.1-1 Cycle of the baseline engine (Max Climb, 11 km, Mach 0.8, ISA)

Station	W kg/s	T K	P kPa	WRstd kg/s	FN	=	
amb		216.65	22.632				3.41 kN
1	22.186	244.44	34.509		TSFC	=	20.1043 g/(kN*s)
2	22.186	244.44	34.509	60.000	WF	=	0.06853 kg/s
13	18.153	294.47	60.818	30.573	BPR	=	4.5000
21	4.034	297.90	63.842	6.510	s NOx	=	0.2590
25	4.034	297.90	63.203	6.575	Core Eff	=	0.4472
3	4.034	646.64	758.439	0.807	Prop Eff	=	0.7496
31	3.452	646.64	758.439		P3/P2	=	21.98
4	3.520	1350.00	735.686	1.049	P2/P1	=	1.0000
41	3.702	1318.27	735.686	1.090	P16/P13	=	0.9800
43	3.702	978.49	172.646		P25/P21	=	0.9900
44	3.762	973.45	172.646		P45/P44	=	0.9800
45	3.762	973.45	169.193	4.141	P6/P5	=	0.9800
49	3.762	710.16	41.094		A8	=	0.06443 m ²
5	3.762	710.16	41.094	14.562	A18	=	0.13248 m ²
8	3.802	709.51	40.272	15.012	P8/Pamb	=	1.77943
18	18.153	294.47	59.602	31.197	P18/Pamb	=	2.63351
Bleed	0.300	646.64	758.438		WBld/W25	=	0.07437
Efficiencies:	isentr	polytr	RNI	P/P	CD8	=	0.97757
Outer LPC	0.8600	0.8707	0.413	1.762	CD18	=	0.97600
Inner LPC	0.8800	0.8899	0.413	1.850	XM8	=	0.95562
HP Compressor	0.8600	0.8985	0.600	12.000	XM18	=	1.00000
Burner	0.9995			0.970	V18/V8,id=	=	0.81000
HP Turbine	0.8800	0.8598	1.225	4.261	Loading	=	100.00 %
LP Turbine	0.9001	0.8822	0.399	4.117	e444 th	=	0.87427
HP Spool mech Eff	0.9900	Nom Spd	32000 rpm		PWX	=	50.00 kW
LP Spool mech Eff	1.0000	Nom Spd	13497 rpm		WCHN/W25	=	0.04500
hum [%]	war0	FHV	Fuel		WCHR/W25	=	0.01500
0.0	0.00000	43.124	Generic		WLc1/W25	=	0.00000

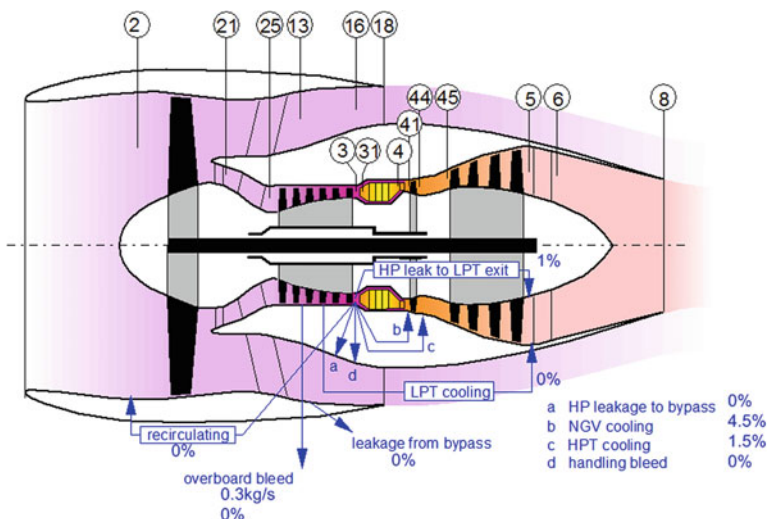
**Fig. 2.1-1** Station nomenclature for the baseline engine

Table 2.1-2 Important differences

	Max Climb	Take Off
N _H [%]	100	105
T ₂₅ [K]	279.9	356.06
T ₃ [K]	647	743
T ₄ [K]	1350	1416
T ₄₅ [K]	973	1027
F _N [kN]	3.41	12.0

point is defined by the conditions where stresses are greatest. Max Climb is not the mechanical design point of our engine because during Take Off on a Hot Day all temperatures, pressures and spool speeds are higher. In our example, mechanical spool speed is 5% higher at Take Off than at Max Climb which results in 12 kN Take Off thrust and the temperatures listed in Table 2.1-2.

2.2 Derivative Engine

The design objective for the new derivative engine is an increase of 25% thrust at both Max Climb and Take Off and a reduction of the specific fuel consumption. We intend to achieve this with a minimum modification of the core by limiting changes to the LP-system.

The changes considered are an increased diameter fan, an additional booster and a re-designed low pressure turbine. The core should be unchanged aerodynamically within the same annulus with minimum increase in mechanical speed, temperatures (T₃, T₄), flow capacity and cooling flows. The new engine architecture is shown in Fig. 2.2-1. (Ignore the gearbox—we will calculate the cycle with a gear ratio of 1.)

Modeling the derivative engine becomes a combination of design calculations for the components on the low pressure spool with off-design calculations for the core components. The cycle design point is Max Climb for the same flight conditions as used for the baseline engine. The data in Table 2.1-1 serve as reference against which we will compare our derivative engine design.

2.2.1 Fan and Booster

We design the new fan with the same aerodynamic loading $\Delta H/U^2$ as that of the baseline engine fan. Therefore, fan efficiency remains the same for all cycles examined, but fan tip speed will differ depending on fan diameter and rotational speed.

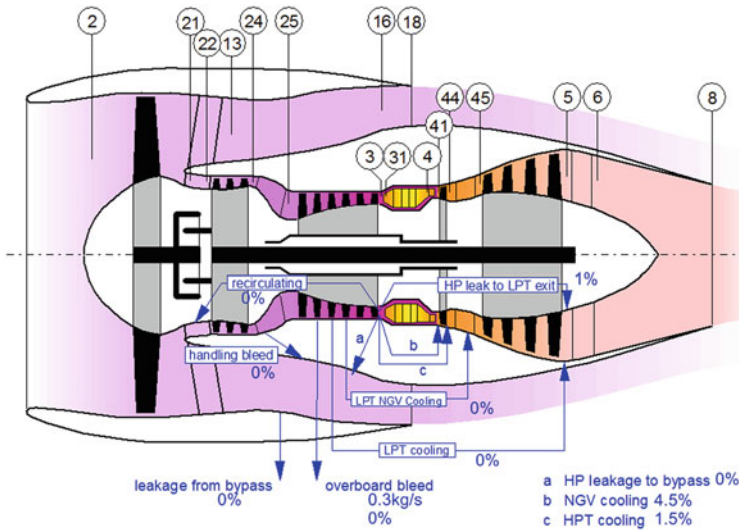


Fig. 2.2-1 Station nomenclature for the growth engine

Fan tip diameter varies with engine inlet mass flow. Mach number at the fan face and rotor inlet radius ratio are the same as in the baseline engine.

We describe fan off-design performance in the baseline engine model with a single compressor map. Total mass flow W_{2Rstd} , bypass pressure ratio P_{13}/P_2 and bypass efficiency η_{2-13} are stored in tables. Core stream pressure ratio P_{21}/P_2 and core stream efficiency η_{2-21} are calculated as

$$\frac{P_{21}}{P_2} = 1 + \frac{(P_{21}/P_2)_{ds}-1}{(P_{13}/P_2)_{ds}-1} * \left(\frac{P_{13}}{P_2} - 1 \right) \quad (2.2-1)$$

$$\eta_{2-21} = \left(\frac{\eta_{2-21}}{\eta_{2-13}} \right)_{ds} * \eta_{2-13} \quad (2.2-2)$$

In the growth engine, the fan map defines only the bypass stream performance. The core stream pressure ratio (P_{21}/P_2)_{ds} in Eq. (2.2-1) is set to 1.0. Fan hub performance is considered as part of the booster for which we use a separate map. Booster efficiency at its design point is the same for baseline and derivative engines.

2.2.2 Core Compressor

The derivative engine uses essentially the same gas generator as the baseline. No compressor modification is intended, so the baseline compressor map (Fig. 2.2-2) is also valid for the growth engine.

Using the same compressor does not necessarily mean that the pressure ratios of both engine cores are the same. The Max Climb compressor operating point cannot be at the same point on the map as in the baseline engine. This is because the booster increases T_{25} which leads to lower $N_H/\sqrt{T_{25}}$ if the mechanical spool speed N_H is kept constant.

The cycle design point calculation of an unmixed flow turbofan is straightforward and does not require iteration. This is also true for the growth engine, but there is one difference: HPC pressure ratio and efficiency are no longer direct input quantities; they are read from the baseline engine compressor map shown in (Fig. 2.2-2). Input values for $N_H/\sqrt{T_{25}}$ and the auxiliary coordinate β define the operating point.

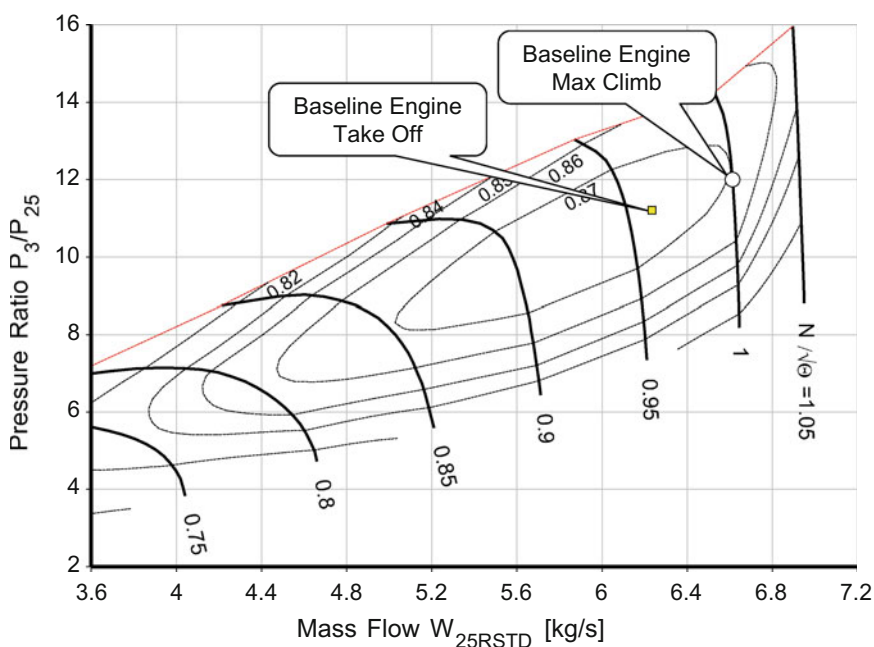


Fig. 2.2-2 Compressor map of the baseline and the derivative engines

Reading the map with these coordinates yields the corrected gas generator flow W_{25Rstd} in addition to pressure ratio P_3/P_{25} and efficiency η_{25-3} . This determines the engine inlet mass flow W_2 as well as the design bypass ratio, T_{25} and P_{25} .

The compressor map from the baseline engine (Fig. 2.2-2) contains absolute values for corrected flow W_{25Rstd} , pressure ratio P_3/P_{25} and efficiency η_{25-3} . The numbers for corrected spool speed $N_H/\sqrt{\Theta_{25}}$, however, are relative. The reference value for the corrected speed in the map originates from the baseline engine cycle design point data in Table 2.1-1:

$$\left(\frac{N_{H,\text{rpm}}}{\sqrt{\theta_{25}}}\right)_{ref} = \frac{32,000 \text{ rpm}}{\sqrt{\frac{T_{25}}{288.15 \text{ K}}}} = \frac{32,000 \text{ rpm}}{\sqrt{\frac{297.9 \text{ K}}{288.15 \text{ K}}}} = 31,472 \text{ rpm} \quad (2.2-3)$$

The reference (mechanical) speed $N_{H,\text{ref}}$ is 32,000 rpm, the reference corrected speed $N_{H,\text{corr,ref}}$ is 31,472 rpm.

We need the reference corrected speed for the calculation of the absolute spool speed $N_{H,\text{rpm}}$ from known values for $N_H/\sqrt{\Theta_{25}}$ and Θ_{25} . If the map is read with the relative corrected speed $N_H/\sqrt{\Theta_{25}} = 0.9604$, for example, and the compressor inlet temperature is 356.06 K, then the absolute spool speed is

$$N_{H,\text{rpm}} = \frac{\frac{N_{H,\text{rpm}}}{\sqrt{\theta_{25}}}}{\frac{N_{H,\text{ref}}}{\sqrt{\theta_{25,\text{ref}}}}} \sqrt{\theta_{25}} N_{H,\text{ref}} = 0.9604 \sqrt{\frac{356.06}{288.15}} 31472 = 33,600 \text{ rpm} \quad (2.2-4)$$

Relative absolute spool speed is $N_H = 33,600/32,000 = 1.05$.

2.2.3 Combustor

The increased thrust engine may run at higher burner exit temperature than the baseline engine. Some modifications to the burner cooling air distribution and to the fuel injectors might be necessary. We assume that these changes have negligible influence on burner pressure loss. Possible improvements in burner efficiency are also neglected in our engine growth study.

2.2.4 High Pressure Turbine

Turbine flow capacity changes of plus or minus 5% can be achieved by re-staggering the turbine inlet vanes. Such a modification of the existing hardware has almost no effect on turbine efficiency. In our cycle studies, we make use of this degree of freedom.

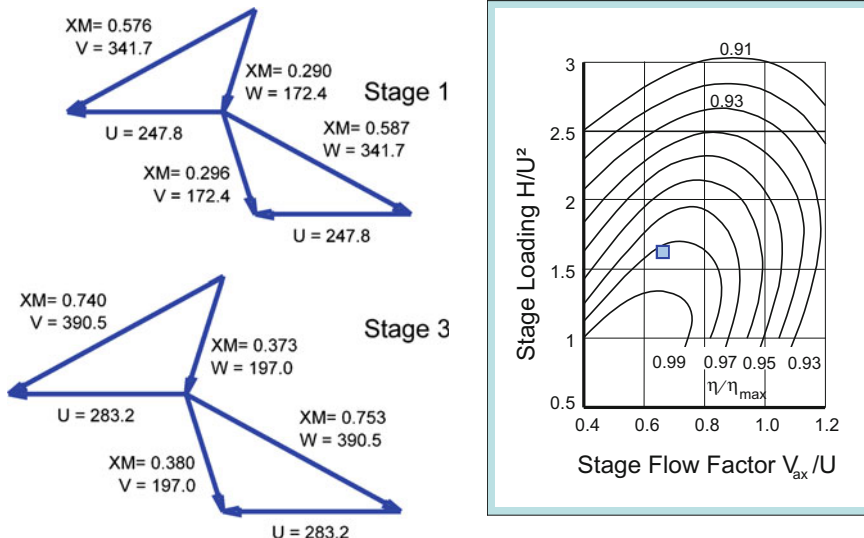


Fig. 2.2-3 LPT velocity triangles for the baseline engine

2.2.5 Low Pressure Turbine

The design point efficiency of the low pressure turbine varies with aerodynamic stage loading and flow factor. We estimate it by employing the simplified version of the preliminary turbine design routine from [1] which is included in GasTurb. Figure 2.2-3 shows the velocity triangles and the location of the design point in the Smith Chart. Here we assume common stage flow factor and loading coefficient.

2.3 Optimizing the Growth Engine

2.3.1 Design Variables

Design variables are input data for the cycle design point calculation. The design variables of our derivative engine are the pressure ratios of the fan and the booster, the bypass ratio and the burner exit temperature. Further cycle design point variables are the map coordinates of the gas generator operating point $N_H/\sqrt{T_{25}}$ and β .

Table 2.3-1 Design variables

1	Fan pressure ratio P_{13}/P_2
2	Booster pressure ratio P_{24}/P_{21}
3	Bypass ratio BPR
4	Burner exit temp. T_4
5	Corrected spool speed $N_H/\sqrt{T_{25}}$
6	Map coordinate β

Altogether we have six cycle design variables for our derivative engine (Table 2.3-1).

2.3.2 Design Constraints

Design constraints can exist as lower and upper limits of design variables and for calculated quantities. Seven constraints exist in our derivative engine:

1. Since only minor modifications of the high pressure turbine (HPT) are allowed, its flow capacity must remain similar to that of the baseline engine.
2. No big changes in HPT pressure ratio are permitted. When taken with constraint no. 1 this implies that the low pressure turbine (LPT) flow capacity will also be similar to that of the baseline engine.
3. The LPT inlet temperature T_{45} must remain lower than say 1150 K because we are hoping to make this turbine from inexpensive materials.
4. There is a temperature limit at the core compressor exit. This comes from the temperature capability of the disk material used for the last stage of the baseline engine.
5. The nacelle limits the fan diameter of the growth engine.
6. Disk stress limits core spool speed. Nevertheless, a moderate increase of 1% in absolute spool speed is feasible.

Table 2.3-2 Constraints

1	HP turbine flow capacity	Reference value $\pm 5\%$	
2	LP turbine flow capacity	Reference value $\pm 5\%$	
3	LP turbine inlet temp T_{45}	<1150 K	Hot Day Take Off
4	Compressor exit temp T_3	<750 K	Hot Day Take Off
5	Fan tip diameter	<0.75 m	
6	Core spool speed N_H	<Reference + 1%	
7	Max Climb thrust	>4.26 kN	=3.41 kN + 25%
8	Hot Day Take Off thrust	>15 kN	=12 kN + 25%

In our example, the objective is to increase the Max Climb and Hot Day Take Off thrusts by 25%. Engine designs with less thrust than that are not acceptable and therefore the minimum Max Climb and Take Off thrust values are further constraints for the growth engine. Table 2.3-2 summarizes the design constraints for the derivative engine.

2.3.3 *Figure of Merit*

The specific fuel consumption (SFC) for Max Climb is the *figure of merit* which is to be minimized. This will automatically result in low cruise fuel consumption. SFC at Take Off is not considered. It makes sense to design the engine at the condition where most of the fuel will be burned!

2.3.4 *Ranges for the Design Variables*

Running the numerical optimization algorithm makes no sense with arbitrary numbers for the design variables. We can easily define reasonable ranges for all of them. These should be narrow because then the search for the optimum will require less effort. However, when a range is too narrow, the true optimum might be excluded from the search unintentionally.

Note that either the lower or the upper range limit can in fact represent a technical constraint for the engine design. In our example, this is the case for the pressure ratio of the single stage fan. All the bold figures in Table 2.3-3 are technical limitations.

Table 2.3-3 Ranges for the design variables

		Min.	Max.
1	Fan pressure ratio	1.1	1.9
2	Booster pressure ratio	1.4	2.3
3	Bypass ratio	4	6
4	Burner exit temp. T_4	1300 K	1600 K
5	Rel. spool speed N_H	0.9	1.02
6	Map coordinate β	0.3	0.8

2.3.5 Starting Point

Many optimization algorithms require that a set of design variables which fulfills all constraints must be known before the optimization can commence. The baseline engine cycle is within the ranges of all design variables; however, it obviously does not meet the minimum thrust constraints.

So how can we get a valid cycle to start with? One possible approach would be to do a rough parametric study which must find a feasible solution only. However, such a parametric study would take more effort than necessary. We can define a provisional figure of merit as Max Climb thrust and run this optimization. The minimum Max Climb thrust constraint is dropped for that preliminary exercise. After maximizing thrust we have a valid start point—provided we can get more than 4.26 kN Max Climb thrust.

Next, we redefine the figure of merit as specific fuel consumption and introduce the minimum thrust constraint. The final optimization can commence.

2.3.6 Graphical User Interface

Figure 2.3-1 shows the optimization window of GasTurb for this exercise with six horizontal gauges for the design variables on the left and six gauges for the constraints on the right. The gauges are continuously updated while the optimization is running. One can immediately see when a variable or a constraint is at a lower or upper limit.

The portion of the figure below the gauges shows how the figure of merit develops. The screenshot of Fig. 2.3-1 was taken during an endless random search

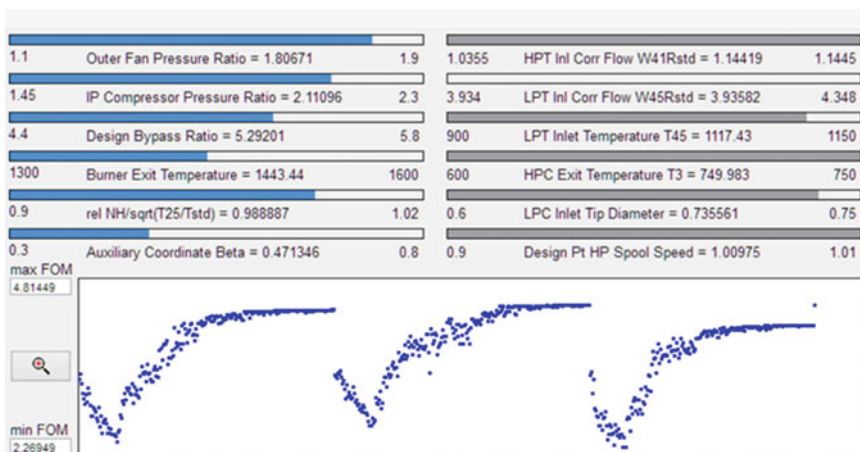


Fig. 2.3-1 Search for a valid starting point—maximizing thrust

for the maximum thrust. As can be seen, the search for the highest thrust does end after the algorithm finds a maximum. But this might be a local maximum rather than the global maximum we are looking for. Which valid solution is found—from several candidates—depends on the starting point of the search. Therefore, after a successful search, the algorithm automatically inverts the figure of merit and searches for a low thrust solution. This solution serves as a new starting point for the next highest thrust search.

Three restarts occurred during the search for maximum thrust in Fig. 2.3-1, and they each ended with a different result. The highest thrust solution, which was found during the endless search, is the final result of the provisional optimization; all local maxima are discarded.

Now we have a valid starting point for the true engine optimization. The minimum Max Climb thrust of 4.275 kN is an additional constraint and the figure of merit is re-defined as SFC. Figure 2.3-2 shows the history of an endless random search for the minimum SFC. Again, we can observe several local optima. Confidence in having found the global optimum increases with the number of optimization runs!

The final solution should be scrutinized very closely—it is not sufficient to look only at the values of design variables and constraints. The calculated properties for both the engine design point (Max Climb, ISA, 11,000 m, Mach 0.8) and the off-design condition (Take Off, ISA + 15 K, sea level, Mach 0.2) must be checked. We should also examine the low pressure turbine velocity diagrams and the off-design operating points in all component maps. Table 2.3-4 compares the growth engine performance with that of the baseline.

The optimum growth engine is influenced by three of the design constraints. Firstly, it has a fan diameter of 0.75 m, i.e. it uses the largest fan which was allowed

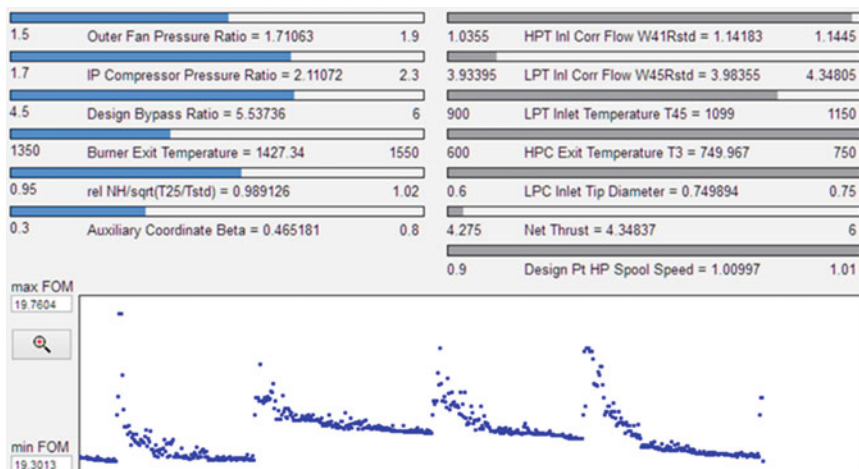


Fig. 2.3-2 Minimizing SFC

Table 2.3-4 Main cycle data comparison

	Baseline engine		Growth engine	
	Max Climb	Take Off	Max Climb	Take Off
Thrust [kN]	3.41	12.0	4.29 (+26%)	15.12 (+26%)
SFC [g/(kN * s)]	19.86	13.51	19.33 (-2.7%)	12.78 (-5.4%)
Bypass ratio	4.5	4.62	5.59	5.77
Fan P ₁₃ /P ₂	1.762	1.573	1.679	1.517
Ideal jet vel. ratio (V ₁₈ /V ₈) _{id}	0.81	0.938	0.737	0.862
Booster P ₂₄ /P ₂	1.85	1.639	2.086	1.828
HPC P ₃ /P ₂₅	12	11.21	11.59	10.72
T ₄ [K]	1350	1416	1423	1477
W _{41Rstd}	1.09	1.089	1.135 (+4%)	1.134
W _{45Rstd}	4.141	4.12	3.989 (-3.7%)	3.973
LPT η _{is} (3 stages)	0.9000	0.9113	0.8806	0.8917
T ₃ [K]	647	743	662	750
T ₄₅ [K]	973	1027	1048	1092
Fan diameter [m]	0.655		0.75	
Core spool speed [rpm]	32,000	33,600	32,320 (+1%)	33,936 (+1%)

in this exercise. The second constraint is the compressor exit temperature, which was limited to 750 K for the Hot Day Take Off case. The third constraint is the absolute gas generator spool speed which could increase by only 1%.

All the design variables remained within the predefined ranges during the optimization. The thrust increase for Max Climb and Take Off is 26%. Note that at Take Off both engines run with 5% more absolute gas generator spool speed than at Max Climb. The specific fuel consumption of the growth engine is reduced by 2.7% at altitude and by 5.4% at Take Off.

Table 2.3-4 also contains values of the ideal jet velocity ratio. This ratio indicates how the gross thrust is split between bypass and core streams. Theory says that the thrust distribution is optimal when the jet velocity ratio is equal to the product of fan and low pressure turbine efficiency. Note that the numerical optimization algorithm has automatically found a cycle for which the jet velocity ratio is near its best theoretical value (0.737): At the cycle design point of the growth engine the efficiency product is $\eta_{\text{Fan}} \times \eta_{\text{LPT}} = 0.757$.

2.4 Exploring the Design Space

Doing a parameter variation about the optimum solution is quite useful. It gives insight into the robustness of the result. Three parametric studies, each with two of the six design variables active, illustrate how the figure of merit—SFC—changes in the region around the best engine cycle.

Figure 2.4-1 shows the influence of Burner Exit Temperature T_4 and Bypass Ratio BPR with boundaries for Max Climb thrust, HP turbine flow capacity W_{41Rstd} and fan diameter. The point with the lowest SFC—the black square—rests on the maximum fan diameter line (Bypass Ratio = 5.6). The mathematical optimum is an engine which produces 1% more Max Climb thrust than required.

Figure 2.4-2 addresses the two variables which define the operating point of the high pressure compressor. The black square is situated at the crossing of the maximum fan diameter line with the T_3 boundary at Take Off.

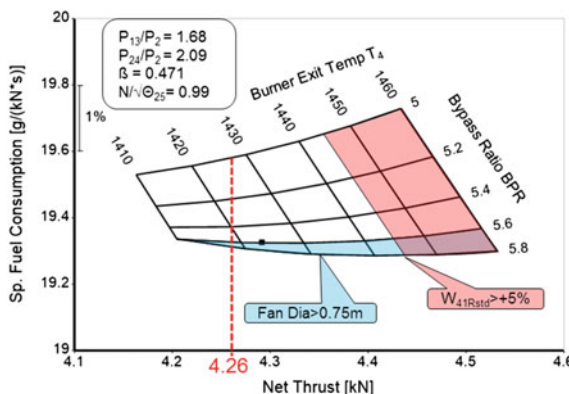


Fig. 2.4-1 Burner exit temperature and bypass ratio

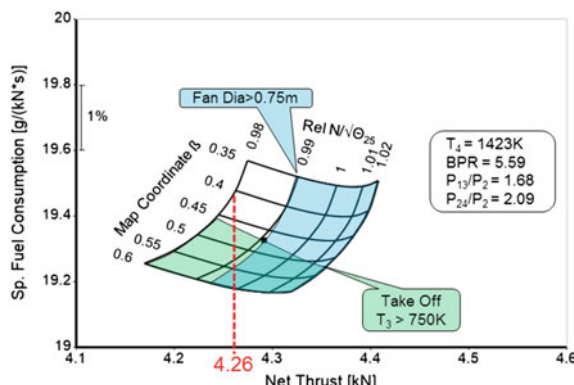


Fig. 2.4-2 Map coordinates of the compressor operating point

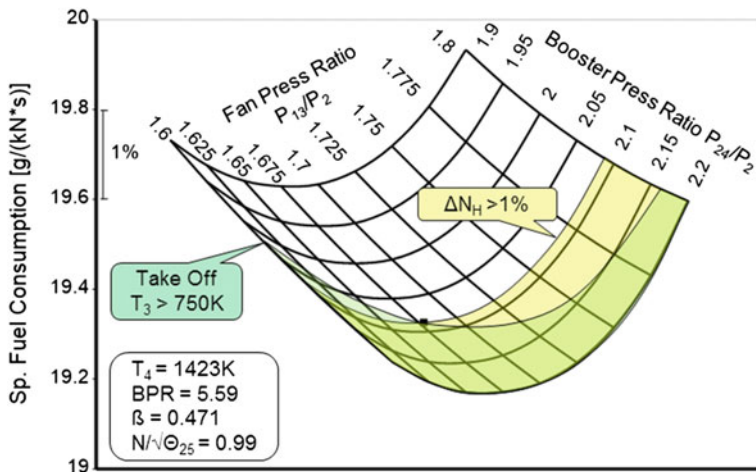


Fig. 2.4-3 Fan and booster pressure ratio

The last two design variables to be examined are fan and booster pressure ratios. In Fig. 2.4-3, the point with the lowest SFC is at the crossing of two boundaries for Take Off: T_3 is not allowed to exceed 750 K and the spool speed increase ΔN_H must not exceed +1% relative to the baseline engine.

Seemingly these figures describe completely the growth engine design space with its boundaries. However, that's not in fact the case. Only two design variables have been changed in each of the figures; four parameters were fixed at their respective optimum values. Each of the figures would have looked different if even one of the fixed parameters had been modified. It is obvious that the complete exploration of the design space with parametric studies would require a huge number of carpet plots!

In real life, the growth engine optimization would not end after finding a first solution or be limited to cycle studies only. For example, specific fuel consumption could be improved even further by adding a fourth stage to the low pressure turbine but would have a weight penalty. An additional special study would also be done to clarify whether the required thrust increase of 25% could be achieved without adding a booster (answer: this is not possible). Another possible question is *What would the thrust and SFC be if the imposed T_3 limit of 750 K at Take Off is replaced by a higher value?*

Keep always in mind: the optimization algorithm finds only the best solution for the mathematical model. The integrity of the result depends on the detail and the quality of the engine model and especially on the applied constraints. Also think about the definition of the figure of merit. Is it really Max Climb specific fuel consumption alone or should a penalty be introduced for candidate engines with more Max Climb thrust than required?

2.5 References

1. Stewart, W.L.: A study of axial-flow turbine efficiency characteristics in terms of velocity diagram parameters. ASME Paper 61-WA-37 (1961)
2. Kurzke, J.: Gas turbine cycle design methodology: a comparison of parameter variation with numerical optimization. ASME Paper 98-GT-343 (1998)

Chapter 3

Modeling an Engine



Engine manufacturers model their engines in great detail. They have all the information about the compressors and turbines and know the specifics of the secondary air system. During engine development testing, as well as thrust or power, many pressures and temperatures are measured together with spool speeds, air mass flow and fuel flow. There is a huge amount of data available which is helpful for understanding and modeling what happens in the engine.

A good performance model is built up from well understood elements. Any deviations between predictions or component rig tests and reality may be explained by differences in the component environment and known modifications of engine parts.

The situation is quite different for gas turbine users, engine maintenance shops and others in need of an engine performance model. There are never enough data for building a simulation which agrees in every detail with what happens in the engine. However, this is not necessarily required. If specific fuel consumption and thermal efficiency agree with the known data then the global parameters in the model cannot be far from the truth. Maybe one overestimates the efficiency of the compressor and underestimates the turbine efficiency, but often this does not really matter.

Simulating the performance of a competitor's engine is a typical situation in which not much information is available. It does not make sense to create a very sophisticated model with many details. It is not especially important to know the secondary air system and the amount of turbine cooling air precisely. This is because the general performance characteristic of any gas turbine depends mainly on the shape of the compressor and turbine maps.

Before we discuss ways to get good approximations for the characteristics of compressor and turbine maps let us first comment on the potential sources of data. Their value in calibrating a performance model varies widely.

3.1 Sources of Data

3.1.1 Magazines and Marketing Brochures

Do you believe all statements made in advertising? Certainly not—and therefore you should also regard the numbers published in magazines and marketing brochures with care. Often it remains unclear for which flight condition the quoted cycle data are valid. Moreover, the data are not necessarily consistent because they may belong to different operating conditions. In such a case, it is impossible to reconcile the thermodynamic cycle calculation with the published parameters.

Marketing brochures aimed at the power generation industry contain much more performance information than those for jet engines. Shaft power, thermal efficiency (heat rate), exhaust gas temperature and mass flow are often shown as functions of ambient temperature. With such information available, it is quite feasible to build and calibrate a useful performance simulation.

3.1.2 Official Engine Data

More data are available for those who are potential customers. The manufacturer provides them with tabulated performance data for a range of operating conditions. Generally, no engine internals are given, only data which are indispensable for the installation of the engine like thrust and fuel flow, air flow, exhaust gas temperature, bleed air and power offtake. The data are generated with a cycle program which calculates the performance of an average new production engine.

Instead of providing tables with data, the potential customer may get a computer program which allows the customer to calculate performance for any operating condition. Such a computer program is sometimes called a *performance deck*. This term originates from the old days where computer programs were delivered as a stack of punched cards.

As mentioned above, the thermodynamic cycle calculation describes an average new production engine, however, the manufacturing tolerances in production result in a performance scatter. Roughly half the engines are worse than average. For obvious reasons, the engine manufacturer wants to deliver all engines he manufactures, including the poor performers. Therefore, a difference is made between average and minimum (guaranteed) performance.

In the *performance deck*, there is no thermodynamic cycle for the minimum engine. The worst production engine is defined as an average engine which needs more fuel. In the performance table which the customer gets (and in the output of the performance deck) the fuel flow is simply factored up by 2.5%, for example. This process makes the number quoted for fuel flow inconsistent with the rest of the data.

Be careful with guaranteed performance data. Some of the numbers might be influenced by commercial considerations. If you try to reproduce such data with a pure cycle program, you will fail.

3.1.3 Calculated Engine Cycle Data

Companies, research institutes and universities frequently collaborate in research projects. Often the partners each use their own legacy performance program in such a context, without exchanging compressor and turbine maps. Of course, this leads to discrepancies between the performance predictions. Typical controversial topics include gas properties, polytropic compressor efficiency, secondary air system, efficiency definition for cooled turbines and mixer simulation methods for turbofan engines.

The question is: what are the reasons for the differences? Can they be reduced to the use of different input data or are the formulas different? Try to reproduce your partner's data with your own cycle code. This task has some similarities with a true engine test analysis: in this case the measured data are the results of the other performance program. This sort of measured data must agree very well with the in-house cycle code because there is no random measurement error in the given data.

The program "GasTurb Details" helps to compare the various definitions and component simulation methodologies. It gives access to the elements of the thermodynamic cycle calculations without calculating the cycle itself. Thus, cycle re-matching effects—which might dilute the effect you are looking for—are avoided.

3.1.4 Measurements Made by the Gas Turbine User

Data acquired by the operator of a gas turbine or in a pass-off test in an engine maintenance shop are very well suited for calibrating a performance simulation model. However, on the cold side of the engine there are very few sensors at each thermodynamic station. On the hot side, downstream of the combustion chamber, many thermocouple elements are employed to obtain a representative value for the mean gas temperature of the flow field with a non-uniform temperature distribution.

With the limited number of sensors, it is not possible to evaluate the absolute efficiencies and flow capacities of all the engine components. This is not always required; it is often sufficient for the measurements to be repeatable. The diagnosis of the differences between engines (due to damage or deterioration, for example) is more important than their source.

A performance model calibrated with measured data from the engine of interest can be very helpful. The simplest application of such a model in an engine

maintenance shop could be to do “What if...?” studies. How much EGT margin will be gained if the high pressure compressor is replaced by a new one? Must the high pressure turbine also be exchanged to get enough EGT margin? Can a stuck bleed valve explain the observed peculiar behavior?

3.1.5 Measurements in an Engine Maintenance Shop

In the following discussion, imagine we are in a jet engine maintenance shop. Many of the arguments are also applicable to data from test cells for engines that produce shaft power.

3.1.5.1 Contractual Performance

The aim of a pass-off test in an engine maintenance shop is to ensure that the engine is fit for flight. The test analysis procedure follows a set of rules defined by the engine manufacturer. Various adjustments are applied to the measured data before they are compared with the pass-off criteria. As well as correcting to *ISA Standard Day* operating conditions, the adjustments include the application of test cell calibration factors and possibly corrections for differences in the hardware between the engine tested and a nominal engine.

A performance model based on the data as they are used for calculating pass-off performance will not necessarily agree with what is happening inside the engine. When doing your own analysis, you are more interested in the thermodynamics than in the contractual performance. You want to know how the engine operates and why this specific engine is different from a reference engine. To make this comparison, you first need to create a thermodynamic model of the reference engine.

3.1.5.2 Thermodynamic Performance

The standard performance test in an engine maintenance shop is often limited to two operating points only: Max Continuous and Take Off. The calibrated operating range of a model which is based on only these two operating points would be very limited because they are near to each other in the compressor and turbine maps. The pass-off data from only one engine are not sufficient to calibrate a useful model.

The location in the component maps of the two pass-off test points depends on the ambient temperature on the day of the test. On a cold day, the corrected spool speeds will be high, on a hot day they will be low. It seems reasonable to enlarge the data base for the model calibration by combining data from pass-off tests done on a hot summer day with those from a cold winter day. The problem with this approach is that the data are not from the same engine. The hardware differences

due to manufacturing tolerances, variances between the sensors and deterioration introduce scatter and possibly misleading trends. A model calibrated with such data is of debatable quality.

A better basis for calibrating a performance model is the test cell calibration report. Such a report is available for any engine/test cell combination. It contains consistent data for the full operating range from Idle to Take Off.

Apply a constant test bed calibration factor to the measured thrust and correct the fuel flow for differences in lower heating value. Do not apply any other correction even though it might be part of the official test data adjustment procedure.

3.2 Data Correction

The aim of an engine performance test is to determine the thrust which the engine would deliver in a free field environment. The force measured on the engine mount in an indoor test is less than the thrust that would be recorded on a free field outdoor test bed. The necessary thrust correction consists of three main components:

- The most significant is the inlet momentum drag which is analogous to an inlet momentum effect in flight. For usual cell dimensions, it represents 70–90% of the total thrust correction.
- Cradle drag is generated by the cell bypass airflow scrubbing the exposed surfaces area of the engine casing, and “pushing against” the exposed structure which supports the engine on the thrust measurement device. Cradle drag accounts for 5–25% of the total thrust correction.
- Local acceleration of cell bypass airflow results in static pressure gradients along projected surfaces of the engine, particularly the bellmouth and exhaust nozzle. These pressure gradients generate horizontal forces which affect the measured thrust of the engine.

All three thrust correction terms grow with engine thrust itself. The dominant term—the inlet momentum drag—increases linearly with thrust over the full power range. The correlations between cradle and pressure drag with thrust are strictly speaking non-linear. However, only a very small error is introduced when a straight line approximates these two correlations, since these two drag terms constitute only a small part of the total thrust correction.

Correcting the measured force by applying a constant factor yields a pretty accurate result for all power levels. This statement is in line with the theoretical and experimental results reported in [1], for example.

The official data correction procedure described in an engine manual may contain a non-constant facility modifier for thrust. Be careful when the thrust correction factor f is not very-nearly constant and varies by more than a few percent over the full power range. In such a case, the facility modifier probably contains some elements of “contractual performance”. Do not apply a doubtful thrust correction when preparing the data for the calibration of a thermodynamic model.

3.2.1 Correction to Standard Day Atmosphere

Why should the measured data be corrected to *ISA Standard Day* conditions? If the measured data are only from one single engine, then a model could be calibrated with the raw data as they are. A problem arises as soon as there are data from more than one engine. For sure, each data set is from a test with different engine inlet temperature and pressure. It is unreasonable to compare the raw data because T_2 and P_2 are basic input parameters for the thermodynamic cycle. Calculate the same thermodynamic cycle (in *cycle design mode*) for altered inlet conditions: Thermal efficiency and power per unit of mass flow will be different even if all component efficiencies, pressure ratios and burner exit temperature are the same. It does not make sense to compare the measured data directly. They must be corrected to data which one would measure on the same engine, operated at the same power level, in a test done on a *Standard Day*.

Standard Day temperature and pressure as defined as the *International Standard Atmosphere ISA* are for sea level $T_2 = 288.15$ K and $P_2 = 101.325$ kPa. Dry air is used for aircraft engines while the power generation community assumes moist air with 60% relative humidity.

The basic idea of the correction procedure is to calculate the parameter values for standard day conditions in such a way that the velocity triangles in terms of Mach numbers everywhere in the machine are the same as tested. Since Mach number accounts for compressibility effects and flow angles dictate incidence losses and the work done in the turbomachinery, the efficiencies, temperature ratios and pressure ratios will remain unchanged during this parameter correction procedure.

Correct to ISA conditions using the traditional method which is based on non-dimensional performance parameters (see Chap. D3). Accuracy of the exponents is less important if T_2 is near to the Standard Day Temperature of 288.15 K.

3.2.1.1 Humidity Corrections

Gas turbine component performance is affected by humidity in two ways: the primary effect comes from the change in gas constant, a much smaller effect from the change in isentropic exponent. The change in gas constant can be considered in a straightforward manner.

First calculate the humidity ratio (=water/air mass ratio war) from relative humidity RH, static pressure P_s and saturation pressure P_{sat} :

$$war = 0.622 \frac{P_{sat}}{\frac{P_s}{RH} - P_{sat}} \quad (3.2-1)$$

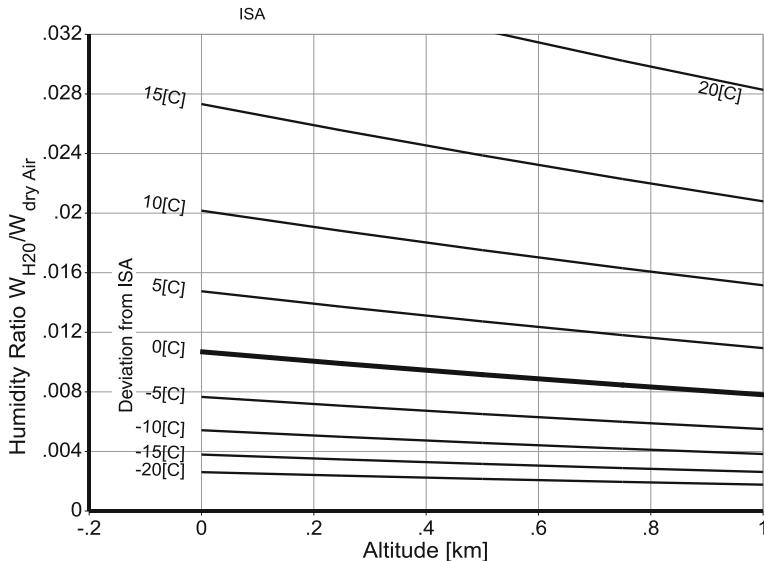


Fig. 3.2-1 Saturated humidity ratio

The gas constant for humid air then follows from

$$R_{mix} = \frac{287.06 + 461.52 * war}{1 + war} \quad (3.2-2)$$

The correction formula for corrected spool speed is

$$\left(\frac{N}{\sqrt{T}} \right)_{dry} = \left(\frac{N}{\sqrt{T}} \right)_{humid} * \sqrt{\frac{R_{dry}}{R_{humid}}} \quad (3.2-3)$$

Figure 3.2-1 shows the humidity ratio for saturated air as a function of altitude and deviation from ISA temperature. For example, correction of the speed data measured on an ISA day with 100% relative humidity to dry air conditions will reduce the corrected speed value by 0.8%.

The effect of changes in isentropic exponent due to humidity need not to be considered in the performance analysis because they are much smaller than those due to compressor inlet temperature.

3.2.1.2 Condensation Corrections

When humid air is drawn into the inlet of a gas turbine, the increase in velocity which occurs in the inlet duct, and the associated reduction in static temperature and



Fig. 3.2-2 Condensation in an aero-engine intake

pressure can result in the condensation of water droplets, (Fig. 3.2-2). The condensation process is irreversible thermodynamically and results in an increase in entropy. The released heat of vaporization raises the total temperature and reduces the total pressure of the air entering the engine, adversely affecting the performance.

Figure 3.2-3 shows the ambient relative humidity versus inlet Mach number necessary for inlet condensation to occur at ideal (i.e. equilibrium) conditions. Realistically, the liquid phase does not appear immediately after crossing the saturation line. The condensation delay occurs when there are rapid changes in temperature and pressure because it involves heat transfer, the rate of which is limited by various factors. The magnitude of the condensation delay depends on the amount and size of condensing nuclei on which the water vapor condenses out. The nuclei can be small particles in the air like salt, dust, pollen, combustion products and smog. The concentration in the atmosphere varies with geographic location, season, and weather conditions.

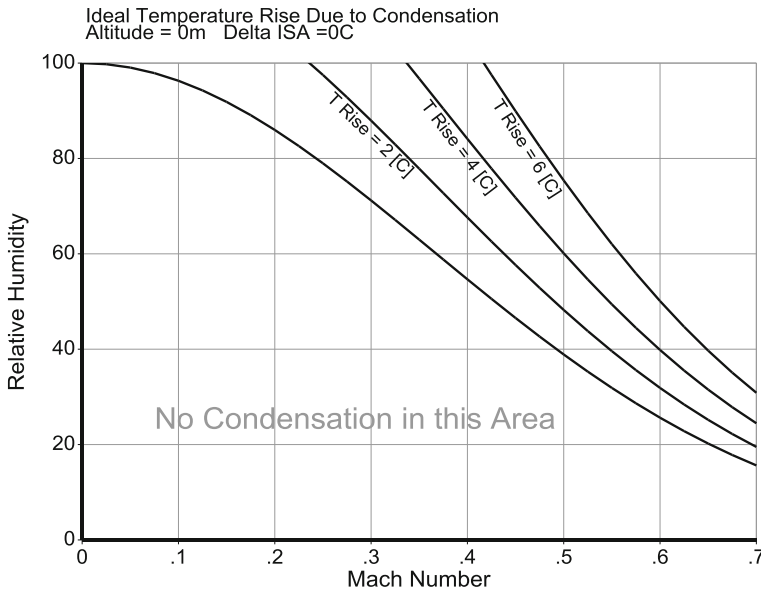


Fig. 3.2-3 Ideal temperature rise due to condensation

Condensation effects are difficult to quantify due to the problems of ascertaining the extent to which the condensation has occurred. Therefore, no performance correction method exists that is reliable and generally applicable. Applying condensation corrections when condensation has not happened, is just as much an error as not applying them when it has.

The only way out of this dilemma is not to do performance tests when condensation is expected. Reference [2] recommends an ideal temperature rise of $7 [^{\circ}\text{C}]$ as a limit for such testing. Check whether this limit has been observed before using engine test data to calibrate your model.

3.2.2 Data Enrichment

Most of the directly measured data are either pressures, temperatures, or spool speeds—except thrust (or power) and fuel mass flow. A calibrated bellmouth is the tool for accurately calculating air mass flow. The calibration curve is a correlation between the bellmouth discharge coefficient and the total-static pressure ratio or Mach number.

When no calibration curve is available, a generic correlation like the one in Fig. 3.2-4 can serve as substitute. This curve is based on data found in [1, 3–5]. The gray area indicates the range of uncertainty of the generic correlation.

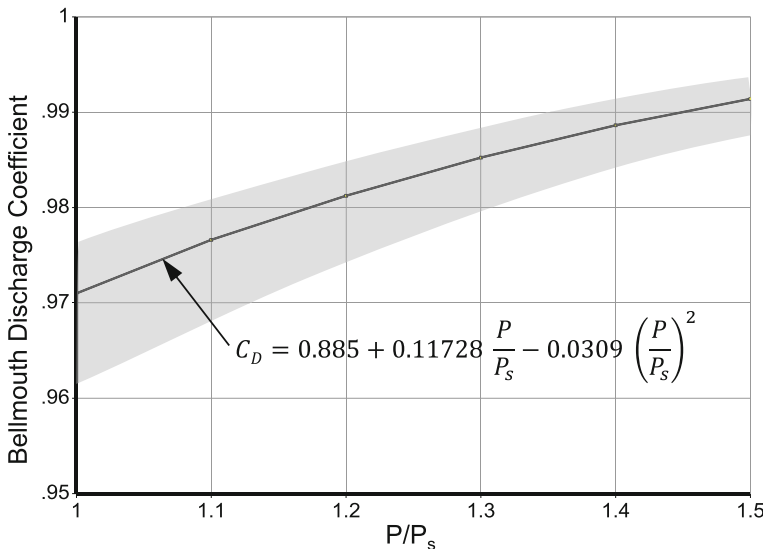


Fig. 3.2-4 Generic bellmouth calibration curve

3.2.2.1 Indirect Test Data

Directly measured pressure, temperature and spool speed data are not very helpful in the model calibration process. Tuning a model requires the adjustment of derived properties like component efficiencies, pressure ratios, corrected mass flows and spool speeds. Comparison of the model with reality and drawing conclusions from the differences is much easier if such indirectly measured (i.e. derived) quantities are combined with the test data.

The indirect test data must be calculated in the manner used in the performance program. Otherwise the comparison with the model is compromised. For example, calculating compressor efficiency with Excel is inaccurate when the gas property model in Excel is different to that used in the performance program.

The solution to this problem is: calculate the indirect test data within the performance program! This requires a capable formula editor for writing the algorithm that yields consistent derived data. Pressure ratios, compressor efficiencies and corrected spool speeds can often enrich the set of directly measured data. It is important that the overall pressure ratio P_3/P_2 is included in the indirect data because this quantity is usually accurate and is also very well suited to be the x-axis in figures containing comparisons of the model with reality.

3.2.2.2 Hybrid Test Data

Another helpful data enrichment method creates a sort of hybrid test data. Hybrid data are values interpolated from a correlation within the model, read at a given directly or indirectly measured value. As an example, take the HPC inlet corrected flow W_{25Rstd} , which is never a measured value, but nevertheless is needed for placing an operating point in the HPC map. Running the model creates the correlation between overall pressure ratio P_3/P_2 and W_{25Rstd} . We get a hybrid value for W_{25Rstd} by reading the correlation $W_{25Rstd} = f(P_3/P_2)$ with the (indirectly) measured value of P_3/P_2 .

The accuracy of the hybrid test data is not the best at the beginning of the model calibration process. But at the end, when the model lines up with all the directly measured pressures, temperatures, mass flows, thrust (or power) and spool speeds, the accuracy of the hybrid data will be as good as that of all other test data.

3.3 Cycle Reference Point

The model calibration process begins with a *cycle reference point*. This will serve as an anchor for the off-design model tuning. The performance calculation mode is “Cycle Design”. In this mode, the thermodynamic cycle calculation determines all flow areas, including those of the nozzle, and the reference flow capacities for the turbines.

Check the data before selecting your cycle reference point. Plot all known corrected spool speeds, pressure ratios, temperatures, and corrected flows with overall pressure ratio as x-axis. Do all the correlations look reasonable? A condensation shock in the inlet can be the reason for inconsistencies at the high-power end of the operating line.

Select a high-power test point which is consistent with the surrounding data points as the cycle reference point. Try running your performance calculation program in “cycle design” mode to reproduce all the known data. If all the data are consistent and a good representation of the respective thermodynamic stations, then it is easy to align the simulation with the real thing.

3.3.1 Trial and Error Method

You can use some of the given data directly as input for the cycle design calculation. If you know compressor pressure ratio, inlet and exit temperature, you can find the compressor efficiency by iteration. Similarly, you can iterate turbine efficiency in such a way that the calculated turbine exit pressure is in line with the given data.

Knowing the main cycle parameters and the thermal efficiency of the engine (or the specific fuel consumption of a turbofan) allows component efficiencies to be estimated.

Be careful if values of burner exit temperature are offered. This temperature simply is not relevant for the cycle calculation because no work is done in the turbine inlet guide vane. An unknown amount of cooling air is invariably added to the mainstream. Consequently, you know neither the decisive temperature at the inlet to the first rotor nor the turbine mass flow.

Knowledge of the exhaust gas temperature is much more helpful. At the exhaust, all the cooling air has rejoined the mainstream. Play with either burner exit temperature or bypass ratio to get the exhaust gas temperature right. Often you can identify the most important elements of the cycle input data in this way. However, many details, such as the secondary air system flow rates, duct pressure losses and mechanical efficiencies, can remain undetermined. Make reasonable assumptions for these quantities. Do parametric studies to determine how they influence the currently imperfect agreement with the data available.

It is also helpful to do sensitivity studies. These can tell us which input quantities are most important for reconciling the model with reality. Moreover, sensitivity studies show which of the questionable input quantities has no effect at all on the details of interest in the model output.

Note that in GasTurb you can highlight input quantities which influence a selected output property, a feature that helps immensely with the formulation of fruitful parametric studies.

3.3.2 *Multi Point Analysis*

This method is appropriate if you have data which have been calculated by a cycle program. Official data issued by the engine manufacturer falls into this category. Be careful: manufacturer's data might not be fully consistent. Guaranteed performance might have been calculated by running the performance model of an average engine, however, a factor on the calculated fuel flow was applied to represent the performance of a minimum performance engine. Thus, the fuel flow is not consistent with the rest of the cycle data.

3.3.3 *Optimized Data Match*

If the trial and error method does not produce satisfactory results, try numerical optimization. Declare the unknown input data as variables. Use the sum of the deviations between model and given data squared as a figure of merit. It is not necessary to define constraints for such an optimization.

Check the results carefully. Do they look right? If an optimization variable runs to its lower or upper limit, then either the limits are too stringent, or the variable has either no effect at all or only a minor influence on the data match.

3.3.4 *Unable to Create a Reasonable Model?*

The cycle program is never in error, it makes sure that all the flow and energy balances are fulfilled and that the working fluid is modeled properly. If you cannot get agreement between the model and the data, then something is wrong with your model input or with the data. The “garbage in—garbage out” syndrome!

Check the assumptions you have made: is all your information about the test vehicle correct? Was it really engine x or was it engine y which was tested? Was the test vehicle equipped with a special nozzle while you assumed it was with a nominal nozzle? Are you sure about the position of bleed valves, active tip clearance control and power offtake?

Do you know exactly where the various sensors are located and what they are measuring? Is the indicated value representative of the relevant thermodynamic station or is it only a single local value? Have the data been properly corrected to ISA conditions? Is the lower heating value of the fuel considered? Are all the unit conversion factors which have been used for processing the data correct? If anything can go wrong, it will!

Do not proceed with off-design modeling work before you have a reasonable thermodynamic model of the cycle reference point—it really would be a waste of time!

3.4 Off-Design

At the *cycle reference point*, the model fits all the data within measurement tolerance. This point is the foundation for all off-design modeling work, it will not be modified anymore.

Suitable component maps are required to predict the component efficiencies at conditions that deviate from the cycle reference point. Since the genuine component maps are not accessible, substitutes must be created during the model generation process.

At the cycle reference point, the match between the given data and the simulation should be good, since the model was tuned as well as possible in the cycle design mode. Other data points along an operating line will deviate somewhat from those of the simulation, depending on the data read from the component maps. The part-load characteristic in terms of specific fuel consumption is highly dependent on the efficiencies read from the compressor maps.

3.4.1 Compressor Maps

One should start building the off-design model with maps from compressors similar to that of the engine to be simulated. For instance, a map from a radial compressor is not suitable for describing the performance of an axial compressor. Especially for the latter the pressure ratio and the shape of the map are correlated and therefore a good match between the map and engine design pressure ratios is important.

Each compressor map yields two correlations along an operating line:

1. Corrected mass flow—efficiency
2. Corrected mass flow—corrected speed

In the final model both correlations must be in line with the given data. It is a good idea to deal with each correlation separately, beginning with the corrected mass flow vs. efficiency case, which means that the spool speed data are initially ignored.

There is a temptation to concentrate on spool speeds because they are often the most accurately measured data available. However, there are two reasons not to use them in the first step of creating an off-design model:

1. Thermodynamically, spool speed is irrelevant. Thermodynamics deals with pressure and temperature ratios, mass flows and component efficiencies. Spool speed does not show up in any of the fundamental thermodynamic correlations and is not needed for the calculation of cycle efficiency, thrust or shaft power delivered.
2. When beginning to build the simulation, the corrected mass flow—spool speed correlation is prone to errors.

To convince yourself that spool speeds are not very meaningful thermodynamically, imagine an engine with an axial compressor with variable guide vanes. Run the engine at constant pressure ratio and then change the compressor guide vane setting. The consequence of the change will be a relatively big change in spool speed, but only a very small change in any of the thermodynamic parameters because compressor efficiency at the fixed pressure ratio will remain (nearly) constant. Thus, in this imaginary experiment, the cycle has not changed, but the spool speed has, which demonstrates that spool speeds are only of secondary importance for thermodynamics.

3.4.1.1 Corrected Flow—Efficiency Correlation

At the cycle reference point, we scale the compressor map values for mass flow, pressure ratio and efficiency to agree with the engine values. By careful selection of its position in the map, the compressor part power can be matched to the data available.

For example, locating the cycle reference point in a map region with poor efficiency will allow the efficiency to increase towards part load, while locating the reference point in the peak efficiency region of the map yields an efficiency decrease at any off-reference operation.

Plot and compare your compressor efficiency data at a given compressor inlet corrected flow if that is feasible. If you do not have any information on component efficiency or flow, then plot specific fuel consumption against shaft power or thrust. If you cannot get satisfactory agreement between the model and the data by shifting the location of the cycle design point in the map, then try with another map or modify the efficiency in the map.

Eventually you should achieve a reasonable match between the given data and the simulation in a plot which employs a thermodynamic parameter as the x-axis. Calculated specific fuel consumption plotted against shaft power or thrust, will match the given data as well as all the temperatures and pressures.

Map scaling is discussed in Sect. C1.2 for compressors and in Sect. C1.3 for turbines.

3.4.1.2 Corrected Flow—Corrected Speed Correlation

Once you are happy with the flow—efficiency correlation you can start the final model adjustment step: getting the spool speeds right. This can be achieved with only minor impact on the already adjusted correlations by re-labeling the speed lines in the compressor maps.

This does not influence the efficiency at a given compressor flow and pressure ratio. The corresponding operating point of the turbine on the same spool will move in its map according to the speed change. Since the turbine operating point is normally in a region with optimum efficiency, where efficiency gradients are small, the shift of the operating point has only a small effect on the turbine efficiency. Therefore, re-labeling the speed lines in a compressor map has little influence on the agreement between the thermodynamic cycle simulation and the given data.

3.4.2 Turbine Maps

Generally, the map of any turbine which is followed by another turbine (like the high pressure turbine (HPT) of any gas generator) is not of importance to the quality of the simulation because the operating range of such a turbine is very narrow. The pressure ratio is practically constant and any changes in turbine efficiency are caused by tip clearance effects, rather than a movement on the map.

The low pressure turbine (LPT) in a turbofan behaves similarly to the HPT as long as the downstream nozzle is critical (pressure ratio > 1.8). However, when the

nozzle pressure ratio becomes sub-critical, the LPT pressure ratio decreases with the corrected LPT speed. In the map, the operating line follows the peak efficiency contour approximately. Mostly there is only a small efficiency decrease with pressure ratio.

Different behavior is seen on LPTs of turboshaft engines, turboprops and gas turbines employed for power generation that are operated with constant mechanical spool speed. Towards part-load the corrected spool speed increases which results in an operating line perpendicular to the peak efficiency contour. Since LPT efficiency varies very much, the shape of the map and the optimally selected correlation of the cycle reference point with the map are important.

3.4.3 More Simulation Details

Sophisticated performance codes used by the gas turbine manufacturers can contain a lot of detail, such as models of the secondary air system with a multitude of gas paths, Reynolds corrections to maps, tip clearance and blade untwist models, gearbox, and accessory simulations etc. It is recommended that the model creation process be started with a simple model that includes only a rough estimate of the secondary air system and where the parasitic losses are stated as percentages of the spool power. Only if it is proven that the required accuracy is not achievable, should additional secondary effects be considered.

3.5 References

1. Al-Alshaikh, A.: An Experimental and Numerical investigation of the effect of aero gas turbine test facility aspect ratio on thrust measurement. Ph.D. thesis, Cranfield University, School of Engineering (2011)
2. Propulsion and Energetics Panel Working Group 24: Recommended practices for the assessment of the effects of atmospheric water ingestion on the performance and operability of gas turbine engines AGARD advisory. Report No. 332 (1995)
3. Smith, S.C.: Airflow calibration of a bellmouth inlet measurement of compressor airflow in turbine-powered propulsion simulators. NASA TM-84399 (1985)
4. Lahti, D.J.: Verification of the theoretical discharge coefficient of a sub-critical flow meter. GE Technical Information Series R90AEB406 (1990)
5. CFM56-3 Engine Shop Manual (2012)

Chapter 4

Engine Model Examples



In this chapter, we describe the calibration of three engine performance models, employing measured data and information from the public domain. We recommend that you approach engine modeling tasks in general with these steps:

- Check input data.
- Create a *Cycle Reference Point*.
- Select suitable maps.
- Identify prime suspects for discrepancies in off-design simulation.
i.e. ignore components where operating conditions change little (HPT, LPT etc.).
- Modify efficiency trends in the suspect components.
- Look for secondary effects where test environment changes, variable geometry is adjusted, or switchable bleed flows vary.
- Finally, adjust the speeds.

As you will see, the model examples reproduce the measured data precisely. That does not mean that every model detail is correct. Nevertheless, these performance models are a sound basis for model-based test analysis (see Chap. 5) and creating input data for aircraft performance programs like APP™ (<http://aircraftperformance.software/>).

4.1 J57-19W

Engine data measured in an altitude test facility are published only rarely. An exception is the AGARD Advisory Report No. 248 [1] which presents and compares the results of testing a Pratt & Whitney J57-19W in several different test facilities.

The engine is a two-spool turbojet with a nine-stage low pressure compressor, a seven-stage high pressure compressor, a single-stage high pressure turbine and a two-stage low pressure turbine. The original exhaust system, in which the tail cone

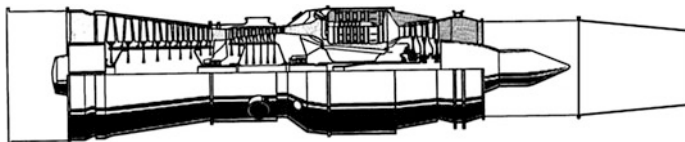


Fig. 4.1-1 J57 Cross section [2]

extends through the nozzle exit, was replaced by a cylindrical tailpipe and a convergent nozzle as shown in Fig. 4.1-1.

The model creation process begins with the thermodynamic cycle of a selected operating point, the *cycle reference point*. The calculation mode is “Cycle Design”. Neither compressor nor turbine maps are needed for this sort of calculation. The cycle reference point serves as an anchor point for off-design simulation.

4.1.1 Cycle Reference Point

The AGARD Report contains the test summary sheet for a single operating point at the altitude test facility of the Royal Aircraft Establishment RAE in Pyestock, England. It contains data for P_3 and T_3 which allow the overall compression efficiency to be computed. Temperatures and pressures between the compressors and the turbines were not measured.

The test summary sheet (Table 4.1-1) contains the most detailed information. For the other operating conditions, only the following correlations between the measured parameters are published:

- $T_8/T_2 = f(P_8/P_2)$
- $W_{2Rstd} = f(N_{LR})$
- $W_F = f(N_{HR})$
- $F_N = f(P_8/P_2)$

These data are available for the following operating conditions (Table 4.1-2).

The data originate from several different altitude test facilities. Since the AEDC data could be read from the graphs most accurately they were preferred over the Pyestock data. The combination of the engine inlet conditions and the ram ratio with the graphical data yields numbers for P_2 , P_{amb} , T_2 , W_2 , W_F , P_8 , T_8 , F_N , N_L and N_H .

Normally, the preferred cycle reference point would be in the middle of the tested range, at test conditions such as 7 or 8. A better choice would be condition 6 since the two low pressure conditions might be influenced by Reynolds number.

Most information is available for test condition 1 so this point was selected. The first cycle model matches the data of the test summary sheet (Tables 4.1-1 and 4.1-3).

The distribution of the overall compression between the low and the high pressure compressors in this cycle calculation is a guess based on information from Ref. [2]. The numbers which agree exactly with those from the test summary sheet

Table 4.1-1 Test summary sheet

UNIFORM ENGINE TESTING PROGRAM			
LOCATION:	RAE PYESTOCK, ENGLAND	FACILITY:	Cell 2
	RECORDED:	84-10-2	11-49-56
	PROCESSED:	84-10-8	13-55-55
POINT: 101			
SUMMARY OF TEST CONDITIONS			
STA	STATION AVERAGES T(K) P(kPa)	AIRFLOW (KG/S)	THRUST (KN)
00	253.82	81.051	55.567
2	253.82	82.291	45.4545
13	584.87	1060.86	55.667
31	834.82	230.628	45.4545
8	828.66	220.372	42.2470
04			
05			
08			
ENGINE PRESS. &TEMP. RATIOS			
P5Q2	2.0026	13.0011	
T5Q2	3.2891	2.3043	
P2QAMB	1.0153	0.82454	
P7QAMB	2.7109		
P8Q2	2.6700		
T8Q2	3.2648		
COMPRESSOR PERFORMANCE			
P3Q2			
T3Q2			
EC			

Table 4.1-2 Test condition summary

Test Condition	Inlet Pressure P ₂ [kPa]	Ram Ratio P ₂ /P _{amb}	Inlet Temp T ₂ [K]
1	82.7	1	253
2	82.8	1	268
3	82.7	1	288
4	82.7	1	308
5	82.7	1.06	288
6	82.7	1.3	288
7	51.7	1.3	288
8	34.5	1.3	288
9	20.7	1.3	288
10	82.7	1.7	288

Table 4.1-3 Cycle matched to the measured data from Ref. [1]

Station	W kg/s	T K	P kPa	WRstd kg/s	FN	=	42.24 kn
amb		252.72	81.051		TSFC	=	23.7787 g/(kN*s)
1	69.395	253.81	82.285		FN/W2	=	608.73 m/s
2	69.395	253.81	82.285	80.200	WF_Burner	=	1.00448 kg/s
24	69.395	400.08	323.945		Core_Eff	=	0.3503
25	69.395	400.08	317.466	26.098	Prop_Eff	=	0.1346
3	68.007	584.88	1069.860	9.176			
31	60.721	584.88	1069.860		P2/P1	=	1.0000
4	61.725	1185.64	1011.018	12.548	P25/P24	=	0.9800
41	65.195	1155.88	1011.018	13.086	P3/P2	=	13.0019
43	65.195	984.35	456.496		P45/P44	=	1.0000
44	68.665	965.26	456.496		P6/P5	=	0.9555
45	68.665	965.26	456.496	27.895	w_NG/w25	=	0.05000
49	68.665	834.69	230.624		WHC1/w25	=	0.05000
5	70.053	828.65	230.624	52.193	WLCL1/w25	=	0.02000
6	70.053	828.65	220.368		WBBLD/w25	=	0.00500
8	70.053	828.65	220.368	54.622	A8	=	0.23890 m ²
Bleed	0.347	584.88	1069.860		WB1d/W2	=	0.00500
						=	0.00
Efficiencies:							
isentr polytr RN1 P/P							
LP Compressor	0.8300	0.8590	0.943	3.937	CD8	=	0.96000
HP Compressor	0.8739	0.8929	2.119	3.370	P8/pamb	=	2.71888
Burner	0.9893				W1kLP/W25	=	0.00000
HP Turbine	0.8456	0.8324	1.957	2.215	Loading	=	100.00 %
LP Turbine	0.8600	0.8491	1.086	1.979	e444_th	=	0.82251
					w1ko/w25	=	0.00000
					far7	=	0.01455
HP Spool mech Eff	0.9900	Nom Spd	9223 rpm		PWX	=	0.0 kw
LP Spool mech Eff	0.9950	Nom Spd	5942 rpm		FHV	=	43.187 MJ/kg

are highlighted in yellow. Note that the spool speeds are of no relevance for this type of cycle model. Figure 4.1-2 shows the station designation and a schematic of the secondary air system.

It is very important to check the data for plausibility and consistency before finally selecting the cycle reference point. Note that the AGARD report mentions some unexpected scatter between the results from the various test facilities for the thrust coefficient and nozzle discharge coefficient data.

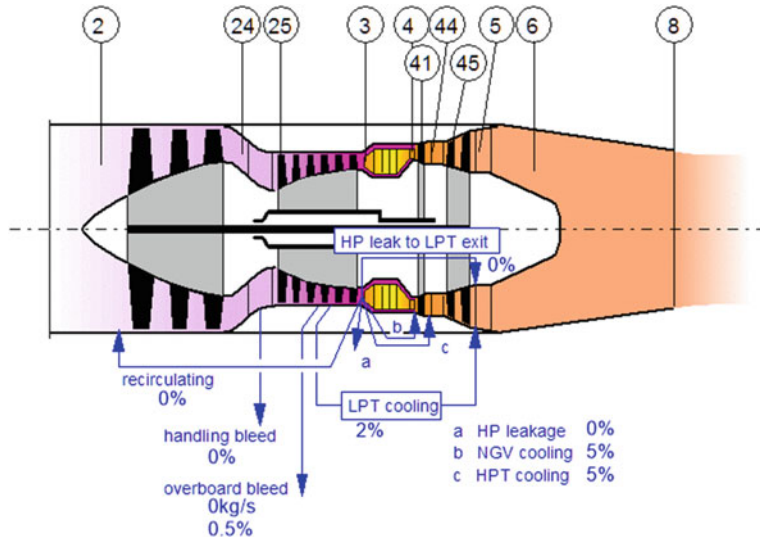


Fig. 4.1-2 Station nomenclature

The gross thrust coefficient is defined in the report as the ratio of measured thrust over thrust calculated from W_8 , T_8 , P_8 , A_8 and P_{amb} . This ratio does not infer nozzle performance, it is a sort of “facility modifier” for thrust. This facility modifier corrects the measured force for inlet momentum, external static pressure distribution on the engine structure and stray forces acting on the engine test frame, as well as differences between the ideal and the real nozzle thrust. We will compare our simulation results with the corrected thrust values from the facility. The gross thrust in our model is that of an ideal convergent nozzle.

The second problem with the data is the scatter in the nozzle discharge coefficient, apparent in Fig. 4.1-3. Our data check uses the measured values W_2 , W_F , T_8 and P_8 for calculating the corrected flow through the nozzle. Theoretically, all the $(W_2 + W_F)\sqrt{T_8/P_8}$ values should collapse onto a single line when plotted over nozzle pressure ratio P_8/P_{amb} .

Figure 4.1-3 shows the relevant data from AEDC. Most of the points fall into a narrow band. Only those from the low pressure test case number 9 are a little bit on the low side. These corrected flow values deviate approximately 1% from the other data—this is not much and therefore acceptable. Thus, we have convinced ourselves that the AEDC nozzle discharge coefficient data are consistent and a good basis for establishing an off-design simulation.

However, there is another problem: the SFC data from Pyestock are about 1.6% higher than those from AEDC in Fig. 9-11 of Ref. [1]. We cannot use the cycle from Pyestock as our reference case because it is inconsistent with the data from AEDC data. So we select the AEDC data for the highest thrust measured for test case 1 as our cycle reference point (Table 4.1-4).

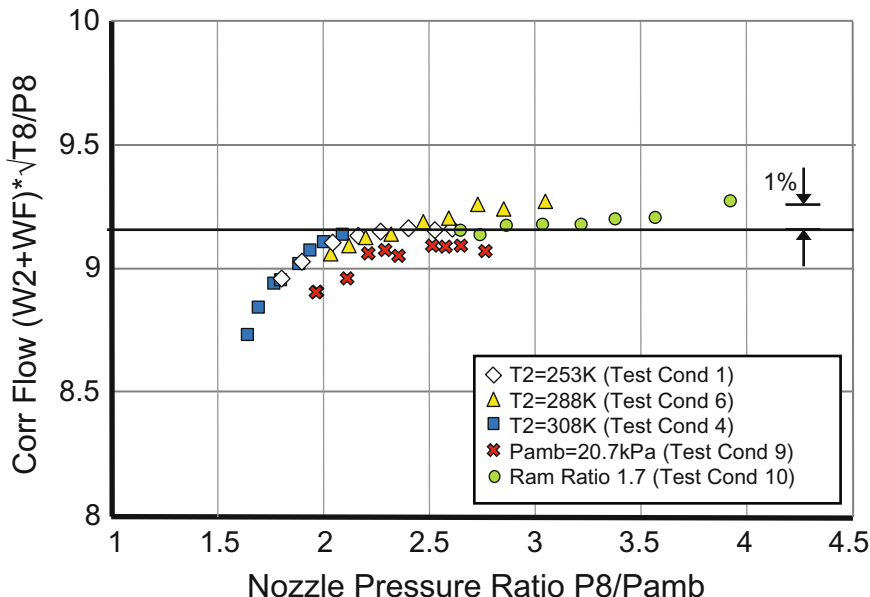


Fig. 4.1-3 Data check for AEDC

Table 4.1-4 Cycle reference point

Station	W kg/s	T K	P kPa	WRstd kg/s	FN	=	46.85 kN
amb		253.03	82.705		TSFC	=	22.1311 g/(kn*s)
1	70.955	253.03	82.705		FN/W2	=	660.32 m/s
2	70.955	253.03	82.705	81.460	WF_Burner	=	1.03684 kg/s
24	70.955	401.05	326.684		Core_Eff	=	0.3551
25	70.955	401.05	320.151	26.493	Prop_Eff	=	0.0000
3	69.749	598.40	1120.528	9.089	P5/P2	=	2.8745 EPR
31	62.440	598.40	1120.528		P2/P1	=	1.0000
4	63.477	1199.00	1058.899	12.390	P25/P24	=	0.9800
41	67.024	1169.34	1058.899	12.920	P3/P2	=	13.5485
43	67.024	985.25	462.389		P45/P44	=	1.0000
44	70.430	967.53	462.389		P6/P5	=	0.9555
45	70.430	967.53	462.389	28.281	w_NGV/w25	=	0.05000
49	70.430	836.52	237.732		WHC1/w25	=	0.04800
5	71.636	831.49	237.732	51.866	wLC1/w25	=	0.01700
6	71.636	831.49	227.160		WBBLD/w25	=	0.00500
8	71.636	831.49	227.160	54.280	A8	=	0.23750 m ²
Bleed	0.355	598.40	1120.527		WB1d/w2	=	0.00500
						=	0.00
Efficiencies:	isentr	polytr	RNI	P/P	CD8	=	0.96000
LP Compressor	0.8200	0.8507	0.952	3.950	P8/pamb	=	2.74663
HP Compressor	0.8500	0.8732	2.131	3.500	w1kLP/w25	=	0.00000
Burner	0.9945				Loading	=	100.00 %
HP Turbine	0.8650	0.8527	2.022	2.290	e444_th	=	0.84230
LP Turbine	0.8820	0.8728	1.097	1.945	w1ko/w25	=	0.00000
HP Spool mech Eff	0.9820	Speed	9235	rpm	far7	=	0.01468
LP Spool mech Eff	1.0000	Speed	5955	rpm	PWX	=	20.0 kw
					FHV	=	42.960 MJ/kg

The main differences between these cycle data and those matching the test summary sheet (Table 4.1-3) are highlighted in yellow. Corrected mass flow W_{2Rstd} and overall pressure ratio P_3/P_2 are slightly higher, LPC efficiency is 1% lower than in Table 4.1-3. The other model details are adjusted in such a way that F_N , W_2 , W_F , T_8 , and P_8 agree with the respective values reported by [1].

Note that burner and turbine efficiencies are higher (and more plausible) than in Table 4.1-3. Increasing these numbers was necessary for getting SFC right.

4.1.2 Off-Design Simulation

4.1.2.1 Simulation with GasTurb Standard Maps

The general rule for component map selections is: use maps from machines of similar design. All GasTurb Standard Maps are from axial turbomachines and therefore suited for a first attempt at engine simulation.

In our first simulation, we use the default values of GasTurb for the coordinates of the map scaling point and switch off Reynolds number corrections. For the nozzle discharge coefficient, we use a correlation $C_{D8} = f(P_8/P_{amb})$ consistent with the data in Fig. 4.1-3.

Figure 4.1-4 shows a SFC comparison of the initial model with the measured data from test cases 1 ($T_2 = 253$ K) and 4 ($T_2 = 308$ K). The ellipse around each of the test data points indicates the measurement uncertainty quoted by [1]. This result is surprisingly accurate—the calculated SFC agrees with nearly all the measured data within measurement accuracy.

SFC is an important thermodynamic parameter, but not the only one. A good simulation must agree with all the known test data, otherwise the engine is not really understood. It does not take long to detect significant differences between our initial model and the given data. The calculated nozzle throat temperature T_8 agrees with the measurements only at the cycle reference point (Fig. 4.1-5). Note that the quoted measurement accuracy for T_8 is quite good—the value compared with the simulation is based on more than 36 thermocouple readings for each single operating point.

How can we correct this deficiency in the simulation? Obviously, the component efficiencies in the model deviate from reality at part load. We must modify the efficiency changes along the operating line in one or several component maps. Which of the four maps (two compressor maps and two turbine maps) should we consider first?

The length of the operating lines in the four maps are quite different. The high pressure turbine (HPT) operates at constant pressure ratio since the corrected flow of the low pressure turbine is constant. Corrected HPT speed varies only a little and therefore the operating line is very short. Consequently, we always read the same efficiency from the HPT map in our simulation; modifying the HPT map does not affect part load SFC characteristics.

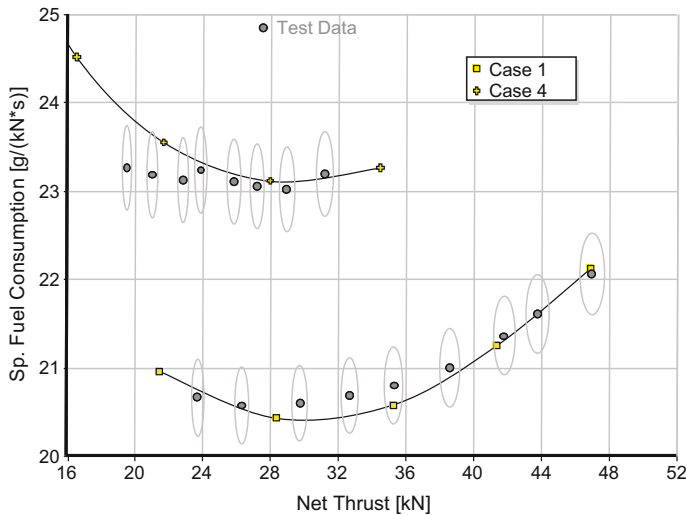


Fig. 4.1-4 Initial SFC simulation results

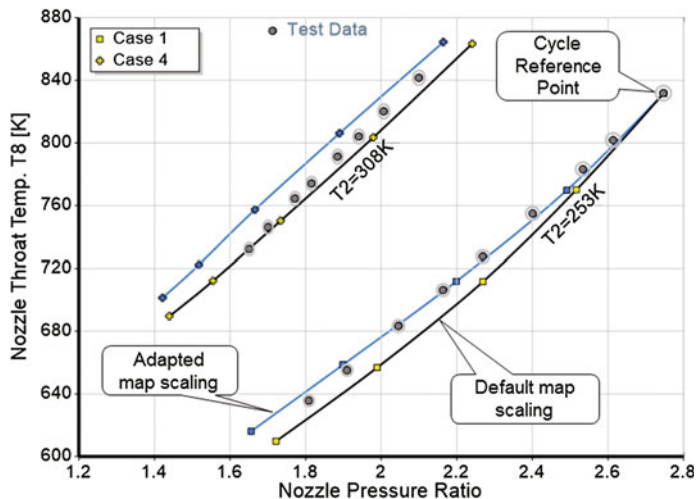


Fig. 4.1-5 Nozzle throat temperature

In the map of the low pressure turbine the situation is very similar, since the nozzle downstream of the LPT is choked in all test cases except for the lower thrust part in case 4 (see Fig. 4.1-3). The operating line is longer than in the HPT, but still not long enough to justify more than minor efficiency changes.

The dominant influence on part load T_8 originates from the efficiency variations along the compressor operating lines. For the low pressure compressor (LPC), we can expect a bigger efficiency variation than for the HPC since the LPC operating line is significantly longer than that in the HPC map. The efficiency change along the LPC operating line is the prime candidate for the cause of deviation between the simulation and the test results.

Let us try to improve the quality of the simulation by changing the LPC map scaling. We move the map scaling point in the unscaled map to a higher pressure ratio, where the efficiency is better, as indicated in the right half of Fig. 4.1-6. Now the efficiency increases towards part load from the cycle reference point value 0.82 to 0.862 ($\Delta\eta = 0.042$). In the left half of Fig. 4.1-6 the efficiency increases to the unrealistically high value of 0.892 ($\Delta\eta = 0.072$).

The effect of this change is a nearly perfect agreement between measured and simulated T_8 for test case 1, as shown in Fig. 4.1-5. However, the initial good match for test case 4 is now gone. Figure 4.1-7 shows that quality of the SFC simulation also got worse.

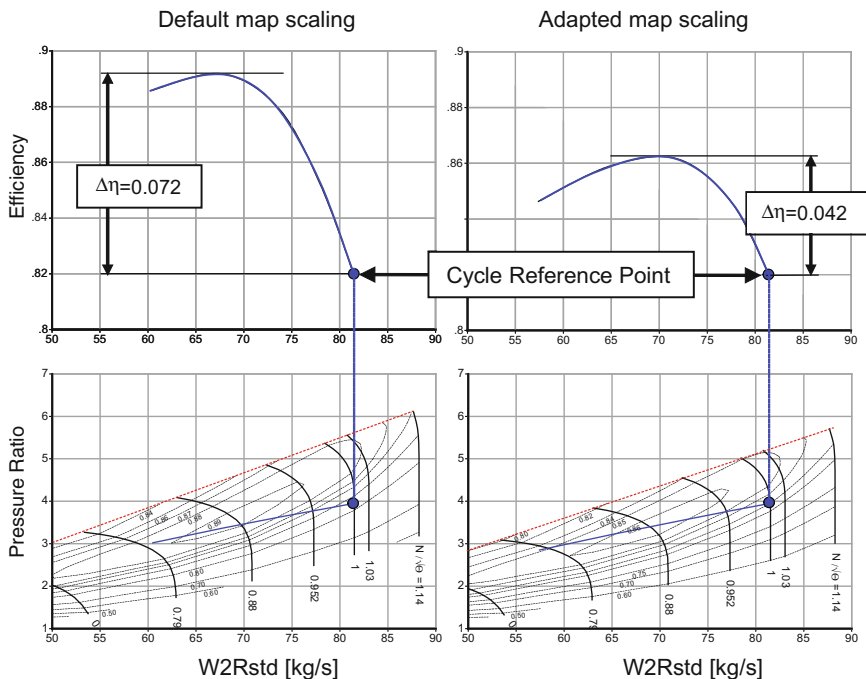


Fig. 4.1-6 Default and adapted scaling of the GasTurb Standard Map for the LPC

What is the reason for the different SFC deviations for cases 1 and 4? A look at the locations and lengths of the two operating lines in the LPC map makes it immediately obvious; the two operating lines are in different regions of the

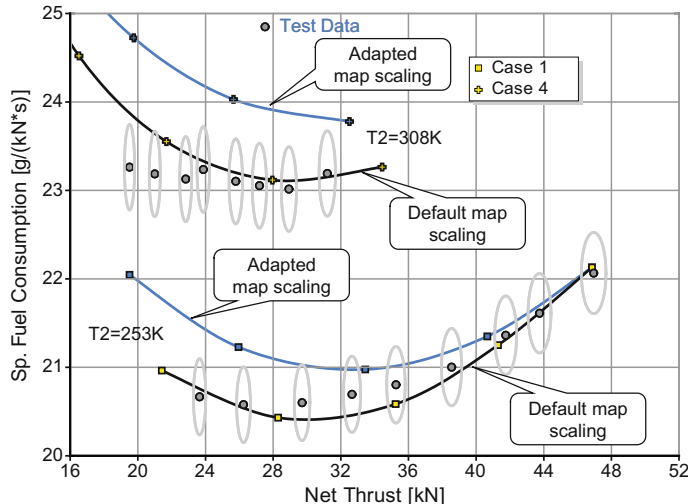


Fig. 4.1-7 SFC for two different map scaling point settings in the GasTurb Standard LPC map

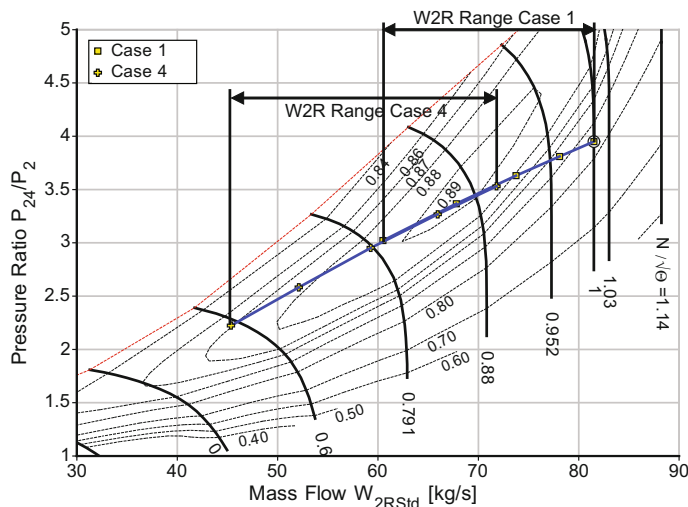


Fig. 4.1-8 Case 1 and 4 operating lines in the LPC map

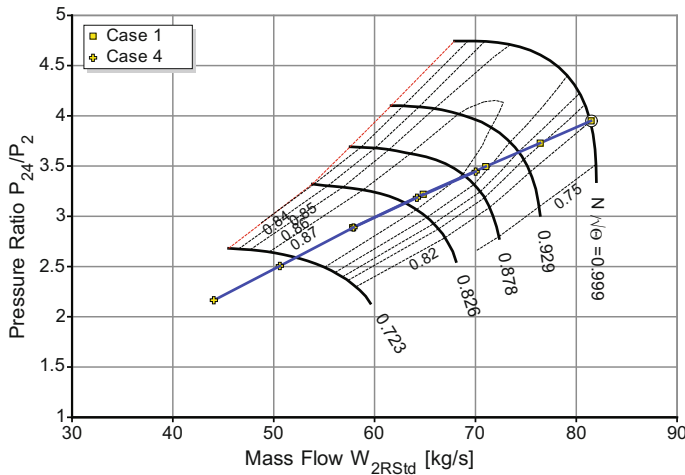


Fig. 4.1-9 LPC map, scaled from the map in Ref. [4]

map. High inlet temperature (case 4, $T_2 = 308 \text{ K}$) shifts the operating line to lower corrected flows (Fig. 4.1-8).

For case 1, the modified map scaling produces a good T_8 match combined with acceptable agreement of the SFC numbers in the high thrust range (Figs. 4.1-5 and 4.1-7). SFC is too high at the low W_{2RStd} end of case 1 and over the full W_{2RStd} range of case 4. Increasing LPC efficiency at lower mass flows, beginning in the region where the two operating lines overlap, is a big step in the right direction.

We could improve the model slightly by repositioning the cycle design point in the HPC and the LPT maps, but we cannot match the data from test cases 1 and 4 simultaneously without modifying the LPC map in the manner explained above. We need a LPC map whose efficiency contours have a different shape.

4.1.2.2 Replacing the LPC Map

Note that the speed lines are vertical in the high-speed range of the GasTurb Standard map for the LPC. This indicates that the map is from a transonic compressor. Another clue to the presence of high Mach numbers is the shape of the efficiency contour lines in this map: the peak efficiency region at high corrected flow is nearer to the surge line than it is at low and medium corrected flow.

However, both J57 compressors, are subsonic designs. The pressure ratio per stage is only 1.17 for the LPC and 1.2 for the HPC. For comparison: the EJ200 fan achieves a higher pressure ratio in only 3 stages than the 9 stage LPC of the J57! For a better simulation, we need to replace both compressor maps with maps from a subsonic compressor.

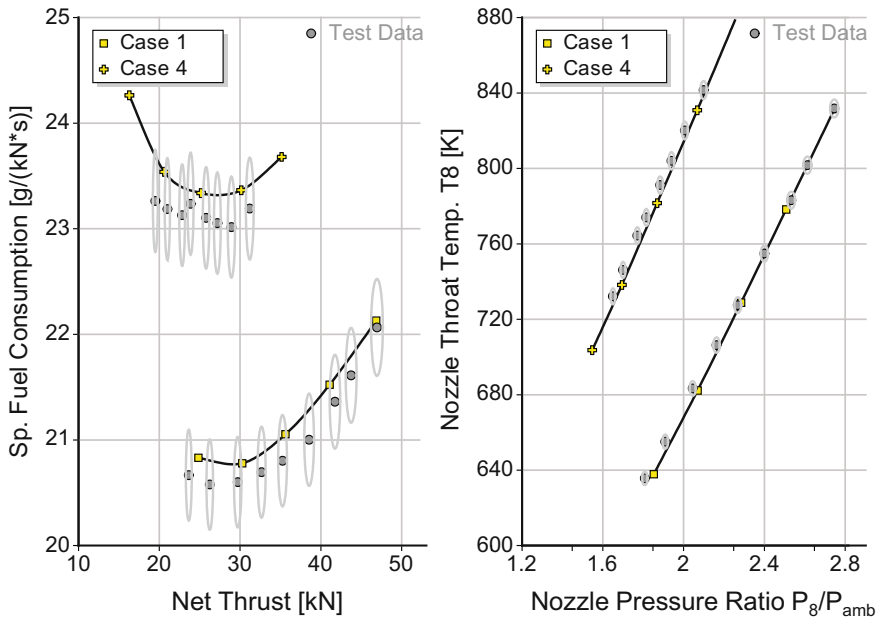


Fig. 4.1-10 Result with LPC and HPC maps scaled from the map shown in Fig. 4.1-9

A map suitable for our task has been published in Ref. [4]. There, the design point pressure ratio of the three-stage compressor tested is only 2.4. The pressure ratio per stage is 1.34 and the maximum Mach number at the inlet of the first rotor is only 0.8285.

With this map scaled to the respective J57 LPC and HPC pressure ratios, mass flows and efficiencies, we get better results for SFC and T_8 for both test cases 1 and 4, as seen in Fig. 4.1-10. Both SFC and T_8 are within measurement tolerance.

4.1.2.3 The High Altitude Case

Next, we check our simulation against all the other available data. Test cases 6 and 10 are in the middle of the temperature range ($T_2 = 288$ K), the engine inlet pressure is $P_2 = 82.7$ kPa. The difference between these two operating conditions is in the ram ratio which is 1.3 for case 6 (corresponds with flight Mach number $M = 0.624$) and 1.7 for case 10 ($M = 0.905$). Additionally, we check our model against test case 9 which has the lowest inlet pressure ($P_2 = 20.7$ kPa).

The performance model based on the scaled compressor map from [4] agrees very well with all the test cases, except for the low inlet pressure case 9. There are two possible reasons why this simulation does not agree with the measurements:

Table 4.1-5 Reynolds correction for the highest thrust of test case 9

	Efficiency	Capacity	Comment
LPC	-6%	-4.7%	RNI = 0.2
HPC	-4.3%	-3%	RNI = 0.44
Burner	-3.3%	n/a	Loading = 300% rel Cycle Ref Pt
HPT	-3.2%	-3.2%	RNI = 0.39
LPT	-2.8%	-2.8%	RNI = 0.2
Nozzle	n/a	-1%	See Fig. 4.1-3

1. poor burner efficiency
2. Reynolds number effects

We can evaluate burner efficiency from the measured values of W_2 , T_2 , W_F and T_8 using an energy balance. For the top thrust point of the case 9 operating line we find $\eta_{\text{Burner}} = 0.967$; there the burner loading is 300% of that at the cycle reference point. When thrust is reduced, burner loading increases up to 540%. For the lowest thrust point of test case 9, we can deduce a burner efficiency of $\eta_{\text{Burner}} = 0.9$.

The burner efficiency model of GasTurb reproduces these values from an input of $\eta_{\text{Burner}} = 0.9945$ at the cycle reference point combined with the default value for the burner part-load constant B of 1.6.

Modeling the Reynolds number effects is more difficult. The question is: how to distribute the losses between the compressors and turbines? We must find two correction factors for each of the four turbomachines: one for efficiency and one for flow capacity. There are not enough measured parameters available to create an unambiguous model. Nevertheless, we found a reasonable looking set of factors based on “engineering judgement”, see Table 4.1-5.

Figures 4.1-11 and 4.1-12 show that the correspondence between the simulation and the test data is nearly always within the quoted uncertainty of the measured values.

4.1.2.4 Spool Speed Model

The agreement between the simulation and the measured data is certainly acceptable, but what about the spool speeds? We ignored them because they were not needed for the thermodynamic model. No wonder that the spool speeds of our preliminary simulation don't agree with the measurements!

Figures 4.1-13 and 4.1-14 show that there are big discrepancies, with a close match only at the cycle design point (top point of case 1).

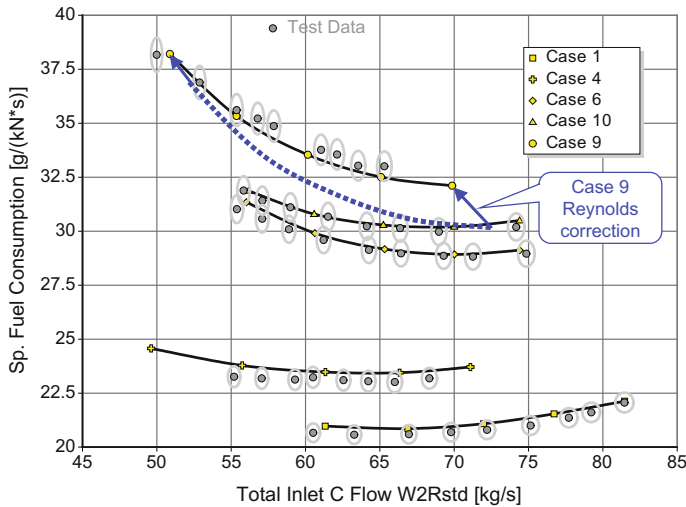


Fig. 4.1-11 SFC for all test cases

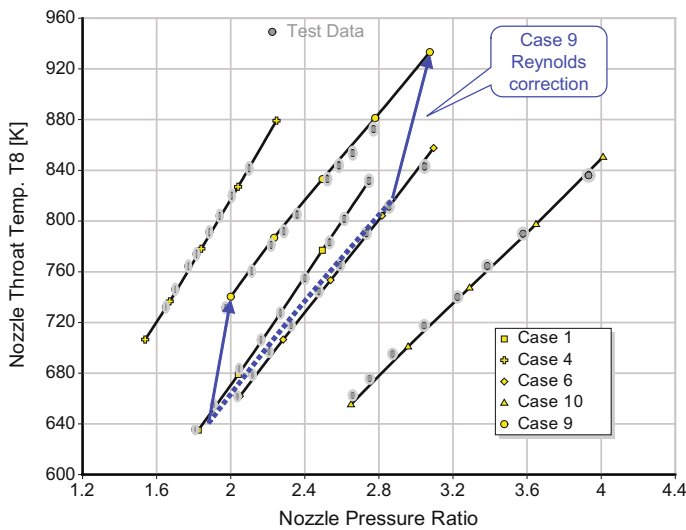


Fig. 4.1-12 T_8 for all test cases

We can correct this model deficit with only minor impacts on the thermodynamic model. We only need to re-label the speed lines in the LPC and HPC maps to get a satisfactory alignment of the spool speed model and the corresponding measured data (Figs. 4.1-15 and 4.1-6). Compare Figs. 4.1-11 and 4.1-12 with Figs. 4.1-17 and 4.1-18 to see that re-labeling the speed lines has not disturbed the SFC and T_8 agreement between model and measurement.

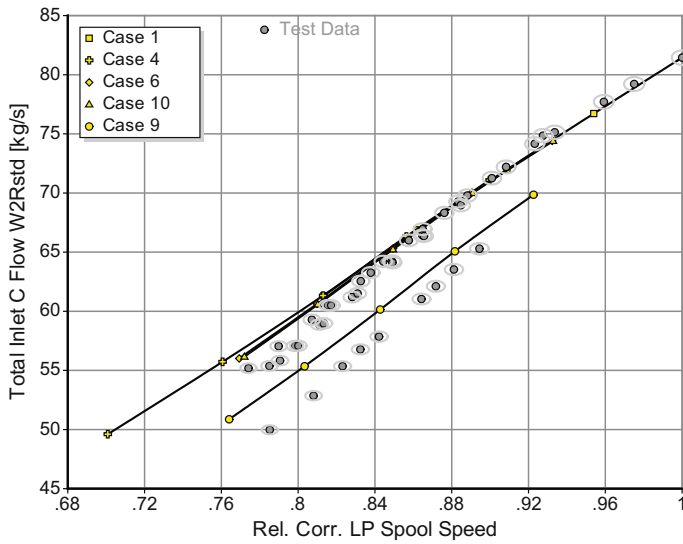


Fig. 4.1-13 Uncalibrated relative corrected LP spool speed for all test cases

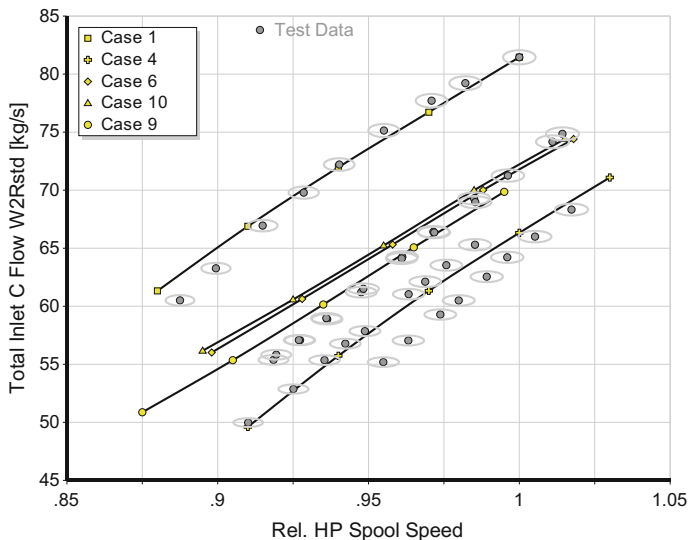


Fig. 4.1-14 Uncalibrated relative HP spool speed for all test cases

You might assume that re-labeling the speed lines of a map is an arbitrary act. Remember, however, that the speed-flow relationship in the maps we have scaled is most probably different from that in the true J57 compressor maps. There is some scatter around the general trend of the speed-flow relationship in compressor maps and within that scatter it is legitimate to play with the numbers.

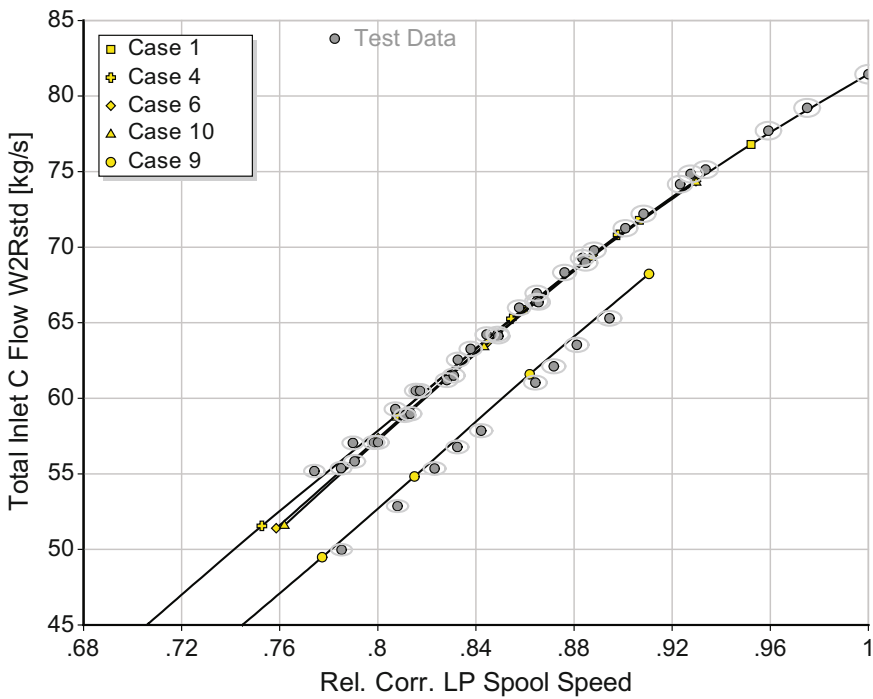


Fig. 4.1-15 Calibrated relative corrected LP spool speed for all test cases

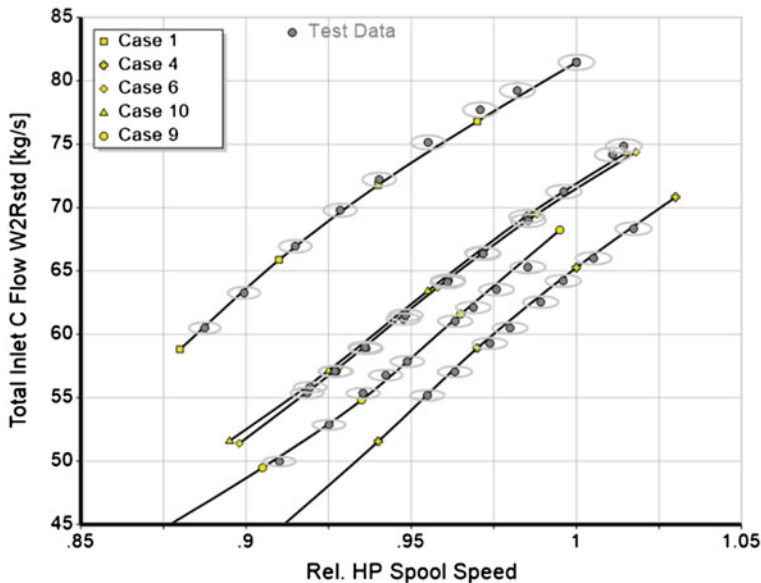


Fig. 4.1-16 Calibrated relative HP spool speed for all test cases

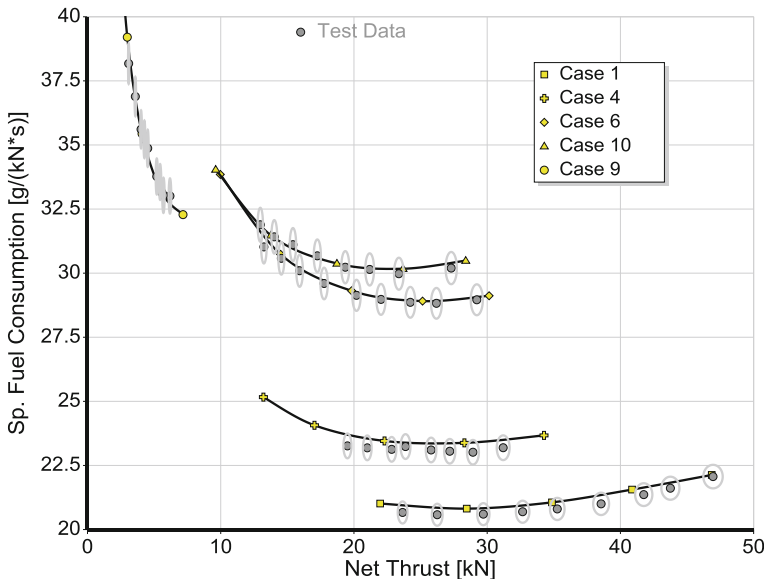


Fig. 4.1-17 SFC for the final model

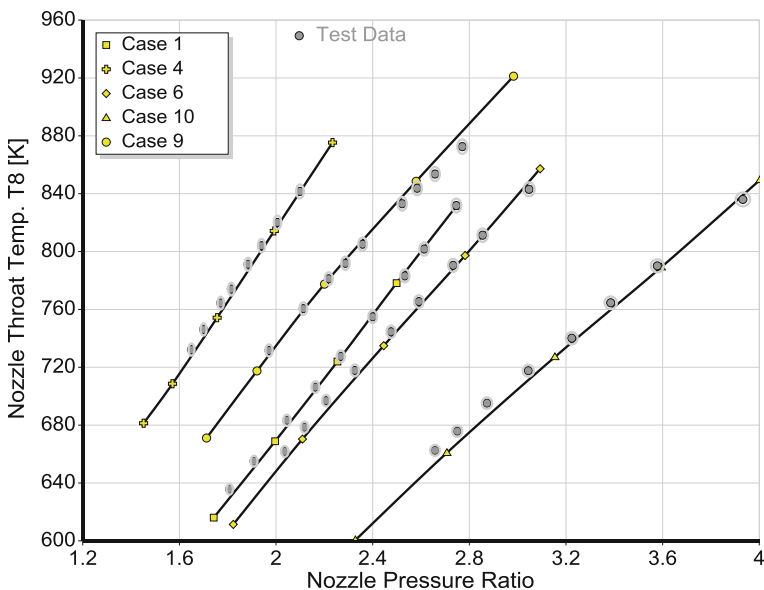


Fig. 4.1-18 Nozzle throat temperature for the final model

The next two figures (Figs. 4.1-19 and 4.1-20) show the operating lines in the two compressor maps. Two values are written next to the speed lines, except for the speed line $N/\sqrt{\Theta} = 1$. The speed values of the unscaled map are in brackets; the other speed numbers are those used in the J57 model.

Note that the revised speed values are valid only near the operating lines. Nothing is known about the true curvature of the speed lines. Since we have scaled

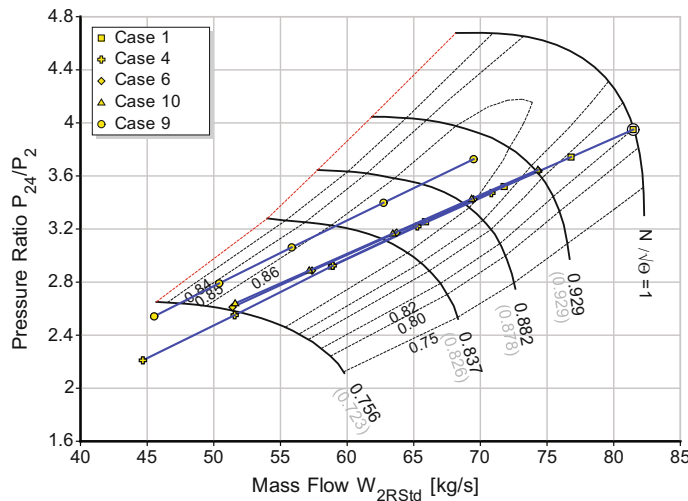


Fig. 4.1-19 Operating lines in the LPC map

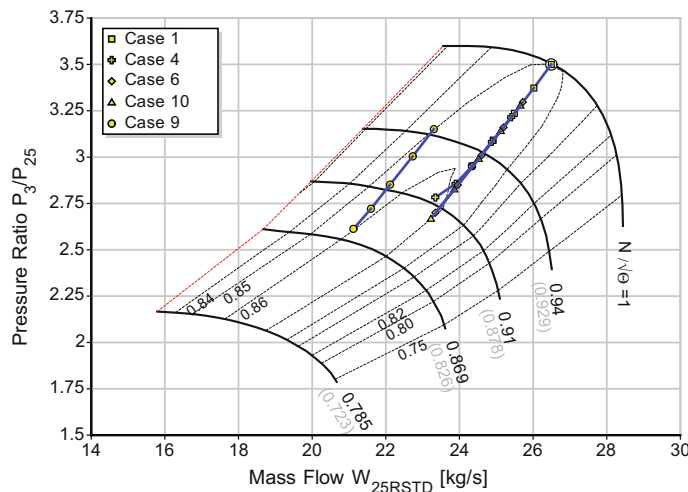


Fig. 4.1-20 Operating lines in the HPC map

the map from a compressor with similar Mach number level, we can have some confidence in our compressor performance model.

The model would not be complete without the turbine maps and these are shown in Figs. 4.1-21 and 4.1-22. The operating lines in the HPT map are very short, which is to be expected from theory. Test case 9 is an outlier because of the Reynolds number effects.

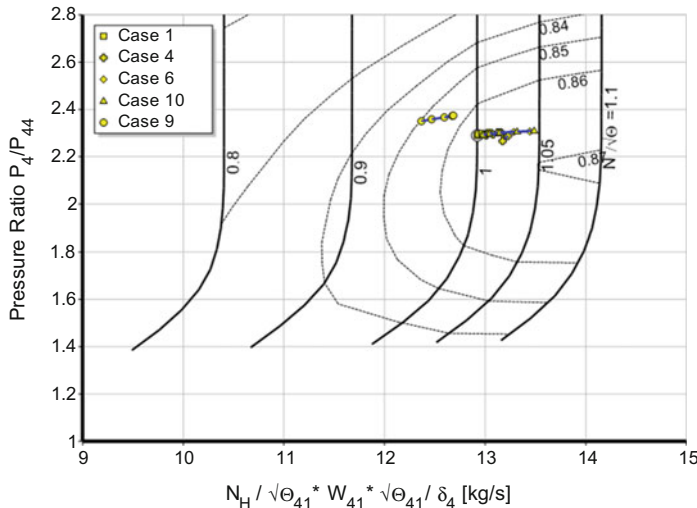


Fig. 4.1-21 Operating lines in the HPT map

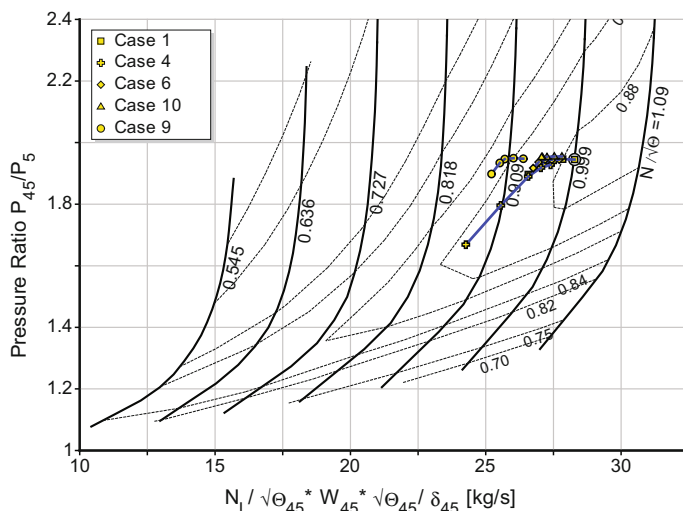


Fig. 4.1-22 Operating lines in the LPT map

4.1.2.5 Final Remarks

If instead of W_2 , either the LP or HP spool speed had been used as the x-axis for the comparison between the simulation and measured data, the task would have been much more difficult. Until the speed lines in the compressor maps are labeled correctly, discrepancies would be seen between the model and the thermodynamic data—even if the thermodynamic model is correct. Therefore, it is not a good idea to compare spool speed simulation results with the measured value at the beginning of the model creation process. It would make the model adjustment process a very frustrating task.

4.2 CFM56-3

You have almost certainly flown in an Airbus A320 or Boeing 737 equipped with CFM56 engines. These turbofans are in the 100 kN Take Off thrust class. The CFM56-3 is the variant installed on the Boeing 737-400.

CFM56 engines are overhauled not only by the OEM but also in various independent maintenance shops around the world. One of these maintenance shops, owned by T.A.P. Air Portugal, is in Lisbon. The Portuguese fleet takes up around 60% of the repair capacity, the remainder is dedicated to external customers.

The data measured on a CFM56-3 engine in the Lisbon test cell (Fig. 4.2-1) were correlated with those from the SNECMA production test cell data in October 1991. Running the same engine in both facilities yields different raw data because the general layout and the dimensions of the Lisbon cell are different to those of SNECMA. Reconciling the corrected data from each test cell requires the application of so-called facility modifiers which are a form of calibration factors. The result of a CFM56 test cell correlation campaign are facility modifiers for thrust, exhaust gas temperature EGT, fuel flow, core spool speed N_2 and mass flow.

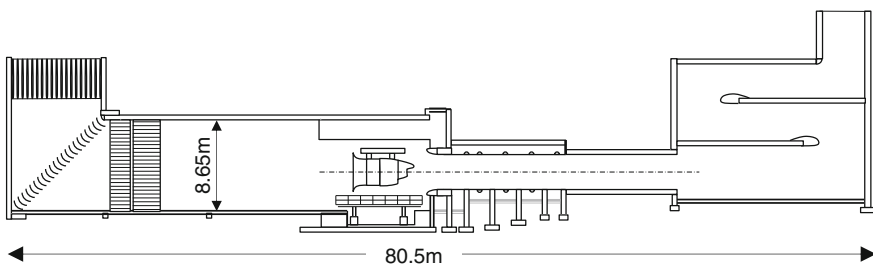


Fig. 4.2-1 Test cell of T.A.P. Air Portugal, Lisbon

Before an engine is declared fit for flight it must pass the acceptance test. The raw data from this test are analyzed using a standardized procedure which includes the application of the facility modifiers. Performance wise, the engine is OK when it has sufficient EGT margin and meets an SFC criterion. The official acceptance test result contains no statement about the quality of the engine components. This, however, is of great interest to the maintenance shop.

Having a thermodynamic model of the cycle can be of great help for analyzing engine component performance. Creating such a model is the topic of this section.

How to calibrate the model? Should we use the corrected data from the official test analysis procedure as a model reference? Or is it better to start with the raw data? As a performance engineer, you should not rely on the official test analysis procedure for two reasons:

1. The official procedure may do more than correct to standard day conditions. Possibly there are terms that address differences in the engine built standard or between test cell and aircraft installation, etc.
2. Facility modifiers are only applied to a few of the data. However, among the measurements there are additional unmodified parameters like compressor exit temperature and pressure. The mixture of corrected and uncorrected facility data is not consistent thermodynamically.

Lessons are: Do your own raw data correction to standard day conditions. Do not apply facility modifiers. Do not apply any correction to the raw data which you do not fully understand. Create a model which is based purely on physics: build a true thermodynamic model.

We use the data from the test cell correlation report [5] as a baseline for our CFM56-3 model. Thanks to Air Portugal for providing a copy of the report and additional information about the data correction procedures. Besides the above-mentioned facility modifiers, the report contains printouts for 40 scans with detailed raw data and the official corrected data.

4.2.1 Check of the Data

The pressures measured in the bellmouth are a very good starting point for our data check. There are six total pressures and four wall static pressure measurements which show little scatter. We can calculate the total to static pressure ratio P_2/P_{s2} from the averaged data, which in turn yields the bellmouth Mach number M_2 .

In the bellmouth, the total temperature is measured by 24 thermocouples. While the average value of all these measurements might be expected to agree with the temperature T_{amb} measured in the test cell, this is not the case. The difference between T_{amb} and T_2 increases with bellmouth Mach number, as shown in Fig. 4.2-2.

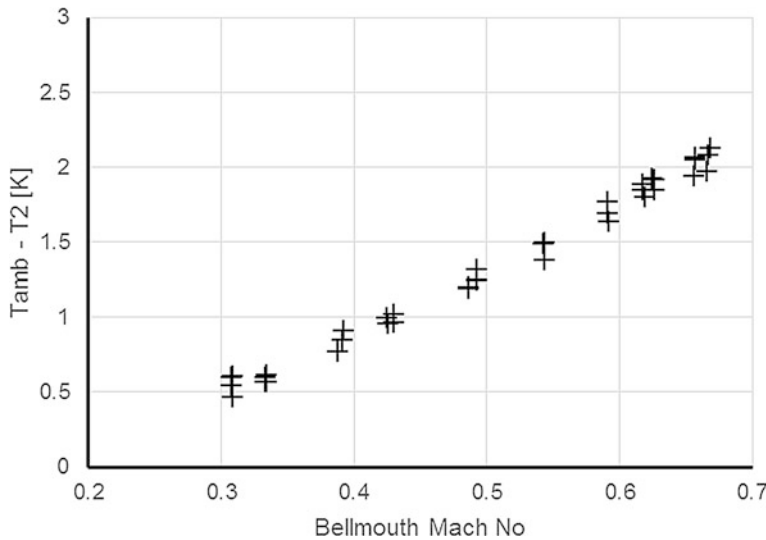


Fig. 4.2-2 Ambient temperature minus bellmouth measured T_2

The explanation for this is that the T_2 probes do not indicate the true temperature. This is quite normal for total temperature probes. The recovery factor r describes the difference between the indicated total temperature and true total temperature:

$$r = \frac{T_{ind} - T_s}{T_{true} - T_s} \quad (4.2.1)$$

Let us assume that T_{amb} (measured with a single probe in the test cell) indicates the true total temperature of the incoming air. We can calculate the static temperature T_s from the pre-determined bellmouth Mach number and T_{amb} . The recovery factor r can be determined for each of the scans and the results are shown in Fig. 4.2-3.

The scatter between the crosses is remarkably low, which indicates highly accurate raw data. On average, the recovery factor is 0.91. We apply this average recovery factor $r = 0.91$ to the indicated total temperature of the probes in the bellmouth and we end up with an accurate value of T_2 as the basis for the data correction to ISA conditions.

P_2 is measured with four bellmouth rakes each reading six total pressures. P_2 is lower than the ambient pressure measured in front of the engine. The pressure ratio correlates well with bellmouth Mach number, and the scatter in the data is extremely small, see Fig. 4.2-4.

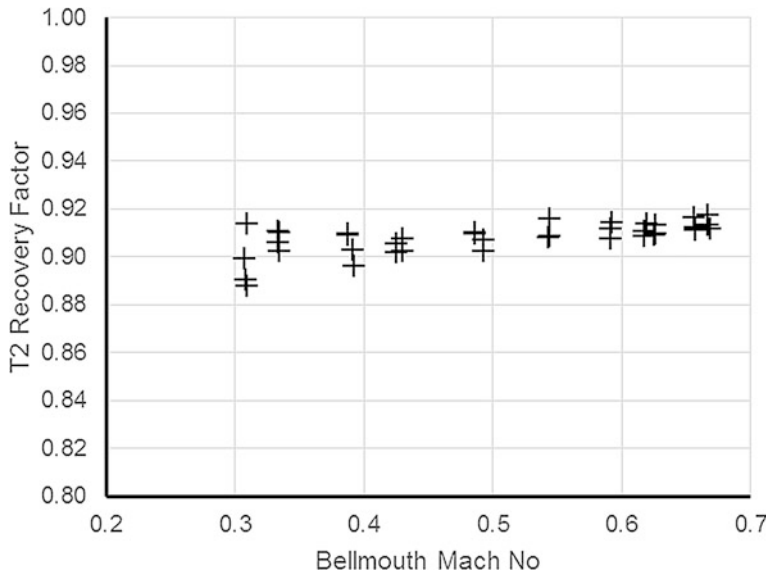


Fig. 4.2-3 Recovery factor for the bellmouth T₂ probes

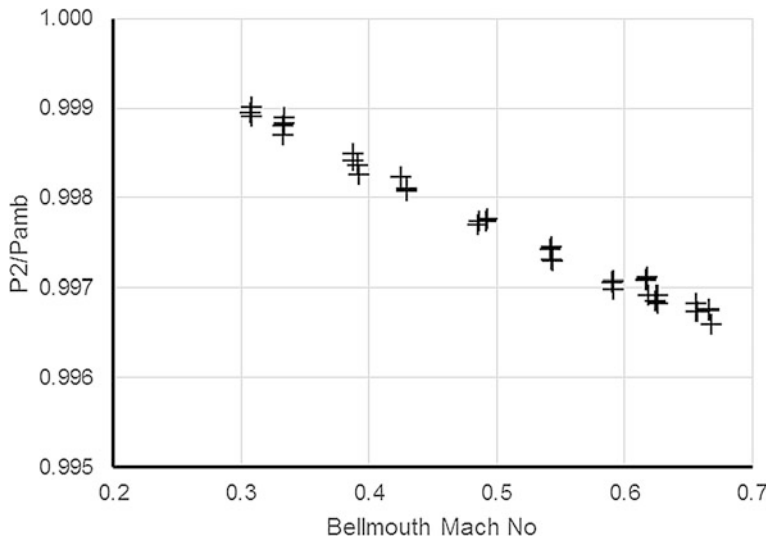


Fig. 4.2-4 Bellmouth total pressure P₂ over P_{amb}

4.2.1.1 Humidity

The raw data are from two different operating lines. The ambient temperature of the first operating line decreases during the test from 20.8 °C (Take Off) to 18.5 °C (Idle). During the second calibration run, the ambient temperature was constant and equal to 21.7 °C. A relative humidity of 40% is reported for both operating lines. The water/air mass ratio is 0.006, which results in a slightly higher gas constant than for dry air. Condensation shocks are highly unlikely under these circumstances. Thus, all the raw data are suitable for engine performance analysis.

4.2.1.2 Mass Flow

The mass flow is found from the raw data for P_2 , the recovery corrected T_2 , the bellmouth area and the bellmouth flow coefficient given in the Engine Shop Manual. The Standard Day corrected mass flow W_{2Rstd} is highly consistent since all the input data for the mass flow calculation show very little scatter.

4.2.1.3 Thrust

The thrust measured at the engine cradle is different from that measured on an open-air test bed. The thrust mismatch depends on the size and the design of the test cell. Therefore, each test cell is calibrated, and the ratio of free stream thrust to measured thrust, the facility modifier for thrust f_{FN} , is determined. The magnitude of the thrust modifier is defined by a polynomial.

The thrust facility modifier in the calibration report is derived from the ratio of a CFMI baseline thrust and the thrust measured by T.A.P. The report contains thrust ratios for three different CFMI baselines. The plus symbols in Fig. 4.2-5 represent the first of the thrust ratios and the circles mark the average of the thrust ratios 2 and 3.

Note that four of the plus symbols do not follow the general trend, they are obvious outliers. Nevertheless, it looks like all the base 1 data points have been used to define the official thrust facility modifier polynomial (the thin dashed line).

There are no outliers among the circles—which are the mean values of the base 2 and base 3 data. These look more reasonable than the base 1 data, represented by the plus signs.

The main reason for the thrust difference between an open air and a closed test facility is that, in the latter, the air approaches the engine in a stream tube, as it does on an aircraft engine in flight. In both of those cases the outer streamlines of the stream tube are parallel some distance upstream of the engine, see Fig. 4.2-6. There, the momentum can be calculated as the product of mass flow and velocity V_0 . This provides an opportunity to calculate the momentum which constitutes most of the difference between the measured and true thrusts.

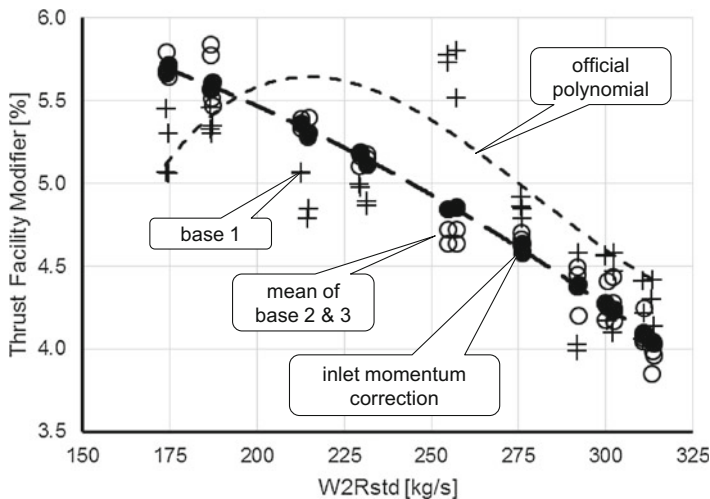


Fig. 4.2-5 Various thrust facility modifiers

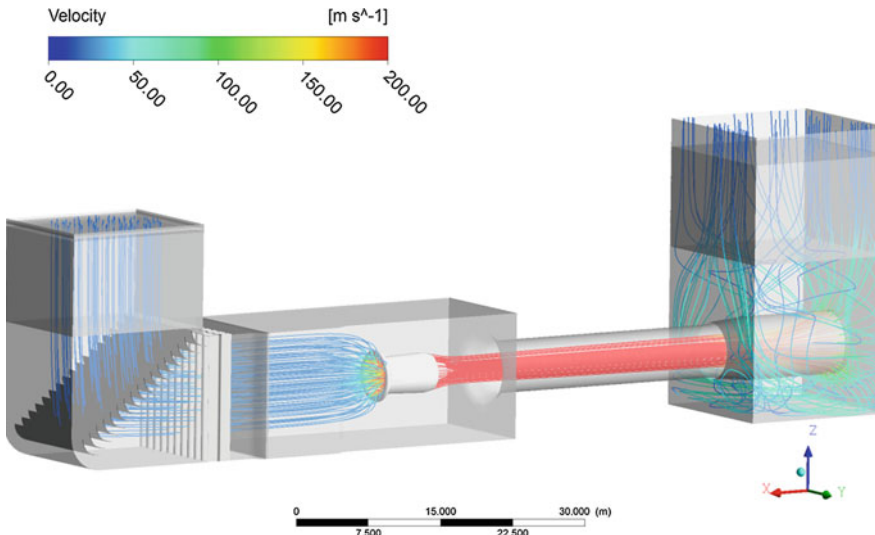


Fig. 4.2-6 Velocity distribution in a test cell (courtesy of MDS Aero Support)

However, how can we determine the representative stream tube diameter which gives results consistent with the data from the correlation report? In fact, this is easy: we adjust the stream tube cross section in such a way that the momentum-based thrust correction agrees with the mean value from the other three corrections. This procedure yields a stream tube diameter of 6 m for $W_{2\text{Rstd}} = 310 \text{ kg/s}$ which decreases slightly to 5.8 m when $W_{2\text{Rstd}} = 170 \text{ kg/s}$.

These numbers look plausible: the test cell is 8.65 m high and 9.75 m wide. There is room left for the secondary air which bypasses the engine and joins the exhaust gases in the detuner at the test section exit.

The scatter in the calculated values of inlet momentum is very small, since the mass flow is determined accurately from the measurements in the bellmouth. Therefore, the inlet momentum based facility modifier is also very accurate, as can be seen from Fig. 4.2-5. It is a much better representation of physics than the official polynomial.

This thrust correction method is based only on measurements. Scatter and peculiar polynomials for the facility modifier are avoided. The procedure can also be applied with confidence outside the calibration range of the test facility.

4.2.1.4 Fuel Flow

Understanding the fuel flow measurement is very important. The first step of the test analysis is the correction to standard day conditions and to the nominal fuel heating value FHV_{nom} :

$$W_{FR} = \frac{W_{F,meas}}{\delta * \theta^{0.68}} * \sqrt{\frac{R_{dry\ air}}{R}} * \frac{FHV}{FHV_{nom}} \quad (4.2-2)$$

The corresponding equation in the Engine Shop Manual contains 0.58 for the Θ exponent. However, the data from the two operating lines (with different Θ values) collapse better if we use 0.68 as the Θ exponent in the equation for W_{FR} . The square root of the gas constant ratio corrects the result from humid to dry air.

The official procedure employs additional terms in the equation: an inlet condensation correction factor (not applicable for these test conditions), a fuel flow facility modifier and a correction for the HPT active clearance control. Figure 4.2-7 compares W_{FR} , as determined by T.A.P. following the official procedure, with W_{FR} as calculated via (4.2-2). The percentage differences are generally small and very consistent, except for the two red points marked A and B. They deviate by 1 and 0.25% respectively from the general trend. What is the reason for this abnormality?

It relates to the HPT active clearance control of the CFM56 engine. The temperature of the clearance control air which is blown on the HPT shroud structure affects its thermal expansion and hence the turbine blade tip clearance. This has a remarkable influence on the engine performance, as reducing the tip clearance by 1% of the blade length increases turbine efficiency by 2%.

The HPT clearance control valve has two inlet ports, one from the 5th stage and one from the 9th stage of the HP compressor. The engine control unit determines which of the air supplies is used—it can also be a mixture of 5th and 9th stage air. A nominal cooling air mode schedule for operating the HPT clearance control valve is part of the official test analysis procedure. In this nominal schedule, the valve

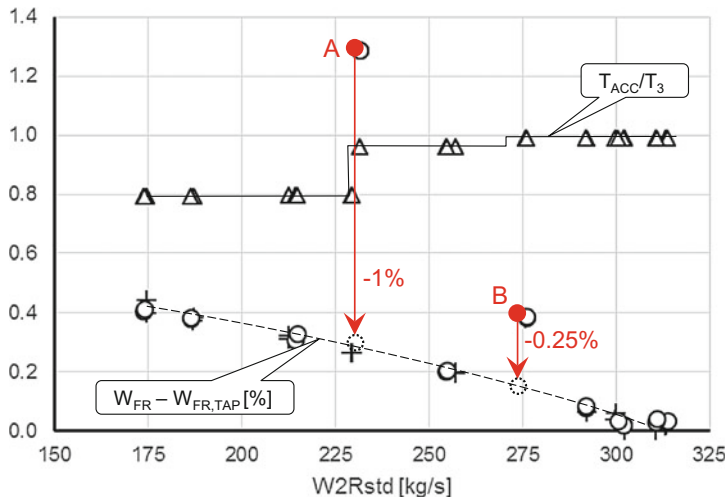


Fig. 4.2-7 Corrected fuel flow and temperature of the HPT ACC air

position changes from stage 5 air at $N_{2R} = 13,200$ rpm to a mixture of 5th and 9th stage air. Above $N_{2R} = 13,760$ rpm all air is taken from the 9th stage.

Near to the switch points in the schedule, it can happen that the valve is not in its nominal position. In such a situation, the measured fuel flow will be adjusted for the deviation of the HPT ACC (Active Clearance Control) valve position from the schedule. Have a look at the upper part of Fig. 4.2-7, which shows the temperature of the shroud cooling air downstream of the valve normalized by T_3 . There are two steps in the T_{ACC}/T_3 data which indicate that the valve position has changed. It is conspicuous that W_{2Rstd} of the T_{ACC}/T_3 steps coincides with the corrected flows of the points A and B.

It is quite clear that the official test analysis procedure has erroneously adjusted the measured fuel flow of point A by +1% and that of point B by +0.25%. When these two adjustments are removed, then points A and B agree perfectly with the other data.

Figure 4.2-7 also shows how the fuel flow difference changes with W_{2Rstd} . This trend and its magnitude also appears in a table of the calibration report which compares the flowmeters of T.A.P. and SNECMA. We could use this knowledge for defining a fuel flow facility modifier. However, we do not know the absolute accuracy of either flowmeter and therefore we use the result of (4.2-2) for the modeling work without applying a facility modifier to W_{FR} .

Specific fuel consumption—the quotient of fuel flow and thrust—is a very sensitive measure of overall engine efficiency. The difference between thermodynamic (true) and contractual performance in Fig. 4.2-8 is significant.

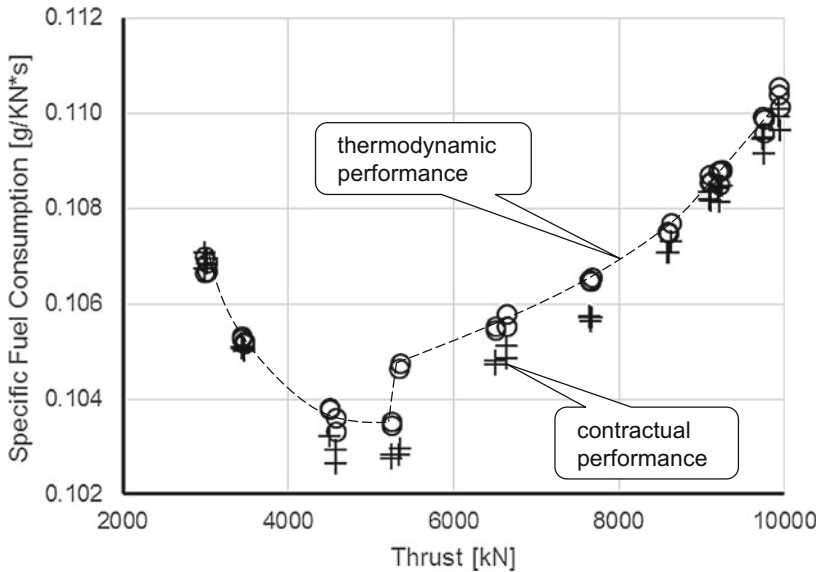


Fig. 4.2-8 Thermodynamic and contractual performance

4.2.1.5 Temperatures

Switching between the sources of the clearance control air affects not only the official fuel flow analysis result but also the main flow path gas temperatures T_{495} (EGT, measured in the second stage vane of the LPT) and the exhaust gas temperature T_{54} . In Fig. 4.2-9 there are steps in the lines connecting the T_{495}/T_3 and the T_{54}/T_3 data points where the clearance control valve switches between the air sources.

If the influence of the clearance control system on the main gas temperatures was not known, then it might be concluded that the EGT and T_{54} measurements contain random scatter.

EGT plays a big role in the official test analysis procedure. The measured value is corrected with $\Theta^{0.91}$ and factors for humidity and condensation. A facility modifier and the clearance correction are applied additionally.

No correction procedure is given for T_{54} in the Engine Shop Manual. This makes it impossible to reconcile EGT and T_{54} in a thermodynamic model if the official EGT correction procedure is used. Therefore, we correct both EGT and T_{54} simply by Θ .

We have already discussed how we interpret the T_2 measurements in the bell-mouth correctly. T_3 is measured by a single probe at the outer wall of the combustion section, as shown in Fig. 4.2-10. No recovery correction is applied there because the Mach number at the probe location is low, but it should be noted that the signal might be biased because of the proximity of the hot combustion chamber. Maybe the temperature measured in the HPT ACC delivery pipe (the offtake is from stage 9.) is a better indicator of the true compressor exit temperature?

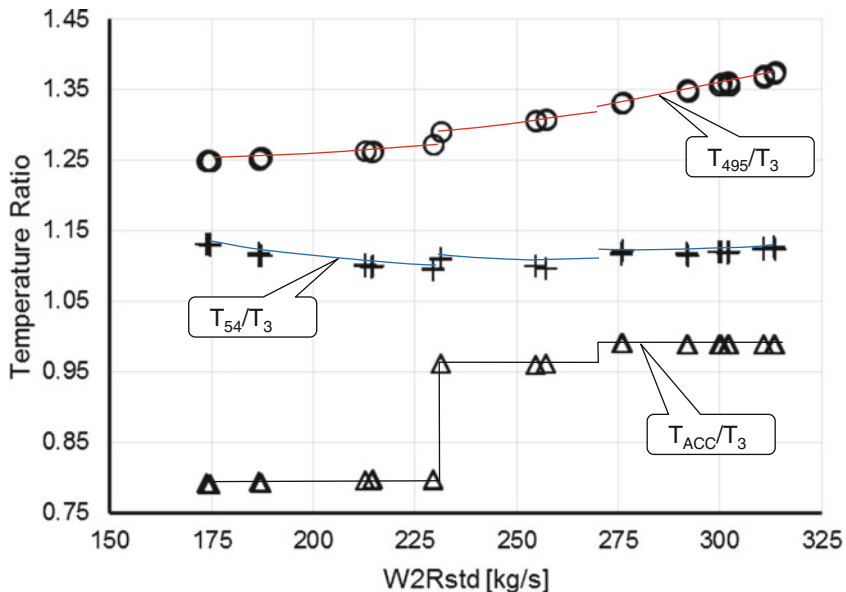


Fig. 4.2-9 Gas temperature ratios

Figure 4.2-11 shows the difference between the indicated T_3 and T_{ACC} as a function of W_F/P_{s3} , which reflects the heat release in the combustion chamber. The clearance control air originates from the 9th stage for all these data. Interpreting T_{ACC} as the true compressor delivery temperature is plausible.

However, T_{ACC} cannot be used as the true T_3 indicator while part of or even all the clearance control air is taken from the 5th stage. For these cases, we can use the linear correlation between $(T_{3,ind} - T_{ACC})$ and W_F/P_{s3} to correct $T_{3,ind}$ to the true compressor exit temperature T_3 .

Two T_{54} probes measure the temperature downstream of the LPT. The difference between the two T_{54} signals is significant and illustrated in Fig. 4.2-12. Note that scans at the same W_{2Rstd} lead to the same (or very similar) results. Thus, the temperature differences are not random, but have a cause—the circumferential temperature distribution must change with W_{2Rstd} .

4.2.1.6 Pressures

All pressure probes in the engine indicate total pressures except the one for P_{s3} , which is a static value at the combustion chamber wall, see Fig. 4.2-10. The ratio between total pressure at the compressor exit P_3 and P_{s3} remains constant within the operating range of the test because the Mach number at this location is low and is also fairly constant. We assume $P_{s3}/P_3 = 0.97$, which takes into account the local velocity at the pickup point as well as the loss in the compressor exit diffuser.

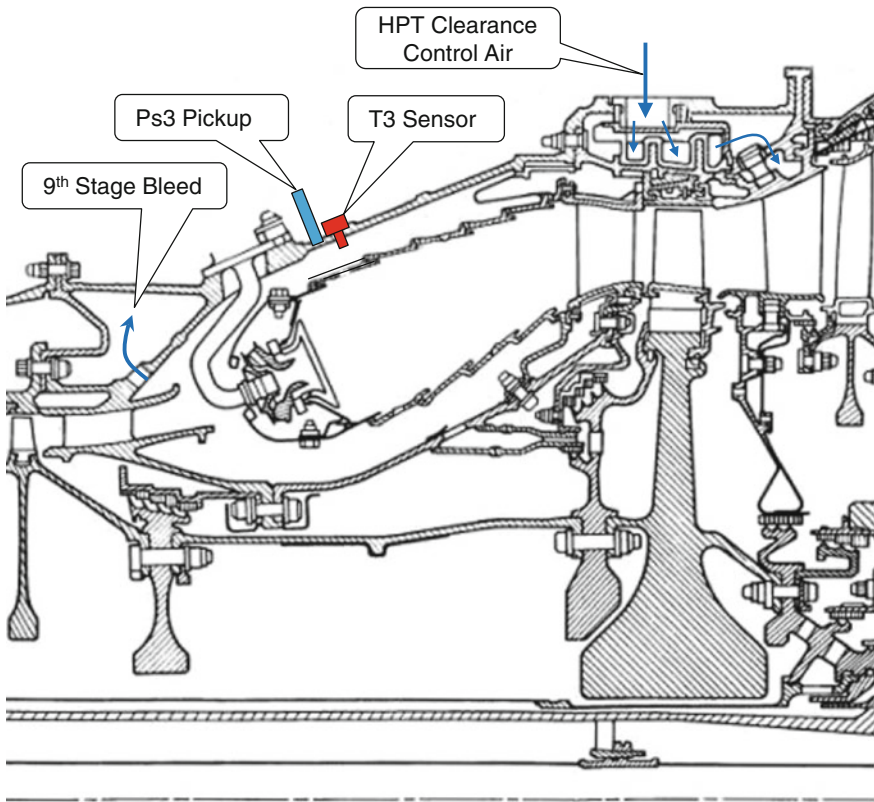


Fig. 4.2-10 Ps₃ and T₃ sensor locations

Pressure ratios and spool speeds are plotted against corrected flow to check the reported numbers. No abnormalities are found in the data from the T.A.P. test cell calibration report.

4.2.1.7 Spool Speeds

Fan speed N₁ is corrected for temperature and humidity deviations from the standard day conditions:

$$N_{1R} = \frac{N_1}{\left(\frac{R}{R_{dryair}} * \frac{T_2}{T_{std}} \right)^{0.47}} \quad (4.2.3)$$

The exponent 0.47 is taken from the Engine Shop Manual. It yields a better data collapse for the two operating lines than the theoretical exponent of 0.5.

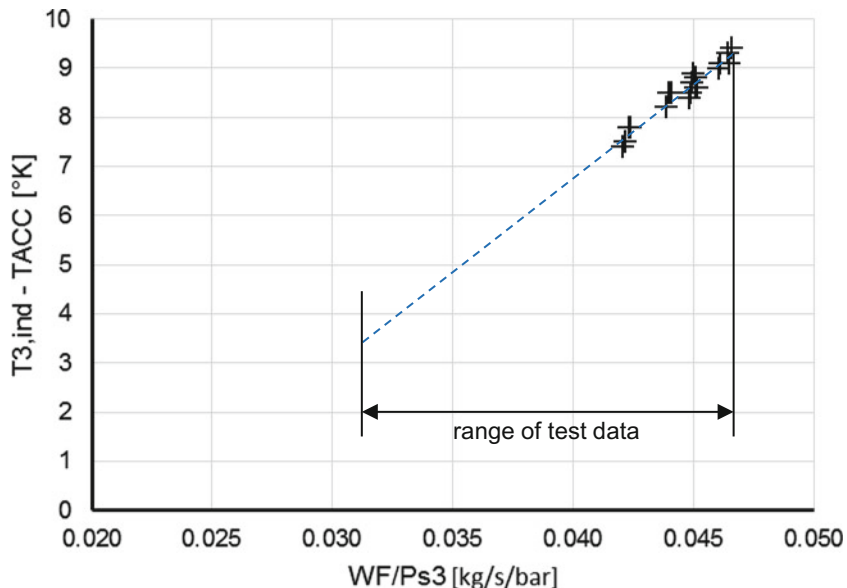


Fig. 4.2-11 Difference between T_3 and TACC

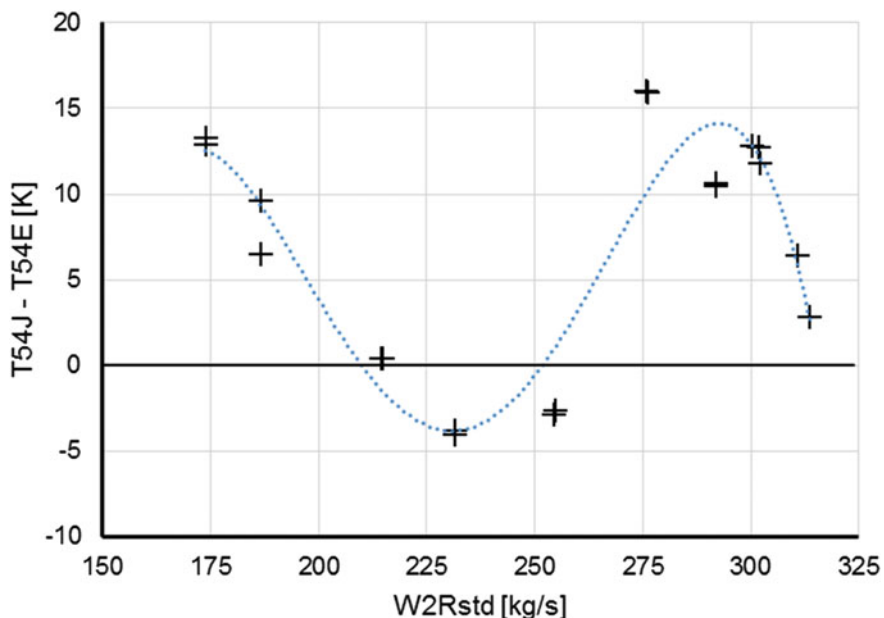


Fig. 4.2-12 Temperature differences downstream of the LPT

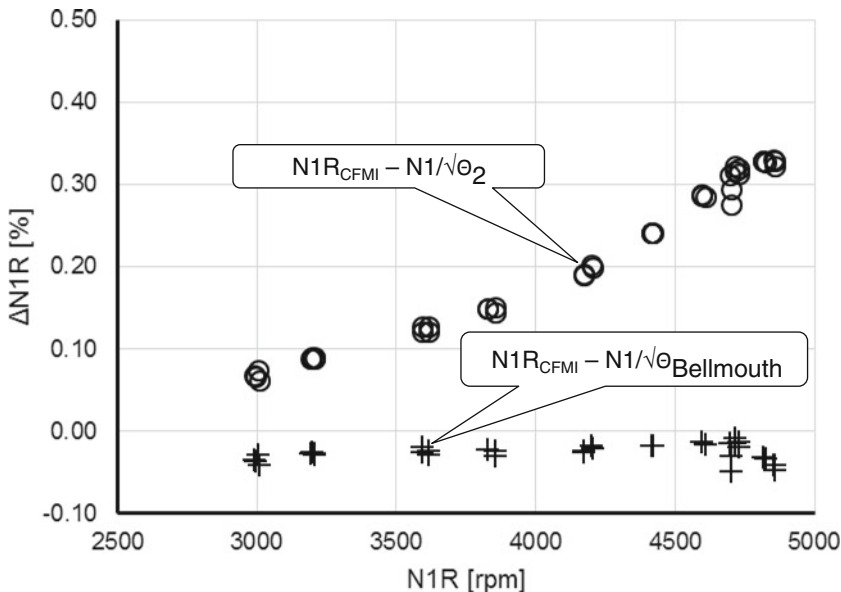


Fig. 4.2-13 Influence of T_2 selection on N_{1R}

The $N_{1R_{CFMI}}$ results, calculated with the Engine Shop Manual procedure, deviate significantly from those derived using the true T_2 values (the circles in Fig. 4.2-13). We define true T_2 values as those measured in the bellmouth, corrected for recovery. When we employ the indicated temperature $T_{2\text{ind}}$ (T_2 without recovery correction) in (4.2-3), we get very good agreement between the two results, as indicated by the crosses in Fig. 4.2-13, with an almost constant result.

Obviously the CFMI procedure does not consider any recovery correction for T_2 and consequently, all of the corrected parameters which contain T_2 are biased. This is another difference between true thermodynamic performance and contractual performance.

HPC corrected spool speed is calculated from (4.2-4) employing the exponent 0.45 from the Engine Shop Manual.

$$N_{2R25} = \frac{N_2}{\left(\frac{R}{R_{\text{dry air}}} * \frac{T_{25}}{T_{std}} \right)^{0.45}} \quad (4.2-4)$$

To check the consistency of the spool speed data, N_{1R} could be plotted against bellmouth Mach number. Prior to beginning the modeling work, it would be a good idea to plot N_{2R} against N_{1R} also.

4.2.2 Cycle Reference Point

The engine modeling work begins with the reproduction of the measured data from a single point, the cycle reference point. Neither component maps nor speed values are needed for this sort of calculation. Select a high thrust point where you have confidence in all the measured parameter values. If you are not sure whether inlet condensation has occurred, then it is better to select a point with a lower thrust.

In the first calibration run, only one of the two T_{54} probes measured reasonable values. Therefore, we select the first point of the second operating line, because it is at the highest thrust. The corresponding Standard Day corrected data are listed in Table 4.2-1.

Note that all temperature corrections use the recovery-corrected T_2 .

We simulate the CFM56-3 with GasTurb as a geared turbofan with a gear ratio of 1. We can use some of the parameters in the table directly as input for the cycle reference point simulation, while other parameters are target values for an iteration. The following assignments work very well without any convergence problems (Table 4.2-2).

Table 4.2-3 shows the simulation results for our high-thrust point in Scan 22. Numbers agreeing with those in Table 4.2-1 are highlighted in yellow.

Thrust F_N was not an iteration target, therefore it deviated initially by 0.3%. We have eliminated this small discrepancy with an appropriate nozzle thrust coefficient. Note that core nozzle area A_8 agrees with the given value also.

Table 4.2-1 Standard day corrected data of scan 22

CFMI Name	GasTurb Name	Units	Value	Comment
F_N	FN	kN	99.43	Measured force, inlet momentum corrected
W_2	W2Rstd	kg/s	313.7	From bellmouth measurements
W_F	WF	kg/s	1.0951	Corrected to $FH_{V_{nom}} = 42.769 \text{ MJ/kg}$
T_{25}	$T_{24} = T_{25}$	K	369.4	Calculated value: $T_{25} - T_2 = f(N_{IR})$ as defined in the Engine Shop Manual
T_3	T3	K	770.8	Corrected to T_{ACC} for sensor position
T_{495}	–	K	1058	EGT harness in LPT second stage vane
T_{54}	T5	K	862.6	2 single element rakes
P_3/P_2	P3q2	–	24.178	Assumption: $P_{s3}/P_3 = 0.97$
P_{25}/P_2	P24q2	–	2.182	single element rake
P_{54}	P5	kPa	148.14	2 single element rakes
P_{17}/P_2	P13q2	–	1.655	4 rakes, each reading 6 pressures
A_8	A8	m^2	0.2933	Core nozzle throat area
A_{18}	A18	m^2	0.74236	Bypass nozzle throat area
N_1	CXN_L	rpm	4837	For reference only, not needed for the cycle calculation
N_2	CXN_H	rpm	14,324	

Table 4.2-2 Iteration scheme for the cycle reference point

Variable	Target
Isentropic IPC efficiency	Booster exit temperature T24
Isentropic HPC efficiency	HPC exit temperature T3
Burner Exit temperature	Fuel flow
Isentropic LPT efficiency	LPT exit pressure
Bypass ratio	LPT exit temperature T5
Bypass duct pressure ratio	Bypass nozzle throat area

Table 4.2-3 Cycle reference point

station	w kg/s	T K	P kPa	WRstd kg/s	FN	=	99.43	KN
amb		288.15	101.325		TSFC	=	11.0146	g/(kN*s)
2	313.798	288.15	101.325	313.798	WF	=	1.0952	kg/s
13	260.946	338.15	167.686	170.811	s_NOX	=	0.7838	
21	52.852	288.24	101.426	52.807	P5/P2	=	1.4619	EPR
22	52.852	288.24	101.426	52.807	Core_Eff	=	0.4131	
24	52.852	369.92	221.130	27.439	Prop_Eff	=	0.0000	
25	52.852	369.92	221.130	27.439	BPR	=	4.9373	
3	52.852	770.82	2447.654	3.578	P2/P1	=	1.0000	
31	45.400	770.82	2447.654		P3/P2	=	24.16	
4	46.495	1577.55	2325.268	4.741	P5/P2	=	1.4619	
41	50.195	1522.91	2325.268	5.028	P16/P13	=	0.9787	
43	50.195	1162.74	541.359		P16/P6	=	1.11905	
44	53.366	1140.92	541.359		P16/P2	=	1.61962	
45	53.366	1140.92	541.359	19.875	P6/P5	=	0.99000	
49	53.366	862.58	148.131		A8	=	0.29325	m ²
5	53.366	862.58	148.131	63.157	A18	=	0.74236	m ²
8	53.947	861.63	146.649	64.454	XM8	=	0.75978	
18	260.946	338.15	164.108	174.536	XM18	=	0.85949	
Bleed	0.000	770.82	2447.654		WBld/w2	=	0.00000	
Efficiency	isentr	polytr	RNI	P/P	CD8	=	0.97899	
Outer LPC	0.8901	0.8976	1.000	1.655	CD18	=	0.99224	
Inner LPC	0.9001	0.8994	1.000	1.001	PWX	=	0.0	kW
IP Compressor	0.8777	0.8903	1.001	2.180	V18/v8,id	=	0.70788	
HP Compressor	0.8677	0.9025	1.621	11.069	WBld/w22	=	0.00000	
Burner	0.9995			0.950	Wreci/w25	=	0.00000	
HP Turbine	0.8250	0.7985	3.281	4.295	Loading	=	99.98	%
LP Turbine	0.9000	0.8843	1.064	3.655	WCHN/w25	=	0.07000	
HP Spool mech Eff	0.9900	Speed	14324	rpm	WCHR/w25	=	0.06000	
LP Spool mech Eff	1.0000	Speed	4835	rpm	WCLN/w25	=	0.00000	
P22/P21=1.0000	P25/P24=1.0000	P45/P44=1.0000			WCLR/w25	=	0.00000	
hum [%]	war0	FHV	Fuel		WBld/w25	=	0.00000	
0.0	0.00000	42.769	Generic		WLkBy/w25	=	0.00000	
					WLkLP/w25	=	0.01099	

One topic needs still to be discussed. Why have we used $T_{5,\text{mea}}$, based on only two single probes, as the iteration target instead of EGT, which is measured by 9 probes?

T_{495} (EGT) is measured in the vane of the 2nd LPT stage (Fig. 4.2-15). The temperature at this location is not among the normal GasTurb output parameters, but we can calculate it as a so-called composed value from T_{45} and T_5 . At the inlet of the 2nd LPT rotor, the mean total temperature is

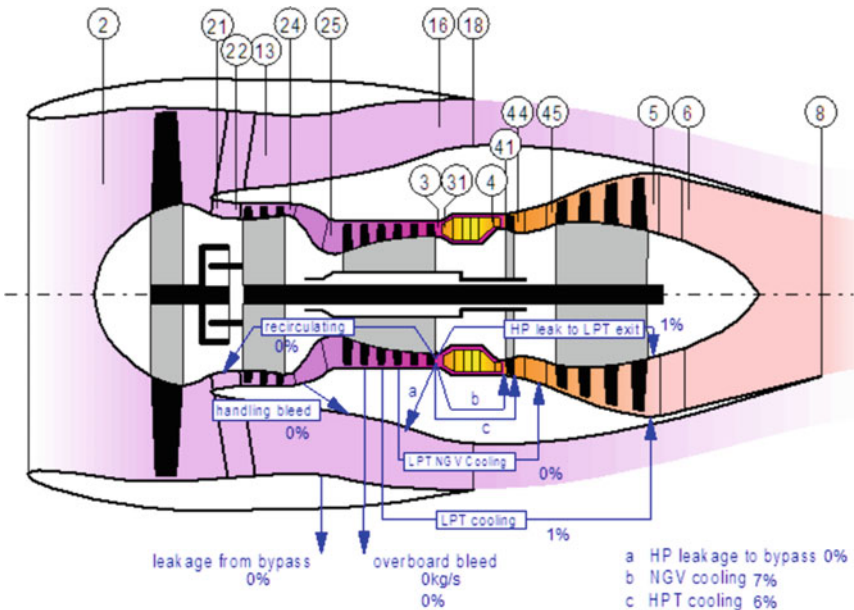


Fig. 4.2-14 GasTurb nomenclature

$$T_{451} = T_{45} - 0.3 * (T_{45} - T_5) \quad (4.2-5)$$

The factor 0.3 is derived from the measured EGT = 1058 K at the cycle reference point where $T_{45} = 1141$ K and $T_5 = 863$ K. Note that the temperature drop in the first stage is bigger than the average fractional value of 0.25. That is beneficial with respect to the metal temperatures in the following stages. Furthermore, stage 4 can be unloaded to produce low values of absolute exit swirl angle and Mach number in the downstream duct as the flow enters the exhaust system.

During part-load operation the LPT pressure ratio decreases, as does the gas density difference between LPT entry and exit. This leads to an increase of the axial velocity component in the first stage which, in turn, increases the work done by the stage. Why that happens is explained in Sect. B3.2 which discusses velocity diagrams.

The change in the fraction of the work done by the first stage as we move along the operating line could be determined theoretically if we could run a turbine map calculation program. But since we do not have the detailed information required for such an exercise, we need to employ an empirical correction to our equation for T_{451} .

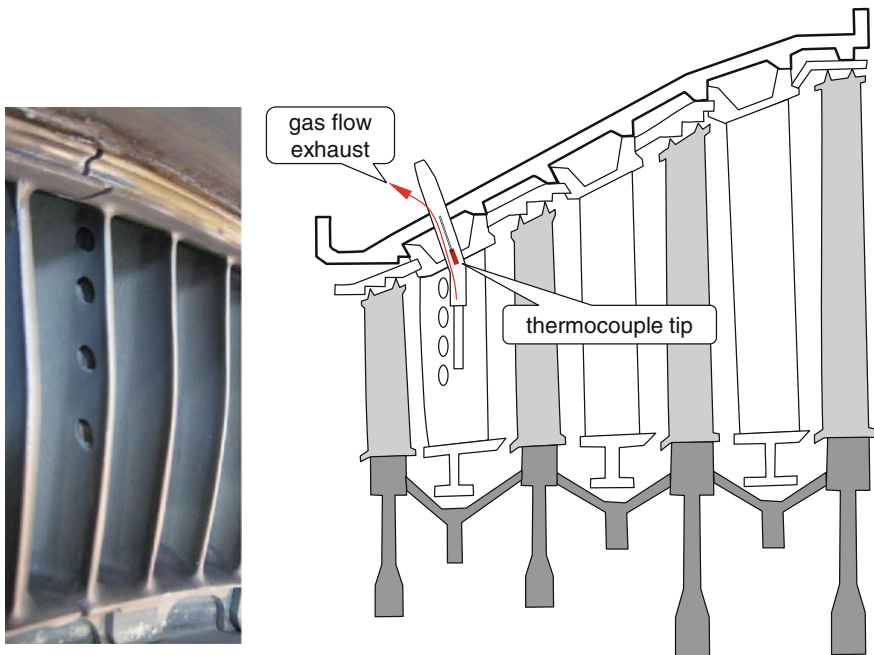


Fig. 4.2-15 EGT measurement in CFM56 engines

The exponent 0.4 in the following equation for EGT reconciles theory with off-design measurements perfectly as we will see later in Fig. 4.2-30:

$$EGT = T_{45} - 0.3 * (T_{45} - T_5) \left(\frac{1141}{T_{45}} \right)^{0.4} \quad (4.2-6)$$

All the data of the cycle reference point look reasonable. That does not mean that every detail is absolutely correct. Slightly different assumptions about the secondary air system, external gearbox losses (HP spool mechanical efficiency), duct losses and nozzle discharge coefficients would lead to different values.

Note that Fan, HPT and LPT efficiencies are interconnected. Assuming higher Fan or HPT efficiency results in lower LPT efficiency. The selected combination of these efficiencies feels right: the very low HPT efficiency is explained with the very high pressure ratio of this highly cooled turbine. Moreover, while scan 22 was taken, the clearance control air was hot (from the 9th stage) which results in big turbine tip clearance.

4.2.2.1 Some Remarks

Creating this cycle reference point was quite easy and straightforward, thanks to the extensive check of the data. In other engine modeling exercises, this is not always the case. Experience tells us that something is wrong with the data whenever it is difficult to get a good agreement with the cycle calculation. Have you really understood what was measured? Do you know what the sensors and their environment look like? Is your data preprocessing based on physics only or have you unintentionally used some elements of *contractual performance*?

A reason for spending excessive time on setting up the cycle reference point is an exaggerated and inappropriate demand for accuracy in less important elements of the model, an example of this being the secondary air system. Concentrate on the main component performance descriptors; that is sufficient for a good performance simulation.

4.2.3 Off-Design

We have selected one of the engine operating points as the cycle design point. Let us call this the *Cycle Reference Point* to avoid any confusion with the engine design point. We could have selected a different operating point, so what is special about the cycle reference point? It is the anchor point—the foundation—for our off-design model.

In the cycle design point calculations, the compressor pressure ratios and efficiencies, as well as the turbine efficiencies, are given data. During off-design simulations these data are read from compressor and turbine maps. The calculation processes are different, however; at the cycle reference point both algorithms must yield the same result.

Usually the true component maps are not available. We must use calculated maps, maps from literature or measured maps from similar components. At the cycle reference point we select the operating points in the compressor and turbine maps and then scale the map values to match the cycle values. This means that at the operating conditions of the cycle reference point both the design and off-design calculations produce the same result.

Off-design calculations at other operating conditions will not agree with the given data initially. This is resolved by rescaling or tweaking the maps until the simulation agrees with the test results. In this calibration process, we repeatedly compare the simulation results with the measured data. Before we discuss the map-tweaking process, let us talk about preprocessing the measured data.

4.2.3.1 Test Data Enrichment

Adapting a model to measured data requires the adjustment of component efficiencies, pressure ratios, corrected mass flows and corrected spool speeds. The measured data, however, consist of pressures, temperatures, and spool speeds.

Calculating pressure ratios, corrected flow and corrected spool speed with a spreadsheet program is straightforward. Efficiencies are a special case; inconsistencies are introduced if the spreadsheet gas property model differs from that used in the performance analysis program. Avoid this difficulty by including the test data pre-processing into the performance analysis program. In GasTurb, you can use the embedded formula editor to create so-called *Composed Values* to enrich your test data. Among other quantities, add all meaningful pressure ratios to the measured data, especially the overall pressure ratio P_3/P_2 .

You should also use *hybrid test data* to further enrich your data base. In this way, you can get a value of the HPC inlet corrected flow W_{25Rstd} , for example for each test point. This value is needed for locating the operating point in the HPC map.

In this context, the term *hybrid* means that we interpolate the test analysis result for W_{25Rstd} from the *measured* overall pressure ratio $(P_3/P_2)_{mea}$ and the *simulated* correlation between W_{25Rstd} and P_3/P_2 . The simulated correlation is that of our currently best available performance model.

Over time the performance model will improve. The hybrid test data should be updated whenever the model calibration process has progressed.

4.2.3.2 Fan Map

The *GasTurb Standard Map* is suitable as a starting point for the CFM56-3 model calibration process because it is from a similar fan [7]. The question is: where in this map should we place the cycle reference point? There are no strict rules, only some rough guide lines:

- The corrected flow (the x-axis value) relates to the Mach number at the fan face. At our cycle reference point, this is calculated as 0.57 from the fan dimensions and the corrected flow. Setting the map scaling point to a corrected flow value of 0.9 in the unscaled map implies that for $N/\sqrt{\Theta} = 1.1$ the fan face axial Mach number is 0.78. This is certainly a high value which should not be exceeded.
- The efficiency at the cycle reference point has a value which remains unchanged during the map scaling process. Placing the map scaling point in a low efficiency region of the unscaled map can create unrealistically high values in the peak efficiency region.

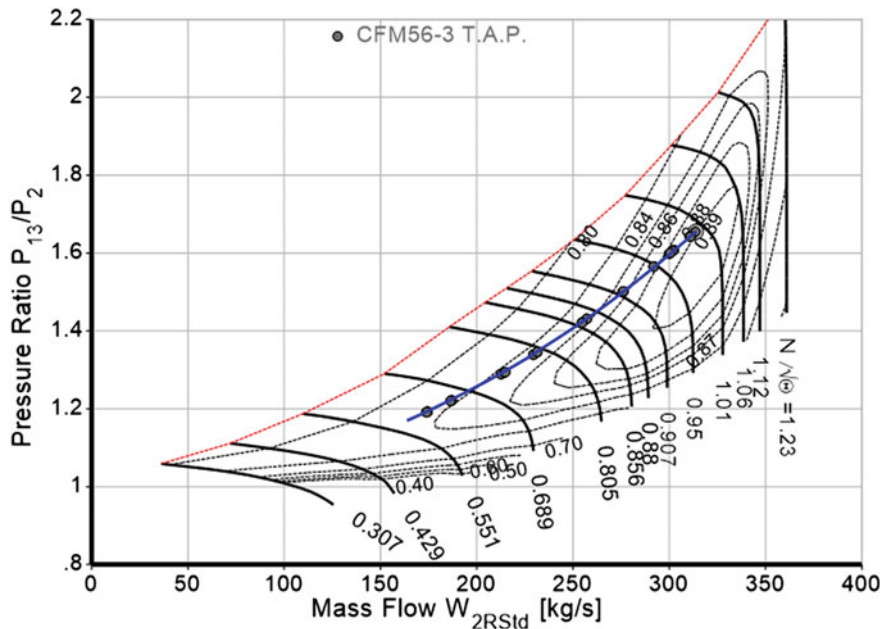


Fig. 4.2-16 Fan map with operating line

- There is some freedom with respect to surge margin. At cruise, the fan operating line certainly passes through the map region where efficiency is highest. The sea level operating line has less surge margin due to the lower bypass nozzle pressure ratio. Therefore, we place the map scaling point slightly above the high efficiency region (Fig. 4.2-16).

4.2.3.3 Booster Map

The first attempt to model the booster operating line is with its corresponding *GasTurb Standard Map*. Figure 4.2-17 shows that the operating line does not pass through the given data points. Why is that?

The GasTurb Standard map is apparently from a compressor designed for a higher Mach number. We can conclude this both from the shape of the efficiency islands and from the range of mass flow values at high corrected speeds. In a transonic compressor map, the region with high efficiencies is at high corrected speed near to the surge line, and the speed lines in the right-hand part of the map are very steep.

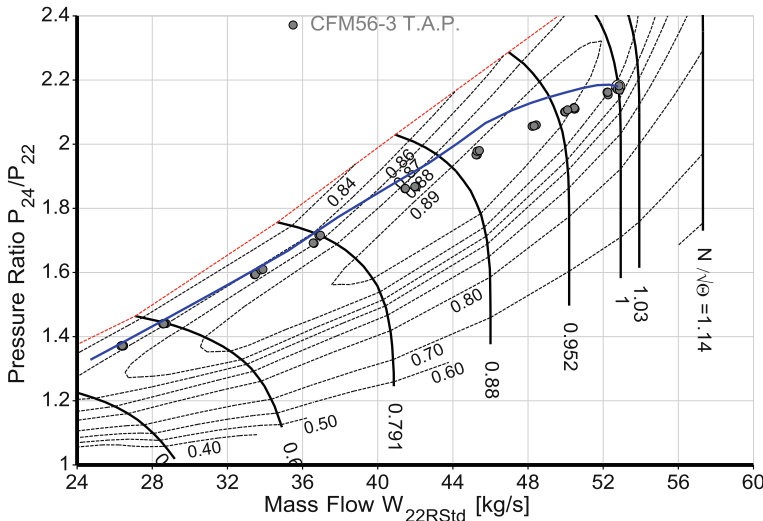


Fig. 4.2-17 Booster operating line with the GasTurb Standard booster map

The relative Mach number level in the CFM56-3 booster is low, due to the low circumferential speed. The map of such a subsonic compressor, in Fig. 4.2-18, looks very different.

Figure 4.2-18 is a scaled version of the map published in [8]. The title of that paper is somewhat misleading: in describing the test vehicle as a high speed compressor. Actually, the maximum rotor Mach number at the design point is only 0.8285—clearly a subsonic device. The highly loaded three stage compressor has a pressure ratio of 2.4. At our cycle reference point the CFM56-3 booster pressure ratio is 2.18. So, the map from [8] is very well suited for our purposes. The only drawback of this map is that rig-measured data are only available for speeds from 0.728 upwards. The lower speed lines have been extrapolated with Smooth C.

Figure 4.2-19 compares the two maps. The operating line in both maps passes through the cycle reference point. The bold operating line is the one from Fig. 4.2-18 while the dotted line is copied from Fig. 4.2-17.

The operating point found with the Standard map for speed 0.93 shows a significantly higher pressure ratio. That is because the gray speed line of the transonic compressor is much steeper than the equivalent speed line of the subsonic compressor. Note that the shape of the speed lines becomes similar at lower speeds and the pressure ratio differences decrease.

The GasTurb Standard booster map is not a good candidate for simulating a conventional bypass ratio 5 turbofan. However, it is appropriate for simulating the booster of a turbofan with gearbox, for example, because such compressors run at higher circumferential speeds and Mach numbers.

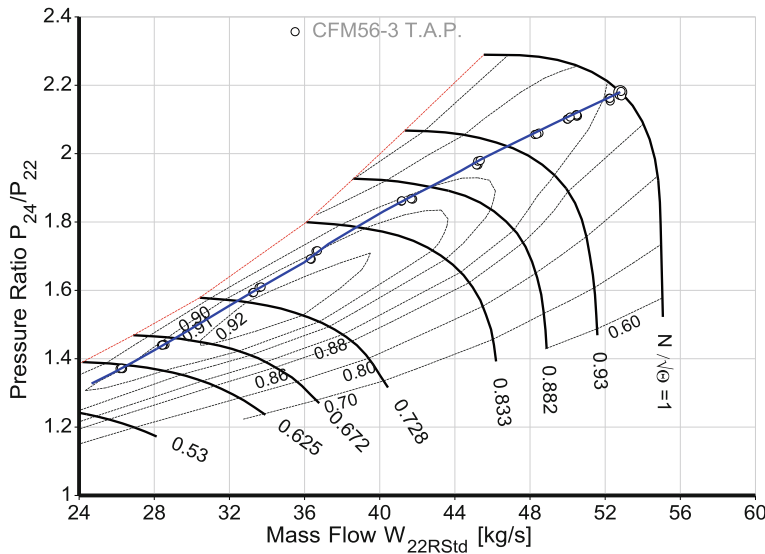


Fig. 4.2-18 Booster operating line in the map of a subsonic compressor map

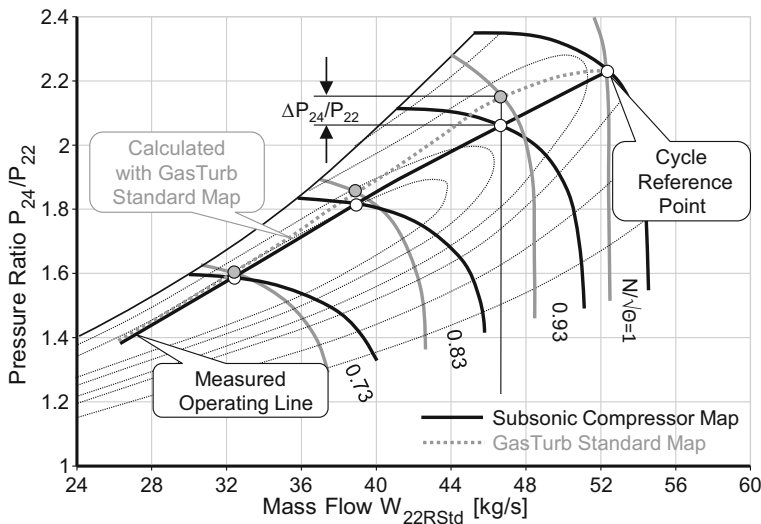


Fig. 4.2-19 Booster map comparison

4.2.3.4 HPC Map

The GasTurb Standard Map is from a compressor with variable guide vanes. It is well suited as a starting point for the model calibration. Add a few speed lines to minimize interpolation errors in the speed-flow correlation. Smooth C is the tool of choice for that task. Set the map scaling point to the default coordinates. Figure 4.2-20 shows the operating line in the HPC map.

4.2.3.5 HPT Map

The pressure ratio of the CFM56-3 HP turbine is constant, as it is in any gas generator turbine. Corrected speed $N_H/\sqrt{\Theta_4}$ varies only a little bit. The operating line is very short and that is why reading the HPT map nearly always yields the same efficiency. Therefore, the shape of the efficiency islands in the map does not influence the simulation accuracy. In our case, use of the GasTurb Standard map together with the default coordinates of the map scaling point is appropriate.

4.2.3.6 LPT Map

The LPT operating line in its map is much longer than that in the HPT map. Efficiency changes with pressure ratio and corrected speed $N_L/\sqrt{\Theta_{45}}$ and

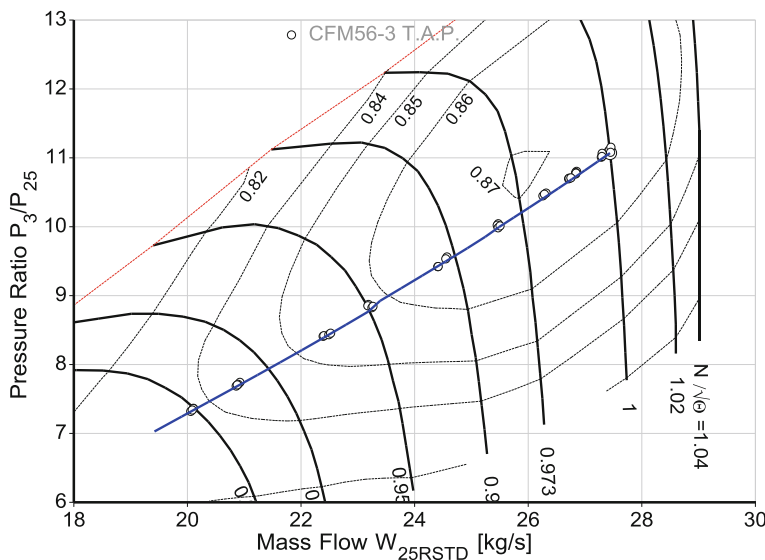


Fig. 4.2-20 HP compressor map

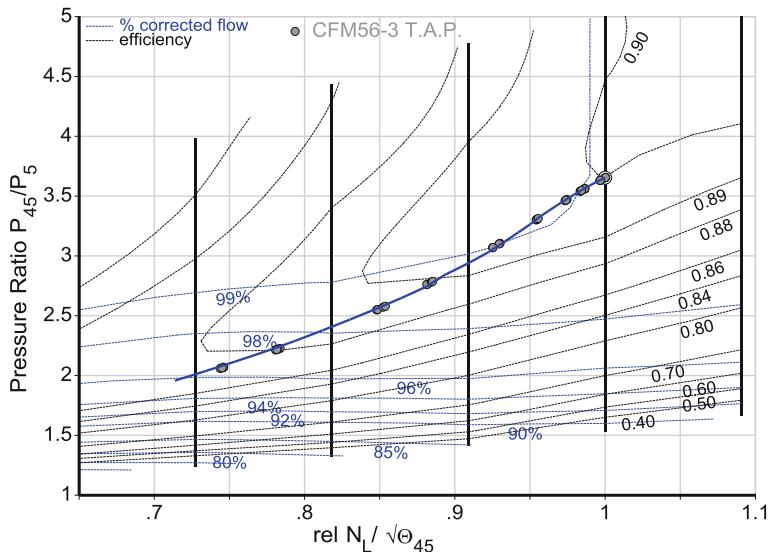


Fig. 4.2-21 LP turbine map

therefore the shape of the map matters. As a starting point for the model calibration we can use the GasTurb Standard map. Select the map scaling point on the speed line 1.1 of the unscaled map in the middle of the efficiency island.

For a low pressure turbine, the efficiency is not the only topic of interest. The change of corrected flow W_{45Rstd} along the operating line affects the position of the HP compressor operating line. Decreasing W_{45Rstd} at constant $N_H/\sqrt{\Theta_{25}}$ not only increases HPC pressure ratio but also increases all temperatures in the hot end of the engine. The shape of the function $W_{45Rstd} = f(P_{45}/P_5)$ is the key to a good simulation of EGT and T_5 .

Figure 4.2-21 shows the efficiency islands as well as the lines of constant corrected flow W_{45Rstd} . At the low power end of the operating line, W_{45Rstd} is only 3% smaller than at high power. If you use the GasTurb Standard map, then you get more than 5% flow reduction along the operating line. The simulated EGT is 20 K higher than measured at the low power end.

4.2.4 Preliminary Model Calibration

We selected the best suited compressor and turbine maps from our library. Running the corresponding model for an arbitrary off-design condition will not yield perfect agreement with the given data because the efficiency gradient and the speed-flow correlation along the operating line differ from reality. We will get that right next.

4.2.4.1 Booster Map

Let us begin with the booster map, which includes the fan root performance, i.e. fan root pressure ratio is set to 1. It is easy to adjust efficiency along the operating line using GasTurb: First we shift all efficiency values on each tabulated speed up or down until the efficiency on the operating line agrees with the targeted given value.

In the second step, we will get the speed-flow correlation right. For that purpose, we need to know the corrected flow W_{22Rstd} of the booster. Unfortunately, we do not have measured values for that. As a substitute, we use “hybrid measured data” which stem from the model correlation between W_{22Rstd} and P_3/P_2 . We assign a model derived flow $W_{22Rstd,mea}$ to each of the measured P_3/P_2 values.

Now we can compare the flow $W_{22Rstd,map}$ read from the map tables at the measured speed $N_L/\sqrt{\Theta}$ with $W_{22Rstd,mea}$. We can get agreement there by modifying the speed values in the map table appropriately. Again, this can be done in GasTurb.

Clearly this is a manipulation of the map which is not necessarily in line with the laws of compressor physics! The modified map will yield the correct data along the operating line, but what about the neighborhood?

4.2.4.2 Second Thoughts About the Booster Map

The simulated booster operating line in Fig. 4.2-18 passes through the measured data. The efficiency variation along the operating line is also in line with the test. However, the position of the operating line in the map does not look right. The line lies somewhere in the region between the peak efficiency and the surge line.

For sure, the booster is designed so that its operating line passes through the map region with the highest efficiencies, provided sufficient surge margin is also available. For a more realistic performance model we need a different map, one in which the region with highest efficiency is above the operating line.

Load the booster map from Fig. 4.2-18 into Smooth C. Define a new beta line grid in which the new $\beta = 1$ line is well above the $\beta = 1$ line of the provisional map. Edit the data in such a way that the backbone of the map (i.e. the line which connects the peak efficiency points on the speed lines) lies above the operating line. The backbone of the map should approximately follow a line of constant work coefficient because this is typical for any map of a subsonic compressor.

Do not modify the shape of the speed lines in the map; edit only the efficiency values. Check the trends of efficiency, torque, specific work, and other physical quantities while working on the map. When you are happy with your editing work then load the revised map into your performance program for a preliminary check.

You will see that the operating line passes through the measured data points even if the efficiency values along the operating line differ from those from the tests. You can produce a physically sound map like the one shown in Fig. 4.2-22 within a few iterations. This map looks much better than the one shown in Fig. 4.2-18.

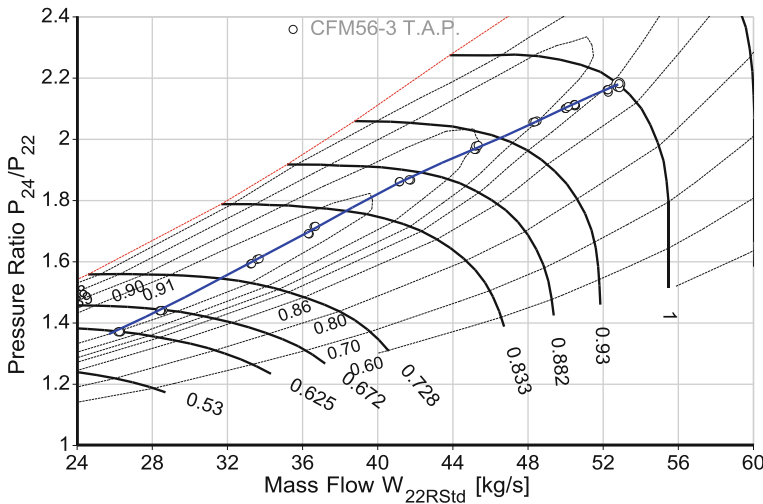


Fig. 4.2-22 Second booster map version

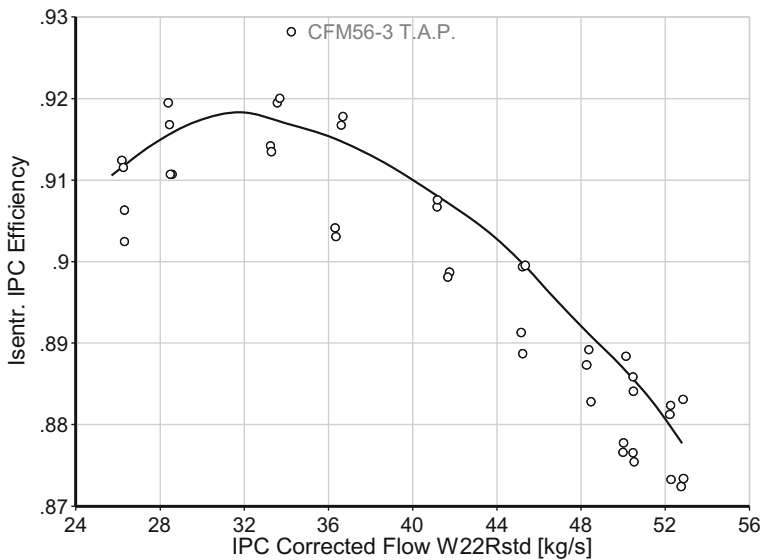


Fig. 4.2-23 Efficiency along the operating line with the second version of the booster map

The efficiency variation along the operating line agrees well with the measurements in both versions of the map; Fig. 4.2-23 shows this for the second map. The difference between the two performance models is that the one using the first map is only valid for the measured booster operating line. There, changes in booster efficiency due to an operating line shift will not be predicted correctly.

Performance models using the second map will at least predict the correct trends even around the measured operating line. The limitation is that neither of the two models will yield credible numbers for surge margin.

4.2.4.3 HPC Map

Adjusting the map of the HPC to the measured data is a similar process as in case of the booster. We shift the efficiency values in the map table up or down as required. The results of the exercise are shown in Fig. 4.2-24.

4.2.4.4 Bypass Ratio

Before we look at the fan efficiency we make sure that we are on the measured operating line given by the measured values of mass flow and fan pressure ratio. We can achieve this with an appropriate correlation between the bypass nozzle discharge coefficient C_{D18} and nozzle pressure ratio P_{18}/P_{amb} . Of course, the curve passes through the point given by C_{D18} and P_{18}/P_{amb} of the cycle reference point.

After having adjusted the fan operating line, we know the bypass ratio and can calculate the core exit mass flow W_5 . Among the measured values are the LP turbine exit pressure P_5 and temperature T_5 . So, we know the core nozzle entry

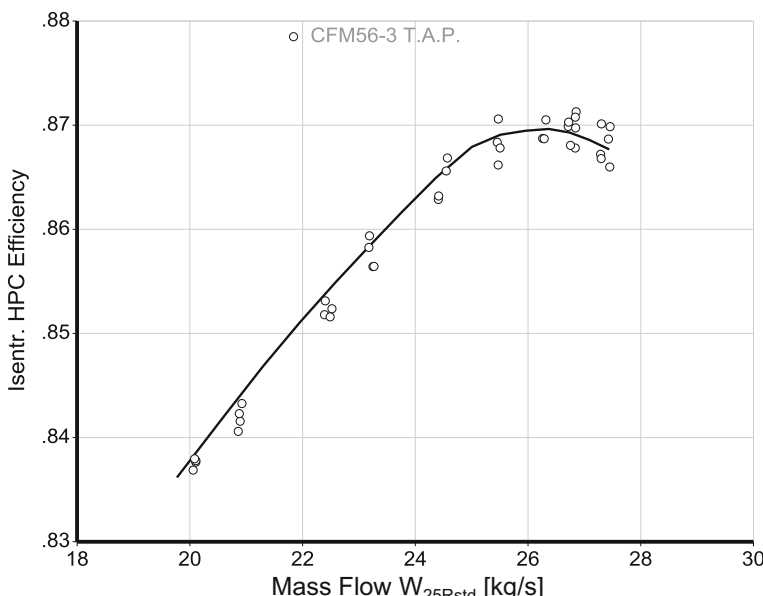


Fig. 4.2-24 Efficiency along the operating line in the HPC map

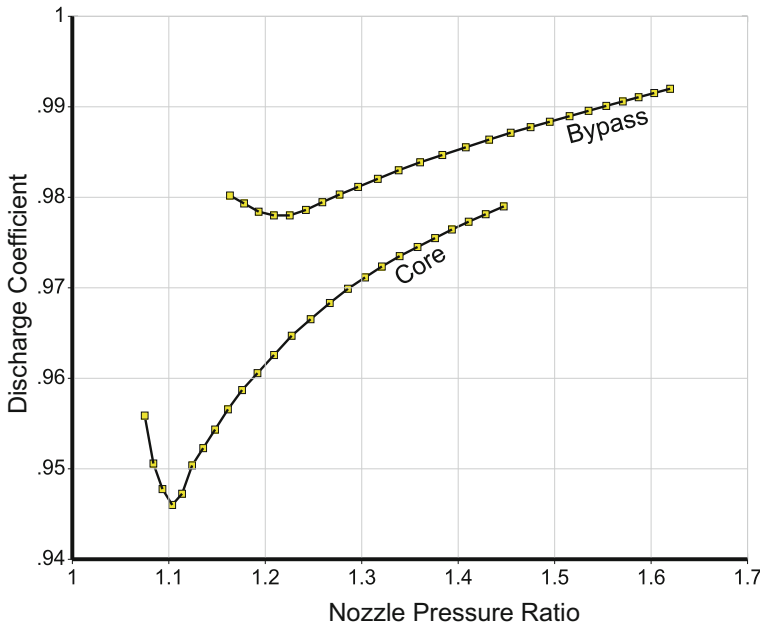


Fig. 4.2-25 Nozzle discharge coefficient derived from the measured data

conditions and we can calculate the discharge coefficient C_{D8} for each of the data points. For our model, we use the relationship between C_{D8} and core nozzle pressure ratio P_8/P_{amb} from Fig. 4.2-25.

4.2.4.5 Fan and LPT Map

Efficiencies along the operating lines of the booster and the HPC are in line with the measured data. The HPT efficiency is nearly constant. Those three components are modeled correctly. There are now only two properties available to adjust the engine simulation, so it accommodates the measured SFC values; the efficiencies of the fan and the LPT. Both affect SFC in a similar way, as can be seen in Fig. 4.2-26. But note that the efficiency has nearly no impact on the simulation of the EGT signal and only a minor influence on T5.

In Fig. 4.2-26, the middle curve shows that a change of $\Delta\eta_{\text{LPT}}$ from -2% to $+2\%$ requires a change of $\Delta\eta_{\text{LPC}}$ from $+2.7\%$ to -2.7% to keep SFC constant. We could decide to improve the fan efficiency somewhat, but then we would have to decrease LPT efficiency accordingly.

In our model, as speed is reduced, both the LPC and the LPT efficiency fall along the operating line (Figs. 4.2-16 and 4.2-21) at approximately the same rate. This balance seems reasonable. If we were to increase part-load efficiency of the

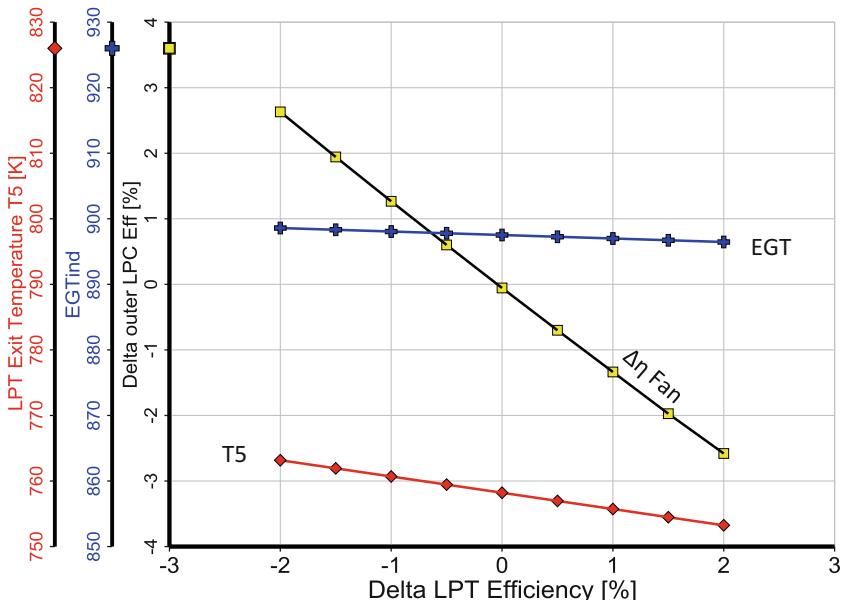


Fig. 4.2-26 Trends for $SFC = 11.5 \text{ g}/(\text{kN} \cdot \text{s})$ @ $FN = 60 \text{ kN}$

fan, for example, then the efficiency islands would no longer look like those of the original unscaled fan map. Also, the efficiency islands in the LPT map would lose their similarity with the original.

4.2.4.6 Spool Speeds

Getting spool speeds right is the last step of the model calibration process. Let us first explain the principle of the speed calibration in more detail.

Any compressor map consists of tables in which corrected spool speed is a parameter. During the GasTurb map scaling process, all speed values in the tables are multiplied by a constant factor such that at the map scaling point the corrected speed is equal to 1.0. Now all the tabulated speed parameter values represent relative corrected spool speed.

Using this map within a thermodynamically calibrated performance model gives the correct answers for mass flow, efficiency, and pressure ratio. Only the speed parameter value—which has been used for reading the map at a given operating point—is not necessarily correct because in the true map the correlation between corrected speed and corrected mass flow might be different. To get the speed-flow characteristic right we adjust the speed parameter values in the map tables.

Finding the N_L model is easy in this case because we know the fan operating line from the measured values of W_{2Rstd} and P_{17}/P_2 . Run an operating line and check how much the simulated corrected speed deviates from the measured one. Adjust the values of tabulated speed parameter so that you get agreement with the measured data. This is straightforward and can be done with GasTurb.

Strictly speaking, there is no justification for modifying the speed values in the fan and booster map tables by more than a small amount. In case of the HPC, however, we can justify bigger changes in the speed numbers because the HPC has variable guide vanes. Unfortunately, we do not know the VGV schedule for which the unscaled HPC map is valid. The VGV schedule of the CFM56-3 is certainly different and that is the main reason why the speed-flow correlation needs adjustment. We need not feel guilty when we change the speed numbers in the HPC map table.

To get the speed-flow correlation right, we use hybrid W_{25Rstd} values and modify the speed values in the map table as necessary. After adapting the speed parameter values more than a small amount you should check the map with Smooth C for consistency with compressor physics. The speed-flow correlation in the fan map must be smooth, while that of the CFM56-3 HPC has a distinct kink which is caused by a similar feature in the variable guide vane schedule.

4.2.4.7 Model Check

Now let us compare the quality of our preliminary model with the measured data. We have three important criteria:

1. The so-called SFC loop, which is a measure of thermal efficiency (Fig. 4.2-27).
2. Accuracy of the exhaust gas temperature EGT.
3. Accuracy of the LPT exit temperature T_5 .

The simulated SFC agrees well with the measurements for thrust values above 53kN. This is no surprise as we have adapted fan and LPT efficiency so that the model matches the measured values in the high thrust range. The simulated SFC at low thrust is significantly higher than measured.

Of course, we could have adjusted fan and LPT efficiencies differently to get the “compromise model” SFC loop. With this alternative approach, we would assume implicitly that the SFC step at $W_{2Rstd} = 230 \text{ kg/s}$ in Fig. 4.2-27 is a random effect caused by measurement noise.

As a second check look at Fig. 4.2-28, which shows how well EGT agrees with reality. The simulation is very accurate at high mass flow, a bit worse in the intermediate range and not useful at all at mass flows lower than 230 kg/s—that is where the SFC step is.

This model deviation is essentially independent of assumptions about fan and LPT efficiencies. In the lower left part of the figure, the SFC compromise model is as bad in its EGT prediction as the high thrust model.

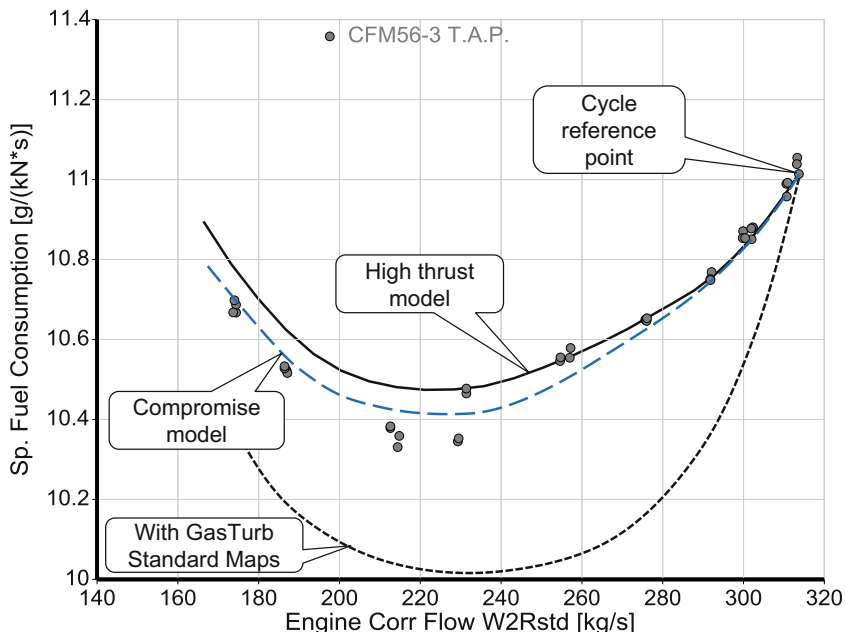


Fig. 4.2-27 SFC loop for various models

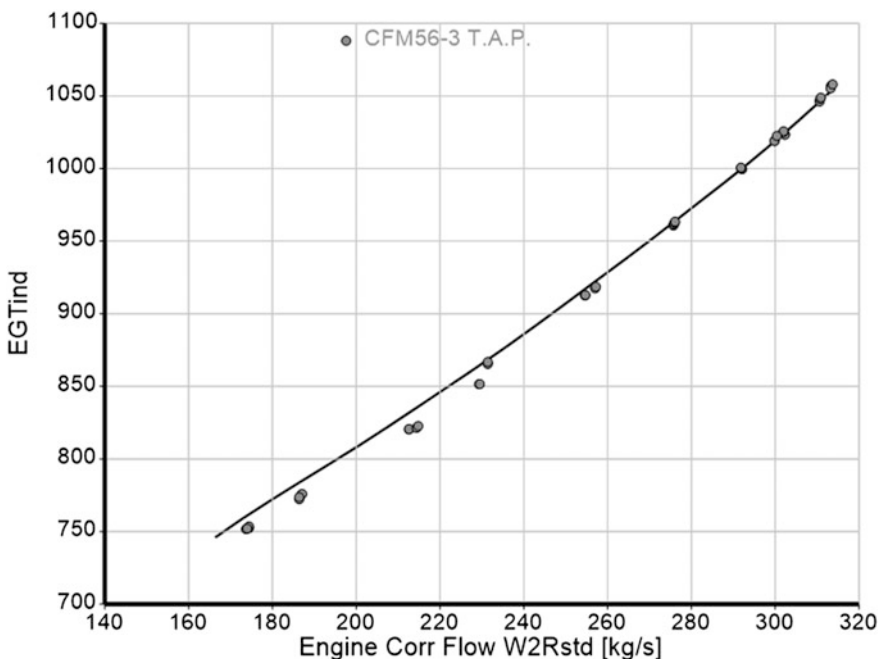


Fig. 4.2-28 Simulated and measured EGT, high thrust and compromise models

4.2.5 Refined Model

Until now we have ignored an interesting parameter—the temperature of the HP turbine clearance control air. Figure 4.2-9 shows that the Temperature Ratio T_{ACC}/T_3 changes in two steps: at $W_{2Rstd} = 230$ and at 270 kg/s. The steps are caused by switching between the three turbine clearance control modes active in the CFM56-3 engine [6].

In mode 1 (corrected core engine speed $N_H/\sqrt{\Theta_2}$ between 12,000 and 13,200 rpm) the turbine shroud cooling air is taken from stage 5 of the HPC. Mode 2 covers the speed range from 13,200 to 13,760 rpm (W_{2Rstd} between 230 and 270 kg/s). In this mode, a mixture of stage 5 and stage 9 compressor air cools the shroud. Mode 3 corresponds to the speed range above 13,760 rpm—all shroud cooling air is from compressor stage 9 (HPC exit).

Why do we want to control turbine tip clearance? Reducing thrust means reducing spool speed and temperature and under those circumstances, both the centrifugal forces and the thermal expansion of the rotating parts get smaller and the disk and the blades shrink. During thrust reduction, tip clearance increases if the liner diameter shrinks less than the blade tip diameter. Extra cooling of the liner support structure reduces the liner diameter and thus the running tip clearance. This is very effective, since 1% reduction of relative tip clearance (the ratio of absolute clearance and blade length) typically yields a 2% efficiency increase.

How do we model the turbine tip clearance control of the CFM56-3? We know neither the amounts of stage 5 and stage 9 cooling air nor the change in tip clearance. Nevertheless, we can create a performance model which fits the measured data.

As a first step, we create a baseline model which agrees as well as possible with the measured data of SFC and EGT when in the mode 3 of the turbine clearance control. The aim of the baseline model is to simulate the engine behavior with tip clearance control inoperative.

In Fig. 4.2-29 the baseline SFC in mode 2 is about 0.25% higher than measured; in mode 1 the SFC difference is 1.35%. The corresponding EGT differences (see Fig. 4.2-30) are 2 and 12 K.

Adapting the model to the measurements is quite simple: constant HP turbine efficiency modifiers of 1% in mode 1 and 0.2% in mode 2 do the job. These modifiers correct SFC, EGT and T_5 simultaneously while this model trim hardly affects the other model parameters.

The agreement of the final model with the measurements in Figs. 4.2-29 and 4.2-30 is excellent but the comparison in Fig. 4.2-31 does not look so good. There, the calculated T_5 deviates from the given data much more than EGT. There are good reasons for ignoring these differences between theory and measurement: Have another look at Fig. 4.2-12, which shows the temperature differences between the two T_5 sensors. The mean value of these sensor temperatures certainly does not always represent the thermodynamic average predicted by the simulation.

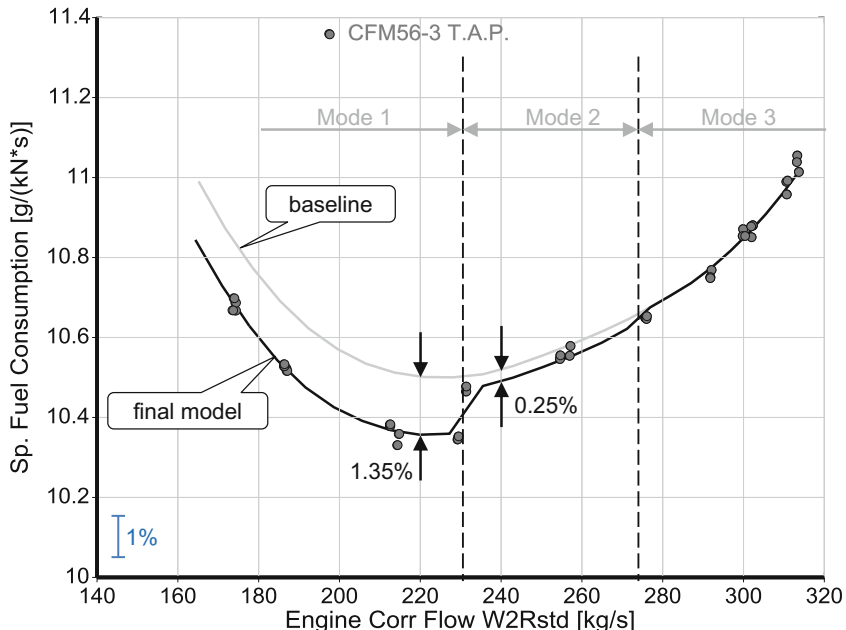


Fig. 4.2-29 SFC loop with and without clearance simulation

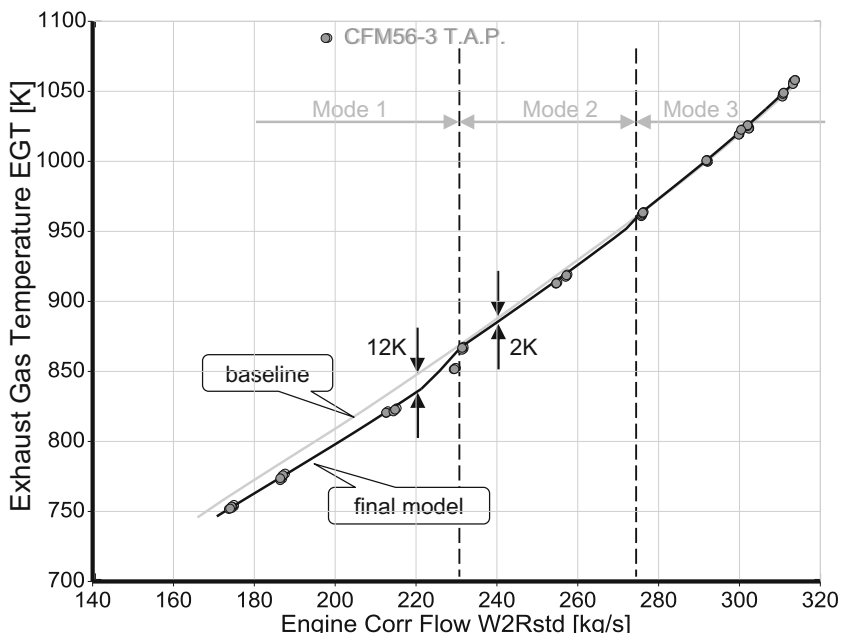


Fig. 4.2-30 EGT with and without clearance control simulation

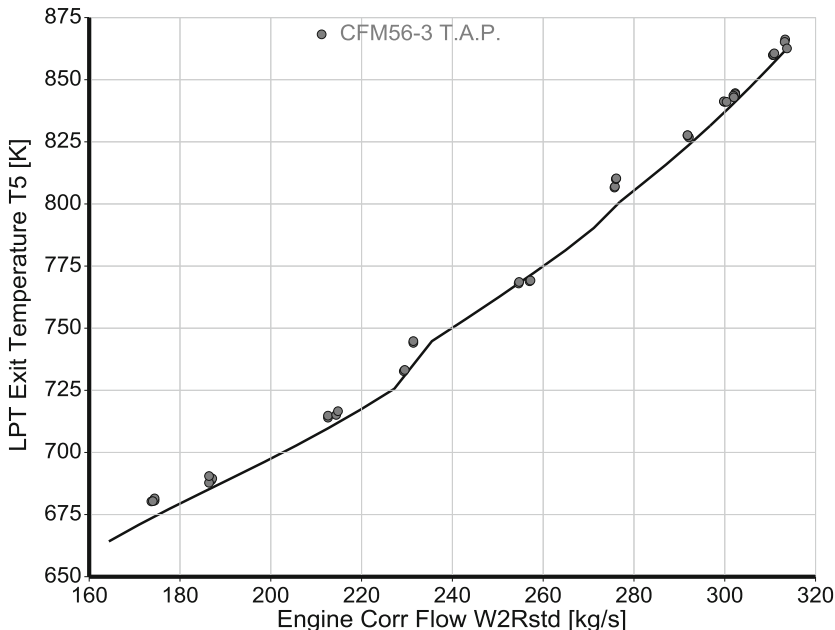


Fig. 4.2-31 The most inaccurate match with the data

A full check of the model consists of many figures with all sorts of parameters. Among those are thrust, mass flows, spool speeds, temperatures, and pressures. Figure 4.2-32 is a typical example, the agreement between theory and reality is of the same quality in all the other correlations.

By the way, the operating lines and the maps of the fan (Fig. 4.2-16), the booster (Figs. 4.2-18 and 4.2-22), HPC (Fig. 4.2-20) and LPT (Fig. 4.2-21) are those from the final model.

4.2.6 Some Final Remarks

The first look at the SFC loop (Fig. 4.2-27) might have given you the impression that there is much scatter in the data. You make a compromise model and regard your job as finished. By doing this you do not realize much of the potential accuracy of the model.

It is obvious that the 1.2% step in SFC near to 53 kN thrust ($W_{2Rstd} \approx 230 \text{ kg/s}$) is not due to random measurement noise. However, how do you reconcile the SFC step in the model? If you do not know about the turbine tip clearance control, you might be tempted to tweak fan efficiency until you get agreement. You would end

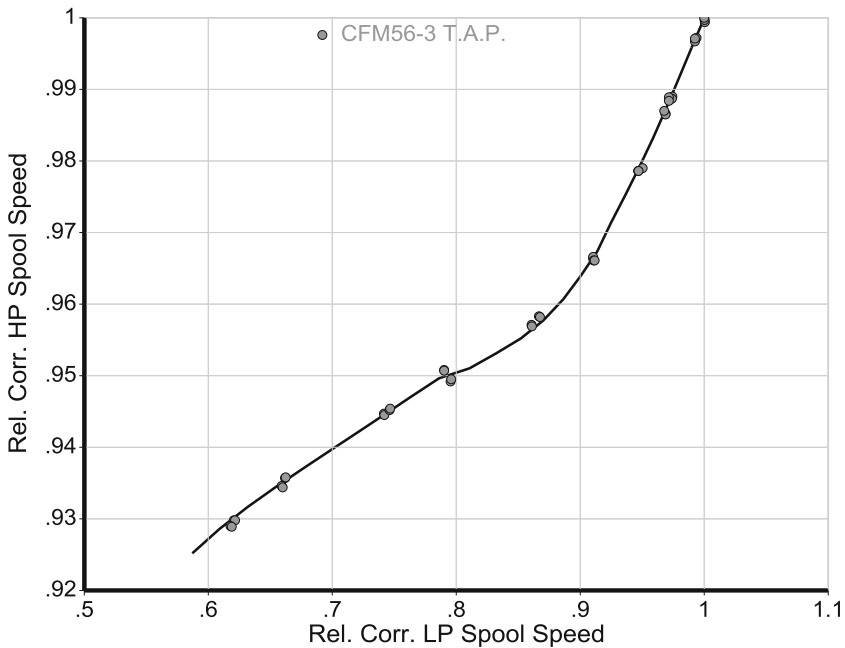


Fig. 4.2-32 One example from many similar correlations

up with a distorted fan map and that cannot be justified in terms of compressor physics.

We have chosen to simulate turbine tip clearance effects very simply. You might be tempted to model the turbine tip clearance control system in much more detail, with varying amounts of stage 5 and stage 9 air, for example. Be careful: you do not have enough knowledge about the secondary air system. Whatever you put in your model would be speculation, not based on facts. In effect, you would create a more complex model without any added value!

The quality of a model becomes important when you calculate operating conditions in which the component operating points are not on the calibrated operating line. This is the case if you run our model at cruise conditions, for example. The fan operating line will be much further from the surge line there than at sea level because the bypass nozzle pressure ratio is higher.

One last piece of advice: Try out many different ideas during model development, but be aware of models that are too complex. When you are done, check whether all the bells and whistles you may have added are necessary. A good model is accurate, and is based only on elements you really understand and are simple to handle.

4.3 F107-WR-400

The F107-WR-400 is a turbofan engine designed by Williams International for cruise missile propulsion. Some performance data of this engine are publicly available. We use these data to calibrate a model which can predict thrust and fuel consumption across the full flight envelope.

4.3.1 Cycle Reference Point Max Continuous ISA SLS

Figure 4.3-1 shows the architecture of the F107-WR-102 which is the same as that of the -400. Guaranteed ratings for sea level static and three flight conditions of the F107-WR-400 have been published in [11]. Most cycle details are available for Max Continuous rating at ISA SLS. Therefore, we use this operating condition as the cycle reference point.

In Table 4.3-1 there are two values for the exhaust gas temperature EGT: maximum rated EGT is 869 K, guaranteed EGT is 14 K higher. First cycle calculations make it obvious that EGT cannot be the nozzle inlet temperature as indicated in the cut-away view (Fig. 4.3-1), it must be the LP turbine exit temperature T_5 .

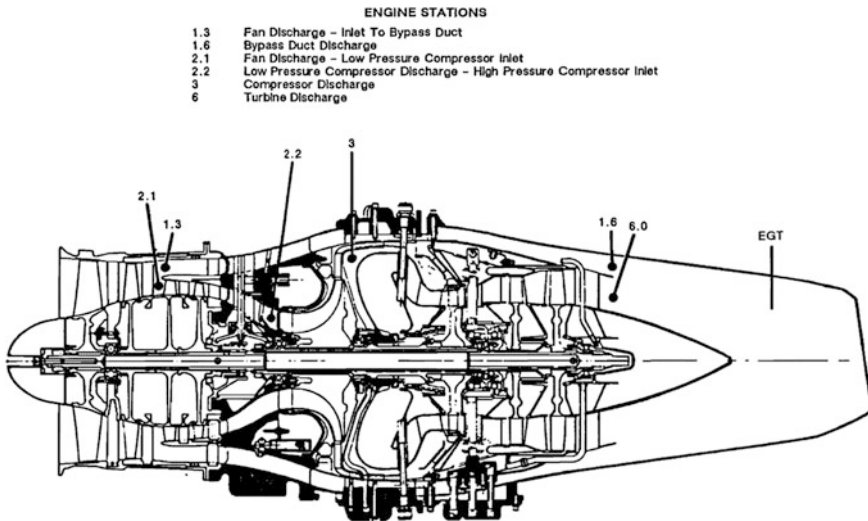


Fig. 4.3-1 Cutaway view of the F107-WR-102 [10]

Table 4.3-1 Summary of given Max Continuous data for ISA SLS

Thrust	kN	2.846	Guaranteed
SFC	g/(kN*s)	19.35	
Airflow	kg/s	6.17	
EGT	K	883	
N _L	RPM	33,100	
N _H	RPM	63,200	
Fuel RJ-4 heating value	MJ/kg	42.54	
Fan		2.1	Max design pressure ratios
Fan + Booster		3.6	
HPC		3.9	
Overall pressure ratio		13.8	
Bypass ratio		1	Max rated values
Airflow	kg/s	6.17	
Turbine inlet temperature	K	1283	
Exhaust gas temperature	K	869	

There are few degrees of freedom for re-engineering the cycle. Fan and radial compressor pressure ratios are given, the power required to drive these compressors varies only with the assumptions for the efficiencies. EGT (T_5) follows from the given values for bypass ratio, T_4 and the power required for the compressors. When EGT is simulated correctly, the calculated thrust depends only on assumptions about the turbine efficiencies and the pressure losses in the bypass duct.

After a few trial cycle calculations, assuming max rated EGT = 869 K is the correct value, we come up with the data listed in Table 4.3-2.

All the data from Table 4.3-1 are reproduced, except SFC which is 5.8% too low. What can we do to get SFC right? We cannot decrease the compressor efficiencies because T_5 would then become lower than the given EGT value. If we decrease the turbine efficiencies (which are already assumed to be very low) then we would lose thrust. The only way to increase SFC is to lower the compressor pressure ratios. We justify that with the wording in the comment on the pressure ratios: “Max Design” can mean that the true pressure ratios are somewhat lower.

Next, we do a parametric study in which we decrease all compressor pressure ratios simultaneously. This we do with the factor f:

$$\pi = \pi_{max} - f * (\pi_{max} - 1)$$

At off-design, the pressure ratio of the gas generator compressor generally changes less than the pressure ratio of the fan. Therefore, we correct the pressure ratio of the HPC by the factor f/2.

We do not know the efficiencies of the compressors and turbines, but we know something about the relationships between them. The fan outer efficiency is usually lower than the inner efficiency for two reasons: the Mach numbers are higher, and the

Table 4.3-2 Max continuous ISA SLS matched to T5 = 869 K

Station	W kg/s	T K	P kPa	WRstd kg/s	FN	=	2.84 kN
amb		288.15	101.325				
1	6.170	288.15	101.325		TSFC	=	18.2381 g/(kN*s)
2	6.170	288.15	101.325	6.170	WF Burner	=	0.05182 kg/s
13	3.085	368.46	212.783	1.661	s NOX	=	0.3992
21	3.085	435.75	364.770	1.054	BPR	=	1.0000
25	3.085	435.75	358.569	1.072	Core Eff	=	0.3408
3	3.085	683.19	1398.419	0.344	Prop Eff	=	0.0000
31	3.039	683.19	1398.419		P3/P2	=	13.801
4	3.091	1283.00	1328.498	0.497			
41	3.091	1283.00	1328.498	0.497	P16/P6	=	1.02759
43	3.091	1066.83	529.255		A63	=	0.01673 m ²
44	3.091	1066.83	529.255		A163	=	0.01000 m ²
45	3.091	1066.83	521.317	1.156	A64	=	0.02673 m ²
49	3.091	869.48	196.612		XM63	=	0.46353
5	3.091	869.48	196.612	2.767	XM163	=	0.49731
6	3.091	869.48	194.646		XM64	=	0.49998
16	3.116	371.66	200.016		P63/P6	=	1.00000
64	6.206	628.98	194.849		P163/P16	=	1.00000
8	6.206	628.97	192.901	4.816	A8	=	0.02118 m ²
Bleed	0.015	683.19	1398.414		CD8	=	0.94884
					Ang8	=	25.00 °
Efficiencies:	isentr	polytr	RNI	P/P	P8/Pamb	=	1.90378
Outer LPC	0.8448	0.8600	1.000	2.100	WLkBy/W25	=	0.01000
Inner LPC	0.8571	0.8800	1.000	3.600	WCHN/W25	=	0.00000
HP Compressor	0.8028	0.8350	2.162	3.900	WCHR/W25	=	0.00000
Burner	0.9995			0.950	Loading	=	100.00 %
HP Turbine	0.8545	0.8400	2.282	2.510	WCLN/W25	=	0.00000
LP Turbine	0.8651	0.8500	1.106	2.651	WCLR/W25	=	0.00000
Mixer	0.3000				WBHD/W21	=	0.00000
					far7	=	0.00842
HP Spool mech	Eff 0.9900	Nom Spd	63200 rpm		WBLD/W25	=	0.00500
LP Spool mech	Eff 1.0000	Nom Spd	33100 rpm		PWX	=	0.0 kw
P2/P1= 1.0000	P25/P21= 0.9830	P45/P44= 0.9850			P16/P13	=	0.9400
					P6/P5	=	0.9900
hum [%]	war0	FHV	Fuel				
0.0	0.00000	42.540	Generic				

tip clearance causes losses which do not exist in the core stream. Centrifugal compressors tend to have lower efficiencies than axial compressors. Usually the efficiencies of uncooled turbines are higher than compressor efficiencies. LP turbine efficiency is a bit higher than HPT efficiency due to the lower hub/tip-radius ratio.

Fan efficiencies especially depend not only on the technology level but also on the location of the operating point in the map. Efficiency drops quickly at high corrected spool speed $N_L/\sqrt{T_2}$ with the consequence that SFC increases. The slope of SFC versus thrust indicates how quickly the fan efficiency drops with increasing of $N_L/\sqrt{T_2}$.

Figure 4.3-2 shows that the slope of SFC versus thrust reveals a clear trend with engine inlet temperature T_2 at Max Continuous rating. The slope is biggest for the flight cases 15,000 ft/M = 0.7 and Sea Level Static and smallest for Sea Level Mach 0.7. From this, we can conclude that at our cycle reference point (Sea Level Static), the fan operates in the high speed region of its map. There the efficiency is significantly less than at part-load operation.

The design point efficiency of the axial low pressure compressor is certainly several points better than that of the centrifugal high pressure compressor. At the cycle reference point—where the LPC operates in the region of high corrected

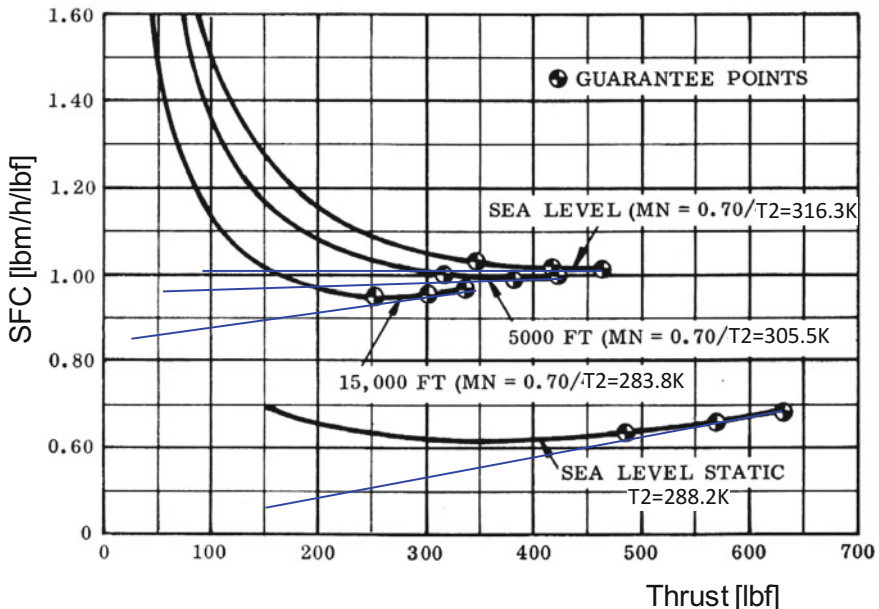


Fig. 4.3-2 Guaranteed performance of the F107-WR-400

speeds—the efficiency difference is certainly smaller. We use the following hypothesis for the efficiencies at the cycle reference point:

Fan inner efficiency	Base
Fan outer efficiency	Base -0.02
HPC efficiency	Base -0.01
HPT efficiency	Base +0.01
LPT efficiency	Base +0.02

The parametric study varies the compressor pressure ratio factor f and the fan inner efficiency to generate new base values for the efficiencies of all the other components.

Figure 4.3-3 shows that with the given EGT = 869 K (T_5), the max pressure ratios ($f = 0$) and guaranteed thrust of $F_N = 2.84$ kN, the SFC value is underestimated by 5.6%. With the alternate EGT of 883 K we get only a 4% SFC deficit from the guarantee value. The component efficiencies are not very different, but the compressor pressure ratios are lower.

We have questioned the rated EGT and the values for the Max Design Pressure Ratios, why not look for further opportunities to get a closer SFC match? The bypass ratio is given as exactly 1. Might the BPR number of 1 be a rounded figure? If we assume a slightly lower bypass ratio of 0.98, then the debit from the target SFC shrinks to only 3.2%, as indicated in Fig. 4.3-4.

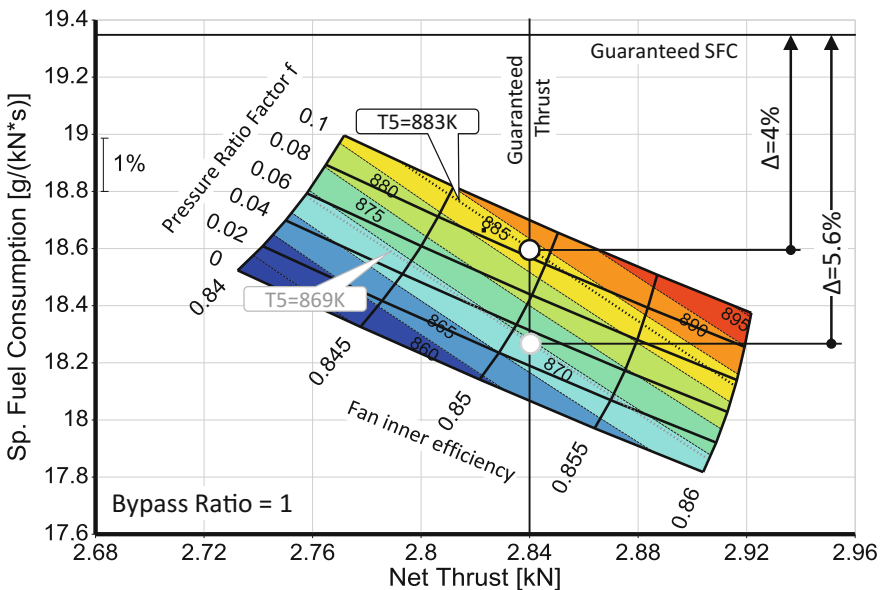


Fig. 4.3-3 Parametric study with component efficiency and compressor pressure ratio changes for BPR = 1

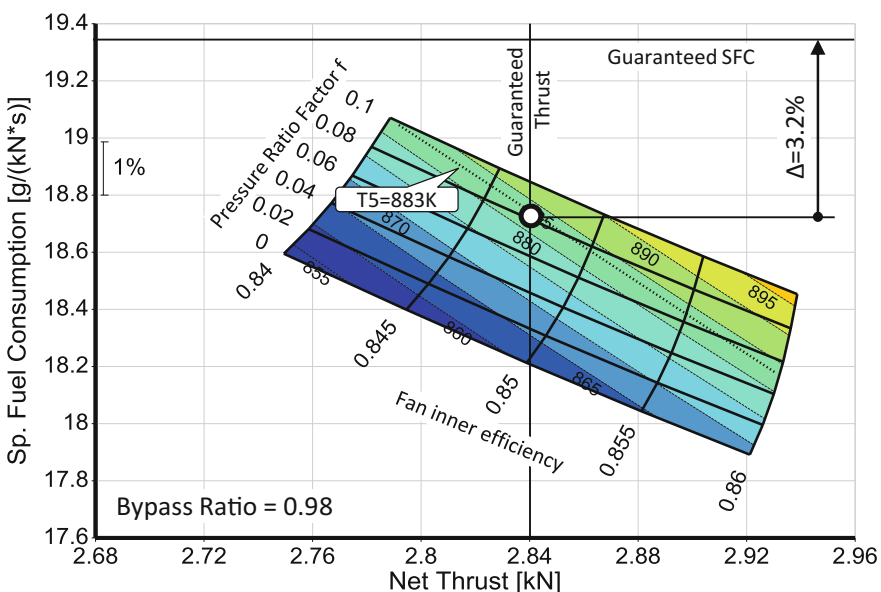


Fig. 4.3-4 Parametric study with component efficiency and compressor pressure ratio changes for BPR = 0.98

It is not possible to get a perfect match of the simulated and the given SFC values without deviating from the other given data much more than we already did. We need a non-technical explanation—and there is one.

The given data are guarantee values. How does the engine manufacturer generate these numbers? He has a model of the average new production engine and must consider the manufacturing tolerance. Even the minimum production engine will deliver the guaranteed thrust, but it will need more fuel than an engine of average quality.

The simplest way to consider that in the performance guarantees is to scale up the fuel flow number. That might have happened with the F107 guarantee numbers we have obtained. A 3.2% SFC margin for covering production tolerance looks reasonable. Therefore, we select the point marked with a circle in Fig. 4.3-4 as the cycle reference point: Table 4.3-3 lists the details. The model we are going to generate will represent an average new production engine.

Table 4.3-3 Cycle reference point

Station	W kg/s	T K	P kPa	WRstd kg/s	FN	=	2.84 kN
amb		288.15	101.325				
1	6.170	288.15	101.325		TSFC =	18.7384 g/(kN*s)	
2	6.170	288.15	101.325	6.170	WF Burner =	0.05322 kg/s	
13	3.054	366.41	203.477	1.715	S NOX =	0.3640	
21	3.116	433.72	342.774	1.130	BPR =	0.9800	
25	3.116	433.72	336.947	1.150	Core Eff =	0.3352	
3	3.116	672.54	1273.300	0.379	Prop Eff =	0.0000	
31	3.069	672.54	1273.300		P3/P2 =	12.566	
4	3.123	1283.00	1209.635	0.552	P16/P6 =	0.96924	
41	3.123	1283.00	1209.635	0.552	A63 =	0.01589 m ²	
43	3.123	1074.87	508.586		A163 =	0.01131 m ²	
44	3.123	1074.87	508.586		A64 =	0.02720 m ²	
45	3.123	1074.87	500.957	1.220	XM63 =	0.50034	
49	3.123	883.00	199.331		XM163 =	0.44042	
5	3.123	883.00	199.331	2.779	XM64 =	0.50000	
6	3.123	883.00	197.338		P63/P6 =	1.00000	
16	3.085	369.58	191.268		P163/P16 =	1.00000	
64	6.208	637.77	192.966		A8 =	0.02155 m ²	
8	6.208	637.77	191.036	4.898	CD8 =	0.94836	
Bleed	0.016	672.54	1273.300		Ang8 =	25.00 °	
<hr/>							
Efficiencies:	isent	polyt	RNI	P/P	P8/Pamb =	1.88538	
Outer LPC	0.8093	0.8270	1.000	2.008	WLkBy/W25=	0.01000	
Inner LPC	0.8193	0.8470	1.000	3.383	WCHN/W25 =	0.00000	
HP Compressor	0.8058	0.8370	2.043	3.779	WCHR/W25 =	0.00000	
Burner	0.9995			0.950	Loading =	100.00 %	
HP Turbine	0.8694	0.8570	2.078	2.378	WCLN/W25 =	0.00000	
LP Turbine	0.8798	0.8670	1.054	2.513	WCLR/W25 =	0.00000	
Mixer	0.3000				WBHD/W21 =	0.00000	
<hr/>							
HP Spool mech	Eff 0.9900	Nom Spd	63200	rpm	far7 =	0.00865	
LP Spool mech	Eff 1.0000	Nom Spd	33100	rpm	WBLD/W25 =	0.00500	
<hr/>							
P2/P1=	1.0000	P25/P21=	0.9830	P45/P44=	PWX =	0.0 kw	
<hr/>							
hum [%]	war0	FHV	Fuel		P16/P13 =	0.9400	
0.0	0.00000	42.540	Generic		P6/P5 =	0.9900	

4.3.2 Off-Design Model

At the cycle reference point, our cycle agrees as well as possible with the given data. We freeze this cycle and make it the anchor point of our off-design model.

For off-design simulations we need performance maps for the compressors and turbines. Since we do not have the genuine maps we must invent them. We will scale maps from similar compressors and turbines in such a way that at the map scaling point they fit perfectly to the cycle reference point. The question is: where do we place this map scaling point in the unscaled map?

From earlier discussions, we know we must place that point in the upper corrected speed region of the compressor maps, where efficiency decreases with increasing corrected flow. With this choice, we get an increase in efficiency when we reduce thrust at sea level static. SFC will decrease in the high power range—and that's what we need to reconcile the simulation with the given data in Fig. 4.3-2.

By trial and error, we find where to place the map scaling point best. It is not difficult to get a good match of SFC in the high power region. Further away from the cycle reference point it might be necessary to modify the efficiency in the compressor maps as a function of corrected spool speed.

The slope of $SFC = f(F_N)$ in the upper thrust range is independent of the location of the scaling point in the turbine maps. Just place it on or near to the 100% corrected speed line in the high efficiency region.

When the simulated SFC matches the given data at sea level static, then also check the SFC at other flight conditions. The circles in Fig. 4.3-5 represent the given data from Fig. 4.3-2. The thrust values are the same in both figures, only the units are different. The guaranteed SFC from Fig. 4.3-2 is converted to the SFC of an average new production engine—it is 3.2% lower.

In the case of the F107-WR-400 it is easy to get a good agreement between the model and the given data because the flight conditions are not far apart.

The next three figures show the component maps of the F107-WR-400 model. In the fan map (Fig. 4.3-6) we see the influence of the flight Mach number on the position of the operating line. In the map of the HP compressor, all the operating lines nearly collapse, see Fig. 4.3-7. The HP turbine map is not worth showing:—the efficiency is nearly constant along the short operating lines, which all collapse. The operating lines in the LPT map are longer but the efficiency varies little (Fig. 4.3-8).

We have got SFC right, but that is not sufficient. Additionally, we need a model of the power control. We know the rated Maximum Continuous thrust at four flight conditions—that's not much but let's make best use of this piece of information.

We run our model in such a way that it produces exactly the rated thrust for each of the four points. This yields four EGT values which we plot against T_2 in Fig. 4.3-9. We notice that the three cases with flight Mach number 0.7 are on a perfectly straight line. The sea level static EGT is significantly higher.

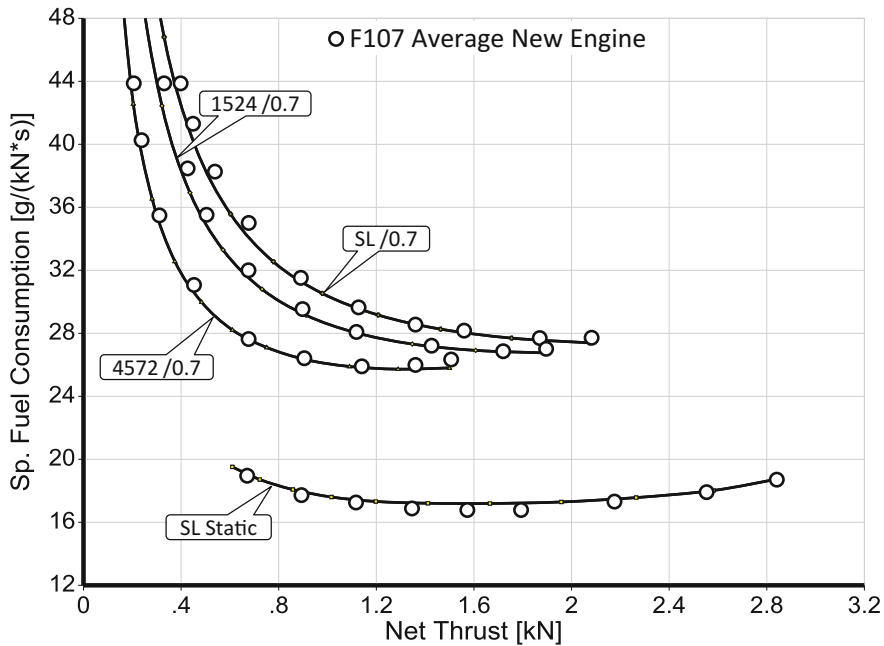


Fig. 4.3-5 Comparison of given data (the circles) with the simulation (the lines)

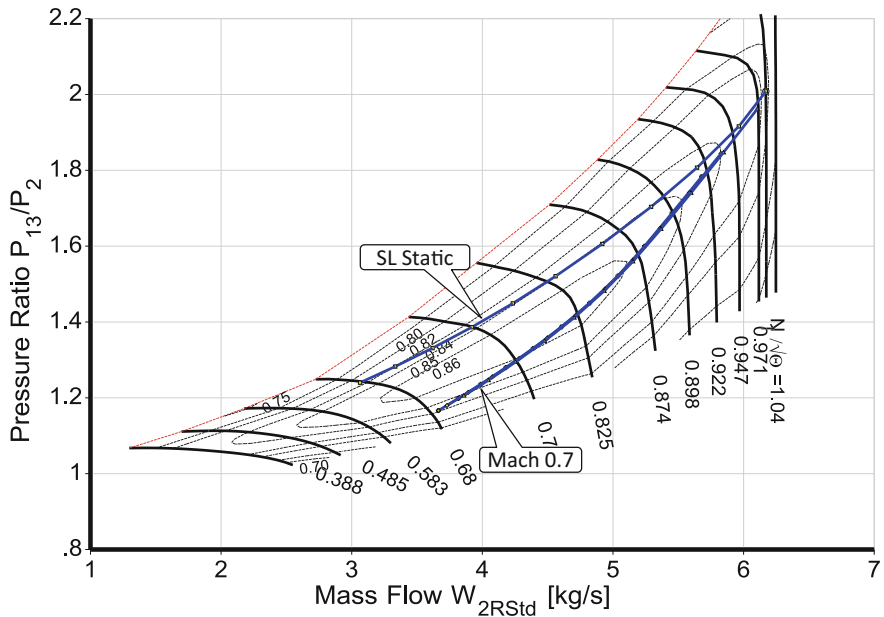


Fig. 4.3-6 Operating lines in the fan map

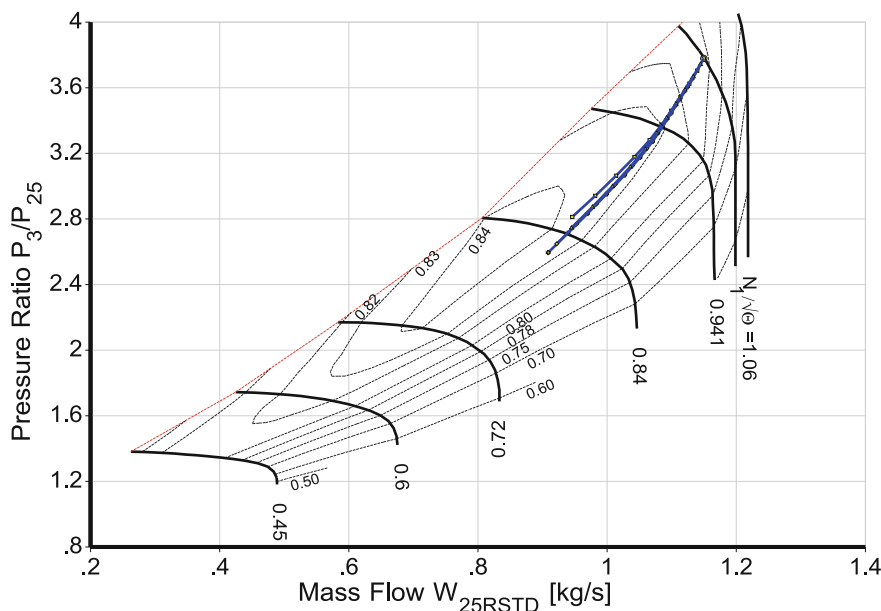


Fig. 4.3-7 Operating lines in the HPC map

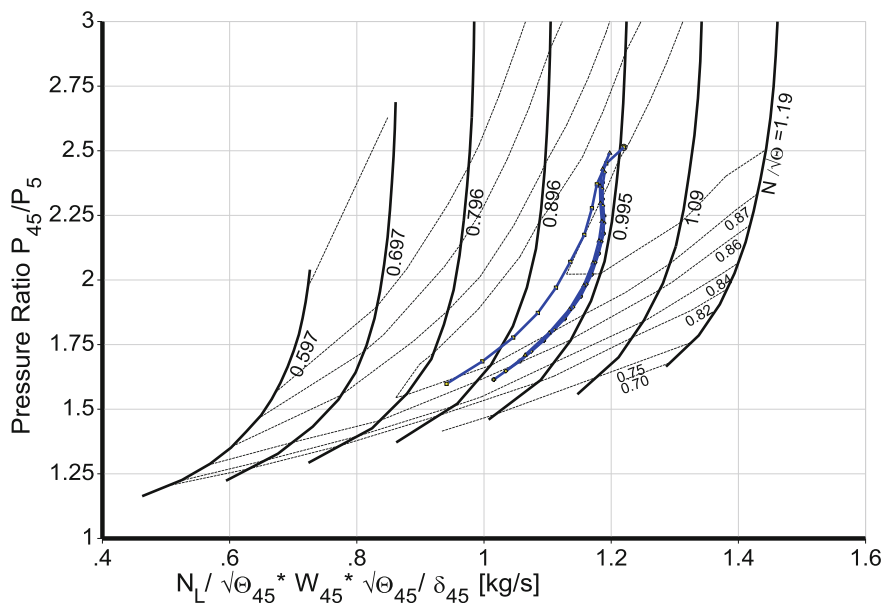


Fig. 4.3-8 Operating Lines in the LPT Map

The power control of the F107-WR-400 is a hydro-mechanical system. Nothing is known about how it works; we must invent something. Our hypothetical power control logic must work over the full flight envelope and at the same time agree with the four given thrust points.

We complement Fig. 4.3-9 with the following limiters:

- A straight line connects the three cases with $M = 0.7$.
- For lower Mach numbers, we shift the line upwards so it passes through point 1 at $M = 0$.
- The maximum permissible EGT is 883 K.
- The maximum permissible corrected fan speed $N_L/\sqrt{T_2}$ is 106%.

Making the rated EGT a function of T_2 and flight Mach number is common practice in modern digital control systems. The $N_L/\sqrt{T_2}$ limiter is set in such a way that the maximum design overall pressure ratio is approximately 13.8, as mentioned in [11].

Figure 4.3-10 shows the thrust of an uninstalled new production engine on an ISA day. At high altitude and low Mach numbers, the thrust is limited by $N_L/\sqrt{T_2}$, in the other flight cases it is limited by the EGT schedule.

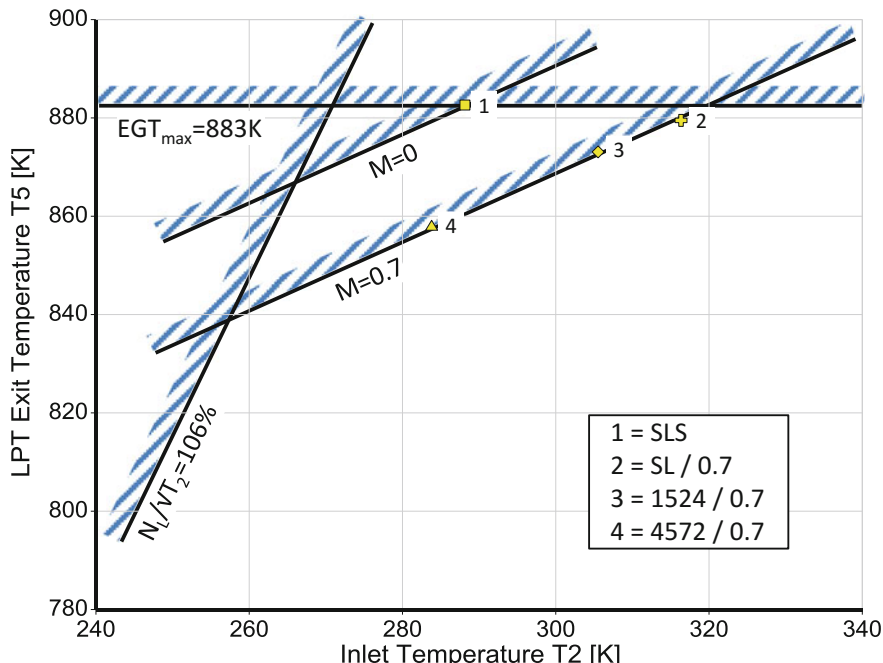


Fig. 4.3-9 Assumed thrust control logic

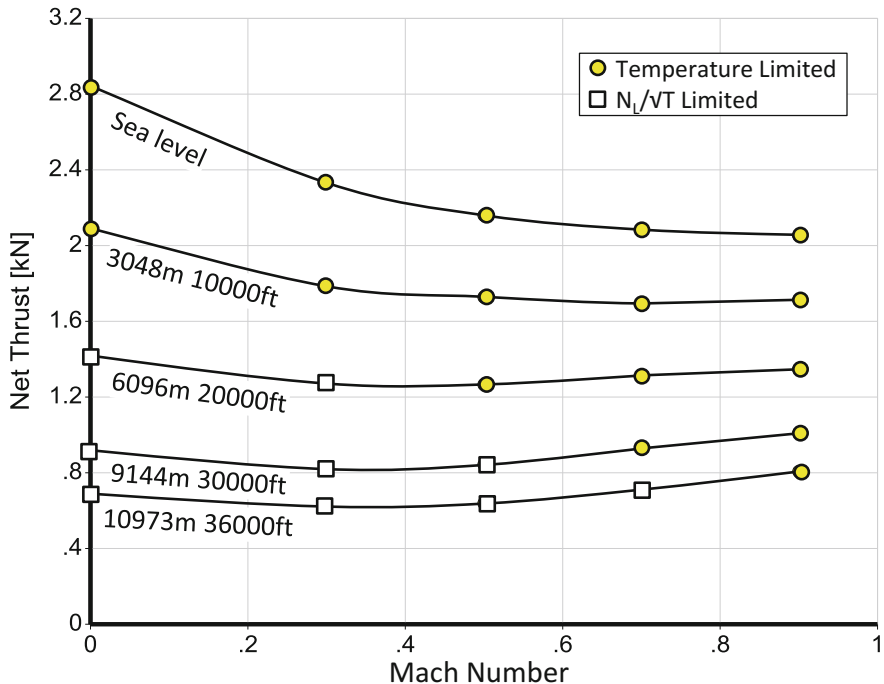


Fig. 4.3-10 Uninstalled Thrust ISA

We could find out more about the power control if we knew thrust throughout the flight envelope. If that were so, we would run the model with the known thrust values and then search in the results for correlations between potential control parameters. Certainly, there are limiters for $N_L/\sqrt{T_2}$, N_H and EGT. The latter might be a function of T_2 and Mach number, as we have assumed here. Maximum EGT may be a fixed value, while thrust is adjusted to the demand of the flight vehicle and a schedule is set for engine pressure ratio.

The re-engineering process always consists of the following steps:

1. Select and model a cycle reference point
2. Adjust the off-design simulation to known SFC data
3. Look for a hypothetical thrust control logic

When the task is to model the performance of an engine with an afterburner, model the dry engine first. Deal with the afterburner performance after you have found the Max Dry operating conditions for the appropriate flight condition. Reheat SFC depends mainly on engine mass flow, and afterburner inlet and exit temperatures. Afterburner efficiency plays a secondary role—expect low efficiencies at very high altitude and low flight Mach numbers—the famous upper left hand corner in the flight envelope.

4.4 References

1. Ashwood, P.F.: The uniform engine test programme. AGARD-AR-248 (1990)
2. Bloomer, H.E., Miller, R.R.: Preliminary altitude performance of the J57-P-1 turbojet engine with fixed-area exhaust nozzle. NACA RM SE54D30 (1954)
3. Kurzke, J.: How to create a performance model of a gas turbine from a limited amount of information. ASME GT2005-68537
4. Lippert, D., Woollatt, G., Ivey, P.C., Timmis, P., Charnley, B.A.: The design, development and evaluation of 3D aerofoils for high speed axial compressors. Part 1: test facility, instrumentation and probe traverse mechanism. ASME GT2005-68792
5. CFMI correlation report of TAP air Portugal for CFM56-3 ENGINE. Prepared by P. Compenat and F. Trimouille Approved by R. Mouginot (Oct. 1991)
6. CFMI. CFM56-3 engine shop manual—Engine test—Test 003—Engine acceptance test task 72-00-00-760-003-0 (2011)
7. Freeman, C.: Method for the prediction of supersonic compressor blade performance. J. Propul. **8**(1) (1992)
8. Lippert, D., Woollatt, G., Ivey, P.C., Timmis, P., Charnley, B.A.: The design, development and evaluation of 3D aerofoils for high speed axial compressors ASME GT2005-68792 (2005)
9. http://www.air.flyingway.com/books/engineering/CFM56-3/ctc-142_Line_Maintenance.pdf
10. Baran, A.J., Dunn, M.G.: The response of an F107-WR-102 engine to “Most Probable” Nuclear Dust Environment (U) Defense Nuclear Agency Technical Report DNA-TR-93-111, July 1993, Declassified July 2010 <http://www.dtic.mil/cgi-bin/GetTRDoc?Location=GetTRDoc&docType=GetTRDoc&docID=GetTRDoc&GetTRDocId=c050749.pdf>
11. http://www.alternatewars.com/SAC/F107-WR-400_Turbofan_PCS_-_October_1984.pdf

Chapter 5

Model-Based Performance Analysis



During the operation of the gas turbine a controller measures spool speeds, fuel flow and a few pressures and temperatures. In addition to these indispensable quantities, some controllers record additional data which are helpful for diagnosing the overall performance and the health status of the engine. Hundreds of temperatures and pressures are recorded during engine development tests.

Spool speeds, pressures and temperatures are the raw data for test analysis which tries to answer questions like how do the components of the gas turbine perform? Do they operate as intended? What will the performance of the engine be on a Standard Day?

There are two fundamentally different ways to analyze the raw data. The traditional approach is to compute specific fuel consumption, component mass flows, pressure ratios, efficiencies and duct pressure losses from the measured data. The calculation requires some a priori knowledge about the secondary air system and parasitic losses. The result of such test analysis computations are ISA corrected component and overall performance data.

The comparison of the test result with the nominal performance or an engine development target is left to the engineer. The problem is that the analyzed compressor efficiency number alone does not tell you much. Imagine you have analyzed a compressor efficiency to be 0.845. Whether this is a good or a bad test result depends on the engine operating point, see Fig. 5.1-1.

The engineer checks the numbers against those from his performance prediction program to assess the compressor performance as being above or below expectation. However, the number comparison is strictly valid only if the secondary air system and other calculation details are the same in both the test analysis and the performance prediction programs. If this is not the case, then the predicted compressor operating line is not consistent with the test. It obviously needs some effort to make the two programs compatible.

Model-based performance analysis combines test analysis and performance prediction within a single program. The prerequisite of the method is a performance model of the tested engine. Run the model for a performance analysis with the same

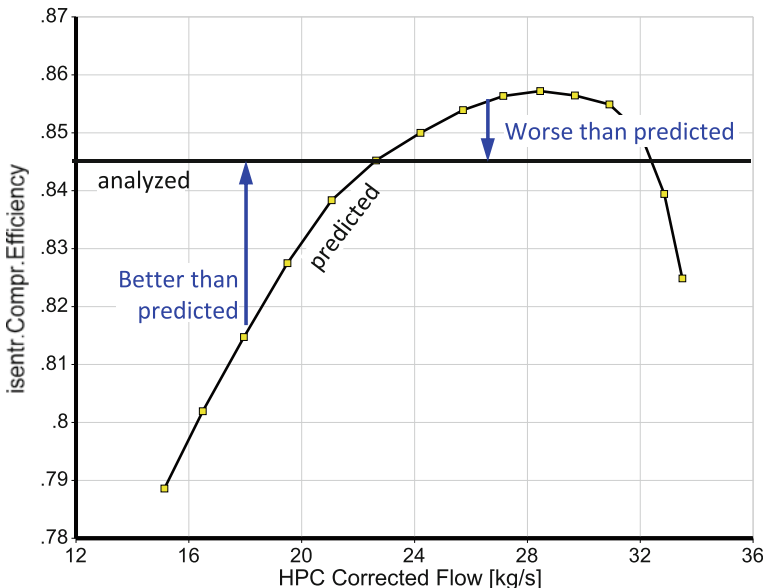


Fig. 5.1-1 Interpretation of a test result

entry conditions and the same command input as the engine on the testbed. The program calculates modifiers for the component maps in a special test analysis mode which make the model agree exactly with the measured data. The magnitude of the model adjustment factors is the actual component performance test result: the tested engine is better or worse than expected.

5.1 The Analysis by Synthesis Methodology

Model-based performance analysis is also known as Analysis by Synthesis, abbreviated to *AnSyn*. The noun Synthesis refers to a combination of two or more entities that together form something new; alternately, it refers to the creation of something by artificial means (Wikipedia).

A performance prediction program synthesizes the overall engine performance from the performance of its compressors, turbines, burners, nozzles, ducts, the secondary air system and other elements. It is an engine performance synthesis program. In test analysis mode, this program reconciles the performance synthesis with the measured data.

5.1.1 *The Model*

Building a useful model is feasible even when only a limited amount of information about the engine is available. Chapter 3 describes the approach to model creation and Chap. 4 provides details of its application in examples. The model describes the engine to be analyzed as effectively as possible, sometimes with a great deal of engineering judgement. All models contain assumptions due to simplifications in the component performance description and lack of information about the test vehicle. The fidelity of the model affects the output of the model-based test analysis.

5.1.1.1 **Degree of Detail**

Basic performance synthesis models of jet engines employ compressor and turbine maps for the main gas path behavior, quantify pressure losses in ducts and combustion chambers and consider discharge and thrust coefficients in exhaust nozzles. The main gas path model is complemented with a not-too-sophisticated description of the secondary air system and simple correlations for the power consumption of the external gearbox.

Some additional details should be considered when the model is intended for use with flight data. Power offtake and bleed air for aircraft purposes are easy to simulate. Reynolds number effects are more difficult to quantify but indispensable nevertheless. The effect of active clearance control (ACC) can be modeled simply as a change in efficiency.

Do not model phenomena which you know to exist without knowing their magnitude. A simple model is easier to understand and creates fewer mathematical problems.

5.1.1.2 **Calibration**

Calibrate the model with the best information available. This can be the testbed calibration report, as in the case of the CFM56 model described in Sect. 4.2. Note, however, that the hardware of the engine to be analyzed is often different to that of the engine used to calibrate the model. Use engineering judgement to make the best test prediction you can.

5.1.2 *Data Preprocessing*

Model-based analysis is a mathematical process with a multi-dimensional system of iterations. If the analysis program is provided with unreasonable raw data, then the

mathematical algorithm will not converge. Avoiding this requires a thorough check of the raw data before the model-based analysis commences.

5.1.2.1 Data Correction to Standard Day Conditions

A few problems with the raw data are easy to detect like engine internal pressure probes which indicate ambient pressure, for example. Other suspicious sensor readings become obvious after correcting the data to Standard Day conditions in plots against overall pressure ratio P_3/P_2 or corrected spool speed. Plotting $N_H/\sqrt{\Theta_2}$ versus $N_L/\sqrt{\Theta_2}$ is another good initial credibility check.

Analysis by Synthesis does not require Standard Day corrected data as input, it works with data measured at any engine inlet temperature—pressure combination. If the data are corrected, this serves as a quick first comparison with previously acquired data.

5.1.2.2 Comparing the Measurements with the Model

Running the model in parallel to the test is convenient. The model operating point is defined by the actual inlet conditions and one of the measured quantities. Fuel flow, engine pressure ratio and N_L are suitable as model control parameters. All indicated measured quantities should agree with the model values within a certain tolerance. Strange probe readings are easy to detect, missing or obviously incorrect data can be replaced by synthesized data (Fig. 5.1-2).

5.1.3 Definition of the AnSyn Factors

AnSyn factors account for differences between the model and the measurement. A factor of 1.0 means there is perfect agreement between the model and the measurement. An efficiency scaling factor greater than one, for example, indicates that the component performs better than predicted.

These statements are very general—how exactly are the AnSyn factors defined and how are they calculated? This is different for compressors and turbines.

5.1.3.1 Compressor

Let us assume we have measured the total pressures and temperatures at the compressor inlet and exit, the spool speed and the true mass flow. From these, we can calculate pressure ratio P_3/P_2 , corrected mass flow W_{2Rstd} , corrected spool

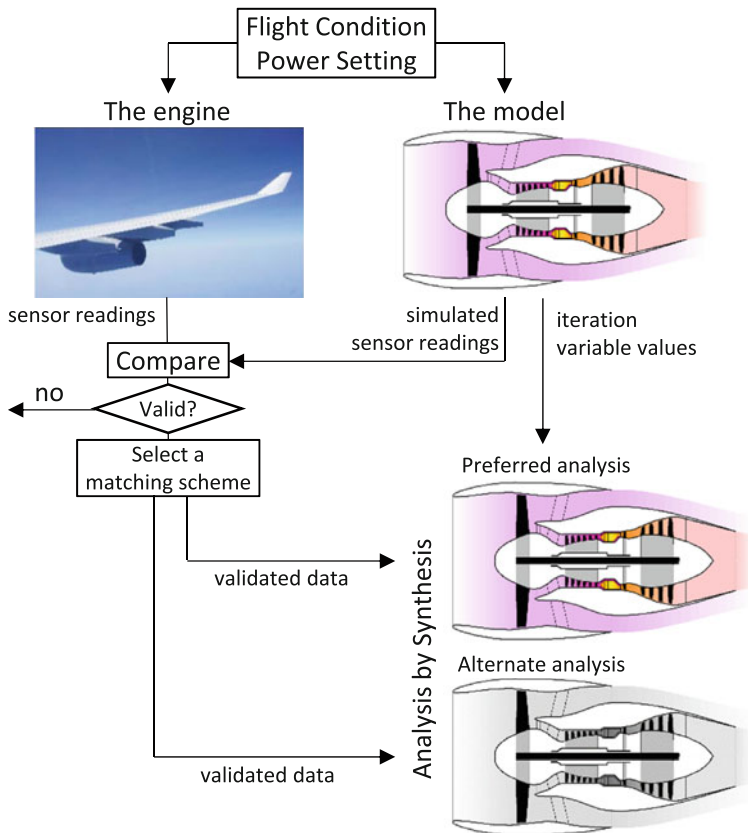


Fig. 5.1-2 Model-based data checking and analysis

speed $N/\sqrt{\Theta_2}$ and efficiency. P_3/P_2 and W_{2Rstd} together define point M in the compressor map (Fig. 5.1-3). The map speed line $N/\sqrt{\Theta_{map}} = 0.9$ is not consistent with the measured pressure ratio and corrected mass flow.

How can we quantify the difference between the map and the measured data with factors on pressure ratio, mass flow and efficiency? The location of point M in the map is unambiguous, but where is its counterpart on the map speed line? We could select point P, which has the measured pressure ratio and calculate the AnSyn factor for corrected flow as the ratio of measured corrected flow and that at point P.

The problem with this AnSyn factor definition is that it would not work in cases where the measured pressure ratio is 11.1 or higher. There is no point on the map speed line $N/\sqrt{\Theta_{map}} = 0.9$ with such a pressure ratio. Alternatively, we could think of defining an AnSyn factor for pressure ratio which would compare two pressure ratios at the measured corrected flow. This does not work with the map in Fig. 5.1-3 because the speed line does not reach the measured mass flow. We must find a definition between these two extremes.

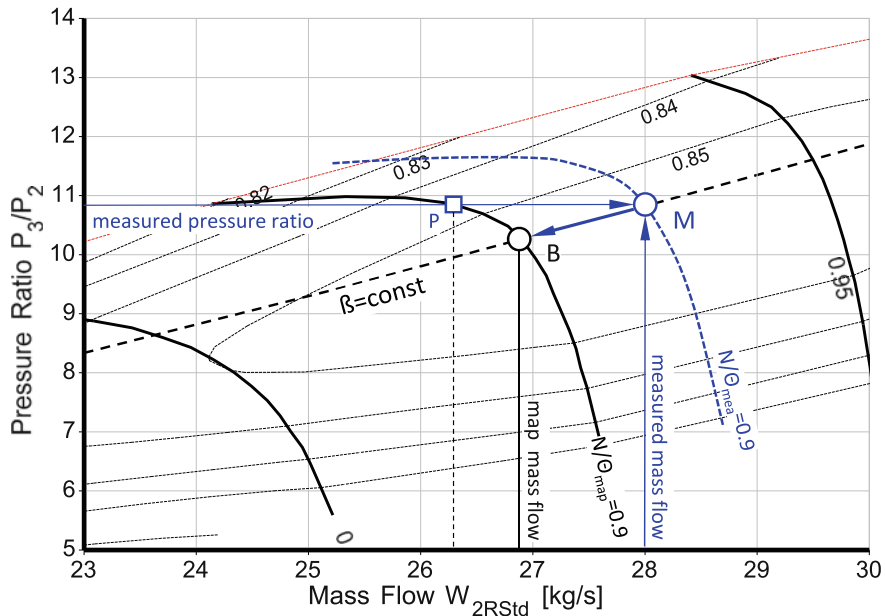


Fig. 5.1-3 Measured data in the compressor map

GasTurb compares the measured data of point M with the map data of point B on the same β line. Critics of this choice may claim that there is no physical law which justifies this decision because the β lines have no physical meaning. Remember, the primary purpose of introducing the β lines is to avoid numerical problems in off-design performance calculations.

However, we can give the β lines a meaning in terms of physics, if we define them as lines of (approximately) constant specific work H/U^2 . With β lines which are parabolas this is easy, especially with the compressor map preparation program Smooth C.

We define the mass flow AnSyn factor as

$$f_{W2RStd} = \left(\frac{W_2 \sqrt{\Theta_2}}{\delta_2} \right)_M / \left(\frac{W_2 \sqrt{\Theta_2}}{\delta_2} \right)_B \quad (5.1-1)$$

Another common name for the mass flow AnSyn factor f_{W2RStd} is flow capacity factor. Note that we need not define an extra pressure ratio AnSyn factor because the difference in pressure ratio between measurement and map implicitly describes the β -line.

The efficiency AnSyn factor is calculated as

$$f_{e23} = \eta_M / \eta_B \quad (5.1-2)$$

5.1.3.2 Turbine

It seems reasonable to define turbine AnSyn factors the same way as compressor AnSyn factors. This would not be a good choice however, because small changes in measured corrected mass flow would translate into big changes in the efficiency read from the map in Fig. 5.1-4. Consequently, we would see a big scatter in the AnSyn efficiency factors.

The problem goes away when we locate the turbine operating point in the map with pressure ratio and corrected speed (Fig. 5.1-5). Scatter in these data causes only small changes of the efficiency read from the turbine map. The AnSyn factors for corrected flow (=turbine flow capacity) and efficiency describe the difference between prediction and measurement accurately.

In reality, the compressor and turbine test analysis algorithm is not as simple as described above. Map modifiers which consider hardware modifications or component deterioration are frequently applied. Reynolds number corrections and tip clearance simulations complicate the algorithm further.

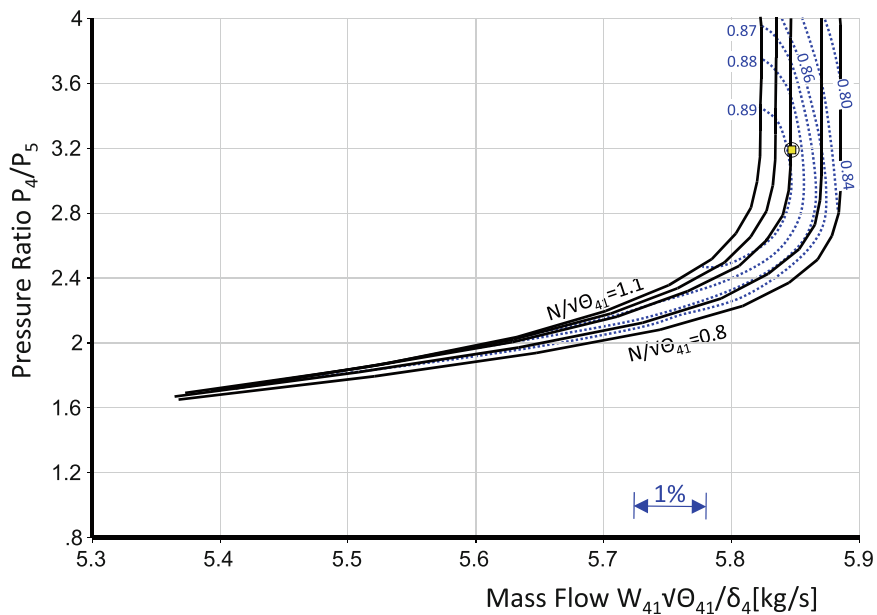


Fig. 5.1-4 Compressor AnSyn methodology applied to a turbine map

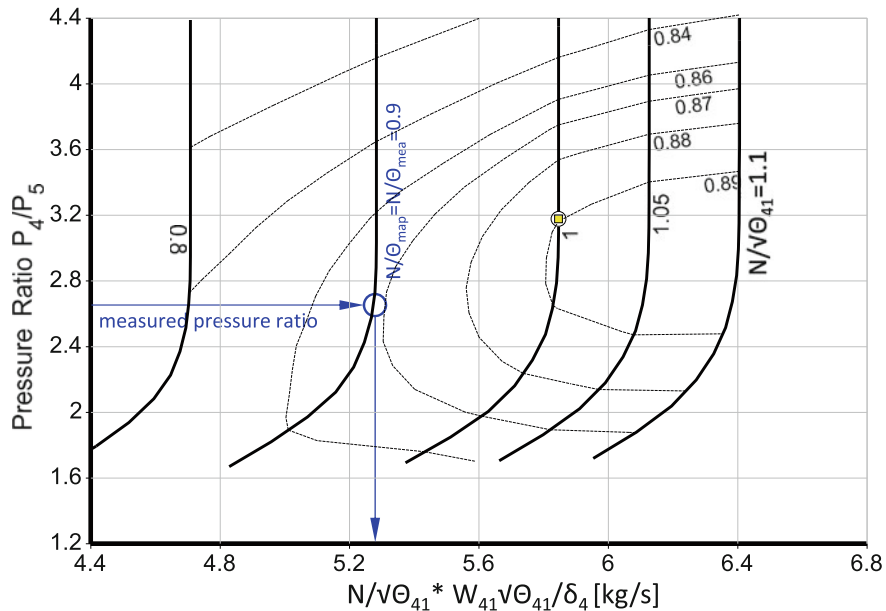


Fig. 5.1-5 Locating the operating point in the turbine map

5.1.4 A Simple Analysis Example

Let us consider the analysis of the sea level performance test of a turbojet (Fig. 5.1-6). Table 5.1-1 lists the quantities measured at any steady state operating point. The lower fuel heating value has been determined in advance, all the data have passed a quality check.

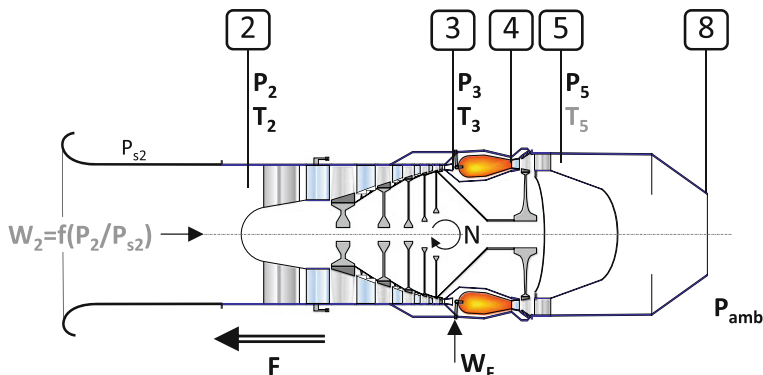


Fig. 5.1-6 Turbojet nomenclature

Table 5.1-1 Measurements on a sea level testbed

Mass flow W_2	kg/s
Spool speed N	RPM
Inlet total temperature T_2	K
Inlet total pressure P_2	kPa
Compressor exit total temperature T_3	K
Compressor exit total pressure P_3	kPa
Fuel flow W_F	kg/s
Turbine exit total pressure P_5	kPa
Ambient pressure P_{amb}	kPa
Thrust F	kN

The synthesis program runs in an off-design mode during the model-based test analysis. That requires a multidimensional iteration with many variables. The off-design iteration commences with guessed values for the variables. In an integrated analysis system, we can use the iteration variable values from the data check run of the model as guesses (see Fig. 5.1-2). We run the model for the analysis by synthesis with the measured spool speed N , the actual compressor entry conditions described by T_2 and P_2 and ambient pressure P_{amb} .

In test analysis mode, we calculate the pressure ratio P_3/P_2 , the corrected flow W_{2Rstd} and the compressor efficiency η_{23} from the measured quantities. Factors for compressor flow capacity f_{W2Rstd} and efficiency f_{e23} match the model with the measured compressor data.

The air mass flow entering the burner W_3 is equal to the compressor mass flow minus the parasitic and cooling air streams as they are defined in the secondary air system model. The heat addition from the fuel yields the burner exit temperature T_4 , and the burner pressure loss models the turbine inlet pressure P_4 . Turbine pressure ratio is the ratio of the calculated inlet pressure P_4 to the measured exit pressure P_{5m} . From P_4/P_{5m} and the work done by the turbine (the sum of compressor and gearbox power) the turbine efficiency e_{4-5} is derived. We can calculate the turbine AnSyn factors for flow f_{W4Rstd} and efficiency f_{e45} after reading the turbine map at the coordinates for corrected speed $N/\sqrt{T_4}$ and the pressure ratio P_4/P_{5m} . The turbine exit conditions of the model are the calculated total temperature T_5 and the measured total pressure P_{5m} .

The model of the turbine exit duct and the jet pipe yields the nozzle entry mass flow W_8 , total pressure P_8 and temperature T_8 . Next, we calculate the nozzle throat area A_{8req} required to pass the mass flow W_8 through the nozzle at the pressure ratio P_8/P_{amb} . The ratio of calculated throat area A_{8req} and model throat area A_8 is the nozzle area AnSyn factor f_{A8} . Finally, we determine the AnSyn factor for thrust as the ratio of measured thrust to calculated gross thrust. This model-based test analysis calculation is straightforward and delivers unambiguous results.

5.1.5 How to Deal with Missing and Additional Measurements

Not every turbojet performance test provides measurements for all the input quantities needed by the program in its test analysis mode. What if engine mass flow W_2 simply isn't available? Could we make use of an additional exhaust gas temperature (EGT = T_5) measurement?

We have several options for analyzing the engine mass flow. If we have a trustworthy compressor map, then we can iterate the program input for mass flow W_2 in such a way that the compressor flow factor f_{W2Rstd} is equal to 1.0. Alternatively, we could believe the model value for turbine flow capacity and iterate W_2 for $f_{W4Rstd} = 1$. A further option is to believe the nozzle discharge coefficient of the model and the nozzle throat area.

We can also derive the engine mass flow from the exhaust gas temperature (EGT) signal. In our baseline analysis technique, the calculated T_5 was a by-product which we did not scrutinize. If we did, then we most probably would find a discrepancy between the model and the indicated EGT value. There are many possible reasons for this temperature difference, one of them could be a mass flow measurement error.

How can we find the mass flow from EGT? Let us consider the engine as a black box and apply the first law of thermodynamics. Just for now, we neglect any heat exchange with the surroundings, and any power offtake, bleed air and leakages. There are two energy flows into this box, engine mass flow W_2 with total enthalpy $H_2 = h(T_2)$ and the energy of the fuel $W_F \times FHV$. The only energy output is the exhaust gas flow $W_8 = W_2 + W_F$ which has the total enthalpy $H_8 = h(T_8) = h(T_5)$. For the energy balance in Eq. 5.1-3, the enthalpies must be expressed relative to the temperature for which the lower heating value of the fuel is valid, usually 25 °C

$$W_2H_2 + W_F FHV = (W_2 + W_F)H_8 \quad (5.1-3)$$

There is only one value of W_2 which fulfills the energy balance with the known values of fuel flow, fuel heating value FHV and exhaust gas temperature $T_8 = T_5$.

What can we do if the T_3 sensor fails? We can assume that the compressor efficiency is on target (or 2% below target) and iterate the program input for T_3 in such a way that the AnSyn factor for efficiency is 1.0 (or 0.98).

What if the P_5 signal is missing? We iterate the program input for P_5 in such a way that the nozzle area AnSyn factor f_{A8} is 1.0. The model-based test analysis is a very flexible tool, missing or failed sensor readings are no problem.

It is advantageous to work with a pre-defined list of sensors. When all the postulated sensor readings are available, the standard off-design matching scheme does not need to be modified. For convenience, the program can opt to switch between several methods for calculating the mass flow: W_2 as measured, from turbine flow capacity or from EGT.

The normal off-design matching scheme needs to be amended when one or more values from the list of sensors are not available. It requires engineering judgement to decide how to deal with the missing measurements and failed sensors. The model-based analysis is still feasible, even if only a few sensor readings are available.

5.1.6 AnSyn and Optimization

No measured value is absolutely correct; each measurement has an uncertainty (Table 5.1-2). The sensor readings and hardware information which we use as input into the performance analysis program are no exception. The uncertainty of an analysis result depends on the methodology which we apply.

In our analysis example, the air mass flow depends on the way we calculate it. We can calculate W_2 from total and static pressures measured in the bellmouth, we can derive it from a known turbine flow capacity or determine it from a heat balance based on the measured exhaust gas temperature EGT, for example. Whenever we select one of these three analysis methods, we will create inconsistencies with respect to two quantities. If we believe the turbine flow capacity analysis, then our mass flow result will differ from that based on the bellmouth pressures and the model EGT deviates from the measured EGT.

How can we reconcile the three mass flow values which we get from the three different paths through the analysis program? One solution is to calculate the weighted sum Σ_{dev} of the deviations between measurement and model and use this as a figure of merit in a numerical optimization which searches for a compromise W_2 value:

$$\Sigma_{dev} = f_B|W_2 - W_{2m}|^n + f_T \left| \frac{W_4\sqrt{T_4}}{P_4} - \left(\frac{W_4\sqrt{T_4}}{P_4} \right)_m \right|^n + f_{EGT}|T_5 - T_{5m}|^n \quad (5.1-4)$$

Table 5.1-2 Typical measurement uncertainty

	Uncertainty
Pressures	$\pm 0.5\%$
Total temperature	± 1.5 K
Spool speed	$\pm 0.1\%$
Air mass flow	$\pm 0.5\%$
Fuel mass flow	$\pm 0.5\%$
Fuel heating value	$\pm 0.5\%$
Thrust	$\pm 1\%$
Shaft power	$\pm 1\%$
Variable Geometry	$\pm 0.1\text{--}0.5\%$

The weighting factors f_B , f_T and f_{EGT} reflect the confidence we have in the bellmouth-derived mass flow, the turbine flow capacity and in the EGT measurement.

Numerical optimization yields the most likely mass flow if we have a perfect model and only random noise in our data. All differences between model and measurement will be small. However, what W_2 will we get if one of the three measurements, for example turbine flow capacity, is plainly wrong? The optimization algorithm will search for the minimum in the weighted sum Σ_{dev} . The solution will not be composed of two small deviations (bellmouth and EGT) and one big deviation in turbine flow capacity. All three elements of the minimized weighted sum Σ_{dev} will be much bigger than in case of correct measurements and an accurate model. The measurement error in turbine flow capacity is distributed over all engine components and blurs the root cause of the problem.

The solution is three analyses—each of which employs only one of the three alternative measurements. This will result in two similar mass flow values and one outlier and the diagnosis of the problem becomes easy.

5.1.7 Application of the AnSyn Factors

5.1.7.1 ISA Correction

Correcting the results from a gas turbine test to ISA Standard Day conditions makes the results comparable with those from other engines or with acceptance test criteria. The basic question to be answered is: What would the engine performance be if the test had been at Standard Day conditions? This question applies not only to measurements taken on a sea level test bed where the local altitude and the weather conditions dictate the conditions of the incoming air but also to experiments in an altitude test facility (ATF) if, due to facility limitations, the conditions at the engine face or the back pressure are not as desired.

The correction of the measured performance to ISA Standard Day conditions is very easy after a model-based test analysis. The AnSyn factors found become part of the model. Running the model calibrated in this way at the same corrected spool speed as measured and at the ISA engine inlet conditions produces the ISA corrected performance.

The model-based performance correction tries to keep all engine internal Mach numbers exactly the same as they were during the test. However, this theoretical aim is not exactly achievable because many small effects prevent precise Mach number similarity between the test and the ISA corrected performance. Among the nuisance factors are, for example, gearbox drag, fuel, oil and hydraulic pump power, changes in gas properties and Reynolds number effects.

5.1.7.2 EGT Margin

Commercial engines are “flat rated” up to a certain ambient air temperature, the “flat rating” or “kink point” temperature. This temperature is usually expressed as relative to the International Standard Atmosphere temperature: ISA + 15 °C, for example. The engine controller makes sure that thrust is constant on days with temperatures lower than the flat rating value and keeps turbine inlet temperature constant on hotter days. The EGT margin is the temperature difference between the red line temperature (the certified maximal admissible temperature) and the exhaust gas temperature one would measure on the considered engine during a sea level Take Off on a day with flat rating ambient temperature.

The calculation of the EGT margin is easy: Just run the model with the AnSyn factors applied at sea level ISA + 15 °C ambient temperature and the Take Off engine rating parameter (scheduled engine pressure ratio EPR respectively N_L). Compare the model output for EGT with the certified redline EGT; $\text{EGT}_{\text{redline}} - \text{EGT}$ is the EGT margin. This margin describes the quality of the tested engine in a manner like specific fuel consumption being a measure of thermal efficiency.

5.1.7.3 Rated Power

The *Rated Power* of engines used in commercial aviation is the power that the engine delivers at ambient temperatures up to the flat rated temperature for an officially declared rating like Take Off or Max Continuous. Max Dry and Max Reheat are equivalent terms from the military world. However, the thrust management of fighter engines differs from that of transport aircraft; there is no flat rating. The control parameter defining power (an engine pressure ratio, spool speed, exhaust gas temperature etc.) is frequently scheduled as a function of engine inlet temperature T, altitude and flight Mach number. Rated power of military engines is usually quoted for an ISA day.

It may happen that the control system prevents the scheduled corrected spool speed of the ISA day from being reached. This is quite normal if the test is done while the ambient temperature is higher than the ISA temperature and a turbine temperature limit is encountered. Deriving the rated performance from such a test on an ISA day is very simple and straightforward. The model, calibrated using the measured data in step one of the analysis procedure is run with ISA day inlet and exhaust conditions at rated power—this yields the rated performance.

Of course, all details that differ from the nominal values during the test for some reason, like bleed air and power offtake, can be taken into account. Even the effect of intended hardware modifications can be considered. There is a smooth transition between performance analysis and performance prediction which cannot be achieved with the old-fashioned way of analyzing gas turbine test data.

5.2 AnSyn During Engine Development

Understanding how a newly designed engine behaves is one of the major aims of a development test run. The analyzed performance needs to be compared with the component and the overall engine development targets. Component designers tend to look only at the performance of their piece of engineering art. Their interpretation of the measured data at the entry and exit of their component is often biased. Then, not too surprisingly, a performance model built from component specialists' analysis results happens to predict a much better SFC than the tested engine!

Performance engineers have the task of reconciling all the component performance analysis results with the overall engine performance as determined by the measured thrust and specific fuel consumption. If the engine has a performance deficit, which component is to blame? To answer this question, we need extensive and accurate pressure and temperature measurements at various thermodynamic stations.

Downstream of a compressor or a turbine, both radial and circumferential profiles of both pressure and temperature exist. Measuring a representative value at a thermodynamic station requires many sensors. Figure 5.2-1 shows the arrangement of 20 pressure pickups on four rakes placed in a low bypass ratio turbofan, downstream of the low pressure turbine. The indicated hub and tip pressures on all four rakes are lower than average. The total pressure in the boundary layers along the annulus walls are not captured.

Why do we need more than one rake? The flow field should be uniform circumferentially—but it is not! Downstream of the turbine rotor we can see the total pressure wakes of the turbine nozzle guide vane, see Fig. 5.2-2. The sensors on the rake will indicate a mean pressure lower than the station average when placed in such a wake. Consider the expected pressure distribution when deciding on the circumferential position of the rakes.

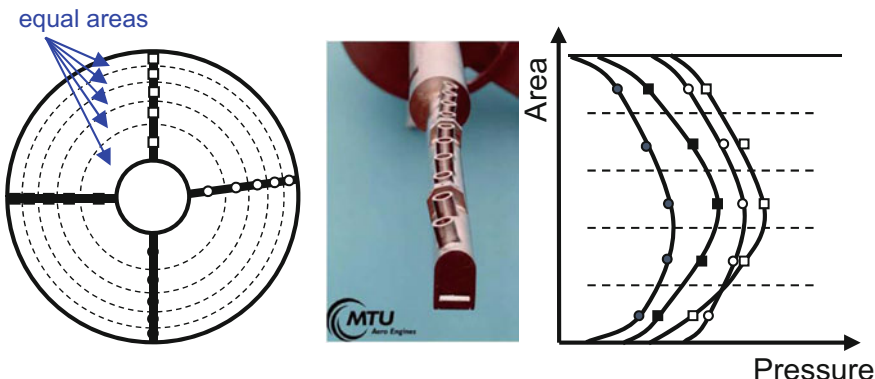


Fig. 5.2-1 Pressure measurement with rakes

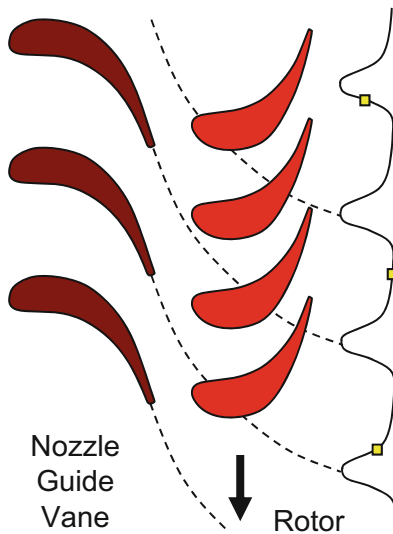


Fig. 5.2-2 Total pressure distribution downstream of a turbine

5.2.1 Sensor Checking

Sensor readings from rakes should be checked in a three-step process. First perform a *Range Check*, and look for numbers which are obviously incorrect. This can be a single reading on a compressor exit rake which indicates ambient pressure because the pressure pipe from the engine to the load cell is broken. Thus, we detect the false reading A marked in Fig. 5.2-3. Next is the *Coarse Filter* check: Calculate the mean value of all remaining 19 readings (ignoring reading A) and look for values outside the coarse filter tolerance band. From this we detect the suspicious reading B. The *Fine Filter*—the third step of the rake checking process—is based on the mean of all sensor readings from the same radius. We detect the reading C as being too high for whatever reason and exclude it from the further analysis. Finally, we replace the three false readings with the mean value on the respective radius.

The interpretation of static pressures measured on a casing can be difficult if the wall pressure is not uniform, as in case of Fig. 5.2-4. To get a representative value, we need several pickups for cross-checking and averaging the individual values.

The performance analysis of development engine tests is based on hundreds of carefully-checked temperature and pressure measurements. One would expect all the numbers to make up a consistent picture of what happens in the engine. However, it remains difficult to assign performance problems to individual engine components. The model-based performance analysis is the only way to reconcile seemingly contradictory measurements.

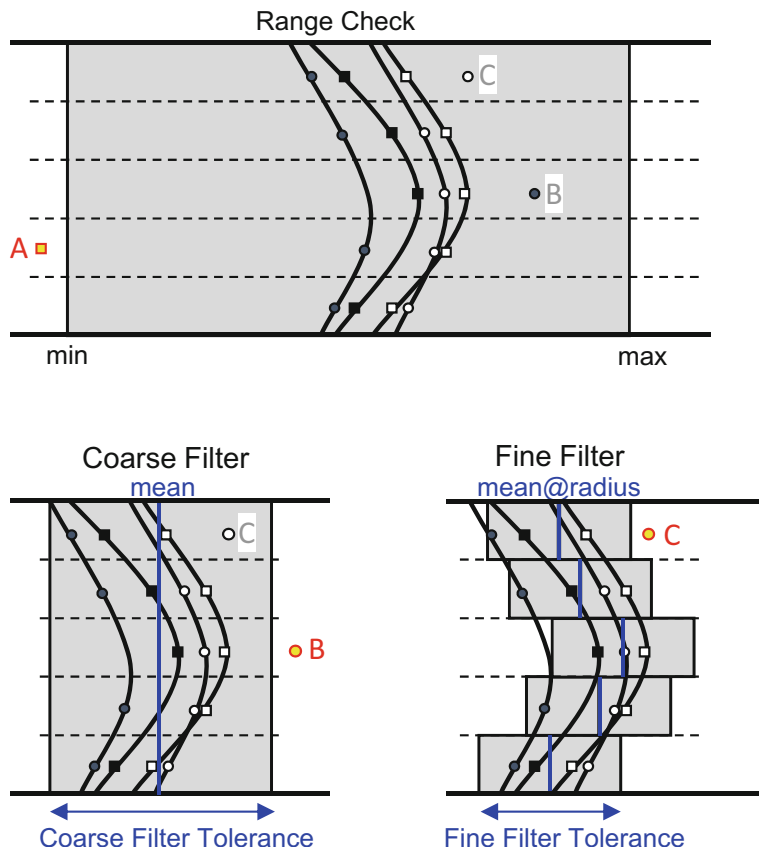


Fig. 5.2-3 Range check, coarse and fine filter

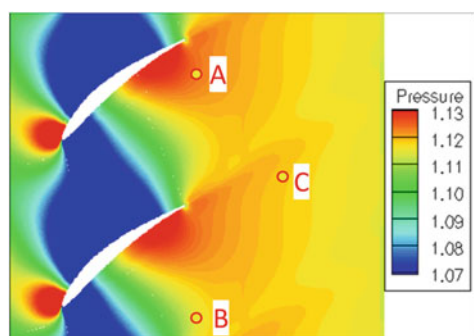


Fig. 5.2-4 Static pressure distribution on a casing

5.2.2 Test Analysis

Figure 5.2-5 shows the main performance instrumentation used in EJ200 development engines. The blue pressures and temperatures were measured with rakes, the other properties with at least two single probes each. If the measurements in the secondary air system are included, there were up to 500 signals available for the performance analysis.

Total temperature and pressure have been measured at all the main thermodynamic stations except burner exit (station 4), low pressure turbine inlet (station 45) and in the nozzle (station 8). Additionally, there were data available for the high pressure turbine rotor blade temperature TBT (measured with an optical pyrometer) and the static pressures P_{s6} , P_{s16} , P_{s7} and P_{s9} .

In such a situation, several alternatives for determining the bypass ratio exist. We can use knowledge about the high pressure turbine flow capacity or employ the measured core exit temperature T_6 in a heat balance. Core compressor and low pressure turbine flow capacity are other options. Each core flow analysis method yields a slightly different bypass ratio and different turbine entry temperature. It is the task of the performance team to reconcile the different analyses. For that purpose, we must use all knowledge from component rig tests, secondary air system analysis and measurement uncertainty considerations.

5.2.3 Model Improvement Potential

We need the performance model for many purposes. One of the most important applications of the model is quantifying the improvement potential through hardware modifications. The quality of the model becomes evident whenever a positive

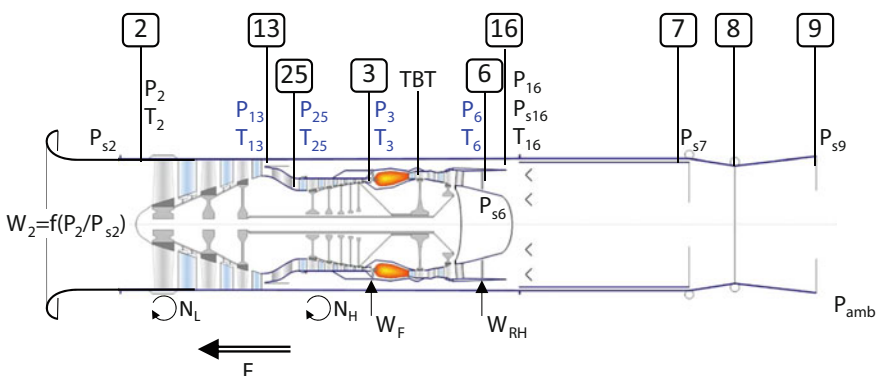


Fig. 5.2-5 Instrumentation for a development engine

effect of a hardware modification is predicted and then checked with a test. Was the modification a success?

If not, what could be the reason? Was the effect so small that it became invisible? Was it a true back-to-back test or were there other engine modifications (possibly initiated by people from non-performance disciplines) which counteracted the modification? Was the performance prediction over-optimistic?

Precise performance predictions require a physics-based model. Wishful thinking is not helpful; again and again improving the model is the right way to go, especially if a prediction did not lead to success. Plotting AnSyn factors for selected quantities can help to detect effects which are not modeled correctly. Take, for example, the data shown in Fig. 5.2-6 from an EJ200 turbofan test in the ATF (altitude test facility). Numerous HPC Efficiency AnSyn factors from three test series are plotted as a function of relative corrected speed. There are clear trends in the SLS and the 36,000 ft/0.7 data; the model HPC under-predicts efficiency slightly at low corrected speed and over-predicts it at high corrected speed.

Is it possible that the compressor behaves differently in the engine than during a rig test? There are many imaginable reasons for that. First, even in a so-called engine parts rig, there are frequently differences between the numbers and positions of the temperature and pressure probes. Second, the component environment is different in the engine than in the rig environment. In the engine the temperature of the compressor case is influenced by the bypass air temperature, while on the

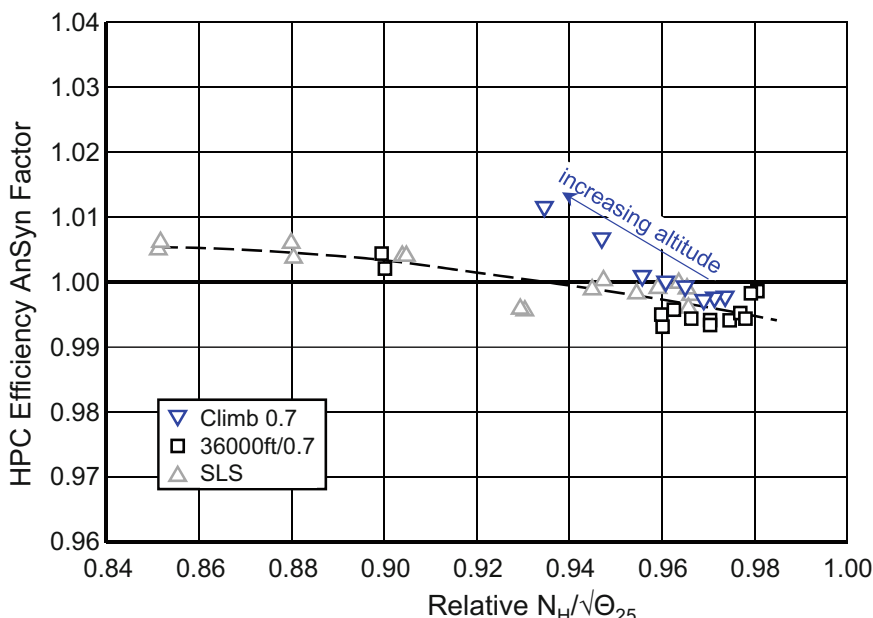


Fig. 5.2-6 HPC efficiency AnSyn factors for three flight conditions

compressor rig there is no such effect. Therefore, at the same spool speed, tip clearances will be different in the engine and the rig test.

We can use the test result shown in Fig. 5.2-6 to improve the compressor map in the model. Scale all map efficiency numbers down by 0.5% at $N_H/\sqrt{\Theta_{25}} = 0.85$, make no change at $N_H/\sqrt{\Theta_{25}} = 0.93$ and increase the values by 0.5% at $N_H/\sqrt{\Theta_{25}} = 0.98$. Using the map modified in this way for analyzing the same test data would make the HPC Efficiency factor scatter around 1.00.

We have not yet discussed the blue downwards-pointing triangles in Fig. 5.2-6. They are the results from a vertical climb simulation at flight Mach number 0.7. Turbine inlet temperature was constant during the test. The climb begins at 36,000 ft, the altitude above which ambient temperature remains constant. The only engine inlet parameter which changes during this climb simulation is the total pressure P_2 , and it gets smaller and smaller with increasing altitude. In terms of flow physics: the Reynolds number decreases during this test.

Lowering pressure and Reynolds number weakens the cycle and therefore lowers the corrected HPC spool speed with increasing altitude. The blue triangles at the two highest altitudes are well above the other test data. That means that the Reynolds number correction for HPC efficiency—which is part of the model—is too severe. At the lowest Reynolds number, the model predicts an efficiency loss which is 1% too big, and this is compensated by an AnSyn factor that is 1% above unity. We can easily improve the performance model by adapting the Reynolds number correction for the HPC efficiency.

There are many more opportunities for scrutinizing the AnSyn factors: Do they show remarkable trends when plotted against a physically meaningful parameter? When looking for corrections to compressor maps, plot corrected speed, corrected mass flow or pressure ratio on the x-axis. Reynolds number effects become visible when plotted against the Reynolds number index at the entry of the component.

Isolate the effect of centrifugal forces on tip clearance by plotting data at (almost) the same corrected spool speed against the square of true spool speed N^2 . This approach is especially suited when plotting HP turbine efficiency AnSyn factors because the data are usually all in a narrow range of corrected speed $N_H/\sqrt{\Theta_4}$ values.

Centrifugal forces are also responsible for the untwist of fan blades at high rotational speed. How much blade untwist affects fan mass flow depends on engine inlet temperature, i.e. on $N_L/\sqrt{\Theta_2}$.

Plot nozzle area AnSyn factors against nozzle pressure ratio on the x-axis. All the data should collapse on a single line, but maybe there is an effect of flight Mach number that causes an inconsistency?

What else can be wrong with the model? Air leakages, parasitic power, gearbox efficiency and other small details could be the culprit. There is no general answer to whether these details are important in your case or not. If you cannot explain the characteristics of your engine with the laws of physics, then you should live with the remaining scatter in the AnSyn factors. This is better than introducing correlations which have only a statistical justification.

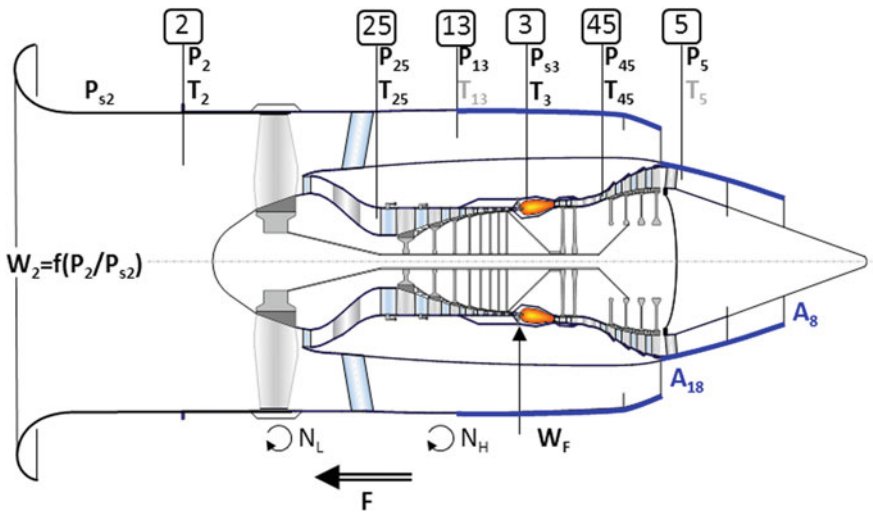


Fig. 5.2-7 Instrumentation in an engine maintenance shop

5.3 AnSyn in Engine Maintenance Shops

After arrival of an engine in the maintenance shop comes the question of which components need repair. This may be obvious, but it is not always. An inbound test run with the aim of determining the most cost-effective work scope is sometimes meaningful.

During installation in the testbed, the bare engine is fitted with a bellmouth and a calibrated exhaust system, which can contain special instrumentation. The bleed ports are sealed, and the external power offtake is zero. Figure 5.2-7 shows typical instrumentation on a high bypass turbofan engine. In most places we have only one or two sensors, with only engine pressure ratio and exhaust gas temperature based on many individual measuring points. The quality of the measurements is poorer than in development engines. Sensor cross-checking is difficult or impossible because only a few pickups are available. Missing measurements are quite common.

We cannot determine absolute values of component flow capacities and efficiencies because the instrumentation is not sufficiently accurate for that. However, we can compare the results with data from other engines or with those from the model of a nominal engine. The AnSyn factors are ideally suited for that purpose.

A major problem for performance diagnosis in a maintenance shop is that not only do the compressors and turbines deteriorate during service due to fouling, erosion, increased tip clearance, foreign object damage FOD etc. but the sensors also degrade over time, all of which makes data interpretation difficult. References [1, 2] present excellent overviews about all the problems connected with gas path analysis. Among other analysis methods, they also discuss the model-based performance

analysis described here. The common conclusion is that model-based methods can be of great help in gas turbine performance analysis—but they are not a cure-all.

5.3.1 Baseline Model for Diagnostics

The baseline model should be calibrated with the best data available, preferably those measured during the test cell calibration. All the calibration data should be from the same engine, otherwise there is additional scatter in the numbers due to the engine manufacturing tolerances. The data from only those two operating points which are considered during the typical acceptance test (Take Off and Max Continuous) are not sufficient, we need data for a range of corrected spool speed $N_L/\sqrt{\Theta_2}$. Keep in mind that we need a valid model for test analysis during all seasons of the year, on cold winter and hot summer days. The engine inlet temperature should be lower than the flat rating temperature (typically ISA +15 °C). Additionally, it should be ensured that neither icing of sensors nor inlet condensation has happened during the test.

Section 4.2 describes in detail how to calibrate a CFM56-3 engine model with data from the test cell calibration report. Note that the interpretation of the measurements deviates in some details from the official acceptance test analysis procedure, which does not consider the engine mass flow, for example. For the calibration of the model, all available measurements are employed, including W_2 derived from the static and total pressure measurements in the bellmouth.

Engines arriving at the maintenance shop can be a mixture from fully overhauled modules to modules that have experienced lengthy service with no refurbishment. Special models can be derived from the baseline model which generate the expected performance of a deteriorated engine on the test bed. Also use information from the visual inspection of the engine to create such a model.

5.3.2 Engine Diagnostics

Figure 5.2-7 shows which sensors are usually installed during a test run on a high bypass turbofan. Engine inlet mass flow is known; bypass ratio and hence core mass flow are not. There are two popular options to separate the core and bypass mass flows: The HP turbine flow capacity method and the heat balance based on the exhaust gas temperature EGT.

Both methods should yield the same result. However, this is usually not the case in practice because incorrect assumptions about the secondary air system disturb the flow capacity method and possible changes in the radial and circumferential temperature distributions due to burner degradation (one or more blocked fuel nozzles) jeopardize the heat balance method. Anyway, decide on one method and keep the other in mind.

We can calculate all pressure ratios and efficiencies from the pressures and temperatures measured around the compressors if the engine has no booster, like in the example of Fig. 5.2-7. In a turbofan engine with a booster, there are generally no sensors that allow fan core and booster performance to be separated. The model provides us with surrogates for the missing sensor values.

We can calculate the full set of compressor AnSyn factors from the measured pressure and temperature values and the corrected compressor mass flows which are a result of the core flow analysis. The compressor calculations also calculate the power to be delivered by the turbines, whose pressure ratios are determined by the P_{45} and P_5 measurements. That is all we need for the calculation of the AnSyn factors for the turbine flow capacity and efficiency.

A few problems may arise when we apply this approach. An accurate measurement of the temperature rise in the fan in a high bypass engine is difficult because it is so small (Fig. 5.3-1). Measurement inaccuracies show up in the power balance between fan and low pressure turbine (LPT). T_{13} measurement uncertainty can be of the same order of magnitude as the effects that are expected to be observed. It is better not to use such a measurement when calculating the fan AnSyn factors because it would distort the values of the other AnSyn factors, especially those for the LPT efficiency.

The efficiency of the outer fan is not expected to change much during service. Erosion, increased tip clearance due to severe rotor tip rubbing and fouling are detectable by visual inspection. If none of that has happened, then assume that fan efficiency is equal to the model efficiency and iterate the “measured value” T_{13m} in such a way that the AnSyn factor for fan outer efficiency becomes unity.

Theoretically, we can base the heat balance on the temperature measurement downstream of the LPT. But this is not a good idea if the number of individual

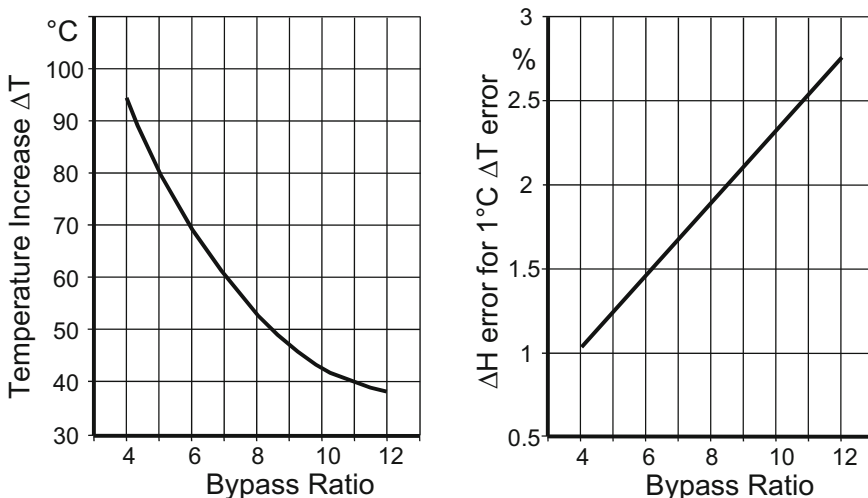


Fig. 5.3-1 Effect of T_{13} uncertainty on fan work uncertainty

temperature pickups in station 5 is much less than that used for determining EGT. Do not expect much from T_5 data if there are only one or two sensors. In such a case, expect deviations between the measured and the simulated T_5 since the local temperature can deviate from the station average significantly.

The thick blue lines in Fig. 5.2-7 indicate hardware dedicated to test bed use only. The geometrical bypass and core nozzle throat areas are known precisely. We can use this information to cross-check the measured total pressures P_{13} and P_5 . If one of these appears to be inaccurate, the corresponding model value could replace it.

Analysis by Synthesis can be done with the test data of the day; there is no absolute necessity to correct the data to ISA conditions first. The essential result of the model-based analysis are the differences between the model and the measurements which are described by the AnSyn factors. However, ISA corrected data for thrust and specific fuel consumption are always of interest for comparisons between engines. Communication with all the stake holders is simpler when you present corrected data.

5.4 AnSyn for Engine Performance Monitoring

We can also apply model-based analysis to performance monitoring while the engine is installed on the aircraft. Such an analysis is less accurate than for a test run in the engine maintenance shop since two important measurements are missing: thrust and total engine mass flow. Additional uncertainties are less accurate on-board fuel flow measurements and variation in the fuel heating value. The latter is measured at the maintenance shop, but it can vary from airport to airport where the aircraft is refueled. During flight, power and bleed air offtake for aircraft purposes are not exactly known; both offtakes are definitely zero during the shop test.

Humidity in the air does not play a role at cruise, but too much humidity can cause condensation shocks during take off. Water vapor condensation invalidates the performance analysis because it affects engine inlet temperature T_2 by an unpredictable amount (see Sect. 3.2.1.2).

5.4.1 Baseline Model for Monitoring

Use the same performance model as during test analysis in the testbed of the maintenance shop. If you know the differences between the nozzle throat areas of the shop and the flight hardware, then adjust the flight engine model accordingly. For performance monitoring from snapshots, during both take off and cruise, use the same baseline model with slightly different input data. Insert your best guesses for power and bleed offtake. Make sure that active clearance control is deactivated in the Take Off simulation.

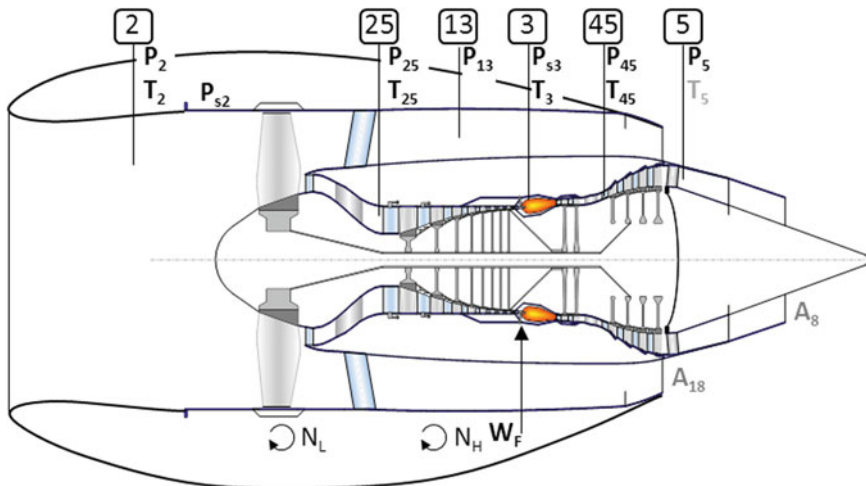


Fig. 5.4-1 Instrumentation on an installed engine

For performance analysis, run the model with the observed fan corrected speed $N_L/\sqrt{\Theta_2}$. Assume that the model accurately predicts fan mass flow. Apart from that, apply one of the analysis methods described above for use in the engine maintenance shop. The available in-flight measurement suite (Fig. 5.4-1) dictates what is best.

The AnSyn factors from a take off analysis are not fully consistent with those from a cruise analysis for several reasons. During take off, some engine parts are not yet stabilized thermally, especially the last compressor disks and the turbine disks. This increases tip clearance—which has a negative effect on efficiency—in comparison with the carefully controlled testbed run with thermally stabilized engine hardware. During cruise we have a thermally stabilized engine, but our model is less accurate because it contains Reynolds corrections of doubtful accuracy. Moreover, the mass flow—speed correlation from the sea level testbed might not be exactly the same during take off and cruise, due to a shift of the operating line in the fan map. All model inaccuracies manifest themselves in changed AnSyn factors.

5.4.2 Trend Monitoring

The result of a model-based test analysis is a set of AnSyn factors for component efficiencies and flow capacities. The absolute numbers are not of interest; we merely observe how these factors change with time. We want to see if engine malfunction or mechanical damage causes any sudden changes. Data trending and filtering methods are helpful for differentiating between random noise in the data and true events.

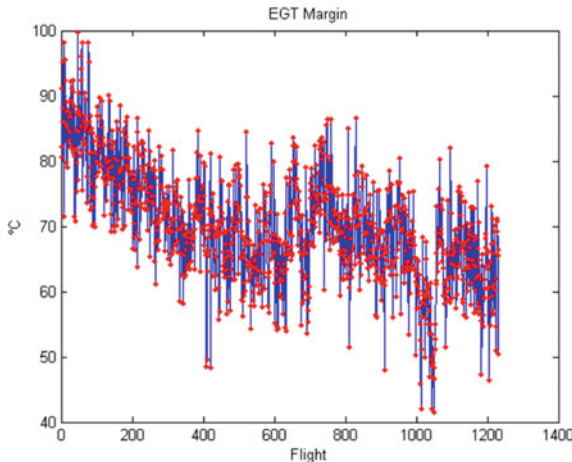


Fig. 5.4-2 Exhaust gas temperature margin for an example engine [7]

The model represents a new engine; the engine to be monitored deteriorates over time. Would it make sense to adapt the model to the observed engine automatically? Updating the model during monitoring would be beneficial if it was highly non-linear. Fortunately, that is not the case. The magnitude of the AnSyn factors would change, the message hidden in them would not.

The AnSyn factors describe the degradation of the components during service but they do not reflect the overall performance status of a deteriorated engine. The loss of thermal efficiency can be expressed as a decrease in the EGT margin—the temperature difference between the red line temperature (the certified maximal admissible temperature) and the EGT required for achieving the rated thrust with that engine during a sea level Take Off on an ISA + 15 °C day. Figure 5.4-2 shows not only the EGT margin decrease in service but also the scatter to be expected. The margin usually decreases steadily, but water washing the engine—decided by the airline—restores a part of the lost margin from time to time.

From such scattered data, it is a challenge to isolate the contribution of each component to the loss in the EGT margin. Regardless of the difficulties—let us do our very best.

5.5 Interpretation of the AnSyn Factors

Interpretation of the AnSyn factors is easy when the model is perfect; the sensors indicate correct values and there is no random noise in the data to disturb the analysis process. We get the exact diagnosis when we analyze “measured” data created by the performance prediction synthesis program.

It is always worthwhile to do some preliminary checks of your model. Try the following: introduce a modifier of -2% for turbine efficiency into your model, run it and note all the pressures and temperatures needed as input for the model-based analysis. Next, remove the modifier from the model, enter the numbers you have just recorded as measured data, and run the program in test analysis mode. The result must show that all the AnSyn factors are unity, except the factor for turbine efficiency which must be 1.02. If that is not the case, then either there is a bug in the code or you have made a typing error while entering the data.

5.5.1 Component Degradation

The main aim of model-based engine test analysis is the diagnosis of the compressor and turbine performance relative to a baseline. How does component degradation manifest itself in the AnSyn factors? What happens typically to an engine during service?

Compressor performance is affected by dirt aggregation (fouling), corrosion, erosion, changes of the airfoil shape due to repair, deteriorating surface quality and tip clearance increase. All these influences lead to a simultaneous loss of similar magnitude in efficiency and corrected flow. Compressors with variable guide vanes (VGV) may suffer from control problems which are relatively easy to detect. Deviations of the VGV position from the baseline schedule will show up in the compressor flow capacity AnSyn factor, but not in the efficiency factor.

Reference [8] shows real data for compressor efficiency AnSyn factors from two CFM56-5C turbofans. The maintenance shop operator interprets Fig. 5.5-1 as follows:

The sample engine shows a typical deterioration behavior for CFM56-5C engines operated in benign environment. A comparably steep initial deterioration is followed by a relatively long operation period with low average deterioration rates. The initial deterioration is primarily caused by seal and tip-clearance effects, whereas the slowly progressing deterioration in the mid area is driven by erosive effects (mainly deterioration of leading edge contour of forward stages). Finally, the deterioration increases in the last phase due to wear effects on the variable stator vane bushings. This behavior is hardly visible in the data since the intention is to avoid severe deterioration of the VSV system, by performing an on-wing or onsite VSV bushing replacement before reaching a critical deterioration level.

Overlaid on this pattern are yearly fluctuations, which show lower efficiency values during winter and higher efficiency during summer. Since the data is cruise data, and the engines operate in a long-haul fleet on routes from Europe to various destinations in the world, the observed efficiency variations are not entirely caused by actual changes in ambient conditions. Variations of the physical HP spool-speed for example result in variations in the actual tip and seal clearances, and thus in the measured efficiency. In addition, secondary effects occur, such as increased fouling during the winter due to the use of de-icing liquids. The deterioration caused by fouling is typically recovered after core engine washes.

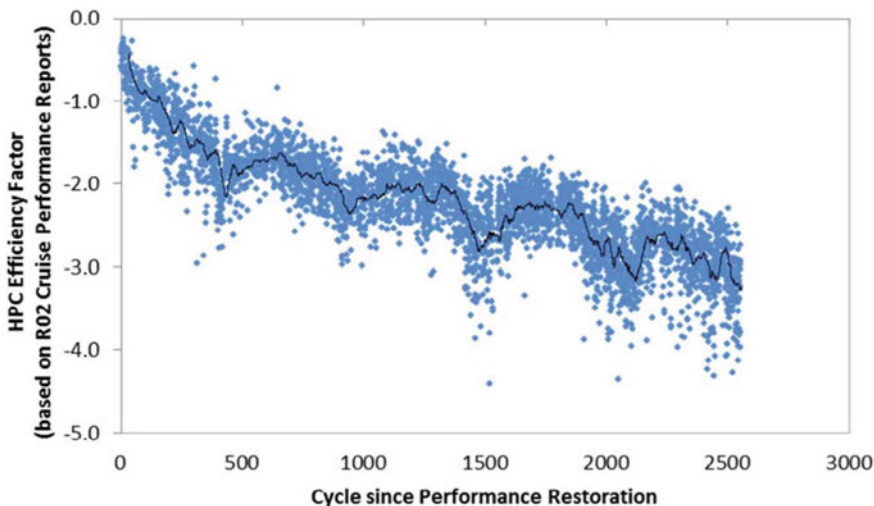


Fig. 5.5-1 Figure 18 from Ref. [8]

In Fig. 5.5-2, the HPC efficiency factor of engine E before and after the partial HPC refurbishment is shown. The partial performance recovery through the applied repair is clearly visible. In addition, the initial deterioration after such repair is comparably low, since most of the seal and tip-clearances were not refurbished. The shift in the data between approximately 300 and 1000 cycles was caused by the customer bleed system of the aircraft. The root cause was an imbalance between the two engines on one wing, which feed one air-conditioning pack. A higher bleed offtake results in a drop in indicated HPC performance.

Turbine efficiency deteriorates mainly due to corrosion, erosion and tip clearance increase. Airfoil shape changes have an influence on turbine flow capacity: Vane trailing edge bowing and erosion increase flow capacity. Turbine capacity decreases when deposits accumulate on the airfoil surface. With turbines—in contrast to compressors—there is no generally valid connection between efficiency and flow capacity changes. Existing experience may indicate what happens in your special case.

Check the efficiency AnSyn factors of the individual compressors and turbines against the overall compression and expansion efficiency ratios $\eta_{\text{measured}}/\eta_{\text{model}}$! We can calculate these efficiency ratios more accurately than the component AnSyn factors because the measurements between compressors and turbines are often of doubtful quality. The overall efficiency ratios also help to detect problems with sensors in intermediate ducts: Any efficiency factor decrease in the downstream component combined with an efficiency factor increase in the upstream component, while the overall efficiency ratio is constant, is a hint to a measurement problem.

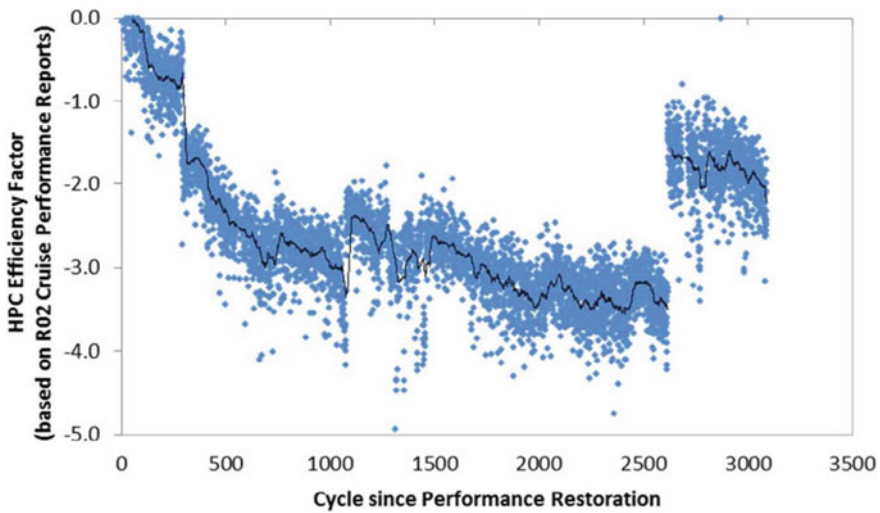


Fig. 5.5-2 Figure 19 from Ref. [8]

5.5.2 *Model Faults*

The baseline model contains elements for which no AnSyn factor exists. Among them are the numbers which describe the secondary air system. We have a model fault if we do not recognize that a seal has deteriorated and leaks more than is assumed in the baseline model. Engine defects like Active Clearance Control (ACC) malfunctioning, unexpectedly leaking thrust reverser doors and bleed valve leakages are also not part of the baseline model. The analysis based on an incorrect model yields misleading values for the AnSyn factors.

Examine how model faults manifest themselves in how AnSyn factors deviate from unity. For that purpose, use as “measured” data the numbers produced by the baseline model. Running the model-based test analysis with these data yields no deviation from the model. Next modify one of the model elements, for example the amount of bleed air or the amount of cooling air bypassing the high pressure turbine. As a consequence, some of the AnSyn factors will deviate from unity. The magnitude of the deviations is a sort of fingerprint of the model fault. Build a library of such fingerprints; they may be of help for the interpretation of the AnSyn factors from true engine tests.

5.5.3 *Sensor Faults*

Not only do AnSyn factors show how components degrade over time, their values also reflect ageing of the sensors. For slowly drifting AnSyn factors, it is difficult to

distinguish one from the other. Detecting a sudden sensor failure is much easier. We limit our thoughts to large defects of a single sensor; failure of two sensors at the same time is very unlikely.

Use the model to learn how sensor errors manifest themselves in the AnSyn factors. The model gives you exact answers, no random noise in the “measured” data disturbs the picture. To begin your studies, run the baseline model in performance prediction mode and note all the parameters which are input quantities for the test analysis. Then switch to test analysis mode and enter the predicted numbers as measured data. The result must be that all AnSyn factors are unity, otherwise something is wrong with your software or your input data.

Now you are ready to study the effect of sensor errors. Only disturb one input for the sensor reading at a time and document how much the AnSyn factors change. You will get three answers from this exercise:

1. How sensitive is the result of the analysis to errors in the various sensor readings?
2. Which of the AnSyn factors are affected by the error?
3. What is the influence of the selected core flow analysis method?

Table 5.5-1 summarizes the effects of single sensor errors on the Take Off analysis result for the CFM56-3 turbofan. The model details and its calibration are described in Sect. 4.2. Most sensor errors affect only those two or three of the AnSyn factors shown in the table. Note that the selection of the core flow analysis method also influences the analysis result. Inappropriate core flow analysis methods produce changes in many AnSyn factors as consequence of a single sensor error.

We can detect single sensor errors easily, provided that we use an appropriate core flow analysis method. Then only two or three AnSyn factors indicate deviations from the model. A compressor exit temperature sensor fault of +5 K is a good example. The excessive T_3 leads to exaggerated compressor work in the analysis by synthesis process. We calculate the compressor AnSyn efficiency factor as 0.987 and hence get a compressor efficiency deficit of 1.3%. At the same time, we see an AnSyn factor for turbine efficiency of 1.01 (an efficiency increase of 1%) because the turbine work is exaggerated by the same amount as the compressor work.

In the bar chart of Fig. 5.5-3 we see the characteristic pattern—a “fingerprint”—of a T_3 sensor error. Other sensor errors go along with different—but equally typical—AnSyn factor fingerprints. Comparing observed AnSyn factor patterns with the model-derived fingerprints can hint at a sensor problem. Create your library of AnSyn factor “fingerprints” and use them in the examination of curious AnSyn results.

Table 5.5-1 Effects of single sensor errors on the AnSyn factors
(Example: CFM56-3 Take Off rating)

Sensor error	Affected AnSyn factors			Core flow analysis method
T ₂ + 1 K	Fan η 1.024	LPT η 0.982	T ₅ -4.9 K	Clear result, except for T ₅ heat balance
P ₂ - 1%	Fan η 1.023	Fan W 1.012		Clear result for all methods
T ₁₃ + 1 K	Fan η 0.980	LPT η 1.015	T ₅ +4.3 K	Clear result, except for T ₅ Heat balance and A ₁₈ method
P ₁₃ - 1%	Fan η 0.976	Fan W 0.993	A ₁₈ 1.013	Clear result, except for A ₁₈ method which yields totally unreasonable factors for the core components
T ₂₄ + 2 K	Booster η 0.976	HPC η 1.01	HPC W 1.008	All methods yield similar results, HPT η factor is analyzed as 0.995
P ₂₄ - 1%	Booster η 0.987	HPC W 1.01	HPC η 1.006	All methods yield the same result
T ₃ + 5 K	HPC η 0.987	HPT η 1.01		All methods yield the same result
P ₃ - 1%	HPT W 1.011	HPT η 1.006	HPC η 0.995	Clear result, except for HP turbine capacity method which yields many deviations for the core stream
P ₄₄ - 1%	LPT W 1.01	LPT η 1.007	HPT η 0.995	Clear result, except for LP turbine capacity method which yields many deviations for the core stream
T ₄₅ + 10 K				Affects only T ₄₅ heat balance which yields many deviations for the core stream
P ₅ - 1%	A ₈ 1.016	LPT η 0.993		Clear result, except for A ₈ method which yields many deviations for the core stream
T ₅ + 10 K				Affects only T ₅ heat balance which yields many deviations for the core stream
W ₂ - 1%	A ₁₈ 0.987	LPT η 0.991	Fan W 0.995	Similar result for all methods, except for A ₁₈ which yields totally unreasonable factors for the core components
W _F - 1% or FHV - 1%				Result depends on core flow analysis method. Similar results only for the heat balance methods. All core component flow factors are ≈0.984...0.99, efficiency factors ≈0.999
N _L - 1%	Fan W 1.013	Booster W 1.013		Clear result for all methods
N _H - 1%	HPC W 1.013			Clear result for all methods

Fan Flow Factor	0.9998		
Fan Outer Efficiency Factor	0.9999		
Fan Inner Efficiency Factor	1		
Booster Flow Factor	1		
Booster Efficiency Factor	0.9997		
HPC Flow Factor	1		
HPC Efficiency Factor	0.9872		█
HP Turbine Flow Factor	1.002		█
HP Turbine Efficiency Factor	1.011		
LP Turbine Flow Factor	0.9999		
LP Turbine Efficiency Factor	1		
Core Nozzle Area Factor	1		
Bypass Nozzle Area Factor	1		
Gross Thrust Factor	1		
T45 measured - T45 calculated K	0.15		
T5 measured - T5 calculated K	0.19		

Core Flow Analysis Method:
Core Nozzle Area A8

Fig. 5.5-3 Effect of a T_3 sensor error of 5 K

5.5.4 Measurement Errors

We created the correctly measured data used in the previous section by running the engine model. Using these input data for the analysis by synthesis yields exactly 1.0 for all AnSyn factors. We simulated the sensor errors by disturbing just one of the measured values. Of course, this scenario is hardly realistic because true measured data always show some scatter. How do measurement errors affect the result of the model-based analysis? (Fig. 5.5-4).

Let us first explain what a measurement error is. It is composed of a random error and a systematic error. The random error is caused by numerous effects in the measurement system that are outside the direct control of the user. Figure 5.2-6 shows that repeated scans from the very same engine test run lead to very similar HPC efficiency AnSyn factors. In this case, the random error is equivalent to the repeatability of the model-based test analysis.

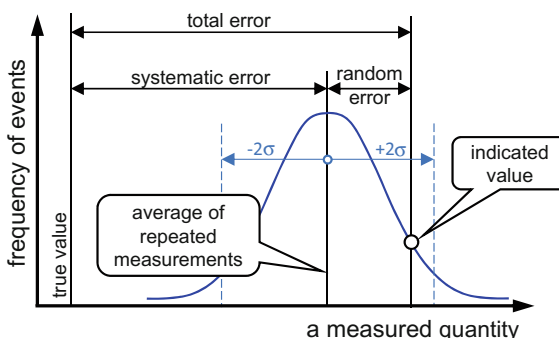


Fig. 5.5-4 Elements of a measurement error

What about the systematic error? Questions about absolute performance are rare. Usually, comparisons are made with previous results. People are interested in why specific fuel consumption (SFC) has gone up by 1.5% or why EGT has risen by 10 °C. Therefore, we limit the object of our test analysis to performance comparisons; systematic errors in our analysis cancel out and become irrelevant.

We can find out how random errors affect the results of the model-based analysis with a Monte Carlo study. For this exercise, we commence with the same data as in the previous section. We repeat the analysis many times with slightly perturbed sensor readings. The average of the sensor readings is the correct value; the random errors follow a Gaussian distribution. This means that 95.4% of all sensor values are within $\pm 2\sigma$ of the correct value (Table 5.5-2).

The results of a Monte Carlo study are standard deviations for the AnSyn factors and the T_{45} respectively T_5 temperature differences. As an example, Fig. 5.5-5 shows the statistical distribution of the HPC Efficiency (AnSyn) Factor after a simulation of 2500 engine performance analyses.

Some of the AnSyn factor standard deviations depend on the core flow analysis method, others not, as indicated in Table 5.5-3. Six methods have been examined: in addition to the already mentioned turbine flow capacity and heat balance methods we have also derived the core flow from the two nozzle areas A_8 and A_{18} . The fan and LPT efficiency results are most affected by the random scatter in the measured data. The reason for that is the scatter in fan work which originates from the scatter in T_2 and T_{13} .

Under the circumstances, it is obviously impossible to diagnose the fan efficiency accurately. A visual inspection of the fan is more meaningful than the model-based test analysis. If the fan blades look good (clean, without signs of erosion or FOD) and the tip clearance is as it should be, then the efficiency will be as that of a new fan. In the analysis it is better to ignore the measured T_{13} and replace it with the value which leads to a fan efficiency AnSyn factor of unity. Now we get a much-reduced scatter for the LPT efficiency factors, as in Table 5.5-4.

Table 5.5-2 2σ of the random sensor errors

T_2 (K)	0.2	T_{45} (K)	1.5
P_2 (%)	0.1	P_5 (%)	0.5
T_{13} (K)	0.6	T_5 (K)	1.5
P_{13} (%)	0.15	W_2 (%)	0.5
T_{24} (K)	1	W_F (%)	0.2
P_{24} (%)	0.15	FHV (%)	0.1
T_3 (K)	1	NL (%)	0.1
P_3 (%)	0.3	NH (%)	0.1
P_{44} (%)	0.5	Humid (%)	30

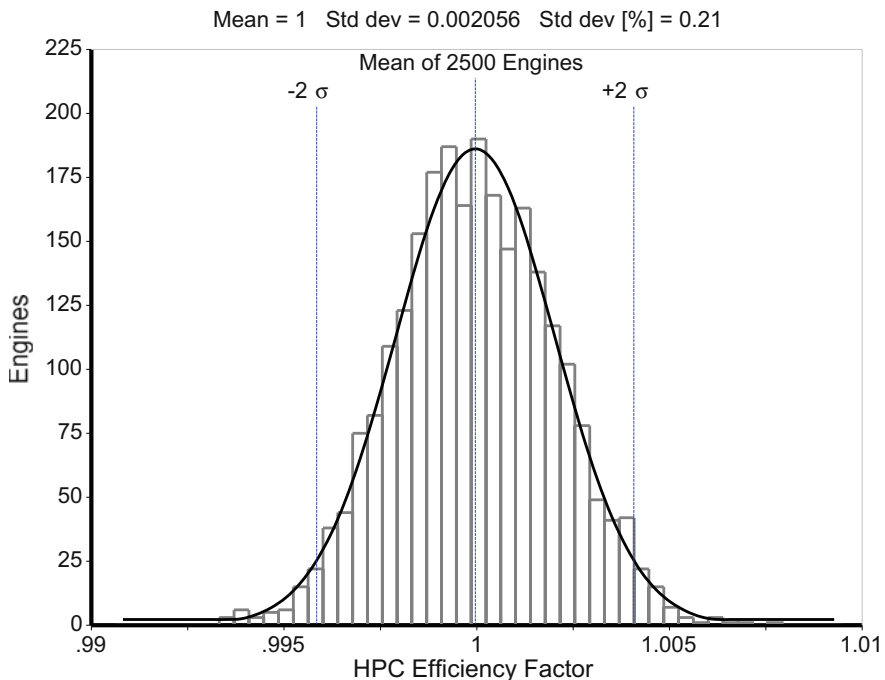


Fig. 5.5-5 Monte Carlo result

Table 5.5-3 2σ of the AnSyn factors, all sensors considered

AnSyn factors and Δ temperatures	Core flow analysis method					
	HPT Flow	LPT Flow	T_{45}	T_5	A_8	A_{18}
Fan η	1.24	1.22	1.22	1.22	1.22	1.24
Fan flow	0.24	0.24	0.24	0.24	0.24	0.24
Booster η	0.7	0.7	0.68	0.7	0.72	0.7
Booster flow	0.3	0.44	0.22	0.42	0.62	0.7
HPC η	0.42	0.4	0.42	0.42	0.42	0.4
HPC flow	0.5	0.74	0.42	0.7	1.04	1.12
HPT η	0.42	0.7	0.38	0.48	0.68	0.74
HPT flow	0	0.68	0.46	0.76	0.94	0.98
LPT η	1.02	1.1	1.04	1.18	0.92	0.96
LPT flow	0.54	0	0.56	0.72	0.86	0.86
T_{45} (K)	3.4	5.2	0	4.2	7.4	8.2
T_5 (K)	3.8	4.8	2.8	0	6.4	7.2
A_8	0.78	0.86	0.82	1.02	0	1.02
A_{18}	0.24	0.28	0.26	0.34	0.3	0
Thrust	0.18	0.18	0.18	0.18	0.2	0.2

Table 5.5-4 2σ of the AnSyn factors if T_{13} is ignored

AnSyn factors and Δ temperatures	Core flow analysis method					
	HPT flow	LPT flow	T_{45}	T_5	A_8	T_{18}
Fan η	0	0	0	0	0	0
Fan flow	0.24	0.24	0.24	0.24	0.24	0.24
Booster η	0.7	0.68	0.68	0.7	0.7	0.7
Booster flow	0.28	0.44	0.22	0.28	0.6	0.6
HPC η	0.42	0.4	0.42	0.42	0.42	0.42
HPC flow	0.5	0.72	0.44	0.5	0.99	0.98
HPT η	0.4	0.7	0.38	0.42	0.68	0.68
HPT flow	0	0.68	0.46	0.58	0.46	0.41
LPT η	0.58	0.68	0.6	0.66	0.48	0.66
LPT flow	0.54	0	0.56	0.64	0.84	0.76
T_{45} (K)	3.5	5.4	0	2.8	7.4	7.2
T_5 (K)	3.2	4.2	2	0	5.5	5
A_8	0.78	0.86	0.8	0.86	0	0.94
A_{18}	0.2	0.24	0.22	0.24	0.28	0
Thrust	0.18	0.18	0.18	0.18	0.2	0.2

5.6 Concluding Remarks

Superficially, the model based test analysis process looks easy; in practice, the process is corrupted by the errors in the measurements and unknown hardware differences between the actual engine and the engine used for calibrating the model.

When we apply the model based analysis process to the individual scans used for model calibration, we get an idea about the minimum scatter—the random error—in the AnSyn factors. Using the same model for the analysis of data from other engines of the same build standard will show bigger scatter because of additional random effects which originate from manufacturing tolerances or the engine usage history.

Even more random effects exist when the data are from an engine which was tested in the maintenance shop testbed prior to repair. There might be unknown hardware differences which are not considered in the model like worn seals, blocked fuel nozzles, degraded sensor performance etc.

Performance analysis results determined in an engine maintenance shop are more accurate than those from an engine installed on an aircraft. This is because calibrated hardware is used in the test cell and the engine is thermally stable when the scan is taken. Nozzle areas are known, power-offtake and bleed for aircraft purposes do not exist.

On-wing engine performance monitoring is based on a smaller number of measurements than those available in the maintenance shop test cell. Neither thrust nor mass flow are among the data available on-wing; there the power-offtake and

bleed air used for aircraft purposes are only estimated values. When recording a Take Off snap shot the engine is not thermally stable and a condensation shock may exist in the inlet. Cruise scan analysis suffers from Reynolds number corrections of dubious quality if the model has been calibrated with sea level test cell data only.

Every piece of information about the engine and the sensors should be used for the interpretation of any performance test analysis result. Visual inspection of the hardware can give valuable hints. Do “what if...?” studies and generate ‘signatures’ for potential errors, examine how a modification of the model affects the AnSyn factors. Does the assumption of a worn seal result in a more plausible result? Could it be that the active clearance control valve did not operate as it should? Was the handling bleed valve fully closed at rated power or was there some leakage?

Model-based test analysis is a powerful tool, but it cannot explain every ostensible performance difference automatically.

5.7 References

1. Doel, D.L.: Interpretation of weighted-least-squares gas path analysis results. ASME GT-2002-30025 (2002)
2. Volponi, A.J.: Gas turbine engine health management—past, present and future trends. ASME GT2013-96026
3. Bauer, M., Staudacher, S.: Fully automated model based performance procedure for online and offline applications. GT2006-91050
4. Canalias, X., Köpf, F., Sahm, P.: Generation of physically based analysis factors to improve synthesis models of jet engines. ASME GT2005-68617
5. Walsh, P.P., Fletcher, P.: Gas Turbine Performance, 2nd edn. Blackwell Science Ltd., (2004)
6. AGARD Working Group 19. Recommended Practices for Measurement of Gas Path Pressures and Temperatures for Performance Assessment of Aircraft Turbine Engines and Components. AGARD-AR-245 (1990)
7. Lacaille, J., Gouby, A., Piol, O.: Wear prognostic on turbofan engines. In: Annual Conference of the Prognostics and Health Management Society (2013)
8. Kraft, J., Kuntzagk, S.: Engine fleet management—The use of digital twins from a MRO perspective. ASME GT2017-63336 (2017)

Chapter 6

Inlet Flow Distortion



For optimum operation as well as ease of design, engine operators and designers prefer a uniform flow field at the face of the fan or first compressor. However, varying distributions of total pressure, total temperature and velocity are encountered quite frequently in practice and are referred to as “distortion”. In service, circumferential and radial variations in pressure are common, especially in aircraft engines and circumferential velocity components can complicate the inlet flow field.

The main problem with inlet flow distortion in aircraft engines is its adverse effect on the stability of the compression system. As we have already discussed, stable compressor operation even under adverse conditions is essential to the success of any gas turbine engine but, owing to the very nature of its diffusing flow fields, the compressor is most vulnerable to flow field unsteadiness because of its potential to stall or surge. Compressor surge results in a total loss of thrust and is of course a much more dangerous event than a partial loss of thrust due to a reduction of compressor efficiency.

Nevertheless, it is of interest to consider how much thrust and SFC are affected by inlet flow distortion. There are two fundamentally different reasons for a change in engine performance in this context. The first is due to the direct impact of flow distortion on component efficiencies and hence the thermodynamic cycle while the second is due to actions of the control system.

So how do we model the effects of inlet flow distortion? One method is via the parallel compressor theory, which describes the effect of inlet pressure or temperature distortion on both stability and performance. In its simplest form, it consists of two compressors working in parallel. The maps of these two compressors differ only in corrected mass flow. Both maps are mass flow-scaled versions of the same map which is employed for the standard performance simulation, when no inlet flow distortion exists. We can integrate this approach into the performance program and develop a tool that simulates not only the effects of distortion in a first compressor but also the transfer of the distortion to subsequent compressors. This enhanced performance program delivers fundamentally correct answers since even

the most complex flow structures still obey the simple laws of mass and energy conservation—and that is what the overall system simulation is all about.

If we compare two operating conditions (with clean and distorted inlet flow respectively) at the same average inlet total pressure P_2 and the same corrected spool speed $N/\sqrt{\Theta_2}$, inlet pressure distortion has only a minor impact on the thermodynamic cycle. The parallel compressor theory yields operating points in two maps, one in the map of the clean sector and one in the map of the spoiled sector. The compressor is assumed to surge when the surge margin in the map of the spoiled sector becomes zero—this answers the question about being able to simulate compressor stability.

So why is the effect of distortion on engine performance small? To address this, let us consider the operating points in the compressor maps. The efficiency values in the two sectors cannot be very different because both operating points are on the same corrected speed line. The mass-averaged efficiency with distorted inlet flow is only slightly lower than that with clean inlet flow. The consequences of this small efficiency loss are equally small changes in the thermodynamic cycle. There can be neither a significant thrust loss nor SFC increase due to inlet pressure distortion if nothing changes other than the distortion level.

However, the control system of the engine can react to the inlet flow distortion in such a way that thrust does change noticeably. This is particularly true if a compressor bleed valve or the exhaust nozzle is opened to counteract possible compressor stability problems. Re-circulation of bleed air to the engine inlet—with the aim of shifting the compressor surge line—affects the performance of the engine adversely because it causes the engine inlet total temperature T_2 to increase.

Performance changes can be large if distortion affects the input signals to the control system. Williams [1] describes the test of a turbojet engine which was controlled by a single turbine temperature sensor. In the test, a screen, which could be rotated, generated a total pressure distortion at the engine face. This pressure distortion manifested itself as a temperature distortion at the inlet to the combustor. (The parallel compressor theory explains why this happens.) In turn, the circumferential temperature variations at combustor inlet resulted in uneven temperature distributions at turbine inlet and exit. The single turbine exit temperature probe employed in the control system kept its indicated value constant, which resulted in significant spool speed changes when the distortion screen was rotated.

6.1 Types of Inlet Flow Distortion

6.1.1 Pressure Distortion

Non-uniform pressure at the engine face can be due to many different reasons. Some of the most common are flow detachment from intake lips at high angles of attack and flow separation from walls of curved inlet ducts. The engine may also be forced to accept unsteady flow conditions such as wakes from stalled wings, ground

vortices, supersonic intake “buzz” and turbulence. We shall concentrate on the steady state type of distortion in order to understand the basic features of the distortion pattern and gain some insight into the mechanism of the compressor’s response.

In the 1960s and earlier Rolls-Royce did much work on flow distortion in the first generation of lift engines, where a VTOL (Vertical Take Off and Landing) application called for the tolerance of extremely high levels of distortion. A high degree of success was achieved in correlating surge margin with intake conditions empirically. Two valuable observations were that

- radial distortion was much less detrimental to the surge line than circumferential distortion
- the critical condition appeared to be related to the lowest area-mean total pressure to be found in any 60° sector at the compressor face.

So how can we describe the complex total pressure pattern of Fig. 6.1-1 with the least possible effort? One approach is to split the circumference into two unequal segments, each with constant—but different—pressures. The low pressure sector represents the “spoiled” or “distorted” part of the flow field, the high pressure sector represents the “clean” part. A plot of the radial average of total pressure over the circumference serves as the basis for setting the two pressure levels indicated by the blue line in Fig. 6.1-2. There are two pressure spikes, the first is restricted to a very small segment, the second extends over a much bigger sector. Small sector pressure spikes do not endanger compressor stability; we can ignore them when evaluating the distorted pressure field.

The pressure distortion coefficient DC_{60} describes the intensity or magnitude of the flow non-uniformity as the pressure difference between the mean total pressure

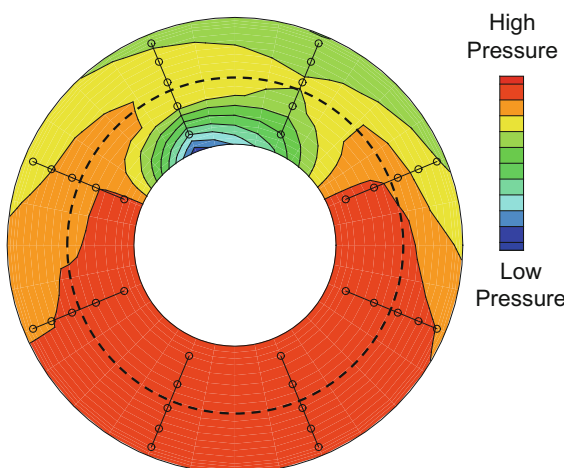


Fig. 6.1-1 Pressure distortion example (Reproduced with permission from Rolls-Royce Deutschland)

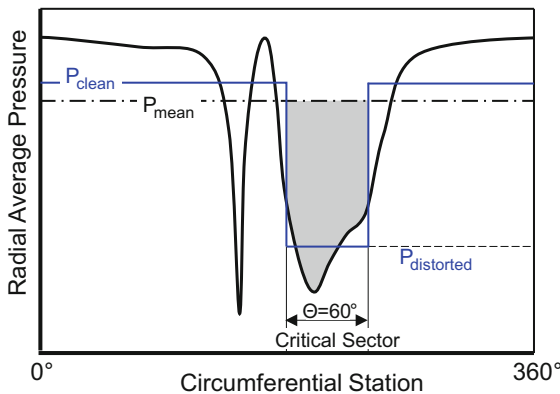


Fig. 6.1-2 Definition of the distortion coefficient DC_{60}

and the average total pressure in the spoiled sector (which we define as 60°), in terms of the dynamic head:

$$DC_{60} = \frac{P_{mean} - P_{60^\circ\text{Sector}}}{\frac{\rho}{2} V_{mean}^2} \quad (6.1-1)$$

Dynamic head is the relevant value in the Aerodynamic Interface Plane AIP, an unobstructed area upstream of the spinner. P_{mean} is the value in the AIP from the general intake pressure recovery model. We simulate the effects of pressure distortion in the AIP with various DC_{60} values using screens like those shown in Fig. 6.1-3.

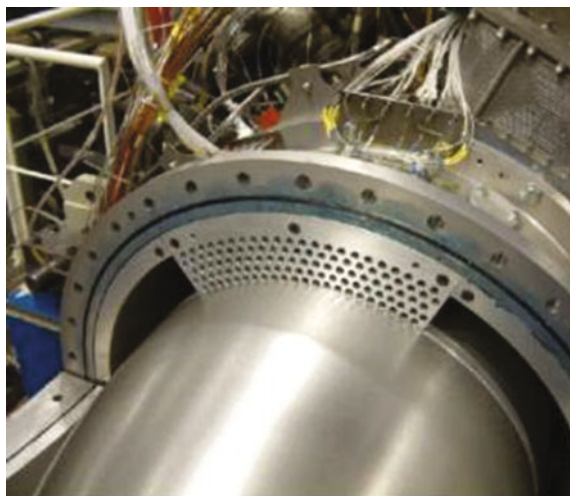


Fig. 6.1-3 Sector distortion screen on a compressor rig (Reproduced with permission from Rolls-Royce Deutschland)

6.1.2 Temperature Distortion

Inlet temperature distortion is relevant for military applications where gun or missile gas ingestion needs to be considered. Carrier-borne airplanes are subject to steam ingestion from the catapult and vertical take-off planes can ingest hot exhaust gases. Commercial aircraft engines may ingest the exhaust gases from other aircraft or, during thrust reverser operation, their own exhaust gases.

We define the temperature distortion coefficient for a sector width of 60° as

$$DT_{60} = \frac{T_{2,60^\circ} - T_2}{T_2} \quad (6.1-2)$$

The total temperature in the spoiled sector $T_{2,60}$ is higher than T_2 , the temperature under normal undistorted circumstances. The average inlet total temperature increases with the temperature distortion level.

6.2 Parallel Compressor Theory

According to the parallel compressor theory the distorted flow field upstream of the compressor consists of two streams with different, but uniform, total pressures. Two imaginary compressors operate in parallel. We describe the performance of these two compressors with mass flow scaled versions of the map used for our standard performance calculations. If the spoiled segment extends over 60° , for example, the flow capacity of the first imaginary compressor is $60^\circ/360^\circ = 1/6$. The second compressor then covers a 300° sector and has $300^\circ/360^\circ = 5/6$ of the real compressor's flow capacity. Both compressors discharge to the same static pressure in the common exhaust duct and this determines how they work in combination and where the operating points are located in the map. The concept is illustrated in Figs. 6.2-1 and 6.2-2.

The compressor with the lower inlet pressure operates with a higher than average pressure ratio and for the other compressor the converse occurs. All high and low operating point pairs (designated as H and L respectively in Fig. 6.2-2) are on the same corrected speed line as the undistorted point M0.

As the distortion increases, the two operating points move away from each other. The stability limit of the total compressor is reached when the local distortion is so high that point L2 encounters the surge line. Consequently, compressor surge is predicted even though the mean operating point M2 is still far from the (clean) surge line.

Figure 6.2-3 shows the circumferential pressure distributions at the inlet and exit of the compressor. Inlet total temperature is the same all around the circumference.

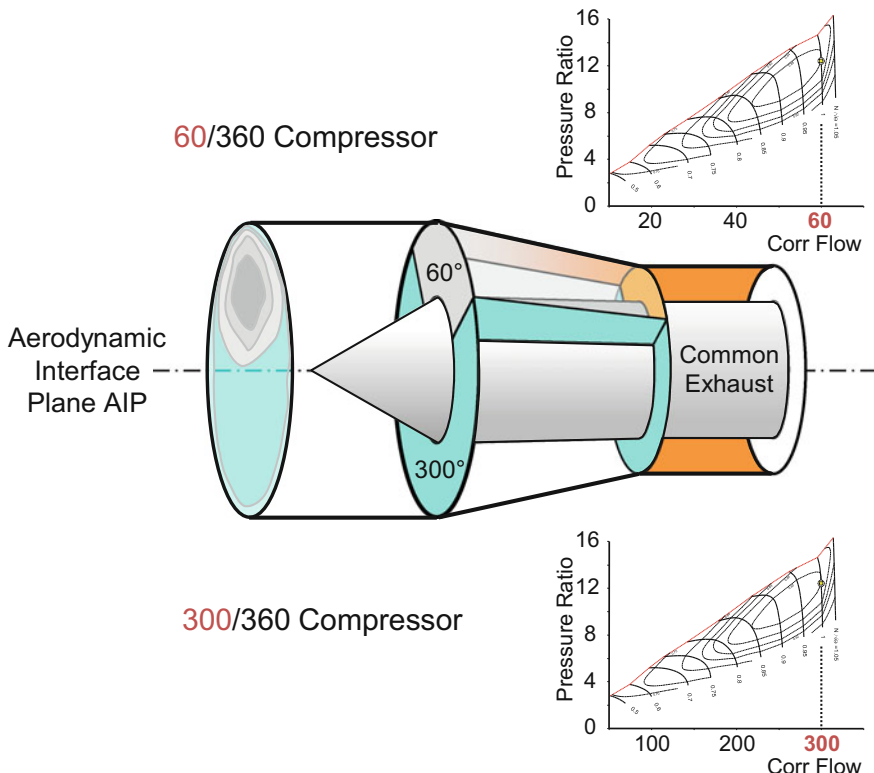


Fig. 6.2-1 Parallel compressor model

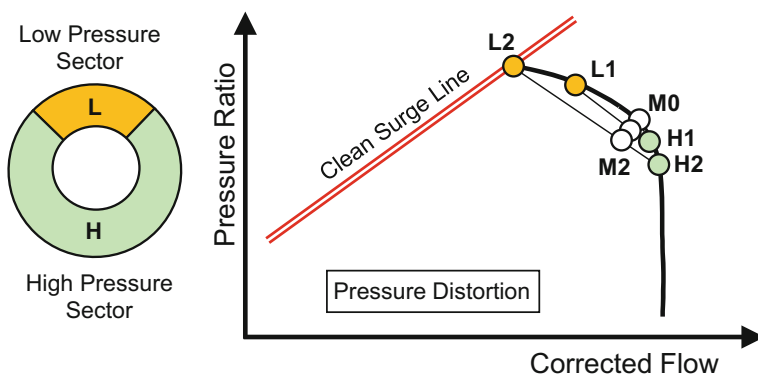


Fig. 6.2-2 Operating points of the clean and the distorted sector in case of pressure distortion

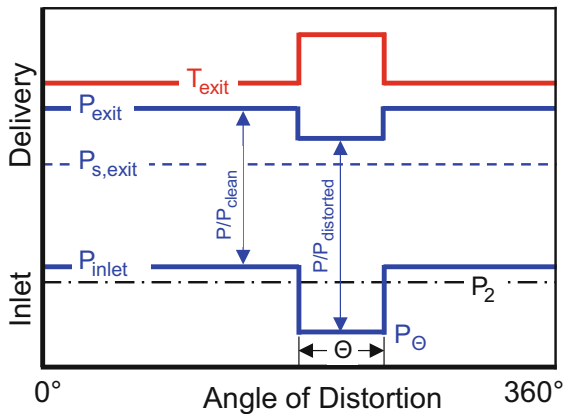


Fig. 6.2-3 Pressure distortion creates temperature distortion

The inlet pressure distortion creates temperature distortion at the compressor exit because the pressure ratios in the clean and distorted sectors are different, temperature and pressure being linked through efficiency.

We can plot the operating points of the distorted and the clean sector, together with the average operating point, on the compressor map in Fig. 6.2-4. There it can also be seen that the distance between the two sector operating points is proportional to total compressor mass flow because DC_{60} relates the total pressure

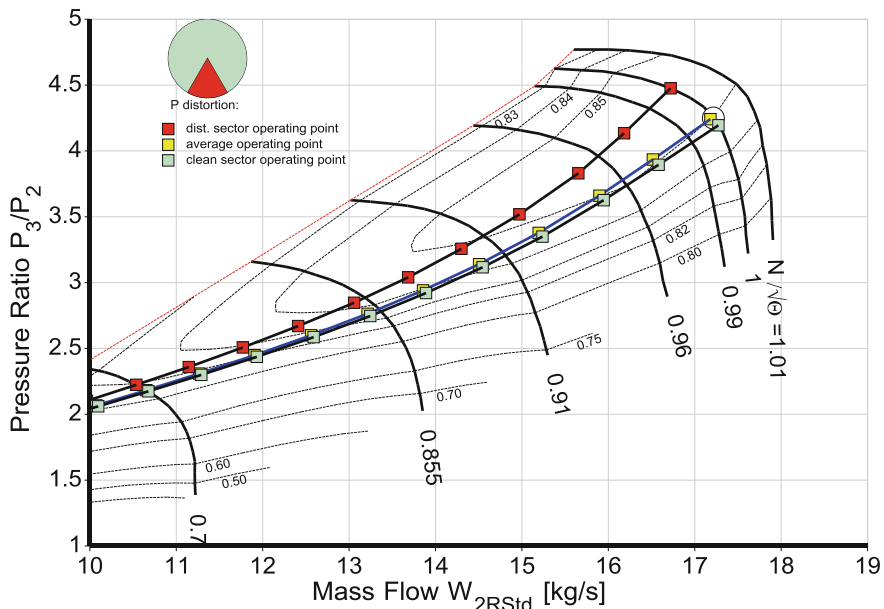


Fig. 6.2-4 Turbojet operating line with distortion (constant DC_{60})

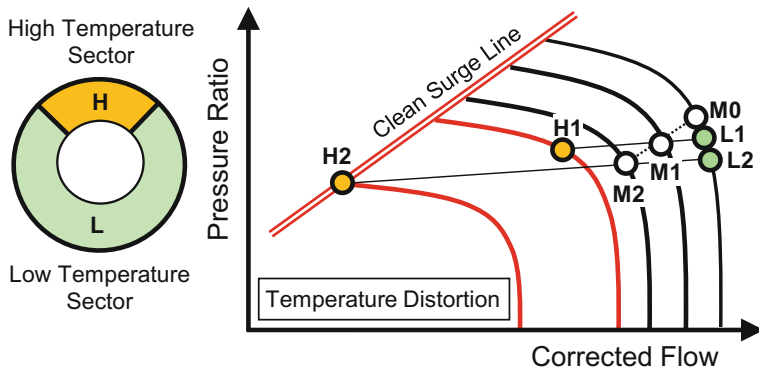


Fig. 6.2-5 Operating points of the clean and the distorted sector in case of temperature distortion

difference between the sectors to the dynamic head in the aerodynamic interface plane AIP for the whole machine.

We can also apply the parallel compressor theory to temperature distortion. In this case, the pressure ratios of the two compressors are equal but the operating points are on different corrected speed lines. This is shown in Fig. 6.2-5. The temperature in sector L remains constant when the temperature distortion increases and the temperature level in sector H rises. The points M0 (no distortion), L1 and L2 are on the same speed line. The compressor is predicted to surge when point H2 approaches the surge line. Note that as the temperature in the distorted sector H is increased, the mean temperature also rises and causes the operating point M2 to shift to a lower corrected speed line than in the case of uniform inlet temperature.

Figure 6.2-6 shows circumferential pressures and temperatures at the inlet and exit of the compressor for a case of inlet temperature distortion only.

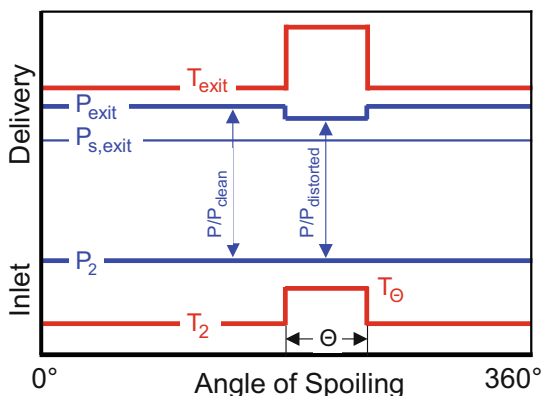


Fig. 6.2-6 Temperature distortion amplifies temperature differences

6.2.1 Theory and Experiment

Does this simple theory produce reasonable results? Let us check with test data presented in a conference many years ago [2]. The experimental set-up consisted of a 6-stage axial compressor with various distortion screens similar to the one shown in Fig. 6.1-3. Table 6.2-1. lists the leading parameters of this compressor, which was designed for a lift engine.

We complement this compressor with dummy models of the burner, turbine and nozzle to make it a complete turbojet engine. The integration of the parallel compressor theory into the turbojet performance program is not difficult: we need only one additional iteration variable—the beta value in the map of the distorted sector. The corresponding additional condition is the static pressure balance downstream of the compressor.

The application of the parallel compressor theory requires the map of the compressor. Unfortunately, the map is not part of the test report of Ref. [2] but that is not a real problem because we can simply take a map from an axial compressor with similar pressure ratio [3] and scale it. Now we are ready to implement the distortion simulations with the parallel compressor model. The task is to simulate the effect of distortion screens with various spoiled-segment angles on compressor stability for two spool speeds 100 and 94%.

We set the pressure upstream of the screen to $P_{\text{clean}} = 101.325 \text{ kPa}$, the ISA value. First we calculate the distortion coefficient for a segment angle Θ and the pressures upstream and downstream of the screen. The pressure ratio over the blocked region of the screen is at 100% spool speed and $P_{\text{dist}}/P_{\text{clean}} = 0.93$. Reference [2] contains no pressure loss number for 94% speed but that is not a problem since we can use our turbojet simulation, along with the standard duct pressure loss model, to calculate it: the pressure difference through the screen $P_{\text{clean}} - P_{\text{dist}}$ is proportional to dynamic head and this leads to a screen pressure ratio of $P_{\text{dist}}/P_{\text{clean}} = 0.943$.

The distortion coefficient DC_Θ changes with the screen segment angle, as indicated in Fig. 6.2-7. It is obvious that distortion intensity is zero when the screen covers the compressor entry completely (segment angle $\Theta = 360^\circ$). Total pressure will then be equal to P_{dist} , which is 93% of P_{clean} . Now we decrease the sector angle from 360° to 180° . The mean pressure is then $P_{m,180} = (P_{\text{clean}} + P_{\text{dist}})/2$ and the pressure loss is cut in half. The distortion coefficient is now greater than zero:

Table 6.2-1 Compressor design parameters

Pressure ratio	4.25
Number of stages	6
Diameter [m]	0.381
Inlet hub/tip radius ratio	0.431
Rotor 1 tip speed $U/\sqrt{\Theta}$ [m/s]	335
Flow per unit frontal area [$\text{kg}/\text{m}^2\text{s}$]	151
Screen pressure ratio @ 100% $N/\sqrt{\Theta N/\Theta}$	0.93

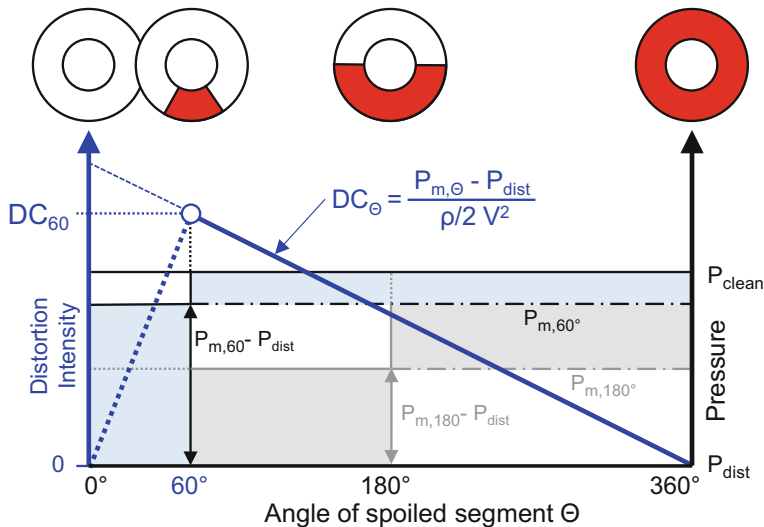


Fig. 6.2-7 Distortion coefficient and sector angle

$$DC_{180} = \frac{P_{m,180} - P_{dist}}{\frac{\rho}{2} V_m^2} = \frac{\frac{(P_{clean} + P_{dist})}{2} - P_{dist}}{\frac{\rho}{2} V_m^2} = \frac{\frac{P_{clean}}{2} - \frac{P_{dist}}{2}}{\frac{\rho}{2} V_m^2} \quad (6.2-1)$$

Further decreases of the sector angle increase the mean pressure and the distortion coefficient in proportion to $\Theta - 360^\circ$. If we know the distortion coefficient for one sector angle, then we know it for any sector angle. For $\Theta = 0$ the correlation yields a distortion coefficient of $DC_0 = 2 * DC_{180}$.

However, $\Theta = 0$ means there is no screen—so there is no distortion! Below a certain segment angle, the distortion coefficient is no longer valid as a definition of distortion intensity. This angle is known as the critical segment angle. Experience has shown that this critical segment angle is approximately 60° and this justifies the use of DC_{60} as a practical measure of distortion intensity.

$$DC_{60} = \frac{P_{m,60} - P_{dist}}{\frac{\rho}{2} V_m^2} = \frac{\frac{300}{360} P_{clean} + \frac{60}{360} P_{dist} - P_{dist}}{\frac{\rho}{2} V_m^2} \quad (6.2-2)$$

So in our example, how big is the distortion coefficient? On an ISA day, the pressure in the clean segment P_{clean} is 101.325 kPa and the pressure in the distorted segment P_{dist} is 94.232 kPa. In the aerodynamic interface plane AIP, the cycle calculation yields the value $q = 9.923$ kPa for the dynamic head. These numbers together result in $DC_{60} = 0.6$. Repeating the DC_{60} calculation with the corresponding numbers from the 94% speed operating point leads to the same outcome.

Figure 6.2-8 shows the reduction in outlet static pressure at surge for the complete range of spoiling angles and two speeds. Reference [2] states: “As the spoiled angle was increased from 0 to 90° , the surge delivery static pressure fell rapidly and stabilized at a constant minimum value from 90° to 360° ”. This is true for the measured data points. The dashed blue lines in Fig. 6.2-8 indicate another, equally justified, interpretation of the data. They highlight the importance of the 60° sector distortion and the relevance of DC_{60} .

Before we can examine the effects of the spoiling segment angle on compressor stability, we must include one more element in our analysis, namely the position of the surge line in the compressor map. We cannot rely on the surge line location that we obtained by scaling the map from Ref. [3]; we need more accurate information. However, the parallel compressor theory also provides us with a solution to this problem: we run the model with a spoiled-segment angle $\Theta = 60^\circ$ and distortion intensity $DC_{60} = 0.6$ for 100 and 94% spool speeds. The pressure ratios in the distorted segment are—according to the parallel compressor theory—two points on the surge line, as shown in Fig. 6.2-9.

Now we can run our model over a range of spoiled-segment angles from 60° to 180° and compare the results with the measurements in Fig. 6.2-10. The simulation yields constant surge delivery static pressures for distortion screens with angles higher than 60° . This general trend agrees with the measurements. The difference in the surge pressures for 94 and 100% spool speeds is predicted almost correctly.

Note that these results are based on the new surge line from the parallel compressor model. The measured data points in Fig. 6.2-10 are on average 2% lower

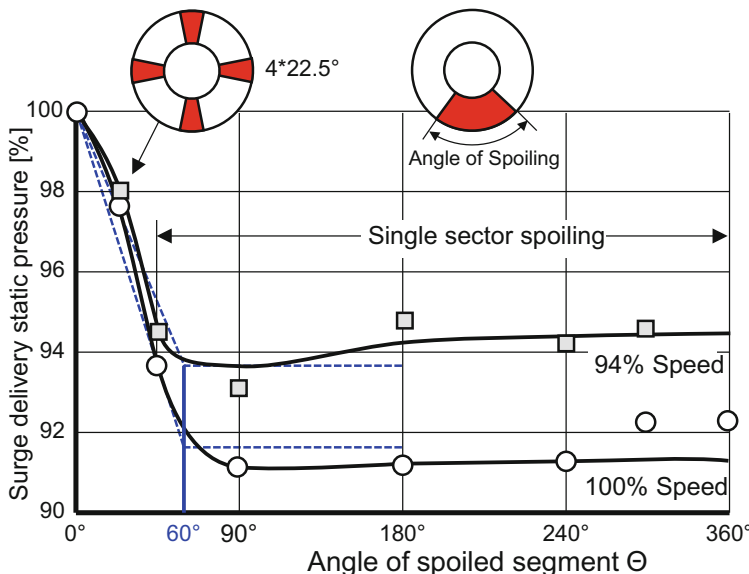


Fig. 6.2-8 Effect of varying circumferential angle of spoiling (adapted from Ref. [2])

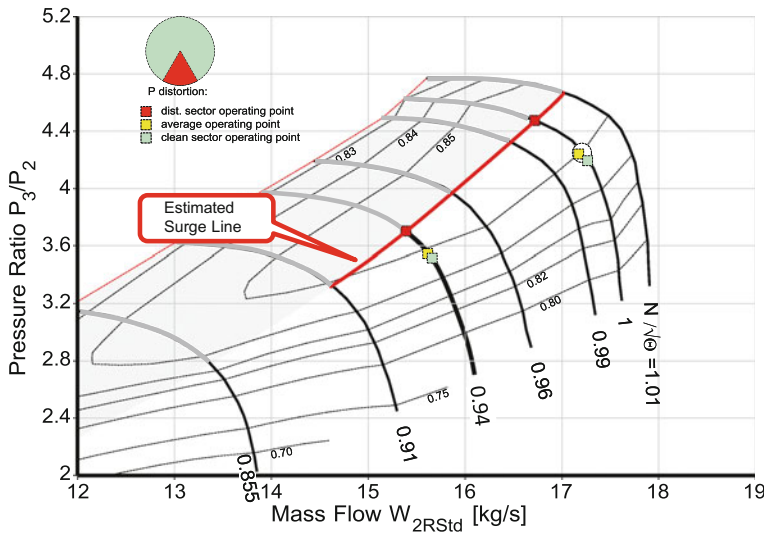


Fig. 6.2-9 Surge line in the scaled map

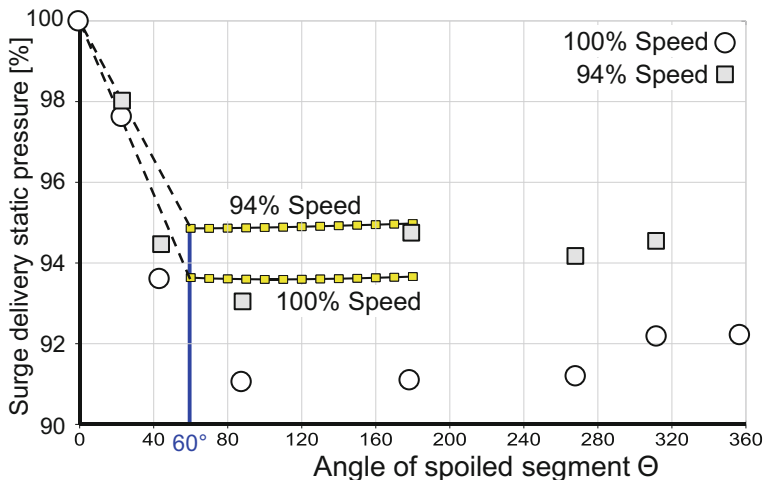


Fig. 6.2-10 Simulation and measurements

than the simulated data. That means the true surge pressure ratio is 2% higher than the calculated surge pressure ratio. Such a small discrepancy between simulation and experiment is not a bad result for such a simple theory!

When integrated into the performance program, the parallel compressor model predicts the impact of flow distortion on both surge margin and performance, although it is acknowledged that the results are only a rough approximation of

reality. The simulation does not predict the distortion-induced mass flow decrease evident from compressor rig tests when the speed line is vertical in the map. However, this shortfall could be remedied by applying an empirical correction factor expressed as a function of the distortion intensity and corrected speed.

6.2.2 Compressor Coupling

The basic parallel compressor theory has been developed for single compressors, but it must be emphasized that care must be taken in its application to multi-spool gas turbine engines or it can lead to serious errors in distortion tolerance estimates and in the diagnosis of the “critical” compressor. Compressors can either be uncoupled with virtually nothing in between or can be connected by short, swan-neck shaped ducts perhaps with many vanes or struts. Even though these parts are crucial to mechanical integrity, they can impact the circumferential static pressure balance quite severely.

Let us examine this situation with the parallel compressor theory applied to a two-spool turbojet example. The design pressure ratios of the LPC and HPC are 4 and 7 respectively. The two compressors are joined by an inter-compressor duct, which causes 2% total pressure loss. The mass flow rate is 100 kg/s at standard day conditions.

Operation with 96% intake pressure recovery and $DC_{60} = 1$ serves as numerical example. In the parallel compressor model, the static pressures at the HPC inlet are assumed to be equal. This implies that there are no struts in the inter-compressor duct to prevent the balance of the static pressures between the two parallel segments. We refer to these compressors as uncoupled. Table 6.2-2 summarizes pressures, temperatures and mass flows for this operating condition.

Table 6.2-2 Two spool turbojet distortion details (uncoupled, $P_2/P_1 = 0.96$, $DC_{60} = 1$)

	P_{inlet} kPa	T_{inlet} K	Corrected flow kg/s	Pressure ratio	Absolute flow kg/s
<i>LPC</i>					
Clean	99.518	288.15	83.453	3.951	81.965
Distorted	86.036	288.15	16.683	4.388	14.166
Average	97.272	288.15	100.136	4.019	96.131
<i>HPC</i>					
Clean	385.118	451.75	26.617	6.944	80.798
Distorted	371.133	457.43	5.274	7.190	15.332
Average	383.057	452.66	31.839	6.979	96.130

However, we can see from the numbers in the last column that some of the air ($81.965 - 80.798 = 1.167 \text{ kg/s}$) must flow from the clean segment of the LPC to the distorted segment of the HPC in the interduct, and this is indicated in Fig. 6.2-11. In reality, there is limited opportunity for this mass transfer between the segments to occur, especially if the inter-compressor duct is short and contains many struts which prevent circumferential balance of the static pressure. No mass flow transfer over the segment borders means that the compressors are referred to as aerodynamically close-coupled.

In the performance program, it is quite simple to switch from the simulation of uncoupled to close-coupled compressors. We replace the numerical condition of “equal static pressures in the interduct” (no coupling) by the condition “no mass flow between sectors” (full coupling).

However, doing that would mean going from one extreme to another. A compromise would be to use a weighted mean between the “equal static pressures” and “no flow between sectors” conditions. Under those circumstances, static pressures in both segments would be matched if the coupling factor CF is zero. This implies that air flows from the clean segment to the distorted segment in the duct. If the coupling factor CF is unity, then no air crosses the segment boundaries in the duct and the static pressures between the segments differ. CF = 0.5 describes a combination half way between the two extremes.

Figure 6.2-12 illustrates the influence of the coupling factor on the stability of a two-spool turbojet. For zero or limited coupling, the surge-critical component is the first compressor (the LPC). For full coupling, the surge margin of the second compressor (the HPC) determines the stability of the combined compression system. The shaded regions of Fig. 6.2-12 tell us when the system is in trouble.

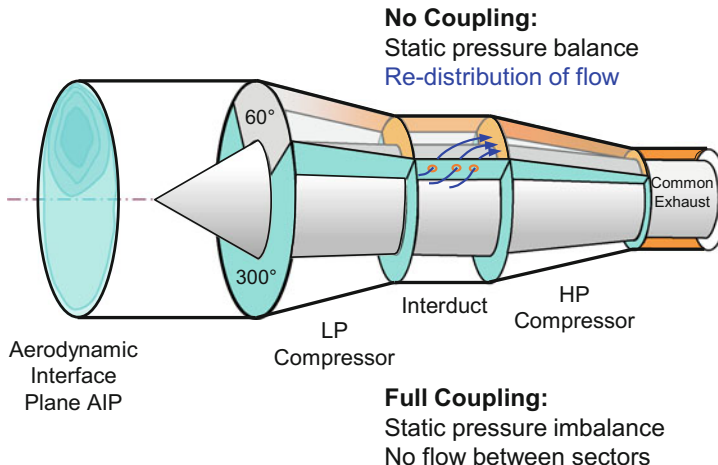


Fig. 6.2-11 Compressor coupling

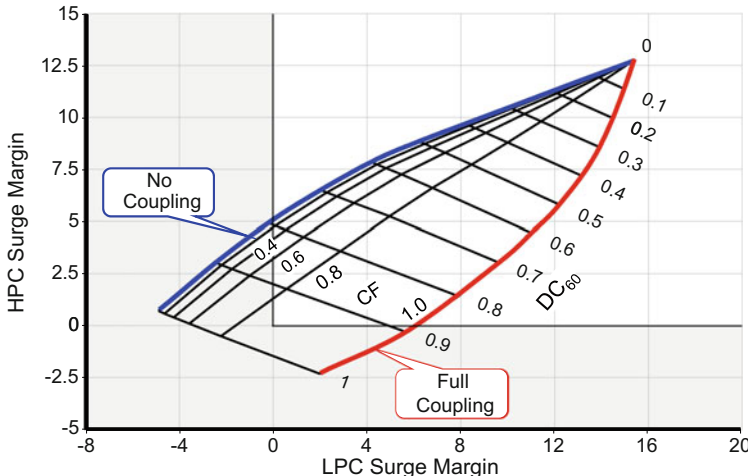


Fig. 6.2-12 Importance of the coupling factor for the compression system stability assessment

6.3 Impact of Distortion on Thermodynamics

Inlet flow distortion affects not only the stability of the compression system but also the performance of the engine. Let us simulate the two-spool turbojet from the previous section with a low-speed spool N_L control. Intake pressure recovery is constant but the distortion intensity increases from $DC_{60} = 0$ to 1. We consider both uncoupled and fully coupled parallel compressors.

The parallel compressor theory creates three spots on the map for each engine operating point: one for the clean segment (light blue), one for the distorted segment (red) and another for the average operating point (yellow). For the LPC in Fig. 6.3-1, the operating points of the two segment compressors are on the same speed line, but the average operating point is not. Engine mass flow decreases and pressure ratio moves upwards on the map as distortion intensity rises; the amount of flow reduction depends on the shape of the speed line.

The efficiency of the average operating point is lower than that for unspoiled inlet flow conditions; how much lower depends on the shape of the efficiency islands on the map and the precise location of the operating points. The changes in LPC efficiency due to inlet flow distortion are very small in any case.

Figure 6.3-2 shows the corresponding operating points on the HPC map. They are on different speed lines because the LPC created some temperature distortion for the HPC from its inlet pressure distortion. Again we see some compressor flow reduction and now it is combined with an efficiency loss of up to one point because the mass-weighted average efficiency is less than that of the average operating point in the map.

There is a distinct shift of the operating point in the distorted compressor segment when we switch from uncoupled to fully coupled compressors. If the

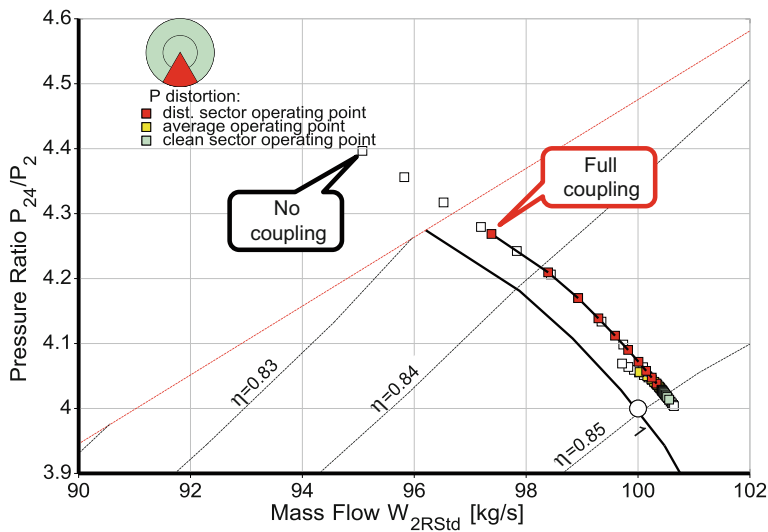


Fig. 6.3-1 LPC operating points with DC₆₀ from 0 to 1, NL control

compressors are uncoupled, then the LPC will surge even though the HPC still has some surge margin left. With fully coupled compressors, it is the other way round.

The parallel compressor theory predicts that only small changes in engine thermodynamics are caused by inlet flow distortion. Thrust and SFC are affected only slightly because the average compressor efficiencies remain nearly constant.

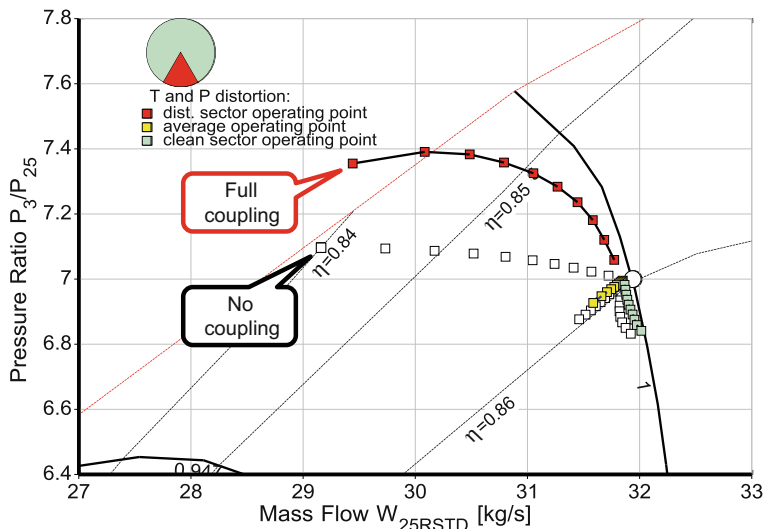


Fig. 6.3-2 HPC operating points with DC₆₀ from 0 to 1, NL control

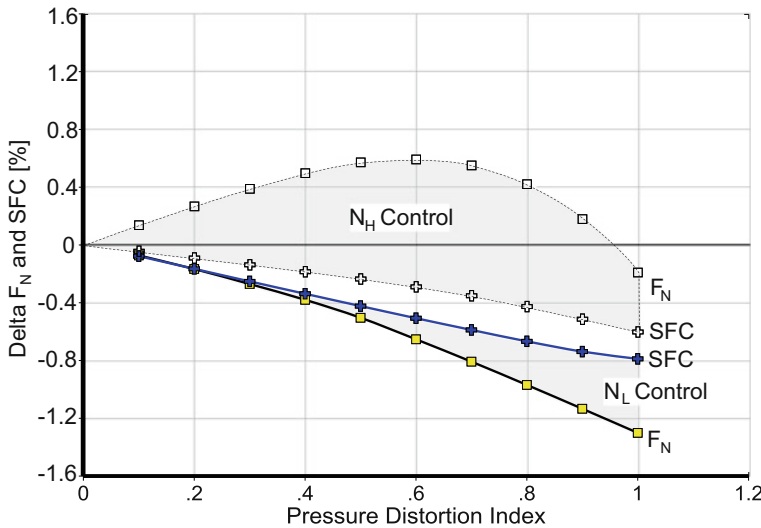


Fig. 6.3-3 Performance changes due to distortion (uncoupled compressors)

The approach to thrust management also influences the sensitivity of thrust and specific fuel consumption to inlet flow distortion. Percentage changes in net thrust and SFC as functions of pressure distortion index are shown in Fig. 6.3-3 for uncoupled parallel compressors as high and low spool speeds are controlled. The biggest difference is observed in the net thrust at around $DC_{60} = 1.0$, where the magnitude is only 1.2%. The simulation yields even smaller thrust and SFC changes due to distortion when we consider the compressors as fully coupled. Thrust does not change at all if the engine is controlled to pressure ratio P_5/P_2 !

However, care should always be taken when comparing measurements against performance results from the parallel compressor theory. In analysis of the test data, the effect of inlet pressure recovery should be separated from the effect of flow distortion. Measured data should be corrected for changes in mass-averaged total pressure at the engine face P_2 before any pronouncements are made about big detrimental effects of inlet flow distortion on engine performance!

6.4 Changes Due to Control System Actions

Figure 6.3-3 shows how the thrust changes due to inlet flow distortion depend on the engine control logic, the chosen thrust management system. Sometimes engines react to inlet flow distortion in an unintended manner because either the control system is unaware of the distortion or there is no actuator available which can counteract.

6.4.1 Unintended Reactions

If a multi-spool engine is controlled by N_L , then any loss in flow capacity of the low pressure compressor due to inlet flow distortion will lead to a thrust loss. Turbofan engines that are controlled by a pressure measured downstream of the core compressor are less sensitive to inlet flow distortion when the distortion does not affect the indicated value of the average engine inlet pressure.

In the hot end of the engine the use of multiple temperature sensors is common practice. An averaged output signal is always available to the engine control system and this is independent of the magnitude of inlet flow distortion. At the cold end, however, single sensors for engine inlet and compressor exit temperature are frequently employed and, the measurement then can affect the rated performance when inlet temperature distortion is present.

An example is the control of variable compressor guide vanes, where their scheduled stagger angle setting is a function of corrected spool speed. Here, the temperature signal needed for calculating the corrected speed might be affected by inlet temperature distortion.

Another example is control of the exhaust nozzle area in a mixed flow turbofan with an afterburner. The scheduled A_8 may be a function of N_L , P_2 and T_2 . Any disturbance of the P_2 and T_2 signals will affect the scheduled A_8 and consequently the thrust.

6.4.2 Intended Actions

If the engine control system is aware of any inlet flow distortion, then compression system stabilizing actions can be mandated.

Bleed from the HPC is used to lower its operating line and thus create additional surge margin. If the air is injected into the bypass channel, then the performance loss is smaller than with overboard bleed. However, air injected into the bypass duct will reduce the surge margin of the fan. The magnitude of this effect will depend on the bypass ratio and whether or not the engine exhaust is mixed.

Low bypass mixed flow turbofan engines with afterburners are equipped with variable area nozzles. During dry operation, the nozzle area does not necessarily need to be modulated, however, opening the nozzle may well help the low pressure compressor if it encounters inlet flow distortion. Such an action generally causes a loss of thrust or an increase in specific fuel consumption.

6.5 Reprise

The parallel compressor theory is a very simple way to describe and quantify the fundamental effects of inlet flow distortion on the stability of a compression system. Two compressors operate with different inlet total pressures and discharge their

flow to the same static pressure in a common duct. Results from the parallel compressor model agree quite well with those obtained from measurements in a compressor rig. DC₆₀ is a suitable distortion descriptor.

The static pressure balance downstream of the compressor, postulated by the parallel compressor theory, cannot occur if the compressor discharges the flow into a short duct with many struts, as is the case with multi-spool engines. Circumferentially constant static pressure at exit requires that some of the mass flow from the clean compressor be transferred to the exit of the spoiled compressor (the one with lower inlet pressure). If this mass transfer cannot occur then we have what we refer to as aerodynamically coupled compressors.

We can describe compressor coupling with a coupling factor CF which is zero for full static pressure balance (no coupling) and unity for no mass flow transfer between segments in the intermediate duct (full coupling). Intermediate degrees of aerodynamic coupling may be simulated by using a weighted average of the two conditions “static pressure balance” and “no mass flow between segments”. This approach is analytically simple, inexpensive and easy to implement in any performance program. In addition to an assessment of compression system stability, the integrated parallel compressor model also provides an indication of the effect of inlet flow distortion on engine performance. As long as the distortion intensity does not affect the flow field within the compressor significantly due to large local flow separation zones, its effect on the average component efficiencies remains small and the thermodynamic performance suffers only marginally. Engine performance is primarily affected by inlet flow distortion only when the control system reacts either unintentionally or takes deliberate actions, such as opening a bleed valve.

Further information on inlet distortion and its effects may be found in Ref's. [4–8]

6.6 References

1. Williams, D.D.: Review of current knowledge on engine response to distorted inflow conditions. In: Engine Response to Distorted Inflow Conditions, AGARD Conference Proceedings No. 400 (AGARD-CP-400), 1986
2. Reid, C.: The response of Axial Compressors to Intake Flow distortion. ASME Paper 69-GT-29 (1969)
3. Cumpsty, N., Heyes, A.: Jet Propulsion, 3rd edn, Fig. 11.5. Cambridge University Press, Cambridge (2015)
4. Inlet Total-Pressure-Distortion Considerations for Gas-Turbine Engines, Aerospace Information Report, Society of Automotive Engineers, AIR 1419, Rev. A, 1999
5. Cousins, W.T.: History, Philosophy, Physics, and Future Directions of Aircraft Propulsion System/Inlet Integration, ASME GT2004-54210 (2004)
6. Kurzke, J.: Effects of Inlet Flow Distortion on the Performance of Aircraft Gas Turbines, ASME GT2006-90419 (2006)
7. Korn, J.A.: Estimated Effect of Circumferential Distortion on Axial Compressors Using Parallel Compressor Theory and Dynamic Stall Delay, AIAA Paper 74-233 (1974)
8. Performance Prediction and Simulation of Gas Turbine Engine Operation, NATO Research and Technology Organization, Technical Report RTO-TR-044 (2002)

Chapter 7

Transient Performance Simulation



The turbine of any gas generator delivers—while the engine runs in steady state—exactly the power required for driving the compressor plus the power needed for the accessory drive, bearing losses and disk windage. Transient maneuvers affect this power balance: an acceleration needs additional power for overcoming the inertia of the spool while during a deceleration some of the power stored in the rotor returns to the cycle. The rotor works like a flywheel which stores energy during accelerations and releases it during decelerations.

Even for the simplest transient simulation we need numbers for the polar moment of inertia. We can make a guess, based on what we may know from similar engines. Using polar moments of inertia determined with a preliminary mechanical engine design of the engine is an alternative.

The mechanical model yields more information than only the inertia of the spools. Simple disk stress calculations also reveal diameter changes due to centrifugal stress. Additionally, the thermal expansion of the disks, blades and casings is predictable. Thus, everything we need for calculating tip clearance at off-design conditions is known. This is important knowledge because compressor surge margin reduces quickly with increasing tip clearance. Statements about engine operability are not meaningful without considering tip clearance changes.

The mechanical model also provides guesses for the blade and vane masses in the flow path and those of the flow annulus boundaries (blade platforms and casings). Heat is stored in and released from these engine parts during transient operation.

Running such an enhanced transient model yields quite different answers compared to the poor man's approach, which considers only the effects of rotor inertia. The following sections describe first simple transient simulations and introduce the commonly applied transient control philosophy. The description of the mechanical model of a turbofan follows before we discuss heat transfer to and from engine parts. Finally, we show and discuss results for two transient maneuvers with a turbofan.

7.1 Transient Basics

7.1.1 Overcoming Rotor Inertia

The power needed to accelerate a rotor with a polar moment of inertia I_{rotor} and a rotational speed N is

$$PW_{acc} = \frac{\partial N}{\partial t} NI_{rotor} \quad (7.1-1)$$

The impact of PW_{acc} on the thermodynamic cycle is the same as that of ordinary power offtake during steady state operation: Turbine inlet temperature rises if power offtake increases at constant corrected spool speed. We can best explain that with the movement of the operating point in the compressor map of a turbojet engine. In Fig. 7.1-1, point A without any power offtake is on the steady state operating line, while the location of point B shows what happens when power offtake is activated. This map includes additional contours of constant T_{41}/T_2 values. The latter are derived by considering mass flow continuity between the compressor and the turbine, where corrected flow is constant. T_{41}/T_2 is much higher at point B than at point A. The pressure ratio is also higher, with the increase depending on the shape of the speed line.

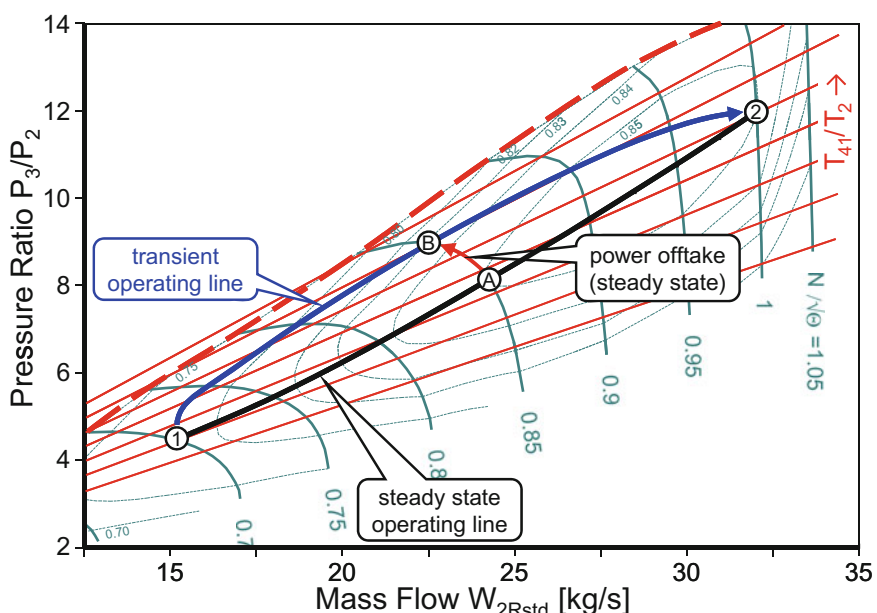


Fig. 7.1-1 Transient operating line in the compressor map of a turbojet

The compressor operating point of a turbojet and/or gas generator moves during an engine acceleration from point 1 on the $N/\sqrt{\Theta_2} = 0.7$ line to point 2 along the blue line. All transient operating points are above the steady state operating line due to the excess power required to overcome the inertia of the rotor. The turbine inlet temperature T_{41} during the transient maneuver is higher than during steady state operation and surge margin is reduced.

What Fig. 7.1-1 shows for a turbojet engine applies equally to the gas generator of any turbofan or turboshaft with free power turbine.

7.1.2 Transient Control Strategies

During an acceleration from idle to full power, the control system must ensure that the turbine inlet temperature remains within acceptable limits and that the gas generator compressor does not surge. The problem is that during fast transient maneuvers, we cannot measure either turbine temperature or surge margin with reasonable accuracy, so we must decide how to operate the engine safely from measurable quantities that can be acquired both quickly and precisely.

Some basic reflections on non-dimensional power offtake lead to a solution of the problem. Operating line shifts in the compressor map are the same when the corrected power offtake is the same.

$$PW_{corr} = \frac{\Delta PW_{acc}}{\sqrt{\Theta_2 \delta_2}} = \frac{\partial N / \partial t}{\delta_2} \frac{N}{\sqrt{\Theta_2}} I_{rotor} \quad (7.1-2)$$

Corrected acceleration power varies with the rate of corrected speed change $(\partial N / \partial t) / \delta_2$ and corrected speed $N / \sqrt{\Theta_2}$. Therefore, in the compressor map, we can plot lines of constant corrected acceleration rate $(\partial N / \partial t) / \delta_2$. Limiting the speed change per time can protect the compressor from surge and this can be seen from Fig. 7.1-2. It is common practice to call this acceleration control mode “N dot” control because $\partial N / \partial t$ is frequently abbreviated as \dot{N} .

There is one problem with the \dot{N} control philosophy. If, for some reason, the compressor surges the speed will drop. The controller reacts to the speed drop by increasing fuel flow with the aim to recover. However, that aggravates the situation; fuel flow must be reduced when the engine surges!

We need a control parameter which reduces fuel flow automatically in the event of surge. Corrected fuel flow divided by corrected speed and compressor pressure ratio is the formula of choice.

$$\frac{W_F}{NP_3} = \frac{\frac{W_F}{\sqrt{T_2} P_2}}{\frac{N}{\sqrt{T_2}} P_3} \quad (7.1-3)$$

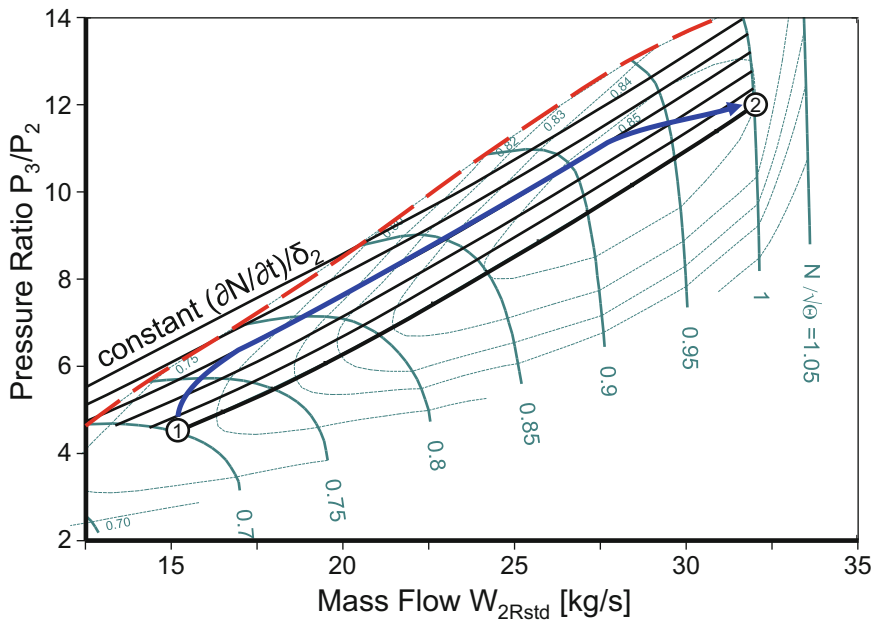
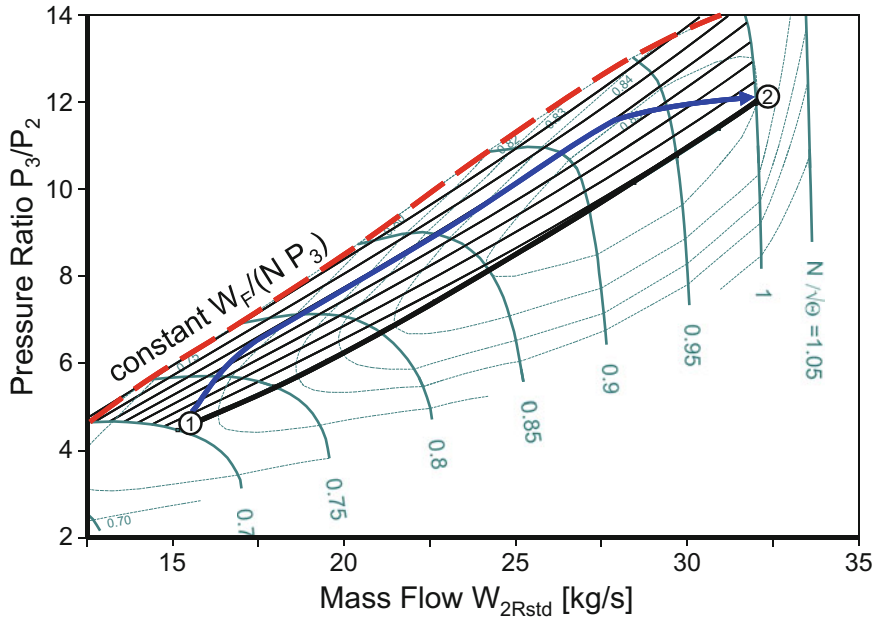


Fig. 7.1-2 N dot control

When the engine surges, P_3 drops sharply and so does the mandated fuel flow. Since $W_f/(N P_3)$ is a combination of three non-dimensional parameters, it is also a non-dimensional parameter itself and we can show lines of constant $W_f/(N P_3)$ in the compressor map. Figure 7.1-3 indicates that these lines are like the $(\partial N / \partial t) / \delta_2$ lines in Fig. 7.1-2. Acceleration along a line of constant $W_f/(N P_3)$ is feasible in our example.

Restricting transients to a constant value of $W_f/(N P_3)$ solves the surge recovery problem, but has a severe disadvantage: The time needed for an acceleration from idle to full power depends on the temperature of the engine parts. A significant amount of fuel is needed to warm up a cold engine. Only part of the fuel energy remains for accelerating the rotor; it takes some additional time to reach full power. A warm engine reacts quicker to throttle movements; acceleration time is less than with a cold engine. Pilots don't like such behavior, they want consistent thrust response to their power lever movements. Therefore, \dot{N} is the method of choice in digital engine controllers because it provides consistent thrust response, for both cold and warm engines. $W_f/(N P_3)$ control is also implemented in modern controllers and serves as a fallback solution in case of surge.

Fig. 7.1-3 $W_F/(N P_3)$ control

7.2 Engine Geometry

For serious examinations of aircraft engine operability, we need more than values of polar moments of inertia. Heat exchange between gas and metal affects the temperature of the engine hardware. For calculating thermal expansion, we must know at least approximate numbers for the mass of engine parts and their heat storage capacity. How centrifugal forces affect the disk diameters and the length of blades also needs to be known. Only then are we able to estimate how tip clearances in compressors and turbines vary during steady state and transient operation. In short, we need at least an idea about the engine geometry.

Creating a model of engine geometry begins with the thermodynamic cycle which defines mass flow, total pressures and total temperatures at the component boundaries. Stage numbers and spool speeds influence the aerodynamic loading and hence the component efficiencies employed in the thermodynamic cycle calculation. Therefore, some engine geometry iterations are necessary to find a compromise usually between many conflicting requirements.

7.2.1 Steady State Geometry

Engine geometry is not the same even in steady state simulations. Casing diameters change with gas temperature—how much depends on the thermal expansion

coefficient of the material. Also blade and disk dimensions adapt to gas temperature. Additionally, there is the effect of centrifugal stress on the dimensions of disks and blades. Consequently, tip clearance varies significantly between idle and full load, for example. (Blades and vanes respond to aerodynamic loads also, but we can neglect that here.)

The steady state performance model is, by definition, consistent with the tip clearance variations generated by the mechanical engine model. This hypothesis is only an approximation to reality because tip clearance changes due to centrifugal forces, which in turn are driven by absolute spool speed N , while compressor efficiency, for example, is a function of corrected spool speed $N/\sqrt{\Theta}$. Compressor maps measured on a rig contain the effects of tip clearance variations with speed on mass flow and efficiency. Therefore, no tip clearance corrections to the map are necessary if the prevailing compressor inlet temperature is the same as during the rig test.

Gas generator turbines generally operate at constant pressure ratio and in a very narrow range of $N/\sqrt{\Theta}$ values. That means that reading the HPT turbine map always yields more or less the same efficiency value. Mechanical spool speed N_{HPT} varies significantly between idle and full load and that leads to significant tip clearance variations. These cause efficiency changes which can be significant since 1% change in relative tip clearance results in about 2% efficiency change.

7.2.2 A Turbofan Example

The example is based on a V2500 cross section published in 1984 [2]. At that time, the engine had only one booster stage, while production V2500 turbofans have three or four of them. Fig. B4.6-1 in the chapter on mechanical design compares the GasTurb model with the cross section of Ref. [2].

The main cycle parameters, supplemented by the fan diameter, are:

Thrust	25000 lbf
Fan tip diameter	63 in
Fan pressure ratio	1.6
Bypass ratio	5.4
Overall pressure ratio	29.8

The performance model employs the compressor maps from Refs. [3, 4] and the turbine maps from Refs. [5, 6]. The geometric model was created with the conceptional design features of GasTurb, as described in Chap. B4.

Tip clearance in all compressors and turbines is assumed to be 1.5% of the blade height at Take Off, ISA SLS conditions which is our mechanical design point. Figure 7.2-1 shows how the first stage geometry changes between 70% (~Idle) and 100% gas generator spool speed. Tip clearance is 1% bigger at Idle due to the lower disk temperatures and stresses. Note that this has nothing to do with transient behavior—it is a property of the steady state off-design simulation.

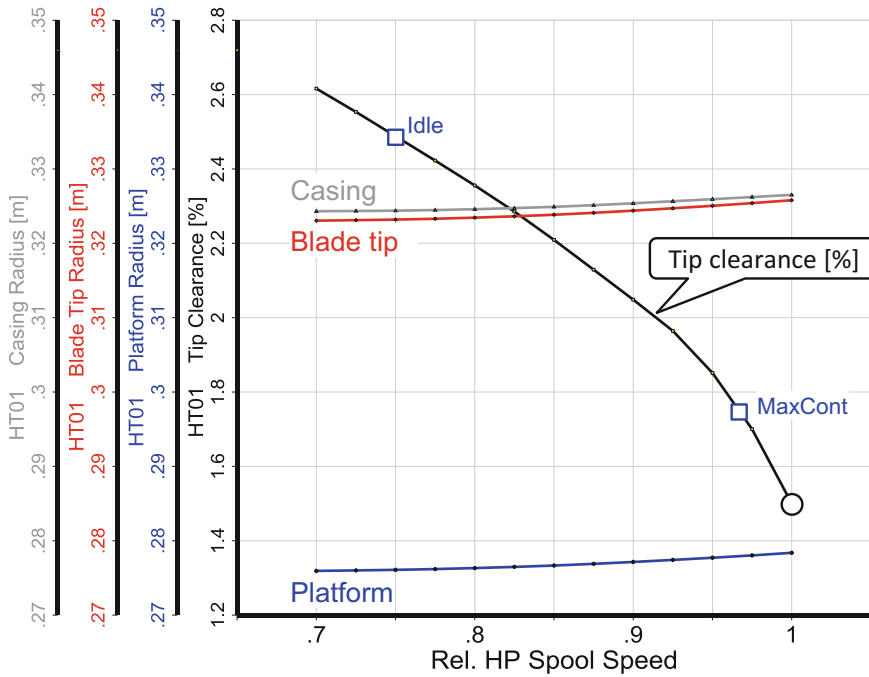


Fig. 7.2-1 Steady state HPT Stage 1 tip clearance

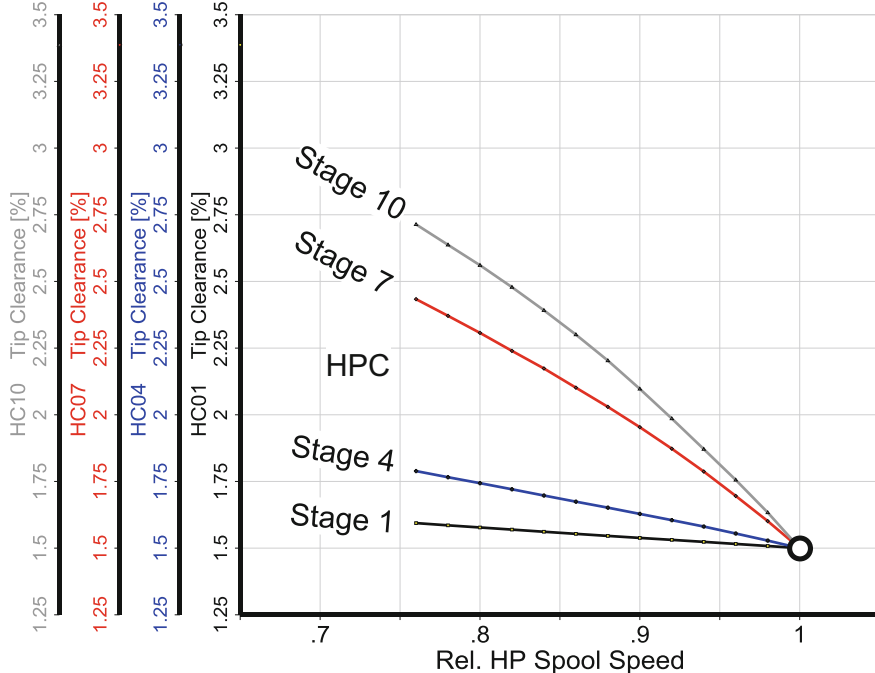


Fig. 7.2-2 Steady state HPC stage tip clearances

At idle, the relative tip clearances in the rear stages of the HPC are bigger than in the front stages (Fig. 7.2-2). This is due to larger temperature changes, greater disk diameters and shorter blades in the rear stages.

In the LPT, the idle relative tip clearance of the first stage is bigger than that of the last stage (Fig. 7.2-3). The explanation is that in this component the temperature variations at the entry are bigger and the first stage blades are shorter.

Figure 7.2-4 shows the steady state efficiencies of the HPC, HPT and LPT. The HPT efficiency model is a special case. It consists of two elements: the first is the efficiency read from the turbine map, the second is a correction term which takes tip clearance variations with relative spool speed into account.

The corrected spool speed of the HPT varies between idle and take off by only 5%. The operating line is short, and the efficiency read from the map varies less than one percent. The much bigger mechanical speed difference of 25% from idle to take-off goes along with a tip clearance difference of approximately 1% (see Fig. 7.2-1) which causes an efficiency loss at idle of approximately 2%.

Both the maps employed for the HPC and LPT are scaled versions of rig measured maps. The effect of decreasing tip clearance from low to high speed is contained in the map efficiency numbers. In the engine the tip clearance varies in a different way than on the rig. This difference, however, is neglected in our turbofan performance model.

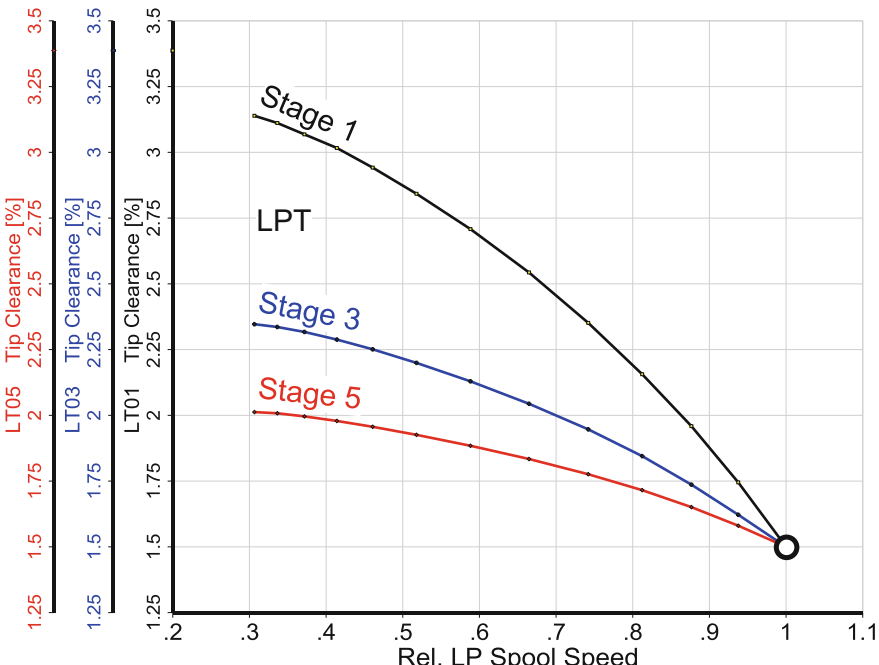


Fig. 7.2-3 Steady state LPT stage tip clearances

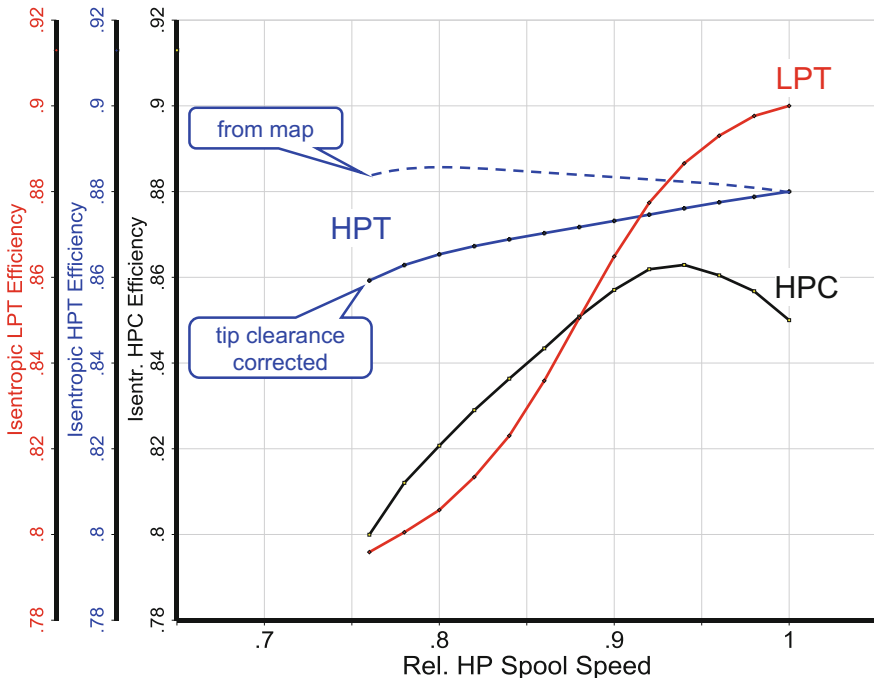


Fig. 7.2-4 Efficiencies of HPC and turbines

7.3 An Enhanced Approach

In the simple simulation of a transient maneuver we only consider the effect of rotor inertia in addition to the steady state power balances. The enhanced model also takes into account the effects of transient tip clearance variations as well as heat transfer to and from the engine parts.

7.3.1 Tip Clearance

When an engine accelerates from Idle to Take Off power, the centrifugal forces on the disks and blades increase. Gas temperatures rise, the blades and vanes are heated quickly, and they expand. Disk temperatures adapt very slowly to the new conditions; their diameter grows during short events primarily due to the centrifugal forces. The thermal expansion of the casing accommodates the growth of the disks and blades during the acceleration, however the casing diameter grows slower than the blade tip diameter and consequently tip clearance reduces. After Take Off spool speed is reached, the casing continues to expand until equilibrium with the gas temperatures is reached. At this point the clearance is at a maximum.

In our simulation we concentrate on short events of less than one minute duration. Disk temperatures will adapt very little during that time. We assume for simplicity that disk temperatures remain constant. That does not mean that the disk dimensions remain constant—they change with spool speed due to centrifugal stress.

Before we can calculate tip clearance, we need to know metal temperatures. For that purpose, we need to know something about heat transfer.

7.3.2 Heat Transfer

In steady state performance calculations, i.e. for stabilized conditions, we do not consider heat flow between gas and engine hardware. We postulate that gas and hardware temperatures are in an equilibrium state. This equilibrium does not exist in transient operation. There is significant heat exchange between the main gas flow, the secondary air system and the metal parts. The amount of heat transferred depends on numerous details.

For the overall system simulation, however, it is not necessary to know the details about local heat transfer, it is sufficient to consider the heat flow in general. It is standard practice that the very complex ‘real’ engine parts are substituted by geometrically simple bits and pieces. The engine parts in contact with the main gas flow are modeled as plates (the airfoils) and cones of constant thickness (ducts and casings).

As a further simplification, we assume that the thermal conductivity within these parts is infinite, which implies the temperature distribution is completely uniform.

Convective heat transfer from a gas with temperature T_{gas} to such an idealized engine part creates a heat flux Q , which is proportional to the heat transfer coefficient h , the surface area A_s and the difference between the temperature of the part T (which is a function of time t) and the temperature of the gas T_{gas} :

$$Q = hA_s(T(t) - T_{gas}) \quad (7.3-1)$$

This heat flux leads to a rate of temperature change of the idealized part dT/dt which is proportional to the product of the mass m of the part and its specific heat C :

$$Cm\frac{dT}{dt} = -hA_s(T(t) - T_{gas}) \quad (7.3-2)$$

This equation can be re-written with $\tau = C * m / (h * A_s)$ as time constant:

$$\frac{dT}{dt} + \frac{1}{\tau}T(t) = \frac{1}{\tau}T_{gas} \quad (7.3-3)$$

For $\Delta T(t) = T(t) - T_{\text{gas}}$, integration yields

$$\Delta T(t) = \Delta T_0 e^{-t/\tau} \quad (7.3-4)$$

ΔT_0 is the temperature difference between the engine part and the gas at time $t = 0$. With progressing time ($t > 0$) the temperature of the part T follows the gas temperature T_{gas} with a first order lag. This lag is fully described by the time constant τ .

For a given engine part of known material, mass and surface area, the time constant only varies with the heat transfer coefficient h . The assumption that the heat transfer in the gas turbine behaves as in a pipe with turbulent flow, leads to the conclusion that the heat transfer coefficient varies with Reynolds number to the power of 0.8.

Absolute Reynolds numbers need not to be determined, it is sufficient to know the Reynolds Number Index RNI, which relates the true Reynolds number to that at ISA Standard Day conditions. Knowing the time constant for one operating condition (the engine design point, for example), allows it to be calculated at another operating point:

$$\tau = \frac{\tau_{ds}}{\left(\frac{RNI}{RNId_s}\right)^{0.8}} \quad (7.3-5)$$

We model heat flow in compressors and turbines separately for (1) airfoils, (2) blade platform including root and (3) for casings, see Fig. 7.3-1. The temperatures of the live disks are assumed to remain unchanged during the short time of a simulation run.

We employ a different time constant for each of the model element types. The magnitude of the time constant $\tau = C * m / (h * A_s)$ depends on the mass of the part m , its surface area A_s , its specific heat C and the heat transfer coefficient h . The mass and the surface area of the airfoils, blade platform (including root and the casing) are determined during engine mechanical design. Specific heat depends on the materials. Knowing the heat transfer coefficient allows us to calculate the time constant.

However, remember the high degree of abstraction in the heat transfer model. To be in line with reality, the model needs to be calibrated and this could be achieved by adjusting numerous heat transfer coefficients. But it is simpler to use the time constants themselves for model calibration. Therefore—instead of the heat transfer coefficients—we use the time constants as input quantities for transient simulations.

Heat transferred in either direction between hardware and gas affects the thermodynamics of the compression and expansion processes. For example, cooling during the compression process reduces the power needed for achieving a given pressure ratio.

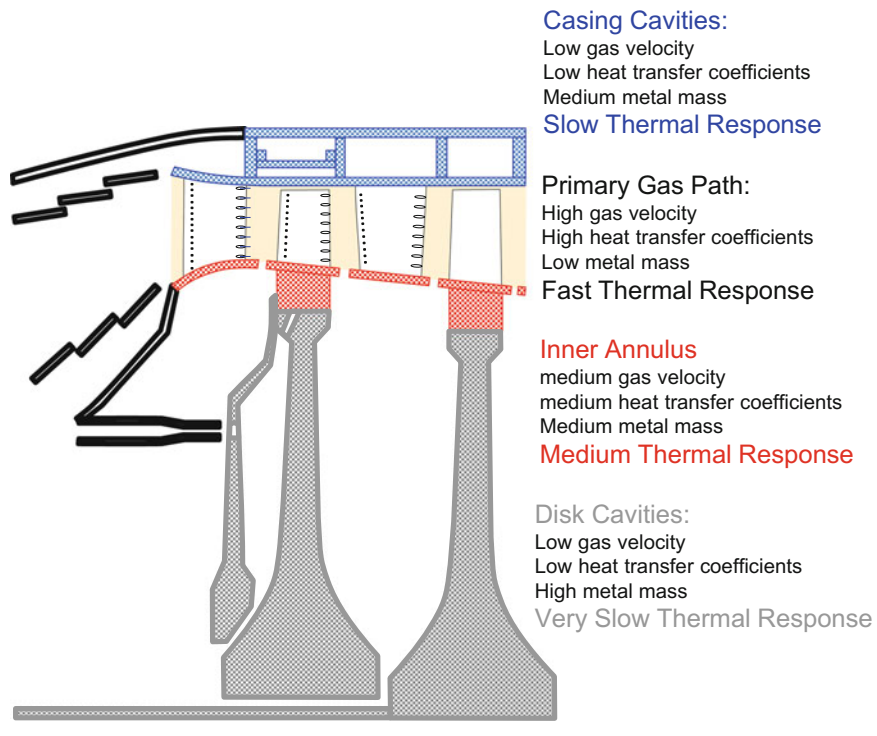


Fig. 7.3-1 Thermal response model

An adiabatic compression can be described by

$$\frac{T_{2,ad}}{T_1} = \left(\frac{P_2}{P_1} \right)^{\frac{n-1}{n}} \quad (7.3-6)$$

This formula can be expanded to describe a compression with heat transfer:

$$\frac{T_{2,ad}}{T_1} = \left(\frac{P_2}{P_1} \right)^{\frac{n}{n-1} \left(1 - \frac{q}{\Delta H_{ad}} \right)} \quad (7.3-7)$$

In that expression, q is the heat flow (positive if heat flows from the gas to the hardware) and ΔH_{ad} is the specific work of the adiabatic process.

So, the total change in compression exit temperature is composed of two elements: the heat flow and a change in specific work. We need the latter in the power balance with the turbine. For a non-adiabatic compression process, specific work is given by

$$\Delta H_c = \Delta H_{ad} \frac{T_2 + \frac{q}{C_p} - T_1}{T_{2,ad} - T_1} \quad (7.3-8)$$

The heat flow on the turbine side is split into two parts: half of it is transferred to the main stream before the expansion process, the rest is transferred downstream. This methodology is consistent with how we consider turbine cooling in steady state performance calculations, as in Chap. D6.

7.3.3 *Burner*

We model heat soakage in burners only for the flame tube and ignore the heat exchange with the external casing. The flame tube is made from sheet metal, which in our model is in contact on both sides with gas of the same temperature—the mean gas temperature in the burner $(T_4 + T_3)/2$. We describe heat soakage with a single time constant and account for Reynolds number effects as described above. Heat flow from the gas into the flame tube reduces the burner exit gas temperature T_4 .

7.3.4 *Other Transient Phenomena*

Rotor inertia, tip clearance alterations and heat exchange with the engine parts are the most relevant differences between steady state and transient simulations. There are more disparities, however, but either they contribute little to the accuracy of the simulation or they are difficult to quantify.

Volume filling belongs to the less important elements of a transient simulation unless very small time-steps are employed in the simulation. Anyway, mass storage in the engine is mainly perceptible during the first instants of the transient but is small afterwards. It is difficult to quantify how the map of a multi-stage compressor is affected by heat transfer to and from the engine hardware. The overall map changes because, for example, the inlet temperature to the rear stages is reduced while a cold engine is accelerating because some heat goes into the metal. Therefore, the rear stages run transiently with a higher corrected speed than in steady state. This affects both the efficiency and the surge margin of the overall compressor. The influence of these changes disappears within the overall accuracy limits of transient performance simulations.

Modeling active tip clearance control of compressors and turbines and the transient clearance changes of seals which control the amount of turbine cooling air requires detailed knowledge about the mechanical design of the engine. We do not have this knowledge, therefore we do not consider its effects in the following simulation example.

7.4 Transient Behavior of a Turbofan

We examine the transient behavior of the V2500 described in Sect. B4.6. The geometry model contains dimensions and masses of all disks, casings, blades and vanes. These data allow the rotor inertias to be calculated. We need only a few additional inputs for an enhanced transient model which addresses more than rotor inertia: it covers

- specific heat of the parts
- three time constants for each compressor and turbine
- a burner flame tube time constant
- tip clearance exchange rates for efficiency, flow capacity and surge margin.

The time constants determine the thermal expansion of the parts and their heat soakage. We use the values in Table 7.4-1 for our example.

Our model neglects tip clearance and heat soakage effects for the fan, all the ducts and the exhaust parts. Also, we consider only relatively short time spans during which the live disk temperatures remain constant.

7.4.1 Accelerating the Cold Engine

Prior to the actual transient simulation, we run a series of steady state (thermal equilibrium) performance points which will serve as a reference. This yields the tip clearance (expressed in percent of the blade height) for each of the compressor and turbine stages at each operating point.

First, we examine an acceleration from Ground Idle to about Max Continuous. The control input demands $N_L = 90\%$; the HP spool acceleration rate is limited to 6% per second.

Figure 7.4-1 shows what happens with thrust, spool speeds and burner exit temperature T_4 . A simulation which considers only spool inertia (no tip clearance and no heat soakage effects) results in nearly the same spool speed and thrust behavior over time. The burner exit temperature T_4 , however, is significantly different. In the first seconds, this temperature is higher in the simple model compared to the enhanced model because no energy is consumed by heating up engine parts.

Table 7.4-1 Time constants [seconds]

	Casing	Blades & vanes	Platform & blade root
Booster	5	1	2
HPC	5	1	2
Burner		1 (can only)	
HPT	5	1	2
LPT	5	1	2

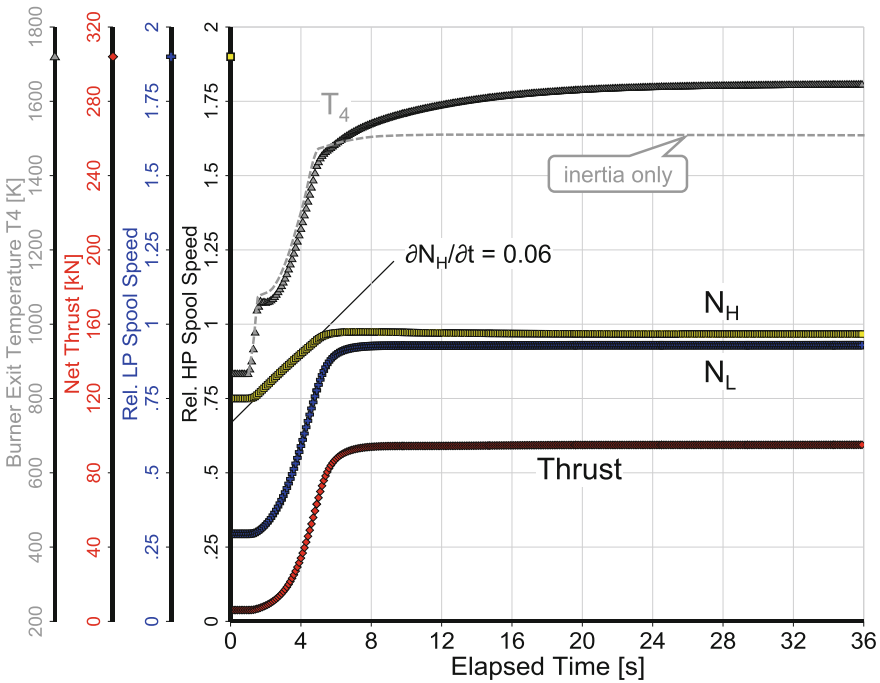


Fig. 7.4-1 Acceleration from Idle to about Max Continuous

After about seven seconds, nothing more happens in the simple simulation, the engine is stabilized.

The burner exit temperature of the enhanced model continues to rise after the target thrust has been reached. This is due to the increasing tip clearances of HPC and HPT which reduce their efficiencies.

The steady state tip clearance of the first HPT stage at Idle is 2.48% and at Max Continuous only 1.75%, as we can see in Fig. 7.2-1. This reduction in tip clearance happens incompletely in the transient simulation: admittedly we observe the effects of centrifugal forces and thermal expansion of blades and casings, however, the radius of the turbine disk does not change. This is justified by the short simulation duration of only 36 s. In the end, the tip clearance of the first HPT stage is 3% bigger than the reference tip clearance, which we have found before for steady state at the same spool speed. The difference between the two tip clearance values is converted to compressor efficiency, flow and surge margin modifiers that employ constant exchange rates. A one percent increase in tip clearance lowers compressor efficiency and flow by 2% and surge margin by 5%. Turbine tip clearance affects efficiency only; one percent increase lowers efficiency by 2% in case of the unshrouded HPT and by 1% for the shrouded LPT. The stage performance modifiers are averaged for each compressor and turbine and then applied to the thermodynamic cycle calculation. The results are shown in Fig. 7.4-2.

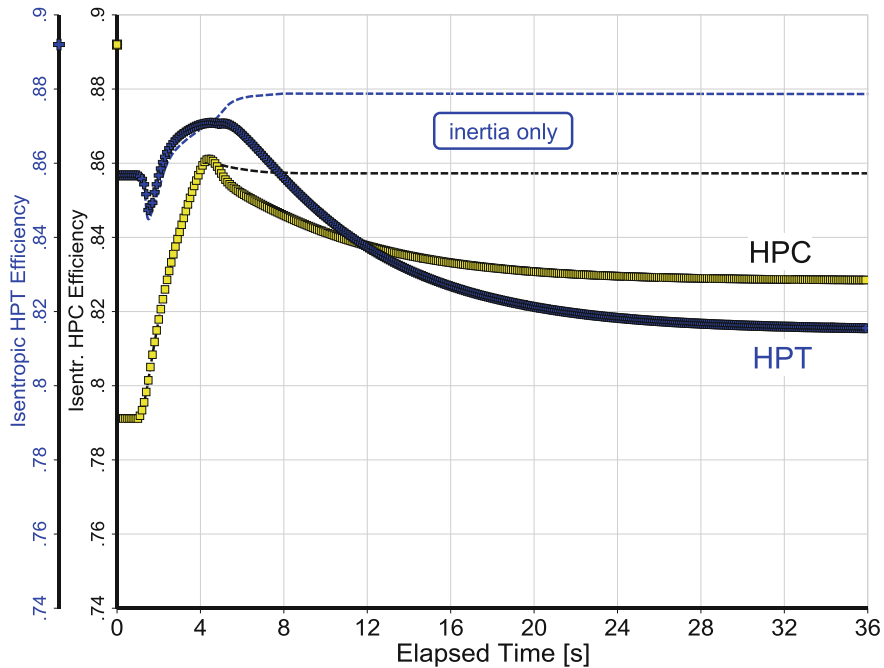


Fig. 7.4-2 Compressor and turbine efficiencies for the acceleration of a “cold” engine

Figure 7.4-3 shows what happens in the gas generator compressor (HPC) map. Squares denote the steady state operating line. Circles represent the enhanced transient simulation and the blue dashed line shows what happens if we consider spool inertia only. It is notable that the blue line ends in the center of the red circle while the other operating line turns to the left. This turn is the effect of the significant compressor and turbine efficiency losses shown in Fig. 7.4-2 and these come from the increased transient tip clearances relative to the steady state values for the same spool speed.

We can judge the surge margin differences better in Fig. 7.4-4 than in the compressor map. At the beginning of the acceleration both the simple and the enhanced simulation indicate similar surge margin consumption. At the end of the acceleration, however, only the enhanced model, denoted by the yellow squares, can predict the significant loss in surge margin after the target thrust is reached. This result agrees with a statement found in Ref. [7]: “Typically the largest tip clearances, and hence the point of minimum surge margin, occur between 30 and 80 s after the engine has achieved maximum rating.”

Figure 7.4-5 confirms this fact, with test data taken from a turbofan during acceleration from stabilized idle to the EGT limit. After around 10–15 seconds, most of the heat flow into the engine hardware has been completed. Beyond that, the engine would run at constant core speed if the clearances did not change over time. However, the core speed drops for about 50 s before it begins to recover

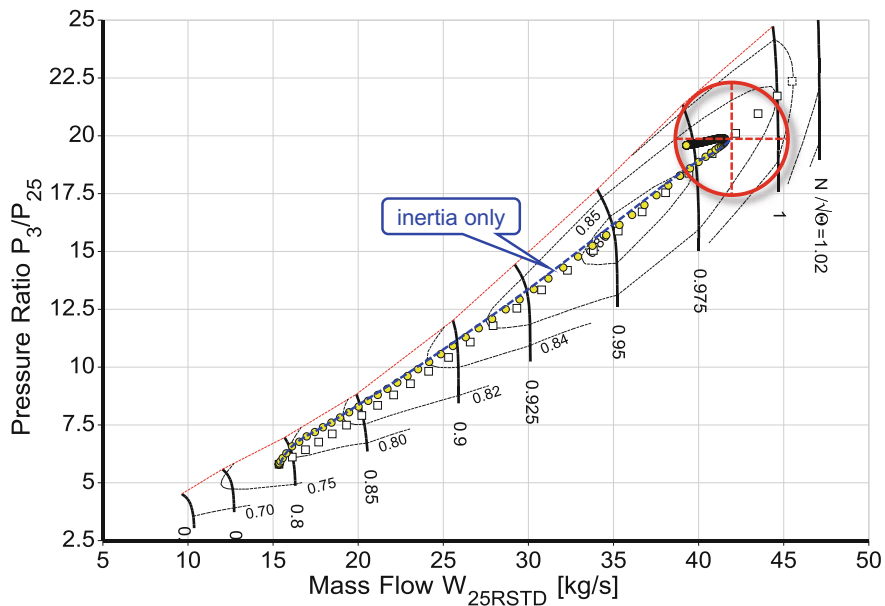


Fig. 7.4-3 Gas generator operating line

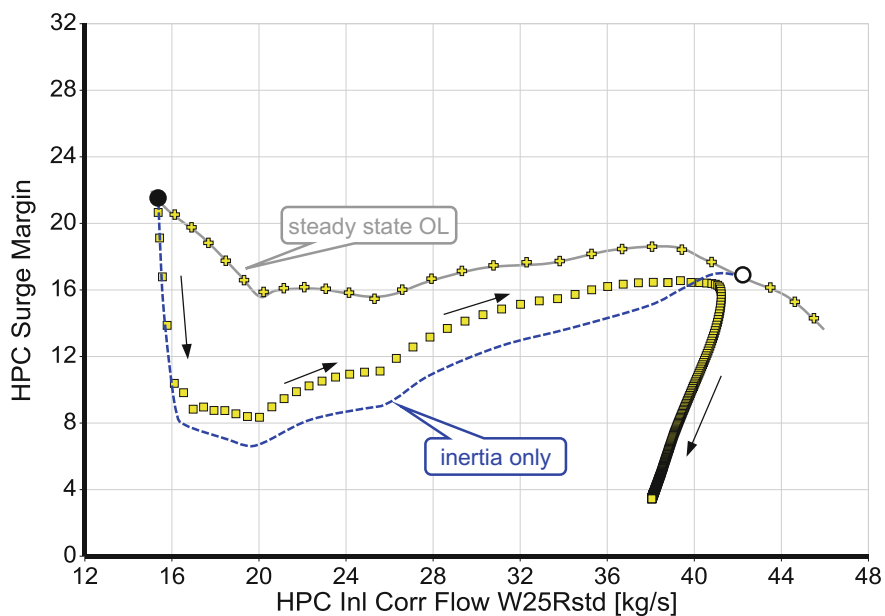


Fig. 7.4-4 Accelerating the cold engine

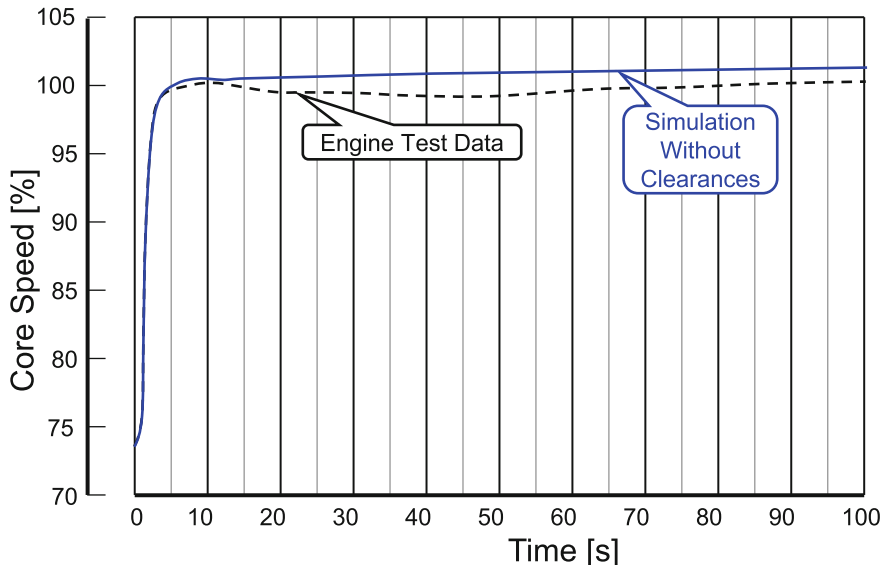


Fig. 7.4-5 Acceleration to the EGT limit of a turbofan (adapted from Ref. [9])

slowly. Reference [9] explains this with a short-term clearance increase. Core speed drops because the losses increase while EGT remains constant.

Loss of HPC surge margin is not the only hazard during the acceleration of a cold engine. There is also the possibility of a blade tip rub shortly before the target spool speed is reached. The centrifugal forces and the heat transfer to the blades increase the blade tip radius immediately, the casing radius, however, grows slowly. Figure 7.4-6 shows the clearance pinch-point at 4–6 seconds for the last HP compressor stage.

7.4.2 Decelerating the Hot Engine and Re-slam

The starting point of any transient simulation is a steady state operating point. If we begin with Ground Idle, as in the previous section, then the metal temperatures are generally low and the steady state tip clearances are big. In contrast, when we begin the simulation at Max Continuous power, then the metal temperatures are high and the tip clearances modest.

Decelerating a hot engine moves not only the operating point in the HPC map away from the surge line but, after a very brief increase, also decreases tip clearances in relation to those at steady state because the disk temperatures remain high. The only operability problem may be flame out in the burner.

Figure 7.4-7 shows the transient maneuver we are going to consider. It is named a “Bodie” after a US air force pilot who first used it during engine flight trials. We will see why this is a particularly severe maneuver.

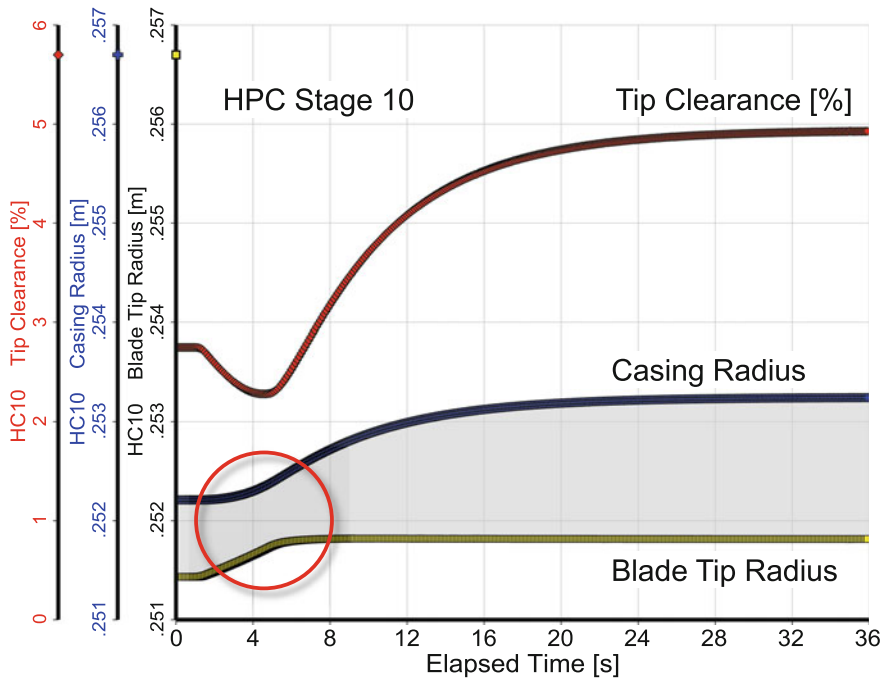


Fig. 7.4-6 HPC Stage 10 tip clearance

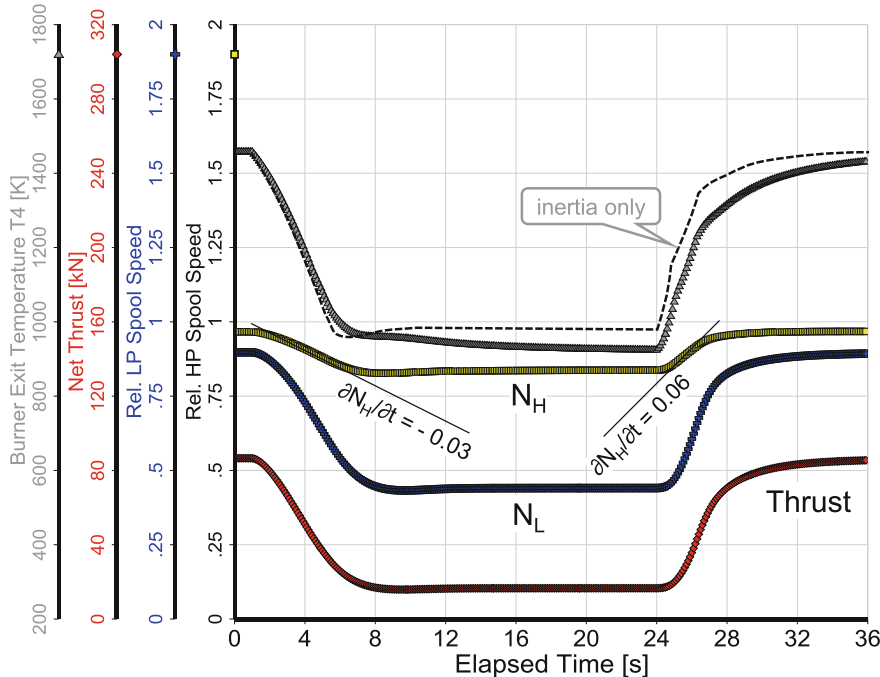


Fig. 7.4-7 Bodie

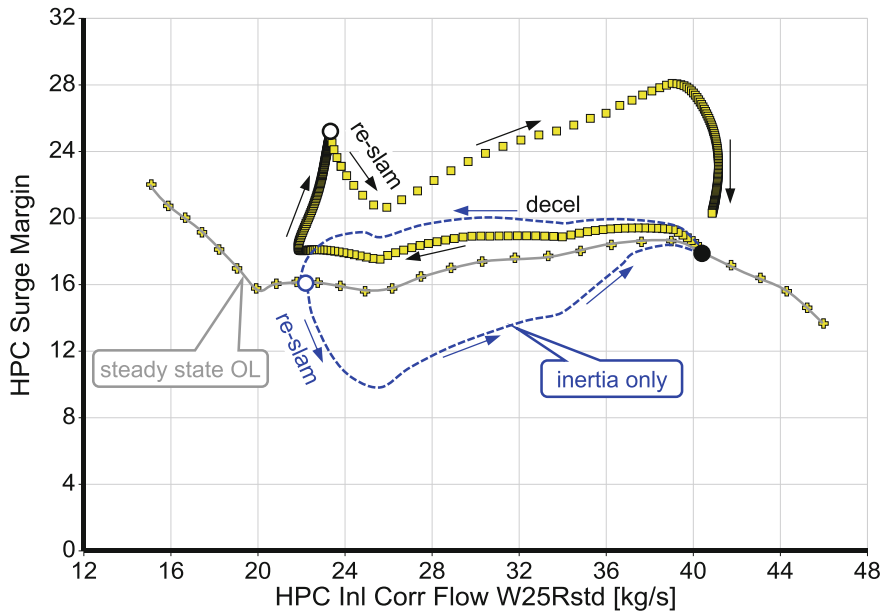


Fig. 7.4-8 HPC surge margin deceleration and re-slam

The simple model shows some loss in surge margin at the begin of the re-acceleration. The enhanced model, predicts significantly bigger margins throughout the maneuver, and this is illustrated in Fig. 7.4-8, so there are no surge problems.

What about the transient heat exchange between the engine hardware and the gas; could that be a problem? Remember that the transient controller keeps $\partial N_H / \partial t$ constant. Heat soakage of the gas generator parts affects the amount of fuel flow needed for a certain $\partial N_H / \partial t$, but does not influence how the HP spool speed changes with time.

The LP spool speed change with time $\partial N_L / \partial t$ is affected by heat soakage. Energy going into the hardware during an acceleration is not available for overcoming LP rotor inertia, so the commanded N_L change is delayed. Energy going from the hardware to the gas during a deceleration also retards N_L . The reaction of N_L (and thus thrust) to a thrust change command is a little more sluggish when heat soakage is considered.

Figure 7.4-9 shows the quantities of heat that are exchanged between gas and HPC and HPT hardware during the examined transient maneuver. Note that thermal equilibrium is attained after a longer time period following a deceleration than during an acceleration because the heat transfer coefficients are reduced at the lower mass flows and rotational speeds.

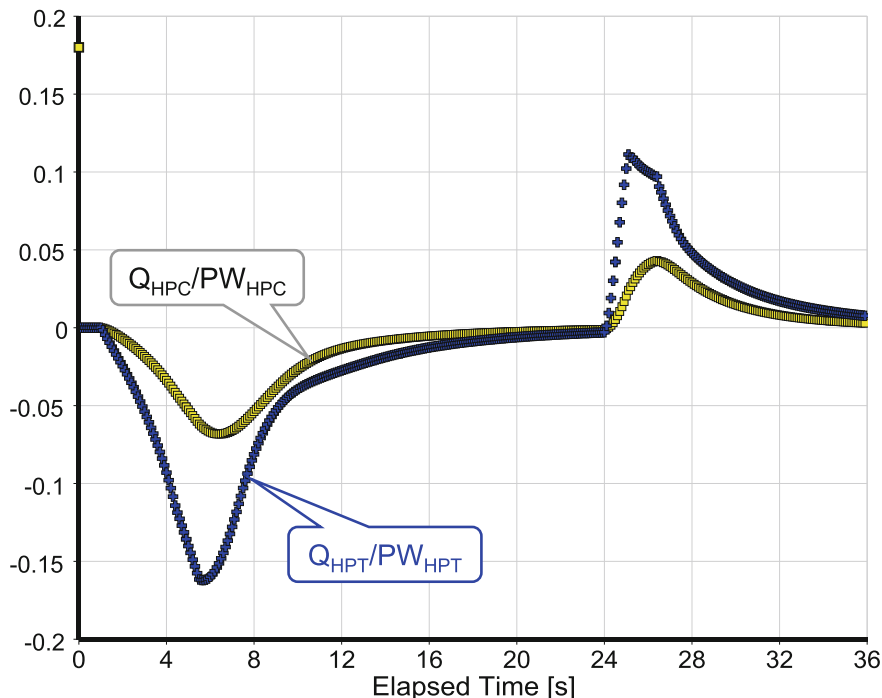


Fig. 7.4-9 Relative heat flows

If neither compressor stability nor heat soakage cause problems, then why is the “Bodie” a severe maneuver which is only used in service during an emergency? It is again a problem of tip clearance.

At the beginning of the re-slam, the disks are still hot, the casing, however, has already cooled down somewhat. Tip clearance is smaller than the design point value of 1.5%. In our example of Fig. 7.4-10 the HPT stage 1 tip clearance is nearly zero when the re-slam begins. The disk radius grows immediately once the spool speed begins to increase. The tip clearance becomes negative, which means that the blade tips come in contact with the casing. Blades and casing are damaged, and the rub increases the tip clearance permanently. Engine performance is deteriorated after the “Bodie” until the engine is repaired during the next visit to the maintenance shop.

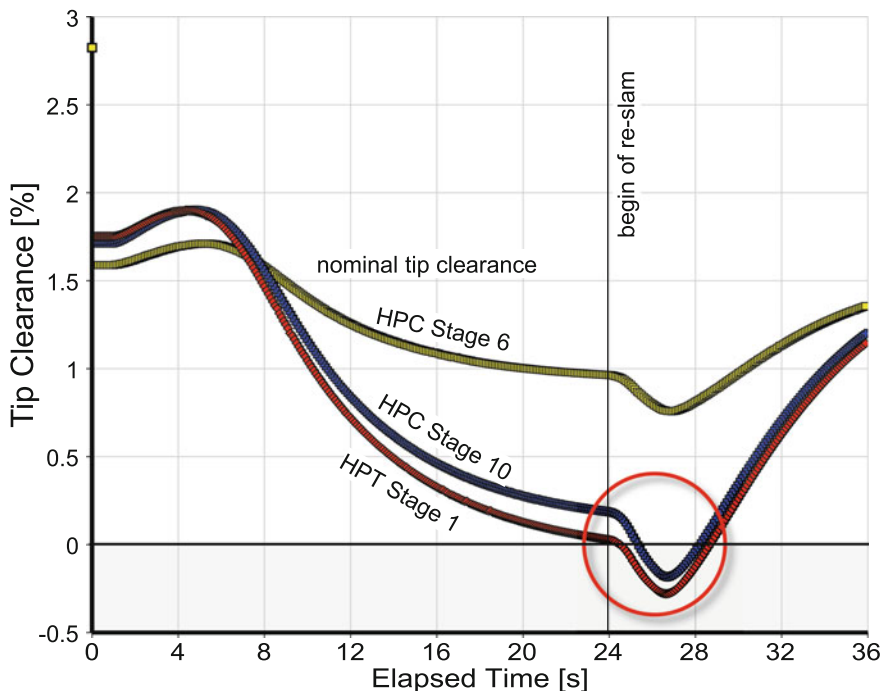


Fig. 7.4-10 Tip clearance changes during a “Bodie”

7.5 Concluding Remarks

In our example neither heat soakage nor transient tip clearance changes affect the duration of a transient maneuver. This is due to our way of controlling the engine with prescribed values of spool speed change per time. Heat soakage and tip clearance variations affect the amount of fuel needed for a given $\partial N / \partial t$. This is only a secondary effect with respect to thrust development over time because fuel mass flow is only a small fraction of the total exhaust gas mass flow.

We could also run the enhanced transient simulation with a controller that employs $W_F/(N P_3)$ as the main control parameter. Then we would get different thrust response times for cold and hot engines.

The quality of the enhanced transient simulation methodology is sufficient for examinations of basic effects as well as for all sorts of “what if ...” studies during the preliminary design phase of a new engine project. The absolute values will not be correct, but trends can be predicted.

When data from a real engine are available, it is feasible to calibrate a model with much better transient simulation capability without much effort. The first step is to reproduce the geometry of the real engine with the preliminary design tool as

well as possible. The second step is to adjust the time constants for the heat flows between the engine hardware and the fluid.

Valid comparisons between engines of different design are only feasible if the quality and degree of detail of the respective models are the same. That can best be achieved if the transient simulation is an integral part of the conceptional engine design and performance program. It is true that the geometry model in such a program is only a crude approximation, but it can be calibrated using any of the much more detailed engine outlines created by the aerodynamicists and designers.

7.6 References

1. Tong, M.T., Halliwell, I., Ghosn, L.J.: A computer code for gas turbine engine weight and disk life estimation. *J. Eng. Gas Turbines Power* **126**, 265–270 (April 2004)
2. Erinnerungen: 1934–1984 Flugtriebwerkbau in München, Herausgegeben von der MTU Motoren- und Turbinen-Union München GmbH, Zweite Auflage (1985)
3. Cornell, W.G.: Experimental Quiet Engine Program, Summary Report, NASA CR-2519 (1975)
4. Cline, S.J. et al.: Energy Efficient High Pressure Compressor Component Performance Report, NASA CR-168245 (1983)
5. Wilfert, G., Kriegl, B., Wald, L., Johanssen, O.: CLEAN—Validation of a GTF High Speed Turbine and Integration of Heat Exchanger, Technology in an Environmental Friendly Engine Concept, ISABE-2005-1156
6. Stabe, R.G., Whitney, W.J., Moffit, T.P.: Performance of a High-Work Low Aspect Ratio Turbine Tested with a Realistic Inlet Radial Temperature Profile, NASA TM 83665 (1984)
7. Walsh, P.P., Fletcher, P.: Gas Turbine Performance, 2nd edn. Blackwell Science Ltd, (2004)
8. Kurzke, J.: Transient Simulations During Preliminary Conceptual Engine Design, ISABE-22011-1321
9. Khalid, S.J., Hearne, R.E.: Enhancing Dynamic Model Fidelity for Improved Prediction of Turbofan Engine Transient Performance, AIAA-80-1083 (1980)

Part B
Preliminary Design

Chapter 1

Engines



Engineering design is how we turn ideas into hardware. Modeling or simulation is used to describe or “capture” the concept & show how a component—and a system—operates before hardware is produced. The “build and test” approach was used in the past and we all know that it is fraught with difficulties, time-consuming, very risky and very expensive. Today’s technology field is fairly level, so the company who can deliver its products most quickly will be most successful. As our mathematical tools and techniques improve, it has become recognized that the simulation and modeling approach is the quickest and the most cost-effective way to get a product to market.

1.1 The Role of Preliminary Design in Systems Studies

Preliminary design is important in a new engine program because many decisions are made which are critical to a successful outcome and the results determine how significant corporate resources are to be committed for many years. Preliminary engine design is where a multitude of technologies and disciplines—many of which have all been taught completely separately at college—are first brought together. This broad technical background enables component models to be assembled to form an engine.

As indicated in Fig. 1.1-1, the skills of an engine designer must include an awareness of the design methods for individual components, a knowledge of thermodynamic cycles to ensure achievement of the overall performance objectives, the ability to assemble the components in a limited geometric envelope, and a familiarity with relevant trade studies to ensure the correct variables are considered and an efficient plan is set up and followed. Moreover, an engine designer must work within both internal (corporate) and external (legislative) design limits.

Following preliminary design, things quickly become very complex and costly, so it is necessary to ensure as early as possible that we are headed down the right

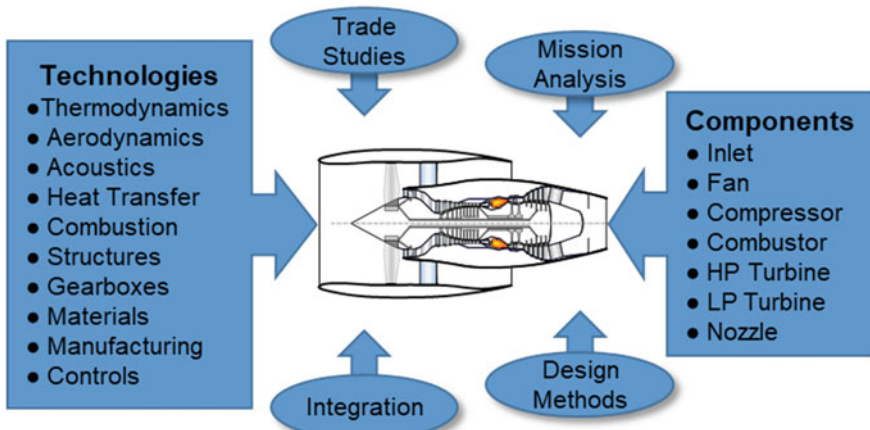


Fig. 1.1-1 Integration of technologies

path before applying more expensive detailed design and analysis techniques. A return to the starting point is both expensive and extremely embarrassing!

One general objective of preliminary engine design is to reduce risk, and this depends on the quality of the tools available and on the skill and knowledge used in applying them. Preliminary design codes are mostly used for trade studies to determine which design candidates should be pursued from what is often a large field of contenders. Some questions to be answered are:

- What does it look like?
- Will it fit?
- Will it work?
- What does it weigh?
- What will it cost?
- Will it be competitive?

We also need a means to assess the level of risk quantitatively. A successful preliminary design is a demonstration of some level of technical readiness. To achieve this, the following, as a minimum, need to be evaluated:

- Engine performance
- Aerodynamic design and component matching
- Flow path characteristics
- Mechanical integrity
- Environmental impact.

Figure 1.1-2 is a rough schematic of the complete design process for a new engine from concept to first engine to test. Preliminary design activities are enclosed in the dark grey envelope, where mission considerations, cycle analysis and engine model construction form an iterative loop. Estimates of weight and

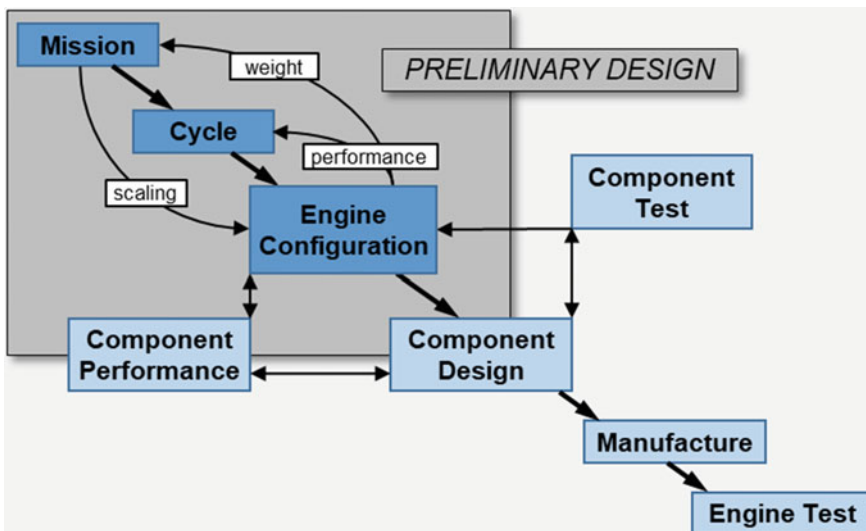


Fig. 1.1-2 Engine design—from concept to manufacture

performance replace earlier assumptions and scaling of the complete new system can occur to meet mission thrust requirements.

Mission analysis is primarily systems-oriented, dealing with Mach number, altitude, thrust and fuel burn. A mission analysis is first carried out, based on a detailed mission profile, assumed characteristics of the aircraft with the engines installed, an assumed take off gross weight (which also includes engines) and values of thrust required from the engine(s) for the mission segments. Experience is used to select a basic engine configuration for the mission. The results of the mission analysis include the fuel burn over each mission segment. A typical trade study is for range (or MTOW) vs SFC and propulsion system weight.

Cycle analysis deals with the conversion of mission conditions to engine parameters, such as local temperatures and pressures. It entails the study of a whole engine, treating each component as a “black box” whose operation may be characterized by a small number of design parameters. The objective is to obtain estimates of performance parameters in terms of design limitations, the flight conditions, and design choices. The parameters are presented in terms of a component map which defines a component’s operation at both the design point and off-design.

Component design and *component performance* go beyond preliminary design as they continue into the detailed design process. Significant improvements to the early versions are communicated back to the design team, depending on the timeline. Component testing is not necessarily related directly to preliminary design but, depending on the importance of a program, component rig tests may occur where significant new technologies have been introduced and relevant findings may

also be fed back to influence performance and operability and may even be used to modify component loss correlations.

The thermodynamic cycle model generates values of the thermodynamic flow properties of interest at every station within the engine, at every engine operating point, and at every point in the aircraft mission. Data is also produced at many other conditions on the extreme edges of the flight envelope that the engine may never see. The outer limits are defined to ensure that there is always an adequate margin of safety built into the final engine design.

The cycle model is used to estimate the overall engine performance as well as that of individual components and their interactions, based on performance maps embedded within the cycle program. Although cycle analysis is never exact, close approximations to engine behavior may be obtained. At this stage of the exercise, the component efficiencies are based on previous experience.

The output from the cycle analysis is an extremely large table of thermodynamic property values—mass flow rates of air, fuel and combustion products, temperatures, pressures, and various overall performance descriptors—and it is from this data that engine hardware must be generated analytically creating the *engine configuration* model. Only a limited number of cycle cases are used to characterize the engine physically and these key points are selected so that a reasonable representation of the mission is taken, with any special segments being included.

To provide meaningful results, designs of every component and the complete engine assembly must be derived to a predefined level of fidelity. This very interesting work of building a complete engine model is the focus of Fig. 1.1-2. As each component takes shape, its performance must be estimated and compared against whatever has been assumed in the cycle analysis. This means that loss models and the ability to estimate efficiencies must be included in the design codes for all the components. The results allow the cycle model to be updated, as implied in the figure. Once an engine weight has been calculated, this may be used to replace the initial guess in the mission analysis for further iteration, together with any associated changes in aircraft performance. If the engines are heavier than was first assumed, more thrust may be needed to power the aircraft, so the engines will be scaled up, re-weighed and re-installed for another analytical “flight” in the mission analysis. This whole process is iterative—gradually converging to an acceptable solution.

All the work described above constitutes *conceptual* or *preliminary engine design* and takes place within the darker shaded box in Fig. 1.1-2. Outside of those activities, in an industrial context, the detailed design of components would follow. This would then be linked to the production of hardware for component rig tests and, ultimately, to engine manufacture and testing. In our consideration of conceptual/preliminary design, we concentrate only on the initial derivation of component and engine hardware designs.

For compressors and turbines, up until the last decade or so, this would have taken us to the definition of the flow path, velocity diagrams for the blades, and blade numbers, but would have stopped short of actual blade profiles. Since that time, however, increased computer power in conjunction with better design codes

and understanding have enabled preliminary design to be extended to airfoil shapes and often to a first cut at predictions of the 3-D flow field. The significance of this is that it significantly reduces the inherent risks in the early phases of a new engine program, allowing the subsequent phases to be pursued with greater confidence.

Preliminary engine design is essentially a part of the overall system study. In the search for an optimum design solution to a specific aircraft mission requirement, many different versions of an engine configuration will be considered and a preliminary design will be carried out for each one.

1.2 Approach and Implementation

Configuration design—building a complete engine model—is summarized in more detail in Fig. 1.2-1. It is during this phase of a new engine program that multiple branches of technology must be brought together and applied simultaneously. The engine model is built up from a library of generic component models that are representative of the appropriate level of technology being considered e.g. current, future near-term, future far-term. Technology levels also often correspond to a year of entry-into-service of the engine under consideration. They might also be designated as *GEN-5*, *GEN-6*, and *GEN-7*, corresponding to different *generations* of technology. Using this notation, *GEN-5* might refer to existing engines whose designs were being replicated or “reverse-engineered” for any number of reasons.

1.2.1 Building an Engine Model

In the preliminary phase of a new engine program, the design tools must be able to deliver the following:

- Construction of models for each component of the system.
- Prediction of its steady-state performance and its interaction with the other components at design point conditions.
- Prediction of steady-state behavior at off-design conditions.
- Prediction of transient behavior.

1.2.2 Component Models

A library of component models is shown in the table on the lower left part of Fig. 1.2-1. Most of these categories contain a whole family of components. For instance, the fan section has a high bypass ratio, low fan pressure ratio, single-stage fan model for use in large subsonic turbofan engines. It would also contain a low

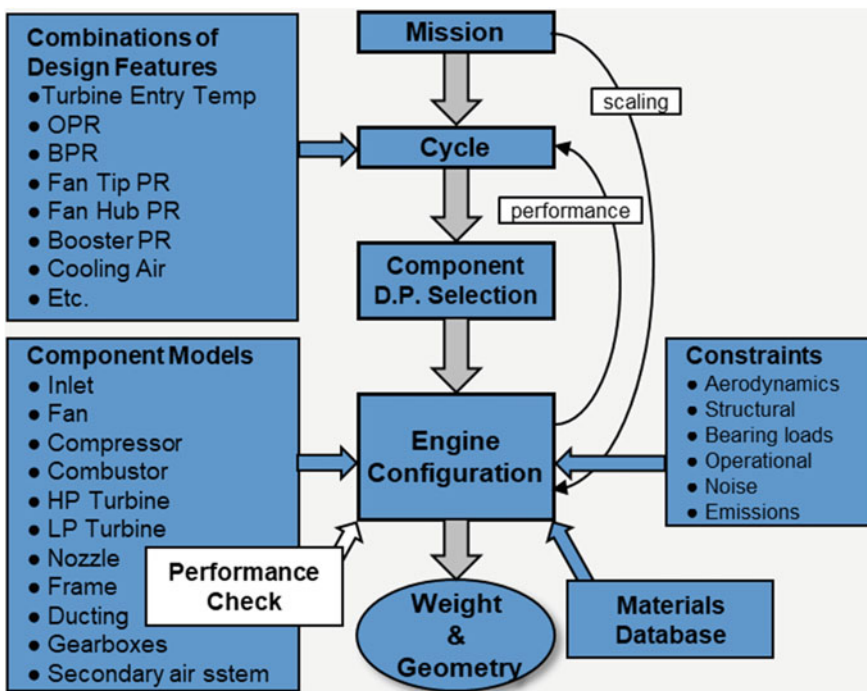


Fig. 1.2.1 Building an engine model

bypass ratio, high pressure ratio multi-stage fan for say a military or supersonic turbofan engine. Each of these sub-categories would ideally be broken down further into fans with different values of fan pressure ratios and rotational speeds, as well as different design styles such as metallic/composite, different inlet radius ratios and blade count. All this would depend on the extent of the available database.

Component models are generic yet specific in terms of technology. They should not contain absolute dimensions but be scalable according to an input value of mass flow rate. Geometry should be specified via non-dimensional parameters, such as inlet radius ratio and aspect ratio. Empirical curve-fitting for the determination of weights should be avoided since such reliance is over-restrictive unless we are designing well within a known conventional range.

It is potentially misleading and therefore quite dangerous to use empiricism for new engine ventures, especially those where extrapolation of empirical rules would have to be done. In contrast, analytical component models should be based on fundamental principles—basic aerodynamics and structural analysis. It is convenient if component models can “stand alone”, since minor adjustments can then be made to say an LP turbine without having to run the whole engine design, and single component studies are often useful and necessary. When built up into an engine, the relevant pieces of information should be passed automatically from one

component model to another. For instance, the rotational speed of a fan should be transferred to the LP turbine that is driving it, with adjustments for different design points if necessary (see Sect. 1.2.5 *Component Hierarchy*).

Component weights or more correctly, component masses, are based on *effective* thicknesses of casings, which account for flanges, ribs, and other non-uniformities. Effective material volume is estimated, and this is then multiplied by the appropriate material density. Blade weights are found from simplified geometric models, with a correction for cooling volumes and passages.

1.2.3 Design Constraints

The risks in a new engine program are high because of the extreme complexity of modern systems and the fact that complex interactions between components and sub-systems preclude the possibility of anticipating completely how the overall system will behave. Preliminary design codes are used in trade studies to determine which candidate designs should be pursued from what is often a large field of contenders. It is important, therefore, that the preliminary design method captures the technological discriminators as accurately and succinctly as possible. The key skill in preliminary engine design lies not in merely assembling the parts within the complete system or engine model, but in doing so under a great many design constraints, both internal and external, as depicted in the *constraints* box to the right of Fig. 1.2-1.

To be competitive an engine must approach the limits of technology in aerodynamics, thermodynamics, structural design, and material properties as well as in many other branches of propulsion systems engineering. Success depends therefore on being able to approach as many of the design limits closely, whilst attempting to satisfy several conflicting requirements. The overall design must also be robust, meaning that a small shortfall in one or more design targets does not lead to exceeding any permissible design limits.

A specific level of technology is applied to an engine design, which defines the design limits. These should be “packaged in sets” to be agreed by all concerned. Any changes to the limits must be communicated by a formal procedure to ensure that all the design groups are working to a consistent standard.

Design constraints fall into two general categories. *Internal design limits* are those set within a company or a design organization. This category contains aerodynamic, thermal and structural constraints. Aerodynamic limits restrict the Mach numbers encountered within ducts and turbomachinery, usually in the interests of improving performance by reducing friction losses. They also impose both upper and lower limits on such features as radius ratios, tip speeds, and exit swirl values from say an LP turbine. Thermal limits such as temperature for the chosen turbine material are used to define the cooling flows. An example of a structural limit is the term AN^2 , which besides being a measure of the rim stress in a

turbine disk, also provides an important and very useful link between the aerodynamics and structural integrity in a turbine for the preliminary designer.

External design limits are those imposed upon a design organization from outside the company. Such restrictions are frequently legislated by national and international bodies, and the most common address protection of the environment. With the huge growth in air transportation over the past sixty years or so, noise attenuation has understandably become critical, particularly at take off and approach. Exhaust emissions make up another important environmental issue, both at take off and at cruise segments of a mission. Different pollutants are targeted for the two mission phases. Legislation will come into force in 2020 for CO₂, classifying aircraft according to their fuel burn during cruise.

During a design exercise, an engineer must be able to keep track of many design parameters simultaneously, ensuring that no prescribed limits are exceeded. In practice—and from personal experience—we all begin by recording observations of the effects of changes on the back of an envelope or even in a design log book. But this approach is only manageable for maybe half a dozen parameters. Beyond this, sooner or later, something (let's say a rotor exit Mach number) will fall through the cracks! Then, after perhaps a week of work, the results are shown triumphantly to the boss, who will say “But what about the rotor exit Mach number?” and the exercise must then be repeated. So, a simple visual representation of where we are relative to all the design limits is essential. In fact, most companies do this in some form or other and we refer to the plots as design envelopes and this topic will be discussed further in Chaps. 2 and 3.

1.2.4 Trade Studies Revisited

A systems study is one in which a few major design parameters are perturbed to determine the optimum combination from many possible candidates. In the case of a turbofan engine, the primary design variables are turbine entry temperature (T₄₁), overall pressure ratio (OPR), fan pressure ratio (FPR), and bypass ratio (BPR).

In a typical systems study T₄₁ and OPR would be held constant, while FPR and BPR would be varied in turn to form a study matrix of maybe twelve points. The activities covered by Fig. 1.1-2 will therefore be repeated twelve times in a systems study, as a candidate engine is designed at each FPR/BPR combination to meet the thrust required at the selected engine design point.

In such a study, not all combinations of fan pressure ratio and bypass ratio make sense. In a mixed flow turbofan, core and bypass exit pressures must be similar ($P_{16}/P_6 \approx 1$), otherwise we get high mixing losses. In a turbofan with separate jet exhaust, we know from theory the optimum ratio of the jet velocities ($V_{18}/V_8 \approx 0.8$). If we introduce these dependencies between FPR and BPR then we have one design parameter less.

Seldom is it possible to predict the results of a preliminary design study, especially for a new type of engine or even just a new version of an established

configuration. The vast number of component interactions often springs surprises, and it is this that makes the work so interesting and a great learning experience.

The engine configuration selected from a design trade study is the one which best meets the aircraft mission requirements. An engine in a subsonic transport aircraft may spend most of its life at cruise conditions, with its major requirement being minimum specific fuel consumption consistent with delivery of a given payload over a certain distance. This could be considered, somewhat simplistically, as a single design point application. In contrast, an engine in a fighter aircraft must be capable of a multi-mission role, which may involve numerous combinations of mission segments, varying from day to day. For each of the above mission types, some of the engine requirements are mandatory, while others may be traded in the interests of overall capability of the aircraft.

Compromise to optimize! The optimization of the overall propulsion system involves a great deal of compromise in the design of individual components. Early questions about any new engine design are “What does it look like?” and “How much does it weigh?” While it is *relative* weights and performance figures that are of immediate interest to the engine preliminary designer (*i.e. is one candidate system lighter or more fuel-efficient than another?*), the demand for absolute accuracy and fidelity in propulsion system modeling still exists and is becoming stronger. This is because of the increasing need to discriminate between the effects of quite subtle differences that are usually present in the leading contenders in a trade study of today’s complex propulsion systems. It is important to have the means of identifying an optimum system design because the ensuing choices and decisions may ultimately be very significant. Risk reduction in any new engine program correlates absolutely with the quality of the results of preliminary design studies.

For each component in any new engine, both aerodynamic and structural requirements must be met, although the function of the component usually dictates where the emphasis lies. If aerodynamics is compromised, the engine performance may be less than desired. If structural integrity is compromised, the engine may fail! Obviously, the latter takes precedence, nevertheless, no stone should be left unturned in the quest for excellence, and therefore both sets of characteristics must be addressed fully.

Expected component lives are usually set in advance, based on maintenance schedules, which are an important ingredient in direct operating costs of the aircraft. If the life of a component is less than the target value, the result could be disastrous. If the life is greater than the target, the component will be too conservative in design, too heavy, and most likely too expensive. While the designer should err inevitably on the side of safety, the competitive marketplace demands narrow design margins, and it is in the navigation of such margins that our preliminary design methods must perform with precision.

Even though preliminary design codes may be very reliable and design limits well-defined, the work habits of individual engineers can affect results significantly. Many years ago, I once did a trade study using a matrix of twenty engines. Time was short and my boss volunteered to do the last one. When the results were plotted

—in various formats—nineteen data points fell on curves that were perfectly smooth, with one outlier! It turned out that, despite the difficulty involved, I had stayed rigidly within the design limit for absolute Mach number at rotor exit. My boss, however, had allowed himself a little leeway... The message here is for consistency *Have one person do it all!*

1.2.5 Component Hierarchy

While it is certainly possible to design an engine by starting at the front—the inlet, and working through to the back—the nozzle, this is inadvisable. There is a better approach that will require less iteration!

Aerodynamically, the HP compressor is probably the most difficult and compressors are very capricious compared to other components. Completely new compressors are quite rare. A great deal of company resources is invested in the design of a new compressor and once a satisfactory design has been established by the component detailed design group, the design is crystallized in a preliminary design model, to be jealously guarded and used with a high degree of respect.

The HP compressor can be said to be the heart of an engine and therefore has highest priority. Once a satisfactory design has been determined, with relatively little adjustment on the part of the humble preliminary designer, this sets the rotational speed for the HP spool and it is sensible to continue by addressing its turbine counterpart. A similar rationale drives the design of the LP spool, which begins with the fan and/or compressor and follows with the LP turbine, again linked through the rotational speed.

The order in which the remaining components are considered can be left to the preference of the designer. Since the frames form the structure and so often define the feasibility of a new engine, it may be convenient to fix them next. Ducts connect all the important stuff, are sized based on limiting friction losses, and are quite numerous, so it is satisfying to make the connections.

In terms of their effect on engine performance, the exhaust nozzle and inlet probably out-rank the turbomachinery, so once the duct areas and locations are known, these two primary components may be designed.

The combustor fits between the HP compressor and HP turbine, so its inlet and exit areas are already known and its length and inclination remain to be determined. The combustor design is completed by defining its internal characteristics.

The remaining significant components or rather collection of components and secondary assemblies, are the *Secondary Air System* and *Accessories*—often not accounted for in a regular preliminary design process. Usually, since accessories do not influence the engine layout or overall geometry, it is safe to estimate their weight as a simple fraction of the overall engine weight, despite earlier warnings about empiricism. Think of a complex high-speed nozzle model which might have its own controls and accessories sub-element. The general sequence is shown in Fig. 1.2-2.

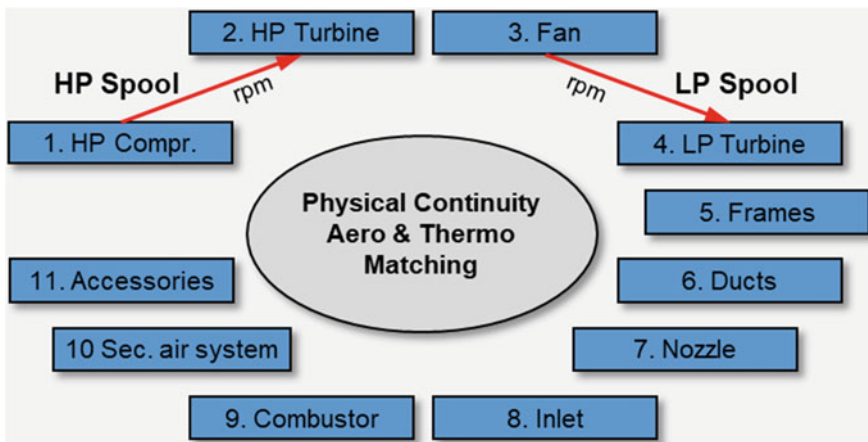


Fig. 1.2-2 Component hierarchy

A new engine component must meet all the demands made of it, but no more because that would lead to extra cost, extra weight and—possibly—extra design time. For components in the engine flow path, aerodynamics governs the external shape or geometry. Structural integrity defines the method of construction, the choice of material(s), and perhaps the internal geometry. However, there are sometimes overlapping areas of interest in such instances as the flexural behavior of fan blades under dynamic load or the details of the cooling passages in turbine blades.

For components or constituent parts outside of the flow path, shape does not necessarily follow function, except in providing strength and endurance, and it is primarily the structural needs that dictate the size of the object and choice of material, with aerodynamics/fluid flow playing a relatively small role.

1.2.6 *The Cycle Design Point*

The immediate objective of cycle analysis is to generate a complete description of thermodynamic gas properties throughout the engine at all the chosen operating conditions. The first cycle case is the *cycle design point*, any additional cycle cases being referred to as *off-design* cases. Outside of this context it is important to distinguish between design and off-design analyses to reconcile our use of the terminology.

For design point analysis, all design choices are still open and controllable, the engine size has yet to be chosen, since usually, a “rubber” engine is designed whose performance is known in specific terms (e.g. thrust per unit mass flow, kN/(kg/s)). Each complete set of design choices results in a different piece of hardware with its own operating conditions.

Design point analysis is much less tedious than off-design, and often provides mathematical optima that can be exploited directly. The combinations of design choices that offer the best performance at each flight condition reveal trends that lead to the best overall solution. On completion of the design point analysis, the type of cycle and possible range of each design choice will have been established. In summary, at the design point, for either the engine or a component, the performance requirements are known, the optimum set of design variables is selected, and the geometry is defined from analysis.

Off-design analysis cannot begin until the design point has been selected, the engine has been sized and the conceptual hardware has been established. Once the design point has been fixed, all other operating conditions become off-design. Then the geometry is known, and values of the design variables are specified; engine conditions, as well as values of performance parameters, may be determined.

The final choice for an engine is based on its off-design characteristics over the entire mission. A winner will be selected from a design trade study because of its balanced behavior over the whole mission and a new engine is seldom designed to match just one of the major flight conditions. An *engine design table* lists all mass flows, total pressures, temperatures at the thermodynamic stations which defined the interfaces between the components. Moreover, it contains all properties that characterize the component operating points like pressure ratios, corrected flow, absolute and corrected spool speeds, shaft power, specific work etc.

Labeling of cycle cases as “design” and “off-design” is significant, firstly, because of component sizing and, secondly, because specification of design conditions sets up points of entry to performance maps for many components. This determines not only the behavior of individual components but ultimately the operability of the complete propulsion system.

1.2.7 *Individual Component Design Points*

To optimize a new engine for its intended mission, an aerodynamic design point should be selected individually for each major flow path component from the available cycle information. The objective is to avoid over- or under-design of any component or assembly. The former would add to the overall engine weight and lead to the excessive consumption of expensive materials and manufacturing resources for both initial supply and replacement, while the latter could contribute to failure, or to inadequate safety margins, at worst. If the whole engine were to be designed at a single mission point, there is a good chance that one or the other would occur, and an optimum solution would not be achieved.

For some components, a single design point cannot define all the aerodynamic and structural requirements and the two facets must be assessed separately and independently, although the combined result will, of course, be captured in the end-product. It is necessary to ensure that we design all components so that every

mission point can be reached, without overdue emphasis on conditions that will be encountered only rarely.

1.2.7.1 LP Compressor

It is necessary to identify and retain the engine cycle case containing the maximum value of corrected inlet flow, and it is customary to use this as the aerodynamic design point of the first compressor. High bypass ratio turbofans of subsonic aircraft usually have the highest corrected flow at end of climb to altitude because there T_2 is much lower than at sea level.

For many engine applications, the maximum value of corrected inlet flow occurs at an engine inlet temperature near to standard day temperature at sea level ($T_2 = 288.15\text{ K}$). In such cases Take Off at ISA sea level static is the preferred cycle design point. Particularly for supersonic applications, the maximum corrected inlet flow will not occur at take off and another mission point should be sought as the design case.

Compressor efficiency drops quickly if the corrected speed is raised above the design value. Furthermore, the increase of corrected flow with corrected speed diminishes. The aerodynamic design point of any compressor must be selected such that the highest corrected flow required by the flight mission is achievable with reasonable efficiency. So, we can select the aerodynamic design point of the compressor from the list of points in the engine design table. It is worth emphasizing that the *aerodynamic design point* is selected to optimize the performance of the turbomachinery blading and to provide good specific fuel consumption throughout the mission.

The *mechanical design point* is selected to guarantee structural integrity throughout the mission, by considering the most severe structural operating conditions. In commercial engines for subsonic aircraft these are encountered during Take Off, Mach 0.25 on a day with flat rating outer air temperature, e.g. ISA + 15 °C.

There is a significant difference in LPC corrected speed between the aerodynamic and the mechanical design point. This is due to the change from the low engine inlet temperature at end of climb (high $N_L/\sqrt{\Theta}$) to that during hot day Take Off (moderate $N_L/\sqrt{\Theta}$). Pressure ratios, temperature ratios and corrected mass flow can differ significantly between the two design points.

1.2.7.2 HP Compressor

The operating line of the HPC in its map is short, the non-dimensional operating conditions of the aerodynamic and the mechanical design point are much nearer to each other than in the LPC map. There is no big difference between the non-dimensional parameters of the aerodynamic and mechanic design point.

1.2.7.3 Combustion Chamber

Design criteria of a combustion chamber differ from those of turbomachines. Mach numbers play a minor part, high altitude relight and high absolute pressure differences from the combustion chamber and its surrounding (bypass or engine bay) constitute the problem.

1.2.7.4 HP Turbine

The pressure ratio of the gas generator turbine remains constant if another turbine or a choked nozzle follows downstream. Corrected speed varies little, the operating point in the map is essentially fixed. Whatever the mechanical design point is, the aerodynamics of the cycle design point is applicable.

For the turbine, structural integrity at the condition with highest turbine entry temperature is of paramount concern. This is usually at take off but for supersonic aircraft may occur at high speed climb. It is taken care of primarily by good design of the disk, means of blade attachment and cooling of all parts. It has little to do with blade profile, numbers, spacing, etc. or with slightly broader characteristics such as stage loading coefficient and flow coefficient. These parameters ultimately define performance and are fixed by the aerodynamic design point. They may be chosen independently of structural requirements, and common sense tells us that they should be.

1.2.7.5 LP Turbine

The length of the operating line in the map of an LPT depends on the downstream component. If this is a choked nozzle (turbojet or low bypass ratio turbofan) then—like in the HPT—the pressure ratio is constant, and all operating points collapse in a narrow map region. There is no change in the aerodynamics in the upper power range.

In high bypass ratio engines, the nozzle pressure ratio during many flight phases is less than critical ($P_8/P_{amb} < 1.86$). The LPT pressure ratio varies, we get an operating line along which the non-dimensional aerodynamic parameters change. Nevertheless, the aerodynamics of the mechanical design point will not differ much from those at the cycle design point.

Both the temperatures and the circumferential speed of LP turbines in conventional turbofans are moderate and cooling is not required except sometimes for the first stage. Thus, the mechanical design of a LPT is less challenging than that of the HPT. The aerodynamic design can be optimized nearly irrespective of mechanics.

However, when we introduce a gearbox between the LPT and the fan, the mechanical design especially of the last LPT stage becomes challenging and aerodynamicists must show consideration for mechanics.

The centrifugal stress σ of a blade at its root is

$$\sigma = \frac{F}{A_h} = \rho\omega^2 \int_{r_h}^{r_t} \frac{A_{blade}(r)}{A_{blade,h}} r \, dr \quad (1.2-1)$$

ρ is the density of the material, ω the angular speed and r stands for radius between hub and tip. With a linear decrease of cross-sectional area, it can be shown that the blade root stress for any hub/tip radius ratio will not exceed the value

$$\sigma_{\max} = \frac{\rho\omega^2 A}{4\pi} \left(1 + \frac{A_{blade,t}}{A_{blade,h}} \right) \quad (1.2-2)$$

In this equation A is the turbine exit area, and since N is proportional to ω , AN^2 is an upper limit for the blade root stress. The allowable AN^2 value can be increased by using a material like titanium aluminide (which has low density) and extreme blade taper $A_{blade,t}/A_{blade,h}$ (which affects aerodynamics negatively).

The aerodynamic design point of a LPT for a turbofan with gearbox should be the same as the mechanical design point. That makes compromises between aerodynamicists and stress engineers easier.

1.3 Engine Development—The Role of Performance

Performance as an engineering discipline accompanies the engine throughout its entire life, from preliminary design, detailed design, the first engine to test, entry into service, performance monitoring, maintenance, and repair. Most preliminary design studies never become reality and just end with a report. Seldom is the decision made to launch the project and make commitments to a customer. Guaranteed values for thrust and SFC at important operating conditions are among these.

Figure 1.3-1 describes the basic workflow for the performance department of an engine manufacturer from preliminary design to production engine. The aircraft mission defines the requirements which lead (as result of conceptional engine design studies) to the preliminary engine performance model, comprised of an *engine design point* and off-design performance characteristics of all engine components. The compressor and turbine performance maps are either calculated or scaled versions of maps from similar turbomachines.

An *engine design table* is calculated—which is part of the engine performance specification—at the outset of the development program. This table contains the cycle details for important operating conditions which originate from the missions the aircraft is designed for. Among them are all flight cases for which thrust and SFC and possible other features are guaranteed to the customer. The table also

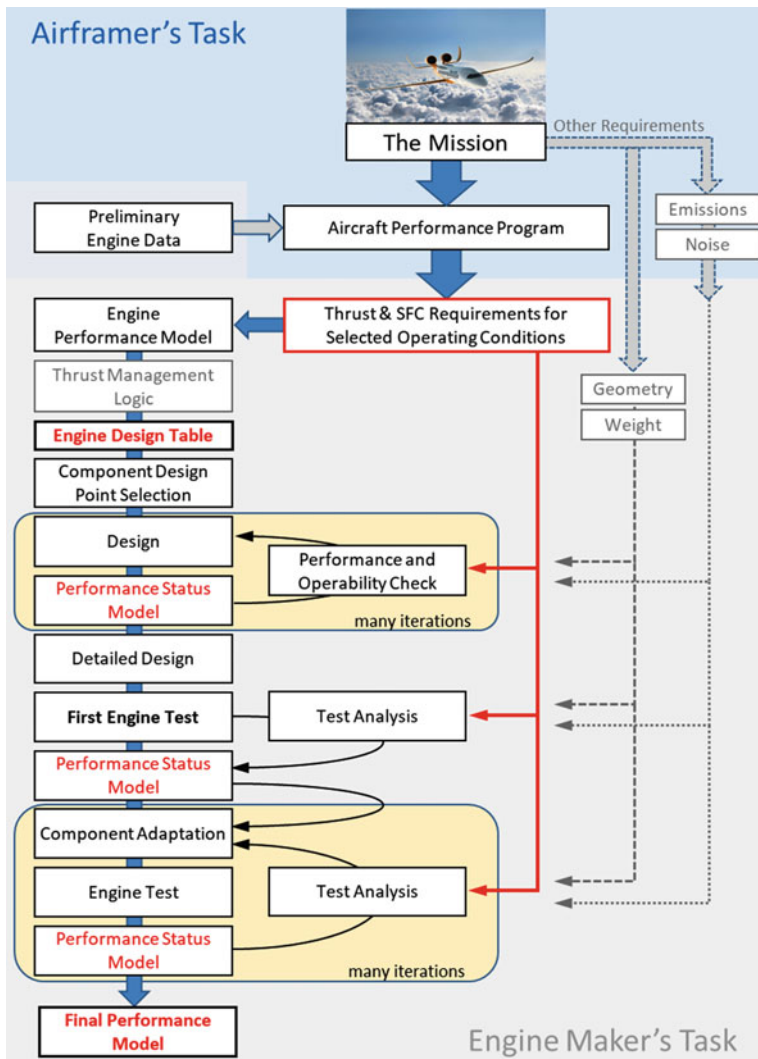


Fig. 1.3-1 Engine performance workflow (aircraft picture © Bauhaus Luftfahrt e.V.)

contains extreme operating cases, for example the conditions at the corners of the flight envelope.

Before the engine design table can be calculated, a preliminary thrust management system must be chosen. The flat rating temperature (ISA + x degree) is the corner stone of the schedules (whether engine pressure ratio or N_L) for *Take Off*, *Max Continuous*, *Max Climb* of an engine for a commercial airliner. Preliminary schedules for *Flight Idle* and *Ground Idle* are indispensable.

The thrust management of military engines employs schedules for a temperature in the hot part of the engine as function of engine inlet temperature T_2 and flight Mach number. The hot end temperature might be the HP or LP turbine inlet temperature, a metal temperature measured with a pyrometer or the exhaust temperature. Moreover, there might be schedules for nozzle area as functions of, for example, corrected fan speed and flight Mach number.

The chosen thrust management system makes sure that all thrust requirements of the aircraft are fulfilled in a consistent manner. The engine will deliver exactly the required thrust at the most demanding flight conditions, at other points in the flight envelope there might be more thrust available than the aircraft designer directly requests. This is unavoidable because the thrust characteristic of a gas turbine differs from that what an aircraft typically needs.

The first point in the design table for a new engine should be the *cycle design point*. The calculation of this point yields the engine geometry implicitly, especially the turbine flow capacities and nozzle areas. It is advantageous to call the spool speeds (in rpm) for this operating point 100%. The turbine flow capacities as well as the nozzle areas should be declared also to be 100%, the nominal values. This avoids communication problems and misunderstandings between the various specialists—provided the 100% values are never changed during the whole engine life, including derivatives. All other operating points in the design table are calculated as off-design points.

Component designers may select any point from the engine design table as their *component design point*. There is no need to choose the *cycle design point*. When quoting percentages to people outside of the component specialist community, make sure that the reference value is that of the cycle design point.

The next step in the engine development process is the design of the engine components. Compressor and turbine aerodynamicists may generate new maps based on the more detailed engine geometry and other boundary conditions. A rig test may provide a measured compressor map which surely will differ from that used for calculating the design table. Refinement of the engine design may also lead to revisions of other component performance assumptions. The consequence of all this: Engine performance is affected and differs from the design aim as given by the engine design table. A performance synthesis considering the most recent knowledge about the component performances is called a *Status Model*.

Running this model with the operating conditions of the engine design table shows where you are potentially in trouble with respect to the engine design aim, especially the guaranteed performance. Use the *Status Model* to determine what can be done to come back on track. If you diagnose a surge problem, you might find that an increase of a turbine flow capacity solves the problem more cheaply than the re-design of the compressor.

A new performance status model should be created whenever new information from the component designers becomes known. The cycle design point remains unaltered; the new information modifies the performance characteristics of one or more components. The effect of engine modifications is found with an off-design calculation.

The first engine test is a highlight of any new engine development program. The measurements will certainly deviate from the pre-test predictions made with the latest performance status model. Model-based test analysis helps with understanding what happens in the engine and for generating a new performance status model.

Employ the new status model to define any engine modifications necessary for achieving the guaranteed performance or to relieve any problem which might show up. Repeat the test, update the status model, modify whatever is adequate...

At the end of the engine development a final performance model ensues. The guaranteed performance is (hopefully) achieved, but there are many differences in the details between the engine design table and the final performance status model. However, that does not matter.

Chapter 2

Compressors



2.1 Function, Environment, and Basic Efficiency

2.1.1 Introduction

The compression system in a gas turbine engine generates the pressure ratio required by the engine cycle as efficiently as possible. The compression process is the first major part of the Joule respectively Brayton cycle, in which power is applied to the working fluid by the rotating compressor blades. A compressor stage consists of a moving rotor blade followed by a stator or vane. The blade is driven by the shaft, using power from the turbine rotor blades. In the absolute frame of reference, work is done on the air, increasing its kinetic energy and raising its total pressure by increasing the dynamic head. In the stator, the air is turned towards the axial direction, and the effective flow area is increased. This causes the flow to decelerate and the corresponding reduction in velocity means that some of the total pressure increase is converted to higher static pressure. Not all the rotor work appears as increased total pressure because there are losses in the imperfect compression process through the compressor rotor blade passages. Similar losses in the stator result in a slight drop in total pressure there.

Not all the air at compressor inlet reaches the combustor because bleed air is taken from intermediate stations for various operational purposes. Examples of these are cooling air for the turbines and exhaust system in an augmented engine, cabin air for passenger comfort and de-icing air for the inlet and nacelle. Bleed air is also used to heat components such as the turbine rear frame to reduce thermal gradients and improve component life. It is also used to pressurize the cavities upstream or downstream of the disks to offset the axial loads generated by the blades and vanes to relieve axial bearing loads, to pressurize certain cavities to seal and prevent ingestion of hot gas, to purge certain systems to remove debris or for local cooling, to cool oil supplies, and to provide tip clearance control for turbine blades. It may be vented overboard to improve engine starting.

It is worth noting at this point, that any diversion from the primary engine flow path of air that has been worked on by the compressor is a penalty to the cycle. Optimum use of this air is to allow it to reach the combustion chamber and attain the maximum cycle temperature, having been mixed with fuel. To minimize the penalties associated with bleed air, it is extracted from the compressor as early as possible, having achieved the pressure needed for its intended purpose. For instance, only air taken from the compressor exit has the pressure needed for it to be used as HP turbine cooling air because it must be expelled from the HPT blade surface, where the local pressure is only a little less than compressor delivery. Even though compressor delivery air may be very hot (about 950 K), in a modern engine, there is sufficient difference between that and the blade metal temperature to result in effective cooling in a turbine. In contrast, air from the early compressor stages or from the fan exit can be used to heat the nacelle leading edge (It is just hot enough.) and ventilate the cabin (It is still cool enough.).

Figure 2.1-1 shows an axial compressor with constant tip diameter, whose flow path is converging. All compressors have a convergent flow path, which enables the axial component of the air velocity to be kept roughly constant, despite a reduction in the volumetric flow rate and an increase in density (mass flow rate = $\rho A V_{ax} = \text{constant}$). The retention of a roughly-constant ratio of axial velocity to blade speed is so that sensible velocity diagrams—hence air and metal angles—may be maintained for sequential stages. In the early years of axial compressors, repeating a stage to form a multi-stage machine meant that a good stage design could be reused by simple scaling, and this saved additional laborious design effort. The axial air speed can be controlled simply by varying the area of the flow path. This is independent of how the circumferential velocities change—the method by which work is done on the air by the compressor blades. The axial and circumferential effects are combined in velocity diagrams and we shall examine their interaction in Sect. 2.2.

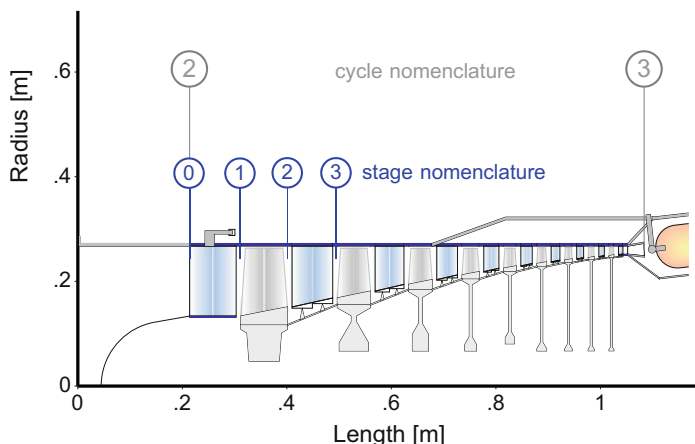


Fig. 2.1-1 A multi-stage axial compressor

For a perfect gas, the specific work (work per unit mass) of the compressor stage in Fig. 2.1-1 is expressed by

$$\Delta H_{1-3} = C_P \Delta T_{1-3} \quad (2.1-1)$$

No work is done in the inlet guide vane, so $T_1 = T_0$. This relation is usually sufficiently accurate for real gases in gas turbine engines if a mean value of C_P is used for the process.

The fluid mechanics through a compressor stage can be traced in Fig. 2.1-2, which shows the compression process in an enthalpy (h)—entropy (s) diagram. Starting at stagnation condition 1, the rotor blade turns the air towards the axial direction and accelerates it to stagnation condition 2 in the absolute terms. Work is done on the air, so its enthalpy increases to $h(T_2)$ and its pressure to P_2 . Static properties change from those at status s1 to those at s2. When static pressures, P_{s2} and P_{s3} , are considered, the increase in kinetic energy in accelerating the flow from V_1 to V_2 in the absolute frame of reference can be seen from the vertical intervals that represent the respective kinetic energies, $\frac{1}{2}V_1^2$ and $\frac{1}{2}V_2^2$. This contrasts with the associated deceleration of the flow in the relative frame. The air decelerates through the vane from status 2 to 3, turning towards the axis. The kinetic energy emerging from the stage, $\frac{1}{2}V_3^2$, is similar in magnitude to that at stage entry, $\frac{1}{2}V_1^2$. The stage work—the change in specific enthalpy from station 1 to station 3—is also indicated, and this corresponds to the expression in Eq. (2.1-1) above. All these features can be associated with the velocity diagram, presented later in Sect. 2.2.

Work from the rotor blades is done usefully in compressing the working fluid and wastefully in overcoming various losses. The efficiency of a compressor is the ratio of *ideal* and *actual* work transfers. Since fans and compressors are essentially adiabatic devices (no heat transfer), the *ideal* (frictionless or reversible) process is *isentropic* in all cases (Note: *isentropic* = *reversible* + *adiabatic*). This is particularly true at steady-state conditions, where conditions have stabilized thermally. Performance may then be quantified in terms of *isentropic efficiency*, usually expressed in terms of stagnation conditions. The use of stagnation conditions (expressed here by properties without a suffix) means that any changes due to kinetic energy effects are accounted for intrinsically. Any increase in entropy or lateral shift across the h-s diagram corresponds to a departure from a (vertical) isentropic process, so the quality of the compression can be determined roughly from the slope of the line. Various forms of thermodynamic efficiency are apparent in Fig. 2.1-2.

Total-to-total isentropic compressor stage efficiency is given by

$$\eta_{is} = \frac{\text{ideal enthalpy rise}}{\text{actual enthalpy rise}} = \frac{h(T_{3is}) - h(T_1)}{h(T_3) - h(T_1)} \quad (2.1-2)$$

Regardless of the engine application, compressor efficiency is always important to the engine cycle and to the fuel burn. Useful compressor work—indirectly represented via the pressure ratio—is what we get; temperature ratio is what we

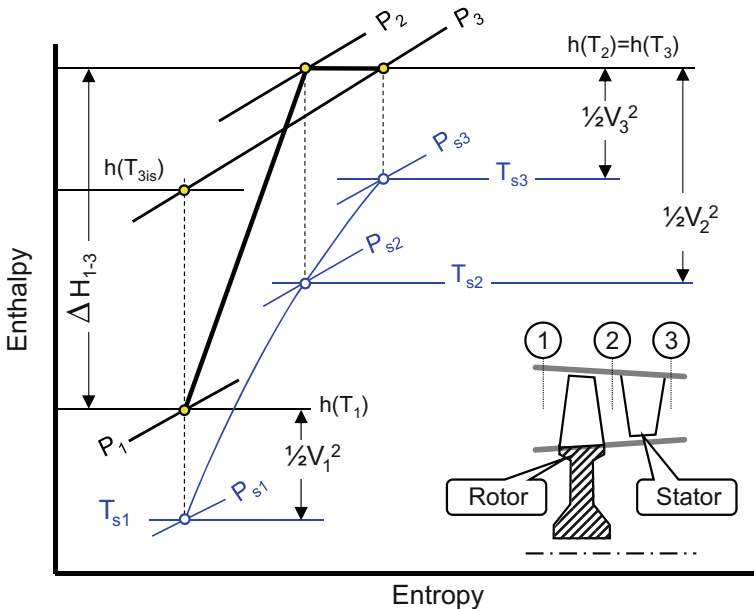


Fig. 2.1-2 Single-stage compressor process in an enthalpy-entropy diagram

pay! In an aircraft engine, the pressure ratio is a fixed requirement and sufficient power is generated by the turbine to drive the compressor and overcome bearing losses. This determines the compressor temperature ratio via the efficiency. High compressor efficiency means that less work must be taken from the turbine so that there is either more energy available for thrust or less fuel may be burned. A quick sketch of an $h-s$ or $T-s$ diagram can often tell us how much we could gain by improving the aerodynamic design for a compressor.

Achieving the required exit pressure is made more difficult than it would be ideally because of the inherent pressure losses. Therefore, in the real process, a temperature ratio greater than ideal must be accepted. Conveniently, the actual pressure rise may be related to the ideal temperature rise, while the actual temperature rise is a measure of the work done. Simple logic tells us which is in the numerator and which is in the denominator in the expression for efficiency, because one is smaller than the other and efficiency is invariably less than unity! This is a useful mnemonic in deriving Eq. (2.1-2) without looking it up.

If we assume a perfect gas and use a constant average value of C_P for the compression process, the isentropic efficiency may be expressed in terms of actual and ideal total temperatures.

$$\eta_{is} = \frac{\text{ideal temperature rise}}{\text{actual temperature rise}} = \frac{T_{3is} - T_1}{T_3 - T_1} \quad (2.1-3)$$

Dividing through by the inlet total temperature (T_2) results in

$$\eta_{is} = \frac{\frac{T_{3is}}{T_1} - 1}{\frac{T_3}{T_1} - 1} \quad (2.1-4)$$

The ideal total temperature ratio in the numerator may be expressed in terms of the actual total pressure ratio to define the turbine isentropic efficiency in terms of actual conditions, to give us

$$\eta_{is} = \frac{\left(\frac{P_3}{P_1}\right)^{\gamma-1/\gamma} - 1}{\frac{T_3}{T_1} - 1} \quad (2.1-5)$$

2.1.2 Limitations of Isentropic Efficiency

So far, we have considered the isentropic efficiencies of compressors as being constant, without regard to the magnitudes of the corresponding changes in pressure and temperature. In practice, as the design pressure ratio increases, the overall isentropic efficiency for a compressor tends to fall. Let us examine what happens to the performance of a multi-stage compressor—for stages of similar quality—as the overall pressure ratio increases. The situation is represented in a T - s diagram in Fig. 2.1-3:

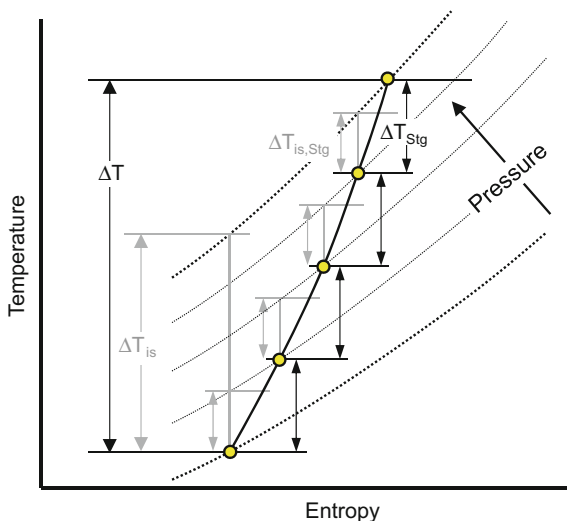


Fig. 2.1-3 Polytropic efficiency in a multi-stage compressor

If we denote the isentropic efficiency of a single compressor stage by η_{Stg} and sum across the total number of stages, the actual overall temperature rise (ΔT) can be written as

$$\Delta T = \sum \frac{\Delta T_{is,Stg}}{\eta_{Stg}} = \frac{1}{\eta_{Stg}} \sum \Delta T_{is,Stg} \quad (2.1-6)$$

However, by definition

$$\Delta T = \frac{\Delta T_{is}}{\eta_{is}} \quad (2.1-7)$$

Therefore, combining (2.1-6) and (2.1-7),

$$\frac{\eta_{Stg}}{\eta_{is}} = \frac{\sum \Delta T_{is,Stg}}{\Delta T_{is}} \quad (2.1-8)$$

By considering the changes in ideal temperature in Fig. 2.1-3, it may be seen that

$$\sum \Delta T_{is,Stg} > \Delta T_{is} \quad (2.1-9)$$

because the vertical distance between lines of constant pressure increases as entropy increases. It may be concluded, firstly, that

$$\eta_{is} < \eta_{Stg} \quad (2.1-10)$$

and, secondly, that the difference between them will become greater as the overall pressure ratio and hence the number of stages are increased. The reason for this is that any increase in temperature above the ideal value means that more work is required to achieve the required pressure ratio, a condition also known as the *pre-heat effect*!

2.1.3 Polytropic Efficiency

The difficulty in making equitable comparisons between different compressors and turbines led to the concept and the use of small-stage or polytropic efficiency. Polytropic efficiency η_{pol} is defined as the isentropic efficiency of a small or elemental stage in a compression or expansion process such that it remains constant over the complete process. Although we do not do so here, the frequent use of the suffix ∞ is a reference to the fact that the overall process is split up into an infinite number of infinitesimal processes each of which can be made isentropic.

For a compression it can be stated that

$$\eta_{pol} = \frac{dT_{is}}{dT} = \text{constant} \quad (2.1-11)$$

But for an isentropic process

$$\frac{T}{P^{\frac{1}{\gamma-1}}} = \text{constant} \quad (2.1-12)$$

and this can be written in differential form as

$$\frac{dT_{is}}{T} = \frac{\gamma-1}{\gamma} \frac{dP}{P} \quad (2.1-13)$$

Substituting for dT_{is} from (2.1-11) results in

$$\eta_{pol} \frac{dT}{T} = \frac{\gamma-1}{\gamma} \frac{dP}{P} \quad (2.1-14)$$

With η_{pol} constant, if we integrate between conditions 1 and 3, which by convention are our start and finish points for a compression process, we obtain

$$\eta_{pol} = \frac{\ln(P_3/P_1)^{\frac{1}{\gamma-1}}}{\ln(T_3/T_1)} \quad (2.1-15)$$

This is the form needed if polytropic efficiency is to be calculated from measured quantities. A more explicit statement is

$$\frac{T_3}{T_1} = \left(\frac{P_3}{P_1} \right)^{\gamma-1/\gamma\eta_{pol}} \quad (2.1-16)$$

If the exponent of the pressure ratio is rewritten in the following form

$$\frac{\gamma-1}{\gamma\eta_{pol}} = \frac{n-1}{n} \quad (2.1-17)$$

Equation (2.1-16) takes the familiar form of the relationship between P and T for a polytropic compression process, namely

$$\frac{T_3}{T_1} = \left(\frac{P_3}{P_1} \right)^{\frac{n-1}{n}} \quad (2.1-18)$$

The definition of η_{pol} signifies that the non-isentropic process under discussion is polytropic—and this is the origin of the term *polytropic efficiency*. $(n-1)/n$ is

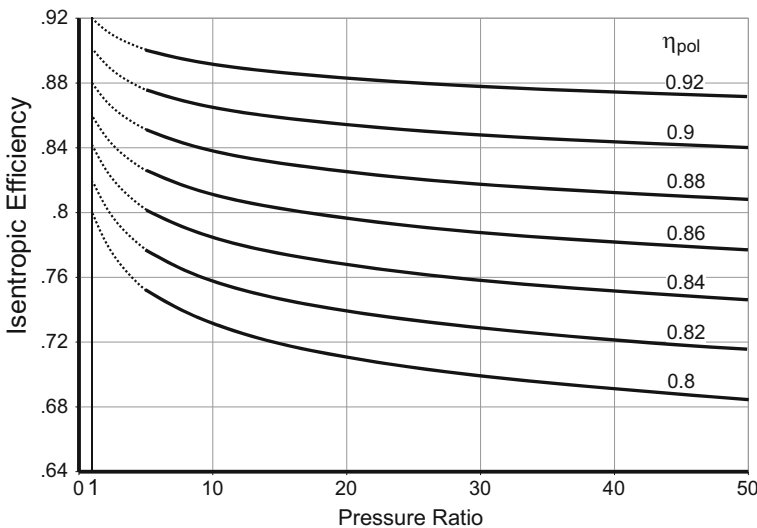


Fig. 2.1-4 Isentropic efficiency versus pressure ratio over a range of polytropic efficiency in a compressor

known as the polytropic index and may be used in place of the isentropic exponent to relate gas properties when *polytropic efficiency* has been specified.

The relationship between isentropic efficiency (η_{is}) and polytropic efficiency (η_{pol}) for a compressor may finally be written as

$$\eta_{C_isen} = \frac{T_{3is}/T_1 - 1}{T_3/T_1 - 1} = \frac{(P_3/P_1)^{(\gamma-1)/\gamma} - 1}{(P_3/P_1)^{(\gamma-1)/\gamma}\eta_{pol}} \quad (2.1-19)$$

The results shown in Figs. 2.1-4 and 2.1-5 have been calculated with GasTurb for dry air and 288.15 K compressor inlet temperature.

2.1.4 Additional Operational Functions

The volumetric flow rate determines the through-flow velocity and hence the air angles incident on the vanes and blades. Since a compressor runs often at conditions other than those it was designed for, any departure from its intended role by an early stage may lead to difficulties in subsequent stages. Typically, this happens at engine start-up, where at rotational speeds much lower than the design value, the compression is also low. This means that the later stages receive air at a lower density, a higher axial velocity and a lower swirl angle. The compressor may surge or be unable to start.

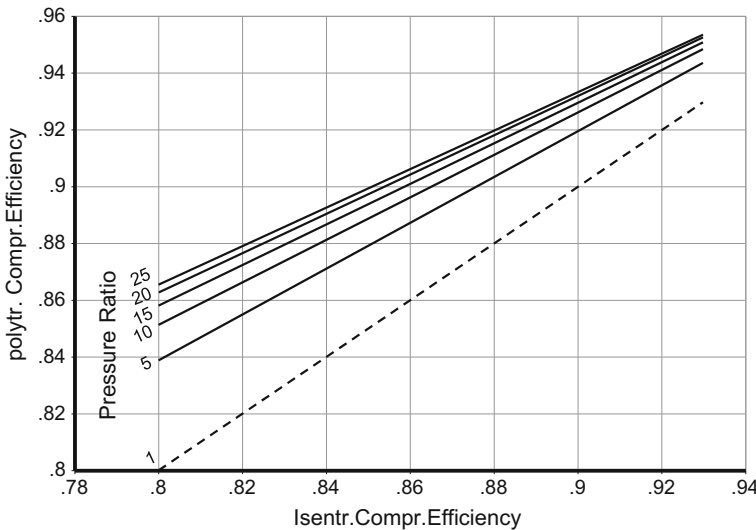


Fig. 2.1-5 Variation of polytropic efficiency with isentropic efficiency for a range of pressure ratios

One remedy for this is to bleed air from the annulus from some of the early stages. This can be done sequentially. A bleed schedule is set up based on a measurable parameter such as rotation speed. Sometimes a large fraction of the primary stream must be removed temporarily to allow the compressor to operate continuously with a satisfactory stall margin.

Variable stators may also be used to alleviate starting problems. The stagger angles of the inlet guide vanes and possibly later stator rows can be scheduled so that the throat area is increased at low rotational speeds. Much attention must be paid to stage matching under these circumstances.

Multiple spools, where the engine core runs much faster than the LP system also provide a solution in large turbofan engines. On turbojet engines, a variable nozzle may be used to control the compressor operating line.

2.2 Velocity Diagrams

2.2.1 Introduction

Figure 2.2-1 shows a section through a compressor stage. An inlet guide vane is included for completeness, although that usually appears only in a first stage and is used either to control the flow rate, to optimize the incidence into the first rotor blade or to reduce the inlet relative velocity. To understand vanes and stators, we use the absolute frame of reference but for rotors we use the relative frame of reference. In relative and absolute frames of reference respectively, the flow

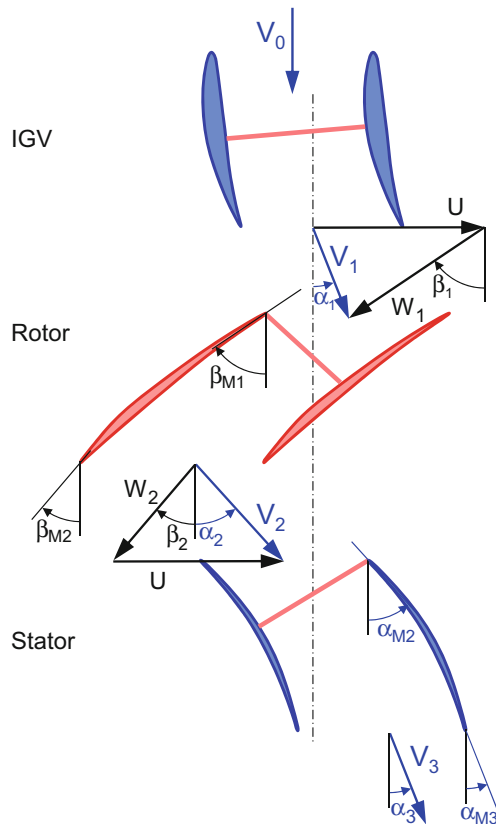


Fig. 2.2-1 Compressor airfoil section

decelerates through blade and vane passages by being turned towards the axial direction. In contrast, the flow accelerates through the IGV passage, being turned away from the axis; the IGV passage is a nozzle rather than a diffuser.

The work done on the air by a compressor stage was defined in thermodynamic terms in Eq. 2.1-1. However, we cannot design vanes and blades from the thermodynamics alone because no information about blade and vane shapes is available there. The shapes of the rotors and stators are determined initially from flow inlet and exit angles, which essentially define the camber line. For a rotor blade, the inlet metal angle matches the relative inlet flow angle; the exit metal angle is equal to the relative exit flow angle. For a stator, the inlet metal angle is approximately equal to the absolute inlet flow angle; the exit metal angle follows from the turning needed to align the flow with the downstream rotor leading edge.

The work done per unit mass flow on the air in a compressor stage (ΔH_{Stg}) is equal to the change in angular momentum. If we refer to Fig. 2.2-2 and stay in the

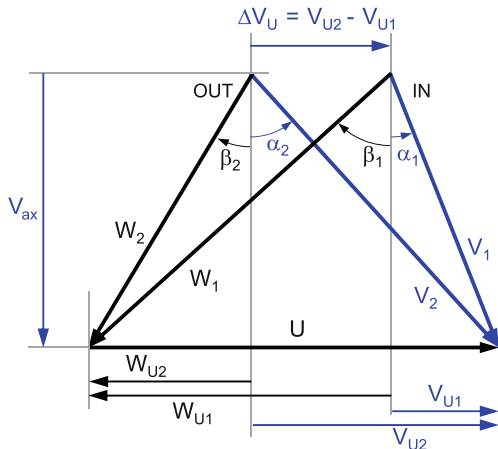


Fig. 2.2-2 Compressor velocity diagram

relative frame, we see that this is given by the product of the blade speed and the difference between the relative swirl velocities at inlet and exit, namely

$$\Delta H_{Stg} = U(W_{U1} - W_{U2}) \quad (2.2-1)$$

Since the swirl velocity usually does not change direction in a compressor and the inlet and exit values have the same sign, their magnitudes are subtracted, and this is illustrated clearly by the vectors in Fig. 2.2-2. It can also be seen there that the same result is obtained when the absolute swirl velocities are used, so we may also write.

$$\Delta H_{Stg} = U(V_{U2} - V_{U1}) \quad (2.2-2)$$

The importance of a sign convention for turning angles and swirl velocities will be discussed in the next section.

If we assume that the axial velocity is kept constant by contraction of the annulus, so that \$V_{ax1} = V_{ax2} = V_{ax}\$, we can express the stage work in terms of either the absolute or relative flow angles using Fig. 2.2-2, as

$$\Delta H_{Stg} = U V_{ax}(\tan \alpha_2 - \tan \alpha_1) = U V_{ax}(\tan \beta_1 - \tan \beta_2) \quad (2.2-3)$$

Since the blade metal angles are defined by the relative angles of the gas, the second part of Eq. (2.2-3) is more useful to us. It may be seen that we need high blade speed, high axial velocity of the working fluid and high deflection in the rotor blades to obtain a high stage work and a minimum number of stages.

To a practiced eye, a velocity diagram contains maybe ninety percent of everything we would ever wish to know about a compressor stage! Neither tables nor plots of blade characteristics have the same impact or carry the same clear

message, especially when it comes to span-wise variations of stage characteristics in a single stage and trends through multiple stages. Unfortunately, incidence and deviation are not represented, they are discussed in the following sub-section.

2.2.2 Sign Convention for Angles and Circumferential Velocities

In quantifying and establishing the direction of both flow angles and metal angles, a sign convention is needed. The concept of positive flow velocity in the direction of an engine axis is accepted universally. Negative values tell us immediately that flow reversal—usually an undesirable phenomenon—has occurred! When it comes to tangential motion, the direction of rotation is extremely important; there have been instances in industry, where communication between compressor and turbine offices has not been crystal clear and whole blade sets have been manufactured as the mirror image of those intended!

We shall measure flow angles or swirl angles, relative to the axial direction or meridional plane in a compressor rather than with respect to a transverse plane. But then, which direction is positive? Frequently, the sign of angles is omitted, and common sense is used to evaluate quantities such as flow turning through a blade row or the relationship between flow inlet angle and incidence. Turbomachinery may be designed without a formal sign convention for flow swirl angles and airfoil metal angles; absolute values are used in the context of either a blade or a vane by a designer who knows what to expect. That's fine for hand calculations, especially if a picture exists, but for setting up a spreadsheet or writing a piece of mean line code, it is best if the engineer is left out of the loop and angle calculations are taken care of automatically by trigonometry and algebra.

Frequently, radial motion can be neglected since magnitudes of both velocity and angles are small, but nevertheless, acknowledgment of radial components is essential for consideration of radial equilibrium. Fortunately, the definition by which positive values of radial velocities and angles correspond to motions in the outward radial direction is an obvious choice and needs no further explanation.

In calculating flow and metal angles through a stage or a series of stages, where, for example, the inlet angles switch from one side of the axial direction to the other, a sign convention is valuable. A good approach for tangential velocities and angles is to adopt a *positive in the direction of blade rotation* sign convention. Then, in Fig. 2.2-1, the gas enters the inlet guide vane axially ($\alpha_0 \approx 0^\circ$) at a modest value of absolute velocity V_0 , is accelerated and turned—but only slightly—through the IGV passage and exits at a somewhat higher absolute velocity V_1 and a modest positive swirl α_1 . The rotor leading edge metal angle β_{M1} is negative and the relative inlet swirl angle β_1 —which aligns roughly with the blade—is also negative.

Since the turning through the blade is limited by the level of diffusion that can be tolerated, the relative exit swirl from the blade β_2 is also negative, the flow having

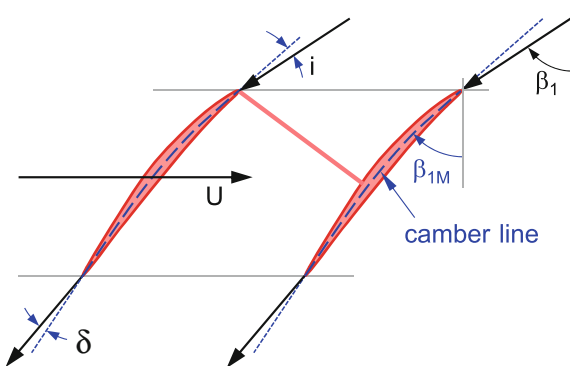


Fig. 2.2-3 Incidence and deviation in a compressor blade

been turned at most to the axial direction. Since the flow has turned from a certain negative swirl angle to a smaller negative swirl angle, the relative turning angle is positive, as indicated in Fig. 2.2-2.

We all know positive or negative incidence when we see it! Traditionally, incidence is interpreted as positive for both blades and vanes when the flow approaches beneath the camber line, i.e. onto the pressure side of the airfoil, as in Fig. 2.2-3.

Blade incidence is defined by:

$$i_{blade} = \beta_{M1} - \beta_1 \quad (2.2-4)$$

Note that in Fig. 2.2-3, both β_1 and β_{M1} have negative values.

As the pressure side of a vane usually faces against the direction of rotation of the blade, both α_1 and α_{M1} are positive and the definition of vane incidence is given by

$$i_{vane} = \alpha_1 - \alpha_{M1} \quad (2.2-5)$$

It should be noted that the sign convention may vary from one engine company to another and from one software vendor to another, so we need to know exactly what we are dealing with in any specific situation!

In almost all compressors, the angle of the flow at a blade or vane trailing edge is not the same as the metal angle. The angle by which the flow apparently fails to follow the blade camber is known as deviation, δ . Although not shown explicitly in velocity diagrams, deviation is still accounted for, since velocity diagrams correspond to the turning angle that the flow actually undergoes rather than blade or vane camber. This does not imply that the flow fails to follow the suction surface of the blade because the *average* exit flow angle is used to define deviation, and this is also used to determine work.

Deviation is due predominantly to inviscid effects, because the flow must adjust itself to the elimination of any transverse pressure difference before the trailing edge

is reached. This can only be achieved by a reduction in streamline curvature, a process which is gradual and begins forward of the trailing edge. Viscous effects also play a part, so deviation is affected by boundary layer growth. More detailed accounts appear in Refs. [1, 2].

2.2.3 Construction

There is a single simple rule for constructing velocity diagrams:

$$\text{Relative velocity}(W) = \text{absolute velocity}(V) - \text{blade velocity}(U) \quad (2.2-6)$$

Let's consider this as we look at Fig. 2.2-2. Flow enters the rotor blade with an absolute velocity of V_1 from the upstream inlet guide vane. Subtraction of the blade speed vector, U , from the vector V_1 results in an inlet velocity relative to the blade of W_1 . The flow then decelerates through the blade passage—clearly in a relative sense—and emerges with a relative velocity of W_2 . If we follow the rule in Eq. (2.2-6), we obtain the absolute exit velocity of V_2 by adding the blade speed vector, U , to the relative flow velocity vector, W_2 . The algebra will always produce correct answers, regardless of the direction of rotation.

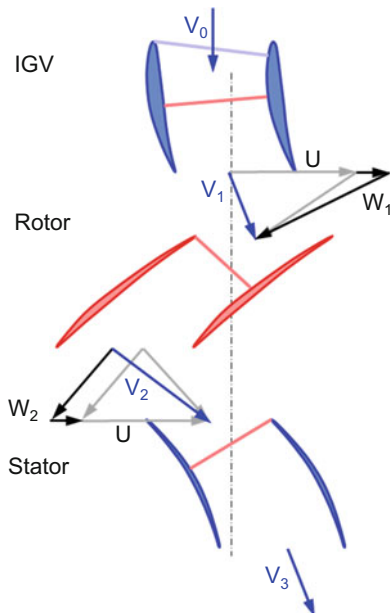
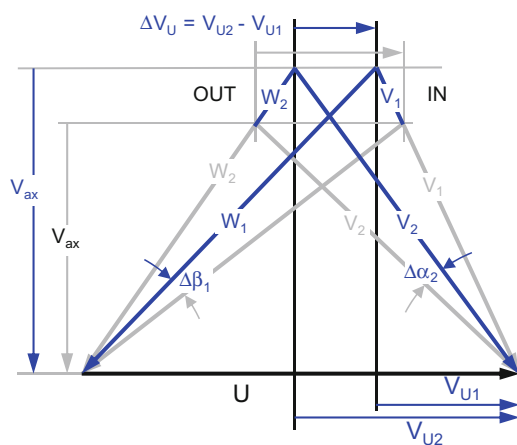
2.2.4 Use of Velocity Diagrams

So, what can we learn from velocity diagrams? We discuss the effect of blockage on stage work in Sect. 2.3-4. Other common elementary questions might be, “What are the effects on a compressor blade of changing the mass flow?” and “What are the effects of changing the blade speed?” Both can be answered by sketching the velocity diagrams.

Let's look at what happens to Fig. 2.2-1 when the flow is increased. The outcome is indicated in Figs. 2.2-4 and 2.2-5, where the vectors change from grey to blue. Higher flow means higher axial velocity V_{ax} in Fig. 2.2-5. Since the IGV exit angle does not change, the absolute swirl at rotor inlet, α_1 is also unchanged. As the blade velocity is constant the relative swirl at rotor inlet, β_1 , must increase (remember the sign convention) and the rotor incidence becomes lower; in Fig. 2.2-4, it changes from almost zero to negative. The blade metal angle is unchanged, so the rotor exit angle, β_2 , is also constant and combined with the higher V_{ax} this results in α_2 reducing, causing a lower incidence for the downstream stator. A reduction in ΔV_U is also seen in Fig. 2.2-5, which means the specific power applied to the air, ΔH_{Stg} , also reduces see Eq. (2.2-2).

So overall, increasing the mass flow at constant speed leads to a reduction in incidence at both the rotor and stator as well as lower specific work.

If we begin again with Fig. 2.2-1, but now increase the blade speed, we generate the velocity diagrams in Figs. 2.2-6 and 2.2-7.

**Fig. 2.2-4** Increased flow**Fig. 2.2-5** Effect of increased flow on velocity diagram

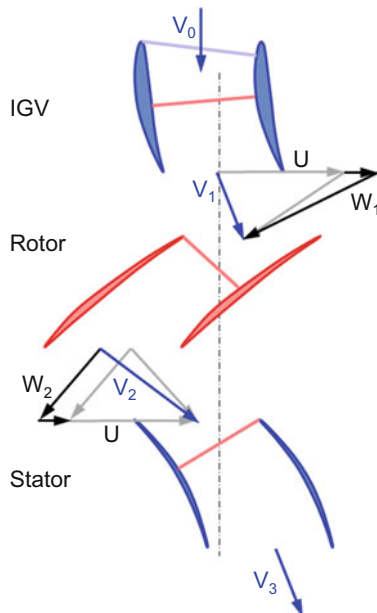


Fig. 2.2-6 Increased blade speed

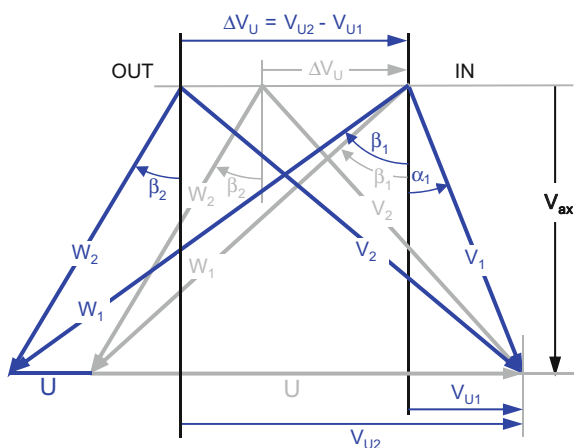


Fig. 2.2-7 Effect of increased blade speed on velocity diagram

The absolute velocity, V_1 , from the IGV is unchanged in magnitude and direction. We determine W_1 , the inlet flow velocity relative to the blade, by subtracting the higher blade speed, U , from the absolute flow velocity, V_1 . The relative inlet swirl angle to the blade, β_1 , is reduced (remember sign convention) and the rotor incidence increases. Regardless of the inlet angle, the exit flow is forced to follow the blade exit metal angle (neglecting any deviation), so the relative exit swirl β_2 is unchanged. As the axial velocity V_{ax} is unchanged so is W_2 , but shifted to the left in the velocity diagram. Adding the increased blade speed, U , to W_2 generates the new absolute exit velocity, V_2 . Increasing the blade speed has also increased the downstream stator incidence. We might expect the increased blade speed to have required more power, and Fig. 2.2-7 shows that this is the case; the increase in blade speed has resulted in an increase in ΔV_U , to deliver more power to the flow.

If we apply our sign convention, the power is positive, and this is power applied to the working fluid. The power taken from the shaft is therefore negative and this aligns with the more general convention, whereby we consider power delivered by the engine as positive.

2.2.5 Stage Characteristics

Three non-dimensional parameters are commonly used to describe or define a stage velocity diagram, if we neglect the inlet guide vane in Fig. 2.2-1.

Loading coefficient, ψ , is expressed as

$$\Psi = \frac{\Delta H_{Stg}}{U_m^2} \quad (2.2-7)$$

where ΔH_{Stg} is the specific stage work (J/kg) and U_m is the mean blade speed (m/s). Strictly, this should be the local area average but for quick estimates, the geometric mean is often used. Note that the mean velocity is also averaged between the leading and trailing edges. In compressors, the tip speed may often replace the mean value.

Some organizations include 2 in the denominator of a compressor loading coefficient. This may be complemented by a $\frac{1}{2}$ in the numerator for a turbine, so that compressor and turbine values are closer numerically and indicate how much more work may be done by a turbine stage than by its compressor equivalent. We can use Eq. (2.2-3) to write

$$\Psi = \frac{U V_{ax} (\tan \beta_2 - \tan \beta_1)}{U_m^2} = \frac{V_{ax} (\tan \beta_2 - \tan \beta_1)}{U_m} = \frac{\Delta V_U}{U_m} \quad (2.2-8)$$

and it can be seen from Fig. 2.2-2 that the loading coefficient represents the distance between the peaks of the *IN* and *OUT* velocity triangles divided by the common base. The stage loading definition may be extended to hub and casing, where it can be implemented to illustrate span-wise variations in stage loading. Note that the sign convention for angles makes the stage work positive in (2.2-8) and we are considering the work done on the air.

Flow coefficient, Φ , is defined as

$$\phi = \frac{V_{ax}}{U_m} \quad (2.2-9)$$

where V_{ax} is the axial velocity of the gas, usually at the blade inlet and U_m is the mean blade speed, as before. Figure 2.2-2 tells us that the flow coefficient represents the ratio of the height of the velocity triangles to their common base. Of course, this is strictly true only if the axial velocity of the working fluid remains constant through the blade, but it does not diminish the usefulness of the parameter.

Knowing how the separation of the peaks and height of the velocity triangles are related to the base, supplies much of what we need to know to define a velocity diagram completely, but we still lack one feature—and that is how the peaks are located laterally in relation to the base. The value of the *stage reaction* gives this information.

Stage reaction, Λ , is defined as the ratio of the increase of static enthalpy through the blade to that through the stage, namely

$$\Lambda = \frac{\Delta h_{s\text{ rotor}}}{\Delta h_{s\text{ stage}}} = \frac{h(T_{s1}) - h(T_{s2})}{h(T_{s1}) - h(T_{s3})} \quad (2.2-10)$$

Relative to the rotor, the flow does no work, and the steady flow energy equation tells us that *through the rotor* the change in static enthalpy is equal to the change in kinetic energy. Referencing Fig. 2.2-2, the numerator of (2.2-10) can be written as

$$h(T_{s1}) - h(T_{s2}) = \frac{1}{2}(W_1^2 - W_2^2) = \frac{1}{2}V_{ax}^2(\sec^2 \beta_1 - \sec^2 \beta_2) \quad (2.2-11)$$

From elementary trigonometry

$$\sec^2 = 1 + \tan^2 \quad (2.2-12)$$

So (2.2-11) becomes

$$h(T_{s1}) - h(T_{s2}) = \frac{1}{2}V_{ax}^2(\tan^2 \beta_1 - \tan^2 \beta_2) \quad (2.2-13)$$

Through the stage, the change in static enthalpy is given by

$$\begin{aligned} h(T_{s1}) - h(T_{s3}) &= (h(T_1) - \frac{1}{2}V_1^2) - (h(T_3) - \frac{1}{2}V_3^2) \\ &= (h(T_1) - h(T_3)) - \frac{1}{2}(V_1^2 - V_3^2) \end{aligned} \quad (2.2-14)$$

If we assume, for convenience, that we have a repeating stage, where the velocity at exit is equal to that at inlet (i.e. $V_3 = V_1$), then (2.2-14) becomes

$$h(T_{s1}) - h(T_{s3}) = h(T_1) - h(T_3) \quad (2.2-15)$$

From (2.2-15), we can write the denominator of (2.2-10) as

$$h(T_{s1}) - h(T_{s3}) = h(T_1) - h(T_3) = UV_{ax}(\tan \beta_1 - \tan \beta_2) \quad (2.2-16)$$

Re-formulating (2.2-10) from (2.2-13) and (2.2-16), we obtain

$$\Lambda = \frac{\frac{1}{2}V_{ax}^2(\tan^2 \beta_1 - \tan^2 \beta_2)}{UV_{ax}(\tan \beta_1 - \tan \beta_2)} = \frac{V_{ax}}{2U}(\tan \beta_1 + \tan \beta_2) \quad (2.2-17)$$

In an engine or a compressor test rig, having stage reaction in terms of static enthalpy is not especially useful, because static enthalpy is not particularly easy to measure. However, we can express Eq. (2.2-10) in a more practical form. If we take the standard entropy equation

$$T ds = dh - v dp \quad (2.2-18)$$

and consider the process to be isentropic and incompressible, then $ds = 0$ and we can state that

$$dh = v dp = \frac{dp}{\rho} \quad (2.2-19)$$

where v is specific volume and ρ is density. Integrating from condition 1 to condition 2 for the numerator and from 1 to 3 for the denominator, we can re-write Eq. (2.2-10) as

$$\Lambda = \frac{P_{s1} - P_{s2}}{P_{s1} - P_{s3}} = \frac{\Delta P_{s\text{rotor}}}{\Delta P_{s\text{stage}}} \quad (2.2-20)$$

A stage with 50% reaction is a special case. The symmetry of its velocity diagram is immediately obvious in Fig. 2.2-8, with $V_1 = W_2$, $\alpha_1 = \beta_2$, etc. It is very common to begin a mean line design of a compressor stage by setting the reaction at 50%, where V_1 and W_2 are at their lowest common value for fixed values of stage work and mean blade speed, since this tends to minimize total pressure losses in both blade and vane. However, we shall see later, when we consider span-wise variation, that 50% reaction is not always best.

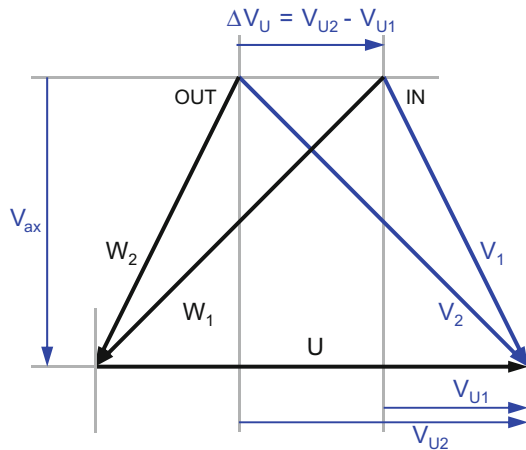


Fig. 2.2-8 A symmetric velocity diagram with 50% reaction

Figure 2.2-9 shows a more general case, where the flow path has converged more, and the axial velocity has increased.

In the generation of the expression of stage reaction in Eq. 2.2-17, the axial velocity was assumed to be constant. If the conditions of Fig. 2.2-9 are used, where V_{ax2} is greater than V_{ax1} , stage reaction is given by

$$\Lambda = \frac{\frac{1}{2}(V_{ax1}^2 \tan^2 \beta_1 - V_{ax2}^2 \tan^2 \beta_2)}{U(V_{ax1} \tan \beta_1 - V_{ax2} \tan \beta_2)} = \frac{(V_{ax1} \tan \beta_1 + V_{ax2} \tan \beta_2)}{2U} \quad (2.2-21)$$

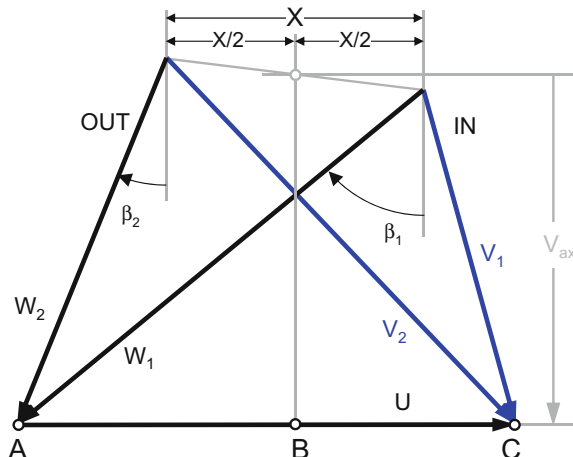


Fig. 2.2-9 General velocity diagram for a compressor

If we use a ruler and protractor to evaluate the parameters in (2.2-17), taking the average value of the axial velocity, the stage reaction turns out to be about 0.54.

There is also a simple graphical method to determine stage reaction from a velocity diagram; connect the peaks of the inlet and exit triangles, bisect that line and drop a perpendicular to the blade speed vector. The fraction of the blade speed at the point of intersection determines the reaction.

If we follow this in Fig. 2.2-9, the reaction is given by AB/AC, which is 0.55 and is very close to the analytical estimate above.

2.3 Preliminary Compressor Design

Design-build-test was once the only route to new engine development but numerical modeling at various levels of fidelity is now recognized as being a necessary part of a more efficient and cost-effective approach. The aerodynamic challenges posed by a compressor have always been more severe than in a turbine because of the predominant adverse pressure gradients encountered by the flow and the difficulty in predicting flow behavior and compressor performance. For that reason, early progress was more rapid in our understanding of turbine flows than of those in compressors. Consequently, more turbine information was made available in the literature than for compressors and mean line design codes for turbines evolved more quickly. (In those early days, turbine cooling was not yet an issue.) At the same time, the commercial value of aerodynamic data came to be appreciated and this led to a reluctance—at least by corporate researchers—to release compressor information so freely. Inevitably, much contemporary compressor data became company proprietary.

Prior to that, however, a great deal of seminal work had been done by NACA researchers at the Lewis Research Center; a resulting compilation was published in Ref. [3]. The contents of this document became the foundation of many of the compressor mean line design codes still used today.

A *1-D mean line model* is the simplest useful representation of an axial compressor. The flow field is inviscid and total pressure losses are accounted for by empirical correlations, based on flow properties and geometric characteristics of the airfoils. It runs very quickly and can be used to answer “what-if” questions and predict the effect of broad changes.

A *2-D streamline model*—also known as a *through-flow model*—is an intermediate level model that runs fairly rapidly. Streamline models are usually based on streamline-curvature solutions that produce circumferentially-averaged flow-field

solutions. Solutions are inviscid, so they rely on the same loss correlations used in mean line analysis. The number of airfoil sections and streamlines may be varied, so changes may be made to individual sections to effect span-wise re-designs—e.g. bow, lean, twist.

Modern commercial software can also use real gases, with an elaborate mixture of ingredients as well as humidity being accounted for. If even only 11 streamlines are used to represent the blade shapes and capture flow features, the run times can be excessive for compressors in industrial gas turbines with 16 or 17 stages, as fluid properties are updated repetitively. So, it is strongly recommended that an ideal gas be used initially to establish the model. If you wish to go with 21 streamlines, you should probably think about using 3-D CFD.

A *3-D CFD model* is the most sophisticated model of a compressor. It produces a very precise representation of the 3-D flow field, provided great care is taken with mesh-generation, selection of viscous fluid model, selection of turbulence model and suitability of the models to the application. CFD models can consume large amounts of time and resources. With continuous improvements in speed, capacity and cost, we move inexorably towards numerical test cells.

2.3.1 *Flow in a Blade Passage*

Knowledge of flow field features was obtained initially from measurements on two-dimensional cascades. Data from compressor test rigs was only added later and was used to characterize flow-field characteristics related to moving blades, such as vortices due to over-tip leakage. Initially, stage efficiency was calculated directly from measurement of relevant inlet and exit data and shaft work absorbed.

When we speak of compressor work being equal to the change in angular momentum of the working fluid and depict it using a velocity diagram, both statements are an idealization in which streamlines remain at constant radii or at constant percentages of the annulus height and work is generated by lateral (tangential) changes in streamline direction. However, it can be shown that there must be some radial motions to balance radial static pressure forces against radial inertia forces along curved streamlines. Flow turning in the vane or blade channel itself causes transverse pressure gradients and complementary flows in the channels, despite the relatively small turning angles and high radii of curvature of the streamlines. Slow-moving boundary layer fluid is transported from blade and vane pressure surfaces to the adjacent suction surfaces. Span-wise deflection results in these elements rolling up to form passage vortices. Superimposed on these general, relatively large-scale motions are more complex smaller-scale structures, resulting from viscous interactions between blade/vane and casing boundary layers, which generate corner vortices. Over-tip leakage also causes vortices, as the leakage flow—close to axial in direction—interacts with the mainstream flow following the blade suction surface. Finally, the vane and blade wakes mix with the passage fluid.

Recognition and description of these flow features are the results of the decades of experimental investigation and analysis discussed above.

2.3.2 *Mean Line Analysis*

Mean line performance models are founded on our recognition and understanding of the features of a compressor flow field. These have evolved continually since the 1950s, as our knowledge has grown. To model the general behavior of turbomachinery flows and the associated loss mechanisms we must first identify their physical characteristics and interactions and then express their effects quantitatively.

For preliminary design, mean line codes are relevant and are still used extensively to simulate a new system at its design point, to define the range of a design region and to explore alternatives, enabling limited resources to focus on cases that align with program objectives. A simple mean line analysis code is integrated in GasTurb.

Mean line design is used to determine the flow path dimensions, the number of stages and the interstage division of pressure ratio, initial estimates of the number of blades and vanes and a provisional prediction of performance. In preliminary design, trends are often more important than absolute values, so the limitations of the pressure-loss correlations in mean line codes are acknowledged and the accuracy of their solutions is accepted—supported by their ease of application.

The construction of a mean line model is based on the ability to generate velocity diagrams at the mean streamline. Usually, the “mid-height” radial location is determined by having half the mass flow on either side, although the average radius may be used occasionally. The ability to estimate total pressure is essential and the quality of any compressor mean line code is assessed primarily by its ability to account for pressure losses adequately.

Initially, it is reasonable to design a compressor in which the stage loading, $\Delta H/U^2$, is roughly constant. Since the blade speed is also roughly constant, this implies equal temperature increases. As a result, the stage pressure ratios will steadily reduce. Work in the first and last stages is then reduced to allow for variations in inlet conditions and the need to make special adjustments in the final stage to limit exit swirl.

2.3.3 *Three-Dimensional Flow and Radial Equilibrium*

It should be noted that the viability of a mean line design often rests on behavior of the flow at hub and tip. Velocity vectors cannot be determined without knowing the pressures at the corresponding radii. Relative tip speed and hub reaction are

frequently of interest, with maximum and minimum limiting values respectively being mandated. The relative tip Mach number is of great interest because of potential shock losses and typically, the hub reaction must be greater than about 15% at design to preclude the possibility of it being negative at any off-design condition.

Mean line codes usually contain a free-vortex assumption in which the whirl velocity varies inversely with radius

$$V_U r = \text{constant} \quad (2.3-1)$$

This is a flow phenomenon that is seen in water going down a drain or in a tornado. A more vivid demonstration of what is conservation of angular momentum is seen in a spinning figure skater, where the speed of rotation increases as the arms are brought inward. In a compressor or a turbine, the simple free-vortex condition results from the assumption that both specific work and axial velocity are constant with radius.

While a free-vortex condition provides a simple basis for turbomachinery design that ensures radial equilibrium, major problems can occur due to radial variations. Firstly, the blades tend to be highly-twisted and secondly, the hub reaction can be very low in low radius ratio designs. A limit in mean line reaction is usually set at design to avoid the hub reaction becoming negative at off-design operation. This might be the adoption of a mean line reaction value more than 50%. Alternative approaches to a combination of constant work and constant axial velocity with radius are useful. A fixed radial variation of reaction might be one; a fixed radial variation of work is another. Combining either of those with constant axial velocity would lead to a solution.

Consideration of radial equilibrium offers a first glimpse into the use of streamline curvature for two-dimensional modeling and analysis, and opens the door to more sophisticated two-dimensional through-flow models, in which flow properties are averaged circumferentially and to two- and three-dimensional CFD methods, both of which are discussed in detail in [1] and [2].

Strictly speaking, a mean line analysis is only appropriate for large values of radius ratio and in early compressor and booster stages the radius ratio is certainly not large. Nevertheless, the approach allows us to generate results of sufficient accuracy in the early stages of a new engine program or derivative study.

2.3.4 Diffusion, Turning and Blockage

The working environment of a compressor is much less demanding than that of a turbine in terms of temperature and corrosion, but this is off-set significantly by the severe aerodynamic challenges imposed. We have already stated that the primary role of a compressor is to generate pressure but in doing so, the flow must move against an adverse pressure gradient, so the more successful we are, the harder the

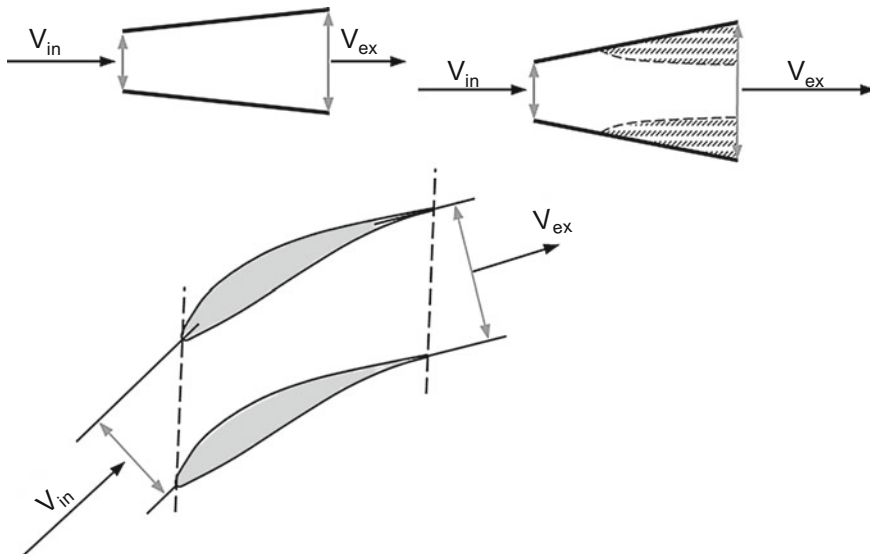


Fig. 2.3-1 Comparison of a straight diffusing channel and a vane passage in an axial compressor

task becomes. Pushing water uphill is an illustrative analogy; for a fixed slope, the broom speed is critical—too little speed and nothing much happens, too much speed and all the water spills out the sides!

In Fig. 2.3-1, we show the process through a compressor stage in absolute terms, with velocities V . The flow decelerates through the blade and accelerates through the vane. However, relative to each of the airfoils, the flow always decelerates and diffuses, and it does so by turning towards the axis. In any diffusing process, instability is an issue, and this can be examined by considering flow in a straight divergent channel, as shown in Fig. 2.3-1.

If the flow is subsonic at the inlet and the divergence angle is modest, it will decelerate smoothly as the area increases and the static pressure will rise. If the divergence angle is increased, the static pressure gradient becomes so large that the boundary layer separates. The resulting blockage causes the effective flow area to reduce and the diffuser becomes a nozzle—a duct in which the flow accelerates—and static pressure is no longer enhanced. In practice, this is influenced by flow speed, surface roughness and boundary layer characteristics. The situation in a curved channel of a compressor blade row is similar, where the geometric passage width is increased as it turns towards the axial direction. Now the shape of the sides of the passage, formed by the blade suction and pressure surfaces, also influences whether the flow remains attached. Increasing the turning angle entails a reduction in V_{ex} and an increase in diffusion and static pressure. Clearly the turning is limited, since if it goes beyond axial, the passage area will become convergent. A very simple criterion for limiting diffusion is the *De Haller* number, defined as V_{ex}/V_{in} . A typical minimum value is 0.72. In preliminary design, the De Haller number is an

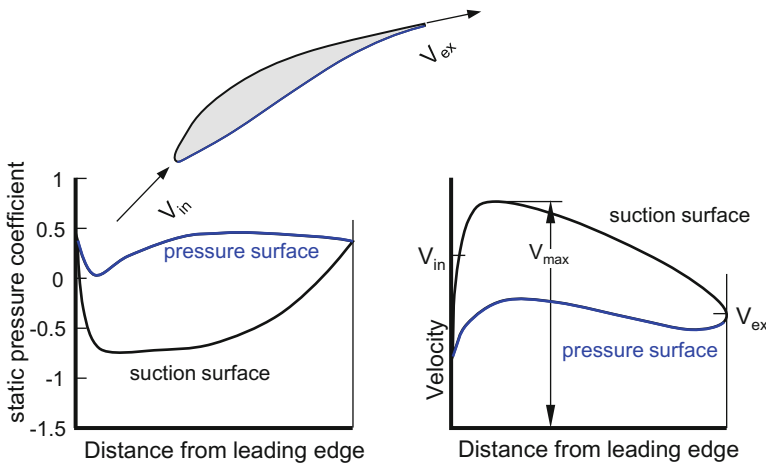


Fig. 2.3-2 Surface static pressure coefficient and velocity around a profile

adequate check on flow quality, but more sophisticated expressions for diffusion factor are normally used.

In practice, parameters subtler than the De Haller number are used to quantify blade or vane loading and the associated degree of diffusion. *Diffusion Factors* (D) are expressed in various forms but all measure flow turning, the deceleration of the air through a blade or vane passage, and the increase of static pressure.

Initially, let's consider a vane in Fig. 2.3-2. A diffusion factor relates the suction surface diffusion to the average surface velocity around the profile. The emergence of this characteristic is attributed to Lieblein in [3]. Lieblein recognized that boundary layer separation on the suction surface of a compressor blade or vane was the limiting ingredient in its ability to turn the flow, and the associated local diffusion was quantified by the deceleration from the peak velocity V_{\max} on the suction surface to that at the trailing edge. From Fig. 2.3-1 we can express this local diffusion as

$$D_{local} = \frac{V_{\max} - V_{ex}}{V_{\max}} \quad (2.3-2)$$

But the average surface velocity is usually close to that at the leading edge, so we can write.

$$D \approx \frac{V_{\max} - V_{ex}}{V_{avg}} \approx \frac{V_{\max} - V_{ex}}{V_{in}} \quad (2.3-3)$$

where V_{\max} is the peak velocity on the suction surface, and V_{in} and V_{ex} are the average velocities into and out of the blade. The evaluation of V_{\max} is difficult in a mean line design study because the blade profile does not exist yet and more

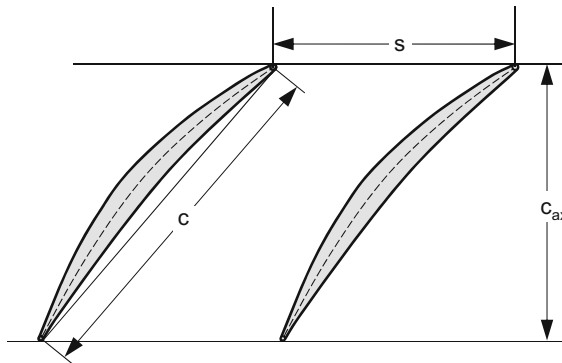


Fig. 2.3-3 Compressor cascade terminology

detailed aerodynamic codes would be needed to predict the velocity distribution in Eq. (2.3-2). But V_{\max} can be expressed empirically as

$$V_{\max} \approx V_{in} + f \left(\frac{\Delta V_U}{\sigma} \right) \approx V_{in} + \frac{\Delta V_U}{2\sigma} \quad (2.3-4)$$

where ΔV_U is the change in swirl velocity and σ is solidity (the ratio of blade chord length to pitch, the distance between the blades, shown in Fig. 2.3-3). Therefore, the diffusion factor can be defined as

$$D = 1 - \frac{V_{ex}}{V_{in}} + \frac{\Delta V_U}{2\sigma V_{in}} \quad (2.3-5)$$

where

V_{in} relative velocity at inlet,

V_{ex} relative velocity at exit,

ΔV_U change in swirl velocity,

σ vane solidity (chord-to-space ratio c/s) at the leading edge.

Values of diffusion factor greater than 0.6 are believed to indicate blade stall and 0.45 is recommended as a typical design choice.

Solidity, in the denominator, acknowledges the influence of the cross-passage pressure gradient, which in turn is dependent on the centripetal acceleration of the fluid elements as they follow the streamlines through the passage [3]. In practice, minimum limiting values of rotor tip diffusion (0.4) and stator hub diffusion (0.6) are of interest to avoid separation, but blade and vane diffusions must be high enough to reach the target values of stage pressure ratios. It should be noted that Eqs. (2.3-3), (2.3-4) and (2.3-5) require absolute values of the velocities; our sign convention is inappropriate! Note that this implies that a maximum value of

diffusion is encountered when V_{U2} is zero and this is indeed borne out because that is where the vane exit velocity becomes axial!

Solidity plays a major role in how much diffusion, and consequently turning, can be sustained. It is reasonable to assume that more turning can be accomplished, and separation avoided by using either larger chords or more blades to guide the flow through the turning angle. Suitable initial design values of solidity may be obtained from empirical relationships used in the CSPAN mean line code [4], described in Sect. 2.3-5. For the rotor tip

$$\sigma_{R_tip} = 0.5M_1 + 0.7 \quad (2.3-6)$$

works quite well—a higher inlet Mach number requires a higher solidity to avoid separation—and for a stator hub

$$\sigma_{S_hub} = \frac{\Delta\alpha}{30} + 0.5 \quad (2.3-7)$$

is satisfactory, where $\Delta\alpha$ is the vane turning angle and the units are degrees—more turning requires higher solidity for a blade to operate well. Both will be adjusted repeatedly during a design exercise.

The development of Eq. (2.3-5) as a convenient measure of compressor blade capability was largely based on the behavior of blades and vanes at minimum-loss incidence, while avoiding the estimation of W_{max} . A broader definition of diffusion that brought rotational speeds other than the design value into play and helped off-design and stall line prediction was also defined by Lieblein in [3]. This is the *equivalent diffusion factor* D_{eq} , which is based on correlation of the boundary layer momentum thickness with incidence different from that for minimum loss, as well as leading and trailing edge flow angles and solidity.

$$D_{eq} = \frac{\cos \alpha_2}{\cos \alpha_1} \left[1.12 + a(\Delta i)^{1.43} + 0.61 \frac{\cos^2 \alpha_1}{\sigma} (\tan \alpha_1 - \tan \alpha_2) \right] \quad (2.3-8)$$

α_1 and α_2 are the inlet and exit flow angles and a is a constant that varies with blade type. For a rotor blade, Eq. (2.3-1) would be expressed in terms of relative angles, the definition of solidity being the same.

D_{eq} is in fact a correlation of boundary layer momentum thickness against flow angles, where the constant a varies from 0.0117 for NACA series blades to 0.007 for the C4 circular arc family. It is commonly found that values of D_{eq} more than 2.0 are a fairly reliable prediction of stall and indicate the upper limits of speeds lines in compressor performance maps.

Boundary layers introduce losses near the hub and casing but, more seriously, introduce blockage because of the displacement thickness on the end walls. The blockage is equivalent to a reduction in the flow area and quite small reductions have a very large effect on stage performance because they affect the mass flow at choke and the work done by the rotor. Unfortunately, there is no accurate method to

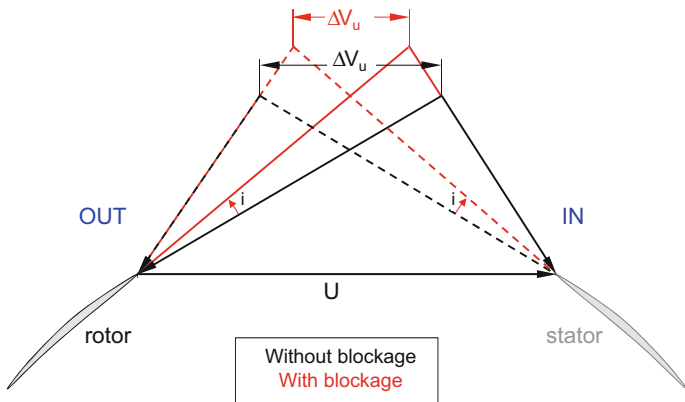


Fig. 2.3-4 Effect on blockage on compressor work

predict blockage and errors in its estimation are probably the greatest source of inaccuracy in predicting performance of multi-stage machines [1].

In the discussion of diffusion, we have implied that blockage occurs in the hub and tip regions of the blade and vane and surfaces, whereas in fact most blockage losses are due to boundary layer growth on the inner and outer walls. Blockage reduces the work done by the rotor in the central portion of the flow path by raising the through-flow velocity, while within the boundary layer, viscous and turbulent action wastefully absorbs energy.

One guideline often used with mean line design tools is that each blade or vane row causes 0.5% flow area blockage but once 4% is generated, it remains constant—a reasonable assumption since a new boundary layer begins to grow on each inner platform of a rotor and on each outer platform for a vane. Blockage changes the flow angles significantly and leads to incidence problems and ultimately, flow separation and stall.

Although increased blockage means that the average axial velocity is greater, Fig. 2.3-4 shows that a reduction in flow turning means less work $\Delta H = U \times \Delta V_u$ is done. Higher boundary layer losses exacerbate the problem.

Achieving the design incidence for all blade and vane rows is desirable for successful compressor operation. Matching the exit angle from a blade row with the inlet angle of the following vane is essential. Clearly this does not happen at all operating conditions and there is some leeway. HP turbines, where the leading edges are much rounder, can tolerate maybe ± 20 degrees of incidence, but for compressors, whose blade leading edges are so much sharper, the margin of error is slight. Figure 2.3-4 indicates typically how incidence changes may occur. Overcoming or avoiding large incidence excursions is crucial to compressor stage matching. Most problems in compressors arise because of a combination of blockage and incidence.

2.3.5 Mean Line Loss Models

A diffusing passage is one which is diverging; the exit area is greater than the inlet area, and—for incompressible flow—the kinetic energy falls, and the static pressure rises, while the total pressure is reduced relatively little by friction and remains essentially constant. The diffusion process can be described simply by the Bernoulli equation for Mach numbers less than about 0.4

$$P = P_s + \rho \frac{V^2}{2} \quad (2.3-9)$$

while for higher Mach numbers, the appropriate compressible expression is

$$P = P_s \left(1 + \frac{\gamma - 1}{2} M^2 \right)^{\gamma / (\gamma - 1)} \quad (2.3-10)$$

Except for an IGV, the passages in all blade and vane rows of a compressor are diffusers, in the relative sense for the former and in the absolute sense for the latter. In contrast, all vane and blade passages in a turbine are nozzles, where the velocity increases and static pressure falls.

In a compressor diffusion dominates, whereas in a turbine, diffusion is local and usually occurs only on the back surface of vanes and blades as the flow decelerates from its peak value to that at the trailing edge. Blockage and deviation occur in both compressors and turbines, but as they are both exacerbated by diffusion, they are significantly larger and more influential in compressors. Since they affect the flow angles and performance, their influence must be quantified and accounted for in a mean line model. These special features have been discussed in Sect. 2.3-4.

Mean line design codes incorporate a detailed appraisal of losses. The quality of a mean line code depends primarily on its ability to do this accurately. Essentially, all mean line codes contain the same velocity diagram calculations, undertaken in the same sequence; they differ only in how the losses are modeled.

Two different approaches are found in the literature. In the first approach the losses are defined by loss coefficients X , based on inlet energy:

$$X = \frac{\Delta H_{s, \text{Loss}}}{\frac{1}{2} W_1^2} \quad (2.3-11)$$

An overall loss coefficient X_T is calculated for each blade and vane row as the sum of profile, trailing edge, shock, and tip clearance losses. Losses due to the axial gap between blade and vanes are considered with an additional loss factor.

$$X_T = X_P + X_{TE} + X_{TC} + X_G \quad (2.3-12)$$

where

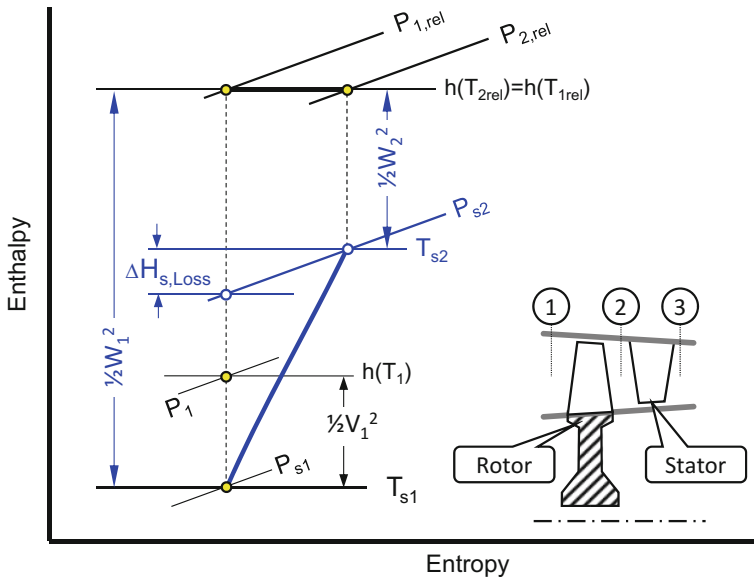


Fig. 2.3-5 Rotor loss description options

X_P basic profile loss coefficient,

X_{TE} trailing edge loss coefficient,

X_{TC} tip clearance loss coefficient,

X_G axial gap loss coefficient

The second approach accounts for loss components using pressure and their loss coefficients, Y —the total pressure loss divided by the inlet dynamic head for a blade or vane row.

$$Y = \frac{P_{1,rel} - P_{2,rel}}{\frac{1}{2}\rho W_1^2} \quad (2.3-13)$$

The overall loss for either a blade or a vane is given in the form

$$Y_T = (Y_P f_{RE} + Y_S + Y_{TE}) \text{corr}_{TC} \quad (2.3-14)$$

where

Y_P basic profile loss coefficient,

f_{RE} a Reynolds number correction,

Y_S secondary loss coefficient,

Y_{TE} trailing edge loss coefficient,

corr_{TC} tip clearance loss correction

2.3.6 *The Structure of the Mean Line Design Code CSPAN*

An example that may be used to discuss the structure of a typical compressor mean line design code is CSPAN (Compressor SPanwise ANalysis), a code written initially by Allison Engines, under NASA sponsorship [4]. At the time, the objective was to enable the study of the effects of a wide range of design parameters on stage pressure ratio and compressor length, with a view to increasing the former and reducing the latter. Originally, pressure losses were not estimated intrinsically, and the pressure field was related to temperature and work by specifying polytropic values of rotor and stage efficiency.

CSPAN was used at the NASA Glenn Research Center for many years and improved by the addition of internal correlations to estimate end-wall blockage and pressure loss coefficients for blade- and vane-rows as functions of mean line diffusion, end-wall clearance, and shocks [5–7]. Prediction of stall margin was also introduced. Calculations are done at an odd number of radial locations from tip to hub, and this may vary from three to eleven. Simple radial equilibrium is used as calculations move from tip to hub. Eventually, the mean line values of relevant flow properties are obtained by integrating across the annulus and mass-averaging.

CSPAN input includes the following:

- Inlet mass flow rate
- Inlet total temperature
- Inlet total pressure
- IGV pressure drop
- Compressor pressure ratio
- Number of stages
- Number of radial stations
- Flow path slope switch (Setting to unity = constant tip radius.)
- First stage blade tip speed
- Flow angle into first rotor tip
- First guesses at rotor tip diffusion factors
- Tip blockage factor at first rotor inlet
- Hub blockage factor at first rotor inlet
- First blade hub/tip radius ratio
- Bleed flows.

Numerous additional inputs may be used to control the design, but most are not mandated, and default values are available for the innocent and unwary! Examples of these are solidities, aspect ratios, axial gaps, hub and tip blockage factors and stage reactions.

Hub radii are determined from the relevant inlet radius ratio values and an input distribution of tip radii, an approach which simplifies the continuity solution. A constant tip radius will result in higher average mean line values of mean velocity, higher average blade speeds, higher stage temperature rises, lower deflections, and possibly the ability to reduce the number of stages.

Stage energy addition is controlled by specifying maximum allowable values of several aerodynamic design variables: rotor-tip and stator-hub diffusion factors, rotor-hub turning, and stator-inlet-hub Mach number. Stage and overall efficiencies are estimated from standard loss correlations. The output contains a meridional view of the flow path, blades and vanes.

A combination of user inputs and program procedures define flow path geometry. The mass flow rate determines the first stage blade inlet geometry from flow per unit area, and the given hub/tip radius ratio.

The hub and tip radii at exit are found by satisfying the mass continuity equation in the following manner. First, the stage exit radii are set equal to the inlet values, but this leads to excessive mass flow due to the pressure increase through the blade. The exit hub radius is then increased iteratively to satisfy continuity. However, there is a limit to the blade hub slope specified by the user ($\alpha_{\text{hub}} \leq 40^\circ$ by default). If this is reached, a similar iteration on the tip exit radius is initiated, whereby it is reduced sequentially.

The blade-tip slope also has a user-specified limit ($\alpha_{\text{tip}} \geq -20^\circ$ by default) and if this is violated and less flow area is still needed, it activates a reduction in the blade aspect ratio that overrides the input value. If either the exit Mach number (M_{exit}) or the hub turning angle ($\Delta\beta_{\text{hub}}$) exceed the maximum design limits, the rotor tip diffusion factor is reduced, and the iteration is repeated. Vane exit radii are determined in the same way until continuity is satisfied.

Stator hub diffusion factor is checked, and blade tip diffusion is reduced if necessary, following the iterative steps for the rotor. The process is repeated for subsequent stages, with blade inlet area being taken from the exit of the preceding vane.

The aerodynamic conditions at rotor exit are determined iteratively, in parallel with the geometric exercise. The absolute tangential velocity at rotor tip is obtained through the tip diffusion factor, tip solidity, blockage factors and axial velocity ratio. This is then passed inwards to the other radial stations via the radial equilibrium assumption, and the energy transfer and pressure rise are obtained by integration. Integration of the corresponding axial velocities, and knowledge of temperatures and pressures provides an estimate of mass flow rate for comparison with the blade inlet value. An unacceptable discrepancy invokes the geometric iteration described above. A similar process is followed for the vane.

CSPAN was reconfigured for the generation of design envelopes, discussed in Sect. 2.4. In its normal operation, the rotor tip diffusion factor is iterated to achieve a target value of stage pressure ratio and whenever its limiting value is reached, a stage is added, unless the limit on the number of stages has also been encountered—in which case, the run will stop with an error message.

This approach is unsuitable for generation of a design envelope, because the number of stages may vary over the design space and because one or more of the four datum design cases may not converge. A revised process was implemented, that allows the user to specify both the number of stages and the overall pressure ratio. The price for this more definitive procedure is the possible infringement of the rotor tip diffusion limit, which is driven by an assumed level of technology. But this can be easily captured by a constraint line in the design envelope.

2.3.7 Structure of the Mean Line Analysis in GasTurb

GasTurb has an integrated mean line analysis for multistage axial compressors. Mass flow, total pressure and temperature at the inlet and pressure ratio originate from the thermodynamic cycle. Inlet and exit areas are specified via input values of local Mach numbers. Interaction with the turbine yields the spool speed.

The interfaces to the adjacent components are fixed during *Conceptual Design*, they define the hub and tip radii for the compressor inlet and exit and the compressor length. The number of stages, and the axial position of all leading and trailing edges are also determined in this phase of preliminary design. The basic shape of the annulus is given as a distribution of hub, mean or tip radius against length.

The compressor is calculated sequentially stage by stage with the output of one stage being the input for the next. Ultimately, the properties at the last stage exit, and therefore at the compressor exit, are found. The calculated total pressure at the exit is the same as the total pressure from the cycle because the pressure ratio is an input for the mean line calculation. Automatic adjustment of the stage loading achieves this.

The calculated total temperature at the compressor exit differs from the value given by the cycle because it is calculated using the loss assumptions. The compressor efficiency calculated by the mean line flow analysis can be fed back to the cycle.

The compressor design calculation begins with the mean line velocity triangles for each stage. Three triangles represent each stage: at stage inlet, between rotor and stator, and at stage exit. It is assumed the radius of the three stage triangles is constant and equal to the mean radius at stage inlet, which is the radius that divides

Table 2.3-1 Origin of input data

Parameter	Origin
Mass flow	Thermodynamic cycle
Inlet total pressure and temperature	Local Mach numbers
Pressure ratio	Interaction with the turbine
Inlet and exit area	
Spool speed	
Number of stages	Conceptual design
Hub and tip radii at the inlet and exit	
Annulus shape	
Row inlet and exit axial positions	
Solidity	Additional input
Tip clearance	
Blockage	
Trailing edge thickness	
A guess for loading	

the annulus into two equal areas. Changes of the mean radius within the stage are ignored - the circumferential speed U is the same in the three triangles of a stage.

The axial velocity V_{ax} is the same in the triangles of any stage. Moreover, all the velocity triangles are geometrically identical—the compressor consists of “repeating” stages. With these simplifications, the three triangles of a stage are uniquely defined by the *stage loading*, the *flow coefficient* and *stage reaction*. (These three terms and their relation to the velocity triangles are explained in Sect. 2.2.4)

Once the velocity triangles are known, the enthalpy changes within the stage are also known. Therefore, these dimensionless coefficients are the main design variables of each individual stage.

In contrast to all other stages, the flow coefficient of the first stage is not a freely selectable input parameter. It is pre-determined by the compressor inlet Mach number, the rotational speed, and the inlet radii, all of these having been obtained from the cycle results and the component interface.

Further inputs are solidity, tip clearance and blockage. The losses are described with *Loss Coefficients X* from which the stage efficiency follows. With this efficiency, the stage exit pressure is calculated which is then used as the inlet pressure of the next stage. After a stage-by-stage calculation of the compressor, the overall compressor efficiency is found.

The blade and vane loss coefficients are either calculated by loss models or are prescribed directly by the user. The *Analytical* loss model is based on the methods of Denton [8]. This model avoids the use of empirical data in accounting for a wide range of applications. The input for calculating the various loss coefficients is based on geometric parameters at the mid section. The stagger angles are calculated as the averages of the respective inlet and exit flow angles. This gives the relationship between the axial chord (given from conceptual design) and the true chord (used in loss calculations).

As the input values for the loading are only guesses, the pressure ratio does not match the input value. Therefore, all input loading values are multiplied by a scaling factor and the design calculation is repeated until matching pressure ratios are obtained.

2.4 Compressor Design Envelopes

2.4.1 Introduction

The design of a new compressor involves the manipulation of the appropriate geometric and aerodynamic parameters within the constraints set by the technology limits so that the resulting design delivers the required pressure ratio and corrected mass flow rate at its design point with an efficiency acceptable to the engine cycle. A compressor design envelope determines an *acceptable design-space* and displays it graphically.

Several selected aerodynamic and mechanical limits are presented in terms of two major design variables, within which the designer must work to meet the demands of the engine cycle, the available compressor technology, material strength, and other internal or external constraints. It limits the range of design choices and offers the preliminary designer a means of considering several parameters and their interactions simultaneously.

Design limits are applied by restricting design choices to manageable ranges, based on an appropriate level of technology. No variables of interest are forgotten or neglected. By assigning real, practical values to the selected design limits, an inexperienced designer is more likely to arrive at an acceptable solution in an efficient manner, and the design process is accelerated for all users, regardless of their expertise. For best effect, the method should be coupled to a reliable compressor design code which incorporates a performance model and delivers estimates of efficiency and stall margin.

There is nothing unique about the approach. It is merely a formalization of the notes and observations of trends that any compressor designer would make in a logbook as the work progresses. The benefits accrue from being able to capture almost the whole design scenario in one view so that no parameters of significance are neglected. Interactions between design variables are illustrated, enabling difficult decisions and practical compromises to be made rapidly and confidently. The key to achieving a realistic preliminary design is the use of design limit values appropriate to the study in hand. A conventional design will assume conventional limiting values, while an advanced design concept will apply more aggressive standards. A preliminary choice of major parameters is determined, and the selection and values of the design limit parameters is established. Such decisions are based on typical performance figures for a conventional axial compressor.

The design scenario, in which design envelopes are so useful, is illustrated in Fig. 2.4-1. The skill in constructing a viable compressor design occurs not merely in bringing all the relevant technologies together (The central box labeled *Engine Configuration*) but in doing so within the restrictions that are imposed (The box on the right labeled *Constraints*).

The current design envelope method considers compressor aerodynamic constraints and performance, but it could easily be extended to include additional objectives and concerns, such as *cost* and *weight*.

2.4.2 Specification of Design Space

Let us consider the design of a compressor, based on engine cycle data, for which mean line solutions may be obtained using seven stages with a suitable “generic” flow path, which fixes the areas. Acceptable blade and vane geometries are also assumed for the purposes of the exercise. The cycle pressure ratio at its chosen design point is the primary objective. Mass flow rates, total temperatures and total pressures at inlet and exit are known, as is the target compressor efficiency.

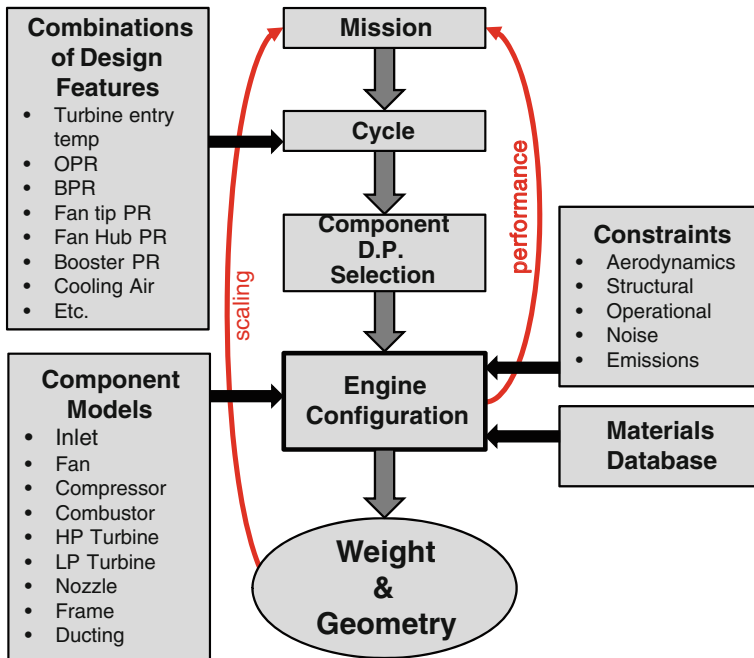


Fig. 2.4-1 Building an engine model

Let us assume that the radial location of the flow path is variable, controlled by the hub/tip radius ratio at the inlet, and rotational speed (N) is an output. (The rotational speed at design, N_{design} , of a compressor is usually taken as its *aerodynamic design point value rather than the mechanical design speed, which accounts for structural issues and allows for overspeed operation.*) If the stage count (n) is held at 7 and two values of inlet radius ratio, rr_{in} are chosen, in the two nominal design solutions generated it will be observed that as the flow path moves outwards, the speed falls. If the final stage of the compressor mean line model is removed and the process is repeated for a 6-stage compressor, it will be seen that for corresponding values of rr_{in} , the speed of the 6-stage machine will be higher, since the average stage loading must be higher to achieve the target value of overall pressure ratio and only minor changes to the blades and vanes are intended. Using only two values of rr_{in} , the results may be plotted, as in Fig. 2.4-2. A straight line connects the points.

Now let us assume that a maximum value of tip speed and a minimum value of hub speed are two design limits of interest. If the exercise above is repeated, each of the four nominal design points will correspond to a different value of $U_{\text{tip,max}}$. Regardless of the values of $U_{\text{tip,max}}$ on the 6-stages line, we can locate $U_{\text{tip,max}}$ by linear interpolation and we can do the same for the 7-stages line. Then, by connecting the two points, the $U_{\text{tip,max}}$ limit line may be identified. The process can be repeated for the $U_{\text{hub,min}}$ limit line and Fig. 2.4-3 can be constructed. Knowing that

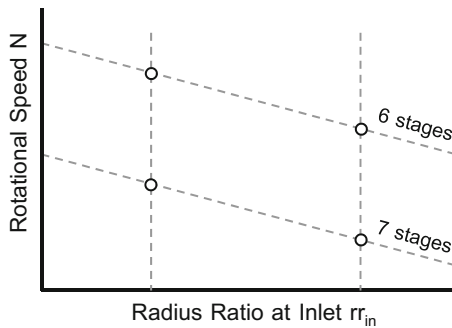


Fig. 2.4-2 Construction of design space for an axial compressor (1)

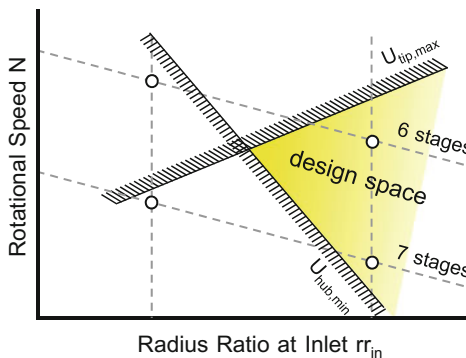


Fig. 2.4-3 Construction of design space for an axial compressor (2)

moving upwards on the plot corresponds to increasing blade speed, enables the upper side of the $U_{tip,max}$ limit line and the lower side of the $U_{hub,min}$ limit line to be shaded to indicate forbidden regions.

Of course, a compressor can only be designed with a finite number of stages, so the small amount of data presented in Fig. 2.4-3 informs us that only two locations correspond to viable designs, while exploiting the permitted limits on $U_{tip,max}$ and $U_{hub,min}$, and those occur where the two stage count lines intersect the two design limit lines.

2.4.3 Primary Design Variables

Completely new compressor designs are relatively rare in industry. Almost all compressors used in modern engines are the result of many years of investment and development by individual organizations, and the associated technology is highly

proprietary. Certain design details are usually embodied in generic preliminary design models handed down to preliminary designers from specialist aerodynamics groups. Examples of such details are blade numbers, aspect ratios, stage loading coefficients, diffusion factors, and internal Mach numbers and angles. The values of these parameters have been chosen carefully to deliver the required performance in terms of pressure ratio, efficiency, and stall margin over a complete range of operation. Consequently, the preliminary designer has limited choices if the performance inherent in the generic model is to be retained, although the possible combinations may still be overwhelming and warrant the use of design envelopes.

Parameters that the designer can and usually must change to install the generic model in a new engine are rotational speed, radius ratio, size (i.e. scale), and possibly stage count—he or she may be allowed to add or subtract one stage. Although designers in academia or other research establishments may have greater freedom than their counterpart in industry in terms of the design options, the general approach is still quite sound and the commonality with industry is also useful. Rotational speed (N) and inlet radius ratio (rr_{in}) are chosen as the primary design variables in the present exercise and these form the coordinates in which the design envelope is defined. Design limit lines for the parameters of interest are superimposed on this framework.

2.4.4 A Core Compressor with 11 Stages—An Example

In this example, the design envelope generator code is based on a modified version of the *CSPAN* compressor performance code written originally by *Allison Engines* under NASA sponsorship [4] and subsequently modified by NASA-Lewis [5–7], but any compressor mean line design code may be used and design envelopes can also be generated using *GasTurb*.

A combination of user input and program procedures define the flow path geometry. The first stage blade inlet geometry is determined by the inlet flow per unit area or Mach number, and hub/tip radius ratio. These define the hub and tip radii at the leading edge of the first blade row. The corresponding exit radii are determined by satisfying the mass continuity equation as follows. Initially the exit radii are set to the inlet values, but this leads to excessive mass flow due to the pressure rise and the reduction in volumetric flow through the machine. The exit hub radius is then increased sequentially to satisfy mass continuity. However, there is a limit to the blade hub slope and this is usually specified by the user to be greater than or equal to typically 40° . If this limit is reached, it triggers a similar iteration in the tip exit radius. The blade tip slope also has a user-specified limit of -20° , which, if violated, causes a reduction in the blade aspect ratio that overrides the value supplied and causes an increase in the chord of the blade, which is carried over to the axial value.

CSPAN presumes that there are no gaps between the blades and vanes, which is unacceptable for constructing the flow path and predicting the length and weight of

a compressor. Therefore, provision was added to the code to allow user-specified gaps that default to 20% of the upstream axial root chords. The vane exit radii are determined in the same way as those for the blade—by an area iteration to satisfy mass flow continuity involving the hub radius, possibly the tip radius, and possibly the vane aspect ratio. Subsequent stages are treated similarly to the first except that the blade inlet area is taken from the preceding vane exit area.

The CSPAN design process is outlined in more detail in Sect. 2.3.6. Originally, the code was set up either to determine the stage count for a required overall pressure ratio (the code would run till the pressure ratio target had been exceeded) or to predict how much pressure ratio could be generated by a fixed number of stages. This procedure is not very useful for design envelope calculations because the number of stages will vary over the design-space diagram and because one or more of the four nominal design cases may not converge at all. So, the code structure was modified slightly to permit the user to specify the number of stages as well as the overall pressure ratio, without the risk of a non-solution [9]. The price for this more definite procedure is the possible violation of the rotor tip diffusion factor limit, which is driven by the assumed level of technology. But since a constraint line on the design envelope can represent this limit, its influence is still captured.

Assume that the selected design constraints for an 11-stage core compressor that has a constant mass flow rate of 54.4 kg/s, is designed at sea-level static conditions and produces an overall pressure ratio of 23 are as follows:

Design Constraint	Value
• Minimum hub/tip radius ratio at inlet	0.35
• Maximum hub/tip radius ratio at inlet	0.65
• Maximum blade tip radius	0.36 m
• Maximum blade tip speed	518 m/s
• Minimum overall isentropic efficiency	0.80
• Minimum stall margin	15%
• Minimum diffusion factor at blade tip	0.50
• Minimum diffusion factor at vane hub	0.60
• Maximum flow turning angle at blade hub	40°

The design envelope in Fig. 2.4-4 is for the final stage of the compressor. It was obtained by running the mean line design code four times, at combinations of $rr_{in} = 0.4$ and 0.5 and $N = 14,000$ and $15,000$ rpm. The inlet radius ratio range and the speed range are both quite narrow, in keeping with the comments in Sect. 2.3 regarding the freedom of preliminary designers. The vertical limit lines for rr_{in} speak for themselves but the maximum tip radius limit falls between these two, so that was a good choice and the design space is bounded on the left by the minimum inlet radius ratio rr_{in} of 0.35 and on the right by the maximum tip radius of 0.36 m. The 15% stall margin limit line—the lower left boundary—also affects the design

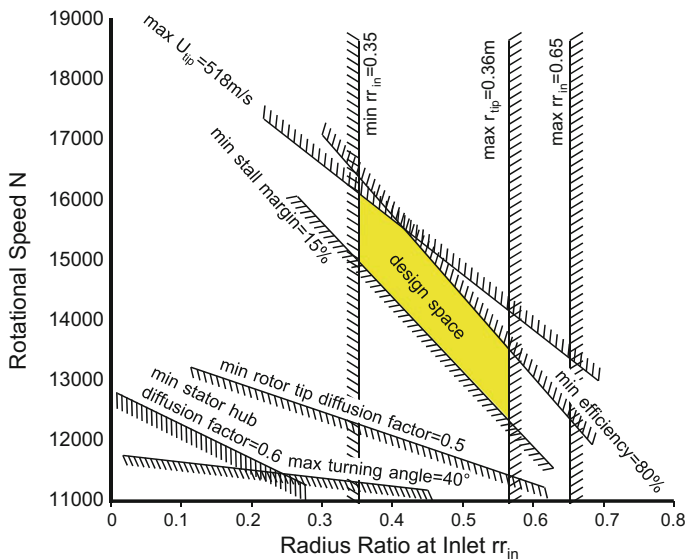


Fig. 2.4-4 A design envelope for an 11-stage axial compressor

quite strongly and prohibits speeds less than about 12,300 rpm. The upper right limit of the envelope is defined by the maximum tip speed line at 518 m/s right at the top and, a little further down, by the minimum isentropic efficiency limit of 80%. Limits on the minimum rotor tip diffusion factor, the maximum turning angle and the minimum stator hub diffusion factor are never encountered in the design of this compressor, so need not concern the designer.

Figure 2.4-5 is a plot of the compressor for the nominal design point corresponding to $rr_{in} = 0.4$ and $N = 14,000$ rpm. The constant tip radius is a choice made in the input file.

Because changes in any of the parameters under consideration may not be linear across the design space, it should be noted that linear interpolation or extrapolation is not strictly correct over the whole region, although for preliminary design purposes the results are still valid. It is recommended, however, that some thought be given to the selection of the four nominal design points so that, if possible, they are reasonably close to where the final compressor design point is expected to be. If that is not possible, an iterative procedure may be adopted, whereby the design envelope is refined in a second pass, by relocating the datum design points. The characteristics of the envelope will change but will result in a more plausible analysis. In any case, it should also be remembered that the generation of the envelope is never the final objective, but only a means to an end, by which the design point is determined. The compressor design code is run subsequently for a single selected design point to generate specific relevant information.

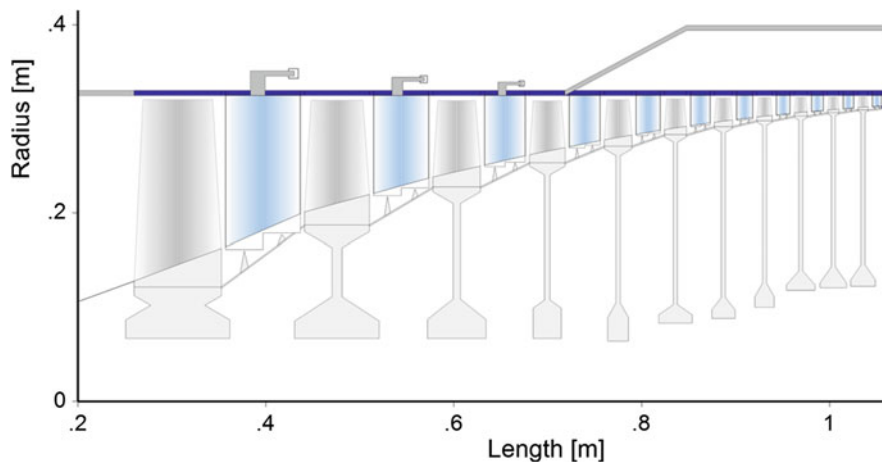


Fig. 2.4-5 The nominal 11-stage axial compressor at $rr_{in} = 0.4$

Running the code should be structured to generate the four nominal cases of the compressor design sequentially to produce the information needed to construct a design envelope. A single-run option should be retained to produce the final design point selection once it has been established. For multi-stage compressors, a design envelope should be plotted automatically for each stage, but it should be noted that the axes in every case must be the same, namely rr_{in} for stage 1 and N. This enables the design envelopes for multiple stages to be superimposed in a meaningful manner to determine if a design space exists for the complete compressor. Then, only if there is a clear design space remaining on the overlaid plots, is there an overall design solution. Sometimes the design limits overlap so that no clear design space is shown, but this provides useful information because the plot tells the user which parameters are impeding a successful design solution and which have least influence. The design variables whose limit lines form the envelope are the biggest drivers. Those that are further away influence the design relatively little and conversely, are less likely to be affected by changes to the influential parameters. At that point it is usually fairly obvious what needs to be changed.

Reaction has not been included as a variable in our example and in fact it is fixed. Typically, the design of a compressor stage will include an assumption of 50% reaction at the mean line. Frequently, however, the mean line reaction will be modified to effect span-wise changes in flow angles and velocities or to maintain a hub reaction greater than some minimum value (usually greater than 15% to avoid negative values at off-design conditions, at which point the compressor would become a turbine!) Since reaction is held constant in the current approach to design envelopes, another envelope or set of envelopes for multi-stages would need to be generated if the stage reaction was changed. In general, from experience, an increase in reaction will cause many of the limit lines in Fig. 2.4-4 to move to the right and rotate in a clockwise direction. They will not all move by the same

amount, however, and this will lead to changes in the location, the shape, and the extent of the design space. Unless a design strategy has been determined previously, it is often very useful to explore the implications and the range of the effects of such changes early in the design program to establish a database.

2.4.5 A Core Driven Fan—A More Complex Example

A variable-cycle engine, in Fig. 2.4-6, contains a front fan, and an HP compressor preceded by a core driven fan (CDF), similar to a booster. Such a configuration has more independent design variables than a conventional propulsion system and its design is very complex. A design envelope with suitable variables and appropriate limiting values may be used to simplify the design problem.

Compared with a traditional engine, the designer has additional choices which include the pressure ratio across the hub of the CDF and the radius ratio at CDF inlet, rr_{23} , as well as the radius ratio at HPC inlet, rr_{25} . Knowing the overall pressure ratio and that of the front fan, determination of the pressure ratio across the hub of the CDF defines that of the HPC. $PR_{CDF\ hub}$ is an important parameter—so important that it can be used as a primary variable in the construction of a design envelope (Figs. 2.4-8).

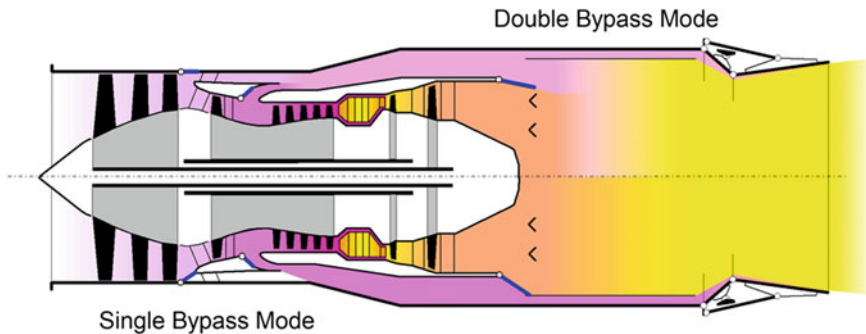


Fig. 2.4-6 A variable cycle engine with a core driven fan

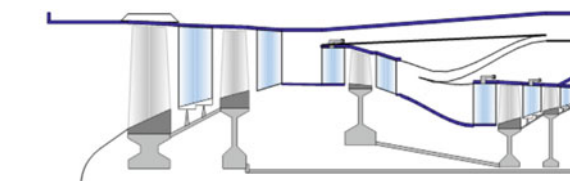


Fig. 2.4-7 A core driven fan stage

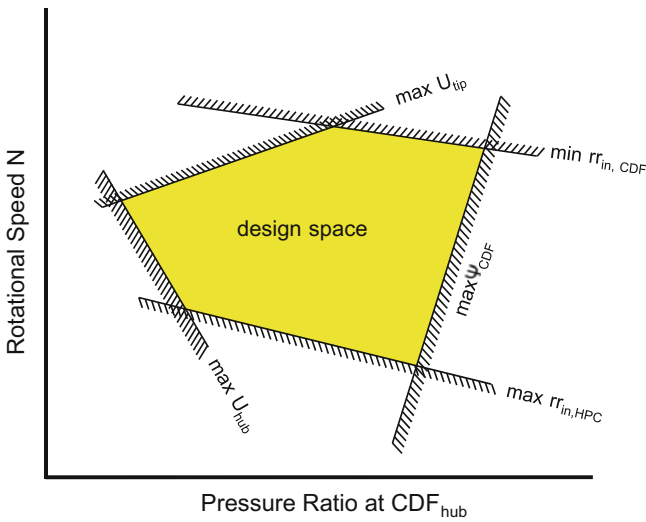


Fig. 2.4-8 Design envelope for a core driven fan stage

2.5 References

1. Cumpsty, N.A.: Compressor Aerodynamics. Krieger Publishing Company, Malabar (2004)
2. Lakshminarayana, B.: Fluid Dynamics and Heat Transfer of Turbomachinery. Wiley, New York (1996)
3. Johnsen, I.A., Bullock, R.O. (eds): Aerodynamic Design of Axial-Flow Compressors. NASA SP-36 (1965)
4. Bryans, A.C., Miller, M.L.: Computer Program for Design of Multistage Axial-Flow Compressors. NASA CR-54530, 1967
5. Glassman, A.J.: Users' Manual for Updated Computer Code for Axial-Flow Compressor Conceptual Design. NASA CR 189171, 1992
6. Lavelle, T.M.: Improvement of a design point compressor analysis tool. M.S. thesis, Case Western Reserve University, May 1994
7. Glassman, A.J., Lavelle, T.M.: Enhanced Capabilities and Modified Users' Manual for Axial-Flow Compressor Conceptual Design Code CSPAN. NASA TM 106833, 1995
8. Denton, J.D.: Loss Mechanisms in Turbomachines ASME 93-GT-435, 1993
9. Strack B., Halliwell, I.: CDE—a preliminary design code to generate compressor design envelopes contract NAS3-27577: propulsion systems modelling. September 1997

Chapter 3

Turbines



3.1 Function, Environment and Basic Efficiency

The expansion process is another major part of the Brayton cycle, where power used to drive the compressor is taken from the flow path via a change in the circumferential momentum of the working fluid as it passes through the turbine rotor blades. In a multi-stage machine, work is done on the moving blades by the gas, with stationary vanes re-aligning it between stages. In aircraft engines, excess energy and pressure remain in the flow and thrust is generated by further expansion through a nozzle. While the aerodynamics of the turbine expansion process is more simple and predictable than that of the diffusing process in the compressor—mainly because the flow is now moving in the direction of the prevailing pressure gradient—the high-pressure turbine still presents immense design challenges. As turbine technology tests its own aerodynamic limits continually to meet unrelenting demands for improved engine performance, it must also incorporate advances in heat transfer and blade cooling methods to ensure structural integrity and guarantee component life. In contrast to a compressor, the high-pressure turbine operates in an environment which is extremely hot, extremely corrosive and even more unstable. Low pressure turbines are subjected to cooler gas temperatures but, aerodynamically, they require more care to sustain a given standard of engine performance.

In single spool turboshafts, turboprops and industrial gas turbines, the flow through the turbine is expanded almost to ambient pressure, with some 60% of the power generated going to drive the compressor. The remaining shaft power constitutes the output, which is used to drive a propeller, or a lift rotor or to generate electricity. For land-based systems, the demand for low weight is relieved considerably, but remember—we still sell engines by the kilo!

In the passage of a gas through a turbine, there is a need to maintain a certain relationship between the blade speed and the air speed, so to maintain its axial velocity as the gas expands, the annulus area becomes larger. In the early years, soon after the advent of the axial turbine concept, repeating a stage to form a multi-stage

machine meant that a good stage design could be reused, perhaps by simple scaling, and this saved additional laborious design effort—usually with a slide rule! This *continuity characteristic* is still essential in that a reasonable relationship must be maintained through the turbine between the mean blade speed and the mean gas speed. Without any significant change in mean radius, the rotational speed of the blades (m/s) would remain fairly constant, but in an annulus of constant area, the gas speed would increase quite rapidly because of its reducing pressure, reducing density and increasing volume (mass flow rate = $\rho A V_{ax} = \text{constant}$). For this reason, the annulus area increases so that the gas speed in the axial direction remains roughly the same. But this can be considered separately from the *rate of change of angular momentum* by which work is done on the turbine blades to drive the compressor and provide shaft power. The axial and angular effects are combined in velocity diagrams and we shall examine those in Sect. 3.2.

From a thermodynamic point of view, T_4 is one of two key parameters in a turbojet cycle, the other being overall pressure ratio. T_4 is the highest temperature occurring in the engine cycle and a high value is called for to maximize cycle efficiency. However, in a real engine cycle with turbine cooling, T_{41} is often more important to a turbine designer than T_4 because station 41 is where the hot working fluid first encounters a moving blade under extreme centrifugal load. T_{41} is also a very meaningful cycle parameter because it coincides with the start of power extraction (see the discussion of mean line turbine in Sect. 3.3).

Here, we focus on an uncooled turbine, shown in Fig. 3.1-1, as we discuss the expansion through a single turbine stage. The working fluid—a mixture of combustion products and air—leaves the burner with an average swirl angle fairly close to zero and the vane turns and accelerates it so it aligns with the blade leading edge. Note that, unlike in Fig. 3.1-1, the annulus area though the vane may be reduced, enabling acceleration to be achieved with reduced swirl at its exit. Shaft or stage work is generated by the rotor blade turning the gas and causing a change in its angular momentum. Specific stage work ΔH [J/kg] becomes stage power PW [W] when it is multiplied by the mass flow rate [kg/s].

For a perfect gas, the specific stage work (work per unit mass) is expressed very simply by

$$\Delta H_{0-2} = C_P \Delta T_{0-2} \quad (3.1-1)$$

This relation is usually sufficiently accurate for real gases in gas turbine engines if a mean value of C_P is used for the process in question.

The fluid mechanics through a turbine stage can be traced in Fig. 3.1-2, which shows the expansion process in an enthalpy (h)–entropy (s) diagram. Starting at stagnation condition 0, the vane turns and accelerates the flow to stagnation condition 1. No work is done, so the temperature does not change but total pressure is lost, and we move transversely on the h – s diagram from the P_0 isobar to that of P_1 . When static pressures, P_{s0} and P_{s1} , are considered, the increase in kinetic energy in accelerating the flow from V_0 to V_1 in the absolute frame of reference can be seen from the vertical intervals that represent the respective kinetic energies, $\frac{1}{2}V_0^2$ and

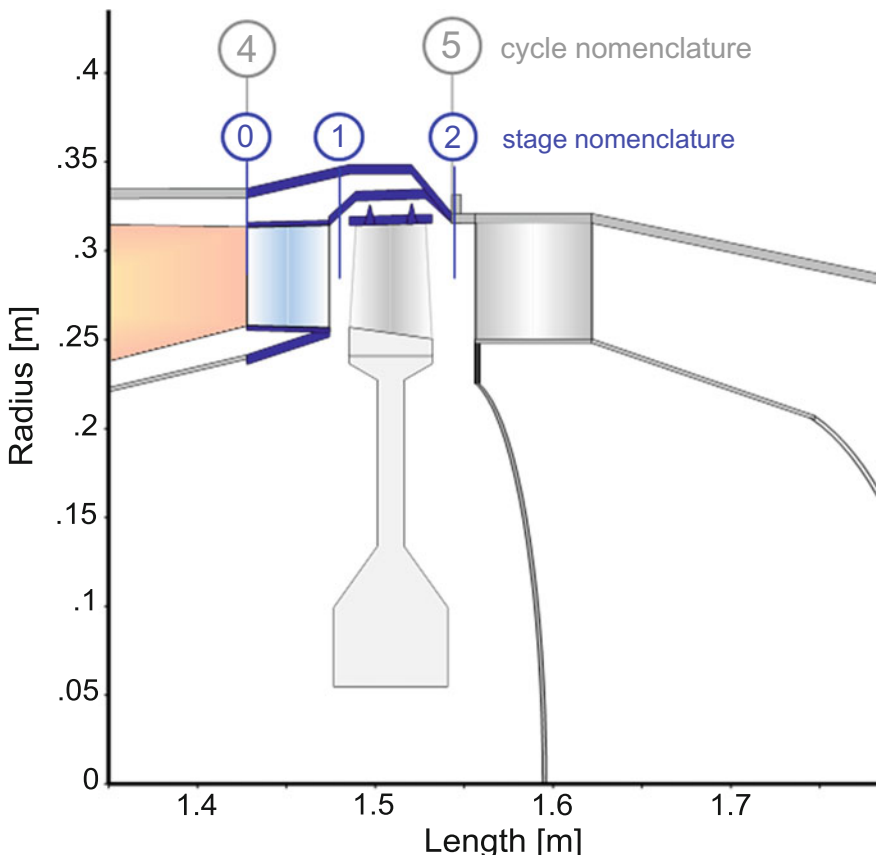


Fig. 3.1-1 Single stage turbine

$\frac{1}{2}V_1^2$. Then, in the rotor blade, stage work $h(T_1)-h(T_2)$ is taken from the flow in expanding from condition 1 to condition 2, accompanied by a loss in total pressure from P_1 to P_2 , as shown on the right of Fig. 3.1-2. Using the corresponding static pressures, the acceleration through the rotor is seen in the change in relative kinetic energy through the rotor, from $\frac{1}{2}W_1^2$ to $\frac{1}{2}W_2^2$. This contrasts with the associated deceleration of the flow in absolute terms, which is indicated by the reduction in absolute kinetic energy from $\frac{1}{2}V_1^2$ to $\frac{1}{2}V_2^2$. The kinetic energy emerging from the stage, $\frac{1}{2}V_2^2$, is similar in magnitude to that at stage entry, $\frac{1}{2}V_0^2$. The stage work—the change in specific enthalpy from station 0 to station 2—is also indicated, and this corresponds to the expression in (3.1-1) above. All these features can be associated with the velocity diagram, presented later in Sect. 3.2.

The efficiency of a turbine is the ratio of *actual* to *ideal* work transfers. However, since fans, compressors and turbines are essentially adiabatic devices (no heat transfer), the *ideal* (frictionless or reversible) process is *isentropic* in all cases (Note: *isentropic* = *reversible* + *adiabatic*). This is particularly true at steady-state

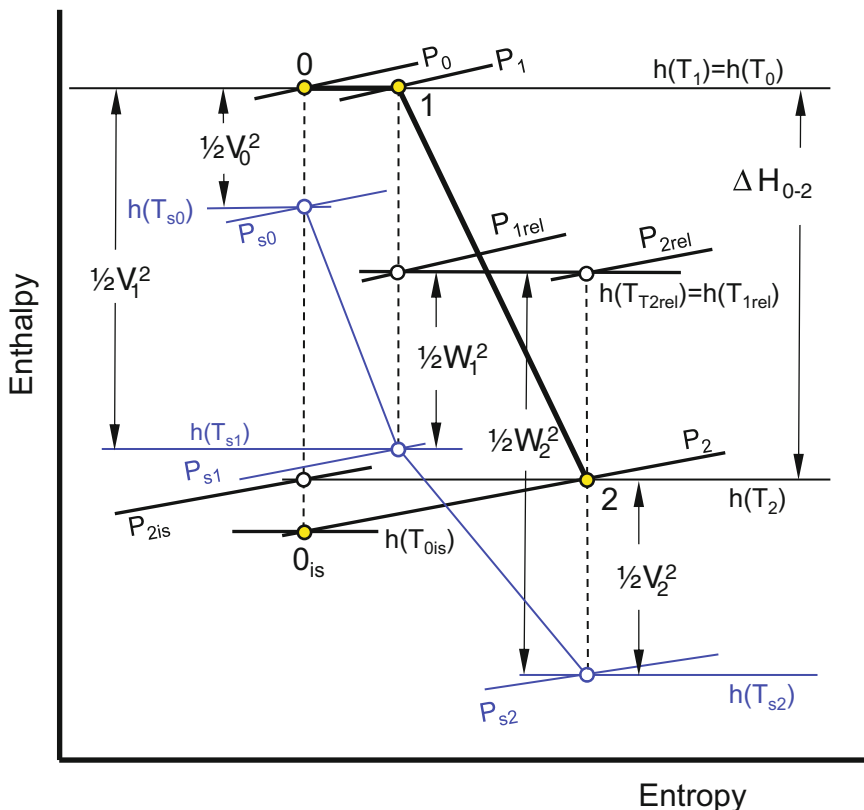


Fig. 3.1-2 Single-stage turbine expansion process in an enthalpy-entropy diagram

conditions, where conditions have stabilized thermally. So performance may be quantified in terms of *isentropic efficiency*, usually expressed in terms of stagnation conditions. The use of stagnation conditions (expressed here by properties without a suffix) means that any changes due to kinetic energy effects are accounted for intrinsically. Any increase in entropy or lateral shift across the h-s diagram corresponds to a departure from a (vertical) isentropic process, so the quality of the expansion can be determined roughly from the slope off the line. Various forms of thermodynamic efficiency are apparent in Fig. 3.1-2.

Total-to-total isentropic stage efficiency is given by

$$\eta_{is} = \frac{\text{Actual enthalpy change}}{\text{Ideal enthalpy change}} = \frac{h(T_0) - h(T_2)}{h(T_0) - h(T_{0is})} \quad (3.1-2)$$

This is normally used when the expansion of the working fluid is close to its full potential and no further work can be extracted as thrust, as in an industrial gas turbine.

Since no work is done on the vane, vane efficiency is inappropriate but the associated vane pressure loss is evaluated by a *vane loss coefficient*. This may be defined in terms of either total temperature (λ_{vane}) or total pressure (Y_{vane}), each expressed as a fraction of the exit dynamic head, and the values are fairly close. Since we are considering the expansion process in terms of enthalpy rather than temperature, we shall use the latter. So

$$Y_{vane} = \frac{P_0 - P_1}{P_1 - P_{s1}} \quad (3.1-3)$$

Rotor loss coefficient is given by

$$Y_{blade} = \frac{P_1 - P_2}{P_2 - P_{s2}} \quad (3.1-4)$$

Regardless of the engine application, turbine efficiency is always important to the engine cycle and to the fuel burn. Turbine work—obliquely measured by temperature ratio—is what we get; pressure ratio is what we pay! In an aircraft engine, just enough power is generated by the turbine to drive the compressor. This determines the turbine pressure ratio via the efficiency. High turbine efficiency means that more pressure ratio is left for expansion through the nozzle. In an industrial gas turbine engine, the flow through the turbine expands almost all the way to ambient and this sets the turbine pressure ratio. The compressor uses around 60% of the turbine power, with the remainder being delivered by the shaft as net engine output. By maximizing turbine efficiency, the power output is also maximized. A simple sketch of an h–s or T–s diagram can often tell us how much we can gain by spending resources on finding the best aerodynamic design for a turbine.

If the specific heat of the working fluid is assumed to be constant, we can use temperature very conveniently in developing expressions for isentropic efficiency. We cannot measure ideal exit temperature, but we can measure exit pressure, so we use this. Achieving the required exit temperature is made more difficult than it would be ideally because of the “reheat” effect of friction in the expansion process, in addition to other non-isentropic phenomena that also produce pressure losses. Therefore, in the real process, a pressure ratio greater than ideal must therefore be accepted. Again, conveniently, the ideal temperature ratio may be expressed in terms of the actual pressure ratio, while the actual temperature ratio is a measure of the work done. Logic tells us once more which is in the numerator and which is in the denominator in the expression for efficiency. Starting again from Eq. (3.1-2)

$$\eta_{is} = \frac{\text{Actual enthalpy change}}{\text{Ideal enthalpy change}} = \frac{h(T_0) - h(T_2)}{h(T_0) - h(T_{0is})} \quad (3.1-5)$$

Assuming a perfect gas and using a constant value of C_P for the expansion process, turbine isentropic efficiency may be expressed in terms of actual and ideal total temperatures.

$$\eta_{is} = \frac{\text{Actual temperature change}}{\text{Ideal temperature change}} = \frac{T_0 - T_2}{T_0 - T_{0is}} \quad (3.1-6)$$

Dividing through by the inlet total temperature (T_0) results in

$$\eta_{is} = \frac{1 - \frac{T_2}{T_0}}{1 - \frac{T_{0is}}{T_0}} \quad (3.1-7)$$

The ideal total temperature ratio in the denominator may then be expressed in terms of the actual total pressure ratio to define the turbine isentropic efficiency in terms of actual conditions, to give us

$$\eta_{is} = \frac{1 - \frac{T_2}{T_0}}{1 - \left(\frac{P_2}{P_0}\right)^{\frac{\gamma-1}{\gamma}}} \quad (3.1-8)$$

3.1.1 Limitations of Isentropic Efficiency

In our design and analysis work on gas turbine engine cycles, we have frequently needed to assume values of overall efficiency for fans, compressors and turbines in order to generate thermodynamic models that are realistic. Up to now, we have used constant values of *isentropic efficiency* and assumed that they were valid regardless of the ranges of temperature and pressure covered by the thermal process. We are now about to show that the use of constant values of isentropic efficiency to describe the quality of thermodynamic processes that span large ranges of temperature and pressure is, in fact, erroneous.

In any turbine, even though re-heating by friction is partially recovered as work in the subsequent stage, this makes it harder to achieve the temperature reduction needed to extract the required work from the flow. Doing so results in a pressure loss even greater than would occur in the equivalent ideal expansion process. This is reflected in the divergence of the constant pressure lines on an enthalpy—entropy or temperature—entropy diagram as each of those properties increases. Therefore, we need a better performance criterion to enable us to make equitable comparisons between different turbines.

Let's consider the expansion process in a four-stage turbine in Fig. 3.1-3, where the suffix ‘Stg’ denotes a stage value.

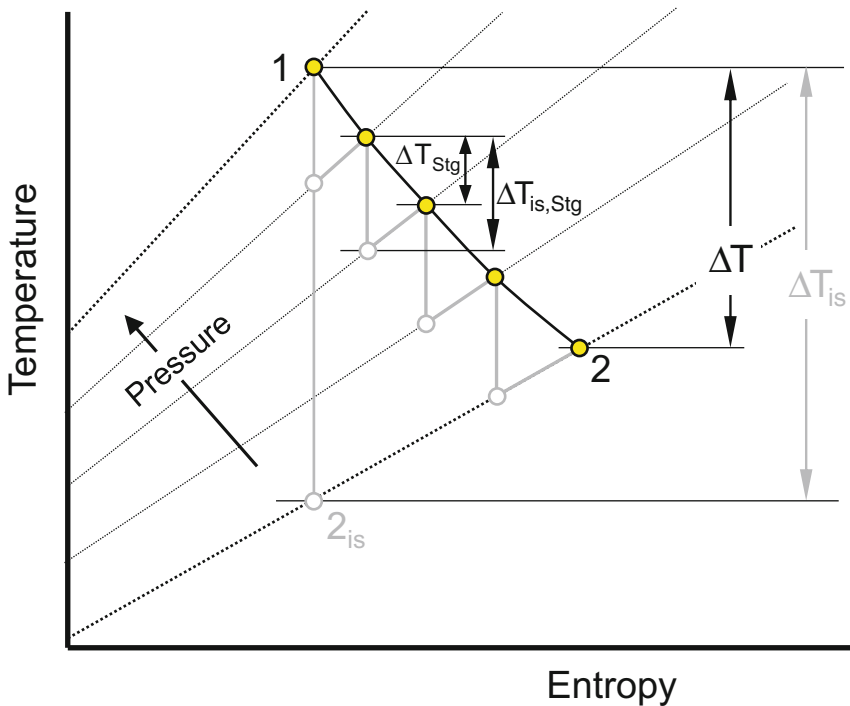


Fig. 3.1-3 Polytropic efficiency in a multi-stage turbine

From Fig. 3.1-3, the overall temperature drop is the sum of the stage values, i.e.

$$\Delta T = \sum \Delta T_{Stg} \quad (3.1-9)$$

Stage efficiency is defined by

$$\eta_{Stg} = \frac{\Delta T_{Stg}}{\Delta T_{is,Stg}} \quad (3.1-10)$$

So the overall temperature drop may be expressed as

$$\Delta T = \sum \eta_{Stg} \Delta T_{is,Stg} = \eta_{Stg} \sum \Delta T_{is,Stg} \quad (3.1-11)$$

Again, by definition, the overall isentropic efficiency of the turbine is

$$\eta_{is} = \frac{\Delta T}{\Delta T_{is}} \quad (3.1-12)$$

So

$$\Delta T = \eta_{is} \Delta T_{is} \quad (3.1-13)$$

Combining (3.1-11) and (3.1-13), we obtain

$$\eta_{Stg} \sum \Delta T_{is} = \eta_{is} \Delta T_{is} \quad (3.1-14)$$

Then

$$\frac{\eta_{Stg}}{\eta_{is}} = \frac{\Delta T_{is}}{\sum \Delta T_{is}} \quad (3.1-15)$$

It can be seen from Fig. 3.1-3 that the sum of the ideal stage temperature drops is greater than the overall ideal temperature drop (because each individual $\Delta T_{is,stag}$ is greater than its counterpart on the ideal 1–2_{is} line to the left) on account of the divergence of the isobars as entropy increases. Therefore

$$\frac{\Delta T_{is}}{\sum \Delta T_{is,Stg}} < 1 \text{ and } \frac{\eta_{Stg}}{\eta_{is}} < 1 \quad (3.1-16)$$

So

$$\eta_{is} > \eta_{Stg} \quad (3.1-17)$$

This difference grows with the overall pressure ratio, stage count and distance between isobars.

The reason for this is that re-heating by friction is partially recovered as work in the subsequent stage. This makes it harder to achieve the temperature reduction needed to extract the required work from the flow and doing so results in an even greater pressure loss than would occur in the equivalent ideal process.

3.1.2 Polytropic Efficiency

The difficulty in making equitable comparisons between different compressors and turbines led to the idea and use of small-stage or polytropic efficiency. Polytropic efficiency in a turbine is defined as the isentropic efficiency of an infinitesimally small step in the expansion process such that its magnitude is constant throughout. It accounts for the fact that the inlet temperatures of the rear stages of a turbine are higher than they might have been expected to be and hence more work is able to be extracted for a constant pressure ratio across each of the stages. In practice, polytropic efficiency is often used in design point calculations, where comparisons are sought, between different engines (perhaps at wide and different ranges of pressure

ratio) since relative performance is of primary interest in that context. At off-design, however, where comparisons are sought between different operating points of the same propulsion system, isentropic efficiency is clearly the arbiter. This is one reason why component maps use isentropic efficiency contours as a measure of performance.

The suffix ∞ is often used and this is a reference to the fact that the overall process is split up into an infinite number of infinitesimal processes each of which can be made isentropic!

For an expansion process through a turbine, between planes 0 and 2 as shown in Fig. 3.1-2, we can write

$$\frac{T_0}{T_2} = \left(\frac{P_0}{P_2} \right)^{\frac{(\gamma-1)\eta_{pol}}{\gamma}} \quad (3.1-18)$$

From which

$$\frac{(\gamma-1)\eta_{pol}}{\gamma} = \frac{(n-1)}{n} \quad (3.1-19)$$

This equation takes the form of the relationship between P and T for a polytropic expansion process, which is

$$\frac{T_0}{T_2} = \left(\frac{P_0}{P_2} \right)^{\frac{(n-1)}{n}} \quad (3.1-20)$$

The relationship between isentropic efficiency (η_{is}) and polytropic efficiency (η_{pol}) for a turbine is found in

$$\eta_{is} = \frac{1 - \left(\frac{P_2}{P_0} \right)^{\frac{(\gamma-1)\eta_{pol}}{\gamma}}}{1 - \left(\frac{P_2}{P_0} \right)^{\frac{(\gamma-1)}{\gamma}}} \quad (3.1-21)$$

The previous equations are valid for constant specific heat C_p . In rigorous calculations for temperature dependent gas properties use Eq. (3.1-2) for determining isentropic efficiency and the following equation for polytropic efficiency:

$$\eta_{pol} = \frac{\ln(P_0/P_{2is})}{\ln(P_0/P_2)} \quad (3.1-22)$$

The results shown in Figs. 3.1-4 and 3.1-5 have been calculated with GasTurb for dry air, fuel/air ratio zero and 1500 K turbine inlet temperature:

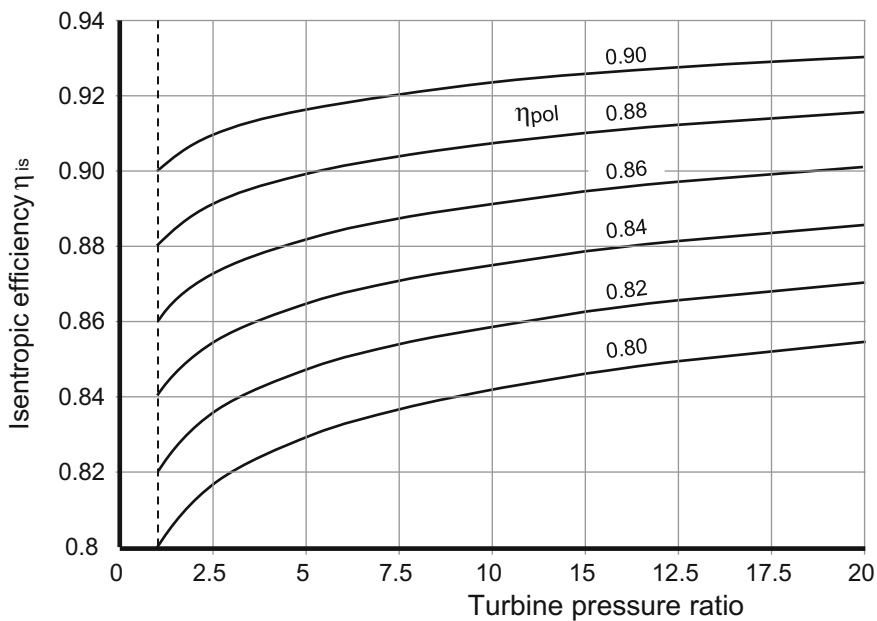


Fig. 3.1-4 Isentropic efficiency versus turbine pressure ratio over a range of polytropic efficiencies

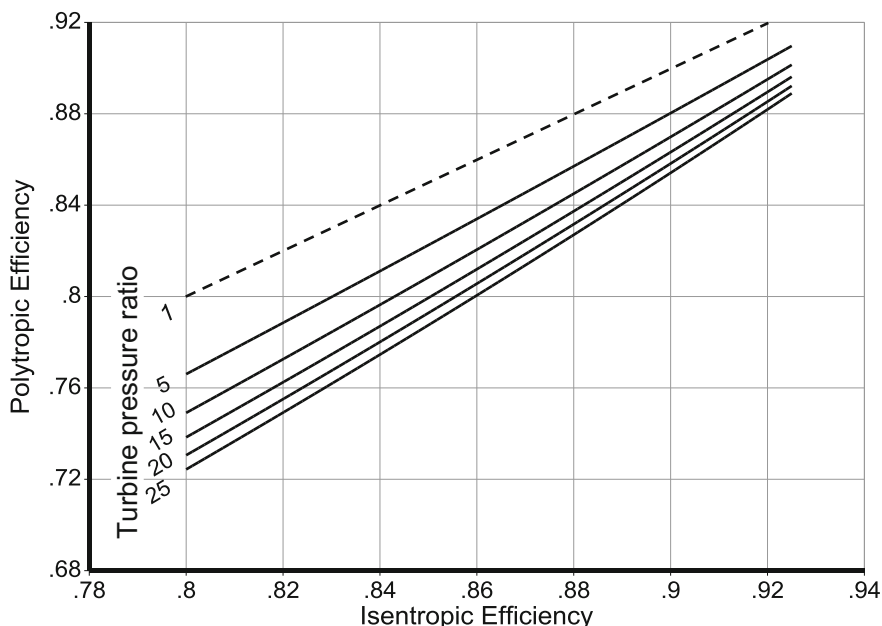


Fig. 3.1-5 Polytropic efficiency versus isentropic efficiency over a range of turbine pressure ratios

3.2 Velocity Diagrams

3.2.1 Introduction

We cannot design vanes and blades from the thermodynamic descriptions of the turbine part of an engine cycle because no information about vane and blade shapes is included. Airfoil shapes are determined initially from flow inlet and exit angles, which essentially fix the camber line. For a vane, the inlet metal angle is obtained from the absolute inlet flow angle; the exit metal angle follows from the turning needed. For a rotor blade, the inlet metal angle matches the relative inlet flow angle closely; the exit metal angle aligns with the relative exit flow angle, which is determined by the turning angle needed to provide the power. Figure 3.2-1 shows a turbine stage with velocity vectors relative to the vane and the blade. For a vane, relative velocities are the absolute values.

Figure 3.2-2 contains the velocity diagram corresponding to Fig. 3.2-1. We have stated previously that stage work (ΔH_{Stg}) per unit mass of flow is equal to the change in angular momentum. If we refer to Fig. 3.2-2 and stay in the relative

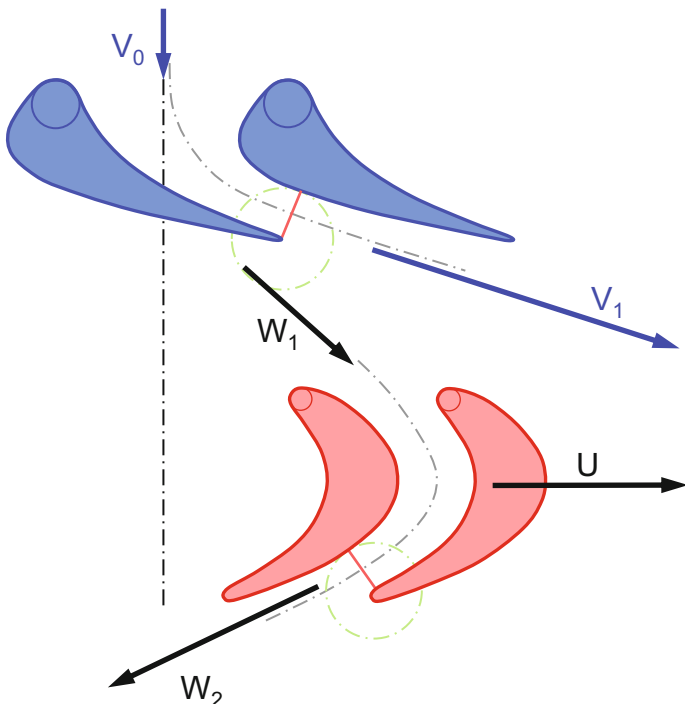


Fig. 3.2-1 Turbine airfoil sections

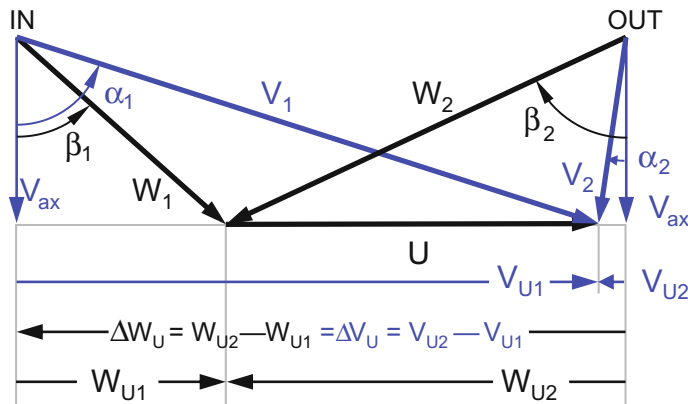


Fig. 3.2-2 Velocity diagram

frame, we see that this is given by the product of the blade speed and the difference between the relative swirl velocities at inlet and exit, namely

$$\Delta H_{Stg} = U(W_{U2} - W_{U1}) \quad (3.2-1)$$

Since the swirl velocity usually changes direction in a turbine and the inlet and exit values have different signs, their magnitudes are added, and this is illustrated clearly by the vectors in Fig. 3.2-1. It can also be seen there that the same result is obtained when the absolute swirl velocities are used, so we may also write.

$$\Delta H_{Stg} = U(V_{U2} - V_{U1}) \quad (3.2-2)$$

The importance of a sign convention for turning angles and swirl velocities will be discussed in the next section.

If we assume that the axial velocity is kept constant by expansion of the annulus, so that $V_{ax2} = V_{ax3} = V_{ax}$, we can express the stage work in terms of either the absolute or relative flow angles by reference to Fig. 3.2-2.

$$\Delta H_{Stg} = UV_{ax}(\tan \alpha_2 - \tan \alpha_1) = UV_{ax}(\tan \beta_2 - \tan \beta_1) \quad (3.2-3)$$

The change in the enthalpy of the working fluid is negative, which corresponds to positive work being transmitted to the shaft by the turbine. Since the blade metal angles are defined closely by the relative angles of the gas, the second part of Eq. (3.2-3) is more useful to define a blade shape.

As for compressors, an experienced designer can learn a lot about the suitability and quality of a turbine stage from a velocity diagram. Almost all “What happens if ...” questions can be answered and for a young turbomachinery engineer, time spent messing about with velocity diagrams is never wasted; it has something to do with a picture and a thousand words!

As for compressors, incidence and deviation are not represented directly in velocity diagrams. Incidence is the angle between the flow at the airfoil leading edge and the extension of the camber angle and is discussed in the following sub-section. Deviation, often referred to in turbines as under-turning and designated by the symbol δ , occurs when the exit angle of the gas does not match the exit angle of the blade or vane. The exit flow angle is less than the exit metal angle and the flow-turning corresponding to the blade profile is not achieved. This is the same as deviation in a compressor and is caused by similar flow behavior. Although not shown explicitly, deviation is accounted for in velocity diagrams, since they represent the turning angle that the flow actually undergoes rather than that corresponding to blade or vane camber. Moreover, the blades and vanes are designed to account for it. This does not mean that the flow fails to follow the suction surface of the blade because it is the *cross-passage average* exit flow angle rather than that on the surface that is used to define deviation and to determine work. As in a compressor, deviation in a turbine is due mainly to inviscid effects, caused by the flow streamline curvature adjusting itself in anticipation of the sudden elimination of any transverse pressure difference before the trailing edge is reached and the rear stagnation point being established. The effect is exacerbated by viscosity, in the form of boundary layer growth and wake mixing, by back-surface curvature and by the local Mach number. More detailed accounts appear in Refs. [1, 2].

An additional feature of a turbine airfoil, closely associated with deviation, is “uncovered turning” on the aft region of the suction surface. It may be seen in Fig. 3.2-3, that downstream of the throat the flow on the suction surface is no longer controlled by an adjacent blade. This means that deviation or even separation are no longer discouraged and subsonic flow is liable to decelerate and supersonic flow is liable to accelerate. Such behavior is made worse by increased uncovered back-surface curvature and is partly the reason why “flat-back” designs are often favored.

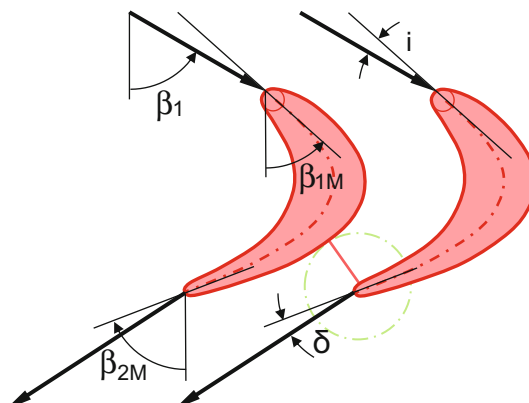


Fig. 3.2-3 Incidence, uncovered turning and under-turning on a turbine blade

3.2.2 Sign Convention for Angles and Circumferential Velocities

Just as for compressors, in quantifying and establishing the direction of both flow angles and metal angles, a sign convention is needed—the same one, in fact. A good approach for tangential velocities and angles is to adopt a “*positive in the direction of blade rotation*” sign convention. Then, in Fig. 3.2-1, the gas enters the vane axially ($\alpha_1 \approx 0^\circ$) at a modest value of absolute velocity V_0 , is accelerated and turned significantly through the vane passage and exits at a high absolute velocity V_1 and high positive swirl α_1 . The rotor leading edge metal angle β_{1M} is positive and the relative inlet swirl angle β_1 —which aligns roughly with the blade—is also positive. The relative exit swirl from the blade β_2 is then negative, the flow having been turned to the axial direction and then beyond to an angle greater in magnitude than the inlet value. The negative turning angle, $\beta_2 - \beta_1$, is shown clearly in the velocity diagram in Fig. 3.2-2.

A sign convention for angles is especially important in the design of vaneless, counter-rotating systems—a relatively new turbomachinery architecture.

Just as for compressors, we all know positive or negative incidence when we see it! Incidence is positive when the flow approaches the airfoil leading edge from beneath a forwards-extension of the camber line, i.e. onto the pressure side of the airfoil, as in Fig. 3.2-3 and, again, this applies to both blades and vanes.

Blade incidence is defined by:

$$i_{blade} = \beta_1 - \beta_{1M} \quad (3.2-4)$$

As the pressure side of a vane usually faces in the direction of rotation of the blade, both α_0 and α_{0M} are negative and the definition of vane incidence is given by

$$i_{vane} = \alpha_{0M} - \alpha_0 \quad (3.2-5)$$

where the subscript M denotes a metal angle.

The case of a vaneless counter-rotating turbine blade, is a special case. If the same direction of rotation is taken as positive for all stages, the signs for the gas angles and metal angles are reversed.

It should be noted that the sign convention may vary from one engine company to another and from one software vendor to another, so we need to know exactly what we are dealing with in any specific situation! There can also be a disconnect between a turbine department and a compressor department; whole blade sets have had to be scrapped because attention was not given to the direction of rotation, with or without a sign convention! Moreover, some commercial design codes can run perfectly well with a negative rpm but if only positive rpm is accepted, it may be necessary to “flip” the airfoils so the code runs. Then, it is critical that the blades be flipped back before manufacturing drawings are produced!

3.2.3 Construction

There is a single simple rule for constructing velocity diagrams, namely:

$$\text{Relative velocity } (W) = \text{absolute velocity } (V) - \text{blade velocity } (U) \quad (3.2-6)$$

Let's consider this as we look at Fig. 3.2-2. Flow enters the rotor blade with an absolute velocity from the upstream vane of V_1 . Subtraction of the blade speed vector, U , from the vector V_1 results in an inlet velocity relative to the blade of W_1 . The flow then accelerates through the blade passage—clearly in a relative sense—and emerges with a relative velocity of W_2 . If we follow the rule in (3.2-6) again, we obtain the absolute exit velocity of V_2 by adding the blade speed vector, U , to the relative flow velocity vector, W_2 . The algebra will always produce correct answers, regardless of the direction of rotation.

3.2.4 Use of Velocity Diagrams

So, what can we learn from velocity diagrams? One common and very elementary question might be, “What is the effect on incidence of changing the mass flow?” Another frequent question is, “What is the effect on incidence of changing the blade speed?” Both can be answered by sketching the velocity diagrams.

Let's look at what happens to Fig. 3.2-2 when the flow is increased. The outcome is indicated in Figs. 3.2-4 and 3.2-5, where the vectors change from grey to black. Flow rate and continuity are reflected in the axial component of velocity, so higher flow means higher axial velocity V_{ax} , which is the height of the pertinent velocity triangle. As the vane exit angle has not changed α_1 is also the same but V_1 is increased. The new relative flow velocity, W_1 , is determined by subtracting the blade speed vector, U , from the new V_1 . The relative swirl angle at blade inlet β_1 has increased and so has the incidence. The blade exit metal angle is unchanged, so the relative exit swirl remains the same and the new W_2 is obtained by extending the initial W_2 vector to account for the higher axial flow. Notice that because of the higher relative inlet swirl and despite no change in the blade metal angles, the flow turning is higher. However, since the incidence has increased, there will most likely be an incidence penalty when it comes to total pressure loss.

The absolute exit swirl angle has reduced, which—as it had a negative value—means more swirl and will lead to higher pressure losses in any downstream duct or conduit. The work per unit mass flow from the stage, is expressed by

$$\Delta H_{Sfg} = U \Delta V_U \quad (3.2-7)$$

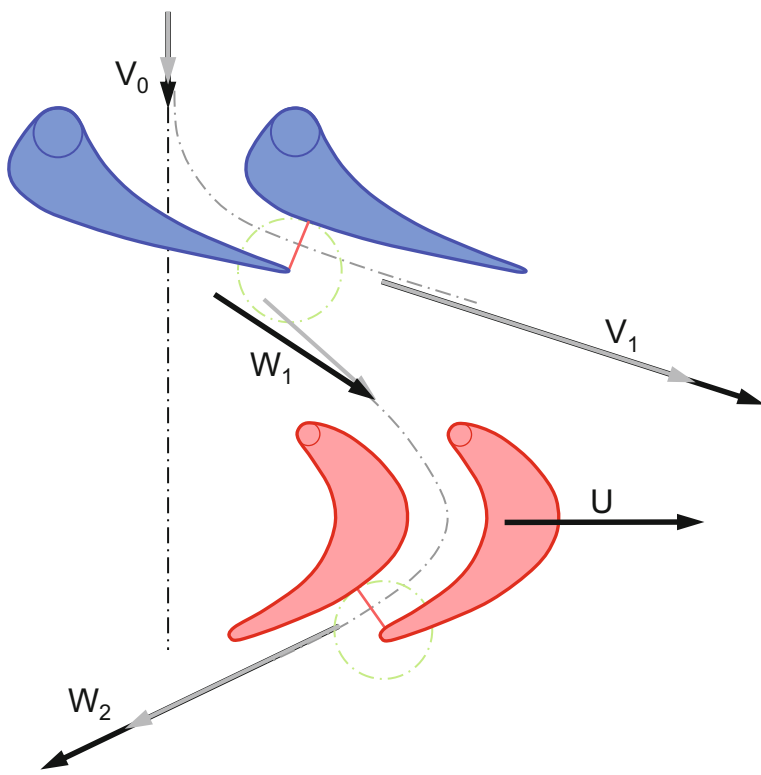


Fig. 3.2-4 Effect of flow increase on velocities

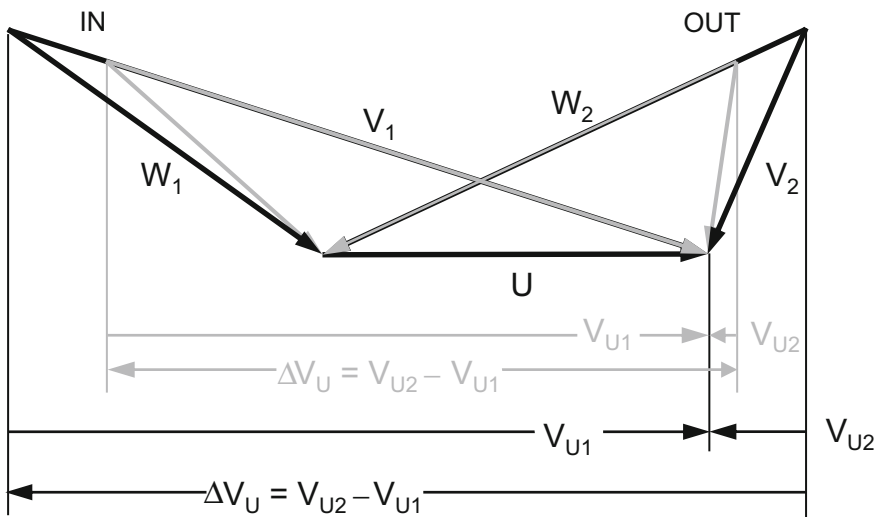


Fig. 3.2-5 Effect of flow increase on velocity diagram

and has increased due to higher turning—that is, a greater change in the angular momentum of the flow, as given by the change in whirl velocity. The higher flow rate will increase absolute power additionally.

If we begin again with Fig. 3.2-2, but now increase the blade speed, we generate the black velocity vectors in Figs. 3.2-6 and 3.2-7. The absolute velocity, V_1 , from the vane is unchanged in magnitude and direction. We determine W_1 , the inlet flow velocity relative to the blade, by subtracting the higher blade speed, U , from the absolute flow velocity, V_1 . The relative inlet swirl angle, β_1 , to the blade is reduced, as is the incidence. Regardless of the inlet angle, the exit flow is forced to follow the blade exit metal angle (neglecting any under-turning), so the relative exit velocity, W_2 , is unchanged but is shifted to the left in Fig. 3.2-7. Adding the increased blade speed, U , to W_2 generates the new absolute exit velocity, V_2 .

Increasing the blade speed has reduced the rotor incidence, causing it to become negative in our example. We might expect the increased blade speed to have produced more power, but in the rough sketch of Fig. 3.2-6 the increase in blade speed has been offset by a reduction in ΔV_U , so the outcome is uncertain without a more accurate calculation.

We can write Eq. (3.2-3) in terms of relative flow angles as

$$\Delta H_{Stg} = U(W_2 \sin \beta_2 - W_1 \sin \beta_1) \quad (3.2-8)$$

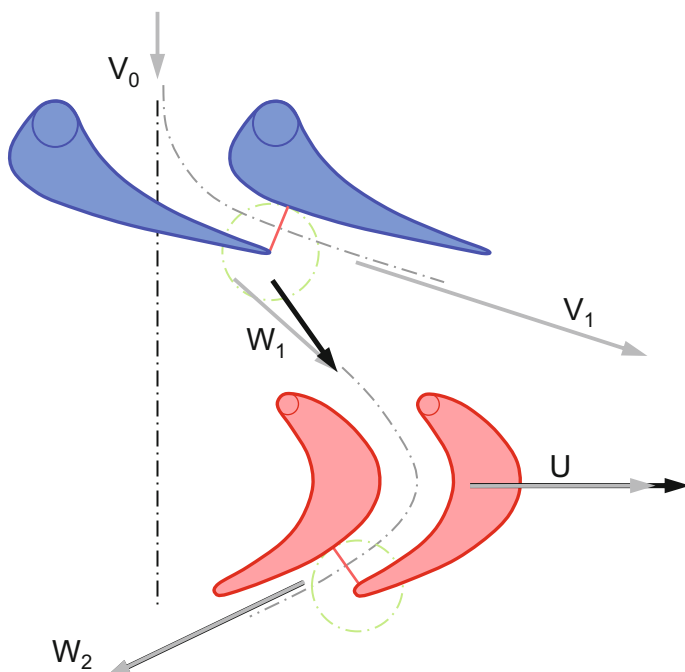


Fig. 3.2-6 Effect of increased blade speed on velocities

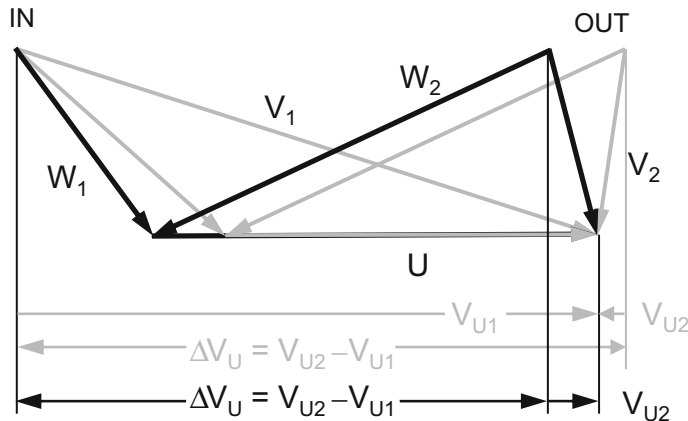


Fig. 3.2-7 Effect of increased blade speed on velocity diagram

If we apply our sign convention, the power is negative, and this is power extracted from the working fluid. The power supplied to the shaft is therefore positive and this aligns with the more general convention whereby we consider power delivered as positive.

3.2.5 Stage Characteristics

Three non-dimensional parameters are commonly used to describe or define a stage velocity diagram.

Loading coefficient, ψ , is expressed as

$$\Psi = \frac{\Delta H_{Stg}}{U_m^2} \quad (3.2-9)$$

where ΔH_{Stg} is the specific stage work (J/kg) and U_m is the mean blade speed. The mass-averaged value is strictly correct, but a simple geometric average may be used conveniently for a quick estimate. Unlike in compressors, blade tip speed is never used to evaluate turbine stage loading. It should be noted that, for a turbine, some organizations include $\frac{1}{2}$ in the denominator and this is often complemented using 2 in the denominator for a compressor, where the tip speed also may replace the mean value. We can use (3.2-3) to write

$$\Psi = \frac{UV_{ax}(\tan \beta_1 - \tan \beta_2)}{U_m^2} = \frac{V_{ax}(\tan \beta_1 - \tan \beta_2)}{U_m} = \frac{\Delta V_U}{U_m} \quad (3.2-10)$$

and it can be seen from Fig. 3.2-2 that the loading coefficient represents the distance between the peaks of the “IN” and “OUT” velocity triangles divided by the common base. The stage loading definition may be extended to hub and casing, where it can be implemented to illustrate span-wise variations in stage loading.

Flow coefficient, Φ , is defined as $\frac{V_{ax}}{U_m}$

$$\phi = \frac{V_{ax}}{U_m} \quad (3.2-11)$$

where V_{ax} is the axial velocity of the gas, usually at the blade inlet and U_m is the mean blade speed, as before. Figure 3.2-2 tells us that the flow coefficient represents the ratio of the height of the velocity triangles to their common base. Of course, this is strictly true only if the axial velocity of the working fluid remains constant through the blade, but it does not diminish the usefulness of the parameter.

Knowing how the separation of the peaks and height of the velocity triangles are related to the base, supplies much of what we need to know to define a velocity diagram completely, but we still lack one feature—and that is how the peaks are located laterally in relation to the base. The parameter *stage reaction* gives this information.

Stage reaction, Λ , is defined as the ratio of the change in static enthalpy through the blade to that through the stage, namely

$$\Lambda = \frac{\Delta h_{srotor}}{\Delta h_{stage}} = \frac{h(T_{s1}) - h(T_{s2})}{h(T_{s0}) - h(T_{s2})} \quad (3.2-12)$$

Relative to the rotor, the flow does no work, and the steady flow energy equation tells us that through the rotor the change in static enthalpy is equal to the change in kinetic energy. Referencing Fig. 3.2-2, the numerator of (3.2-12) can be written as

$$h(T_{s1}) - h(T_{s2}) = \frac{1}{2}(W_2^2 - W_1^2) = \frac{1}{2}V_{ax}^2(\sec^2\beta_2 - \sec^2\beta_1) \quad (3.2-13)$$

From elementary trigonometry

$$\sec^2 = 1 + \tan^2 \quad (3.2-14)$$

So (3.2-13) becomes

$$h(T_{s1}) - h(T_{s2}) = \frac{1}{2}V_{ax}^2(\tan^2\beta_2 - \tan^2\beta_1) \quad (3.2-15)$$

Through the stage, the change in static enthalpy is given by

$$\begin{aligned} h(T_{s0}) - h(T_{s2}) &= (h(T_0) - \frac{1}{2}V_0^2) - (h(T_2) - \frac{1}{2}V_2^2) \\ &= (h(T_0) - h(T_2)) - \frac{1}{2}(V_0^2 - V_2^2) \end{aligned} \quad (3.2-16)$$

If we assume, for convenience, that we have a repeating stage, where the velocity at exit is equal to that at inlet (i.e. $V_2 = V_0$), then (3.2-16) becomes

$$h(T_{s0}) - h(T_{s2}) = h(T_0) - h(T_2) \quad (3.2-17)$$

And, from (3.2-3), we can write the denominator of (3.2-12) as

$$h(T_{s0}) - h(T_{s2}) = UV_{ax}(\tan \beta_1 - \tan \beta_2) \quad (3.2-18)$$

Re-formulating (3.2-12) from (3.2-15) and (3.2-18), we obtain

$$\Lambda = \frac{\frac{1}{2}V_{ax}^2(\tan^2 \beta_2 - \tan^2 \beta_1)}{UV_{ax}(\tan \beta_1 - \tan \beta_2)} = -\frac{V_{ax}}{2U}(\tan \beta_1 + \tan \beta_2) \quad (3.2-19)$$

In an engine or a turbine test rig, having stage reaction in terms of static enthalpy is not especially useful, because static enthalpy is not particularly easy to measure. However, we can modify Eq. (3.2-11) to a more practical form. If we take the standard entropy equation

$$Tds = dh - vdp \quad (3.2-20)$$

and consider the process to be isentropic and incompressible, then $ds = 0$ and we can state that

$$dh = vdp = \frac{dp}{\rho} \quad (3.2-21)$$

where v is specific volume and ρ is density. Integrating from condition 1 to condition 2 for the numerator and from 0 to 2 for the denominator, we can re-write Eq. (3.2-12) as

$$\Lambda = \frac{P_{s1} - P_{s2}}{P_{s0} - P_{s2}} = \frac{\Delta P_{srotor}}{\Delta P_{sstage}} \quad (3.2-22)$$

A stage with 50% reaction is a special case. The symmetry of its velocity diagram is immediately obvious in Fig. 3.2-8, with $V_1 = W_2$, $\alpha_1 = \beta_2$, etc. It is very common to begin a mean line design of a turbine stage by setting the reaction at 50%, where V_1 and W_2 are at their lowest common value for fixed values of stage work and mean blade speed, since this tends to minimize total pressure losses in both vane and blade. However, we shall see later, when we consider span-wise variation, that 50% reaction is not always best.

Figure 3.2-9 contains a more general velocity diagram, where the flow path is less divergent than in our previous cases and the axial velocity has increased.

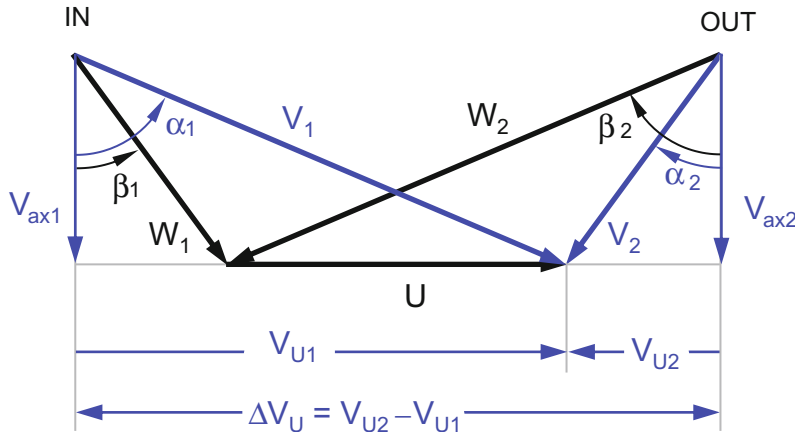


Fig. 3.2-8 A symmetric velocity diagram with 50% reaction

For different values of V_{ax1} and V_{ax2} we can modify (3.2-19) to express stage reaction as

$$\Lambda = \frac{\frac{1}{2}(V_{ax1}^2 \tan^2 \beta_1 - V_{ax2}^2 \tan^2 \beta_2)}{U(V_{ax1} \tan \beta_1 - V_{ax2} \tan \beta_2)} = -\frac{(V_{ax1} \tan \beta_1 + V_{ax2} \tan \beta_2)}{2U} \quad (3.2-23)$$

If we use a ruler and protractor to evaluate the parameters in (3.2-23) from Fig. 3.2-9, the stage reaction turns out to be about 0.62.

There is also a simple graphical method to determine stage reaction from a velocity diagram; connect the peaks of the inlet and exit triangles, bisect that line and drop a perpendicular to the blade speed vector. The fraction of the blade speed at the point of intersection determines the reaction. This is the ratio AB/AC in Fig. 3.2-9, which gives a reaction of 0.62.

An additional useful parameter usually calculated in a mean line design code is the *Zweifel loading coefficient* [1] and it is convenient to introduce it here. The Zweifel coefficient, Z_w , is a measure of the actual tangential force on a vane or blade as a fraction of the ideal value. For a given turning angle, since all the flow in the annulus must be turned, the more airfoils there are, the lower their loading. The loading coefficient is also inversely proportional to chord. Figure 3.2-10 is a sketch of the pressure distribution around a typical turbine airfoil.

The Zweifel loading coefficient is given by the ratio of the actual tangential force on a blade section to the ideal tangential force. The former may be obtained from the velocity diagram. The latter would occur if the static pressure on the pressure surface corresponded to the stagnation pressure at the leading edge and the static pressure over the suction surface corresponded to the exit value. In Fig. 3.2-10, the actual tangential blade load corresponds to the enclosed area of the static pressure distribution while the ideal value corresponds to the light blue rectangle.

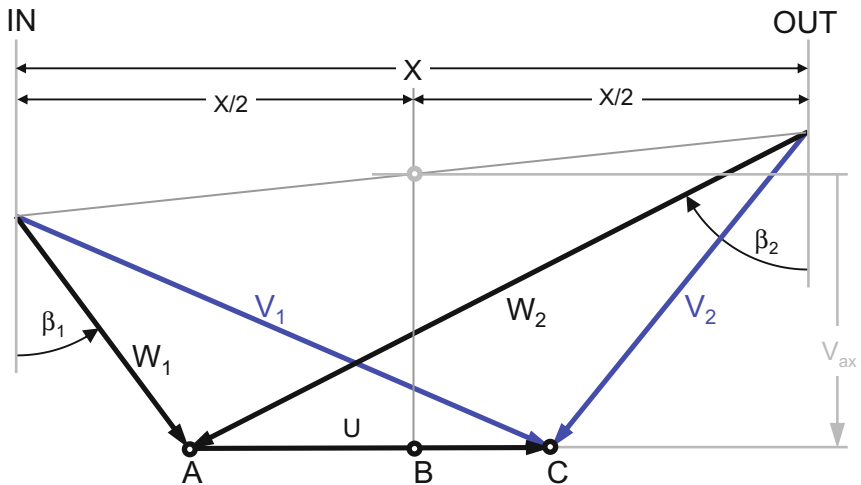


Fig. 3.2-9 General velocity diagram for a turbine

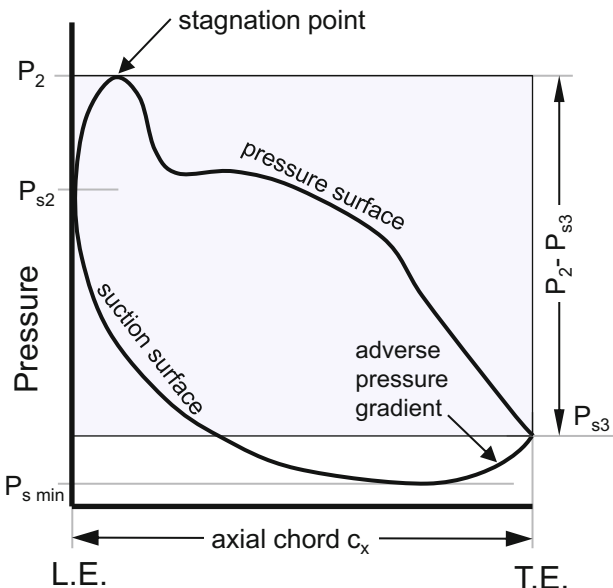


Fig. 3.2-10 Pressure distribution around turbine airfoil

The Zweifel coefficient is of interest because it influences the spacing or pitch and hence the number of airfoils. The axial chord also determines it. Ultimately, it drives the weight and the cost of a turbine stage. It is defined, per unit height or span, by

$$Z_w = \frac{2F_U}{\rho W_2^2 c_{ax}} \quad (3.2-24)$$

where F_U = tangential force, ρ = gas density, W_2 = trailing edge relative velocity, and c_{ax} = axial chord.

If we assume incompressible flow, the axial velocity is constant and the tangential force per passage per unit height, F_U , is given by

$$F_U = \text{Passage flow} \times \Delta V_U = V_{ax} \rho s [V_{ax} (\tan \beta_1 - \tan \beta_2)] \quad (3.2-25)$$

where V_{ax} = axial velocity and s = blade pitch.

Substituting in (3.2-24) gives us

$$Z_w = \frac{2V_{ax} \rho s [V_{ax} (\tan \beta_1 - \tan \beta_2)]}{\rho V_2^2 c_{ax}} \quad (3.2-26)$$

But

$$\frac{V_{ax}^2}{V_2^2} = \cos^2 \beta_2 \quad (3.2-27)$$

So, from (3.2-26) we obtain

$$Z_w = 2 \cos^2 \beta_2 \frac{s}{c_{ax}} (\tan \beta_1 - \tan \beta_2) \quad (3.2-28)$$

We can apply the same process to a vane in the absolute frame to obtain a similar equation for the Zweifel loading coefficient in terms of α_1 and α_2 , using its trailing edge velocity V_2 .

In 1954, experimental results indicated that an optimum Zweifel coefficient would be encountered between 0.8 and 1.0 and this leads to suitable values of airfoil count and solidity. Farokhi [2, pp. 715–717], examines the effect of inlet and exit flow angles on airfoil solidity ($\sigma = s/c$) based on a recommended value of Zweifel loading parameter. Coull and Hodson [3] address the suitability of Zweifel coefficients in optimizing the performance of LP turbines. They present an enlightening comparative study of different loss models using a *Smith Chart* as a vehicle and offer an alternative parameter—the circulation coefficient—as an improved assessment of loading for high-lift blades in modern LP turbines.

Circulation coefficient, C_O , is defined as the ratio of the circulation around the blade to the ideal value and is expressed as

$$C_O = \frac{\text{actual circulation}}{\text{ideal circulation}} = \frac{\oint V_S}{V_2 S_O} = \oint \left(\frac{V_S}{V_2} \right) d \left(\frac{S}{S_O} \right) \quad (3.2-29)$$

where V_S = local surface velocity, S = surface distance, V_2 is trailing edge velocity, S_O = total surface distance around profile.

It should be noted that a more complicated expression for a compressible Zweifel coefficient may be derived, where the axial velocity changes across the vane or blade row, and this is most often used in industry.

3.3 Preliminary Turbine Design

3.3.1 HP Turbine

Turbine performance may be quantified most directly by either isentropic or polytropic efficiency. However, this is a *result* of the turbine design as opposed to an *input*, and it is best that the turbine designer knows what he or she is up against.

There are several parameters that capture the severity of the turbine's task by combining only a few basic thermodynamic quantities. Examples of these are *stage loading coefficient* $\Psi = \Delta H/U^2$, *reduced flow* $W \sqrt{T}/P$, and *work coefficient* $\Delta H/T$.

- The stage loading coefficient is very important because it is a direct link to the velocity diagram and hence to all the relevant velocity components and flow and blade angles, in absolute and relative frames of reference. It compares the extraction of thermodynamic energy (change in specific enthalpy) with mean “blade energy”, and is recognized by turbine designers for its correlation with flow coefficient and isentropic efficiency.
- The value of reduced flow is that it relates directly to Mach number and is a measure of the capacity of the turbine and of its proximity to choking. The vane row capacity is usually considered in this context, although relative conditions in the blade row should also be addressed. If severe choking is encountered, the required work extraction will not be met, except by over-sizing, and then only at the expense of increased profile losses, not to mention the increase in turbine weight.
- The work coefficient, $\Delta H/T$, compares work extraction with the inlet conditions, T usually being T_{41} , the turbine rotor inlet total temperature. The higher the inlet temperature, the easier it is to deliver the necessary power.

Once the number of stages has been decided, based on work split and stage loading, the vane and blade rows can be defined. In order that the turbine is not too heavy,

the stage loading must be somewhere near the high limit, but not necessarily at the extreme. This process may be made easier using turbine design envelopes, as described in Sect. 3.4.

The turbine inlet area can either be derived from a preferred value of Mach number or stated directly. Since the specific stage work is pre-determined and the rpm has been fixed by the HP compressor, the blade mean radius is the only remaining variable. Fixed values of the stage-loading limit can be associated with specific levels of turbine technology; hence this parameter may be used as a major design characteristic. Varying stage loading moves the turbine in or out.

Increasing the radial dimensions (moving the turbine outwards) will effect a general reduction in gas velocities—work extraction is aided by increased blade speed—although this is almost invariably at the expense of weight, largely because the disk sizes increase! While a reduction in stage loading will lead to improved efficiency, it needs to be balanced against higher sensitivity to tip clearance (shorter blades) and windage losses. An additional, useful piece of information is the trade-off between turbine efficiency and weight, which should be evaluated at an aircraft level.

The overall turbine geometry is obtained simply by joining the inlet to the exit, and the best method of fixing exit dimensions is via an upper limit on AN^2 . The background of this term is explained in subsection 1.2.7.5 Thus, a vital connection is made with the structural integrity of the machine. The distribution of annulus area through the turbine may be manipulated via local geometric parameters, and via an increase in the value of AN^2 at the exit, subject to the imposed limit.

To minimize total pressure losses due to friction, excessive Mach numbers should be avoided. These are caused by small annulus areas and high values of swirl, compounded by reductions in static temperature (\approx speed of sound squared) and density associated with high work extraction. Velocities at vane and blade trailing edges may be traded via stage reaction.

3.3.2 LP Turbine

Many of the design guidelines for HP turbines also apply to their LP counterparts, except that, within the component hierarchy, the geometry of the HP turbine exit defines the LP turbine inlet dimensions. Unless the two are close-coupled, as in the case of a vaneless LP unit, an inter-turbine duct affords some freedom and an outward shift results in more LPT blade speed and lower loading at a fixed value of LP spool rpm.

On high bypass engines the LP turbine usually has more stages than an HP turbine, so possible variations of interstage work split make life more interesting for the preliminary designer. Knowing the rpm, it would be reasonable to assume a constant mean blade radius, fixed at a ratio to the HP turbine exit value, to make an initial estimate of the number of stages. The design process is also similar to that above, with a reduction of loading being applied in the final stage as a concession to

reduced exit swirl and low exhaust losses prior to the final expansion. An adjustment to the final stage reaction may also assist in achieving minimal exhaust loss.

Low Reynolds numbers, typically around 200,000, are prevalent in LP turbines and when this is combined with the high turning angles needed for high loading and low blade thickness, difficulties arise with flow transition and separation. Although the general approach to HP and LP turbine design may be similar, attention must be paid to significant differences in the details of the flow structure. Additionally, the higher aspect ratios present in LP turbines means that, compared to HP turbines, secondary flow effects are often reduced in the mid-span region of the blading passages. For many years this resulted in emphasis being given to research on the former. However, having recognized the problem, secondary flows and their associated losses have been given more attention.

References [4–6] describe the design problems further and indicate potential solutions but still underscore the need for further work. For example, specific mention is made in Ref. [4] to the origins of corner vortices and the interaction between suction surface separation bubbles and the flow on the end wall. Reference [5] examines our ability to distinguish the primary design parameters from more general guidelines and this is closely connected with the knowledge needed to expand the usable design space for LP turbines, outlined in Ref [5]. Reference [6] also demonstrates that the Zweifel loading coefficient may no longer be adequate to assess blade loading in LP turbines, since similar values of that coefficient can quite easily apply to a broad range of blade loadings and to both laminar and turbulent boundary layers. A new circulation coefficient is proffered in its place.

Reference [5] also tests the efficacy of established mean line loss models for LP turbines and recommends that some be replaced. Reference [6] shows that front-loaded, high lift blades offer improvements in mid-span performance which is off-set by higher end-wall losses than rear-loaded designs.

Progress in the past few years has led to significant reductions in the total number of LP turbine vanes and blades over the complete range of LP turbine pressure ratios. This has been due partly to new design features such as non-axisymmetric end wall contouring, to modern computer-aided optimization methods and to the improved prediction of transition by CFD.

3.3.3 Mean Line Analysis

The *Smith Chart* [7] was introduced in 1965 and is one of the earliest and simplest empirical turbine performance models, based on extensive measurements from turbine rig tests at Rolls-Royce in the nineteen-fifties and -sixties. In this model, contours of isentropic stage efficiency are plotted against flow coefficient and stage loading coefficient. By intent, the data is limited to stages with 50% reaction and the values of efficiency are corrected to zero tip clearance (Fig. 3.3-1).

Stage loading coefficient (ψ) is the change in angular momentum (ΔV_U or ΔW_U) normalized by the mean blade speed U . It is also known as the stage loading factor

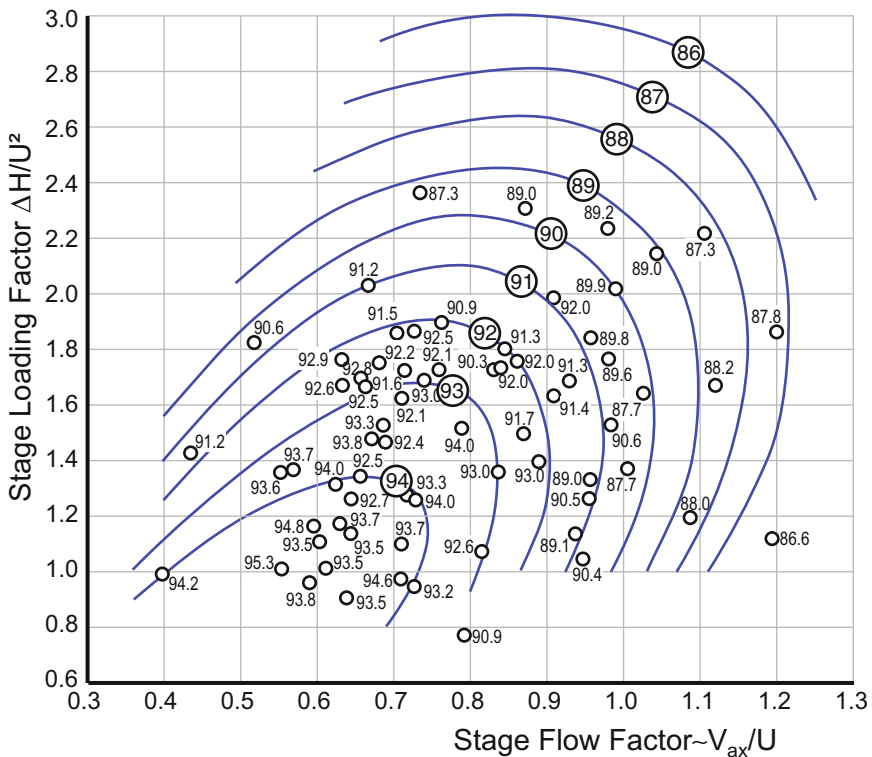


Fig. 3.3-1 The original Smith Chart [7]

$\Delta H/U^2$ because—according to Euler's law, $\Delta H = U \times \Delta V_U$. For a constant mean blade speed, it is an indicator of how much work is generated per unit of mass flow and, for a constant axial velocity, how much flow turning is done in the rotor blade.

High loading capability in a multi-stage machine means that fewer stages can be used, leading to reduced weight and cost. For a given blade speed, a high flow coefficient ($\phi = V_{ax}/U$) means that more flow can be accepted through an annulus of a given size, again resulting in reduced weight and cost.

Numerous updates have been made to the original 1965 *Smith Chart* to relocate and re-form the efficiency contours because of improved turbine designs, moreover, contemporary versions often include additional contours of parameters of interest to a specific program or study. As turbine aerodynamics has improved, for fixed coordinates, the same efficiency contours have moved outwards away from the origin. A lateral shift of the contours to the right indicates our ability to pass more flow through the annulus without performance penalty. A vertical shift upwards is a measure of our ability to increase stage loading and hence reduce the stage count without penalty.

Our understanding has increased immensely over the past six decades or so due to the development of improved instrumentation, combined with more effective data acquisition and processing techniques. Knowledge of turbine flow field features was obtained initially from measurements on two-dimensional cascades. Data from test rigs was only added later and was used specially to characterize how flow elements relate to moving blades, such as vortices due to over-tip leakage. Stage efficiency was calculated directly from measurements of relevant inlet and exit data and shaft work.

The development of three-dimensional flow structures and their contribution to losses in compressors has been outlined in Sect. 2.3.5. These also appear in turbine blade passages, where secondary flows are often magnified by higher turning and more streamline curvature. While the rapid growth of boundary layers—the source of many problems in compressors—is not as severe a problem in turbines, boundary layer behavior is often influenced adversely by the ejection of cooling flows from blade surfaces. All departures of the flow from uniform cylindrical or conic surfaces are essentially secondary flows; recognition and description of them are the results of the decades of experimental investigation and analysis.

One interpretation of coherent features of the flow in a turbine blade passage is shown in Fig. 3.3-2. While friction loss over the vanes and blades constitute a major performance deficit in the form of profile loss, most of the features in Fig. 3.3-2 contribute to secondary loss. Over-tip leakage loss is usually book-kept separately.

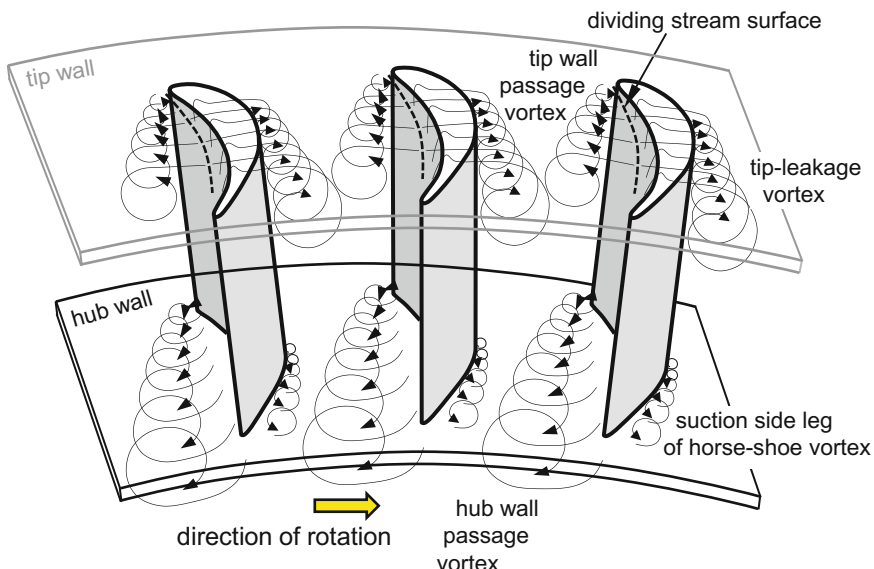


Fig. 3.3-2 Vortices in a turbine Blade passage with tip clearance (adapted from Ref. [16])

Numerical modeling at various levels of fidelity is now recognized as being a necessary complement to a more efficient and cost-effective approach. Mean line codes are relevant and used extensively to simulate a new system at its design point, to define the range of a design region and to explore alternatives, enabling limited resources to focus on cases that align with program objectives. At the preliminary design stage, trends are often more important than absolute values.

3.3.4 Development of a Mean Line Code

Mean line performance models are founded on our recognition and understanding of the flow field features and they have evolved continually since the 1950s, as our knowledge has grown. To model the general behavior of turbomachinery flows and the associated loss mechanisms we must first identify their physical features and interactions and then express their effects quantitatively. Since their inception, development and implementation of a design tool for a turbine or compressor has followed the sequence in Fig. 3.3-3.

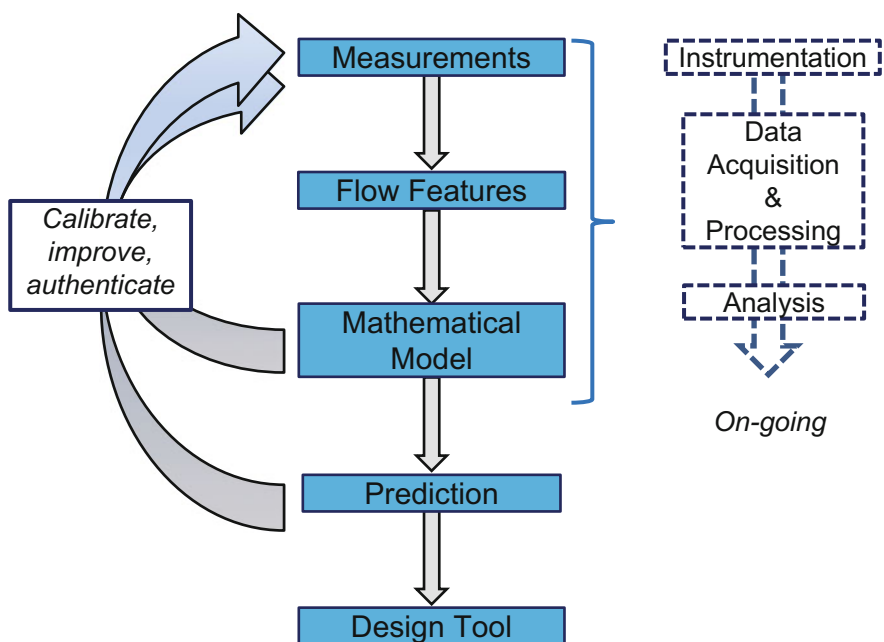


Fig. 3.3-3 Development of a mean line design code

In more detail, the sequence presented in Fig. 3.3-3 for the generation of design tools from flow measurements is:

- Interpretation of the measurements leads to identification and improved understanding of the primary flow field features and the associated physical processes.
- A more advanced approach, used to this day, is to express components of either total pressure loss or total enthalpy loss by correlating them empirically with suitable combinations of geometry and flow field characteristics.
- As knowledge improves, the loss models are tested and calibrated against additional, more specific, measurements. Improvements are made, and the verification process continues. This is an on-going process for engine manufacturers and others with the resources and financial incentives.
- We finally become sufficiently confident (or desperate) to use the models to predict turbine performance without measurements.
- At this stage, the models become design tools.

3.3.5 *Structure of a Mean Line Code*

The construction of a mean line model is based on the ability to generate velocity diagrams at the mean streamline. Usually, the “mid-height” radial location is determined by having half the mass flow on either side, although the average radius may be used occasionally.

The ability to estimate total pressure is essential and the quality of any turbine mean line code is assessed primarily by its ability to account for pressure losses accurately. Total pressure is a convenient currency because we can measure it easily. Changes in enthalpy are also used for loss accounting and the two properties can be interchanged. The resulting loss coefficients are expressed in terms of either ideal exit dynamic head or ideal exit kinetic energy.

Figure 3.3-4 shows the structure of a typical turbine mean line design code and the sequence in which the subroutines are run. Turbine work is obtained from the engine cycle at the selected design point from the *INPUT* file. The Input file also supplies the work split between the stages, which is usually based on practical experience, although without such knowledge an equal division is a good starting point. Reducing the work in first and last stages often enables unwelcome conditions delivered by combustor to be accommodated and exit swirl to be reduced.

No major assumptions are made about the turbine geometry. *FLOWPATH* represents a subroutine where the flow path is generated, and the blading is laid out, based initially on axial chords, and axial gaps. The mean radius of the first blade is obtained from the input values of stage loading coefficient, rotational speed, and stage work. Knowing the rpm and the overspeed factor f_{os} , the turbine exit area is

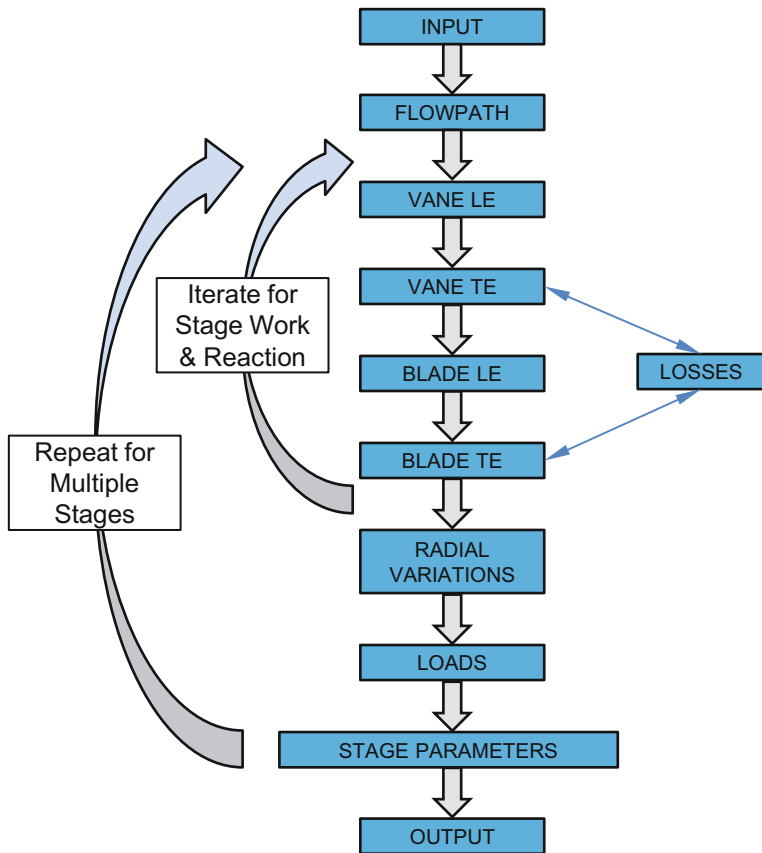


Fig. 3.3-4 Structure of a typical turbine mean line design code

derived from the maximum value of AN^2 at the turbine exit, where A is the exit area and N is the mechanical design speed (*design rpm* \times f_{os}). Axial gaps are provided in INPUT as fractions of the relevant upstream airfoil axial chords. The remaining flow path dimensions are obtained from the distribution of flow area through the complete machine via mean, stage slopes, blade slopes. Having generated a smooth flow path, the vane and blade coordinates are adjusted to account for prescribed values of airfoil taper (axial chord at tip/axial chord at hub) although the mid-height chord remains constant. Further adjustments are made to the flow path coordinates to account for constant blade tip diameters, if appropriate. A constant blade tip diameter is usually needed for an HP turbine blade where shrouds and seals are unable to be carried, since an axial shift would not cause a change in tip clearance.

Subroutines *VANE_LE* and *BLADE_LE* calculate all aerodynamic and thermodynamic parameters needed to construct the velocity diagrams, with initial guessed

values of axial velocity and swirl angle leading into an iterative procedure. Mean line inlet values for the first vane are directly or indirectly provided by the *INPUT* file; data for the remaining cases comes from calculations at the preceding trailing edges. The exit velocity diagrams are generated in *VANE_TE* and *BLADE_TE* based on the input work required form each stage, the calculations being done in the appropriate frames of reference. Exit temperatures are determined initially from the work extraction but these are adjusted subsequently as any cooling flow is mixed in. The corresponding exit pressure is obtained by estimating the total pressure losses through the vane or blade row. The *LOSSES* subroutine is called from each of the exit calculations, again ensuring that the flow angles and velocities are either absolute or relative, as appropriate.

Having calculated mean line parameters, a free-vortex condition is assumed to enable flow parameters to be estimated at hub, tip and other radial locations defined in the input. This is applied in the sub-routine *RADIAL VARIATIONS*. Axial and tangential loads are often needed in preliminary design, so these are also estimated for each vane and blade row in *LOADS*, based on changes in static pressure.

STAGE_PARAMETERS calculates and summarizes the overall parameters of interest for individual stages. Average inlet and exit values of pressure and temperature, various forms of pressure ratio, various forms of efficiency, corrected flow, corrected speed, power, torque, stage loading coefficient, stage flow coefficient, loss break-down (a rule of thumb for optimum performance is to make profile loss and secondary loss roughly equal), Zweifel coefficient are all examples. Some may be legacy parameters and others derived specially for a new program. Finally, the output is presented in a usable format.

Figure 3.3-5 contains geometric characteristics of vanes and blades commonly used in design codes and loss models.

The stagger angle (ϕ) for a vane or blade may be estimated reasonably well from either gas angles or metal angles. Maximum thickness to chord ratios (t_{max}/c) are also determined empirically, based on the airfoil turning angle or camber angle. It is reasonable to assume that the greater the turning, the greater t_{max}/c will be. The true chord, c , is easily obtained from the axial chord and the stagger angle.

3.3.6 Mean Line Loss Models

Variations of the *Smith Chart* offer a rapid but approximate method of estimating turbine stage efficiency from velocity diagrams. Mean line design codes incorporate an improved approach to performance evaluation by incorporating a detailed appraisal of losses. Their quality depends primarily on their ability to do this accurately. Essentially, all mean line codes contain the same velocity diagram calculations, undertaken in the same sequence; they differ only in how the losses are modeled.

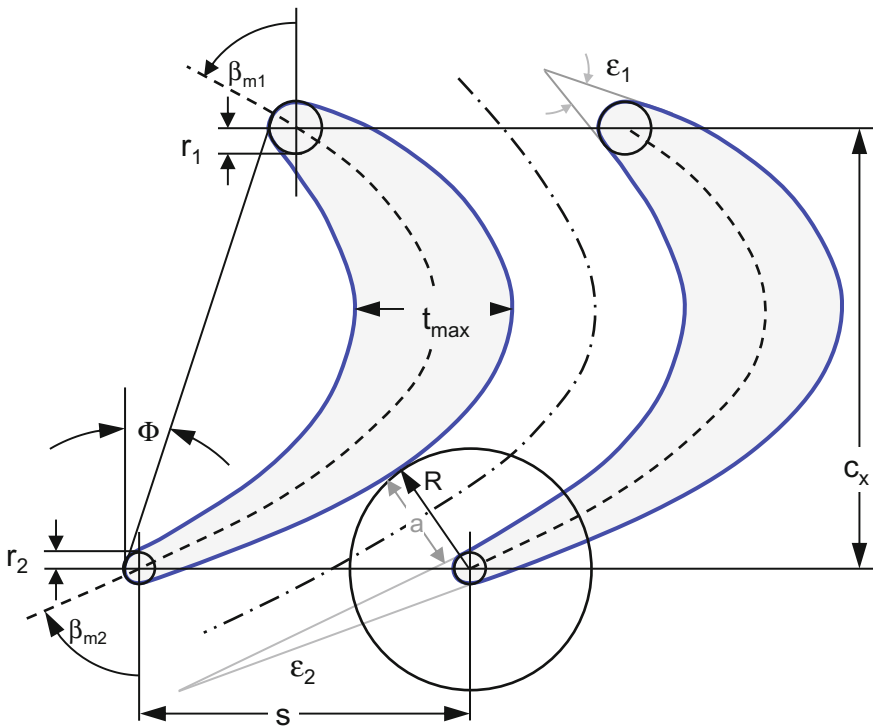


Fig. 3.3-5 Turbine cascade terminology.

β_{m1}	L.E. metal angle	β_{m2}	T.E. metal angle	ϵ_1	L.E. wedge angle	ϵ_2	T.E. wedge angle
c	chord	$\Delta\beta_m$	camber angle	s	pitch	a	throat opening
r_1	L.E. radius	r_2	T.E. radius	R	section radius		
Φ	stagger angle	c_x	axial chord	t_{max}	max thickness		

Two different approaches are taken in Refs. [8–11], which are examples of mean line loss models that span the early history of the development of mean line design codes for axial turbines and upon which most current mean line codes are based. The first approach, used in Refs. [8–10] accounts for loss components using pressure loss coefficients, Y —the total pressure loss divided by the exit dynamic head for a vane or blade row.

The overall loss for either a vane or a blade is given in the form

$$Y_T = (Y_P f_{RE} + Y_S + Y_{TET}) \times \text{corr}_{PTC} \quad (3.3-1)$$

where

- Y_P basic profile loss coefficient,
- f_{RE} a Reynolds number correction,
- Y_S secondary loss coefficient,
- Y_{TET} trailing edge loss coefficient,
- corr_{TC} tip clearance loss correction.

The second approach, used in Ref. [11], quantifies loss components using energy loss coefficients, X—the reduction in enthalpy divided by the exit kinetic energy for vane or blade row.

$$X = \frac{\Delta H_{s,loss}}{\frac{1}{2}V_{ex}^2} = \frac{\frac{1}{2}V_{is,ex}^2 - \frac{1}{2}V_{ex}^2}{\frac{1}{2}V_{ex}^2} = \frac{V_{is,ex}^2 - V_{ex}^2}{V_{ex}^2} - 1 \quad (3.3-2)$$

Experience has allowed each loss element to be attributed to some combination of the blade geometric parameters shown in Fig. 3.3-5 and relevant flow parameters. Examples of geometric features are airfoil solidity, aspect ratio and thickness/chord ratio. Flow characteristics of interest are turning angle and exit flow velocity or Mach number. Loss elements also may be corrected for Reynolds number and Mach number, where appropriate. Expressions for the loss elements developed in Refs. [8–10] are discussed in subsection 3.3.7 but comments on the effects of cooling air will be made later in subsection 3.3.8. Simplified examples of the application of turbine mean line loss models can be found in Refs. [2, 12]. Figure 3.3-6 illustrates how the two types of loss coefficient relate to the turbine expansion process.

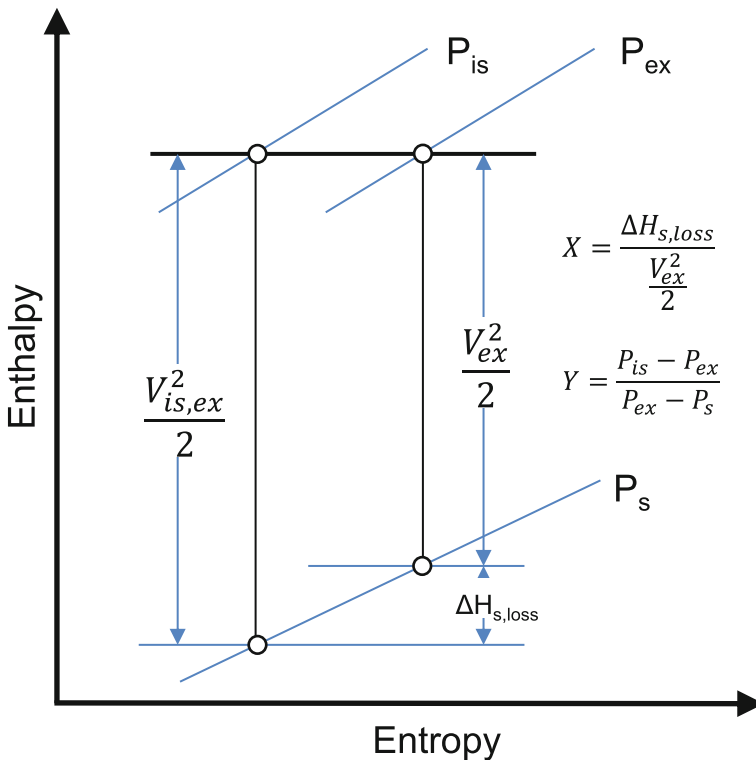


Fig. 3.3-6 Cascade loss description alternatives

Almost all codes in current use have been derived either from these or from similar numerical simulations. Industrial versions have been modified considerably with data derived from research programs using cascades and turbine test rigs, supplemented by results from engine tests. This proprietary information has been used either to change the format of the loss correlations or to alter the coefficients in the loss component equations often to such an extent where, if we were able to view the source codes, we would find the original models hard to recognize. Development of mean line performance models is still underway with improvements to individual loss components continually being generated. References [13–16] are examples of progress made relatively recently to enable these simple turbine design codes to keep pace with practical developments and aerodynamic advances.

3.3.7 *Loss Components*

Losses are categorized as follows. We shall refer to the larger units as *components* and the smaller units as *elements*.

-
- Profile, Y_{P_TOTAL}
 - Basic profile, Y_{P-BASE}
 - Shock, Y_{SHOCK}
 - Cooling air ejection, Y_{COOL}
 - Reynolds number correction, f_{Re}
 - Secondary, Y_S
 - Trailing edge, Y_{TET}
 - Overtip leakage, Y_{TCL}
 - Cooling air mixing, Y_{MIX}
-

3.3.7.1 Profile Loss

Profile losses are incurred because of viscous and turbulent dissipation due to motion of the flow field relative to the vane and blade rows. This is confined to the boundary layers and can include separation. Profile loss is the most complex part of the loss model. A basic profile loss coefficient, Y_{P-BASE} , is quantified in terms of leading and trailing edge flow angles, and maximum thickness-to-chord ratio.

Shock losses address the possible impact of supersonic drag rise due to the formation of trailing edge shocks. Depending on the Mach number at the leading edge and the acceleration through the vane or blade passage, shocks may occur near the trailing edge. Since, in general, incident Mach numbers are highest at the hub, the potential shock loss is applied to account for local high-speed effects at hub inlet Mach numbers greater than 0.4.

Release of the coolant from the blade surface causes growth of the boundary layer and increased turbulence and may also result in boundary layer separation. Note that this is independent of and additional to the kinetic energy mixing effects between the coolant and the free stream. Its influence on profile loss can be minimized by selective location of the cooling holes and careful tailoring of their shapes.

Up to this point, it has been assumed that the profile loss coefficient has been calculated at a reference Reynolds number of 200,000, based on true chord. For significant deviations from this, a Reynolds number adjustment is applied to the overall profile loss, Y_{PO} .

3.3.7.2 Secondary Loss

Secondary loss is closely influenced by the shape of the passage cross section, and are quantified conveniently in terms of the aspect ratio of the airfoil. In addition to the transverse flows caused by curvature of the blade passage and radial forces, the more detailed secondary flow patterns are the result of viscous interaction between the boundary layers on the vane or blade and the inner and outer casings.

For HP turbine blades with aspect ratios close to unity, the large vortex structures tend to fill the passage and secondary losses are high. For LP turbine blades, the mid-passage flow remains relatively undisturbed and the secondary losses are relatively low.

3.3.7.3 Trailing Edge Loss

Trailing edge loss is expressed as a pressure loss coefficient, Y_{TET} , which is a function of trailing edge thickness expressed as a fraction of throat opening—in other words, a function of trailing edge blockage.

3.3.7.4 Over-Tip Leakage Loss

The simplest over-tip leakage loss model considers the tip leakage flow as being unavailable to do work. Its effect is estimated very simply by applying a factor to the work term in the efficiency equation that expresses the clearance area as a fraction of total annulus area to the net work from the turbine stage after the other loss components have been allowed for. The effect of tip seals may also be considered.

A better estimate of the leakage flow could be obtained by considering the tip clearance in relation to the boundary layer profile and thickness. An even more realistic approach includes the estimation of the leakage flow over the unloaded blade tip, its interaction with the primary flow, the generation of a “scraping” vortex and its subsequent dissipation but that will not be attempted here.

At this point in the code, the profile, secondary, and trailing edge loss coefficients are summed to produce Y_T , the stage efficiency is calculated and the adjustment for blade tip clearance is applied.

3.3.8 Effects of Cooling Air

Cooling air is used to sustain the life of turbine vanes and blades in regions where the gas temperature is too close to a value safe for the material. Since the advent of gas turbine engines, turbine entry temperatures have risen steadily in pursuit of improved cycle performance and—despite significant advances in material properties—the quantity of cooling air used has increased accordingly. Therefore, the importance of estimating accurately how cooling loss affects performance has become increasingly important.

Cooling loss is unlike other loss components in that its evaluation is less amenable to empirical correlations based on combinations of airfoil geometry and freestream flow conditions and relies more on direct calculations based on several of its properties. It should be noted that, typically, the cooling air supplied to a vane or blade in an aircraft engine seldom exceeds 5% of the turbine inlet flow, whereas in an industrial gas turbine, the cooling air for the first vane alone might be more than 20% of the turbine inlet flow. So it could be argued that the accuracy in estimating the cooling penalty is more important in the latter case.

One practical approach to multi-stage cooled turbine efficiency is discussed in Chap. D5, where secondary air flow properties are combined with those of the primary flow to account for the detailed effects of cooling on turbine efficiency. Cooling loss or rather the inability of the coolant to produce work is accounted for by identifying the secondary flow as either “working” or “non-working”—an approach validated extensively by measurements.

The method is enhanced by the derivation and use of an equivalent single stage; this is especially valuable for the generation of performance maps for multi-stage cooled turbines. Many mean line codes still use this, but some modern software includes detailed calculations that account for the contributions to the turbine work by each of the cooling flow elements as well as the penalties due to their corresponding losses as they mix with the primary stream. The effects on profile loss of cooling air ejection is a small part of this and is mentioned above.

Contributions of the cooling air to the turbine work through a change in angular momentum of the working fluid and losses due to mixing will now be addressed. Overall flow continuity is very important as the departure from and return to the flow path of leakage air must also be accounted for carefully in the combined compressor/turbine system.

Cooling flows and their relevant properties must be considered in detail to account for their influence on turbine performance. Knowing the source of the coolant in the compressor, the source temperature and pressure is determined but the loss of pressure and increase in temperature in reaching the turbine blade must

also be estimated. The work done on the coolant to deliver it to the cooling cavities in the turbine blade must also be estimated and this presents a debit to turbine performance.

The contribution to turbine work of each cooling element is calculated based on its contribution to angular momentum. In a mean line model, cooling flows are not distributed radially; the overall contribution of each row of cooling holes is addressed. The precise tangential angle of a cooling hole row is used, together with the coolant mass flow and its temperature, to determine its work contribution. The ejection velocity must also be calculated based on the size of the holes and the coolant supply pressure. Clearly the location of the cooling hole row on the blade profile is critical to determining the ejection angle. Such estimates are usually handled by “secondary flow” experts, who also estimate heat transfer within the turbine, along with blade life.

The mixing loss of each cooling flow element is estimated. The ejection loss owing to boundary layer disturbance is estimated for each cooling flow element and this has been mentioned earlier, as part of the profile loss.

3.4 Turbine Design Envelopes

3.4.1 *Introduction*

A turbine design envelope is a simple graphical representation of several aerodynamic and mechanical limits within which the turbine designer must work to meet the demands of the engine cycle, the available turbine technology, and material strength. The value of a design envelope is that it assists the design engineer in applying the design limits by restricting design choices to manageable ranges, based on an appropriate level of technology. The technique thereby alleviates an onerous burden for a designer and improves the rate of convergence to an acceptable, realistic solution for any user. An overall benefit is that the design cycle time may be reduced considerably. For successful application, the method should be coupled to a reliable turbine design code which incorporates a performance model.

There is nothing unique about the techniques that are employed. They are merely a formalization of the notes and observations of trends that any turbine designer would make in the margin of a logbook as the work progresses. The benefits accrue from being able to capture almost the whole design scenario in one view. Interactions between design variables are illustrated, enabling difficult decisions and practical compromises to be made rapidly and confidently. The key to achieving a realistic preliminary design is the use of design limit values appropriate to the study in hand. A conventional design will assume conventional limiting values, while an advanced design concept will apply more aggressive standards. A preliminary choice of major parameters is determined, and the selection and values of the design limit parameters are established. Such decisions are based on typical performance figures for a conventional axial turbine.

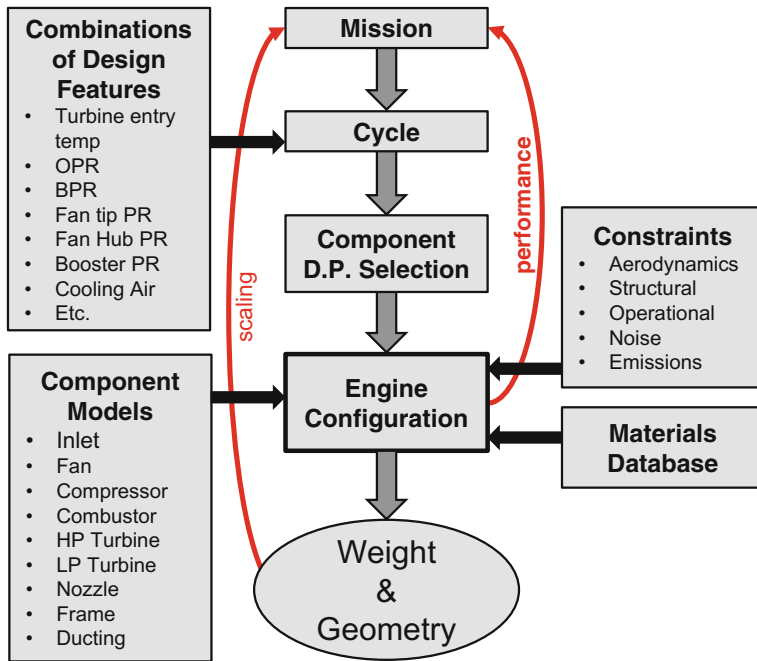


Fig. 3.4-1 Building an engine model

The design scenario, in which design envelopes are so useful, is illustrated in Fig. 3.4-1. The skill in constructing a viable turbine design occurs not merely in bringing all the relevant technologies together (the central box labeled *Engine Configuration*) but in doing so within the restrictions that are imposed (the box on the right labeled *Constraints*).

The current design envelope method addresses turbine aerodynamic and structural constraints directly but there is no reason why it could not be extended to account for additional objectives and concerns. For example, *cost* might also be considered.

3.4.2 Specification

In the design of any turbine, the required power output at its chosen design point is given by the engine cycle. If an assumed or desired value of isentropic efficiency is also taken from the cycle, the following are known:

- Mass flow rate, total temperature, and total pressure at inlet
- Mass flow rate, total temperature, and total pressure at exit

For a given level of technology, specific limiting values of a number of design parameters are also known. For a traditional axial turbine, examples are:

- Stage loading coefficient, $\psi = \Delta H/U^2$
- Flow coefficient, $\phi = V_{ax}/U$
- Stage reaction, $\Lambda (= \Delta P_s \text{ rotor} / \Delta P_s \text{ stage})$
- AN_{\max}^2 at turbine exit. This is a measure of the maximum blade root stress that occurs at the rim of the disk and is a vital mechanical consideration. It is important to note that N_{\max} may not correspond to the turbine design speed, since the aerodynamic design point may not be at the maximum rotational speed condition. N_{\max} is the product of N_{design} and $XNOS$, the overspeed factor defined in the input file. N_{\max} is known as the mechanical design speed. The role of AN^2 is discussed in Chap. 4
- Absolute and relative Mach numbers
- Blade aspect ratios
- Zweifel coefficients.

The design of a new turbine requires that the appropriate geometric, aerodynamic, and structural parameters be manipulated within the constraints set by the technology limits (and by increasingly stringent environmental regulations), so that the resulting machine delivers the required power output at its design point, with an efficiency acceptable to the engine cycle.

Only a limited number of independent design parameters are at our disposal, and one suitable selection for a conventional turbine is:

- Number of stages
- Stage loading coefficient, ψ
- Stage reaction, Λ
- AN_{\max}^2 at exit.

The rotational speed, N_{design} , of a turbine at its *aerodynamic design point*—both magnitude and direction—must be matched to that of the corresponding compressor, whose aerodynamic design may have precedence.

3.4.3 Primary Design Variables

For a conventional turbine, AN_{\max}^2 and stage loading coefficient, ψ , are taken as the coordinates in which a design envelope is defined. Design limit lines for the parameters of interest are superimposed on this framework. In practice, since the rotational speed, N , is fixed, it is only the turbine exit area, A , that varies in the abscissa. The turbine exit area influences many internal features of the turbine either directly or indirectly, in addition to its exit characteristics. The choice of exit area influences the area distribution throughout the machine, which in turn affects Mach numbers, swirl angles, flow coefficients, stage reactions, and blade tip speeds. It is

appropriate therefore, that the exit area, A_{exit} , be used as one of the primary design variables and is therefore reflected in the abscissa for the construction of design envelopes. AN_{max}^2 provides a powerful link between the turbine aerodynamics and the structure, so this becomes the second primary variable. N_{max} is the mechanical design speed of the turbine, as opposed to the aerodynamic value. It corresponds to the maximum speed the machine will encounter and is accounted for by inclusion of an overspeed factor (usually called XNOS) in the input to a mean line code.

The stage loading coefficient is used as the ordinate, because it is generally accepted as being an indicator of technological achievement. There is a very strong traditional correlation between stage loading coefficient ($\psi = \Delta H/U^2$), flow coefficient ($\phi = V_{ax}/U$), and isentropic efficiency (η) in the form of a loading diagram or *Smith Chart*.

Stage loading coefficient is the parameter that links stage work to mean blade speed. As turbine technology improves, stage loading coefficients can be increased without loss of efficiency and turbines can be designed with fewer stages. Consequently, both weight and performance are changed in a beneficial manner.

3.4.4 Solution and Interpretation

To generate the data needed for construction of a design envelope the turbine design code is run four times, using combinations of two values of the two primary variables—stage loading coefficient (ψ) and AN_{exit}^2 . The design limit lines are positioned in terms of AN_{exit}^2 by linear interpolation at each of the two selected values of stage loading coefficient. The rotational speed is fixed (usually by the compressor) and stage reaction is also fixed, for convenience.

Suppose we have an upper limit on the absolute Mach number at rotor blade exit, ($M_{ex,blade}$) of 0.65. If the turbine design code is run at design points 1 and 2 in Fig. 3.4-2, two values of $M_{ex,blade}$ will result. Regardless of the validity of these values, the location of $M_{ex} = 0.65$ at the chosen value of stage loading coefficient may be determined by interpolating linearly between points 1 and 2. This corresponds to point A in Fig. 3.4-2. The location, B, of $M_{ex,blade} = 0.65$ at the lower value of stage loading coefficient may be identified in a similar manner from the design points 3 and 4 in Fig. 3.4-2. The locus of the $M_{ex,blade} = 0.65$ design limit is obtained by joining points A and B. It may be determined easily that M_{ex} increases as we move upwards and to the left in Fig. 3.4-2, so that side of the limit line is shaded to denote its prohibition.

The interpolation process may be repeated between the pairs of design points 1 & 2 and 3 & 4 for any design variable of interest, provided it is calculated in the design program. Depending on the variable, extrapolation may be required to locate the limit line. Figure 3.4-3 contains a typical, completed design envelope. There, limit lines have been constructed for the following design parameters, with values typical of those in an HP turbine:

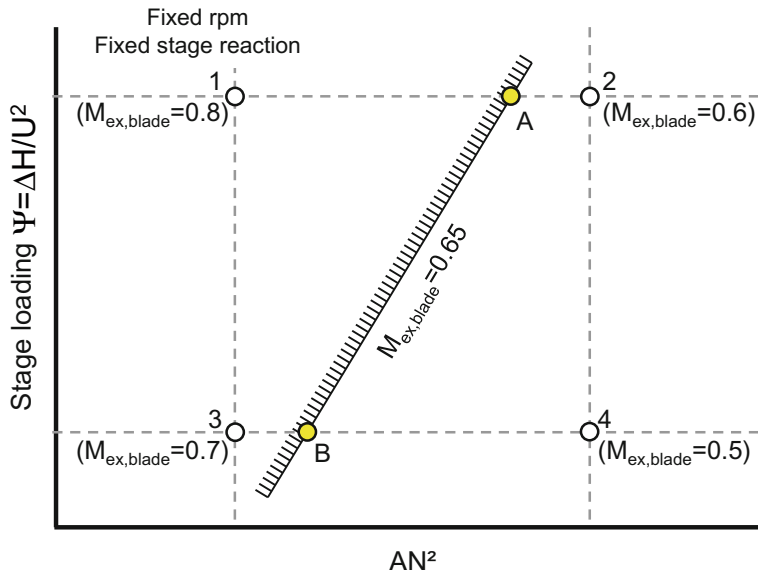


Fig. 3.4-2 Construction of a limit line in a design envelope for an axial turbine

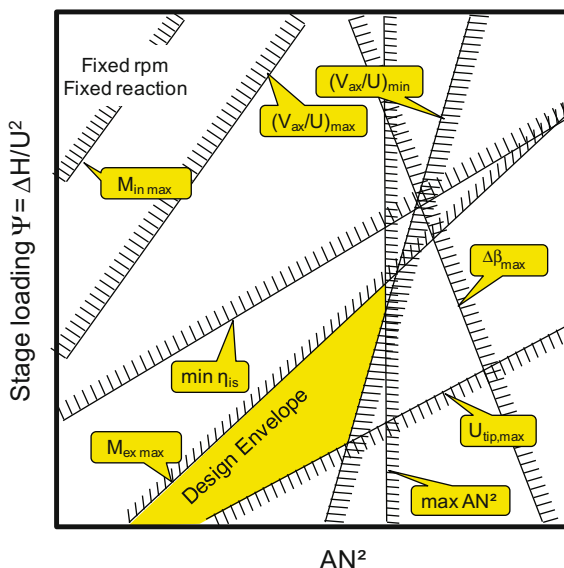


Fig. 3.4-3 A design envelope for an axial turbine

• Maximum relative Mach number at blade inlet, $M_{in,max}$	0.52
• Maximum absolute Mach number at blade exit, $M_{ex,max}$	0.67
• Minimum flow coefficient, $(V_{ax}/U)_{min}$	0.5
• Maximum flow coefficient, $(V_{ax}/U)_{max}$	1.0
• Min isentropic efficiency $\eta_{is,min}$	0.85
• Maximum blade turning angle, $\Delta\beta_{max}$	134°
• Maximum AN^2 (A in inches ² , N in rpm)	45×10^9
• Maximum tip speed, $U_{tip\ max}$ (m/s)	580

It should be noted that linear interpolation or extrapolation is not strictly correct over the whole region considered, although for preliminary design purposes the results are still quite valid. It is recommended therefore that some thought be given to the selection of the four datum design points so that, if possible, they are reasonably close to where the final turbine design point is expected to be. If that is not possible, an iterative procedure, whereby the turbine design envelope is refined in a second pass—by relocating the datum design points—will result in a more plausible analysis. In any case, it should also be remembered that the generation of the envelope is never the final objective, but only a means by which the design point is determined. The turbine design code is then run subsequently for a single selected design point to generate specific relevant information.

It is preferable to have an independent means of establishing turbine efficiency beyond the engine cycle case at the selected design point. Our knowledge of the turbine inlet and exit conditions implies that an assumption concerning turbine performance has already been made in the cycle analysis and verification that this is reasonable should be provided. The turbine design envelope code *TDE* [17, 18] was used for the current example and this contains the *Kacker and Okapuu* loss model [10]. A limit line for an acceptable value of efficiency may also be plotted on the turbine design envelope.

In *TDE*, the main program has been structured to run the four datum cases of the turbine design code repetitively to produce the information needed to construct a design envelope. A single-run option was retained to generate the detailed output for a regular turbine design run, once the design point has been established. A design envelope is plotted automatically for each stage of a multi-stage machine, but it should be noted that the axes in every case are the same, namely first-stage Ψ and final-stage AN_{exit}^2 for the turbine in question. This enables the design envelopes for multiple stages to be superimposed meaningfully. Then, only if there is a clear design space remaining on the overlaid plots, is there a design solution. It should be noted that a design envelope may also be used to indicate which flow parameters are impeding a successful design solution and which have most or least influence.

- Some general observations are worthwhile regarding the contrived example in Fig. 3.4-3, where the selected design limit lines form a closed envelope of finite area.
- Any turbine with design values of stage loading coefficient and AN^2 inside the envelope will comply with all the design limits being considered.

- The possible ranges of loading coefficient and exit area are indicated. It should be remembered that although AN_{\max}^2 is plotted, N is fixed and so it is only the turbine exit area that is changing. This is the geometric area at the final blade exit plane, not the downstream mixed-out plane.
- The design variables whose limit lines form the envelope are those with the most powerful influence. Those that are further away influence the turbine design relatively little and conversely, are less likely to be affected by changes to the influential parameters.
- While the generation of a design envelope makes the designer's task significantly easier, it is sometimes made easier still in practice by the fact that the design search is usually restricted to one edge of the envelope. For example, the numerical values of the limits in Fig. 3.4-3 are typical of those used for a conventional axial HP turbine. In an associated LP turbine, difficulty may be encountered in achieving the desired low value of Mach number at inlet to the vane. Under such circumstances, we may find ourselves needing to design the HPT at the maximum value of AN^2 (i.e. maximum exit area)—in other words, against the right-hand edge of the design space. The trade-off then becomes simple—on one hand, if the stage loading is raised the turbine moves inwards towards the centerline and becomes lighter—on the other hand, if the stage loading is reduced the efficiency improves. Usually it is known whether performance or weight is more important and often an “exchange rate” may be provided by cycle analysis. It is then relatively easy to locate the design point at its optimum location within the envelope.
- Typically, the design of a turbine stage will begin with an assumption of 50% stage reaction at the mean line. Frequently, however, the mean line reaction will be modified to effect changes in flow angles and velocities or to maintain a hub reaction greater than some minimum value (usually greater than 15% to avoid negative values at off-design conditions, at which point the turbine would become a compressor!) Since reaction is held constant in the current approach to design envelopes, another envelope or set of envelopes for multi-stages would need to be generated if the stage reaction was changed. In general, from experience, an increase in reaction will cause many of the limit lines in Fig. 3.4-3 to move to the right and rotate in a clockwise direction. They will not all move by the same amount, however, and this will lead to changes in the location, the shape, and the extent of the design space. Unless a design strategy has been determined previously, it is often very useful to explore the implications and the range of the effects of such changes early in the design program to establish a database.
- The rotational speed is the second major variable that is kept constant in the construction of a design envelope. It has a very powerful influence on the turbine design space, since it is a key feature of the velocity diagrams, and changes in rpm are reflected in gas velocities and angles. Adjustment of the rotational speed is a very significant alteration, since it is usually defined by the appropriate compressor. Such a measure is taken only when other approaches have failed.

Often this implies re-selection of the turbine design point from the available cycle data, or a change in the design speed of the corresponding compressor or fan. Again, the characteristics of the design envelope will change significantly.

3.5 Vaneless Counter-Rotation

For many decades, a great deal of time and resources have been spent in pursuit of improved turbomachinery efficiencies, this being one way to reduce fuel burn and the resulting emissions. Traditional aerodynamic approaches have led to incremental improvements, demonstrating the law of diminishing returns, as increasing investment has produced decreasing benefits and escalating costs. The adoption of vaneless, counter-rotating stages is a “thinking-out-of-the-box” approach that offers significant potential gains in efficiency for both turbines and compressors, in contrast to the traditional incremental approach. Elimination of all “non-working” vane rows corresponds to the removal of roughly half the loss sources! A nominal efficiency target for a modern turbine is no longer around 90% but closer to 95%. While 5% efficiency improvement may be too ambitious for compressors, combining a more modest gain with what the turbine offers yields very impressive advances in SFC and fuel burn. Vaneless counter-rotation (VCR) leads to turbomachinery designs with roughly half the length and half the weight of their traditional counterparts, and only half the “traditional” design and production times are necessary. Clearly, cost could be reduced quite dramatically—although this also depends on practical issues. The risks may be too high currently for commercial enterprise but the high potential benefits warrant closer examination of the concept.

We are all familiar with how a conventional multi-stage turbine stage works and a VCR device is only slightly more complex. In a traditional turbine, a first vane accelerates the flow and—in the relative frame—aligns it with the leading edge of a rotor blade. The rotor turns the flow through a chosen angle to extract power via the rate of change of angular momentum. A second vane then aligns the flow relative angle with the leading edge of the second blade, and the process is repeated. But suppose that rather than the flow encountering a second vane, it is intercepted by another blade—suitably aligned—but rotating in the opposite direction. Additional power is extracted, but now via a spool that is rotating counter to the first. Depending on the application, separate shafts may be retained or a single-rotation output may be obtained through a gearbox.

Vaneless counter-rotation was used in the mid-1980s by GE Aircraft Engines in the *GE36* or *Unducted Fan (UDF)* engine in response to a prevailing oil crisis. In the GE36, most of the thrust was provided by a counter-rotating prop-fan at the rear of the engine, supported and driven directly by a free counter-rotating power turbine. A simplified drawing is shown in Fig. 3.5-1. Vaneless counter-rotation was not used anywhere else in the engine.

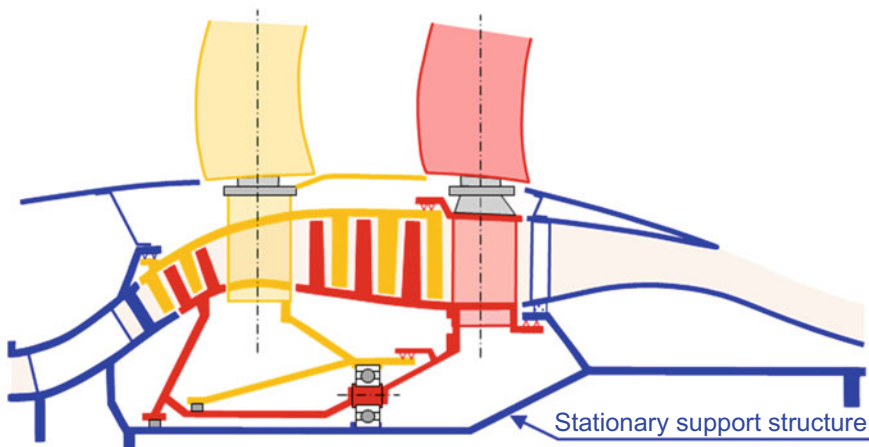


Fig. 3.5-1 The free counter-rotating power turbine in the GE36 unducted fan engine

Counter-rotating unducted fans are still of interest for their potential contribution to reduced fuel burn in subsonic commercial engines [19, 20]. There is a need not only to design, analyze and predict the performance of turbines that drive them but also to address vaneless counter-rotating turbomachinery in general. In this section, a mean line code for axial VCR turbines, named *VCR-AXT* [21] has been used to investigate the efficiency improvement potential, using the *Kacker and Okapuu* loss model [10]. The code includes an option to design a conventional turbine with vanes, so a baseline model of an LP turbine was generated first and this was followed by a VCR derivative. A comparison that demonstrates significant improvements in turbine efficiency and engine specific fuel consumption is presented.

At this point, a comment on previous design and analytical approaches to vaneless counter-rotating turbines is felt to be worthwhile. While there are very few references in the literature on this topic, I have encountered informal material that attempts to superimpose the velocity diagrams from two counter-rotating blades with the purpose of illustrating that “twice the work can be generated” when compared to an orthodox vane/blade combination. While this is not totally untrue, it misses the point as well as makes some unnecessarily restrictive assumptions. What should be established up-front, is that the turbine must still be designed one blade at a time—so don’t go jumping in with two at once! The key to success from the design logic point of view, is the establishment of a sign convention for the direction of rotation and swirl angle. Once the sign convention is set, firm adherence to it via simple algebra and trigonometry, will take care of (almost) all potential difficulties.

Let's look at a comparison of a mean line model of a VCR turbine based on an existing conventional LP machine. Our baseline design models the 4-stage low pressure turbine from a *CFMI CFM56* engine. This is a mid-size subsonic commercial turbofan that produces about 115kN of thrust. All input data is either available in the public domain or values have been guessed. The mass flow rate at turbine entry is 57 kg/s; cooling flow is omitted for this exercise. Inlet temperature and pressure are 1202 K and 814 kPa respectively. Fuel/air ratio is 0.0218. The mean inlet swirl angle to the first vane is -45.3° . The fractional work split between stages is 0.30, 0.27, 0.26 and 0.17; stage 1 is more loaded than the middle two, so that stage 4 can be unloaded to produce low values of absolute exit swirl angle and Mach number in the downstream duct as the flow enters the exhaust system.

Figure 3.5-2 shows the flow path, vanes (in yellow) and blades (in green) for the baseline 4-stage LP turbine. The flow path is very close to section drawings of the real thing, despite the somewhat limited number of parameters used in its reproduction. A free-vortex mean line design ensures radial equilibrium in the VCR-AXT code; axial velocity and specific work are constant with radius, while whirl velocity varies inversely with radius.

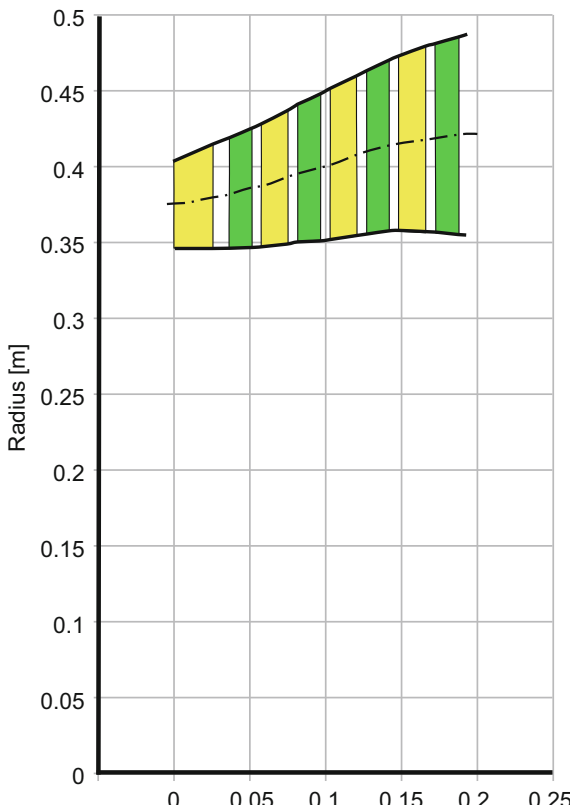


Fig. 3.5-2 Flow path for the baseline LP turbine

The mean line velocity diagrams for the baseline turbine are given in Fig. 3.5-3. They reflect the uneven work split and show that all stages have a mean line reaction of 50%. The isentropic stage efficiencies are of obvious interest and are estimated to be 82.8, 88.1, 91.4 and 93.2% respectively. The overall adiabatic efficiency is 89.7%

The flow path of an equivalent vaneless counter-rotating turbine is shown in Fig. 3.5-4. The same overall power output and the same split between stages have been used. The turbine length has been reduced from 0.196 to 0.085 m.

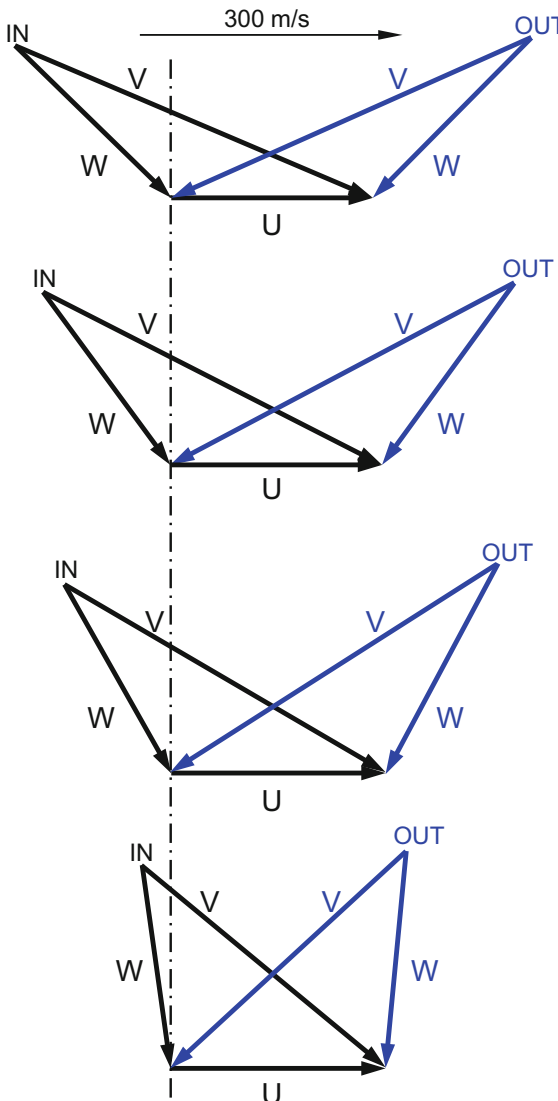


Fig. 3.5-3 Mid-height velocity diagrams for the baseline LP turbine

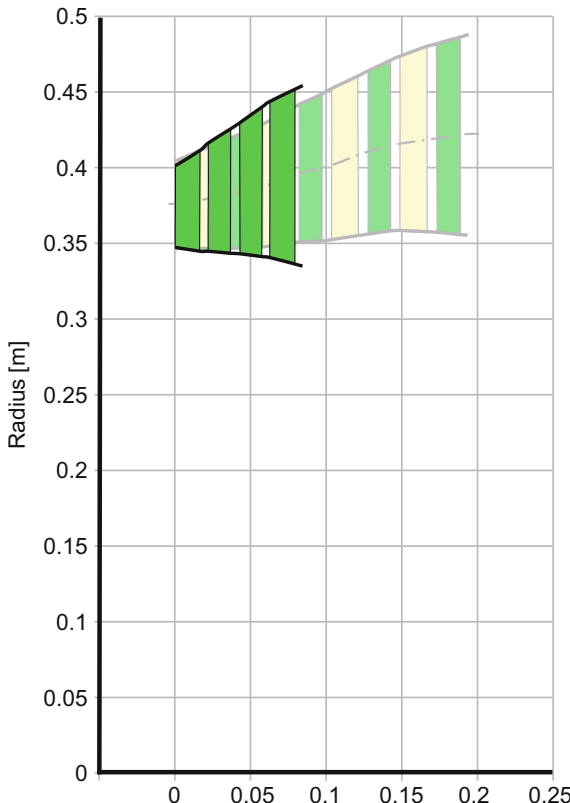


Fig. 3.5-4 Flow path for the VCR LP turbine

In the VCR model, values from the baseline turbine of inlet conditions, mass flow rate, blade counts, and inlet swirl were all retained. The absolute inlet swirl to the first rotor has been held at 45° , just as it was initially.

The velocity diagrams for the VCR turbine are presented in Fig. 3.5-5. The most obvious difference between these and the corresponding baseline figures is how the “stage” velocity diagrams flip from one side of the vertical axis to another, as the blade speeds change from positive to negative. But a distinct general asymmetry can also be seen; the exit triangles for the first and third blades contain velocities that are much higher than the stage 2 and 4 equivalents. The asymmetry is reflected exactly in the stage efficiency values, namely 90.3, 96.9, 90.0 and 98.7%. The corresponding relative mean exit Mach numbers are 1.019, 0.675, 1.121 and 0.552. Clearly, the high flow velocities at exit in rotors 1 and 3 are damaging! This tells us that a “symmetric” design—in terms of the appearance of the velocity diagrams—is what we should aim for when it comes to optimized performance. The key to achieving this is setting an appropriate inlet swirl angle. However, despite the gross asymmetry, the overall isentropic efficiency of the VCR machine is now 93.9%—an

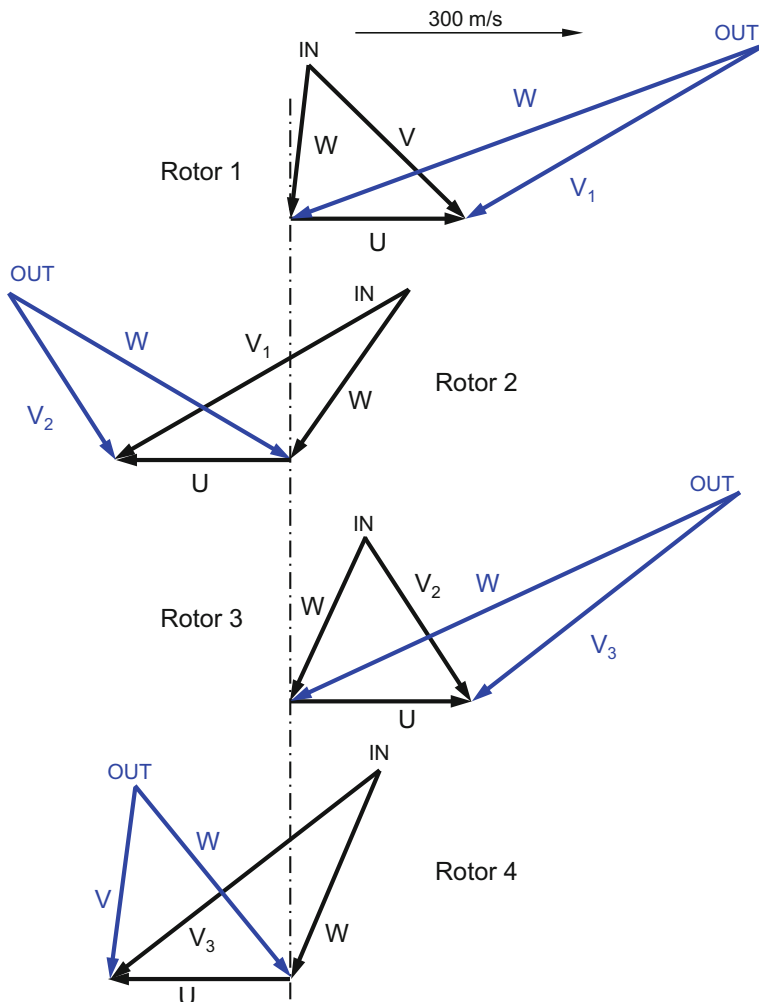


Fig. 3.5-5 Mid-height velocity diagrams for the initial VCR LP turbine

improvement of 4.2% when compared with the baseline turbine and consistent with our expectations!

Adjustment of the inlet swirl angle leads us to what we shall refer to as the optimized VCR LP turbine. A brief trial-and error survey led us to an optimized inlet mean swirl of 56.4° and this resulted in the velocity diagrams shown in Fig. 3.5-6.

It is felt that an even more symmetric state could have been reached had it not been for the retention of the stage fractional work split (0.30, 0.27, 0.26 and 0.17); a smoother distribution of work, with higher loading on stage 4 might have been better; the velocity and swirl angle at the exit from rotor 4 are both quite modest!

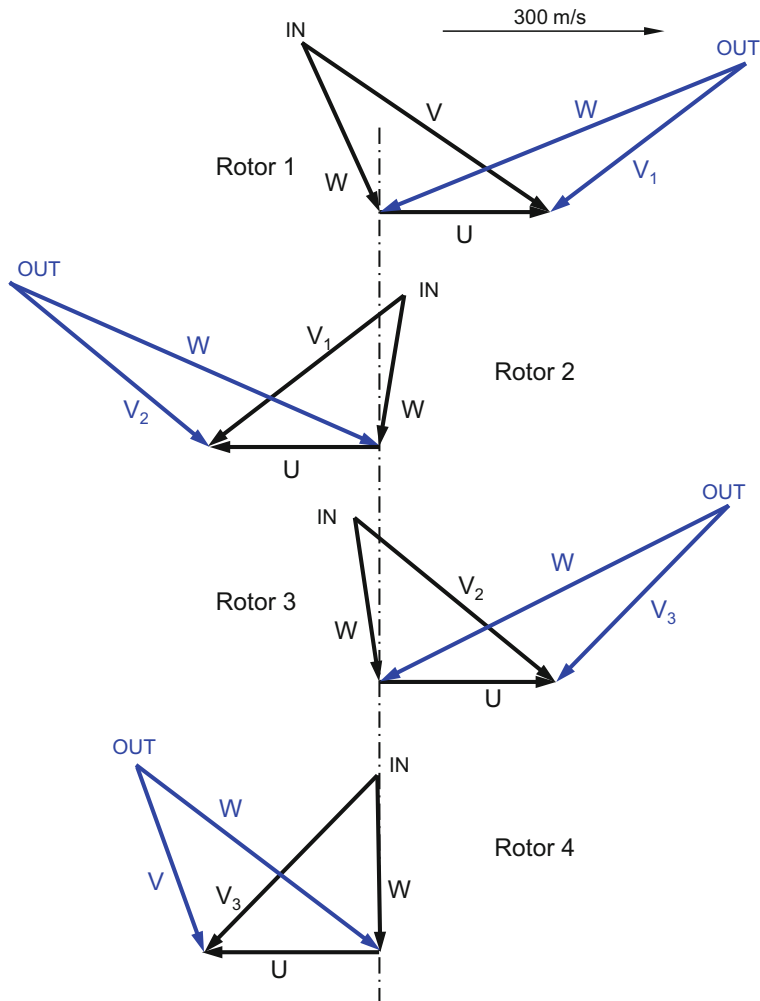


Fig. 3.5-6 Mean line velocity diagrams for the optimized VCR LP turbine

However, the variation of isentropic stage efficiency that corresponds to Fig. 3.5-6 is now 94.5, 94.8, 96.0 and 97.2% while the overall value is 95.9%. Compared to the baseline, elimination of the vanes with some optimization has given us 6.2% improvement in efficiency—or 60% of the overall baseline loss.

The stage performance comparison is illustrated in Fig. 3.5-7. The optimized performance could be improved by shifting the stage 2 data point on the red curve to produce a linear variation. When the overall efficiency values are inserted into a cycle model, with no other changes, the specific fuel consumption improves by 2.5%. However, this is probably overshadowed by the reductions in length, weight

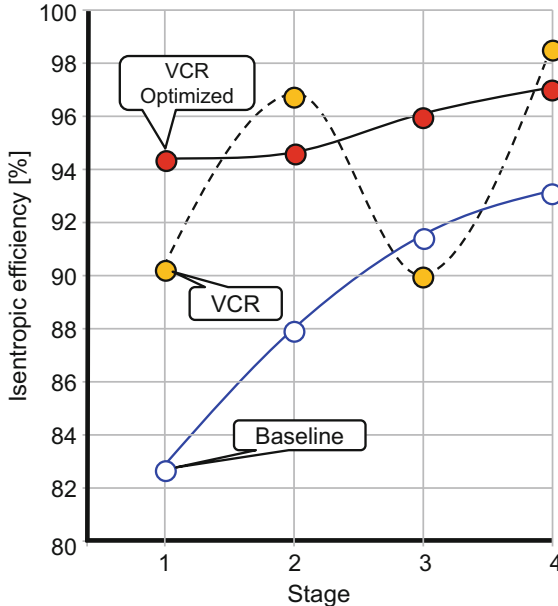


Fig. 3.5-7 Improvements to isentropic stage efficiencies in an LP turbine using vaneless counter-rotation

and cost of the turbine! It must be noted that an inlet guide vane is essential to control the inlet swirl, so we should penalize our result accordingly.

If we accept the aerodynamic approach, several mechanical issues must be addressed to make vaneless counter-rotating turbomachinery viable. Design of the frames and location of the bearings are critical to the blade rows cantilevered from the outer casing. In motion, they will be under compression and the use of new ceramic materials will help there. Usually turbine blade tip sections have relatively little camber; to provide the necessary stiffness, a spanwise redistribution of work may be warranted. Vaneless counter-rotation complements the exoskeletal engine concept [21]. An exoskeletal VCR engine offers an opportunity for an open duct through the engine centerline that could accommodate a ram-jet or could lead to significant noise reduction via an inverted velocity profile at exit. Potential benefits make the pursuit of VCR quite attractive to those of us interested in new engine architectures.

3.6 References

1. Zweifel, O.: The spacing of turbomachine blading, especially with large angular deflection. *Brown Boveri Rev.* **32**(12), 436–444 (1945)
2. Farokhi, S.: Aircraft Propulsion, 2nd edn. Wiley, New York (2014)

3. Coull, J.D., Hodson, H.P.: Blade loading and its application in the mean-line design of low pressure turbines. ASME Paper GT2011-45238
4. Hodson, H.P., Dominy, R.G.: Three-dimensional flow in a low-pressure turbine cascade at its design condition. Paper 86-GT-106 31st International Gas Turbine Conference and Exhibit, Dusseldorf, Germany
5. Coull, J.D., Hodson, H.P.: Blade loading and its application in the mean-line design of low pressure turbines. In: GT2011-45238. Proceedings of ASME TurboExpo, Vancouver, Canada, 6–10 June 2011
6. Praisner, T.J., Grover, E.A., Knezevici, D.C., Popovic, I., Sjolander, S.A., Clark, J.P., Sondergaard, R.: Toward the expansion of low-pressure turbine airfoil design space. In: GT2008-50898. Proceedings of ASME Turbo Expo, Berlin, Germany, 9–13 June 2008
7. Smith, S.F.: A simple correlation of turbine efficiency. *J. R. Aeronaut. Soc.* **69**, 467 (1965)
8. Ainley, D.G., Mathieson, G.C.R.: A Method of performance prediction for axial flow turbines. *Aeronautical Research Council R&M* 2974 (1951)
9. Dunham, J., Came, P.M.: Improvements to the Ainley-Mathieson method of turbine performance prediction. Paper No. 70-GT-2. ASME Gas Turbine Conference and Products Show, Brussels, Belgium, May 21–28, 1970.
10. Kacker, S.C., Okapuu, U.: A mean-line prediction method for axial turbine efficiency. ASME Paper 81-GT-58, ASME International Gas Turbine Conference and Products Show, Houston, Texas, USA, March 9–12, 1981.
11. Craig, H.R.M., Cox, H.J.A.: Performance estimation of axial flow turbines. In: Proceedings of the Institution of Mechanical Engineers, vol. 185 (1971)
12. Saravanamuttoo, H.H., Rogers, G.F.C., Cohen H.: *Gas Turbine Theory*, 5th edn. Pearson Education Limited, Cambridge (2001)
13. Benner, M.W., Sjolander, S.A., Moustapha, S.H.: Influence of leading-edge geometry on profile losses in turbines at off-design incidence; experimental results and an improved correlation. *ASME Trans J. Turbomach.* **119**, 193–200
14. Benner, M.W., Sjolander, S.A., Moustapha, S.H.: An empirical prediction method for secondary losses in turbines: part I—A new loss breakdown scheme and penetration depth correlation. *ASME GT2005-68637*
15. Benner, M.W., Sjolander, S.A., Moustapha, S.H.: An empirical prediction method for secondary losses in turbines: part II—A new loss secondary loss correlation. *ASME GT2005-68639*
16. Zhu, J., Sjolander, S.A.: Improved profile loss and deviation correlations for axial-turbine blade rows. *ASME GT2005-69077*
17. Halliwell, I.: TDE—A Preliminary Design Code to Generate Turbine Design Envelopes. Volume I: The Turbine Design Code. Contract NAS3-27577: Propulsion Systems Modelling, Sept 1997
18. Halliwell, I.: TDE—A Preliminary Design Code to Generate Turbine Design Envelopes. Volume II: Turbine Design Envelopes. Contract NAS3-27577: Propulsion Systems Modelling, Sept 1997
19. Halliwell, I.: Performance Benefits of a Vaneless Counter-rotating LP Turbine. Northwind Propulsion Inc., Heath, Ohio, USA, Feb. 2006
20. Halliwell, I.: Exoskeletal engine concept: feasibility studies for medium and small thrust engines. NASA/CR-2001-211322, 2001
21. Chamis, C.C., Blankson, I.M.: Exo-skeletal engine a novel concept. NASA/TM-2004-212621, 2004

Chapter 4

Mechanical Design



4.1 Introduction

Engine weight is a key design parameter for any new aircraft engine. It affects aircraft range and is a key element in fuel burn. Weight is also considered an indicator of engine cost. Overly simple correlations of engine weight with parameters like thrust, mass flow, bypass ratio, compressor pressure ratio etc. do not help much to select the best engine concept from several candidates. We must go into more detail and consider the weight of the individual engine modules (Fig. 4.1-1).

The well-known NASA code WATE (Weight Analysis of Turbine Engines, [1]) calculates the weight and dimension of each major engine component, such as compressor, burner, turbines and frames, primarily using a semi-empirical method augmented with analytical calculations for specific component elements.

Reference [2] describes the enhanced, object oriented computer code WATE++ in which many of the empirical relationships have been replaced with analytical weight and dimension calculations. The primary method used to calculate weight throughout the code is to determine material volume and multiply it by the appropriate density. Stress level, maximum temperature and pressure, material, geometry, stage loading, hub/tip ratio, blade/vane counts, and shaft speed are taken into account for each component.

Accurate absolute weight numbers are impossible to get at the conceptual design stage. However, algorithms which correctly predict weight trends are a valuable tool for the subsequent preliminary design phase.

Estimating weight and dimensions of an aircraft engine is indispensable for calculating fuel burn during an aircraft design mission. However, this is not the only application of a detailed engine geometry model. For serious examination of aircraft engine operability, we need to know more than the values for the polar moments of inertia (which we might get from comparisons with other engines, for example). We need to know how compressor and turbine tip clearances vary during transient maneuvers. This demands that we consider the heat exchange between gas and

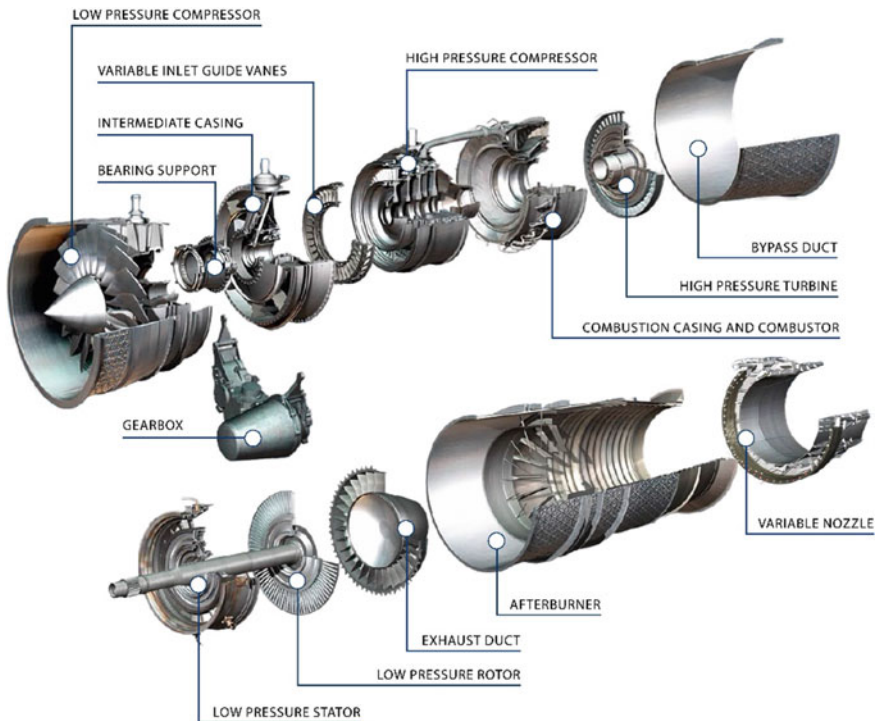


Fig. 4.1-1 Modules of the EJ200 turbofan (© EUROJET Turbo GmbH)

metal which affects the temperature of the engine hardware. To calculate thermal expansion, we must obtain at least approximate values for engine parts mass and heat storage capacity. The effect of centrifugal forces on disk diameters and the length of blades also needs to be known. Only then are we able to estimate how tip clearances in compressors and turbines vary during steady state and transient operation.

In the following sections we describe the elements of the basic engine geometry model implemented in GasTurb. It consists of the flow annulus walls, modeled as combinations of cylindrical and conical sheet metal elements, blades and vanes represented by small flat plates, disks, and shafts. A stress calculation method is employed for estimating the weight and the polar moment of inertia of disks. The shape of the disks can be optimized for weight.

The basic engine geometry model does not describe bearing structures, engine mountings, accessory gearboxes, fuel pipes, hydraulic and bleed air offtake systems, active tip clearance control devices, control units and actuators. These objects can be included either by factors or adders applied to the basic module weights or by project-specific models that are generated on-the-fly by the user and designated as *composed values*.

4.2 Flow Path

Creating a geometric engine model begins with the thermodynamic cycle which defines mass flow, total pressures and total temperatures at the component boundaries. Mach numbers at the inlet and exit of the components are not needed for the thermodynamic cycle, but they define the flow areas at the component boundaries. Selecting the hub/tip radius ratios at the inlet and exit of the compressors and turbines yields the cornerstones of the annulus. When Mach numbers and hub/tip radius ratios are set, then we know the general flow path layout. The exact shape of the flow annulus within the compressors and turbines may be optimized later, during the design of these components.

4.2.1 Compressors

The primary demands for any compressor are generation of total pressure ratio and delivery of mass flow rate. Within the constraints of the relevant technology limits, the number of stages, rpm of the spool, pressure ratios of individual stages, compressor efficiency, and stall margin define the geometry of the flow path implicitly.

In an aircraft engine, the hub/tip radius ratio at the inlet to the first compressor should be low because this results in a small front diameter. Remember that compressor inlet Mach numbers relate to the engine growth potential. Therefore, they should not be set too high at the beginning of a new project.

The LP compressor has a number of unique design challenges, partly due to its exposure to the elements. The design must take into account ingestion of rain, hail and ice as well as a range of different sizes of bird. It is also the only component required to demonstrate that a rotor failure is contained by completing a fan blade-off test.

4.2.2 Low-Bypass-Ratio Fan or LP Compressor

The LP compressor can be considered as the compression system in a single-spool engine, or with a stratified flow, as a low or medium bypass ratio fan in a two-spool engine for military or other high-speed applications. In the fan configuration, the number of stages is usually limited to two or three. The LPC of many turbofans is located between a front frame—which supports the front bearing and can include variable guide vanes—and the engine main frame, see Fig. 4.2-1.

Take off conditions impose the most extreme demands in terms of rotational speed, stall margin, and overall operability and reliability. For those reasons, take-off conditions are normally selected as the mechanical design point for the LP compressor.

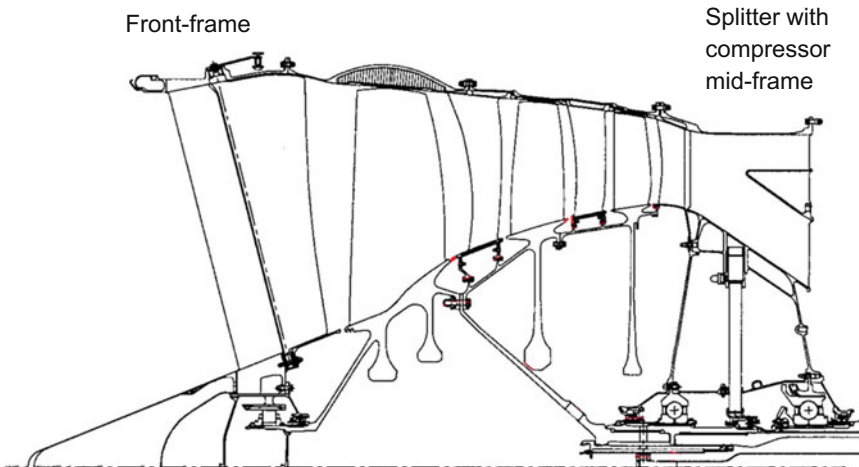


Fig. 4.2-1 Low pressure compressor between front and rear frame [1]

The material of choice for high performance low bypass ratio turbofans are Titanium alloys. Traditionally the rotors are an assembly of a disk and a set of removable blades. In modern engines some or all of the rotors are manufactured as single parts which combine the disk and the blades in a so-called blisk (bladed disk).

4.2.3 High-Bypass-Ratio Fan

This type of fan is typically used in engines powering today's subsonic commercial transport aircraft. Tip diameters are large, and there is a close physical link with the splitter and the booster, which are immediately downstream (Figs. 4.2-2 and 4.2-3).

The flow through a high bypass ratio fan is stratified, that is divided into a bypass stream and a core stream. The pressure ratio is typically lower in the core stream than the bypass stream due to the low circumferential speed at the hub. Within the cycle calculation, the bypass pressure ratio is specified uniquely, but the fan hub pressure ratio is often combined with that of the booster, and the preliminary designer is permitted to determine the pressure ratio split for the core stream.

Nowadays, blades of high bypass ratio fans are made from either hollow titanium or carbon fiber composites. The shape of these blades is very complex. Nevertheless, during preliminary design we model them as flat plates of constant thickness. The fan casing structure above the fan blades is strengthened. This is required for containing a fan blade in case of failure due to a bird strike, for example. The fan containment structure is usually made from a highly-ductile steel casing, which can deflect to absorb energy and this is reinforced by a ring of continuously-wound Kevlar fibers.

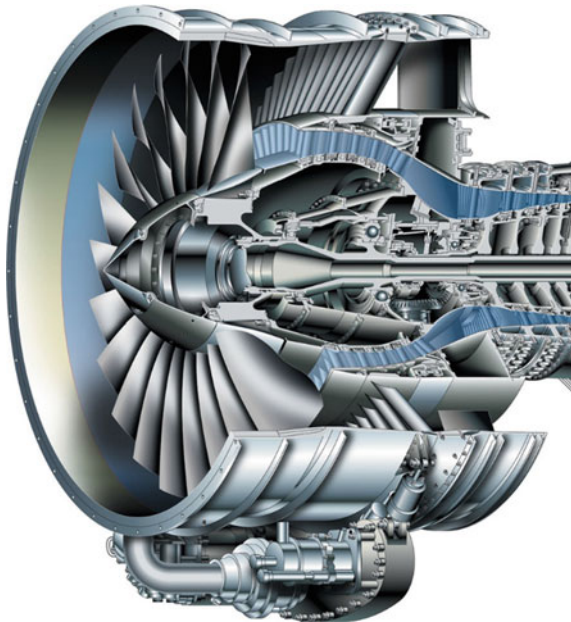


Fig. 4.2-2 High bypass ratio fan and booster (© 2014 United Technology Corporation—Pratt & Whitney Division)

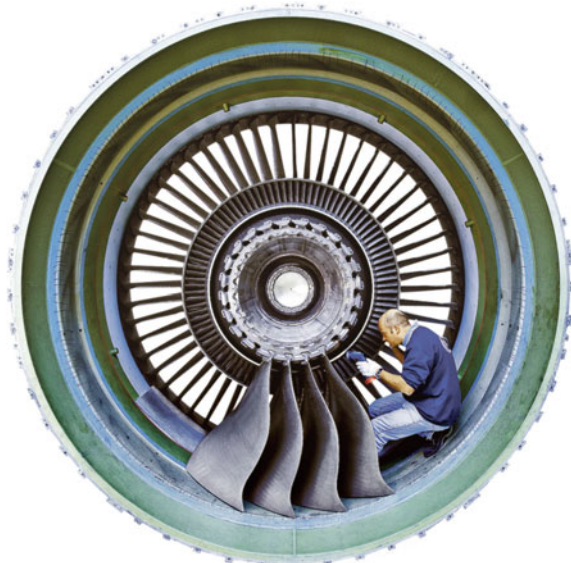


Fig. 4.2-3 GP7000 fan blades (© Copyright MTU Aero Engines)

4.2.4 *Splitters*

In terms of design, flow splitters tend to be passive devices. Typically, many of their input parameters regarding flow area are received from adjacent components. In the case of a splitter immediately downstream from a high bypass fan, the fan inlet area would correspond to the total flow through the fan, the booster flow would drive the inner exit area, while only the inlet area of the bypass duct might remain as a design variable.

In an industrial environment, a single-function splitter is seldom used, the splitter usually being combined with a strut, a frame, and a handling bleed valve. Under such circumstances the overall role of the component needs to be considered to ensure that it fulfills its intended function especially at off-design conditions.

4.2.5 *Booster*

A booster in a high bypass ratio engine “boosts” the pressure in the core stream. A booster is employed when the combined fan hub and HP compressor pressure ratio is insufficient to meet the required overall pressure ratio. To match the core flow to the HP compressor demand, most boosters incorporate a handling bleed, which opens at low speed. In engines without a gearbox, the speed is the same as that of the fan, because the components are on the same shaft. The booster and LPT rpm is higher than that of the fan in engines with a gearbox. Since the temperatures within the booster are moderate, titanium is an appropriate lightweight material.

4.2.6 *HP Compressor*

The rotational speed of the engine core results from an integrated design with the HP turbine. This is done primarily by adjusting the number of compressor stages, although the more limited influence of inlet radius ratio may also be used to advantage. Design limits are imposed on a great many parameters, such as tip speed, stall margin, Mach numbers, radius ratios at inlet and exit, with empirical values established via test results from research rigs and engines. A few of the design limits will dominate, and a successful solution will most likely occur by full exploitation of as many limits as possible.

Aerodynamically, a multi-stage compressor is always too fast at the inlet and too slow at the exit. This drives the designer to a minimum bore diameter at the front, limited by space requirements for the LP and maybe IP shafts. At the exit of the gas generator compressor, the desire for high circumferential speed pushes out the diameter and frequently, also encourages a constant-tip HPC design. This leads to high hub/tip ratios and short blades, which increase the sensitivity to tip clearance.

For combustion stability, the Mach number at gas generator compressor exit must be low because the inlet velocity to the burner must not exceed certain limits.

The length of the compressor follows from the chosen blade and vane aspect ratios. Low aspect ratios lead to lower engine parts count, reduced cost, improved strength and better aeroelastic stability. These permit higher aerodynamic loading levels, which deliver higher efficiency, and improved vibrational characteristics. Low aspect ratio designs are more distortion tolerant due to larger chords in the rotor blades. Disadvantages of low aspect ratio designs include high disk rim loads and large axial length.

The upper part of Fig. 4.2-4 illustrates the cross section of a real compressor while the lower part shows the much simpler GasTurb model. Cones of constant wall thickness represent the casing and the inner air seals. The casing thickness in the model is bigger than the value which might be obtained from a drawing because

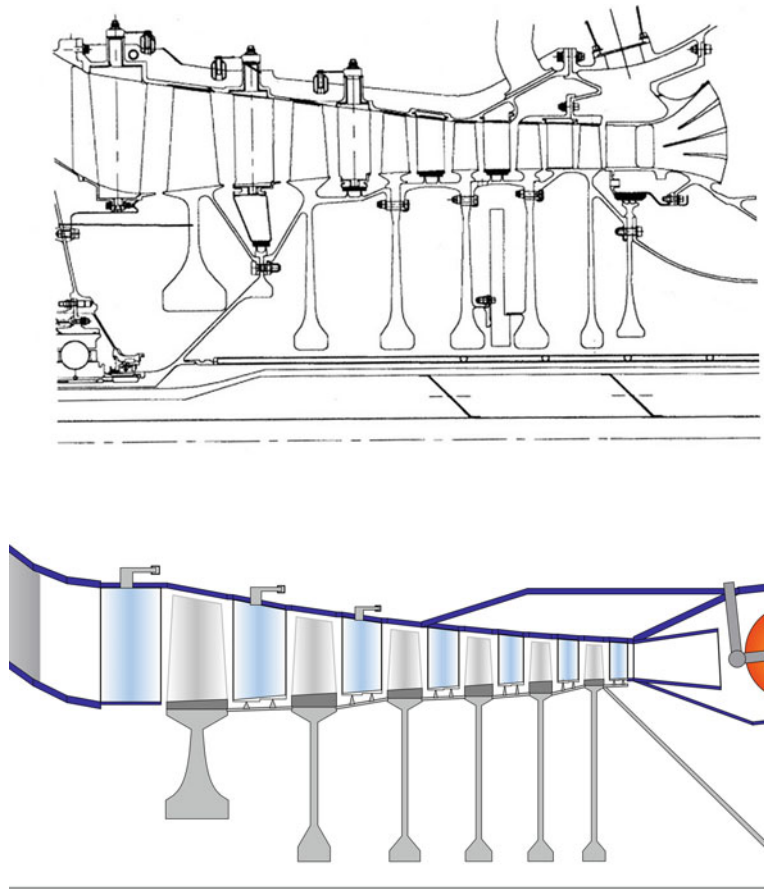


Fig. 4.2-4 High pressure compressor [4]

flanges, nuts, bolts, and non-axis symmetric elements like bleed offtake pipes must be considered by an adequate adder to the true casing thickness. We use *effective thickness* in a model

Front stages of HP compressors may be designed as blisks, manufactured from a titanium alloy. The temperature level in the rear HPC stages requires the use of nickel alloy or stainless-steel blades, vanes and disks.

4.2.7 Combustor

The combustor connects two primary flow path components—the HP compressor and the HP turbine. Since these have priority in the design hierarchy, the combustor inlet geometry is obtained from the compressor and the exit geometry from the turbine (Fig. 4.2-5).

In preliminary design, the combustor is usually considered to be made up of the outer casing, the pre-diffuser, and the burner. The pre-diffuser picks up the HP compressor exit dimensions and diffuses the flow to a velocity level deemed suitable. The cant angle can normally be adjusted as part of the diffuser such that the combustion chamber lines up with the turbine vane inlet. The combustion process determines the volume and hence the internal dimensions of the combustor itself.

The dome height and burner length are the primary influences on geometry. Dome height controls the transverse dimension of the system and is dependent on the reference velocity and the combustor bypass flow. To obtain an estimate of weight, preliminary definitions of the combustor liner and the inner and outer casings are required together with, at least, an empirical estimation of fuel handling and ignition hardware.

The maximum pressure differential ($P_3 - P_{\text{amb}}$) is an additional consideration. This is needed to determine wall thickness and avoid excessive weight. In addition to the internal static value, the pressure differential also depends on the ambient pressure, which is an inverse function of altitude.

Nickel-chromium-iron alloys are used for combustion-can liners, diffuser assemblies and containment rings.

4.2.8 HP Turbine

The HP turbine combines with the HP compressor and combustor to form the core of the engine. As part of the HP spool, it is linked to the compressor both aerodynamically and mechanically, see Fig. 4.2-5. It is worth emphasizing that the mechanical design point is selected to guarantee structural integrity throughout the mission, by consideration of the worst possible circumstances. The structural

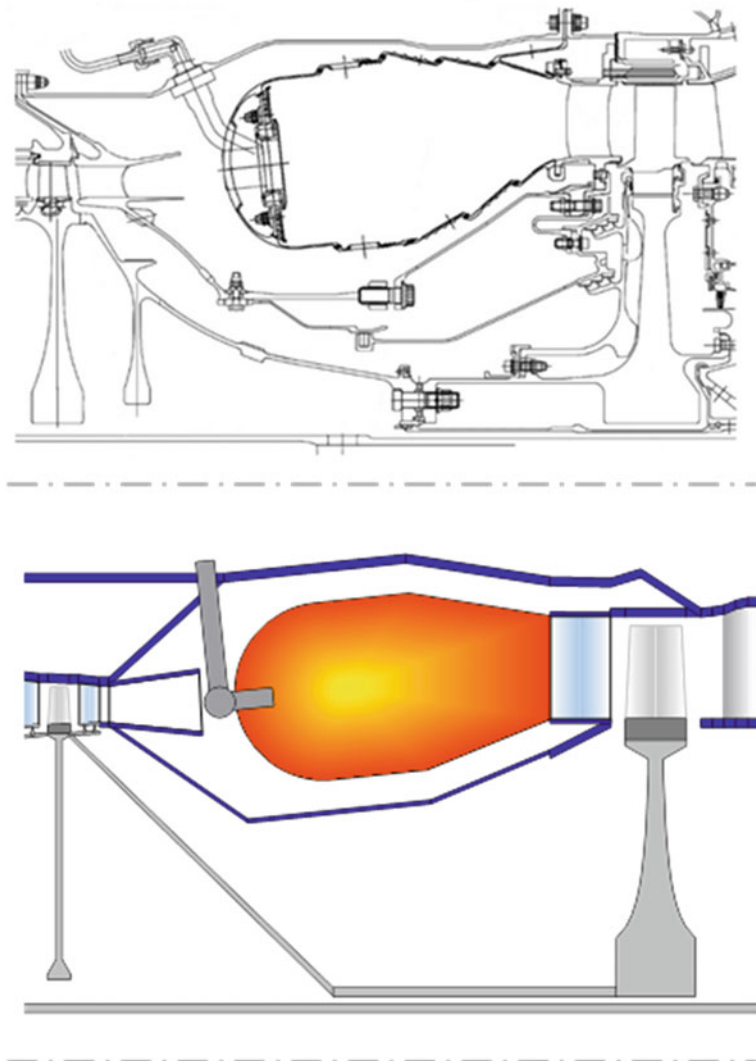


Fig. 4.2-5 Combustor and HP turbine [5]

integrity during kink-point day take off (the highest ambient temperature with maximum thrust) is of paramount concern. This is taken care of primarily by good design of the disk and means of blade attachment.

The overall turbine geometry is obtained simply by joining the inlet to the exit, and the best method of fixing exit dimensions is via an upper limit on AN^2 . Here, A is the annulus area at turbine exit and N is the rpm corresponding to the mechanical design speed (i.e. the maximum value). AN^2 is a measure of rim stress (whose

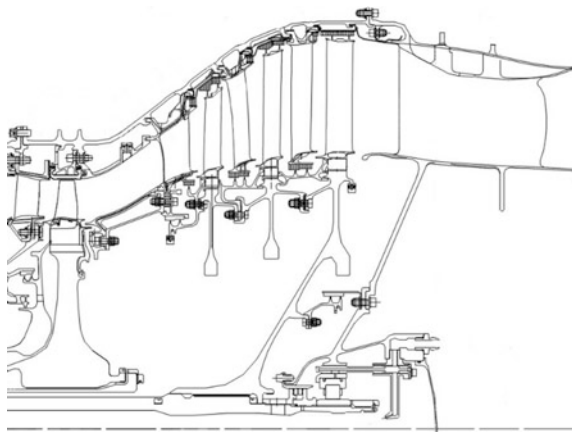


Fig. 4.2-6 HP and LP turbine

allowable limits may be related to material properties) and its selected upper limiting value is able to be correlated with temperature and hence blade cooling capability.

Note that the exit Mach number of the gas generator turbine relates to its aerodynamic loading: with highly loaded single stage turbines it will be higher than with moderately loaded two stage turbines.

Active clearance control increases the turbine casing weight. Whether the turbine blades are shrouded or not affects not only the weight of the blades themselves but also that of the turbine disk which sees a bigger rim load when the blades are shrouded.

Be sure to use a representative value for the thickness of the flat plate which represents the complex shape of a cooled turbine blade. Figure 4.5-3 indicates that the blade wall thickness is much less than the profile thickness value as used during the aerodynamic design. Using an inappropriate value for the mean blade thickness leads to an incorrect disk rim load and finally to a non-representative disk mass.

Another influential factor for turbine disk stresses is the diameter of the disk bore: it must be big enough to accommodate the shaft connecting the LP turbine with the fan (Fig. 4.2-6).

4.2.9 LP Turbine

Many of the design guidelines for HP turbines also apply to the LP variety, except that, within the component hierarchy, the HP turbine exit defines the LP turbine inlet dimensions. An inter-turbine duct affords some freedom, unless the two are close-coupled, as in the case of a vaneless LP unit. The LP turbine usually has more stages than an HP turbine, so possible variations of interstage work split make life more interesting for the preliminary designer. This enables a reduction in the work across the final stage to achieve reductions in exit swirl, exit velocities, and exhaust loss.

In LP turbines nickel-iron-chromium alloys are usually used for turbine disks, shafts and cases. The LP turbine of turbofans with a gearbox run with much higher AN². The blade material of choice is titanium aluminide (TiAl) which has mechanical properties that are almost equivalent to the nickel alloys in use today, although its density is much lower. Turbine blades in TiAl are only about half the weight of comparable nickel alloy components.

4.2.10 Afterburners

The most common type of afterburner is found in a low bypass ratio turbofan engine used in military applications, where burning is carried out in the mixed exhaust stream. In other engine configurations, augmentation can be used in the core and bypass streams separately. When it occurs in the bypass or fan stream it is referred to as “duct burning”.

In preliminary design, where early estimates of afterburner weight and dimensions are needed, the sub-components that must be considered are diffuser, spray ring, flame holder, the augmenter duct itself, and the duct liner. The latter is used as screech damper (screech is a high frequency oscillation which can destroy the afterburner quickly) and also ducts cooling air to the nozzle.

4.2.11 Nozzles

The purpose of the exhaust nozzle is to produce the required thrust at all phases of an aircraft mission. It is fair to say that the influence of nozzle performance on engine net thrust and specific fuel consumption is higher than that of any other single component. It is crucial, therefore, to achieve the optimum performance with due regard to weight, complexity, maintainability, and cost.

Nozzles or exhaust systems may be divided into two major types, according to their application.

Subsonic nozzles are those for low speed applications, commercial transport being the most common, and they are usually convergent and conic. Their geometry is usually fixed and therefore they are the simplest.

Supersonic nozzles are required to perform at high flight speeds, but must also be able to deliver the appropriate levels of thrust at all other phases of a mission. These nozzles usually have variable geometry and are always complex, relatively heavy, and very expensive. They have been developed mainly for use on military aircraft, but currently are the focus of attention in many supersonic civil aircraft programs, where the major requirements are high efficiency at supersonic cruise and low noise at take off.

Mixed and *unmixed* nozzles also occur in both high and low-speed categories.

4.2.11.1 Subsonic Nozzle

Subsonic nozzles (or nacelles) can be considered as two types. Separate flow nozzle configurations are the most common on high bypass ratio engines and usually mounted on the wing via a pylon. Fuselage-mounted engines are frequently used on smaller aircraft and mostly have a long duct, mixed flow nozzle. This has superior performance at cruise conditions, and better thrust reversing and noise suppression, however it is heavier than the separate flow nozzle.

4.2.11.2 Supersonic Nozzle

Supersonic or, more correctly, *multi-functional* exhaust systems are especially important for military operations. Performance requirements for advanced weapons systems have increased significantly over the past two decades, and there is additional incentive in the form of *supersonic civil* applications. This is reflected in component efficiencies and operational characteristics, as a result of which, emphasis has been placed on improved engine-airframe integration and nozzle flexibility. In future, it is likely that the functional operation of the exhaust nozzle will be shared by the engine and aircraft control systems.

Finally, if the maximum pressure differential across the nozzle flaps and side-walls does not occur at take off, then this must be investigated. Maximum “ Δp ” may well occur at altitude, where the ambient pressure is less than that at ground level, even though the internal pressure may be somewhat less than at other points in the mission. Subsonic climb conditions are typical candidates for this effect.

4.3 Frames and Ducts

4.3.1 Front Frame

A front frame is used in many modern, low bypass ratio, high pressure ratio turbofan engines to provide structural support for a front bearing. This is needed whenever the number of fan or LP compressor stages becomes too heavy to be supported in a cantilevered fashion from the main or mid frame. Typically, two stages may be overhung, while more than two stages necessitate the use of a front frame. However, there are exceptions: both the RB199 and the EJ200 have three stage fans and no front frame.

A multi-stage fan is usually associated with a high pressure ratio, low aspect ratio engine, with the overall axial dimension of the fan being greater than its diameter. The structural support requirements are satisfied by the design of an array of struts with suitable stiffness and minimum aerodynamics loss. Typically, such engines are for military applications, although these configurations are also encountered in the NASA HSR program.

Since the role of the front frame is to connect the fan with the engine inlet, its dimensions are set mostly by those of the fan. In addition to the struts and/or variable inlet guide vanes, the additional sub-element of a front frame is the bullet nose. In the absence of a front frame, a conical or elliptical bullet nose is used for leading edge closure of the fan hub.

4.3.2 *Main Frame*

In a turbofan engine, the main frame or mid frame is located between the booster and HP compressor, and spans the bypass duct and the core flow path. In addition to forming a principal structural element and carrying bearings for the HP and LP spools, the mid-frame is also the route for services to the interior of the engine and for power offtake shafts.

Apart from the structural requirements, which may be supplied independently, the inlet and exit geometry for the definition of a main frame is passed in from the adjacent components, namely the bypass duct inlet flow area and radial dimensions, the booster exit area, and the HP compressor flow inlet area. The corresponding radial dimensions are defined via slopes and axial locations.

4.3.3 *Turbine Center Frame*

The turbine center frame is situated between the HP turbine and the LP turbine of a turbofan (Fig. 4.3-1). It connects the HP and sometimes the LP shaft's rear bearing with the housing and forms an aerodynamic transition duct between the two turbines. In addition, there may be pipes through which oil flows to the bearing. The



Fig. 4.3-1 Turbine center frame of the GEnx (© MTU Aero Engines)

turbine center frame defines the position of the bearing, which is important for maintaining component clearance in the entire HP system.

4.3.4 Rear Frame

The rear frame is an integral part of the structure in most gas turbine engines, although occasionally an overhung or cantilevered LP turbine will be encountered. In addition to structural rigidity, the rear frame provides support for the rear bearings, and usually includes a row of exit guide vanes to alleviate the exit swirl, thereby reducing losses in the downstream diffuser.

In a turbofan, the rear frame does not incorporate vanes or struts in the bypass stream, but the outer limits of the bypass duct are usually set via the radial spacing between the core and the outer duct. The radial spacing is defined as a function of the strut chord or height. Fuselage mounted engines have struts (A-frames) from the rear frame across the bypass duct.

For the engine core, the rear frame connects the LP turbine with the downstream diffuser, and as such, the slopes of the diffuser casings are often set by input parameters to the frame. Input to the rear frame also affords the opportunity to adjust the radial height of the bypass duct (and hence the flow area) so as to control the Mach number and minimize losses.

In the case of a low bypass turbofan engine, the rear frame must be configured with the downstream mixer in mind. For an unmixed high bypass ratio engine, the rear frame serves only to center the core flow path structure. The bypass duct is supported via the main frame and is therefore not associated with the rear frame structure.

4.4 Shafts

In a gas turbine engine, the HP shaft is a complex multi-part structure that does not resemble a cylinder in the slightest. In preliminary design the HP shaft is usually addressed in terms of its contributions to two major rotating components, namely the HP compressor and the HP turbine. In the case of a drum construction for a compressor, the shaft is made up of the inner casing sections held together by web disks to which the blades are attached. For an HP turbine the rotating components outside of the main disk are made up of a complex array of webs, seals, and supporting disks, with stub shafts running forward and aft to the respective bearings. The preliminary designer is not too concerned with the geometric details, and the weight of an HP shaft is usually accounted for by using empirical constants that are functions of the weights of the compressor and turbine rotor assemblies. In GasTurb, the HP shaft model consists of a cone and a cylinder as shown in Fig. 4.2-5

An LP shaft does however resemble a cylinder—somewhat! Its weight is usually accounted for in the mechanical design of the LP turbine or power turbine, as appropriate, and not the compressor. The length of the shaft is determined by the distance between the front and rear bearings and it is unlikely that this will be known until all the turbomachinery and the combustor have been designed and the overall length of the flow path is fixed. The details are extremely important, however, since they can have a surprising impact on the overall weight.

The weight of the shaft is determined, firstly, by its length and this depends on the distance between the bearings. Shaft weight is also related to its outer diameter and the thickness of the cylinder, which are driven by the maximum torque to be transmitted. But the outer diameter and cylindrical thickness also depend on the length, since the shaft must not bend under its own weight. If we can save on length we can save also on the other two dimensions. In this regard, a short combustor can reduce the engine weight by a few hundred kilograms! Accurate estimates of LP shaft and HP disk dimensions are important, since this determines whether the disks can accommodate the LP shaft within their bore. Failure in this respect has often been the source of embarrassment since it leads to major revisions in the overall design.

The LP shaft should be designed at the cycle operating conditions that correspond to maximum torque.

4.5 Disks

The requirement for higher gas generator compressor and turbine stage work without additional stages has resulted in increased blade tip speeds in advanced commercial aircraft engines. High speed, low aspect ratio designs result in significant increases in compressor disk rim loading.

Traditionally the compressor rotors consist of a disk with attached airfoils. A more modern compressor design uses *blisks* in the first stages—blades and disk are manufactured as a single piece. The term blisk is an acronym composed of the words “blade” and “disk”. Figure 4.5-1 shows a HPC compressor blisk which is part of the PW1000G PurePower® Geared Turbofan™.

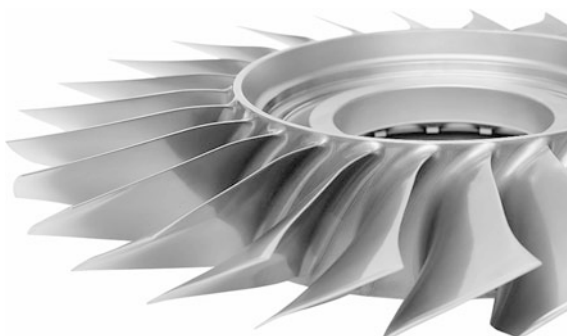


Fig. 4.5-1 Bladed disk (© MTU Aero Engines)

High turbine inlet temperatures create a severe thermal environment, thereby making it difficult to design turbine disks for a specific life requirement that meets the goals. The current trend indicates that gas generator compressor and turbine tip speeds, as well as turbine inlet temperatures, will continue to increase in advanced commercial engines as higher work levels are achieved.

Equally important, aircraft engines must meet safety demands. Fatigue loading of turbine components associated with repeating aircraft take off/cruise/landing cycles is a principal source of degradation in turbomachinery. A disk burst cannot be contained and is potentially the most catastrophic failure possible in an engine, therefore disks are designed as life-limited parts with overspeed capability and low cycle fatigue life as primary objectives.

4.5.1 Disk Design Methodology

A typical disk design is based on the blading geometry, weight, and rotational speed that will already have been specified in the design of the turbomachinery flow path. Figure 4.5-2 shows how blades are typically attached to a disk, and introduces some of the nomenclature.

A disk must be designed to withstand the centrifugal stresses generated by the rotating blades at the maximum rotational speed of the spool and to transmit the torque generated by the turbine blading to the appropriate compressor rotor. Only that portion of the disk inboard of the blade root is considered to carry the stresses,

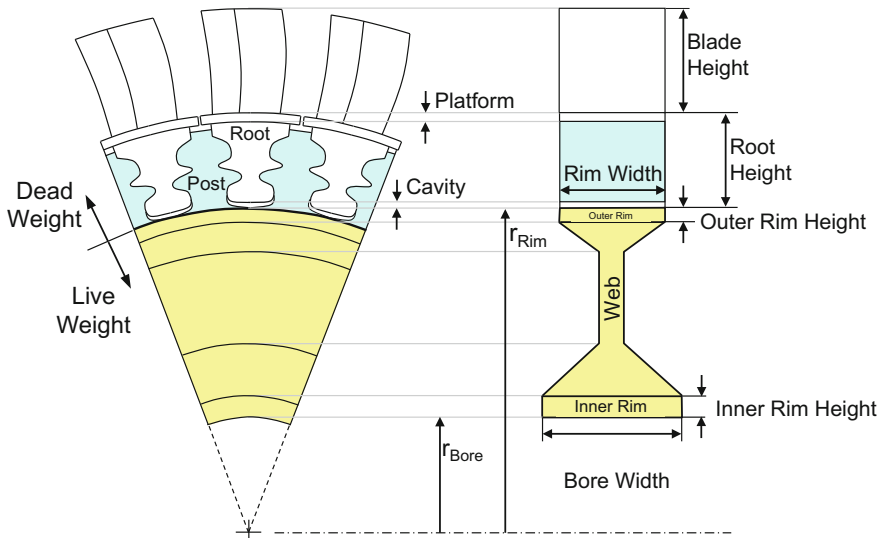


Fig. 4.5-2 Disk nomenclature

and this is referred to as the live disk. The parts of the disk between the blade roots (posts), as well as the blade roots themselves and the airfoils, constitute dead weight. Although it is the design of the live disk which is being addressed here, the posts must not be neglected when the total disk weight is quoted. The dead weight produces the pull stresses on the rim of the live disk, but moving inwards towards the bore, the disk must also support an increasing proportion of the centrifugal stress generated by its own weight.

The average stress at the outer radius of the live disk is estimated by smearing the total centrifugal force of the dead weight around the circumference. The weight of the blades, including platforms and roots, and the axial chord at the root should already be known from the flow path design. The radial location of the center of gravity of the combined dead weight must also be known. However, to calculate the radial pull stress at the live rim, certain assumptions are made regarding the height and weight of the blade root, and the weight of the posts.

The disk stress calculation deals only with the “live” disk which carries the rim load caused by the blades (including shroud, inner platform, and root) and the posts that are holding the blades.

By the way, we can get blade numbers without doing a detailed aerodynamic compressor design. Making assumptions about the aspect ratio = blade span/chord and the pitch/chord ratio is sufficient.

It is recognized that actual disk lives depend upon countless details of a highly localized nature. Such details cannot be known until a final design has been reached, and therefore cannot be accounted for during the early stages of design that are of concern here.

4.5.2 Rim Load

The rim load is calculated considering the individual masses of the blades (including the shroud), the blade roots (including the blade platforms) and the posts. For each of these elements the product of mass, the radius of the center of gravity and rotational speed yield a contribution to the radial forces pulling at the rim of the live disk. The rim stress $\sigma_{r,rim}$ is the sum of all the forces divided by the live disk rim area.

For the estimation of the rim load estimation, only a few more quantities are needed besides the flow annulus dimensions and the number of blades. The *Root/Blade Height Ratio* is usually much higher for high pressure turbines than for low pressure turbines. Note that the *mean blade thickness*, which is usually supplied as a percentage of the chord in these calculations, must be the *effective mean thickness* of the metal that accounts for the mass. In case of cooled or hollow blades, it is much less than the actual mean profile thickness, compare Figs. 4.5-3 and 4.5-4. Don’t mix up the profile thickness quoted by the aerodynamicists with the mean blade thickness employed here.

Airfoils are modeled as flat plates with the dimension *chord* \times *annulus height* \times *thickness*. Blade taper is accounted for by using an appropriate value for the effective mean blade thickness. The center of gravity is at a lower radius than



Fig. 4.5-3 Cooled turbine blades

the local mean radius of the annulus radius because of blade taper. This is important for the calculation of the polar moment of inertia.

Blade shrouds, if they exist, are assumed to have a constant thickness. The center of gravity of the shroud is located just outside the flow path, since the shroud is not only a simple plate; there are also tip fences or seals outside of it. The blade attachment is comprised of the blade platform, the neck and the fir tree. The neck does not necessarily exist details are shown in Fig. 4.5-4.

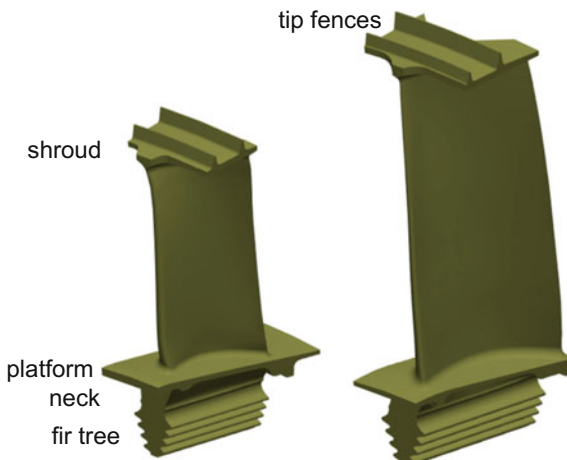


Fig. 4.5-4 Uncooled low-pressure turbine blades [5]

4.5.3 Disk Temperature

Rim and bore temperatures influence both stress and dimensions of a disk; Exact values for these temperatures are impossible to get during the preliminary design phase, only first estimates are feasible. GasTurb defines the temperature gradient from the platform towards the disk center with a single number which stands for the temperature difference from the platform to the center point of the disk. The temperatures in the live disk are interpolated linearly between the platform temperature and that of the imaginary disk center.

In compressors the inner platform temperature is equal to the local gas temperature during steady state operation. The first rotor sees compressor inlet temperature, the last compressor rotor sees exit temperature. Intermediate rotor blade platform temperatures are interpolated linearly between compressor inlet and exit. The casing temperature above each rotor is the same as the platform temperature.

The platform temperature of turbine disks is determined using a more sophisticated algorithm. At first, the program calculates an approximate value for the relative temperature at the rotor inlet for each stage by applying a factor of 0.9 to the absolute stage inlet temperature T_i . Considering the radial temperature distribution factor RTDF leads to the inner platform temperature being $T_{plt} = 0.9 T_i (1 - RTDF)$. If the turbine is uncooled, then this temperature serves as the anchor point from which the temperature decreases linearly towards the disk center point with a given gradient.

With cooled turbines, we need to consider the path of the cooling air. It is usually injected into the cavity in the front of the turbine disk with a tangential velocity component. This lowers the temperature of the cooling air that enters the rotor in a manner similar to the main stream gas temperature—which is lower in the relative (rotating) system compared to the absolute (non-rotating) system. Depending on the amount of cooling air and how it is routed to the rotor, the temperature at the live disk rim can be significantly lower than the platform temperature. To take that effect into account, the anchor point for the disk temperature calculation is placed between the platform temperature of an uncooled turbine and the cooling air delivery temperature (T_3 in case of high pressure turbines).

If a cooled turbine has more than one cooled stage, then two thirds of the total cooling air is led to the first rotor and one third goes to the second stage. If the turbine has more than two stages, then the rest of the stages are regarded as uncooled.

The temperature of the casing around the turbine rotors depends on the absolute rotor inlet temperature, corrected by the radial temperature distribution factor RTDF to $0.9 T_i$ and the temperature of the shroud cooling air. The latter is T_3 for gas generator turbines and T_{13} for turbofans. Shroud cooling effectiveness depends on the specific design of the turbine case.

4.5.4 Disk Stress

The disk stress calculation should be done for the maximum steady state rotational speed and the highest operating temperatures. If the operating point with the highest temperature does not coincide with the operating point which has the highest rotational speed, then both conditions should be checked.

The disk stress analysis (nomenclature see Table 4.5-1) is based on the following differential equations:

Equilibrium of forces for a disk element:

$$\frac{d(tr\sigma_r)}{dr} - t\sigma_t + t\rho\omega^2r^2 = 0 \quad (4.5-1)$$

Radial stress:

$$\sigma_r = \frac{E}{1-v^2} \left[\frac{du}{dr} + v \frac{u}{r} - (1+v)\alpha\Delta T \right] \quad (4.5-2)$$

Tangential Stress:

$$\sigma_t = \frac{E}{1-v^2} \left[\frac{u}{r} + v \frac{du}{dr} - (1+v)\alpha\Delta T \right] \quad (4.5-3)$$

The live disk is divided into many rings for the stress calculation. The differential equations above are converted into finite difference equations. In the disk bore (the inner area of the innermost ring) the radial stress σ_r is zero. The displacement of the bore is estimated at the beginning of the calculation. The differential equations yield the radial and the tangential stresses as well as the displacement at the outer radius of the first ring. These quantities then allow the conditions in the second and the further rings to be calculated. Finally, all the rings have been covered and the radial stress at the outer radius of the live disk is found.

Table 4.5-1 Disk stress calculation nomenclature

E	N/m ²	modulus of elasticity
r	m	radius
t	m	disk thickness
u	m	radial displacement
α	1/°C	coefficient of thermal expansion
v	—	Poisson's ratio
σ_r	N/m ²	radial stress
σ	N/m ²	tangential stress
ω	rad/s	rotational speed
ΔT	°C	temperature above reference (room) temperature

If this radial stress is not equal to the rim load, the estimated bore displacement is corrected iteratively until the rim load is equal to the calculated radial stress at the outer radius of the live disk.

4.5.5 Material Properties

Many different material properties influence the disk stress calculation. All of them change with temperature, except material density. The most important temperature-dependent property is tensile strength.

Tensile strength measures the force per cross sectional area required to pull a test specimen to the point where it breaks. While the stress is low, the length of the material will increase proportionally to the force applied. When the force is removed, then the material will relax back to its original shape.

During a tensile stress test, the reduction in cross sectional area is proportional to the increase in length in the elastic range. The ratio of transverse contraction to longitudinal extension of the material is Poisson's ratio. During the test, when a certain stress is exceeded, a plastic deformation happens, and the shape of the material changes permanently (Fig. 4.5-5).

Figure 4.5-6 shows the ultimate strength of four alloys frequently used in gas turbines as functions of material temperature. AM 350 is a chromium-nickel-molybdenum stainless steel which has been used for compressor components such as blades, disks and shafts. Greek Ascoloy (418) is a stainless steel designed for services at temperatures up to 650 °C. Typical applications in gas turbines are for

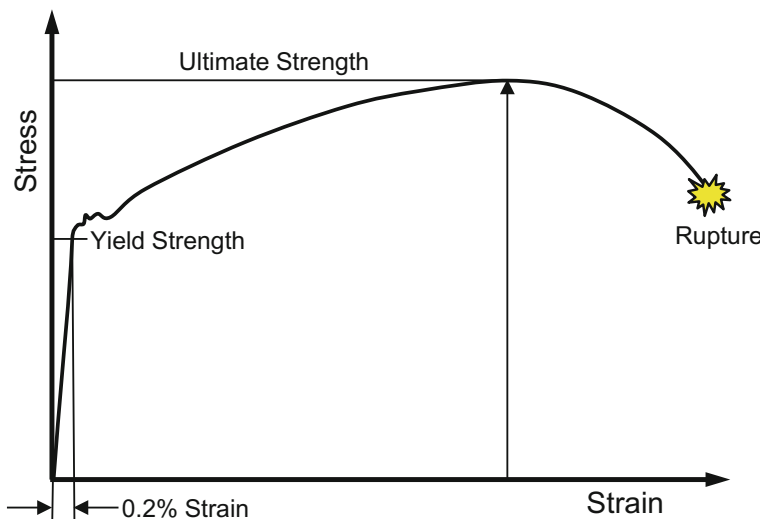


Fig. 4.5-5 Tensile stress test

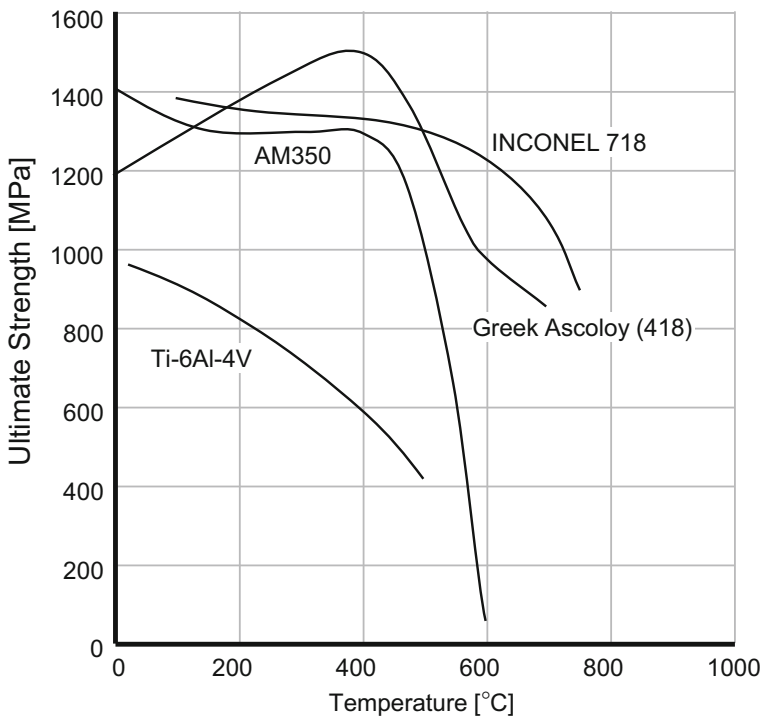


Fig. 4.5-6 Ultimate strength of four materials

compressor parts. INCONEL 718 is a high strength, corrosion-resistant nickel chromium material used up to 700 °C for rings and casings. Ti-6AL-4 V is the workhorse alloy of the titanium industry; it is used up to approximately 400 °C for compressor blades, disks and rings.

4.5.6 Design Margins

The disk design margin (expressed in %) compares the *yield strength* $\sigma_{0.2 \text{ local}}$ of the material at the local temperature with the local *von Mises* stress $\sigma_{\text{von Mises}}$:

$$DM = \left(\frac{\sigma_{0.2 \text{ local}}}{\sigma_{\text{von Mises}}} - 1 \right) 100 \quad (4.5-4)$$

Von Mises stress is a combination of stresses in two or three dimensions which can be compared to the tensile strength of a material loaded in one dimension. In our work, the web stress (at the web outer diameter, just below the disk rim) is possibly critical.

No safety margins are considered, it is up to the disk designer to select an appropriate positive stress margin, 10...30% are reasonable numbers.

The disk burst margin (in %) compares the *ultimate strength* of the material σ_{ultimate} (evaluated at the average disk temperature) with the average tangential stress:

$$BM = \left(\frac{0.47 \sigma_{\text{ultimate}}}{\sigma_{t,\text{average}}} - 1 \right) 100 \quad (4.5-5)$$

The factor 0.47 (taken from Ref. [3]) is a sort of safety margin and therefore a burst margin ≥ 0 is a reasonable design target.

The disk burst speed—which should be greater than 130...150% of the operating speed—is calculated as

$$\frac{\omega_{\text{burst}}}{\omega_{\text{op}}} = 100 \sqrt{\frac{\sigma_{\text{ultimate}}}{\sigma_{t,\text{average}}}} \quad (4.5-6)$$

4.5.7 Stress Distribution

GasTurb offers a choice of two different disk shapes, shown in Fig. 4.5-7. In a web disk, the middle section—the web—is of constant thickness. Both the hub and rim sections are thicker, the thickness transition towards the web in the middle is linear. In a hyperbolic disk, the thickness beyond the hub is a hyperbolic function of the radius (Fig. 4.5-7).

The upper part of Fig. 4.5-6 compares radial, tangential and von Mises stress distributions from a web and a hyperbolic disk. In this example the stress is highest in the bore. That does not necessarily mean that the bore stress margin is critical because in the disk bore, the material temperature is low and yield strength is high.

It must be acknowledged that this disk stress calculation method has its limitations. In an actual disk, the local stresses—which are relevant for disk life—depend on countless details which are not yet known in the preliminary design phase of an engine.

4.6 Engine Weight

Precise engine weight predictions are very difficult. Specialists calculate engine weight during development as the sum of the few big parts and the countless small parts, including all pipes, nuts and bolts. During the preliminary design phase such a calculation is not feasible. The details of the mechanical design—especially of the static parts—are not known. Thus, any number for the absolute weight will be

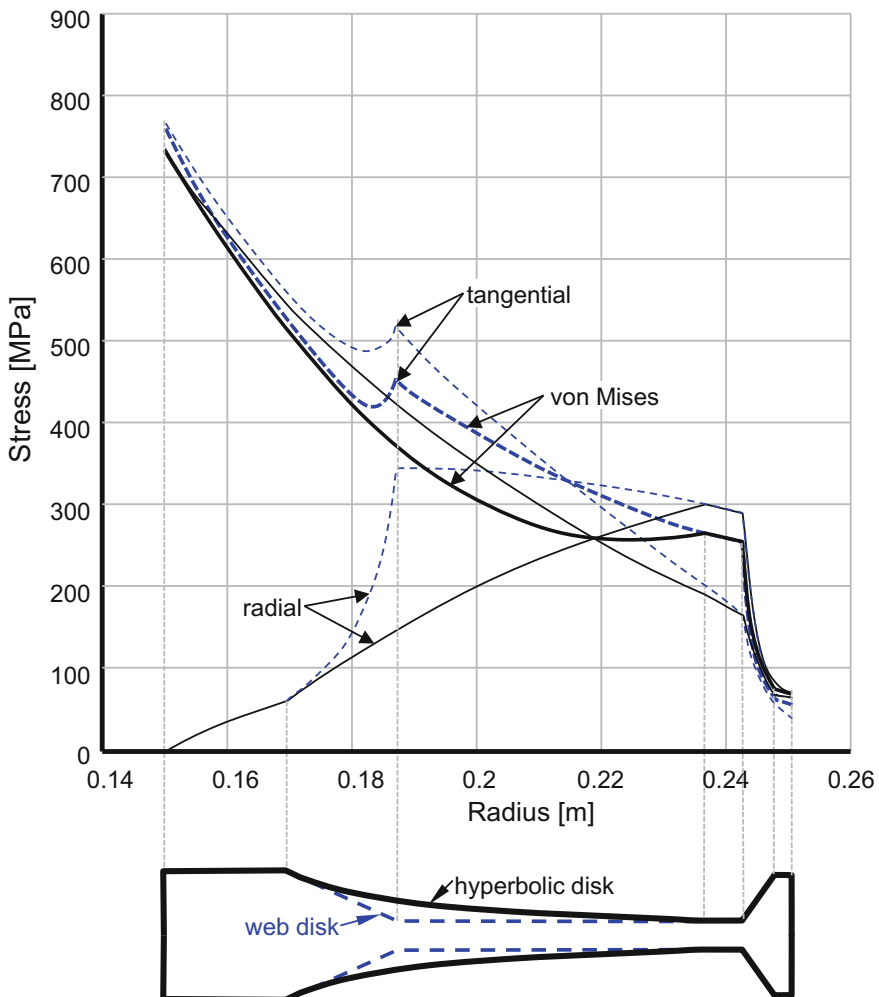


Fig. 4.5-7 Stress distribution in web and hyperbolic disks

inaccurate. However, if the model considers many engine components in some detail, the effects of modifying important design parameters relative to a reference engine design can be predicted.

As an example, Fig. 4.6-1 shows a GasTurb model based on a V2500 cross section, published in 1984. At that time, the engine had only one booster stage while the production V2500 turbofans now have three or four. The agreement between this model and the engine picture published in Ref. [7] is very good.

The basic GasTurb model does not consider all engine parts. Bearing structures, engine mountings, the external gearbox and its drive from the gas generator spool, the control unit, actuators and external dressings (pipes and mechanical links) are

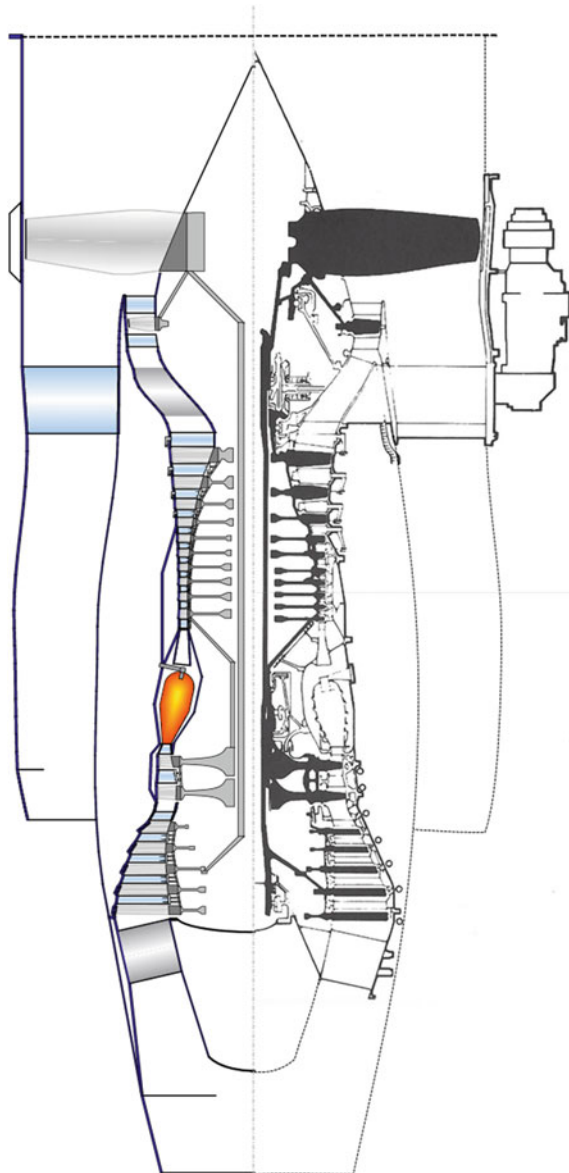


Fig. 4.6-1 GasTurb geometry model of a V2500 engine

not modeled. Therefore, the sum of the modeled component weights is only around 60% of the total engine weight. This shortfall was the result of Ref. [8] which compared the GasTurb 11 weight model with the true V2500 engine parts weight, measured in the MTU maintenance shop. Most of the weight model enhancement proposals have been implemented in later GasTurb versions.

For each of the component models there is a weight factor which can be used to reconcile the calculated component weight with reality. Additionally, there are factors and adders for the total calculated weight. Thus, the GasTurb model can be calibrated with data from real engines.

Instead of using the component weight factors and adders for considering parts that are not modeled explicitly, their weight can be modeled with additional correlations in the formula editor of GasTurb (*Composed Values*). This is a way to enhance the mechanical model and to define a more realistic model for any specific project of interest.

The accuracy of the rotating mass model is better than that of the stationary parts. There are only a few elements, such as turbine cover plates and small disks that carry inner air seals which are neglected. Consequently, the GasTurb model tends to estimate polar moment of inertia of rotors on the low side.

4.7 References

1. Onat, E., Klees, G.W.: A Method to Estimate Weight and Dimensions of Large and Small Gas Turbine Engines, NASA CR-159481, 1979
2. Tong, M.T., Naylor, B.A.: An Object-Oriented Computer Code for Aircraft Engine Weight Estimation ASME GT2008-50062, 2008
3. Tong, M.T., Halliwell, I., Ghosh, L.J.: A computer code for gas turbine engine weight and disk life estimation. J. Eng. Gas Turbines Power **126**, 265–270 (2004)
4. Pratt & Whitney.: General Electric Aircraft Engines Critical Propulsion Components Volume 1: Summary, Introduction, and Propulsion Systems Studies NASA/CR 2005-213584/VOL1, May 2005
5. Abdullahi, H., Kotulla, M., Staudacher, S.: A New Method for Online Monitoring and Trimming of Pyrometer Measurements in High Performance Turbo Engines AIAA Paper 2003-1195
6. de la Calzada, P., Parra, J., Villanueva, M.A., Ruiz-Goepgui, J.I.: Design and Development of the Inter-turbine Structure and Power Turbine for the MTR390E Turbohaft Engine GT2013-94021, 2013
7. Erinnerungen.: 1934–1984 Flugtriebwerkbau in München (Memories: 1934–1984 Aero Engine Production in Munich) Herausgegeben von der MTU Motoren- und Turbinen-Union München GmbH Zweite Auflage 1985 Published by MTU Motoren- und Turbinen-Union München GmbH Second Edition 1985
8. Donus, F.: Ermittlung der Genauigkeit und Erarbeitung von Verbesserungsvorschlägen bei der Gewichtsabschätzung mit GasTurb 11 (Evaluation of the accuracy and development of improvement proposals of the GasTurb 11 weight estimation) Diplomarbeit Institut für Luftfahrtantriebe der Universität Stuttgart, 2008

Part C

Off-Design

Chapter 1

Component Performance



Part A of this book describes solutions to overall system simulation requirements. The material presented are mainly examples in which the component models are not always described in detail. Part B deals with component design issues. Here, in the first section of Part C, we discuss the performance of gas turbine components like inlets, compressors, turbines, combustors, mixers, afterburners and nozzles. In a second section, we describe how these components work together in an engine.

While Part B describes how to design the geometry of a component for given requirements, here we assume that the geometry of the component is known. We show how well the component performs when the operating conditions deviate from those for which the geometry was optimized.

1.1 Inlet

The gas turbine manufacturer usually does not design nor build the inlet of aircraft engines or the air intake of power stations. Thus, the inlet is essentially not a gas turbine component and we could ignore it in this book as not being our business. However, the losses in the inlet depend on the operating conditions of the gas turbine, on how much air is ingested by the engine. We need to know how the operating conditions affect the losses in the inlet to calculate the so-called installed performance.

Aircraft engine inlets are quite different to those designed for gas turbines in power stations. Therefore, we devote separate sections to each of them.

1.1.1 Aircraft Engines

The installed performance of any gas turbine propulsion system depends greatly on the inlet. The pressure loss and distortion of the flow to the engine, and

consequently the installed thrust and fuel consumption, are determined by the general configuration and the specific geometry of the inlet. Typically, in a subsonic environment, a 1% reduction in inlet total pressure recovery will reduce net thrust by about 1.3%, while for supersonic operations the penalty can be much higher.

Traditionally, specification of the inlet used to be the prerogative of the airframer, with guarantees of performance being accepted by the engine designer. Nowadays, with the increased demands by more complex aircraft on inlet performance, the integration of engine, nacelle and airframe has become more critical, along with a more equitable sharing of responsibilities. The inlet is an important part of the nacelle, and it can never be designed as an afterthought. Indeed, it must be considered in parallel with, if not in advance of, the other propulsion system components. Engine integration is now regarded as a technology in its own right. The following discussion of inlet performance is mainly based on Ref. [1].

1.1.1.1 Loss Description

The stagnation or total pressure at the fan face is needed for use in the cycle calculations. If the aircraft is moving, it is the ram pressure rise, $P_2 - P_{amb}$, which is of interest and the inlet should conserve or recover as much of the dynamic head $\frac{1}{2}\rho V_0^2$ as possible. At subsonic conditions, inlet performance may be defined in three ways:

- Inlet pressure ratio, which is expressed simply as P_2/P_0 , where P_0 is the free-stream stagnation pressure.
- Inlet isentropic efficiency, η_i , is the fraction of the inlet dynamic head retained. It is included in the definition of total pressure at the compressor face

$$P_2 = P_{amb} \left(1 + \eta_{in} \frac{\gamma - 1}{2} M_0^2 \right)^{\gamma/\gamma-1} \quad (1.1-1)$$

- Ram efficiency is the ratio of ram pressure rise to inlet dynamic head

$$\eta_{Ram} = \frac{P_2 - P_{amb}}{\frac{1}{2} \rho V_0^2} \quad (1.1-2)$$

Performance of a supersonic inlet is usually expressed in terms of pressure recovery P_2/P_0 . A typical definition is found in the military specification MIL-E-5008B which is a very general estimate of the characteristics of an oblique shock system.

$$\left(\frac{P_2}{P_0}\right)_{shock} = 1 - 0.075(M_0 - 1)^{1.35} \quad (1.1-3)$$

The AIA Standard estimates ram recovery for less sophisticated inlets:

$$\left(\frac{P_2}{P_0}\right)_{shock} = 1 - 0.1(M_0 - 1)^{1.5} \quad (1.1-4)$$

None of these loss descriptors take variations in corrected mass flow into account.

1.1.1.2 Subsonic Aircraft

Commercial subsonic airliners like the Airbus A320 have only a short duct as an inlet. It is sized such that it is always able to admit the quantity of airflow required by the engine. The cycle condition selected as the inlet design point should therefore be that at which the corrected mass flow is maximum to ensure that the engine always receives the flow that it needs (Fig. 1.1-1).

The operating point in the compressor map determines the corrected flow at the face of the engine. Corrected flow is connected inseparably with compressor inlet Mach number. Its value does not exceed 0.6–0.7 at high values of corrected spool speed and is lower than the cruise Mach number of commercial airliners. Thus, the inlet must decelerate the flow and work as a diffuser. In contrast, during take off the flight Mach number is lower than at the engine face—the flow accelerates upstream of the inlet throat.

The flow distribution at the fan or compressor face must be as uniform as possible and the total pressure losses must be minimized.



Fig. 1.1-1 Intake on an airbus A320

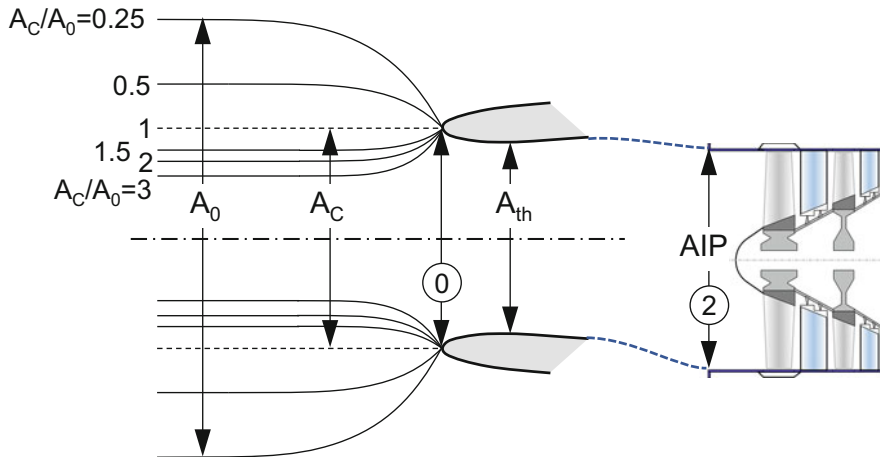


Fig. 1.1-2 Streamlines upstream of the nacelle

The boundary between the intake and the engine is the *Aerodynamic Interface Plane* AIP (see Fig. 1.1-2). Usually this coincides with the front flange of the engine or it is just a short distance upstream. Total pressure P_2 and total temperature T_2 in the AIP are, by definition, the entry conditions for the gas turbine.

Over the full range of forward speed, from zero to cruise value, the total pressure loss (other than that due to skin friction) is determined by the occurrence and resulting size of flow separation at the lip and the magnitude of the throat Mach number, which is a measure of the corrected flow W2RStd. In general, at zero and low forward speed (except at very low throat Mach numbers) the ingested stream tube will be larger than the intake capture area ($A_C/A_0 < 1.0$) and separation will occur on the inside of the lip if the lip is sharp like that of a fighter aircraft inlet (Fig. 1.1-3). Following separation, the magnitude of the loss rises rapidly with throat Mach number.

As forward speed increases, the cross sectional area of the incoming streamtube, A_0 , decreases for a given throat Mach number. When it becomes less than the capture area A_C , ($A_C/A_0 > 1.0$), lip separation does not occur, and losses rapidly return to the skin friction level of the basic duct loss. With increasing incidence, such as under cross-wind or high angle of attack maneuvers, lip separation can occur at all values of A_C/A_0 and not just at low values of A_C/A_0 as at zero incidence.

The lip contraction A_C/A_{th} ratio can markedly affect the magnitude of total pressure loss due to lip separation. Figure 1.1-4 illustrates the effect of changing A_C/A_{th} from 1.078 to 1.25 at 20° incidence and low forward speed conditions. In this case, differences in performance between the contraction ratios are due principally to separation.

Not all inlets are as short as those on the A320 (Fig. 1.1-1). Long S-shaped ducts lead the air to the AIP when inlets are mounted at the side or on top of the fuselage.

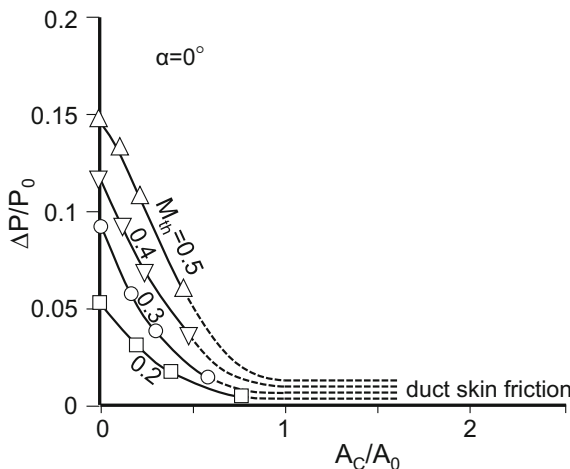


Fig. 1.1-3 Straight ducts: variation of loss with throat Mach number, zero incidence [1]

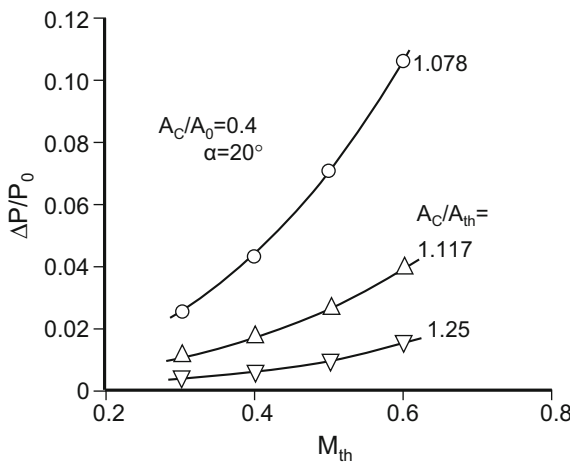


Fig. 1.1-4 Effect of lip contraction ratio on total pressure loss at subsonic speeds

Figure 1.1-5 illustrates the basic total pressure loss due to skin friction on duct walls, as measured in a duct with a bellmouth intake where the range of throat Mach number is controlled by varying the downstream pressure. The total pressure loss increases with duct length, duct curvature and changes in the shape of its cross section.

Any asymmetric flow separation in a straight duct creates uneven total pressure distribution and thus inlet flow distortion in the AIP. Curved inlets are especially susceptible to distortion in the area profiles of swirl and total pressure. Total pressure distortion and total pressure loss are linked inseparably. Distortion affects engine operability and total pressure loss affects engine performance.

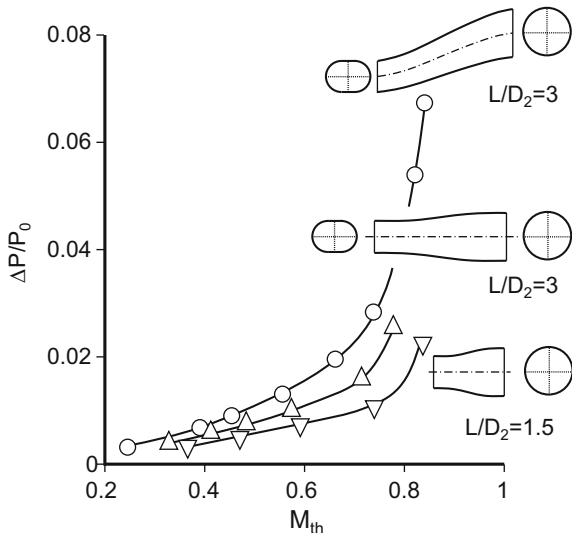


Fig. 1.1-5 Flow in subsonic diffusers

The former can be examined with the parallel compressor model (see Chap. A6), the latter is amenable to basic non-dimensional performance considerations.

It should be noted that inlet distortion leads to a total pressure loss. The distortion descriptor DC₆₀ (defined in Sect. 6.1) shows a correlation between the distortion level and the total pressure loss, P₂/P₁. It is the pressure loss that leads to a reduction in thrust rather than the distortion itself.

To evaluate the reduction in thrust due to an increase in intake pressure loss, we consider a series of operating points at a constant corrected spool speed N/ $\sqrt{\Theta_2}$. Corrected net thrust F_N/ δ_2 would remain constant during a test in the ATF (altitude test facility) if the pressure ratio P₂/P_{amb} was kept constant. An increase in the intake loss of 1 % would cause a similar loss in gross thrust.

If P_{amb} is kept constant, any decrease of P₂ reduces the nozzle pressure ratio and F_N/ δ_2 decreases in such a way that 1% total pressure loss results in a greater loss in net thrust.

1.1.1.3 Supersonic Aircraft

The analysis of a supersonic inlet is different from that of its subsonic equivalent because pressure waves warning of its presence cannot be propagated upstream to allow the streamlines to adjust. Locally the flow is dominated by oblique and normal shocks, and boundary layer separation is very likely due particularly to the sharp leading edges. For these reasons there are many different types of supersonic inlets. Fixed and variable geometries are two general categories. Internal

compression, external compression, and mixed compression describe types of inlet, based on the location of oblique shock waves through which the compression process takes place. These may also be delineated roughly by the corresponding Mach number regimes in which they are used. Within the latter two types, different numbers of oblique shocks can be utilized depending on the incident Mach number, the pressure recovery required, and the length, weight, complexity, and cost that are tolerable.

Variable geometry must be incorporated into the design to accommodate the range of flow rates from static take off to high speed, high altitude cruise of supersonic transport aircraft. Variable geometry is also used to incline the oblique shock system correctly and to control the total pressure recovery. Bypass and bleed doors may be required at high-speed cruise, and auxiliary doors to supplement the inlet flow may be needed at take off (Fig. 1.1-6).

For a military application, the designer must consider the very significant differences in the multi-phase mission requirements. Hence there is a need for levels of performance that are at least adequate at every condition between static take off and supersonic cruise. Such conditions may include take off, subsonic climb, supersonic, high-altitude cruise, high-speed, low-level penetration, and transonic maneuvering, in addition to whatever range of supersonic flight speeds are also demanded. There are many different intake designs, from simple Pitot intakes to complex variable geometry.

Figure 1.1-7 shows the intake recovery data of many fighter aircraft over a range of Mach numbers, taken from Ref. [1]. The figure is complemented with lines for the total pressure recovery of a vertical shock, the AIA Standard and the MIL-E-5008B Standard intake recovery.

Note the agreement between the intake recovery of a vertical shock and the data from the F-16 with a pitot inlet. Another remarkable curve is that of the F-104. This aircraft has a single fixed geometry cone, designed for $M = 1.8$.

Attempts at improving performance over the fixed geometry F-104 inlet were made in the F-4. Acceptable performance was obtained over a wider range of Mach number, but the full benefit of variable ramps was not realized until the advent of the F-111, F-14 and F-15 aircraft.

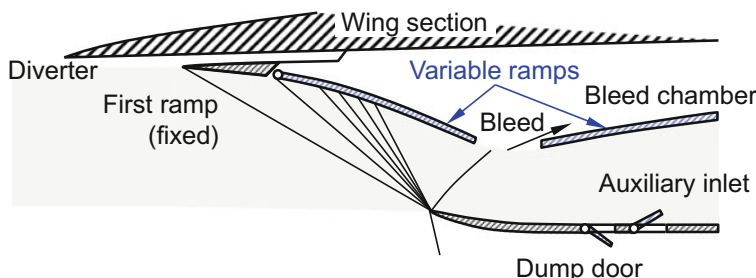


Fig. 1.1-6 Concorde inlet

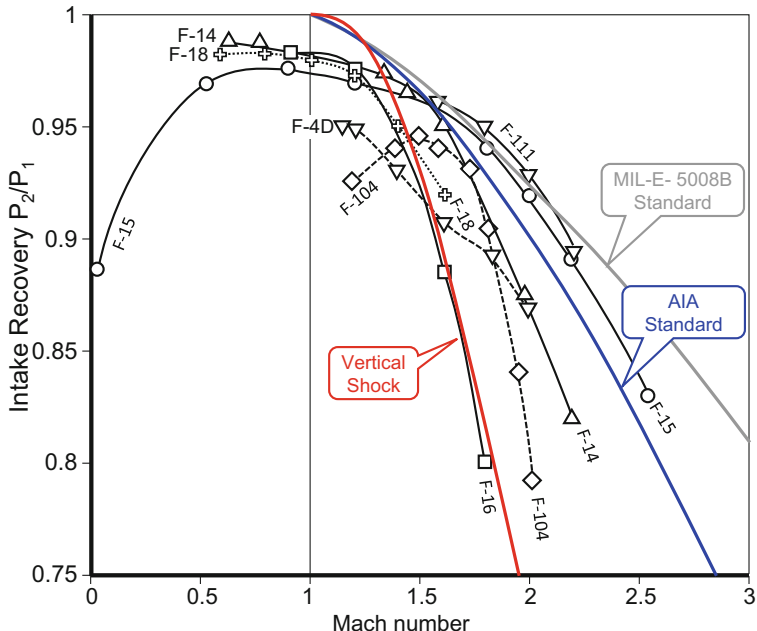


Fig. 1.1-7 Intake recovery of fighter aircraft

The concept of sustaining intake performance at high angles of incidence by positioning an intake beneath a body or a wing forming a shield, applies to both subsonic and supersonic aircraft and has been used on a number of aircraft projects varying from Concorde to F-16. When incidence is varied, airflow direction is controlled by the aircraft surface, so to that extent, the intake is not aware of a change of aircraft attitude. Additionally, at supersonic speeds, advantage can usually be taken of a reduction in local Mach number and hence a reduction in shock losses occurs as incidence increases.

The response to the requirement for increased maneuverability of supersonic fighters, had a major impact on the design and development of many current aircraft. Whereas the drive for increased speed in earlier years had caused aircraft intakes to become more complex with time, there has been a conscious effort to keep complexity to a minimum in current aircraft. European and Soviet designers sometimes tend to place greater value on simplicity and/or light weight than upon high pressure recovery and low drag. Of course lower cost is always attractive.

High pressure recovery and low distortion over a wide range of flight conditions, including high angles of attack, can be achieved with a hinged lower lip of the cowl. The European Fighter Aircraft (EFA)—a predecessor of the Eurofighter (Fig. 1.1-8) —used both underbody shielding and a hinged lower cowl lip. There is a favorable effect on losses at subsonic speed and high incidence and also a favorable effect on intake efficiency at take off conditions (Fig. 1.1-9).



Fig. 1.1-8 Eurofighter intake (copyright Eurofighter—Jamie Hunter)

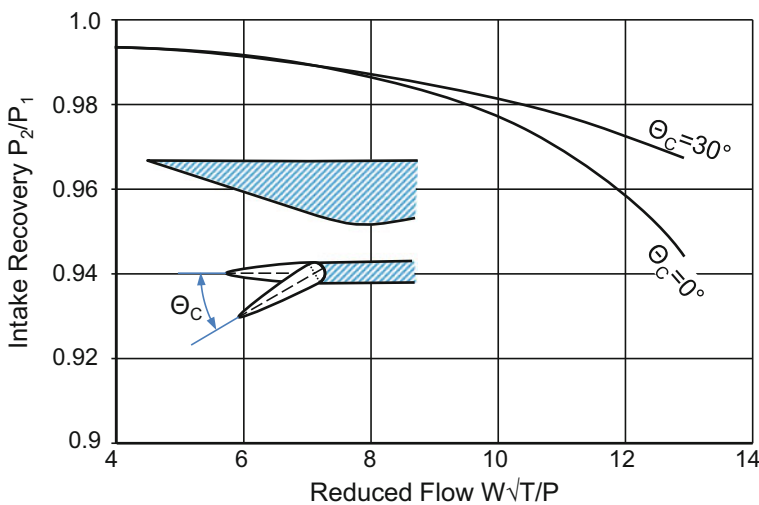


Fig. 1.1-9 Performance of supersonic intake with hinged cowl lip at static conditions (take off)

1.1.1.4 Spillage Drag

All the external forces on an engine nacelle are considered a part of the aircraft drag. However, these forces depend on the mass flow through the intake, the shape of the intake in the immediate vicinity of the cowl lip and—in case of supersonic intakes—the strength and disposition of compression surface shock waves.

It is common practice to split the nacelle drag in two parts: a constant fraction is part of the aircraft drag, and a variable fraction which changes with engine mass flow. The inlet force due to the departure of A_C/A_0 (see Fig. 1.1-2) from a reference

condition is the spillage drag. The reference inlet mass flow for zero spillage drag of a typical scoop intake might be defined as that for which $A_C/A_0 = 1$.

During subsonic flight, a reduction of A_C/A_0 below the design value results in an increase in the pre-entry drag force and a corresponding increase in cowl forebody thrust force [1]. These two forces are equal and opposite in a potential (i.e. frictionless) flow field and therefore result in no spillage drag.

In viscous subsonic flow, the change in cowl pressure gradients result in a thickening of the cowl boundary layer and ultimately, as area ratio A_C/A_0 increases further, to separation of the flow from the cowl lip. Under these circumstances cowl thrust is decreased from the potential flow value and a rapid rise in spillage drag from the datum flow value is observed.

Vertical and oblique shocks exist upstream of the inlet during supersonic flight. Their position relative to the intake entry affects spillage drag. Variable inlet geometry helps to minimize spillage drag.

1.1.2 Power Generation

The qualifying properties of an aircraft engine inlet are the total pressure loss and the distortion level, only in exceptional cases do total temperature changes play a role. In power generation, just the opposite is true; total pressure losses at maximum mass flow are usually no higher than 1%, but total temperature changes significantly if inlet air chillers, evaporation coolers or fogging are applied. An inlet cooling system is a useful gas turbine option for applications where significant operation occurs in the warm months. This is a cost-effective way to add machine capacity during the period when peaking power periods are usually encountered on electric utility systems.

The air supply for the gas turbine in a power station needs a much bigger device than an aircraft engine. Due to its enormous size it is called the *air inlet house*. The blue construction to the left of the gas turbine building in (Fig. 1.1-10) is the air inlet of a combined cycle power plant near Bangkok, Thailand.

Downward pointing weather hoods are located just upstream of the entrance to the air inlet house, so the ambient air must turn upwards to flow into the inlet filtration system. The turning of the air is effective in minimizing rain and snow penetration. After the weather hood is a trash or insect screen. Trash screens capture large pieces of paper, cardboard, bags, and other debris. The screens also deflect birds, leaves, and insects.

There are two basic systems currently available for inlet cooling. An *inlet chiller* is basically a heat exchanger through which the cooling medium (usually chilled water) flows. Perhaps the most widely accepted system is the *evaporative cooler* in which the air passes through a wet porous medium. Part of the water is evaporated, absorbing heat from the air and increasing its relative humidity.



Fig. 1.1-10 Combined cycle power plant

A more efficient way to evaporate water is an inlet fogging system. This is the least expensive cooling option and has low operating costs, particularly when one accounts for the fact that fog systems impose only a negligible pressure drop on the inlet airflow when compared to evaporative coolers.

Fog nozzle manifolds are typically located just downstream of the air filters, but other locations can be desirable, depending on the design of the inlet duct and the intended use of the fog system. Figure 1.1-11 shows the basic arrangement of filters, cooling devices and the silencer in an air inlet house.

In addition to the advantage of achieving extra power, the use of an evaporative cooler or inlet fogging improves the environmental impact of the machine. Increasing water vapor in the inlet air tends to lower the amount of oxides of nitrogen produced in the combustion process and, therefore, lowers the emissions of the machine.

The various inlet air cooling options are best studied with a psychrometric chart. On a hot afternoon in a desert climate, when the relative humidity is 20%, it is possible to cool by as much as 15 °C, while in a humid climate hot-afternoon the cooling potential can be just 5.5° or less, see Fig. 1.1-12.

The chiller can reduce the air temperature more than wetted technologies because the air can be chilled below the wet bulb temperature, indifferent to the weather conditions.

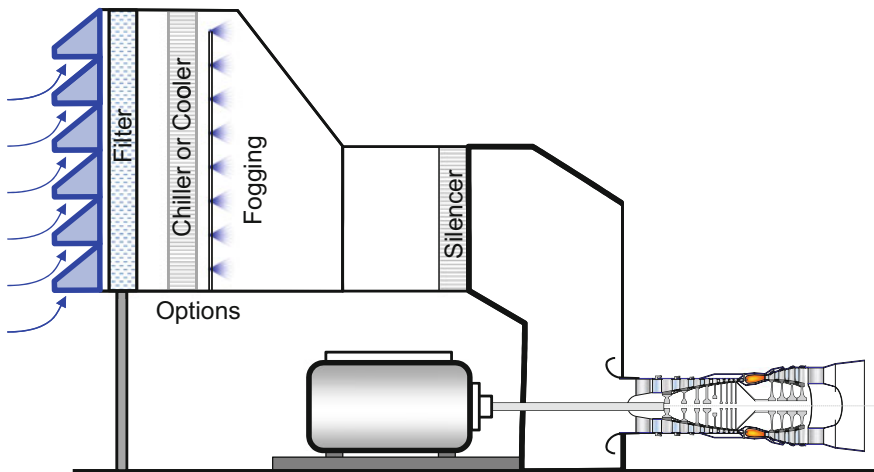


Fig. 1.1-11 Air inlet house

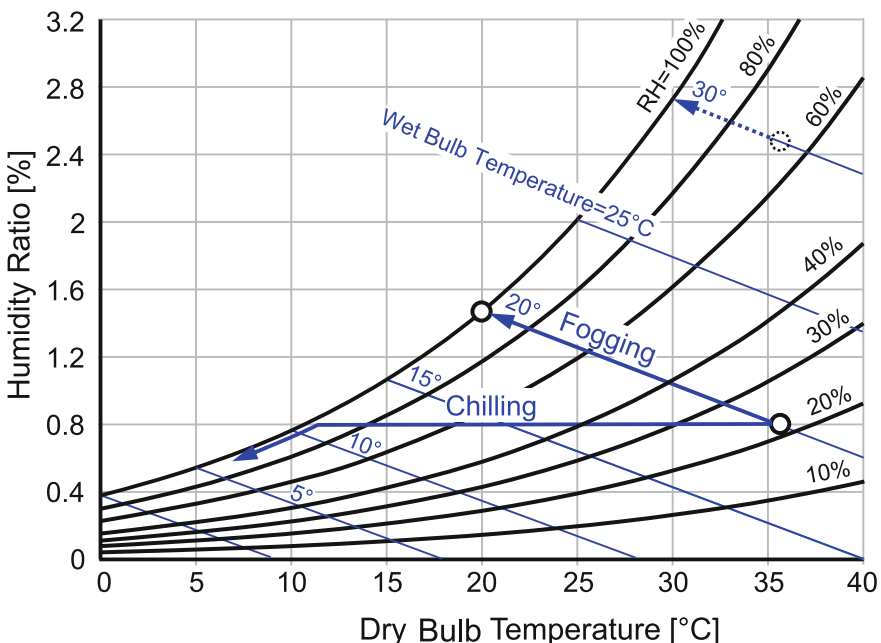


Fig. 1.1-12 Chilling and evaporation in the psychrometric chart

Figure 1.1-13 shows the magnitude of power increase which may be achieved with an inlet fogging system. On a day with outer air temperature of 40 °C and 20% relative humidity, power can be increased by 9.3% and heat rate reduced by 1% simultaneously with evaporation of water.

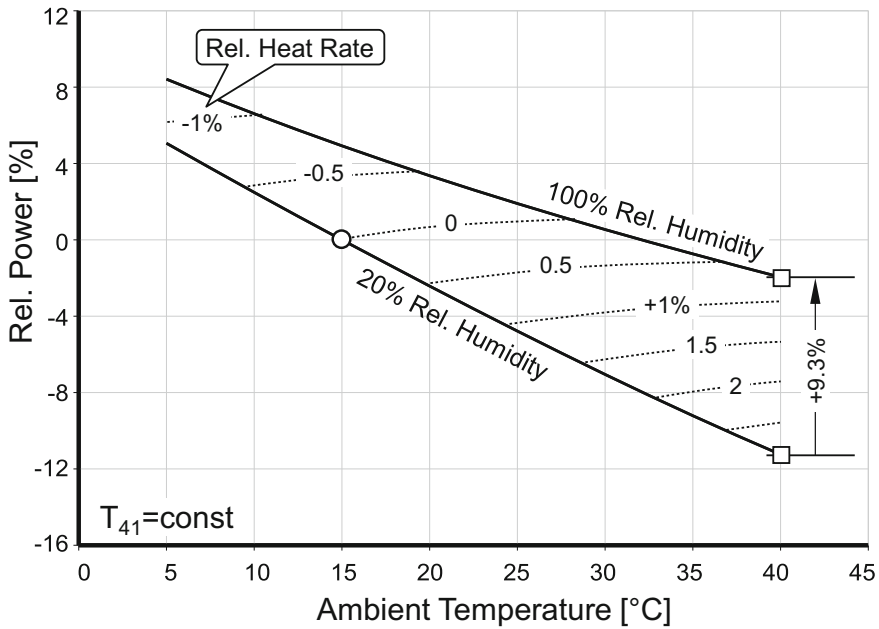


Fig. 1.1-13 Effects of fogging (single spool engine)

1.2 Off-Design Behavior of Compressors

Realistic compressor maps are the key to high quality gas turbine performance calculations. Map prediction requires knowledge of the detailed geometry and results from even the most sophisticated current codes are not accurate enough to predict the performance map of a newly designed compressor precisely. Only if the code has been calibrated with rig data from a similar compressor, can adequate maps be constructed.

The best results are obtained from a dedicated compressor rig using engine parts. Such a map can then be scaled to represent slightly modified versions of the same compressor. Realistically, however, true and direct compressor map generation is only feasible for engine manufacturers and research organizations; it is not an option for the gas turbine user. For him the only way to achieve that objective is to adapt an existing map from the literature in such a way that it matches any available data.

Many publications address map manipulation processes, ranging from simple to more sophisticated physics-based scaling rules. There are also reports that describe the use of statistics, genetic algorithms, neural networks and morphing techniques (a graphical procedure that changes one image into another through a seamless transition) for re-engineering compressor maps. These approaches do not consider

the laws of physics while modifying the shape of the speed and efficiency lines; consequently, at best, the resulting maps are valid only in the region where they have been calibrated and, at worst, they are invalid everywhere! The valid region is frequently very restricted, especially in the case of gas generator compressors which run in steady state always on a single operating line.

In this chapter, we describe which physical phenomena influence the shape of speed and efficiency lines in compressor maps. For machines operating at relatively low speeds (so that the flow into each stage is subsonic), there is usually considerable variance between the values of corrected flow at choke and stall. As the speed of the machine is increased the range narrows until the speed lines are vertical over a wide range of pressure ratios.

The flow at a certain speed can also be limited by choking in the compressor exit guide vanes. For high pressure ratio single-stage centrifugal compressors this is normal, but it can also happen, for example, with low pressure ratio multi-stage boosters of turbofan engines. If the compressor chokes at its exit, then the specific work remains constant along the speed line while the overall pressure ratio varies and consequently the efficiency contours in the map have special characteristics.

In other parts of the map, the efficiency varies in a different systematic manner along speed lines. Peculiar shapes of specific work and corrected torque contours can reveal physical impossibilities that are difficult to see in the standard compressor map formats. Compressor maps generated without considering the inherent physical phenomena can easily result in misleading performance calculations if used at operating conditions outside of the region where they have been calibrated. Whatever map adaptation method is used, the new maps created should be checked thoroughly for violations of the underlying laws of compressor physics.

1.2.1 About Compressor Maps

Let's discuss the correlations between pressure ratio, flow, speed, specific work, torque and efficiency inherent in any compressor map in the context of various compressor design features. The thoughts presented are an updated version of Ref. [2] entitled *Correlations Hidden in Compressor Maps*.

A compressor map is usually a carpet plot with lines of pressure ratio versus corrected flow over a range of corrected spool speeds. Additionally, there may be contour lines of constant efficiency either shown in the same plot or presented separately, again for a range of corrected speed lines but plotted against either corrected flow or pressure ratio.

Let us first clarify what is meant by the terms *corrected flow* and *corrected spool speed*. *Corrected flow* usually is defined as $W\sqrt{\Theta/\delta}$ with $\Theta = T/288.15$ K and $\delta = P/101.325$ kPa. The essential content of this quantity is $W/\sqrt{T/P}$, the so-called *reduced flow*.

To simplify matters we consider the inlet of a compressor without inlet guide vanes. $W/\sqrt{T/P}$ can be expanded usefully by introducing the axial Mach number M_{ax} :

$$W \frac{\sqrt{\Theta}}{\delta} \propto W \frac{\sqrt{T}}{P} = \frac{A M_{ax} \sqrt{\gamma/R}}{\left(1 + \frac{\gamma - 1}{2} M_{ax}^2\right)^{\frac{\gamma+1}{2(\gamma-1)}}} \quad (1.2-1)$$

If we consider dry air at Standard Day temperature only, then the isentropic exponent γ and the gas constant R are constant values and it is obvious that $W\sqrt{T/P}$ represents the axial flow Mach number in the compressor face annulus area A .

Note that the relation between $W\sqrt{T/P}$ and M_{ax} is not a linear one. As Mach number approaches the sonic condition, the flow parameter becomes very flat and reaches a maximum at the exactly sonic condition. Therefore, at high airflows the speed lines become closely bunched together.

Corrected spool speed is given by $N/\sqrt{\Theta}$ which differs only by a constant factor from *reduced speed* N/\sqrt{T} . The latter is proportional to corrected circumferential speed U/\sqrt{T} . Introducing the static temperature T_s leads to

$$\frac{U}{\sqrt{\gamma R T_s}} = \frac{U}{\sqrt{T}} \frac{\sqrt{1 + \frac{\gamma-1}{2} M_{ax}^2}}{\sqrt{\gamma R}} \quad (1.2-2)$$

where $U/\sqrt{(\gamma R T_s)}$ is the circumferential speed U divided by the local velocity of sound—it is the circumferential velocity expressed as the Mach number M_U .

$$\frac{N}{\sqrt{\theta}} \propto \frac{U}{\sqrt{T}} = M_U \frac{\sqrt{\gamma R}}{\sqrt{1 + \frac{\gamma-1}{2} M_{ax}^2}} \quad (1.2-3)$$

Thus at a given corrected flow (i.e. a given compressor face Mach number M_{ax}), U/\sqrt{T} is a measure of the circumferential Mach number M_U .

The circumferential Mach number M_U can reach any value. The corrected flow through a compressor, however, is limited since the axial Mach number M_{ax} cannot exceed unity. This knowledge can be used for map extrapolation to extremely high corrected spool speeds, provided the annulus area at the compressor face is known. Thus, a hidden correlation between corrected speed and flow exists in the maximum speed region of the map. This correlation, however, is not of much practical value because, in reality, compressor face Mach numbers are seldom higher than about 0.7.

Finally, pressure ratio can also be expressed as a Mach number because $\Delta H_{is}/(\gamma R T_1)$ is equivalent to a Mach number squared.

$$\frac{P_2}{P_1} = \left(1 + \frac{\Delta H_{is}}{C_P T_1}\right)^{\frac{\gamma}{\gamma-1}} = \left(1 + \frac{\gamma - 1}{2} M^2\right)^{\frac{\gamma}{\gamma-1}} \quad (1.2-4)$$

1.2.1.1 The Shape of Speed Lines

Much of the off-design performance behavior of a multi-stage compressor is determined by how well or how poorly the stages match from front to rear. In particular, far from design conditions at very low or high airflows the local flow parameters vary considerably in magnitude, causing the front, middle and rear stages to operate simultaneously over the range from stall to choke at the same rpm. Overall compressor performance reflects the cumulative performance of all stages, from front to rear.

Nevertheless, it is useful to consider the basic shape of a speed line (i.e. a line with constant corrected speed) of a single stage compressor operating at comparatively low Mach numbers: this can be derived from the analysis of the velocity diagrams in Fig. 1.2-1.

Let us introduce two useful quantities—often referred to as stage characteristics—the *flow coefficient* $\Phi = V_{ax}/U$ and the *work coefficient* $\Psi = \Delta H/U^2$. If the velocity triangles are symmetric and the flow angle at the exit of each blade and vane is independent of the incidence angle and equal to the exit metal angle, these two quantities are related linearly:

$$\Psi = 1 - \phi(\tan \alpha, + \tan \beta) \quad (1.2-5)$$

Symmetrical triangles : $\alpha_1 = \beta_2$

$$\beta_1 = \alpha_2$$

Flow follows blade exit angle: $\alpha_1 = \alpha_3 = \text{const.}$

$$\beta_2 = \text{const.}$$

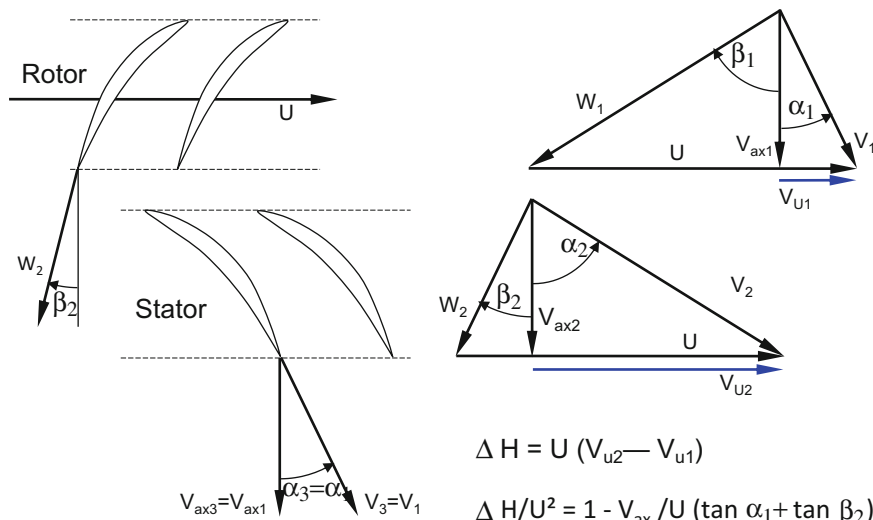


Fig. 1.2-1 Velocity triangle analysis

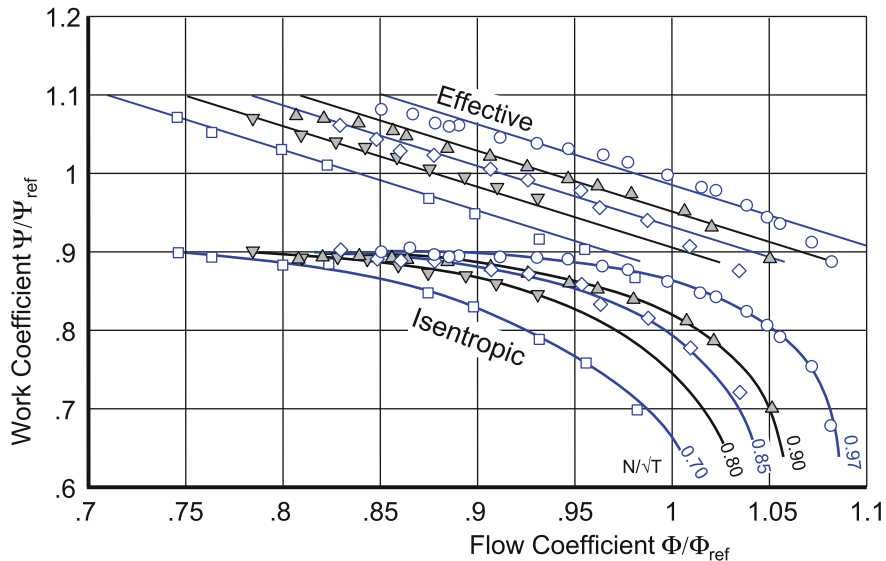


Fig. 1.2-2 The effects of work and flow coefficient in the measured map of a three stage axial compressor [4]

In a real compressor map the correlation between the effective work coefficient and the flow coefficient is essentially linear only in the low flow region, as can be seen from Fig. 1.2-2. We distinguish between the effective or actual Ψ , associated with the work input, and the ideal or isentropic Ψ_{is} , associated with the corresponding pressure ratio. The difference between Ψ and Ψ_{is} is caused by the losses, which are lowest in the middle of the flow coefficient range (near to the design conditions) and increase towards both ends, i.e. surge and choke respectively.

Since the spool speed does not appear in the $\Psi - \Phi$ correlation above one might expect all speed lines plotted as functions of Ψ and Φ to agree. However, this is usually not the case, as we can see from the example in Fig. 1.2-2.

There are two regions in a compressor map where the $\Psi - \Phi$ correlation is neither very meaningful nor very helpful and they are where speeds are either very low or very high (supersonic). We discuss this further in the next two sections.

1.2.1.2 The Zero-Speed Line

At very low spool speeds the $\Psi - \Phi$ correlation becomes very sensitive to changes for numerical reasons. If the spool speed is zero, Ψ is undefined (because work input is zero) and Φ is infinite—so the correlation cannot be used. However, the basic shape of the zero-speed line may be derived from simple considerations.

A non-rotating compressor is nothing other than a pipe with a complex internal geometry that creates pressure losses! Imagine a test with constant inlet pressure P_1

and steadily decreasing downstream exit pressure P_2 . As long as the resulting flow velocity through the compressor is not too big, the pressure loss is proportional to the square of the compressor inlet velocity:

$$P_1 - P_2 = k \frac{\rho}{2} V_{ax}^2 \quad (1.2-6)$$

Conversion to compressor map coordinates yields:

$$\frac{P_2}{P_1} = 1 - k \frac{\gamma * M_{ax}^2}{2 * \left(1 + \frac{\gamma-1}{2} M_{ax}^2\right)^{\frac{\gamma}{\gamma-1}}} \quad (1.2-7)$$

This formula describes a line passing through the point {pressure ratio = 1; mass flow = zero}. With moderate Mach numbers, while k is truly constant, the shape of the zero-speed line resembles a parabola. We obtain the maximum inlet Mach number when sonic velocity is reached in the exit vanes, where the flow area is small and the pressure is relatively low due to the losses created by the upstream stages. Lowering P_2 further has no effect on the flow field, the inlet Mach number remains constant and that means that speed line zero becomes vertical.

In reality, the precise shape of the speed line zero is known only rarely. Nevertheless, even knowing it approximately can be of help when extrapolating and adapting a compressor map to low speed data. A smooth transition of the low speed line shape towards that of the zero-speed line should be made in any case.

1.2.1.3 “Supersonic” Speed Lines

Supersonic velocities can exist in the flow relative to the rotor of the first compressor stage. In such a case, the lines for higher corrected blade speed are vertical over a wide range of pressure ratios because the flow field upstream of the first rotor does not change. The map of a single stage fan shown in Fig. 1.2-3 is an example in which supersonic flow in the rotor is the reason for the speed lines being vertical in the high-speed region.

But supersonic flow fields upstream of and within the rotor passages are not the only reason for vertical speed lines in a compressor map. High pressure ratio, single stage centrifugal compressors have inherently high circumferential tip velocities and these result in high inlet Mach numbers to the diffuser. When sonic flow at the inlet to the exit vanes is reached due to low back pressure, the same flow structure appears in the vane passages as described above. Changing the backpressure affects only the position of the terminal shock in the vanes but not the flow field in the rotor. So the speed lines are vertical over a large region of the map, as can be seen in Fig. 1.2-4.

Boosters of ungeared turbofan engines, for example, operate with very low circumferential speeds and will never see supersonic flow at their entry. Figure 1.2-5 shows the predicted map of a 5-stage low pressure compressor [3] and just as in the

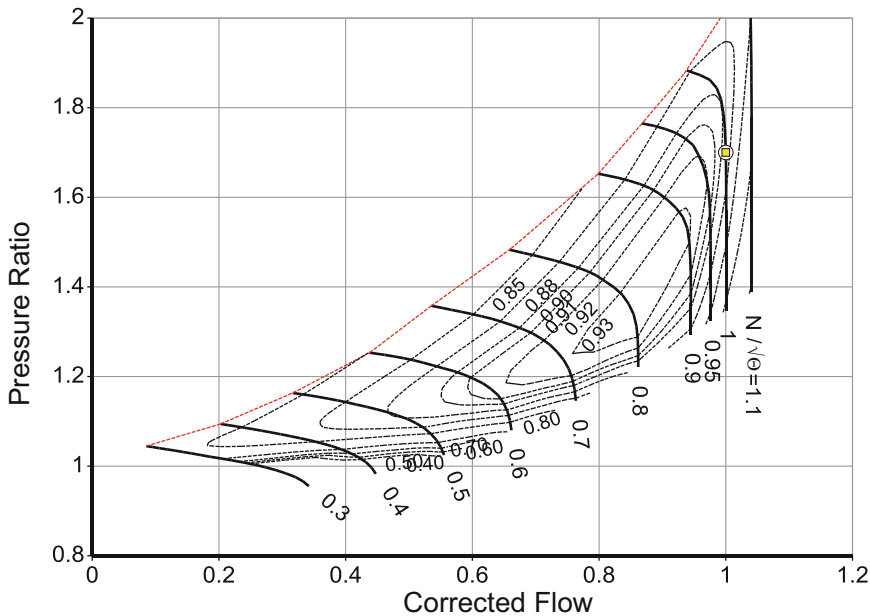


Fig. 1.2-3 Fan map with vertical speed lines (Refs. [5, 6])

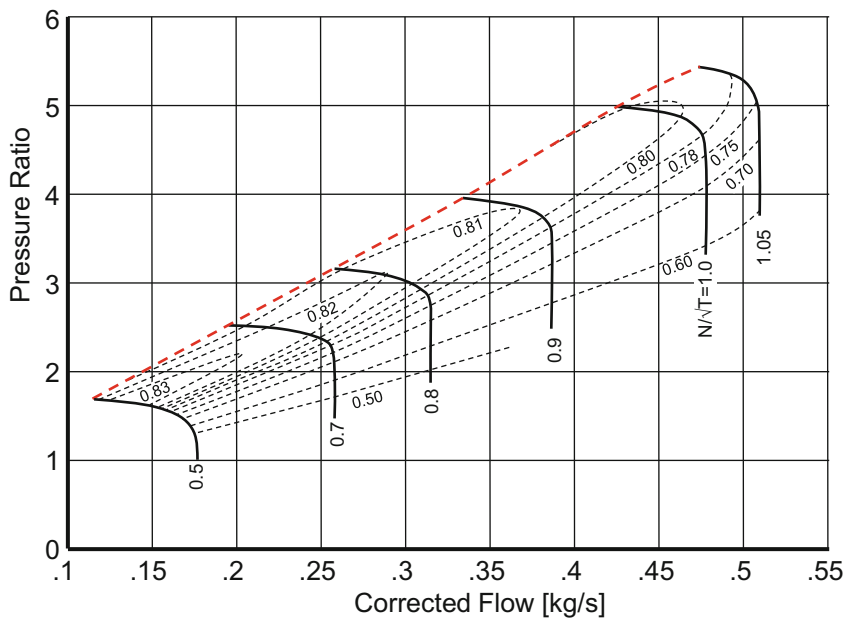


Fig. 1.2-4 Map of a high-speed centrifugal compressor [34]

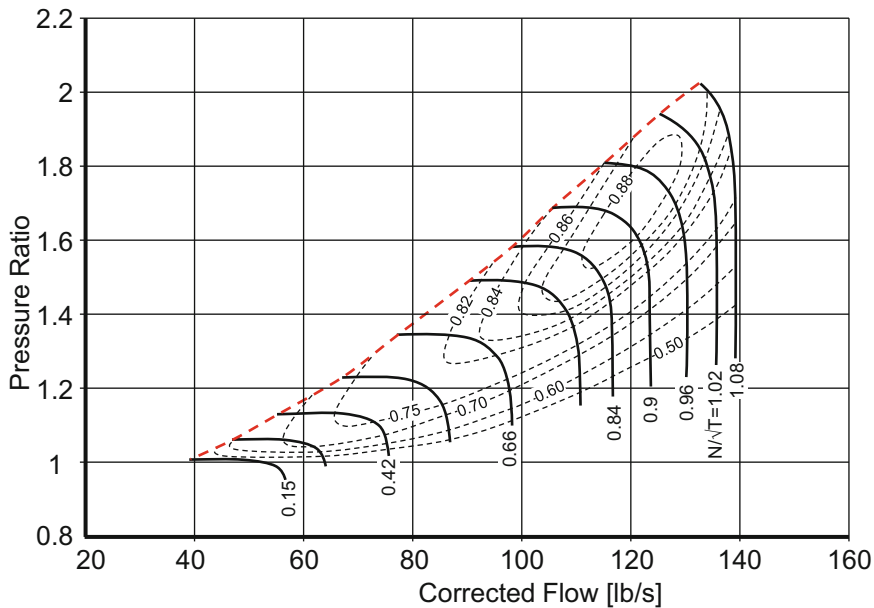


Fig. 1.2-5 Map of a 5-stage booster [3]

case of Fig. 1.2-3, the speed lines are vertical in the high-speed region. The reason for these vertical sections in this case is that sonic velocity is reached in the exit guide vanes.

1.2.1.4 Specific Work

If a compressor map contains speed lines with vertical sections, is it possible to find out whether this is due to supersonic flow in the first rotor or due to a choked blade row at the compressor exit? For a given speed, a plot of specific work against pressure ratio tells a clear story.

If specific work is a horizontal line in such a plot, we can deduce that the compressor exit is choked. This is because work is done only in the rotor(s) and if the rotor flow fields are unaffected as the backpressure is reduced below the critical value specific work remains constant and the constant flow is indicative of choked exit vanes. Figure 1.2-6 shows this effect for the booster map presented in Fig. 1.2-5.

If we return to the centrifugal compressor map presented in Fig. 1.2-4 and plot specific work against pressure ratio in Fig. 1.2-7, we see the same behavior over a much wider speed range, as the diffuser vanes choke.

If the specific work variation is not a horizontal line when plotted against pressure ratio (as in Fig. 1.2-8) even though the speed line is vertical in the conventional map, then it can be said that a supersonic flow field must exist in the first

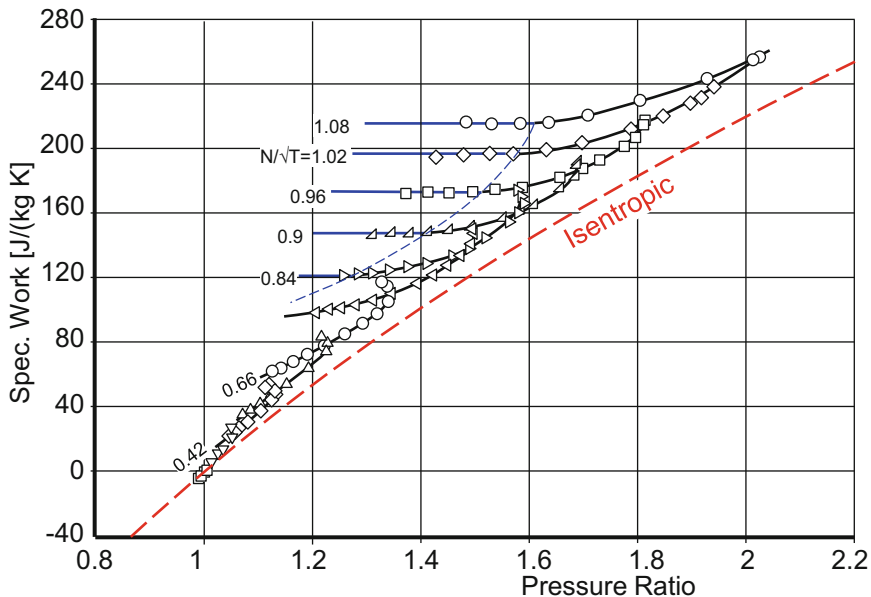


Fig. 1.2-6 Specific work for the 5-stage booster [3]

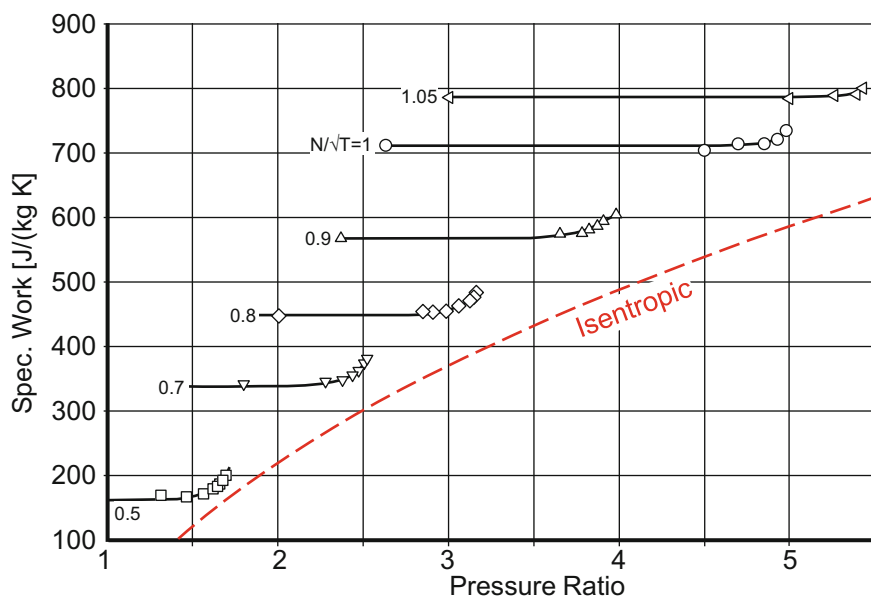


Fig. 1.2-7 Specific work for the centrifugal compressor [34]

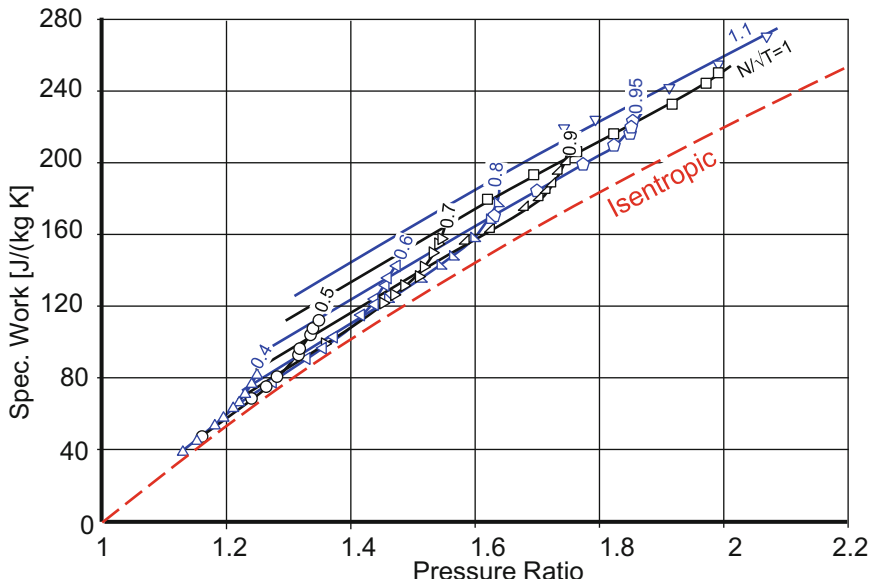


Fig. 1.2-8 Specific work for the single stage fan [3]

rotor. This can be attributed to different terminal shock positions in the rotor causing changes in relative rotor exit velocity leading to changes in the circumferential component of the absolute velocity at rotor exit (because both U and V_{ax} are constant). Consequently, specific work depends on pressure ratio.

1.2.1.5 Torque

Let us have a second look at Fig. 1.2-2 in conjunction with Fig. 1.2-1. In the low to medium flow range of a speed line, where the flow is subsonic, the $\Psi_{eff} - \Phi$ correlation is essentially a straight line. At a given spool speed, Ψ_{eff} is proportional to specific work. For low Mach numbers (incompressible flow) the axial velocity V_{ax} is proportional to corrected flow. Therefore Φ is proportional to corrected flow and specific work, and when plotted as a function of flow, is a straight line in that region of the map.

In case of high pressure ratio centrifugal compressors, the lines of specific work against flow are straight over the complete flow range. This can be seen in Fig. 1.2-9, which is just another version of the map in Fig. 1.2-4.

Instead of looking at corrected specific work $\Delta H/T_1$, we can consider corrected torque $Trq/(W\sqrt{T_1})$. These two properties are connected because compressor shaft power can be expressed in two ways, namely:

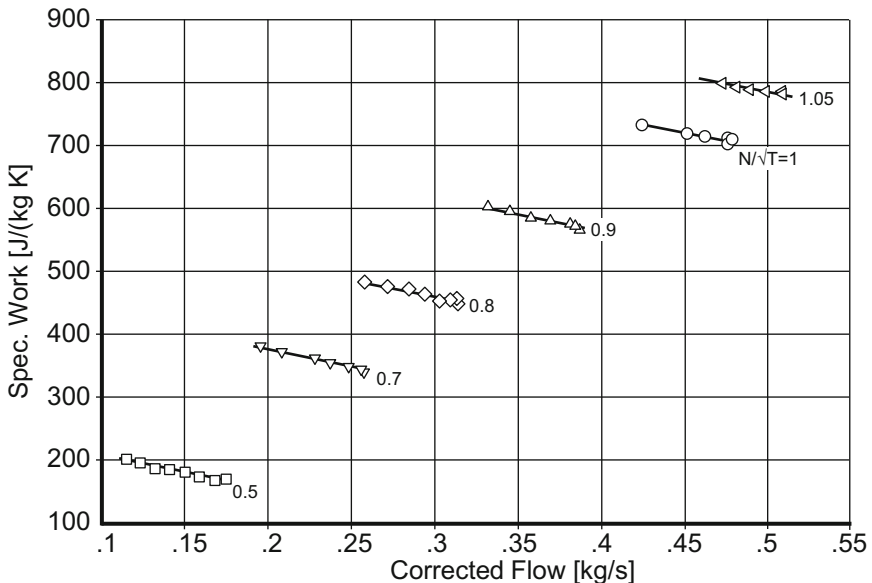


Fig. 1.2-9 Specific work for the centrifugal compressor [34]

$$PW = kNTrq = W_1 \Delta H \quad (1.2-8)$$

Rewriting the second relationship gives us

$$\frac{Trq}{W_1 \sqrt{T_1}} = \frac{\frac{\Delta H}{T_1}}{k \frac{N}{\sqrt{T_1}}} \quad (1.2-9)$$

For the single stage fan example, Fig. 1.2-10 shows that the torque lines as functions of corrected flow are linear over a significant part of the map, in the region left of the blue dashed line.

1.2.2 Compressor Map Coordinates

In off-design cycle calculations we need to evaluate the compressor map numerically. This is easy and straightforward in the middle of the map shown in Fig. 1.2-11. Corrected speed and mass flow define point A and so does the combination of corrected speed and pressure ratio. However, the use of co-ordinates corrected speed and corrected flow is ambiguous in regions where the speed lines are vertical, such as where the blue arrow is shown pointing upwards. Is the pressure ratio for that flow to be evaluated at C_1 or at C_2 ?

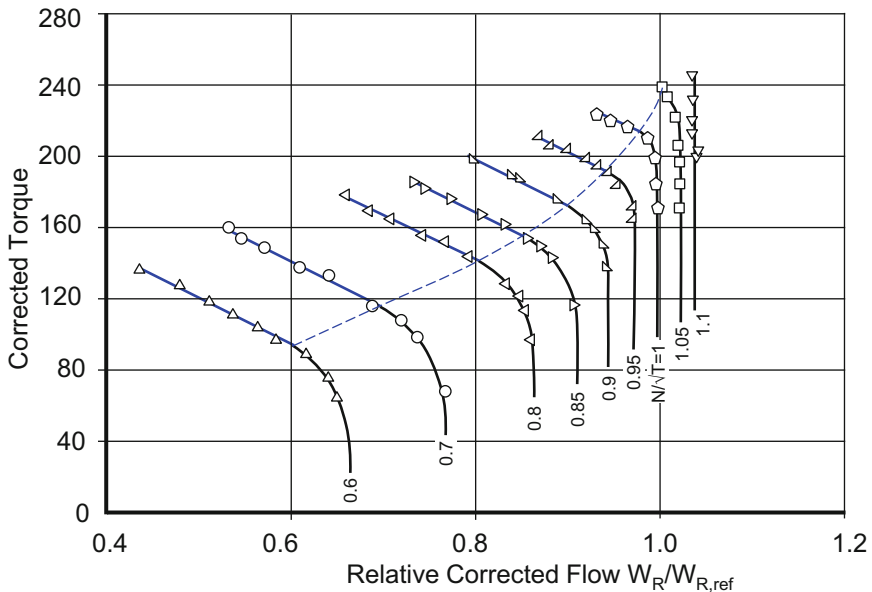


Fig. 1.2-10 Corrected torque for the single stage fan (Refs. [4, 5])

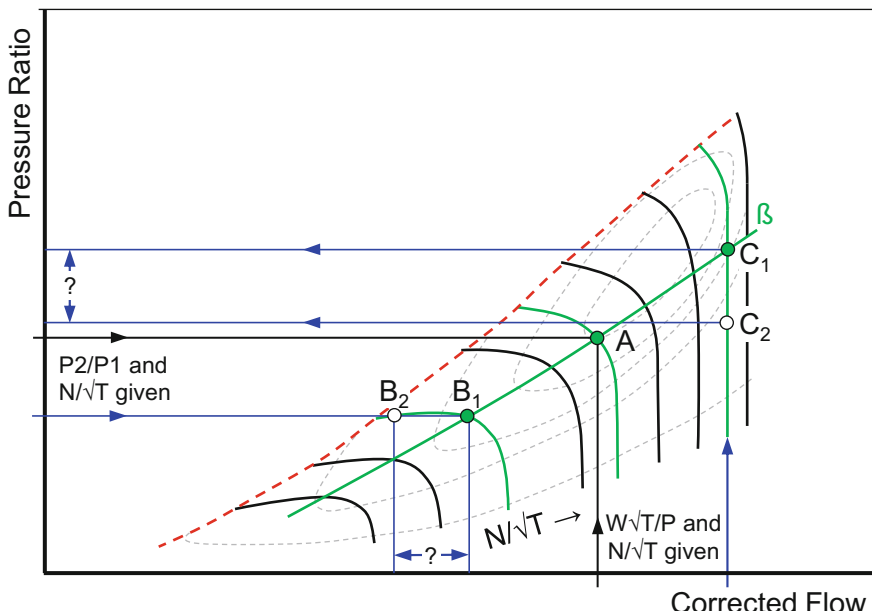


Fig. 1.2-11 The compressor map reading problem

Nor can we read the map from co-ordinates *corrected speed* and *pressure ratio* because in the low flow region the speed lines tend to roll over so that two solutions exist for corrected mass flow at B_1 and B_2 .

We solve the map-reading problems and eliminate the uncertainty by introducing auxiliary coordinates, the so-called β -lines that have unique crossings with each of the speed lines. Now we can evaluate the maps unambiguously for any given pair of *corrected speed* and β .

The shape of these new auxiliary coordinates is arbitrary; linear or parabolic shapes are in use as well as lines parallel to the so-called backbone of the map—a line which connects the peak efficiency values of each speed line (Fig. 1.2-12).

Smooth C—a program which prepares compressor maps for the use with GasTurb and other performance programs—produces maps with equally spaced parabolic β -lines which do not necessarily represent any real physical value. The lower boundary of the map is the $\beta = 0$ line; the upper boundary is the $\beta = 1$ line. In between these two boundaries there are typically 20–30 equally-distributed parabolas with β values between zero and unity.

Parabolic β -lines enable any type of compressor map to be covered completely. In case of subsonic compressors without variable geometry, parabolic β -lines can be selected in such a way that they have the shape of constant $\Psi = \Delta H/U^2$ lines in the region with unchoked exit guide vanes. In the region with choked exit guide vanes, the β -lines can be equally spaced auxiliary coordinates and again do not represent any real physical value.

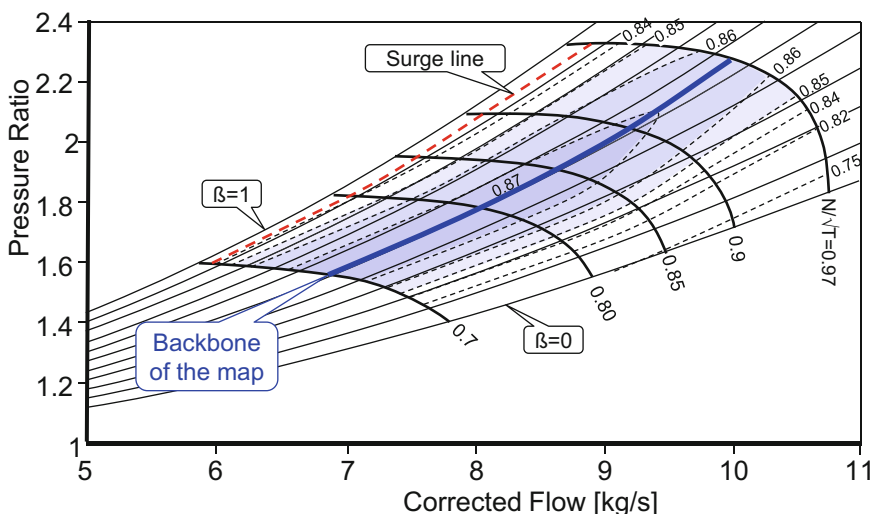


Fig. 1.2-12 β -lines in the compressor map from Ref. [4]

1.2.2.1 Efficiency Correlations

For subsonic inlet Mach numbers, the variation of efficiency for compressor blades and vanes depends on the Mach number itself and on the incidence. Figure 1.2-13 shows that the useful incidence range decreases rapidly as the inlet Mach number increases.

Consequently, if the general level of Mach number in a compressor is high, the efficiency islands in the corresponding map are narrower than in those where Mach numbers are more moderate. This can be seen, for example, in a comparison of Fig. 1.2-14 with Fig. 1.2-15. Both maps are from compressors with approximately the same design pressure ratio, but their Mach number levels differ significantly. The map in Fig. 1.2-14 is for a single-stage fan, where the stage loading (and Mach numbers) is high, while that of Fig. 1.2-15 is for a three-stage, compressor, where the stage loading is more modest.

Now let's look at how compressor efficiency varies along speed lines, but rather than examining a conventional map with co-ordinates of corrected flow and pressure ratio and struggling with efficiency directly, we introduce two not so common expressions for the loss.

The first expression avoids the numerical problems which exist with efficiency when pressure ratio is very close to unity—because efficiency is the ratio of $H_{1-2}/H_{1-2,is}$ and $H_{1-2,is}$ is zero when pressure ratio is 1. If we think of the losses as a simple duct pressure loss, we encounter no numerical difficulty. Figure 1.2-16 contains compression loss expressed as $1-P_2/P_{2is}$ and plotted as a function of β for a series of speed lines. This is yet another form of the single-stage fan map from Ref. [4] but it ensures that the efficiency of the process is captured for any pressure ratio and any spool speed.

The second expression considers how the losses increase to both sides of the point with the highest efficiency on the speed line. Figure 1.2-17 shows $|\Psi - \Psi_{\min \text{ loss}}|$ as function of $\Phi - \Phi_{\min \text{ loss}}$. The location of the *min loss* point is the peak efficiency point on each speed line, i.e. on the *backbone* of the map.

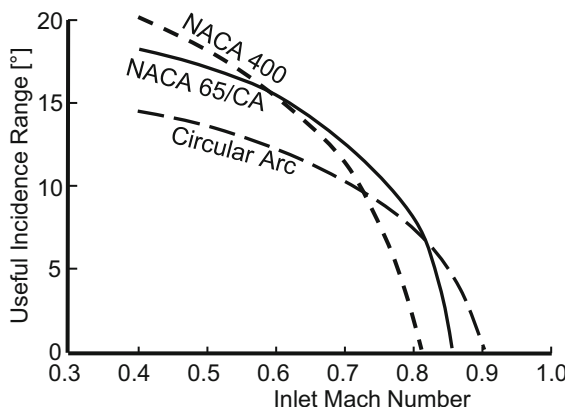


Fig. 1.2-13 Incidence range of standard series airfoils [35]

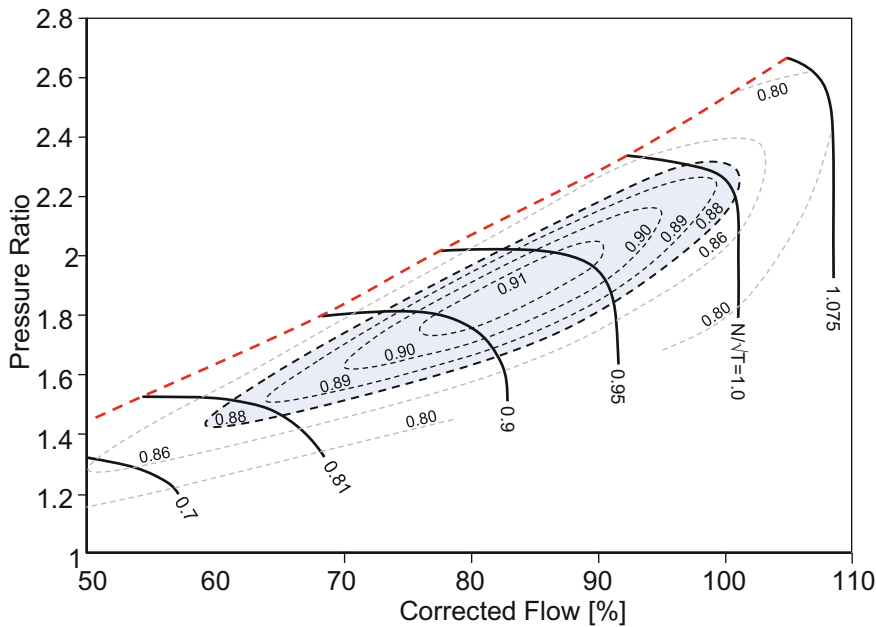


Fig. 1.2-14 Single stage fan map [36]

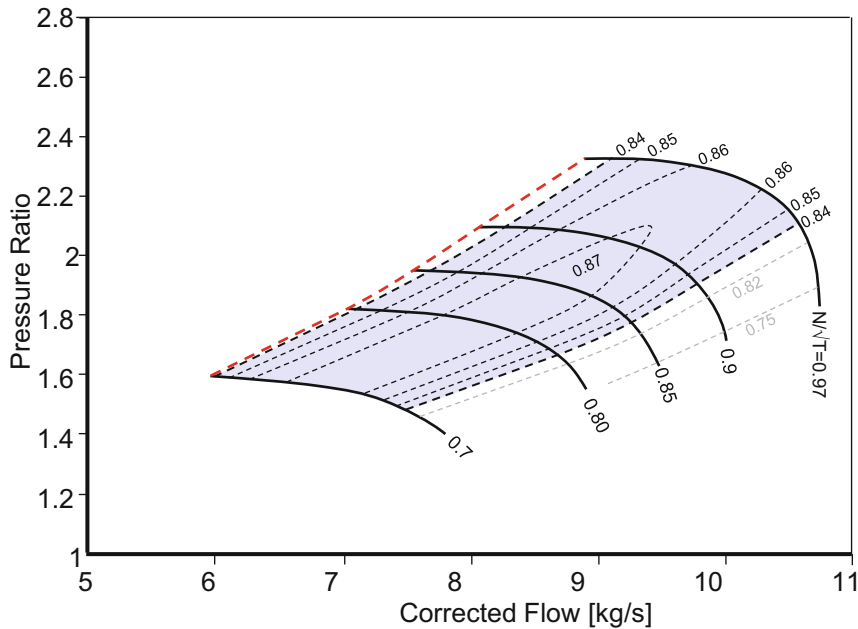


Fig. 1.2-15 3-stage compressor map [4]

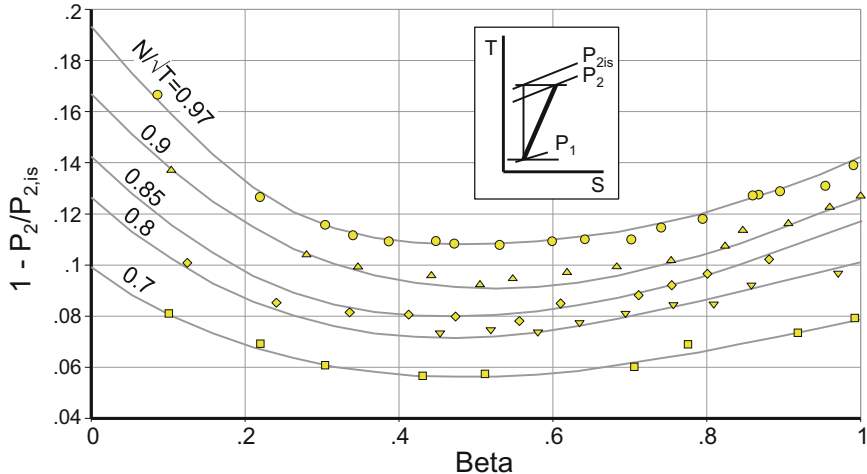


Fig. 1.2-16 Compression pressure loss in the map from Ref. [4]

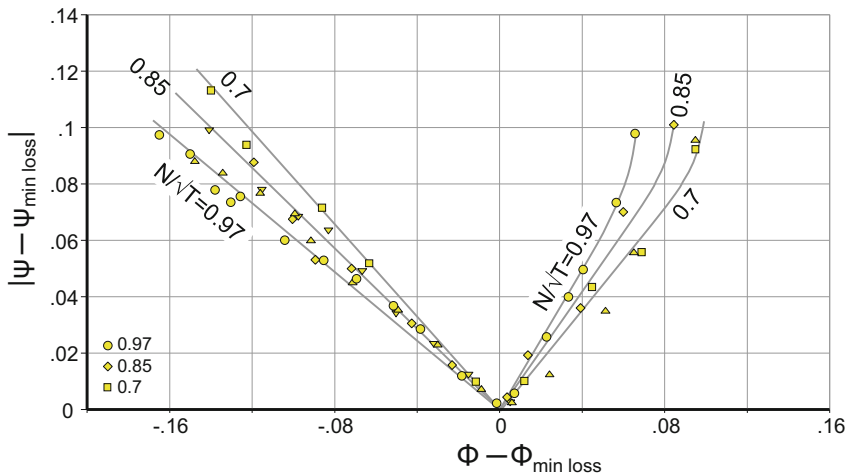


Fig. 1.2-17 Losses expressed as ψ difference to the backbone ψ of the map

We observe that the speed lines are essentially linear functions of work coefficient Ψ over flow coefficient Φ in the left part of the figure. In the right part they are linear initially but tend to become vertical at higher Φ values.

This loss description works fine in the high speed region of the map. In the low speed region both work coefficient and flow coefficient become increasingly sensitive to scatter in the data. Of course, neither Ψ nor Φ are computable for the speed line zero.

1.2.2.2 Work and Flow Correlations with Spool Speed

In the previous sections, we have discussed the variations of pressure ratio, flow rate, specific work, torque and efficiency at constant corrected speeds. Now we will have a look at correlations of those parameters between different corrected spool speeds. The β -lines we have just introduced are an ideal tool for showing trends in a compressor map. In the examples we show, the β -lines correspond approximately to lines of constant aerodynamic loading, $\Delta H/U^2$.

The β -line grid for the example in Fig. 1.2-12 enables us to show how the various map parameters change with rotational speed. Along the backbone of the map (the peak efficiency line) the effective work coefficient Ψ is essentially constant; the velocity triangles are very similar, which implies that the incidences to the blade and vanes are low.

If we re-plot the map as shown in Fig. 1.2-18, we see that specific work is a linear function of speed squared for all β -lines, which indicates that $\Psi = \Delta H/N^2$ is constant along all β -lines. The uppermost β line passes through the origin; the lowest one crosses the zero specific work line at some positive speed. This is because in a small region of the map, at very low speed, the compressor can operate as a turbine and deliver work instead of consuming it.

Figure 1.2-19 shows corrected flow as a function of corrected speed for the single stage fan from Refs. [5, 6]. For low to medium speed values, flow increases linearly with speed along any β -line. In the top right, the flow increase with speed diminishes which indicates that the axial velocity approaches Mach 1. Since the rightmost speed line in Fig. 1.2-3 is vertical, all β -lines converge for this speed in Fig. 1.2-19.

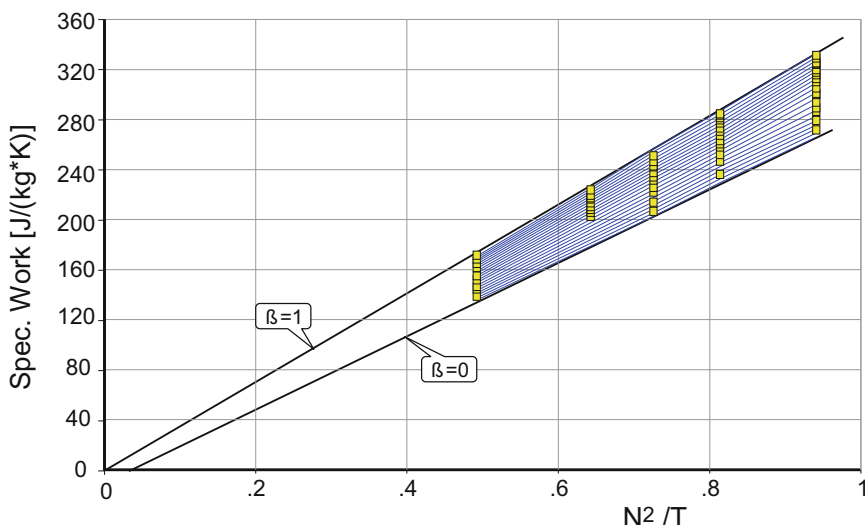


Fig. 1.2-18 Specific work is a linear function of speed² in the map from Ref. [4]

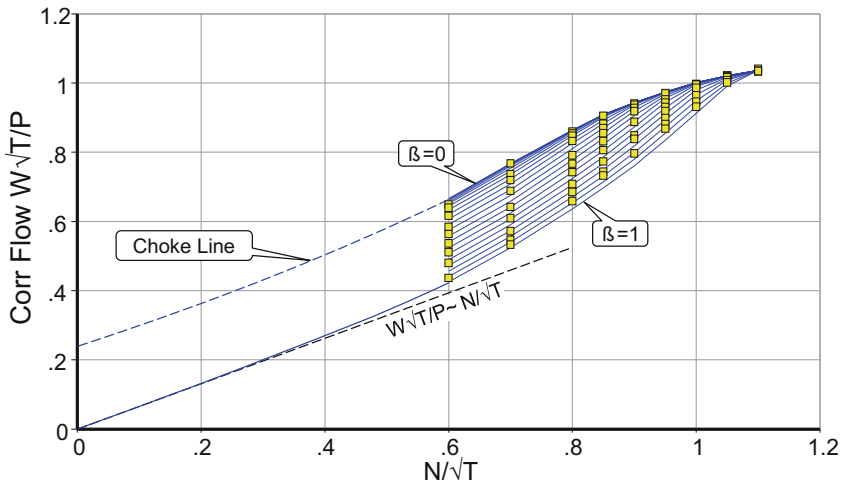


Fig. 1.2-19 Flow—speed correlation for $\beta = \text{constant}$ in the map from Ref. [5, 6]

1.2.3 Compressors with Variable Guide Vanes

All compressors with fixed stators have linear $\Delta H^2 - N^2$ correlations, similar to those of Fig. 1.2-18. The $W-N$ correlation shown in Fig. 1.2-19 is also typical but for subsonic compressors, the top right part—where the β -lines level out—is missing. In any case, the β -lines are smooth when plotted against corrected speed.

Compressors with high design pressure ratio often need variable guide vanes to ensure acceptable operation at part load. This is because the increase in density of the working fluid from inlet to exit is much less at low corrected speed than at the design value. The exit annulus area is then too small to pass the resulting flow volume and so the flow is reduced. Let's look at the process more closely in Fig. 1.2-20, where inlet velocity triangles for R1 and R10 are drawn. For the moment, we assume that there are no variable inlet guide vanes.

At R1 inlet, comparison of the grey triangle (design speed) with the black triangle (reduced speed) shows a reduction in the axial velocity of the flow. Completion of the triangles with the relative velocities shows a rotation which produces a positive incidence change for R1. Let us also examine the velocity triangles at the inlet to R10. We see that the axial flow velocity at reduced blade speed is now only slightly less than it was at design speed—the effect of reduced flow having been offset by the effects of reduced pressure ratio. The flow still leaves S9 at its exit metal angle and the magnitude of the absolute velocity is determined by the axial velocity (continuity). Construction of the relative velocity shows a reduction in the relative swirl and a reduction in R10 incidence. In general, a speed reduction tends to cause the first stage to stall because of incidence and the last stage to choke because of high volumetric flow.

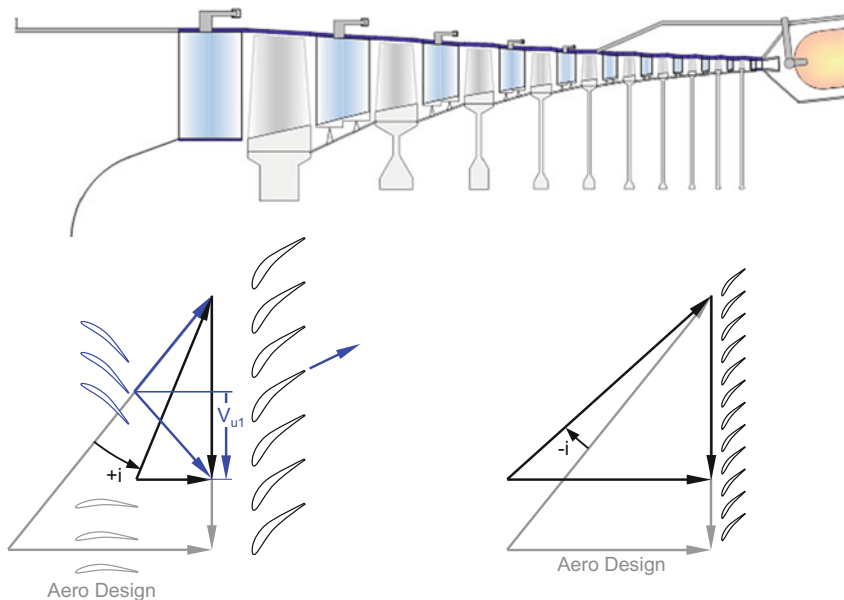


Fig. 1.2-20 The off-design problem of a multistage compressor

Introducing variable inlet guide vanes resolves the stall problem of the first stage by controlling the incidence of the first rotor. At the aero design point the IGV's are in fully open position (the gray vanes in Fig. 1.2-20) with axial exit flow. Closing the IGV's (moving to the blue position) restores the aero design incidence of R1 (blue triangle) and reduces the work done by the first stage because we increase V_{U2} and $\Delta H = U(V_{U2} - V_{U1})$; bear in mind that without an IGV, V_{U1} is always zero.

Re-staggering the variable guide vanes affects the whole map, so a series of IGV setting angles implies a series of maps! Closing the IGV's makes the map shrink: the speed lines move towards lower pressure ratios and lower mass flows, as shown in Fig. 1.2-21. The position of the map backbone is not affected very much; the peak efficiency suffers only when corrected speed is high.

As well as IGV's, compressors with high design pressure ratios often need additional variable stators. During compressor development, the settings (i.e. stagger angles) of each row of VGVs are optimized for efficiency and surge margin at each corrected speed. The result is a VGV schedule, similar to the one shown in Fig. 1.2-22, for example. At a given corrected spool speed all the VGV's are at specific stagger angle settings.

Figure 1.2-23 shows the mechanics of a typical VGV control. The single hydraulic actuator not only moves the IGV unison ring but also the bell crank that connects it with all the other unison rings.

The map of a compressor with VGV's combines corrected speed lines from different VGV positions to form a single map. The VGV positions are controlled with a single actuator as a function of corrected speed.

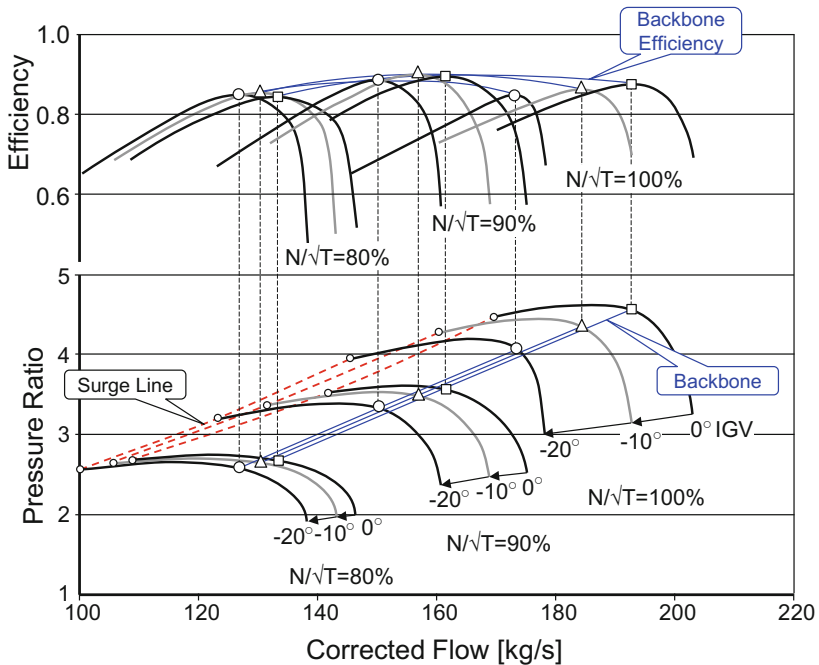


Fig. 1.2-21 Calculated effect of the IGV position on the map of a 10-stage compressor [37]

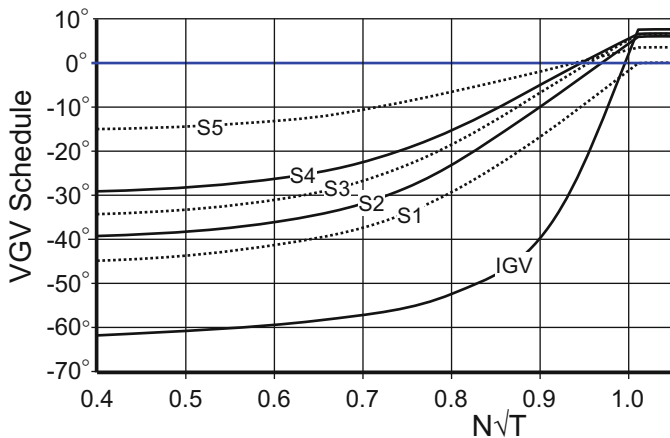


Fig. 1.2-22 Variable guide vane schedule for a 10-stage compressor (adapted from Ref. [38])

Such a map looks like any other map at first sight, see Fig. 1.2-24. However, if we plot specific work against the square of corrected speed, it becomes obvious that this is a map with an embedded VGV schedule. This is indicated in Fig. 1.2-25 by how all the β -lines sag relative to the linear relationship $\Delta H \sim (N/\sqrt{T})^2$ in

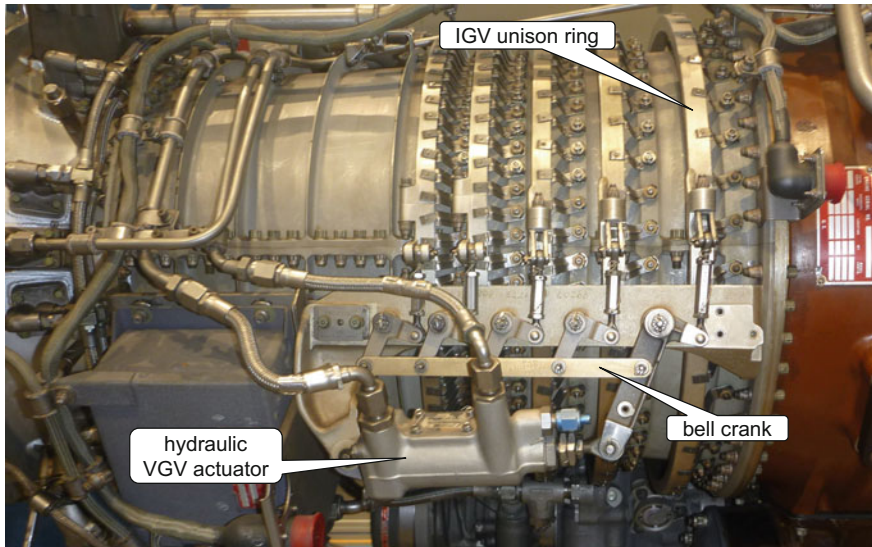


Fig. 1.2-23 VGV positioning mechanism

Fig. 1.2-25. At a given corrected speed, the specific work is lower than that for a fixed geometry compressor while the VGV's are not fully open. In Fig. 1.2-25 at the speed 1.015, a sharp bend occurs in all the β -lines and this is a consequence of the kink in the VGV schedule of Fig. 1.2-22 at the same speed. The kink is also visible in plots of corrected flow versus corrected speed.

What happens if we deviate from the VGV schedule embedded in the map? Such an event might be caused by a malfunction of the engine control system or it might be an intended action with the aim of improving surge margin during a transient.

Small deviations from the nominal VGV schedule result primarily in a proportional change in corrected mass flow. But bigger deviations also affect compressor efficiency, as shown for example in Fig. 1.2-26.

Variable guide vanes are an important control element for single spool gas turbines when they are used for power generation. These machines run at a constant mechanical spool speed N dictated by the electrical generator. With variable guide vanes, it is possible to control the mass flow and thus the power which the gas turbine delivers at a given burner exit temperature.

For the simulation of a single spool gas turbine in a power station we use a baseline compressor map which is valid for a reference guide vane position. Power is controlled by varying the mass flow, which is effected by the VGV's. Mass flow is directly proportional to their stagger angle, as shown in the upper part of Fig. 1.2-26. Compressor efficiency remains nearly constant around the reference VGV position within a range of $\pm 20^\circ$.

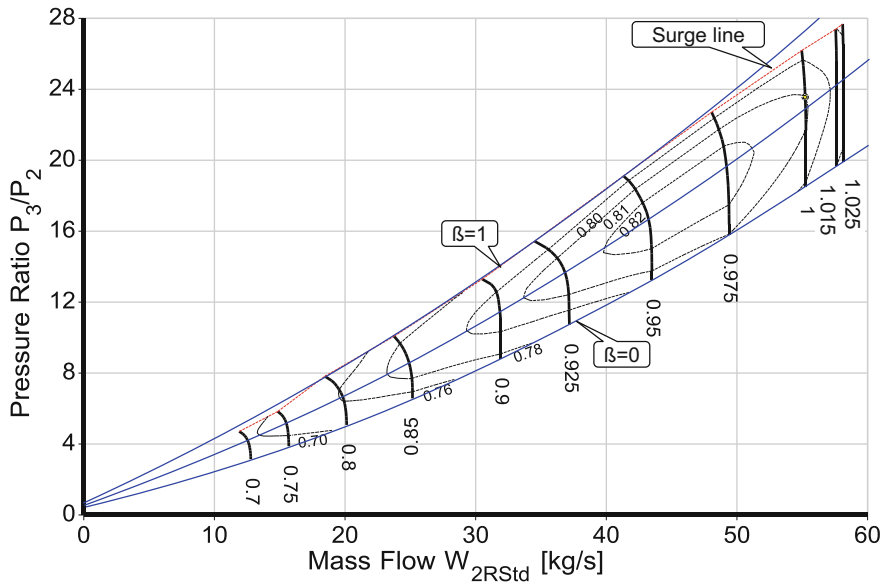


Fig. 1.2-24 Map of a compressor with scheduled variable guide vanes [38]

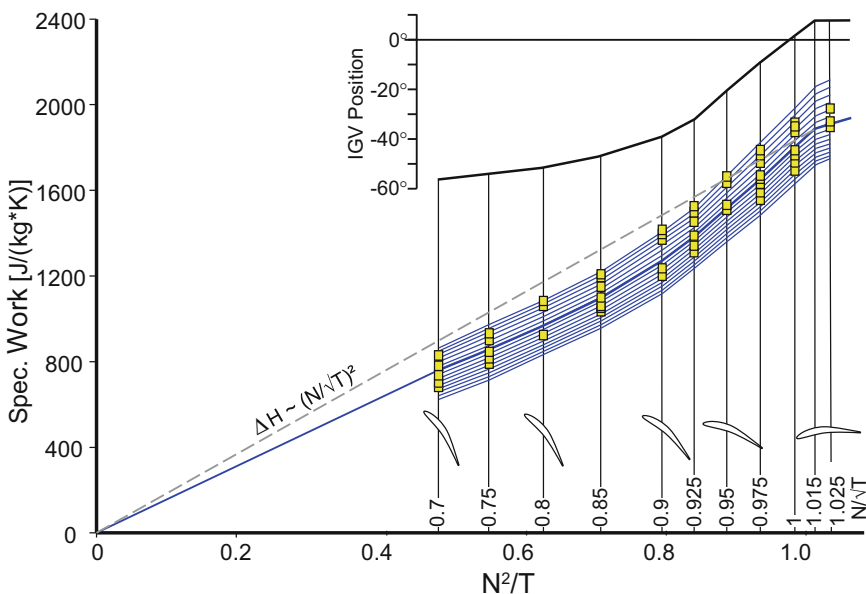


Fig. 1.2-25 Specific work of the Ref. [38] compressor

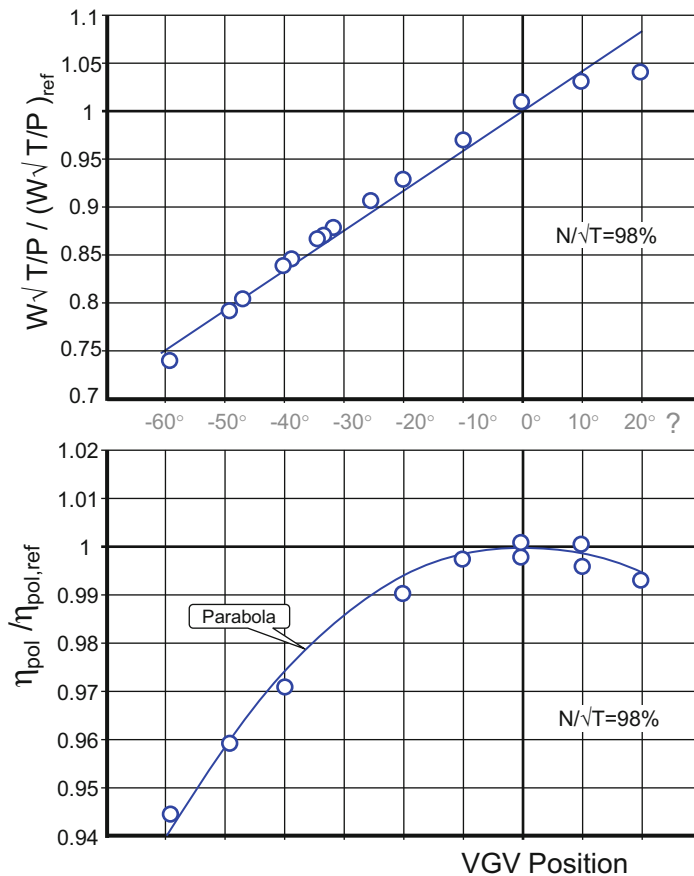


Fig. 1.2-26 Mass flow control with VGV in single spool gas turbines (adapted from Ref. [39]). The VGV scale is a guess by the author

1.2.4 Fan Maps

An ordinary compressor map consists of tables of corrected mass flow, pressure ratio and efficiency as functions of corrected speed and the auxiliary coordinate β . Such a map yields the average compressor exit pressure ratio and efficiency. However, in an accurate model we must differentiate between exit conditions from the core and bypass duct. This is especially important for a single stage fan in a high bypass ratio engine.

The bypass ratio varies significantly within the flight envelope from idle to full thrust. The position of the dividing stream line varies, as indicated in Fig. 1.2-27, even though the average fan performance remains the same. Since both pressure ratio and

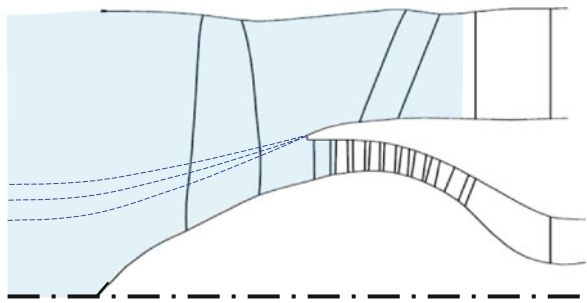


Fig. 1.2-27 Bypass ratio varies during off-design

efficiency vary with fan radius, for the same point in the average map we get different core and bypass pressure ratios and efficiencies, when the bypass ratio changes.

So why does the efficiency vary with radius? At high fan speeds, the relative inlet velocities near the blade tip are usually supersonic. So, the supersonic flow field of the bypass stream is very different from the subsonic flow field of the core stream. The rotor blade profile of the outer part is designed for supersonic flow while the profile near the core stream region is optimized for subsonic flow.

The simplest way to account for differences in pressure ratio and efficiency between the core and the bypass streams is as follows. Interpret map pressure ratio and efficiency values initially as those in the bypass stream. (P_{13}/P_2 and η_{2-13}). Then derive the core stream values, P_{21}/P_2 and η_{2-21} from the bypass map values by applying constant factors:

$$\frac{P_{21}}{P_2} = 1 + f_{P/P} \left(\frac{P_{13}}{P_2} - 1 \right) \quad \text{and} \quad \eta_{2-21} = f_\eta \cdot \eta_{2-13} \quad (1.2-10)$$

Another simple model considers the fan root as part of the booster and in this case we assign only the outer stream values to the fan map tables—the bypass pressure ratio P_{13}/P_2 and the bypass efficiency η_{2-13} . The inner fan performance is incorporated into the booster map. Both these simple methodologies ignore the effect of bypass ratio variations.

A more accurate account of fan performance consists of the above mentioned bypass map tables with P_{13}/P_2 and η_{2-13} complemented by two more tables which contain P_{21}/P_2 and η_{2-21} . Generating such a so-called “split map” is not trivial because the bypass ratio in the engine is not the same for all operating conditions. Therefore, a pre-calculated representative bypass ratio is assigned to each point in the fan map. Two independent throttles downstream of the test vehicle are required for achieving this bypass ratio on a compressor rig.

An even more rigorous (and potentially expensive) fan performance model is recommended in Ref. [7]. Multiple maps at intervals of 0.5 bypass ratio are used to quantify the efficiency and pressure ratio in the core and bypass stream for any operating condition in the engine.

We found neither split maps nor fan maps with bypass ratio as an additional parameter in the open literature; these map types cannot be used outside industry with access to measured rig data. Therefore, in academic and research communities and for preliminary design studies an approach is needed which characterizes the effect of changing bypass ratio on fan performance in a simple manner. In the following we describe a simulation method that addresses the variable bypass ratio effect but uses only one additional map table, the main fan dimensions, and the spool speed.

1.2.4.1 The Flow Field in a Single Stage Fan

This special fan performance model is based on the characteristics of the flow field. As an example, Fig. 1.2-28 shows the Mach numbers in the blade passages of a highly three-dimensional modern fan operating at an average pressure ratio of 1.382. It illustrates very large span-wise changes in the rotor blade profiles and relative Mach number contours at tip, mid-span and hub sections. While the flow is transonic with visible shock structures in the tip region, the flow in the hub region is completely subsonic. Additional examples can be found in Ref. [8].

1.2.4.1.1 Core Section

The flow in the fan hub region is always subsonic due to the low hub/tip radius ratio, even though the relative Mach numbers sometimes exceed 1.5 in the tip region. Therefore, we can use subsonic (incompressible) compressor theory to model the core flow of a high bypass fan.

An off-design simulation begins with a cycle design calculation which yields some important engine geometry details. In the case of a single stage fan of known hub/tip radius ratio, fan face axial Mach number and blade tip speed we can calculate a representative rotor blade trailing edge angle in the core stream. Here is how we do that:

We calculate the specific work ΔH_{core} of the core stream from the design point efficiency $\eta_{2-21,\text{ds}}$ and the core stream pressure ratio $(P_{21}/P_2)_{\text{ds}}$. The axial flow

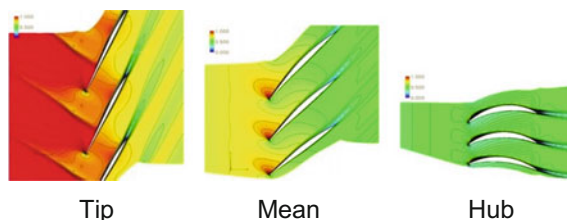


Fig. 1.2-28 Relative Mach number contours [40]

velocity at the fan face V_{ax} follows from the given corrected mass flow and assumptions about fan tip speed, fan face Mach number and hub/tip radius ratio. The mean radius of the core stream r_{core} results from the fan radii and bypass ratio; The circumferential speed U_{core} equals $U_{Tip} * r_{core}/r_{tip}$.

With these data we can determine the flow coefficient $\Phi_{core} = V_{ax}/U_{core}$ and the work coefficient $\Psi_{core} = \Delta H_{core}/U_{core}^2$. Analysis of the rotor velocity diagram in Fig. 1.2-29 yields an equation for the rotor blade exit angle $\beta_{2,core}$:

$$\beta_{2,core} = \tan^{-1} \left(\frac{1 - \Psi_{core}}{\Phi_{core}} \right) \quad (1.2-11)$$

During off-design simulations we postulate that the flow always follows the blade exit metal angle $\beta_{2,core}$. The flow coefficient $\Phi_{core} = V_{ax}/U_{core}$ is easily found and allows the work coefficient for the core stream to be calculated:

$$\Psi_{core} = 1 - \Phi_{core} \tan \beta_{2,core} \quad (1.2-12)$$

Specific work done in the core stream is $\Delta H_{core} = \Psi_{core} U_{core}^2$, so if we know the core stream efficiency η_{2-21} , then we can calculate the core stream pressure ratio P_{21}/P_2 .

At the cycle design point we know the efficiency in the core stream, but we do not know how η_{2-21} varies with fan operating conditions. But if we have neither a measured value nor a calculated value for core stream efficiency, we can at least get a reasonable estimate. Let us go back to the basics of compressor cascade flow to understand what happens in the subsonic fan hub region during off-design. Figure 1.2-30 shows that compressor cascade loss coefficients remain constant while the inlet flow is subsonic, say below a Mach number of 0.75. These cascade losses

Flow follows blade exit angle: $\beta_2 = \text{const.}$

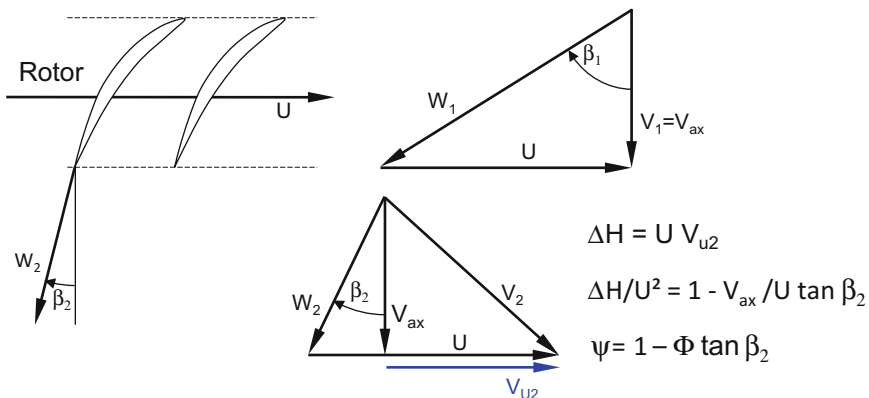


Fig. 1.2-29 Core stream velocity triangles

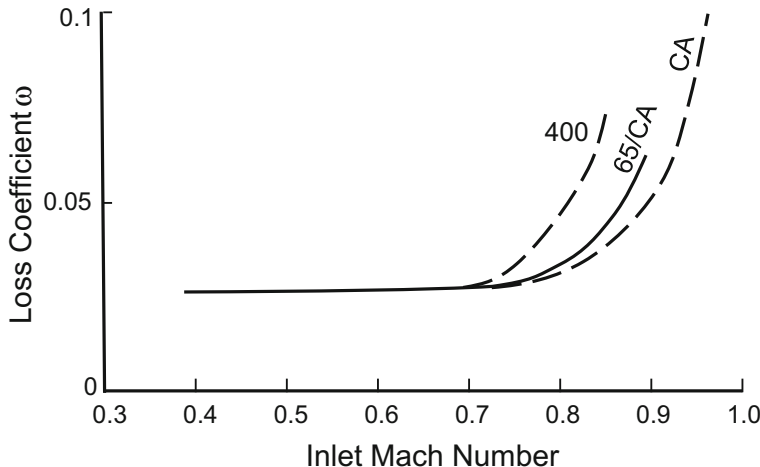


Fig. 1.2-30 Cascade loss coefficient as a function of Mach number for three blade profile types [41]

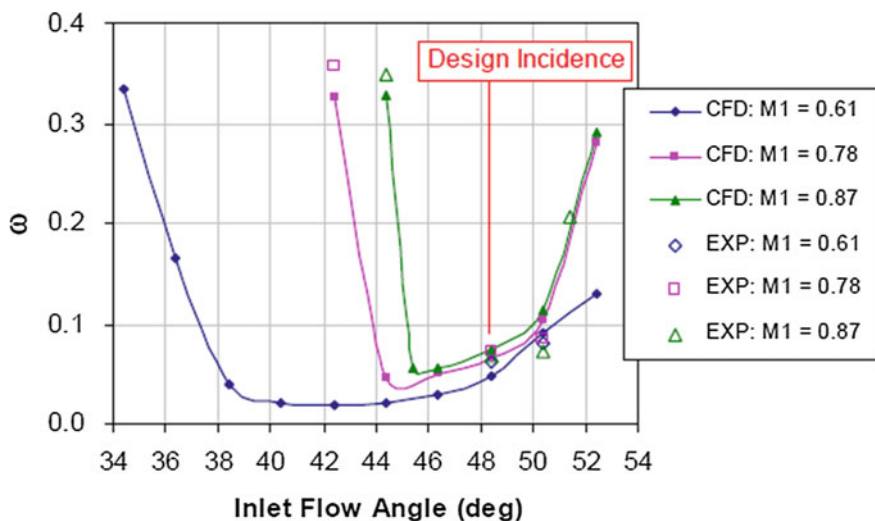


Fig. 1.2-31 Loss—incidence characteristic [42]

depend not only on inlet Mach number but also on incidence and Fig. 1.2-31 includes that. Note that the lower the Mach number, the wider the range of low loss incidence.

For a single stage fan rotor with axial inlet flow, the swirl angle and hence the incidence is given by the velocity ratio V_{ax}/U , i.e. the flow coefficient Φ . Flow coefficient and work coefficient in the core stream region are connected through Eq. (1.2-12) because $\beta_{2,\text{core}}$ is constant during off-design (It follows the blade exit

metal angle.). That means that in the fan map—complemented with lines of constant $\Psi = \Delta H/U^2$ —a line of constant power coefficient Ψ_{core} is simultaneously a line of constant incidence. We find the peak core stream efficiency on the Ψ_{\min} loss line for which incidence is optimal.

From this we can figure out how the core efficiency map must look. The efficiency peak value is at the same value of $\Psi_{\text{core}} = \Delta H_{\text{core}}/U_{\text{core}}^2$ on all speed lines. The efficiency will decrease only slightly when it deviates from the minimum loss value on the speed line because of the wide low loss incidence range in the subsonic flow regime.

1.2.4.1.2 Bypass Section

As we said earlier, close to the fan design point the flow in the bypass section, near to the blade tip, is supersonic. The incidence angle is unique and the efficiency varies with the position of the terminating shock as shown in the example in Fig. 1.2-32. This shock moves downstream from the design position and creates higher losses when the fan pressure ratio is decreased. The operating point with the highest efficiency is near the surge line. The location of the maximum efficiency point on a speed line of the average fan map—in contrast to the maximum efficiency in the core stream—is not at the same $\Delta H/U^2$ value for each speed.

The average relative Mach number of the fan rotor is much higher than the relative Mach number in the core stream region. Therefore, the average low loss incidence range is smaller than that in the core region. Consequently, along a speed line, the average fan efficiency decreases more quickly than the core stream efficiency when the operating point deviates from the optimum incidence point. In other words, the efficiency islands in the core stream map are wider than those in the average fan map.

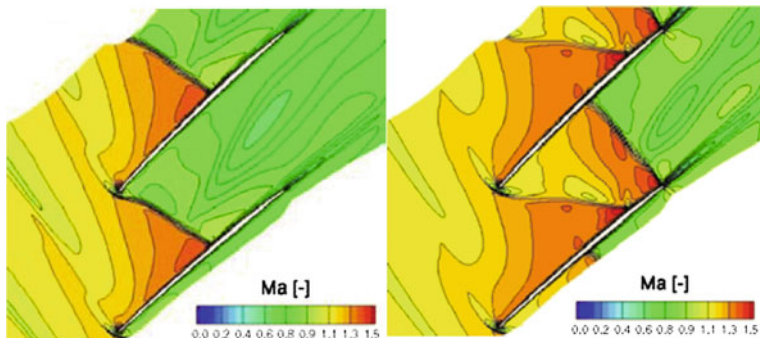


Fig. 1.2-32 Rotor shock system at approximately 90% blade height near design conditions (left) and at choked flow conditions at 100% corrected speed [43]

In general, tip clearance losses and supersonic shock losses lead to lower than average efficiency in the bypass stream. Therefore, the core stream efficiency is higher than the average efficiency in all parts of the map.

1.2.4.2 Extended Fan Map

As [50] shows, we extend the average fan map (which consists of the usual tables for total corrected mass flow, average pressure ratio P_{21a}/P_2 and average efficiency η_{2-21a}) by adding a table with core stream efficiency η_{2-21} . A few details of fan geometry are needed for off-design simulation: hub and tip radius for calculating the circumferential speed plus the rotor blade exit angle in the middle of the core stream. These quantities were used previously in the cycle design calculation and can be retrieved.

1.2.4.2.1 The Algorithm

During each pass through the off-design engine model we know the (estimated) values for the map coordinate β and the corrected spool speed. The map itself yields the total corrected flow, from which we can calculate the velocity V_{ax} at the fan face. Dividing this velocity by the circumferential speed U_{core} gives us the flow coefficient Φ_{core} ; then the power coefficient Ψ_{core} follows from Eq. (1.2-12). The specific work done on the core stream is $\Delta H_{core} = \Psi_{core} U_{core}^2$.

We can calculate the core stream pressure ratio P_{21}/P_2 after reading the core stream efficiency η_{2-21} from the added fan map table. Now we have all we need to calculate the bypass pressure ratio P_{13}/P_2 and bypass efficiency η_{2-13} from the average pressure ratio P_{21a}/P_2 and efficiency η_{2-21a} :

$$\frac{P_{13}}{P_2} = \frac{(BPR + 1) \left(\frac{P_{21a}}{P_2} - 1 \right) - \left(\frac{P_{21}}{P_2} - 1 \right)}{BPR} + 1 \quad (1.2-13)$$

$$\eta_{2-13} = \frac{(BPR + 1) \eta_{2-21a} - \eta_{2-21}}{BPR} + 1 \quad (1.2-14)$$

1.2.4.2.2 How to Get Such a Map

This approach is not problematic when values of either measured or calculated core stream efficiency are available. However, this is rarely the case and usually a map with only average pressure ratio and efficiency is available.

Nevertheless, we can make an educated guess about the shape of core stream efficiency islands in the average map. For that purpose, let us assign a physical

meaning to the auxiliary map coordinate β by declaring that all β lines are parallel to lines representing constant average work coefficient $\Psi = \Delta H/U^2$.

Figure 1.2-33 shows a map of a typical single stage fan. The peak efficiency line connects the points with the highest efficiency on each of the speed lines. The same map is shown in Fig. 1.2-34, where lines of constant Ψ have replaced the efficiency contours. It is found that these Ψ lines can be approximated very closely by parabolic β -lines, as used in GasTurb.

Note that in the low speed region the peak efficiency line is parallel to one of the constant Ψ lines. This characteristic is typical for a subsonic compressor. In the high speed region, the peak efficiency line turns upwards towards the surge line. This is because (as mentioned before in the discussion of Fig. 1.2-32) in a supersonic flow field the highest efficiency region is near to the surge line.

If we hypothesize that the peak efficiency line of the core stream coincides with the peak efficiency line of the average map in the low speed region of the map, where the flow field is subsonic, this fixes the β value as equivalent to a constant core stream work coefficient Ψ_{core} . The peak efficiency line of the core stream is a β line in the average fan map, see Fig. 1.2-35.

The core stream efficiency islands in the average fan map show the following characteristics

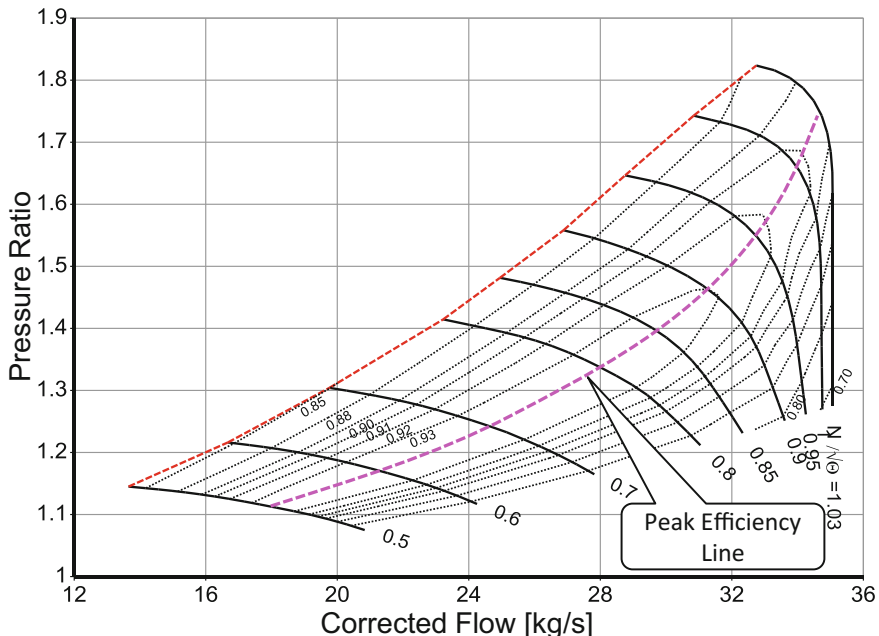


Fig. 1.2-33 Single stage fan map [44]

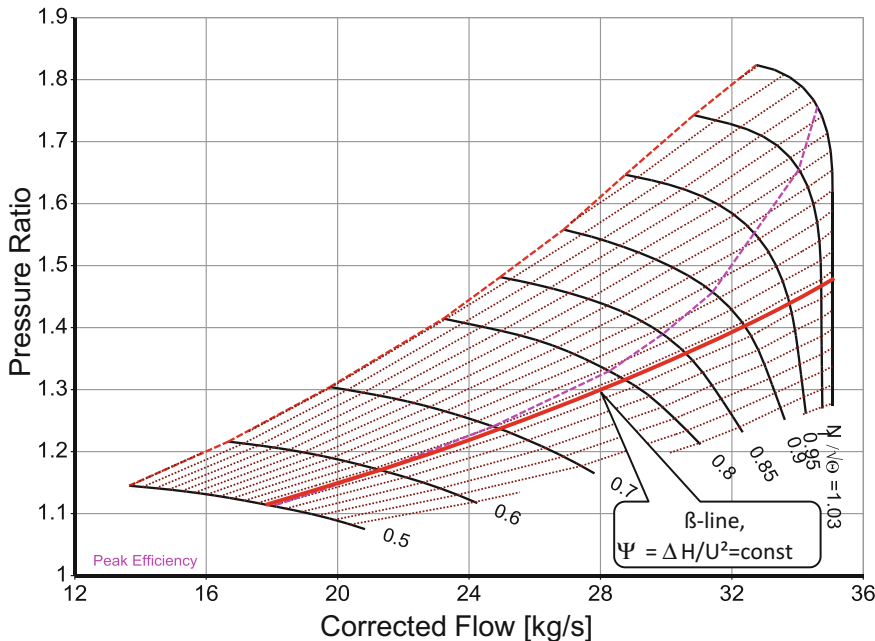


Fig. 1.2-34 Fan map with lines of constant power coefficient $\Psi = \Delta H/U^2$

- η_{2-21} is generally higher than η_{average}
- The core stream efficiency islands are broader than those in the average efficiency map
- At high corrected speed, η_{2-21} decreases less than η_{average}

All these trends result from the fact that the flow in the fan hub region is always subsonic and the effects of tip clearance losses are absent. These considerations have been applied while generating the core stream efficiency islands in Fig. 1.2-36.

By the way: inaccuracies in the core efficiency guess only have a minor impact on the overall performance, especially for high bypass turbofans.

We have explained how the effect of bypass ratio variations on fan performance can be modeled from an example of a single stage fan. The algorithm can also be applied to multistage fans. The addition of a table with core stream efficiency to those for a basic average performance map certainly yields more accurate results than the poor man's approach which accounts for the difference between core and bypass performance with simple factors for pressure ratio and efficiency.

Creating the core stream efficiency table for a given average fan map is supported by the program Smooth C, which is introduced in the next section. In GasTurb the input of an extended fan map with a core stream efficiency table automatically invokes an algorithm that retains the average performance and adjusts pressure ratio and efficiency according to the prevailing bypass ratio.

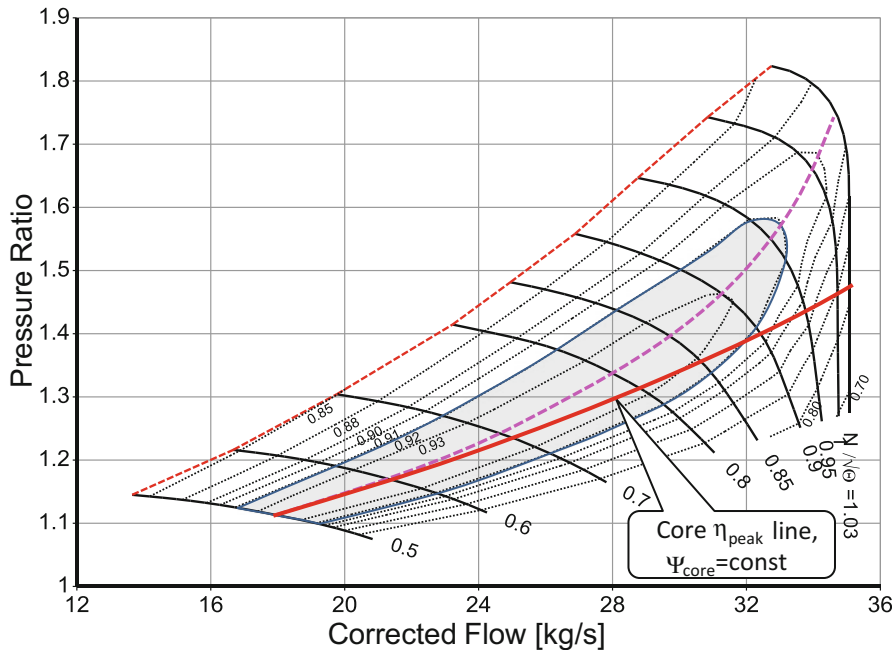


Fig. 1.2-35 Location of the core stream peak efficiency in the average map

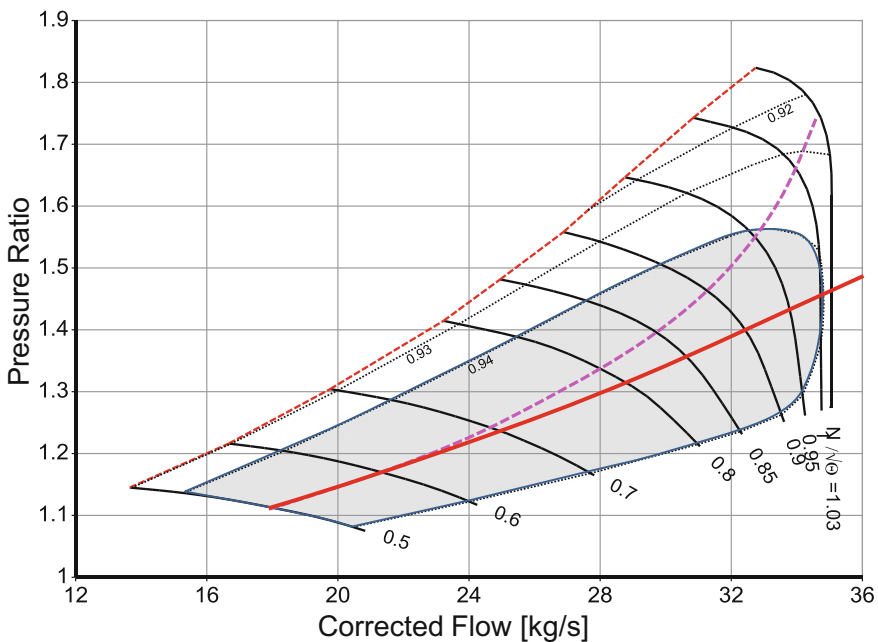


Fig. 1.2-36 Average fan map with core efficiency contour lines

1.2.5 Secondary Effects

Until now we have only discussed basic fundamentals of compressor performance and its simulation. There are several secondary effects which may need to be considered, especially in accurate aircraft engine performance models. Among them are the influences of Reynolds number and inlet flow distortion which are discussed in their own sections. Here we limit our remarks to three other phenomena: interstage bleed air offtake, tip clearance and blade untwist.

1.2.5.1 Bleed Air from an Intermediate Stage

Compressor interstage bleed is quite common. Often relatively small amounts of air are taken from intermediate stages for instance to cool rearward turbine stages or seal bearing chambers. For certain engines, “handling bleeds” may be used to reduce the need for variable guide vanes with much larger fractions of the compressor flow extracted early in the compression process to maintain stall margins, especially during start-up. The work done on the bleed air is considered within the standard cycle calculation under the assumption that the compressor map is not affected by the air offtake. This is only correct if the bleed air amount is a constant percentage of the total flow at any operating point but when bleed is used for operability, a bleed schedule is normally set up and that can vary quite considerably.

Changing the amount of bleed is equivalent to changing the compressor annulus. If during a rig test less bleed is taken off than occurs in the engine, the final compressor stages will operate at higher flow and the surge margin will increase. So for an accurate performance model, it may be necessary to use different compressor maps if the amount of interstage bleed (as a percentage of the compressor inlet flow) changes much during engine operation.

1.2.5.2 Tip Clearance

The impact of tip clearance on compressor and turbine behavior is so severe that every effort is made to minimize it during engine operation. That can be done to a limited degree by passive means, i.e. an optimal thermal match of static and rotating parts. An active clearance control (ACC) system blows cold air on the casing which shrinks and thus reduces the running tip clearance. For a correct simulation of an engine with active clearance control we need to model the change in tip clearance and its effects on the component behavior with some precision.

Tip clearance affects efficiency, mass flow and—especially pronounced—the surge margin of compressors. Figure 1.2-37 gives an idea of the magnitude of the tip clearance effects on efficiency of multistage axial compressors. The solid symbols represent data from machines with shrouded stators, the open symbols from those with cantilevered stators.

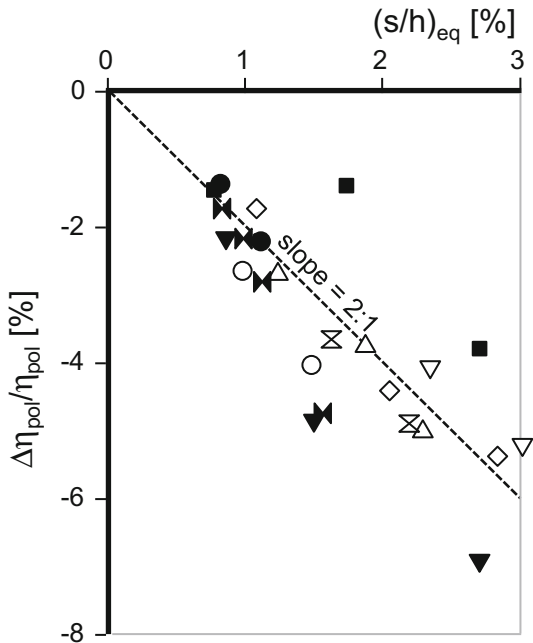


Fig. 1.2-37 Efficiency loss in multistage axial compressors (re-formatted version of Fig. 12.1 in Ref. [11])

The correlating parameter in Figs. 1.2-37 and 1.2-38 is the equivalent tip clearance $(s/h)_{eq}$ which is defined as

$$\left(\frac{s}{h}\right)_{eq} = \frac{\left(\frac{s}{h}\right)_{Rotor} + A\left(\frac{s}{h}\right)_{Stator}}{1+A} \quad (1.2-15)$$

Absolute tip clearance s is related to the local annulus height h . The relative rotor and stator tip clearances are mean values of all blade or vane rows. The weighting factor A is 0.8 for cantilevered and 0.3 for shrouded stators.

Figure 1.2-38 shows that the exchange rate of corrected flow versus equivalent tip clearance is the same as that of efficiency: 1% change in tip clearance corresponds to an efficiency loss of 2%. This is a severe effect on engine performance, but the simultaneous loss of 8% in surge margin is much more important when it comes to engine operability.

Whether or not tip clearance corrections are applicable in the performance simulation depends on the tip clearance embedded in the map. Constant tip clearance is usually the assumption in simple compressor map calculation programs. In a map measured on a compressor rig the tip clearance is usually a function of spool speed.

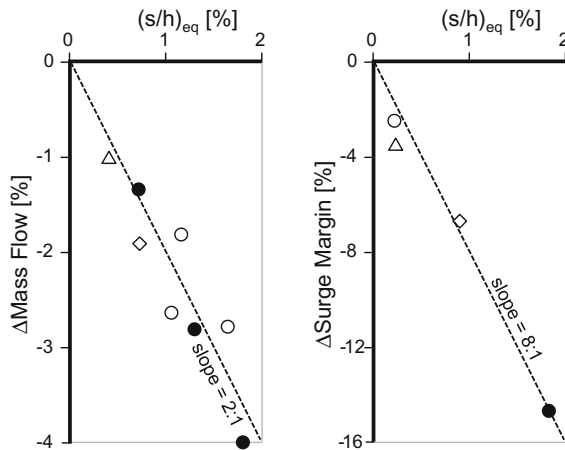


Fig. 1.2-38 Impact of tip clearance on mass flow and surge margin [45]

There are two types of compressor rigs: specific development rigs and engine parts rigs. Development rigs are heavy designs with lots of additional instrumentation and features not available in the engine. For example, in the rig compressor there might be more adjustable stators than intended for the engine.

Engine parts rigs are built from engine parts—as the name says. However, the surroundings or the environment of the actual compressor in the engine cannot be simulated during the rig test. High pressure compressors in bypass engines have quite different heat transfer to the bypass when operating in the engine. There will be air of varying temperature flowing around the compressor casing which does not exist on the rig. This causes a difference in tip clearance behavior when the speed is changing. An example for this effect is shown in Fig. 1.2-39.

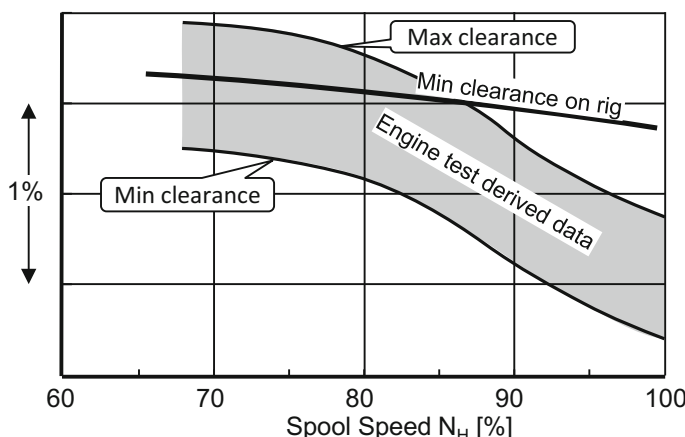


Fig. 1.2-39 Running tip clearance in an engine and during a rig test

1.2.5.3 Blade Untwist

Blade untwist is a mechanical phenomenon where the leading edge blade angle varies with operating condition. This is due to the loads from centripetal force, aerodynamic pressure forces on the blade and also perhaps thermal loads. Clearly untwist is primarily of concern for low hub/tip radius ratio fans and damaging effects can be exaggerated in modern engines where precise three-dimensionality is critical in airfoil design. The blade is designed at “hot” rotating conditions with some nominal untwist which changes with both engine power setting and environmental conditions. Since it is manufactured at cold stationary conditions, great care must be taken in predicting the changes. It is fortunate that fans run over a fairly narrow range of temperatures. Figure 1.2-40 shows the magnitude of rotor blade untwist to be expected.

So how do such changes in fan rotor geometry affect a compressor map? At a given corrected speed N/\sqrt{T} , the mechanical speed N varies within the flight envelope significantly. Imagine a fighter engine which has to operate at high altitude, low Mach number with an inlet temperature of say $T_2 = 240\text{ K}$ and at low altitude and high ambient temperatures with $T_2 = 380\text{ K}$. The ratio of the mechanical speeds N_1 and N_2 follows from

$$\frac{N_1}{\sqrt{240K}} = \frac{N_2}{\sqrt{380K}} \quad (1.2-16)$$

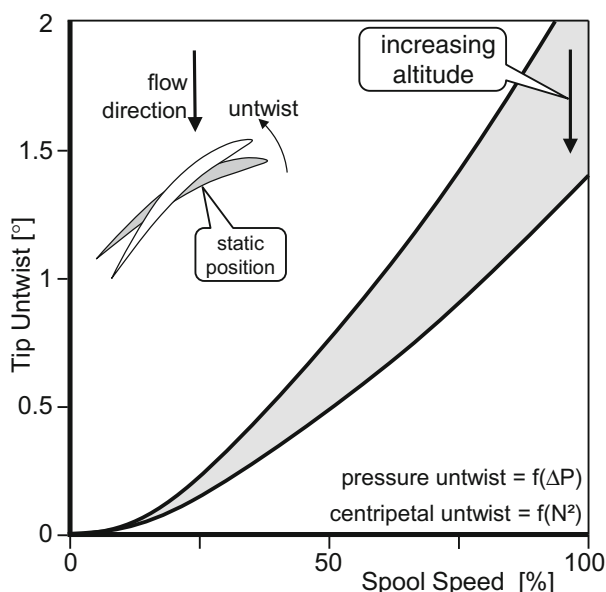


Fig. 1.2-40 Tip untwist of a single stage fan [9]

$N_1/N_2 = 0.8$ in this example. That means the centripetal forces at low inlet temperatures are only about 64% of those at high inlet temperatures. According to Fig. 1.2-40, this speed difference leads to almost 1° difference in blade untwist—a change that can affect flow and efficiency quite substantially.

In fact, the primary impact of untwist is on flow capacity of high bypass ratio fans. At high corrected speed and supersonic relative Mach number the phenomenon of unique incidence exists which manifests itself as vertical speed lines in the map. The metal angle of the rotor leading edge determines the corrected flow. So untwist causes increased corrected flow in the high speed region of the map. The blade untwist effect is typically of the order of 2% flow capacity per degree untwist at high corrected speed and half of that at low speed [9].

The magnitude of the actual blade untwist correction for a specific map depends on the blade untwist for which the map is valid. In a very simple compressor map calculation program, blade untwist might not be considered at all; the reduction of untwist at spool speeds lower than design is ignored. On the other hand, blade untwist happens inevitably during a compressor rig test. The measured map is valid for a varying blade untwist. The applicable magnitude of blade untwist corrections depends on the conditions for which the map is valid.

A problem with untwist modeling is that its effects are replicated by those of tip clearance and Reynolds number. Since all three results are functions of engine inlet conditions— T_2 , P_2 and mechanical spool speed—inadequacies in the individual models are difficult to separate. A good model for one will be misleading when its outcome is compared with test data where the others have been ignored [9].

1.2.6 Scaling Compressor Maps

Compressor maps are indispensable for accurate gas turbine performance predictions. The true maps are usually not available but this problem may be solved by using scaled maps from compressors of similar design. Map scaling may be done outside the performance program in a special input data pre-processing process. GasTurb scales the maps automatically in such a way that the calculation of the cycle design point in the off-design simulation mode agrees with the results of the cycle design calculation in every detail.

Let us study the automatic map scaling of GasTurb with an example. Reference [6] contains the map from a modern civil fan for a corrected speed range from 110% down to 65%. The original map contains only efficiency differences, so the absolute efficiency numbers in Fig. 1.2-41 are only a guess. This map has been re-generated and extrapolated to lower speed values in *Smooth_C*.

Calculation of the cycle design point has yielded values for fan pressure ratio, polytropic or isentropic efficiency and corrected flow. Since the combination of these three numbers will not be found in the map available the question arises: “Where in the unscaled map is the map scaling point corresponding to the cycle design point?”

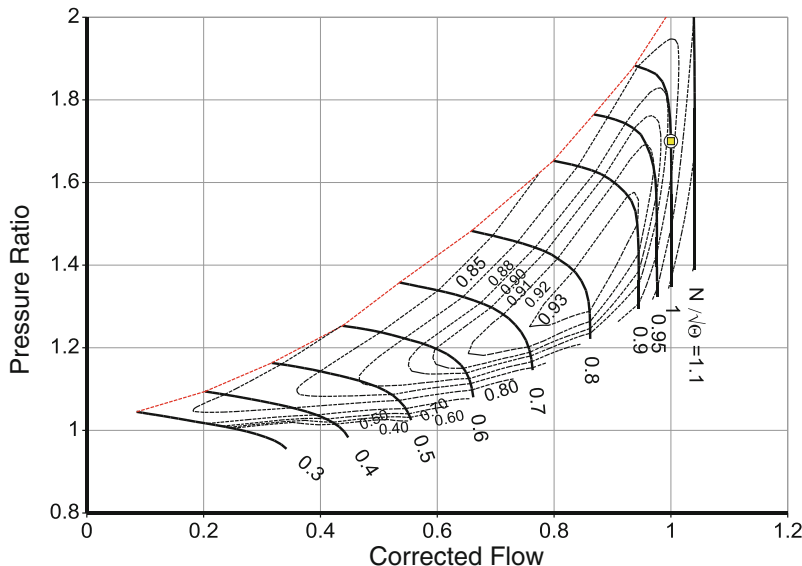


Fig. 1.2-41 GasTurb Standard Map for turbofans, unscaled

When *Standard Maps* are selected in GasTurb, the program locates the scaling point using preset map coordinates. For example, in the fan map under discussion, the default map scaling point is on the line for 100% corrected speed, i.e. $N/\sqrt{\Theta} = 1.0$. The auxiliary map coordinate $\beta = 0.5$ fixes the pressure ratio. Figure 1.2-42 shows an automatically-scaled version of the GasTurb Standard Fan Map as an example. The *map scaling point* is also often called the *map entry point*.

Of course, the default selection of the map scaling point cannot be right for all engines. Its correct location is strongly related to the position of the cycle design point within the engine operating envelope.

If the cycle design point is a cruise case, it is tempting to locate the scaling point within the peak efficiency region of the map. With such a selection, the relative corrected speed in the unscaled *Standard Map* would be 0.9, for example. This scaling point choice results in Map B (Fig. 1.2-43) for the same cycle design point as before. When compared to Map A, the speed values are different, the general level of efficiency is lower and the maximum corrected flow is higher.

The differences in speed come from the fact that—in GasTurb, by definition—the corrected speed of the cycle design point is 100% in all compressor and turbine maps. When scaling a map, all the speed values in the unscaled map are divided by the speed at the map scaling point. This procedure yields a corrected speed value of 1.0 for the cycle design point.

When it comes to off-design efficiency, even though the efficiency in both maps is identical to the design point value at the map scaling point, the peak efficiency in Map A (Fig. 1.2-42) is much higher than that in Map B (Fig. 1.2-43).

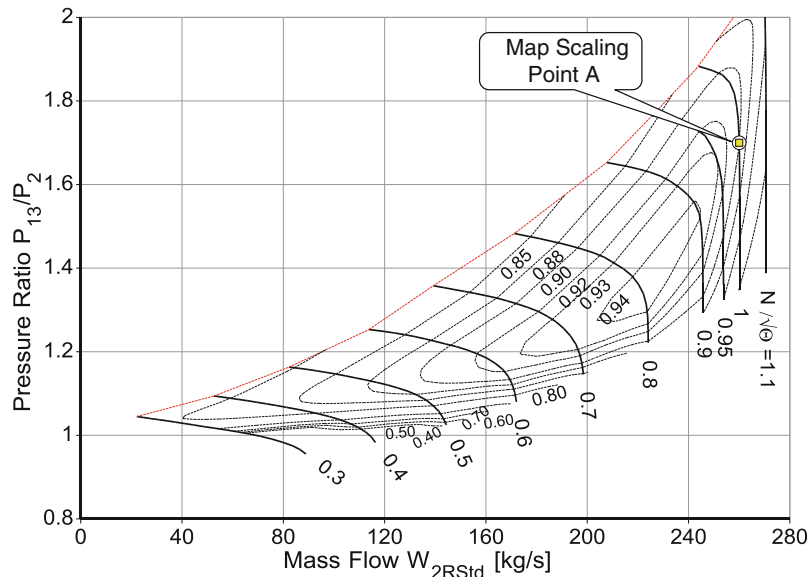


Fig. 1.2-42 Map A—the Gasturb standard map for turbofans, scaled for the cycle design point with $P_{13}/P_2 = 1.7$, $W_{2R\text{Std}} = 260 \text{ kg/s}$, $\eta = 0.9$ using the default map scaling point setting $N = 1$ and $\beta = 0.5$

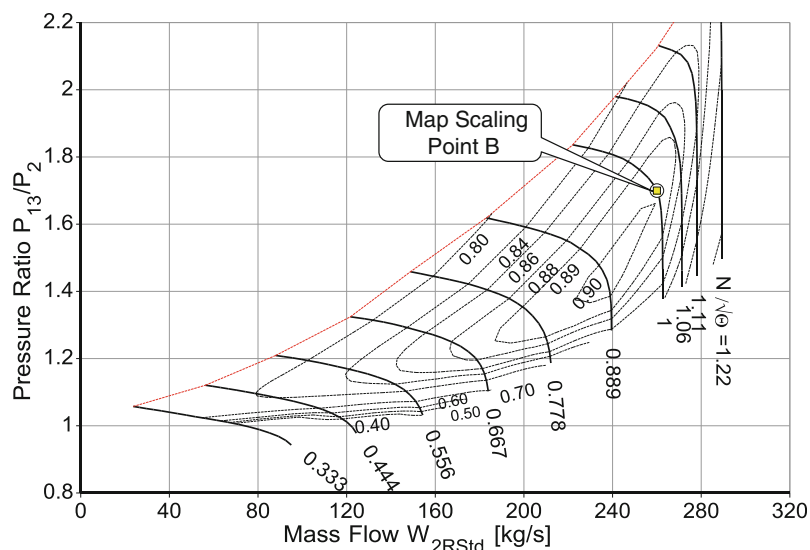


Fig. 1.2-43 Map B: GasTurb Standard Map for turbofans, map scaling point $N = 0.9$ and $\beta = 0.4$

But we can also see that pressure ratio and corrected flow are generally higher in fan B than fan A. So, it looks like everything is different in the two scaled versions of the same baseline map!

However, there is one hidden quantity which is not affected by scaling: the axial Mach number at the compressor face and this can be determined unambiguously from the corrected flow divided by the area of the compressor face if these are known.

In the fan map of Fig. 1.2-41, corrected flow is not expressed absolutely but as a fraction of its value at design and the area of the compressor face is unknown. Therefore, we cannot calculate the inlet Mach number scale for this map; we must guess initially. Let us assign a Mach number of 0.7 to the relative corrected flow value of 1.0. This is typical for transonic fans of modern large civil aero engines.

From the Mach number, we can calculate a corrected flow per unit area. Using the value 1 for corrected flow yields a reference value for the fan face area. From this, we can calculate the corrected flow per area and hence the Mach number at the engine face for any point on the x-axis. So we can plot the unscaled map with Mach number as the x-axis, as shown in Fig. 1.2-44. The next section describes how this scale can help set the map scaling point.

In a pure thermodynamic cycle study—where engine size does not matter—it is not necessary to consider the Mach numbers in the flow path. The map scaling point can be positioned in such a way that the desired performance characteristic is achieved.

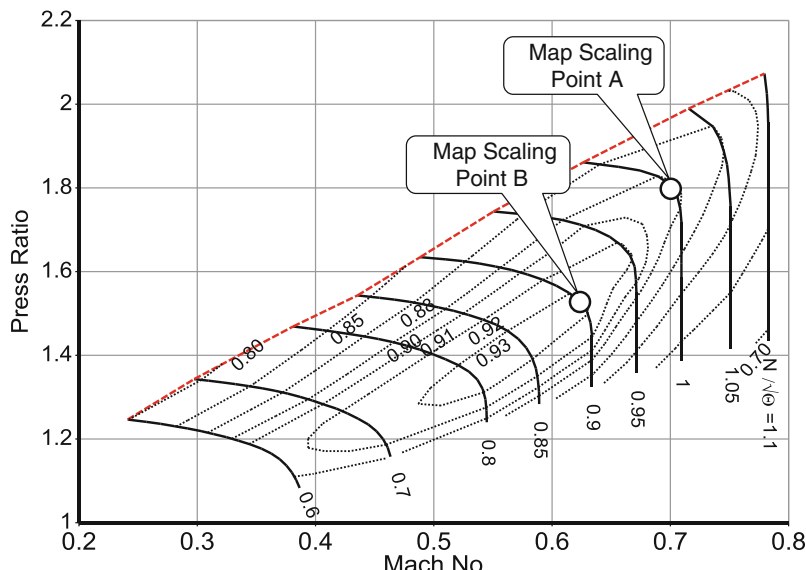


Fig. 1.2-44 Unscaled GasTurb Standard Map with Mach number as X-axis

Higher fidelity simulations go beyond thermodynamics and account for the size of the engine. The dimensions of the annulus are either calculated or even known in advance—when an existing engine is to be modeled, for example.

During the cycle design calculations, the axial Mach number can be determined unambiguously from the flow annulus area and the corrected flow. The abscissa of the map scaling point must be consistent with this Mach number in any true performance model.

In our cycle design point example, let us assume that for the known fan tip diameter the fan face Mach number is 0.7. The map scaling point coordinates $N = 1$ and $\beta = 0.5$ are consistent with this Mach number and therefore Map A (Fig. 1.2-42) is consistent with the cycle design point. If the fan tip diameter was bigger, consistent with a fan face Mach number of only 0.62, then Map B would be correct.

1.2.6.1 How to Find the Mach Number Scale in a Fan Map

To set the map scaling point correctly, we need to know the axial Mach number. To create the Mach number scale in Fig. 1.2-44 we used a guess. For transonic fans without inlet guide vanes, we do not need to guess because we can derive what we need from the shape of the speed lines.

Let us look at the flow field in the high speed/low pressure ratio region of Fig. 1.2-44. There, all the speed lines are at least partially vertical, which means that the axial Mach number at a given corrected speed is constant. The velocity triangles at the rotor inlet are invariant in terms of Mach number. The reason for that is that rotor inlet flow conditions are supersonic, as shown in Fig. 1.2-45. Note that the flow field upstream of the throat is unaffected when the pressure ratio is reduced.

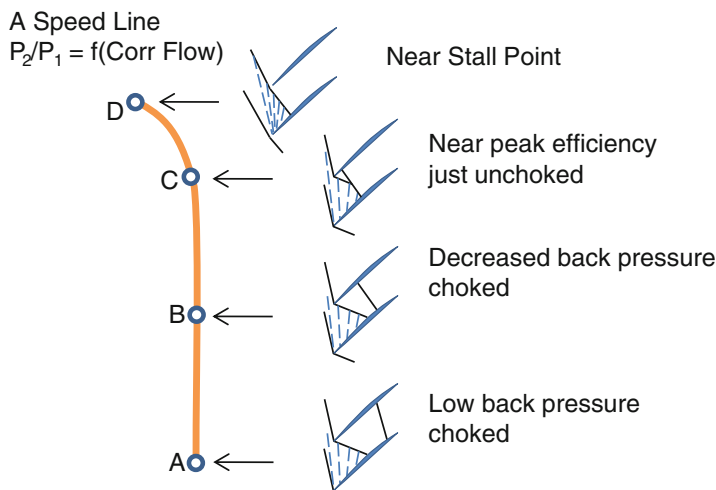


Fig. 1.2-45 Supersonic flow field at four points on a speed line

What happens when speed is reduced compared to this operating condition? As long as the speed reduction is small, part of the speed line will be vertical, just as before and the flow field will remain supersonic.

It is easy to calculate the supersonic flow field if the rotor blade consists of a flat wedge upstream of the passage throat. In Fig. 1.2-46 the Mach numbers upstream and downstream of the oblique shocks as well as the shock angles have been determined for a wedge angle of 4.1° and for two blade speeds.

The flow direction upstream of the oblique shocks is the same for both speeds; the incidence to the rotor blade is unique. Changes in corrected speed do not affect the angles in the fan inlet velocity diagram. Therefore, the axial Mach number is proportional to the corrected spool speed, which is a direct measure of the circumferential Mach number.

If we look at the vertical parts of the two speed lines N_1 and N_2 in Fig. 1.2-44, we can read two values of corrected flow from the unscaled map and determine the ratio W_1/W_2 . As shown above, circumferential speed is proportional to axial Mach number and therefore M_1/M_2 must be equal to N_1/N_2 . So, the velocity triangles are similar and we know how the corrected flow changes with Mach number in the map.

Now recall some isentropic flow basics: there is a fixed relationship between corrected flow per unit area and Mach number, as shown in Fig. 1.2-47. The slope

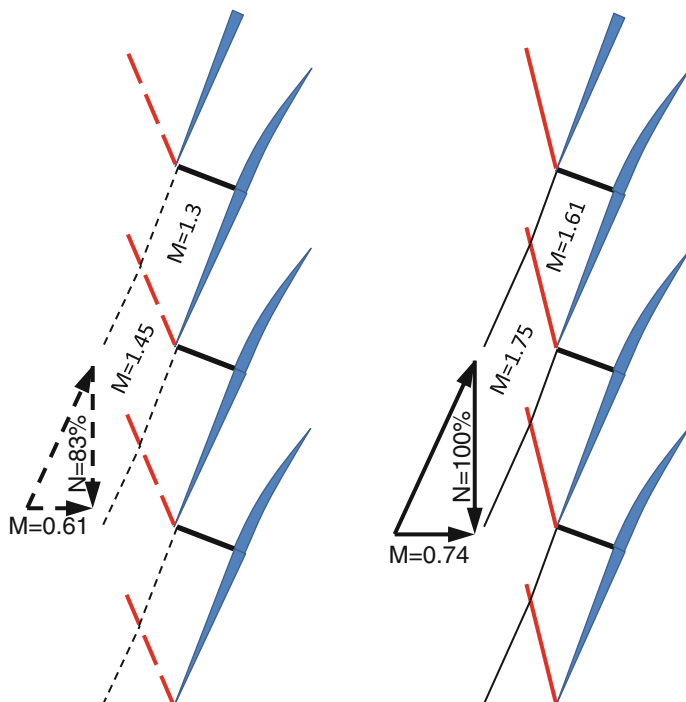


Fig. 1.2-46 Effect of speed on the velocity triangles

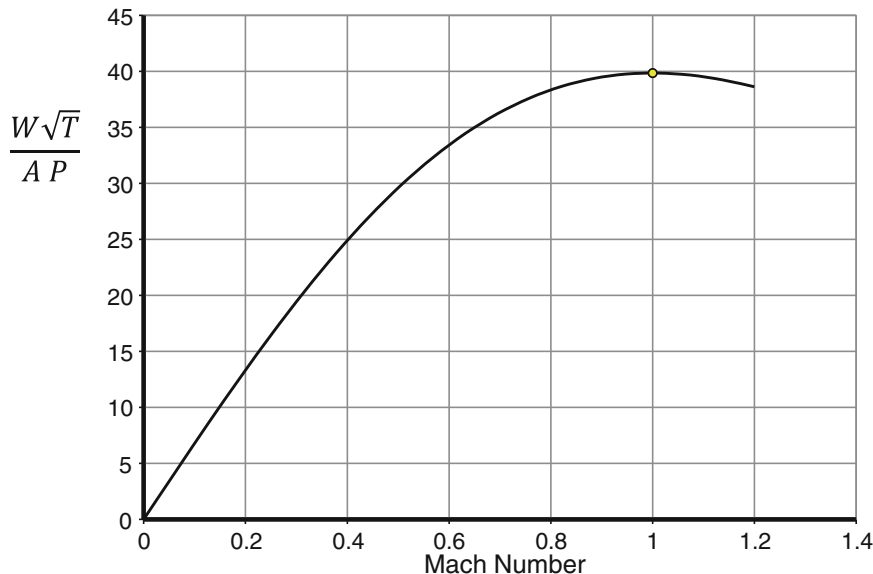


Fig. 1.2-47 Corrected flow per area as function of Mach number

of this curve depends on the absolute Mach number. With increasing Mach number, the exchange rate between Mach number and corrected flow per area goes down. The curve has a maximum at $M = 1$; there the exchange rate between Mach number and corrected flow is zero.

Let us return to the problem of setting the map scaling point correctly. The Mach number of the map scaling point is that at the fan face. Selecting a map scaling point connects a corrected flow value from the map with this Mach number. We can draw a second x-axis—which has a non-linear scale—for the Mach number parallel to the corrected flow axis and this is done in Fig. 1.2-48.

Figure 1.2-48 shows what we get for the Mach number axis if we locate the map scaling point ($M = 0.7$) on the highest speed line ($N = 1.1$). For the vertical part of the line $N = 1$, we read a Mach number of 0.66. As explained in the discussion of Fig. 1.2-46, a 10% increase in corrected speed must correspond to an equal axial Mach number increase of 10% (from 0.66 to $0.66 * 1.1 = 0.73$). So, if we now check how much speed increase would be needed to reach an axial Mach number of 0.73, we find in Fig. 1.2-48 that it could only be achieved with $\Delta N = 12\%$.

In Fig. 1.2-49, with the map scaling point chosen, the problem is eliminated. The increase in corrected flow in going from speed 1 to 1.1 is consistent with a Mach number increase of 10%, as it should be. The map scaling point is correct.

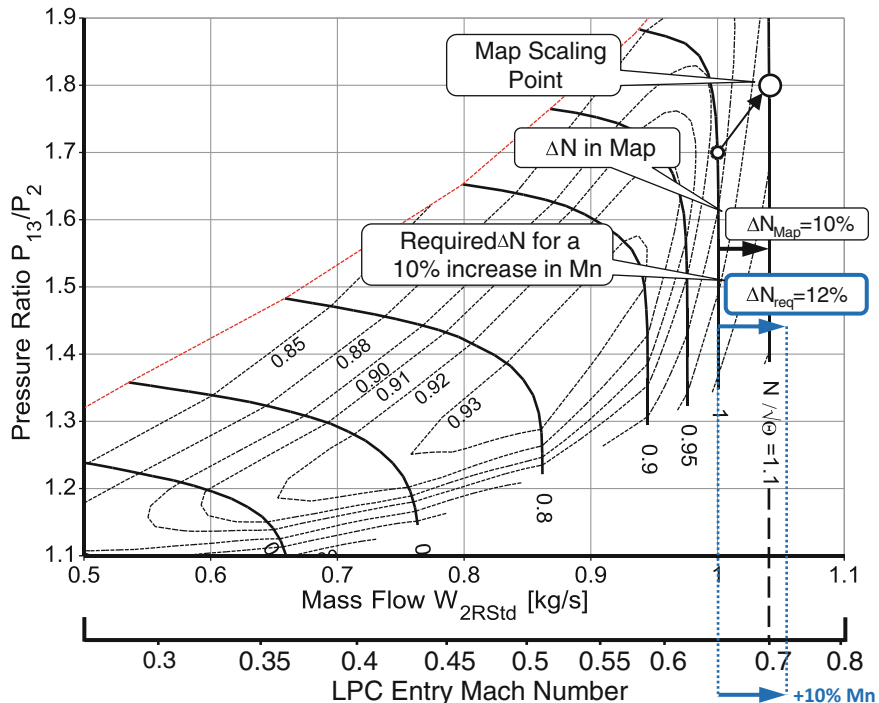


Fig. 1.2-48 Map scaling point on the speed line 1.1

While the map scaling point was set at too high a corrected flow in Fig. 1.2-48, the opposite is true in Fig. 1.2-50, where the map scaling point is on the 0.9 speed line. Here, the Mach numbers in the high-speed region are out of reach and the corrected flow for speed 1.1 would be higher than the theoretical maximum. Scaling the map with this map entry point would be a fault in the simulation.

Up to now we have spoken only about setting the abscissa of the map entry point—in terms of either speed or flow. What about the pressure ratio (the β coordinate)? There is no simple answer to that. On one hand, we want high efficiency at any off-design operating condition and on the other, we always need sufficient surge margin. The surge pressure ratio of gas generator compressors should be at least 20% higher than the design point pressure ratio, at the map scaling point. This surge margin is needed for operating line shifts due to power offtake, Reynolds number effects, inlet flow distortion, transients, efficiency deterioration during service, engine manufacturing and control tolerances. Booster operating lines are flatter than gas generator operating lines and come close to the surge line at low power settings. At the cycle design point, even more surge margin might be needed than for the high-pressure compressor.

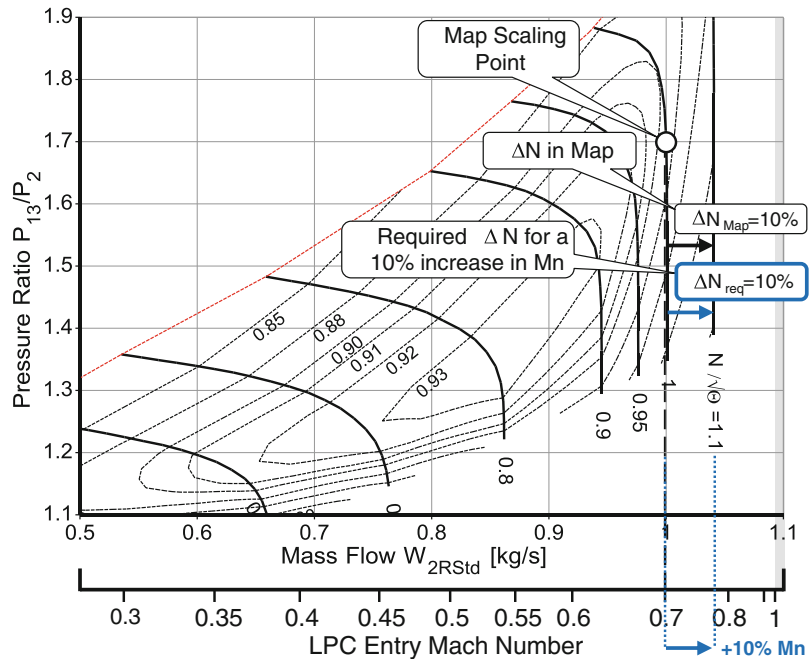


Fig. 1.2-49 Map scaling point on the speed line 1.0

In summary: do not choose the map scaling point casually! Its selection affects efficiency, surge margin and corrected flow at a speed throughout the operating range of your engine.

1.2.6.2 Mach Number Scale for Other Compressor Maps

The method for finding the Mach number scale described in the previous section for fans is also applicable to maps for multi-stage axial compressors without inlet guide vanes. For a compressor with variable geometry, the spacing between the speed lines in a map is controlled not only by the axial Mach number but also by the stagger angle of the variable guide vanes. There is no longer a unique connection between the axial Mach number and corrected flow.

Partially vertical speed lines are also found in maps from radial compressors. This phenomenon can be caused by a supersonic relative Mach number at rotor entry and by choking of the exit guide vanes. In the latter case, we do not know the relationship between corrected flow and speed.

One thing we know for sure is that the Mach number assigned to the highest speed in the map must be lower than 1.0. Otherwise the scaled map is not consistent with compressor inlet Mach number at the cycle design point.

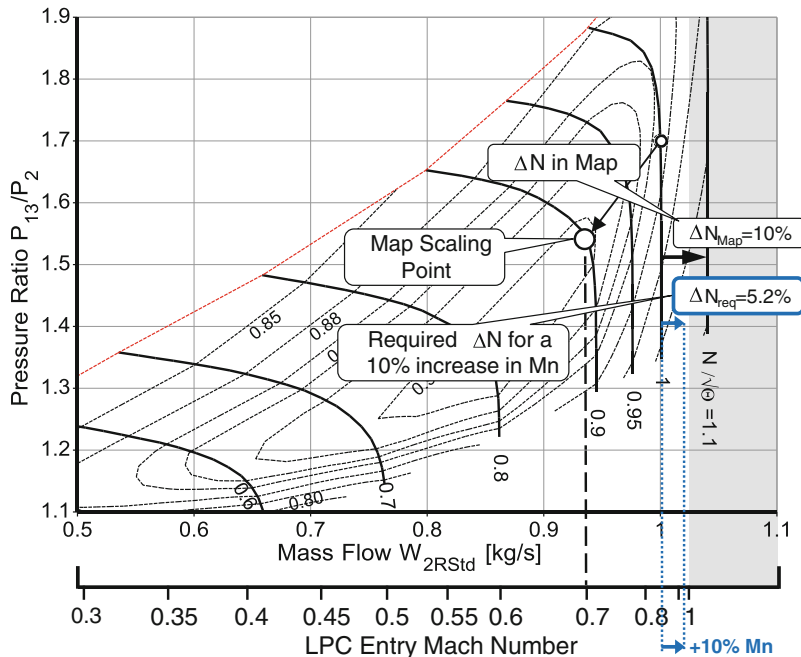


Fig. 1.2-50 Faulty setting of the map scaling point

1.2.7 The Map Preparation Program Smooth C

In performance calculation programs, compressor maps are needed in a special format which employs auxiliary coordinates like the β -lines introduced above. Producing this format “by hand” is a cumbersome task that takes a great deal of time because of the scatter in the data, shown for example in Fig. 1.2-51. These data along speed lines are from a compressor rig test and they are not evenly distributed over the speed range. Interpolation and extrapolation is necessary.

The program *Smooth C* is a tool that quickly produces high quality compressor maps from measured or calculated data. Have a look at Figs. 1.2-2, 1.2-8, 1.2-10, 1.2-12, 1.2-15, 1.2-16 and 1.2-18 to see some of the output which *Smooth C* can produce from the information in Fig. 1.2-51.

Compressor maps can be for more than overall system performance simulation. Employing the same beta line grid for two or more maps allow differences between compressor variants to be evaluated in a consistent manner. Moreover, the effects of inter stage bleed, Reynolds number, tip clearance, blade and vane re-stagger, distortion etc. can be assessed with this approach.

The accuracy of the compressor map representation is very important for precise cycle calculations. Depending on the engine type, it should be remembered that 1% error in compressor efficiency can mean up to 1% error in specific fuel consumption! Such an error can easily be introduced into the cycle calculation by use of a

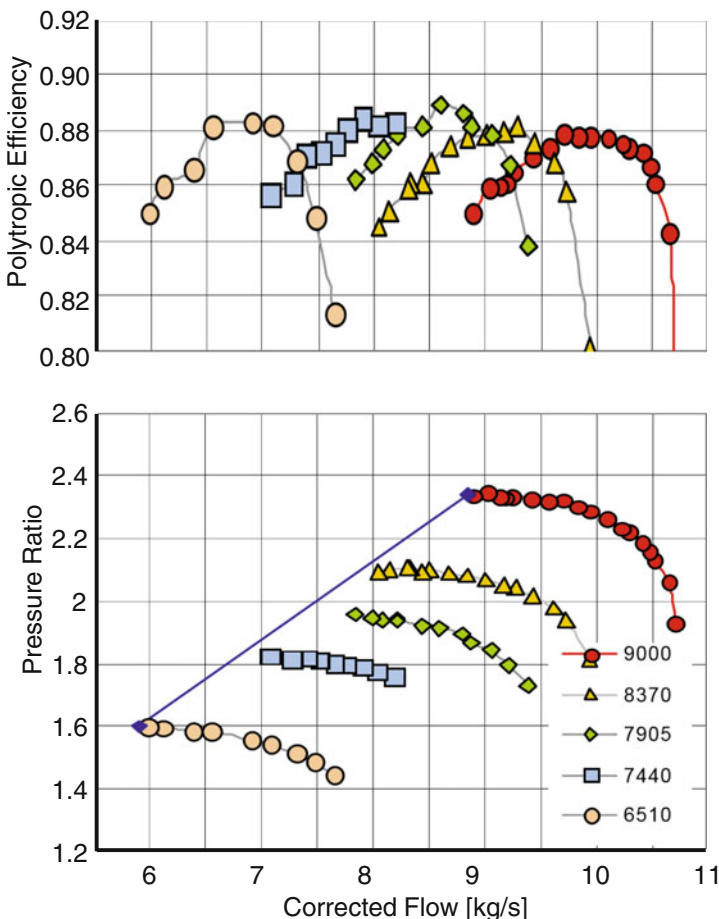


Fig. 1.2-51 Measured data as presented in Ref. [4]

low quality compressor map. The interpolation of data is prone to error if the data are scattered or if there are insufficient speed lines in the map.

However, *Smooth C* is not only a valuable tool for dealing with measured data. It can also be used to check the quality of any compressor map provided as input. Various cross plots allow you to judge whether the map is a reasonable description of compressor physics or not. Deficiencies can be corrected and physically-meaningful interpolations and extrapolations of the map are possible.

Instead of genuine measured data—which seldom are available outside industry and research facilities—one can also take data from figures published in the literature. Even relativized compressor map data can be used.

Smooth C output is tabulated with the same number of points for all speed lines. This format is suitable to use as input to performance programs that simulate the performance of either gas turbines or turbocharged piston engines.

1.2.8 A Simple Map Scaling Procedure

If a compressor is scaled geometrically (i.e. all dimensions—including tip clearance—are factored with the same value), then also the flow field will be scaled geometrically. At a given point in the map, all Mach numbers and all flow angles are the same as for the original compressor (Reynolds number effects neglected). Corrected specific work is the same as well as the efficiency and consequently also the pressure ratio. It is straightforward to derive the map for the scaled compressor by applying constant factors to W_c and N_c of the original map. When the map is plotted employing the quantities $W_c/W_{c,ref}$ and $N_c/N_{c,ref}$ then there is no difference between the maps of the original and the scaled compressor (Fig. 1.2-52).

Scaling a map in pressure ratio and efficiency implies a change in the flow field because specific work relates to the flow angles. If the change in pressure ratio is limited, then the following simple map scaling procedure is applicable.

Pressure ratio scaling

A pressure ratio scaler is defined as $f_{PR} = (PR_{Design} - 1)/(PR_{Map} - 1)$. During map scaling, all values in the pressure ratio map table are replaced by $PR_{new} = 1 + f_{PR} (PR_{old} - 1)$.

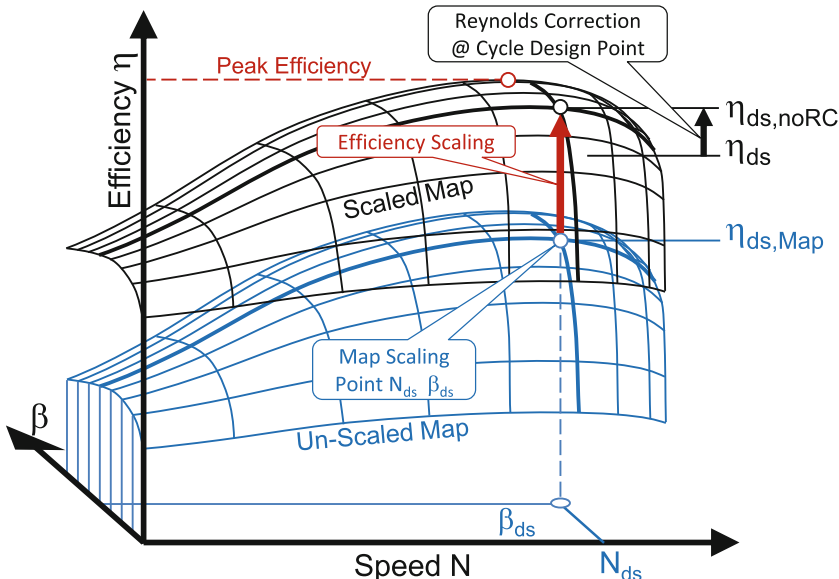


Fig. 1.2-52 Efficiency scaling

Efficiency scaling

The following three efficiency formulations each play a role in efficiency scaling:

- The cycle design point efficiency, η_{ds}
- The efficiency in the unscaled map at the map scaling point, $\eta_{ds,Map}$
- The Reynolds-corrected design point efficiency, $\eta_{ds,RC}$

The Reynolds Number Index, RNI, at the cycle design point determines if an efficiency correction needs to be applied. When the Reynolds correction is removed from the cycle design point efficiency η_{ds} , the efficiency becomes $\eta_{ds,noRC}$ which is higher than η_{ds} in this example.

Efficiency scaling is done by multiplying all the values in the efficiency table of the unscaled map by the factor $f_\eta = \eta_{ds,noRC}/\eta_{ds,Map}$. At the map scaling point during off-design simulations, this yields the exact cycle design point efficiency if the Reynolds number index is the same as at the cycle design point. The peak efficiency is the highest value in the scaled map.

Note that the map scaling point (representing the cycle design point) is normally not at the location of the peak efficiency.

Mass flow scaling

Mass Flow scaling is like efficiency scaling. We have a value for the standard day corrected flow from the cycle design point $W_{Rstd,ds}$ and another value $W_{Rstd,ds,Map}$ from the unscaled map at its scaling point. Furthermore, we know the Reynolds correction for corrected flow. The map scaling is done by multiplying all the values in the mass flow table of the unscaled map by the factor $f_W = W_{Rstd,ds,RC}/W_{Rstd,ds,Map}$.

1.2.9 Advanced Map Scaling

The shape of a compressor map changes with the Mach number level (subsonic or transonic) and the design pressure ratio (compare Fig. 1.2-24 with Fig. 1.2-3, for example). Map shape variations are ignored if the simple pressure ratio scaling of the previous chapter is employed.

Reference [10] derives a more sophisticated scaling procedure from a statistical analysis of many compressor maps. It is based on a few characteristic map properties which describe the location of the peak efficiency line with a reference circle and the mass flow increase from surge to choke for constant speed.

There are three scaling steps:

1. The mass flow range for each of the speed lines is adjusted. The higher the design point pressure ratio, the steeper are the speed lines in the map and the range from surge to choke mass flow decreases.

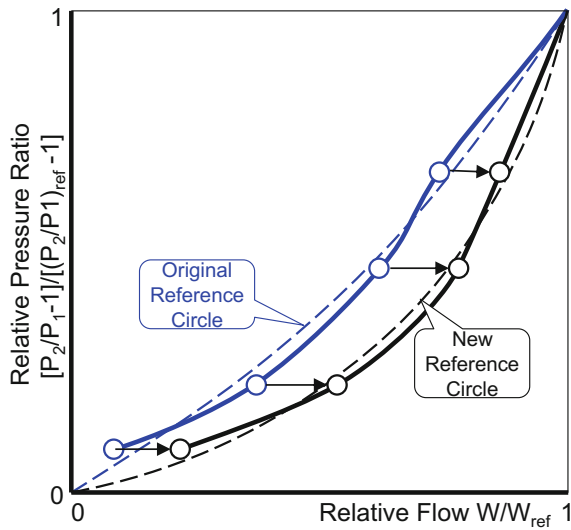


Fig. 1.2-53 The second scaling step [6]

2. In the second scaling step, the mass flow values are scaled for each speed line separately in such a way that the peak efficiency line is shifted according to the difference between the original and the new reference circles.
3. In the third step the speed values associated with the speed lines are modified in such a way that the correlation between pressure ratio and speed is correct.

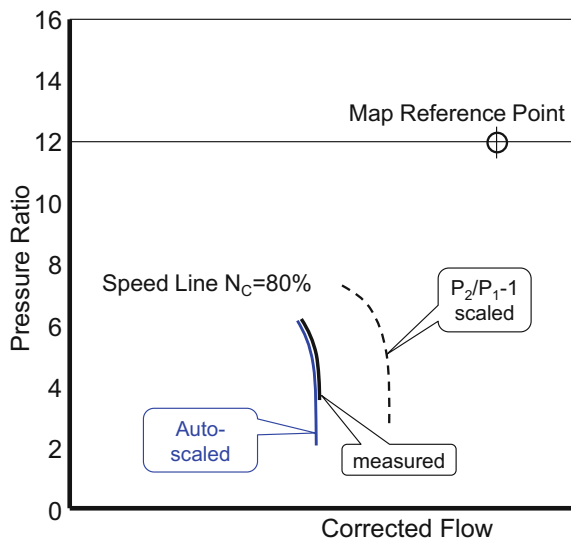


Fig. 1.2-54 Comparison of map scaling procedures (based on Ref. [10])

This map scaling methodology is implemented in the program Smooth C [11] as the automatic scaling option (Fig. 1.2-53).

Figure 1.2-54 highlights the variations caused by the two map scaling procedures with an example. The compressor design pressure ratio of the baseline map is 4, the scaled map is for pressure ratio 1. For comparison we use the measured 80% speed line from a compressor with the same pressure ratio 1. There is an excellent agreement between the measurement and the result from the scaling procedure suggested in Ref. [12].

Note that there is a remarkable mass flow difference between the simple P_2/P_{1-1} scaling result and that from the more sophisticated scaling procedure.

1.2.10 Map Scaling During Off-Design

Sometimes it is desirable to change the shape of a map during off-design simulations. This could be needed to match a compressor model to measured data or other trusted sources.

In the following, we assume that detailed results from the cycle design point agree very well with given data. Running the model in off-design mode at the same operating point produces exactly the same results. At other operating conditions, the simulation will usually not agree with the available data. So can we correct such a defect in the model?

The efficiency value read at part load conditions depends on the shape of the map. Perhaps, along a real operating line, the efficiency falls off more steeply than the calculation predicts. In Fig. 1.2-55, for example, the given efficiencies of points A and B are lower than those read from the original map (the dashed line). To match the simulation to the data from points A and B we can scale the tabulated

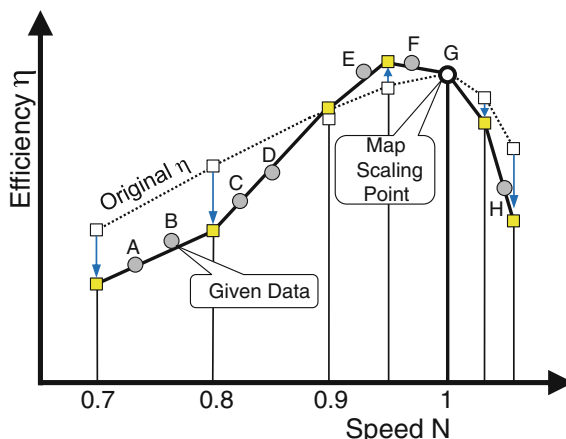


Fig. 1.2-55 Efficiency scaling along the operating line

efficiency values for the speed lines 0.7 and 0.8 downwards. Then, when we adjust the tabulated efficiency values for the speed lines 0.9 and 0.95 upwards, agreement is reached for points C, D, E and F also. Point G does not need to be adjusted because there we have matched our cycle design point to the data already. The efficiencies for the two speed values above 1.0 need to be scaled downwards to align point H.

GasTurb offers this sort of map scaling in the *Operating Line* window. Along an operating line, we can get perfect agreement between the available data and the simulation with this approach. When the data are not all on a single operating line, then the accuracy of the model depends not only on the corrected spool speed but also on how efficiency changes at constant speed from $\beta = 0$ to $\beta = 1$. If the deviations between data and model are more than tolerable, then the efficiency slope along the speed lines must be modified. Smooth C is a perfect tool for this job.

Two more deviations between model and data are possible in a map—for corrected flow and pressure ratio. We eliminate the differences by scaling the speed values.

Let us explain the process using Fig. 1.2-56. At point B, we know the measured values of pressure ratio P/P_B , mass flow W_B and speed N_{B1} . In our map, however, the speed value N_{B1} is significantly different. If we adjust the first two map speed values from 0.6 to 0.69 and from 0.7 to 0.79 respectively, the revised map contains the correct speed value for point B.

We can apply similar speed value corrections to all the other speed lines, except for the cycle reference point (the map scaling point). There the relative corrected speed is unity, *by definition*. This sort of speed calibration is offered in the *Operating Line* window of GasTurb. Any modified map should be checked thoroughly to ensure that it is in line with the laws of compressor physics! Smooth C is the perfect tool for this.

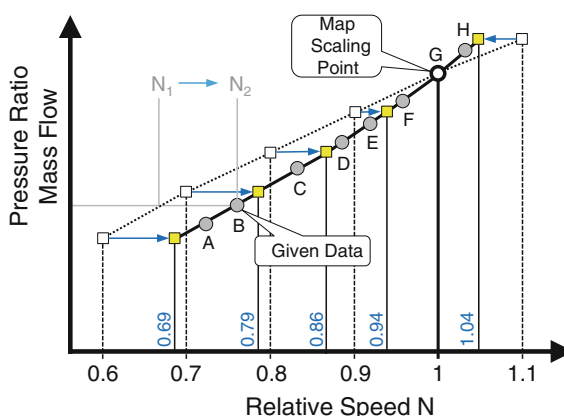


Fig. 1.2-56 Speed scaling along the operating line

1.3 Turbine Performance

The aerodynamic design of a turbine is usually carried out in a way that minimum losses occur at the design point operation. Gas generator turbines operate most of the time at the pressure ratio for which they were designed, but low pressure turbines of aircraft engines, for example, run during idle, take off and cruise at very different operating conditions; efficiency and corrected flow vary with pressure ratio and corrected speed. Additionally, changes in running tip clearances and Reynolds number affect the turbine performance.

The basis of the turbine performance description is a map which tabulates selected dimensionless parameters as functions of corrected spool speed. Possible parameters are pressure ratio, isentropic corrected work, effective corrected work, corrected torque, efficiency, isentropic and effective work parameter $\Delta H/U^2$. There is no generally accepted standard for which of these parameters should be employed. We describe and justify the methodology used in GasTurb in Sect. 1.3.2. Other approaches have their own advantages; there is no right or wrong.

First, we discuss some physical details of turbine performance, then we explain the data arrangement in the turbine map tables. All the explanations assume uncooled axial turbines; cooled turbine modeling is the topic of chapters D5 and D6. Some remarks about modeling variable area turbines and vaneless counter-rotating turbines conclude this chapter.

1.3.1 Operational Behavior

Figures 1.3-1 and 1.3-2 show two popular performance presentations of the same turbine map [13]. The first format is like that of a compressor map. The difference is in the x-axis parameter, which is the product of the relative corrected speed $N_L/\sqrt{\Theta_{45}}$ and corrected flow $W_{45}\sqrt{\Theta_{45}/\delta_{45}}$ in Fig. 1.3-1. If we had used corrected flow as the x-parameter as in a compressor map, the whole map would have collapsed into a very narrow region. The contour lines for efficiency would then be difficult to differentiate; such a map would not be suited for the illustration of turbine operating lines.

The second version of the map in Fig. 1.3-2, shows contour lines for efficiency and corrected flow in a plot with relative corrected speed as x-axis. The highest mass flow number in the map is declared 100% and the contour lines are for constant percentages of this mass flow. Corrected specific work is on the y-axis, but that is not compulsory; we could have used pressure ratio, as in the previous figure.

1.3.1.1 Corrected Mass Flow

The corrected mass flow of the turbine(s) is among the results of any cycle design calculation. It varies during off-design simulations according to the position of the

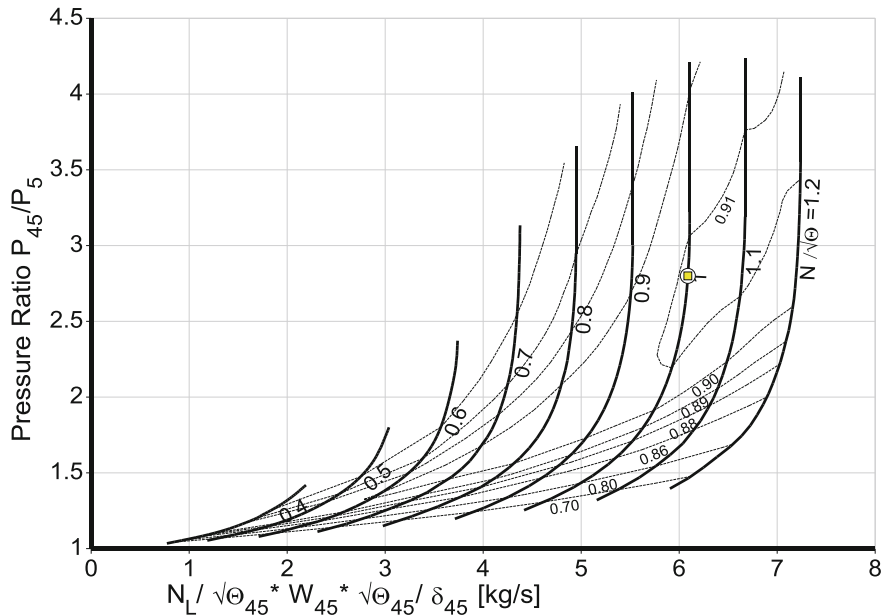


Fig. 1.3-1 Turbine map with pressure ratio and the product of corrected speed and flow as axes

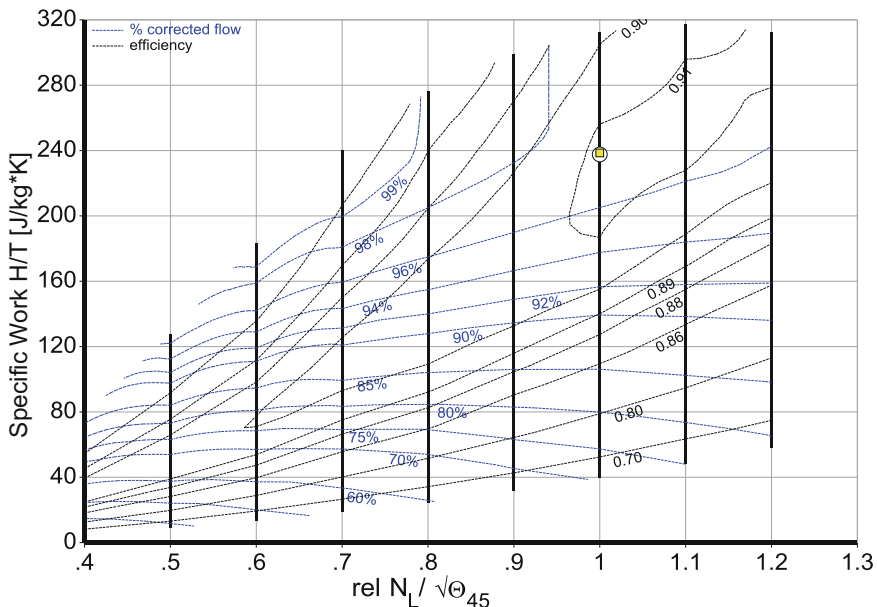


Fig. 1.3-2 Turbine map with corrected speed as x-axis and contour lines for corrected flow

operating point in the turbine map. In a turbofan, the corrected flow of the HP turbine determines the position of T_4/T_{25} lines and the corrected flow of the LP turbine controls the location of the operating line in the gas generator compressor map. The corrected flow of a turbine is to a certain degree more important than its efficiency.

Figure 1.3-3 shows the *reduced flow* $W\sqrt{T}/P$ as a function of turbine pressure ratio. On the speed line $N/\sqrt{\Theta} = 1.0$ the highest reduced flow value is 390 kg $\sqrt{K}/(s \text{ bar})$. This number is difficult to visualize in a meaningful way, but when we convert it to *corrected flow* $W\sqrt{\Theta}/\delta = 23.28 \text{ kg/s}$ we get an impression of the approximate size of this turbine.

If we expand the term $W\sqrt{T}/P$ by the square root of the gas constant R and flow area A , we get the following relation of reduced flow with Mach number and isentropic exponent γ :

$$\frac{W\sqrt{RT}}{AP} = \frac{M\sqrt{\gamma}}{\left(1 + \frac{\gamma-1}{2} M^2\right)^{\frac{\gamma+1}{2(\gamma-1)}}} \quad (1.3-1)$$

At the exit of the nozzle guide vane (NGV) the Mach number is highly subsonic or even sonic. In the range of Mach numbers between 0.9 and 1 the reduced flow per area varies by less than 1% and between Mach 0.8 and 1 only by 3.7%. Ignoring this small variation allows us to calculate the turbine throat area A . Inversely, the NGV throat area, A , defines the value of $W\sqrt{T}/P$, the so-called flow capacity of the turbine.

Whether the maximum corrected flow $W\sqrt{\Theta}/\delta$ in the map is a function of reduced speed $N/\sqrt{\Theta}$ or not depends on the aerodynamic design. Highly loaded single stage turbines often operate with a choked stator at design pressure ratio. In this case the corrected flow remains constant over a significant portion of the

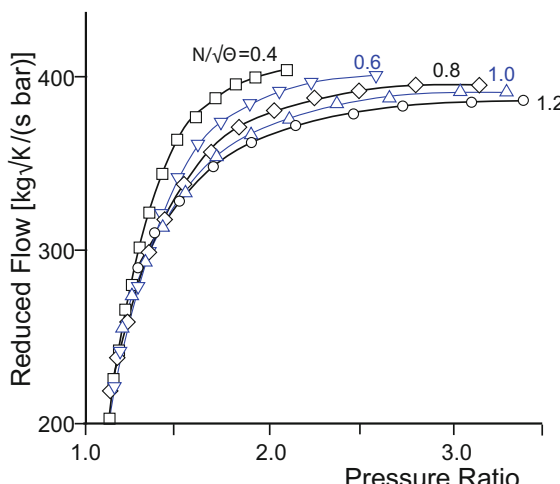


Fig. 1.3-3 Corrected flow of a low pressure turbine

map. If the NGV is unchoked, then the maximum corrected flow is a weak function of corrected speed. $W\sqrt{\Theta}/\delta$ increases slightly with decreasing $N/\sqrt{\Theta}$ as we see in Fig. 1.3-3.

Two gas properties appear in the equation above: the gas constant R and the isentropic exponent γ . Burning hydrocarbon fuels like Kerosene leads to combustion gases with the same gas constant as dry air. Humidity in the air, however, affects the gas constant. That is the reason why GasTurb interprets the corrected flow read from the turbine map as $W\sqrt{(R\Theta)}/\delta$.

What about the effect of varying isentropic exponent γ ? It changes significantly during operation, so if γ increases from 1.3 (high T_4) to 1.35 (low T_4), $W\sqrt{\Theta}/\delta$ increases by 1.3%. This increase in corrected flow is approximately compensated for by the thermal expansion of the hardware—and thus the throat area—which decreases when going from high to low T_4 . Ignoring the influence of γ on turbine flow capacity is a pragmatic solution to the theoretically unsolvable problem of considering γ changes exactly.

At high power, in the region of constant corrected flow in the map, the turbine map itself is not an important element of a precise performance model. That statement changes when we consider the exhaust gas temperatures at low power. Figure 1.3-4 illustrates how LP turbine corrected flow affects the position of the operating line of the gas generator compressor in a turbofan. The disagreement

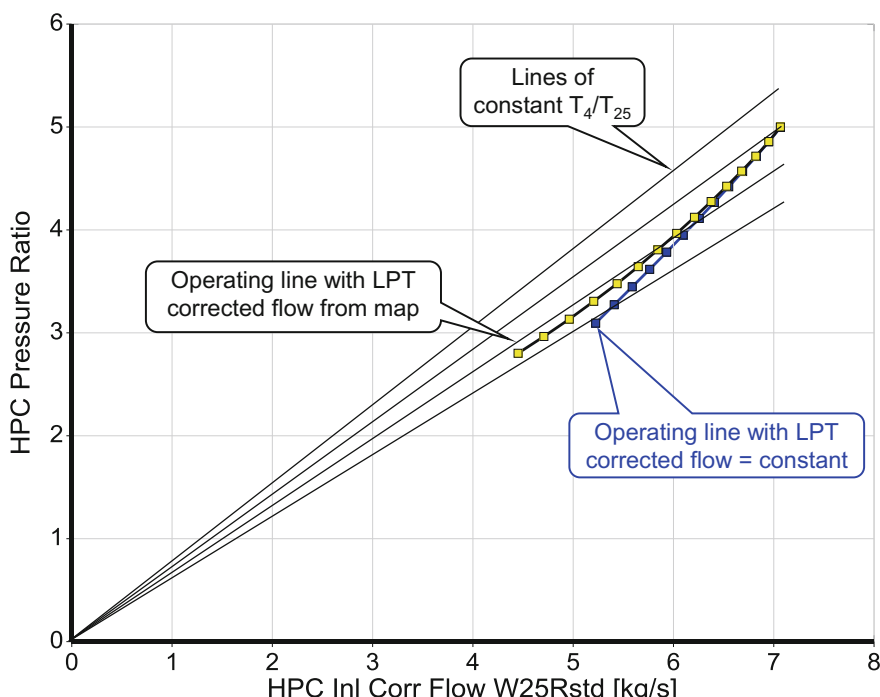


Fig. 1.3-4 Compressor operating line and T_4/T_{25} lines

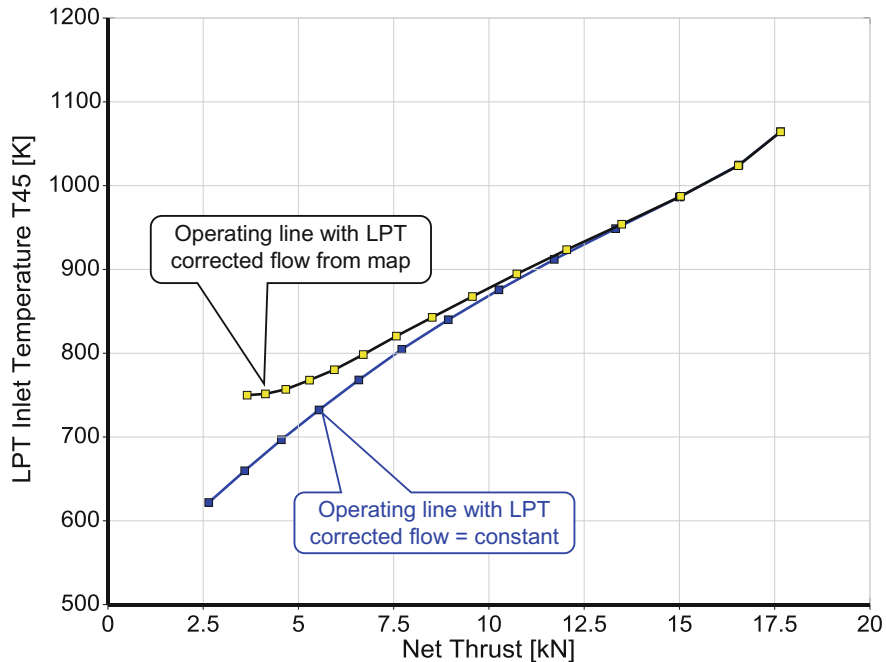


Fig. 1.3-5 Effect of LPT corrected flow on T_{45}

between the two operating lines seems to be insignificant, however, if we look at another version of the operating line in Fig. 1.3-5, we see LPT inlet temperature differences of more than 100 K at the low power end. The corrected flow reduction with pressure ratio in the LPT map becomes important if we want our performance model to line up with measured exhaust gas temperatures at low to medium power.

1.3.1.2 Specific Work

The sequence in cycle calculations is: compressors and combustor first then the turbine calculations. At a certain place in the code, we know how much turbine power we need, so we can use the corrected specific power $H/(R\Theta)$ and the corrected spool speed $N/\sqrt{R\Theta}$ as the coordinates for reading the turbine map. This approach works well in many cases, however, there are exceptions. There might be a region in the turbine map where the desired specific work is not achievable. Figure 1.3-6 shows measured data from Ref. [14] as an example.

How can we explain what happens inside the turbine when specific work no longer increases with pressure ratio? Let us address that for a single stage axial turbine operating at constant spool speed and constant inlet pressure. Within the normal range of the map, a decrease in turbine exit pressure leads to a change in the flow field in the turbine and to a higher power output.

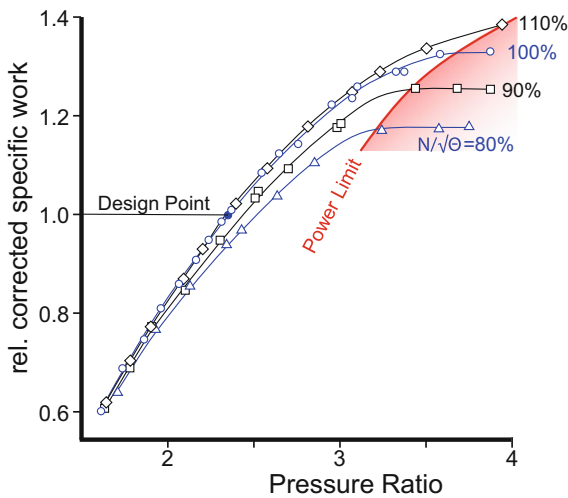


Fig. 1.3-6 Power limit in a turbine map

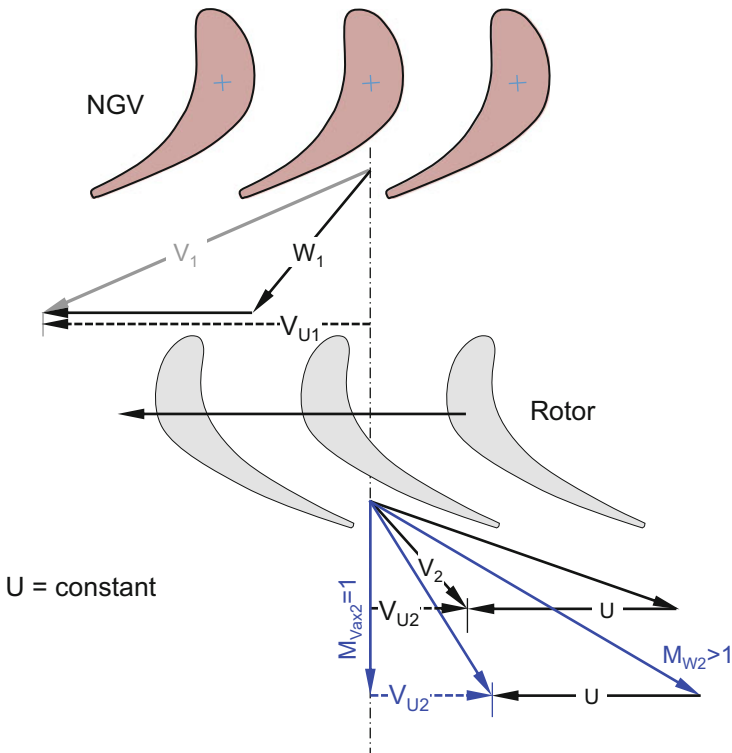


Fig. 1.3-7 Velocity triangles for the turbine power limit

The exit Mach number in the relative frame of the rotor becomes sonic at a certain pressure ratio. The circumferential component of the absolute rotor inlet velocity remains constant if we decrease exit pressure further. Nothing changes inside the turbine anymore, but the turbine outlet velocity increases until the turbine exit annulus chokes. That is the condition at which the circumferential component of the absolute velocity achieves its maximum value and the power limit of the turbine is reached (Fig. 1.3-7).

Our conclusion: do not use the current value of corrected specific work to read the turbine map. Guess the turbine pressure ratio and iterate it till the power balance between compressor and turbine is achieved.

1.3.1.3 Efficiency

Plotting efficiency against pressure ratio paints a picture with lines of very different curvatures at low and high corrected speeds, as seen in Fig. 1.3-8. Such a picture is not well suited for presenting operating points in a turbine map.

We can present the same information more clearly (more usefully) as contour lines which are functions of pressure ratio and corrected speed. We've done this in Fig. 1.3-9, where the map is supplemented with lines of constant blade speed/jet speed ratio (v), whose general format matches that of the efficiency contours quite closely.

So, what is v and how is it related to efficiency? It relates the rotor blade circumferential velocity U to the gas velocity V_{jet} . This is the gas velocity that would occur as the result of an ideal expansion from inlet total to exit static conditions

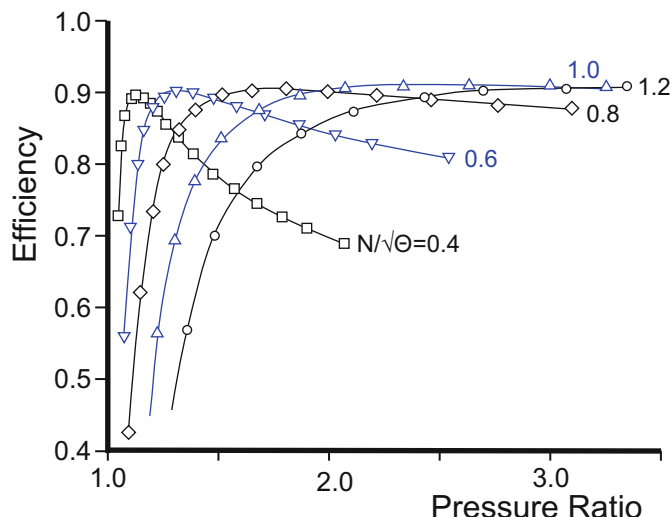


Fig. 1.3-8 Turbine efficiency

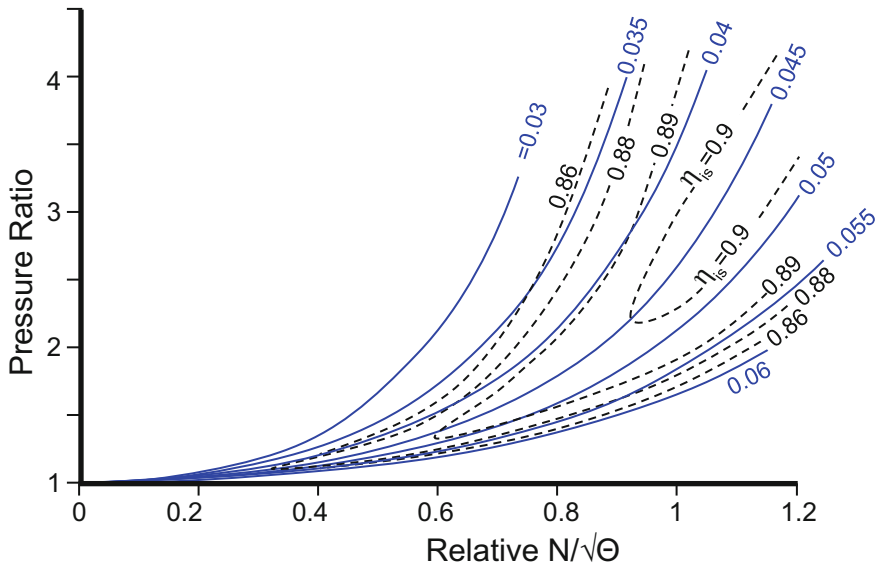


Fig. 1.3-9 Efficiency contours and lines of constant blade/jet speed ratio

through the turbine [14]. We simplify the relationship by calculating the jet velocity from the isentropic inlet total to exit total enthalpy change in the turbine as

$$V_{jet} = \sqrt{2(h(T_1) - h(T_{2,is}))} = \sqrt{2H_{is}} = \sqrt{2\frac{H}{\eta_{is}}} \quad (1.3-2)$$

Use of the *loading parameter* $\Psi = \Delta H/U^2$ leads to an informative formula for the blade/jet speed ratio:

$$v = \frac{U}{V_{jet}} = \sqrt{\frac{\eta_{is}}{2\Psi}} \quad (1.3-3)$$

We conclude—assuming constant efficiency—that a line of constant blade/jet speed ratio in a turbine map is a line of constant turbine loading. Do not be not confused by the labels on the v lines in Fig. 1.3-9; there, we have replaced the unknown value of U with the relative blade speed U/U_{ref} .

In Fig. 1.3-8, the curvature of the efficiency lines changes drastically with corrected speed. However, these curvature differences vanish if we plot efficiency against the blade/jet velocity ratio v , as in Fig. 1.3-10. The efficiency curves coalesce quite closely except at low values of v , and they all reach their maximum at the same blade/jet speed ratio of 0.045.

We can explain the basic shape of the efficiency lines by looking at the turbine velocity triangles. Figure 1.3-11 illustrates how these change during a speed

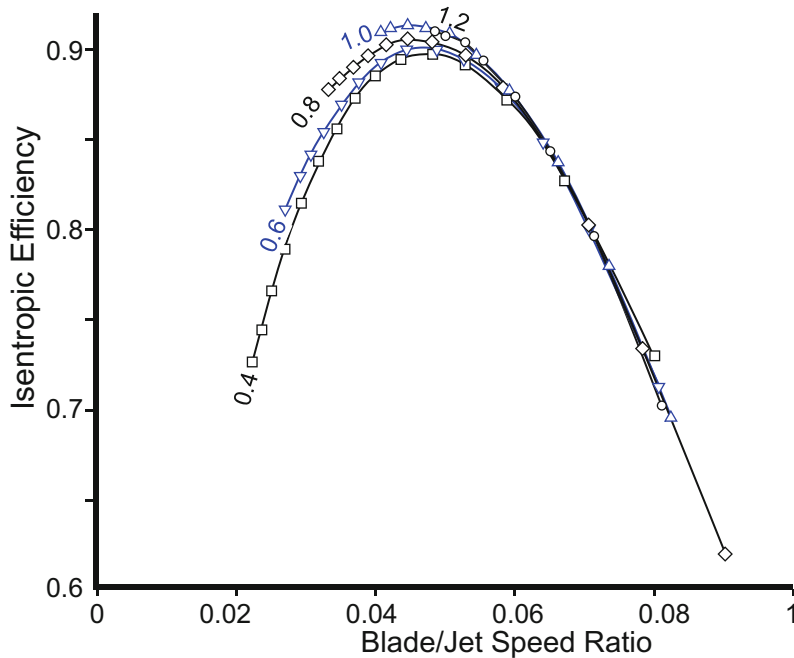


Fig. 1.3-10 Efficiency correlates with blade/jet speed ratio

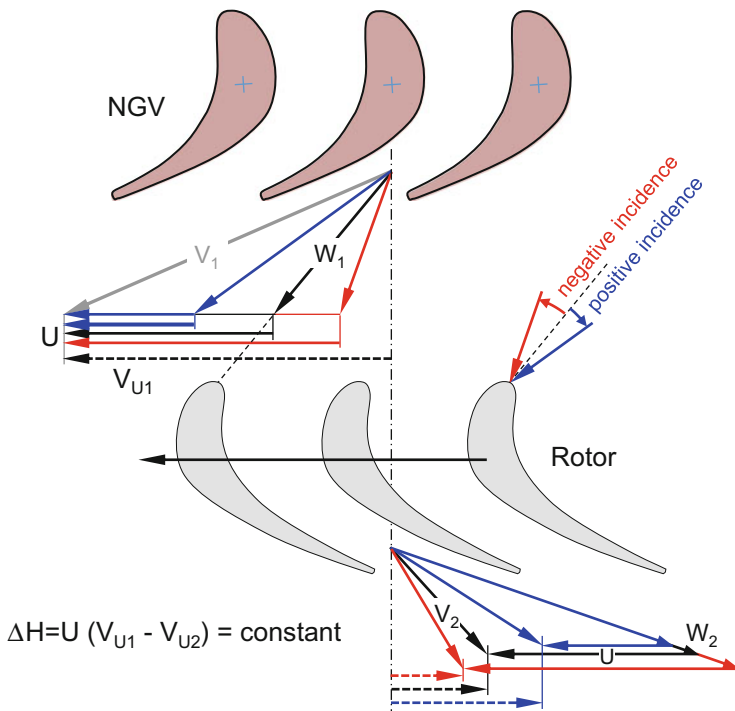


Fig. 1.3-11 Velocity triangles for changing blade speed at constant specific work

increase at constant specific work. According to Fig. 1.3-2 the corrected flow varies only a few percent during this thought experiment. NGV exit velocity V_1 and the circumferential component V_{U1} remain essentially constant.

Let us begin at low speed (the blue triangles in Fig. 1.3-11), where the turbine loading parameter $\Psi = \Delta H/U^2$ and the rotor blade angle of incidence are big, and the efficiency is poor. Both the loading and the incidence decrease when the turbine speeds up. At some speed, the incidence is zero, the profile losses are minimum, and the efficiency reaches its maximum (black triangles). Any further speed increase leads to negative incidence, and the consequent increase in losses causes the efficiency to fall again (red triangles).

The turbine loading parameter for maximum efficiency is linked directly to the turbine geometry; it is Ψ for zero incidence. $\Psi_{\min \text{ loss}}$ is given through the turbine design; it does not change during off-design operation. The efficiency maximum in Fig. 1.3-10 is at the same blade/jet speed ratio for every speed because $v_{\min \text{ loss}}$ and $\Psi_{\min \text{ loss}}$ are connected through Eq. (1.3-3).

1.3.1.4 Exit Angle

Turbine exit flow angle is of interest in a performance program especially if the losses of the component downstream of the turbine depend on it. An example are the strut losses of struts downstream of the power turbine in a helicopter engine, because there the flow angle can vary over a very wide range.

Exit angle may be tabulated or calculated from a known blade metal angle, the axial velocity component and circumferential speed.

1.3.2 *The Map Preparation Program Smooth T*

Smooth_T is a tool for converting turbine data to a format suited for performance programs; it is similar to the compressor map generation program Smooth_C. The input consists of measured or calculated data, either as tables or as pictures. The program makes a proposal for constant speed lines passing through the given points. The user checks if these lines make sense in terms of physics and corrects them if necessary. In the end, all turbine performance parameter correlations should be smooth—hence the program name, Smooth T.

The output consists of many rectangular tables with the same number of points for all speed lines. These tables are suitable as input for programs simulating gas turbine or turbocharged piston engine performance. Smooth T can also be used to check the quality of turbine maps. The program offers many different views of the data; it is easy to see whether the map is a reasonable description of turbine physics or not.

Smooth T is especially helpful if the map includes extreme operational conditions like pressure ratios less than unity or very low corrected spool speeds. Look again at Fig. 1.3-10: All the efficiency curves are consistent in their individual

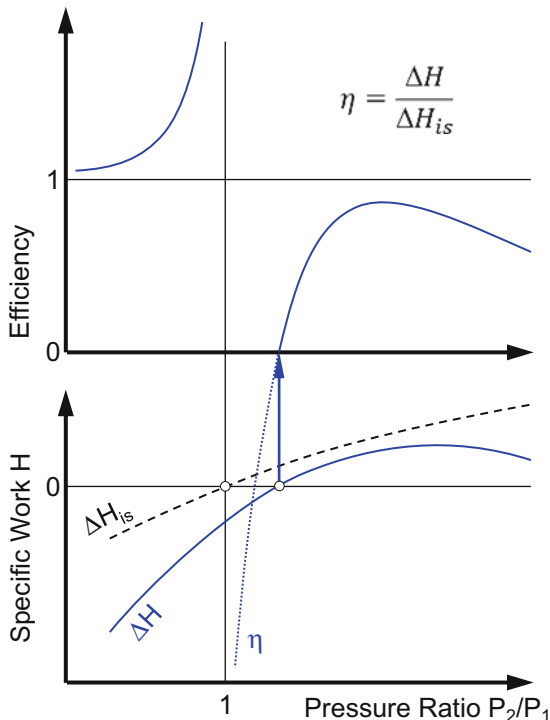


Fig. 1.3-12 Efficiency around pressure ratio 1

profiles and in their variation with blade/jet speed ratio. Seemingly all efficiency display problems are resolved.

However, that is not the case: the jet velocity V_{jet} is zero if turbine pressure ratio is 1.0. We are unable to calculate a blade/jet speed ratio if $P_1/P_2 = 1$. See what happens with efficiency in Fig. 1.3-12: When pressure ratio is 1.0, efficiency jumps from $+\infty$ to $-\infty$ because the isentropic specific work ΔH_{is} is zero.

Do we really need a turbine map which covers pressure ratios less than unity? Normally not—it only has meaning if the task is to simulate windmilling of an aircraft engine. We avoid a lot of numerical pain if we restrict our turbine performance map tables to the region where P_2/P_1 is greater than unity.

The low spool speed region of the turbine performance map is another problem area. Frequently, neither measured nor calculated data exist, and we need to extrapolate the map. A special case is the zero speed line. If we knew its shape, then we could convert the extrapolation problem to an interpolation problem. Fortunately, we know quite a lot about the zero speed line!

Imagine a special turbine test with the rotor blocked. The starting condition is $P_1/P_2 = 1$ and $W\sqrt{T_1}/P_1 = 0$. As soon as we apply a pressure ratio $P_1/P_2 > 1$ gas will begin to flow through the non-rotating turbine. The vanes and blades create a

pressure loss which is proportional to dynamic head q , as long as the Mach number is lower than say 0.6 everywhere in the turbine. Since q/P_1 is proportional to $(W\sqrt{T_1}/P_1)^2$, it follows that

$$\frac{P_1}{P_2} = 1 + k_p \left(\frac{W\sqrt{T_1}}{P_1} \right)^2 \quad (1.3-4)$$

Our first finding is: for moderate Mach numbers (moderate reduced flow), the zero speed line is a parabola passing through the point $P_1/P_2 = 1$, $W\sqrt{T_1}/P_1 = 0$. Increasing the pressure ratio increases the turbine entry Mach number until finally, somewhere in the turbine, a local Mach number becomes sonic. Continuing to increase the pressure ratio will no longer affect the corrected flow, and in the corresponding region of the map, the zero speed line is horizontal, if the map is presented as $W\sqrt{T_1}/P_1 = f(P_1/P_2)$.

What can we say about the force needed to prevent the rotor from rotating? Think of a single airfoil; the lift force is proportional to dynamic head. Consequently, torque (the product of the force and a characteristic length) divided by P_1 is proportional to reduced flow squared.

$$\frac{Trq}{P_1} = k_{Trq} \left(\frac{W\sqrt{T_1}}{P_1} \right)^2 \quad (1.3-5)$$

Dividing both sides of this equation by reduced flow yields a linear relationship between reduced torque $Trq/(W\sqrt{T_1})$ and reduced flow $W\sqrt{T_1}/P_1$.

$$\frac{Trq}{W\sqrt{T_1}} = k_{Trq} \frac{W\sqrt{T_1}}{P_1} \quad (1.3-6)$$

An educated guess regarding the shape of the zero speed line is a great help for extending the turbine map to the low speed region. Figure 1.3-13 shows that the lower parts of the $N/\sqrt{\Theta}$ lines 0.4, 0.6 and 0.8 are essentially straight lines that are equally spaced. Estimating the zero speed line is easy: it must be parallel to the other speed lines and pass through the origin. The line for $N/\sqrt{\Theta} = 0.2$ is an interpolated line between $N/\sqrt{\Theta} = 0$ and $N/\sqrt{\Theta} = 0.4$.

What can we do with our knowledge of $Trq/(W\sqrt{T_1})$? Remember that the product of torque Trq and spool speed N (i.e. the turbine power) is equal to the product of mass flow W and the enthalpy drop ΔH . From that correlation we can write

$$\frac{Trq}{W\sqrt{T_1}} \frac{N}{\sqrt{T_1}} = \frac{\Delta H}{T_1} \quad (1.3-7)$$

We can then calculate turbine efficiency from $\Delta H/T_1$ and pressure ratio (except for $P_1/P_2 = 1$) for any corrected speed.

Smooth T offers many options for smoothing the speed lines. Adjust efficiency as a function of pressure ratio or specific work in the standard operation region;

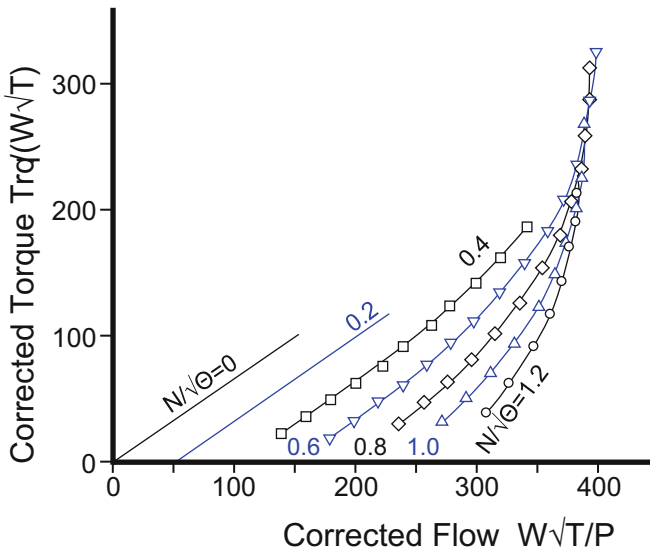


Fig. 1.3-13 The speed line zero helps extrapolating a map

adapt torque lines in exotic map areas. The quality of the result depends somewhat on the user's knowledge of turbomachinery fundamentals and his or her confidence in applying it. Without this knowledge, however, you'll have a bit of a problem in understanding gas turbine performance anyway.

1.3.3 *Turbine Map Format*

Smooth T generates performance tables in many different formats. Generating maps in the format required by GasTurb is one of the output options. Why is a GasTurb turbine map so special anyway?

The efficiency contour lines in a pressure ratio—speed plot, define a landscape with a broad top region at high speed. This high efficiency region, becomes smaller in the mid speed range and deforms to a narrow ridge at low speed (Fig. 1.3-14). Small differences in pressure ratio coincide with big changes in efficiency in this map region. Capturing the details of the efficiency ridge at low speed accurately would require a huge number of equally distributed pressure ratio grid points. Using the rectangular grid marked with the gray circles in Fig. 1.3-14 would lead to severe accuracy problems in the low speed area. Moreover, we would have to store much useless data—especially in the region of high pressure ratios and low speed. We never need to know the turbine performance in that part of the map when we simulate standard gas turbine performance.

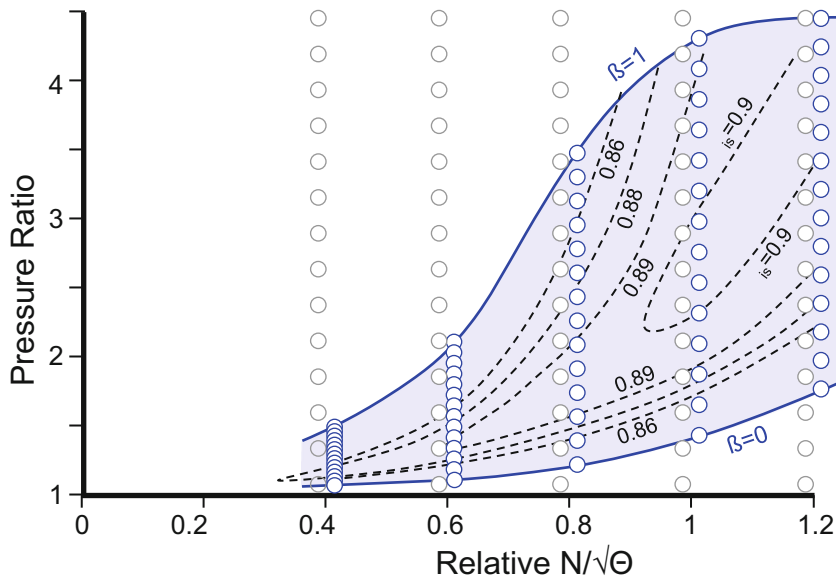


Fig. 1.3-14 The boundaries $\beta = 0$ and $\beta = 1$

We can achieve high accuracy with a minimum number of grid points if we focus on the region of interest, which is the peak efficiency zone. The blue circles in Fig. 1.3-14 are distributed in such a way that we get adequate accuracy for any point of interest in the map.

1.3.3.1 Beta Lines

Let us add two pressure ratio boundaries to our turbine map. We call the low pressure ratio boundary the $\beta = 0$ line and the high pressure boundary the $\beta = 1$ line. All turbine operating points we ever expect to be of interest should be between the two β lines.

The map boundaries (the $\beta = 0$ and $\beta = 1$ lines) are defined in two tables as functions of corrected speed between the minimum and the maximum pressure ratios. Two further tables contain mass flow and efficiency in the same format as in compressor maps: corrected speed is the parameter and β the argument.

Beta is one of the standard iteration variables in the off-design cycle calculation. Its value is known at the beginning of the turbine calculation. Both map boundary pressure ratio tables are read using the corrected speed $N/\sqrt{\Theta}$, which is also known. Linear interpolation between the two pressure ratio boundaries ($\beta = 0$ and $\beta = 1$) yields the turbine pressure ratio. Reading the corrected mass flow and efficiency tables provides the other two turbine performance parameters.

1.3.3.2 Turbine Map Scaling

The true turbine map is rarely known outside the engine designer's community. We have to use a map from a similar turbine and scale it. The question is where to place the map scaling point, the point at which perfect agreement between the cycle design point and the map is established? That depends on the expected position of the operating line.

Gas generator turbines of multi-spool engines mostly run at constant pressure ratio; the operating line in the turbine map is short. We cannot make a big error when we set the map scaling point somewhere in the middle of the high efficiency area. Alterations to gas generator turbine efficiency originate primarily from changes in running tip clearance, not from locating the operating point incorrectly in the map.

In multi-spool engines, the operating lines in the low pressure turbine maps (Fig. 1.3-15) are much longer than in the gas generator turbine map. Their shape and orientation depend on the application of the gas turbine. The power turbine of a turboshaft engine runs at constant spool speed if it drives a helicopter rotor, a propeller or a generator. The corrected spool speed $N_L/\sqrt{\Theta_{45}}$ increases when power is reduced because the turbine inlet temperature T_{45} decreases. The map scaling point should be set to a pressure ratio slightly above the peak efficiency region. Such a selection benefits specific fuel consumption at part load.

The operating line of a low pressure turbine in a turbofan runs more or less parallel to the peak efficiency ridge in the map. In general, efficiency will drop

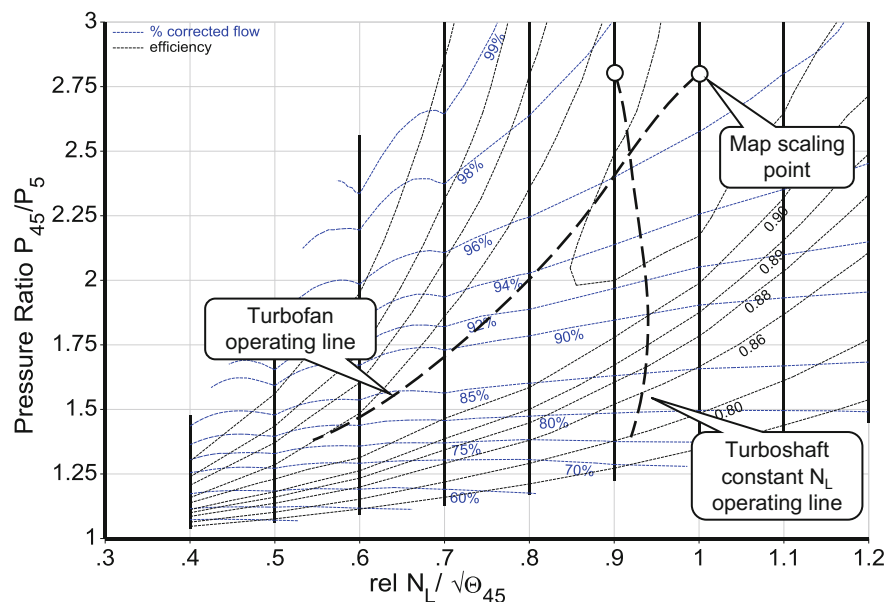


Fig. 1.3-15 Setting the turbine map scaling point

towards part load. This effect is driven, at least partly, by changes in running tip clearance. Reynolds number effects also can play a role.

For an LPT in a turbofan, our advice is to set the map scaling point in the peak efficiency region. If this selection does not yield the expected efficiency drop, adjust either the tip clearance model or the Reynolds correction.

The position of the map scaling point affects not only efficiency but also the part load corrected flow, which in turn determines the exhaust gas temperature, followed by the output shaft power, at low thrust. This effect was explained in the discussion of Figs. 1.3-4 and 1.3-5. The corrected flow will remain constant or decrease only slightly if we set the map scaling point to a higher map pressure ratio point. If we select a lower pressure ratio map scaling point, then we get a steeper decrease of the corrected flow with pressure ratio. This results in higher exhaust gas temperature in the low thrust (low power) region.

1.3.4 Tip Clearance

Not all modifications to efficiency and corrected flow alterations emanate from operating point shifts in the turbine map. Accurate aircraft engine performance simulations employ map correction terms for differences in turbine running tip clearance and Reynolds number. The latter are discussed in Chap. 4.

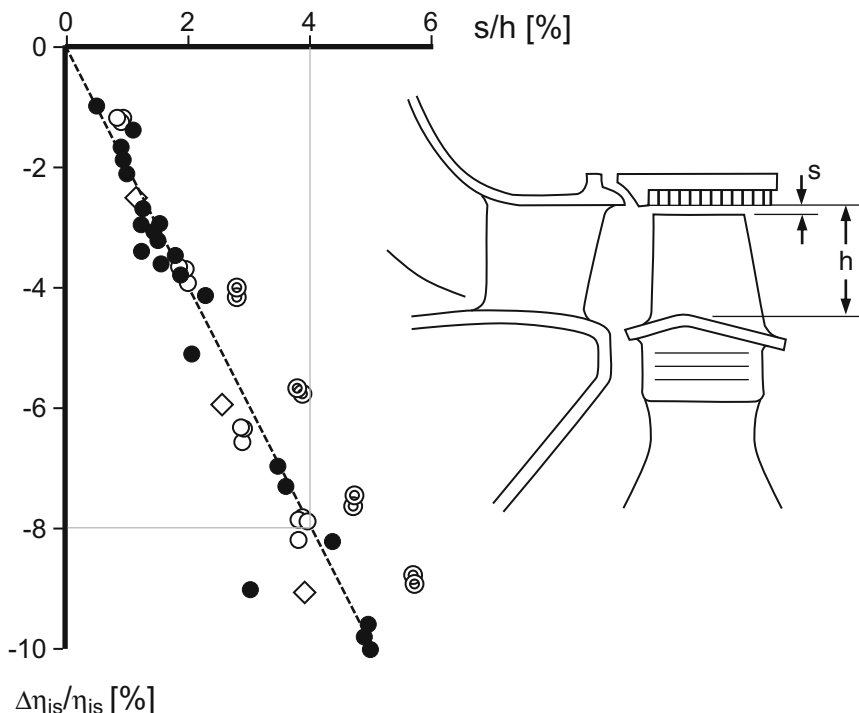


Fig. 1.3-16 Tip clearance effect for unshrouded turbines [15]

Tip clearance alterations are larger in turbines than in compressors due to the higher temperatures, which result in greater thermal expansion of the parts. The effects of tip clearance on efficiency differ for unshrouded and shrouded turbines.

Reference [15] contains data for unshrouded turbines; the efficiency loss is 2% for 1% increase in relative tip clearance. This information is presented in Fig. 1.3-16. Reference [16] compares the effect of tip clearance between shrouded and unshrouded turbines and Fig. 1.3-17 contains those results in the same format as used in Fig. 1.3-16. The data for unshrouded turbines is common to both studies. We conclude that the sensitivity of shrouded turbines to changes in tip clearance is about half that of unshrouded turbines.

If we observe significant variations in gas generator turbine efficiency in measured data which we want to reproduce with a model, then we need to simulate tip clearance as a function of spool speed or temperature. The operating line in the turbine map is very short and the efficiency value read from the turbine map is virtually constant. Changes in efficiency can only come from tip clearance alterations and not from either steep efficiency slopes in the map or Reynolds number effects.

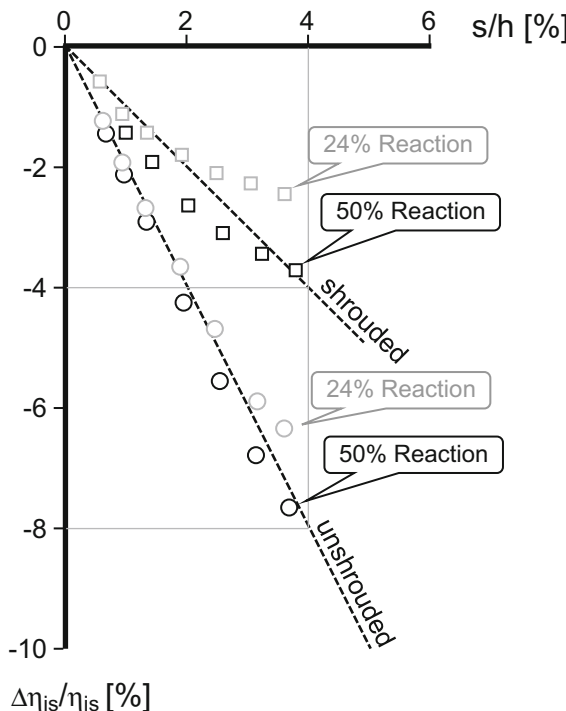


Fig. 1.3-17 Tip clearance effect for shrouded and unshrouded turbines [16], adapted

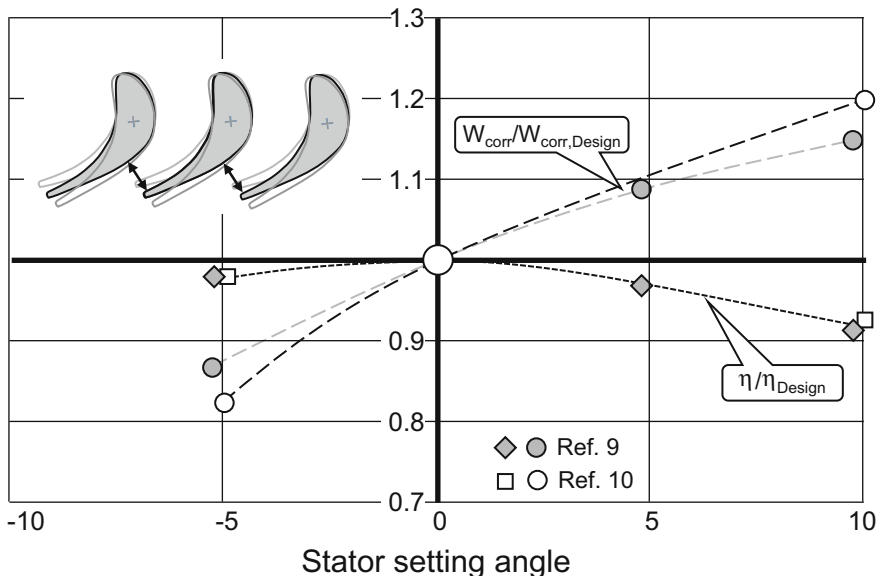


Fig. 1.3-18 Effect of stator setting angle on flow capacity and efficiency of variable geometry turbines

1.3.5 Variable Geometry Turbines

Variable area turbines are used in gas turbines with a heat exchanger. Closing the nozzle guide vane at part load shifts the compressor operating line towards higher T_4/T_2 values. This shift results in a higher heat exchanger inlet temperature and thus more heat transfer from the hot to the cold side. Part load specific fuel consumption improves significantly.

Figure 1.3-18 shows experimental results from [17] and [18], normalized by the design point conditions. Corrected flow increases nearly linearly when plotted against stator stagger angle. Efficiency falls off on both sides of the design point.

Rigorous modeling of a variable area turbines requires a set of turbine maps. If maps for different stator setting angles are unavailable, then we scale the map for the design point stator setting and apply modifiers for efficiency and flow capacity like those shown in Fig. 1.3-18.

1.3.6 Vaneless Counter-Rotating Turbines

The term *vaneless counter-rotating turbine* is somewhat misleading. Counter-rotating of a single turbine is a contradiction in itself. Actually, there are two turbines in sequence, one normal turbine which is composed of the NGV and the

first rotor, followed by a second turbine which consists only of a rotor turning in the opposite direction.

We can describe the performance of the first turbine with its map, nothing special about that. The problem is the performance characterization of the second rotor. The map of this vaneless turbine changes with the flow angle downstream of the first rotor. This flow angle is firmly connected with the operating point of the first turbine; we can superimpose contour lines corresponding to a range of first rotor exit flow angle onto the first turbine's map, see Fig. 1.3-19.

For rigorous modeling of the performance of the second rotor, we need another set of maps. How to get this? If we want to base the maps on measurements from a test rig, then we need a device which allows us to set the inlet flow angle. We could also calculate the set of maps by assuming a variable geometry turbine with a lossless inlet guide vane, for example.

The last thought leads to the idea of using a single map for the nominal performance of the second rotor, together with modifiers for corrected flow and efficiency. Correlations between the exit flow angle of the upstream turbine and the modifiers shown in Fig. 1.3-18 might be a good guess of what happens in two counter-rotating turbines in sequence.

Sometimes it is desirable to program the counter-rotating turbine as a single object. Reference [19] describes this approach in which a set of turbine maps is employed. The corrected spool speed ratio is the key parameter in the set of turbine performance tables.

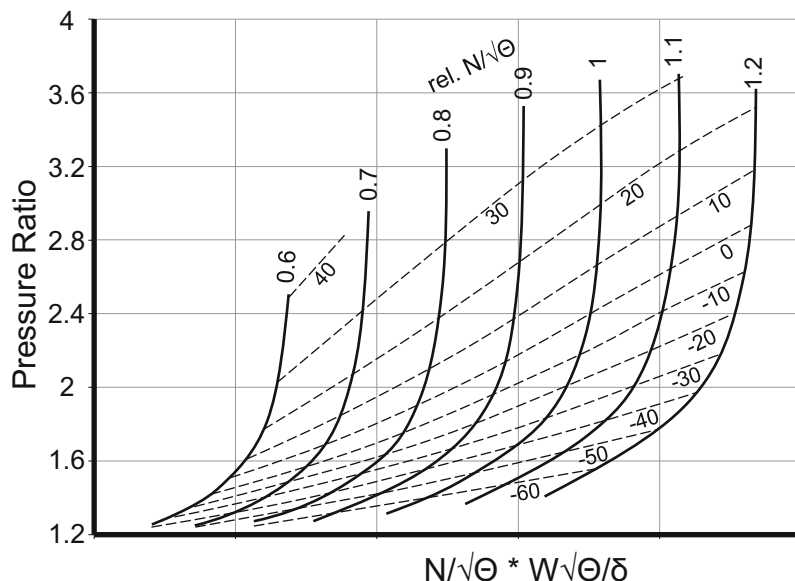


Fig. 1.3-19 Turbine map with exit flow angle contour lines

1.4 Combustor

Two main characteristics of the combustion process affect the performance model of the cycle: the efficiency as it converts the chemical energy of the fuel into thermal energy in the gas path and the pressure loss incurred as it does so. The chemical processes involved may be left to combustion specialists and we will outline a few basics and discuss a typical approach used in preliminary engine design. The methodology used for conventional single-staged combustors is described. Recent developments in combustion technology, known variously as staged and lean-burn combustors, are not considered as they do not affect performance significantly.

1.4.1 Efficiency

Combustion efficiency is the ratio of the fuel needed for an ideal combustion process to that used in a real one. The ideal case assumes chemical equilibrium at the prevailing conditions pressure P_3 and temperature T_4 in the burner. Nowadays, the efficiency of combustion chambers exceeds 99.9% for high power operating conditions. At part load near idle and at very high altitudes, however, the burner efficiency can deviate noticeably from 100%.

Lefevre and Ballal [20] present combustion efficiency as a function of the parameter Θ for a fuel/air ratio of 0.01, which is typical for idle conditions. The dashed line Fig. 1.4-1 is a guess for the efficiency at take off fuel/air ratio of 0.025. The operating line of this combustor begins at take off with an efficiency of 0.99 and ends at idle with the very low value of 0.3.

By modern standards, the general efficiency level of this combustor is very poor. Inefficiency is nothing less than incomplete combustion, it produces mainly carbon monoxide CO and unburnt hydrocarbons, in addition to other atmospheric contaminants. Therefore, much better efficiency values are needed for low emissions combustors.

Data from a modern combustor is shown in Fig. 1.4-2: Combustion efficiency versus loading parameter Θ [21]. Note that in this figure the loading parameter Θ is defined slightly differently from the relationship associated with Fig. 1.4-1

$$\Theta = \frac{P_3^{1.8} e^{T_3/300K} Vol}{W_{31}} \quad (1.4-1)$$

Combustion efficiency in this figure is not only a function of the Θ parameter; it depends on the fuel/air-ratio also. Along an operating line from Take Off to Idle, both Θ and fuel/air ratio decrease. At top of climb conditions for a commercial turbofan, the loading parameter is typically half of the Take Off value, while the fuel/air ratio is about the same. Since the efficiency slope is very flat at higher Θ values, the altitude and the sea level operating lines are almost the same. Therefore,

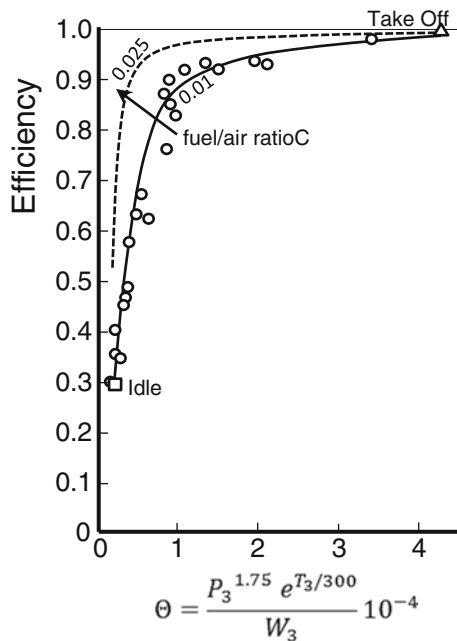


Fig. 1.4-1 Combustion efficiency correlation [20], modified

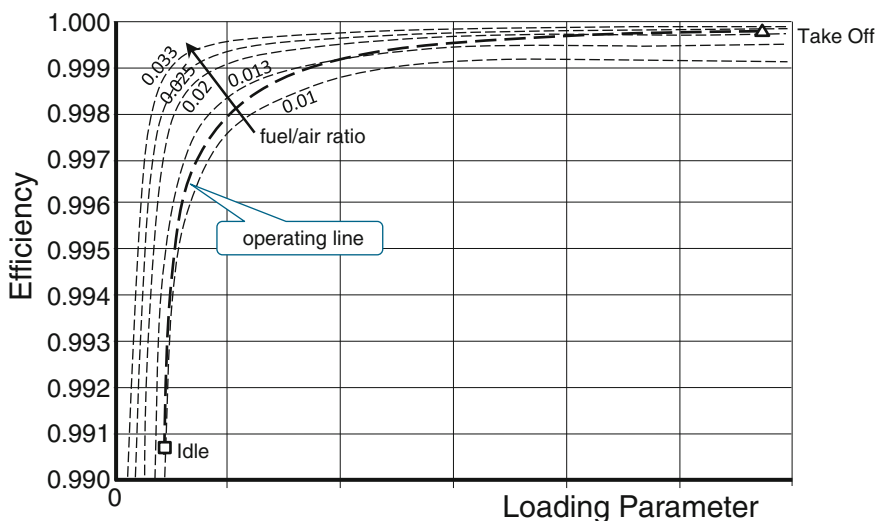


Fig. 1.4-2 Combustion efficiency versus loading parameter Θ [21]

to simplify the performance model, we ignore the difference and in the following outline, we make combustion efficiency a function of Θ only.

In Figs. 1.4-1 and 1.4-2, efficiency does not change much in the region of the high loading parameters, but does so very rapidly in the idle region. We could tabulate such a characteristic, but there is a better solution. Reference [22] shows how a simple correlation can describe the combustion efficiency changes along the operating line. Instead of the loading parameter Θ , this correlation uses the inverse, the burner loading $\Omega = 1/\Theta$:

$$\Omega = \frac{W_{31}}{P_3^{1.8} e^{T_3/300K} Vol} \quad (1.4-2)$$

Reference [7] also mentions burner loading, but defines it slightly differently as

$$\Omega = \frac{W_{31}}{P_3^{1.8} 10^{0.00145(T_3-400)} Vol} \quad (1.4-3)$$

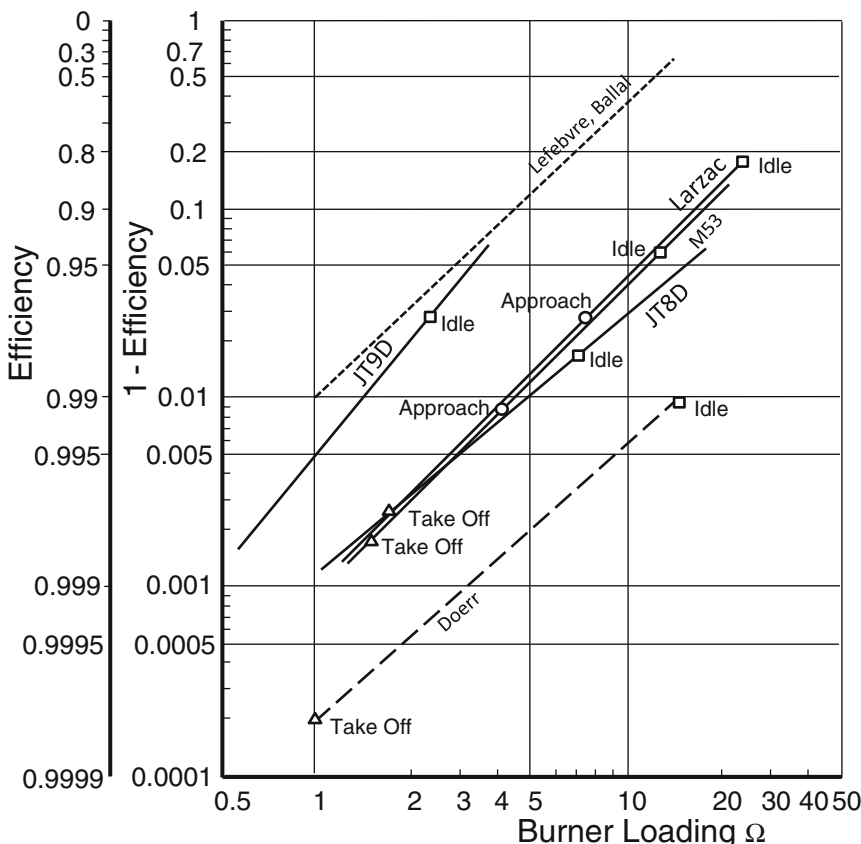


Fig. 1.4-3 Combustion efficiency versus burner loading Ω

Using Ω has the advantage that experimental data from various combustors collapse on straight lines when plotted in a graph with $\log(\Omega)$ as x-axis and $\log(1 - \eta)$ as y-axis, as demonstrated in Fig. 1.4-3. Solid lines are from Ref. [22], the dashed lines represent the data in Figs. 1.4-1 and 1.4-2.

We can describe burner efficiency with the linear formula:

$$\log(1 - \eta) = A + B * \log(\Omega) \quad (1.4-4)$$

The slope of the line defines how burner efficiency changes with loading Ω during off-design operation. Therefore, we call B the burner part load constant, which is in the range from 1.34 to 1.94 in Fig. 1.4-3. The average value of ≈ 1.6 is suited as a default value if no specific knowledge about the burner design is available.

So how do we get a value for A ? That's easy if we relate burner loading to that at the cycle design point:

$$\frac{\Omega}{\Omega_{ds}} = \frac{W_{31}P_{3,ds}^{1.8}e^{\frac{T_{3,ds}}{300K}}}{W_{31,ds}P_3^{1.8}e^{\frac{T_3}{300K}}} \quad (1.4-5)$$

We define this ratio the relative loading and the equation for burner efficiency at part load becomes

$$\log(1 - \eta) = A + B \log(\Omega/\Omega_{ds}) \quad (1.4-6)$$

Since $\log(\Omega/\Omega_{ds}) = 0$ at the cycle design point, the constant A is equal to $\log(1 - \eta_{ds})$. So the efficiency of an average combustor can be calculated for any operating condition from

$$\log(1 - \eta) = \log(1 - \eta_{ds}) + B \log(\Omega/\Omega_{ds}) \quad (1.4-7)$$

The shape of the part load characteristic, plotted as a function of the loading parameter Θ in Fig. 1.4-4, depends mainly on the efficiency at the cycle design point. Figure 1.4-5 shows the influence of the part load constant B for a combustor with a design point efficiency of 0.999.

The accuracy of this simple combustion efficiency model is fully sufficient for performance simulations.

1.4.2 Pressure Loss

First, let us clarify the bookkeeping of the total pressure loss in a combustion chamber. The most accurate burner inlet pressure measurement is obtained with rakes positioned in the diffuser exit plane. If we declare this total pressure to be the

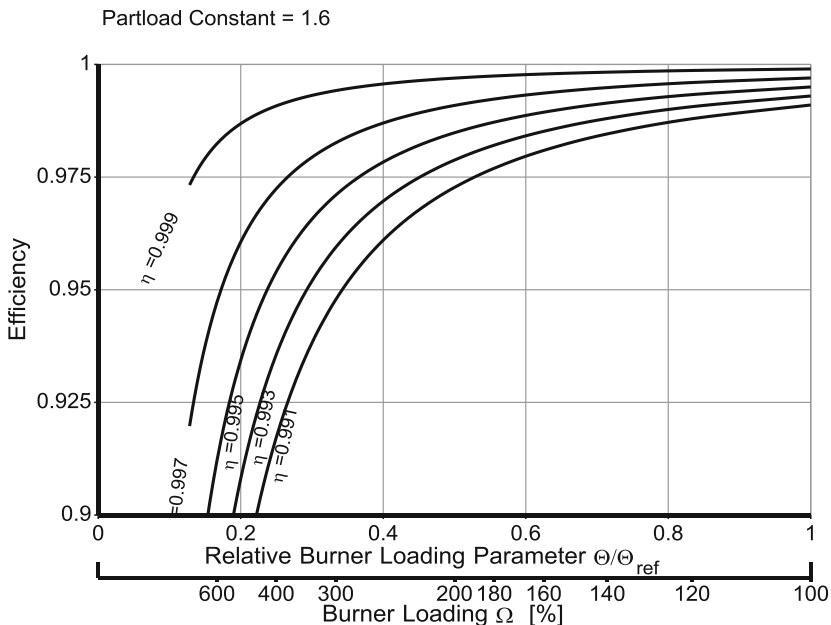


Fig. 1.4-4 Combustion efficiency for part load constant $B = 1.6$

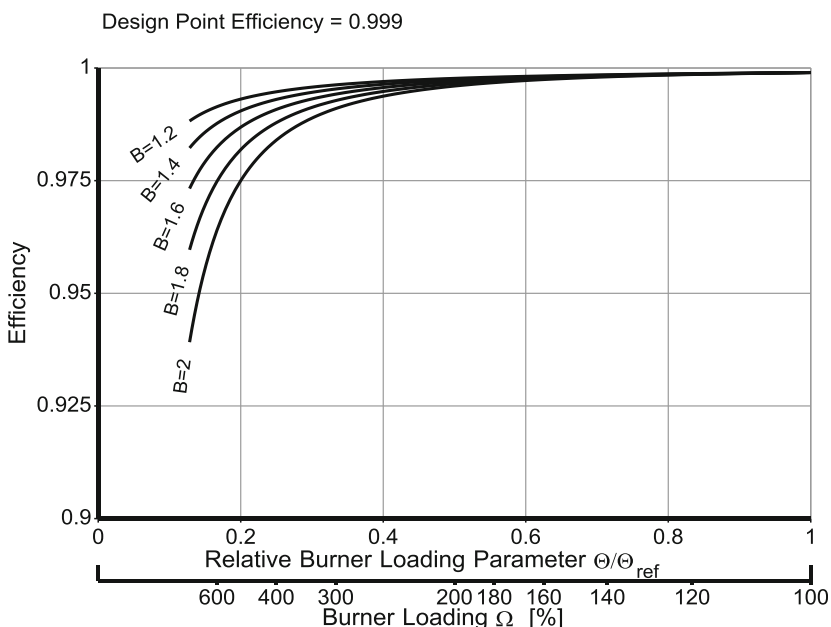


Fig. 1.4-5 Combustion efficiency = f (part load constant B)

burner inlet pressure P_3 , we burden compressor efficiency with the friction and boundary layer separation losses within the diffuser. The compressor designers will not like that, but separating these losses from those in the combustor, based on measurements within an engine, is not practical.

The dump loss downstream of the diffuser exit plane is the first element of the combustor pressure losses. More pressure loss contributions are caused by cooling the flame tube and by turbulent mixing in the dilution zone. Together, these losses make up the so-called cold pressure losses. Their magnitude varies during off-design operation in proportion to the corrected inlet flow W_{3Rstd} squared [7].

References [7, 20], as well as other books, refer to further sources of pressure loss elements, the so-called fundamental pressure loss. This loss has nothing to do with friction and flow separation, it is a basic feature of thermodynamics. Heat addition in a frictionless pipe of constant area accelerates a gas that enters the pipe with a subsonic Mach number. The amount of heat which can be added is limited by sonic flow at the pipe exit.

High Mach numbers at the pipe entry, combined with maximum heat addition, result in total pressure losses of the order of 15–20%. In the combustor, however, we encounter extremely low Mach numbers. Reference [23] shows data from many engines, the burner reference Mach number is found to be in the range from 0.012 to 0.04. According to Fig. 1.4-6, the fundamental pressure loss for such low Mach numbers is less than 0.15%.

The temperature ratio T_4/T_3 does not change very much during off-design operation. Therefore, for a given engine, the fundamental pressure loss varies less

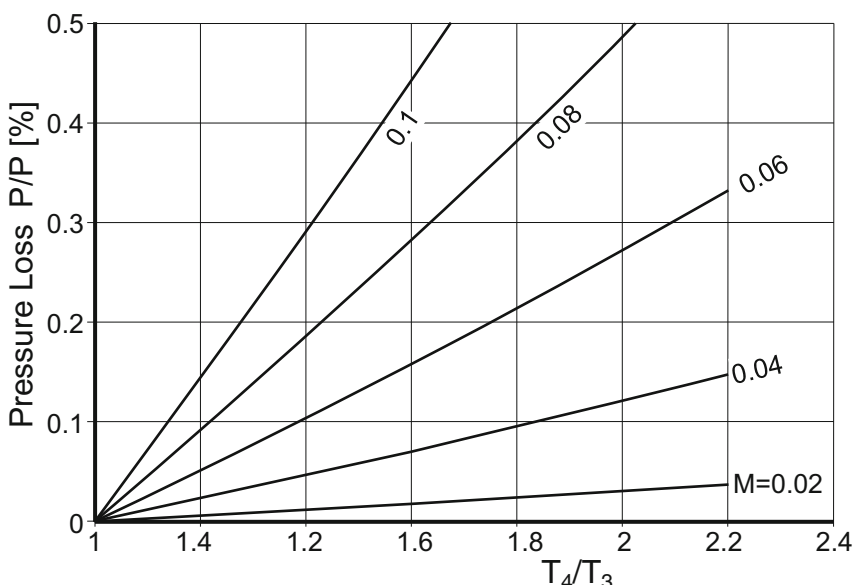


Fig. 1.4-6 Fundamental pressure loss in combustors

than 0.02% from idle to maximum power. In the light of the uncertainty in the value of the cold pressure loss, it is not worthwhile to consider the hot pressure loss in combustors, at least not at the preliminary design level.

Note that this is very different in afterburners because there the inlet Mach number is approximately 0.2, a hundred times bigger than in the main combustor.

1.4.3 Temperature Distribution at the Combustor Exit

At the combustor outlet the temperature is neither circumferentially nor radially constant. Each fuel injector is visible as a hot spot, and the flame tube cooling results in lower than average temperatures at hub and tip, see Fig. 1.4-7.

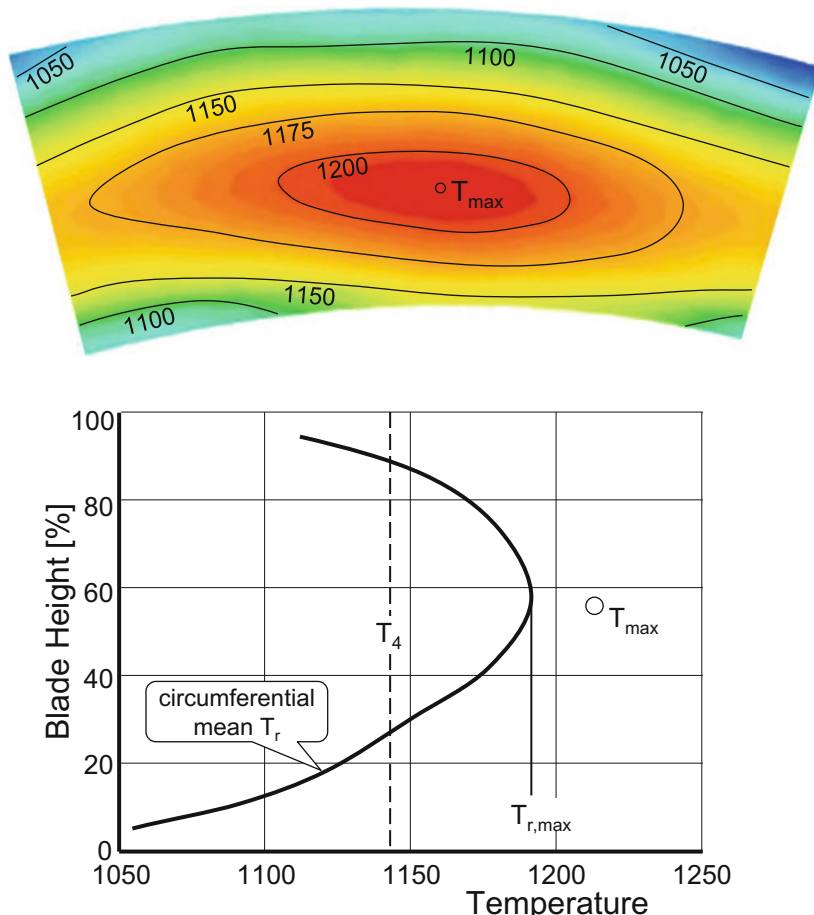


Fig. 1.4-7 Combustor exit temperature distribution (adapted from Ref. [46])

The turbine inlet guide vane must endure the hot spot temperature T_{max} ; the turbine blade sees a lower temperature for two reasons. Firstly, the circumferential temperature variations are averaged out. Secondly, the relative total temperature in the rotating system is about 10% lower than the absolute rotor inlet temperature.

Two factors describe the magnitude of the temperature variation at the combustor exit. The Overall Temperature Distribution Factor OTDF and the Radial Temperature Distribution Factor RTDF. They are defined as

$$\text{OTDF} = \frac{T_{max} - T_4}{T_4 - T_3} \quad (1.4-8)$$

and

$$\text{RTDF} = \frac{T_{r,max} - T_4}{T_4 - T_3} \quad (1.4-9)$$

OTDF is also called the pattern factor and RTDF is known as profile factor [20].

1.5 Mixer

Mixing the hot and cold exhaust jets of a turbofan can enhance the performance of an exhaust system, and hence that of the engine, in several ways. Firstly, it can increase thrust, provided the total pressures at the core and bypass exits are similar and the mixing process is not accompanied by significant pressure losses. The turbofan cycle needs to be especially tailored for the mixer, since the optimum fan pressure ratio for a single mixed stream is lower than that for separate hot and cold streams. The mixer is a highly efficient way to transfer energy from the hot to the cold stream avoiding losses in the LPT and fan. We should note that at cruise speeds a small increase in gross thrust gives a much bigger percentage increase in net thrust.

Secondly, mixing can lead to less noise at take off. This, along with reductions in emissions, has become a crucial mandate for engine designers in the last two or three decades because of increased traffic from urban airports. Mixing is very effective in this regard because jet noise is proportional to the eighth power of jet velocity and the mixed velocity is significantly less than that of the hot core stream. Mixing effectiveness is likely to be higher in low bypass ratio turbofans than in high bypass ratio types, so it is very appealing for business jets and military aircraft. In the latter, mixing is necessary for afterburning engines, where it enables a single reheat system to be used. Additionally, the reduction in exhaust temperature corresponds to a reduced infrared signature for stealth considerations.

Mixing is used to advantage quite frequently in high bypass ratio turbofans for long range commercial operations, which leads us to consider a disadvantage. Mixers are quite heavy! In trans-oceanic flights where the overall fuel burn is great

and the vehicle itself is heavy, the additional weight and cost of mixers to save fuel can be justified easily in trade studies. The use of the CFM56-5C2 on the Airbus A340 is an example.

1.5.1 How Mixing Increases Thrust

Before we discuss the performance of real mixer-nozzle combinations, let us look at a simplified graphic example as an illustration of how mixing increases thrust. Let us assume a bypass ratio of unity and equal pressures in the core and bypass duct prior to mixing. Then

$$W = W_{hot} = W_{cold} \quad (1.5-1)$$

and

$$P_{hot} = P_{cold} \quad (1.5-2)$$

The temperature of the core stream is considerably higher than that of the bypass stream, so their enthalpy values are similarly different.

If the hot and cold streams are each expanded completely to the prevailing ambient pressure so that $P_{s9} = P_{amb}$, the changes in enthalpy will be equal to the respective changes in kinetic energy. The total thrust will then be given by

$$F_{unmixed} = F_{hot} + F_{cold} = W\sqrt{2}\left(\sqrt{\Delta H_{hot}} + \sqrt{\Delta H_{cold}}\right) \quad (1.5-3)$$

If the hot and cold streams are mixed completely

$$H_{mixed} = \frac{(H_{hot} + H_{cold})}{2} \quad (1.5-4)$$

and the total thrust will then be

$$F_{mixed} = 2W\sqrt{2\Delta H_{mixed}} \quad (1.5-5)$$

Figure 1.5-1 shows the enthalpy-entropy diagram for separate hot and cold streams as well as a mixed stream for the current situation. It may be seen that the mixed specific enthalpy is the average of the hot and cold stream values, but because the isobars diverge as enthalpy increases, the mixed stream kinetic energy (ΔH_{mixed}) is closer to that of the hot stream than to the cold stream and twice its value is always greater than the sum of hot and cold. Therefore

$$F_{mixed} = 2W\sqrt{2\Delta H_{mixed}} > W\sqrt{2}\left(\sqrt{\Delta H_{hot}} + \sqrt{\Delta H_{cold}}\right) = F_{unmixed} \quad (1.5-6)$$

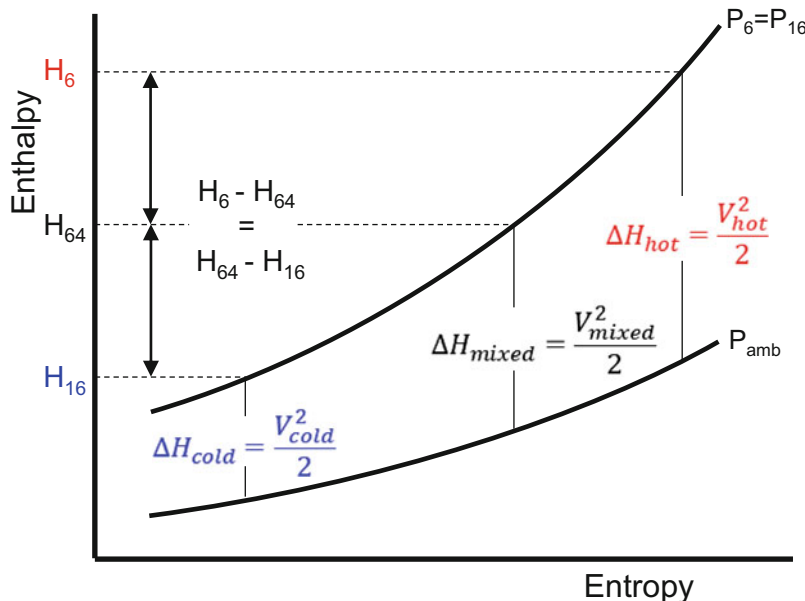


Fig. 1.5-1 Enthalpy-entropy diagram for unmixed and mixed nozzles

This reasoning can easily be applied to more practical cases where the hot and cold flows are not equal.

In the following we discuss the performance of mixer-nozzle combinations as they are used for business jets and commercial airliners.

1.5.2 *Mixer Geometry*

For simulating the mixer of a turbofan in a performance program we need a simple geometry model like the one sketched in Fig. 1.5-2. Mixer inlet conditions are those at the core exit (station 6) and the bypass exit (station 16). Pressure losses caused by the chute are bookkept between stations 6 and 63 in the hot core stream and 16 and 163 in the cold stream.

The essence of the mixer algorithm is the assumption that the mixing happens in a frictionless duct of constant cross section. The figure shows that the process occurs between the inlet stations 63 and 163 and the mixing plane station 64. The nozzle throat is located further downstream at station 8.

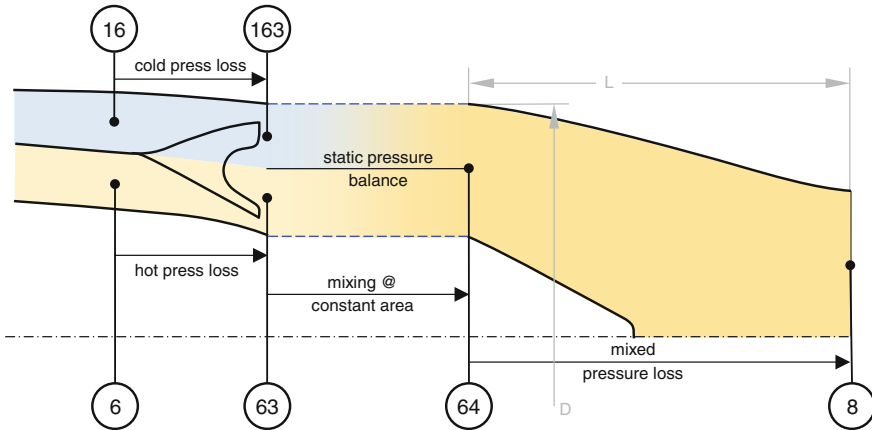


Fig. 1.5-2 Mixer nomenclature

1.5.3 Fully Mixed Thrust

The ideal mixer has no pressure losses from stations 6 to 63, 16 to 163 and 64 to 8. At station 64 both streams are fully mixed and expand through the nozzle as a single stream without any losses. The total pressure and temperature of the cold stream in station 163 are the same as at station 16 and the equivalent is true for the hot stream.

The following laws of physics apply:

Conservation of mass

$$W_{64} = W_{63} + W_{163} \quad (1.5-7)$$

Conservation of energy

$$W_{64}H_{64} = W_{63}H_{63} + W_{163}H_{163} \quad (1.5-8)$$

Conservation of momentum

$$W_{64}V_{64} + P_{s64}A_{64} = W_{63}V_{63} + P_{s63}A_{63} + W_{163}V_{163} + P_{s163}A_{163} \quad (1.5-9)$$

The sum of the cold and hot mixing areas is equal to the combined area and the static pressures of both streams are equal:

$$A_{64} = A_{63} + A_{163} \quad (1.5-10)$$

$$P_{s63} = P_{s163} \quad (1.5-11)$$

The ideal gas equation applies to all three mass flows:

$$W = A\rho V = A \frac{P_s}{RT_s} V \quad (1.5-12)$$

This system of equations can only be solved by iteration but doing that within a spreadsheet calculation is cumbersome.

Fully mixed gross thrust can be defined in two ways. Reference [24] calculates it as an ideal expansion from station 64 to ambient conditions, i.e. $F_{G64} = W_8 * V_9$. This implies an ideally-matched convergent-divergent nozzle with variable area ratio A_9/A_8 . In practice, for a high nozzle pressure ratio, A_9/A_8 —as well as the nozzle length and weight—becomes excessive and the ideal thrust is unattainable, except with a 2D nozzle design.

We use the ideal thrust of a convergent nozzle as reference because such nozzles are used in most practical mixer applications. Thus, the fully mixed thrust is given by:

$$F_{G64} = W_8 V_8 + A_8 (P_{s8} - P_{amb}) \quad (1.5-13)$$

1.5.4 Unmixed Thrust

We call the gross thrust which could be developed by expanding the hot flow from station 6 through an ideal convergent nozzle the hot thrust $F_{G,\text{hot}}$. Similarly we call the thrust of the cold stream expanded from station 16 the cold thrust $F_{G,\text{cold}}$. The unmixed combined thrust is simply the sum of $F_{G,\text{hot}}$ and $F_{G,\text{cold}}$.

1.5.5 Mixer Efficiency and Mixer Velocity Coefficient

Mixer efficiency expresses the actual gross thrust gain as a fraction of the fully-mixed gross thrust gain:

$$\eta_{mix} = \frac{F_G - F_{G,\text{unmixed}}}{F_{G,\text{fullymixed}} - F_{G,\text{unmixed}}} \quad (1.5-14)$$

Instead of mixer efficiency, a thrust coefficient is often used and this is the ratio of the actual thrust to the ideal thrust. The ideal thrust may be that from either an ideal convergent nozzle or an ideal convergent-divergent nozzle where the flow expands to ambient pressure.

$$C_{FG} = \frac{F_{G,\text{measured}}}{F_{G,\text{fullymixed,ideal}}} \quad (1.5-15)$$

In Ref. [24] the ideal case is defined as the thrust achievable with an isentropic expansion to ambient conditions. This thrust is higher than that of a lossless convergent nozzle when the nozzle pressure ratio is supercritical. Losses are expressed by the velocity coefficient C_V :

$$C_V = \frac{F_{G,\text{measured}}/W_8}{V_{\text{ideal}}} \quad (1.5-16)$$

This definition of thrust coefficient is adequate in the selection of a nozzle type but is unsuitable as a measure of mixer performance. If the nozzle pressure ratio is higher than the critical value, then the thrust coefficient will be less than unity even if the mixer—nozzle combination has no losses at all!

We measure the quality of the mixer—nozzle combination by the mixer efficiency defined in Eq. (1.5-14). The ideal gross thrust is that of a lossless convergent nozzle.

1.5.6 Thrust Gain Potential

Now we will examine, in a more general way, the thrust gain due to mixing that is achievable theoretically.

Figure 1.5-3 shows the cruise thrust gain potential of a frictionless mixer in a turbofan for a commercial airliner. The values of gross thrust gain on the x-axis do not look impressive. However, if we express the thrust benefit as a percentage of net thrust, then we get more attractive numbers because

$$\frac{\Delta F_G}{F_N} = \frac{\Delta F_G}{F_G - W_2 V_0} > \frac{\Delta F_G}{F_G} \quad (1.5-17)$$

From this equation, it is obvious that a mixer improves the thrust at take off ($V_0 = 0$) much less than it does at cruise. The percentage SFC improvement at take off is also much less than the percentage improvement in cruise SFC.

The main driver for the mixer benefit is the temperature ratio T_6/T_{16} . Mixing brings no benefit when the temperatures of the core and bypass streams are equal.

Mixing the two streams becomes less attractive when the bypass ratio is high. The gross thrust gain potential decreases with increasing bypass ratio. Mixers for high bypass ratios are inherently heavy.

The Mach number in the mixing plane, M_{64} , plays a secondary role, as we can see from Fig. 1.5-4. Low mixer Mach numbers yield the biggest thrust gain. However, they also imply bigger mixer areas A_{64} , which lead to bigger nacelle diameters and higher engine and installation weights.

At a given value of P_{16}/P_6 greater than unity, the optimum mixer velocity ratio V_{163}/V_{63} is unity. In contrast, when P_{16}/P_6 is less than unity, $V_{163}/V_{63} = 0.3$ is a good choice.

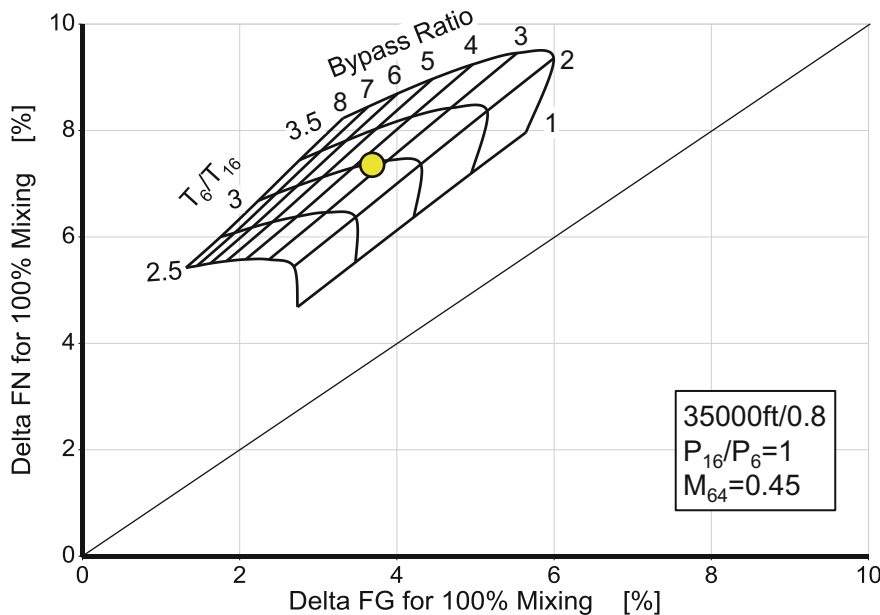


Fig. 1.5-3 Thrust gain for fully mixed conditions, no friction pressure loss

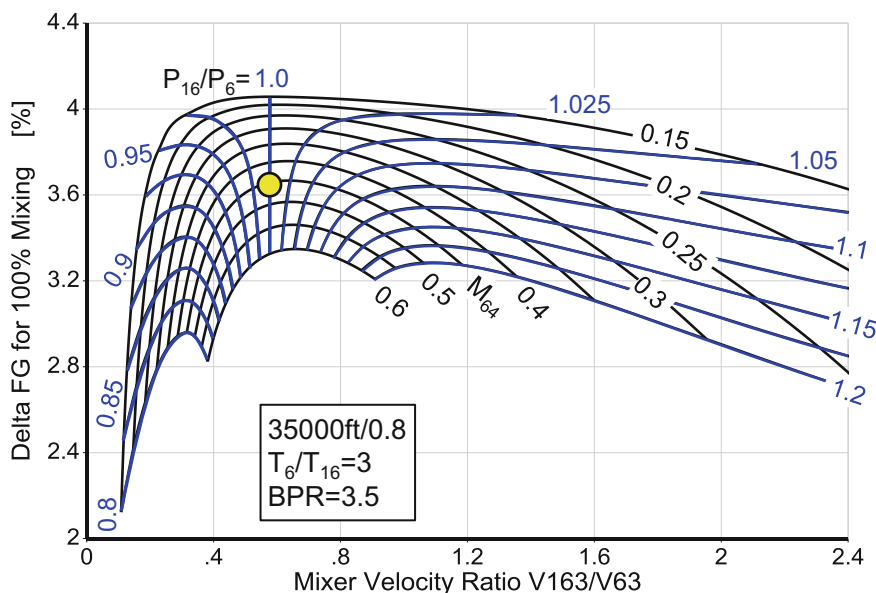


Fig. 1.5-4 Mixer Mach number and P_{16}/P_6 effect

1.5.7 Practical Mixers

The theoretical thrust gain from mixing the two streams of a turbofan looks attractive. How much of this improvement potential can we exploit? Figure 1.5-5 shows how mixer chutes look in a real engine. Per Ref. [24], such mixers achieve a mixing efficiency between 60 and 80%.

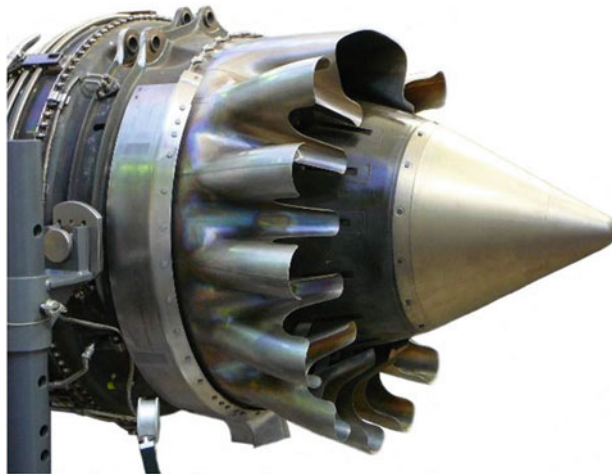


Fig. 1.5-5 Mixer chute example

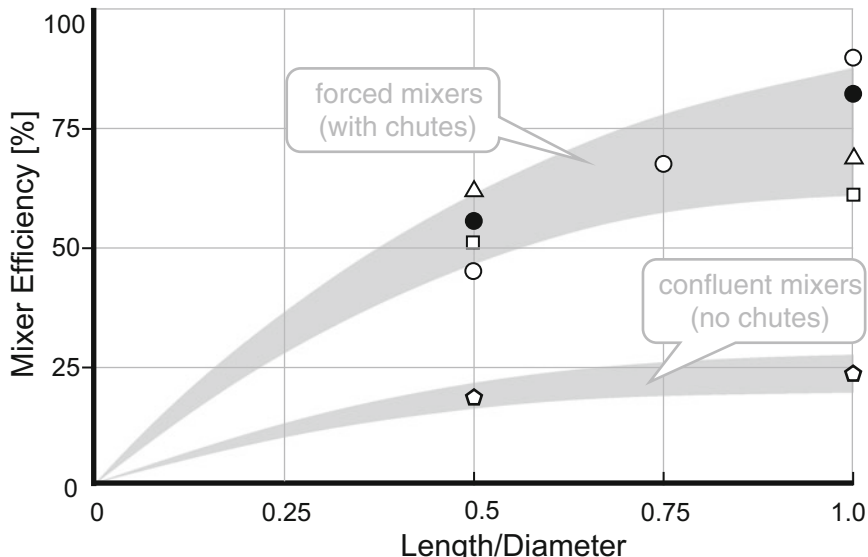


Fig. 1.5-6 Mixer efficiency for various chute designs (data from Ref. [24])

Mixers without chutes (*confluent mixers*) reach 20–30% mixing efficiency. Higher length/diameter ratios enhance mixing, as we see from Fig. 1.5-6.

1.5.8 Mixer Design Example

Mixers are often used with small engines for business jets. For example, a cycle optimization study for such an engine yields the following mixer inlet conditions.

Table 1.5-1 Mixer inlet conditions @ 40,000 ft/0.8

Station	Mass flow (W)	Total temperature (K)	Total pressure (kPa)
16	11.2	294	46.9
6	3.14	801	43.1

What is the best mixer geometry for this cycle? The only variables which we can play with under the boundary conditions of the cycle are the Mach number in the mixing plane M_{64} and the mixer efficiency. The simplest mixer design consists of a conical splitter between the fan and primary streams and Fig. 1.5-6 indicates a mixer efficiency of up to 25%.

Better mixer efficiencies require chutes and sufficient tailpipe length downstream of the mixing plane but it should be borne in mind that increasing the wetted surface results in more friction loss, i.e. more total pressure losses.

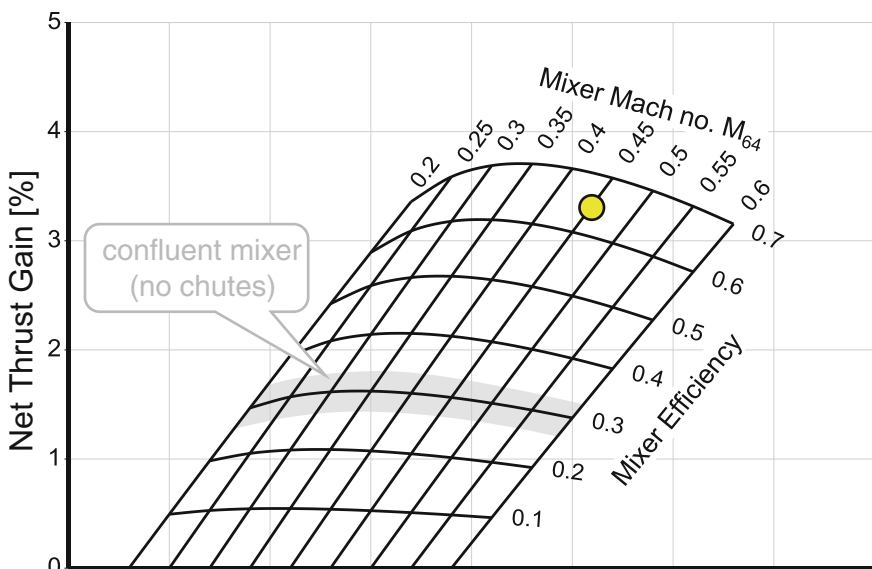


Fig. 1.5-7 Net thrust gain due to mixing—effect of mixer Mach number

For our business jet engine, let us select a forced mixer with chutes like those in Fig. 1.5-5. The design aim for the mixer is 65% efficiency with 1% total pressure loss downstream of the chutes. The length of the mixer, measured from the chute exit to the nozzle throat, then needs to be approximately 80% of the bypass exit diameter, if we refer to Fig. 1.5-6.

We choose $M_{64} = 0.45$ as mixer Mach number from the correlation in Fig. 1.5-7, which uses the mixer entry temperatures and pressures from Table 1.5-1. This is a compromise between performance and weight: lower Mach numbers would yield more gross thrust gain but also increase the mixer area and thus the diameter of engine and nacelle. Cost, weight and drag would also increase.

Table 1.5-2 lists the aero-thermodynamic details for the design point of the selected mixer. The mixer inlet conditions, the Mach number after mixing and the nozzle back pressure are highlighted.

Table 1.5-2 Mixer details for 65% efficiency, 1% mixed pressure loss and mixer Mach no $M_{64} = 0.45$

Station	Mass flow W (kg/s)	Total temperature (k)	Total pressure (kPa)	Static pressure (kPa)	Mach	Velocity (m/s)	Area (m ²)
16	11.2	294	46.9				
163	11.2	294	46.43	39.43	0.489	164.2	0.1333
6	3.14	801	43.1				
63	3.14	801	42.67	39.43	0.345	190.0	0.0914
BPR	3.567						
64	14.34	410.9	44.63	38.87	0.450	178.9	0.2340
ambient				18.75			
8, cold	11.2	294	46.9	24.77	1	313.8	0.1013
8, hot	3.14	801	43.1	23.09	1	515.0	0.0517
8,mixed	14.34	410.9	44.6	23.61	1	370.8	0.1613
P63/P6	P163/P16	P64/P63	P64/P163	P8/P64	P8/Pamb		
0.99	0.99	1.046	0.957	1	2.380		
	P16/P6			V163/V63			
	1.088			0.8342			
Fn	Fg	Fg,ideal	Fg,unmixed	efficiency	Fg,gain	Fn,gain	
kN	kN	kN	kN		%	%	
2.668	6.054	6.102	5.965	0.65	1.47	3.33	

Next, we examine the design space around our chosen design point. Figure 1.5-8 shows the influence of mixer efficiency and total pressure loss due to friction in the jet pipe on net thrust gain. With a confluent mixer, we could get 1.7% improvement. This is matched by a 1.7% SFC improvement, since the fuel flow did not change during our mixer study, which also had constant mixer inlet conditions.

A forced mixer is certainly more expensive and adds some weight to the engine. However, it contributes significantly to the performance of the engine. Net thrust and SFC improvements of more than 3% are attractive, so a more extensive trade study is warranted!

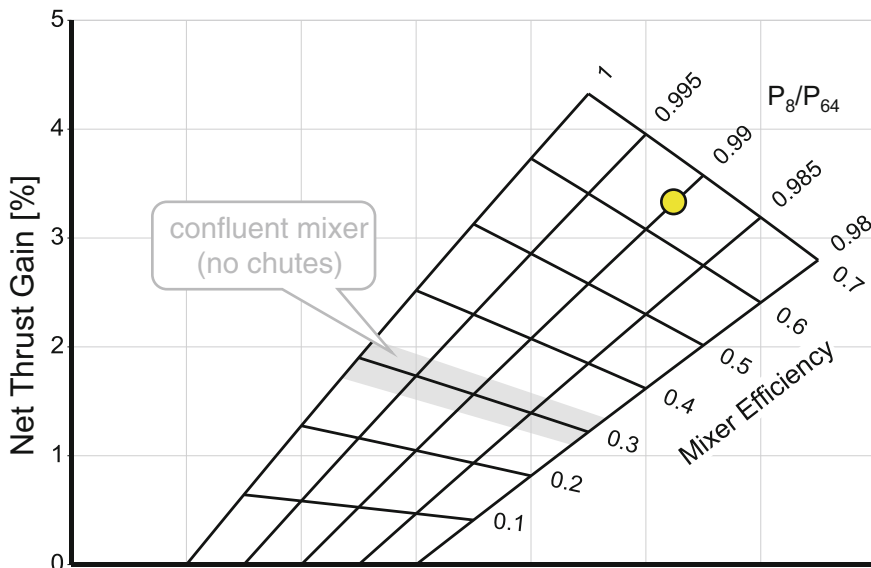


Fig. 1.5-8 Net thrust gain due to mixing—effect of pressure losses

Figure 1.5-8 tells us about the influence of friction pressure losses. When mixer efficiency is high, then 1% total pressure loss will reduce the net thrust gain of the mixer by the same percentage.

1.5.9 Mixer Off-Design

During off-design simulations we apply basically the same methodology as we did for the design of the mixer. However, there is one important difference: in an off-design simulation, the geometry—in terms of the areas A_{63} , A_{163} and A_{64} —is known. The velocities at these thermodynamic stations depend on the exit conditions for the core and bypass streams and these vary considerably within the flight envelope and with thrust. We have “target values” for each of these velocities.

So, what are the differences when it comes to off-design simulations of a separate flow turbofan and a mixed flow turbofan? As described in Chap. 7, any off-design calculation is iterative, with many guesses for the selected variables (spool speeds, burner exit temperature and the coordinates of the operating points in each of the component maps).

An off-design iteration begins with initial guessed values being set for the iteration variables, which usually means that none of the target values is fulfilled. For each of the conditions, an *error* is calculated which quantifies the magnitude of the discrepancy. The Newton Raphson algorithm modifies the values of the iteration variables in such a way that, in the end, all conditions are fulfilled, i.e. all *errors* are zero.

In any gas turbine simulation, each exhaust nozzle imposes a condition: namely, the total pressure at the exit of the upstream component must be such that the mass flow passes through the given nozzle area at the prevailing back pressure. The “error” is the difference between the upstream total pressure and the required total pressure.

The mixed flow turbofan has the same number of iteration variables as the separate flow turbofan, however, one condition is missing since there is only one exhaust nozzle instead of two. We need another condition to replace the bypass nozzle flow condition. The mixer aero-thermodynamic model provides this: the static pressures P_{s63} and P_{s163} must be in balance.

Experience shows that the assumption of equal static pressure in the mixing plane works well in the performance simulation for any mixed flow turbofan. Coding of the off-design mixer model is challenging because the iteration error must operate so that it directs the Newton Raphson algorithm for any combination of core and bypass exit mass flows, temperatures and pressures towards a converged solution.

Staying with off-design operations, how does a mixed flow turbofan behave when we pull back the power lever? All temperatures and pressures at the mixer entry decrease (Fig. 1.5-9). While the temperature ratio T_{16}/T_6 decreases, the pressure ratio P_{16}/P_6 goes up. Both events make the mixer worse. At very low power, the mixer even destroys thrust!

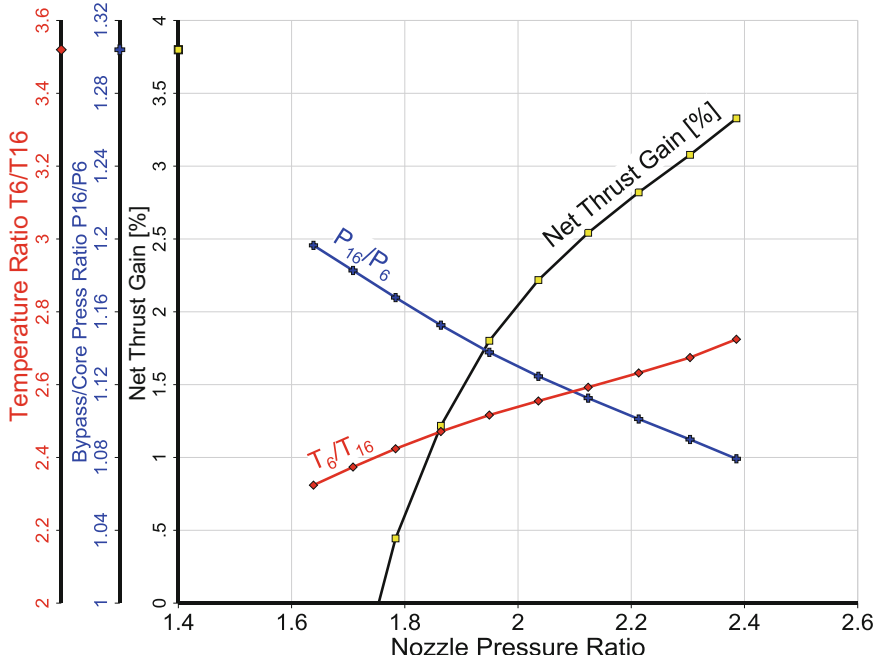


Fig. 1.5-9 Mixer performance at part load

The trends in Fig. 1.5-9 are universal, the exact numbers deviate only slightly. As in any nozzle, discharge and velocity coefficients vary with nozzle pressure ratio; empirical values for C_D and C_V are used to reconcile theory and measurement.

Problems with simulation accuracy of engine matching (how bypass ratio changes with engine rating) can be solved by slightly manipulating the mixer areas A_{63} and A_{163} . If possible, the sum of the areas should be kept constant, i.e. $A_{63} + A_{163} = A_{64\text{design}}$.

1.6 Afterburner

An afterburner (also named augmenter or reheat system) is a simple device, and it consists of only a few basic parts: a diffuser section, fuel injectors, flame-holders, a jet pipe with a liner which controls the cooling air distribution and a nozzle with variable throat area.

To minimize pressure losses in the diffuser, the turbine exit guide vanes eliminate or at least reduce residual swirl downstream of the low-pressure turbine rotor. For the same reason, and also to increase flow residence time in the combustion zone, the Mach number is reduced from approximately 0.4 to 0.2. Fuel injectors are placed in this region in such a way that the fuel can be distributed as required.

The flame-holders stabilize the flame in the relatively high velocity environment, and the jet pipe serves as a combustion chamber, which provides time for the chemical reaction. A screech damper is necessary to suppress high-energy, destructive acoustic frequencies. The screech damper is part of the liner that protects the outer case from high temperatures. Downstream of the afterburner a variable area nozzle is required to control the operating conditions of the turbomachinery.

The flow characteristics in an active afterburner are extremely complex, and it is not feasible to simulate them on a purely theoretical basis with sufficient accuracy. Development of an afterburner is still an empirical task that includes an old-fashioned cut-and-try approach. Accurate simulation of afterburner performance will always include empirical correlations, derived from the analysis of engine test data.

An afterburner must operate over a wide range of conditions. To obtain the maximum thrust the fuel should be injected in such a way, that all the available oxygen in the main stream is consumed. That means that the fuel/air ratio must be very uniform at the nozzle inlet. When the fuel is distributed unevenly, there are rich and lean regions with fuel/air ratio ratios that are above and below the stoichiometric value. In both cases the heat release is less than maximum.

At minimum afterburner rating the fuel should be distributed in the now small combustion region such that a stoichiometric zone always exists to prevent the

flame from being blown out. In contrast to the maximum thrust situation, an uneven fuel distribution is now required!

Simulation of the afterburner requires models for:

- Pressure losses in dry and reheated operation
- Heat release from a given amount of fuel
- The effect of variable nozzle geometry on the operation conditions of the turbomachinery
- Power requirement of the afterburner fuel pump.

The following paragraphs deals with modeling the steady state afterburner operation in mixed flow turbofans. The methods described are also applicable to the afterburners of straight turbojets. Practical afterburner models are all semi-empirical.

1.6.1 The Need for a Precise Afterburner Simulation

Control of the afterburner fuel flow for mixed flow turbofan engines is very complex. For a given nozzle area, burning too much afterburner fuel can throttle the fan so that it surges. In contrast, insufficient heat release causes the fan pressure ratio to decrease and the gas velocity in the jet pipe to increase, thereby causing the flame to be extinguished. Ideally, the operating point of the fan should not be affected by the afterburner operation.

Two different methods are used to achieve this—at least approximately. In some engines, the afterburner fuel has a *closed loop* control so that a prescribed fan pressure ratio is always achieved. The problem with this approach is that in the event of a delay in afterburner ignition, the nozzle would close to keep the fan pressure ratio at the target level. If the afterburner was then to ignite the nozzle probably would be unable to open quickly enough to avoid a sharp rise in afterburner pressure and again this would lead to a fan surge.

In principle, this problem can be avoided with an *open loop* afterburner fuel control. In such a system, the pilot selects a nozzle area and the afterburner fuel flow is calculated within the control system as a function of the measured nozzle position. The fuel injected into the afterburner will heat the exhaust gas so that the desired fan pressure ratio is achieved. Now however, since no pressure signal is fed back to the afterburner fuel flow control, an ignition delay will not cause the nozzle to close and the danger of a fan surge when the fuel finally ignites is eliminated.

In practice, with the open loop afterburner fuel control one needs a precise method to calculate the fuel flow from the control system inputs. On one hand, when the heat release from the fuel injected is too high, the fan surge margin will be less than desired. On the other hand, when the heat release is lower than desired, thrust will be lost. Any inaccuracy in the fuel schedules or fuel monitoring will affect thrust, specific fuel consumption and fan surge margin directly.

Deducing the afterburner control laws from engine tests at sea level and altitude is neither practical nor economic. Therefore, schedules for nozzle area and fuel flow must be derived from a model. Any defect in this model means that, at certain flight conditions, greater fan surge margins must be incorporated for safety reasons and, at other flight conditions, greater turbine inlet temperature margins must be included to compensate for potential thrust losses.

The primary function of the control system is to ensure safe operation of the engine and, as a consequence, the model must predict the fan operating point as precisely as possible.

Setting up a good simulation requires much more than an accurate representation of the afterburner burning efficiency. In fact, all elements of the model have either a direct or an indirect impact on a calculated fan surge margin.

1.6.2 Geometry and Nomenclature

Turbofan afterburner hardware differs widely. There are two basic approaches to its design: *mix first, then burn* and *mix/burn simultaneously*. The pros and cons of each are discussed in Ref. [25]. For performance simulation, it is common to calculate first the mixing and then the heat addition.

We commence by addressing the upstream pressure losses between stations 6 and 63 in the core stream and between stations 16 and 163 in the bypass stream. The architecture and stations are shown in Fig. 1.6-1. Note that a substantial part of the bypass flow enters the annulus behind the liner and a portion of this rejoins the main stream through the many holes that make up the screech damper.

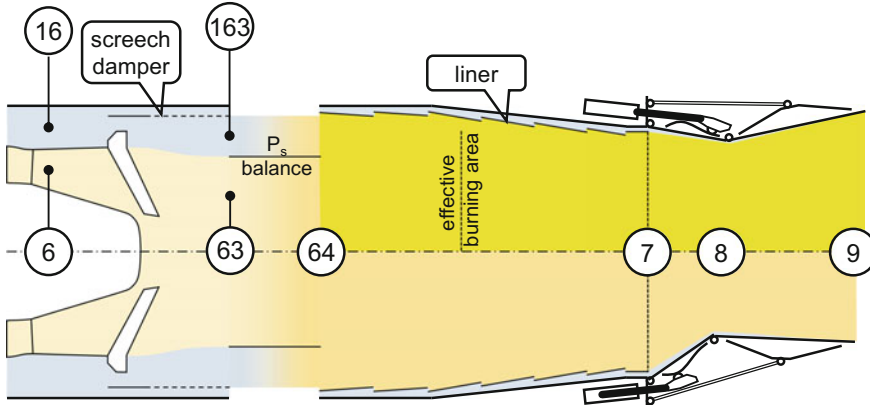


Fig. 1.6-1 Afterburner nomenclature. Upper part with reheat on, lower part for dry operation

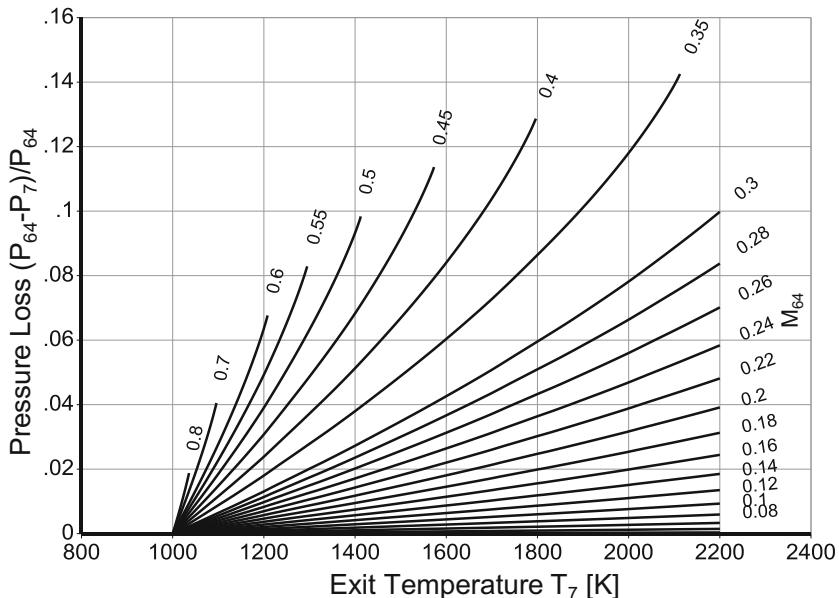


Fig. 1.6-2 Fundamental pressure loss due to heat addition in a frictionless pipe

Mixing of the core and bypass streams is calculated through a model that yields the properties at station 64. The model postulates a frictionless constant-area pipe of infinite length in which two streams mix completely. Conservation of mass flow, energy, and momentum is mandated. The cycle matching calculation makes sure that the static pressures P_{s63} and P_{s163} are in balance. See Sect. 1.5 for further details.

When the afterburner is lit, the static pressure on the mainstream side of the liner is lower than it is in dry operation and therefore the cooling flow through the screech damper and the liner increases compared with dry operation.

Combustion begins with the thermodynamic state of station 64 and ends with that of station 7, the nozzle entry. The fundamental pressure loss—the total pressure loss due to heat addition in a frictionless constant area pipe—depends on the Mach number M_{64} and the temperature ratio T_7/T_{64} . If the jet pipe (between stations 64 and 7) is not cylindrical, then M_{64} can be replaced by the Mach number in an imaginary *effective burning area* (Fig. 1.6-2).

1.6.3 Afterburner Operation

When no fuel is injected, the afterburner behaves as a mixer, and the calculation described in Sect. 1.5 applies.

1.6.3.1 Pressure Losses

Flame holding and propagation requires a flame-holder configuration that creates a low velocity, re-circulating air region. Such a system intrinsically generates significant pressure losses. Additional losses originate from the fuel injectors (spray rings or spray bars) placed upstream of the flame-holders and from the turbine exit diffuser. Often, all these losses are lumped together and modeled as one. Since the flow Mach number in this part of an engine is invariably subsonic, the pressure losses in the core stream will be proportional to the square of the corrected flow at turbine exit.

Modeling the pressure losses in the bypass flow can be more difficult, especially in engines where the bypass ratio is low. However, with some effort, the pressure downstream of the bypass flame-holders can usually be derived from the bypass exit pressure with the help of an empirical correlation.

The loss due to wall friction in the jet pipe is small compared to that caused by the flame-holders. Mixing the liner cooling air with the main stream causes some pressure loss in the jet pipe. Usually these three losses are not accounted for separately and they are combined with the bypass flame-holder loss characteristic.

1.6.3.2 Flow Field

In a high bypass engine without an afterburner, the whole bypass stream joins the core stream at the trailing edge of the mixer. When the mixer is confluent, both streams are essentially flowing in parallel and their respective static pressures are equal. The shape of a forced mixer is quite complex, however, and this influences the flow field heavily in the region where the two streams meet. Nevertheless, in reconciling the turbomachinery conditions in such an engine, it is sufficient to calculate the mean static pressures from the fixed effective flow areas and subsequently ensure that they are equal.

Frequently, the geometry at entry to the afterburner is very complex. The flame-holders create re-circulation zones of significant size just within the region where the simple mixer model assumes a static pressure balance. Two questions arise: what are the effective mixer areas, and do they vary over the operating conditions? In modeling real engines, some empirical corrections to the simple static pressure balance assumption are unavoidable.

A typical nozzle and liner requires 8–13% of total engine airflow for cooling. With a low bypass ratio engine, this means that up to 50% of the bypass air flows outside the liner and does not participate in the burning process. Its momentum is normally neglected when it is mixed with the mainstream. Moreover, the total cooling air is split: one part is mixed before the heat addition calculation, and the remainder is mixed afterwards, beyond station 7.

When the amount of injected fuel is increased from minimum to maximum, the Mach number rises at the afterburner exit and, consequently, the static pressure in

the jet pipe falls. The driving pressure ratio of the liner cooling air rises and therefore more of the bypass air flows outside, leaving less air for combustion.

1.6.4 Reheat Efficiency

The fuel distribution affects reheat efficiency very much. It is important that the fuel should be vaporized and thoroughly mixed with the combustion air upstream of the flame holders. Usually, the fuel is injected through plain-orifice atomizers (i.e. plain holes) located in stub pipes. Ideally, it is injected in an upstream direction to improve atomization by increasing the relative velocity between the fuel and air. The distribution of fuel/air ratio in the plane of the flame holders varies with fuel flow. In the core stream, complete evaporation of the fuel is assured. In the bypass stream, low evaporation rates associated with low air temperatures make good atomization of critically importance.

1.6.4.1 Definition

It seems natural to define efficiency of an afterburner as the ratio of actual to real temperature rise:

$$\eta_{T1} = \frac{T_7 - T_{64}}{T_{7,id} - T_{64}} \quad (1.6-1)$$

The efficiency value that ensues depends on what we consider the ideal afterburner exit temperature $T_{7,id}$ to be. This can be the temperature of complete combustion which—in the case of burning hydrocarbons—produces nothing other than carbon dioxide and water. However, such a chemical process only happens theoretically. Carbon monoxide (CO) will be formed even when there is more than sufficient oxygen in the air to oxidize the carbon and hydrogen in the fuel completely. NO_x and partially-burnt hydrocarbons also exist in the gas mixture in the chemical equilibrium state. The equilibrium temperature $T_{7,equi}$ is lower than $T_{7,id}$. The difference between $T_{7,equi}$ and $T_{7,id}$ is caused by dissociation—an equilibrium process by which the products of combustion achieve the minimum Gibbs function for the mixture. Figure 1.6-3 shows that dissociation reduces the achievable afterburner exit temperature significantly.

No afterburner can achieve local exit temperatures higher than the chemical equilibrium value. It is misleading to use $T_{7,id}$ in the definition of afterburner efficiency because that would indicate that even a perfect fuel distribution in a long afterburner with large diameter (i.e. long residence time for the combustion process) would have much room for improvement. Therefore, the temperature-based afterburner efficiency should be defined as

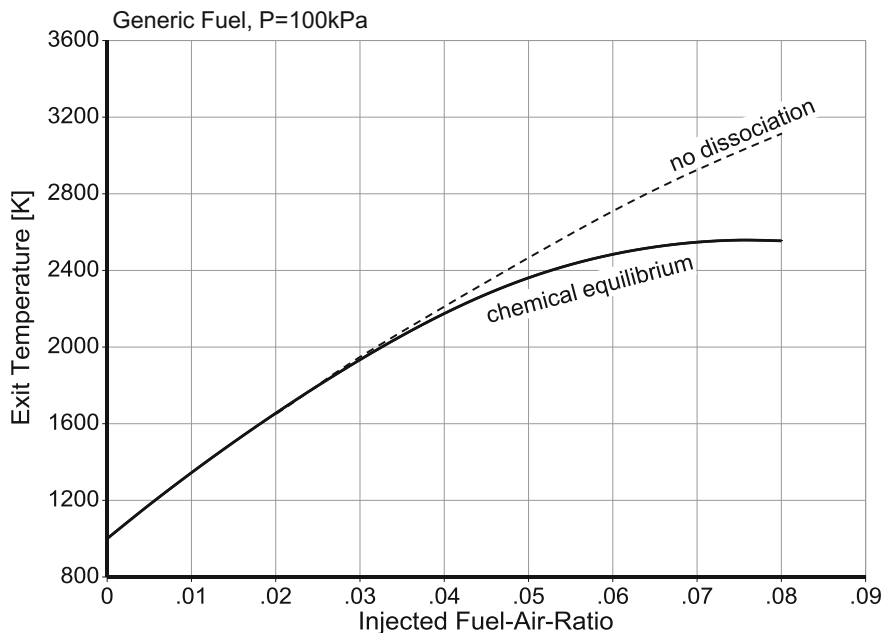


Fig. 1.6-3 Effect of dissociation for a hydrocarbon burning at 100 kPa

$$\eta_{T2} = \frac{T_7 - T_{64}}{T_{7,equi} - T_{64}} \quad (1.6-2)$$

However, there is a problem even with this statement. If very much fuel is injected into a poorly designed afterburner, then the fuel/air ratio at station 7 can be far in excess of stoichiometric. The equilibrium temperature for such a mixture could be lower than the actual temperature T_7 . From Eq. (1.6-3), the efficiency would then be greater than 100% for a device which is performing extremely poorly!

This problem goes away when we define afterburner (or reheat) efficiency as a ratio of fuel mass flows, namely:

$$\eta_{W2} = \frac{W_{F,RH,equi}}{W_{F,RH}} = \frac{far_{7,equi} - far_{64}}{far_7 - far_{64}} \quad (1.6-3)$$

Here, $W_{F,RH,equi}$ is the fuel flow required by an ideal afterburner to achieve the chemical equilibrium temperature $T_{7,equi}$.

Figure 1.6-4 shows how we can get efficiency values between 0.864 and 0.953 for the same afterburner. Our preferred definition yields $\eta_{RH} = \eta_{W2} = 0.926$.

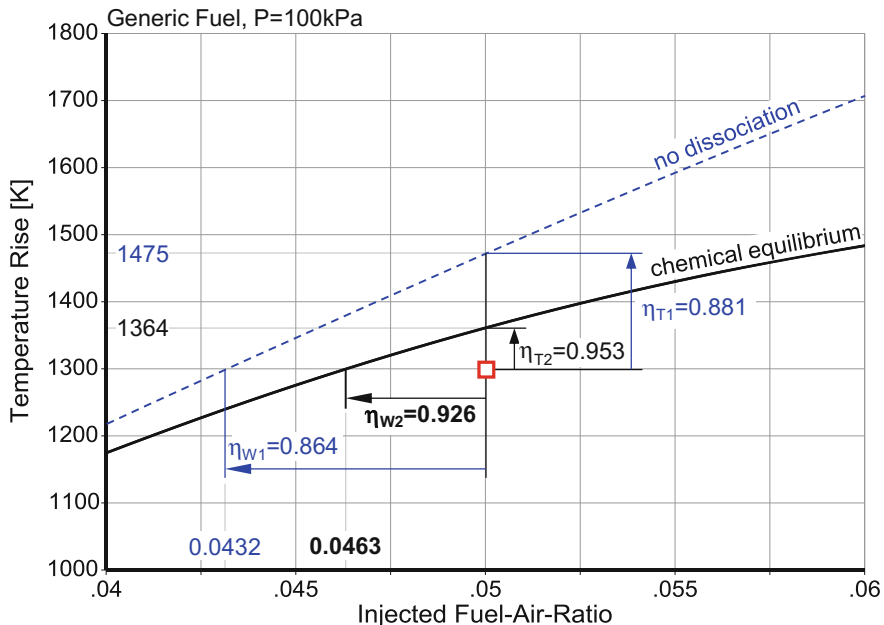


Fig. 1.6-4 Evaluations of various afterburner (reheat) efficiency definitions

Obviously, it is very important to know how afterburner efficiency is defined. However, not all publications explain what they regard as the ideal afterburner exit temperature unambiguously. Quoted efficiency values below about 0.9 might be justified by them being based on ideal combustion (i.e. without dissociation) rather than reality.

None of our references contain a clear definition of afterburner efficiency. The numbers quoted vary widely: Ref. [26] cites values between 0.8 and 0.9, while Ref. [27] quotes a range between 0.85 and 0.9 for favorable operating conditions. Reference [7] offers 0.93 as a typical value. It seems natural to assume that the lower values are based on ideal combustion with no dissociation.

1.6.4.2 Methods of Determining Efficiency

Afterburner rig

Special rigs are sometimes designed for the development of afterburners. The supply of bypass air with the appropriate temperature and pressure does not pose too much of a problem. However, the core inlet air must be preheated to turbine exit temperature in a burner, and this requires a smaller fuel/air ratio than at the same location in the engine. Consequently, there will be more oxygen available in the rig than in the engine when no corrective measures are taken (e.g. by injection of steam or nitrogen).

In the analysis of an afterburner rig test, the nozzle inlet mass flow is well known and the total pressure at this location may be derived from static pressure measurements at the liner exit. The static pressure sensors can be calibrated with the help of—for example—CFD calculations. When the effective nozzle throat area is known, the nozzle throat temperature may be calculated, followed by the burning efficiency. Note that this test analysis method requires an accurate measurement of the geometric nozzle area and that is very difficult for a variable area nozzle!

When the burning efficiency found from rig tests is used in total engine simulations, extreme care should be taken. The numbers quoted for the efficiency depend critically on the model of liner cooling used in the analysis of the rig test.

Gas analysis

Gas analysis is a tool that provides information about local fuel/air ratio and local efficiency. The measured values are normally very high but they cannot be used for performance simulations because the effect of cooling air is not accounted for. So, we suggest that gas analysis is more a tool for checking the fuel distribution and for optimizing the fuel injection system rather than estimating augmenter efficiency.

Engine Test

There are two methods of evaluating the afterburner efficiency from measurements taken during an engine test. The first is the same as that for the afterburner rig. In the second, instead of using the nozzle throat area measurement, the measured thrust is used to derive the nozzle inlet temperature. This method requires a high-quality simulation of the nozzle performance because any defect will change the evaluation and give a wrong impression of the afterburner performance. Overestimating nozzle performance goes along with an underestimation of afterburner exit temperature (and thus afterburner efficiency) and vice versa.

As a result we get the reheat *thrust efficiency* $\eta_{RH,F}$. By virtue of its derivation, when used in the overall engine simulation $\eta_{RH,F}$ will yield the correct nozzle flow and also the correct gross thrust.

1.6.4.3 Efficiency at Part Load

There is no way to calculate afterburner efficiency purely from theoretical considerations with sufficient accuracy. Therefore, only empirical correlations can be used.

References [7] and [28] recommend that we use a correlation based on burner loading since this is common practice with primary combustion chambers. Remember, we can determine the part-load efficiency of a main burner using the simple correlation introduced in Sect. 1.4 and repeated here in Eq. (1.6-4).

$$\log(1 - \eta) = \log(1 - \eta_{ds}) + B \log(\Omega/\Omega_{ds}) \quad (1.6-4)$$

Thus, efficiency is a function of the part load constant B and the burner loading parameter Ω :

$$\Omega = \frac{W_{31}}{P_3^{1.8} e^{T_3/300K} Vol} \quad (1.6-5)$$

For the afterburner (reheat system) we define the loading parameter Ω_{RH} similarly as

$$\Omega_{RH} = \frac{W_{64}}{P_{64}^{1.8} e^{T_{64}/300K} Vol_{RH}} \quad (1.6-6)$$

Ω_{RH} characterizes the combined effects of pressure P_{64} , temperature T_{64} and mass flow W_{64} . Since reheat volume is the product of area A_{64} and jet pipe length, W_{64}/A_{64} is a measure of the gas velocity.

We can describe the part load behavior of a typical main combustion chamber by employing a part load constant B of 1.6 in Eq. (1.6-4). This value accounts for a reduction of the fuel/air ratio with increasing loading parameter. The efficiency drop for a constant fuel/air ratio is less and therefore, lower B values are appropriate.

1.6.5 EJ 200 Example

The EJ200 is the engine used in the Eurofighter Typhoon aircraft. It has been developed in Europe during the last decade of the 20th century. Table 1.6-1 lists the main design parameters of this fighter engine.

Table 1.6-1 EJ200 engine specifications (uninstalled ISA SLS) Ref. MTU Product Leaflet

EJ200 engine specifications (uninstalled, ISA, SLS)		
Max. thrust, reheated	90 kN	20,000 lbf
Max. thrust, dry	60 kN	13,500 lbf
Overall pressure ratio	26:1	26:1
Fan pressure ratio	4.2:1	4.2:1
Bypass ratio	0.4:1	0.4:1
Specific fuel consumption, reheated	47–49 g/kNs	1.66–1.73 lb/lbf h
Specific fuel consumption, dry	21–23 g/kNs	0.74–0.81 lb/lbf h
Air flow rate	75–77 kg/s	165–170 lb/s
Length (approximate)	4000 mm	157 in.
Max. inlet diameter	740 mm	29 in.

1.6.5.1 Modeling Results from the Altitude Test Facility

Reference [29] contains comprehensive results from an EJ200, installed in an altitude test facility. The data plots in the references have no scales for reheat efficiency and bypass ratio. While it is not difficult to figure out the efficiency values, the exact scale for bypass ratio remains a secret—even to those of us who like to *reverse-engineer* things!

To analyze the test data, we need to know the conditions at reheat inlet for each of the test points. Therefore, we create a generic performance model of the engine, based on data from the public domain like those in Table 1.6-1.

The reheat inlet conditions in the simulation are those from station 64 in Fig. 1.6-5. It is impossible to evaluate the gas properties in the hypothetical mixing plane 64, however we can estimate the static pressure on the liner wall $P_{s,wall}$ and correlate it with P_{s64} . This has been done in Ref. [29], which contains a plot of $P_{s64}/P_{s,wall}$ against a measure of reheat, expressed as the temperature ratio T_7/T_{64} . This plot is reproduced here in Fig. 1.6-6. The ratio of the two static pressures increases linearly with the temperature ratio. We can explain this with the fact that the heat addition has already begun upstream of the location of the liner wall pressure sensor. Due to the lower density of the burning gases, the local Mach number here is higher than M_{64} and consequently $P_{s,wall}$ is lower than P_{s64} , the static pressure before the heat release.

Reheat efficiency data from four different test series are available, and these are presented in Fig. 1.6-7. The first series of points is a thrust modulation from minimum to maximum reheat at SLS. The second and the third series are similar thrust modulations at altitude 36,000 ft for Mach 1.8 and Mach 0.7. The last series of tests simulates a vertical climb with maximum reheat thrust at Mach 0.7, starting at an altitude of 36,000 ft.

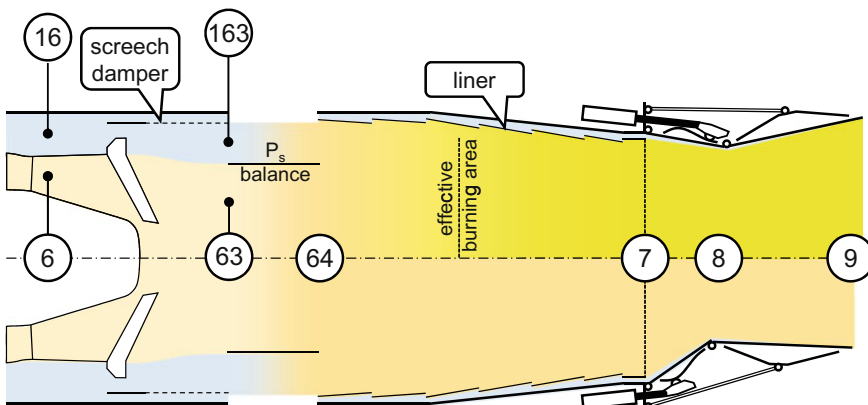


Fig. 1.6-5 EJ 200 afterburner nomenclature

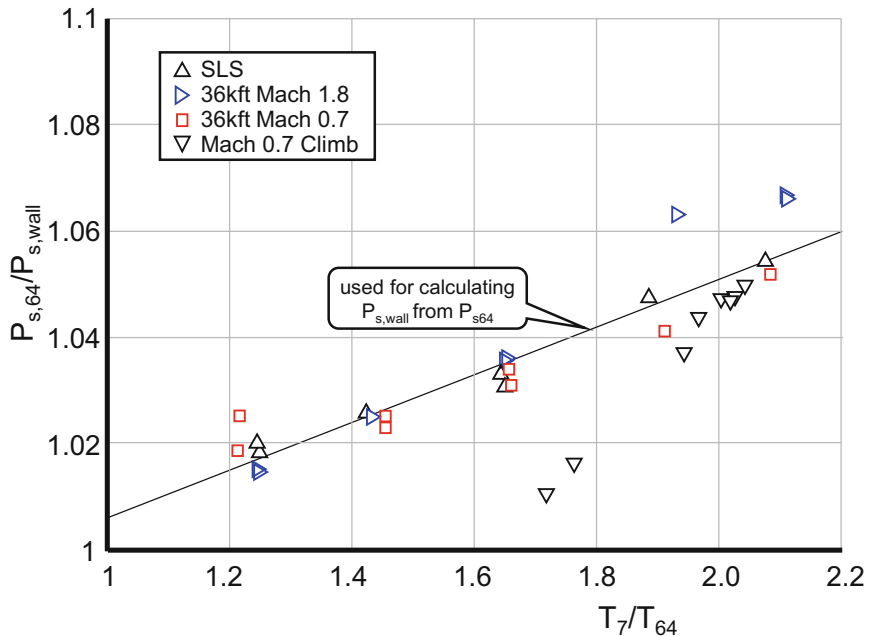


Fig. 1.6-6 Correlation between the calculated pressure $P_{s,64}$ and the measured static pressure $P_{s,wall}$

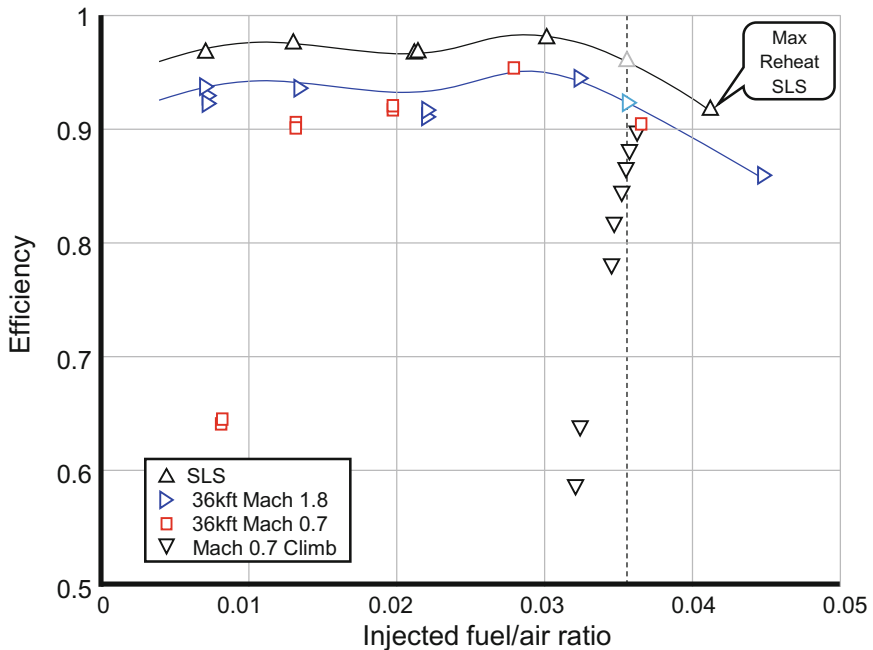


Fig. 1.6-7 Reheat efficiency for all test points (Ref. [29], efficiency scale guess added)

Our aim here is to reproduce these results within our performance simulation. We base our model on the correlation of efficiency with the reheat burner loading Ω_{RH} :

$$\log(1 - \eta_{RH}) = \log(1 - \eta_{RH,ref}) + B_{RH} \log(\Omega_{RH}/\Omega_{RH,ref}) \quad (1.6-7)$$

There are three constants in this equation: the reference values for efficiency $\eta_{RH,ref}$, reheat loading $\Omega_{RH,ref}$ and reheat part load constant B_{RH} . For reference values in Eq. (1.6-7), we choose the data from our model that simulates the uninstalled ISA SLS performance for *Max Reheat*.

The test analysis begins with the simulation of the reheat inlet conditions. First, we consider only the data with an injected fuel/air ratio of about 0.036. Reheat efficiencies for SLS and 36,000 ft/Mach 1.8 are interpolated from Fig. 1.6-7; for the other test points we use the efficiency at the measured $\text{far}_{RH,\text{inj}}$ value. We run the model with the measured reheat efficiency in such a way that the calculated static pressure $P_{s,wall}$ agrees with the corresponding measurement. For the SLS and the 36,000 ft/Mach 1.8 cases we achieve this by adjusting the intake recovery factor, the burner exit temperature and the nozzle throat area. The aim is to reconcile the known differences in bypass ratio and temperature ratio T_7/T_{64} for each test point. For the vertical climb test series simulation, we assume that the engine runs with constant corrected fan speed and the nozzle throat area increases with altitude. Opening the nozzle in low Reynolds number flight conditions increases fan surge margin.

This preliminary performance model yields a value for the relative reheat burner loading $\Omega_{RH}/\Omega_{RH,ref}$ for each test point. Now we can complement the figure shown in Sect. 1.4 that we used for correlating the efficiency of main combustion chambers with burner loading. The blue circles in Fig. 1.6-8 correspond to the reheat efficiency and loading parameter results from the altitude test facility.

It is obvious that all data points—except one—follow a straight line in the double logarithmic figure. That means that Eq. (1.6-7) describes the efficiency behavior of this reheat system very well. The reference efficiency $\eta_{RH,Ref} = 0.975$ and the part load constant $B = 0.9$ define the location of the blue line.

The only outlier is the flight condition 36,000 ft/Mach 1.8. This point differs significantly in nozzle pressure ratio, which is around 12 for the supersonic flight case, while all the other cases correspond to much lower nozzle pressure ratios varying from 3 to 4.

Note that all the reheat efficiency values presented in Ref. [29] have been calculated from measured thrust. So the accuracy of this calculation depends on the nozzle performance simulation. Any imperfection of the model and uncertainties in the true nozzle area ratio A_9/A_8 show up as ambiguities in T_7 and affect the reheat efficiency.

We think that the much higher nozzle pressure ratio at Mach 1.8 is the reason why the reheat efficiency does not follow the general trend. Most probably, the apparent reheat efficiency difference between SLS and 36,000 ft/Mach 1.8 is not real but due to an inaccuracy in the nozzle performance analysis.

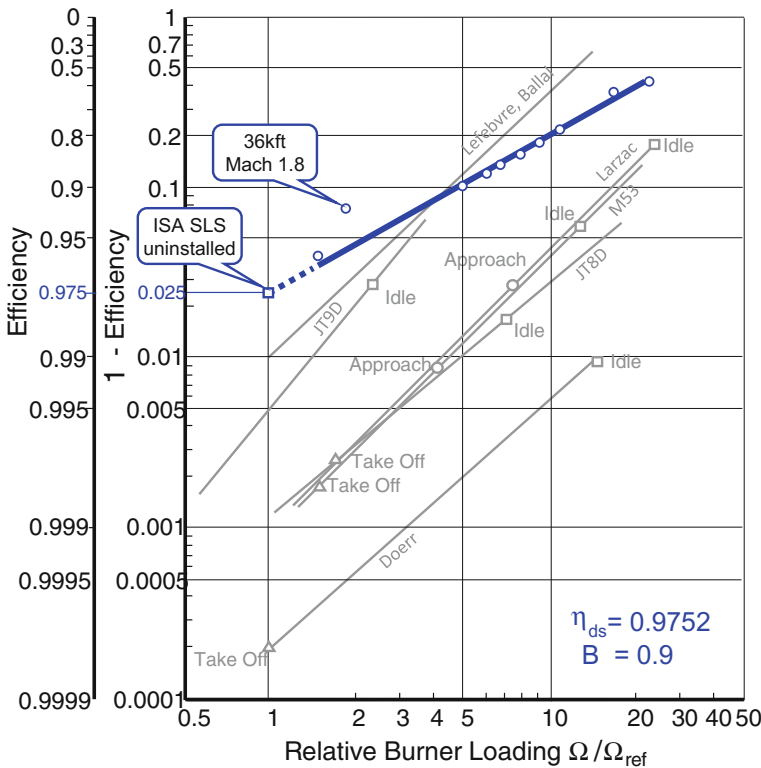


Fig. 1.6-8 Reheat efficiency characteristic

The slope of the reheat efficiency line in Fig. 1.6-8 is shallower than all the other lines, but they describe the characteristics of conventional combustors. So, the change in slope can be explained by the differences in fuel/air ratio: it is constant for an augmenter but for a main combustion chamber it decreases as the loading goes up.

We have already seen in Fig. 1.6-7 that reheat efficiency varies with fuel/air ratio. Let us have a closer look at the fuel injection process and explore why this happens. In the EJ200 afterburner, shown in Fig. 1.6-9, there are three places where fuel is introduced. During a thrust modulation from minimum to maximum reheat, first the primary zone (which is located at the outer part of the radial flame holders, see Fig. 1.6-9) is ignited. The fuel supply is through vaporizers in the centers of the primary baskets. Next the reheat fuel is added to the core stream. This is done through 15 spray bars upstream of each of the flame holders (not visible in Fig. 1.6-9); the fuel flow is increased but is limited to a certain level. Last, the bypass fuel injectors start to operate and supply an increasing portion of fuel to the bypass stream.

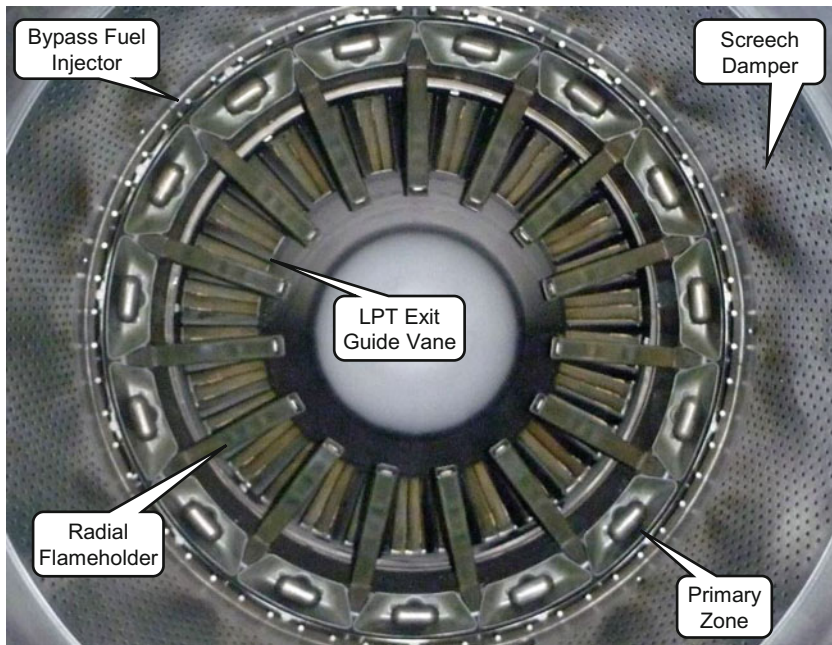


Fig. 1.6-9 Fuel injection in the EJ200 afterburner

From tests, this fuel injection sequence leads to the wave-like curve of the efficiency correction term derived from Ref. [29] and shown in Fig. 1.6-10. The sharp efficiency drop at the high fuel/air ratio end of the curve is typical for any afterburner. It comes from an imperfect fuel distribution: the higher the average

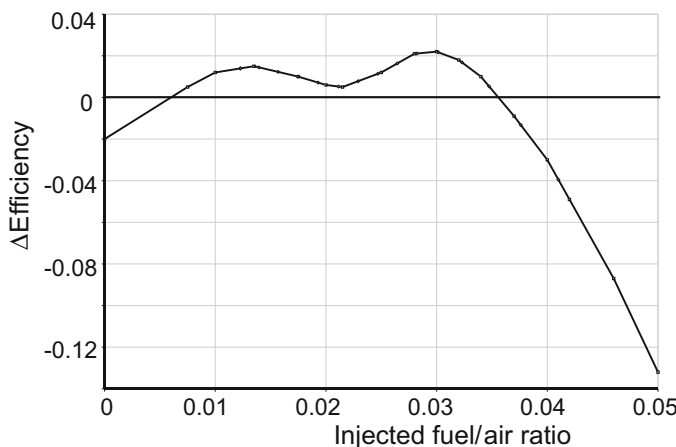


Fig. 1.6-10 Fuel/air ratio correction term

fuel/air ratio, the more probable is the existence of local rich (over-stoichiometric) regions with a lack of oxygen.

The blue line in Fig. 1.6-8 is the relationship

$$\log(1 - \eta_{RH}) = \log(1 - 0.9752) + 0.9 \log(\Omega_{RH}/\Omega_{RH,ref}) \quad (1.6-8)$$

for the test data with $far_{inj} = 0.036$. Applying the fuel/air ratio correction term from Fig. 1.6-10 complements and enhances our model. The following figures show how this very simple model performs. The circles are the results of the simulation, the other symbols represent measured data from Ref. [29]. Generally, the simulation agrees well with the measured data. The model deviates from the test data of the supersonic flight case 36,000 ft Mach 1.8, as to be expected.

Reference [5] interprets the data differently. No attempt was made to correlate efficiency with burner loading. The flight condition 36,000 ft/Mach 1.8 was not detected as an outlier. A bypass ratio correction term is proposed to reconcile the model with the measurements. The problem with this proposal is that there is no explanation of how bypass ratio affects reheat efficiency.

It could be argued that the reason for decreasing reheat efficiency with increasing bypass ratio is poor fuel atomization and evaporation in the cold bypass stream. However, the reduction in reheat efficiency exists even when no fuel is injected into the bypass, i.e. when the injected fuel/air ratio is less than 0.02. The curves of efficiency versus injected fuel/air ratio for SLS and 36 k ft/1.8 are parallel over the full fuel/air ratio range.

The only influence of an increasing bypass ratio is the higher velocity in the jet pipe. This is reflected in an increased value of reheat burner loading. So the effect of bypass ratio is considered in the suggested simple reheat efficiency model.

The dashed lines in Figs. 1.6-11, 1.6-12 and 1.6-13 connect the reheat efficiency points calculated from our model for the climb data series (the yellow symbols). We observe reasonable agreement between model and experiment except for the two points with the lowest pressure in Fig. 1.6-13.

Figure 1.6-11 compares three thrust modulations from minimum to maximum reheat with the test data. The sea level static simulation agrees quite well with the measurements over the full range. For the 36,000 ft/Mach 0.7 case, the minimum reheat test point is an obvious outlier and the high efficiency at $far_{inj} = 0.028$ is also suspicious. The model describes the general efficiency trend with injected fuel/air ratio fairly well.

We have already elaborated why the supersonic flight case test data (36,000 ft/Mach 1.8) are inconsistent. The test efficiency level is simply too low and the model produces more plausible results. Otherwise, the simulated efficiency variations with reheat are in line with the test results.

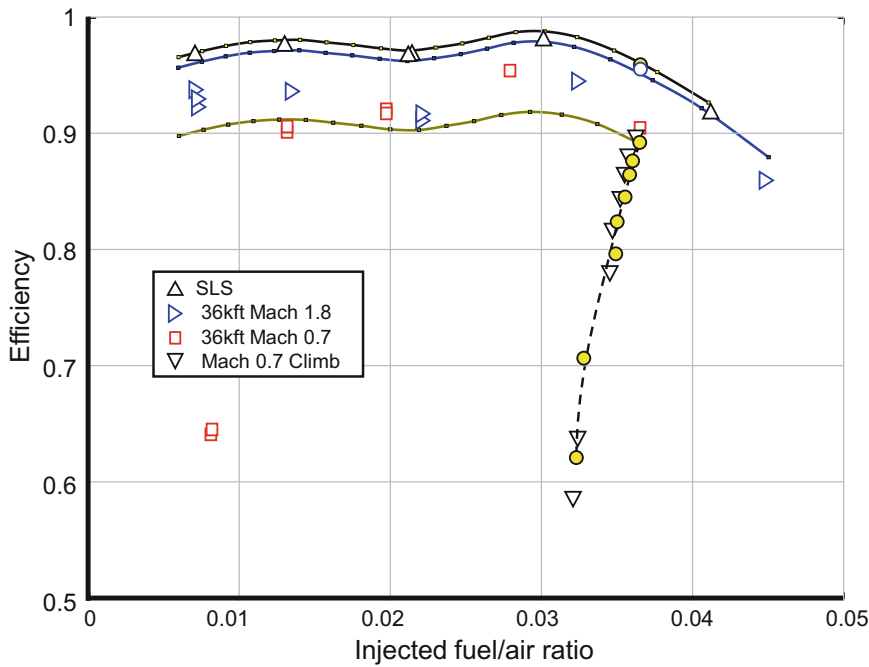


Fig. 1.6-11 Test data and simulation

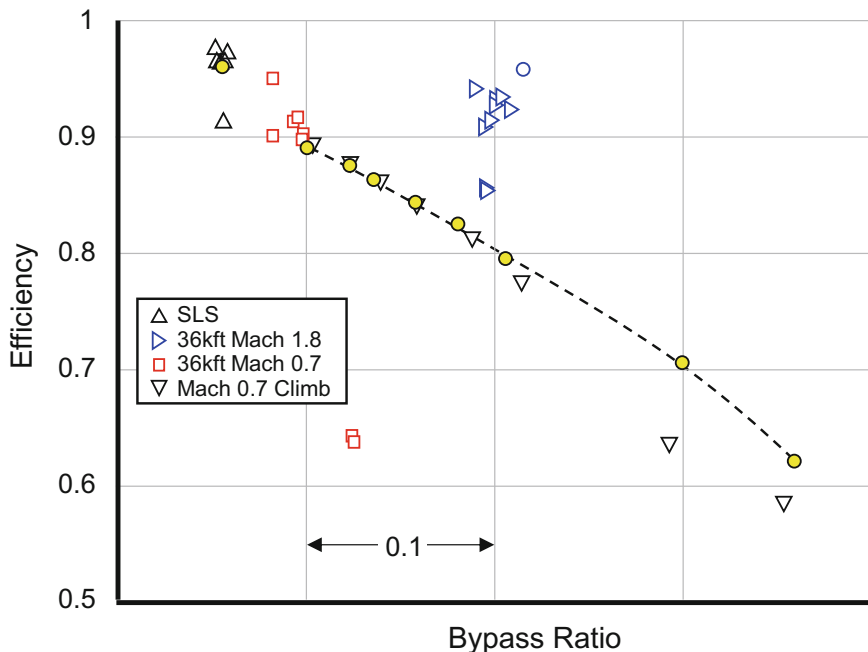


Fig. 1.6-12 Efficiency correlation with bypass ratio

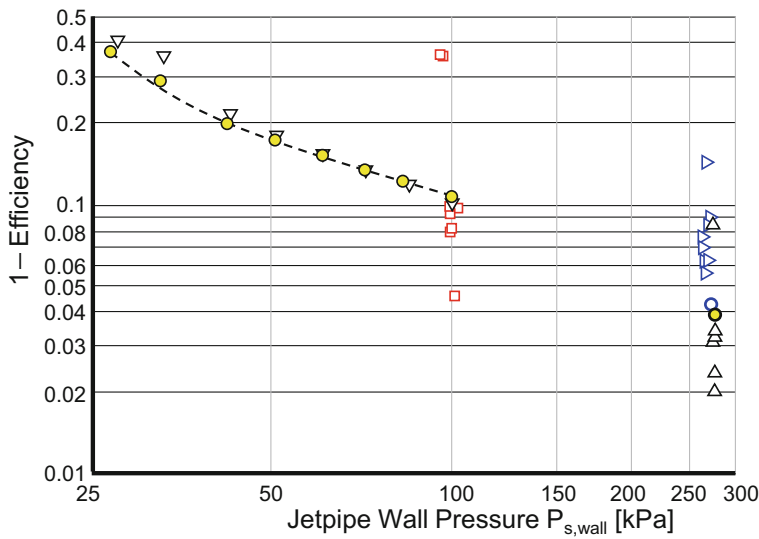


Fig. 1.6-13 Test data and simulation

1.6.5.2 Conclusions

The model we used for this analysis did not contain many details of the cooling air flows through the screech damper, the liner and the nozzle. For this reason, and others, perfect agreement with the measured data should not to be expected.

We believe that the test results from the EJ200 are useful for simulating the afterburner performance in preliminary engine design studies. The absolute level of reheat efficiency depends on the design of the mixer and fuel injection system as well as on the length of the jet pipe. The part-load characteristic is composed of two elements: the basic efficiency change with reheat burner loading and a correction term which is a function of the injected fuel/air ratio.

1.7 Nozzles

One or two nozzles terminate the flow path of turbojets and turbofans. Many of them are conical subsonic nozzles because they are simple, inexpensive to manufacture and the configuration is inherently strong and rigid. Engines for supersonic fighter aircraft frequently employ convergent-divergent nozzles.

To describe the nozzle performance, two characteristics are generally required: a thrust coefficient C_{FG} which describes the effectiveness of converting pressure energy to velocity and the discharge or flow coefficient C_D .

1.7.1 Convergent Nozzles

1.7.1.1 Discharge Coefficient

The discharge coefficient compares the actual mass flow with the theoretical value, calculated from the geometrical exit area A_8 , total pressure and temperature at the nozzle entry and the ambient pressure to which the flow expands (Fig. 1.7-1).

Discharge coefficients of conical nozzles for a range of cone angles α , exit to inlet area ratios A_8/A_7 and pressure ratios P_7/P_{amb} are reported in Ref. [30]. Figure 1.7-2 shows, as a typical example, the data for $A_8/A_7 = 0.828$ (diameter ratio $D_8/D_7 = 0.91$).

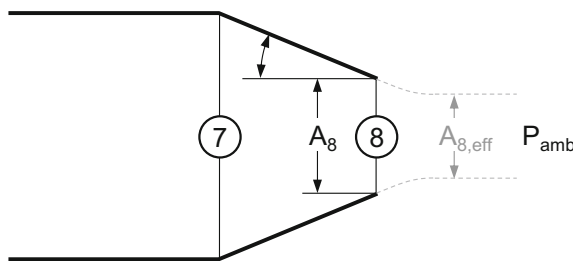


Fig. 1.7-1 Conical nozzle nomenclature

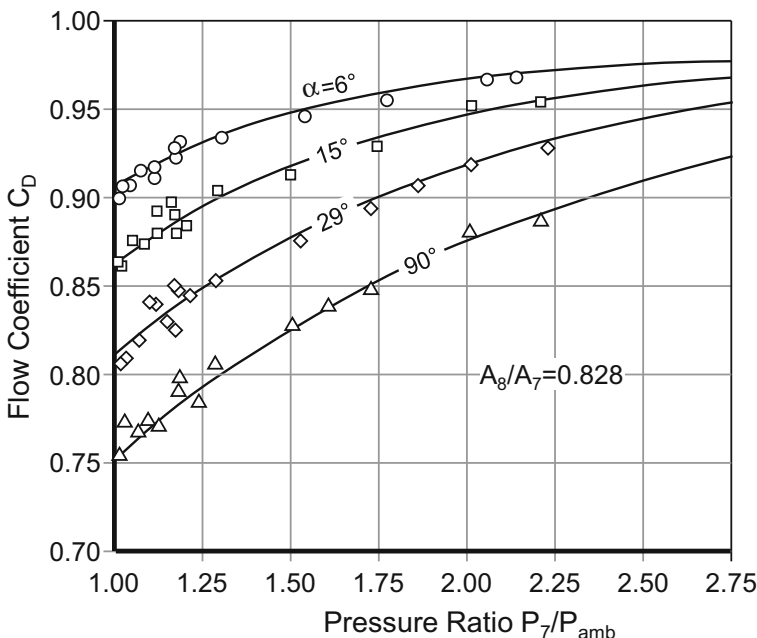


Fig. 1.7-2 Flow coefficient of conical nozzles (adapted from Ref. [30])

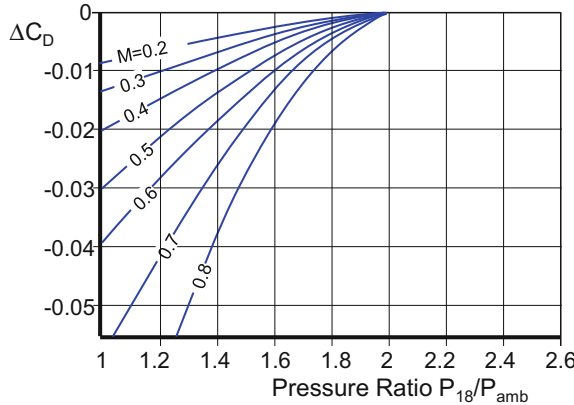


Fig. 1.7-3 Nozzle flow coefficient suppression for an isolated nacelle [31]

External flow can affect the flow coefficient through the interaction between the engine exhaust flow and the external freestream flow. We can characterize this suppression effect by a discharge coefficient modifier ΔC_D as a function of free-stream Mach number and nozzle pressure ratio (Fig. 1.7-3). Reference [31] mentions that the degree of suppression is extremely dependent on the aircraft configuration.

For separate flow exhaust systems, we need two flow coefficient correlations: one for the core stream and another for the bypass stream. The core flow coefficient is established in a wind tunnel test by operating the model with zero fan flow. This determines the upper line in the core nozzle flow coefficient plot in Fig. 1.7-4. With both the fan and the core stream flowing, we get the variation of C_{D8} with P_{18}/P_8 . The variation of C_{D8} is due to the interaction between the fan and core streams near the core nozzle exit plane.

1.7.1.2 Thrust Coefficient

The second descriptor of nozzle performance is the thrust coefficient, the ratio of actual thrust to ideal thrust. There are two options for defining the ideal thrust. Either it is the thrust developed by a loss-less expansion with the boundary condition of the actual geometry or that of an ideal expansion to ambient pressure. Thus we get two versions of the thrust coefficient C_{FG} and $C_{FG,id}$.

There is no difference between C_{FG} and $C_{FG,id}$ as long as the velocity at station 8 is subsonic. However, if the nozzle pressure ratio is above the critical value of $P_8/P_{\text{amb}} \approx 1.86$, we get a pressure term in the thrust equation for loss-less expansion if we take the actual nozzle geometry into account:

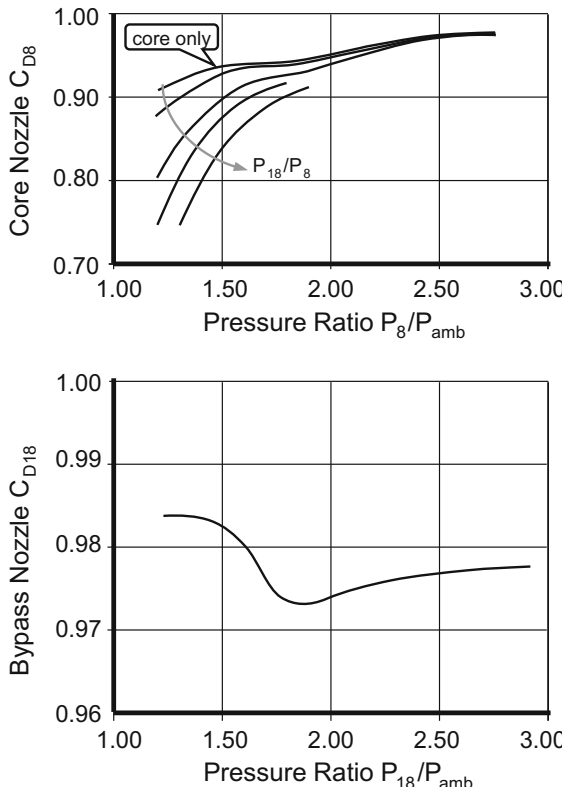


Fig. 1.7-4 Typical separate flow exhaust system nozzle flow coefficients [31]

$$F_8 = W_8 V_8 + A_8 (P_{s8} - P_{amb}) \quad (1.7-1)$$

If we characterize the losses with the thrust coefficient C_{FG} , then we get the true gross thrust from

$$F_{G8} = W_8 V_8 C_{FG} + A_8 (P_{s8} - P_{amb}) \quad (1.7-2)$$

The thrust coefficient C_{FG} describes on one hand, total pressure losses upstream of the nozzle exit and on the other hand, effects of unequal radial temperature, pressure, velocity, and flow angle distributions in the nozzle exit plane. We can characterize a part of the losses as a decrease in total pressure as they happen in any duct with friction. Separating the total pressure loss from station 7 to station 8 from the effects of non-uniform distribution of flow properties simplifies the calculation of the static pressure and the velocity in station 8. There is no need to employ a nozzle efficiency value $\neq 1$ in our calculation if we do that.

The ideal thrust coefficient $C_{FG,id}$ compares the actual thrust with that of an ideal expansion to ambient pressure. Full expansion to ambient pressure yields the ideal velocity V_{id} .

$$C_{FG,id} = \frac{F_{G8}}{W_8 V_{id}} \quad (1.7-3)$$

We prefer the use of the thrust coefficient C_{FG} which describes the quality of the conversion of pressure energy to velocity. Deviations of the nozzle geometry from the one required for the ideal process is a different topic and should be bookkept separately.

Besides the flow coefficients, Ref. [30] also presents model test results for a velocity coefficient C_V . This coefficient is equivalent to the thrust coefficient C_{FG} as we define it. Figure 1.7-5 is a reproduction of figure 9 from Ref. [30]. The various symbols stand for different nozzle geometries in terms of cone angle α and exit to inlet area ratios A_8/A_7 . The thrust coefficient C_{FG} , which relates the thrust to that of a loss-less convergent nozzle, is constant over the full range of pressure ratio within measurement accuracy.

Thrust coefficients for separate flow turbofans are also essentially constant. The same model test that determined the discharge coefficients in Fig. 1.7-4, also established the thrust coefficients for the core and bypass streams. The variations of C_{FG8} and C_{FG18} were smaller than 1% over the full range of pressure ratio.

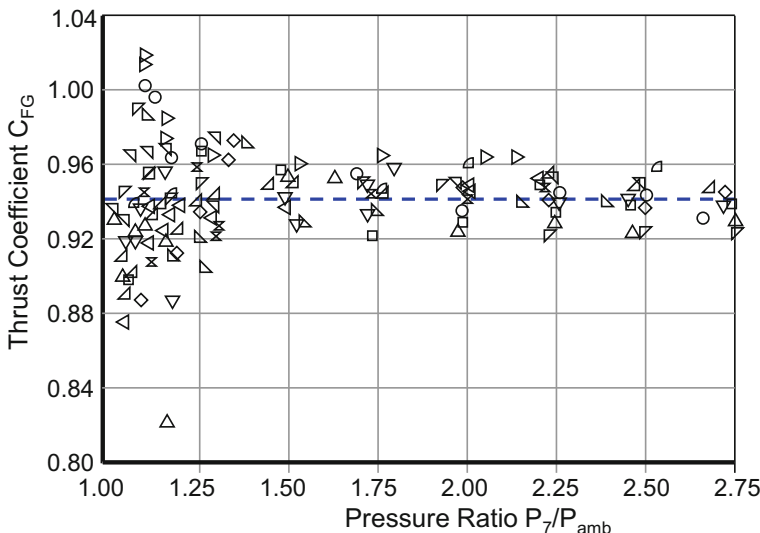


Fig. 1.7-5 Model test results from Ref. [30]

1.7.2 Convergent-Divergent Nozzles

Ideal full expansion to ambient pressure requires a convergent-divergent nozzle if the pressure ratio is higher than the critical value. The ideal area ratio of the divergent nozzle part A_9/A_8 depends on the nozzle pressure ratio.

1.7.2.1 Theory

The isentropic expansion of the flow in a convergent nozzle is a simple process. Velocity and Mach number increase from the nozzle inlet (station 7) to the exit station 8. The higher the pressure ratio P_7/P_{amb} , the higher the jet velocity at the nozzle exit as long as the exit Mach number is less than unity. The maximal velocity which can exist at the nozzle exit is the velocity of sound, i.e. $M_8 = 1$.

The divergent part of a convergent-divergent nozzle continues downstream of the throat. What happens there depends on the pressure ratio P_7/P_{amb} . Figure 1.7-6 shows several variants of static pressure evolution from inlet to exit of the nozzle. The static pressure downstream of the nozzle exit (Station 9) determines which of these variants defines the development of static pressure.

The simplest case is that the ambient pressure corresponds to point B in the figure. The static pressure decreases continuously from point A to point S (sonic

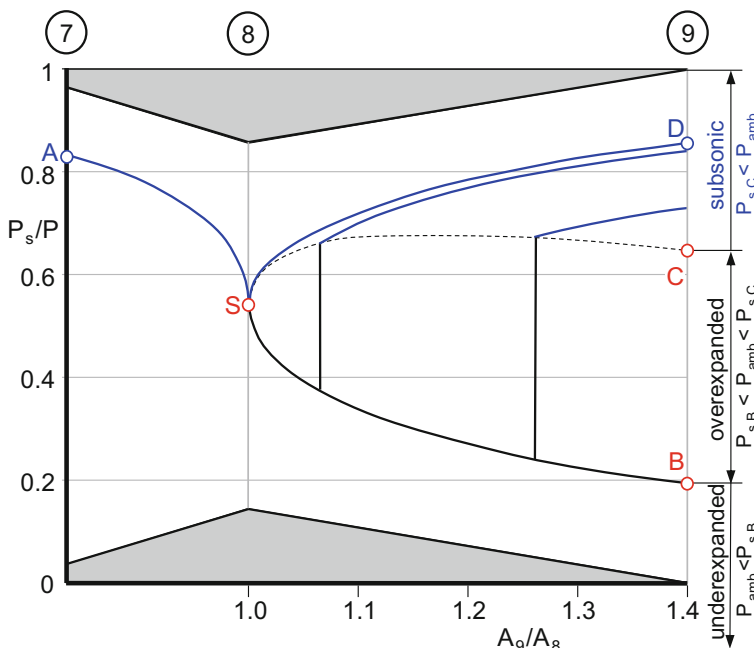


Fig. 1.7-6 Static pressure behavior in a perfect convergent-divergent nozzle

velocity) and further to point B. The flow is isentropic; the pressure ratio is ideal for that geometry. The thrust is simply $F_9 = W_9 V_9$.

If the ambient pressure is lower, then the static pressure evolution inside of the nozzle remains the same as before. The thrust equation, however, must be complemented with a pressure term:

$$F_9 = W_9 V_9 + A_9(P_{s9} - P_{amb}) \quad (1.7-4)$$

Nothing dramatic happens when ambient pressure is a bit higher than P_{s9} . The pressure term in the thrust equation becomes negative, but that's all. However, if the ambient pressure rises to that corresponding with point C, then suddenly a vertical shock appears in the nozzle exit. This shock decelerates the velocity to subsonic Mach number and consequently the thrust is much lower than before. Increasing ambient pressure further moves the vertical shock towards the nozzle throat. When the ambient pressure is an epsilon higher than indicated by point D then the velocity is subsonic throughout the nozzle. In other words: in the region above the line A-S-D the flow behaves as a venturi.

The performance of a convergent-divergent nozzle can be characterized by a suitably defined thrust coefficient. The ideal thrust coefficient $C_{FG,id}$ compares the actual thrust with the one produced by an ideal expansion to ambient pressure, whatever the actual nozzle area ratio is. $C_{FG,id}$ is equal to unity only when there are no losses and the nozzle area ratio “matches” the pressure ratio. This definition of a thrust coefficient is well suited for nozzle design studies.

Figure 1.7-7 shows the relation of ideal thrust coefficient with nozzle area ratio and pressure ratio. Each of the curves with constant A_9/A_8 reaches $C_{FG,id} = 1$ at a distinct value of pressure ratio. When the pressure ratio is higher, the flow is under expanded and $C_{FG,id}$ drops moderately. To the left of the optimum pressure ratio, however, $C_{FG,id}$ decreases more rapidly especially if the nozzle area ratio is well above the optimum for the pressure ratio. This is the region of an over expanded and subsonic nozzle exit flow.

Operating a convergent-divergent nozzle which was designed for a high nozzle pressure ratio at low pressure ratio is very inefficient. Compare the two points A and B in Fig. 1.7-7. At a pressure ratio of 2, the nozzle with area ratio $A_9/A_8 = 1.28$ generates approximately 6.4% less thrust than a nozzle with $A_9/A_8 = 1.05$.

1.7.2.2 Reality

Until now we have only spoken about the performance of a perfect convergent-divergent nozzle without friction, leakage, and other imperfections. Let us now consider the performance of real nozzles, as they are used on fighter aircraft engines with an afterburner. The latter demands that the throat area is variable: dry operation requires a much lower throat area than operation with afterburner lit, where the volumetric flow rate is increased tremendously.

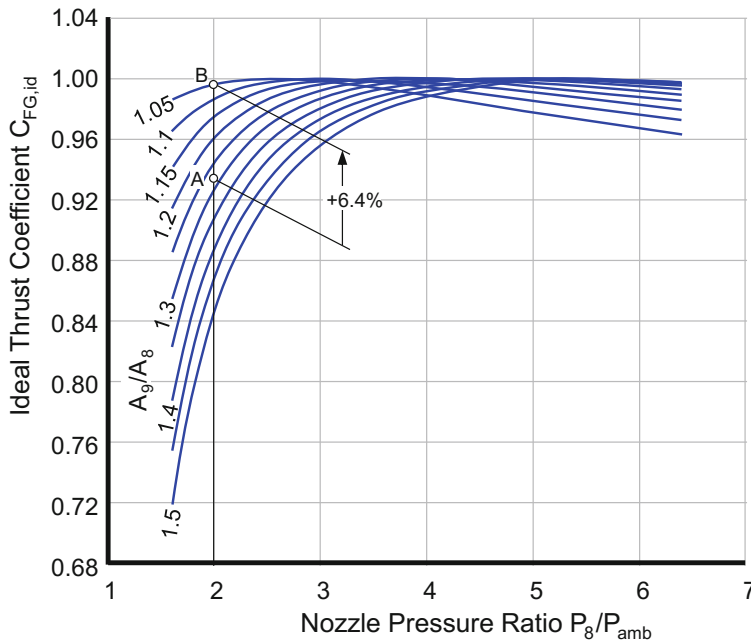


Fig. 1.7-7 Ideal thrust coefficient of perfect convergent-divergent nozzles

Nearly all convergent-divergent nozzles on existing engines are of circular design. The throat and exit area control is achieved with various mechanical arrangements of actuators, struts, and rings. Figure 1.7-8 shows as a typical example the basic design of the GE F101 and the EJ200 nozzles. An actuator ring with rollers controls the position of the primary petals and thus the throat area A_8 . The nozzle is fully open when the actuator ring is in the rear position and closes when a set of hydraulic actuators pulls the ring forward. The master petals of the divergent nozzle section are hinged directly to the primary petals and supported by external struts.

Slave petals close the gap between the master petals which open when the nozzle exit diameter increases. The maximum width of the slave and master petals is restricted by the circumference of the nozzle in the closed position; the petals touch each other. The sum of the width of all petals limits the circumference of the nozzle in the most open position.

The actual area ratio depends not only on the roller track shape and the geometric arrangement of petals and struts. The temperature of the primary petals also plays a role. Even a small thermal expansion of the primary petals causes a significant change in A_9/A_8 , as illustrated in Fig. 1.7-9. It makes a difference whether the afterburner is off or on! Nevertheless, we can describe the complex geometric relations between petal movement, roller track shape and strut positions with a simple nozzle area schedule as shown, for example, in Fig. 1.7-10.

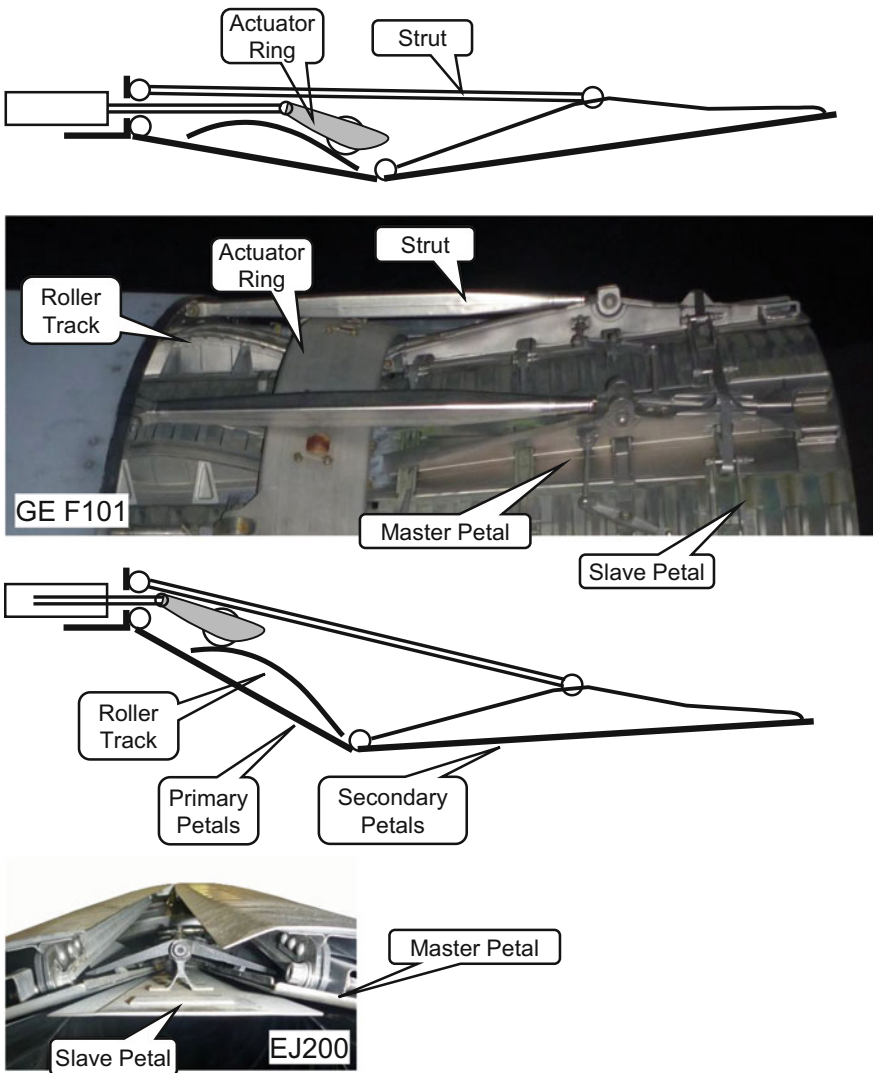


Fig. 1.7-8 Geometry of circular convergent-divergent nozzles

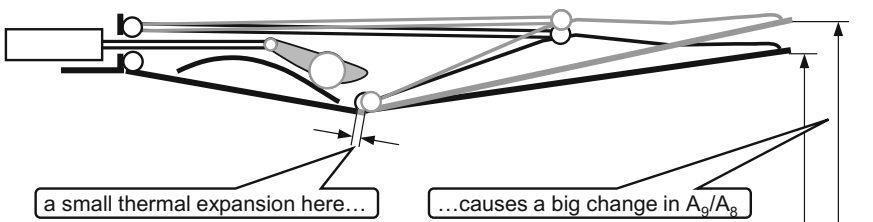


Fig. 1.7-9 Primary petal temperature effect on nozzle area ratio

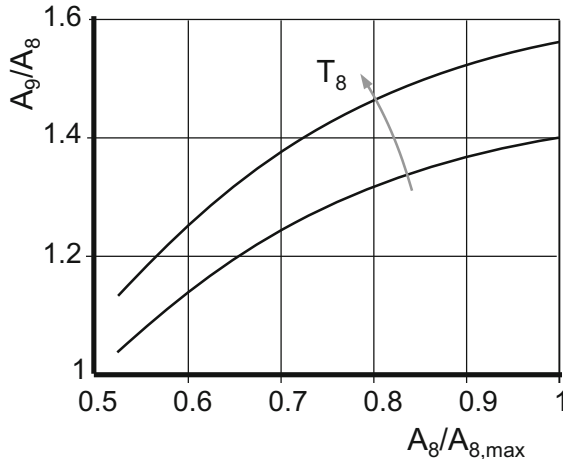


Fig. 1.7-10 Nozzle area ratio as function of relative throat area and temperature

Now let us examine the flow inside the convergent-divergent nozzle and compare theory with reality. Reference [32] contains test data from the EJ200 turbofan which are suited for this purpose. Three pressure measurements are key to understanding the behavior of the nozzle: inlet total pressure P_8 (derived from a static pressure pickup at the nozzle entry P_{s7}), the static pressure measured on the inner side of the master petals near to the nozzle exit (P_{s9}) and the pressure to which the flow expands, P_{amb} . Figure 1.7-11 contains these data which are all from dry operation (afterburner not lit), complemented with lines for constant area ratio which represent theory.

Let us examine what happens along the line $A_9/A_8 = 1.05$, starting at point U. The nozzle pressure ratio is high, the static pressure P_{s9} is higher than P_{amb} and the flow is under-expanded. The two pressures are equal at point M, where we have a perfect alignment of pressure ratio P_8/P_{amb} and area ratio $A_9/A_8 = 1.05$. Reducing the pressure ratio to lower values than at point M leads to over-expanded flow conditions with $P_{s9} < P_{\text{amb}}$. The nozzle exit static pressure decreases until point S where a vertical or normal shock appears, which increases the pressure to P_{amb} (point A).

It immediately strikes the eye that none of the measured data points is in the lower part of the over-expanded region. The nozzle exit pressure is never less than 90% of the ambient pressure. Why is that?

The shape of the roller track defines how the area ratio A_9/A_8 varies from the closed to the open nozzle position. Low area ratios are appropriate during subsonic cruise, when the nozzle is closed, because then the nozzle pressure ratio is small. High supersonic Mach numbers are achievable only with the afterburner on. In this flight phase, both nozzle pressure ratio and optimum area ratio are high. Therefore,

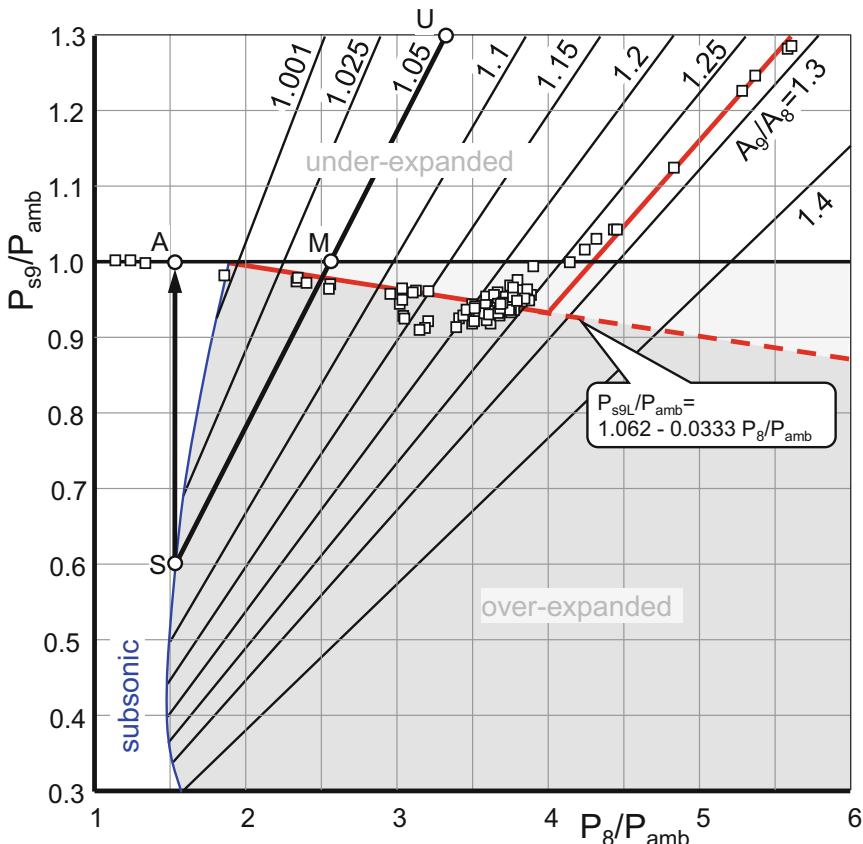


Fig. 1.7-11 Nozzle exit static pressure P_{s9}/P_{amb} as function of nozzle pressure ratio

the roller track and the hinge positions of the strut are selected in such a way that the closed nozzle has a low area ratio A_9/A_8 and the open nozzle a high area ratio.

The explanation of this scenario is simple. When the pressure outside the nozzle is higher than that inside the divergent section, then the slave petals detach from the master petals and create a path for ambient air. This reduces the effective nozzle exit area A_9 , the effective area ratio A_9/A_8 becomes smaller than the geometric area ratio. Figure 1.7-12 shows this feature clearly during a maximum reheat operation on a sea level testbed. The slot between slave and master panels is also visible in the lower part of Fig. 1.7-8.

The slave petals touch the master petals provided that P_{s9} is greater than ambient pressure. Now the flow follows the hardware geometry; the data points with pressure ratios higher than 4.5 are all on the $A_9/A_8 = 1.28$ line in Fig. 1.7-11.

Figure 1.7-11 includes an empirical correlation for the over-expansion limit. For each nozzle pressure ratio, we can read what the effective nozzle area ratio is from the limit line. We can locate this area ratio in the drawing of a nozzle with the

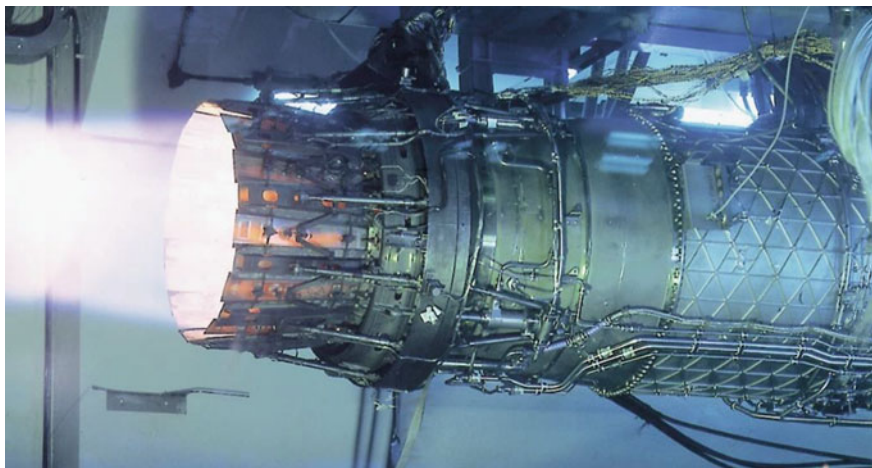


Fig. 1.7-12 Maximum reheat on a sea level testbed (© EUROJET Turbo GmbH)

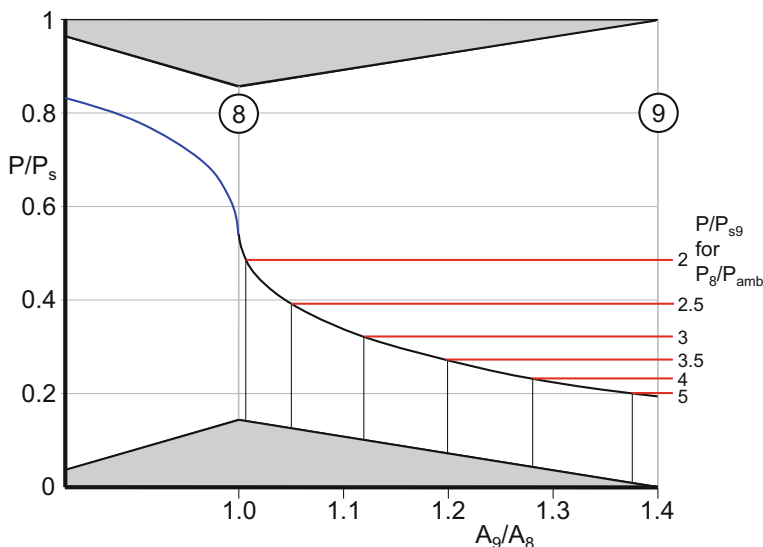


Fig. 1.7-13 An imaginary flow detachment position

geometric area ratio of $A_9/A_8 = 1.4$, for example (Fig. 1.7-13). In a simplified view of the complex reality, we can interpret the axial position of the over-expansion limit as the location where the flow detaches.

Figure 1.7-14 explains the difference between the two simulations. Without restriction of over-expansion, the jet velocity remains constant almost over the complete range of pressure ratios (the black line). Below a pressure ratio of 1.5, a vertical shock occurs within the nozzle which decreases the velocity dramatically.

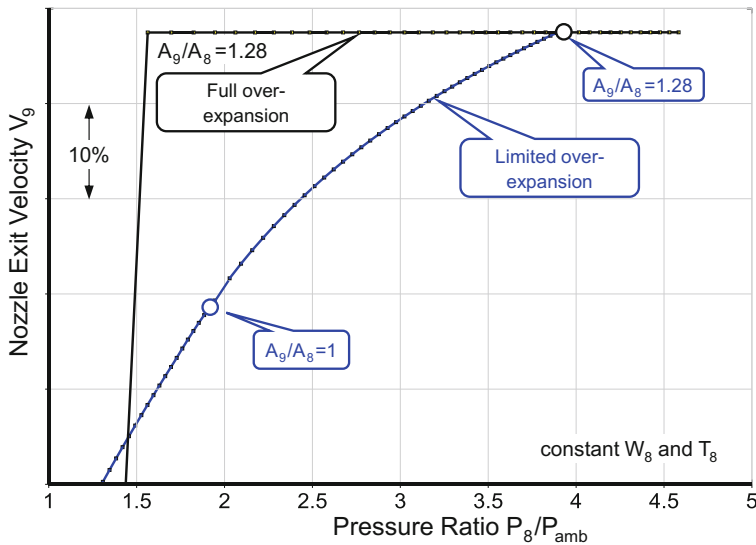


Fig. 1.7-14 Nozzle exit velocity with and without flow detachment simulation

The blue line represents the simulation with limited over-expansion. Beginning at pressure ratio 3.9 and ending at pressure ratio 2.1, the nozzle area ratio decreases from 1.28 to unity. In parallel with the area ratio, the jet velocity decreases and there is a smooth transition from supersonic to subsonic nozzle exit velocity.

More interesting than the jet velocity, is what happens to thrust. Although jet velocity is lower only when limited over-expansion happens, thrust is higher

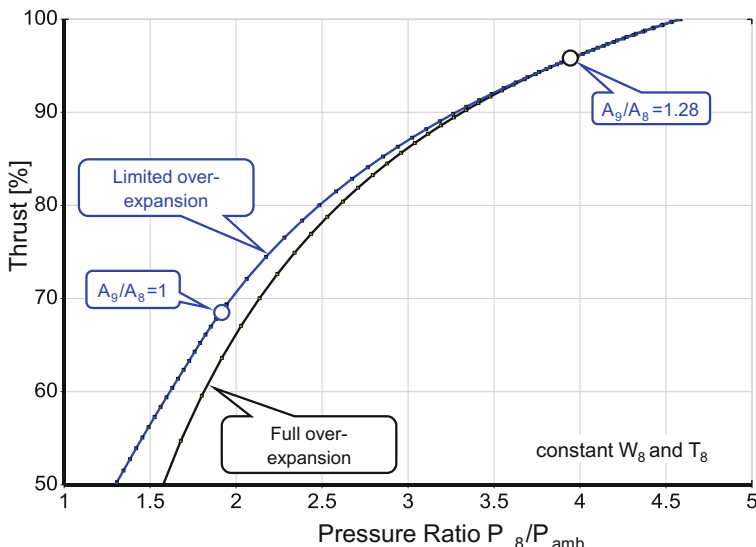


Fig. 1.7-15 Thrust with and without flow detachment simulation

(Fig. 1.7-15). The difference between the two simulations grows with decreasing pressure ratio.

Figure 7 in Ref. [32] contains test data which permit a comparison between our simulation and measurements. The flow conditions of an ideal expansion to the geometric nozzle exit area A_9 serve as an arbiter of the nozzle performance.

Gross thrust is

$$F_9 = W_9 V_9 C_A C_f C_{V9} + A_9 (P_{s9} - P_{amb}) \quad (1.7-5)$$

In this formula, C_A is the angularity coefficient from Ref. [33], Fig. 5.12, which takes into account the losses due to the non-axial exit of the exhaust gases from the nozzle. The coefficient C_f from Ref. [33], Fig. 5.13 accounts for the effects of boundary-layer momentum loss, caused by friction in the nozzle. Both these coefficients depend on the nozzle area ratio and the primary petal angle. The velocity coefficient C_{V9} reconciles the measured thrust with theory.

Note that the definition of the velocity coefficient C_{V9} from Ref. [32] is identical to that of our thrust coefficient C_{FG} .

Figure 1.7-16 shows the nozzle velocity coefficient C_{V9} synergized from engine tests over a wide range of ratings, altitudes, and Mach number. The original C_{V9} data points from Ref. [32] for pressure ratios below 3 are marked with yellow symbols. As the nozzle pressure ratio reduces towards 1, the value of C_{V9} increases well above 1 because the underlying theory of the reference condition includes the full theoretical over-expansion. When the calculated theoretical thrust is too low, velocity coefficients higher than 1 are needed to reconcile this unrealistic model with measurements.

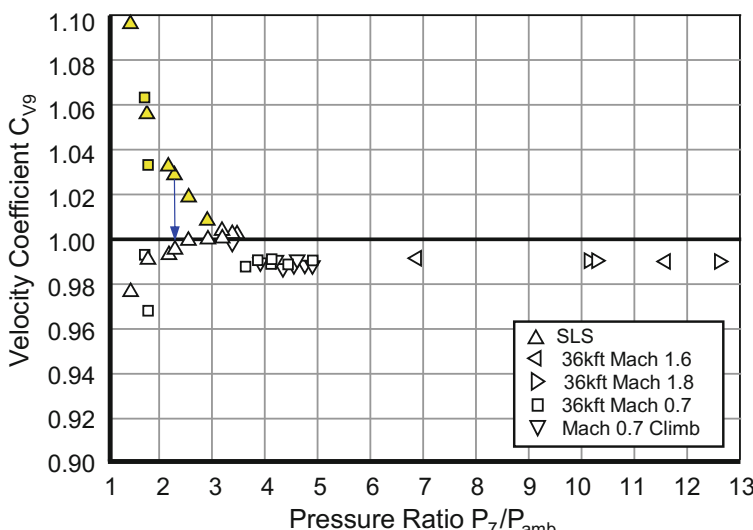


Fig. 1.7-16 Comparison with altitude test facility results

We get a much more meaningful result if we employ the simulation with limited over-expansion as the basis for the C_{V9} calculation. The yellow symbols have white counterparts which represent the test analysis results based on the more realistic theory. All the white symbols are within a very narrow tolerance over the full range of tested nozzle pressure ratios.

Note that such a consistent and plausible test analysis result is only feasible because we use a thrust coefficient definition based on the real nozzle geometry. If we use the thrust coefficient $C_{FG,id}$ (based on an ideal expansion to ambient pressure), we would not get a constant value.

1.7.2.3 Implementation

For the calculation of the flow in the nozzle we need correlations between the geometry and the effective flow area. The nozzle throat flow coefficient C_{D8} of a convergent-divergent nozzle varies only with the primary petal angle, see Ref. [33], Fig. 5.7. C_{D9} is constant and equal to 0.995 in our model, if the flow is under-expanded.

Figure 1.7-17 shows how the nozzle area ratio varies along the limiting line in Fig. 1.7-11. This is the highest effective area ratio which occurs in a real nozzle. Before we begin with the calculation of the convergent-divergent nozzle flow, we compare the geometric nozzle area ratio with that in the figure. If the geometric area

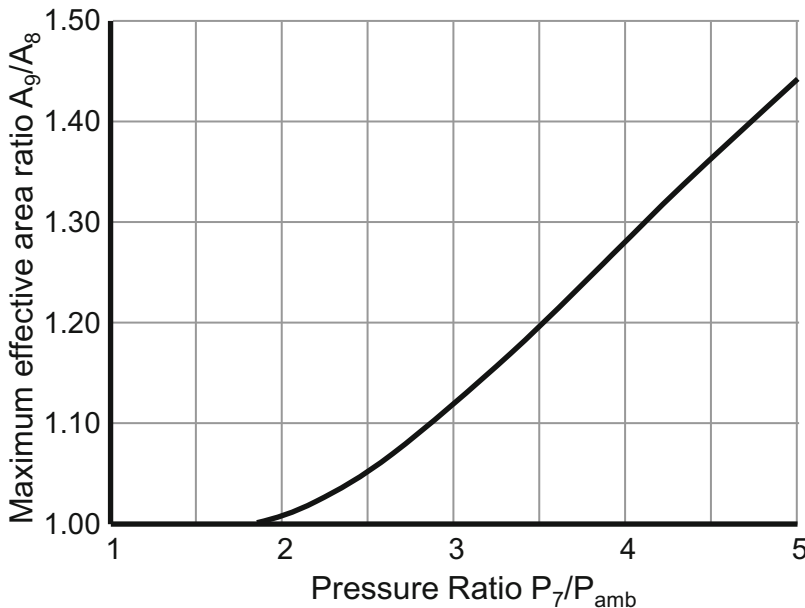


Fig. 1.7-17 Area ratio along the over-expansion limit line

ratio is bigger than the maximum effective area ratio, then we use the value from Fig. 1.7-17 in the calculation. With this procedure, we get values for the static pressure at the nozzle exit that are never lower than those on the limiting curve in Fig. 1.7-11.

We think that this nozzle performance model is not only applicable to the EJ200. The reason for the over-expansion limit is the gap between the master and the slave petals in the divergent part of the nozzle, which opens when the static pressure surrounding the nozzle is higher than the inside pressure. This phenomenon certainly exists on many engines with convergent-divergent nozzles of circular design.

1.8 References

1. Fluid Dynamics Panel Working Group 13 Air intakes for high speed vehicles AGARD Advisory Report AR 270 (1991)
2. Kurzke, J.: Correlations Hidden in Compressor Maps ASME GT2011-45519 (2011)
3. Michael, C.J. Halle, J.E.: Energy Efficient Engine Low-Pressure Compressor Component Test Hardware Detailed Design Report NASA CR-165354 (1981)
4. Lippett, D., Woollatt, G., Ivey, P.C., Timmis, P., Charnley, B.A.: The Design, Development and Evaluation of 3D Aerofoils for High Speed Axial Compressors: Part 1—Test Facility, Instrumentation and Probe Traverse Mechanism ASME GT2005-68792 (2005)
5. Freeman, C.: Method for the prediction of supersonic compressor blade performance. *J. Propul.* **8**(1) (1992)
6. Cumpsty, N., Heynes, A.: Jet Propulsion—A Simple Guide to the Aerodynamic and Thermodynamic Design and Performance of Jet Engines, 3rd edn. Cambridge University Press, Cambridge (2015)
7. Walsh, P.P., Fletcher, P.: Gas Turbine Performance, 2nd edn. Co-published by Blackwell Science Ltd. and ASME Press (2004)
8. Mårtensson, H., Edin, N.: Performance Test and Analysis of the Highly Loaded 1½ Stage Transonic Test Compressor HULDA AIAA Paper 2013-1127, ISABE (2013)
9. RTO Applied Vehicle Technology Panel Task Group AVT-018 Performance Prediction and Simulation of Gas Turbine Engine Operation RTO Technical Report RTO-TR-044 (2002)
10. Kurzke, J., Riegler, C.: A New Compressor Map Scaling Procedure for Preliminary Conceptional Design of Gas Turbines Aircraft Engine Committee Best Paper Award ASME 2000-GT-0006 (2000)
11. Kurzke, J.: Calculation of installation effects within performance computer programs. In: AGARD Lecture Series 183 (1992)
12. Kurzke, J.: Preparing Compressor Maps for Gas Turbine Performance Modeling Manual to Smooth C 8.3 (2013)
13. Broichhausen, K.: Aerodynamic Design of Turbomachinery Components—CFD in Complex Systems AGARD Lecture Series 195 (1994)
14. Stabe, R.G., Whitney, W.J., Moffit, T.P.: Performance of a High-Work Low Aspect Ratio Turbine with a Realistic Inlet Radial Temperature Profile AIAA-84-1161 (1984)
15. Hourmouziadis, J., Albrecht, G.: An Integrated Aero/Mechanical Performance Approach to High Technology Turbine Design AGARD CP 421 (1987)
16. Yoon, S., Curtis, E., Denton, J., Longley, J.: The effect of clearance on shrouded and unshrouded turbines at two levels of reaction. *J. Turbomach.* **136**(2) (2013)
17. McLallin, K.L., Kofskey, M.G., Wong, R.Y.: Cold-Air Performance of a 15.41-cm-Tip Diameter Axial-Flow Power Turbine with Variable-Area Stator Designed for a 75 kW Automotive Gas Turbine Engine NASA TM-82644 (1982)

18. Razinsky, E.H., Kuziak, Jr., W.R.: Aerodynamic performance of a variable nozzle power turbine stage for an automotive gas turbine. *J. Eng. Power*, Page 587ff (1977)
19. Alexiou, A., Roumeliotis, I., Aretakis, N., Tsalavoutas, A., Mathioudakis, K.: Modeling contra-rotating turbomachinery components for engine performance simulations: the geared turbofan with contra-rotating core case. *J. Eng. Gas Turbines Power* **134** (2012)
20. Lefevre, A.H., Ballal, D.R.: *Gas Turbine Combustion*, 3rd edn. CRC Press (2010)
21. Doerr, T.: Rolls Royce Deutschland introduction to aero-engine gas turbine combustion. In: *Aero-Engine Design: From State of the Art Turbofans Towards Innovative Architecture Von Karman Institute for Fluid Dynamics Lecture Series 9–12 Apr 2013*
22. Münzberg, H.G., Kurzke, J.: *Gasturbinen—Betriebsverhalten und Optimierung*. Springer Verlag Berlin Heidelberg New York (1977)
23. Grieb, H.: *Projektierung von Flugtriebwerken* Birkhäuser Verlag (2004)
24. Kozlowski, H., Larkin, M.: Energy Efficient Engine Exhaust Mixer Model Technology Report NASA-CR-165459 (1982)
25. Sotheran, A.: High Performance Turbofan Afterburner Systems AIAA-87-1830 (1987)
26. Flack, R.D.: *Fundamentals of Jet Propulsion with Applications*. Cambridge University Press, Cambridge (2005)
27. Grieb, H.: *Projektierung von Turboflugtriebwerken* Birkhäuser Verlag (2004)
28. Farokhi, S.: *Aircraft Propulsion*, 2nd edn. Wiley, New York (2014)
29. Kurzke, J., Riegler, C.L: A Mixed Flow Turbofan Afterburner Simulation for the Definition of Reheat Fuel Control Laws Presented at the RTO AVT Symposium “Design Principles and Methods for Aircraft Gas Turbine Engines” RTO MP-8 (1998)
30. Grey, R.E., Wilsted, H.D.: Performance of Conical Jet Nozzles in Terms of Flow and Velocity Coefficients NACA TN 1757 (1948)
31. E-33 In Flight Propulsion Measurement Committee In-Flight Thrust Determination AIR1703A, SAE International (2012)
32. Kurzke, J., Riegler, C.: A mixed flow turbofan afterburner simulation for the definition of reheat fuel control laws. Paper presented at the RTO AVT Symposium on “Design Principles and Methods for Aircraft Gas Turbine Engines”, Toulouse, France 1998 Published in RTO MP-8
33. Aircraft Propulsion Systems Technology and Design Edited by Gordon C. Oates AIAA Education Series (1989)
34. Uchida, H., et alii.: Development of Centrifugal Compressor for 100 kW Automotive Ceramic Gas Turbine. ASME 94-GT-73 (1994)
35. Hobbs, D.E., Weingold, H.D.: Development of controlled diffusion airfoils for multistage compressor application. *J. Eng. Gas Turbines and Power* **106**, p. 271. (ASME Paper 83-GT-211) (1984)
36. Creason, T.L., Baghdadi, S.: Design and Test of a Low Aspect Ratio Fan Stage AIAA-88-2816 (1988)
37. Bernini, E., Toffolo, A.: Axial-Flow Compressor Model Based on a Cascade Stacking Technique and Neural Networks ASME GT2002-30443 (2002)
38. Cline, S.J., Fesler, W., Liu, H.S., Lovell, R.C., Shaffer, S.J.: Energy Efficient Engine High Pressure Compressor Component Performance Report NASA CR-168245 (1983)
39. Savic, S.M., Micheli, M.A.: Redesign of a Multistage Axial Compressor for a Heavy Duty Industrial Gas Turbine (GT11NMC) ASME GT2005-68315 (2005)
40. Kazawa, J., Nishizawa, T., Masaki, D.: Numerical Analyses of Flutter Characteristics of Titanium and Composite Fan Rotor Blade AIAA Paper 2011-1247, ISABE (2011)
41. Hobbs, D.E., Weingold, H.D.: Development of controlled diffusion airfoils for multistage compressor application. *J. Eng. Gas Turbines Power* **106**, p. 271. (ASME Paper 83-GT-211) (1984)
42. Song, B., Ng, W.F.: Performance and Flow Characteristics of an Optimized Supercritical Compressor Stator Cascade ASME Turbo Expo. GT2005-68569 (2005)
43. Schnell, R., Giebmanns, A., Nicke, E., Dabrock, T.: Aerodynamic Analysis of a Fan for Future Ultra-High-Bypass-Ratio Aero Engines AIAA Paper 2009-1149, ISABE (2009)

44. Jerez Fidalgo, V., Hall, C.A., Colin, Y.: A Study of Fan-Distortion Interaction within the NASA Rotor 67 Transonic Stage ASME Turbo Expo, 2010-GT-22914 (2010)
45. Schmücker, J., Schäffler, A.: Performance deterioration of axial compressors due to blade defects. In: AGARD Conference Proceedings 558 (1994)
46. Amrish babu, D., Arun, K.K., Anandanarayanan, R.: Optimization of pattern factor of the annular gas turbine combustor for better turbine life IOSR. J. Mech. Civil Eng. (IOSR-JMCE) (2015)
47. Kurzke, J.: Effects of Inlet Flow Distortion on the Performance of Aircraft Gas Turbines ASME GT-2006-90419 (2006)
48. Loud, R.L., Slaterpryce, A.A.: Gas Turbine Air Treatment GE Company, Schenectady, Report GER-3419A
49. Melissa, W., Kurz, R., Brun, K.: Technology review of modern gas turbine inlet filtration systems. Int. J. Rotating Mach. **2012** (2012)
50. Kurzke, J.: An Enhanced Off-Design Performance Model for Single Stage Fans ASME Turbo Expo, GT2014-26449 (2014)
51. Glassman, A.J.: Turbine Design and Application, Vol. 1 NASA SP-290 (1972)
52. McAulay, J.E., Abdelwahab, M.: Experimental Evaluation of a TF30-P-3 Turbofan Engine in an Altitude Facility: Afterburner Performance and Engine-Afterburner Operating Limits NASA TN D-6839 (1972)
53. Report of the RTO AVT Task Group AVT-018 Performance Prediction and Simulation of Gas Turbine Engine Operation RTO-TR-044 (2002)

Chapter 2

Understanding Off-Design Behavior



The ability to work through a gas turbine engine cycle by hand—at least for the design point—is something that should be acquired by all young engineers. Manipulation of the theoretical thermodynamic process (using simple tables of C_p and γ for air and combustion products at various fuel/air ratios) provides valuable insight into flow- and energy-balance, how ideal and real temperatures and pressures are related via efficiency, and the overall iterative approach which must be taken. In fact, such an exercise constitutes the most basic foundation for all performance codes. However, the iterative calculation sequence is quite cumbersome and very time-consuming—even more so when we move to off-design examples and complex engine cycles. So once the basic knowledge has been established, the next logical step, soon taken by most propulsion engineering students, is to capture those same, simple calculations in a spreadsheet. Fortunately, if we are serious about doing this, a number of quite sophisticated computer programs are now available and their use enables us to progress rapidly towards understanding the influence of the relevant design parameters & variables on engine performance without having to focus on specific theoretical details. It is critical that a gas turbine designer or performance specialist does more than enter input data and believe the output! Fortunately, current commercial design codes give us answers within fractions of seconds and enable us to explore appropriate *design spaces* and the consequences of design decisions in acceptable time frames.

Before running any computer program, an aspiring designer or performance analyst should first think *What do I want to accomplish?* For example, if the surge margin of the core compressor is marginal, the question is *What is the reason for it and what can be done to improve the situation?* If a growth variant of an engine is of interest, then *what design options are open?* If measurements on a test bed indicate a degraded engine performance, *which compressor or turbine is the most likely source?* Just playing with the input data and hoping that the solution will somehow manifest itself is usually in vain. The well-known phrase *garbage in—garbage out* should now spring to mind! You should have an idea about what will

happen if you modify the input to your program, but such thoughts can only be based on knowledge and we hope to accelerate the learning experience here.

This chapter describes the principles of gas turbine off-design behavior. Understanding these principles is the prerequisite of the effective and professional use of any gas turbine performance program. When you know something of how the gas turbine works, then you can ask reasonable questions of your performance program.

We begin with a look at the off-design behavior of some jet engine components and after that we describe how they work together.

2.1 Turbojet

The straight turbojet is the simplest gas turbine and it consists of the four main components—compressor, burner, turbine and nozzle, as shown in Fig. 2.1-1. Understanding the performance and component-matching of a turbojet is the key to understanding the behavior of the gas generator in any multi-spool engine.

2.1.1 *Off-Design Behavior of the Components*

2.1.1.1 Compressor

Figure 2.1-2 shows the map of a compressor. It describes how total pressure ratio and efficiency vary with spool speed and mass flow.

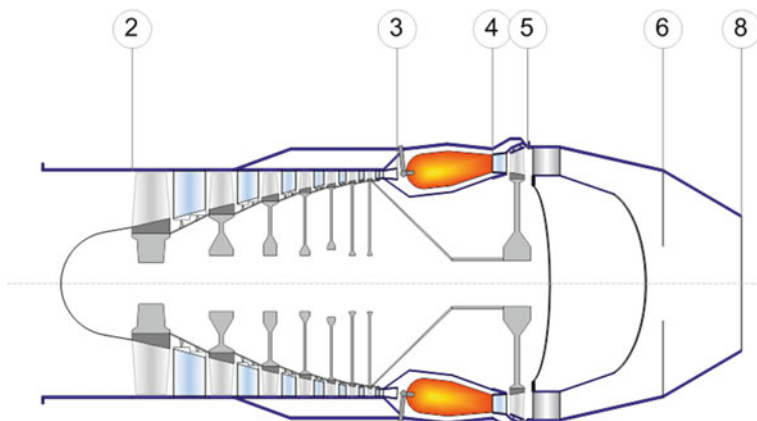


Fig. 2.1-1 Turbojet thermodynamic station nomenclature

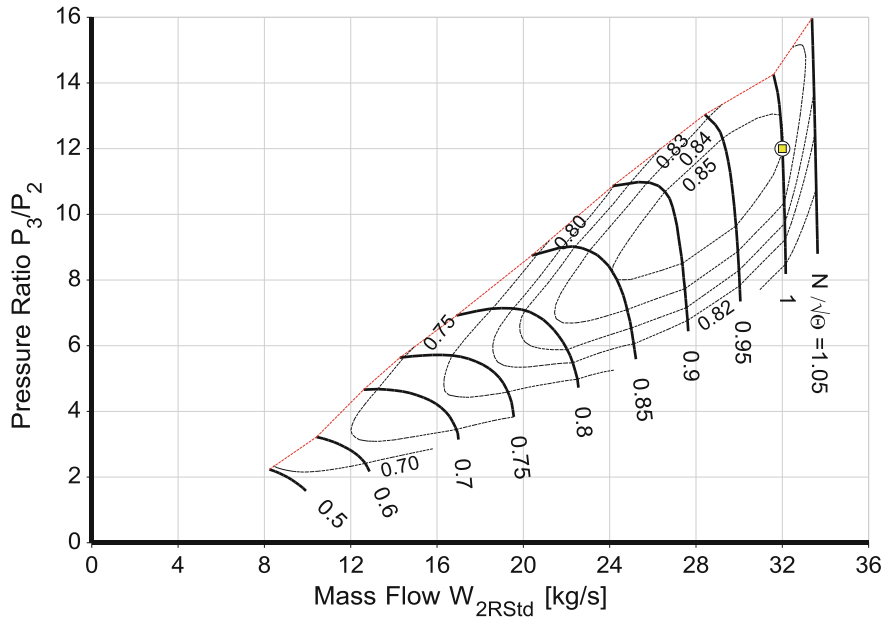


Fig. 2.1-2 Compressor map

Let us first discuss the numbers along the x-axis. This is not simply mass flow; it is the mass flow the compressor would deliver on a standard day—the so-called standard day corrected mass flow W_{2RStd} which is defined as

$$W_{2RStd} = \frac{W_2 \sqrt{\Theta_2}}{\delta_2} = W_2 \sqrt{\frac{T_2}{T_{Std}} \frac{P_{Std}}{P_2}} \quad (2.1-1)$$

It is convenient to use the ratios $\Theta_2 = T_2/T_{Std}$ and $\delta_2 = P_2/P_{Std}$ rather than T_2 and P_2 themselves because the units of the corrected flow are then the same as those of the true flow. The dimensions of standard day corrected mass flow are kg/s in SI units. On an ISA day, the true mass flow is equal to the standard day corrected value W_{2RStd} .

So what is the significance of corrected mass flow and why do we use it? It is an indirect measure of the Mach number in the compressor entry area A and therefore is valuable as a determinant of aerodynamic similarity. Mach number is the ratio of true flow velocity $V = W/(A \rho)$ to sonic velocity $V_{sonic} = \sqrt{(\gamma RT_s)}$:

$$M = \frac{V}{V_{sonic}} = \frac{W}{A \rho \sqrt{\gamma RT_s}} = \frac{WRT_s}{AP_s \sqrt{\gamma RT_s}} = \frac{W \sqrt{\frac{R}{\gamma}} T \sqrt{\frac{T_s}{T}}}{AP \frac{P_s}{P}} \quad (2.1-2)$$

From the last expression in this equation—because the total/static ratios P/P_s and T/T_s depend only on the isentropic exponent γ and Mach number—it follows that

$$\frac{W\sqrt{RT}}{AP} = f(M, \gamma) \quad (2.1-3)$$

If we ignore possible variations in the gas constant R (due to humidity, for example), then we can say that the both the reduced mass flow parameter $W * \sqrt{T}/P$ and the corrected mass flow $W\sqrt{\Theta}/\delta$ are measures of the Mach number at compressor entry.

While the corrected mass flow is an indication of the flow Mach number in the axial direction, the corrected speed is related to the rotor blade Mach number in the circumferential direction:

$$M_U = \frac{U}{V_{sonic}} = c \frac{N}{\sqrt{\gamma RT_s}} = c \frac{N}{\sqrt{\gamma RT}} \frac{T}{T_s} \quad (2.1-4)$$

If we neglect the influence of the gas constant R then we get

$$\frac{N}{\sqrt{T}} = f(M, \gamma) \quad (2.1-5)$$

The compressor map co-ordinates, corrected mass flow and corrected spool speed, together set the Mach number and the flow angle relative to the first rotor. In turn Mach number and incidence determine the losses in the compressor and hence its efficiency.

Compressor performance changes also due to changes in Reynolds number, tip clearance, interstage bleed air offtake etc. For the moment, we neglect these secondary effects.

2.1.1.2 Burner

Apart from its influence on the residence time of combustion products in the burner and the successful completion of the process, velocity does not play much of a role in its design and operation. The chemical reaction between fuel and air dominates the process. Of course the quality or effectiveness of the process is very important and that depends largely on how well the fuel and oxygen can be mixed and brought into contact.

We are willing to accept a significant loss in total pressure—typically around 4%—to ensure that. The temperature rise in the burner depends primarily on the fuel/air ratio and secondarily on the pressure in the burner if burner exit temperature is above 1600 K. At 2000 kPa pressure, the hydrocarbon fuel used in aircraft engines creates the temperature rise shown in Fig. 2.1-3.

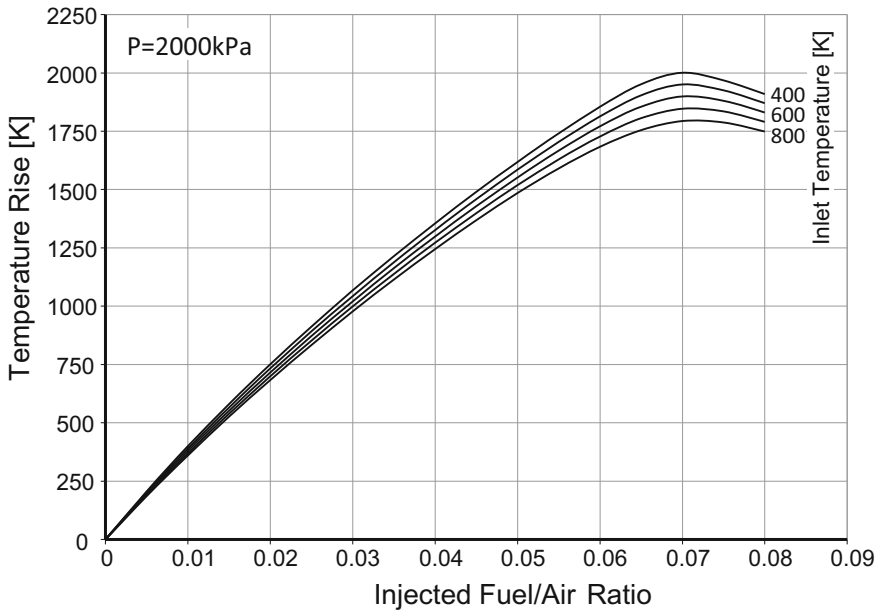


Fig. 2.1-3 Temperature rise capability with hydrocarbon fuel at a pressure of 2000 kPa

2.1.1.3 Turbine

When we plot the performance of a turbine employing the same co-ordinates as used in the compressor map, it looks like Fig. 2.1-4. The turbine is located between thermodynamic stations 4 and 5 of the turbojet; thus the turbine pressure ratio is P_4/P_5 . The corrected flow of the turbine is composed from mass flow, temperature and pressure at the rotor inlet, the intermediate station 41. No work is done between stations 4 and 41, but total temperature decreases due to the introduction of cooling air to the nozzle guide vane NGV. T_{41} and W_{41} are the relevant parameters for the work transfer in the turbine. Therefore, we calculate the corrected turbine mass flow as $W_{41}\sqrt{\Theta_{41}/\delta_4}$ with $\Theta_{41} = T_{41}/T_{\text{std}}$ and $\delta_4 = P_4/P_{\text{std}}$. The corrected mass flow at the turbine design point is called the turbine capacity. Station 41 is especially important to a turbine designer, because it is there that the very hot working fluid first encounters a rotating component.

The narrow range of corrected mass flow above the pressure ratio 2.8 stands out. The range of corrected flow can become a single value if the turbine nozzle guide vane chokes and causes the speed lines to coalesce. It is difficult to read efficiency values from this map because all the corrected speed lines are so close to each other. A turbine map in the form of Fig. 2.1-4 is not really suitable for practical use.

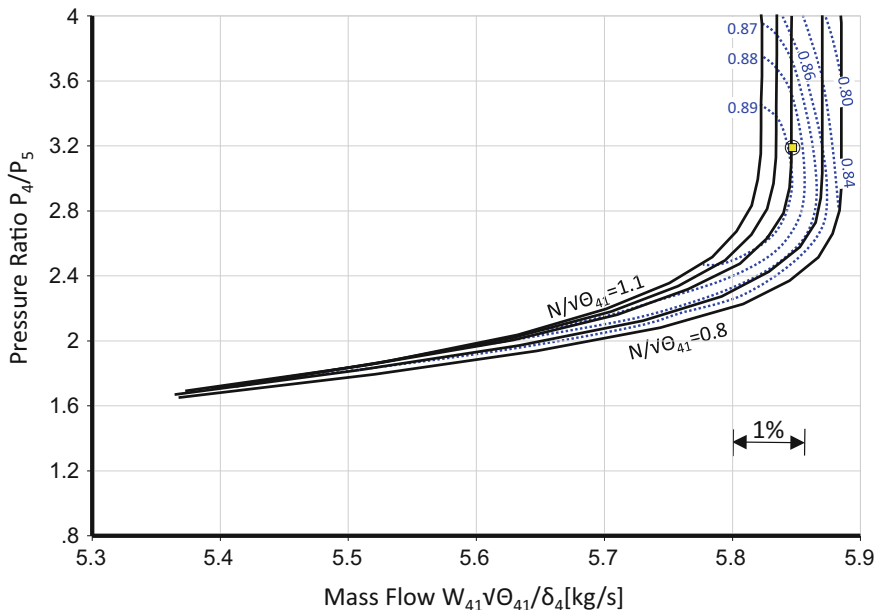


Fig. 2.1-4 Turbine map in the format of a compressor map

We can easily eliminate this difficulty with a mathematical trick: we simply multiply corrected mass flow by the corresponding corrected speed and use the product on the x-axis. Then the turbine map looks like Fig. 2.1-5 and we can assess the operating line much easier from this format.

2.1.1.4 Exhaust Nozzle

The corrected flow per unit area through a nozzle reaches its maximum at sonic conditions, where Mach = 1. Note that for a given area the corrected flow reaches 90% of its maximum value when Mach number is only 0.68, as shown in Fig. 2.1-6. Theoretical considerations based on the assumption of sonic flow are useful also for high subsonic Mach number.

2.1.2 Component Synergy

There are a few simple correlations which are the key to understanding the off-design behavior of a turbojet engine. We will show later that those very same principles apply to the gas generator of any multi-spool gas turbine.

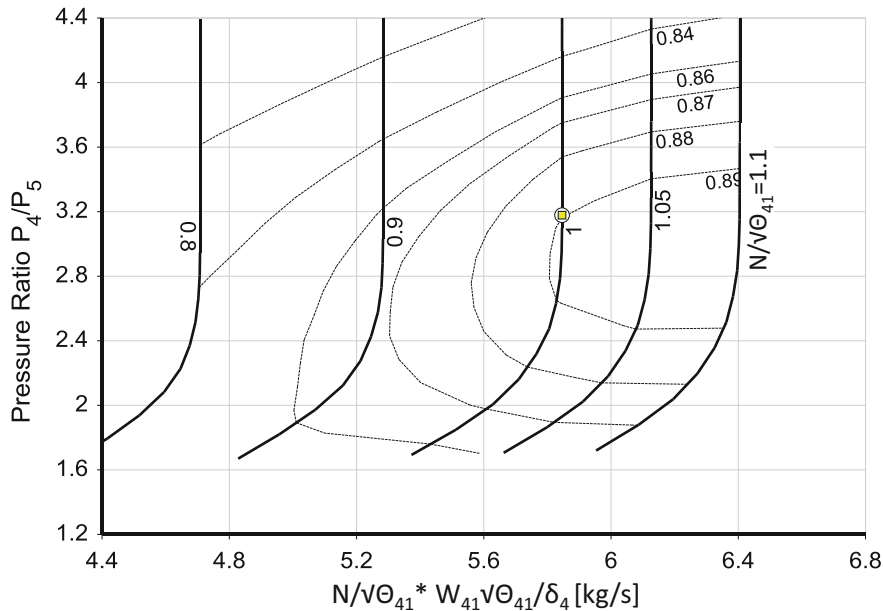


Fig. 2.1-5 Turbine map

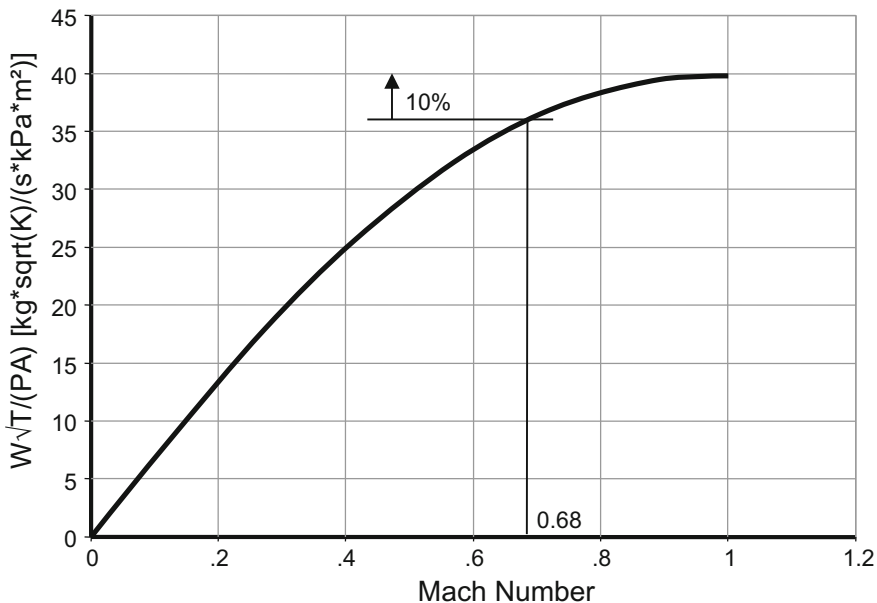


Fig. 2.1-6 Reduced flow per area through a nozzle

2.1.2.1 Flow Conservation Between Compressor and Turbine

Let us make some simplifications first:

1. We limit our considerations to high power operation.
2. The fuel mass flow is small compared to the total mass flow.
3. The pressure losses in the combustion chamber are small and a constant fraction of the entry pressure.
4. The bleed and cooling air elements are constant fractions of the compressor inlet mass flow.

$$W_{41}/W_2 = \text{const} \quad (2.1-6)$$

We can expand this relationship in such a way that it consists only of an area ratio, pressure ratios, a temperature ratio and corrected flows.

$$\frac{W_2\sqrt{T_2}}{A_2P_2} = \frac{W_{41}\sqrt{T_{41}}}{A_{41}P_4} \frac{A_{41}}{A_2} \frac{P_4}{P_3} \frac{W_2}{W_{41}} \frac{P_3}{P_2} \sqrt{\frac{T_2}{T_{41}}} \quad (2.1-7)$$

Three terms on the right side of this equation are constant:

- $W_{41}\sqrt{T_{41}}/(A_{41}P_4)$ is constant because the velocity in the NGV throat is (nearly) sonic
- P_4/P_3 and W_2/W_{41} are constant because of simplifications 3 and 4 respectively.

We can rearrange Eq. (2.1-7) as follows:

$$\frac{P_3}{P_2} = \frac{1}{\frac{W_{41}\sqrt{T_{41}}}{A_{41}P_4} \frac{A_{41}}{A_2} \frac{P_4}{P_3} \frac{W_2}{W_{41}}} \sqrt{\frac{T_{41}}{T_2} \frac{W_2\sqrt{T_2}}{P_2}} \quad (2.1-8)$$

In this format the equation describes a family of linear relationships between pressure ratio and corrected flow that pass through the origin {0,0}; for each, the change in slope is driven by the temperature ratio T_{41}/T_2 , since the first term is constant.

We can draw two important conclusions from this equation:

- Efficiency variations do not influence the position of the T_{41}/T_2 lines in the compressor map because neither compressor nor turbine efficiency appear in the equation.
- The slopes of the T_{41}/T_2 lines are reduced when bleed air is taken from the compressor, increasing the mass ratio W_2/W_{41} .

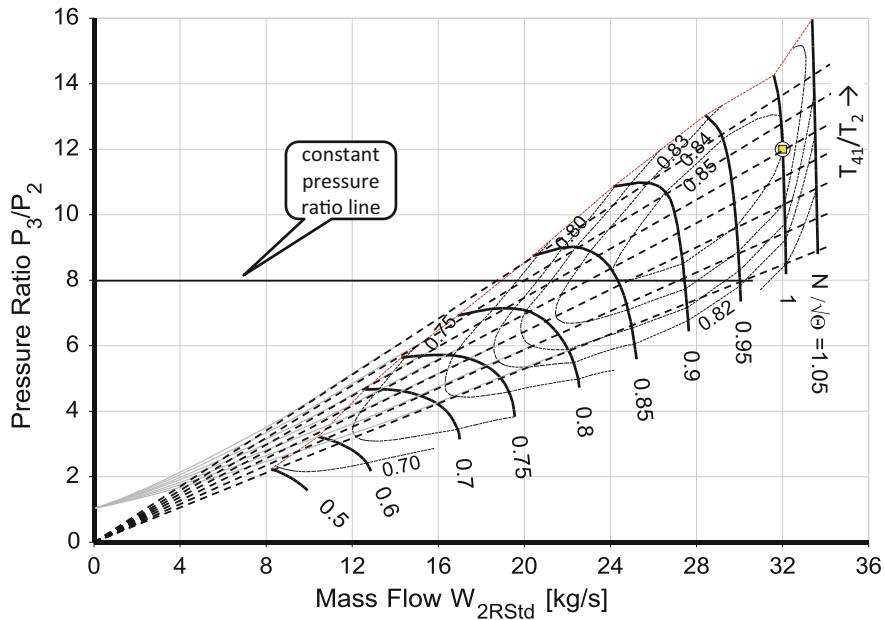


Fig. 2.1-7 Lines of constant T_{41}/T_2 in the compressor map

Note that the assumption of constant $W_{41}\sqrt{T_{41}}/(A_{41}P_4)$ is not valid over the full thrust range. At low power $W_{41}\sqrt{T_{41}}/(A_{41}P_4)$ decreases according to Fig. 2.1-7 with the consequence that P_3/P_2 increases. Therefore, in reality, the family of T_{41}/T_2 lines does not pass through the origin but through the point $\{0,1\}$.

2.1.2.2 Flow Conservation Between Turbine and Nozzle

We now evaluate the mass flow continuity between turbine and nozzle to get another important insight into the off-design behavior of a turbojet engine. We expand and arrange the equation $W_8 = \text{const} * W_{41}$ in a similar manner as the approach above to get another equation which consists only of pressure, temperature, mass flow and area ratios, as well as corrected flow terms:

$$\frac{W_{41}\sqrt{T_{41}}}{A_{41}P_4} = \frac{W_8\sqrt{T_8}}{A_8P_8} \frac{W_{41}}{W_8} \frac{A_8}{A_{41}} \frac{P_8}{P_5} \sqrt{\frac{T_5}{T_8}} \sqrt{\frac{P_5}{P_4}} \sqrt{\frac{T_{41}}{T_5}} \quad (2.1-9)$$

We have mentioned before, that we limit our theoretical considerations to the high power range. However, we did not say what we exactly mean by *high power*. Now we clarify the term *high power operation* by applying it only to operation with sonic flow in the nozzle throat. The corrected flow per area $W_8\sqrt{T_8}/(A_8P_8)$ is constant and equal to $W_{41}\sqrt{T_{41}}/(A_{41}P_4)$ because we have the sonic velocity in the NGV throat.

Let us make a few further assumptions which will not impair or compromise our final conclusion. The turbine NGV throat area A_{41} is constant. The total pressure loss between the turbine exit and the nozzle throat P_5/P_8 is usually small, therefore P_5/P_8 is close to 1.0. The total temperature ratio T_5/T_8 is unity because there is no energy exchange with the flow between turbine exit and nozzle inlet.

The last two terms in the equation are the turbine pressure and temperature ratios. They are linked through the turbine efficiency η_{4-5} :

$$\frac{T_5}{T_{41}} = 1 - \eta_{4-5} \left(1 - \left(\frac{P_5}{P_4} \right)^{\frac{\gamma-1}{\gamma}} \right) \quad (2.1-10)$$

Turbine efficiency is constant in the map region near to the turbine design point, see Fig. 2.1-5. We can use the turbine design efficiency to calculate the turbine temperature ratio from the turbine pressure ratio.

Now we know the values of all the terms in Eq. (2.1-9), except turbine pressure ratio P_4/P_5 and the area ratio A_8/A_{41} . But the product of A_8/A_{41} and P_5/P_4 is constant. Reducing the area ratio results inevitably in a decrease of turbine pressure ratio. In other words, as long as we have sonic flow in the nozzle throat and $W_{41}\sqrt{T_{41}}/(A_{41}P_4)$ is constant, turbine pressure ratio is solely a function of nozzle area:

$$\frac{P_4}{P_5} = f \left(\frac{A_8}{A_{41}} \right) \quad (2.1-11)$$

2.1.2.3 Flow Conservation Between Compressor Exit and Turbine Inlet

The mass flow continuity between compressor exit and turbine inlet, i.e. in the burner, yields

$$\frac{W_3\sqrt{T_3}}{P_3} = \frac{W_{41}\sqrt{T_{41}}}{P_4} \frac{P_4}{P_3} \frac{W_3}{W_3 + W_F} \sqrt{\frac{T_3}{T_{41}}} \quad (2.1-12)$$

The corrected flow $W_{41}\sqrt{T_{41}}/P_4$ and the pressure ratio P_4/P_3 are constant and the fuel flow W_F is small compared to the air mass flow W_3 . Therefore, the product of the corrected flow at the compressor exit and the square root of the temperature ratio T_{41}/T_3 is also constant:

$$\frac{W_3\sqrt{T_3}}{P_3} \sqrt{\frac{T_{41}}{T_3}} = const \quad (2.1-13)$$

We can calculate $W_3\sqrt{T_3}/P_3$ for each point in the compressor map unambiguously:

$$\frac{W_3\sqrt{T_3}}{P_3} = \frac{W_2\sqrt{T_2}}{P_2} \frac{W_3}{W_2} \frac{P_2}{P_3} \sqrt{\frac{T_3}{T_2}} \quad (2.1-14)$$

The temperature ratio T_3/T_2 is a function of pressure ratio and efficiency. From Eq. (2.1-13), it follows that lines of constant $W_3\sqrt{T_3}/P_3$ are simultaneously lines of constant temperature ratio T_{41}/T_3 .

2.1.2.4 Energy Balance Between Compressor and Turbine

The turbine provides shaft power to the compressor and drives accessories like fuel and oil pumps. The aircraft needs additional electric and/or hydraulic power PW_X .

$$PW_T = PW_C + PW_X \quad (2.1-15)$$

The shaft power of the two turbomachines is equal to the product of mass flow W and enthalpy difference ΔH . We can rewrite the power balance as

$$W_2 \Delta H_C = W_{41} \Delta H_T - PW_X \quad (2.1-16)$$

With isentropic efficiencies for the compressor and the turbine, this becomes:

$$\frac{W_2 \Delta H_{is,C}}{\eta_C} = W_{41} \Delta H_{is,T} \eta_T - PW_X \quad (2.1-17)$$

Isentropic compressor work and pressure ratio are related thus:

$$\frac{\Delta H_{is,C}}{T_2} = C_{P,C} \left[\left(\frac{P_3}{P_2} \right)^{R/C_{P,C}} - 1 \right] \quad (2.1-18)$$

In this equation $C_{P,C}$ is mean specific heat in the compressor. The isentropic turbine work is similarly related with its pressure ratio:

$$\frac{\Delta H_{is,T}}{T_{41}} = C_{P,T} \left[1 - \left(\frac{P_5}{P_4} \right)^{R/C_{P,T}} \right] \quad (2.1-19)$$

Inserting Eqs. (2.1-18) and (2.1-19) into Eq. (2.1-17) yields

$$C_{P,C} \left[\left(\frac{P_3}{P_2} \right)^{R/C_{P,C}} - 1 \right] = \frac{T_{41}}{T_2} \eta_C \eta_T \frac{W_{41}}{W_2} C_{P,T} \left[1 - \left(\frac{P_5}{P_4} \right)^{R/C_{P,T}} \right] - \frac{\eta_C PW_X}{T_2 W_2} \quad (2.1-20)$$

In the previous section we learned that the turbine pressure ratio P_4/P_5 is set by the nozzle throat area. Equation (2.1-20) relates compressor pressure ratio P_3/P_2 to the temperature ratio T_{41}/T_2 . It is this equation, together with Eq. (2.1-8), which defines the position of the operating line in the compressor map.

2.1.2.5 Compressor and Turbine Operating Lines

Now we are ready to draw some conclusions. If we look at a constant pressure ratio line in the compressor map with embedded T_{41}/T_2 lines in Fig. 2.1-7, we can deduce that

- T_{41}/T_2 increases when the product of compressor and turbine efficiency falls. The compressor operating point moves to the left.
- T_{41}/T_2 decreases if the turbine pressure ratio P_4/P_5 increases. This happens when the nozzle throat area is increased.
- T_{41}/T_2 must increase when power offtake PW_X increases. The compressor operating point moves to the left.
- The compressor operating point moves to the left also (T_{41}/T_2 increases) when some air is bled off (W_{41}/W_2 gets smaller).

Both pressure ratio P_3/P_2 and temperature ratio T_{41}/T_2 increase as we move up the compressor operating line. That means that the compressor operating line must be steeper than the T_{41}/T_2 lines.

Along a line with constant temperature ratio T_{41}/T_2 pressure ratio increases according to Eq. (2.1-8) linearly. The constant $W_3/\sqrt{T_3/P_3}$ lines in the compressor map (see Fig. 2.1-8) are also (nearly) straight lines through the origin, as the T_{41}/T_2 lines are. The remarkable difference between the two families of lines is that—at constant corrected flow—the T_{41}/T_2 family parameters increase while the $W_3/\sqrt{T_3/P_3}$ parameter decreases with raising pressure ratio.

The value of $W_3/\sqrt{T_3/P_3}$ decreases along an operating line from low to high thrust as we can see in Fig. 2.1-8. The slope of the compressor operating line is not only steeper than the T_{41}/T_2 lines but also steeper than the $W_3/\sqrt{T_3/P_3}$ lines. Equation (2.1-13) relates the declining $W_3/\sqrt{T_3/P_3}$ values with the increase of the temperature ratio T_{41}/T_3 along the operating line.

The operating line in the turbine map is a line with constant turbine pressure ratio as long as the nozzle is choked. Note that this condition is not fulfilled for the 5 white points in Figs. 2.1-8, 2.1-9 and 2.1-10.

2.1.2.6 How Accurate Are These Equations?

When we derived the Eqs. (2.1-6)–(2.1-20) we made many assumptions. We used constant values for specific heat instead of temperature-dependent gas properties and we ignored variations of pressure losses in ducts and the burner. Also, for

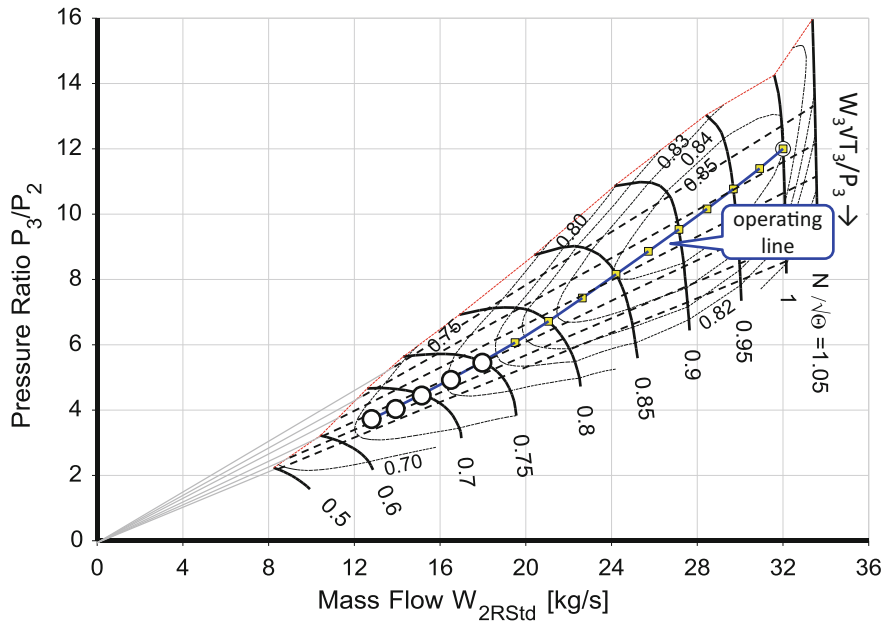


Fig. 2.1-8 Compressor operating line calculated with GasTurb

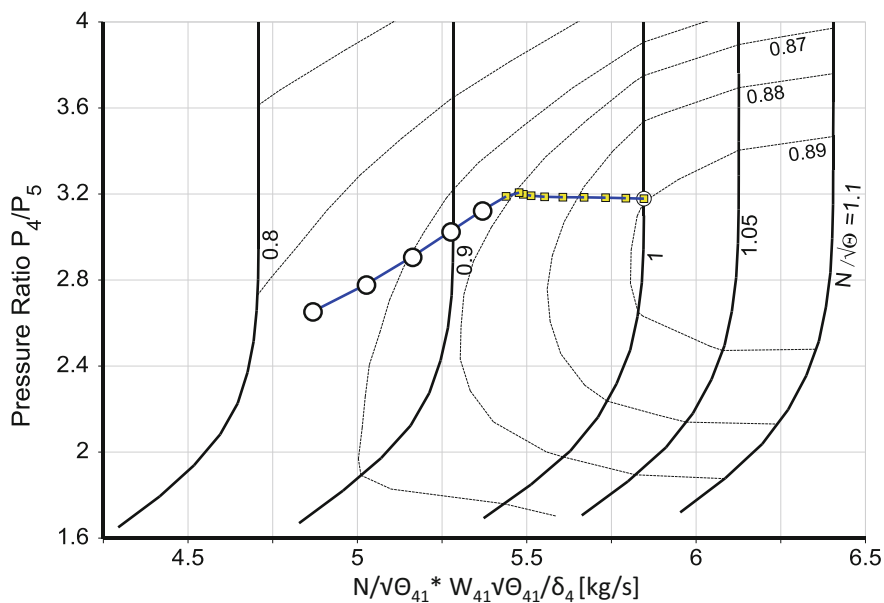


Fig. 2.1-9 Turbine operating line

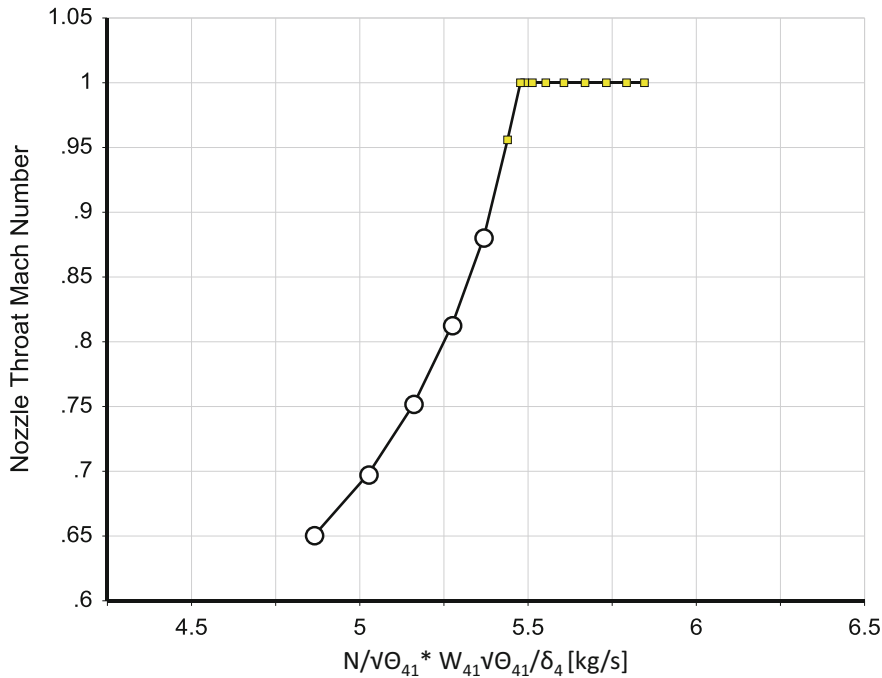


Fig. 2.1-10 Nozzle throat Mach number

example, we had no interest in the amount of fuel and did not even mention the nozzle discharge coefficient. So are the conclusions which we derive from the simplified equations accurate enough to be useful? Let us examine that further.

Figure 2.1-11 supplements the information in Figs. 2.1-8, 2.1-9 and 2.1-10 and shows how temperature ratios T_{41}/T_2 and T_{41}/T_3 as well as $W_3\sqrt{T_3}/P_3$ vary along the operating line of our turbojet. No simplifying assumptions are used in these off-design cycle calculations.

The equations describe realistically what happens in the upper power range, while the nozzle throat is choked. Both T_{41}/T_2 and T_{41}/T_3 increase nearly linearly with compressor pressure ratio along the operating line. The product of T_{41}/T_3 and $W_3\sqrt{T_3}/P_3$ is constant according to Eq. (2.1-13)—that's what we see in Fig. 2.1-11. This demonstrates that the relatively simple correlations are a good guide to understanding what happens during off-design operation of a turbojet engine.

2.1.2.7 Variable Compressor Geometry

Axial compressors designed for pressure ratios above 4 to 5 usually have variable inlet guide vanes (VIGV's) and perhaps one or more stages with variable stators. This begs the question *if we have insufficient surge margin in our engine, can*

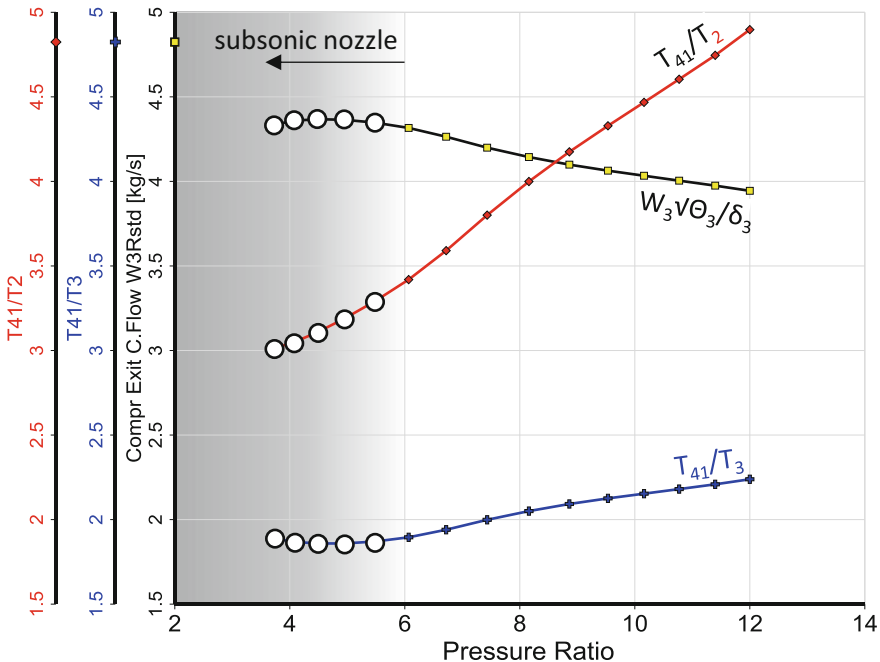


Fig. 2.1-11 Temperature ratios and corrected flow at the compressor exit

we shift the operating line of the compressor with the help of the variable guide vanes?

Resetting the variable inlet guide vanes primarily changes the relationship between corrected spool speed $N/\sqrt{\Theta}$ and corrected mass flow. This is demonstrated in Fig. 2.1-12, where the VIGV has been closed by 10° . The relation between corrected flow and efficiency is affected very little.

If we recall the equations which define the position of the operating line in the compressor map, neither true nor corrected spool speeds show up in any of the correlations. We can conclude that resetting the variable guide vanes has no effect on the location of the operating line in the map in Fig. 2.1-13. Turbine inlet temperature T_{41} remains the same, but spool speed increases.

What happens in the turbine map when we close the compressor guide vanes? The turbine spool speed is the same as that of the compressor, which increases. So the corrected turbine spool speed $N/\sqrt{T_{41}}$ will also increase. The turbine operating line in Fig. 2.1-14 shifts to the right, with the turbine pressure ratio not being affected.

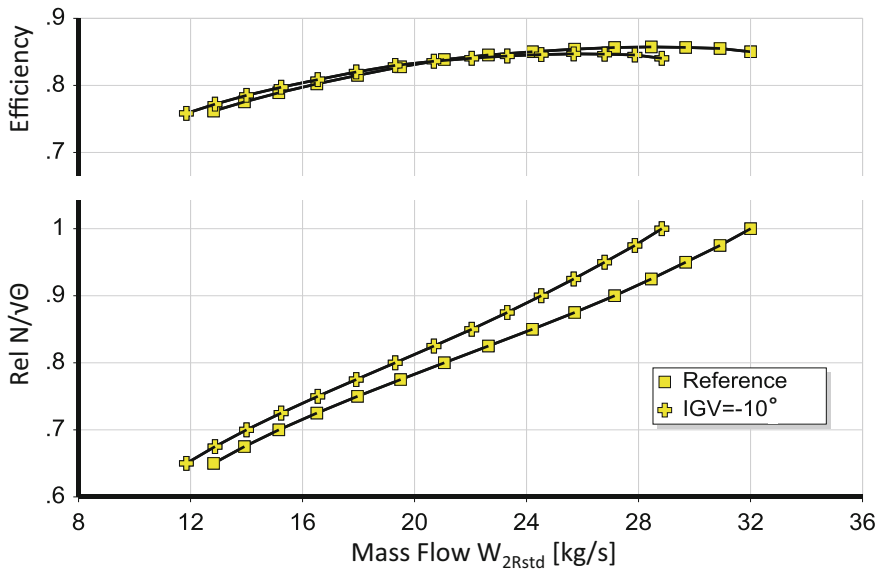


Fig. 2.1-12 Effect of variable guide vane setting on corrected speed and efficiency

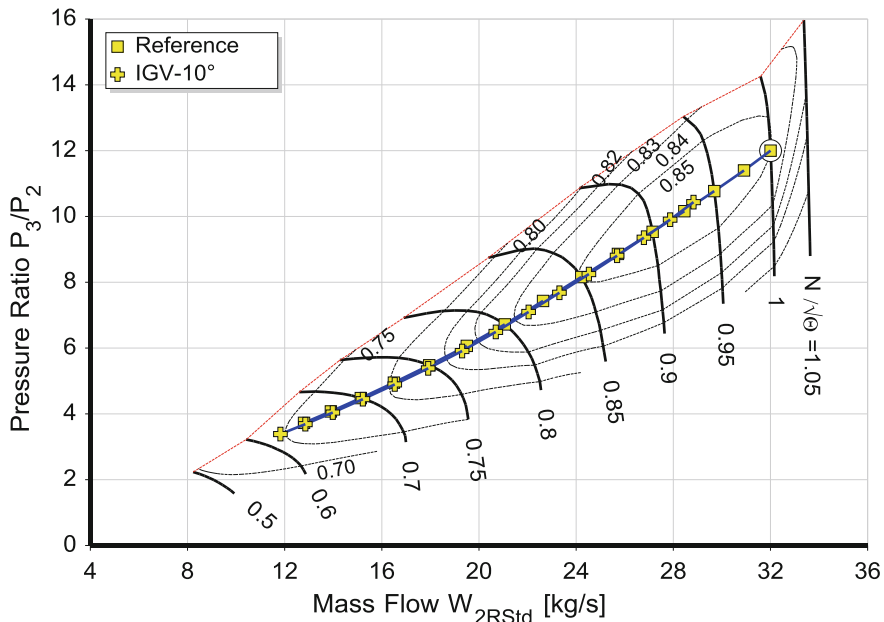


Fig. 2.1-13 Compressor operating lines for two IGV settings

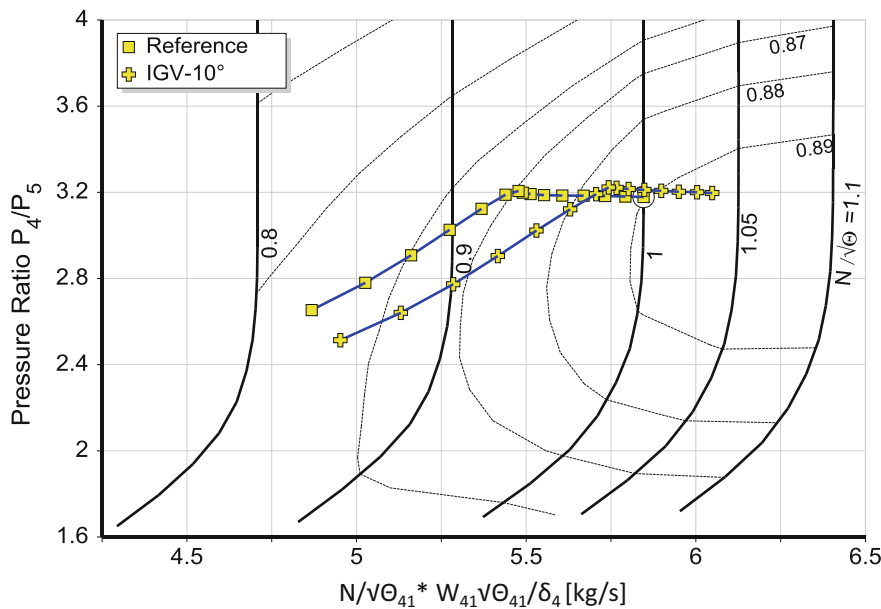


Fig. 2.1-14 Turbine operating line shift due to change in compressor VIGV stagger angle

2.1.3 Booster Operating Line

A booster is a compressor upstream of the core engine. The operating line of the gas generator compressor (the high pressure compressor HPC) is the major influence on the location of the operating line in the booster map. This is because the corrected inlet flow of the HPC, $W_{25}\sqrt{T_{25}/P_{25}}$, is the corrected exit flow of the booster.

Let us compare the slopes of the booster and HPC operating lines in the same map. We know from previous considerations that the HPC corrected exit flow $W_3\sqrt{T_3/P_3}$ increases along the operating line when we reduce both power and the core entry flow $W_{25}\sqrt{T_{25}/P_{25}}$ (see Figs. 2.1-8 and 2.1-11). So, the corrected exit flow from the booster goes down while the corrected exit flow of the HPC goes up.

The HPC operating line is steeper than the lines of constant corrected exit flow in the HPC map in Fig. 2.1-15. However, the gradient of the booster operating line is quite the opposite. It is less steep than the lines of constant corrected exit flow in the map and it tends to run into the surge line (Fig. 2.1-15). Insufficient booster surge margin at low power is often a problem which we can solve only with a bleed valve between the two compressors.

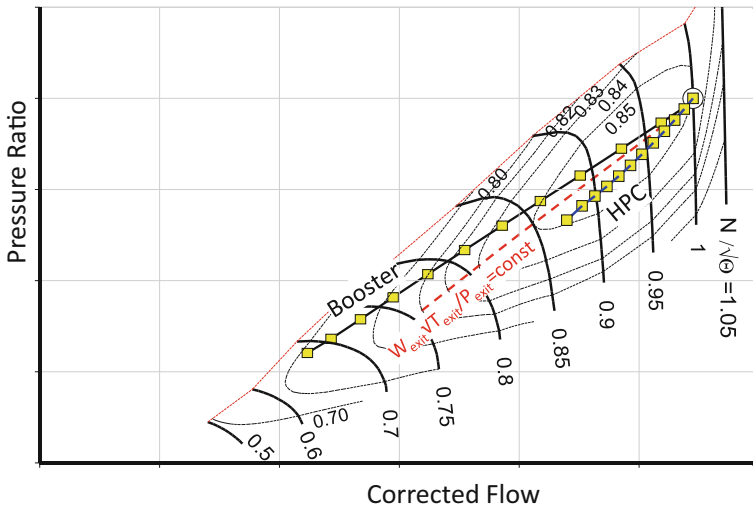


Fig. 2.1-15 Booster and high pressure compressor (HPC) operating lines

2.2 Turbofan

So why have we studied the off-design behavior of a turbojet engine in such detail, since such an engine is rarely used for aircraft propulsion these days? Our interest stems from the fact that the off-design behavior of the turbofan core—the gas generator—follows that of a complete turbojet engine very closely. And the reason for this is because the flow characteristics of a low pressure turbine are very similar to that of a nozzle (Fig. 2.2-2).

We can easily translate the turbojet equations into those for a turbofan gas generator. We replace the parameters from the engine inlet station 2 with those from station 25, the gas generator inlet station. Equation (2.1-8) becomes Eq. (2.2-1), which describes a family of straight P_3/P_{25} lines over a range of $W_{25}\sqrt{T_{25}/P_{25}}$; with the temperature ratio T_{41}/T_{25} as the variable.

$$\frac{P_3}{P_{25}} = \frac{1}{\frac{W_{41}\sqrt{T_{41}}}{A_{41}P_4} \frac{A_{41}P_4}{A_{25}P_3} \frac{W_{25}}{W_{41}}} \sqrt{\frac{T_{41}}{T_{25}} \frac{W_{25}\sqrt{T_{25}}}{P_{25}}} \quad (2.2-1)$$

The power balance between the core compressor and turbine yields the equation for the operating line

$$C_{P,C} \left[\left(\frac{P_3}{P_{25}} \right)^{R/C_{P,C}} - 1 \right] = \frac{T_{41}}{T_{25}} \eta_{HPC} \eta_{HPT} \frac{W_{41}}{W_{25}} C_{P,T} \left[1 - \left(\frac{P_{45}}{P_4} \right)^{R/C_{P,T}} \right] - \frac{\eta_{HPC} P W_X}{T_{25} W_{25}} \quad (2.2-2)$$

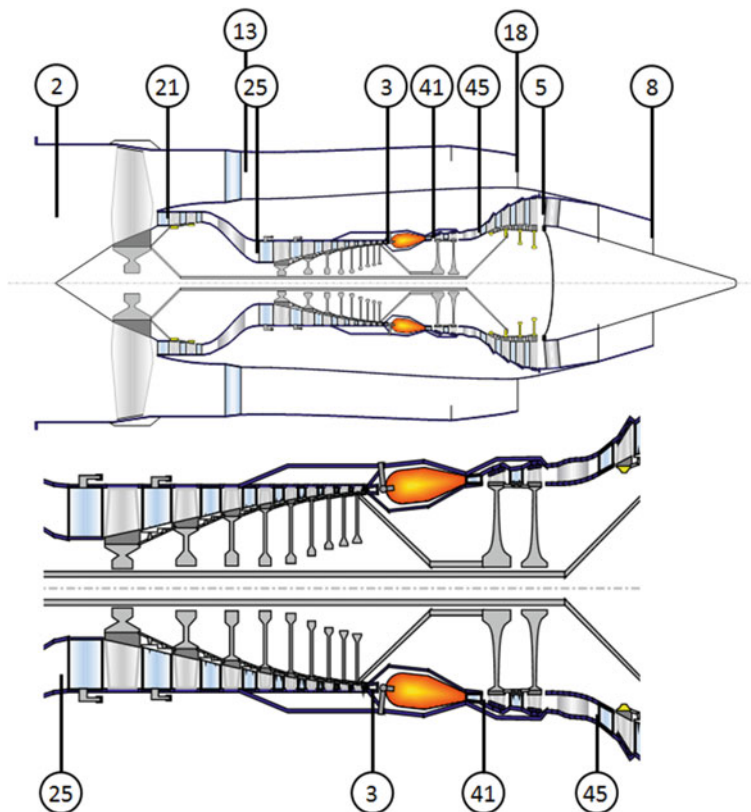


Fig. 2.2-1 Turbofan gas generator nomenclature

2.2.1 Fan Operating Line

The bypass nozzle dominates the fan operating line of a high bypass ratio turbofan with separate cold and hot nozzles. The corrected flow through the bypass nozzle depends on the pressure ratio P_{18}/P_{amb} and that has an inverse relationship to the bypass ratio. During cruise—at least in the high power range—the bypass nozzle pressure ratio is above the critical value, i.e. the flow is sonic even for very high bypass ratio engines. At Take Off conditions, however, the nozzle pressure ratio becomes sub-critical, the corrected fan exit flow gets smaller, and the operating line moves towards the surge line.

Figure 2.2-3 compares the fan operating lines at altitude (cruise conditions) and sea level static (take off conditions) of two high bypass ratio engines. The upper map is from a bypass ratio 6 engine which has a fan design pressure ratio of $P_{13}/P_2 = 2$. The bypass nozzle pressure ratio P_{18}/P_{amb} is 2.94 at Max Climb, the nozzle is choked and $W_{18}\sqrt{T_{18}/P_{18}}$ is as big as it can be. The bypass nozzle Mach

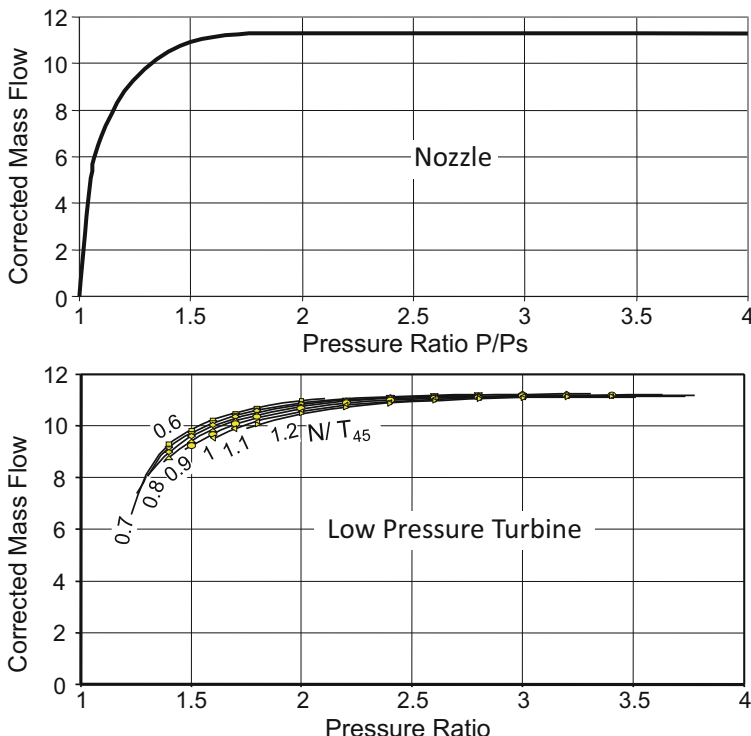


Fig. 2.2-2 Corrected flow of nozzles and low pressure turbines

number at sea level static Take Off is $M_{18} = 0.9$, the corrected flow $W_{18}\sqrt{T_{18}/P_{18}}$ is only slightly less than at Max Climb (see Fig. 2.1-6). The Take Off point in the fan map is very near to the cruise operating line.

The lower map is that of a bypass ratio 12 engine, in which the Max Climb fan pressure ratio is only 1.48. The bypass nozzle pressure ratio P_{18}/P_{amb} of 2.19 is not much above its critical value. The bypass nozzle Mach number at sea level static Take Off is only $M_{18} = 0.64$ and $W_{18}\sqrt{T_{18}/P_{18}}$ is around 12% smaller than at Max Climb. The fan operating point at Take Off is on an operating line of lower corrected fan exit flow $W_{13}\sqrt{T_{13}/P_{13}}$ than at Max Climb (again recall the trend of $W_3\sqrt{T_3/P_3}$ lines in Fig. 2.1-8). In the map, operating lines of low corrected fan exit flow $W_{13}\sqrt{T_{13}/P_{13}}$ are above operating lines with high $W_{13}\sqrt{T_{13}/P_{13}}$. The sea level operating line in the fan map of a high bypass ratio engine is much nearer to the surge line than is the cruise operating line.

If necessary, there are two options for avoiding the fan operability problem of a very high bypass ratio turbofan. Either we use a variable area bypass nozzle, which opens at sea level conditions and shifts the operating line to the right, or we adjust the fan rotor blade angle and shift the surge line to the left.

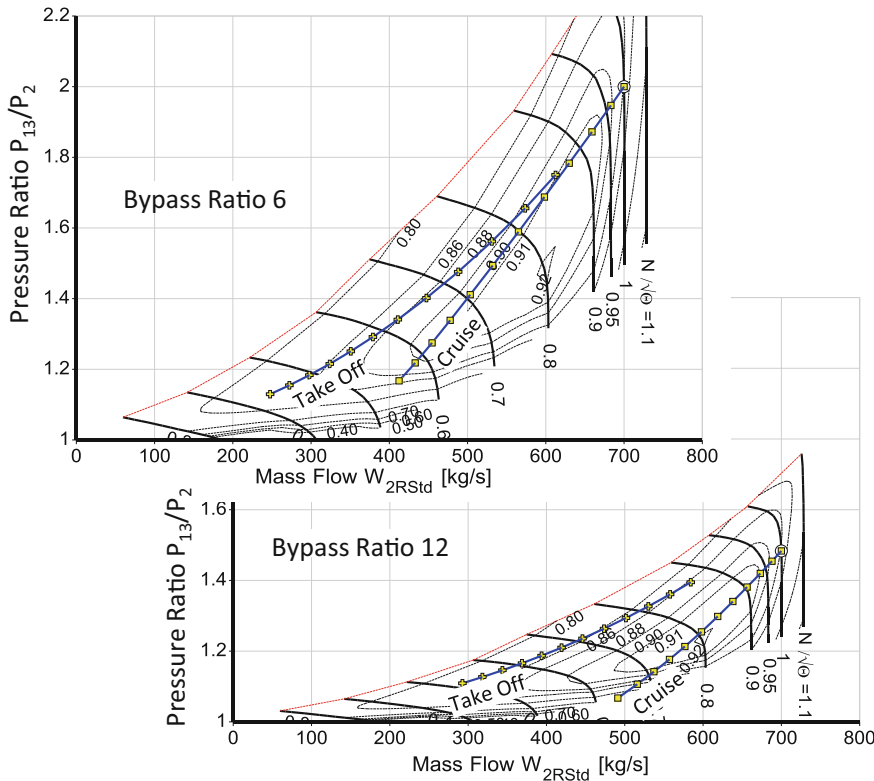


Fig. 2.2-3 Fan operating lines for low and high bypass ratio turbofans

2.2.2 Turbofan Booster Operating Line

The operating line of the booster (or intermediate pressure compressor IPC) in a turbofan is not only determined by the downstream compressor, the HPC, but also by the fan. This is because both the fan and the booster rotate at the same spool speed. In case of a turbofan with gearbox the ratio between fan and booster spool speed is constant.

We examine the booster part-load behavior by taking the example of a high bypass turbofan. The cycle design point is top of climb at 35000 ft Mach 0.8. The main cycle design point parameters are listed in Table 2.2-1.

In our off-design studies, we use GasTurb Standard Maps for all components except the booster. For simulating the booster performance, we use four different maps, all scaled to the same cycle design point pressure ratio of 3:

1. The GasTurb Standard booster map, scaled by GasTurb to the cycle design pressure ratio employing a constant factor to the P/P-1 values of the original map [1].

Table 2.2-1 Main data of a turbofan example

Thrust	kN	38.4
SFC	g/(kN s)	14.7
Mass flow	kg/s	332
Bypass ratio		10
T ₄	K	1600
OPR P ₃ /P ₂		53
Fan outer pressure ratio P ₁₃ /P ₂		1.525
Fan inner pressure ratio P ₂₁ /P ₂		1.5
Booster pressure ratio P ₂₄ /P ₂₁		3
HPC pressure ratio P ₃ /P ₂₅		12

2. The same map, scaled with the procedure described in Ref. [4].
3. A generic map of a subsonic compressor (typical for the booster of a conventional turbofan), scaled with the procedure of Ref. [4].
4. A map of a transonic compressor [3] (typical for the booster of a turbofan with gearbox), scaled with the procedure of Ref. [4].

The map scaling procedure of Ref. [4] is implemented as *automatic scaling* in the compressor map preparation program Smooth C [5].

Figure 2.2-4 shows the four booster operating lines for cruise at 35000 ft/Mach 0.8 from the cycle design point down to about 50% thrust. Fan and booster spool speed are approximately 80% of the design point value at that thrust.

2.2.2.1 Shape of the Operating Line

The four operating lines diverge towards part-load significantly. What is the reason for that and how can we influence the slope of the booster operating line?

We consider now operating points at 80% fan speed and examine the effect of fan and booster efficiency changes of $\pm 2\%$ on the booster pressure ratio. The fan outer pressure ratio remains constant in this exercise because the bypass nozzle controls the fan pressure ratio.

Figure 2.2-4 shows that fan outer efficiency affects booster pressure ratio, but booster efficiency does not.

In a second parametric study, we examine the effect of fan and booster flow capacity. Note that fan flow capacity does not affect fan pressure ratio because that is determined by the bypass nozzle. The main effect of a fan capacity increase is an increase in booster pressure ratio. Booster flow varies only by 1.7% for a change in fan flow capacity from -2% to $+2\%$. Increasing booster flow capacity by the same amount decreases booster pressure ratio and increases booster flow by 4.5%.

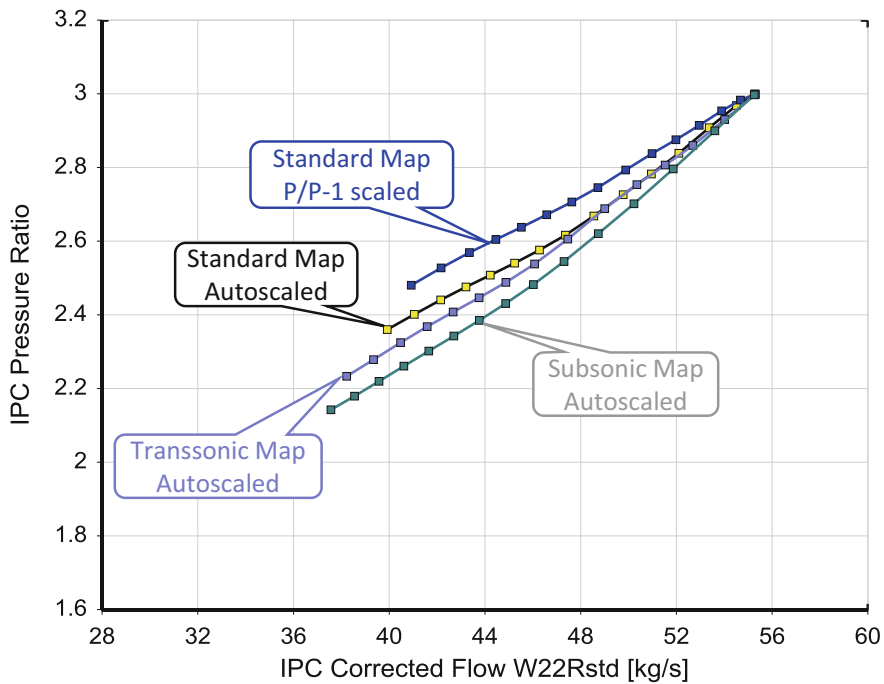


Fig. 2.2-4 Booster operating lines in four different maps

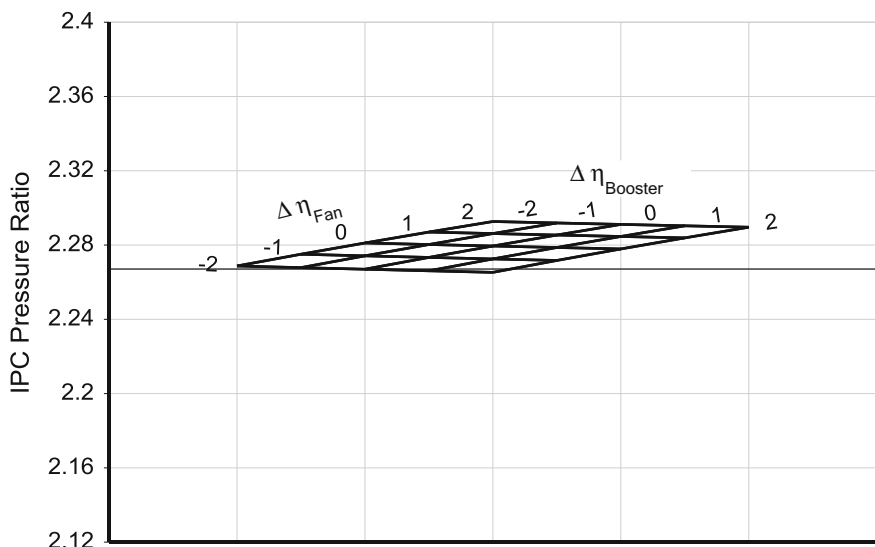


Fig. 2.2-5 Effect of fan and booster efficiency changes on booster pressure ratio (NL = const)

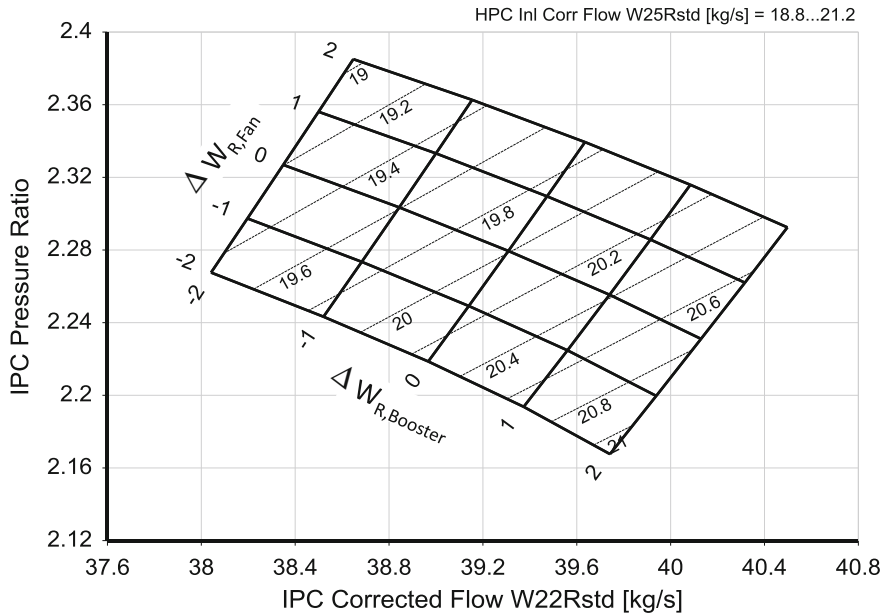


Fig. 2.2-6 Effect of fan and booster flow capacity

We concentrate now on the booster and assume that the fan map yields the correct fan flow and efficiency. As we have seen in Fig. 2.2-5, booster efficiency does not affect booster pressure ratio. Thus, the driving parameter for the booster pressure ratio at constant corrected spool speed is its flow capacity. The shape of the booster operating line depends solely on the correlation of corrected flow with corrected speed in the booster map. This correlation differs from map to map, therefore we got four different booster operating lines in Fig. 2.2-4.

The contour lines in Fig. 2.2-6 are those of constant HPC inlet corrected flow W_{25Rstd} which is equal to the booster exit corrected flow. Decreasing W_{25Rstd} goes along with decreasing HPC pressure ratio.

2.2.2.2 Map Selection and Scaling

Scaling makes one point in the map, the map scaling point, line up exactly with the cycle reference point. What is the difference between the four maps? The origin of the first and the second map is the same [1], the only difference between them is the scaling procedure, see section C1.2.9.

If we employ the scaling procedure $P2/P1-1$ rather than *Automatic Scaling* to generate the booster map for our turbofan simulation then the corrected flow numbers for the 80% speed lines will not be the same. The difference in corrected flow is equivalent to a change in booster flow capacity which in turn leads to a

difference in booster pressure ratio (see Fig. 2.2-6). Consequently, we get two different booster operating lines from the same unscaled map, see Fig. 2.2-4.

There are two more booster operating lines in Fig. 2.2-4: One which we get when the map is a scaled version of the booster map from a conventional turbofan [2]. The circumferential speed of such a booster is low and the flow field is subsonic in general. The other map [3] is a scaled version of that from a compressor running at high circumferential speed in which the flow field is transonic.

The speed lines in the map of the subsonic compressor are flat and the mass flow range from surge to choke is remarkable. This contrasts with the speed lines in the map of the transonic compressor which are steep, with much less mass flow increase from surge to choke. The map from Ref. [1] (the GasTurb Standard booster map) and the map from Ref. [3] have some similarity. Both maps are apparently from transonic compressors and therefore it is not surprising that the corresponding operating lines in Fig. 2.2-4 are near each other.

The operating line calculated with the map from the subsonic compressor is the lowest in Fig. 2.2-4. That indicates that the booster operating line of a conventional turbofan is steeper—and less prone to running into the surge line—than that of a turbofan with gearbox.

Let us now study a second operating line, that for SLS. We compare again the slowly rotating booster of a conventional turbofan (subsonic flow) with the fast running booster (transonic flow) of a turbofan with gearbox. In the transonic map the SLS operating line is farther apart from the cruise operating line: the pressure ratio difference at $W_{22Rstd} = 40 \text{ kg/s}$ is much bigger than in the map of the subsonic booster, compare Fig. 2.2-7 with Fig. 2.2-8. This comes from the different slopes of the speed lines which affect the mass flow—speed relationships along the operating lines.

2.2.2.3 Variable Geometry

All operating lines in Fig. 2.2-4 are nearly straight with steadily increasing pressure ratio over flow. In Fig. 2.2-9, however, the operating line in the properly scaled GasTurb Standard map looks quite different: at high flows the pressure ratio decreases! How can that be?

The reason lies in the selection of the map scaling point. Remember: this is the point in the unscaled map which becomes through the map scaling process the cycle design point. The map scaling point of the map used for the calculation of the operating line marked “Standard map auto-scaled” in Fig. 2.2-4 was selected to be on the speed line marked $N/\sqrt{\Theta} = 0.998$ in the unscaled map.

The map scaling point used for creating the map of Fig. 2.2-9, however, was selected to be at $N/\sqrt{\Theta} = 1.05$. It is astonishing that such a small change causes such a big difference in the shape of the booster operating line.

From Fig. 2.2-6 it is seen that a difference in the flow-speed relationship could be the reason. The blue lines are the β -lines of the map which have been defined in such a way that they are simultaneously lines of constant work coefficient $\Delta H/U^2$ (Fig. 2.2-10).

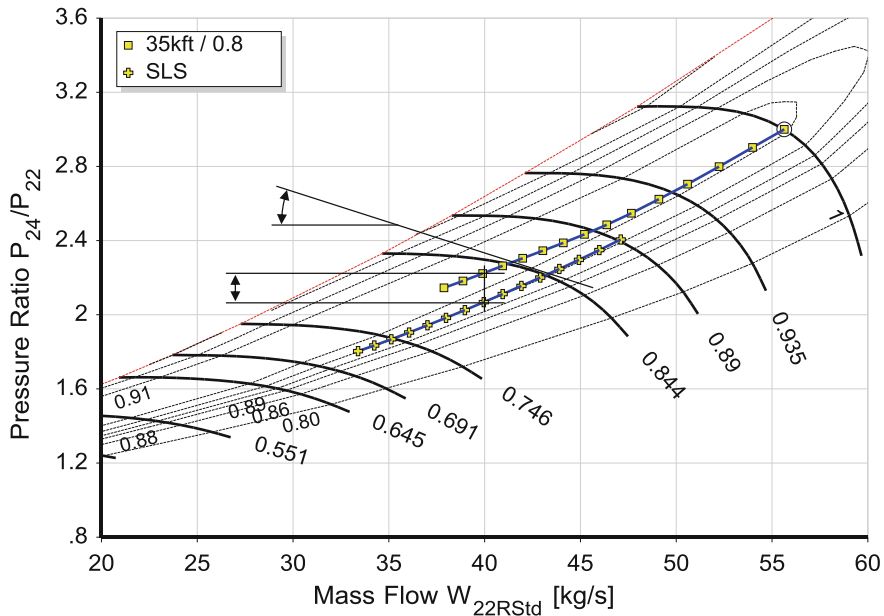


Fig. 2.2-7 Cruise and SLS operating lines in the subsonic booster map

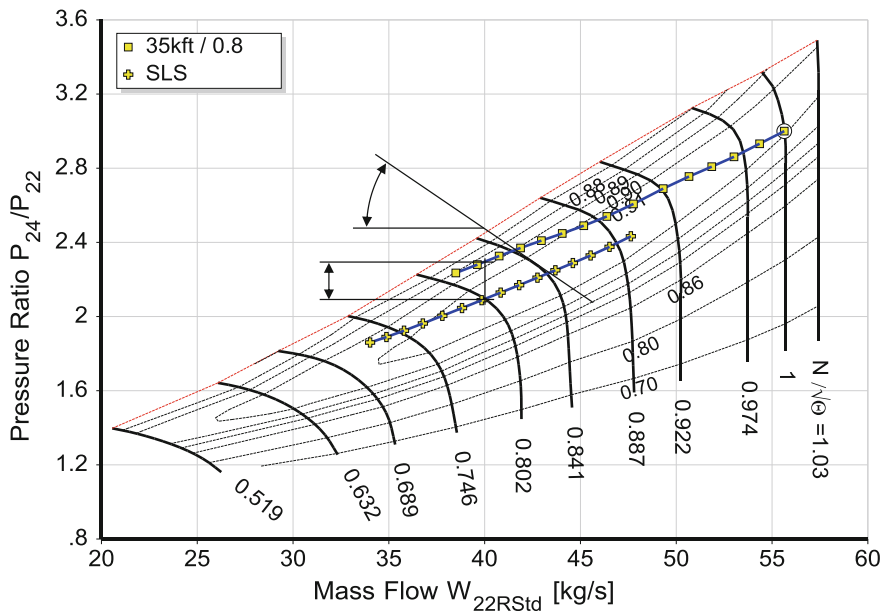


Fig. 2.2-8 Cruise and SLS operating lines in the transonic booster map

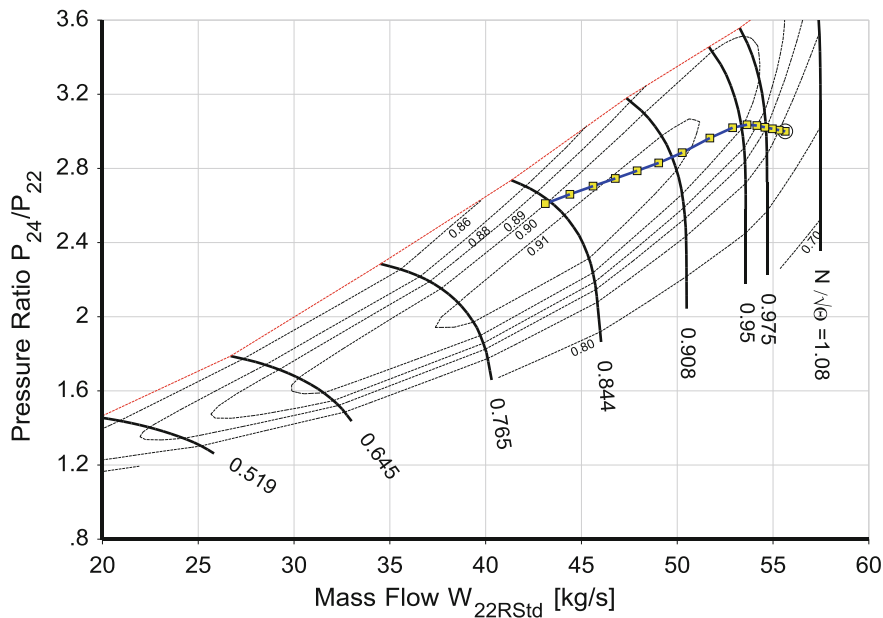


Fig. 2.2-9 Map scaling point at $N/\sqrt{\Theta} = 1.05$

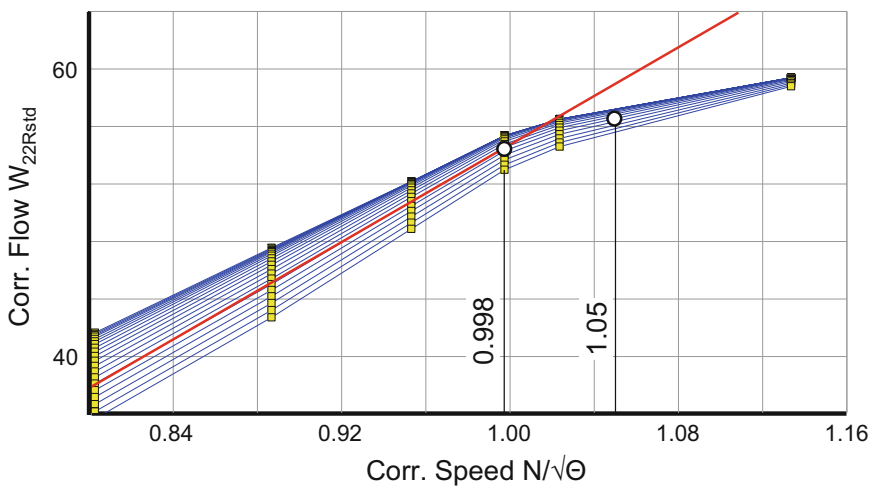


Fig. 2.2-10 Flow-speed relationship in the unscaled map

The slope of corrected flow versus corrected speed for constant β changes abruptly at $N/\sqrt{\Theta} = 0.998$. Such a sudden change is typical for compressors with variable guide vanes. The kink in the flow-speed correlation is a consequence of a kink in the VGV schedule $\alpha_{IGV} = f(N/\sqrt{\Theta})$.

Reference [1]—the origin of the GasTurb booster Standard map—does not discuss variable compressor geometry. The reason for the kink in the flow—speed relationship of this map is unknown to us. Our conclusion and strong recommendation is: examine the map before using it for simulating the performance of a booster in a turbofan engine!

For checking the flow-speed correlation in a map define the β -line grid between two parabolas which both pass through the origin. Then plot W_R over $N/\sqrt{\Theta}$ and $\Delta H/\Theta$ over N^2/Θ . If these lines are straight, then the compressor geometry is invariant. If not, then the map is from a compressor with variable geometry.

Using the map from a compressor with variable geometry for simulating the performance of a booster without variable guide vanes is an error. In contrast, we can use the map from a compressor without VGV's to simulate the performance of a booster with variable guide vanes by adding a VGV schedule. This has been done to generate the blue operating lines in Fig. 2.2-11. The dashed lines are shown for comparison, they are a copy of the operating lines in Fig. 2.2-8.

This example shows that VGV's can shift the booster operating line and thus optimize both efficiency and surge margin. If the booster operating line in a turbofan with gearbox poses an operability problem at high power then this can be

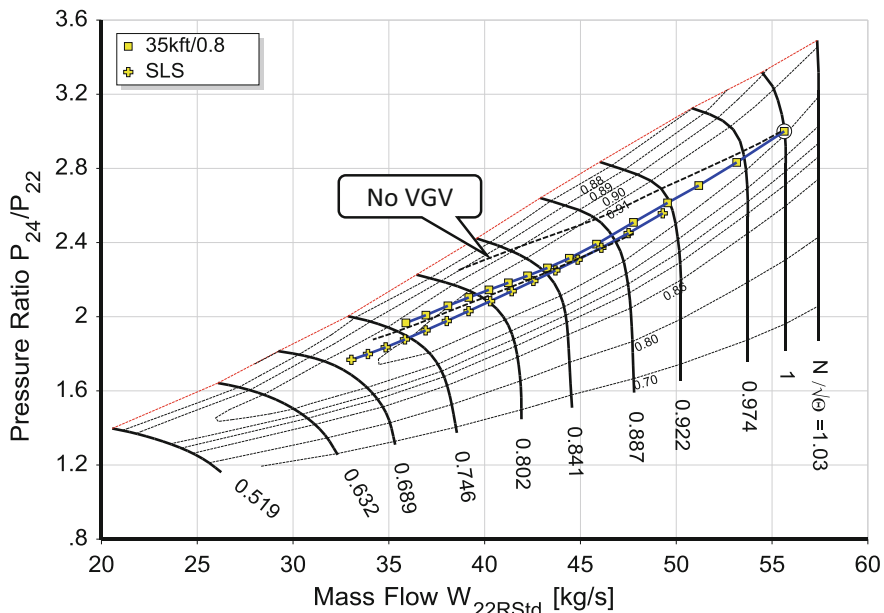


Fig. 2.2-11 Booster operating lines with scheduled VGV's

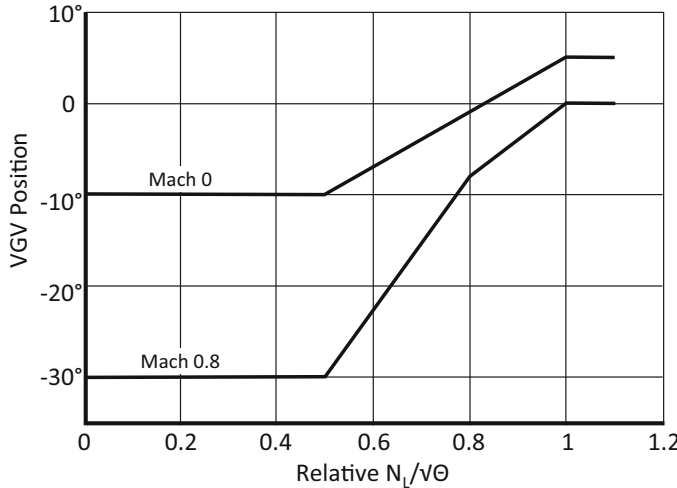


Fig. 2.2-12 VGV schedule for the operating lines in Fig. 13.26

solved with properly scheduled VGV's (Fig. 2.2-12). A handling bleed downstream of the booster is commonly used for solving operability problems at lower speeds and well above Idle.

2.2.2.4 Wrap up

The position of the operating line in the booster map of a turbofan is determined predominantly by the flow-speed relationship in the booster map. The second most important factor is the flow-speed relationship of the fan. It is important to employ representative booster maps. For conventional turbofans, use a map from a slowly turning compressor with a subsonic flow field. For turbofans with gearbox, utilize a map from a fast running compressor with transonic flow field.

2.2.3 Low Pressure Turbine

The pressure ratio of the low pressure turbine may be characterized through the ratio of the corrected mass flows at its inlet and exit. Ignoring any pressure losses and mass flow changes between turbine exit and core nozzle throat leads to

$$\frac{\frac{P_{45}}{P_8}}{\sqrt{\frac{T_{45}}{T_8}}} = \frac{\frac{W_8 \sqrt{T_8}}{P_8}}{\frac{W_{45} \sqrt{T_{45}}}{P_{45}}} \quad (2.2-3)$$

The LPT pressure ratio does not change as long as the core nozzle is choked because then both the corrected mass flows in the equation are constant. This is the case in the upper thrust range of low bypass ratio turbofans.

The higher the bypass ratio, the lower the design pressure ratio of the fan and subsequently the lower the velocity of the bypass jet. The core jet velocity follows the bypass jet velocity, since the optimum ratio of these is approximately constant in well-designed engines.

So what happens along the LPT operating line? The inlet corrected flow remains constant in the upper thrust range. The corrected core nozzle flow $W_8\sqrt{T_8}/P_8$ decreases with core jet Mach number and so does the pressure ratio of the LPT.

We cannot locate the operating line in the LPT map with pressure ratio alone—we would also need to know how corrected spool speed $N_L/\sqrt{T_{45}}$ changes with pressure ratio. Unfortunately, there is no simple way to calculate $N_L/\sqrt{T_{45}}$ because the spool speed N_L depends on the shape of the speed lines in the fan map, as well as on the position of the operating line.

Figure 2.2-13 shows typical operating lines for take off and cruise in the LPT map—they pass through the peak efficiency region of the map.

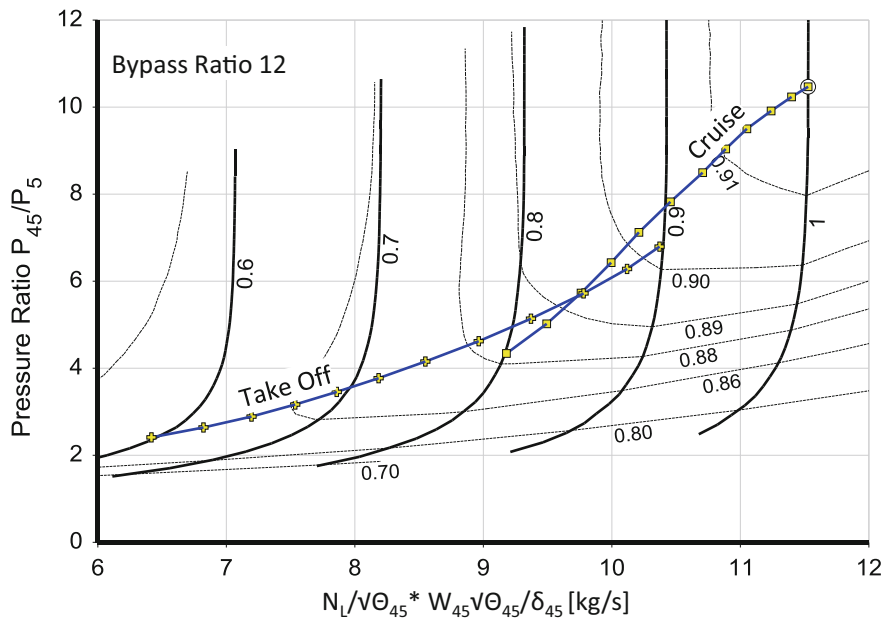


Fig. 2.2-13 Operating line in the low pressure turbine map of a turbofan

2.3 Multi-spool Turboshaft

A two spool turboshaft engine consists of a gas generator followed by a free power turbine. The off-design behavior of the gas generator is essentially that of a turbojet because the flow characteristic of the power turbine is similar to that of the turbojet nozzle—remember Fig. 2.2-2. All the turbojet equations are also valid for the two spool turboshaft.

However, we are free to choose the rotational speed of the power turbine. When we use our turboshaft for land or sea vehicle propulsion then we adjust the power turbine speed to be best for the vehicle. The turbine runs at constant rotational speed if it drives a propeller, a helicopter rotor or an electric generator.

Mass flow W_{45} , temperature T_{45} and pressure P_{45} at the entry to the power turbine vary with the turbine rotor inlet temperature T_{41} of the gas generator. The power turbine pressure ratio P_{45}/P_5 is slightly less than P_{45}/P_{amb} , the corrected power turbine speed is $N_{\text{PT}}/\sqrt{T_{45}}$. These two parameters together locate the operating point in the power turbine map, so we can read efficiency and then calculate the shaft power delivered (Fig. 2.3-1).

If we reduce power while N_{PT} remains constant, then the corrected spool speed $N_{\text{PT}}/\sqrt{T_{45}}$ will increase because the gas generator exit temperature T_{45} falls. The turbine operating line with constant N_{PT} passes through the peak efficiency region, and it is perpendicular to the operating line of the low pressure turbine map in a turbofan (Fig. 2.2-13).

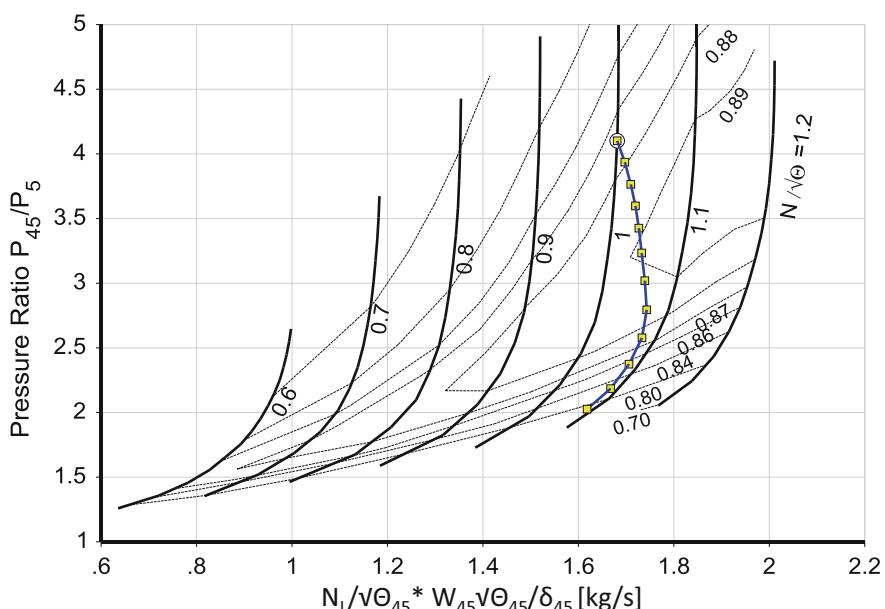


Fig. 2.3-1 Operating line in a power turbine map for $N_{\text{PT}} = \text{constant}$

A three-spool turboshaft has a two-spool gas generator. The first compressor, the booster, is turned by an intermediate turbine which is located between the gas generator and the power turbine. The operating line of the booster is controlled by the high pressure compressor, as explained in the turbofan section. The pressure ratio of the intermediate turbine is constant because the flow capacities of both the high pressure and the power turbine are invariant.

2.4 Single Spool Turboshaft

Some, but not all, of the turbojet equations are also valid for the single spool turboshaft. We can draw a family of straight pressure ratio lines versus corrected flow through the origin (Eq. 2.1-8); the temperature ratio T_{41}/T_2 is the variable. The basis for these lines is the mass flow continuity between compressor and turbine and the knowledge that $W_{41}\sqrt{T_{41}/P_4}$ is constant in the upper power range.

The mass flow continuity between compressor exit and turbine inlet yields another commonality with the turbojet: The product of the corrected flow at the compressor exit $W_3\sqrt{T_3/P_3}$ and the square root of the temperature ratio T_{41}/T_3 is invariable.

Now we address the differences between turbojet and turboshaft configurations. The turbine pressure ratio of a turbojet P_4/P_5 remains constant in the high power operating range because the exhaust nozzle is choked. In contrast to this, the Mach number in the exhaust of a turboshaft is very low. The turbine pressure ratio is related directly to the compressor pressure ratio:

$$\frac{P_4}{P_5} = \frac{P_3}{P_2} \frac{P_4 P_2}{P_3 P_5} \quad (2.4-1)$$

The burner pressure ratio P_4/P_3 and exhaust pressure ratio P_5/P_2 are both close to 1 and do not change much within the operating range. Turbine pressure ratio is proportional to that of the compressor.

In a turbojet, the power offtake plays only a secondary role in the energy balance between compressor and turbine. However, for the single spool turboshaft, power offtake is the most important parameter: the generation of shaft power is the principal objective of the machine:

$$PW_X = PW_T - PW_C \quad (2.4-2)$$

For each point in the compressor map we know pressure ratio, efficiency and mass flow. Therefore, we can calculate how much power the compressor needs for any operating point. Lines of constant temperature ratio T_{41}/T_2 in the map connect the compressor with the turbine. At each compressor map point, we know the spool speed N and the turbine entry temperature T_{41} . The turbine pressure ratio is nearly the same as compressor pressure ratio, see Eq. (2.4-1). The corrected speed

$N/\sqrt{T_{41}}$ and pressure ratio P_4/P_5 determine the operating point in the turbine map and thus determine the turbine efficiency. Turbine power is easy to calculate, and the difference between it and the compressor power is the shaft power delivered.

Many single-spool turboshafts are used for power generation where they operate at constant speed N . This is a requirement of the electrical generator. The ambient temperature of the day determines the corrected spool speed $N/\sqrt{T_2}$. Load variation moves the operating point up or down along the constant $N/\sqrt{T_2}$ line in the compressor map.

The operating line in the turbine map of a turbojet is a very short constant pressure ratio line, turbine efficiency is essentially constant. In contrast, the turbine operating line in a single spool turboshaft is much longer because both the pressure ratio and corrected spool speed $N/\sqrt{T_{41}}$ vary with load. Of course, turbine efficiency depends on the location of the operating point in the map.

Variable compressor inlet guide vanes—which are needed for high pressure ratio compressors anyway—allow us to modify the correlation between corrected speed and corrected flow. We can shift the $N/\sqrt{T_2}$ line by closing the inlet guide vanes (the IGV's) to produce lower pressure ratio and mass flow. This allows us to produce the same power output either with low T_{41} and high mass flow W_{2Rstd} or with high turbine inlet temperature and low mass flow, see Fig. 2.4-1. The single operating line in the compressor map widens to a carpet and the same happens in the turbine map in Fig. 2.4-2.

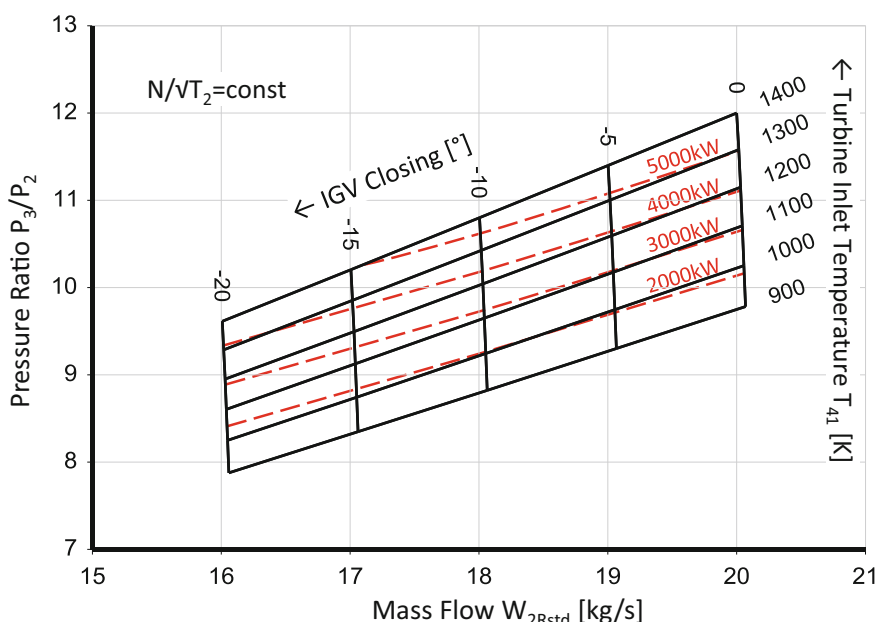


Fig. 2.4-1 Lines of constant shaft power output in the compressor map

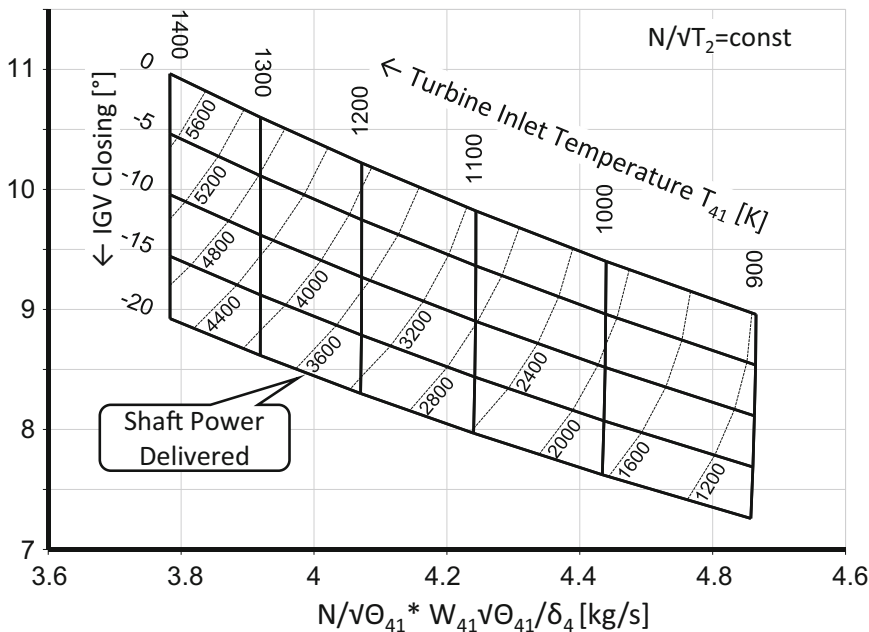


Fig. 2.4-2 Lines of constant shaft power output in the turbine map

But what is the benefit of closing the IGV's compared to reducing the turbine inlet temperature? Running the engine hotter increases the exhaust gas temperature, which can be an advantage in a combined-cycle power station. The variable IGV's can also be used for emission control since the fuel/air ratio, the velocity and the pressure in the burner all change with the IGV angle. Furthermore, we can use the IGV's for maximizing thermal efficiency.

2.5 References

1. Converse, G.L.: Extended Parametric Representation of Compressor, Fan and Turbines vol. III, pp. 24–26, NASA CR-174647, 1984 also in: Map Collection 3, J. Kurzke (2012)
2. Generic map of a subsonic booster in: GasTurb 13 (2017)
3. Suzuki, M., Kuno, N.: Research & Development of Two-stage Fan Component in HYPR Project AIAA 95-2344, 1995 also in: Map Collection 3, J. Kurzke (2012)
4. Kurzke, J., C. Riegler, A.: A New Compressor Map Scaling Procedure for Preliminary Conceptual Design of Gas Turbines, Aircraft Engine Committee Best Paper Award, ASME 2000-GT-0006, (2000)
5. Kurzke, J. : Preparing Compressor Maps for Gas Turbine Performance Modeling Manual to Smooth C 8.3, (2013)

Part D Basics

Chapter 1

Gas Properties and Standard Atmosphere



Any accurate cycle calculation program must utilize a good description of the gas properties. GasTurb uses data created with the NASA Computer program CEA (Chemical Equilibrium with Applications), which calculates chemical equilibrium compositions from any set of reactants and determines thermodynamic and transport properties for the product mixture. CEA represents the latest in a number of computer programs that have been developed at the NASA Lewis (now Glenn) Research Center during many decades. The publicly available program is written in ANSI standard FORTRAN by Bonnie J. McBride and Sanford Gordon. It is in wide use by the aerodynamics and thermodynamics community, with over 2000 copies in distribution.

1.1 The Half Ideal Gas

In GasTurb the working fluid is assumed to behave like a half-ideal gas. The definition of such a gas can be derived from basic thermodynamics as follows.

The state of a thermodynamic system is described fully by two state variables. For example, enthalpy h may be written as a function of temperature T and pressure P .

$$h = f(T, P) \quad (1.1-1)$$

The total differential of this relationship is

$$dh = \left(\frac{\partial h}{\partial T}\right)_{P=const} dT + \left(\frac{\partial h}{\partial P}\right)_{T=const} dP \quad (1.1-2)$$

Specific heat at constant pressure is defined as

$$C_P = \left(\frac{\partial h}{\partial T} \right)_{P=const} \quad (1.1-3)$$

The specific heat at constant pressure C_P of a real gas depends on both temperature and pressure. Furthermore,

$$\left(\frac{\partial h}{\partial P} \right)_{T=const} \neq 0 \quad (1.1-4)$$

For an ideal gas C_P is constant and

$$\left(\frac{\partial h}{\partial P} \right)_{T=const} = 0 \quad (1.1-5)$$

A half-ideal gas has the following characteristics:

$$C_P = f(T) \quad C_P \neq f(P) \quad \left(\frac{\partial h}{\partial P} \right)_{T=const} = 0 \quad (1.1-6)$$

Air behaves very much like a half-ideal gas at temperatures above approximately 200 K. Gaseous combustion products behave similarly; Their properties depend on the chemical composition of the fuel, the fuel/air ratio, and temperature.

1.1.1 Enthalpy

The enthalpy of the half-ideal gas is the integral of $C_P dT$ where C_P is the specific heat at constant pressure and T the temperature. The integration begins at a reference temperature and ends at the temperature of interest:

$$h(T) = \int_{T_{ref}}^T C_P(T) dT \quad (1.1-7)$$

The reference temperature T_{ref} can be selected arbitrarily, but when used for energy balances must be consistent with the reference temperature of other parameters such as fuel heating value (FHV), (Sect. 1.2.3). Its magnitude is not important for isentropic compression and expansion calculations because these involve only enthalpy differences.

Since the specific heat is a function of temperature and fuel/air ratio, the enthalpy also depends on temperature and fuel/air ratio.

1.1.2 Entropy Function

For an isentropic process with the half-ideal gas

$$\frac{dP}{P} = \frac{C_P(T)}{R} \frac{dT}{T} \quad (1.1-8)$$

In integral form this is

$$\int_{P_1}^{P_2} \frac{dP}{P} = \frac{1}{R} \int_{T_1}^{T_2} \frac{C_P(T)}{T} dT \quad (1.1-9)$$

We define the entropy function Ψ as

$$\Psi(T) = \frac{1}{R} \int_{T_{ref}}^T \frac{C_P(T)}{T} dT \quad (1.1-10)$$

Again, the reference temperature can be selected arbitrarily. Just as for the enthalpy, the calculation of isentropic compression and expansion processes uses only differences of entropy function values, not the absolute values themselves.

Use of the entropy function allows us to write the following simple formula for an isentropic change of state:

$$\ln\left(\frac{P_2}{P_1}\right) = \Psi_2 - \Psi_1 \quad (1.1-11)$$

Since the specific heat is a function of temperature and fuel/air ratio, the entropy function is also dependent on them.

1.2 Numerical Values

1.2.1 Specific Heat, Enthalpy and Entropy Function

CEA calculates chemical equilibrium compositions from any set of reactants and determines among others specific heat, enthalpy and entropy for the product mixture. We must run CEA for a representative pressure when creating data tables with specific heat, enthalpy, entropy and gas constant because in a half-ideal gas these properties must be independent from pressure.

Another characteristic of the half-ideal gas is its invariant chemical composition. Therefore, we force CEA to consider only the main combustion products H_2O and CO_2 while calculating C_p , h , Ψ and R for the products of any liquid or gaseous hydrocarbon fuel combustion. Under these circumstances, the composition of the gases is a linear function of fuel/air-ratio. It is sufficient to run CEA at only two fuel/air-ratios and interpolate for other values.

Humidity in the air, inlet fogging and water injection affect the chemical composition of the working fluid. Specific heat, enthalpy, entropy and gas constant all change with water/air ratio; Additional gas property tables are needed for modeling the water content in the air and the combustion gases.

1.2.2 Temperature Rise Due to Combustion

For the calculation of the temperature rise due to combustion, we must consider all sorts of combustion products, and we must take the influence of pressure into account. The main parameters are inlet temperature, fuel/air ratio and pressure. Additionally, we must distinguish between water and steam injection into a combustion chamber and also consider the humidity of the air. Therefore, the tables which contain the numbers for the temperature increase due to combustion are quite extensive.

1.2.3 Fuel

In gas turbines, mostly hydrocarbons are used as fuel. Hydrocarbons with 86.08 mass% of carbon and 13.92 mass% of hydrogen burn with air such that the molecular weight and therefore also the gas constant of the combustion products is exactly that of dry air ($R = 287.05 \text{ J/(kg K)}$). The lower heating value of this generic fuel is 43.124 MJ/kg at $T = 25^\circ\text{C}$.

Kerosene, JP-4 and other fuels used in aviation and for stationary gas turbines have a composition, which comes close to that of the generic fuel.

It should be noted that many aircraft manufacturers use specific values for the fuel lower heating value. Some prefer to use an average value and others a minimum value. When providing performance data to an aircraft customer, the fuel lower heating value should always be identified.

1.3 Standard Atmosphere

Ambient pressure and temperature of a standard day are described by the *International Standard Atmosphere* ISA. Extreme conditions on cold or hot days are defined in the US Military Standard 210 (MIL 210).

Given the flight altitude, both static temperature and pressure are calculated using the international standard atmosphere (ISA). Below 11,000 m the ambient ISA temperature is

$$T_{amb,ISA} = 288.15K - 6.5 \frac{altitude[m]}{1000m} \quad (1.3-1)$$

Ambient pressure in this altitude range is

$$P_{amb} = 101.325kPa \left(1 - 0.0225577 \frac{altitude[m]}{1000m} \right)^{5.25588} \quad (1.3-2)$$

Between 11,000 m and 25,000 m, the temperature is constant and equals 216.65 K.

The corresponding ambient pressure is

$$P_{amb} = 22.632kPa \times e^{\frac{11000m - altitude[m]}{6341.62m}} \quad (1.3-3)$$

Above 25,000 m, the temperature increases again according to

$$T_{amb,ISA} = 216.65K + 3 \frac{altitude[m] - 25000m}{1000m} \quad (1.3-4)$$

and ambient pressure there is

$$P_{amb} = 2.4886kPa \left(\frac{216.15K}{T_{amb,ISA}} \right)^{11.8} \quad (1.3-5)$$

The ISA defines a relationship between altitude, ambient pressure and ambient temperature for a “Standard Day”. It should be noted that the *true* or *geometric* altitude only has the same value as the *pressure altitude* when the temperature is ISA. Certification procedures for aircraft noise are defined for ISA + 10 °C conditions using geometric altitudes for the test conditions. The performance engineer must take account of this when generating cycle data for noise evaluations. More information on the definition of altitude may be found in [1].

Similar care must be taken when quoting airspeeds. There are several commonly used terms for aircraft speeds; indicated airspeed (“IAS”), calibrated airspeed (“CAS”), equivalent airspeed (“EAS”), and true airspeed (“TAS”). Engine performance data should always identify which definition is being used.

Besides the ISA correlation of ambient temperature with altitude there are various other temperature standards in use (Fig. 1.3-1).

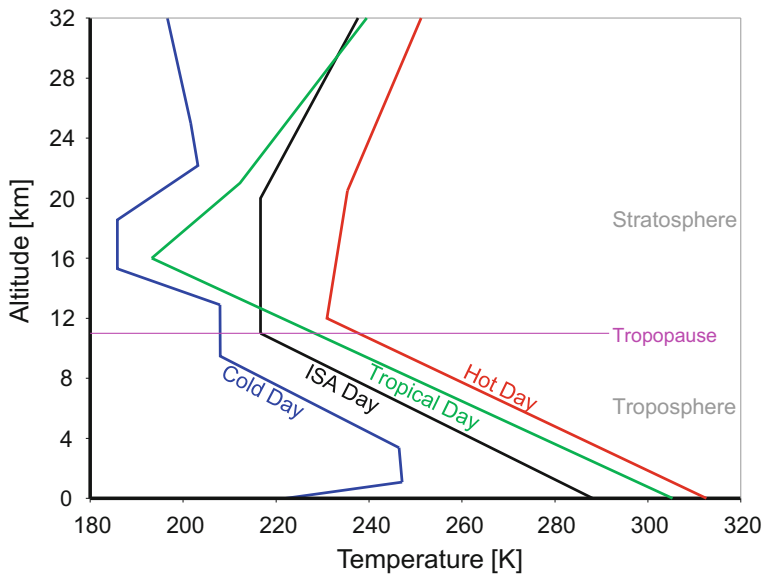


Fig. 1.3-1 Ambient temperature standards

1.4 Reference

1. Brown, F.S.: Subsonic Relationships Between Pressure Altitude, Calibrated Airspeed, and Mach number. Air Force Flight Test Center, Edwards AFB. Report AFFTC-TIH-10-01 (2012)

Chapter 2

Spreadsheet Calculations



2.1 Frequently Needed Equations

2.1.1 Some Simple Correlations

Mass flow

$$W = A\rho V \quad (2.1-1)$$

Density

$$\rho = \frac{P_s}{RT_s} \quad (2.1-2)$$

Mach number

$$M = \sqrt{\gamma RT_s} \quad (2.1-3)$$

Total/static temperature ratio

$$\frac{T}{T_s} = 1 + \frac{\gamma - 1}{2} M^2 \quad (2.1-4)$$

Total/static pressure ratio

$$\frac{P}{P_s} = \left(1 + \frac{\gamma - 1}{2} M^2 \right)^{\frac{\gamma}{\gamma - 1}} \quad (2.1-5)$$

Corrected flow per area

$$\frac{W\sqrt{T}}{A P} \sqrt{\frac{R}{\gamma}} = \frac{M}{\left(1 + \frac{\gamma - 1}{2} M^2\right)^{\frac{\gamma+1}{2(\gamma-1)}}} \quad (2.1-6)$$

Specific heat at constant pressure

$$C_P = \frac{\gamma}{\gamma - 1} R \quad (2.1-7)$$

2.1.2 Compressor

The task: calculate specific work H_{1-2} and exit temperature T_2 for a given compressor inlet temperature T_1 , pressure ratio P_2/P_1 and isentropic or polytropic efficiency.

2.1.2.1 By means of the isentropic exponent γ and specific heat C_P

This is the method of choice for simple gas turbine performance calculation. Taking the temperature dependence of specific heat into account requires iteration.

$$H_{1-2,is} = \frac{\gamma}{\gamma - 1} R T_1 \left[\left(\frac{P_2}{P_1} \right)^{\frac{\gamma-1}{\gamma}} - 1 \right] \quad (2.1-8)$$

Specific work for isentropic efficiency less than unity:

$$H_{1-2} = \frac{H_{1-2,is}}{\eta_{is}} \quad (2.1-9)$$

Exit temperature

$$T_2 = T_1 + \frac{H_{1-2}}{C_P} \quad (2.1-10)$$

A slightly different method for calculating exit temperature is based on

$$\eta_{is} = \frac{C_P(T_{2,is} - T_1)}{C_P(T_2 - T_1)} = \frac{\frac{T_{2,is}}{T_1} - 1}{\frac{T_2}{T_1} - 1} \quad (2.1-11)$$

Re-written

$$T_2 = T_1 \left\{ \frac{\left(\frac{P_2}{P_1}\right)^{\frac{\gamma-1}{\gamma}} - 1}{\eta_{is}} + 1 \right\} \quad (2.1-12)$$

Correlation isentropic—polytropic efficiency

$$\eta_{is} = \frac{\left(\frac{P_2}{P_1}\right)^{\frac{\gamma-1}{\gamma}} - 1}{\left(\frac{P_2}{P_1}\right)^{\frac{\gamma-1}{\gamma\eta_{pol}}} - 1} \quad (2.1-13)$$

2.1.2.2 By means of the entropy function Ψ

This is the method of choice for professional gas turbine performance calculation. The temperature dependence of specific heat is taken exactly into account.

The difference in the entropy function values for T_1 and $T_{2,is}$ equals the logarithm of the pressure ratio:

$$\Psi(T_{2,is}) = \Psi(T_1) + \ln\left(\frac{P_2}{P_1}\right) \quad (2.1-14)$$

When isentropic efficiency is given:

$$H_{1-2} = \frac{h(T_{2,is}) - h(T_1)}{\eta_{is}} \quad (2.1-15)$$

Exit temperature follows from enthalpy $h(T_2)$:

$$h(T_2) = h(T_1) + H_{1-2} \quad (2.1-16)$$

Polytropic efficiency is calculated as

$$\eta_{pol} = \frac{\ln\left(\frac{P_2}{P_1}\right)}{\Psi(T_2) - \Psi(T_1)} \quad (2.1-17)$$

When polytropic efficiency is given:

$$\Psi(T_2) = \Psi(T_1) + \frac{\ln\left(\frac{P_2}{P_1}\right)}{\eta_{pol}} \quad (2.1-18)$$

Specific work:

$$H_{1-2} = h(T_2) - h(T_1) \quad (2.1-19)$$

Isentropic efficiency:

$$\eta_{is} = \frac{h(T_{2,is}) - h(T_1)}{H_{1-2}} \quad (2.1-20)$$

2.1.2.3 Comparing compressors of different pressure ratios

Polytropic efficiency is one way of comparing compressors of different pressure ratios. However, it does not take account of the number of stages N. The simplest approach allowing for stage count is to compare average stage pressure ratio which is defined as:

$$\left(\frac{P_2}{P_1}\right)_{avg} = OPR^{1/N} \quad (2.1-21)$$

Another approach assumes that the aerodynamic loading, $\Delta H/U^2$, and polytropic efficiency are held constant for each stage. As the mean diameter does not vary very much from inlet to exit of a compressor, the circumferential velocity, U, is also roughly constant. The rising temperature from front to rear leads to reducing $\Delta H/T$ or lower stage pressure ratio at the rear. Figures 2.1-1 and 2.1-2 show how the stage pressure ratio varies from 1.59 on stage 1 to 1.22 on stage 10 for a compressor with overall pressure ratio 20 and 0.90 polytropic efficiency.

The pressure ratio of the first stage is called the *pressure ratio parameter*. The difference between pressure ratio parameter and the average stage pressure ratio is shown in Fig. 2.1-2 for 5- and 10-stage compressors across a range of overall pressure ratio.

2.1.3 Turbine

The task: Find from given turbine inlet temperature T_1 , specific work H_{1-2} and efficiency the pressure ratio P_1/P_2 and the exit temperature T_2 .

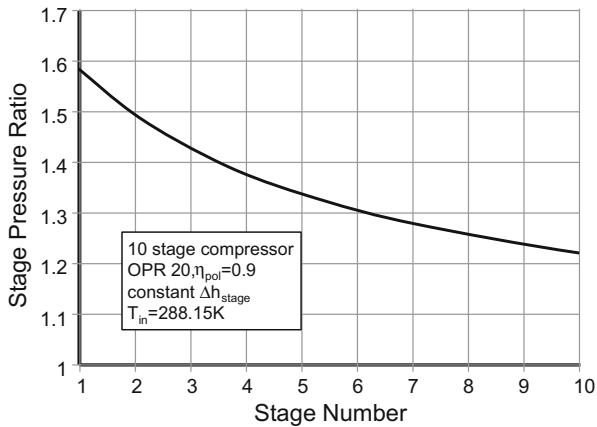


Fig. 2.1-1 Compressor stage pressure ratio versus stage number

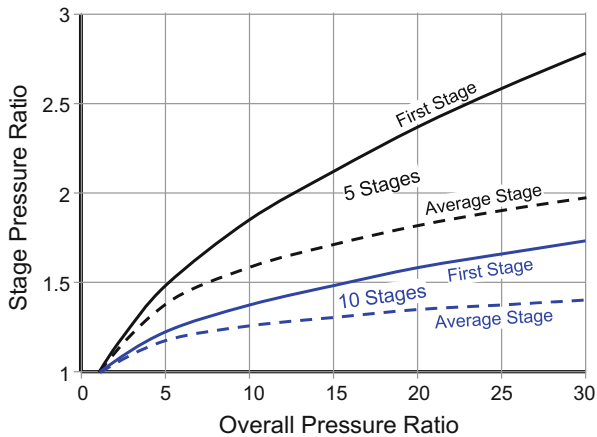


Fig. 2.1-2 Pressure ratio parameter versus average stage pressure ratio

Enthalpy after expansion:

$$h(T_2) = h(T_1) - H_{1-2} \quad (2.1-22)$$

2.1.3.1 When isentropic efficiency is given:

$$h(T_{2,is}) = h(T_1) - \frac{H_{1-2}}{\eta_{is}} \quad (2.1-23)$$

By means of the entropy function Ψ

Pressure ratio

$$\frac{P_1}{P_2} = e^{\Psi(T_1) - \Psi(T_{2,is})} \quad (2.1-24)$$

Polytropic efficiency

$$\eta_{pol} = \frac{\psi(T_1) - \psi(T_2)}{\ln\left(\frac{P_1}{P_2}\right)} \quad (2.1-25)$$

2.1.3.2 When polytropic efficiency is given:

Pressure ratio

$$\frac{P_1}{P_2} = e^{(\Psi(T_1) - \Psi(T_{2,is})) / \eta_{pol}} \quad (2.1-26)$$

Entropy function for $T_{2,is}$

$$\psi(T_{2,is}) = \Psi(T_1) - \ln\left(\frac{P_1}{P_2}\right) \quad (2.1-27)$$

Isentropic efficiency

$$\eta_{is} = \frac{h(T_1) - h(T_2)}{h(T_1) - h(T_{2,is})} \quad (2.1-28)$$

A slightly different method for calculating exit pressure P_2 assumes constant specific heat:

$$\eta_{is} = \frac{C_p(T_1 - T_2)}{C_p(T_1 - T_{2,is})} = \frac{1 - \frac{T_2}{T_1}}{1 - \frac{T_{2,is}}{T_1}} = \frac{1 - \frac{T_2}{T_1}}{1 - \left(\frac{P_2}{P_1}\right)^{\frac{\gamma-1}{\gamma}}} \quad (2.1-29)$$

Re-written

$$P_2 = P_1 \left[1 - \frac{1}{\eta_{is}} \left(1 - \frac{T_2}{T_1} \right) \right]^{\frac{\gamma}{\gamma-1}} \quad (2.1-30)$$

2.1.4 Isentropic and Polytropic Efficiency

We define polytropic efficiency as the isentropic efficiency of an infinitesimally small step in a compression, such that its magnitude would be constant throughout. It accounts for the fact that the inlet temperature to a back stage of a compressor is higher, and hence more work input is required for the same pressure rise.

Polytropic efficiency enables compressors and turbines of different pressure ratio to be compared on an ‘apples to apples’ basis. Those of the same technology level, average stage loading and geometric design freedom will have the same polytropic efficiency regardless of pressure ratio.

Figure 2.1-3 makes it understandable why compressor people prefer quoting polytropic efficiency and turbine designers like to present isentropic efficiency numbers.

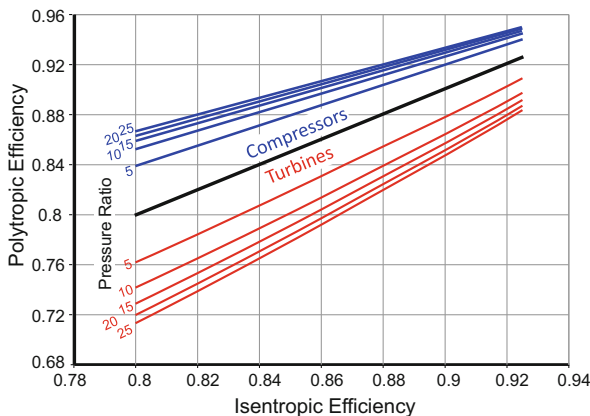


Fig. 2.1-3 Polytropic and isentropic efficiency ($T_{\text{entry}} = 288 \text{ K}$)

2.1.5 Combustor

How much heat is added in the combustion chamber depends on the chemical composition of the liquid or gaseous fuel. The higher fuel heating value is determined experimentally in a bomb calorimeter. The combustion of a stoichiometric mixture of fuel and oxidizer in a steel container at 25 °C is initiated by an ignition device and the reactions allowed to complete. When hydrogen and oxygen react during combustion, water vapor is produced. The vessel and its contents are then cooled to the original 25 °C and the higher heating value HHV is determined as the heat released between identical initial and final temperatures (Ref. Wikipedia).

Any water produced during the test will be in liquid form after the bomb calorimeter has been cooled down to 25 °C. The lower fuel heating FHV value is calculated from the higher heating value for the water being in vapor form. FHV is the quantity of interest for gas turbines.

If the bomb calorimeter test had been done at a different temperature, i.e. not at 25 °C, we would measure a different FHV value.

The energy balance through a combustor is

$$\begin{aligned} W_A [h_A(T_1) - h_A(T_{ref})] + W_F [h_F(T_F) - h_F(T_{ref})] + W_F FHV_{T_{ref}} \\ = (W_A + W_F) [h_G(T_2) - h_G(T_{ref})] \end{aligned} \quad (2.1-31)$$

In this equation stands A for air, F for fuel and G for combustion gases. The reference temperature is the temperature for which the fuel heating value is valid.

We can re-write this equation, employing mean values for specific heat:

$$\begin{aligned} W_A C_{P,A}(T_1 - T_{ref}) + W_F C_F(T_F - T_{ref}) + W_F FHV_{T_{ref}} \\ = (W_A + W_F) C_{P,G}(T_2 - T_{ref}) \end{aligned} \quad (2.1-32)$$

Let us assume that the fuel temperature is $T_F = T_{ref}$ and we introduce the fuel/air mass ratio, $far = W_F/W_A$. The equation changes to

$$C_{P,A}(T_1 - T_{ref}) + far FHV_{T_{ref}} = (1 + far) C_{P,G}(T_2 - T_{ref}) \quad (2.1-33)$$

We can solve the equation for far :

$$far = \frac{C_{P,G}(T_2 - T_{ref}) - C_{P,A}(T_1 - T_{ref})}{FHV - C_{P,G}(T_2 - T_{ref})} \quad (2.1-34)$$

2.1.6 Nozzle

Critical temperature ratio

$$\frac{T}{T_s} = \frac{\gamma + 1}{2} \quad (2.1-35)$$

Critical pressure ratio

$$\frac{P}{P_s} = \left(\frac{\gamma + 1}{2} \right)^{\frac{\gamma}{\gamma - 1}} \quad (2.1-36)$$

2.2 Cycle Calculation for a Turbojet Engine

2.2.1 Requirement

To calculate the thrust and specific fuel consumption for a turbojet engine flying at an altitude of 8000 m at Mach 0.7 and ISA temperature.

2.2.1.1 Data Available

The engine has a mass flow rate of 30 kg/s

Overall pressure ratio = 20.0

The isentropic efficiency of the compressor = 0.85

Combustor efficiency = 0.99

The maximum allowable turbine entry temperature (T_4) = 1700 K

The isentropic efficiency of the turbine = 0.89

Zero overboard bleed flow and power extraction.

2.2.1.2 Assumptions

Inlet isentropic efficiency = 0.965

Combustor pressure loss = 4%

Heating value of the fuel at 25 °C, FHV = 43.124 MJ/kg

Uncooled turbine

The expansion in the convergent exhaust nozzle is isentropic

Mechanical efficiency, η_m = 0.99.

2.2.2 Solution

2.2.2.1 Sketch the engine and identify the calculation planes (Fig. 2.2-1).

2.2.2.2 Consult the “US Standard Atmosphere” tables to obtain ambient conditions.

The ambient conditions at an altitude of 8000 m are T_{amb} = 236.15 K and P_{amb} = 35.60 kPa. Note that any inaccuracy in these values (introduced by rounding the numbers, for example) propagates to all the following calculations.

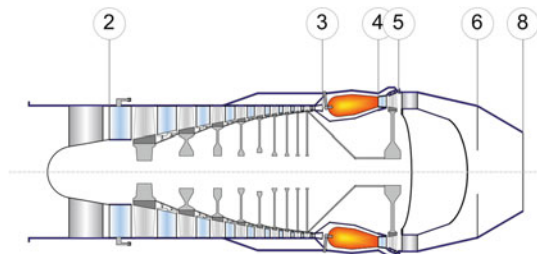


Fig. 2.2-1 Thermodynamic stations (calculation planes)

2.2.2.3 Calculate conditions at the compressor face.

The inlet is essentially an isentropic duct, where no work is done or heat is transferred. Ratio of specific heats, $\gamma = C_P/C_V = 1.4$ for air at prevailing temperature. The total temperature, T_2 , at flight Mach number, M_0 , is obtained from

$$T_2 = T_{amb} \left(1 + \frac{\gamma - 1}{2} M_0^2 \right) = 236.15 (1 + 0.2 \times 0.7^2) = 259.35 \text{ K} \quad (2.2-1)$$

In this example, the stagnation pressure at the compressor face is defined by isentropic efficiency

$$P_2 = 35.60 (1 + 0.965 \times 0.2 \times 0.7^2)^{3.5} = 48.84 \text{ kPa} \quad (2.2-2)$$

2.2.2.4 Calculate conditions at the compressor delivery.

The compressor overall pressure ratio OPR is given by

$$OPR = \frac{P_3}{P_2} = 20 \quad (2.2-3)$$

The total pressure at compressor delivery then becomes

$$P_3 = 48.84 \times 20 = 976.80 \text{ kPa} \quad (2.2-4)$$

In the absence of turbine cooling flow and overboard bleed flow the mass flow at compressor delivery is the same as at the compressor inlet, thus $W_3 = W_2$.

The equation for compressor isentropic efficiency, $\eta_{is,2-3}$ can be used to obtain the exit total temperature through the isentropic relationship between the ideal temperature ratio and actual pressure ratio

$$\eta_{is,2-3} = \frac{\text{Ideal work}}{\text{Actual work}} = \frac{T_{3is} - T_2}{T_3 - T_2} = \frac{\frac{T_{3is}}{T_2} - 1}{\frac{T_3}{T_2} - 1} = \frac{\left(\frac{P_3}{P_2}\right)^{\frac{\gamma-1}{\gamma}} - 1}{\frac{T_3}{T_2} - 1} \quad (2.2-5)$$

For a meaningful value of γ , we need the average compressor total temperature, so initially let us assume a mean value of 1.4 for γ through the compressor and use that to get us a first value of T_3 . Equation (2.1-12) gives us

$$T_3 = T_2 \left\{ \frac{\left(\frac{P_3}{P_2}\right)^{\frac{\gamma-1}{\gamma}} - 1}{\eta_{is,2-3}} + 1 \right\} \quad (2.2-6)$$

Substituting known values into Eq. (2.1-12), we obtain

$$T_3 = 259.35 \left\{ \frac{(20)^{\frac{1.4-1}{1.4}} - 1}{0.85} + 1 \right\} = 672.31 \text{ K} \quad (2.2-7)$$

A better value for γ can now be obtained by considering the inlet and exit temperatures, and then

$$\overline{T_{2-3}} = \frac{259.35 + 672.31}{2} = 465.83 \text{ K} \quad (2.2-8)$$

From the γ versus temperature chart in Fig. 2.2-2, at far = 0,

$$\overline{\gamma_{2-3}} = 1.39 \quad (2.2-9)$$

and for later use from Fig. 2.2-3

$$\overline{C_{P2-3}} = 1024 \text{ J/kg K} \quad (2.2-10)$$

Substituting once more in the compressor efficiency Eq. (2.2.6), the new value of compressor delivery temperature is found to be

$$T_3 = 661.37 \text{ K} \quad (2.2-11)$$

The temperature value has changed by only 1.6%, so further iteration is unnecessary. By the way, GasTurb uses the entropy function for getting the exact result $T_3 = 662 \text{ K}$. For later use, we calculate the total temperature rise through the compressor as being

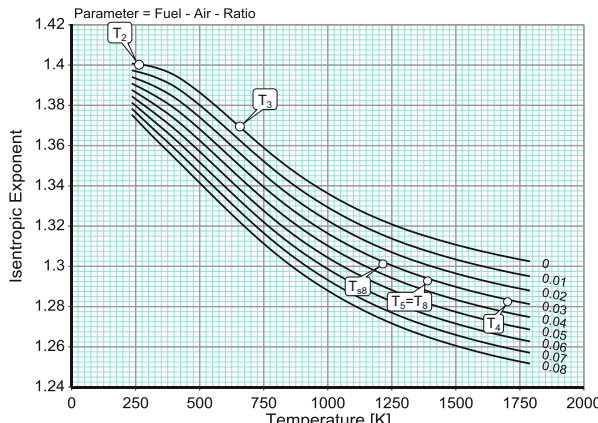


Fig. 2.2-2 Isentropic exponent of air and combustion products from a generic hydrocarbon fuel

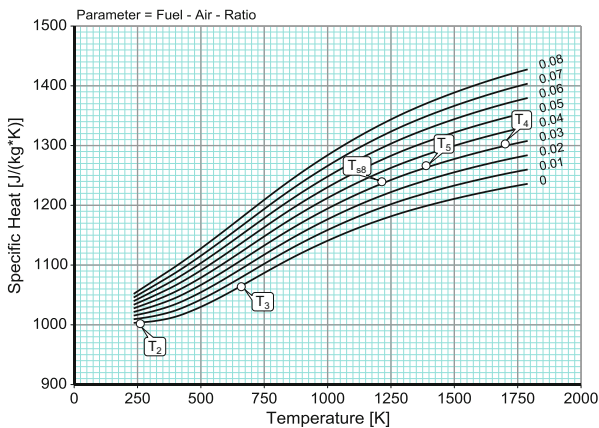


Fig. 2.2-3 Specific heat of air and combustion products from a generic hydrocarbon fuel

$$T_{3-2} = 661.37 - 259.35 = 402.02 \text{ K} \quad (2.2-12)$$

2.2.2.5 Calculate combustor exit conditions and fuel flow rate.

Combustor calculations could be delayed, but now is a good time to calculate the fuel flow rate so it can be included in the turbine mass flow used in the subsequent energy balance calculations.

The compressor delivery total temperature was obtained above ($T_3 = 661.37 \text{ K}$), and the maximum turbine entry total temperature has been given in the input ($T_4 = 1700 \text{ K}$). The fuel heating value of $FHV = 43.124 \text{ MJ/kg}$ is valid for the temperature of $T_{ref} = 25^\circ\text{C}$.

$$far = \frac{C_{P,G}(T_4 - T_{ref}) - C_{P,A}(T_3 - T_{ref})}{FHV - C_{P,G}(T_4 - T_{ref})} \quad (2.2-13)$$

Initially, let us assume a fuel/air-ratio of 0.05 and make adjustments later. For this far, the specific heat of the combustion gases $C_{P,G} = 1347 \text{ J/kg K}$ at 1700 K and 1045 J/kg K at the reference temperature of 298 K. Mean $C_{P,G}$, of the combustion gases is 1196 J/kg K . The respective values for the air are $C_{P,A} = 1066 \text{ J/kg K}$ at 661 K and 1005 J/kg K for 298 K, which yields the mean value $C_{P,A}$ of 1035.5 J/kg K . Inserting these values into the equation above yields $far = 0.03137$.

With the new fuel/air ratio we get improved values for $C_{P,G}$ and from re-evaluation of the equation we get $far = 0.03034$. Fuel flow is

$$W_{F,ideal} = far * W_3 = 0.03034 \times 30 = 0.91 \text{ kg/s} \quad (2.2-14)$$

But this is the ideal value. The actual fuel burn is calculated by considering the combustor efficiency, η_{3-4} . Then

$$W_F = \frac{W_{Fideal}}{\eta_{3-4}} = \frac{0.91}{0.99} = 0.92 \text{ kg/s} \quad (2.2-15)$$

This value is 2.4% lower than the value calculated by GasTurb which reads tables with data that were generated by the NASA CEA Program. One reason for the difference is dissociation, which under the prevailing conditions reduces the equilibrium temperature by 5 K. Working with mean specific heat over the big temperature range from 298 to 1700 K is responsible for the main part of the difference.

In the absence of turbine cooling air, the mass flow rate through the turbine is

$$W_4 = W_3 + W_F = 30 + 0.92 = 30.92 \text{ kg/s} \quad (2.2-16)$$

The total pressure at the combustor exit is obtained from the combustor pressure loss provided. Therefore

$$P_4 = P_3 \times 0.96 = 976.80 \times 0.96 = 937.73 \text{ kPa} \quad (2.2-17)$$

2.2.2.6 Do an energy balance calculation for the spool and find the conditions at the turbine exit.

In general terms, the work balance on an engine spool may be stated as turbine work \times mechanical efficiency equals compressor work plus power offtake. The mechanical inefficiency is caused by power extraction for engine accessories (fuel and oil pumps), in addition to bearing and disk windage losses. In this example power offtake is zero. Expressed more specifically, the energy balance becomes

$$W_{turbine} \times \overline{C_{P4-5}} \times T_{4-5} \times \eta_{mech} = W_{compressor} \times \overline{C_{P2-3}} \times T_{2-3} \quad (2.2-18)$$

from which the temperature drop across the turbine may be expressed as

$$T_{4-5} = \frac{1}{\eta_{mech}} \times \frac{W_2}{W_4} \times \frac{\overline{C_{P2-3}}}{\overline{C_{P4-5}}} \times T_{2-3} \quad (2.2-19)$$

To be accurate, the mass flow rate through the turbine must include the fuel added to the gas stream, and that is why we have already calculated it. As for the compressor, we need an average value of temperature across the turbine to evaluate the corresponding average value of C_p . We guess a value of the turbine exit temperature (T_5) to be 1400 K, and since we already know that $T_4 = 1700$ K, the initial average value of the temperature through the turbine becomes 1550 K. From Fig. 2.2-3, at $\dot{m}_{far} = 0.03034$, we obtain

$$\overline{C_{P4-5}} = 1284.4 \text{ J/kg K} \quad (2.2-20)$$

Then, substituting in Eq. (2.2-19), we obtain

$$T_{4-5} = \frac{1}{0.99} \times \frac{30.00}{30.92} \times \frac{1024}{1284.4} \times 402.02 = 314.22 \text{ K} \quad (2.2-21)$$

This provides a better value of turbine exit temperature ($T_5 = 1700 - 314.22 = 1385.8 \text{ K}$), a better value of average temperature across the turbine (1542.9 K) and improved values of average specific heat through the turbine. From Fig. 2.2-3 at far = 0.03034

$$\overline{C_{P4-5}} = 1283.4 \text{ J/kg K} \quad (2.2-22)$$

Inserting the new value of C_{P4-5} into the power balance Eq. (2.2-19) results in a temperature drop through the turbine of

$$T_{4-5} = \frac{1}{0.99} \times \frac{30.00}{30.92} \times \frac{1024}{1283.4} \times 402.02 = 314.36 \text{ K} \quad (2.2-23)$$

Compared with our previous estimate, the change in the value of the temperature drop is only 0.14 K, from which it may be deemed that the solution has converged. The turbine exit temperature is then

$$T_5 = 1700 - 314.36 = 1385.64 \text{ K} \quad (2.2-24)$$

This value deviates less than 1 K from the GasTurb result which is $T_5 = 1384.73 \text{ K}$.

We now use the expression for turbine isentropic efficiency, which incorporates the isentropic relationship between ideal temperature ratio and actual pressure ratio, to calculate the exit total pressure.

$$\eta_{4-5} = \frac{\text{Actual work}}{\text{Ideal work}} = \frac{T_4 - T_5}{T_4 - T_{5is}} = \frac{1 - \frac{T_5}{T_4}}{1 - \frac{T_{5is}}{T_4}} = \frac{1 - \frac{T_5}{T_4}}{1 - \left(\frac{P_5}{P_4}\right)^{\frac{\gamma-1}{\gamma}}} \quad (2.2-25)$$

The isentropic exponent at the mean turbine temperature is 1.289 (Fig. 2.2-2).

$$P_5 = P_4 \left[1 - \frac{1}{\eta_{4-5}} \left(1 - \frac{T_5}{T_4} \right) \right]^{\frac{\gamma-1}{\gamma}} \quad (2.2-26)$$

$$P_5 = 937.73 \left[1 - \frac{1}{0.89} \left(1 - \frac{1385.64}{1700} \right) \right]^{1.289/0.289} \quad (2.2-27)$$

From which

$$P_5 = 331.84 \text{ kPa} \quad (2.2-28)$$

This value deviates only 0.7% from the GasTurb result which is 329.55 kPa

2.2.2.7 Calculate the thrust from the exhaust nozzle.

Net thrust is determined from the rate of change of momentum between engine inlet (the ram drag) and nozzle exit combined with the effect of any excess (static) pressure acting on the nozzle exit area. This is expressed as

$$F_N = W_8(V_8 - V_0) + A_8(P_{s8} - P_{amb}) \quad (2.2-29)$$

where W_8 is the exhaust mass flow rate and A_8 is the nozzle throat area. (The exit and throat are coincident for a simple convergent nozzle.)

The pressure term only appears if the nozzle is choked, otherwise the flow expands to ambient pressure at the exit and the pressure term in Eq. (2.2-29) disappears. We must calculate the pressure ratio through the nozzle and determine if choking occurs.

The nozzle is isentropic, no pressure is lost between the turbine exit and the nozzle exit, and $P_8 = P_5$. The temperature and pressure at entry to the nozzle are $T_8 = T_5 = 1385.64 \text{ K}$ and $P_8 = 331.84 \text{ kPa}$ respectively.

The nozzle pressure ratio is given by

$$\frac{P_8}{P_{amb}} = \frac{331.84}{35.6} = 9.32 \quad (2.2-30)$$

The nozzle pressure ratio for choking conditions is expressed as

$$\frac{P_8}{P_{s8}} = \left(\frac{\gamma + 1}{2} \right)^{\frac{\gamma}{\gamma-1}} \quad (2.2-31)$$

where P_{s8} is the static pressure in the choked nozzle throat plane and the value of γ corresponds to the gas temperature at that location.

The nozzle throat static temperature is given by

$$T_{s8} = T_{s,sonic} = \left(\frac{2}{\gamma + 1} \right) T_8 \quad (2.2-32)$$

We know that far_8 is 0.03034, so from Fig. 2.2-2

$$\gamma_{T8} = 1.295 \quad (2.2-33)$$

We use this value for estimating the static temperature in the nozzle throat using Eq. (2.2-32) as

$$T_{s8} = 0.87 \times T_8 = 0.87 \times 1385.64 \text{ K} = 1205 \text{ K} \quad (2.2-34)$$

From Fig. 2.2-2 we get an improved estimate for the isentropic exponent

$$\gamma_{Ts8} = 1.304 \quad (2.2-35)$$

Using Eq. (2.1-36), the critical pressure ratio at which the nozzle chokes is given by

$$\left(\frac{P_8}{P_{s8}}\right)_{sonic} = \left(\frac{1.304+1}{2}\right)^{1.304/0.304} = 1.835 \quad (2.2-36)$$

Therefore

$$\frac{P_8}{P_{amb}} \gg \frac{P_8}{P_{s8}} \quad (2.2-37)$$

and the nozzle is severely choked.

Now we calculate the nozzle throat area A_8 . For the choked nozzle, the exit static temperature at its exit is given by

$$T_{s8} = T_{critical} = \left(\frac{2}{\gamma+1}\right) T_8 \quad (2.2-38)$$

So

$$T_{s8} = \left(\frac{2}{2.304}\right) 1385.64 = 1202.8 \text{ K} \quad (2.2-39)$$

The corresponding static pressure is

$$P_{s8} = \frac{P_8}{\left(\frac{P_8}{P_{s8}}\right)_{sonic}} = \frac{331.84}{1.835} = 180.84 \text{ kPa} \quad (2.2-40)$$

Note:

We are interested in static values of temperature and density because static temperature determines the speed of sound in a gas and static density is used in the

continuity equation to determine the mass flow rate and the speed at which it travels through an orifice or duct. Both properties are evaluated by moving with the gas!

The density of the gas, based on known static values of pressure and temperature, is calculated from the equation of state

$$\rho_{s8} = \frac{P_{s8}}{RT_{s8}} = \frac{180.84 \times 1000}{287.05 \times 1202.8} = 0.5238 \text{ kg/m}^3 \quad (2.2-41)$$

Since the nozzle is choked, the speed of the exit exhaust gas is the same as the speed of sound, and is found from

$$V_8 = \sqrt{\gamma RT_{s8}} = \sqrt{1.304 \times 287.05 \times 1202.8} = 671.0 \text{ m/s} \quad (2.2-42)$$

The exit area of the hot nozzle is found from the continuity equation, as follows:

$$A_8 = \frac{W_8}{\rho_8 V_8} = \frac{30.92}{0.5238 * 671.0} = 0.0880 \text{ m}^2 \quad (2.2-43)$$

At a flight speed of Mach 0.7 and an altitude of 8000 m, U.S. Standard Atmosphere tables tell us that the speed of sound at that altitude is 308.15 m/s, so the aircraft is flying at $V_0 = 215.70 \text{ m/s}$. We can now substitute values into Eq. (2.2.29) to get

$$F_N = \frac{30.92 \times 671.0 - 30.00 \times 215.70}{1000} + 0.088 \times (180.84 - 35.6) \quad (2.2-44)$$

that is

$$F_N = 14.276 + 12.78 = 27.06 \text{ kN} \quad (2.2-45)$$

This value agrees perfectly with the GasTurb result.

2.2.2.8 Calculate the specific fuel consumption

Specific fuel consumption is defined by

$$SFC = \frac{W_F}{F_N} \quad (2.2-46)$$

So

$$SFC = \frac{0.92 \times 1000}{27.06} = 34.0 \text{ g/kN s} \quad (2.2-47)$$

This value deviates by 2.3% from the GasTurb result; The reason is the difference in fuel flow.

Station	W kg/s	T K	P kPa	WRstd kg/s	FN	=	27.08 kN
amb		236.15	35.600		TSFC	=	34.7713 g/(kN*s)
1	30.000	259.34	49.389	59.046	FN/W2	=	902.69 m/s
2	30.000	259.34	48.840		Prop Eff	=	0.3318
3	30.000	662.06	976.798	4.717	eta core	=	0.5081
31	30.000	662.06	976.798		WF	=	0.94163 kg/s
4	30.942	1700.00	937.727	8.121	s NOx	=	0.31021
41	30.942	1700.00	937.727	8.121	XM8	=	1.0000
49	30.942	1384.73	329.549		A8	=	0.0888 m ²
5	30.942	1384.73	329.549	20.855	P8/Pamb	=	9.2570
6	30.942	1384.73	329.549	20.855	WBd/W2	=	0.00000
8	30.942	1384.73	329.549		Ang8	=	0.00 °
Bleed	0.000	662.06	976.802		CD8	=	1.0000
					WC1N/W2	=	0.00000
P2/P1 = 0.9889	P4/P3 = 0.9600	P6/P5 = 1.0000			WC1R/W2	=	0.00000
Efficiencies:	isentr polytr	RNI	P/P		Loading	=	100.00 %
Compressor	0.8500	0.8976	0.546	20.000	e45 th	=	0.89000
Burner	0.9900				far7	=	0.03139
Turbine	0.8900	0.8778	1.163	2.845	PWX	=	0.00 kW
Spool mech Eff	0.9900	Nom Spd	9292 rpm				
hum [%]	war0	FHV	Fuel				
0.0	0.00000	43.124	Generic				

Fig. 2.2-4 Cycle overview page of GasTurb

2.2.2.9 GasTurb output

Figure 2.2-4 shows the cycle overview output of GasTurb and Fig. 2.2-5 shows the details at the thermodynamic stations. Compare the numbers with those from the hand calculation results to see differences. By far the biggest deviation between the hand calculation and GasTurb is in the fuel flow. GasTurb does not calculate a fuel/air ratio for the combustion chamber, it reads tables which have been created with the NASA CEA program. This approach describes in effect the chemical

	Units	St 2	St 3	St 4	St 5	St 6	St 8
Mass Flow	kg/s	30	30	30.9416	30.9416	30.9416	30.9416
Total Temperature	K	259.339	662.064	1700	1384.73	1384.73	1384.73
Static Temperature	K	245.022	654.499	1690.4	1352.79	1376.61	1204.85
Total Pressure	kPa	48.8399	976.798	937.727	329.549	329.549	329.549
Static Pressure	kPa	40.0474	936.118	914.008	297.448	321.147	179.622
Velocity	m/s	169.49	126.81	157.88	283.762	143.067	671.228
Area	m ²	0.310862	0.047479	0.104041	0.142351	0.26611	0.088756
Mach Number		0.54	0.25	0.2	0.4	0.2	0.999836
Density	kg/m ³	0.569391	4.98268	1.8837	0.766002	0.812721	0.519368
Spec Heat @ T	J/(kg*K)	1003.82	1065.83	1302.81	1265.61	1265.61	1265.61
Spec Heat @ Ts	J/(kg*K)	1003.48	1064.03	1301.81	1260.96	1264.43	1237.6
Enthalpy @ T	J/kg	-38936.4	374760	1.65841E6	1.25326E6	1.25326E6	1.25326E6
Enthalpy @ Ts	J/kg	-53299.8	366720	1.64595E6	1.213E6	1.24302E6	1.02798E6
Entropy Function @ T		-0.487439	2.85002	6.91866	6.00077	6.00077	6.00077
Entropy Function @ Ts		-0.685924	2.80749	6.89304	5.89828	5.97494	5.39389
Exergy	J/kg	22506.1	413038	1.41817E6	1.00435E6	1.00435E6	1.00435E6
Gas Constant	J/(kg*K)	287.05	287.05	287.045	287.045	287.045	287.045
Fuel-Air-Ratio		0	0	0.031388	0.031388	0.031388	0.031388

Fig. 2.2-5 Properties at stations

equilibrium as the ideal case for a combustor. It is not feasible to describe the heat addition in the combustion chamber accurately with mean values for specific heat. The influence of pressure and water content in the air on the chemical equilibrium cannot be described with the half-ideal gas model which is employed in GasTurb.

2.2.3 Summary

First sketch the engine and number the calculation planes.

Consult the “US Standard Atmosphere” tables to obtain ambient conditions.

Calculate conditions at the compressor face.

Calculate compressor delivery conditions. Calculations are iterative

Find P_3 from OPR

Use efficiency to get to delivery temperature

Calculate fuel flow rate from an energy balance and combustor exit conditions.

Fuel flow contributes to turbine flow

Burner efficiency is important

Turbine entry pressure, P_4 , is needed

Do an energy balance calculation for the spool and find the conditions at the turbine exit.

Note the mechanical efficiency

Use correct mass flows

Need to guess a mean turbine temperature & then iterate, using efficiency equation

Calculate the thrust from the exhaust nozzle.

First check for choking to determine if there is a pressure term in the thrust equation.

Calculate the specific fuel consumption.

Chapter 3

Non-dimensional Performance



What is the background of the non-dimensional parameters which everybody uses for describing the performance of turbomachinery? Where do these parameters come from? We could employ a general method like the Buckingham π theorem to explain how sets of dimensionless parameters may be found for any engineering problem which can be described with a set of measurable quantities. We do not do that—lovers of abstract theory please refer to other books—we begin with the statement that the following three non-dimensional parameters are most important for fluid dynamics in the turbomachinery of gas turbines:

1. The *Mach number* M —the ratio of flow velocity to the local speed of sound.
2. The *Reynolds number* Re —the ratio between inertia forces and viscous forces.
3. The *isentropic exponent* γ —the ratio of the specific heat at constant pressure to the specific heat at constant volume.

3.1 Non-dimensional Compressor Performance

What does non-dimensional mean in our context? We want to describe the flow phenomena in the compressor with non-dimensional parameters, using quantities to which no physical dimension is applicable. Examples for such quantities are velocity ratios, temperature ratios, pressure ratios and efficiencies.

Velocity triangles are a preferred way for describing what happens in turbomachines (Fig. 3.1-1). *Similar* irregular triangles have common angles between the sides. Velocity ratios in similar velocity diagrams are the same.

Another velocity ratio is the Mach number. To explain its connection with the flow field in turbomachines let us compare two rig tests with the same compressor.

Test A is carried out with ideal ISA inlet conditions (dry air, $T_{\text{amb}} = 288.15 \text{ K}$ and $P_{\text{amb}} = 101.325 \text{ kPa}$). During Test B the weather and the location of the test rig determine the inlet conditions of the day.

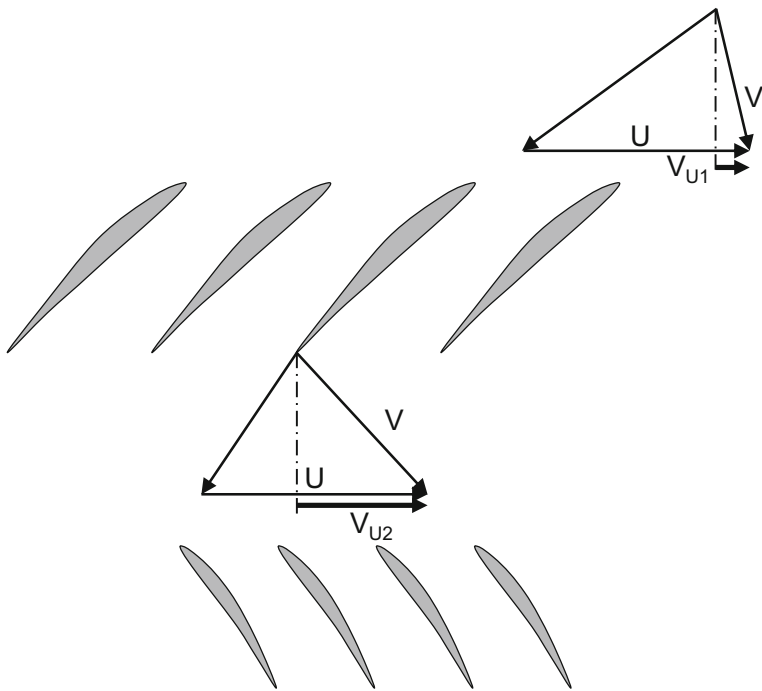


Fig. 3.1-1 Velocity triangles of a compressor stage

What would happen if we run both tests with the same spool speed (same circumferential speed U)? In test B, we adjust the throttle in such a way that we get the same compressor inlet flow velocity V as in the test with ISA inlet conditions (test A). The velocity triangles at the compressor inlet would be the same.

Let us assume for the moment that the exit velocity triangles would also be the same in both rig tests. Euler's law would yield the same specific work $H_C = U(V_{u2} - V_{u1})$ for both tests, the energy balance would result in $H_C = \gamma/(\gamma - 1)R(T_2 - T_1)$.

Since the velocity triangles are the same, the two tests seem to be non-dimensionally the same. However, since the temperature difference $T_2 - T_1$ is the same, the temperature ratio T_2/T_1 cannot be the same because T_1 is different. Thus, the non-dimensional quantity T_2/T_1 would not be the same even if the velocity triangles are identical in both tests. Or the other way round: if temperature ratio is set to the same value in both tests by adjusting the throttle, then the velocity triangles must be different. Running the test with equal spool speeds obviously does not yield consistent results. Either the temperature ratio is different, or the shapes of the velocity triangles are different.

Can we run the two rig tests in such a way that the temperature ratio remains the same? Yes, we can! Divide both equations for H_C by T_1 and the gas constant R :

$$\frac{H_C}{RT_1} = \frac{\gamma}{\gamma - 1} \left(\frac{T_2}{T_1} - 1 \right) = \frac{U}{\sqrt{RT_1}} \left(\frac{V_{u2}}{\sqrt{RT_1}} - \frac{V_{u1}}{\sqrt{RT_1}} \right) \quad (3.1-1)$$

This equation means that we will get the same temperature ratio T_2/T_1 if we run both tests with the same $U/\sqrt{RT_1}$ and adjust the throttle in such a way that $V_{u2}/\sqrt{RT_1} - V_{u1}/\sqrt{RT_1}$ match in each test.

$U/\sqrt{RT_1}$ looks similar to a Mach number, but it is not the true Mach number of the circumferential speed U , which is

$$M_U = \frac{U}{\sqrt{\gamma RT_s}} \quad (3.1-2)$$

$U/\sqrt{RT_1}$ is related to the true circumferential Mach number M_U and the Mach number of the absolute velocity M_{V1} . The ratio of static temperature T_s to total temperature T_1 at the compressor inlet is:

$$\frac{T_1}{T_s} = 1 + \frac{\gamma - 1}{2} M_{V1}^2 \quad (3.1-3)$$

Using this correlation, we can write:

$$\frac{U}{\sqrt{RT_1}} = \frac{U\sqrt{\gamma}}{\sqrt{\gamma RT_s} \frac{T_1}{T_s}} = \frac{U}{\frac{1}{\sqrt{\gamma}} \sqrt{\gamma RT_{s1}} \left(1 + \frac{\gamma-1}{2} M_{V1}^2 \right)} = \frac{M_U}{\frac{1}{\sqrt{\gamma}} \sqrt{1 + \frac{\gamma-1}{2} M_{V1}^2}} \quad (3.1-4)$$

Similarly, we can express the circumferential velocity components in terms of Mach numbers:

$$\frac{V_{u1}}{\sqrt{RT_1}} = \frac{M_{Vu1}}{\frac{1}{\sqrt{\gamma}} \sqrt{1 + \frac{\gamma-1}{2} M_{V1}^2}} \quad (3.1-5)$$

M_U , M_{V1} and M_{Vu1} fully describe the non-dimensional inlet velocity triangle, and M_U , M_{V2} and M_{Vu2} the non-dimensional exit velocity triangle. These non-dimensional velocity triangles are connected inseparably to the temperature ratio T_2/T_1 through Eq. (3.1-1). In other words, equal Mach numbers lead to equal total temperature ratios T_2/T_1 .

What about pressure ratio? Pressure ratio and temperature ratio are connected through the efficiency η :

$$\frac{P_2}{P_1} = \left[1 + \eta \left(\frac{T_2}{T_1} - 1 \right) \right]^{\frac{\gamma}{\gamma-1}} \quad (3.1-6)$$

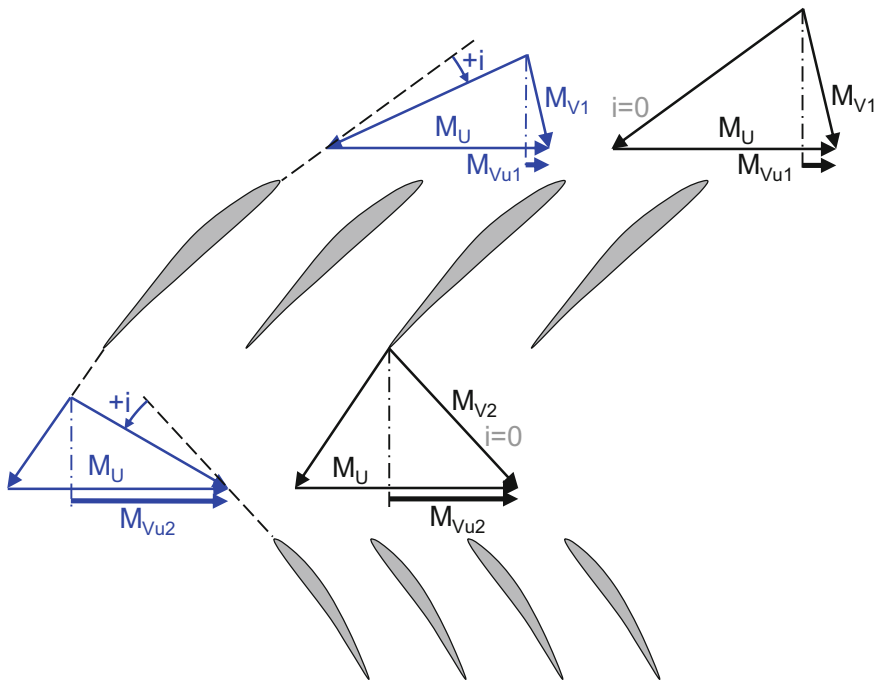


Fig. 3.1-2 Mach number triangles of a compressor stage, definition of incidence angle i

Which parameters influence efficiency? Figure 3.1-3 shows cascade pressure loss coefficients for various blade designs. They depend on incidence angle i and Mach number (Fig. 3.1-2).

If we have the same non-dimensional velocity triangles (i.e. similar triangles), then incidence and the inlet Mach number will be the same for each of the blade and vane rows. Consequently, the pressure loss coefficients will also be the same. That means that not only is the total temperature ratio T_2/T_1 defined by the non-dimensional Mach number triangles but also the efficiency and total pressure ratio P_2/P_1 . These considerations are the origin of the term *Mach number similarity* which plays a big role in gas turbine performance analysis.

In practice, we do not describe the non-dimensional compressor operating point with the terms $U/\sqrt{RT_1}$, $V_{U1}/\sqrt{RT_1}$ and $V_{U2}/\sqrt{RT_1}$. We use *reduced speed* and *reduced flow* for setting the non-dimensional compressor inlet velocity triangle.

It is common practice to replace the circumferential speed U with spool speed N , measured in revolutions per minute:

$$\frac{N}{\sqrt{RT_1}} = k \frac{U}{\sqrt{RT_1}} \quad (3.1-7)$$

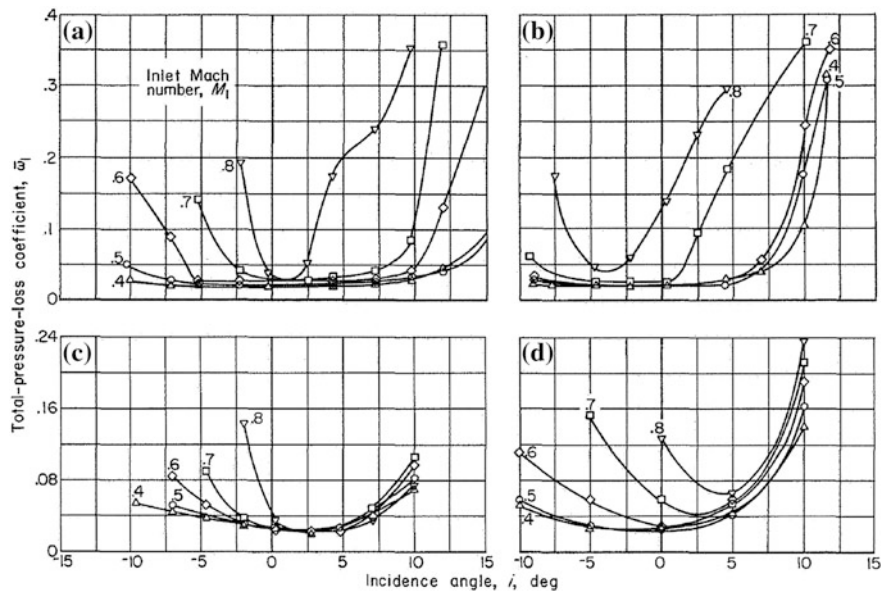


Fig. 3.1-3 Loss characteristics of cascade blade sections [2] **a** Circular Arc, **b** Parabolic Arc, **c** Double Circular Arc, **d** Sharp Nose Blade

Often this relation is simplified further by regarding the gas constant R as invariant. Reduced speed is calculated as N/\sqrt{T} [rpm/ \sqrt{K}] and corrected speed as $N/\sqrt{\Theta}$ [rpm] with $\Theta = T/288.15$ K. Note, however, that the gas constant of air changes with humidity. If you want to simulate the influence of humidity on performance, then R should be retained in the definition of reduced and corrected spool speeds.

Corrected flow is related to the Mach number at the compressor inlet (with the area A), upstream of the inlet guide vane or, without an IGV, it could apply to the first rotor:

$$W_{red} = \frac{W\sqrt{RT}}{P} = A \frac{M\sqrt{\gamma}}{\left(1 + \frac{\gamma-1}{2}M^2\right)^{\frac{\gamma+1}{2(\gamma-1)}}} \quad (3.1-8)$$

There are similar simplifications of the Mach number and reduced mass flow definitions in use, as in case of the reduced spool speed definition. $W\sqrt{T}/P$ [kg/s $\sqrt{K/kPa}$] is a short formula, but the units are complex. These are more simple and more meaningful if corrected flow is defined as $W\sqrt{\Theta}/\delta$ [kg/s] with $\Theta = T/288.15$ K and $\delta = P/101.325$ kPa because this number gives an impression of the compressor size. The most useful definition of corrected flow includes the gas constant R which allows to consider the effects of humidity.

Back to our two rig tests. Test B was done at the ambient conditions of the day. The question could have been: what would we measure for the same operating condition on an ISA day? By “the same operating conditions” we mean that all the Mach numbers and flow angles are the same. This could be made feasible by running the test with the same corrected spool speed, pressure ratio and corrected mass flow. If we did that, we would measure the same efficiency as in test B. So, what is the added value of running test A? Nothing! It is unnecessary to do the test at ISA inlet conditions because we get no new information.

Compressor performance maps contain lines of constant corrected speed and efficiency in a figure with corrected flow as x-axis and pressure ratio as y-axis. The map only contains non-dimensional information. Selecting an operating point in the map is equivalent to selecting the Mach numbers and flow angles everywhere in the compressor.

There are more non-dimensional parameters of interest, for example the *reduced shaft power*. We get it by multiplying reduced flow and reduced specific work:

$$PW_{red} = \frac{W\sqrt{RT}}{P} \frac{H_C}{RT} = \frac{PW}{P\sqrt{RT}} \quad (3.1-9)$$

3.2 Non-dimensional Engine Performance

What we have explained in great detail for the compressor applies, in principle, to turbomachinery in general. Selecting an operating point in a component map determines the Mach numbers and flow angles at the inlet and everywhere in the compressor and the same statement applies to the turbine. Corrected speed, corrected flow, pressure ratio and temperature ratio of the component are fixed by the map point selection.

Mach number and flow direction at the entrance to any duct downstream of a compressor or turbine depend only on the Mach number similarity point in the related component map. Therefore, the pressure losses in the duct are a function of the operating point location in the map of the upstream component. Note that the Mach number at a duct exit is equal to the entry Mach number of a downstream component.

What about the combustion chamber? Let us consider the mass flow balance from entrance to exit, expressed in Mach number corrected values:

$$\frac{W_2\sqrt{T_2}}{P_2} = \frac{W_4\sqrt{T_4}}{P_4} \frac{W_2}{W_4} \frac{P_4}{P_3} \frac{P_3}{P_2} \sqrt{\frac{T_2}{T_3}} \sqrt{\frac{T_3}{T_4}} \quad (3.2-1)$$

The first three terms on the right side of this equation are essentially constant. We can solve this equation for the temperature ratio T_4/T_3 :

$$\frac{T_4}{T_3} = \left(k \frac{\frac{P_3}{P_2} \sqrt{\frac{T_2}{T_3}}}{\frac{W_2 \sqrt{T_2}}{P_2}} \right)^2 \quad (3.2-2)$$

On the right side of the equation there are only Mach number similarity parameters of the gas generator compressor. Thus, we can consider the temperature ratio T_4/T_3 also as a Mach number similarity parameter.

In the combustion chamber, heat is added by burning fuel. Can we relate T_4/T_3 to the fuel mass flow W_F ? Let us try with the simplified energy balance which employs a mean value for the specific heat C_P within the combustion chamber:

$$W_F \eta FHV = C_P [(W_3 + W_F)T_4 - W_3 T_3] \quad (3.2-3)$$

Introducing the fuel/air ratio $far = W_F/W_3$ and rearranging this formula again results in an expression for the temperature ratio T_4/T_3 :

$$\frac{T_4}{T_3} = \frac{1 + \frac{far \eta FHV}{C_P T_3}}{1 + far} \quad (3.2-4)$$

Now we run into a problem: the temperature ratio T_4/T_3 is a function of the absolute value of T_3 . Employing an energy balance for the combustor is therefore incompatible with Mach number similarity.

However, there is a work-around for this problem. Remember that mechanical energy and heat are equivalent. If we consider the fuel mass flow as an energy stream and not as a mass flow, we can write—in analogy to corrected shaft power established in Eq. (3.1-9)—the following expressions for *reduced fuel flow*:

$$W_{F,red3} = \frac{W_F}{P_3 \sqrt{RT_3}} = \frac{P_2}{P_3} \sqrt{\frac{T_2}{T_3}} \frac{W_F}{P_2 \sqrt{RT_2}} \quad (3.2-5)$$

Both P_3/P_2 and T_3/T_2 are Mach number similarity parameters, thus fuel flow reduced to engine inlet conditions $W_{F,red2}$ is also a Mach number similarity parameter.

$$W_{F,red2} = \frac{W_F}{P_2 \sqrt{RT_2}} \propto W_{F,corr2} = \frac{W_F}{\delta_2 \sqrt{\frac{R}{R_{dry air}} \Theta_2}} \quad (3.2-6)$$

With this definition of corrected fuel flow, we assume that the heat supplied to the burner is proportional to the fuel mass flow. In reality, the heat released by the chemical reaction also depends on the absolute values of burner inlet temperature and pressure. Note also that differences in the fuel heating value FHV must be taken care of.

One important non-dimensional parameter is still missing: *reduced thrust*. Its derivation is easy: reduced thrust is the product of reduced flow and a term representing the Mach number of the jet:

$$F_{G,red} = \frac{W_9 V_{9eq}}{P_9} = \frac{W_9 \sqrt{RT_9}}{P_9} \frac{V_{9eq}}{\sqrt{RT_9}} \quad (3.2-7)$$

The equivalent jet velocity V_{9eq} is equal to specific thrust F_9/W_9 . In practical applications, we prefer reducing thrust to the engine inlet conditions P_2 and T_2 . This is no problem, as we can express F_G/P_2 as a combination of Mach number similarity parameters:

$$F_{G,red2} = \frac{F_G}{P_2} = \frac{W_2 \sqrt{RT_2}}{P_2} \frac{W_9 P_2}{W_2 P_9} \sqrt{\frac{T_9}{T_2}} \frac{V_{9id}}{\sqrt{RT_9}} \propto \frac{F_G}{\delta_2} \quad (3.2-8)$$

Reduced net thrust is the difference between $F_{G,red2}$ and reduced inlet momentum $F_{0,red2}$.

Combining corrected fuel flow with corrected thrust yields an expression for *corrected specific fuel consumption* SFC_{corr2} :

$$SFC_{corr2} = \frac{W_{F,corr2}}{F_{N,corr2}} = \frac{W_F}{\frac{F_N}{\delta_2} \sqrt{\frac{R}{R_{dry air}}} \Theta_2} = \frac{SFC}{\sqrt{\frac{R}{R_{dry air}}} \Theta_2} \quad (3.2-9)$$

All of the corrected parameters discussed are connected directly or indirectly with Mach numbers in the turbomachinery. This justifies calling them *Non-Dimensional Parameters* in spite of the fact that the numerical values are often not dimensionless.

Table 3.2-1 summarizes the most widely used parameter correction formulae, which are all of the following mathematical form:

$$Par_{corr} = \frac{Par}{(X\Theta)^a \delta^b} \quad (3.2-10)$$

Table 3.2-1 Parameter correction parameter overview

Parameter	Corrected	Humidity corrected	a Θ exponent	b δ exponent
Pressure	$P_{corr} = \frac{P}{\delta}$	$P_{corr} = \frac{P}{\delta}$	0	1
Temperature	$T_{corr} = \frac{T}{\Theta}$	$T_{corr} = \frac{T}{X\Theta}$	1	0
Spool speed	$N_{corr} = \frac{N}{\sqrt{\Theta}}$	$N_{corr} = \frac{N}{\sqrt{X\Theta}}$	0.5	0
Gas mass flow	$W_{corr} = \frac{W \sqrt{\Theta}}{\delta}$	$W_{corr} = \frac{W \sqrt{X\Theta}}{\delta}$	-0.5	1
Shaft power	$PW_{corr} = \frac{PW}{\sqrt{\Theta}\delta}$	$PW_{corr} = \frac{PW}{\sqrt{X\Theta}\delta}$	0.5	1
Fuel flow	$W_{F,corr} = \frac{W_F}{\sqrt{\Theta}\delta}$	$W_{F,corr} = \frac{W_F}{\sqrt{X\Theta}\delta}$	0.5	1
Thrust	$F_{corr} = \frac{F}{\delta}$	$F_{corr} = \frac{F}{\delta}$	0	1
SFC	$SFC_{corr} = \frac{SFC}{\sqrt{\Theta}}$	$SFC_{corr} = \frac{SFC}{\sqrt{X\Theta}}$		

In this expression Θ stands for the temperature ratio T/T_{ISA} and δ for the pressure ratio P/P_{ISA} with $T_{ISA} = 288.15\text{ K}$ and $P_{ISA} = 101.325\text{ kPa}$. In the humidity corrected version, X stands for the humidity correction term $R/R_{\text{dry air}}$ with $R_{\text{dry air}} = 287.04(\text{J/kg}\cdot\text{K})$.

3.2.1 Practical Correction to Standard Day Conditions

For the derivation of the non-dimensional parameters, we have made some simplifying assumptions. Many small effects result in discrepancies between pure theory and reality. First of all, the isentropic exponent is not constant. Its variation influences the structure of the flow field within the turbomachinery because the isentropic exponent is a similarity parameter in itself, see Ref. [1].

We can take into account the changes in the gas constant due to different absolute humidity of the incoming air by using the more rigorous formulations of the Mach number similarity parameters shown in the middle column of Table 3.2-1.

Another reason why the flow field may change is the Reynolds number, the ratio of inertia forces to viscous forces in a fluid moving over a surface, which affects the boundary layer, see Chap. 4). Reynolds number depends on pressure and temperature; its influence on the flow field depends on both the surface roughness and the magnitude of the Reynolds number itself.

Mechanical deformations due to stress and thermal expansion change the geometry of the engine. Especially variations in tip clearance can significantly change the flow field, efficiency and corrected flow.

In the combustion chamber, the chemical processes dominate and they are not a function of Mach number. Mixing and friction pressure losses are not affected by compressibility effects because the Mach numbers in the combustor are very low.

In the definition of the corrected fuel flow we have supposed that the amount of heat released is proportional to fuel flow. This is a crude description of the chemical process in the combustion chamber, especially for higher fuel/air ratios.

All these reasons make it impossible to keep the Mach numbers and flow angles in a gas turbine strictly constant everywhere while applying the parameter correction procedure. The pure theory does not yield satisfying results, however, there is a work-around for this problem also. If we calculate the Mach number similarity parameters with Θ and δ exponents slightly different to those listed in the last two columns of Table 3.2-1, then we get acceptable results. This simple empirical approach is very popular and is used frequently in engine maintenance shops for correcting the raw data from the test cell to ISA conditions.

3.2.2 How to Determine the Exponents

Evaluating the exponents from engine tests requires a big and consistent data base which rarely exists. Therefore, the exponents for δ and Θ are determined by running a thermodynamic model of the engine with constant corrected thrust or shaft power over a range of inlet temperatures and pressures.

Let us explain how the Θ exponent for the fuel flow correction is found. We start with the following:

$$\frac{W_F}{\Theta^a \delta^b} = \frac{W_{F,ISA}}{\Theta_{ISA}^a \delta_{ISA}^b} = W_{F,ISA} \quad (3.2-11)$$

This yields

$$\Theta^a = \frac{W_F}{W_{F,ISA} \delta^b} \quad (3.2-12)$$

The final formula for the fuel flow Θ exponent is

$$a_{WF} = \frac{\ln \left[\frac{W_F}{W_{F,ISA} \delta^b} \right]}{\ln(\Theta)} \quad (3.2-13)$$

How do we get rid of the unknown δ^b term? That is simple: do the calculation at sea level—then δ equals 1 and thus δ^b is also equal to 1. For calculating the δ exponent b_{WF} , change the altitude, but keep the engine inlet temperature constant:

$$b_{WF} = \frac{\ln \left[\frac{W_F}{W_{F,ISA} \Theta^{a_{WF}}} \right]}{\ln(\delta)} \quad (3.2-14)$$

The exponents for other parameters like mass flow, spool speed, thrust, shaft power etc. can be found analogously. Most of the exponents closely follow the theory, as for example, the Θ exponent for fan speed in Fig. 3.2-1. The figure also shows that Θ exponent for fuel flow behaves differently; it is well above the theoretical value of 0.5 and increases with fuel/air ratio. Why is that?

The x-axis values are proportional to the temperature difference in the combustor. Mach number similarity, however, requests constant T_4/T_3 . This inconsistency leads to the non-constant Θ exponent.

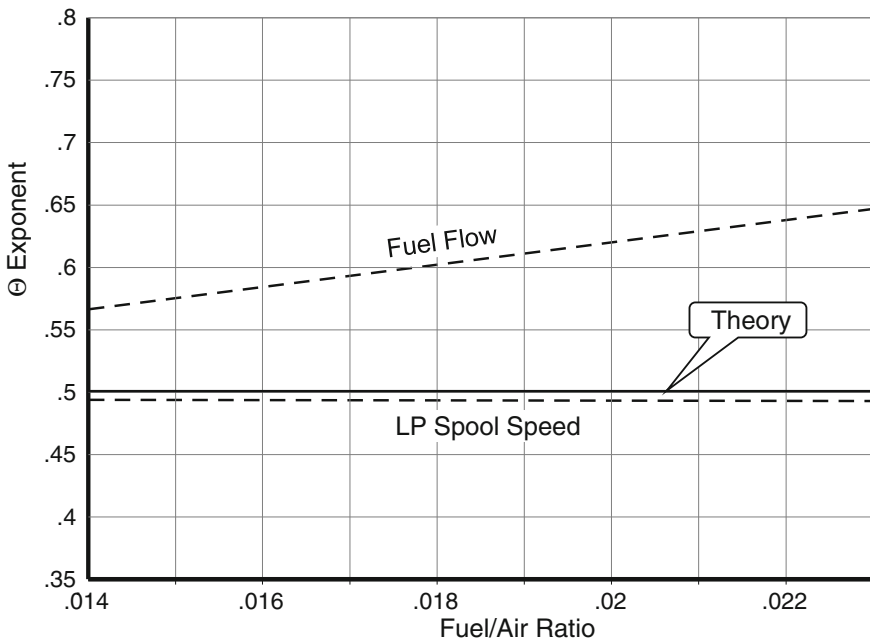


Fig. 3.2-1 Θ exponents for a commercial turbofan

3.2.3 Aircraft Engines with Afterburners

An afterburner (reheat system, augmenter) is a special sort of combustor. At full power, the system typically operates at approximately the same nozzle throat temperature T_8 —irrespective of the engine inlet temperature T_2 . Keeping the temperature ratio T_8/T_2 constant while correcting data from a test done on a cold day, for example, would lead to ridiculously high corrected T_8 value. Moreover, the afterburner efficiency is mainly a function of the fuel/air ratio, which is in turn a function of temperature difference, but not a function of temperature ratio. Thus, during the parameter correction with constant temperature ratio, the afterburner efficiency would not remain constant. Conclusion: it is not possible to use the modified exponent method for correcting thrust and fuel flow of aircraft engines with an afterburner.

3.2.4 Gas Turbines with Heat Exchanger

Test data from a gas turbine with a heat exchanger could be corrected to Standard Day conditions with the modified exponent method if there were not the variable turbine geometry. This device is required to keep the heat exchanger inlet temperature high at part-load and thus to maximize the amount of heat transferred to the combustor, which in turn results in low SFC. The variability of the geometry in this case prevents the successful application of the parameter correction procedure based on Mach number similarity.

Note also that the heat exchanger is a component whose effectiveness is not dependent on Mach number but on Nusselt number and Reynolds number. Therefore, the data correction procedure based on Mach number similarity is not valid.

3.3 References

1. Roberts, S.K.: Effects of Fluid Properties on the Aerodynamic Performance of Turbomachinery for Semi-Closed Cycle Gas Turbine Engines Using O₂/CO₂ Combustion. Master Thesis 2001 Ottawa-Carleton Institute for Mechanical and Aerospace Engineering (2001)
2. Lieblein, S.: Experimental flow in two-dimensional cascades chapter VI in aerodynamic design of axial flow compressors NASA SP-36 (1965)
3. Volponi A.J.: Gas Turbine Parameter Corrections. ASME Paper 98-GT-947 (1998)
4. Kurzke, J.: Model Based Gas Turbine Parameter Corrections ASME GT2003-38234 (2003)

Chapter 4

Reynolds Number Corrections



Compressor and turbine maps describe the performance of turbomachinery with dimensionless parameters, which represent Mach numbers. This means that the compressibility of the working fluid is taken into account. The influence of varying Reynolds number—the ratio of inertia and friction forces—on turbomachinery is a secondary effect. Reynolds number plays no role in simulations of gas turbines used for power generation, since the inlet pressure and temperature do not deviate much from the standard day conditions.

In the flight envelope of aircraft engines, the Reynolds number changes significantly. Figure 4.1-1 shows the engine inlet Reynolds Number Index RNI—a relative Reynolds number—in the flight envelope of a fighter engine. RNI decreases from 1.4 along the right envelope boundary down to 0.25 in the upper left-hand corner.

4.1 Reynolds Number Index

The Reynolds number for axial turbomachinery is usually defined as

$$Re = \frac{LV}{v} = \frac{\rho LV}{\mu} \quad (4.1-1)$$

In this definition L is the blade chord length, V the velocity relative to the blade, v the kinematic viscosity and μ the dynamic viscosity. Further details on kinematic viscosity and dynamic viscosity and how to derive their values for air and combustion products may be found in Ref. [1].

In radial compressors the mean flow velocity is approximately half of the tip speed U_2 and the hydraulic diameter is twice the rotor exit tip width b_2 . Thus, the Reynolds number of a centrifugal compressor is

$$Re = \frac{U_2 b_2}{v} = \frac{U_2 b_2 \rho}{\mu} \quad (4.1-2)$$

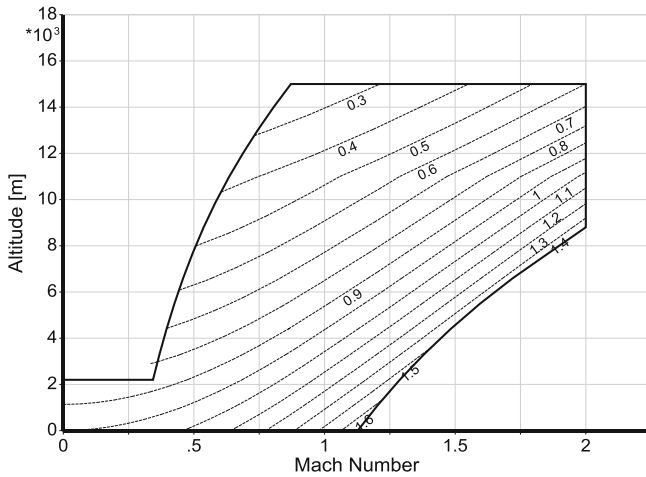


Fig. 4.1-1 Reynolds number index in the flight envelope

In performance simulations, instead of the true Reynolds number, it is convenient to use the *Reynolds Number Index RNI*, which is the ratio of the actual Reynolds number and a reference Reynolds number for the same Mach number:

$$RNI = \frac{\rho LV}{\rho_{ref} L_{ref} V_{ref}} \frac{\mu_{ref}}{\mu} \quad (4.1-3)$$

There are no length changes between actual and reference conditions, therefore $L = L_{ref}$. Inserting the expression $P_s/(R T_s)$ for the density ρ , yields

$$RNI = \frac{P_s}{RT_s} \frac{R_{ref} T_{s,ref}}{P_{s,ref}} \frac{V}{V_{ref}} \frac{\mu_{ref}}{\mu} \quad (4.1-4)$$

$$RNI = \frac{P_s}{P_{s,ref}} \frac{V}{\sqrt{\gamma RT_s}} \frac{\sqrt{\gamma}}{\sqrt{RT_s}} \frac{\sqrt{\gamma_{ref} R_{ref} T_{s,ref}}}{\sqrt{V_{ref}}} \frac{\sqrt{R_{ref} T_{s,ref}}}{\sqrt{\gamma_{ref}}} \frac{\mu_{ref}}{\mu} \quad (4.1-5)$$

The *Reynolds Number Index* compares conditions at the same Mach number, therefore:

$$M = \frac{V}{\sqrt{\gamma RT_s}} = \frac{V_{ref}}{\sqrt{\gamma_{ref} R_{ref} T_{s,ref}}} \quad (4.1-6)$$

This leads to

$$RNI = \frac{P_s}{P_{s,ref}} \sqrt{\frac{T_{s,ref}}{T_s}} \sqrt{\frac{R_{ref}}{R} \frac{\gamma}{\gamma_{ref}} \frac{\mu_{ref}}{\mu}} \quad (4.1-7)$$

The ratios of static and total pressures and temperatures are the same for actual and reference conditions, since the Mach number is the same. Ignoring changes in the isentropic exponent, the ratio of the actual to reference Reynolds number becomes

$$RNI = \frac{P}{P_{ref}} \sqrt{\frac{R_{ref} T_{ref}}{RT} \frac{\mu_{ref}}{\mu}} \quad (4.1-8)$$

Reference conditions are $P_{ref} = 101.325 \text{ kPa}$, $T_{ref} = 288.15 \text{ K}$ and $R_{ref} = 287 \text{ J/(kg*K)}$, hence at ISA sea level static conditions, RNI equals 1.

4.2 Turbomachinery Loss Correlations with Reynolds Number

Let us begin with an extremely simplified model of turbomachinery; we consider it as an arrangement of pipes in which the blade chord is the characteristic dimension. The pressure losses in pipes are illustrated in the so-called *Moody Chart* which describes them as a function of Reynolds number and relative roughness.

Figure 4.2-1 shows a snippet from the Moody chart with three bold straight lines added. Let us concentrate first on the middle line which has a slope of $n = -0.2$.

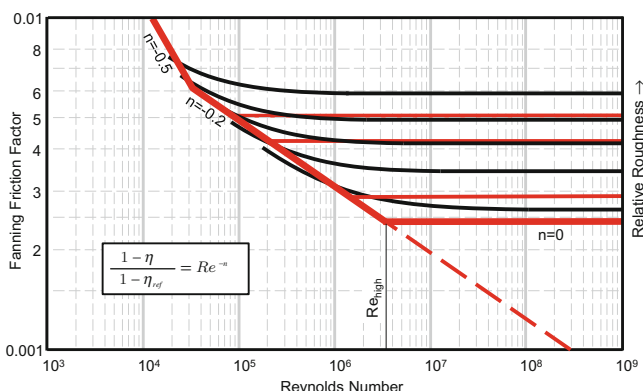


Fig. 4.2-1 Moody chart

This number is also found in Ref. [2], a popular correlation between turbomachinery efficiency and Reynolds number:

$$\frac{1 - \eta}{1 - \eta_{ref}} = \left(\frac{Re_{ref}}{Re} \right)^{-0.2} \quad (4.2-1)$$

The Moody Chart shows that turbomachinery losses vary with Reynolds number similarly to pressure losses in a pipe. We will use this pipe flow analogy to describe, in a simplified way, the Reynolds number effects on the performance of turbomachinery.

There are limits for the validity of Eq. (4.2-1). At a given value of relative roughness, there is a Reynolds number above which the losses remain constant because the boundary layer is turbulent and attached and the blade surfaces are hydrodynamically rough. Since we don't know any better, we estimate this Reynolds number based on the relative roughness values in the Moody chart. For a given relative roughness, the horizontal line marked with $n = 0$ defines the upper critical Reynolds number limit for which Eq. (4.2-1) is valid.

The bold line on the left is much steeper than the middle line, its slope is $n = -0.5$. This is because, below a critical Reynolds number of around 5×10^4 , the losses increase steeply due to the onset of laminar separation.

4.2.1 Compressor

The slope of $n = -0.5$ at subcritical Reynolds number is reported in many references. An example taken from Ref. [3] is shown in Fig. 4.2-2. Many other references report the same slope, the main difference between the various publications is the magnitude of the critical Reynolds number.

Note that Figs. 4.2-1 and 4.2-2 differ in the title and the ordinate. In the Moody diagram the y-axis title is *Fanning Friction Factor* while in Fig. 4.2-2 it is

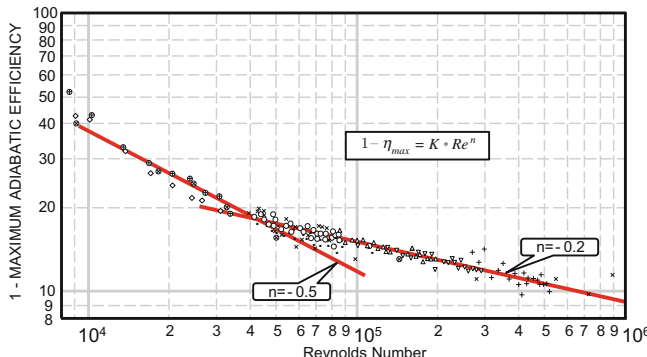


Fig. 4.2-2 Variation of peak stage efficiency (Fig. 22 from Ref. [3])

1—Maximum Adiabatic Efficiency. Both scales are logarithmic, only the numbers are different. The ratio between the Fanning Friction Factor and 1-efficiency, the efficiency loss, is constant. In this example the efficiency losses increase with Reynolds number exactly as the friction factor of a pipe increases.

4.2.2 *Turbine*

Reynolds number primarily affects the low pressure turbine of aircraft engines. The magnitude of the effects on efficiency and flow capacity is significant, even for the large engines of commercial airlines which cruise at 35,000 ft. It is even stronger for the much smaller engines of business jets, which not only have lower overall pressure ratios but also may have cruising altitudes above 50,000 ft.

The most important loss mechanisms with respect to Reynolds number are the profile losses. At lower Reynolds numbers, it becomes increasingly difficult to avoid flow separation on the suction side. The turbine suffers a loss in both efficiency and flow capacity due to thicker boundary layers and higher viscous effects.

Reference [4] describes the rig test of a five-stage low pressure turbine designed for a conventional turbofan cruising at an altitude of 35,000 ft. The reference Reynolds number is 210,000, based on the exit velocity and the chord length of the 1st vane. Within the Reynolds number range from 270,000 to 120,000, efficiency decreased by a factor of 0.987 (Fig. 8 in Ref. [4]). That means that the losses increased by 17.6% if we assume $\eta_{ref} = 0.93$, for example.

$$\frac{1 - 0.987 * 0.93}{1 - 0.93} = 1.176 \approx \left(\frac{120,000}{270,000} \right)^{-0.2} \quad (4.2-2)$$

17.6% loss increase corresponds to the ratio of the Reynolds number to the power of -0.2 . Other assumptions for η_{ref} can be reconciled with a slightly different value for the exponent.

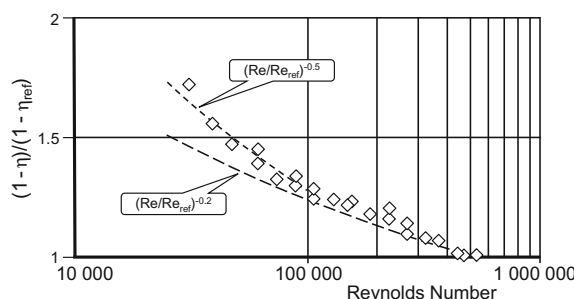


Fig. 4.2-3 Reynolds number effect on low pressure turbine efficiency (adapted Fig. 14 in Ref. [5])

Similar loss increase data are reported in Ref. [5] from a rig test on a three-stage turbine. Reynolds number is based on exit velocity and mean true chord. The Reynolds number range is much wider in these tests than in Ref. [4] and extends into the laminar flow region.

For Reynolds numbers higher than 100,000, both tests agree with the finding that the losses rise proportional to Reynolds number ratio to the power of -0.2 . An exponent of -0.5 describes the loss increase well for Reynolds numbers lower than 100,000 (Fig. 4.2-3).

For both reports, the test results for corrected flow also agree essentially. From Figs. 8 and 9 in Ref. [4], we can derive the ratio between corrected flow and efficiency changes as $5/6.5$, while the authors of Ref. [5] found that ratio to be $5/6$.

In gas generator turbines, the Reynolds number is higher by a factor of two to three than in low pressure turbines. Consequently, the efficiency and corrected flow changes due to Reynolds number effects are inherently much smaller than in low pressure turbines. Moreover, the cooling air injection holes of film-cooled blades make the blade surface rough. Roughness not only increases losses, but also makes efficiency less sensitive to Reynolds number. Therefore, Reynolds number corrections for cooled gas generator turbines are usually not applicable.

4.2.3 *Some Additional Remarks*

The slopes $n = -0.2$ and $n = -0.5$ which we have used to justify the pipe flow analogy are debatable figures. Reference [2] reviews works published before 1967 on Reynolds number effects in axial compressors. A general conclusion from tests is that the value of the exponent can vary significantly from one compressor to another. So, it is not astonishing that Ref. [6] (published 37 years after Ref. [2]) recommends the use of n values between -0.05 and -0.25 , while Ref. [7] endorses the range from -0.1 to -0.14 for compressors and -0.18 for turbines. There are several potential reasons why the values of the exponent may differ so much:

- The data result from tests in the transitional region of the Moody chart where the slope changes gradually from -0.2 to zero.
- Equation (4.2-2) implies that all the losses are dependent on friction. This is not necessarily true. In fact, losses related to high Mach number operation and the presence of shock systems are largely insensitive to Reynolds number.
- Most authors use polytropic efficiency in Eq. (4.2-2), some use isentropic efficiency.

4.3 Applying the Pipe Flow Analogy in Performance Programs

Applying the pipe flow analogy within performance programs is easy and needs only two inputs: the true Reynolds number at the cycle design point and the surface roughness of the blades and vanes. For calculating the Reynolds number, we need a characteristic length L and a representative velocity. Approximate numbers for both of these are easy to obtain from the geometry at the turbomachinery entry. More accurate numbers are among the output of any preliminary engine design calculations.

At the cycle design point we know both the true Reynolds number and the Reynolds Number Index RNI. The ratio between the two is a constant which allows us to calculate RNI for any point on the x-axis of the Moody chart.

The surface roughness of new metallic blades is of the order of 1.5 μm . Reference [6] lists the following typical roughness values:

Precision cast surface	2–3 μm
Typical polished forging	0.75–1 μm
Highly polished	0.25–0.5 μm

The effective surface roughness of cooled turbine blades is certainly much higher. Each film cooling row interrupts the boundary layer and the similarity with the boundary layer in a smooth pipe is also questionable.

Dividing the absolute roughness value by the characteristic length L, yields the relative roughness which we need for reading the Moody chart. Point A in Fig. 4.3-1 is the intersection of the lines for smooth flow and the horizontal line for the relative roughness. The Reynolds number index of point A is RNI_{high} .

Point B marks the critical Reynolds number 0.5×10^5 , below which the losses increase steeply due to the onset of laminar separation. Point C is at Reynolds number 0.25×10^5 which, together with point B, describes the slope in the laminar region. The Reynolds number indices for these two points are RNI_{low} and $\text{RNI}_{\text{lamin}}$. The slopes of the smooth and the laminar regions are $n = -0.2$ and $n = -0.5$ respectively.

In the performance program, the turbomachinery maps are scaled in such a way that no Reynolds correction is applied if RNI is greater than RNI at point A. In other words, the loss correction factor $f_{1-\eta}$ is 1.0 if $\text{RNI}_{\text{design}} > \text{RNI}_{\text{high}}$. The efficiency correction factors at points B and C are:

$$f_{1-\eta,\text{low}} = \frac{\text{loss factor @ point B}}{\text{loss factor @ point A}} \quad (4.3-1)$$

$$f_{1-\eta,\text{lamin}} = \frac{\text{loss factor @ point C}}{\text{loss factor @ point A}} \quad (4.3-2)$$

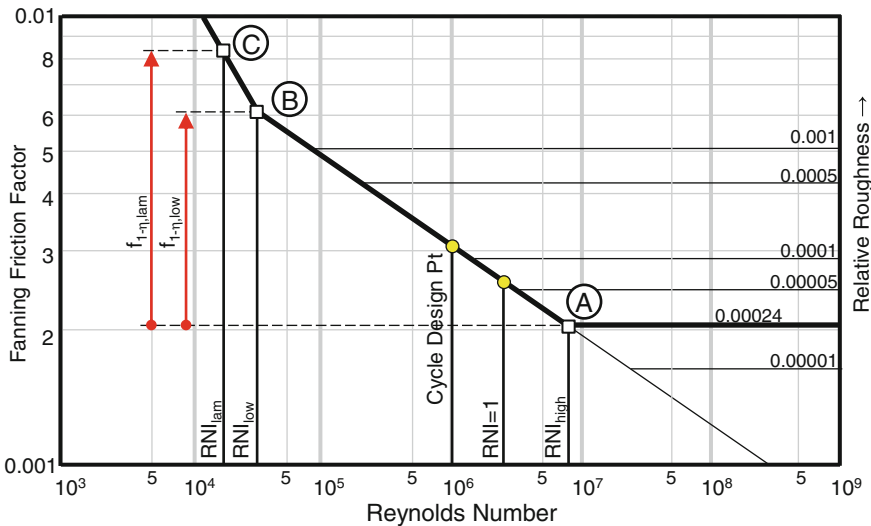


Fig. 4.3-1 Reynolds correction factors

During off-design calculations the efficiency correction factor $f_{1-\eta}$ is interpolated logarithmically at any RNI value. The efficiency read from the map is corrected according to

$$\eta = \eta_{map} (1 - f_{1-\eta}(1 - \eta)) \quad (4.3-3)$$

4.4 Variations of the Pipe Flow Analogy

The advantage of the pipe flow analogy is that it requires very few input data for a Reynolds correction.

As already mentioned, the exponent n in the efficiency correlation with Reynolds number (Eq. 4.2-1) can deviate from the value $n = -0.2$, which is part of the pipe flow analogy. Reference [2] reports that the sensitivity decreases with an increasing number of stages. Using numbers for n between -0.2 and -0.1 can be interpreted such that only a part of the losses are friction losses which vary with Reynolds number. If that is true, then this can be taken into account in the pipe flow analogy in such a way that the factors defined in Eqs. (4.3-1) and (4.3-2) are calculated as

$$f_{1-\eta,low} = 1 + \frac{a}{100} * \left(\frac{\text{friction factor @ point B}}{\text{friction factor @ point A}} - 1 \right) \quad (4.4-1)$$

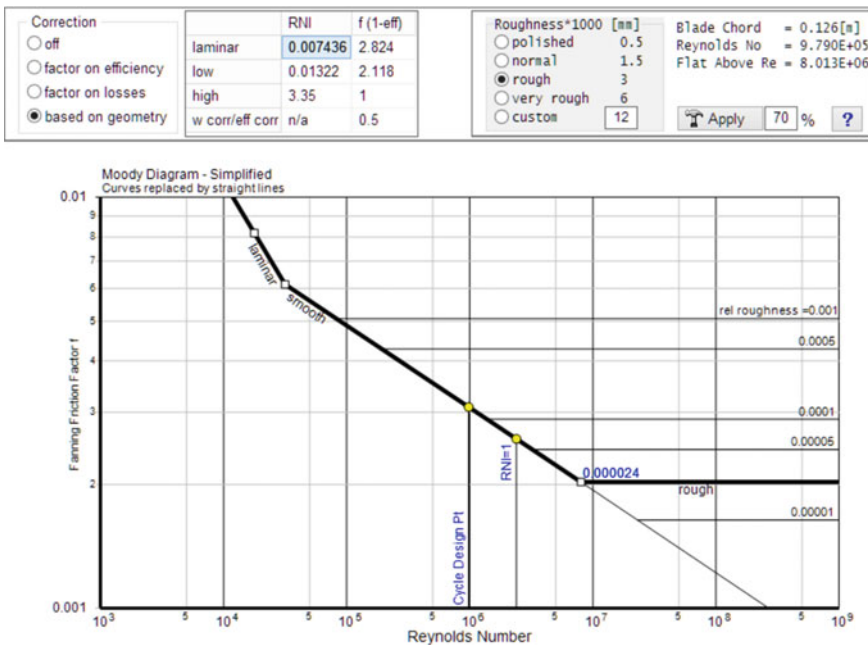


Fig. 4.3-2 Reynolds correction options in GasTurb

$$f_{1-\eta, \text{lam}} = 1 + \frac{a}{100} * \left(\frac{\text{friction factor @ point C}}{\text{friction factor @ point A}} - 1 \right) \quad (4.4-2)$$

In these equations, “a” stands for the percentage of the total losses which is due to friction; $a = 70\%$ seems to be a reasonable value.

If the results of the pipe flow analogy are presented in an editable table (in the top left corner of Fig. 4.3-2, for example), then it is easy to adapt the numbers for the RNI breakpoints as well as the efficiency factors, as required if more accurate information is available.

Most people have a better feel for efficiency numbers than for factors on turbomachinery losses. To help them, we can convert the factor $f_{1-\eta}$ to a factor for efficiency η itself. From a scientific point of view this is not quite correct, but much easier to recognize.

4.5 Mass Flow Correction

Reference [6] connects the Reynolds number correction of flow with the efficiency correction. For compressors, the flow correction factor is derived in a complex way from the efficiency loss and pressure ratio. The turbine flow correction is simply a fraction of the efficiency correction. Certainly, no significant error is introduced if

we apply the same simple method to both compressors and turbines; according to the turbine formula in Ref. [8], the ratio f_w/f_η is between 0.4 and 0.6. For example, if the efficiency is corrected using the factor 0.96, then the mass flow will be corrected by the factor 0.98 if f_w/f_η is input as 0.5.

4.6 References

1. Viscosity: <https://en.wikipedia.org/wiki/Viscosity>, Wikipedia 2017
2. Wassell, A.B.: Reynolds number effects in axial compressors. ASME Paper 67-WA/GT-2. Journal of Engineering for Power (1967)
3. Carter, A.D.S., Moss, C.E., Green, G.R., Annear, G.G.: The effect of reynolds number on the performance of a single-stage compressor. ARC Technical Report R. & M. No. 3184 (1960)
4. Gier, J., Hübner, N.: Design and analysis of a high stage loading five-stage LP turbine rig employing improved transition modeling. ASME GT2005-68971 (2005)
5. Hura, H.S., Joseph, J., Halstead, D.E.: Reynolds number effects in a low pressure turbine. ASME GT2012-68501 (2012)
6. Walsh, P.P., Fletcher, P.: Gas Turbine Performance, 2nd edn. Blackwell Science Ltd., (2004)
7. Grieb, H.: Projektierung von Flugtriebwerken. Birkhäuser Verlag (2004)
8. ICAAMC Working Group: Influence of the reynolds number on the performance of centrifugal compressors. ASME Paper 87-GT-10 (1987)

Chapter 5

Efficiency of a Cooled Turbine



In the aero-engine industry there are many different definitions of turbine efficiency and many methods of bookkeeping are used to account for work contributions and total pressure losses in turbines. Without knowing the precise definition of efficiency, any value quoted is ambiguous and of little value. This is especially true for cooled turbines where, for the same machine (identical geometry, temperatures, pressures, primary & secondary flows) estimates of efficiency might vary by several percentage points. Cooling air is used in modern engines to ensure the life of the turbine components in an extremely hostile environment but it is used very sparingly because it is an expensive commodity. To achieve the pressure needed for its release from holes in the surface of an HPT blade into the adjacent high-pressure primary flow, it must be taken from compressor delivery, where significant compressor work will have been done on it, using energy supplied by the turbine. So cooling air imposes a high penalty on the engine cycle, reflected ultimately in fuel burn. Additionally, power is expended to deliver coolant to a moving blade, coolant pressure is dissipated within the cooling passages as it picks up heat and is delivered to the blade surface and—once it is ejected into the main flow—there are further pressure losses due to mixing and possibly due to local disturbances to the boundary layer. The reduction in pressure of the primary flow through the burner is accepted because not only does it ensure high burner efficiency but it also means that compressor delivery pressure is sufficient to overcome the mainstream total pressure in the turbine inlet guide vane, which enables the system to work. The “upside” is that, generally, some of the ejected cooling air elements have tangential momentum which complements the turbine work.

Having sketched some of the background, it can be seen that calculating and combining the secondary air flow properties with those of the primary flow in order to account for the detailed effects of cooling on turbine efficiency is supported by an extensive research program at most OEMs. So it is not surprising that they are reluctant to reveal details of their cooled-efficiency estimates! Differences in efficiency also occur for non-proprietary reasons, often based on “legacy” codes or traditional ways of doing things. Regardless of the reasons, it is important to

understand the various definitions because today's new engine projects nearly always involve a consortium of two or more companies. There is a high probability of misunderstanding if the partners do not adhere to a unique system with a clearly-defined control volume and associated nomenclature. Turbine designers and performance specialists should not quote numbers for the efficiency of a cooled turbine without clearly defining the methodology and control volume on which it is based. Under such circumstances, the partners may agree to a generic definition of cooled efficiency, to which both sets of results can be converted for comparison.

Corporate partners in a collaborative engine development project should agree on a unique and unambiguous definition of turbine efficiency. It could be argued that it is not important which definition is used, as long as ambiguity is eliminated, however, when picking an efficiency definition, certain practical considerations should be taken into account. When a company switches to a definition not used in previous projects it can be difficult to translate past experience to current design goals. It is also important that the selected efficiency definition is compatible with the overall engine simulation. Exchange rates for turbine efficiency with overall engine parameters like thrust and specific fuel consumption must form reasonable guidelines for the engine development process.

Let us first ask what we mean by the efficiency? It is generally accepted that the efficiency of any machine is a number which describes its technical quality. For a turbine we define the efficiency as the ratio of delivered shaft power PW_{SD} to ideal shaft power $PW_{SD,id}$ —that which the turbine would deliver if there were no losses.

This generic definition is ambiguous since the terms PW_{SD} and $PW_{SD,id}$ can each mean different things. In the delivered shaft power, the disk windage and the bearing losses may or may not be included, and the ideal shaft power $PW_{SD,id}$ may or may not account for the work potential of the cooling air. It is important that we use a clearly defined control volume to identify the gas mass flows that contribute to the power generation. In the performance calculation, the main gas flow enters the control volume at the turbine entry station and leaves it at the turbine exit station. Cooling and sealing air enters the control volume from additional clearly specified stations on the inner and outer walls.

Let us begin with the simplest case, an uncooled turbine. The control volume has only one entry and one exit for the gas. The shaft power delivered is equal to the product of gas mass flow and the change in its total enthalpy. We do not consider heat transfer and define the isentropic turbine efficiency as the ratio of the effective specific enthalpy difference ΔH to the isentropic enthalpy difference ΔH_{is} .

$$\eta_{is} = \frac{\Delta H}{\Delta H_{is}} = \frac{\frac{\gamma}{\gamma-1} R(T_{in} - T_{ex})}{\frac{\gamma}{\gamma-1} RT_{in} \left[1 - \left(\frac{P_{ex}}{P_{in}} \right)^{\frac{\gamma-1}{\gamma}} \right]} \quad (5.1-1)$$

This equation seems to be unambiguous—but it is not. For example, we can employ either a constant value ($\gamma = 1.3$, for example) or the mean value between the inlet and the exit of the turbine ($\gamma_{in} + \gamma_{ex}/2$) for the isentropic exponent of the

gas. The equation is suitable for spreadsheets but is not used in any professional cycle program, where the entropy function is used for modeling the temperature dependency of the gas properties to correlate pressure ratio with isentropic specific work ΔH_{is} . A more sophisticated calculation would also address the effects of chemical reactions that happen downstream of a combustion chamber. So we can immediately quote three different values for efficiency of an uncooled turbine, depending on the gas model we employ.

Modeling a cooled turbine rapidly creates additional problems. Cooling and sealing flows now enter the control volume and mix with the main gas stream. There are two basically different methodologies for defining the efficiency: either we go into the details of the expansion process or we deal with the turbine as a sort of “black box”. Let us begin with the most popular “detailed” approach and explain it, starting with a cooled single stage turbine.

5.1 Single Stage Turbine

5.1.1 *Simulation Principle*

What are the turbine inlet conditions for the performance calculation? You may say: that's simple, we can use the conditions at burner exit station 4 in Eq. (5.1-1) and T_4 is the turbine inlet temperature. However, that is not correct.

Let's look at Fig. 5.1-1, which shows the cooling air flows in a burner and the turbine stator. The latter is also dubbed Nozzle Guide Vane (NGV) because it imparts swirl and accelerates the gas as in any nozzle. There are many cooling air streams in the combustor; they cool the flame tube and mix with the combustion gases, increasing its mass flow and decreasing its temperature. Cooling the NGV's reduces the gas temperature even further and adds to the mass flow. The turbine rotor inlet temperature RIT is significantly lower than the burner outlet temperature. Within the cycle calculation, it is common practice to re-name RIT as T_{41} .

We calculate the enthalpy $h(T_{41})$ from the first law of thermodynamics, assuming that the NGV cooling air W_A has the compressor exit temperature T_3 :

$$h(T_{41}) = \frac{W_4 h(T_4) + W_A h(T_3)}{W_4 + W_A} \quad (5.1-1)$$

No turbine work is done in the NGV and work extraction from the gas begins at station 41. The temperature difference between T_4 and T_{41} is irrelevant for the shaft power extraction process, so why not define station 41 as the turbine entry station? The reason we can't do this is we don't know the corresponding pressure, P_{41} .

Now let us define the region between stations 4 and 45 in Fig. 5.1-2 as the axial extent of our control volume. The radial limits are formed by the annulus walls at hub and tip, through which secondary air flows for cooling and sealing enter.

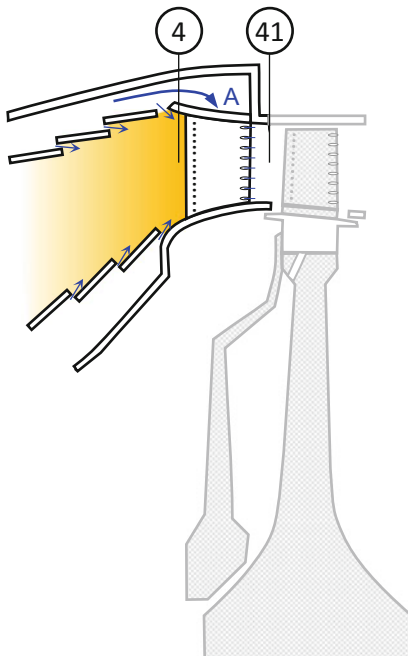


Fig. 5.1-1 Burner exit station 4 and rotor inlet station 41

To determine efficiency, we must decide how much each of the secondary flows contributes to the generation of shaft power, which is simply the product of mass flow and its change in enthalpy. With our way to calculate T_{41} already implicitly decided, we know that the NGV cooling air stream A in Fig. 5.1-2 will do work. It is *non-chargeable* cooling air in our book-keeping system. What about the other secondary flows in Fig. 5.1-2; are they doing work or not?

The NGV platform cooling air W_c and the disk rim sealing air W_d do not have much momentum for generating work. We ignore them when calculating T_{41} ; computationally, they bypass the work extraction process and join the main stream after the turbine rotor. Nor can the rotor cooling air W_D and the liner cooling air W_a do work in the turbine; they are *chargeable* and join the main gas stream downstream of the rotor in the computation.

Figure 5.1-3 represents the thermodynamic expansion process in an enthalpy-entropy diagram. Between stations 4 and 41, mixing of NGV cooling air with the main stream occurs. The work transfer occurs from station 41 to an imaginary station 42. Mixing of all the non-working secondary flows—the *chargeable* cooling air—with the rotor exit mass flow then follows. This last step yields the properties in the turbine outlet station, which is station 45 for single spool gas generators.

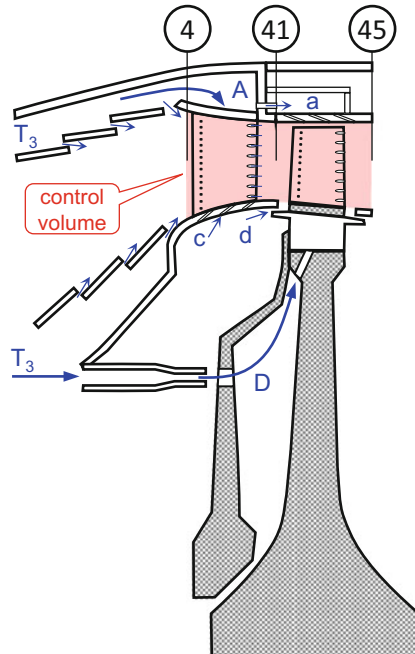


Fig. 5.1-2 Secondary air flows in a single stage turbine

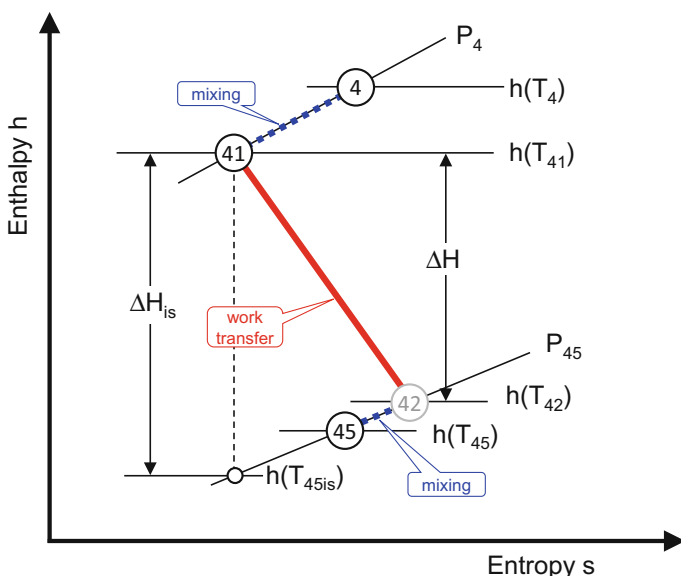


Fig. 5.1-3 Single stage turbine process in the enthalpy-entropy diagram

The actual expansion process in the rotor is the same as that of an uncooled turbine and Eq. (5.1-1) can be re-written as:

$$\eta_{is} = \frac{\Delta H}{\Delta H_{is}} = \frac{\frac{\gamma}{\gamma-1} R(T_{41} - T_{42})}{\frac{\gamma}{\gamma-1} RT_{41} \left[1 - \left(\frac{P_{45}}{P_4} \right)^{\frac{\gamma-1}{\gamma}} \right]} \quad (5.1-2)$$

The power created within our control volume must be greater than the net power required at the shaft because we need some additional power to accelerate the rotor cooling air W_D to the blade velocity U . This corresponds to an enthalpy increase of the cooling air as follows:

$$h(T_D) = h(T_3) + \frac{U^2}{2} \quad (5.1-3)$$

Frequently, the power needed for pumping the rotor cooling air and the resulting change in its enthalpy are both ignored, assuming that the effects more or less cancel each other. However, it is incorrect to account for pumping power while neglecting the corresponding enthalpy increase.

5.1.2 About NGV Cooling Air

Thermodynamically, NGV cooling air behaves like air in the dilution zone of the combustion chamber.

- The mass flow split between burner cooling air and dilution air is irrelevant for the cycle calculation if the resulting burner exit temperature T_4 is the same.
- The mass flow split between dilution air and NGV cooling air is irrelevant for the cycle calculation if the NGV exit temperature T_{41} is the same.

Euler's equation describes the work transfer in an axial turbine:

$$\Delta H = U(V_{U42} - V_{U41}) \quad (5.1-4)$$

The NGV accelerates and turns the flow so that at its exit the vector of the absolute velocity V_{41} has a circumferential component V_{U41} . This process does not generate any turbine work because the circumferential speed U of the NGV is zero. So, the work transfer begins only just in the turbine rotor where the gas temperature is T_{41} . What happened upstream of station 41 does not matter for the work transfer. For constant T_{41} , changing the amount of NGV cooling air cannot have any influence on the power output of the turbine and neither turbine exit temperature nor pressure are affected.

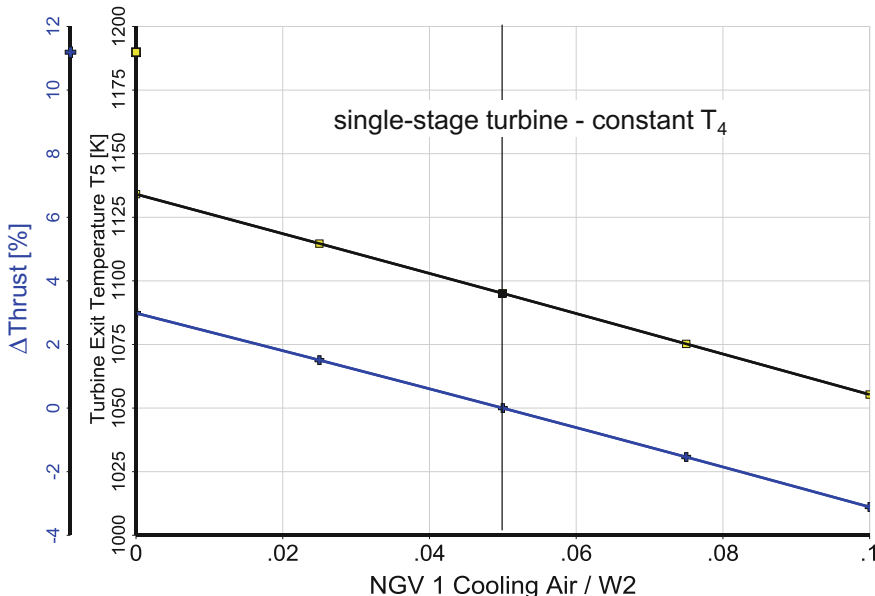


Fig. 5.1-4 Turbojet, single-stage turbine, constant T_4

Be careful with cycle studies in which the amount of NGV cooling air is variable. Increasing NGV cooling air while T_4 remains constant reduces T_{41} . This way you relieve the mechanical design tasks of the NGV and the turbine rotor simultaneously. The turbine exit temperature decreases due to the lower T_{41} and this finally leads to a loss in thrust, see Fig. 5.1-4.

If the design problem is limited to the NGV, then the cycle study must be done with constant T_{41} . Such a study yields a very different result. Neither thrust nor T_5 change while the amount of NGV cooling air varies! This result is consistent with the frequently adopted hypothesis which says that NGV cooling air has no negative influence on the turbine work.

5.1.3 Exchange Rates

How do the various elements of this turbine model affect the results of performance simulation? Let us examine that by means of a cycle design calculation with constant T_{41} (Fig. 5.1-5). Depending on where it is applied, that same numerical difference of 0.02 has very different consequences, namely.

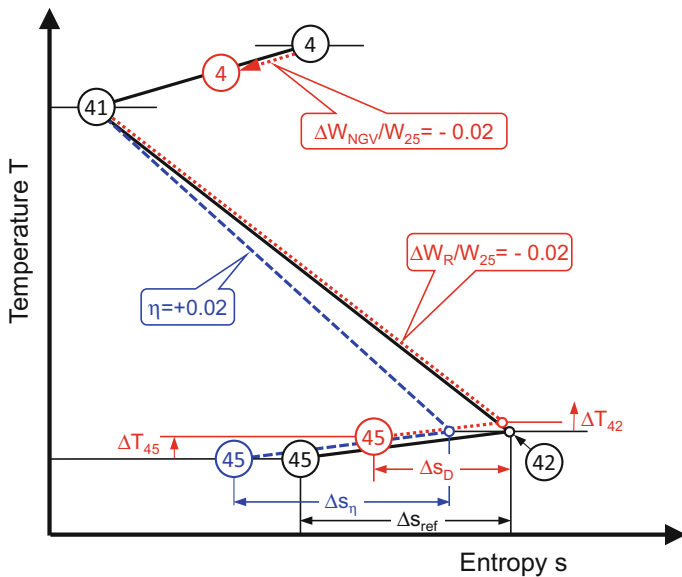


Fig. 5.1-5 Effects of efficiency and cooling air on stage performance (constant shaft power)

- ΔW_{NGV} cooling air has no effect on P_{45} and T_{45}
- ΔW_R cooling air influences both P_{45} and T_{45} . The reduction of 0.02 in rotor cooling air (red dashed lines) causes both temperature and pressure to be higher at exit. This is because the working gas flow rate increases by 2%.
- $\Delta \eta$ efficiency affects only turbine exit pressure P_{45} . An improvement of 0.02 in turbine efficiency (blue dashed lines) causes the turbine exit pressure P_{45} to increase, while the temperatures T_{42} and T_{45} remain unchanged.

The cycle calculation connects the changes in P_{45} and T_{45} with changes in thrust and shows that a 2% reduction in rotor cooling air increases the thrust twice as much as a 2% increase in efficiency.

5.2 Two-Stage Turbine

Figure 5.2-1 shows the control volume for a cooled two-stage turbine with its many secondary air streams. We can apply the same bookkeeping philosophy as before and model the two-stage cooled turbine stage by stage. The secondary air streams join the main gas flow at the appropriate stations. The NGV cooling air is added

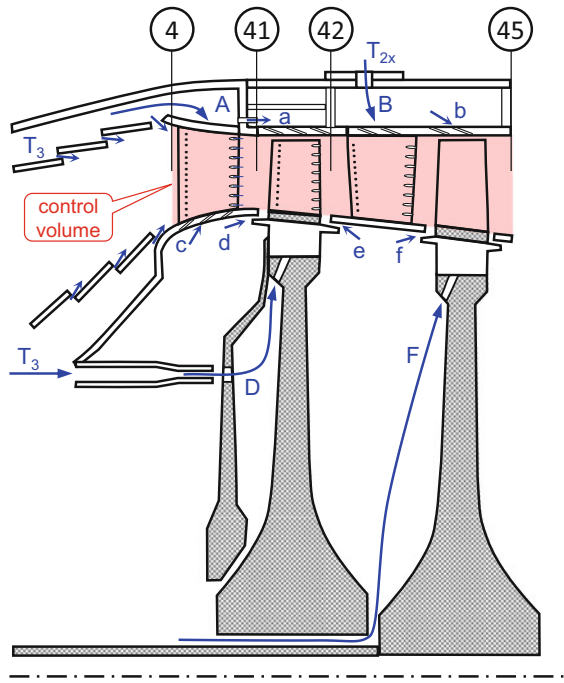


Fig. 5.2-1 Schematic of a cooled two-stage turbine

upstream of the rotor 1, and the rotor 1 cooling air and the other chargeable flows of stage 1 mix with the main stream between stations 415 and 42 (see Figs. 5.2-1 and 5.2-2). Addition of the stator 2 cooling air yields the inlet mass flow W_{421} and temperature T_{421} to rotor 2. The remaining secondary flows join the mainstream at rotor 2 exit, mixing out at station 45.

We could study the effects of cooling air with this model in some detail; however, this would come at a price. We would need to know the individual efficiencies of the two stages as well as the work split between the two rotors. Furthermore, we would need two turbine maps for off-design simulations, one for each stage. Moreover, the changing swirl angle downstream of rotor 1 would affect the map of the second stage, so rigorous modeling would require several maps for the second stage, each corresponding to a different inlet swirl angle. A reasonable conclusion is that modeling a cooled multi-stage turbine stage by stage within performance simulation programs is not very practical!

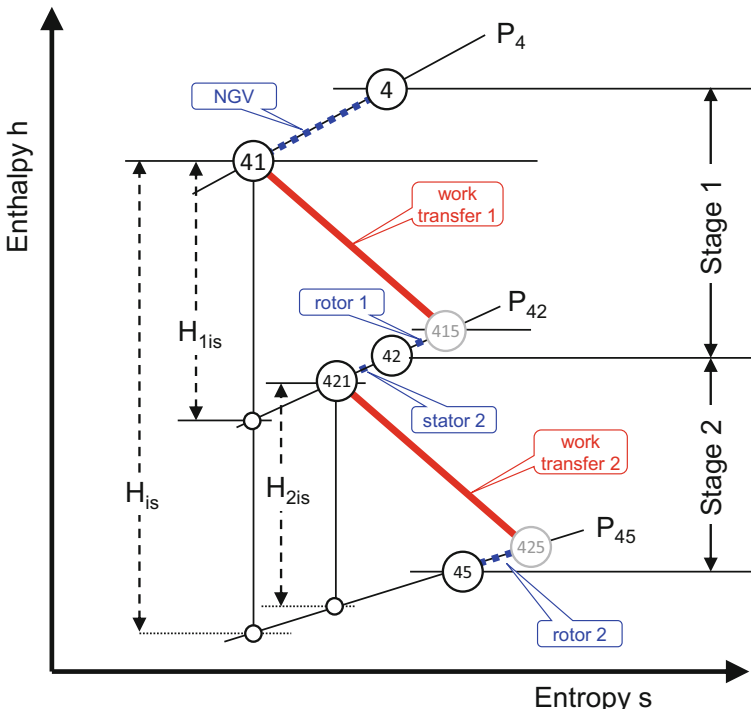


Fig. 5.2.2 Two stage turbine process in the enthalpy entropy diagram

5.3 Equivalent Single Stage Turbine

The alternative to stage-by-stage turbine simulation is that we model multi-stage turbines as an equivalent single-stage turbine and assign an appropriate work potential to each secondary flow. In a two-stage turbine, for example, the work potential of the first rotor cooling air is 50% (as opposed to the 0% for a true single-stage turbine) because this cooling air can do work in the second stage. Note that the 50% number is a simplification assuming equal work split for each stage. The cooling air of the second stator will also do work in the second rotor—its work potential is also 50%.

In a three-stage turbine with cooled first and second stages, the work potential of the rotor 1 and vane 2 cooling air is 66%. For rotor 2, its cooling air can do work in the third stage, so its work potential in the equivalent single stage turbine is 33%. Cooling air which contributes to the work extraction is dubbed *non-chargeable*, non-working cooling air is *chargeable*.

In the following we limit ourselves to cooled two-stage HPTs as they are employed in many turbofan gas generators. Four secondary air streams are considered: two cool the NGV's, two the rotor blades. NGV1 cooling air works in both

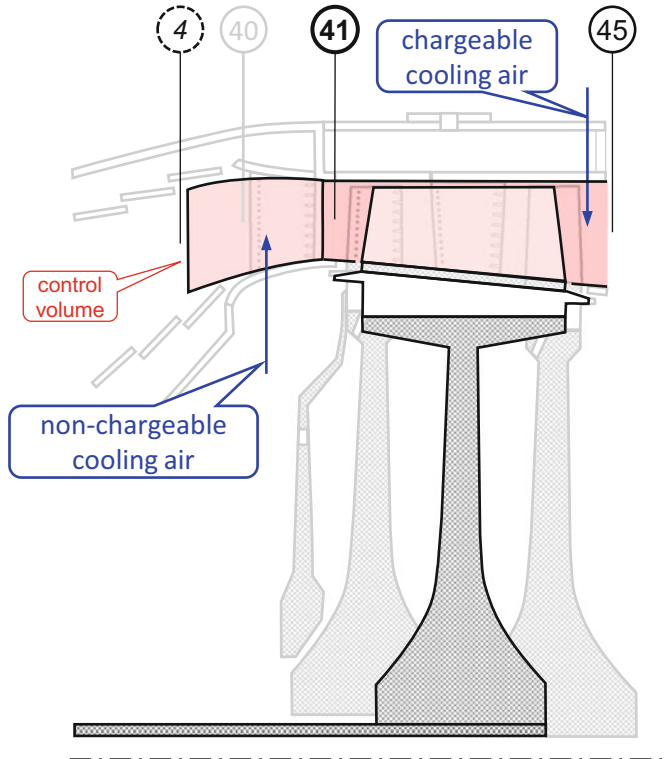


Fig. 5.3-1 Equivalent single stage turbine

Table 5.3-1 Calculation of virtual cooling air streams

		Cooling air of the equivalent single-stage turbine	Working = non-chargeable	Not working = chargeable
Virtual NGV cooling air	$W_{NGV \text{ virtual}}$	$W_{NGV1} + 0.5W_{R1} + 0.5W_{NGV2}$	100%	0%
Virtual rotor cooling air	$W_R \text{ virtual}$	$W_{R2} + 0.5W_{R1} + 0.5W_{NGV2}$	0%	100%

rotors, rotor 1 and NGV2 only in the second rotor. Rotor 2 cooling air does not contribute to the turbine power. The cycle calculation shows the four thermodynamic stations 4, 41, 42 and 45 (Fig. 5.2-1).

In the equivalent single stage turbine model, we combine the four cooling air streams of the two-stage turbine into two virtual cooling air streams $W_{NGV \text{ virtual}}$ and $W_R \text{ virtual}$. The amounts of these two virtual streams are calculated as shown in Table 5.3-1 (Fig. 5.3-1).

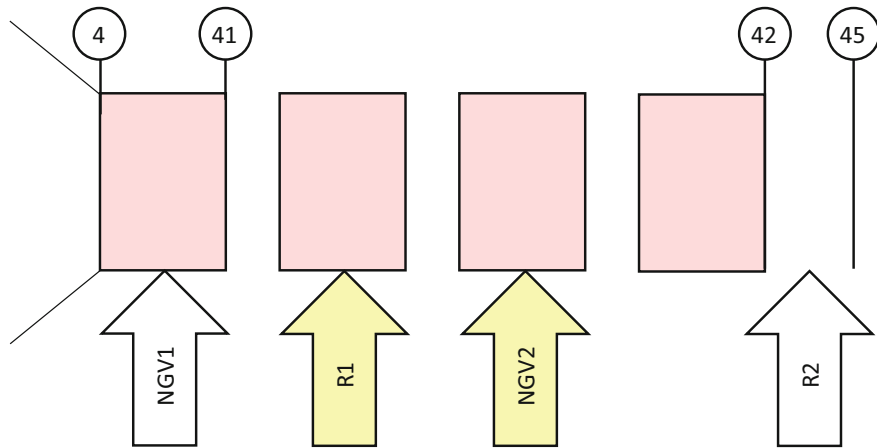


Fig. 5.3-2 Two-stage turbine schematic

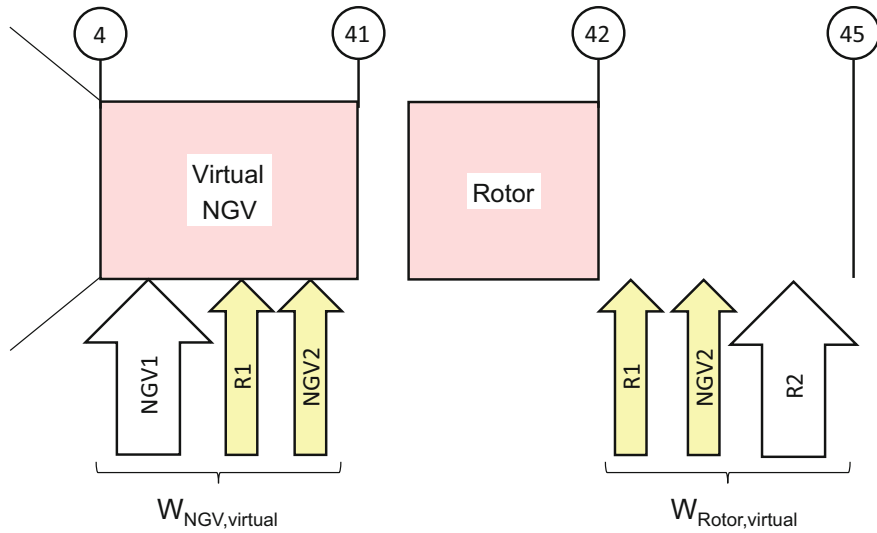


Fig. 5.3-3 Equivalent single stage turbine

Figures 5.3-2 and 5.3-3 show how a two-stage turbine is converted to an equivalent single stage turbine.

The temperature drop in the virtual NGV is bigger than in NGV1 because $W_{NGV, \text{virtual}}$ is bigger than W_{NGV1} . This fact causes a problem when we try to assign the temperatures T_4 and T_{41} to the engine hardware:

- If we declare T_4 to be the turbine inlet (=burner exit) temperature, then T_{41} cannot be the true NGV1 exit temperature.

- If we declare T_{41} to be the NGV1 exit temperature, then T_4 is no longer equal to the burner exit temperature.

Let us have a closer look at the internals of the virtual NGV to resolve that problem. For that purpose, we divide the cooling air $W_{NGV\text{ virtual}}$ in two parts: W_{NGV1} and the sum of the working fractions of the cooling air streams $W_{CL} = 0.5 W_{R1} + 0.5 W_{NGV2}$. This allows us to introduce an intermediate station between the stations 4 and 41. There are two mathematically equivalent options for locating this intermediate station:

- Add W_{NGV1} first, then W_{CL}
- Add W_{CL} first, then W_{NGV1}

It seems logical to go with the first option, however, both options have their advantages.

5.3.1 The Virtual RIT Method

If we add W_{NGV1} first (Fig. 5.3-4) then the stator exit temperature T_{41} is higher than the rotor inlet temperature RIT because $W_{CL} = 0.5 W_{R1} + 0.5 W_{NGV2}$ joins the mainstream between T_{41} and rotor inlet. This is a computational process which in reality does not happen. The thus calculated RIT is not the true rotor inlet temperature, it is a *virtual RIT*. (Ref. [1] calls this temperature *pseudo RIT*)

Thus, the work extraction process begins with a temperature lower than the true stator outlet temperature T_{41} . This discrepancy can confuse people outside the fraternity of the performance specialists. Especially turbine aerodynamicists and turbine cooling specialists will have difficulties to reconcile the numbers published by the performance department with those which they get from their aerodynamics, heat transfer and stress calculation computer programs.

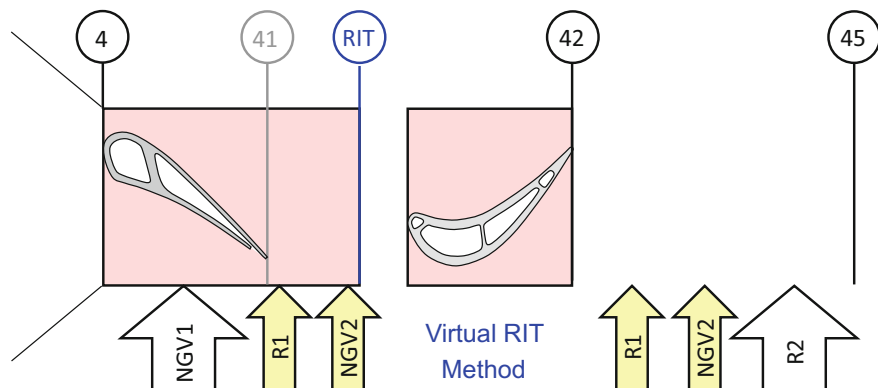


Fig. 5.3-4 Equivalent single stage turbine schematic A

5.3.2 The Virtual T_4 Method

It seems odd to add the NGV1 cooling air after the working part of the rotor 1 and NGV2 cooling air has been added to the main stream (Fig. 5.3-5). However, it makes the communication with the turbine designers easy. There is no difference between stator outlet temperature T_{41} and rotor 1 inlet temperature.

The price for this advantage is the introduction of a *virtual T_4* which differs from the NGV1 inlet temperature T_{40} . When this methodology is applied, then the difference between these two temperatures can confuse people from outside the performance fraternity in a similar way as the difference between T_{41} and the *virtual RIT* described in the previous chapter.

5.3.3 Sensitivity Analysis

Performance programs answer the question: What is the thrust increase if we can live with less turbine cooling air? In a parametric cycle study for a given technology level we can either use the turbine inlet temperature T_4 as the constant value or the NGV1 exit temperature T_{41} .

Using T_4 is intuitive but not compatible with the generally accepted hypothesis *NGV1 cooling air is working, i.e. non-chargeable*. In Fig. 5.3-6 we see a dramatic thrust loss with an increasing amount of NGV1 cooling air, caused by the decreasing stator outlet temperature T_{41} .

Figure 5.3-7 shows what happens if we keep T_{41} constant: Thrust is no longer affected by the increasing amount of NGV1 cooling air. This result is in line with the hypothesis *NGV cooling air is working, i.e. non-chargeable*; it is also consistent with our finding for the single-stage turbine.

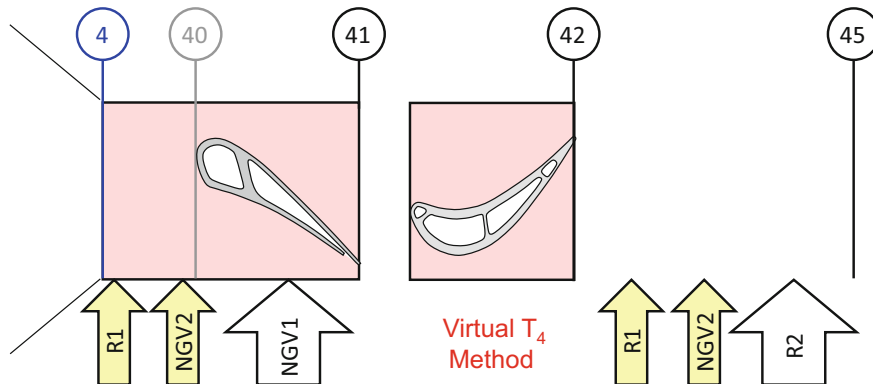
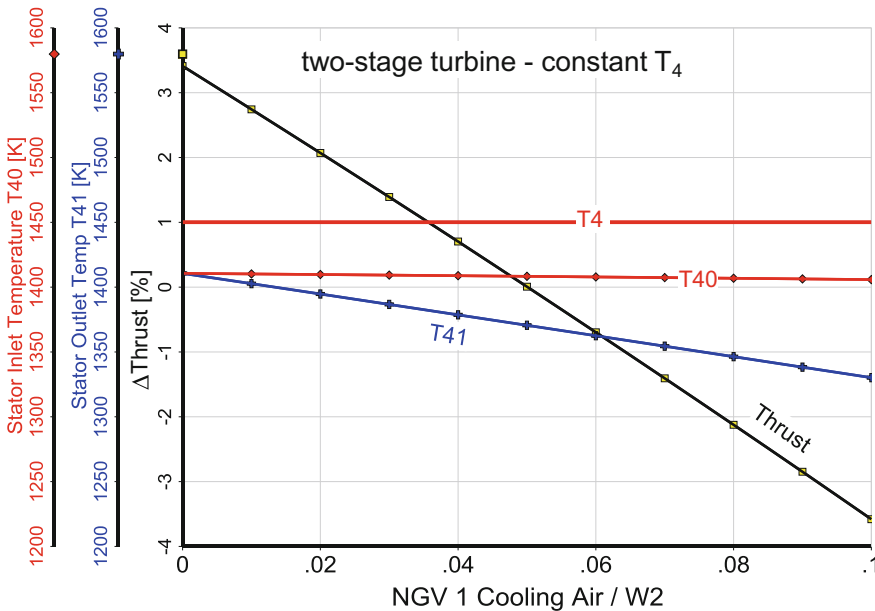
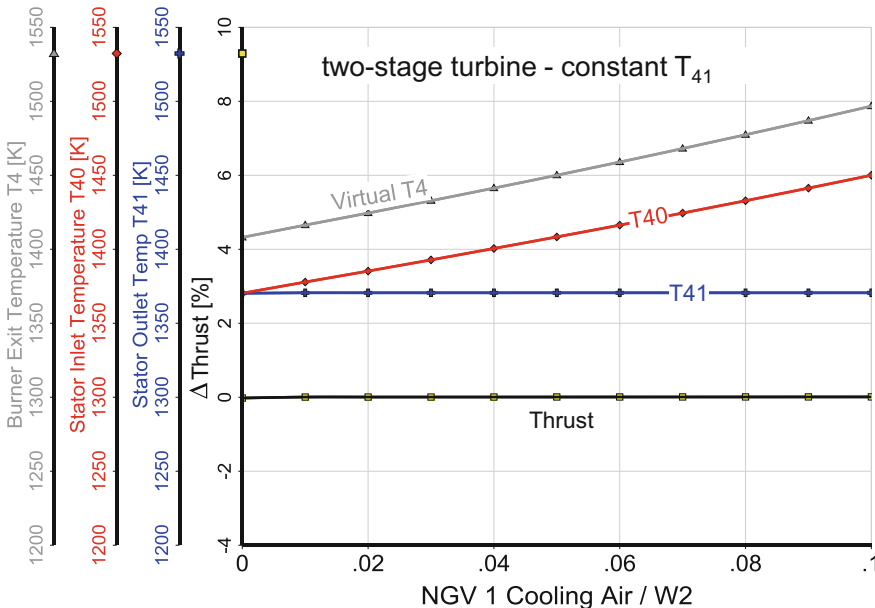


Fig. 5.3-5 Equivalent single stage turbine schematic B

Fig. 5.3-6 Two-stage turbine—constant T_4 Fig. 5.3-7 Two-stage turbine—constant T_{41}

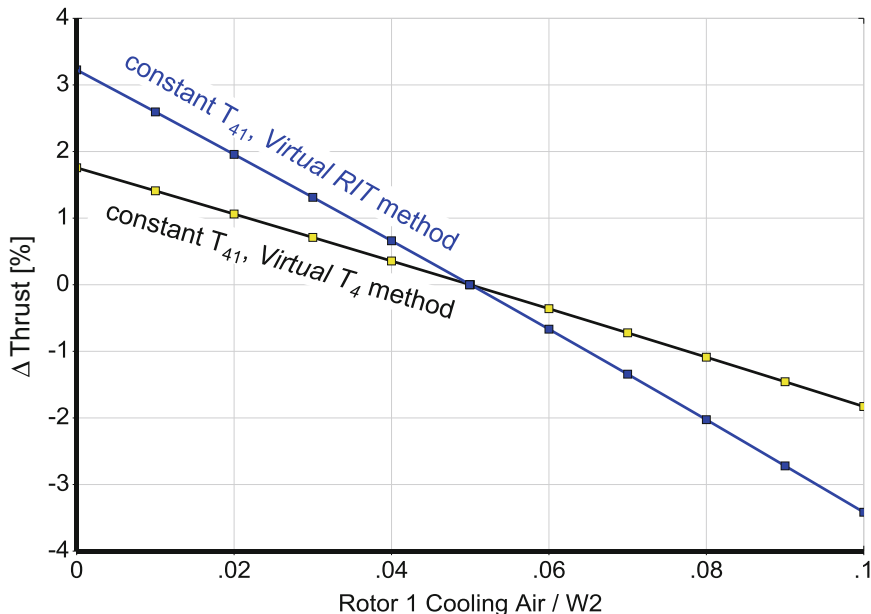


Fig. 5.3-8 The choice of the virtual turbine temperature matters!

In Fig. 5.3-7 the NGV1 inlet temperature T_{40} rises with the amount of NGV1 cooling air. The *virtual T4* is even higher than T_{40} because $W_{CL} = 0.5 W_{R1} + 0.5 W_{NGV2}$ is mixed upstream of the first rotor in addition to the NGV1 cooling air. By the way, if we keep T_{41} or the *virtual RIT* constant makes no difference with respect to NGV1 cooling air changes.

The sensitivity of the simulation result with respect to rotor 1 and stator 2 cooling air variation, however, depends on your choice of the simulation methodology. Keeping T_{41} of the *virtual T4* method constant increases the difference between T_4 and T_{40} proportional to the amount of W_{CL} . The temperature with which the work extraction process begins is not affected.

Keeping T_{41} of the *virtual RIT* method constant yields bigger thrust changes than keeping T_{41} of the *virtual T4* method constant, see Fig. 5.3-8. This is because the gap between the constant stator outlet temperature T_{41} and the *virtual RIT* increases with the amount of rotor1 and NGV2 cooling air. The temperature with which the work extraction begins drops with increasing W_{CL} and that results in an additional thrust loss.

Both the *virtual T4* and the *virtual RIT* methodologies yield the same sensitivity to $W_{CL} = 0.5 W_{R1} + 0.5 W_{NGV2}$ variations if in the first case T_{41} is kept constant and in the second case the *virtual RIT*.

5.3.4 Application

GasTurb can simulate both versions of the equivalent single stage turbine. The *virtual T₄* method requires an iteration with burner exit temperature T₄ as variable and T₄₁ = constant as iteration target. After convergence, T₄ is the virtual turbine inlet temperature and T₄₀ is the true turbine inlet temperature. T₄₁ is the true NGV1 exit temperature which is coincident with the rotor inlet temperature RIT at which the work extraction process begins. (for nomenclature see Fig. 5.3-5).

Simulating the *virtual RIT* method with GasTurb is feasible if we look at the station nomenclature in a slightly different way. T₄₁ remains the temperature at which the work extraction begins. The difference between T₄ and T₄₁ is due to adding the sum of all three working cooling air streams W_{CLNGV1} + W_{CLR1}/2 + W_{CLNGV2}/2.

Let us now introduce a virtual station 405 which is between stations 4 and 41. We calculate the temperature T₄₀₅ (as composed value) assuming that the temperature change between station 4 and 41 is proportional to the amount of cooling air added:

$$\frac{T_{405} - T_{41}}{T_4 - T_{41}} = \frac{W_{CLR1}/2 + W_{CLNGV2}/2}{W_{CLNGV1} + W_{CLR1}/2 + W_{CLNGV2}/2} \quad (5.3-1)$$

The application of the *virtual RIT* method requires an iteration of the burner exit temperature T₄ as variable with the target T₄₀₅ = constant. After convergence T₄ is the turbine inlet temperature, T₄₀₅ the NGV1 exit temperature and T₄₁ the *virtual RIT*.

5.4 Thermodynamic Efficiency

The degree of abstraction of the equivalent single-stage turbine model increases with the number of turbine stages. As an alternative, we can consider the turbine as a black box which converts thermal energy into shaft power. The flow of main stream energy W₄ h(T₄) enters the control volume defined in Fig. 5.2-1, together with many secondary energy streams. The energy output is the useful shaft power PW plus the power needed for the delivery of the rotor cooling air, for example W_D ΔH_P. The thermodynamic efficiency relates this output power to the sum of the work potential of all the streams. The work potential is defined by isentropic expansion from P₃, P_{2x} and P_D respectively to the common turbine exit pressure P₄₅. Figure 5.4-1 shows the details of the expansion process for the two-stage turbine in the enthalpy-entropy diagram. We define the thermodynamic efficiency as

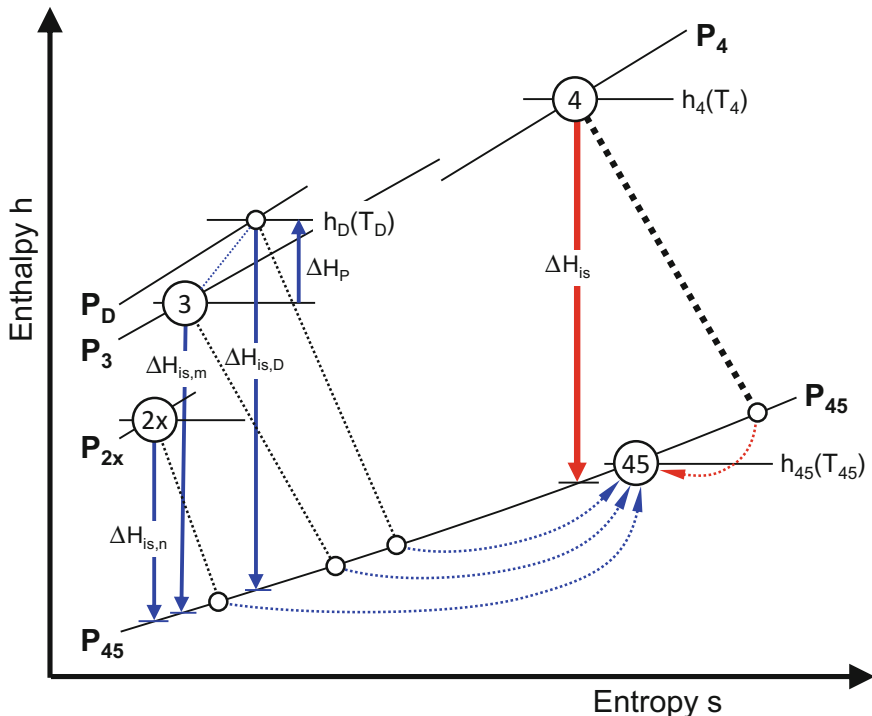


Fig. 5.4-1 Thermodynamic efficiency in the enthalpy entropy diagram

$$\eta_{th} = \frac{PW + W_D\Delta H_P}{W_4\Delta H_{is} + \sum W_m\Delta H_{is,m} + \sum W_n\Delta H_{is,n} + W_D\Delta H_{is,D}} \quad (5.4-1)$$

The expansion process begins at station 4 and no rotor inlet temperature needs to be calculated; the NGV cooling air is one of the many secondary air flows which enter the black box at the compressor exit temperature T_3 .

This definition of turbine efficiency has the advantage that no assumptions need to be made about the work delivered by any of the individual secondary streams. The work potential of each stream is defined via its respective pressure and temperature, all of which—at least theoretically—can be measured. Moreover, the thermodynamic turbine efficiency accounts for the pressure of the secondary streams. The thermodynamic turbine efficiency is less ambiguous than the equivalent single stage value.

5.4.1 Comparison of Turbine Efficiency Estimates

We have already shown how cooling air and efficiency affect the exit conditions of a single-stage turbine. In the simulation of a multi-stage cooled turbine by an equivalent single-stage device the question arises regarding which of the secondary air flows do work (non-chargeable) and do not do work (chargeable). We introduce a simple rule stating that any cooling air does useful work in all rotors downstream of the blade or vane row where it is injected.

The following example assumes 5% cooling air for the NGV and rotor 1, combined with 2.5% cooling air each for the second vane and rotor. The third and later stages are uncooled. The turbine inlet temperature T_{40} , the NGV exit temperature T_{41} and the shaft power are all constant as well as the equivalent stage efficiency, which is 0.87.

Figure 5.4-2 shows the influence of the turbine stage count on thermodynamic efficiency, the chargeable and non-chargeable cooling air fractions and the virtual temperature T_4 . Thermodynamic efficiency is always lower than 0.87, the equivalent single stage value. The difference decreases as stage count rises.

In the single stage turbine, the non-chargeable and the chargeable cooling flow ratios are both 0.05. The chargeable amount decreases and the non-chargeable amount increases with the number of turbine stages as more of the cooling air is able to do work. The imaginary burner exit temperature T_4 increases as more

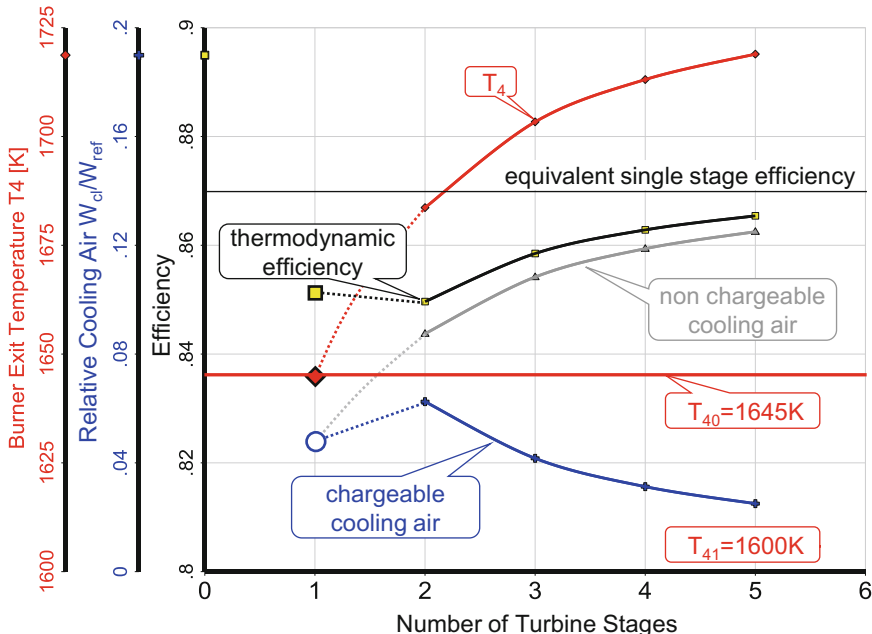


Fig. 5.4-2 Equivalent single stage methodology applied to multi-stage turbines

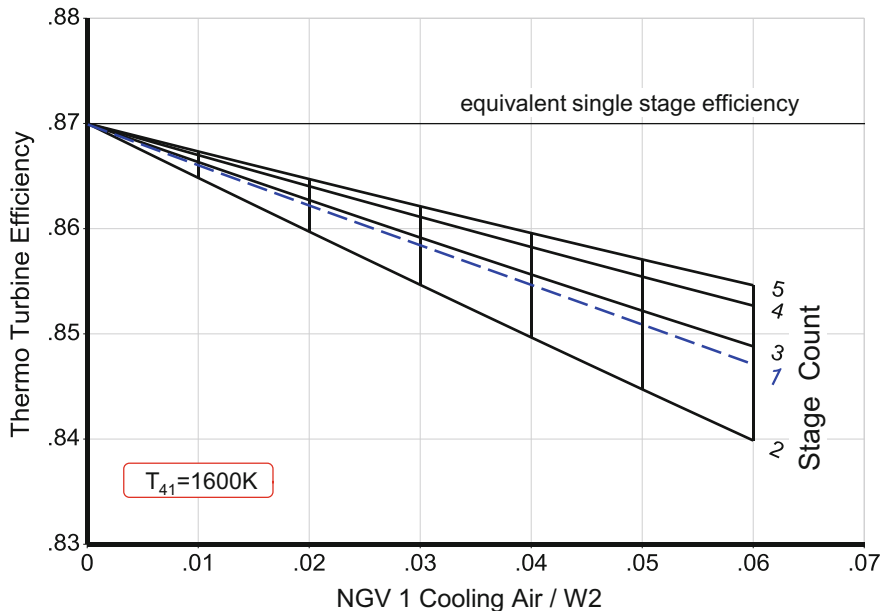


Fig. 5.4-3 Thermodynamic efficiency as function of stage count and degree of cooling

non-chargeable cooling air is mixed with the main stream between stations 4 and 41. Note that the temperature difference between T_4 and T_{41} is quite large—so do not use constant values of T_4 in calculations that involve real turbine hardware!

The difference between turbine stage efficiency and thermodynamic efficiency is approximately 2% in a comparison of single- and two-stage machines. This remarkably high discrepancy emphasizes the importance of common book-keeping when engine performance engineers talk with turbine designers.

While there is no difference between the equivalent single stage efficiency and the thermodynamic efficiency if the turbine is uncooled, the disparity between the two values increases with the amount of cooling air, as shown in Fig. 5.4-3. The amounts of NGV 1 and rotor 1 cooling air are equal; vane 2 and rotor 2 cooling air flows are half the NGV 1 values shown on the x-axis.

The difference between the two efficiency values depends not only on the amount of cooling and the stage count but also on the turbine pressure ratio, as indicated in Fig. 5.4-4. Unfortunately, there is no simple formula for the conversion of one efficiency to another.

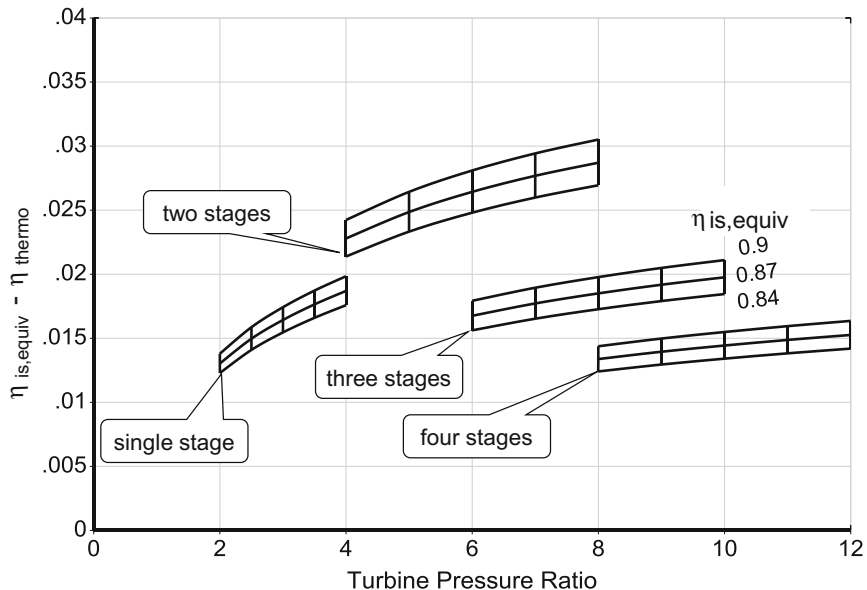


Fig. 5.4-4 Difference between efficiency numbers as function of turbine pressure ratio

5.4.2 Efficiency Definition Affects the Results of Cycle Studies

After having seen the differences when we compare the results of using the various efficiency definitions, it is not too surprising that these have very significant effects on the results of engine performance calculations. Figure 5.4-5 shows the results of two parametric studies of a turbojet. The blue carpet is valid for constant thermodynamic turbine efficiency while the black carpet corresponds to constant isentropic equivalent single-stage efficiency. The calculation was adjusted intentionally to align the top right corner points and emphasize the different shapes of the carpets. The cooling air percentages are constant, but the turbine pressure ratios as well as the cooling air temperatures differ from case to case. In this example, differences are increased as thrust and SFC are reduced. Matching the carpets at some other location would not change the general result that divergence increases with distance from the match point.

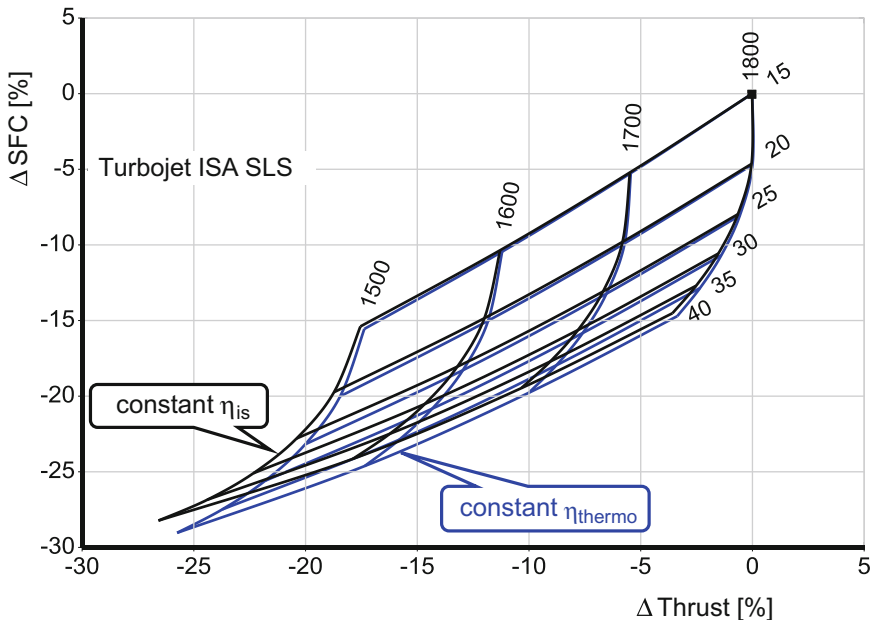


Fig. 5.4-5 Turbojet cycle study results for two turbine efficiency definitions

5.5 Efficiency Losses Due to Cooling

Up to now we have only discussed turbine cooling air bookkeeping systems. However, all cooling techniques involve increased aerodynamic losses and, consequently, decreased efficiency. The losses associated with turbine cooling include increased profile losses due to thicker blade profiles needed for the accommodation of cooling passages, interaction of coolant films with the blade boundary layer, mixing losses between coolant and main flows, modified wakes and corner flow fields.

5.5.1 Some Numbers

A realistic performance model must account for the losses listed above and assign efficiency decrements to specific design features of the turbine cooling system. According to Ref. [1], each percent of cooling air lowers the turbine efficiency by the $\Delta\eta_{\text{stage}}$ amounts listed in Table 5.5-1.

Reference [2] is another source of generic exchange rates between the amount of turbine cooling flow and the decrease in efficiency. The numbers for $\Delta\eta_{\text{stage}}$ in Table 5.5-2 are of the same order of magnitude as those in Table 5.5-1.

Table 5.5-1 Efficiency loss for 1% cooling air, Ref. [1]

	$\Delta\eta_{\text{stage}}$	
	Stator	Rotor
Suction surface cooling	0.0075	0.0150
Rotor shroud cooling by upstream injection	0.0025	0.0050
Trailing edge cooling	0.0025	0.0050
Leading edge or pressure surface cooling	0.00125	0.0025

Table 5.5-2 Efficiency loss for 1% cooling air, Ref. [2]

	% Trailing edge ejection	Rel. cooling flow	$\Delta\eta_{\text{stage}}$	
			Stator	Rotor
	Advanced convection	100	1.5	0.001 0.002
	Film with convection	75	1.4	0.0012 0.0024
	Film with convection	50	1.3	0.0015 0.003
	Film with convection	25	1.0	0.0018 0.0036
	Transpiration with convection	25	0.8	0.005 0.01

5.5.2 A Real-World Example

The turbine cross section in Fig. 5.5-1 shows the cooling and sealing air flows in a so-called “worm diagram”. The values next to the arrows are percentages of core compressor entry mass flow. This type of picture enhances communication between performance engineers and secondary air system specialists. If we were working for an engine manufacturer, then we would have access to the temperatures and pressures of the main gas stream and each of the cooling and sealing air flows. We are unable to calculate thermodynamic efficiency without these data. However, we can translate the information contained in the figure to input data for an equivalent single stage turbine model because, for that approach, we need neither temperatures nor pressures of the secondary gas streams.

First, we define the control volume in the turbine drawing and then we assign a work potential to each cooling flow element. This is straightforward for vane and blade cooling air but somewhat ambiguous for the many small flows entering the control volume along the hub and tip boundaries of the control volume.

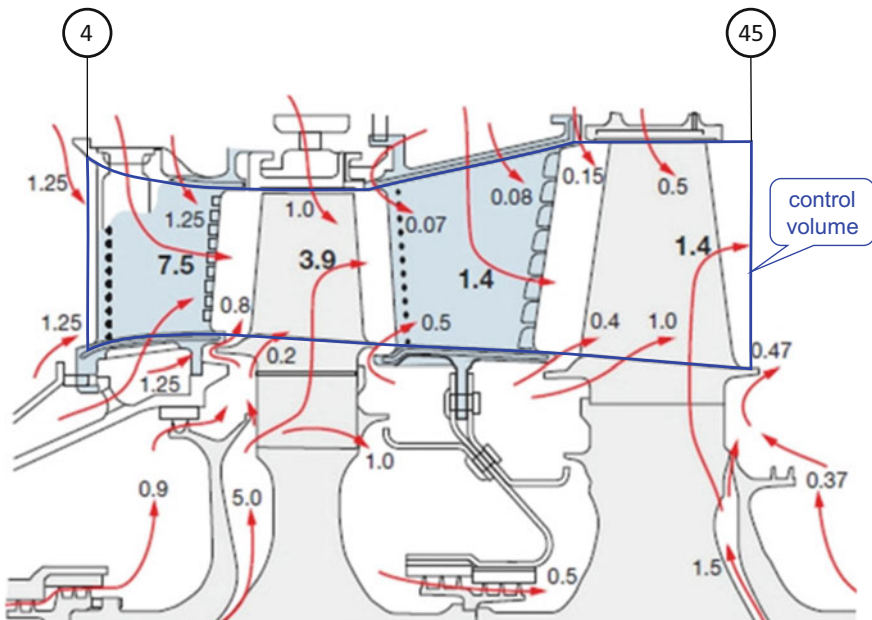


Fig. 5.5-1 A real world example of turbine cooling [3]

The main gas stream enters the turbine control volume at the combustor exit station 4. Two secondary flows upstream of the control volume entry (1.25% each) are part of W_4 ; they are not relevant in our equivalent single stage turbine model. Table 5.5-3 shows our selected distribution of work potential and the efficiency losses due to cooling. The cooling and sealing flows entering the control volume from the inner and outer walls are different. Their orientation makes it easy to identify them and to correlate the content of Table 5.5-3 with Fig. 5.5-1. Our decisions are not unquestionable, especially with respect to the application of efficiency losses from Tables 5.5-1 and 5.5-2. In a real-world situation performance engineers, turbine designers and secondary air system specialists talk to each other and agree to an appropriate, clearly defined accounting system.

The NGV cooling air of 7.5% does work in both rotors. The sum of all secondary flows with 50% work potential is 10.37% and the non-working secondary flows add up to 3.53%. In total this turbine needs 21.4% of the core compressor mass flow for cooling and sealing purposes.

In the equivalent single stage turbine model, we add half of the secondary flow (with 50% work potential) to the NGV cooling air. The other half becomes part of the non-working rotor cooling air. The input for the performance program is $W_{c1NGV}/W_{25} = 0.075 + 0.1037/2 = 0.12685$ and $W_{clrotor}/W_{25} = 0.0353 + 0.1037/2 = 0.08715$.

Table 5.5-3 Work potential and efficiency decrements

	W/W_{25} [%]	Work [%]	$\Delta\eta_{stage}$	Comment
Tip	1.25	50		NGV platform cooling
	1	50		Rotor 1 shroud cooling
	0.07	50		Vane 2 sealing
	0.08	0		Vane 2 platform cooling
	0.15	0		Rotor 2 sealing
	0.5	0		Rotor 2 shroud cooling
Main	7.5	100	0.0135	NGV cooling
	3.9	50	0.0117	Rotor 1 cooling
	1.4	50	0.0021	Vane 2 cooling
	1.4	0	0.0028	Rotor 2 cooling
Hub	1.25	50		NGV platform cooling
	0.8	50		Rotor 1 front seal
	0.2	50		Rotor 1 platform cooling
	0.5	50		Rotor 1 rear seal
	0.4	0		Rotor 2 front seal
	1	0		Rotor 2 platform cooling

The data in Table 5.5-2 enable us to quantify an efficiency loss due to cooling within the main stream. Let us assume film and convection cooling of the NGV with 25% trailing edge ejection, a less sophisticated cooling scheme for rotor 1 and vane 2 (50% trailing edge ejection) and advanced convection cooling for rotor 2. Adding up the four numbers leads to an efficiency loss of 0.0301 along the mean flow path.

The sum of all secondary flows entering the control volume between stations 4 and 45 along hub and tip is 0.072. If we assume from Table 5.5-1 that each percentage of this air causes an efficiency loss of 0.0025 then we get another $\Delta\eta$ of 0.018. If the uncooled turbine has an isentropic efficiency of 0.92, for example, then the in-engine efficiency of the cooled turbine will be only 0.872.

5.6 References

- Walsh, P.P., Fletcher, P.: Gas Turbine Performance, 2nd edn. Blackwell Science Ltd, (2004)
- Gauntner, J.W.: Algorithm for calculating turbine cooling flow and the resulting decrease in efficiency, NASA TM 81453, (1980)
- Van den Braembussche R.A.: Turbomachinery blade design systems, Von Karman Institute for Fluid Dynamics, VKI Lecture Series LS 1999–02
- Kurzke J.: Performance modeling methodology: efficiency definitions for cooled single and multistage turbines, ASME GT-2002-30497, (2002)

Chapter 6

Secondary Air System



The basic thermodynamic cycle describes the process in terms of the primary air flows in a gas turbine. Of course, in addition to the main stream there is a secondary air system which provides the turbine cooling air, sealing air (prevents hot gases entering the turbine disk cavities and bearing chambers) and controls the axial load on the bearings (Fig. 6.1-1). By its nature the secondary air system (SAS) is very complex involving many different sources for the air with flows returning at numerous positions within or leaving the main gas path. This section shows how a greatly simplified SAS can be used in the performance model whilst still providing an accurate simulation of both overall performance and component parameters.

The SAS consists of a multitude of relatively small elements plus a few bigger air flows dedicated to turbine cooling. The SAS consists of two subsystems, the *internal* and the *external* system. The first subsystem deals with the air flows that are required for the safe operation of the engine. These are the turbine cooling air, bearing and rim sealing air, bearing thrust control, active tip clearance control, handling bleeds. These bleeds are usually quantified as percentages of the relevant compressor entry mass flow. The pressure of an individual flow is of no interest, except for computing the thermodynamic efficiency of a cooled turbine.

The second subsystem, the external air system, provides air needed for aircraft purposes (cabin ventilation, de-icing of nacelle and aircraft parts, cross starting of engines). These secondary flows are mostly specified as an absolute value in kg/s. Both air pressure and temperature at the engine interface are of interest to the customer—the aircraft.

6.1 SAS in the Performance Model

It is common practice in a performance model to replace the numerous flow lines by a manageable number of secondary streams. The model remains “fit for purpose” as it maintains energy balances, with realistic flows, pressures and temperatures at the

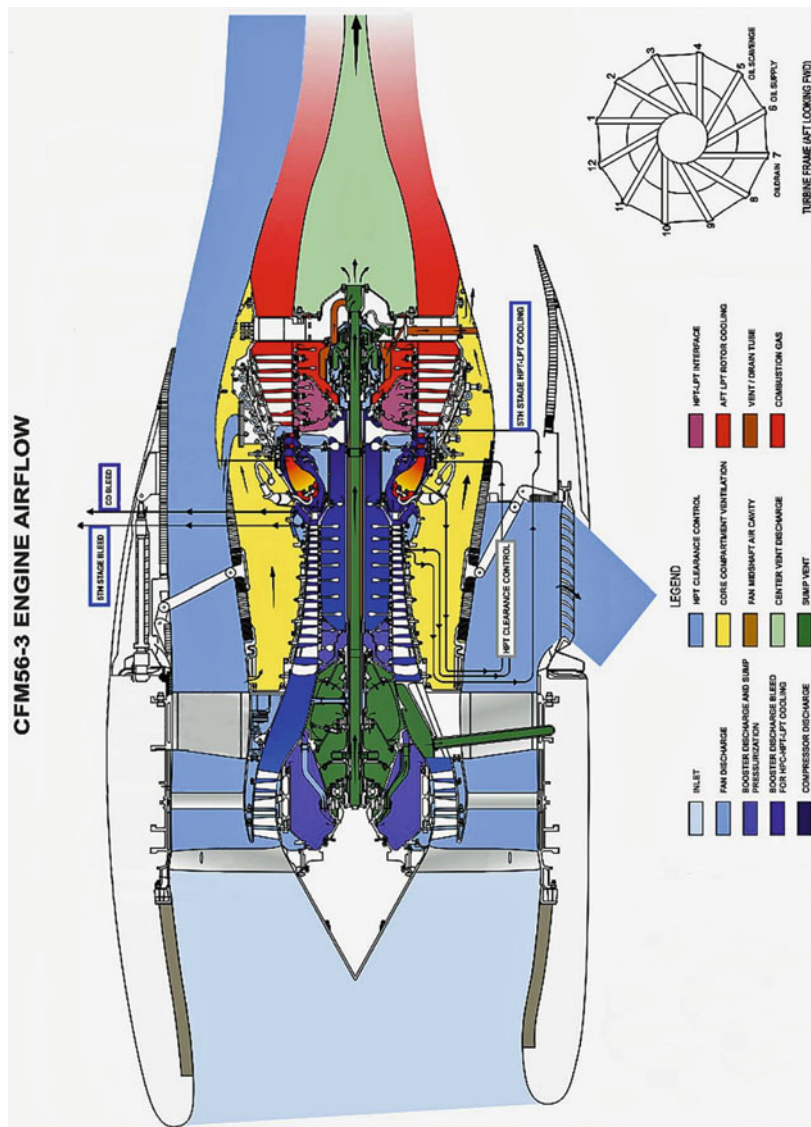


Fig. 6.1-1 Simplified secondary air system

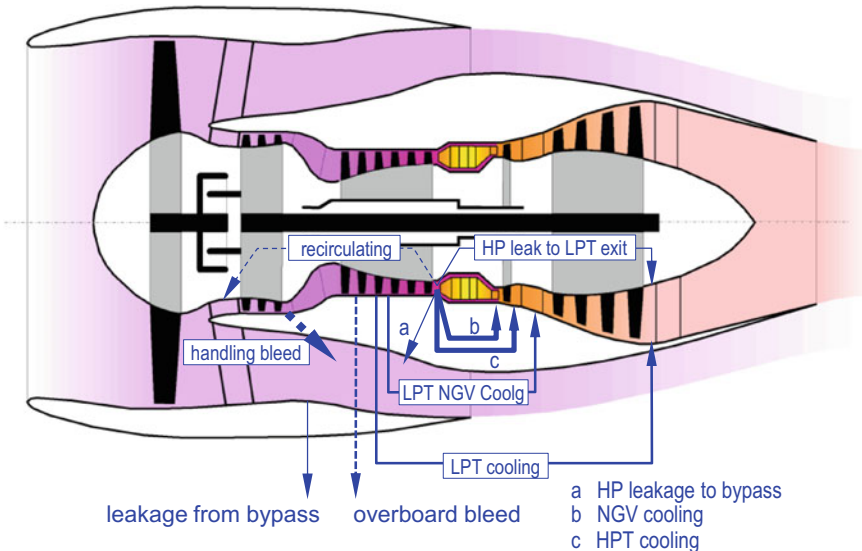


Fig. 6.1-2 Schematic of secondary air system for a 2-shaft turbofan (© Copyright CFMI)

main thermodynamic stations as well as representing the overall process adequately.

Figure 6.1-2 shows the most important secondary air flow paths in a turbofan performance model. Solid lines represent the invariant part of the internal air system: the mass flow is a constant fraction of the HP compressor entry flow for any off-design case. Dashed lines indicate the variable parts of the internal and external air systems.

Performance programs in industry often model the secondary air system in great detail. You might be tempted to consider more secondary flow paths than shown in Fig. 6.1-2 with the aim of a more accurate simulation. What is the effect of simplifying the secondary air system model on the overall performance simulation quality?

Let us examine the influence of two different variants of the SAS model on the performance characteristics of a turbofan. The first one employs a medium complex description of the turbine cooling system while, in the second, all turbine cooling air flows are zero. Figure 6.1-3 shows the enthalpy-entropy diagrams of the two cycle design points.

Turbine temperatures and efficiencies of the cycle without secondary air system have been adjusted in such a way that the HPT pressure ratio, thrust and specific fuel consumption are the same. The differences between the two models are primarily in the turbine: The model without turbine cooling air shows significantly lower turbine

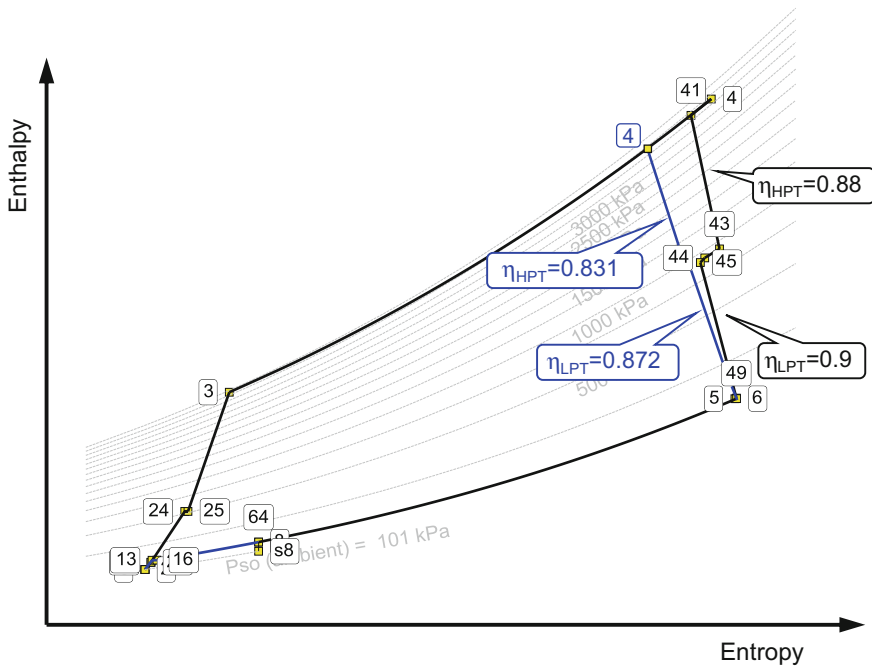


Fig. 6.1-3 Mixed flow turbofan enthalpy—entropy diagram with and without turbine cooling air

inlet temperatures and the turbine efficiency numbers are also lower. Apart from that, there are only very small differences between the two cycle design points.

Figure 6.1-4 shows how the two models behave in an off-design simulation: The turbine temperature levels are different, but their tendencies from full to part load are the same. It is noteworthy that there is no difference in the specific fuel consumption, a measure of thermal efficiency.

The conclusion from this exercise: a simplified secondary air system model does not significantly influence the quality of the overall performance simulation. However, if you are interested in the true gas temperatures or turbine efficiencies the implementation of the SAS must be well understood.

6.2 SAS Calculation

In the following, we limit ourselves to the SAS that corresponds to Fig. 6.1-2. It is simple to derive energy balances, when the flow sources are at thermodynamic stations as the temperatures are known. However, there are exceptions to this with interstage ports used for overboard bleed and LPT flows. Also on multi-stage turbines some SAS flows are returned mid-turbine. We now show how this can be represented in the simplified SAS model.

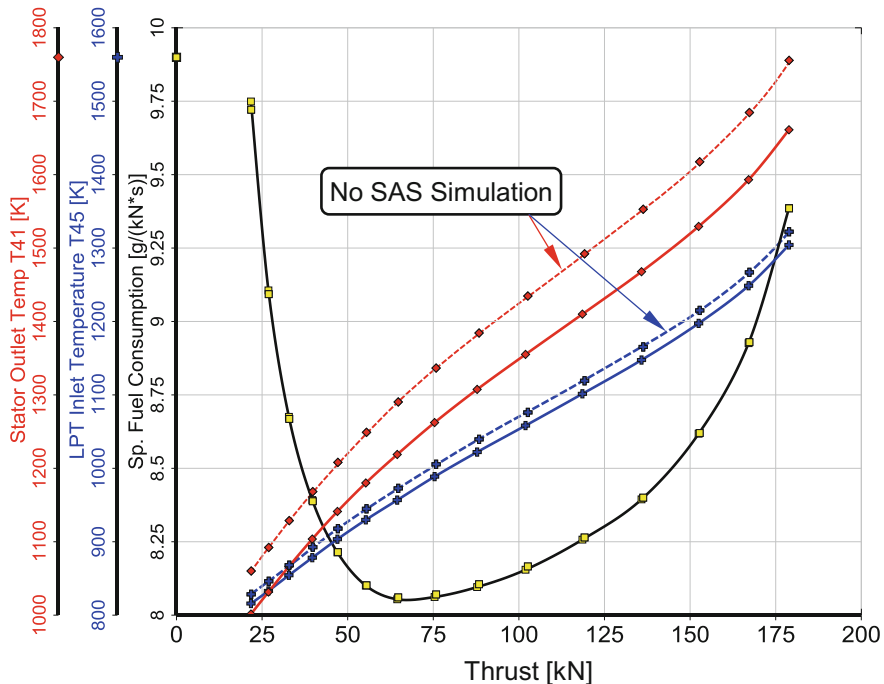


Fig. 6.1-4 Models with and without secondary air system

6.2.1 Interstage Bleed

The specific compression work done on an interstage bleed (station 2x in Fig. 6.3.1) is $H_{2x} - H_2$. We relate this enthalpy difference to the overall specific work of the HPC:

$$\Delta H_{2x,rel} = \frac{H_{2x} - H_{25}}{H_3 - H_{25}} \quad (6.2-1)$$

The relative specific work $\Delta H_{2x,rel}$ is easily estimated. If the bleed port is located at the exit of the 7th stage of a ten-stage compressor, then the relative specific work done on this bleed is $\Delta H_{2x,rel} = 0.7$.

Generally, there is no need to calculate the bleed air pressure. The exception is the overboard bleed needed for aircraft purposes—the customer bleed. For this special case, we employ the polytropic HPC efficiency to calculate the main stream total pressure at the bleed port. The pressure losses of the bleed port and in the pipe to the aircraft-engine interface depend on many geometrical details and the amount of bleed air. If an accurate bleed pressure value is needed then, typically, compute it

using the formula editor of your performance program, but note that these losses do not affect the overall engine performance.

6.3 Turbine Cooling Air

Most secondary air flows recombine with the main stream. There the mass flow is added and the temperature of the mixed stream follows from an energy balance. The bleed air pressure is not considered in the mixing process.

Within the performance program, multi-stage turbines are simulated as equivalent single stage turbines. The turbine cooling air joins the main stream upstream or downstream of the turbine rotor.

Turbine cooling air must have sufficient pressure to allow it to join the main stream. For a single stage HPT, this is simple to model as all HPT cooling flows in the performance model (streams b and c in Fig. 6.1-2) are taken from compressor delivery.

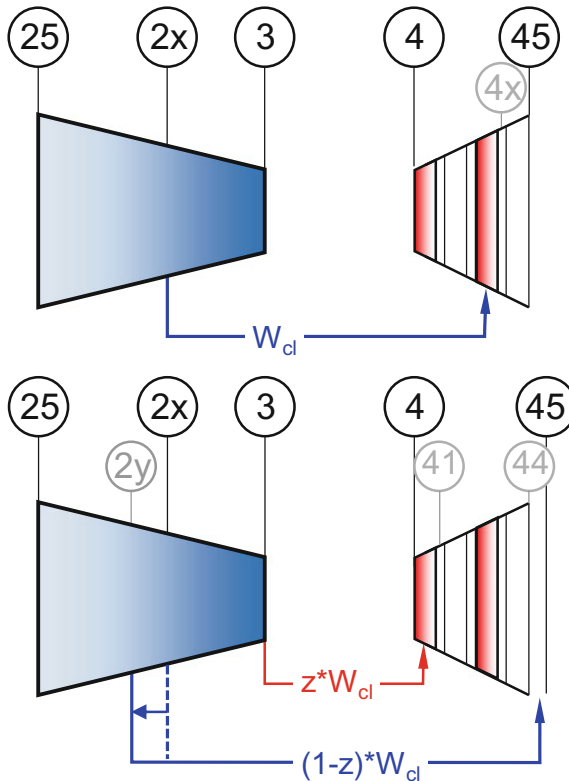


Fig. 6.3-1 HPT cooling with compressor interstage bleed

In a two-stage turbine, the second stage can be cooled with bleed air from an intermediate compressor stage. The cooling air joining the main stream in the second stage vane contributes to the turbine power. How can this flow be modeled using the SAS scheme from Fig. 6.1-2?

In Fig. 6.3-1 there is no route from the compressor interstage station 2x to an imaginary turbine interstage stage 4x; such a station just does not exist in this performance model. We replace the cooling bleed flow W_{cl} by two equivalent flows: one which participates in the power generation (z^*W_{cl}) and a second which bypasses the turbine. $(1 - z)^*W_{cl}$. The value of z is the proportion of the turbine power generated downstream of where the flow is introduced:

$$z = \Delta H_{T4x,rel} = \frac{(H_{4x} - H_{44})}{(H_{41} - H_{44})} \quad (6.3-1)$$

We wish to maintain the compressor work in the cooling flow. The part of the cooling flow taken from station 3 has more work done on it than before, so to compensate we reduce the work on the non-working part by moving the offtake position from station 2x to 2y.

The energy balance for the cooling flow is:

$$W_{cl}(H_{2x} - H_{25}) = zW_{cl}(H_3 - H_{25}) + (1 - z)W_{cl}(H_{2y} - H_{25}) \quad (6.3-2)$$

Which re-arranged into relative specific work gives

$$\Delta H_{2y,rel} = \frac{\Delta H_{2x,rel} - z}{1 - z} \quad (6.3-3)$$

The working flow $W_{cl,3y}$ is added to HPT NGV flow and the non-working flow $W_{cl,2y}$ to the LPT NGV flow in Fig. 6.3-1.

Next, let us look at the practical application of this approach. If the bleed port is located right after the 7th stage of a ten-stage compressor then $\Delta H_{2x,rel} = 0.7$. The relative enthalpy drop from the second vane cooling air injection point to the turbine exit is $\Delta H_{T,rel} = z = 0.5$. The relative work of the first imaginary stream is 1.0, that of the second imaginary stream—the non-working flow—is $\Delta H_{2y,rel} = (0.7 - 0.5)/(1 - 0.5) = 0.4$. We account for this chargeable cooling air by adding it to the input value, which intrinsically stands for the LPT NGV cooling air $W_{C\ LPT\ NGV}/W_{25}$ in Fig. 6.3-1. The non-chargeable (i.e. the working) interstage bleed air may be added to the HPT NGV cooling air in your performance program. Alternatively, you can ignore it completely because this air goes through precisely the same process as the main stream.

6.3.1 Multi-stage Turbines

Single spool gas turbines designed for power generation need many turbine stages because the turbine pressure ratio equals (nearly) the compressor pressure ratio. The Siemens SGT8000H heavy-duty gas turbine, for example, has four turbine stages which are all air-cooled.

The first stage employs air from stage 13 (compressor exit) for cooling, the other three turbine stages are cooled with bleed air taken after the compressor stages 11, 8 and 5. We must also include a corresponding turbine in the performance program and this must be modeled as an equivalent single stage machine because we have only one turbine map. So, in the simulation, the cooling air can join the main stream either upstream or downstream of the sole turbine rotor.

Figure 6.3-2 shows the SAS of the single spool engine configuration of GasTurb. There are two cooling air sources: one is an intermediate stage of the compressor; the other is the exit of the compressor. The interstage bleed air can re-unite with the main stream only downstream of the turbine because it has insufficient pressure for use in cooling the first turbine stage. Air with compressor exit pressure can join the main stream upstream of the first turbine rotor since the sink pressure has been reduced at least by the burner pressure loss.

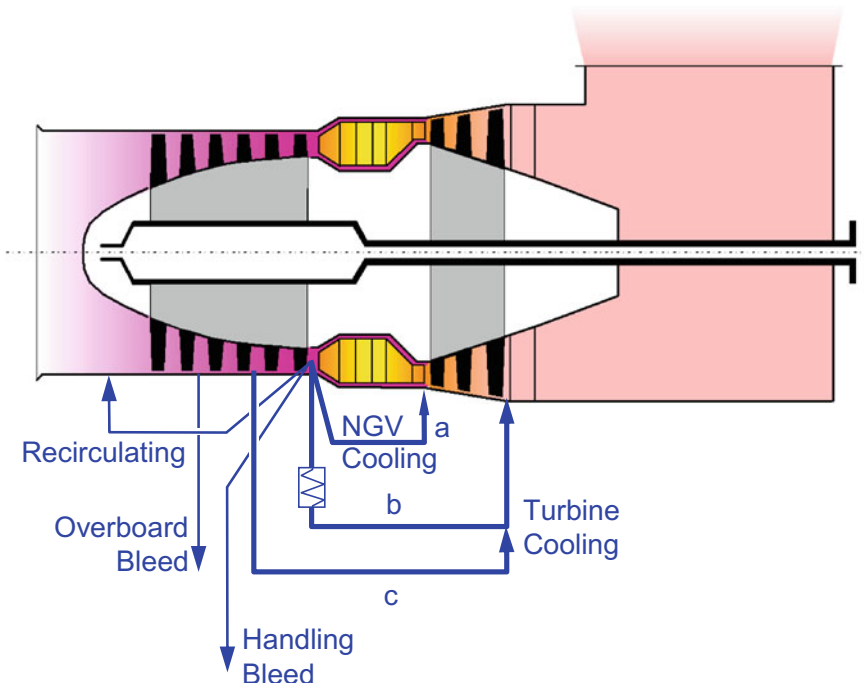
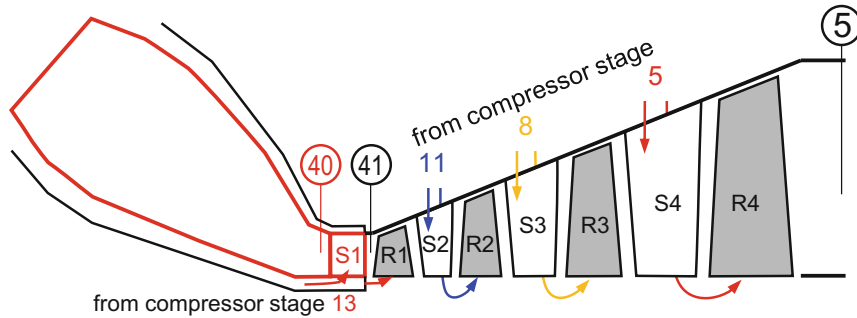


Fig. 6.3-2 GasTurb SAS for the single spool turboshaft



$W_{Cl}/W_2[\%]$	6.3	5.8	4.4	3.4	1.8	1.3	0.7	0.3	$\Sigma = 24\%$
Work potential $\Delta H_{T,rel}$	1	.75	.75	0.5	0.5	0.25	0.25	0	
Working $W_{Cl}/W_2[\%]$	6.3	4.35	3.3	1.7	0.9	0.325	0.175	0	
Not Working $W_{Cl}/W_2[\%]$	0	1.45	1.1	1.7	0.9	0.975	0.525	0.3	

Fig. 6.3-3 Secondary air system for a single spool gas turbine for power generation

Table 6.3-1 Energy balance for compressor interstage bleed

1	Source stage no	13		11		8		5		
2	Work fraction $\Delta H_{Cl2x-4x}$	1		0.846		0.615		0.385		
3	Sink	S1	R1	S2	R2	S3	R3	S4	R4	Total S2-R4
4	Rel. mass flow $W_{Cl2x-4x}/W_2$	6.3	5.8	4.4	3.4	1.8	1.3	0.7	0.3	11.9
5	Turbine work fraction z	1	0.75	0.75	0.5	0.5	0.25	0.25	0	
6	Working mass fraction of W_2	6.3	4.35	3.3	1.7	0.9	0.325	0.175	0	6.4
7	Turbine bypass $1 - z$	0	0.25	0.25	0.5	0.5	0.75	0.75	1	
8	Non-working mass fraction of W_2	0	1.45	1.1	1.7	0.9	0.975	0.525	0.3	5.5
9	Non-working flow: Equivalent compr work fraction $\Delta H_{Cl,y,rel}$	1	1	0.384	0.692	0.23	0.487	0.18	0.385	Mass weighted mean 0.453

The true cooling air scheme is much more complex than that in the performance model. Let us consider as a numerical example the SAS schematic shown in Fig. 6.3-3. It is somewhat similar to the real SGT-8000H cooling configuration; the numbers we are using here have been published for a similar engine in Ref. [2].

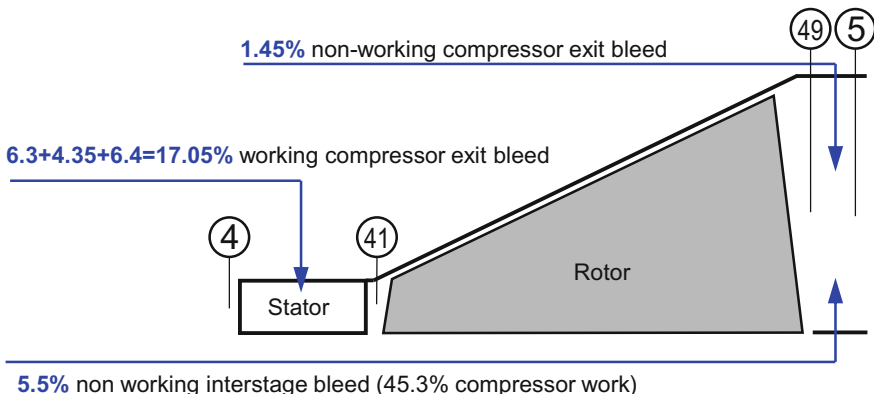


Fig. 6.3-4 SAS of the equivalent single stage turbine

We can transform this detailed SAS to the simple model shown in Fig. 6.3-2. Stator 1 cooling flow is simple to model as it is taken from compressor exit and allocated to the NGV flow a in Fig. 6.3-2. Rotor 1 flow is split into a working and non-working flows according to lines 5 and 7 in Table 6.3-1 and allocated to the flows a and b respectively in Fig. 6.3-2.

Stators and Rotors 2–4 are cooled with interstage air which are split into working and non-working flows. The working flow is taken from compressor exit and included in the flow a in Fig. 6.3-2, with the non-working flows added to flow c in Fig. 6.3-2. For each of the interstage flows the equivalent HPC specific work fraction is calculated according to Eq. (6.3.3) as described in Sect. 6.3. The mean specific work in the total flow c is derived from the mass-weighted mean of the lines 8 and 9 in Table 6.3-1.

The equivalent single stage turbine SAS is shown in Fig. 6.3-4.

It should be noted that the Stator 1 may also be regarded as part of the combustion chamber. This does not change the overall cycle as the flows and temperatures through the turbine rotor are not affected. However, the value for T_4 reduces when the cooling flow is added upstream of the stator in the model.

6.4 References

1. Kurzke, J.: About simplifications in gas turbine performance calculations. Paper presented at Turbo Expo 2007, Montreal, Canada ASME GT2007-27620, 2007
2. H₂IGCC Low Emission Gas Turbine Technology for Hydrogen Rich Syngas Project under the European Union's Seventh Framework Programme for Research and Technological Development SP4—Description of the models adapted or developed ad hoc for the IGCC-CCS plants D4.2.2—final—long version <http://www.h2-igcc.eu/Pdf>

Chapter 7

Mathematics



Design point calculations of simple thermodynamic cycles are straightforward—it is a sequential evaluation of one equation after the other. However, when two streams are mixed in the cycle, an iteration is required as the static pressures at the mixer entry must be equal or at least similar. Also, cycles with heat exchanger need iteration: the heat exchanger exit temperature is needed at the burner entry, but is not known until nearly the whole cycle has been calculated.

Off-design performance calculations deal with the matching of many components. For each of the compressors and turbines we need to find the coordinates of the operating points in the respective performance map. Moreover, mass flow continuity between components, power balances for each spool, mass flow restrictions for the nozzles and pressure balances in mixers must be fulfilled. It is obvious that many iterations are required.

This section begins with the calculation of the off-design performance of a helicopter engine. Four nested and overlapping iteration loops are required to arrive at the solution.

Next, we step back and present basic iteration algorithms and discuss which are best suited for which purpose. The method of choice for overall system simulation is the Newton-Raphson algorithm. Of course, this preferred approach to off-design performance simulation has some peculiarities and pitfalls. Convergence problems are discussed in the last section of this chapter.

7.1 The Off-Design Simulation Task

Let us begin with a simple off-design performance problem. We want to know the power delivered by a turboshaft with free power turbine for a given gas generator spool speed XNH and power turbine speed $XNPT$. The sequence of the calculations is sketched in Fig. 7.1-1.

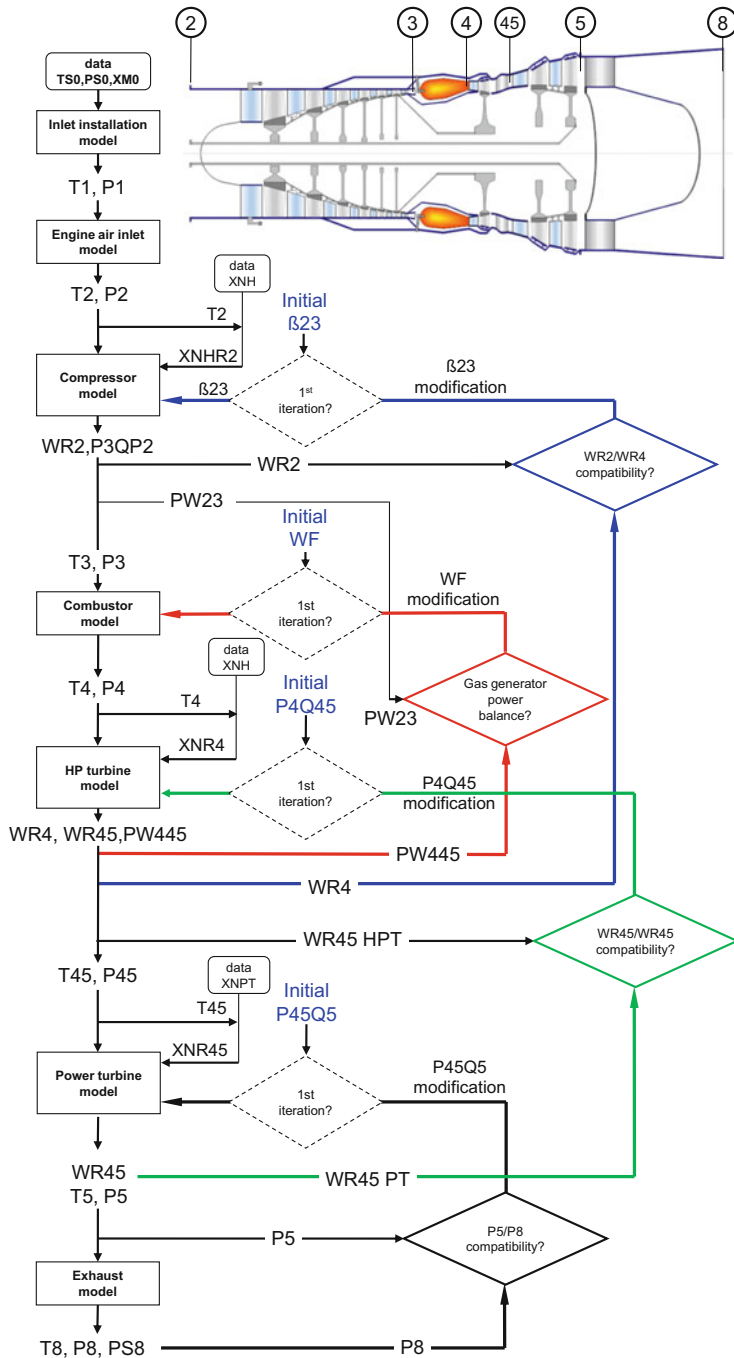


Fig. 7.1-1 Nested loops (adapted from Ref. [1])

Flight conditions define TS_0 , PS_0 and flight Mach number XM_0 . The inlet installation model describes the air intake performance as it is part of the helicopter —this yields T_1 and P_1 . Further pressure losses and total temperature changes might happen in the engine part of the air inlet. The air enters the compressor with total temperature T_2 and total pressure P_2 .

Since compressor spool speed XNH is given in this example, we can easily calculate the corrected speed $XNHR_2$. To read the compressor map we need the auxiliary map coordinate β_{23} in addition to $XNHR_2$, however, we do not yet know it. We begin with an initial estimate of β_{23} and wait until we find the means to correct this guess iteratively.

Reading the compressor map yields corrected flow W_{2R} , pressure ratio P_{3Q2} and efficiency. This enables us to calculate the compressor exit temperature T_3 and pressure P_3 as well as the power needed by the compressor PW_{23} .

Inputs to the combustor model are the air and fuel flows. Since we do not yet know the latter, we begin with an initial guess of WF . The model then provides the conditions at the combustor exit W_4 , T_4 and P_4 .

Inputs to the HP turbine model are the corrected spool speed $XNHR_4$ and another estimated value for locating the operating point in the turbine map. We guess the HP turbine pressure ratio P_{4Q45} and the HP turbine model yields numbers for the corrected flows at the entry (W_{4R}) and exit (W_{45R}), T_{45} and P_{45} as well as the power PW_{445} .

At this point in the calculation sequence, if the turbine power is less than the power required by the compressor, then our guess for fuel flow WF was on the low side. We modify the fuel flow and jump back to the combustor model. The power balance between compressor and turbine will be fulfilled after a few iterations on WF .

However, even when the power balance is OK, there is still a potential problem with the corrected turbine entry flow WR_4 . This may be determined in two ways: either read from the turbine map or calculated from WR_2 , WF , T_4 and P_4 . Any discrepancy between the two results can be eliminated by modifying the compressor map coordinate β_{23} . Thus, we have two nested iteration loops; the WF loop is inside the β_{23} loop.

After convergence of these two loops we proceed with the power turbine model. Again, we need a guess, this time for the pressure ratio P_{45Q5} . Corrected spool speed is easy to calculate, since spool speed $XNPT$ is given and T_{45} is known from the HP turbine model.

After evaluating the power turbine model, we have two values for PT entry corrected flow, the number read from the PT map and the value at HP turbine exit. To make these two numbers agree, we must modify the estimated value for the HP turbine pressure ratio P_{4Q45} and then repeat the evaluation of the HP turbine model. This affects both the power balance between compressor and turbine and the WR_2/WR_4 compatibility. Both iterations described earlier must be repeated until all incompatibilities have vanished.

Once that has been achieved, we can go to the final iteration. We calculate the pressure ratio P_8/PS_0 needed to pass the flow through the exhaust. This must be

matched with the power turbine exit total pressure P5. The initial value of P45Q5 will certainly not be correct; we need to modify it. This leads to a cascade of changes in the values of HP turbine pressure ratio P4Q45, fuel flow WF and compressor map coordinate β23. The job is done after all four compatibility issues have been resolved.

This sort of calculation sequence is easy to understand when applied to simple engine architectures. However, its complexity increases with the number of compressors, turbines, and nozzles. Moreover, it is difficult to adapt to specific simulation tasks. What if you want to know the shaft power for a given fuel flow, or the gas generator spool speed for a given T4, or ...? This kind of performance calculation provokes writing of “spaghetti code” which, in the end, even the programmer has difficulties in understanding. Therefore, it is understandable that this approach has been abandoned by industry many decades ago. Let's look at something better....

7.2 Basic Algorithms

Off-design simulations require iteration: guess the value of a variable, detect an inconsistency in the calculation, improve your guess until the inconsistency has been eliminated or reduced below an acceptable value epsilon. Let us step back a bit and have a look at a few abstract algorithms.

7.2.1 Newton

The Newton algorithm is well suited to simple problems. Begin with a guess x_n and evaluate both the function value f and the derivative f' for x_n . Equation (7.2-1) yields the improved guess x_{n+1} :

$$x_{n+1} = x_n + \frac{f(x_n)}{f'(x_n)} \quad (7.2-1)$$

Finding temperature from a given enthalpy value is a typical application example. The function to be nulled is the difference between the given enthalpy h_0 and the enthalpy for the guessed temperature $h(T_n)$. Enthalpy is a monotonically increasing function of temperature and specific heat $C_P(T)$ is the derivative of enthalpy $h(T)$. Thus, an improved value for temperature at a given enthalpy value h_0 is

$$T_{n+1} = T_n + \frac{h_0 - h(T_n)}{C_P(T_n)} \quad (7.2-2)$$

7.2.2 Regula Falsi

In the case of enthalpy, we know in advance how it behaves mathematically. That is not so clear for other functions which appear in performance programs. If in doubt about the convergence behavior of a one-dimensional iteration, then the *Regula Falsi* algorithm is preferred. Figure 7.2-1 explains graphically how it works. The thick gray line shows how the error E behaves as a function of the variable x .

We begin with the guess V_0 for the iteration variable, where the error is E_0 . To find the local gradient of $E = f(x)$ we make a test step from V_0 to V_1 and this evaluates the error E_1 . The improved guess V_2 is where the straight line through the points $\{V_0; E_0\}$ and $\{V_1; E_1\}$ crosses the line $E = 0$.

The selection of points to improve the guess depends on the shape of $E = f(x)$. In our example, the straight line connecting $\{V_0; E_0\}$ and $\{V_2; E_2\}$ is the best choice for determining V_3 . From there, we go to V_4 which we find on the line connecting $\{V_2; E_2\}$ and $\{V_3; E_3\}$. There, the residual error E_4 is less than ε ; the iteration has converged.

The Regula Falsi algorithm is a good choice for iterations in which upper or lower limits exist for the variable. Within performance programs, such limits are flow areas which cannot be negative or Mach numbers which must be between zero and unity if you search for a subsonic solution. If seeking a supersonic solution, Mach numbers below unity are forbidden. Negative pressures and temperatures are not permitted within performance calculations, negative velocities or mass flows may or may not be valid results.

Look at Fig. 7.2-2 to see what can happen. In this example, the error function $E(x)$ is of the type $E = a+b/x$. That means, when the variable value goes from $x + \varepsilon$

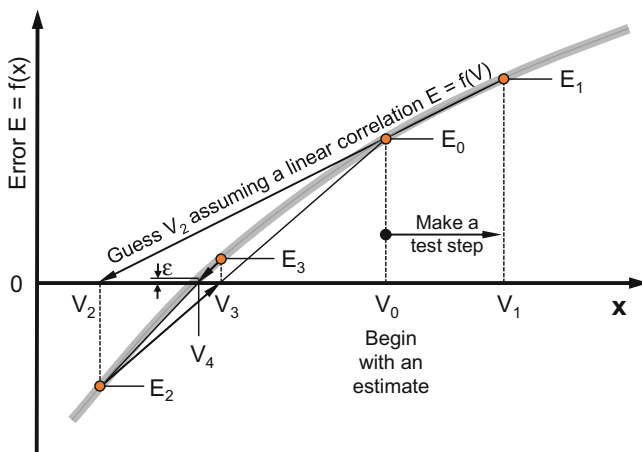


Fig. 7.2-1 Regula Falsi

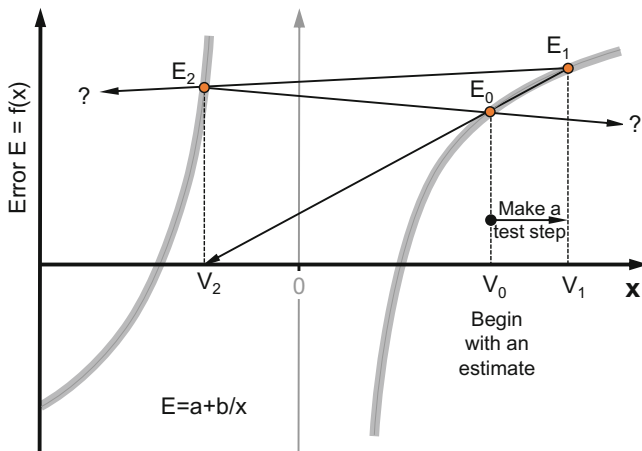


Fig. 7.2-2 A convergence problem

to $x-\varepsilon$, the E error jumps from $-\infty$ to $+\infty$. Neither the guess sequence $\{V_0; E_0\}$, $\{V_1; E_1\}$ $\{V_2; E_2\}$ $\{V_0; E_0\}$ nor the sequence $\{V_0; E_0\}$, $\{V_1; E_1\}$ $\{V_2; E_2\}$ $\{V_1; E_1\}$ results in satisfactory convergence behavior.

Fortunately, we can often exclude invalid x -values by considering the laws of physics. Setting limits for the step size of the variable values can also help to control the behavior of the algorithm.

7.2.3 Newton-Raphson

The Newton-Raphson algorithm manipulates n variables V in such a way that by the end of iterations, the n errors E are insignificant.

$$E_i(V_j) = 0 \quad \begin{matrix} i=1 \dots n \\ j=1 \dots n \end{matrix} \quad (7.2-3)$$

The relationship between the errors and the variables is non-linear. The Newton-Raphson method assumes that changes in E are related to changes in V by first order finite-difference equations:

$$\Delta E = M \Delta V \quad (7.2-4)$$

where ΔV and ΔE are n -vectors denoting changes in V and E from some reference condition, and M is an $n \times n$ matrix of partial derivatives of E with respect to V :

$$M_{i,j} = \frac{\partial E_i}{\partial V_j} \quad (7.2-5)$$

The matrix M (which may be called a Jacobian matrix) is obtained by calculating a reference case and n independent perturbed cases, such that only the j^{th} variable is perturbed from its reference value on the j^{th} case. Then, for the j^{th} case

$$M_{i,j} = \frac{\Delta E_i}{\Delta V_j} \quad \text{for } i = 1 \dots n \quad (7.2-6)$$

Once the Jacobian matrix is obtained, the reference case is improved by using

$$V = V_r - M^{-1}E_r \quad (7.2-7)$$

If the system of equations were linear, this would lead to convergence in one iteration step.

The algorithm works with two variables V_j and two errors E_i , as follows: First, the variable V_1 is changed by the small amount ΔV_1 . Both errors E_1 and E_2 will change, and we will get the influence coefficients $\partial E_1 / \partial V_1$ and $\partial E_2 / \partial V_1$. Then V_1 is reset to its original value and the second variable V_2 is changed by the amount ΔV_2 . Again, both errors will change, and we will get $\partial E_1 / \partial V_2$ and $\partial E_2 / \partial V_2$.

Let us assume for the moment, that the influence coefficients $\partial E_i / \partial V_j$ are constant. Then we can immediately calculate how the variables V_j need to be modified to reduce the errors E_i to zero. ΔV_1 and ΔV_2 are the changes needed to achieve that:

$$\begin{aligned} \frac{\partial E_1}{\partial V_1} \Delta V_1 + \frac{\partial E_1}{\partial V_2} \Delta V_2 &= -E_1 \\ \frac{\partial E_2}{\partial V_1} \Delta V_1 + \frac{\partial E_2}{\partial V_2} \Delta V_2 &= -E_2 \end{aligned} \quad (7.2-8)$$

Let us show how the Newton-Raphson iteration works with a simple numerical example. The errors and variables are related linearly:

$$\begin{aligned} E_1 &= 5V_1 + 3V_2 + 4 \\ E_2 &= -3V_1 + 7V_2 + 24 \end{aligned} \quad (7.2-9)$$

The arbitrary guess of $V_1 = 9$ and $V_2 = 2$ yields $E_1 = 55$ and $E_2 = 11$. The partial derivatives in this correlation between errors and variables are

$$\begin{aligned} \frac{\partial E_1}{\partial V_1} &= 5 & \frac{\partial E_1}{\partial V_2} &= 3 \\ \frac{\partial E_2}{\partial V_1} &= -3 & \frac{\partial E_2}{\partial V_2} &= 7 \end{aligned} \quad (7.2-10)$$

The following linear system of equations must be solved for determining the required changes to the variable guesses

$$\begin{aligned} 5\Delta V_1 + 3\Delta V_2 &= -55 \\ -3\Delta V_1 + 7\Delta V_2 &= -11 \end{aligned} \tag{7.2-11}$$

The Gauss algorithm solves such linear systems of equations and here it generates the solution $\Delta V_1 = -8$ and $\Delta V_2 = -5$. Thus, the improved guesses for the variables are $V_1 = 9 - 8 = 1$ and $V_2 = 2 - 5 = -3$. Insert these variable values into Eq. (7.2-11) to convince yourself that this makes both errors zero.

7.3 Application to Performance Calculations

The calculation of each off-design point requires iteration. As we have seen in the helicopter engine example of Fig. 7.1-1 we must estimate four variable values which need to be modified such that, in the end, the cycle calculation is consistent. We could do so with the nested loop approach, but using the Newton-Raphson algorithm makes the flow of calculations much simpler. In Fig. 7.3-1 we have the same variables for which we need an estimate as in Fig. 7.1-1. The errors are also the same. The difference is that we do not attempt to null the errors while calculating the physics.

We separate the equations which describe the physics from those needed for mathematical and organizational purposes. Figure 7.3-2 illustrates that and also makes clear that the Newton-Raphson algorithm can be easily adapted to any number of variables.

In practical applications to gas turbine performance problems, the influence coefficients are not constant and the changes of the V_j will not lead directly to $E_i = 0$ after the first correction. It is possible to use the same Jacobi matrix for calculating new ΔV_i values from the new E_i numbers, as long as we get a reasonable reduction in the errors with each step. When this becomes inefficient, we recalculate the Jacobi matrix.

7.4 More About the Analytical Technique

As always in real-world applications of mathematical algorithms, the devil is in the details. Should we resolve any tiny discrepancy in the performance model by adding a variable to the Newton-Raphson iteration? At each place in the code, where a temperature needs to be derived from a known enthalpy value, we would need an iteration variable! This would lead to a huge number of variables—and we would need initial guesses for all of them. This is not a practical approach.

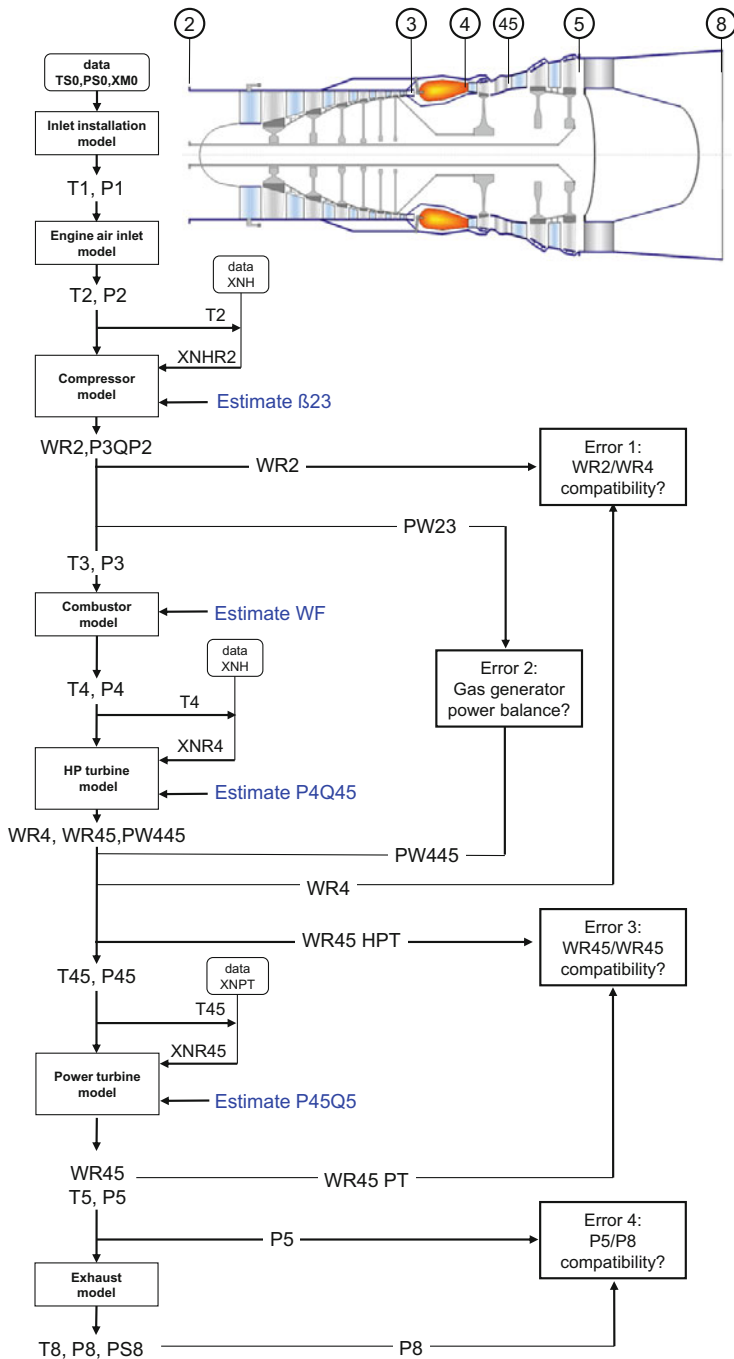


Fig. 7.3-1 Newton-Raphson approach

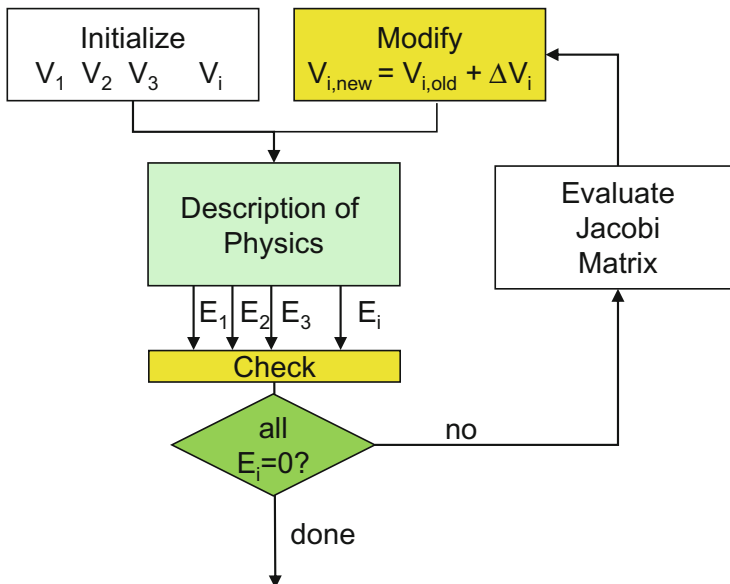


Fig. 7.3-2 Generalized Newton Raphson iteration

7.4.1 Hierarchy of Iterations

Making good estimates for iteration variable values is often simpler if the guess can be delayed to the point in the code where the variable is first needed. Then, some knowledge is available which did not exist during initialization of the overall system simulation. We call this a local iteration in contrast to the global iteration of the Newton-Raphson algorithm.

All one-dimensional iterations, like those connected with the evaluation of gas properties and isentropic processes, are best solved with the simple Newton algorithm. Estimate the corresponding iteration variables with correlations employing an approximate value of the isentropic exponent. Set lower and upper variable limits to make sure that the final value of the iteration variable is valid in terms of physics, even when the iteration did not converge. This procedure ensures that negative temperatures or pressures never appear. It is not possible to continue the performance model evaluation if T is lower than ~ 150 K (the lower limit of the gas property model) or P is less than zero.

The use of the Regula Falsi algorithm is appropriate when things get more complicated. That is the case when two solutions for a problem exist, subsonic and supersonic. The flow in a convergent-divergent nozzle is a good example for this situation. In combustion calculations with a given exit temperature there are also two solutions, under-stoichiometric and over-stoichiometric. Similarly, mixer calculations pose numerical problems which cannot be handled adequately with the simple Newton algorithm.

The Newton-Raphson algorithm is best suited for resolving problems which relate to the matching of the major gas turbine components. The program logic remains simple and straightforward if the initial guesses for the global variables are independent from each other.

A debatable situation occurs in the case of a heat exchanger, whose cold side exit temperature T_{35} really must always be higher than the compressor exit temperature T_3 , otherwise there is no heat transfer. This can be guaranteed with a one-dimensional iteration embedded in the physics part of the program. The variable of this local iteration is T_{35} , which must be higher than T_3 . The latter, however, is only known after the compressor calculation is completed. We can handle the heat exchanger problem with a local Regula Falsi iteration.

Alternatively, we can make T_{35} a global iteration variable and allow $T_{35} < T_3$ while calculating the physics. This implies hypothetical negative heat flows and other numerical conditions which cannot happen in a real engine.

All errors are less than epsilon once the global Newton-Raphson iteration has converged. All laws of physics are fulfilled; there are no inconsistencies left in the result. This may not be the case during the first pass through the performance model and while calculating the Jacobian matrix. We need a robust performance model, which generates all required global error values even when the initial guesses of the global variables are far from the final solution. This is a challenge for the software developer, when writing a gas turbine performance program.

7.4.2 Steady State Performance

Figure 7.3-1 employs four global iteration variables and errors in the simulation of the steady state performance of a helicopter engine. This is a relatively simple engine architecture; for more complex engines we need more global variables. As an example, Table 7.4-1 shows the eight variables and errors appearing in the GasTurb steady state calculation of a two-spool turbofan with a booster and with given HP spool speed.

Table 7.4-1 Global iteration variables for a two-spool turbofan with booster (Ref. GasTurb)

Variable	Compatibility check
Beta value in HPC map	HPT flow
Burner exit temperature T_4	HPT work (HP spool power balance)
Beta value in LPC map	Core nozzle pressure ratio P_g/P_{amb}
Low pressure spool speed	LPT flow
Bypass ratio	Bypass nozzle pressure ratio P_{18}/P_{amb}
Beta value in IPC map	Flow continuity LPC core - IPC
Beta value in HPT map	Flow continuity IPC - HPC
Beta value in LPT	LPT pressure ratio (LP spool power balance)

If, instead of the HP spool speed XNHPC, another parameter is the given value, then we employ XNHPC as an additional variable and the deviation from the target value as an additional error. Nothing is changed within the part of the program that describes the physics. This is the most important advantage of the Newton-Raphson setup outlined in Fig. 7.3-2.

We can easily add global iteration variables to the system. Thus, we could make the nozzle throat area of a turbojet a function of corrected spool speed, the burner exit temperature T_4 a function of engine entry temperature T_2 and flight Mach number or the external gear box losses functions of altitude. Anything is feasible—as long as it makes sense in terms of the physics.

GasTurb comes with global variable and error selections dependent on the engine configuration. You can add more variables to the default matching scheme. For each of the additional variables, lower and upper limits are required. The limits should be used to exclude variable values that are physically meaningless and give the program an order of magnitude. The variable might be a relative amount of cooling air that varies between 0 and 0.2 or it might be the power delivered to a generator which can be several thousand kilowatts, for example *matching scheme*. Narrow ranges support the accuracy of the solution; however, they might also exclude the solution to your particular problem.

To avoid the situation shown in Fig. 7.2-2 you should not use $x = 0$ as an iteration target. If you want x to be zero, make $E = 1$ the target of your iteration and define E as

$$E = \frac{1000 + x}{1000} \quad (7.4-1)$$

7.4.3 Limiters

The control system of an engine must ensure that the engine operates within safe limits. Typically, maximum limits are set for:

- Temperatures—compressor exit (T_3), turbine rotor inlet (T_{41}), inter-turbine or exhaust
- Pressures—burner
- Speeds—both mechanical for stress reasons and corrected (N/\sqrt{T}) to protect compressors against blade flutter.

For each individual limiter, we determine an iteration error in such a way that any exceedance yields a positive error value. From all these limiter errors, we select the highest and employ it in the Newton-Raphson algorithm. Since we add only one error, we need to add only one global iteration variable to the system—*independent* from the actual number of limiters.

After the Newton-Raphson iteration has converged, one of the individual limiter errors is equal to zero (less than epsilon) and all the other errors are lower. That ensures that none of the limiters is exceeded.

All the limiters mentioned above prevent the exceedance of critical values. During idle operation, however, certain values must not fall short of a minimum value. Handle this task by calculating a positive error value for each minimum limit if the relevant quantity is below its limit. From all the individual limiter errors, select the biggest one to use in the Newton-Raphson iteration.

So, if limiters are part of your performance simulation task, there are three options:

1. Search for the maximum performance (max rating).
2. Search for the minimum performance (idle rating).
3. Look for a solution between these boundaries.

Case three requires up to three converged global iteration solutions. First try without limiters and see if the result is within all the limits. If that is the case, then you are done. If the solution violates a minimum limiter, then re-run the simulation with activated minimum limiters while ignoring the maximum limiters. Check whether this newly converged solution violates one or more of the maximum limits. Should that be the case, restart the iteration and consider only maximum limiters.

7.4.4 Dynamic Engine Simulation

Once an initial steady-state solution has been obtained, a time-varying solution may be generated. This requires the solution of a set of differential equations which model the system. In this section, the procedure used to solve the differential equations in DYNGEN [2] as well as in GasTurb will be discussed. The approach is described in more detail in appendix A of Ref. [3]

Consider first the differential equation

$$\frac{dy}{dt} = f(y, t) \quad (7.4-2)$$

To obtain a numerical solution, this differential equation must be replaced by the equation:

$$y_{j+1} = y_j + \Delta t [\varepsilon f(y_j, t_j) + (1 - \varepsilon)f(y_{j+1}, t_{j+1})] \quad (7.4-3)$$

Here, equation y_j stands for the y value at time $t_0 + j \Delta t$; the value of ε is in the range between zero and unity.

The bracketed quantity in Eq. (7.4-3) represents a weighted average of the derivative $f(y, t)$ over the integration interval $[t_j, t_{j+1}]$. For $\varepsilon = 1$, Eq. (7.4-3) becomes

$$y_{j+1} = y_j + \Delta t f(y_j, t_j) \quad (7.4-4)$$

Equation (7.4-4) is known as Euler's method, and allows explicit calculation of y_{j+1} as a function of the previous values y_j and t_j . On the other hand, for $\varepsilon \neq 1$, Eq. (7.4-3) is the modified Euler method, and in general cannot be solved explicitly for y_{j+1} , because of the dependence of function f on y_{j+1} , which appears on the right-hand side of the equation. In this case, some form of iteration must be used at each integration step to solve for y_{j+1} .

From the standpoint of simplicity of the integration formula, Eq. (7.4-4) is clearly preferable to Eq. (7.4-3). However, there are two other important considerations: accuracy and stability. As mentioned in Ref. [2], the use of Eq. (7.4-3) can lead to greater integration accuracy, but stability is more important than accuracy for dynamic engine simulation.

Reference [2] elaborates on these topics and points to the fact that dynamic engine simulations generally contain a mix of high and low frequencies. The high frequencies result from the lumped-volume representation of component dynamics, which includes the storage of mass and energy. The low frequencies result from rotor dynamics, heat transfer to and from metal parts and the slow motion of exhaust nozzle and bleed valves, for example. Frequently, the simulation user is interested in the low-frequency effects, such as overall engine spool-up time, and is not concerned with the high frequency effects at all.

If the simulation uses Euler's method, the integration step size is restricted by the highest frequency in the system, even though the user is not interested in high frequency information. In this case, a step size of 10^{-4} s, or smaller is frequently required. If an implicit (modified Euler) technique is used ($\varepsilon < \frac{1}{2}$), the step size is not restricted. It can be chosen to suit the desired frequency content of the output, which typically allows a step size of 0.1 s or larger.

The difference equation representation used in DYNGEN (and GasTurb) utilizes $\varepsilon = 0$, so that Eq. (7.4-3) becomes

$$y_{j+1} = y_j + \Delta t f(y_{j+1}, t_{j+1}) \quad (7.4-5)$$

Using this approach requires iteration—this is not a burden because we need iterations anyway. We modify the steady state continuity, energy and power equations to get dynamic equations. The resulting dynamic equations are included either as error equations, or used to calculate dynamic power balances, flows and enthalpies at various stations throughout the engine.

7.5 About Convergence Problems

If anything can go wrong, it will. That's also true if you simulate gas turbine performance using iterations. Everyone encounters convergence problems! You can blame your software for not being robust enough, but that will not necessarily solve your problem.

7.5.1 *A Solution Exists, but the Program Does not Find It*

7.5.1.1 Poor Variable Estimates

When a new performance point is to be calculated, the variable values in memory are the guesses with which the Newton-Raphson iteration begins. Often these guesses are appropriate, but not always. If you calculate Idle directly after Take Off performance, then the variable values found for Take Off are generally poor estimates for the Idle operating point.

If the Idle point does not converge, re-start your iteration with the variable values from a converged point and go in small steps into the problem area. Thus, you get estimated values for each point for the iteration variables that are near to the solution for the subsequent step. With this approach, a good performance program will always find the solution—provided it exists.

A failed convergence attempt frequently ends with extreme values of the global variables which are unsuited as starting conditions of the next Newton-Raphson iteration. In this case, go back to the last converged solution or enter guess variable values manually.

7.5.1.2 Reasonable Variable Estimates

It can happen that you run into convergence problems even when your guess values look reasonable. What can you do then? Maybe the Newton-Raphson iteration is stopping prematurely because the number of passes through the performance model has exceeded a prescribed limit. In this case, increase the number of permitted passes! You could also challenge the generation of the Jacobi Matrix. The size of the variable steps employed for calculating the partial derivatives influences the quality of the matrix; too large steps introduce errors due to non-linearities of the problem and too small steps introduce numerical error. Maybe your convergence criterion is too stringent—bigger residuals of the global errors might be acceptable; it depends on your accuracy requirements.

Our advice: do not invest much time in investigations of the solver behavior, as most convergence problems have a different cause.

7.5.1.3 Problem Formulation

Performance calculation convergence may depend on how the task is formulated. Let us look at the part load curve of a turbojet. You may ask what thrust it produces for a certain burner exit temperature T_4 . Figure 7.5-1 shows that this is an ambiguous question; there are two solutions if T_4 is greater than 700 K. Which one the program finds depends on the estimated variable values at the beginning of the Newton-Raphson iteration. If you enter 650 K for T_4 then the iteration will not converge.

You can circumvent this problem by asking what the thrust is for a given fuel flow. There is no minimum in the curve $W_f = f(F_N)$, the ambiguity has vanished.

Adding variables with special targets to the standard off-design iteration scheme can create convergence problems. Think of a variable area nozzle employed for controlling surge margin. Lower and upper limits need to be defined for the iteration variable A_8 . If these limits are too stringent, this might exclude the solution—the iteration will not converge.

Another opportunity for convergence problems is the following. The core stream of a turbofan is compressed firstly by the inner part of fan and secondly by the booster (IPC). You want to simulate these two compressors as a single device because you do not know the individual pressure ratios. For that reason, you set the fan root pressure ratio to 1.0 and the booster pressure ratio to the combined pressure ratio of fan root and booster at the cycle design point. That works without problems if the fan root performance is derived from the bypass performance.

However, you run into problems in off-design mode, if you choose the booster design pressure ratio as 1.0 and fan root pressure ratio as the combined pressure ratio. This is because the booster performance is described by a map and the map

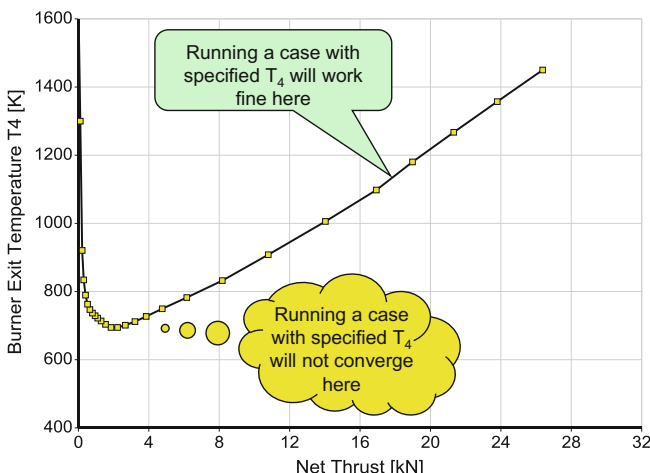


Fig. 7.5-1 About the problem formulation

coordinate β is a variable in the standard iteration scheme. Modifying β has no effect on the global iteration errors in this case—convergence will not happen. The calculation works only at the cycle design point.

7.5.1.4 Problematic Component Maps

We describe compressor and turbine performance with component maps. Reading values from component map tables poses no problem if the maps are smooth and the operating point is within the tabulated range. However, if the maps are not in line with the laws of physics, then you cannot expect the overall system simulation to work correctly.

It is difficult or even impossible to achieve convergence in the region around a compressor pressure ratio of 1.0 if the performance map tables contain efficiency. This is because efficiency decreases to minus infinity near pressure ratio $1 + \varepsilon$ and jumps to plus infinity at pressure ration $1 - \varepsilon$. A map representation in which efficiency does not appear solves this problem.

7.5.2 No Solution Exists

7.5.2.1 Operating Point Is Outside One or More Component Maps

Map extrapolation is problematic and should be limited. Map extrapolation limits can prevent convergence. This is not a real disadvantage because wide-ranging extrapolations lead to inaccurate results anyway.

7.5.2.2 Cycle Is not Feasible

You can create an apparent convergence problem by steadily increasing the power offtake from a turbojet. If you exceed a certain level of power offtake, and limit T_4 , the nozzle pressure ratio reduces to less than 1 and steady state operation is no longer possible.

We try during model-based test analysis (AnSyn) to reconcile a performance model with measured data by iteration. If one of the measured data has a severe fault ($P_3 = P_{\text{amb}}$, for example), then matching the model to this nonsense value is impossible—the iteration fails to converge.

7.5.2.3 Garbage in—Garbage Out

As a performance engineer you frequently ask very special questions of your performance program. You add one or more conditions which the desired operating

point should fulfill. If the imposed requirements are contradictory, then the program will react with non-convergence.

Some examples:

- Try to shift the gas generator compressor operating line by modifying the variable guide vane schedule—that is not feasible.
- Request a certain power offtake while keeping both spool speed and fuel flow constant—that is not feasible either.

Engineering judgement quickly identifies these two examples as nonsensical demands. But sometimes garbage is not easily recognized. Try not to blame your software too soon for not converging if you are searching for a solution which cannot exist.

7.6 References

1. Report of the RTO Applied Vehicle Technology Panel (AVT) Task group AVT-018 Performance prediction and simulation of gas turbine engine operation NATO research and technology organisation technical report RTO-TR-044, 2002
2. Sellers, J.F., Daniele, C.J.: DYNGEN: a program for calculating steady-state and transient performance of turbojet and turbofan engines NASA-TN-D-7901, 1975
3. Sellers, J.F., Teren, F.: Generalized dynamic engine simulation techniques for the digital computer NASA TM X-71552, 1974

Chapter 8

Optimization



Traditionally, performance engineers seek the best thermodynamic cycle for a new gas turbine design using extensive parametric studies. This task takes much time, especially in complex engine studies with many design variables.

The alternative to screening wide ranges of design variables with systematic parameter variations is an automatic search for the optimum engine design using numerical optimization algorithms.

8.1 Parametric Studies

The results of parametric studies are normally presented graphically. A single figure can show the results for at least two parameters. Let us consider compressor pressure ratio and burner exit temperature as design parameters of a single spool turbojet engine, for example. The primary output is a carpet plot, with specific thrust as x-axis and specific fuel consumption as y-axis. We can add contours of other calculated parameters of interest, such as turbine pressure ratio and turbine exit temperature, as in Fig. 8.1-1.

Let us assume that the design objective is a high specific thrust turbojet engine. Two constraints apply:

1. For cost reasons, only single stage turbines are acceptable. This limits the turbine pressure ratio to four.
2. The turbine exhaust case shall be uncooled. So the highest permissible turbine exit temperature is 1200 K.

Figure 8.1-1 shows that the engine with the highest specific thrust, which fulfills both constraints, has a burner exit temperature of 1640 K and a compressor pressure ratio of around 21.

Most gas turbine cycles are much more complex than that of our simple turbojet. One more design variable requires a whole set of figures like the one above to

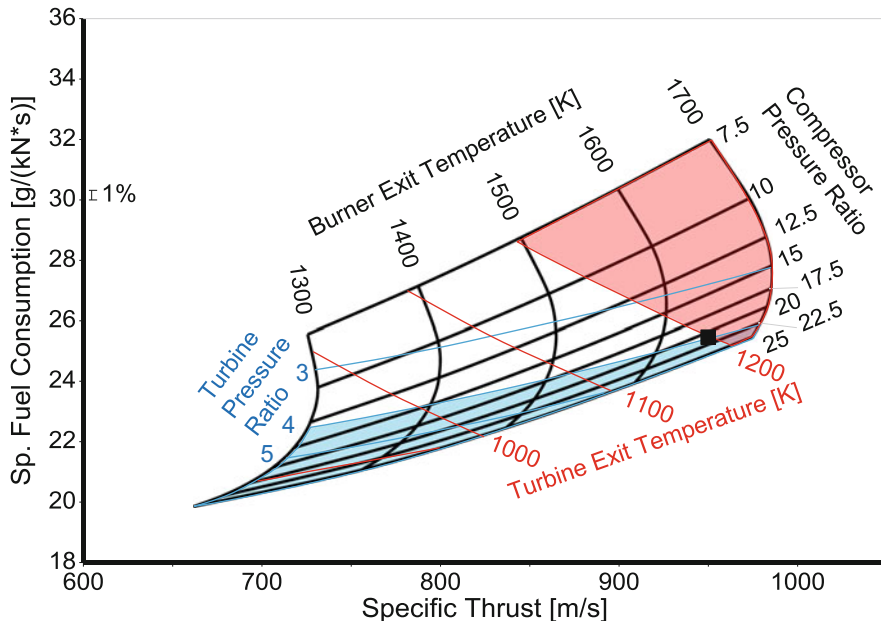


Fig. 8.1-1 Parametric study for a turbojet

present all the results. When we use seven values for each variable, then we get seven figures for three variables, 49 figures for four variables, and 343 figures when our problem has five design variables. Numerical optimization algorithms offer an alternative to time-consuming parametric studies.

8.2 Numerical Optimization

A parametric study explores the design space. We need not define exactly the properties of the “optimum” engine design *a priori*. Later, we can find the best compromise between all the different and often conflicting requirements.

In contrast, numerical optimization algorithms require the definition of a figure of merit before the calculation can commence. The figure of merit might be the specific fuel consumption of a turbofan at cruise, which is to be minimized. For a fighter engine it might be that the specific thrust be maximized. We may also consider a weighted combination of these two quantities.

Numerical optimization algorithms can be classified in two groups: Methods that use gradient information and others.

8.2.1 A Gradient Strategy

The following is a good example of an optimization task: A mountaineer intends to climb the highest peak in a certain region. He has no map and the weather is foggy. His only tool is an altimeter. What is he going to do? He will certainly check his surroundings first and then go in the direction of the steepest ascent. In the end he will come to the top of a mountain—a place where each step leads downwards.

The steepest ascent may lead toward the border (which is either the lower or upper limit of a design variable) of the region. Then our mountaineer will walk along the border until he reaches the place where each step leads downwards or out of the allowed region.

Is that the end of the story? Not necessarily. There might be several summits within the region. Our mountaineer may have found the highest peak by chance, but he cannot be sure of that. He has to check other parts of the region. In mathematical terms there might be “local” optima besides the “global” optimum.

Let us turn to the mathematical algorithm now. The mountaineer who first makes test steps in several directions uses the “gradient strategy” as a search method. With the test steps, he is looking for the partial derivatives $\partial Z / \partial V_i$. For each optimization variable he must do one test step before he can start to move in the “right” direction.

The local gradients will be different after the first step uphill. The test steps could now be repeated to find the new direction. Test steps take time, however, and it is therefore better to go on in the same direction as long as the altitude increases.

The gradient search algorithm implemented in GasTurb was derived from Ref. [2]. The principle is the following and is illustrated in Fig. 8.2-1. We begin at the point marked “Start 1”, looking for the direction of the steepest gradient (“Direction 1”). Following this direction, we walk to the highest point. Then we change the direction by 90° (orthogonal). This can be done without evaluating the local gradient. We again go for the highest point. To define the third direction, we use the experience from the first two directions. We connect the point “Start 1” with the optimum point found along “Direction 2” and this defines “Direction 3”. We follow this, again as long as altitude increases.

This procedure can be applied repeatedly until the search steps or the changes in the “figure of merit” become very small. There is also a maximum limit for the number of optimization steps. In the example in the figure, the optimum is eventually found along search direction 5.

The success and the efficiency of the search depends on where the algorithm starts. Starting at point number 2 leads quickly to the global optimum, yet when we commence at start point 3 we end at a local optimum.

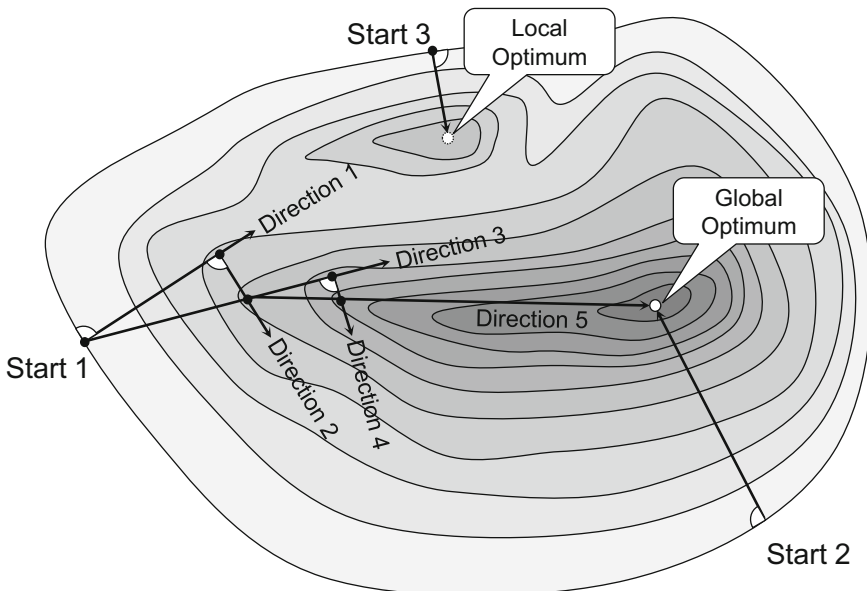


Fig. 8.2-1 A gradient strategy

8.2.2 Adaptive Random Search Strategy

The second optimization strategy offered by GasTurb is based on Ref. [2]. In this algorithm we use random numbers for the optimization variables that are concentrated around the best previous solution. Figure 8.2-2 illustrates the method.

The preliminary search boundary is the red circle around the start point. The diameter of this circle is 10% of the variable range which is to be examined. The search for the optimum begins with random numbers from within this circle as input for the engine model evaluation. Small deviations from the center point of the search region are more probable than bigger deviations.

If the model evaluation yields a valid solution and the figure of merit is better than at the start point, then the search range moves so that the improved solution becomes the center point of the red circle. This random process is repeated a pre-defined number of times. In the end of this phase, the center of the search circle is much nearer to the optimum than it was at the beginning.

Now the diameter of the search circle is reduced. Additionally, the distribution of the random numbers now concentrates more around the center point of the orange circle than it did before. Both these changes reduce the distance between the random numbers and increase the probability of hitting the optimum value directly.

We run the engine model with random numbers from within the orange circle as often as during the first optimization series. The orange search circle moves nearer to the optimum again, but with smaller steps.

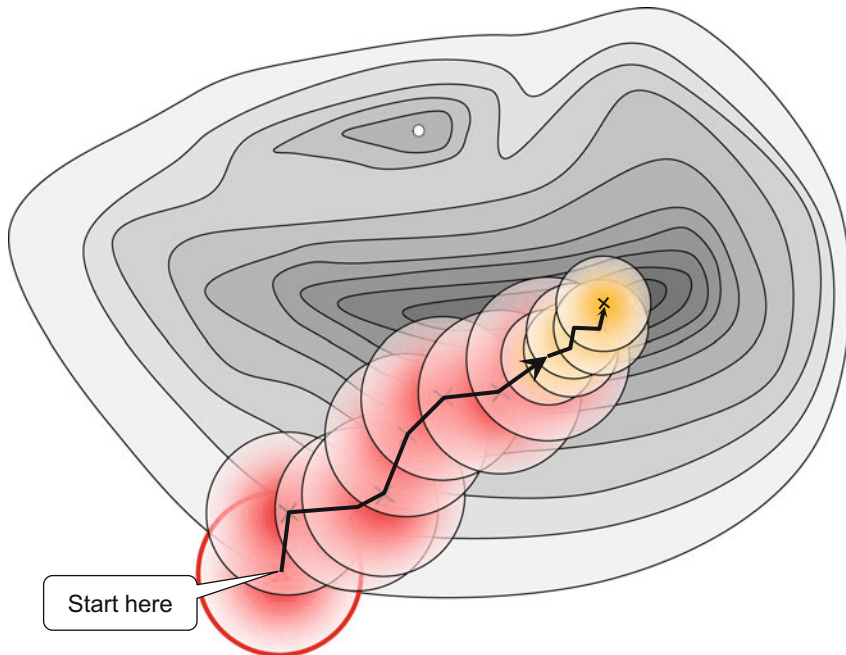


Fig. 8.2-2 Adaptive random search strategy

We repeat the search range reduction and the concentration of the random numbers around the center of the search region two more times. The process ends very near to the numerical solution of the optimization problem.

If you are interested in the mathematical formulation of the method—here it is:

$$V_i = V_i^* + \frac{R_i}{k_R} (2\theta - 1)^{k_v} \quad (8.2-1)$$

The nomenclature in Eq. (8.2-1) is explained in Table 8.2-1.

The search for the optimum begins with $k_R = 10$ and $k_v = 1$. In one search series, the program tries $40 \times n$ random engine model evaluations. After all these engine designs have been examined then k_R is duplicated and k_v is increased by 2. This makes the search region for the next $40 \times n$ engine model evaluations smaller. Then k_R is duplicated again and k_v further increased by 2. This procedure is repeated until all cycles for $k_R = 80$ have been tried. Design variable combinations for which the model evaluation leads to an error or constraints are violated are ignored.

Select the ranges for your design variables carefully. If the variable range is very wide, then the result will become inaccurate. On the other side, a too small variable range can exclude the true optimum unintentionally.

Table 8.2-1 Optimization nomenclature

V_i	New guess for the variable. Becomes the new center of the search region if the figure of merit has improved
V_i^*	Value of V_i which has produced before the best figure of merit (i.e. the center of the search region)
R_i	Search range for variable V_i
k_R	Range reduction coefficient (positive integer)
k_v	Distribution coefficient (positive odd integer)
Θ	Random number between zero and one
n	Number of variables ($i = 1 \dots n$)

8.2.3 Constraints

Let us come back to our mountaineering example. Up to now we have not spoken much of constraints. They are like fences in the landscape which make part of the territory inaccessible. These fences often exclude the summit (where each step leads downwards) as an acceptable solution. They create optima that would not exist without the fences. Constraints make the task of optimization difficult.

Where our mountaineer ends his search for the highest point in a certain region depends on where he begins. If he starts at point A in Fig. 8.2-3, then he will begin with a climb along the steepest gradient until he reaches the fence. He can reach the global optimum quickly when he then follows the fence. However, if he starts at point C—only a little bit to the right of point A—he ends up at local optimum 2, which is quite far away from the global optimum.

Starting at point B, after an initial climb in the open country, leads our mountaineer again to a fence once again. Here he modifies his search strategy and walks along the fence up to the highest point (local optimum 1). That would be the end of a simple gradient search because from there each step leads downwards.

In contrast to the simple gradient search, the adaptive random search can step over the valley and finally reach the global optimum.

8.2.4 Application

The cycle selection for a new or derivative gas turbine is always a task with many constraints. Local optima frequently exist within the design space. How can we make sure that we find the global optimum with a high probability?

It is quite simple: we run the optimization from various start points. GasTurb offers an endless random search strategy for that purpose. Each time an optimum solution is found, the search begins for a new starting point. Temporarily we look for a worse engine design which fulfills all constraints. It is a short search, because

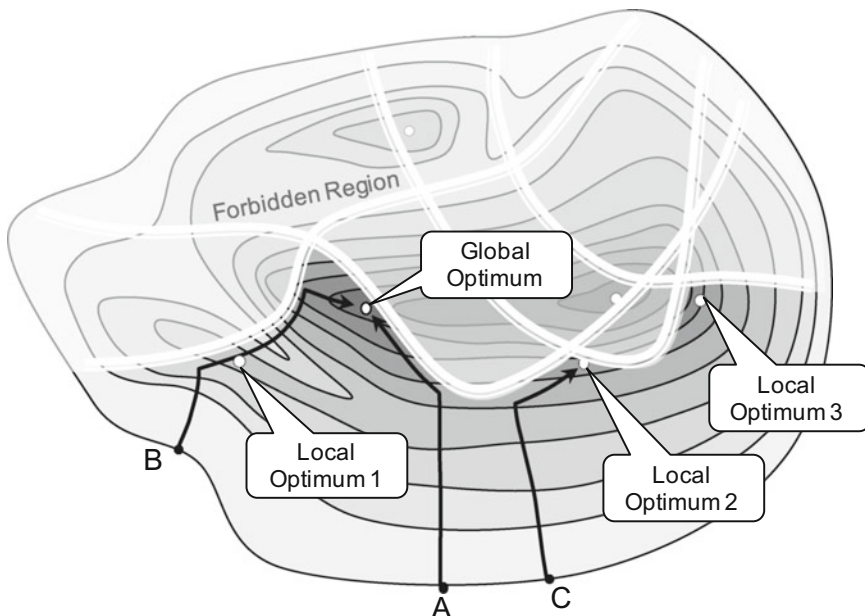


Fig. 8.2-3 Constraints create local optima

no accurate result is needed for the new start point. From the new start point we begin again with the search for the best engine design.

This switching between true optimization and the search for a new starting point continues until the stop button is pressed. The best solution found during all the searches is the final result of an endless random search. The more restarts we try, the higher is the probability that this strategy will find the global optimum.

The endless random search is the best choice if there are many optimization variables and constraints in a complex optimization problem running on a slow computer. You can do other jobs and leave the optimizer alone. Come back later, press the stop button and you will see the best solution your computer has found during the last hour, for example.

Check this solution thoroughly; is it a realistic result? Not necessarily, because the algorithm finds only the mathematical optimum of the model. When you get a peculiar result, this is often a hint to a deficit in the model. Is the definition of the figure of merit adequate? Maybe a constraint is missing?

Improve your model, add more details, scrutinize the constraints and adjust the definition of the figure of merit. Re-run the optimization algorithm until you get a satisfying solution.

Check how the neighborhood of the optimum looks. A parametric study limited to the region of interest makes it obvious which of the design variables and constraints have the biggest impact on the result. This examination might again lead to a modification of constraints and a modified figure of merit.

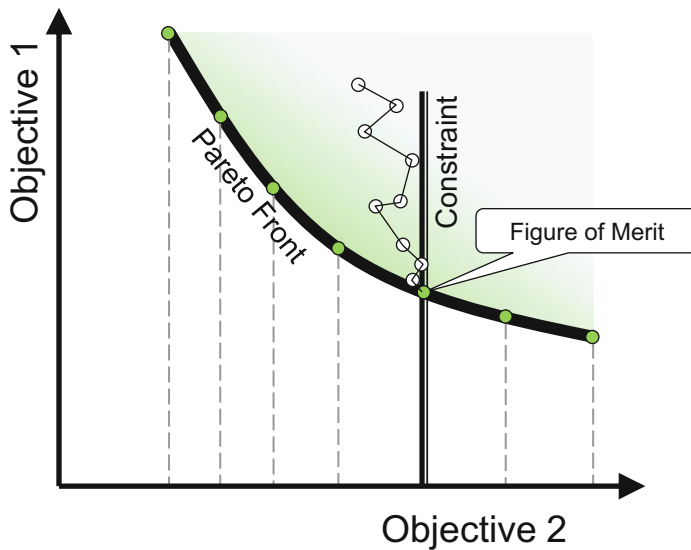


Fig. 8.2-4 Multi-objective optimization

Often, defining an appropriate figure of merit is not easy. Many different criteria can define what a “good” engine is: thermal efficiency, weight, noise, emissions, manufacturing cost and so on. How can these entirely different entities be combined into a single figure of merit?

One solution could be a weighted sum of the relevant parameters. The question is: how are the weighting factors set?

There is another way to deal with several objectives. If there are two of them, for example, then you can restate the problem and declare one of the objectives formally as the figure of merit (objective 1 in Fig. 8.2-4) and the other (objective 2) as a constraint. Run many optimizations, all with different values for the constraint. Each run will yield one point on the so-called Pareto front which is the border line of the design space. All feasible solutions are on one side of this line.

Examine in your model how other important parameters vary along the Pareto front. Take your observations into account when finally selecting the best compromise between the objectives and constraints of your engine design task.

8.3 References

1. Heinrich, G.: Jacob, 1982. *Fachberichte Messen - Steuern - Regeln, Springer Verlag, Rechnergestützte Optimierung statischer und dynamischer Systeme* (1982)
2. Kelahan, R.C., Gaddy, J.L.: Application of the adaptive random search to discrete and mixed integer optimization. *Int. J. Numer. Meth. Eng.* **12**, 289–298 (1978)

Chapter 9

Monte Carlo Simulations



The Monte Carlo method is a powerful and simple-to-use tool for generating statistical information. The method has its name from the casino in Monte Carlo where gamblers make many statistical experiments. The physical experiment with the ball in roulette is replaced in a Monte Carlo study by running a computer model with randomly distributed input data. The simulation yields output properties that are again randomly distributed. The distributions of the output properties can be analyzed for their mean values, standard deviations, confidence levels etc.

Typical examples for the application of Monte Carlo simulations to engine design and performance problems are the analysis of measurement uncertainty and production tolerance estimates.

Let us first recall some fundamentals of statistics and then discuss some application examples of Monte Carlo simulations to gas turbine performance. GasTurb makes Monte Carlo simulations easy, both for cycle design and off-design applications. Specify the probability distribution of the input quantities, run many cases, and finally examine the statistical distributions of the calculated results.

9.1 Statistical Background

9.1.1 Normal Distribution and Standard Deviation

Everybody knows the probability density plot for a so-called *standard (Gaussian) distribution* which looks like a bell. This distribution has the property that approximately 68.2% of the values fall within one standard deviation of the mean. Likewise, 95.4% within 2 standard deviations and 99.7% within 3 standard deviations (Fig. 9.1-1).

The following example has no special meaning in terms of physics. It serves only as a device for some statistical examinations. We consider results from a

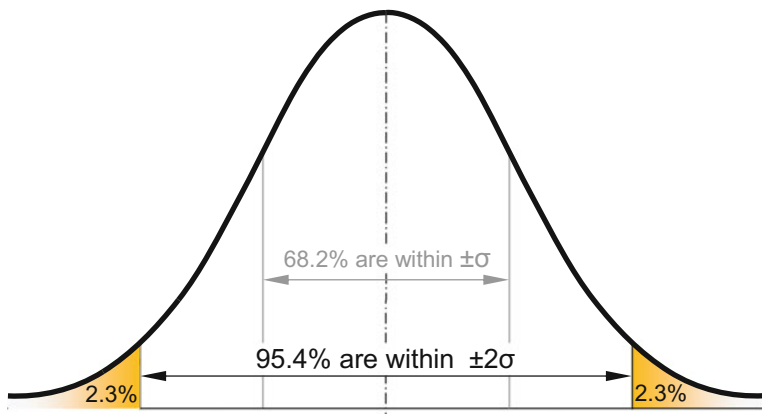


Fig. 9.1-1 Normal distribution

Table 9.1-1 Comparison of root sum squared and Monte Carlo

Column No.	2	3	4	5	6
	Base	ΔBase	$\Delta\text{SFC} [\%]$	$\sigma_{\Delta\text{SFC}}$ Root sum squared	σ_{output} Monte Carlo
Fan efficiency	0.9	-0.015	0.64	0.64	0.566
HPC pressure ratio	12	0.2	-0.24	0.24	0.214
HPC efficiency	0.87	-0.013	0.36	0.36	0.302
Burner exit temp.	1700	10	0.45	0.45	0.403
HPT efficiency	0.89	-0.019	1.13	1.13	0.975
LPT efficiency	0.881	-0.01	0.7	0.70	0.611

turbofan cycle design calculation. Column 2 in Table 9.1-1 lists the base values for six arbitrarily selected cycle input quantities. SFC changes by the percentages listed in column 4 if we modify the respective base value in column 2 by the respective ΔBase value in column 3.

Let us assume now that the six quantities are normally distributed random quantities with standard deviations $\sigma_i = |\Delta\text{Base}|$. The question to be answered is: What will the standard deviation of SFC be? To answer this question, we make use of the following statistical law, the addition theorem for normal distributions:

If n random variables are independent of each other and each follows a Gaussian distribution with the standard deviation σ_i , then any random variable which is a linear combination of the n random variables will also follow a Gaussian distribution. The standard deviation σ of this Gaussian distribution can be calculated as

$$\sigma = \sqrt{\sum_{i=1}^n \sigma_i^2} \quad (9.1-1)$$

The overall SFC change caused by all the ΔBase values together may be calculated as the linear combination of the individual ΔSFC numbers. The sum of all ΔSFC numbers is such a linear combination; it results in $\Delta\text{SFC}_{\text{total}} = 3.04\%$. This is a close approximation to the result of a full cycle calculation, simultaneously combining the component changes which yields 3.13% SFC increase. Thus, the condition for the validity of the addition theorem for normal distributions is fulfilled and we may calculate the standard deviation for SFC from the equation above as $\sigma_{\text{SFC}} = 1.60\%$.

The method we have applied is also known as the *Root Sum Squared* method. The preconditions for the use of this method are

- The random variables follow a Gaussian distribution
- They are independent from each other
- Their effects on the quantity of interest can be combined linearly.

If one or more of these conditions are not fulfilled, then the *Root-Sum-Squared* method must not be applied.

Back to our example. The last column in the table contains standard deviations determined by running Monte Carlo simulations with only one random variable. The standard deviation input for each of the six variables is $\sigma_i = |\Delta\text{Base}_i|$.

It is conspicuous that the results of the six Monte Carlo simulations in column 6 are more than 10% lower than the standard deviations which were employed with the *Root Sum Square* method (column 5). At first glance this is a surprising result—we would expect the numbers in columns 5 and 6 to be very similar. The reason for the discrepancy is that the program does not strictly run the simulations with normal distributed input variables. Indeed, the GasTurb program generates normal distributed random numbers with the specified standard deviation in a first step. In a second step, however, all values outside of the range of mean value $\pm 2\sigma$ are discarded. This avoids exotic input parameter combinations which have no meaning in terms of gas turbine performance.

Thus, the program runs the simulations with numbers that follow a truncated normal distribution with $\sigma_{\text{trunc}} < \sigma_{\text{Gauss}}$. No wonder that the dependent quantities like ΔSFC , for example, have lower standard deviations than expected for unlimited input data.

We can get the overall SFC scatter in two ways: Either we calculate the *Root Sum Squared* value of column 6 or we run a Monte Carlo simulation in which the input data of all six variables are randomly distributed with the (truncated) standard deviation of $\sigma_i = |\Delta\text{Base}_i|$. In both cases, the result is the same: $\sigma_{\Delta\text{SFC}_{\text{total}}} = 1.40\%$. There is no need to calculate the individual ΔSFC_i values first; it is sufficient to run only one Monte Carlo simulation in which all random input properties vary simultaneously.

The result of a Monte Carlo simulation will always be a slightly lower standard deviation than that calculated with the *Root Sum Squared* method because it employs truncated normal distributions.

9.1.2 Probability Distribution and Confidence Level

Up to now we have only discussed the Gaussian normal distributions. The more general case is the non-symmetric probability distribution with the density $p(x)$ as shown in Fig. 9.1-2. The probability $P(x)$, that the performance level is less than x , is given by the dark grey area in the left part of the figure.

If the random event is the achievement of a component efficiency level η_0 , for example, then the probability of missing this efficiency level $P(\eta_0)$ is connected to the probability density $p(\eta)$ by

$$P(\eta_0) = \int_0^{\eta_0} p(\eta) d\eta \quad (9.1-2)$$

Frequently, the confidence level is discussed instead of the probability. The confidence level expresses the probability that a certain performance level is achieved. In the example of Fig. 9.1-2, the confidence level of achieving the minimum performance would be 1 and the confidence level of achieving the maximum performance would be zero. Note that the confidence level of achieving the most probable level is less than 0.5 because the distribution in Fig. 9.1-2 is non-symmetrical.

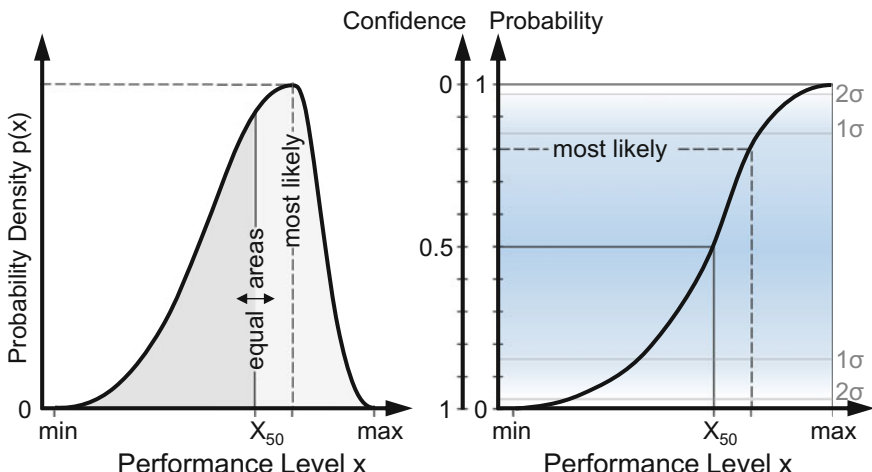


Fig. 9.1-2 Non-symmetrical distribution

9.2 Measurement Uncertainty

Engine tests are performed not only for evaluating the overall characteristics in terms of thrust and specific fuel consumption. The main purpose of performance testing—especially during the development phase—is determining the efficiency of the engine components. Both random and systematic measurement errors affect the accuracy of the analysis result.

In addition to the variations in the measurement chain there are also small random differences in engine geometry and operating conditions. An engine running condition is never fully stable because of small variations in inlet flow conditions, variable geometry settings, thermal expansion of casings and disks etc. Also unintended (and undetectable) changes to the engine during reassembly for a back-to-back test contribute to the uncertainty of an experiment.

9.2.1 Systematic Errors

The random errors are not negligible in a carefully controlled engine performance test, but are smaller than the systematic errors caused by limitations in number and positioning of the probes. Seldom is there space in an engine to put enough pressure and temperature pickups at the component interface planes. Even if every effort is made to correct the measurements for all known effects, some uncertainty remains.

The difference between the measurement (after applying all known corrections) and the true mean value is a bias. It is not possible to calculate the magnitude of the bias exactly—it will always be a guess. Simulate the bias errors with the Monte Carlo method as normally distributed measurement errors.

9.2.2 A Conventional Test Analysis Procedure

During an engine performance test, we usually measure all temperatures and pressures on the cold side of the engine (stations 2, 13, 25 and 3 in Fig. 9.2-1). Furthermore, fan mass flow and fuel flow, as well as the inlet and exit total pressures of the low pressure turbine, are normally available for the test analysis. Temperatures that may be measured around the low pressure turbine are not used in the analysis because the accuracy of the mean values suffer from the severe gradients both circumferentially and radially.

From the pressures and temperatures on the cold side of the engine, we can derive all the compressor efficiencies. For the analysis of the turbine efficiencies we need to know the turbine shaft power. The power balance with the compressors provides that information if either the core flow or bypass ratio is known.

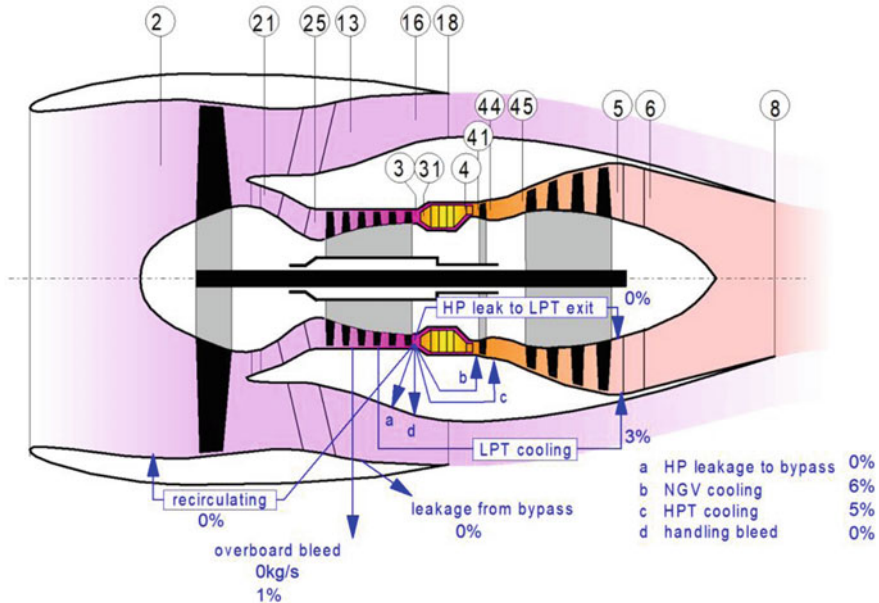


Fig. 9.2-1 Turbofan nomenclature

9.2.3 Core Flow Analysis

We can find the bypass ratio during the test analysis process in several ways. For example, we can calculate the bypass ratio so that mass flow continuity at the bypass nozzle exit is fulfilled. This approach needs the exact dimension of the bypass nozzle area A_{18} and a well-founded value for the nozzle discharge coefficient C_{D18} .

Alternatively, we can use the throat area of the high pressure turbine nozzle guide vane as the basis for the core flow analysis. This so-called HPT flow capacity method requires a good knowledge of the secondary air system because the amount of air that bypasses the turbine throat area influences the core flow calculation.

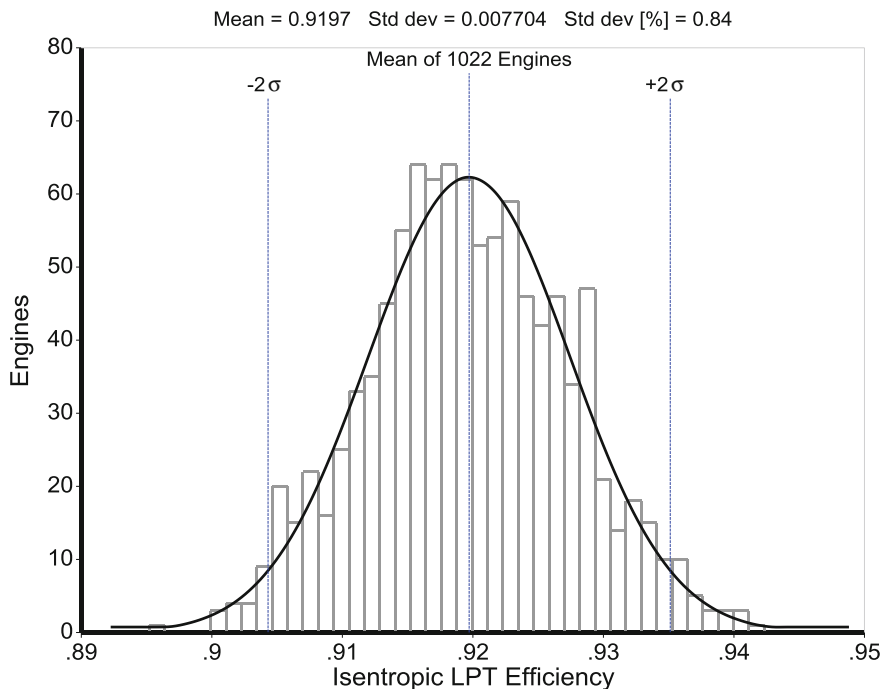
We simulate the test analysis of two engines with bypass ratios of 6 and 10 respectively. The pressure ratios of the booster and the high pressure compressor are the same ($P_{21}/P_2 = 3.5$ and $P_3/P_{25} = 12$) for both engines. The fan pressure ratios are different ($P_{13}/P_2 = 1.87$ for bypass ratio 6 and $P_{13}/P_2 = 1.516$ for bypass ratio 10). All the other details like the burner exit temperature and the component efficiencies are assumed to be the same and typical of modern high bypass engines.

Besides the mean value (the data of the baseline engine cycle), the Monte Carlo simulation input also needs the standard deviations σ of the individual measurements. For this exercise, we use the σ values in Table 9.2-1.

The random errors in the measured data are normally distributed and independent from each other. All pre-conditions of the “Root-Sum-Squared” method are

Table 9.2-1 Assumed standard deviations for the measured data

Parameter	Symbol	σ [%]
Inlet pressure	P_2	0.1
Inlet temperature	T_2	0.1
Fan exit pressure (core)	P_{21}	0.2
Fan exit temperature (core)	T_{21}	0.2
Fan exit pressure (bypass)	P_{13}	0.15
Fan exit temperature (bypass)	T_{13}	0.15
HP compressor exit pressure	P_3	0.2
HP compressor exit temperature	T_3	0.2
Fan mass flow	W_2	0.4
Fuel flow	W_F	0.7
HP turbine exit pressure	P_{45}	0.2
LP turbine exit pressure	P_5	0.2

**Fig. 9.2-2** Test analysis result for BPR = 6

fulfilled. Thus, we could determine the standard deviations of the test analysis results by this method. But for each single quantity, we would have to calculate the sensitivity of the output quantity to each of the individual measurements—and that is relatively cumbersome.

Table 9.2-2 Standard deviation of the test analysis results

Component	Bypass ratio 6 (%)	Bypass ratio 10 (%)
Fan	0.93	1.37
Booster	0.65	0.64
High pressure compressor	0.33	0.32
High pressure turbine	0.42	0.44
Low pressure turbine	0.84	1.11

Running a Monte Carlo simulation is much simpler because it delivers the statistical distributions for all test results in one go. In GasTurb, the random numbers representing the measured data are normally distributed with the prescribed standard deviation σ . Values outside the limits of $\pm 2\sigma$ are not considered. Thus, the random numbers employed as input for the test analysis process follow a truncated normal distribution. All random variations of the various parameters are independent from each other.

In our example, a single Monte Carlo run performs around 1000 test analyses (Fig. 9.2-2). Table 9.2-2 lists the resulting standard deviations for the component efficiencies. It is seen that the measurement tolerances from Table 9.2-1 lead to greater uncertainty in the efficiency of the fan and the low pressure turbine if the bypass ratio is high.

9.3 Engine Design Uncertainty

When a new engine is designed, there is some uncertainty about the component performances that can be achieved. That transfers to an uncertainty in the overall engine performance. If, for example, the design target in specific fuel consumption of the project is met, but with insufficient confidence, the cycle must be modified.

The confidence with which the development targets are achieved can be improved to a certain extent with more time and money spent for engine development. The Monte Carlo method applied to this problem can give an estimate about the exchange rate between confidence and development effort [2].

The input data for such an exercise is derived from interviews with the component specialists. Ask them first for the best value that the efficiency could assume. This value is interpreted as the 2σ limit of a normal distribution. That means, that in only 2.5% of all cases will this value be exceeded. Further questions are for the most probable value and for a pessimistic value which will be achieved in at least two thirds of all component designs. Check the answers for consistency: the difference between the most probable and the best value should be approximately twice as big as the difference between the most probable and the low value estimate.

An alternate set of questions about an efficiency level could be

1. What is the most likely level of efficiency?
 - Most likely
2. What is the efficiency level which is unlikely to be missed?
 - Unlikely to be worse than ...
3. What is the efficiency level which is unlikely to be exceeded?
 - Unlikely to be better than ...

A further way to collect data on the variability is by asking the component design experts the following three simple questions:

1. What is the predicted value?
 - Assume that the predicted value is also the most likely value
2. What are the one-chance-in-a-thousand best and worst possible values?
 - Most people can relate to this as unlikely chance, but a chance nonetheless
 - For modeling purposes, these values can be used as the 0 respectively 100 probability values.
3. If you did ten such designs, how many of them would fall within an interval of the width x ?
 - Provides additional confidence information.

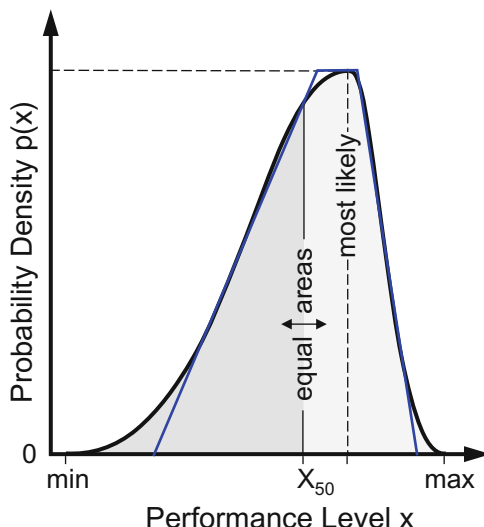


Fig. 9.3-1 Approximation of a non-symmetrical distribution with a trapezoid

Use the answers to these questions to define a trapezoid which describes the probability density, with the most likely value being coincident with the peak of a triangle (Fig. 9.3-1). Generate a trapezoid by cutting off the peak of the triangle, see Fig. 9.3-2. The solid line in that figures shows how a normal distribution with the same mean value would look.

The confidence in LPT efficiency exceeding the most likely value of 0.92 is 17% in the example of Fig. 9.3-3. Or the other way around, the probability of η_{LPT} being less than 0.92 is 83%.

Turbofan cycle design calculations for 35,000/Mach 0.8 and the LPT efficiency input from Fig. 9.3-2 yields the SFC distribution shown in Fig. 9.3-4. Not too surprisingly, this figure looks like a mirror image of the LPT efficiency probability distribution.

In the next study, we assume that not only are the LPT efficiency values non-symmetrically distributed but also those for the fan, booster, HPC and HPT efficiency. For each efficiency the minimum value is 2% lower and the maximum value 0.5% higher than the most likely value.

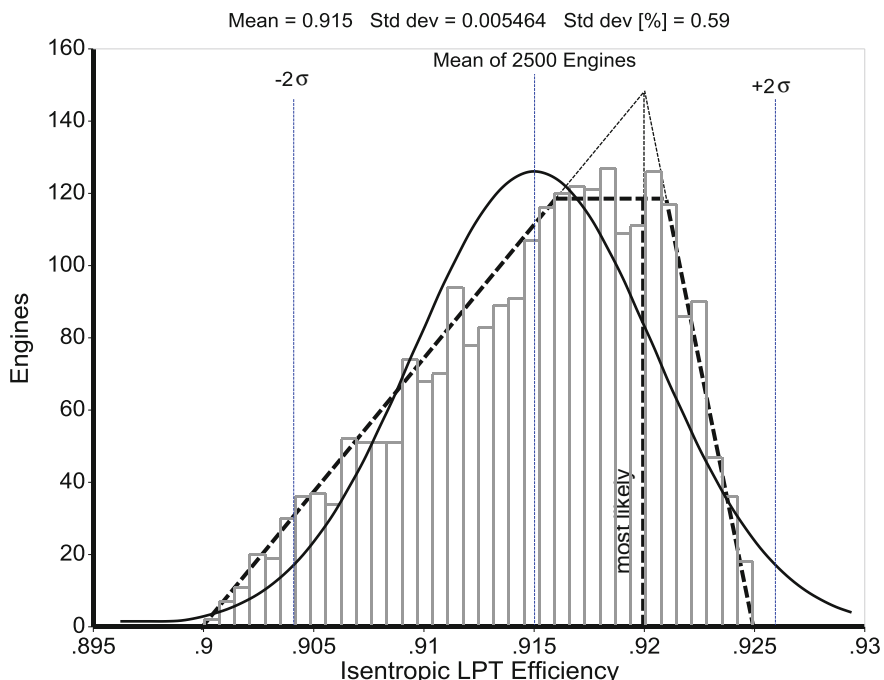


Fig. 9.3-2 Trapezoidal probability distribution

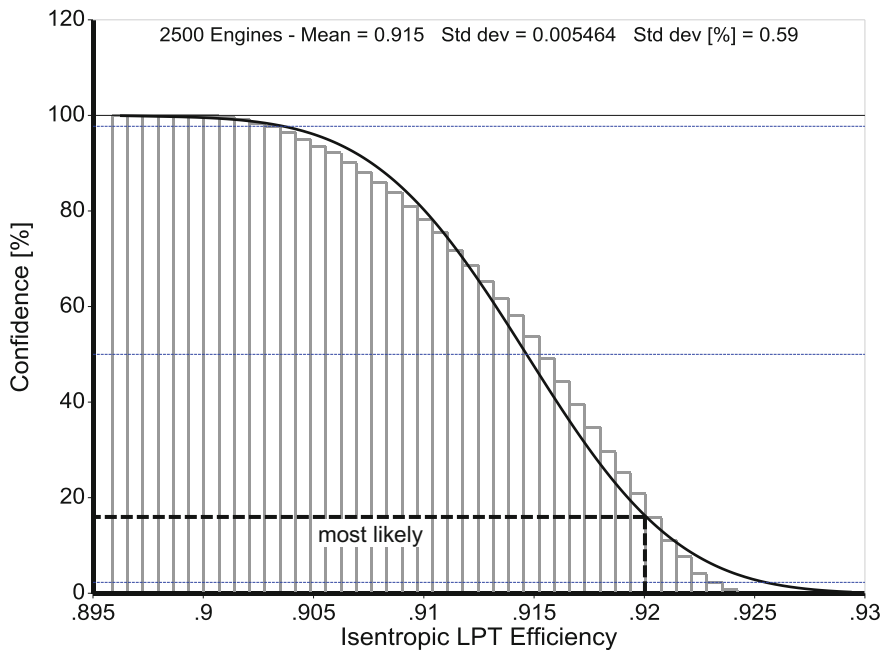


Fig. 9.3-3 Confidence in η_{LPT} being greater than...

The SFC of the engine with the most likely component efficiencies is 15.64 g/(kN s) at flight condition 35,000 ft/Mach 0.8. The Monte Carlo simulation of 2500 engines yields the SFC probability density distribution shown in Fig. 9.3-5.

The distribution is much more symmetric than that in Fig. 9.3-4, in fact it nearly follows a Gaussian distribution. This result is a consequence of a basic statistical law, the central limit theorem. It says that when independent random variables are added, their sum tends toward a normal distribution even if the original variables themselves are not distributed normally.

The mean SFC is 15.86, which is 0.9% higher than in Fig. 9.3-4, and the standard deviation has increased from 0.5 to 0.74% due to adding the four additional random input variables η_{Fan} , $\eta_{Booster}$, η_{HPC} and η_{HPT} .

Figure 9.3-6 shows the probability of reaching a certain SFC value. Achieving the low specific fuel consumption of an engine in which all components have the most likely efficiency is hardly probable. Nevertheless, the most likely SFC value could be the design target. If you want to have a high probability of success, the SFC promised to the customer should not be below 16.

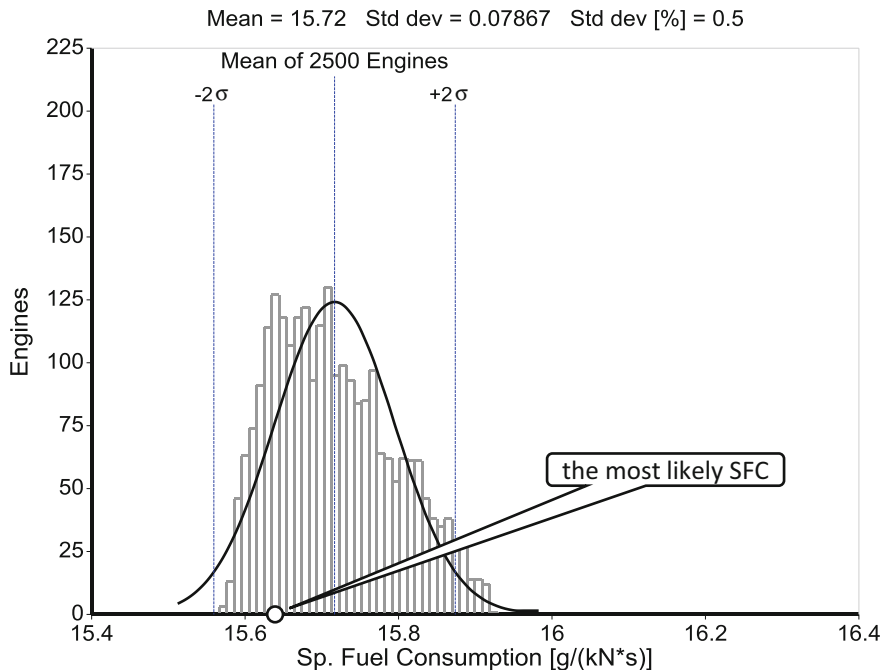


Fig. 9.3-4 SFC probability distribution corresponding with Fig. 9.3-2

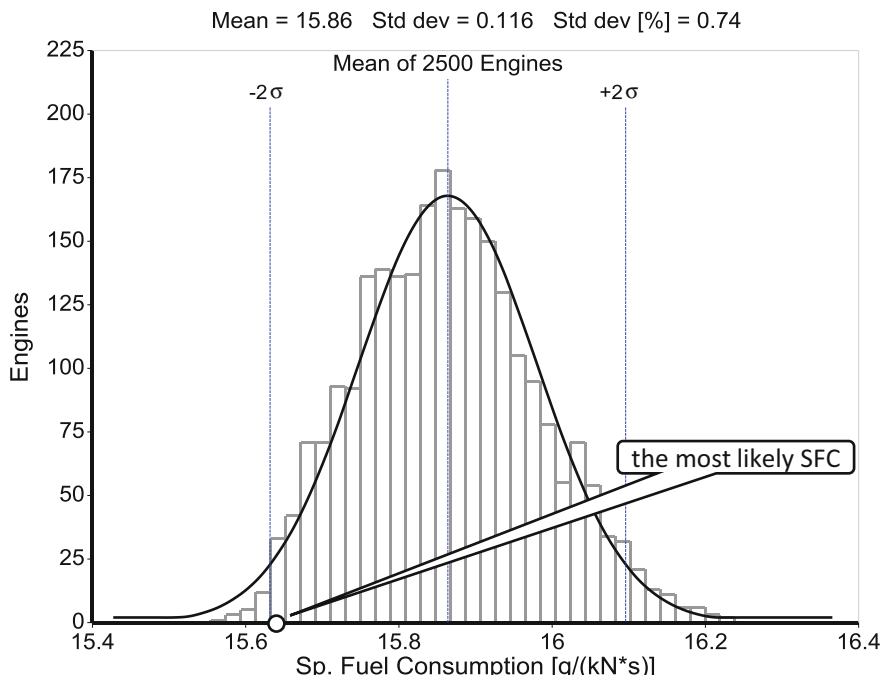


Fig. 9.3-5 SFC distribution for non-symmetrically distributed turbomachinery efficiency

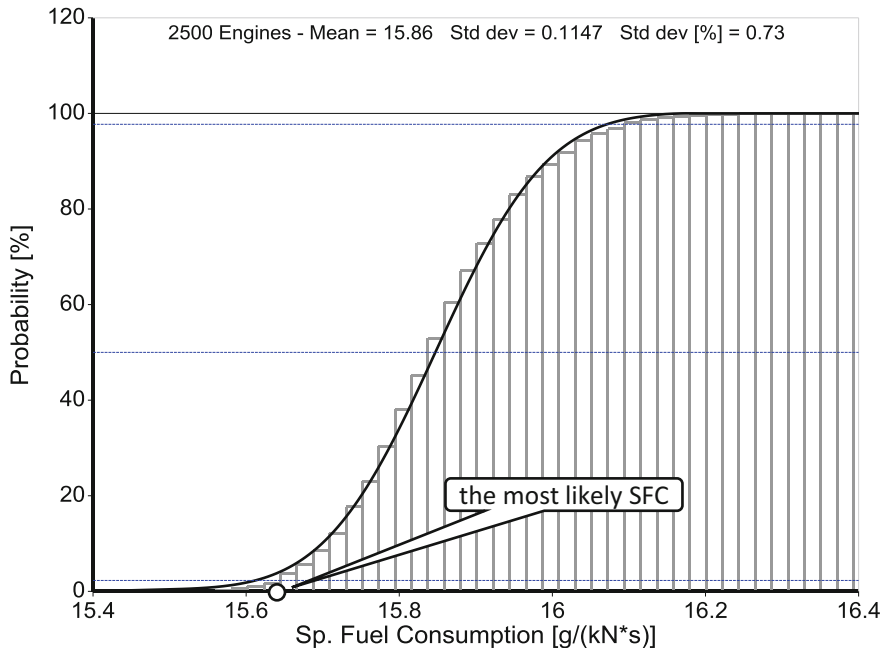


Fig. 9.3-6 Probability of achieving a SFC target

9.4 Engine Manufacturing Tolerance

Even in a well-controlled gas turbine manufacturing process, there are small geometrical differences between the individual compressors, turbines, ducts and nozzles in the assembly. The setting up of the control system during engine pass-off causes additional variations. Consequently, there is a performance scatter in the order of 1–2% in any gas turbine series production.

With the Monte Carlo method, we can simulate a batch of engines with randomly distributed properties. Engine manufacturing tolerance in terms of thrust (respectively shaft power) and specific fuel consumption are derived from component production tolerances (efficiency, flow capacity) and secondary air system variations.

In the previous examples of the Monte Carlo method, we have run the performance program in cycle design mode. Now we need an off-design cycle calculation program. Think of the shift of the HPC operating line due to turbine flow capacity scatter, which affects the surge margin, for example. The simulation of the control system interaction with the operation of the compressors and turbines also requires a full off-design performance model.

In the following we discuss manufacturing tolerances having an impact on the aero-thermodynamics of the gas turbine. Tolerances in the blading and the tip clearance of turbomachines, internal air seals, nozzle areas etc. are of particular interest.

9.4.1 Random Variations

For the Monte Carlo simulation of a batch of engines, we can assume that the various parameters are normally distributed around their nominal values. Estimate the standard deviations from previous experience. The magnitude of the variations in turbine capacity, for example, can be derived from throat area measurements or from cold flow tests on special rigs. Tip clearance of turbomachines is often measured during engine assembly. Variations transfer to scatter in efficiency and mass flow.

Usually we cannot derive all standard deviations reliably from the manufacturing process and we have to make some reasonable guesses. A global check of the estimates can be performed by comparing the results of the Monte Carlo simulation with the scatter in thrust and specific fuel consumption which is observed during engine pass-off.

9.4.2 Correlations

Most of the manufacturing differences are purely random and independent of each other. However, there is an important exception; compressors of poor efficiency generally have less mass flow than an average compressor at a given speed. One percent loss in efficiency (caused by a bigger than average tip clearance, for example), is accompanied by approximately 1% loss in flow capacity. We can apply this correlation within the Monte Carlo simulation in such a way that the same random number is used to scale the compressor map with respect to both the flow capacity and the efficiency. A pressure ratio correction is derived from the efficiency correction, with the assumption that the corrected specific work remains unchanged.

9.4.3 Control System Tolerance

The actual thrust or power delivered by an engine depends not only on its quality, but also on the control system and the sensor tolerances. A turbojet which runs to a preset spool speed, for example, may deliver more than the nominal thrust if it was assembled from components with less than average quality. This is because the high burner exit temperature needed for keeping the spool speed at the scheduled spool speed value increases the nozzle inlet temperature and consequently the jet velocity.

9.4.4 A Turboshaft Example

Let's examine the series production of a two-spool turboshaft engine (gas generator plus free power turbine) and evaluate the expected scatter in the pass-off test. A good compressor may be combined with a bad turbine to give an average engine. A low performing engine is a combination of poor components. The best production engine is a combination of excellent components, which are matched optimally with each other, and a control system which might operate on the extreme of its tolerance band. The performance synthesis automatically takes into account all the re-matching effects due to changes in efficiencies and flow capacities as well as the control system behavior.

Table 9.4-1 lists the input for our Monte Carlo simulation of the manufacturing tolerance in the batch we are going to examine. Compressor flow and efficiency scatter are related, all the other properties are independent of each other. The shaft power delivered is limited either by gas generator spool speed N_H or by the power turbine inlet temperature T_{45} .

Figure 9.4-1 shows the resulting pass-off gas generator spool speeds of 2500 engines plotted against shaft power. There are two distinct groups of data. Most points are within the N_H limiter tolerance band, others are below that band. The latter engines are limited in performance by PT inlet temperature T_{45} . Poor performing engines (those with less than 940 kW shaft power) are either limited by spool speed N_H or by T_{45} , while better than average performing engines are always N_H limited.

It is remarkable that along the 940 kW line there are two clusters of points, one around $N_H = 0.998$ and a second within the N_H limiter tolerance band. Applying the "Root-Sum-Squared" method, (the poor man's approach to statistic problems) would yield only the mean value and the standard deviation of a single Gauss distribution. The mean value might be in the middle of the N_H limiter tolerance band ($N_{H,\text{mean}} = 1.007$) or in the middle of the second cluster ($N_{H,\text{mean}} = 0.998$). This can be a significant difference with respect to turbine disk life, for example.

Table 9.4-1 Estimated manufacturing and control tolerances

	σ
Compressor	0.25%
• Efficiency and flow capacity	
High pressure turbine	0.3%
• Efficiency	0.3%
• Flow capacity	
Low pressure turbine	0.2%
• Efficiency	0.1%
• Flow capacity	
N_H limiter setting	0.1%
T_{45} limiter setting	5 K

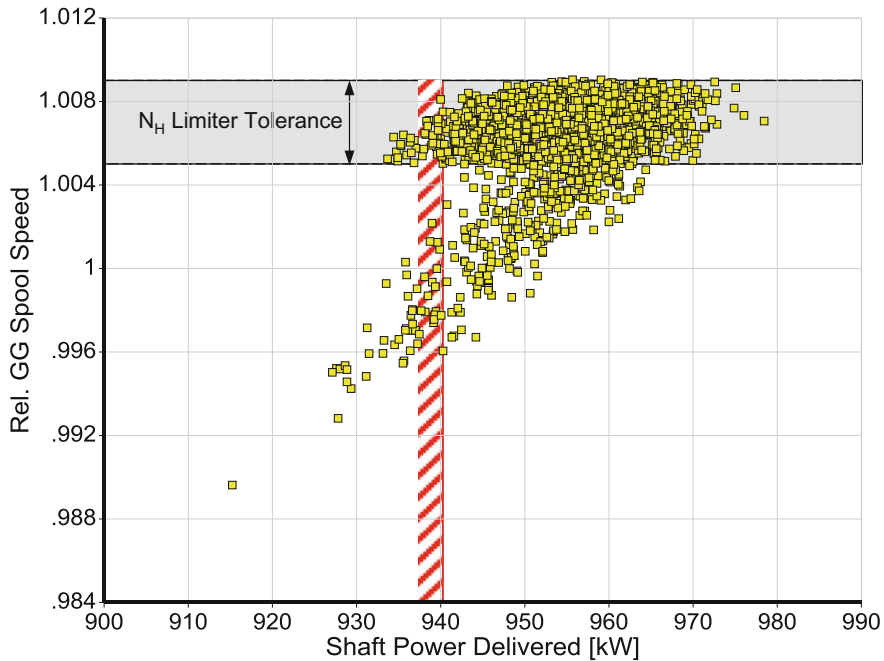


Fig. 9.4-1 Gas generator spool speed and LPT inlet temperature distributions

Clearly the “Root-Sum-Squared” method is not applicable for our example problem. The reason is that the various random variables are not independent. The off-design simulation ties them together in a way which is difficult to look through, especially with respect to control system interactions.

Monte Carlo studies don’t have preconditions with respect to dependencies between random variables. They are easy to apply and yield reliable results in short time.

9.5 References

1. Kurzke, J.: Some Applications of the Monte Carlo Method to Gas Turbine Performance Simulations ASME 97-GT-48 (1997)
2. Younghans, J.L., Johnson, J.E., Csonka, S.J.: A Methodology to Assess Uncertainty in Selecting Affordable Gas Turbine Technology ASME 94-GT-419 (1994)

Appendix

Nomenclature*

Total pressure and total temperature are the most important quantities in thermodynamic cycle calculations; seldom are static pressure and temperature needed. We use the letters P and T for total pressure and temperature with a number as index which designates the thermodynamic station.

We insert the index s before the station number for marking static pressure respectively temperature when static pressure and temperature show up in an equation.

Parameter names

Symbol	SI unit	Stands for	Comment, example
a	m/s	Velocity of sound	
A	m^2	Area	
alt	m, km	Altitude	also expressed in ft or kft
b	m	Width	@ radial compressor rotor exit
B		Burner part-load constant	
BPR		Bypass ratio	
cs	kg/s	Core size	
C		Coefficient	
C_D		Discharge coefficient	
C_{FG}		Thrust coefficient	
C_P	J/(kg K)	Specific heat @ constant pressure	
D	m	Diameter	
e	–	Efficiency	e_{2-3} = compressor efficiency efficiency between stations 2 and 3
EAS	knot	Equivalent air speed	
EGT	K	Exhaust gas temperature	often quoted in °C

(continued)

(continued)

Symbol	SI unit	Stands for	Comment, example
f		A factor	
h	J/kg	Enthalpy	
F	N, kN	Force, thrust	
FHV	MJ/kg	(Lower) fuel heating value	valid for 25 °C
far	–	Fuel-air-ratio	by mass
h	m	Blade height	
h (T)	J/kg	Enthalpy at a temperature	$H_4 = h(T_4)$
H	J/kg, m ² /s ²	Specific work	H_C = enthalpy change in the compr. $H_{2-3} = h(T_3) - h(T_2)$
i	deg	Incidence	
I	kg m ²	Polar moment of inertia	
IGV	–	Inlet guide vane	
ISA		International standard atmosphere	
k	various	A constant value	
L	m	Length	
M	–	Mach number	
n	–	Exponent in loss correlations with Reynolds number	
N	rpm	Absolute spool speed	mechanical spool speed
N	–	Relative spool speed	absolute spool speed related to a reference value
OPR	–	Overall pressure ratio P_3/P_2	
P	kPa	Total pressure	
P _s	kPa	Static pressure	static pressure = the true pressure
PR	–	Pressure ratio	
PSFC	kg/(kW s)	Power specific fuel consumption	
PW	kW	Shaft power	
PWX	kW	Shaft power extracted	for customer purposes
q	kPa	Dynamic head	
Q	kW	Heat flow	
r	m	Radius	
rr	–	Radius ratio r_{hub}/r_{tip}	
R	J/(kg*K)	Gas constant	
Re	–	Reynolds number	
RH	%	Relative humidity	
RNI	–	Reynolds number index	Reynolds number relative to Reynolds number at standard day conditions

(continued)

(continued)

Symbol	SI unit	Stands for	Comment, example
rpm	1/min	Revolutions per minute	
s	J/(kg K)	Specific entropy	
SFC	kg/(kN s)	Specific fuel consumption	
SLS		Sea level static	
t	sec	Time	
T	K	Total temperature	
T _s	K	Static temperature	static temperature = the true temp.
Trq	Nm	Torque	
TSFC	kg/(kN s)	Thrust specific fuel consumption	
U	m/s	Circumferential velocity	
V	m/s	Velocity	absolute velocity in velocity triangles
VGV	–	Variable guide vane	
Vol	m ³	Volume	
W	m/s	Relative velocity	relative velocity in velocity triangles
W	kg/s	Mass flow rate	
war	–	Water-air-ratio	by mass
Y		ΔP/q	describes a cascade loss
α	deg	Absolute flow angle	
α	deg	Nozzle cone angle	
β	deg	Relative flow angle	used in velocity diagrams
β	–	Auxiliary coordinate	used in component maps
δ	–	P/101.325 kPa	
Δ	–	A difference	ΔH = enthalpy difference
ε	–	A very small value	
Λ	–	Stage reaction	
Φ	–	Flow coefficient V _{ax} /U	
Φ	–	Burner loading parameter	
γ	–	Isentropic exponent	
η	–	Efficiency	
μ	kg/(m s)	Dynamic viscosity	
v	–	Blade-jet speed ratio	
ν	m ² /s	Kinematic viscosity	
ρ	kg/m ³	Density	
σ		Standard deviation	
σ		Solidity	chord/pitch
Ψ(T)	–	Entropy function @ a temp.	
Ψ	–	Power coefficient ΔH/U ²	also known as <i>work coefficient</i> , <i>stage loading coefficient</i> and <i>aerodynamic loading</i>
Θ	–	T/288.15 K	
Ω	–	Burner loading	

Indices

a	Air
ad	Adiabatic
amb	Ambient
ax	Axial
B	Burner (main combustion chamber)
corr	Corrected
C	Compressor
cl	Cooling
ds	Design
D	Discharge
eff	Effective
eq	Equivalent
equi	(Chemical) equilibrium
ex	Exit
F	Fuel
FG	Gross thrust
FN	Net thrust
g	Gas
G	Gross
h	Hub
H	High pressure spool
HPC	High pressure compressor
HPT	High pressure turbine
i	Inner annulus
id	Ideal
in	Inlet
inj	Injected
is	Isentropic
IPC	Intermediate pressure compressor
IPT	Intermediate pressure turbine
L	Low pressure spool
LPC	Low pressure compressor
LPT	Low pressure turbine
m	Mean
mea	Measured
mech	Mechanical
mix	Mixing
N	Net
o	Outer annulus
P	Pressure
pol	Polytropic
prop	Propulsive

(continued)

(continued)

PT	Power turbine
R	Reduced (=corrected)
Re	Reynolds
ref	Reference
rel	Relative
RH	Reheat (= afterburner, augmentor)
sat	Saturation
SD	Shaft (power) delivered
std	Standard day conditions
Stg	Stage
t	Tip
T	Turbine
therm	Thermal
thermo	Thermodynamical
u	In circumferential direction
V	Volume
x	In axial direction

Station numbering

0	Free stream air conditions
1	First station of interest to the engine manufacturer, e.g. propulsion system entrance, external/internal interface or vehicle/engine interface
2	First compressor front face
2x	Intermediate compressor stations
3	Last compressor discharge or burner entrance
3x	Intermediate burner stations
4	Burner discharge or first turbine entrance
4x	Intermediate turbine stations
5	Last turbine discharge
6	Available for mixer, afterburner etc.
7	Engine/exhaust nozzle interface
8	Exhaust nozzle throat
9	Exhaust nozzle discharge

Special terms

AEDC	Arnold Engineering Development Complex
Backbone	A line which connects the highest efficiency points on all speed lines in a compressor or turbine map
Corrected flow, Corrected speed	$W\sqrt{\Theta}/\delta = W\sqrt{(T/288.15\text{ K})/(P/101.325\text{ kPa})}$ $N/\sqrt{\Theta} = N\sqrt{(T/288.15\text{ K})}$
GasTurb	A publicly available gas turbine performance program for Windows
Cycle design point	The operating condition which defines the geometry of the engine by means of a cycle design calculation
Incidence	Flow angle with minimum losses Flow angle measured against the minimum loss flow angle
ISA	International standard atmosphere
MBTO	Mean Time Between Overhaul
OEM	Original equipment manufacturer Gas turbine engine manufacturer
Peak efficiency line	Same as backbone
Pitch-line radius	Mean radius, based on equal areas $r_m = \sqrt{(r_t^2 - r_h^2)/2}$
Reduced flow, Reduced speed	$W\sqrt{T}/P$ N/\sqrt{T}
Smooth C	A program for generating compressor map tables from measured or calculated data
Smooth T	A program for generating turbine map tables from measured or calculated data
Uninstalled	No power offtake or bleed for aircraft purposes Subsonic flight: no intake pressure loss Supersonic flight: intake pressure loss as defined in MIL-E-5007

* This is not a complete nomenclature, as sparsely used terminology is described in the text

Index

A

- Acceleration, 269
Acceptance test, 167
Accessories, 304
Active Clearance Control (ACC), 172, 173, 215, 239, 483
Adaptive random search, 718, 720
Advanced map scaling, 499
Aerodynamic design point, 116, 306, 307
Aerodynamic Interface Plane (AIP), 252, 442
Aerodynamic limits, 301
Aerodynamic loading, 60
Aerodynamic spool speed, 108
Aerospace Standard AS755, 3
Afterburner (Augmenter, Reheat)
 Afterburner efficiency, 33, 546
 Afterburner operation, 544
 Afterburner simulation, 542
 Afterburner, 23, 30, 48, 104, 211, 421, 529, 541, 542, 649
 Efficiency at part load, 549
 Flame-holders, 545
 Reheat pipe, 105
 Temperature rise due to combustion, 616
AIA Standard, 441, 445
Airbus A340, 530
Aircraft
 Airbus A340, 530
 Blackbird SR-71, 100, 112
 Business jets, 116, 537
 Concorde, 445
 Eurofighter Typhoon, 550
 Eurofighter, 446
 European Fighter Aircraft (EFA), 446
 F-4, 445
 F-14, 445
 F-15, 445
 F-16, 445
 F-104, 445
 F-111, 445
 Fighter aircraft, 48, 95
 Helicopter propulsion, 56
Aircraft drag, 447
Aircraft mission, 298, 309
Aircraft mission requirements, 303
Aircraft speeds, 617
Air inlet house, 448
Air intake, 439
Altitude test facility, 230
AM350, 431
AN², 82, 309, 396
AnSyn
 Analysis by Synthesis (AnSyn), 214, 235
 AnSyn factors, 216, 218, 219, 221, 232, 234
 Interpretation of the AnSyn factors, 237
Area ratio, 54
Augmented turbofan, 56, 106
Augmenter, *see* Afterburner
Auxiliary coordinate β , 120
Average new production engine, 132
Average stage pressure ratio, 622
Axial Mach number, 453

B

- Backbone, 464, 467
Batch of engines, 736
Bellmouth, 139, 167
Bernoulli equation, 342
 β line, 218, 463, 516
Bias, 727
Blackbird SR-71, 100, 112
Blade aspect ratios, 73
Blade incidence, 325, 370
Blade metal angles, 323
Blade metal temperature, 62
Blade root stress, 60, 309
Blade speed/jet speed ratio, 509

- Blade untwist, 231, 483, 485
 Bleed schedule, 321, 483
 Blisk, 414, 425
 Blockage, 336, 340
 Bodie, 286
 Booster
 Booster, 416
 Booster map, 190
 Booster operating line, 593, 597
 Bore radius, 84
 Bottoming cycle, 19
 Boundary layer, 226, 325, 334, 337, 340
 Brayton, 3
 Brayton cycle, 6, 313, 357
 Burner, *see* Combustor
 Business jets, 116, 537
 Bypass duct, 74
 Bypass ratio, 35, 37, 70, 192, 229, 728
- C**
 Calibrated Airspeed (CAS), 617
 Camber line, 370
 Carnot cycle, 12
 Central limit theorem, 733
 Centrifugal compressors, 203, 651
 CF6, 115
 CFD, 334
 CFM56, 115, 166, 238
 CFM56-3, 241, 403
 CFM56-5C2, 530
 Chargeable cooling air, 664, 670, 679, 693
 Chemical composition, 616
 Chemical equilibrium, 18
 Chemical Equilibrium with Applications (CEA), 613, 615
 Choking, 452
 Circumferential Mach number, 453
 Clearance changes of seals, 281
 Close-coupled, 262
 Closed loop control, 542
 Coarse Filter, 227
 Cogeneration, 19
 Combined cycle, 19
 Combined cycle efficiency, 22
 Combustor (Burner)
 Burner efficiency, 159
 Burner loading, 159
 Burner outlet temperature, 663
 Burner part-load constant, 159
 Combustion Chamber, 308, 525, 647
 Combustion efficiency, 32
 Combustor, 304, 418
 Dilution air, 666
- Flame tube, 281
 Overall Temperature Distribution Factor (OTDF), 529
 Pattern factor, 529
 Pressure loss, 525
 Radial Temperature Distribution Factor (RTDF), 529
 Stoichiometric combustion, 18
 Temperature rise due to combustion, 616
 Commercial airliner, 44 *See also* Aircraft
 Commercial subsonic aircraft, 94 *See also* Aircraft
 Common core, 70, 115
 Component
 Degradation, 238
 Design, 297, 311
 Design points, 306
 Hierarchy, 304
 Models, 299
 Performance map, 713
 Performance, 297
 Synergy, 582
 Component maps, 713
 Compressor
 AnSyn factors, 218, 219
 Compressor, 313
 Coupling, 261, 267
 Design envelopes, 347
 Deviation, 325
 Efficiency correction, 659
 HP compressor, 304, 307, 416
 Incidence, 325
 Number of compressor stages, 622
 Overall compressor performance, 454
 Peak efficiency line, 464, 467, 480
 Pressure ratio of 1, 713
 Rig, 451
 Through-flow model, 333
 Velocity diagram, 323
 Compressor maps
 Auxiliary coordinate β line, 120, 218, 463, 516
 Efficiency contours, 452
 Mach number scale for compressor maps, 491, 495
 Map coordinates, 461
 Parabolic β -lines, 463, 516
 Performance maps, 451, 644
 Pressure ratio scaling, 498
 Re-engineering compressor maps, 451
 Simple map scaling, 498
 Spacing between map speed lines, 495
 Split map, 474

- Compressor map scaling, 487
Conceptual design, 346
Concorde, 445
Condensation, 138, 179, 233, 235
Condenser, 19, 21
Confidence level, 726
Configuration design, 299
Confluent mixers, 537
Constant pressure combustion, 10
Constant volume combustion, 10
Constraints, 720, 721
Continuity characteristic, 358
Contractual performance, 134, 135
Control system, 266, 708
Control volume, 662, 663
Convergence problems, 711
Convergent-divergent nozzles, 53, 102, 563
Convergent nozzles, 53, 559
Cooled Turbines
 Chargeable cooling air, 664, 670, 679, 693
 Cooled turbines, 661
 Cooling air, 393
 Cooling air bookkeeping, 682
 Cooling effectiveness, 61, 63
 Cooling loss, 393
 NGV cooling air, 666
 Non-chargeable cooling air, 664, 670, 674, 679
Core compressor, 68
Core driven fan stage, 355
Core efficiency, 26
Core flow analysis, 728
Core size, 68, 93
Corrected parameters
 Circumferential speed, 453
 Correction exponents, 646
 Flow, 452, 505
 Flow per area, 44, 93
 Fuel flow, 647
 Mass flow, 503
 Parameter correction procedure, 136
 Specific fuel consumption, 646
 Specific power, 507
 Speed, 307
 Spool speed, 94, 452, 507
 Thrust, 646
Counter-rotating, *see* Vaneless counter-rotating turbine
Coupling Factor (CF), 262
Cradle drag, 135
Critical segment angle, 258
Cross section, 274
CSPAN mean line code, 340, 344, 351
Cycle efficiency
Core efficiency, 26
Overall efficiency, 27
Propulsive efficiency, 27, 29, 34, 38, 44, 70
Thermal efficiency, 11, 17, 18, 23, 25, 26, 29, 38, 41, 45, 132
Transmission efficiency, 26
Cycle Analysis, 297
Cycle design mode, 735
Cycle design point, 72, 103, 305, 308, 311
Cycle design point calculation, 66, 93, 100
Cycle reference point, 141, 143, 148, 179, 183, 201
Cycle types
 Bottoming cycle, 19
 Brayton, 6, 313, 357
 Carnot cycle, 12
 Constant pressure combustion, 10
 Constant volume combustion, 10
 Humphrey cycle, 10
 Joule cycle, 3, 6, 313
 Rankine Cycle, 19
 Sequential combustion, 8, 14, 15
 Topping cycle, 19
- D**
- DC₆₀ distortion coefficient, 251
Deceleration, 269, 286
De Haller number, 337
Derivative engines, 92, 115
Design constraints, 123, 301
Design envelopes, 302, 345
Design margins, 432
Design point, 306
Design point analysis, 305
Design process, 296
Design space, 92, 116, 348, 716, 722
Design variables, 122, 302, 350
Deterioration, 99, 133
Deviation, 325, 369
Diffusion, 336
Diffusion Factor, 338, 345
Dilution air, 666
Direct drive turbofans, 70, 72
Discharge coefficient, 192, 559
Disk
 Bore diameter, 85
 Burst margin, 433
 Burst speed, 433
 Design, 426
 Dimensions, 274
 Stress, 430
 Temperature, 429
 Von Mises stress, 432
Dissociation, 546

- Distortion
 Compressor distortion, 496
 Coupling Factor CF, 262
 Critical segment angle, 258
 Distortion Coefficient (DC60), 251
 Distortion intensity, 258
 Full coupling, 262
 Inlet Distortion, 249
 Parallel compressor theory, 249, 253
- Dry engine, 30
 Dry turbofan, 52
 Ducts, 422
 Dynamic head, 4
 DYNGEN, 709, 710
- E**
 Economizer, 21
 Effective burning area, 544
 Effective work coefficient, 455
 EGT, *see* Exhaust Gas Temperature
 EGT margin, 134, 167, 225, 237
 EJ200, 157, 229, 550, 565, 573
 Emissions, 90, 302
 Endless random search, 125, 720
 Energy balance (Heat balance), 13, 222, 229, 233, 242, 587, 614, 640, 687, 692
 Energy-based definition of thermal efficiency, 18
 Engine configuration model, 298
 Engines
 CF6, 115
 CFM56, 115, 166, 238
 CFM56-3, 241, 403
 CFM56-5C2, 530
 EJ200, 157, 229, 550, 565, 573
 F107-WR-400, 201
 GE F101, 565
 GE36, 401
 J57-19W, 147
 LMS 100, 8
 MT30, 115
 MTR390, 56
 PW1000G Geared Turbofan, 81
 PW4000, 115
 RB199, 422
 SGT8000H, 694
 T800, 56
 Trent, 115
 V2500, 274, 434
- Engine design table, 306, 309
 Engine Development, 309
 Engine family, 70, 73, 115
 Engine geometry, 273
 Engine inlet diameter, 39
- Engine maintenance shops, 232
 Engine parts rig, 230
 Engine Pressure Ratio (EPR), 225
 Engine weight, 411, 433
 Enthalpy-entropy diagram, 7, 8, 23, 25, 316, 360, 530, 664, 678, 689
 Entropy function, 615
 Equivalent Airspeed (EAS), 100, 617
 Equivalent diffusion factor Deq, 340
 Equivalent exhaust jet velocity, 38
 Equivalent jet velocity, 30, 646
 Equivalent single-stage turbine, 393, 670, 677
 Equivalent single-stage turbine efficiency, 680, 692
 Equivalent tip clearance, 484
 Erosion, 232
 Euler's method, 710
 Eurofighter Typhoon, 446, 550
 European Fighter Aircraft (EFA), 446
 Evaporation coolers, 448
 Evaporator, 21
 Exhaust emissions, 302
 Exhaust Gas Temperature (EGT), 142, 174, 189, 193, 201, 223, 233, 518
 Exoskeletal engine, 408
 External compression, 445
 External design limits, 302
- F**
 F-4, 445
 F-14, 445
 F-15, 445
 F-16, 445
 F-104, 445
 F107-WR-400, 201
 F-111, 445
 Facility modifier, 135, 166, 170
 Fan
 AnSyn factors, 234
 Diameter, 44
 Operating line, 595
 Tip diameter, 73
 Tip relative Mach number, 88
 Tip speed, 78
 Fan maps
 Bypass section, 478
 Core section, 475
 Extended fan map, 479
 Fan maps, 473
- Fanning Friction Factor, 654
 FHV, *see* Fuel Heating Value
 Fighter engines, 225
 Figure of merit, 142, 716, 721
 Fine Filter, 227

- First law of thermodynamics, 222
First order lag, 279
Flame-holders, 545
Flame tube, 281
Flat-back turbine blade, 369
Flat rated, 225
Flat rating, 310
Flight envelope, 96, 100, 298, 651
Flow annulus, 66
Flow capacity factor, 218
Flow coefficient
 Compressor, 330, 347
 Turbine, 375, 396, 454, 455, 560
Flow correction factor, 659
Flow path, 413
Flow separation, 655
Fogging, 448
Foreign Object Damage (FOD), 232
Fouling, 238
Frame of reference, 321
Frames
 Front frame, 422
 Main frame, 423
 Rear frame, 424
 Turbine center frame, 423
Free-vortex, 336
Front frame, 422
Fuel burn, 297
Fuel flow-based thermal efficiency, 18
Fuel Heating Value (FHV), 17, 38, 172, 614, 625, 626, 645
Full coupling, 262
Fully mixed thrust, 532
Fundamental pressure loss, 50
- G**
- Gas Properties
 Chemical Equilibrium with Applications (CEA), 613, 615
 Dissociation, 546
 Entropy function, 615
 Fuel Heating Value (FHV), 17, 38, 172, 614, 625, 626, 645
 Gas constant, 616
 Generic fuel, 616
 Humidity, 136, 235, 506, 616, 643
 Hydrocarbon, 616
 Ideal gas, 614
 Isentropic exponent, 4, 639, 647
 Psychrometric chart, 449
 Specific heat at constant pressure, 614
 Steam, 19
 Temperature rise due to combustion, 616
- Gas generator, 35, 57, 69, 115, 120, 188, 271
Gas generator turbines, 656
Gas path analysis, 232
GasTurb, 346, 351, 417, 424, 429
GasTurb Details, 133
GasTurb Standard maps, 116, 153, 184
Gauss algorithm, 704
Gaussian distribution, 244, 724 *See also Statistics*
GE F101, 565
GE36, 401
Gear ratio, 82
Gearbox, 70, 72
Geared Turbofan, 81
Generic fuel, 616
Geometric altitude, 617
Geometric model, 274
Global maximum, 126
Global optimum, 717, 720
Gradient search, 720
Gradient strategy, 717
Greek Ascoloy (418), 431
Gross thrust, 56
GT24/26, 8 *See also Engines*
Guaranteed thrust, 206
- H**
- Half-ideal gas, 613
Handling bleeds, 483
Heat balance, *see* energy balance
Heat exchanger, 11, 13, 14, 650, 707
Heat rate, 132
Heat Recovery Steam Generator (HRSG), 15, 19
Heat soakage, 282, 288
Heat storage, 273
Heat transfer, 278, 281
Heat transfer coefficient, 279
Helicopter propulsion, 56
High-Bypass-Ratio Fan, 414
Hot Day Take Off, 94
HP compressor, 304, 307, 416
HP Shaft, 424
HP spool, 304
HP turbine, 304, 308, 380, 418
HP turbine flow capacity, 728
Hub, 309
Hub/tip radius ratio, 66
Humidity, 136, 235, 506, 616, 643
Humidity corrections, 136
Humphrey cycle, 10
Hybrid measured data, 190
Hybrid test data, 141, 184

Hydrocarbon, 616

I

Ideal cycle, 5

Ideal gas, 614

Ideal jet velocity ratio, 37, 43, 127

Ideal thrust coefficient, 562

Idle, 709

IGV, *see* Inlet Guide Vane

Incidence

Compressor, 325

Controlling incidence, 469

Turbine, 369

INCONEL, 432, 718

Indicated airspeed, 617

Indicated total temperature, 168

Infrared signature, 529

Inlet

External compression, 445

Inlet, 439

Inlet air chillers, 448

Inlet condensation, 172

Inlet cooling system, 448

Inlet flow distortion, 99, 249–267, 483

Inlet fogging, 449, 616

Inlet isentropic efficiency, 440

Inlet momentum drag, 135

Inlet pressure ratio, 440

Inlet pressure recovery, 100, 265, 440, 446

Inlet recovery factor, 168

Internal compression, 444

MIL-E-5008B Standard intake recovery, 440, 445

Mixed compression, 445

Oblique shock waves, 445

Pitot inlet, 445

Ram efficiency, 440

Inlet Guide Vane (IGV), 315, 321, 469

Installed SFC, 86

Intake, *see* Inlet

Integration step size, 710

Intercooling, 9, 14

Internal compression, 444

Internal design limits, 301

International Standard Atmosphere (ISA), 67, 136

Interpretation of the AnSyn factors, 237

Inter-stage bleed, 483, 497, 691, 693

ISA corrected data, 235

ISA correction, 224

ISA Standard Day, 136

Isentropic efficiency, 59, 315, 317, 320, 362, 365, 621, 625

Isentropic exponent, 4, 639, 647

Iteration algorithms, 697

J

J57-19W, 147

Jacobian matrix, 703, 704

Jet velocity ratio, 70, 74

Joule, 3, 6, 313

K

Kink point, 225

L

Laminar separation, 654

Limiter, 708

Lip contraction, 442

LMS 100, 8

Loading coefficient

Compressor, 330

Turbine, 374, 380

Zweifel loading coefficient, 377, 396

Local maximum, 126

Local optimum, 720

Loss coefficient

Compressor, 343, 347

Turbine, 361

Low-Bypass-Ratio Fan, 413

Lower Fuel Heating Value FHV, 616, 626

LP Compressor, 413 *See also* Compressor

LP Shaft, 425

LP spool, 304

LP Turbine, 308, 381, 420, 655

M

Mach number scale for compressor maps, 491, 495

Mach number, 4, 639

Mach number similarity, 224, 642, 645

Main frame, 423

Maintenance shops, 166

Manufacturing tolerance, 132, 735

Maps, *see* Compressor maps, Fan maps,

Turbine maps

Map entry point, 488

Map extrapolation, 713

Map manipulation, 451

Map preparation, 496

Map scaling during off-design, 501

Map scaling point, 153, 189, 194, 207, 488, 490

Map-tweaking, 184

Mass flow AnSyn factor, 218

Mass flow scaling, 499

- Mass storage, 281
Materials
 AM350, 431
 Greek Ascoloy (418), 431
 INCONEL 718, 432
 Material properties, 431
 Ti-6AL-4 V, 432
Max Climb, 73, 94
Max Continuous, 225
Max Dry, 225
Max Reheat, 225
Mean line analysis
 CSPAN mean line code, 340, 344, 351
 Mean line analysis, 335, 382
 Mean line code, 385
 Mean line loss model, 333, 342, 388
Measured data, 133, 134
Measurement error, 243
Measurement uncertainty, 723
Mechanical design point, 116, 307, 308, 411
MIL-E-5007, 100
MIL-E-5008B Standard intake recovery, 440, 445
MIL-STD 210, 617
Minimum afterburner rating, 541
Minimum (guaranteed) performance, 132
Minimum production engine, 206
Mission analysis, 90, 297
Mission performance, 90
Mixed compression inlet, 445
Mixed flow nozzles, 422
Mixed flow turbofan, 44, 45
Mixer
 Efficiency, 533
 Geometry, 531
 Mixed cycle, 529
 Off design, 539
 Practical mixers, 536
 Thrust gain, 46
 Velocity coefficient, 534
Model-based performance analysis, 213, 215, 222, 227, 312
Model fault, 239
Monte Carlo, 244, 723
Moody Chart, 653, 657
MT30, 115
MTOW, 297
MTR390, 56
Multi-point Design, 93
Multi-spool turboshaft, 607
Multi-stage compressor, 316, 354, 416
Multi-stage cooled turbine, 393
- N
Nacelle, 44
Nacelle drag, 447
N dot control, 271
Nested loop, 704
Net thrust, 56
Newton algorithm, 700, 706
Newton-Raphson algorithm, 702, 704
NGV cooling air, 666
Noise, 89, 90, 617
Non-chargeable cooling air, 664, 670, 674, 679
Non-dimensional parameter
 Circumferential speed, 453
 Flow, 452, 505
 Flow per area, 44, 93
 Fuel flow, 647
 Mass flow, 503
 Specific fuel consumption, 646
 Specific power, 507
 Speed, 307
 Spool speed, 94, 452, 507
 Thrust, 646
Non-dimensional performance, 300, 639, 644, 646
Non-symmetric probability distribution, 726
Normal Distribution, 723
Nozzles
 Convergent-divergent nozzles, 53, 102, 563
 Convergent nozzles, 53, 559
 Ideal thrust coefficient, 562
 Mixed flow nozzles, 422
 Nozzle area AnSyn factor, 221
 Nozzle discharge coefficient, 153
 Nozzle pressure ratio, 53
 Nozzles, 421, 558
 Subsonic nozzles, 421, 422
Nozzle guide vane (NGV), 663
Nozzle pressure ratio, 53
Number of compressor stages, 622
Number of turbine stages, 64
Numerical analysis
 Iteration algorithms, 697
 Nested loop, 704
 Newton algorithm, 700, 706
 Newton-Raphson algorithm, 702, 704
 Regula Falsi, 701, 706
Numerical optimization, 116, 124, 142, 223, 715
 Constraints, 720, 721
 Figure of merit, 142, 716, 721
 Global maximum, 126
 Global optimum, 717, 720
 Gradient search, 720

Numerical optimization (*cont.*)

Gradient strategy, 717

Local maximum, 126

Local optimum, 720

Pareto front, 722

Nusselt number, 650

O

Oblique shock waves, 445

Off-design analysis, 306

Off-design calculations, 93

Off-design matching scheme, 223

Off-design performance, 305, 306

Open loop, 542

Open rotor, 42

Operability, 484

Operating lines, 97, 494, 588

Optimization, *see* Numerical optimization

Output shaft power, 518

Overall compressor performance, 454

Overall efficiency, 27

Overall engine simulation, 662, 706

Overall pressure ratio, 39, 141, 184, 216

Overall Temperature Distribution Factor
(OTDF), 529

Over-tip leakage loss, 392

P

Parabolic β -lines, 463, 516

Parallel compressor theory, 249, 253

Parameter correction procedure, 136

Pareto front, 722

Pass-off test, 134

Pattern factor, 529

Peak efficiency line, 464, 467, 480

Performance deck, 132

Performance monitoring, 235

Performance prediction, 230

Performance scatter, 735

Performance synthesis program, 214

Pinch point, 21

Pipe flow analogy, 654, 657

Pitch line loading, 74

Pitot inlet, 445

Point performance, 100

Polar moment of inertia, 269

Polytropic efficiency, 59, 318, 320, 363–365,
622, 625

Power control, 211

Power generation, 15, 146

Power off-take, 97

Practical mixers, 536

Preheat effect, 318

Preliminary compressor design, 333

Preliminary engine design, 295, 298, 299

Preliminary turbine design, 122, 380

Preprocessing measured data, 183

Pressure ratio AnSyn factor, 218

Pressure ratio parameter, 622

Pressure ratio scaling, 498

Probability distribution, 726

Production tolerance, 723

Profile factor, 529

Profile loss, turbine, 391

Propulsive efficiency, 27, 29, 34, 38, 44, 70

Pseudo RIT, 673

Psychrometric chart, 449

Pulse detonation engines, 10

PW1000G Geared Turbofan, 81, 425

PW4000, 115

Q

Quality criterion, 69

R

Radial compressor, 495

Radial distortion, 251

Radial equilibrium, 335

Radial Temperature Distribution Factor
(RTDF), 529

Rake, 226

Ram effect, 25

Ram efficiency, 440

Ramjet, 107

Random errors, 727

Range Check, 227 *See also* Sensors

Rankine Cycle, 19

Rated Power, 225

Ratings, 94

Raw data, 216

Rayleigh flow, 50

RB199, 422

Reaction, 336, 354

Real cycles, 15

Rear frame, 424

Red line temperature, 225

Reduced parameters

Flow, 380, 452, 505, 514, 515, 642

Fuel flow, 645

Shaft power, 644

Speed, 642

Thrust, 646

Torque, 514

Re-engineering performance, 211

Regula Falsi, 701, 706

Reheat, *see* Afterburner

Relative humidity, 136

Relative roughness, 653

- Relative velocity, 326, 371
Re-slam, 289
Re-stagger, 496
Reynolds correction, 159
Reynolds number, 229, 483, 488, 496, 499, 639, 647, 650, 651, 657
Reynolds Number Index, 97, 279, 652
Rim Load, 427
Root Sum Squared, 725, 737
Rotor blade metal temperature, 61
Rotor inlet temperature, 663, 673
Rotor loss coefficient, 361
- S**
Screech damper, 421, 541
Secondary air system, 221, 304, 687, 690
Secondary effects, 146
Secondary loss, 392
Sensitivity studies, 142
Sensors
 Checking, 227
 Coarse filter, 227
 Fine filter, 227
 Sensor failure, 241
 Sensor readings, 223
 Sensor tolerances, 736
Separate flow turbofans, 43, 45
Separate flow nozzle, 422
Sequential combustion, 8, 14, 15
SGT8000H, 694
Shafts, 424
Shock losses, 391
Sign convention in velocity diagrams, 324, 370
Simple map scaling, 498
Single Point Design, 91
Single spool gas turbines, 694
Smith Chart, 379, 382, 397
Smooth C, 186, 190, 195, 218, 463, 482, 487, 496, 502
Smooth T, 512
Solidity, 339
Spacing between map speed lines, 495
Specific fuel consumption, (SFC), 27, 297
Specific heat at constant pressure, 614
Specific power, 7
Specific thrust, 39, 48, 100, 102, 646
Specific work, 7, 458, 507
Speed, 100% values, 311
Speed line, 454
Spillage drag, 447, 448
Split map, 474
Splitters, 416
Spool speed, 68, 144
Spray bars, 545
Spray rings, 545
Stage loading coefficient, 380, 396
Stage loading, 347
Stage matching, 321
Stage reaction, 330, 347, 375
Standard Day, 617
Standard deviation, 244, 723
Static pressure, 4
Static temperature, 4
Station numbers, 3
Statistics
 Addition theorem for normal distributions, 724
 Manufacturing tolerance, 132, 735
 Measurement uncertainty, 723
 Monte Carlo, 244
 Non-symmetric probability distribution, 726
 Normal Distribution, 723
 Probability distribution, 726
 Random errors, 727
 Root Sum Squared, 725, 737
 Standard deviation, 244, 723
 Truncated normal distribution, 725
Status Model, 311
Stealth, 529
Steam, 19
Steam turbines, 21
Stoichiometric combustion, 18
Streamline model, 333
Stress distribution, 433
Structural limit, 301
Subsonic nozzles, 421, 422
Super cruise, 55
Supersonic flight, 54
Supersonic nozzles, 421, 422
Supersonic speed lines, 456
Surge, 249
Surge line, 97
Surge margin, 69, 97, 471, 484, 495
Surge pressure ratio, 494
Systematic errors, 727
- T**
T800, 56
Take off, 94, 116, 225, 307, 522
Taper, turbine airfoil, 387
Technology level, 299
Temperature-entropy diagram, 5
Temperature rise due to combustion, 616
Tensile strength, 431
Test analysis, 213, 728
Test cell, 170
Test cell calibration, 232

- Thermal efficiency, 11, 17, 23, 25, 27, 29, 38, 41, 45, 132
 Thermal limits, 301
 Thermodynamic cycle model, 298
 Thermodynamic turbine efficiency, 678, 680
 Three-dimensional flow, 335
 Through-flow model, 333
 Thrust coefficient, 560, 562, 564
 Thrust correction, 135
 Thrust gain, 46, 105
 Thrust gain potential, 534
 Thrust management, 265, 310, 311
 Thrust per frontal area, 48, 53
 Thrust response times, 290
 Thrust/weight ratio, 48, 53
 Ti-6AL-4 V, 432
 Time constant, 279
 Tip clearance, 69, 145, 172, 231, 232, 269, 273, 274, 276, 277, 289, 483, 484, 497, 519, 647
 Top of climb, 45
 Topping cycle, 19
 Torque, 85, 460
 Total pressure, 3
 Total temperature, 3
 Trailing edge loss, 392
 Transient Performance
 First order lag, 279
 Simulation, 269
 Transient control, 269
 Transient performance, 269
 Transmission efficiency, 26
 Trend Monitoring, 236
 Trent, 115
 True airspeed (TAS), 617
 Truncated normal distribution, 725
 Turbines
 AnSyn factors, 219
 Center frame, 423
 Cooling air, 692
 Design envelopes, 394
 Efficiency, 15, 58, 661
 Equivalent single-stage turbine, 393, 670, 677
 Equivalent single-stage turbine efficiency, 680, 692
 Flow capacity, 121, 219, 233, 581
 HP turbine, 304, 308, 380, 418
 HP turbine flow capacity, 728
 Inlet conditions, 663
 LP turbine, 308, 381, 420
 Over-tip leakage loss, 392
 Performance, 503
 Profile loss, 391
 Rotor blade temperature, 229
 Rotor loss coefficient, 361
 Stage count, 679
 Tip clearance, 197, 200
 Turbine function, 357
 Turning, 336
 Two-staged cooled turbine, 668
 Uncovered turning, 369
 Vane loss coefficient, 361
 Velocity triangles, 61, 510
 Zweifel loading coefficient, 377, 396
 Turbine maps
 Turbine map β -lines, 516
 Turbine map format, 512, 515
 Turbine map scaling, 517
 Turbine map shape, 145
 Turbofan
 Augmented turbofan, 56, 106
 Direct drive turbofan, 70, 72
 Dry turbofan, 52
 Mixed flow turbofan, 44, 45
 Separate flow turbofans, 43, 45
 Turbofan, 34, 66, 100
 Turbofan booster operating line, 597
 Turbojet
 Dry engine, 30
 Turbojet, 23, 100, 220, 578
 Wet engine, 30
 Turboprop
 Turboprops, 146
 Unducted Fan (UDF), 401
 Turboshaft, 5, 146, 737
 Two-stage cooled turbine, 668
- U**
 Ultimate strength, 431
 Uncertainty, 223, 727
 Uncovered turning, 369
 Unducted Fan (UDF), 401
 Unmixed thrust, 533
 Untwist correction, 487
 US Military Standard 210, 617
- V**
 V2500, 274, 434
 Vane incidence, 325, 370
 Vaneless counter-rotating turbine, 370, 401, 520
 Vane loss coefficient, 361
 Variable area nozzles, 53, 266, 541
 Variable compressor geometry, 590
 Variable Cycle Engine (VCE), 355
 Variable geometry compressor, 601
 Variable geometry turbine, 520, 650

- Variable guide vanes (VGV), 144, 188, 195, 266, 321, 469, 482
Variable inlet guide vanes, 468
Velocity coefficient, 562
Velocity diagram
 Compressor, 321, 326
 Turbine, 61, 75, 367, 371, 405, 510
 Velocity triangles, 454, 468
Virtual NGV, 673
Virtual RIT, 673, 676
Virtual T4, 674, 676
Volume filling, 281
Von Mises stress, 432
- W**
Water/air mass ratio, 136
Water injection, 616
- Wave rotor, 10
Weight, 90
Weight Analysis of Turbine Engines (WATE), 411
Wet engine, 30
Work coefficient, 380, 454
Worm diagram, 683
- Y**
Yield strength, 432
- Z**
Zero-D performance programs, 66
Zero-speed line, 455
Zweifel loading coefficient, 377, 396